



**GOVT. DIGVIJAY AUTONOMOUS PG  
COLLEGE,  
RAJNANDGAON, CG**  
AFFILIATED TO  
Hemchand Yadav Vishwavidyalaya, Durg  
Reaccredited b++ by NAAC

## Report 2023-24

**3.4.4 - Number of books and chapters  
in edited volumes / books published  
per teacher during the year**

(Session 2023-24)



स्थापना वर्ष

प्राचार्य  
PRINCIPAL  
शासकीय दिग्विजय महाविद्यालय  
DIGVIJAY COLLEGE  
राजनांदगांव (छ.ग.)  
RAJNANDGAON (C.G.)

# CARBON DOTS IN BIOLOGY

SYNTHESIS, PROPERTIES, BIOLOGICAL  
AND PHARMACEUTICAL APPLICATIONS

*Edited by Berdimurodov Elyor Tukhliyivich  
and Dakeshwar Kumar Verma*

G I E



ACS SYMPOSIUM SERIES

# CARBON DOTS

RECENT DEVELOPMENTS AND  
FUTURE PERSPECTIVES



**E. BERDIMURODOV,  
D. K. VERMA & L. GUO**

 ACS Publications

ACS SYMPOSIUM SERIES

# HEAVY METALS IN THE ENVIRONMENT

MANAGEMENT STRATEGIES FOR GLOBAL POLLUTION



**D. K. VERMA, C. VERMA  
& P. K. MAHISH**



ACS Publications



Scanned with OKEN Scanner

DE GRUYTER

STEM

# PHYTOCHEMICALS IN MEDICINAL PLANTS

BIODIVERSITY, BIOACTIVITY AND DRUG DISCOVERY

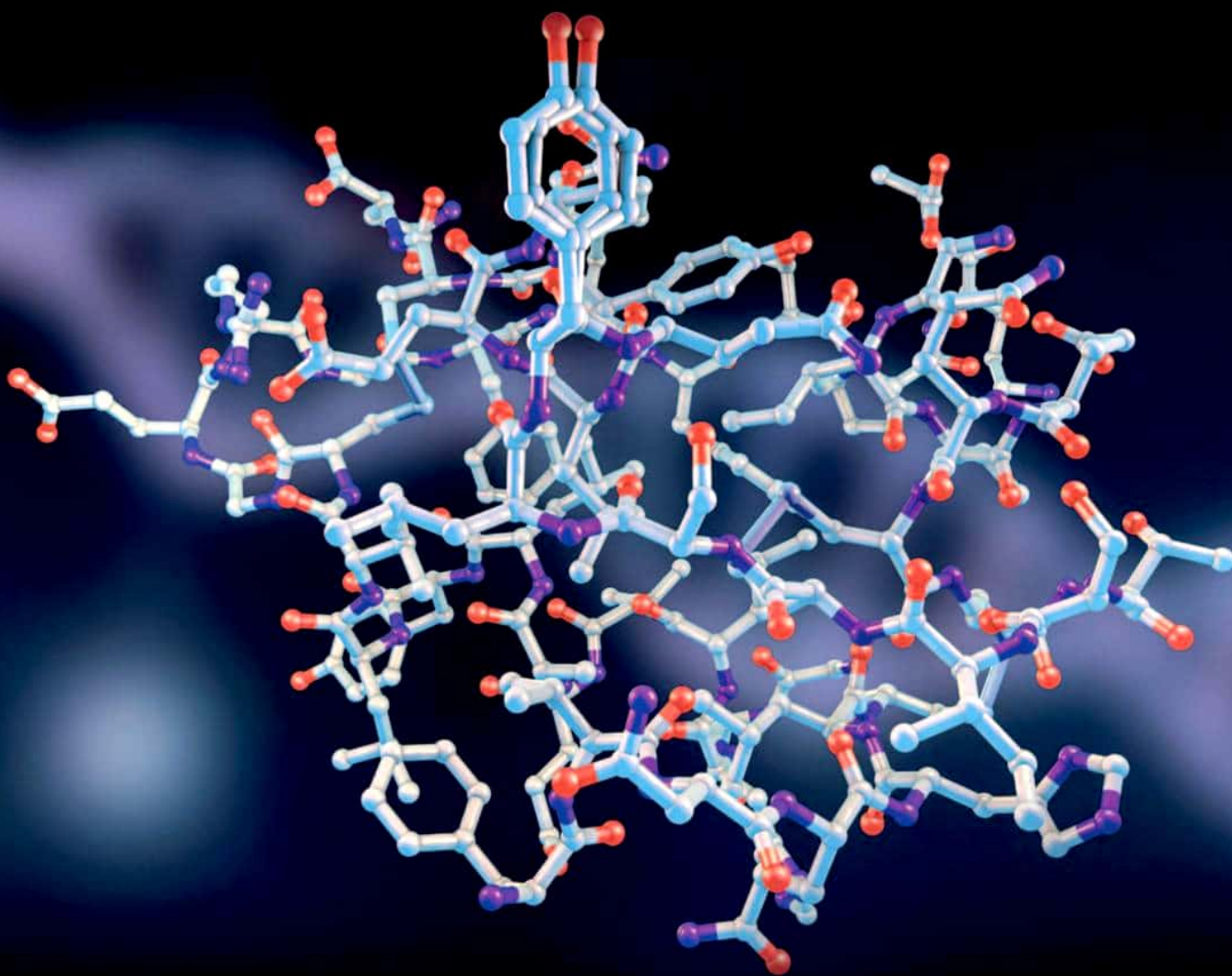
*Edited by Charu Arora, Dakeshwar K. Verma,  
Jeenat Aslam, Pramod K. Mahish*



DE  
G

# COMPUTATIONAL MODELING AND SIMULATIONS FOR DESIGNING OF CORROSION INHIBITORS

Fundamentals and Realistic Applications



Edited by

Dakeshwar Kumar Verma

Chandrabhan Verma

Jeenat Aslam



Copyrighted material



Scanned with OKEN Scanner

# ESSENTIAL OILS

SOURCES, PRODUCTION AND APPLICATIONS

*Edited by Rajendra C. Padalia,  
Dakeshwar K. Verma, Charu Arora  
and Pramod K. Mahish*



DE  
G

WILEY-VCH

Edited by Dakeshwar Kumar Verma,  
Chandrabhan Verma, and Paz Otero Fuertes

# Green Chemical Synthesis with Microwaves and Ultrasound

Green Chemical Synthesis with

WILEY-VCH





# HANDBOOK OF ORGANIC NAME REACTIONS

REAGENTS, MECHANISM AND APPLICATIONS



**Dakeshwar Kumar Verma**  
**Yeestdev Dewangan**  
**Chandrabhan Verma**

Copyrighted material



Scanned with OKEN Scanner

DE GRUYTER

# CARBON ALLOTROPES

NANOSTRUCTURED ANTI-CORROSIVE MATERIALS

*Edited by Jeenat Aslam, Chandrabhan Verma,  
Dakeshwar Kumar Verma, Ruby Aslam*

DE  
G

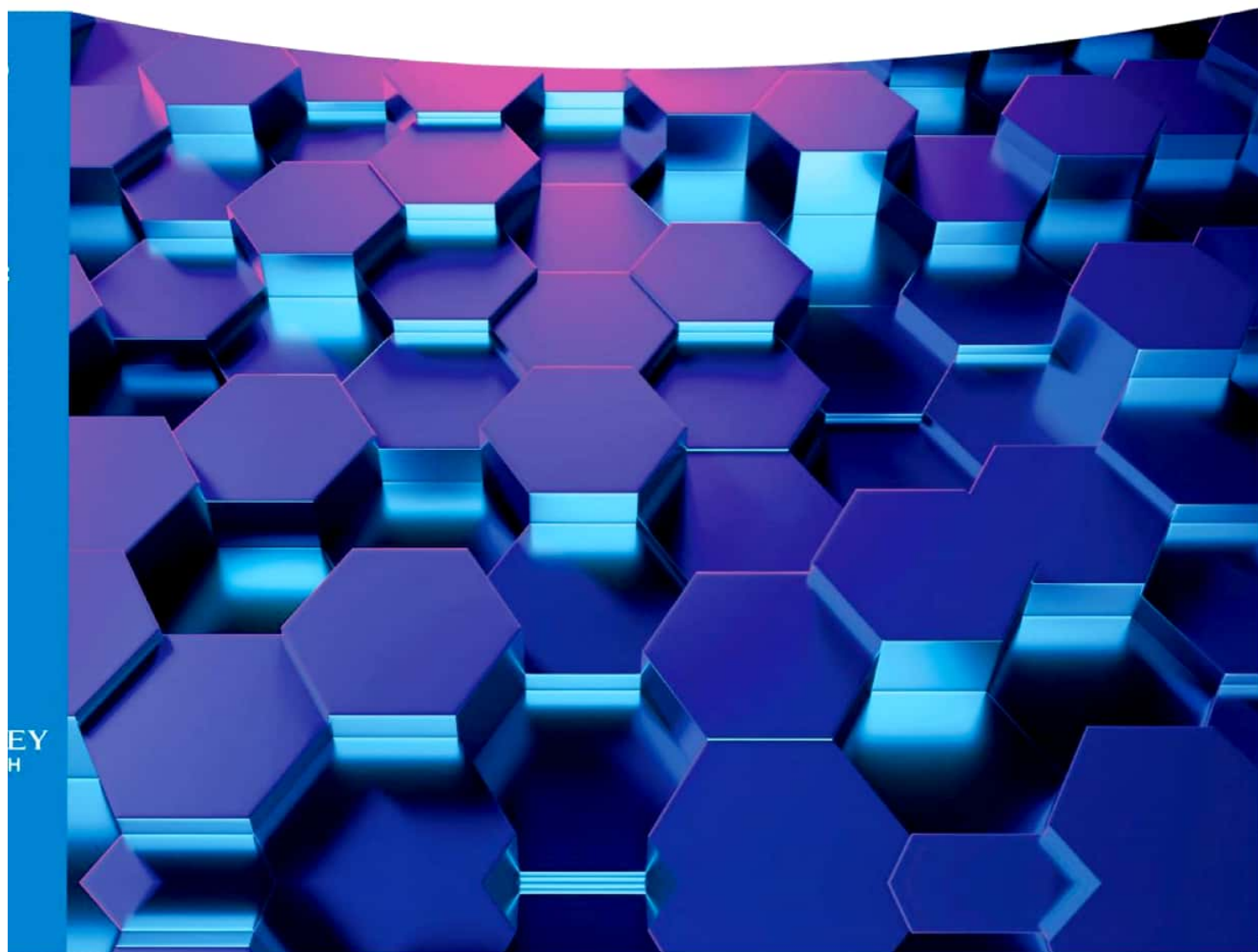


WILEY-VCH

Edited by Dakeshwar Kumar Verma and  
Jeenat Aslam

# Organometallic Compounds

Synthesis, Reactions, and Applications



WILEY-VCH



# Metal Organic Frameworks

Fundamentals to Advanced

Edited by  
Bhawana Jain  
Dakeshwar Kumar Verma  
Ajaya Kumar Singh  
Jai Singh



Copyrighted material



Scanned with OKEN Scanner

EMERGING MATERIALS AND TECHNOLOGIES

# Biosorbents

Diversity, Bioprocessing,  
and Applications

Edited by

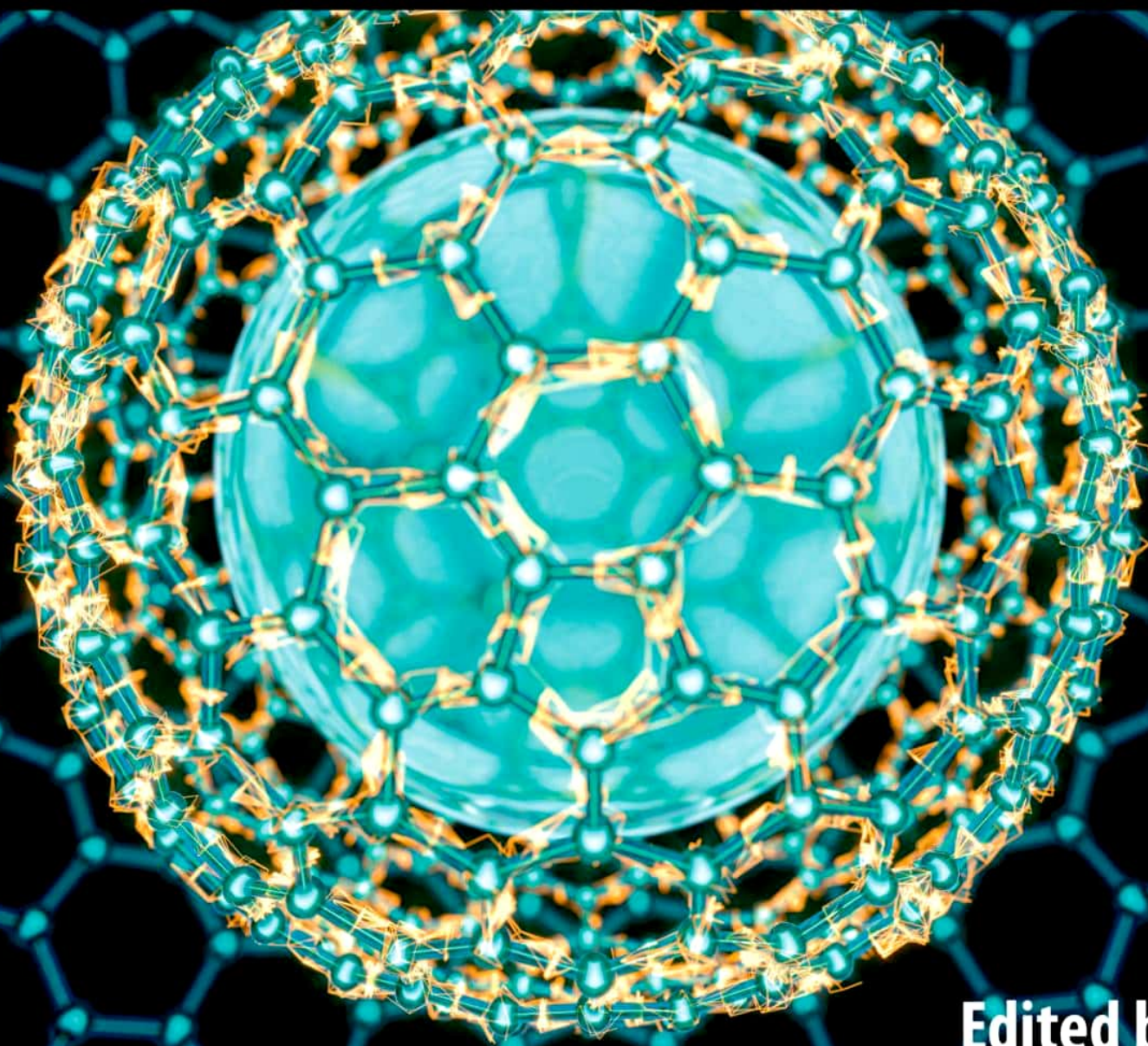
**PRAMOD KUMAR MAHISH,  
DAKESHWAR KUMAR VERMA,  
and SHAILESH KUMAR JADHAV**

 **CRC Press**  
Taylor & Francis Group

Copyrighted material

# HANDBOOK OF BIOMOLECULES

Fundamentals, Properties, and Applications



Edited by  
**Chandrabhan Verma**  
**Dakeshwar Kumar Verma**



Copyrighted material



Scanned with OKEN Scanner

ACS SYMPOSIUM SERIES

# HEAVY METALS IN THE ENVIRONMENT

MANAGEMENT STRATEGIES FOR GLOBAL POLLUTION



**D. K. VERMA, C. VERMA  
& P. K. MAHISH**



ACS Publications

## Chapter 11

# Analyzing Contamination of Heavy Metals—ICP-MS and SEM-EDS

Neeta Gupta,<sup>1</sup> Rakesh Kumar Yadav,<sup>2</sup> Bhawana Jain,<sup>3,\*</sup> Shilpi Shrivastava,<sup>4</sup>  
and Dakeshwar Kumar Verma<sup>5,\*</sup>

<sup>1</sup>Department of Chemistry, Govt. E. Raghavendra Rao P.G. Science College, Bilaspur, Chhattisgarh 495001, India

<sup>2</sup>Department of Chemistry, Dr. C.V. Raman University, Kargi Road, Kota, Bilaspur, Chhattisgarh 495113, India

<sup>3</sup>Siddhachalam Laboratory, Raipur, Chhattisgarh 491001, India

<sup>4</sup>Kalinga University, Kargi Road, Raipur, Chhattisgarh 493221, India

<sup>5</sup>Department of Chemistry, Govt. Digvijay Autonomous Postgraduate College, Rajnandgaon, Chhattisgarh 491441, India

\*Email: bhawanajain123@gmail.com.

\*Email: dakeshwarverma@gmail.com.

Naturally occurring elements with a high atomic weight and a density at least five times higher than that of water are referred to be heavy metals. The widespread use of heavy metals raised the concerns towards effects on human health and pervasiveness in the environment due to usage in large quantity. Present article describes the harm that heavy metals can cause to both living organisms and their environment. Newfangled techniques for analysis were also discussed, including ICP-MS and SEM/EDS. Advanced inductively coupled plasma mass spectrometry (ICP-MS) and energy dispersive spectroscopy (EDS) and scanning electron microscopy (SEM) were utilized to establish a procedure for the detection and elimination of metal contaminants. In conclusion, a number of complementary and cutting-edge methods are presented as the optimal procedure for removing heavy metals from water and soil. We hope this investigation of multistep procedures will inspire researchers to launch brand-new cleanup initiatives.

## 1. Introduction

Greater ecological and global public health worries have been related to pollution from these metals in recent years. Heavy metals are those that have a higher density than water. Assuming



a correlation between mass and toxicity, “heavy metals” also encompass metalloids like arsenic, which can be dangerous even at relatively low concentrations (1). Their widespread dispersion in the environment as a result of their many industrial, residential, agricultural, medicinal, and technical uses has raised questions about their possible consequences on both human health and the environment. Numerous factors, including as the dosage, the method of exposure, the chemical species, as well as the exposed individuals’ age, gender, heredity, and nutritional status, all have an impact on the toxicity of these substances. Priority metals include those with the potential to cause the greatest harm to the general public, such as arsenic (As), cadmium (Cd), chromium (Cr), lead (Pb), and mercury (Hg). These metals are considered systemic toxicants, and even low-level exposure is known to damage multiple organs. Apart from this various heavy metals are natural origin observed in the earth’s crust, the excavation/mining and industrial production and usage, domestic, agricultural based heavy metals, metal based compounds are the primary sources of environmental pollution and human activities (2). Heavy metals can be found in the environment from a variety of different geological, industrial, agricultural, pharmaceutical, and household effluents, as well as the atmosphere. Additionally, corrosion of metals, soil erosion leading to metal ions, air deposition, and stripping of heavy metal ions, deposit resuspension, and metal vaporization from water resources to soil as well underground water may all contribute to contamination/pollution (3). It has also been claimed that natural events like weathering and volcanic eruptions greatly contribute to heavy metal contamination (4). Industrial sources include the reprocessing of metal in refineries, burning of coal in power plants, burning of oil, nuclear power plants, and high tension lines, as well as the production of plastics, textiles, microelectronics, wood preservation, and paper.

Although heavy metals are typically found in low amounts (ppb range to less than 10 ppm) throughout a wide range of environmental matrices, they are also classified as trace elements (5). They are affected by physical parameters like temperature, phase association, adsorption, and sequestration, which all play a role in their bioavailability. Moreover, it is impacted by chemical elements such as complex kinetics, lipid solubility, and octanol/water partition coefficients that alter speciation at thermodynamic equilibrium (6). Other significant biological aspects include species traits, trophic relationships, and biochemical and physiological adaptability (7). The necessary heavy metals influence the biochemistry and physiology of plants and animals. They serve significant roles in several oxidation process and are significant components of several essential enzymes (8). The cell membrane, mitochondria, lysosomes, endoplasmic reticulum, nuclei, and certain enzymes involved in metabolism, detoxification, and damage repair have all been documented to be impacted by heavy metal exposure in biological systems (9). Interactions between metal ions and DNA and nuclear proteins have indeed been observed, leading to DNA damage and conformations that may trigger cell-cycle modulation, carcinogenic, or cell death (10). A number of in-house experiments have shown that ROS generation and oxidative stress are crucial in the carcinogenicity of metals like As, Cd, Hg, Cr and Pb (11, 12). These five components are among the most poisonous and therefore are considered to be of paramount importance to public safety. All of these substances are systemic toxicants, meaning they can cause harm to several organs at even relatively modest doses. There are numerous molecular components of heavy metal-induced toxicity and carcinogenicity, not all of which have been fully explained or understood. Yet, it is well recognized that different metals have different toxicological modes of action due to their individual characteristics and physicochemical qualities. The goal of this study is to obtain information about the heavy metals, distribution, identification, and removal techniques. Also the study aims to brief out advanced techniques employed to analyse heavy metals such as ICP-MS and SEM-EDS. Also we tried to elaborate the removal of heavy metals using various materials employed as removing agents and techniques.

## 2. Impact of Heavy Metals on Organisms and Environment

In any organisms, numerous deficiency disorders or syndromes are brought on by an insufficient supply of certain micronutrients. Vegetation and animals' biochemistry and physiology are affected by the heavy metals essential for their survival. They are crucial parts of several important enzymes and play pivotal roles in a variety of oxidation-reduction reactions. In addition, it has been noted that heavy metals may impact cellular organelles and parts in biological systems, including the cell membrane, mitochondria, lysosomes, endoplasmic reticulum, nuclei, and several enzymes involved in metabolism, detoxification, and damage repair (13). Metal ions have been discovered to interact with nuclear proteins and DNA in cells, resulting in DNA damage and conformational changes that might influence the cell cycle, cause cancer, or trigger apoptosis. Numerous lab studies have shown that the generation of reactive oxygen species (ROS) and oxidative stress are crucial factors in the toxicity and carcinogenicity of metals such as arsenic, cadmium, chromium, lead, and mercury (14–16).

For many years, many levels of biological organization have demonstrated metal's effects on aquatic life. Heavy metals typically reach the food chain through the roots of plants through the adsorption step. Heavy metal absorption by plants is influenced by environmental factors such as temperature, humidity, pH, nutrition and organic matter availability. It has also been shown that summertime absorbent activity is much higher than wintertime absorbent activity. The efficiency of plants to gather certain heavy metals depends on both specific plant species and the metals themselves. There is a wide range in how plants respond to changes occurs in levels of nutrients and heavy metals in soil. These extensive alterations to plant characteristics result in new light absorption and reflectance characteristics that may be used to gauge soil pollution and the plant's physiological health. When the concentration of heavy metals and metalloids in soil reaches a critical level, the metals and metalloids may accumulate in both the roots and the leaves of plants to dangerous levels. Metal poisoning in plants has been linked to a variety of physiological changes, including stunted development, reduced photosynthesis, and increased respiration and transpiration. Utilizing atomic absorption spectroscopy, the status of several heavy metals in seasonal vegetables such as mustard, cabbage, spinach, and cauliflower planted in Kakching-Wabagai was examined (17). It was determined that the samples with no lead levels in them had Fe and Cu concentrations beyond allowable limits. Raphanus and Phaseolus exhibit some of the identifying leaf symptoms, combined with a decreased root, shoot and biomass ratio. Ochoa-Hueso R et al., explored the various elements concentrations for shoots, soil, roots, and fruits collections in diverse plants (18). Pepper has the greater level of Copper (Cu) and Zinc (Zn) rises in plant shoot, accompanied by collard greens, radishes, lettuce, and tomatoes. Tomato plants had much higher concentrations of Cu and Zn than the other examined plants. Such biogeochemical processes in the root exudates resulted in the release of organic acids. As the metal accumulates in the roots of developing plants, it stunts their development.

In the field of water, the majority of rivers are contaminated, particularly water contamination may originate from a wide variety of human activities, such as mining, automobile emissions, industrial emissions, combustion, and garbage incineration. After that, they make their way down to the ocean, where the majority of them sink to the ocean floor and the flow of water slows down. Therefore, biotic components are put at risk due to water pollution since it is often ingested. Additionally, the pH of the water is a major factor in determining which metals are soluble. When metal-rich Rivers enter the ocean, the pH drops and the metals sink to the sea floor as a result of their decreased solubility (19). Heavy metals' propensity to increase environmental toxicity has made them a worldwide issue of particular concern in the context of the aquatic environment. Many

environmental problems, like as river water poisoning, have been made worse by the overexploitation of mines across the globe. Heavier metals, such as Cd, may alter the carbon-to-nitrogen ratio of mangroves by accumulating in the plants' roots and stems. Heavy metals have an influence on carbon storage in estuary plants and mangroves, which has a knock-on effect on the global climate. Figure 1 summarizes the heavy metal sources, migration, and toxicity.

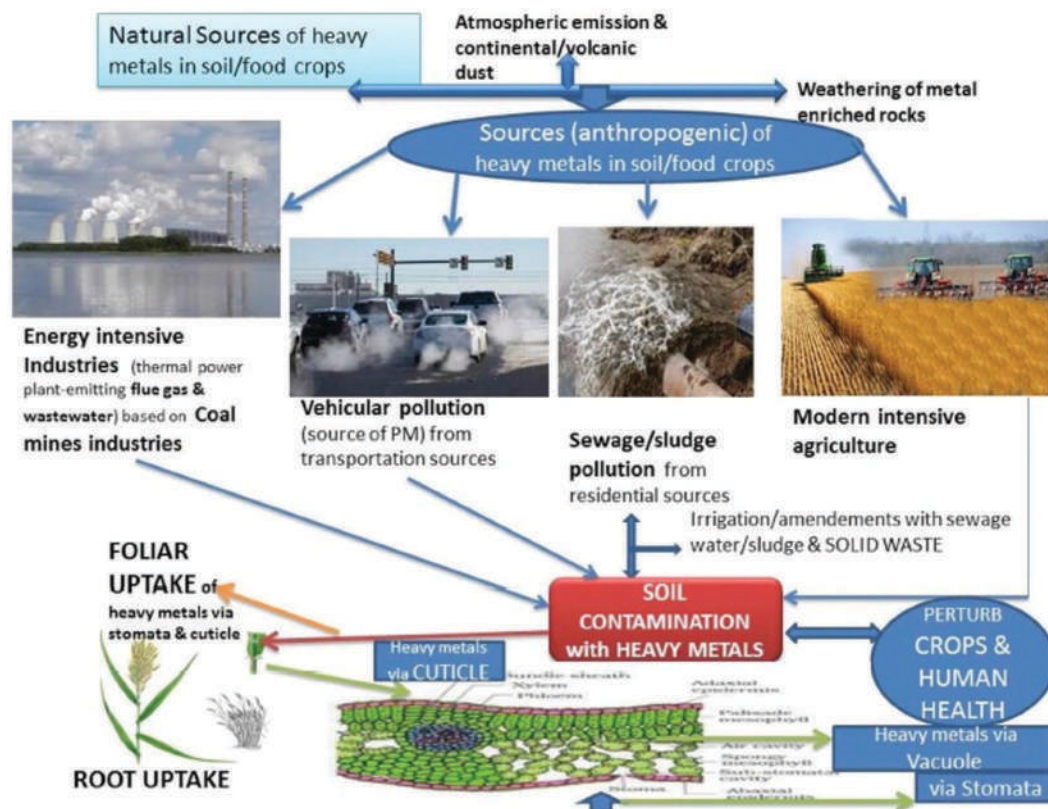


Figure 1. Sources of heavy metal contamination in food crops that are both natural and man-made, their entry points (via stomata/cuticle), and the effects they have on humans and other animals. Reproduced with permission from reference (12), 2019 Elsevier.

The environment of an estuary, as well as the people who eat the seafood caught there, might be negatively impacted by arsenic accumulation in overwhelming quantities. The bioaccumulation of cadmium in marine creatures is affected by factors such as the structure of the cadmium complex, the temperature, and the salinity of the marine environment. Since lead is only marginally soluble in salt water, it has been determined that its presence in aquatic systems is tolerable. Because of this, marine species are shielded from the danger of lead poisoning. Lead's toxicity is systemic, but it tends to accumulate in the lungs and cause damage there, which may eventually progress to cancer (20). The marine environment has been shown to contain mercury, an extremely dangerous heavy metal. Methyl mercury is a very prevalent mercury chemical that may be discovered in seafood, particularly from the Indian Ocean.

Speaking on human health, long-term exposure to high amounts of heavy metals (Nickel, Chromium, Cadmium etc.) may have devastating consequences for human health. Thorough research has shown that pre-chronic toxic nature and carcinogenesis may be induced in living organisms by heavy metals (Mercury (Hg), Lead (Pb), and Arsenic (As)). Epidemiological research

indicates that Cr, As, and Ni are human carcinogens, whereas Be, Pb, and Cd are only suspected to be carcinogenic. Heavy metals are both essential for life's most fundamental processes and very poisonous when present in excess. There is cause for concern about the possible influence on human health as well as environment due to their widespread environmental presence because of their many medicinal, residential, industrial, and agricultural uses. Exposure to heavy metals, whether by ingestion or contact with the skin, is associated with an increased risk of adverse health effects due to the environmental hazards associated with heavy metal pollution. These are exceedingly dangerous to the varied ecosystems, both on land and in water. Due to their retention capabilities, heavy metals tend to build up in the environment and, ultimately, in living organisms through the food chain. For instance, long-term contact with several common industrial chemicals and metals has been associated to an increased risk of cancer. Negative health effects, such as chronic inflammation and an increased risk of cancer, have been linked to long-term exposure to Pb, As, V, Cr, Hg, Cd, Cu, Zn, and Ni. Evidence suggests that eating Cd contaminated in rice and other foods may increase the chance of developing breast cancer after menopause (21). The most severe type of chronic Cd poisoning is known as Itai-itai illness, which is brought on by the ingestion of Cd on a regular basis. Proximal tubular dysfunction is common in the Jinzu River basin population as a result of chronic cadmium exposure, which mostly affects the kidneys. It has been stated that Blackfoot illness was caused by drinking arsenic-contaminated well water in southern Taiwan. This is a rare peripheral vascular disease that occurs along the southern coast of Taiwan, causing dry gangrene and ultimately amputation of the afflicted limbs.

### 3. Analysis of Heavy Metals

Determination of amounts of heavy metal in the environment on a qualitative and quantitative level is also necessary due to the presence of different species of heavy metal and ability to form complexes. The level of toxicity induced by the various heavy metals need to be confirm, verify and propose the control measures for the safety of individual organism or environment is most important. In other words, to obtain high removal efficiency and adsorption capabilities, it is essential to use approaches that may shed light on the structural arrangements of adsorbing materials and their potential interactions with heavy metals.

#### 3.1. Advanced ICP-MS Technique

Spectrophotometry, atomic absorption and fluorescence spectrometry, X-ray fluorescence spectrometry, plasma emission spectroscopy, ICP-MS, etc. are few of the techniques used to investigate trace elements. The most adaptable detection method nowadays is ICP-MS, a potent characterisation technique employed to synthesize and identify novel materials and in the elemental analysis of diverse types of samples (22). It has applications in many fields, including biophysics, environmental research, forensic science, materials science, speciation analysis, etc. and is capable of accurately detecting and quantifying the majority of the elements from the periodic table. Furthermore, a form of ICP-MS can identify metals and a number of non-metals at concentrations as low as 1 part in  $10^{15}$  on non-interfered low-background isotopes. A mass spectrometer is used to extract and quantify the ions after ionising the sample using ICP. In comparison to atomic absorption spectroscopy, ICP-MS is quicker, more accurate, and more sensitive. The instrument has great capabilities, such as the capacity to do various elemental analyses, appropriate accuracy, and reduced detection limits. ICP-MS also provides the capacity to examine isotopes quickly, straightforward spectra, and a larger linear dynamic range (23). As a cutting-edge technique, ICP-MS is the most up-

to-date technique, and it offers several benefits, including a high detection rate, a low detection limit, a high degree of accuracy, and the ability to determine many elements heavy metals.

### 3.1.1. Operating Principle of the ICP-MS

Ions generated in an inductively coupled plasma are collected and analysed in a mass spectrometer using the ICP-MS method. First, the analyte present in liquid form is sucked inside the system using peristaltic pump, later case that initiates a constant uptake-flow-rate. Here, an auto sampler was employed to cut down on wasted reagents and speed up the analysis process. Later it is pushed into a nebulization chamber, where the liquid sample is evaporated into a gaseous aerosol. Argon gas helps transport the tiniest of droplets to the plasma, while the bigger ones are drained away. The second step involves filtering the aerosol before it is put into the plasma, because too much analyte aerosol in the solvent might cause plasma extinction. Argon plasma is created on top of a torch when the gas reacts with the electromagnetic field produced by a radiofrequency generator. Injecting the aerosol into the plasma causes it to instantly dissolve, evaporate, atomize, and then ionise depending on the ionisation potential of the constituent components. High temperatures, between 6,000 and 10,000 K, are supplied by the argon plasma. Argon gas is often employed in ICP because of its chemical stability and increased ionisation potential, which produce a normal spectrum. It has the potential to ionise or excite a wide range of elements without reliably combining with the analyte (24).

The third component is mass spectra and detection, after being vaporised in the ICP torch, the ions and atoms are transported to the interface by a stream of argon gas. The interface's storage space, formed by two conical structures stacked one on top of the other, allows the ions to concentrate in a more condensed region. From being introduced into a mass spectrometer (MS) (quadrupole or a hexapole), the ions will be sorted according to mass to charge ratio before being sent to detection unit. In ICP-MS a detection unit is primarily an electron breeding device which transforms ion signalings into electric pulses (25).

### 3.1.2. Advantages

ICP-MS may be used to accurately quantify the identification of metal ions present in natural sources and drinking water at lower levels; this is especially important in areas where toxicity management is crucial due to possible metal contamination. As a result of its high sensitivity, small sample size need, and low susceptibility to interference from other elements, ICP-MS technique is widely accepted for adsorption/water treatment study. ICP-MS has certain drawbacks, such as its sensitivity to higher level salt concentrations found in metabolite, sweat, and saliva extraction solutions, which may create disturbances of the data, and its high operating expenses due to the significant quantity of argon utilised.

## 3.2. Advanced ICP-MS Technique Employed to Detect Contamination of Heavy Metal Ions

Sung Hwa Choi and colleagues used the ICP-MS, DM), and femtosecond (fs) laser ablation – ICP-MS (fs-LA-ICP-MS) to determine the lead, cadmium, mercury, concentrations in four commercially available cereals (26). Furthermore, Using the ICP-MS method (ICP-MS ELAN 9000 for the analysis (Perkin Elmer)), Nur Azalina Suzianti Feisal et al. determined the levels of nickel, arsenic, cadmium, and lead in a hair sample (27). Author's findings demonstrated that ICP-MS may be more sensitive than other methods, with a detection limit as low as 2.34 g/g and ICP-MS can provide multi-element measurements accurate to within a few parts per billion. Qiang He and

co-workers utilised a dual-cloud point extraction (d-CPE) in conjunction with ICP-MS for pre-concentration and determination of Cr, Ga, Ag, Cd, Mn, Fe, In, Cu, Ni, Co, Pb, and Zn in natural water samples (28). They found that not only does it remove surfactant's effect on ICP during the surfactant-rich phase, but it also mitigates interferences introduced by the sample matrix. Another research reported an on-line separation technique for determining Cu, As, Se, Cd, In, Hg, Tl, Pb, and Bi in water and biological materials using ICP-MS (29). According to the findings of the research The ELAN 6000 ICP-MS from Perkin Elmer-Sciex was used. The research showed that the separation and preconcentration of Cu, As, Se, Cd, In, Hg, Tl, Pb, and Bi may be achieved by the coupling FI-ICP-MS with on-line complexation with DDTP, followed by sorption of the complexes in a minicolumn packed with C18 silica gel and elution with methanol. The suggested approach not only improves sensitivity but also permits matrix separation for external calibration. In addition, the method allows for high sampling frequencies, low relative standard deviations (less than 6%), and minimal sample and chemical consumption (29).

Similar to the previous work, this one used a microwave acid digestion system using ICP-MS and DMA to effectively quantify the 6 heavy metals (Me-Hg, Pb, Sn, Cd, As, and Hg) were observed in the HMR products. The six heavy metals were present at an average quantity of 8.87  $\mu\text{g}/\text{kg}$ . Recalculating the 95 % of food intake data ( $\mu\text{g}$  per day) for each heavy metal required converting heavy metal levels to food intake data at a rate of 0.009  $\mu\text{g}$  per kg (30). The production of fish and aquaculture in Vietnam's coastal region makes a significant contribution to the national economy. However, for both local and foreign markets, concerns about seafood quality and safety, particularly with regard to metal concentrations, are growing. However, certain fish have the capacity to take up and retain trace metals in their systems, which subsequently have an impact on human health when humans eat fish (31). Trace metal elements present in seafood's, particularly in key seafood's items, is of significant attention in tandem with rising demands for food safety and consumption. The various biokinetics of different species are intimately tied to the trace metal elements that accumulate in them. According to an analysis by Wang and Guangyuan, which looked at the levels of many main metal pollutants in bivalve mollusks from throughout the globe, oysters are the hyperaccumulators of copper and Zinc, while scallops are the hyperaccumulators of Cd (32). As a result, many different kinds of animals serve as environmental indicators of water quality. As an example of a bioindicator, oysters are often used to detect copper and zinc pollution.

Nhu Da Le and colleagues conducted four sampling campaigns in 2020 to determine the concentrations of various trace metal elements (TMEs) Fe, Zn, Mn, Cu, As, Cd, and Hg in fishes, crustaceans, and mollusks living in the coastal zone of the Red River (33). ICP-MS analysis of fish, crustacean, and mollusk samples revealed that concentrations of TMEs order as follows  $\text{Fe} > \text{Zn} > \text{Mn} > \text{Cu} > \text{As} > \text{Cd} > \text{Hg}$ . Specifically, the levels of iron, zinc, manganese, copper, arsenic, cadmium, and mercury in seafood samples ranged from 13.13 to 202.73; 7.63 to 82.71; 0.48-22.73; 0.72-15.58; 0.18-5.12; 0.001-1.114; and 0.001-0.923  $\text{mg kg}^{-1}$ . LOD and LOQ values of TMEs evaluated by ICP-MS. The rising level of life in China has shifted the country's attention to food safety and quality. Hongxing Zhang et al. determined the Ca, Mn, Fe, Zn, Cu, Cr, As, Se, Mo, Cd, La, Ce, Pr, Nd in rice grown in Lishu county, Jilin province, using ICP-MS combined with microwave digestion. In terms of its trace components, the findings revealed that northeastern rice is of higher quality. It has more good elements and less heavy metals (34).

Bioaccumulation of metals in rice grains is used as a selection criterion. To aid in variety selection, rice breeding needs a very sensible technique of determining metal concentration in individual rice grains. Xiufen He used a quick and easy approach to assess the presence of four hazardous metals As, Cd, Cr, and Pb in a single grain of rice (35). Therefore, author created a simple

and quick solid sampling platform based on pure multi-walled-carbon-nanotubes (MWCNTs) and aided Matrix-solid-phase-dispersion (MSPD) and analysed by using ICP-MS. Good sensitivity and accuracy were shown by the method's restricts spotting ability, which were observed around 5.0, 0.6, 10, and 2.1 ng/g<sup>-1</sup> (As, Cd, Cr, Pb), with relative-standard-deviations (RSD) n=6 of 7.7 percentage. 30 field samples of rice tested with this technology showed findings that were in agreement with those obtained using the conventional microwave digestion. Giacomo Dugo et al., determined common spices sold on the Italian market were analysed the levels of Cd, Hg, As, and Pb using ICP-MS. With regard to Cd and Hg, the food safety analysis for spices took into account considering the Tolerable-Weekly-Intake (TWI) and the Provisional Tolerable-Weekly-Intake (PTWI), similarly for As and Pb, it used the 95 percentage lower-confidence-limit (LCL) of the bench mark dosage (BMDL) of 1% excess risk. At long last, they were able to confide in one another. All samples tested had concentrations of the components under study that were far below the limits specified by national and international norm-setting bodies (36).

#### 4. Advanced SEM-EDS Technique

The value of traditional imaging methods is sometimes overlooked as a result of the availability of an expanding number of improved imaging instruments. In reality, the basis for drawing reliable conclusions regarding functional connections is the capacity to view structures with the great resolution attained by utilising electron microscopes. The capacity of scanning electron microscopy (SEM) to analyse dimensional topography and the distribution of exposed features remains unique despite advancements in other forms of light (LM), atomic force microscopy (AFM), and electron microscopy (EM). By maximising specimen preparation and instrumental parameters, the final resolution attained is managed. In addition, a SEM paired with an Energy-Dispersive-X-ray spectrometer (SEM/EDS) is one of the important analytical tool used to detect and characterise heavy metals in environmental media. A brand new piece of equipment for micro-scale qualitative and quantitative chemical analysis. The analysis provided by SEM with EDS proved to be extremely helpful in determining the origins and identities of heavy metal-containing phases.

##### 4.1. Basic Operating Principle of the SEM-EDS

Electron microscopes take advantage of the wave-like characteristic electrons to create a micrograph using an electronic beam. A tungsten wire filament is heated in the SEM utilized at GeoZS, emitting electrons which were generally accelerated at very high speed by using an anode. The diameter of the electron emitting beam is adjusted using electromagnetic lenses (condenser lenses), and objective lenses were used to focus the beam on a probe-point located on the specimen surface (37). As wavelength of the electronic beam is shorter than that of visible light, SEM makes it possible to achieve high resolution as well as practical magnification. Electron beam-sample interactions produce several signals, including secondary electrons (SE), backscattered electrons (BSE), distinctive X-rays, and others. SE are electrons with a lower energy that are formed at the surfaces of the material as a result of awakening electrons in the specimen's outer shell that are loosely bound. These electrons can be used to construct a topographical map of the sample. The BSE are the main electronic beam which were forcibly deflected using atomic-nuclei (AN) in the specimen, but they kept the majority of their energy after leaving the sample, which allowed for the creation of a Z-contrast or compositional picture of the sample. Deep inside the sample, the electron beam interacts with an inner shell electron, causing it to be expelled and replaced with an electron from a higher

energy shell, resulting in the emission of a photon of distinctive X-rays. Multiple detectors are used to pick up signals and convert them into a picture or recognisable X-ray spectra.

#### 4.1.1. Advantages

Since it is one of the most distinguishing chemical properties of chemical compounds, the atomic number ( $Z$ ), which is different for each element, serves as the basis for both BSE imaging and X-ray (EDS) identification of heavy metal-bearing phases. The elemental abundance in a sample determines how many BSE are present.  $Z$ -contrast, also known as compositional contrast, allows for the relative differentiation of particles with varied elemental composition by reflecting more BSE than elements with lower  $Z$ . The high atomic number and high electron density of heavy metals make them excellent electron backscatters. The following are the fundamentals of recognising and characterising heavy metals. Samples are first inspected at low magnifications using the BSE mode that permits the heavy metal-bearing phases in the sample to be localised to grains. In a low  $Z$  matrix, their brightness is accentuated (38). Heavy metal-containing grains in the sample are first localised using BSE imaging, and then the chemical composition of those grains is evaluated qualitatively and semi-quantitatively using an energy EDS. EDS is able to detect and analyse the X-rays that are unique to each chemical element based on its atomic number since they are released by the element itself.

#### 4.2. Advanced SEM-EDX Technique Employed to Detect Contamination of Heavy Metal Ions

SEM and EDS work together to do single-particle analyses. Heavy metals whose concentrations are less than the EDS's theoretical-detection-limit (TDL), as established by conventional geological bulk sample analysis, can be identified using this method. Thus, certain metal trace elements may be detected. The atomic proportions of the component elements, as determined by semi-quantitative X-ray microanalysis, are subsequently used to evaluate the mineral phases of heavy metals. Heavy metals may be analysed with a SEM because of its high resolution in a variety of environmental conditions (stream soil and sediments, mining waste deposits, transportation, and atmospheric depositions occurs snow). However, as metals are often found in solid forms, their origins may be determined by examining their connections in specific particles as well as their mineralogy, morphology, and chemical makeup using technologies such as electron microscopy and microanalysis. Milos Miler et al. classified the metal-bearing particles into 19 separate metal-bearing phases after identifying the particles and characterising those using SEM/EDS (39). These phases were divided into three categories based on their elemental makeup and morphology: geogenic-anthropogenic, anthropogenic, and secondary weathering products. In order to analyse the impacts of mangrove wetland restoration on microplastics and examine the connection between microplastics and heavy metals, Peiyong Guo et al. attempted to give data on the abundance, kinds, surface textures, and accumulated heavy metals from the wetland (40). Injuries/fractures, changes, cavities, peels/flakes, and the adhesion of different materials were shown in the SEM pictures to be typical hallmarks of microplastic deterioration, while heavy metals including Cr, Zn, Pb, and Cd were shown to be adsorbed onto their surfaces in EDS images. The accumulation of heavy metals in microplastics occurred in the following order: Zn > Pb > Cu > Cr > Ni > As > Cd > Hg, and microplastics could serve as a heavy metal transporter.

Author Chandrashekar and colleagues collected samples from the Ponnai River in Tamil Nadu, India in order to characterise minerals and heavy metals using various spectroscopic methods (41). They discovered heavy metals using SEM/EDS and SEM/EDS results showed that Zn, Cr, Pb, Ni, Cu, Mn, As, and Hg are present in the sand samples. According to the outcome of multivariate



statistical methods, the examined metals As, Cr, Ni, Mn, Hg, and Pb were deposited in samples as a result of home and industrial effluent discharge, whereas Zn was obtained via transportation operations. As a result, the findings of this study suggest that ongoing monitoring is necessary to determine the degree of contamination in the study area because both natural and anthropogenic activities affect the quality of the sand samples on a daily basis. Rafa Panek et al. investigated the effectiveness of virgin zeolite (Na-X) and a zeolite-carbon-composite (Na-X-C)) as adsorbing material for the removal of the  $Pb^{2+}$  and  $Zn^{2+}$  ions from aq. solutions. Particle size, elemental content, XRD, SEM-EDS, and  $N_2$  adsorption/desorption all used to characterise both materials. According to their research, Zn ions are far better at exchanging places when cations present within the zeolite material structure compared to Pb ions, which are significantly higher. It has been demonstrated that the competition for accessible reactive sites present on the surface of adsorbent proceeds to a significant reduction in the total volume of both heavy metals which are adsorbed when the solutions include both of them together. As an added bonus, while sodium base was more effective at desorbing the heavier metal,  $Pb^{2+}$ , hydrochloric acid was more effective at desorbing both heavy metals (42).

Tailings and other solid waste include a wide variety of heavy metals in concentrated amounts. The potential end result, a glass-ceramic, not only offers superior physical qualities, but also successfully solidifies heavy metal ions. According to Zhang Yunsheng, there has been a comparatively small amount of study conducted for the stabilisation of only one heavy metal in glass ceramics. In this regard, they utilised Zn and Cu, and 2 heavy metals which are found in tailings on a regular basis, as stand-ins in order to evaluate the phase changes and chemical mechanism for stabilising the mixture. The author has confirmed that zinc and copper behave in very different ways during healing phase of glass ceramic. Zn and Cu both stay put in the deposit phase as a solid solution when the heavy metal ions limit is lower than 1.5 weight percentage. Since glass ceramics effectively bind heavy metals, the stripping level is substantially lesser than the standard level, and the stripping rate is rather consistent when heavy metal level is up to 1.5 weight percentage. Finally observed outcome demonstrated the high reliability and possibility of recycling Zn and Cu rich tailings and other solid-wastes in an eco-friendly acceptable glass ceramics (43).

There is an immediate need to upgrade the dated sewage treatment system that cannot eliminate heavy metals. Granular sludge was loaded with bio-mineralizing *Lysinibacillus* using a screening process, and the resulting bacterial consortium was able to self-regulate pH and solid-liquid separation. As such, the bacterial consortium might be made to create stable and innocuous phosphate minerals by having heavy metals fastened on it. According to a study by Yingwen Xue et al., the maximum removal efficiencies for  $Pb^{2+}$ ,  $Cd^{2+}$ , and  $Ni^{2+}$  ions respectively, were 97.9%, 70%, and 40%. Despite the presence of organic matter and other metal ions in the dirty water used in this study,  $Pb^{2+}$  removal efficiency was not significantly affected. The mechanisms were analysed using three dimensional EEM, XPS, XRD, SEM-EDS, FTIR, and high-throughput-sequencing (HTS) techniques. As sequential results proved that bacterial consortium comprised a system in which many different species may coexist, *Lysinibacillus* proved crucial role in the action of  $Pb^{2+}$  reduction. Deducing from the SEM-EDS Proof positive that the AGS has been loaded with bacteria. Carbon, oxygen, phosphorous, chlorine, and potassium were its primary building blocks shown in the Figure 2a. Figure 2b shows the PMBC after 320 hours of  $Pb(II)$  removal, and the sediment surface was not uniform. There were many rod like particles, all having the same crystal development path. The XRD analysis confirmed that the primary components were carbon, oxygen, phosphorus, and lead (C, O, P, Pb). After 720 hours of  $Pb^{2+}$  reduction, the PMBC appeared as shown in Figure 3c. The crystals

grew in various orientations, at a considerable quantity of crystals were encased when formation of precipitate takes place, composed primarily of above said elements. As a part of confirmation results confirms the crystals' pattern/shape, size, and development path shifted in response to the conditions inside the reactor (44).

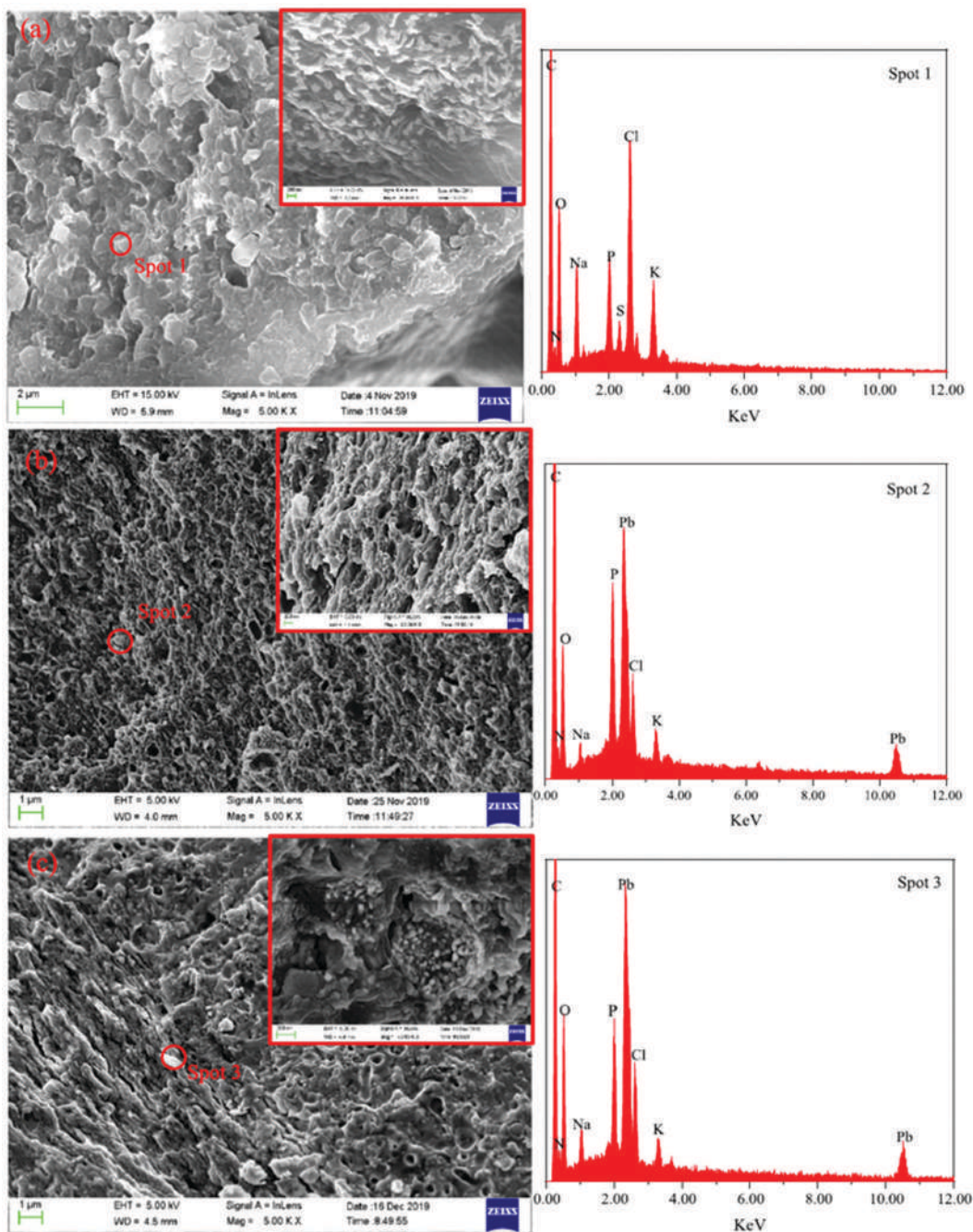


Figure 2. Sediment was analyzed using SEM-EDS before and after lead was extracted, a, b, and c all represent times before, during, and after mineralization. Reproduced with permission from reference (44), 2021 Elsevier.

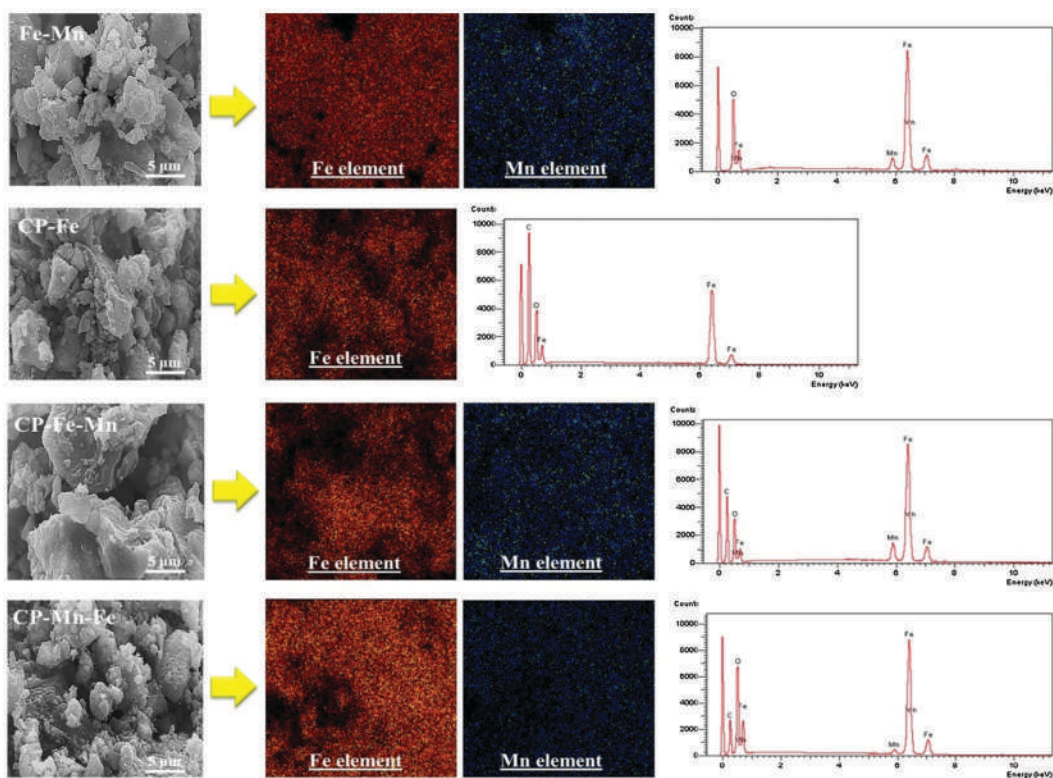


Figure 3. SEM-EDS micrographs of Adsorbents as-prepared. Reproduced with permission from reference (45), 2020 Elsevier.

Researchers led by Panya Maneechakr looked at the adsorption behaviours of heavy metal cations utilising palm kernel cake residue-based active  $\text{MnO}_2$ -modified magnetic biochar (45). They observed that, developed adsorbent, CP-Fe-Mn, exhibited paramagnetic characteristics, as indicated by a saturation magnetization value of 20.94 emu/g. The adsorption procedure for CP-Fe-Mn was found to be simple, allowing for easy recovery of the compound from the aqueous solution. According to Temkin, Langmuir, Redlich-Peterson, and Toth isotherms, Dubinin-Radushkevich the adsorbing behaviours of every heavy metal ions over CP-Fe-Mn were discovered to be a single layer physical absorption process. Similar SEM-EDS findings supported the manufactured magnetic adsorbents' morphologies, and the presence of Fe and Mn elements was displayed in Figure 3. Due to the  $\text{Fe}_3\text{O}_4$  and  $\text{MnO}_2$  covering on each adsorbent's surface, it was discovered that these surfaces were craggy and uneven.  $\text{Fe}_3\text{O}_4$  and  $\text{MnO}_2$  were not modified in the case of CP, and the surface morphology was smooth and flat. The EDS data further demonstrate the presence and even distribution of Fe and Mn elements on the support surface. Final author confirmed that maximum adsorption capacities ( $q_{\text{max}}$ )  $\text{Cd}^{2+}$ ,  $\text{Cr}^{3+}$ ,  $\text{Pb}^{2+}$ , and  $\text{Hg}^{2+}$  were 18.60, 19.92, 49.64, and 13.69 mg/g.

As phosphates are good for the environment, they could be used to make it easier to get rid of clay. By using a simple method, Zinc-Aluminium layered-double-hydroxide (LDH) was intercalated with amino-trimethylene-phosphonic acid (ATMP) and used to remove  $\text{Cu}^{2+}$  and  $\text{Pb}^{2+}$  ions from waste water bodies (46).

Xian Zhou et al. employed mechanochemistry-alkali activation to manufacture a geo-polymer precursor (RG) from a Bayer-red-mud (RM) and coal-gangue (CG) bent having the ratio of 8:2

for solidifying and stabilising fly ash from municipal solid waste incineration (MSWI) (47). When the RG content of geopolymer S/S solids was greater than 60%, the authors confirmed, 99.6% of the heavy metals were immobilised. EDS investigation confirmed that this structure is made of geopolymer, as this class of materials is often made up of Na, Al, Si, and O. Raw RM's ferric oxide-dominated hematite mineral particle is strongly bonded to the geopolymer's surface. This suggests that the impurities may become embedded in the geopolymer's fissures and holes, making the structure more stable than adhesive aggregation. Raw FAs were incorporated into the geopolymer products in a way that nests the loosely agglomerated particles inside the network structure. Since M2-microstructure 3's is more tightly packed than that of M1-3, it is better able to keep heavy metals contained within the hardened samples.

## 5. Removal of Heavy Metal Ions

### 5.1. Removal of Heavy Metals from Water

Numerous studies investigated the removal or absorption of heavy metals from water, wastewater, and soils especially to have in-depth knowledge on harmful impacts of heavy metal ions. As a result of the fact that variability only accounted for 2.5% of the world's freshwater, water is seen as an essential goal of these ecosystems (48). The human body cannot function properly without meeting this requirement on a daily basis. For the objective of removing heavy metals from water, a wide variety of biochar strategies, materials, and applications have been suggested and put into practise. In order to get rid of a number of heavy metals as  $\text{Cd}^{2+}$ ,  $\text{Cu}^{2+}$ , and  $\text{Ni}^{2+}$ , Graphene-oxide (GO) and Go derived composite materials have been investigated then applied as new adsorbents (49). In addition, many materials based on graphene oxide were employed to purify water by removing harmful metals. Polyacrylamide oxide hydrogel grafted sodium alginate was proposed as a new bio-adsorbent by Jiang et al. for the reduction of heavy metal ions (50). Based on result,  $\text{Pb}^{2+}$  &  $\text{Cu}^{2+}$  were eliminated, and after five cycles, confirmation of over 60% of absorption capacity was obtained. For the removal of  $\text{Pb}^{2+}$  and  $\text{Cu}^{2+}$ , a thiosemicarbazide-based nanocomposite containing a modified graphene oxide was also used (51). Zhu et al. examined the potential of electrospun nanofibrous membranes (ELM), as well as their manufacture and the method by which they remove heavy metals (52). Choi et al., also presented thiol-functionalized cellulose nanofiber membranes for the efficient removal of  $\text{Cu}^{2+}$ ,  $\text{Cd}^{2+}$ , and  $\text{Pb}^{2+}$  from aqueous solutions (53).

As knowledge expands and new methods are developed Scientists have used cutting-edge methods to estimate the heavy metals absorption capability of various materials using a variety of perspectives. Apart from conventional approaches removing or treatment procedures still there are various technical challenges, and progressing research has made great contributions to identify, treat and remove heavy metals accordingly. In this regard artificial intelligence (AI) methods are being considered as a possible solution (54). Towards this aim, Singh et al. used a variety of machine learning techniques to forecast the adsorption of chlorophenol ( $\text{CP}^{2+}$ ), including radial-basis-function (RBF) and multilayer-perceptron-neural-networks (MLPN), a support-vector-machine (SVM), and gene-expression-programming (GEP) (55). They analysed the significance of the models' exceptional results and found that MLPN and RBFN models fared well in comparison to the others.  $\text{Cd}^{2+}$  removal efficiency was estimated using an ANN (artificial neural network) model created by Fawzy et al. (56). Their analysis showed a very good fit, with an  $R^2$  of 0.923. In order to foretell the sawdust-based removal of heavy metals from aqueous solutions, Dolatabadi et al.

(57) combined artificial neural networks (ANNs) with an Adaptive-Neuro-Fuzzy-Inference System (ANFIS) model. Based on their findings, these models appear to be useful modelling tools for analysing processes involved in the reduction of heavy metal ions from aq. solutions. Moreover, Fan et al., used a comprehensive review of various machine learning methods to model heavy metal removal processes. These algorithms included artificial-neural-networks (ANN), genetic algorithms (GA), and particle swarm optimization (PSO) (58). Their results suggest that GA-ANNs and PSO-ANNs models might be used to accurately simulate the processes involved in heavy metals' elimination from the environment. A similar approach was taken by Lu et al., who successfully simulated heavy metal ion percentage using ANN and SVM models (59).

Particulate heavy metal concentrations were claimed to be promptly simulated using SVM and ANN models. In order to estimate the rate of absorption for sodium in an aqueous solution, Rahnama et al. created a number of RBFN and ANFIS-based models, such as ANFIS-Grid partition, ANFIS-subtractive clustering, and ANFIS-Forward clustering (60). Last but not least, the RBFN model's predictive power for sodium absorption was established. In addition, El Hanandeh et al. reference some intriguing work wherein they predict the absorbency of heavy metals onto biochar utilizing ANN and MIMO systems, and they get an excellent result (i.e.,  $R^2 = 0.99$ ) (61). Rodriguez-Romero et al., used pyrolysis in combination with  $ZnCl_2$  activation to remove  $As^{2+}$  from water. After that, they used an ANN model to predict absorption kinetics and isotherms (62). In order to get rid of these toxins, many different materials and AI methods have been used and proposed, and the effectiveness with which different materials absorb heavy metals in different environments has also been predicted. A novel technique is also being tested whether halloysite nanotubes extracted from weathered pegmatites could effectively absorb heavy metals. Since the World Health Organization (WHO) has issued warnings about  $Pb^{2+}$  in aqueous solutions being harmful to human health, this element was chosen as a case study, and nanotube-type halloysite weathered pegmatites were explored as a means of removing  $Pb^{2+}$  from the solution (63). Notably, Nano tubes based halloysites derived from weathering igneous rocks were not studied for their potential to remove heavy metal ions, nor has it been used in this capacity.

After that, a cutting-edge intelligent hybrid model known as the Harris-Hawks-Optimization (HHO)-MLP-Neural-Network-Model used to predict the capacity with which nano tube based halloysites absorbs radiation from weathered-pegmatites. The MLP-Neural connectivity and the HHO algorithmic program are the foundations upon which this model was constructed. It is important to note that a tool used to confirm the uptake of heavy metal ions in water using the HHO-MLP-Neural-Structural-Network has not constructed till date. Finally, experimental data were thoroughly examined to determine the  $Pb^{2+}$  absorptivity of the material in an aqueous solution. The accuracy with which the predicted HHO-MLP-Neural-Structural-Network helps to predict  $Pb^{2+}$  absorption capability was rigorously evaluated. For instance, the ability of nano-tube based halloysites derived from weathered-pegmatites to take up  $Pb^{2+}$  ions in water was studied. In addition, unique hybrid intelligent model was presented for estimating  $Pb^{2+}$  absorption from an aqueous solution utilising this new material. This model is constructed using a Harris hawk's optimization (HHO) algorithm and a multiple layers perceptron (MLP) neural network (64).

## 5.2. Removal of Heavy Metals from Soil

Rocks can be broken down into smaller particles or soil by the action of ice, water, temperature, etc. There is a wide variety of binding qualities between soil and heavy metals, making the soil

matrix an important storage or transport medium for these elements. Instead of breaking down like organic contaminants do, metals tend to bioaccumulate in ecosystems. Metal ions in the soil may be removed by adsorption, oxidation, exchange, catalysis, reduction, or precipitation (65). Multiple variables, including pH, moisture, temperature, particle size distribution, metal type, and clay presence, all play a role in these transformations. The soil's heavy metals' mobility, solubility, and toxicity will depend on its specific composition. In most cases, carbonic acid and water are used to dissolve the minerals. Minerals that can't be dissolved are broken up into tiny granules. Metal wastes, gasoline, animal excrement, sludge, irrigation with waste water, air deposition, etc. all contribute to soil contamination, as do other sources of metals and metalloids (66). Typically, Pb, Cr, Zn, Cd, and Hg are the heaviest metals to be discovered in soils. These metals reduce agricultural production and disrupt the food chain because they bioaccumulate and biomagnify. Therefore, remediation steps must be taken to reduce the polluted area and prevent heavy metals from infiltrating the terrestrial, air, and aquatic habitats. Different methods have been discovered so far for cleaning up soil that has been tainted by heavy metals. Soil burning, excavation and landfill, soil washing, solidification, and electric field application are all examples of such mechanical or physio-chemical processes (67).

For instance, Pb, Zn, Cd, and Cu were extracted using a Citrate solution, which is safe for the environment. Effective extraction of heavy metals was achieved at two distinct pH ranges, about two-four. A kinetic analysis shown that equilibrium was attained in 4 hours when washing at a pH of about 2, while washing at a pH of about 4 or 5 gradually climbed towards the end of 24 hours. Extraction percentages for Pb and Cu were raised from 67.6 to 85.9% and from 77.5 to 83.4%, respectively, after washing at pH 2 for 6 h and then washing at pH 5 for 16 h. It has also been investigated whether using ultrasound can enhance the extraction of heavy metals from citrate. Results showed that after only 30 minutes of ultrasonic application at 19.5 KHz, heavy metals were extracted at a higher rate than they had been after 24 hours of washing. This enhanced the efficiency of citrate in its removal of heavy metals (68).

The use of plants to extract and eliminate elemental contaminants or to reduce their bioavailability in soil is called phytoremediation, and it is a plant-based technique. Plant roots may take up ions from the soil even at very dilute levels. Plants recover damaged soil by sending their roots deep into the soil to build a rhizosphere ecosystem, which accumulates heavy metals and reduces their bioavailability (67). In order to clean up heavy metal-contaminated soils, a multitude of phytoremediation techniques can be used, a) phytostabilization, or the use of plants to lessen the soil's bioavailability of heavy metals, b) Phytoextraction is the process of removing metals from the soil by growing plants that absorb them, c) Phytovolatilization, or the process by which plants remove toxic substances from the soil by means of transpiration, is one method d) Heavy metal ions in water can be removed by a process called phytofiltration, in which hydroponically-grown plants are used to filter the water. Phytodegradation and rhizodegradation are two further phytoremediation techniques used to decompose organic contaminants. Here, we zero in on the four most common phytoremediation techniques used to clean up soil contaminated with heavy metals: phytostabilization, phytoextraction, phytovolatilization, and phytofiltration. So soil naturally contains certain metals, but when their concentrations become excessive owing to human actions, the soil becomes contaminated. Heavy metal contamination of soil poses a severe environmental risk to human health and must be remedied effectively.

## 6. Conclusion

Implementation of advanced techniques is gaining increasing prominence in the field of identification and elimination of heavy metals and they are typically looked upon as a potentially effective method for dealing with heavy metal contaminations. ICP-MS and SEM-EDS are two of the most cutting-edge techniques utilized for the detection and quantification of heavy metals in their various forms. Today's cutting-edge methods allow for the quantitative measurement of intangibles such heavy metal content and removal efficiency. This article provides a comprehensive overview of the many existing integrated alternatives for heavy metal removal/recovery from polluted environments, drawing from a wide range of scholarly studies. Also the study provides a comprehensive overview of the many studies conducted on the several integrated approaches for heavy metal removal/recovery from polluted environments. The present article mainly focused on analysis toxic heavy metals using advanced ICP-MS and SEM-EDS methods. It has been claimed that inexpensive adsorbents are crucial in the process of detoxifying water and soil by binding hazardous metals. Heavy metals can be removed from wastewater and soil using a variety of treatment technologies, however the authors noted that many problems and shortcomings exist that must be addressed.

## References

1. Duffus, J. H. "Heavy Metals" a Meaningless Term? (IUPAC Technical Report). *Pure Appl. Chem.* **2002**, 74 (5), 793–807; DOI: 10.1351/pac200274050793.
2. He, Z. L.; Yang, X. E.; Stoffella, P. J. Trace Elements in Agroecosystems and Impacts on the Environment. *J. Trace Elem. Med. Biol.* **2005**, 19 (2–3), 125–140; DOI: 10.1016/j.jtemb.2005.02.010.
3. Raymond, A. W.; Okieimen, F. E. Heavy Metals in Contaminated Soils: A Review of Sources, Chemistry, Risks and Best Available Strategies for Remediation. *ISRN Ecology.* **2011**, 402647; DOI: 10.5402/2011/402647.
4. Shallari, S.; Schwartz, C.; Hasko, A.; Morel, J. L. Heavy Metals in Soils and Plants of Serpentine and Industrial Sites of Albania. *Sci. Total Environ.* **1998**, 209 (2–3), 133–142; DOI: 10.1016/S0048-9697(98)80104-6.
5. Kabata-Pendia, A.; Henryk, P. *Trace elements in soils and plants*, 3rd ed.; CRC: Boca Raton, 2001; p 331.
6. Hamelink, J. L.; Landrum, P. F.; Harold, B. L.; William, B. H. *Bioavailability: physical, chemical, and biological interactions*; CRC: Boca Raton, FL, 1994.
7. Verkleji, J. The effects of heavy metals stress on higher plants and their use as biomonitors. In *Plant as bioindicators: indicators of heavy metals in the terrestrial environment*; Markert, B. , Ed.; VCH: New York, NY, 1993; pp 415–424.
8. WHO/FAO/IAEA. *Trace elements in human nutrition and health*; World Health Organization: Geneva, 1996; pp 343; <https://apps.who.int/iris/handle/10665/37931>.
9. Wang, S.; Shi, X. Molecular mechanisms of metal toxicity and carcinogenesis. *Mol. Cell Biochem.* **2001**, 222 (1-2), 3–9.
10. Beyersmann, D.; Hartwig, A. Carcinogenic metal compounds: recent insight into molecular and cellular mechanisms. *Arch. Toxicol.* **2008**, 82 (8), 493–512; DOI: 10.1007/s00204-008-0313-y.

11. Yedjou, C. G.; Tchounwou, P. B. Oxidative stress in human leukemia cells (HL-60), human liver carcinoma cells (HepG2) and human Jerkat-T cells exposed to arsenic trioxide. *Metal Ions Biol. Med.* **2006**, *9*, 298–303.
12. Rai, P. K.; Lee, S. S.; Zhang, M.; Tsang, Y. F.; Kim, K. H. Heavy metals in food crops: Health risks, fate, mechanisms, and management. *Environment international.* **2019**, *125*, 365–85.
13. Wang, S.; Shi, X. Molecular Mechanisms of Metal Toxicity and Carcinogenesis. *Mol. Cell. Biochem.* **2001**, *222* (1–2), 3–9; DOI: 10.1023/A:1017918013293.
14. Yedjou, C. G.; Tchounwou, P. B. Oxidative Stress in Human Leukemia Cells (HL-60), Human Liver Carcinoma Cells (Hep G2) and Human Jerkat-T Cells Exposed to Arsenic Trioxide. *Biol. Med.* **2006**, *9*, 298–303.
15. Tchounwou, P. B.; Yedjou, C. G.; Foxx, D. N.; Ishaque, A. B.; Shen, E. Lead-Induced Cytotoxicity and Transcriptional Activation of Stress Genes in Human Liver Carcinoma (HepG2) Cells. *Mol. Cell. Biochem.* **2004**, *255* (1–2), 161–170; DOI: 10.1023/b:mcbi.0000007272.46923.12.
16. Sutton, D.; Tchounwou, P. B.; Ninashvili, N.; Shen, E. Mercury Induces Cytotoxicity and Transcriptionally Activates Stress Genes in Human Liver Carcinoma (HepG2) Cells. *Int. J. Mol. Sci.* **2002**, *3* (9), 965–984; DOI: 10.3390/i3090965.
17. Martín-Gámez, C.; Acebal, M. d. C.; Prieto, T. Developing the Concept of ‘Ecosystem’ Through Inquiry-Based Learning: A Study of Pre-service Primary Teachers. *J. Biol. Educ.* **2020**, *54* (2), 147–161; DOI: 10.1080/00219266.2018.1554596.
18. Ochoa-Hueso, R.; Delgado-Baquerizo, M.; Risch, A. C.; Schrama, M.; Morriën, E.; Barmantlo, S. H.; Geisen, S.; Hannula, S. E.; Resch, M. C.; Snoek, B. L.; van der Putten, W. H. Ecosystem Coupling: A Unifying Framework to Understand the Functioning and Recovery of Ecosystems. *One Earth* **2021**, *4* (7), 951–966.
19. Briffa, J.; Sinagra, E.; Blundell, R. Heavy Metal Pollution in the Environment and Their Toxicological Effects on Humans. *Heliyon* **2020**, *6* (9), e04691; DOI: 10.1016/j.heliyon.2020.e04691.
20. Chen, T.; Liu, X.; Li, X.; Zhao, K.; Zhang, J.; Xu, J.; Shi, J.; Dahlgren, R. A. Heavy Metal Sources Identification and Sampling Uncertainty Analysis in a Field-Scale Vegetable Soil of Hangzhou, China. *Environ. Pollut.* **2009**, *157* (3), 1003–1010; DOI: 10.1016/j.envpol.2008.10.011.
21. Gwenzi, W. Rethinking Restoration Indicators and End-Points for Post-mining Landscapes in Light of Novel Ecosystems. *Geoderma* **2021**, *387*, 114944.
22. Beauchemin, D. *Inductively Coupled Plasma Mass Spectrometry Methods*, 3rd ed.; Elsevier Ltd.: 2016.
23. Meermann, B.; Nischwitz, V. ICP-MS for the Analysis at the Nanoscale – A Tutorial Review. *J. Anal. At. Spectrom.* **2018**, *33* (9), 1432–1468; DOI: 10.1039/C8JA00037A.
24. Novaes, C. G.; Bezerra, M. A.; da Silva, E. G. P.; Santos, A. M. P. d.; Romão, I. L. d. S.; Santos Neto, J. H. S. A Review of Multivariate Designs Applied to the Optimization of Methods Based on Inductively Coupled Plasma Optical Emission Spectrometry (ICP OES). *Microchem. J.* **2016**, *128*, 331–346; DOI: 10.1016/j.microc.2016.05.015.
25. Eschnauer, H.; Jakob, L.; Meierer, H.; Neeb, R. Use and Limitations of ICP-OES in Wine Analysis. *Mikrochim. Acta* **1989**, *99* (3–6), 291–298; DOI: 10.1007/BF01244684.



26. Choi, S. H.; Kim, J. Y.; Mi Choi, E.; Lee, M. Y.; Yang, J. Y.; Ho Lee, G.; Su Kim, K.; Yang, J.; Russo, R. E.; Yoo, J. H.; Kang, G.; Su Park, K. Heavy Metal Determination by Inductively Coupled Plasma – Mass Spectrometry (ICP-MS) and Direct Mercury Analysis (DMA) and Arsenic Mapping by Femtosecond (Fs) – Laser Ablation (LA) ICP-MS in Cereals. *Analytical Letters* **2019**, 52 (3), 496–510; DOI: 10.1080/00032719.2018.1471484.
27. Feisal, N. A. S.; Hashim, Z.; Jalaludin, J.; How, V.; Hisham Hashim, J.; Azmi, W. N. F. W.; Fasha, Z.; Anual, Z. F.; Shaharudin, R. The Determination of Heavy Metals Concentration in Hair by Inductively Coupled Plasma Mass Spectrometry (ICP-MS). *J. Environ. Anal. Toxicol.* **2019**, 9, 1; DOI: 10.4172/2161-0525.1000598.
28. Peng, G.; He, Q.; Zhou, G.; Li, Y.; Su, X.; Liu, M.; Fan, L. Determination of Heavy Metals in Water Samples Using Dual-Cloud Point Extraction Coupled with Inductively Coupled Plasma Mass Spectrometry. *Anal. Methods* **2015**, 7 (16), 6732–6739; DOI: 10.1039/C5AY00801H.
29. Dressler, V. L.; Pozebon, D.; Curtius, A. J. Determination of Heavy Metals by Inductively Coupled Plasma Mass Spectrometry After On-Line Separation and Preconcentration. *Spectrochim. Acta B* **1998**, 53 (11), 1527–1539; DOI: 10.1016/S0584-8547(98)00180-3.
30. Hwang, H. J.; Hwang, G. H.; Ahn, S. M.; Kim, Y. Y.; Shin, H. S. Risk Assessment and Determination of Heavy Metals in Home Meal Replacement Products by Using Inductively Coupled Plasma Mass Spectrometry and Direct Mercury Analyzer. *Foods* **2022**, 11 (4), 504; DOI: 10.3390/foods11040504.
31. Nguyen, V. K.; Pham, V. H. Study on Accumulation of Heavy Metals Cadmium (Cd) and lead (Pb) in clam *Corbicula* sp. from estuaries, Da Nang city. *J. Sci. Technol. (Da Nang University)* **2009**, 1 (30), 83–89.
32. Wang, W.-X.; Lu, G. Heavy metals in bivalve mollusks. In *Chemical Contaminants and Residues in Food*, 2nd ed.; Schrenk, D., Cartus, A., Eds.; Woodhead Publishing: 2017; Chapter 21, pp 553–594.
33. Le, N. D.; Hoang, T. T. H.; Phung, V. P.; Nguyen, T. L.; Duong, T. T.; Dinh, L. M.; Pham, T. M. H.; Phung, T. X. B.; Nguyen, T. D.; Duong, T. N.; Le, T. M. H.; Le, P. T. H.; Le, T. P. Q. Trace Metal Element Analysis in Some Seafood in the Coastal Zone of the Red River (Ba Lat Estuary, Vietnam) by Green Sample Preparation and Inductively Coupled Plasma-Mass Spectrometry (ICP-MS). *Journal of Analytical Methods in Chemistry* **2021**, 6649362; DOI: 10.1155/2021/6649362.
34. Zhang, H.; Rui, Y.; Li, Y. Determination of Beneficial Elements, Heavy Metals and Rare Earth Elements in Northeastern Rice Brand of China by ICP-MS. *Asian J. Chem.* **2013**, 25 (4), 2315–2316; DOI: 10.14233/ajchem.2013.12855.
35. He, X.; Chen, L.; Chen, X.; Yu, H.; Peng, L.; Han, B. Analysis of Four Toxic Metals in a Single Rice Seed by Matrix Solid Phase Dispersion -Inductively Coupled Plasma Mass Spectrometry. *Sci. Rep.* **2016**, 6, 38472; DOI: 10.1038/srep38472.
36. Bua, D. G.; Annuario, G.; Albergamo, A.; Cicero, N.; Dugo, G. Heavy Metals in Aromatic Spices by Inductively Coupled Plasma-Mass Spectrometry. *Food Addit. Contam. Part B Surveill.* **2016**, 9 (3), 210–216; DOI: 10.1080/19393210.2016.1175516.
37. Zhou, W.; Apkarian, R. P.; Wang, Z. L.; Joy, D. Fundamentals of Scanning Electron Microscopy. In *Scanning Microscopy for Nanotechnology, Techniques and Applications*; Zhou, W., Wang, Z. L., Eds.; Springer: 2006; pp 1–40.

38. Bernaus, A.; Gaona, X.; Valiente, M. Characterisation of Almadén Mercury Mine Environment by XAS Techniques. *J. Environ. Monit.* **2005**, *7* (8), 771–777; DOI: 10.1039/b502060n.
39. Miler, M.; Gosar, M. Assessment of Metal Pollution Sources by SEM/EDS Analysis of Solid Particles in Snow: A Case Study of Žerjav, Slovenia. *Microsc. Microanal.* **2013**, *19* (6), 1606–1619; DOI: 10.1017/S1431927613013202.
40. Deng, J.; Guo, P.; Zhang, X.; Su, H.; Zhang, Y.; Wu, Y.; Li, Y. Microplastics and Accumulated Heavy Metals in Restored Mangrove Wetland Surface Sediments at Jinjiang Estuary (Fujian, China). *Mar. Pollut. Bull.* **2020**, *159*, 111482; DOI: 10.1016/j.marpolbul.2020.111482.
41. Chandrasekaran, A.; Senthil Kumar, C. K.; Sathish, V.; Manigandan, S.; Tamilarasi, A. Effect of Minerals and Heavy Metals in Sand Samples of Ponnai River, Tamil Nadu, India. *Sci. Rep.* **2021**, *11* (1), 23199; DOI: 10.1038/s41598-021-02717-x.
42. Panek, R.; Medykowska, M.; Wiśniewska, M.; Szewczuk-Karpisz, K.; Jędruchniewicz, K.; Franus, M. Simultaneous Removal of Pb<sup>2+</sup> and Zn<sup>2+</sup> Heavy Metals Using Fly Ash Na-X Zeolite and Its Carbon Na-X(C) Composite. *Materials (Basel)* **2021**, *14* (11), 2832; DOI: 10.3390/ma14112832.
43. Yilin, P.; Wenhua, Z.; Yunsheng, Z.; Wanting, Z.; Zaixiang, Z.; Fan, W. Migration and Transformation of Heavy Metals in Glass-Ceramics and the Mechanism of Stabilization. *Ceram. Int.* **2021**, *47* (17), 24663–24674; DOI: 10.1016/j.ceramint.2021.05.188.
44. Zhang, K.; Zhang, D.; Wu, X.; Xue, Y. Continuous and Efficient Immobilization of Heavy Metals by Phosphate-Mineralized Bacterial Consortium. *J. Hazard. Mater.* **2021**, *416*, 125800; DOI: 10.1016/j.jhazmat.2021.125800.
45. Manechakr, P.; Mongkollertlop, S. Investigation on Adsorption Behaviors of Heavy Metal Ions (Cd<sup>2+</sup>, Cr<sup>3+</sup>, Hg<sup>2+</sup> and Pb<sup>2+</sup>) Through Low-Cost/Active Manganese Dioxide-Modified Magnetic Biochar Derived from Palm Kernel Cake Residue. *J. Environ. Chem. Eng.* **2020**, *8* (6), 104467; DOI: 10.1016/j.jece.2020.104467.
46. Zhu, S.; Asim Khan, M. A.; Wang, F.; Bano, Z.; Xia, M. Rapid Removal of Toxic Metals Cu<sup>2+</sup> and Pb<sup>2+</sup> by Amino Trimethylene Phosphonic Acid Intercalated Layered Double Hydroxide: A Combined Experimental and DFT Study. *Chem. Eng. J.* **2020**, *392*; DOI: 10.1016/j.cej.2019.123711.
47. Zhou, X.; Zhang, T.; Wan, S.; Hu, B.; Tong, J.; Sun, H.; Chen, Y.; Zhang, J.; Hou, H. Immobilization of Heavy Metals in Municipal Solid Waste Incineration Fly Ash with Red Mud-Coal Gangue. *J. Mater. Cycles Waste Manag.* **2020**, *22* (6), 1953–1964; DOI: 10.1007/s10163-020-01082-7.
48. Petersen, L.; Heynen, M.; Pellicciotti, F. Freshwater Resources: Past, Present, Future. In *International Encyclopedia of Geography*; Wiley: 2019; DOI: 10.1002/9781118786352.wbieg0712.pub2.
49. Peng, W.; Li, H.; Liu, Y.; Song, S. A Review on Heavy Metal Ions Adsorption from Water by Graphene Oxide and Its Composites. *J. Mol. Liq.* **2017**, *230*, 496–504.
50. Jiang, H.; Yang, Y.; Lin, Z.; Zhao, B.; Wang, J.; Xie, J.; Zhang, A. Preparation of a Novel Bio-adsorbent of Sodium Alginate Grafted Polyacrylamide/Graphene Oxide Hydrogel for the Adsorption of Heavy Metal Ion. *Sci. Total Environ.* **2020**, *744*, 140653.
51. Abubshait, H. A.; Farag, A. A.; El-Raouf, M. A.; Negm, N. A.; Mohamed, E. A. Graphene Oxide Modified Thiosemicarbazide Nanocomposite as an Effective Eliminator for Heavy Metal Ions. *J. Mol. Liq.* **2020**, *327*, 114790.

52. Zhu, F.; Zheng, Y. M.; Zhang, B. G.; Dai, Y. R. A Critical Review on the Electrospun Nanofibrous Membranes for the Adsorption of Heavy Metals in Water Treatment. *J. Hazard. Mater.* **2021**, *401*, 123608.
53. Choi, H. Y.; Bae, J. H.; Hasegawa, Y.; An, S.; Kim, I. S.; Lee, H.; Kim, M. Thiol-Functionalized Cellulose Nanofiber Membranes for the Effective Adsorption of Heavy Metal Ions in Water. *Carbohydr. Polym.* **2020**, *234*, 115881.
54. Jahed Armaghani, D.; Kumar, D.; Samui, P.; Hasanipanah, M.; Roy, B. A Novel Approach for Forecasting of Ground Vibrations Resulting from Blasting: Modified Particle Swarm Optimization Coupled Extreme Learning Machine. *Eng. Comput.* **2021**, *37* (4), 3221–3235; DOI: 10.1007/s00366-020-00997-x.
55. Singh, K. P.; Gupta, S.; Ojha, P.; Rai, P. Predicting Adsorptive Removal of Chlorophenol from Aqueous Solution Using Artificial Intelligence Based Modeling Approaches. *Environ. Sci. Pollut. Res. Int.* **2013**, *20* (4), 2271–2287.
56. Fawzy, M.; Nasr, M.; Nagy, H.; Helmi, S. Artificial Intelligence and Regression Analysis for Cd(II) Ion Biosorption from Aqueous Solution by Gossypium barbadense Waste. *Environ. Sci. Pollut. Res. Int.* **2018**, *25* (6), 5875–5888.
57. Dolatabadi, M.; Mehrabpour, M.; Esfandyari, M.; Alidadi, H.; Davoudi, M. Modeling of Simultaneous Adsorption of Dye and Metal Ion by Sawdust from Aqueous Solution Using of ANN and ANFIS. *Chemom. Intell. Lab. Syst.* **2018**, *181*, 72–78.
58. Fan, M.; Hu, J.; Cao, R.; Ruan, W.; Wei, X. A Review on Experimental Design for Pollutants Removal in Water Treatment with the Aid of Artificial Intelligence. *Chemosphere* **2018**, *200*, 330–343.
59. Lu, H.; Li, H.; Liu, T.; Fan, Y.; Yuan, Y.; Xie, M.; Qian, X. Simulating Heavy Metal Concentrations in an Aquatic Environment Using Artificial Intelligence Models and Physicochemical Indexes. *Sci. Total Environ.* **2019**, *694*, 133591.
60. Rahnema, E.; Bazrafshan, O.; Asadollahfardi, G. Application of Data-Driven Methods to Predict the Sodium Adsorption Rate (SAR) in Different Climates in Iran. *Arab. J. Geosci.* **2020**, *13* (21), 1160.
61. El Hanandeh, A.; Mahdi, Z.; Imtiaz, M. S. Modelling of the Adsorption of Pb, Cu and Ni Ions from Single and Multi-component Aqueous Solutions by Date Seed Derived Biochar: Comparison of Six Machine Learning Approaches. *Environ. Res.* **2021**, *192*, 110338; DOI: 10.1007/s12517-020-06146-4.
62. Rodríguez-Romero, J. A.; Mendoza-Castillo, D. I.; Reynel-Ávila, H. E.; de Haro-Del Rio, D. A.; González-Rodríguez, L. M.; Bonilla-Petriciolet, A.; Duran-Valle, C. J.; Camacho-Aguilar, K. I. Preparation of a New Adsorbent for the Removal of Arsenic and Its Simulation with Artificial Neural Network-Based Adsorption Models. *J. Environ. Chem. Eng.* **2020**, *8* (4), 103928.
63. Gu, Z.; Song, W.; Yang, Z.; Zhou, R. Metal–Organic Framework as an Efficient Filter for the Removal of Heavy Metal Cations in Water. *Phys. Chem. Chem. Phys.* **2018**, *20* (48), 30384–30391; DOI: 10.1039/c8cp05129a.
64. Bac, B. H.; Nguyen, H.; Thao, N. T. T.; Hanh, V. T.; Duyen, L. T.; Dung, N. T.; Du, N. K.; Hiep, N. H. Estimating Heavy Metals Absorption Efficiency in an Aqueous Solution Using Nanotube-Type Halloysite from Weathered Pegmatites and a Novel Harris Hawks

- Optimization-Based Multiple Layers Perceptron Neural Network. *Eng. Comput.* **2022**, 38 (S5), 4257–4272; DOI: 10.1007/s00366-021-01459-8.
65. Hashim, M. A.; Mukhopadhyay, S.; Sahu, J. N.; SenGupta, B. Remediation Technologies for Heavy Metal Contaminated Groundwater. *J. Environ. Manage.* **2011**, 92 (10), 2355–2388; DOI: 10.1016/j.jenvman.2011.06.009.
66. Khan, S.; Cao, Q.; Zheng, Y. M.; Huang, Y. Z.; Zhu, Y. G. Health Risks of Heavy Metals in Contaminated Soils and Food Crops Irrigated with Wastewater in Beijing, China. *Environ. Pollut.* **2008**, 152 (3), 686–692; DOI: 10.1016/j.envpol.2007.06.056.
67. DalCorso, G.; Fasani, E.; Manara, A.; Visioli, G.; Furini, A. Heavy Metal Pollutions: State of the Art and Innovation in Phytoremediation. *Int. J. Mol. Sci.* **2019**, 20 (14), 3412; DOI: 10.3390/ijms20143412.
68. Furukawa, M.; Tokunaga, S. Extraction of Heavy Metals from a Contaminated Soil Using Citrate-Enhancing Extraction by pH Control and Ultrasound Application. *J. Environ. Sci. Health A Tox. Hazard. Subst. Environ. Eng.* **2004**, 39 (3), 627–638; DOI: 10.1081/ese-120027729.

# CARBON DOTS

RECENT DEVELOPMENTS AND  
FUTURE PERSPECTIVES



**E. BERDIMURODOV,  
D. K. VERMA & L. GUO**



ACS Publications

## Chapter 8

# Carbon Dots in Sensing: Photoelectrochemical, Electrochemiluminescent, Electrochemical, Colorimetric, and Fluorescent Applications

Ashima Sharma,<sup>1</sup> Kavita Tapadia,<sup>\*,2</sup> Rubina Sahin,<sup>3</sup> Dakeshwar Kumar Verma,<sup>\*,4</sup> Paz Otero,<sup>\*,5</sup> and Indu Agrawal<sup>6</sup>

<sup>1</sup>Chhattisgarh Environment Conservation Board, Raipur, Chhattisgarh 492001, India

<sup>2</sup>Department of Chemistry, National Institute of Technology, Raipur, Chhattisgarh 492001, India

<sup>3</sup>Department of Chemistry, NMDC DAV Polytechnic, Dantewada, Chhattisgarh 494441, India

<sup>4</sup>Department of Chemistry, Govt. Digvijay Autonomous Postgraduate College, Rajnandgaon, Chhattisgarh 491441, India

<sup>5</sup>Universidade de Vigo, Nutrition and Bromatology Group, Department of Analytical Chemistry and Food Science, Faculty of Science, Ourense E-32004, Spain

<sup>6</sup>Department of Chemistry, Kamla Nehru College, Korba, Chhattisgarh 495445, India

\*Email: [ktapadia.chy@nitrr.ac.in](mailto:ktapadia.chy@nitrr.ac.in)

\*Email: [dakeshwarverma@gmail.com](mailto:dakeshwarverma@gmail.com)

\*Email: [paz.otero@uvigo.es](mailto:paz.otero@uvigo.es)

Novel carbonaceous nanomaterial carbon dots (CDs) have unique physicochemical properties and attributes for various applications that make them a very precious tool for researchers. The ease of synthesis of CDs has created many research interests because of their large surface area with many functional groups that enhance their binding capacity. Apart from these properties, CDs have a low cost, are eco-friendly, are highly stable, are biocompatible, and are used as good sensors. In this chapter, photochemical, electrochemiluminescent, electrochemical, colorimetric, and fluorescent applications of CDs are described, where CDs have been used as a sensing probe. The electronic and optical properties of CDs—such as absorption, photoluminescence, phosphorescence, and others—have been used for the determination of heavy metals, biomolecules, enzymes, and so forth. The future trends of CDs' importance open new ways in the fields of nanoscience and nanotechnology.

## Introduction

Commonly known as “carbon dots” (CDs), carbon quantum dots (CQDs) are nanoscale carbon-based materials with unique optical and electrical capabilities. They typically have dimensions between a 0 to 10<sup>n</sup> of nanometers and are tiny, semi-spherical nanoparticles (1). The majority of the carbon atoms in the carbon dots have varied structures, such as a structure resembling graphene carbon, amorphous, or a combination of the two. Fundamentally, carbon dots differ from other materials due to the quantum confinement effect produced by their tiny size and the related quantum mechanical events that take place at the nanoscale level (2). This confinement effect leads to the tunable optical properties of these discrete energy levels and quantized electronic states. Carbon precursors from various carbon sources, including as biomass, organic molecules, and waste materials, must be carbonized or car and passivated in order to form carbon dots. Carbon dots are very appealing for a variety of applications because they have several intriguing features (3). Among the essential characteristics are: optoelectronics, bio imaging, drug delivery, sensing, catalysis, and energy storage, are just a few of the domains in which carbon dots are used. They have been utilized as sensors for detecting biomolecules and heavy metals, photocatalysts, fluorescent probes, and as parts of solar cells and super capacitors (4). Due to their electrical qualities carbon dots may be beneficial in electronics, optoelectronics, and energy storage devices, which include strong electrical conductivity. Carbon dots’ surfaces can easily be functionalized with a variety of functional groups, allowing for their incorporation into various matrices and aiding their use in a variety of applications (5). Carbon dots are suitable for biomedical applications like medication administration, bio-imaging, and bio-sensing since they are usually thought to be green and bio-compatible. Carbon dots have strong photo-luminescence, which allows them to absorb light at particular wavelengths while emitting light at various wavelengths. By adjusting the carbon dot size, surface passivation, and doping, this characteristic can be tailored (6). With continued efforts concentrated on enhancing their synthesis processes, comprehending their fundamental features, and exploring novel applications, carbon dot research is a vibrant and quickly developing subject. However, thermal breakdown, hydrothermal processes, microwave-assisted synthesis, or laser ablation techniques are frequently used regardless of the precise synthesis methodologies (7). Bottom-up Synthesis: This process entails the controlled chemical reactions of condensation, hydrothermal carbonization, or carbonization to produce carbon dots from small carbon-containing molecules. For instance, carbon precursors such aromatic compounds can be condensed in the presence of surface passivation agents to produce carbon dots.

Laser ablation: In this technique, a carbon target is exposed to a laser beam while submerged in liquid. Carbon dots develop in the liquid medium as a result of the carbon target’s vaporization by the laser and subsequent cooling. Microwave-Assisted Synthesis: In this technique, a surface passivation agent such as ethylene diamine is combined with a suitable carbon precursor (such as citric acid or glucose) and heated using a microwave source. Carbon dots appear as a result of the carbonization and nucleation processes being facilitated by the quick heating and regulated circumstances. Electrochemical Synthesis: An electrode made of carbon is submerged in an appropriate electrolyte solution and is given an electric potential. Electrochemical oxidation electrochemical etching, or Electrochemical exfoliation, of carbon precursors are some examples of the electrochemical methods that can be used to form the carbon dots (8).

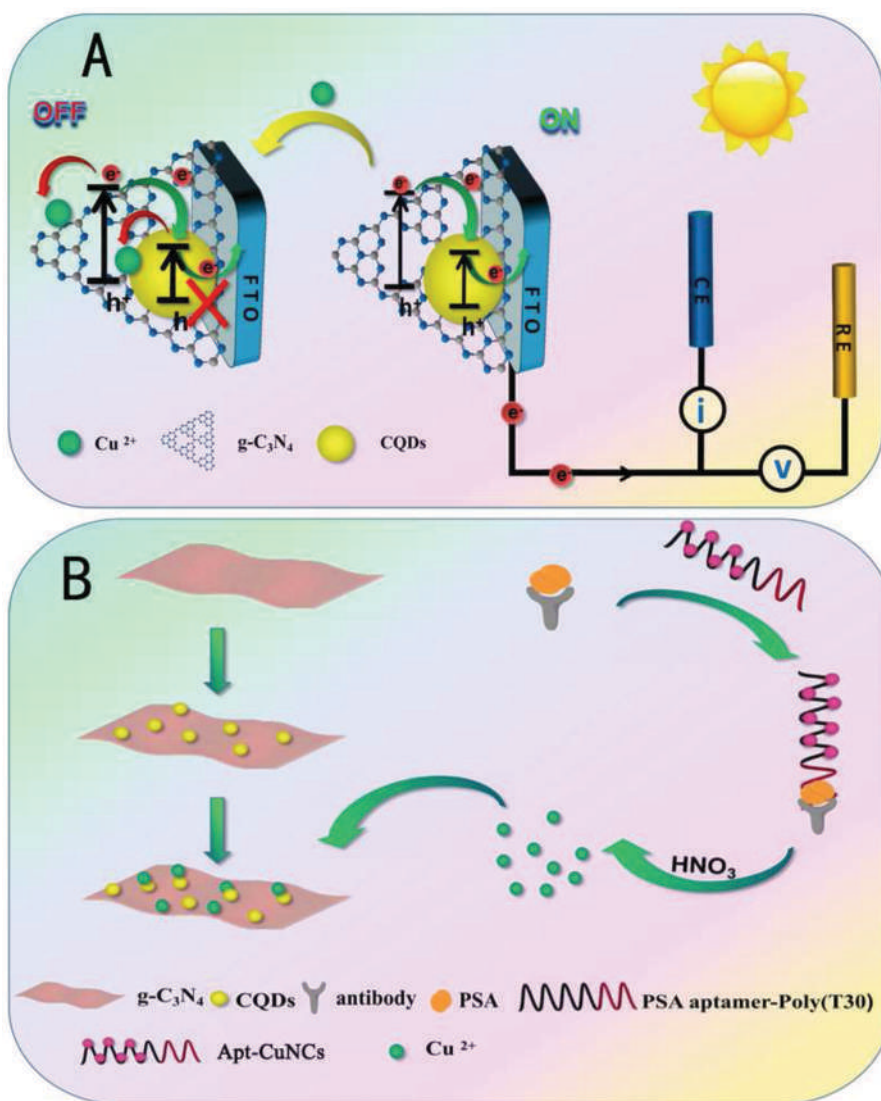


Figure 1. Diagram showing the photoelectrochemical (PEC) immunoassay based on g-C<sub>3</sub>N<sub>4</sub> (CQDs/g-C<sub>3</sub>N<sub>4</sub>) nanoheterostructures functionalized with carbon quantum dots toward the target PSA: (A) The PSA aptamer conjugated with DNA-templated copper nanoclusters (Apt-CuNCs) was used as the tracer in (B) immunoreaction on monoclonal anti-PSA antibody-coated microplate, which illustrates the mechanism of Cu<sup>2+</sup>-quenched photocurrent of CQDs/g-C<sub>3</sub>N<sub>4</sub> nanoheterostructures. Reproduced with permission from reference (18). Copyright 2017 American Chemical Society.

## CDs as Photoelectrochemical Sensors

Recent developments are focused on the development of nanomaterials which bears the better biocompatibility, photostability and ecofriendly properties as well as excellent optical and electrochemical properties. According to previously reported works, it has been observed that CDs are a well known biosensor because they convert concrete evidence about target analytes into evident optical signals as fluorescence intensity and change of colour (9, 10). The fluorescent property of



CDs can be modified from visible to near infrared range through careful selection of doping materials (11–13). Surface of CDs has many more functional groups which provide abundant binding sites for specific analytes. Thus, its chemical inertness and low toxicity makes it perfect nanoprobe for biosensing applications (14).

### **Biosensing Applications of CDs**

Carbon dots have abundance of functional groups containing high surface are used to modify bio receptors. A fast electron conduction takes place between sensory interface and the electrodes which make CDs as good electrochemical sensor. Furthermore, CDs is a fluorescent material which intensify the fluorescence signals arises from the target analytes. Both the properties electrochemical as well as fluorescence makes CDs an excellent tool for the bio imaging. In an experiment direct photoelectrochemical response of CDs was explained where CDs was prepared using Chitosan via solvothermal method. Chitosan prepared CDs was linked via covalent bond to an indium tin oxide (ITO) surface through self-assembled silane monolayer. The photocurrent was generated from ITO-silane-CDs surface was attributed the photocurrent to a photogenerated electron transfer mechanism by CDs, illuminated with 420 to 450 nm wavelength. The surface was used for lateral resolution ac-photocurrent imaging of a surface at the micron scale (15). One important energetic driving force for electron transmission to the ITO is the Fermi energy,  $E_f \approx 4.6$  eV. At anodic potentials, the holes in CDs absorb electrons from an anode. The electrolyte solution's  $\text{OH}^-$  serves as the electron donor (D) in this instance. use of CDs as photocatalysts to produce  $\text{D}^+$  from D photocurrent is produced under illumination. Investigations were done into how the photocurrents of CDs linked to their quantum yields.

There are numerous instances of CDs being utilized as PEC (photoelectrochemical) sensors. Carbon dot-based photoelectrochemical (PEC) sensors were developed in an experiment to detect glutathione (GSH) at ultrasensitive levels without the need for additional catalysts. In this PEC sensing device, CDs showed both photoelectric and catalytic capabilities. Graphene oxide (GO), mesoporous silica (MS), and silver nanoparticles (AgNPs) were added to increase the effectiveness of CDs in detecting GSH. Among the many hybrid nanocomposites, CDs@MS-based PEC sensors had the best sensing capabilities. The PEC sensor was successfully utilized to measure the amount of GSH in the cardiac cells of mice that had experienced various ischemia/ischemia-reperfusion therapies, and to look into the causes of myocardial infarction (MI) (16).

Another example is the development of a unique photoelectrochemical sensor (PEC) that uses WS<sub>2</sub> nanosheets as the photoactive material and boronic acid-fabricated CDs for signal amplification. This sensor is intended for the ultrasensitive detection of T4- $\beta$ -glucosyltransferase ( $\beta$ -GT) and 5-hydroxymethylcytosine (5hmC). In animals, 5-hydroxymethylcytosine (5hmC) functions as a switchpad for genetic control. WS<sub>2</sub> nanosheets were used as the photoactive material in a novel photoelectrochemical (PEC) biosensor for 5hmC detection, and B-CDs, or functionalized carbon dots, were used as the signal amplification unit. The T4- $\beta$ -glucosyltransferase ( $\beta$ -GT) activity can also be measured using this biosensor. WS<sub>2</sub> nanosheets and gold nanoparticles (AuNPs) were first immobilised on an ITO electrode surface. Subsequently, the probe DNA was immobilised on the electrode surface by means of an Au-S bond. Following that, hybridization was used to capture the complementary DNA carrying 5hmC on the altered electrode surface. After glycosylation, the hydroxyl groups of the 5hmC residues were converted to glucose by -GT from uridine diphosphoglucose. B-CDs may subsequently become more immobilised on the modified electrode surface, resulting in a strong photocurrent (17). In another instance, ultrasensitive

photoelectrochemical (PEC) determination of prostate-specific antigen (PSA) was performed by carbon quantum dots (CQDs) and graphitic carbon nitride (g-C<sub>3</sub>N<sub>4</sub>). Combining CQDs and g-C<sub>3</sub>N<sub>4</sub> encouraged the separation of photoexcited electrons and holes and significantly raised the photocurrents of the nanoheterostructures. On a microplate covered with monoclonal anti-PSA antibody, a sandwich-type immunoreaction was first performed utilizing CuNCs coupled with PSA aptamer as the tracer (18). The overall phenomenon is shown in Figure 1.

In addition, the linear range and limit of detections (LODs) of target analytes are shown in Table 1.

**Table 1. Statistical Parameters of Analytes Determined by CDs as Photoelectrochemical Sensors**

<i>Sensor</i>	<i>Target</i>	<i>Linear Range</i>	<i>LOD</i>	<i>Ref.</i>
CDs	GSH	0.02–4 μM	6.2 nM	(16)
WS 2-CDs-AuNPs-DNA	T4-β-Glucosyltransferase	0.1–220 units/mL	0.028 unit/mL	(19)
WS 2-CDs-AuNPs-DNA	5-Hydroxymethylcytosine	0.01–100 nM	0.0034 nM	(19)
CQDs and graphitic carbon nitride (g-C <sub>3</sub> N <sub>4</sub> )	PSA	0.02–100 ng/mL	5.0 pg/mL	(18)

### CDs as Electrochemiluminescent Sensors

By utilizing their distinctive luminous characteristics and surface changes, carbon dots can make efficient electrochemiluminescent sensors. Their potential for use spans a number of industries, including chemical analysis, biomedical diagnostics, and environmental monitoring. To enhance the performance and versatility of carbon dot-based ECL sensors, ongoing research is investigating new synthesis techniques, surface functionalization tactics, and sensing processes.

In the process known as electrochemiluminescence (ECL), an electrochemical reaction results in the emission of light. It includes producing excited states of luminous species at the electrode surface through electron-transfer processes. Electrochemical systems can be used to incorporate carbon dots as ECL sensors. A general description of the application of carbon dots as electrochemiluminescent sensors is given below (20).

Carbon dot-based ECL sensors have a number of benefits, including high sensitivity, a wide dynamic range, a quick reaction time, and good stability. They can be used to find a variety of analytes, such as medicines, biomolecules, heavy metals, and environmental contaminants. Carbon dots are also inexpensive, simple to make, and compatible with a variety of electrode materials and electrochemical processes (20).

**Analyte detection:** The presence of particular analytes can modify the ECL emission of carbon dots. Different techniques, such as direct interaction between the analyte and the carbon dots, modifications to the immediate surroundings of the dots, or control over the electrochemical process, can be used to accomplish this. Depending on the experimental design and analytic needs, analyte detection might be qualitative or quantitative (21).

**ECL Measurement:** The ECL measurement can be carried out once the carbon dots have been immobilised on the electrode. Usually, the working electrode receives voltage from electrode in

order to start an electrochemical reaction and produce the ECL emission. Using the appropriate photodetection methods, such as photomultiplier tubes or charge-coupled device (CCD) cameras, the emitted light is then detected and measured (22).

**Immobilisation on Electrodes:** To make an ECL sensor, modified carbon dots can be immobilised on electrode surfaces. There are several methods that can be used to immobilise the subject, including self-assembly, Carbon Dot Synthesis: There are several ways to make carbon dots, including laser ablation, solvothermal synthesis, hydrothermal synthesis, microwave-assisted synthesis, or carbonization of organic precursors. The production procedure has an impact on the carbon dots' size, surface chemistry, and luminous properties (23).

After being synthesized, carbon dots can have their surfaces changed to improve certain characteristics or add particular functionalities. This can be done via surface coating with different substances, such as polymers, biomolecules, or particular receptors for the target analytes, or by chemically functionalizing anything.

### CDs as Electrochemical Sensors

In the field of the electrochemical analysis, Carbon dots (CDs) have great importance as compared to other nanoparticles. It has a specific  $\pi$ - $\pi$  conjugation structure, solubility in various solvents to a large extent, having high electrical conductivity, intrinsic low toxicity, appropriate chemical & mechanical properties, having a large active site, series of functional group, large edge sites for functionalization, inherent catalytic actions and excellent biocompatibility. In this chapter we focus on the application of carbon nano dots (CNDs) in the field of electroanalytical investigation. CNDs have effective response in sensing

1. Hydrogen Peroxide ( $H_2O_2$ ) and Glucose ( $C_6H_{12}O_6$ )
2. Bio-Organic molecules
3. Heavy Metal Ions

### Application of CNDs for Electrochemical Sensing and Biosensing

Hydrogen peroxide ( $H_2O_2$ ) and oxygen ( $O_2$ ) have been reduced through the application of CDs and Graphene quantum dots' (GQDs') electrochemical activity. When measuring glucose (GLC), CDs and GQDs exhibit parallel activity towards glucose oxidation, simulating the action of the enzyme glucose oxidase. Due to the high reactivity of CDs and GQDs towards a wide range of organic molecules, metal ions, and other pertinent chemicals, these molecules, ions, and compounds can be easily sensed.

### Detection of Hydrogen Peroxide and Glucose

In various industrial process,  $H_2O_2$  used as oxidant, but expose of high concentration of  $H_2O_2$  may leads to trouble in human beings (24). So, it is very important that it should be measured precise and accurate. There are various methods are known for the determination of  $H_2O_2$ , among which electrochemical sensors method found to be most promising because of special features of accurate detection, easy to handle and showing quick response on determination. As a non-enzymatic sensor for the detection of  $H_2O_2$ , CDs & GQDs have shown a maximum possibility of mimicking enzyme activity (25). Nanostructured GQDs-Chitosan (GQDs-CS) has been utilised to effectively immobilise methylene blue (MB) through the amino-hydroxyl reaction. As a result, the combined

action of methylene blue (MB) and GQDs-Chitosan (GQDs-CS) causes an intriguing particular sensor activity in the final product. The combination of silver nanoparticles with CDs (AgNPs/CDs) casted on Glassy Carbon electrode (GCE) was successfully tested as an amperometric  $H_2O_2$  sensor. The ability of AgNPs and CDs to mimic enzyme activity and enhance molecular identification to the highest level of interest is the most intriguing aspect of this approach. Furthermore, intracellular  $H_2O_2$  produced from both diseased and non-cancerous cells during anticancer drug therapy has been measured using a novel electrochemical sensor that uses reduced graphene oxide quantum dots (rGO QDs)/ZnO nanofibers (NFs). High catalytic activity in this biosensor has been observed, indicating the synergistic effect of rGo QDs and ZnO nanofibers (26). Another literature reviews highlight that CDs/MWCNTs/GCE has new electrocatalytic activity towards the reduction of  $H_2O_2$  (27).

Glucose (GLC) in blood has another significant impact on human health. There are so many techniques have been studied to develop advance biosensor for glucose (GLC) detection. Normally, Glucose Oxidase Enzyme (GOx) has been used in electrochemical detection of GLC. High performance glucose biosensor via GQD modified Carbon Ceramic electrode (CCE) has been induced by Razmi et al. 2013 (28). GQDs have large surface area, larger hydrophilic edges and a hydrophobic plane, having high porosity. The nanostructure electrocatalyst of CQDs/ Octahedral-Cuprous Oxide ( $Cu_2O$ ) synthesized by Li et al., 2015 (29). This electrode has construct for non-enzymatic electrochemical sensors for the detection of glucose (GLC) and  $H_2O_2$  (30). CDs/ Octahedra  $Cu_2O$  showed significant electrocatalysis to the glucose (GLC) oxidation and  $H_2O_2$  reduction as compared to octahedral  $Cu_2O$ . Table 2 and Table 3 highlights different kinds of electrochemical sensors for the determination of  $H_2O_2$  and glucose (GLC) by using CDs and GQDs.

**Table 2. A List of Applications of CD- and GQD-Based Electrochemical Sensors for the Detection of  $H_2O_2$**

S.No	Improved Electrode	Method Applied	Linear Range	Detection Limit	Ref.
1	AgNPs/CDs/GCE	Amperometry	0.2–27.0 $\mu$ M	80 nM	(31)
2	Ag/CNC/GCE	Amperometry	5.00 $\mu$ M–11.05 mM	0.51 $\mu$ M	(32)
3	Ag/C/GCE	Amperometry	4–25.5 mM	1.3 $\mu$ M	(33)
4	AuNPs–N-GQDs/GCE	Amperometry	0.25 $\mu$ M–13.327 mM	0.12 $\mu$ M	(34)
5	CDs/MWCNTs/GCE	Amperometry	3.5 $\mu$ M–30 mM	0.25 $\mu$ M	(35)
6	CQDs/GCE	Amperometry	100 nM–1 mM	300 nM	(36)
7	CQDs/ $Cu_2O$ /NF/GCE	Amperometry	5 $\mu$ M–5.3 mM	2.8 $\mu$ M	(37)
8	CS–GODs/AgNCs/Au	Amperometry	10 $\mu$ M–7.38 mM	0.15 $\mu$ M	(38)
9	GQDs-CS/MB/GCE	Amperometry	1 $\mu$ M–11.78 mM	0.7 $\mu$ M	(39)
10	rGOQDs/ZnO NFs/ITO	Amperometry	1–22.48 $\mu$ M	0.025 $\mu$ M	(40)

**Table 3. A List of Applications of CD- and GQD-Based Electrochemical Sensors for the Detection of GLC**

S.No	Improved Electrode	Method Applied	Linear Range	Detection Limit	Ref.
1	GOD-CNDs-rGO/GCE	CV	40 $\mu$ M–20 mM	40 $\mu$ M	(41)
2	GOx-GQD/CCE	Amperometry	5–1270 $\mu$ M	1.73 $\mu$ M	(42)
3	CQDs/AuNPs-GOx/Au	Amperometry	0.05–2.85mM	17 $\mu$ M	(43)
4	GOx-GQD/ GCE	Amperometry	10 $\mu$ M–3 mM	1.35 $\mu$ M	(44)
5	<u>NiO@NCDs/ Ni foam electrode</u>	Amperometry	5 $\mu$ M–12 mM	0.01 $\mu$ M	(45)
6	GQDs/CoNiAl-LDH/CPE	Amperometry	0.01–14.0 mM	6 $\mu$ M	(46)

### Detection of Organic Compounds

The organic compounds which have vital importance for human beings are very important to detect with accuracy. The bio-molecules compounds like Dopamine (DA), Ascorbic Acid (AA), Uric Acid (UA), Nicotinamide Adenine Dinucleotide (NADA), Epinephrine (EP) and so on. The electrochemical sensors of CDs are of low cost, easy to handle and high sensitivity. The modified electrode of CDs can strengthen the rate of electrochemical reaction and be beneficial by increasing the active electrochemical surface sites. The abnormality in Dopamine (DA) can be correlated by neurological disorder. So, detection of DA is very important and essential for diagnosis purposes. An advanced and modified N-doped carbon quantum dots (NCQDs) developed by Jiang et al. for the detection of DA with broad linear range and low detection limit (47). Additionally, a Cuprous Oxide- Carbon dots / Nafion ( $\text{Cu}_2$ )-CDs/ NF) fabricated for the determination of DA. In  $\text{Cu}_2\text{O}$ -CDs/NF electrode,  $\text{Cu}_2\text{O}$  is cable to increase the conductivity and CDs are able to interact with DA through the amine functional group as well as to reduce  $\text{Cu}(\text{OH})_2$  directly. The best part of this electrode that other bio-molecules like UA and AA had no interference during the detection of DA (48). Another electrode made by the N-CDs and ferrocene @  $\beta$ -CDs) are deposited on a GCE. The importance of this materials is higher catalytic activity during the detection of DA accomplished by oxidation of UA as comparison with the unmodified electrode (N-CD and FC@  $\beta$ -CDs) respectively (49). Additional to that, L-AA imprinted polymer film was fabricated in pencil graphite electrode (PGE) modified with carbon dots (CDs), poly-aniline ferrocene-sulphonic acid (PANI- FSA) for separation and measurement of D-AA & L-AA formed in aqueous & biological samples (50). For the determination of NADH (51). Carbon screen printed electrode modified with magnetic nanoparticles and CDs (SPE/MagNP/CDs) has been used (52). This electrode is very effective method for aggregation dynamic qualifier agent and the removal of magnet leads to effective release of nanoparticles.

The CDs have ideal properties like greater surface area and high electrical conductivity, promotes this in the field of drug investigation. For the detection of doxorubicin hydrochloride (DOX) a novel electrochemical sensor developed. It was done by one step electrodeposition method by the deposition of AgNPs, CDs and rGO on GCE electrode. The electrocatalytic activities is directly affected by the concentration of  $\text{Ag}(\text{NH}_3)_2\text{OH}$ . During the experiment, it was observed

that, when the volume ratio of the reagent in CDs-GO was 3:1 (v/v) to Ag (NH<sub>3</sub>)<sub>2</sub>OH was reduced and fixed to 1:1. then, the best result obtained as well as electrocatalytic activities also found considerable.

**Table 4. The Electrochemical Sensing of Heavy Metals by CDs**

S.No	Improved Electrode	Target Metal Ion	Method Applied	Linear Range	LOD	Ref.
1	PANI/GQDs/SPCE	Cr(VI)	Linear sweep voltametry	0.1–10 mg/L	0.097 mg/L	(59)
2	GQDs/GCE	Cu(II)	Differential pulse anodic stripping voltametry	--	0.3 nM	(60)
3	NCQDs-GO/GCE	Cd(II)	Anodic stripping voltametry	11.24–11241 µg/L	7.45 µg/L	(61)
4	CS/GQDs/GCE	Cd(II)	Square wave stripping voltametry	--	1.9 µg/L	(62)
5	GQDs/GCE	Pb(II)	Differential pulse anodic stripping voltametry	0.8–10 µM	7 nM	(63)
6	GNPs/SPGE	Pb(II)	Square wave stripping voltametry	20–200 PPB	2.2 ppb	(64)
7	GQDs/graphene/GCE	Cu(II)	Differential pulse anodic stripping voltametry	0.015–8.775 µM	1.34 nM	(65)
8	OH-GQD@VMSF/ITO	Hg(II)	Differential pulse anodic stripping voltametry	1.0 nM–0.5 µM	9.8 pM	(66)
9	NH <sub>2</sub> -GQD@VMSF/ITO	Cd(II)	Differential pulse anodic stripping voltametry	1.0 µM–20.0 µM	4.3 nM	(67)
10	GQDs/AuNPs/GCE	Hg(II)	Anodic stripping voltametry	--	0.02 nM	(68)

### Detection of Metal Ions

For the detection of heavy metals, there are so many methods are known. Among all detection by nanoparticles based on electrochemical sensor basically CDs and GQDs are most popular. It is simple, easy to operate, fast detection and having affordable are the main reasons for this. For the detection of Cr(VI) (53), developed a nanoparticles sensor by polyaniline/graphene quantum dots (PANI/GQDs) modified screen-printed carbon electrode (SPCE). The electrochemical sensor

(PANI/GQDs/SPCE) has been used for the determination of concentration of Cr(VI) in real samples. Addition to that (54), developed another electrochemical sensor for the determination of Cu(II) ion in the brain of rat by micro-dialysates. An electrode made of graphene quantum (GQDs/PGE) has been used for the sensing of Cu(II) ion (55). As literature reviews indicate, high concentrations of heavy metals like Pb(II), Cd(II), Hg(II), Cr(VI) in groundwater make it unfit for all living organisms. Due to anthropogenic activities its concentration increases day by day. On view of this, Li et al. developed an electrochemical sensor for the detection of Cd(II) and Pb(II) by Anodic Stripping Voltammetry (ASV). This sensor was developed by the combination of N-doped Carbon Quantum dots-graphene Oxide (NCQDs-GO) (56). The (NCQDs-GO) dropped onto GCE. The results obtained from NCQDs-GO/GCE much better than normal (GO/GCE) and NCQDs. Due to accumulation of heavy metal such as mercury leads to neural and renal issues on human beings (57) though its permissible limit is 0.001 ppm. Thus, detection in such low quantity is challenging. In this regard, Ting et al. (58) developed an electrochemical sensor made up of gold nanoparticles (AuNPs) and GQDs and then it was used in Anodic Stripping Voltammetry (ASV) for the detection of Hg(II) and Cu(II) respectively. In addition, Table 4 represents the Electrochemical sensing of heavy metals by CDs.

## CDs as Colorimetric and Fluorescent Sensing Applications

Zero-dimensional carbonaceous materials are called carbon dots. Carbon dots are small fluorescent molecules less than 10 nm in diameter. Good conductivity, strong chemical stability, broadband optical absorption, and luminescence are among the special qualities of carbon dots (69–71). Carbon dots can be broadly classified into three types: carbonised polymeric dots (CPDs) (P1), which are made up of a core carbon atom and surface functional groups, and graphene quantum dots (GQDs). Their different structures determined the optical properties. Hereafter, this property will be described.

## Optical Properties of CDs

### UV Absorption Properties

The CQDs prepared from different precursors show different absorption spectra in different solvents, but they possess similar UV absorption peaks. There are more than one absorption peaks observed in the UV region in the range of 260 to 320 nm. The surface functional groups, tail part covers the complete visible region. The absorption peak of CQDs is found in the wavelength range 220–270 nm due to transition of electrons from  $\pi$  orbital to C=N bonds. In the region of 280–350 nm the absorption peak found due to electronic transition from C-O/C=O bonds to  $\pi^*$  orbital (72). In the range of 350–600 nm, the absorption peak found due to electronic transition in functional groups present on the surface of nanoparticles, shows that moieties present on the surface impart the absorption in UV-Visible zone. In some cases, surface functional groups after binding shows red shift (73). In other cases, if aromatic rings present on the surface of CQDs the absorption peak covers 600–800 nm wavelength range (74).

### Fluorescence Properties

CDs is used as detector due to availability, low poisonousness and low cost. The surface modification of CDs is very easy, which makes them soluble in water. Consequently, high

fluorescence quantum yield makes CDs good fluorescence-based sensors. The binding pattern between CDs and metal ions completely changes the properties of fluorophores and fluorescence intensity and gives good signals of analytes (75).

Fluorescence is the key property of CDs. Functionalization of CDs enhances the fluorescence property of CDs. The structure of CDs is complex. Thus, the description of the CDs fluorescence mechanism is difficult. The optical properties of CDs differ on whether they are prepared from the same materials. The difference depends upon the optimization of different parameters such as temperature, incubation time in the microwave hydrothermal preparation method. Thus, the two different samples of CDs. The surface structure of CDs is compatible with their fluorescence. The CDs prepared from two different mechanisms show give different coloured spectra. Temperature dependent synthesis of CDs as at high temperature and long reaction time, exposed CDs showed a full colour spectrum, while at low temperature and short-duration prepared CDs showed a blue coloured spectrum because the different size of CDs affects the emission profile. As the size decreases, the energy gap between the conduction band and valence shell increases and vice versa condition arises as the size increases. The overall change is due to the presence of functional groups on CDs surface. The abundance of functional groups on the surface of CDs gives full spectrum (76, 77). Fluorescence resonance energy transfer (FRET) phenomenon is responsible for the fluorometric determination of analytes using CDs. FRET is the phenomenon in which fluorescence resonance energy transfer between donor and acceptor molecules (78).

**Table 5. Statistical Parameters of Heavy Metal Ions Using CDs as Fluorescence Sensing Probes**

S. No.	Fluorescent Probe	Metal Ion	Detection Limit	Linear Range	Ref.
1	Carbon dots	Aluminum (III)	113.8 nM	0.15–38.6 $\mu$ M	(80)
2	N-doped GQDs	Fe(III)	90 nM		(81)
3	N-S doped CDs	Hg(II)	0.5 nM		(82)
4	Polyethylene amine functionalized GQDs	Cu(II)		0–9 $\mu$ M	(83)
5	N-doped GQDs	Hg(II)	80 nM	80–100 nM	(84)
6	Green CDs	Pb(III)	0.59 nM	0.01–1 nM	(85)
7	CQD-gold nanocluster (CQDs/AuNCs)	Cd(II)	32.5		(86)

### Colorimetric-Fluorescence-Based Determination of Heavy Metals

There are various heavy metals such as chromium (III), aluminium, iron etc., are nutritious and essential for living organisms but sometimes these may be toxic in its higher concentrations, but some heavy metals, such as chromium (IV), lead (II), arsenic (III), mercury (II) can cause toxicity even in its trace amount. These heavy metals are nonbiodegradables. Carbon dots are developed as fluorescent nano sensor for detecting these environmental contaminants in living organisms. The energy transfer takes place between nano carbons and metal ions due to functional groups and



surface setups. Fluorescence quenching has been seen between donor and acceptor in the overall mechanism where transfer of electrons involves between donor and acceptor. Metal ions are responsible for the quenching of CDs. In the overall determination of metal ions turn on and turnoff of fluorescence spectra takes place. It is attributed to nonradiative electron transfer from the excited state to the d-orbital to the metal ions. The soft-soft and acid-base interactions between CDs moiety and metal ions make the fluorescent tool more effective. The quenching of fluorescence spectra of CDs in presence of Hg(II) ion (79).

Wei et al. shows the determination of Al(III) ion in presence of blue fluorescent CDs synthesized from naringin with emission peak at 420 nm. In the presence of Al(III) ion, a new peak appears at 500 nm due to proximity of adjacent CDs. Also, visual detection of Al(III) based on monitoring of colour changes by a smartphone (80). The statistical parameters of heavy metals, detected by fluorescence method are shown in Table 5.

### **Colorimetric-Fluorescence--Based Determination of Biomolecules**

For the purpose of determining biothiols, CDs are the most sought-after fluorescent probe due to their real-time applicability, crystalline nature, low toxicity, and seamless production. Biothiols like glutathione, homocysteine, and cysteine are essential for maintaining redox homeostasis, decreasing damage from pollution and free radicals, and regulating gene expression, among many other functions. Similarly, aberrant biothiol stages can cause severe illnesses like Alzheimer's disease (AD), neurotoxicity, hair loss, liver/pore damage, and skin damage, among others. Several low-toxic probes, such as fluorescent quantum dots, emissive organic probes, composited nanomaterials, and so on, were cited in real-time programmes to quantify the biothiols in an organic system. Carbon dots (CDs), one of such fluorescent probes, have become more and more appealing for the detection of biothiols due to their smooth manufacturing, nanosize, crystalline housing, low toxicity, and real-time applicability (87). A CDs-based totally biothiols assay may be completed by way of fluorescent "turn-On" and "turn-Off" responses via direct binding, metal complex-mediated detection, composite stronger interaction, reaction-based totally reviews, and so on (88). So far, the supply of an assessment centered on fluorescent CDs-based biothiols detection with data on current developments, mechanistic components, linear stages, LODs, and actual applications is missing, which lets in us to supply this comprehensive evaluation. Furthermore, it has been seen that Gold composite carbon dots are applied for the determination of glutathione with 50nM detection limit (89).

### **Conclusion**

By utilising their distinctive luminous characteristics and surface changes, carbon dots can make efficient electrochemiluminescent sensors, Photoelectrochemical sensors, electrochemical sensors, colorimetric and fluorescent sensing applications. Their potential for use spans a number of industries, including chemical analysis, biomedical diagnostics, and environmental monitoring. To enhance the performance and versatility of carbon dot-based ECL sensors, ongoing research is investigating new synthesis techniques, surface functionalization tactics, and sensing processes.

## References

1. Basavaraj, N.; Sekar, A.; Yadav, R. Review on Green Carbon Dot-Based Materials for the Photocatalytic Degradation of Dyes: Fundamentals and Future Perspective. *Mater. Adv.* **2021**, *2* (23), 7559–7582. DOI: 10.1039/D1MA00773D.
2. Mintz, K. J.; Cilingir, E. K.; Nagaro, G.; Paudyal, S.; Zhou, Y.; Khadka, D.; Huang, S.; Graham, R. M.; Leblanc, R. M. Development of Red-Emissive Carbon Dots for Bioimaging Through a Building Block Approach: Fundamental and Applied Studies. *Bioconjug. Chem.* **2022**, *33* (1), 226–237. DOI: 10.1021/acs.bioconjchem.1c00544.
3. Deshmukh, S.; Deore, A.; Mondal, S. Ultrafast Dynamics in Carbon Dots as Photosensitizers: A Review. *ACS Appl. Nano Mater.* **2021**, *4* (8), 7587–7606. DOI: 10.1021/acsanm.1c01880.
4. Li, Z.; Wang, L.; Li, Y.; Feng, Y.; Feng, W. Frontiers in Carbon Dots: Design, Properties, and Applications. *Mater. Chem. Front.* **2019**, *3* (12), 2571–2601. DOI: 10.1039/C9QM00415G.
5. Zhang, J.; Yu, S. H. Carbon Dots: Large-Scale Synthesis, Sensing and Bioimaging. *Mater. Today* **2016**, *19* (7), 382–393. DOI: 10.1016/j.mattod.2015.11.008.
6. Wang, F.; Pang, S.; Wang, L.; Li, Q.; Kreiter, M.; Liu, C. Y. One-Step Synthesis of Highly Luminescent Carbon Dots in Noncoordinating Solvents. *Chem. Mater.* **2010**, *22* (16), 4528–4530. DOI: 10.1021/cm101350u.
7. Zheng, X. T.; Ananthanarayanan, A.; Luo, K. Q.; Chen, P. Glowing Graphene Quantum Dots and Carbon Dots: Properties, Syntheses, and Biological Applications. *Small* **2015**, *11* (14), 1620–1636. DOI: 10.1002/smll.201402648.
8. Bardhan, S.; Roy, S.; Das, S. Carbon Dots: Fundamental Concepts and Biomedical Applications. In *Nanotechnology for Biomedical Applications*; 2022 March 9; pp 83–108. DOI: 10.1007/978-981-16-7483-9\_5.
9. Sinha, R. P.; Häder, D. P. UV-Induced DNA Damage and Repair: A Review. *Photochem. Photobiol. Sci.* **2002**, *1* (4), 225–236. DOI: 10.1039/b201230h.
10. Zhang, H.; Salo, D.; Kim, D. M.; Komarov, S.; Tai, Y. C.; Berezin, M. Y. Penetration Depth of Photons in Biological Tissues from Hyperspectral Imaging in Shortwave Infrared in Transmission and Reflection Geometries. *J. Biomed. Opt.* **2016**, *21* (12), 126006. DOI: 10.1117/1.JBO.21.12.126006.
11. Zhang, Y. Q.; Ma, D. K.; Zhuang, Y.; Zhang, X.; Chen, W.; Hong, L. L.; Yan, Q. X.; Yu, K.; Huang, S. M. One-Pot Synthesis of N-Doped Carbon Dots with Tunable Luminescence Properties. *J. Mater. Chem.* **2012**, *22* (33), 16714–16718. DOI: 10.1039/c2jm32973e.
12. Zhang, Y. Q.; Ma, D. K.; Zhuang, Y.; Zhang, X.; Chen, W.; Hong, L. L.; Yan, Q. X.; Yu, K.; Huang, S. M. One-Pot Synthesis of N-Doped Carbon Dots with Tunable Luminescence Properties. *J. Mater. Chem.* **2012**, *22* (33), 16714–16718. DOI: 10.1039/c2jm32973e.
13. Jiang, L.; Ding, H.; Lu, S.; Geng, T.; Xiao, G.; Zou, B.; Bi, H. Photoactivated Fluorescence Enhancement in F, N-Doped Carbon Dots with Piezochromic Behavior. *Angew. Chem.* **2020**, *132* (25), 10072–10077.
14. Ji, C.; Zhou, Y.; Leblanc, R. M.; Peng, Z. Recent Developments of Carbon Dots in Biosensing: A Review. *ACS Sensors* **2020**, *5* (9), 2724–2741. DOI: 10.1021/acssensors.0c01556.
15. Zhang, D. W.; Papaioannou, N.; David, N. M.; Luo, H.; Gao, H.; Tanase, L. C.; Degoussé, T.; Samorì, P.; Sapelkin, A.; Fenwick, O.; Titirici, M.; Krause, S. Photoelectrochemical Response

- of Carbon Dots (CDs) Derived from Chitosan and Their Use in Electrochemical Imaging. *Mater. Horiz.* **2018**, 5 (3), 423–428. DOI: 10.1039/C7MH00784A.
16. Li, Z.; Zhang, J.; Li, Y.; Zhao, S.; Zhang, P.; Zhang, Y.; Bi, J.; Liu, G.; Yue, Z. Carbon Dots Based Photoelectrochemical Sensors for Ultrasensitive Detection of Glutathione and Its Applications in Probing of Myocardial Infarction. *Biosens. Bioelectron.* **2018**, 99, 251–258. DOI: 10.1016/j.bios.2017.07.065.
  17. Sui, C.; Wang, T.; Zhou, Y.; Yin, H.; Meng, X.; Zhang, S.; Waterhouse, G. I. N.; Xu, Q.; Zhuge, Y.; Ai, S. Photoelectrochemical Biosensor for Hydroxymethylated DNA Detection and T4-β-Glucosyltransferase Activity Assay Based on WS2 Nanosheets and Carbon Dots. *Biosens. Bioelectron.* **2019**, 127, 38–44. DOI: 10.1016/j.bios.2018.11.054.
  18. Lv, S.; Li, Y.; Zhang, K.; Lin, Z.; Tang, D. Carbon Dots/g-C<sub>3</sub>N<sub>4</sub> Nanoheterostructures-Based Signal-Generation Tags for Photoelectrochemical Immunoassay of Cancer Biomarkers Coupling with Copper Nanoclusters. *ACS Appl. Mater. Interfaces* **2017**, 9 (44), 38336–38343. DOI: 10.1021/acsami.7b13272.
  19. Sui, C.; Wang, T.; Zhou, Y.; Yin, H.; Meng, X.; Zhang, S.; Waterhouse, G. I. N.; Xu, Q.; Zhuge, Y.; Ai, S. Photoelectrochemical Biosensor for Hydroxymethylated DNA Detection and T4-Beta-Glucosyltransferase Activity Assay Based on WS2 Nanosheets and Carbon Dots. *Biosens. Bioelectron.* **2019**, 127, 38–44. DOI: 10.1016/j.bios.2018.11.054.
  20. Chen, Y.; Cao, Y.; Ma, C.; Zhu, J. J. Carbon-Based Dots for Electrochemiluminescence Sensing. *Mater. Chem. Front.* **2020**, 4 (2), 369–385. DOI: 10.1039/C9QM00572B.
  21. Li, L.; Liu, D.; Mao, H.; You, T. Multifunctional Solid-State Electrochemiluminescence Sensing Platform Based on Poly (Ethylenimine) Capped N-Doped Carbon Dots as Novel Co-reactant. *Biosens. Bioelectron.* **2017**, 89 (1), 489–495. DOI: 10.1016/j.bios.2016.03.069.
  22. Niu, W. J.; Zhu, R. H.; Cosnier, S.; Zhang, X. J.; Shan, D. Ferrocyanide-Ferricyanide Redox Couple Induced Electrochemiluminescence Amplification of Carbon Dots for Ultrasensitive Sensing of Glutathione. *Anal. Chem.* **2015**, 87 (21), 11150–11156. DOI: 10.1021/acs.analchem.5b03358.
  23. Shi, C. G.; Shan, X.; Pan, Z. Q.; Xu, J. J.; Lu, C.; Bao, N.; Gu, H. Y. Quantum Dot (QD)-Modified Carbon Tape Electrodes for Reproducible Electrochemiluminescence (ECL) Emission on a Paper-Based Platform. *Anal. Chem.* **2012**, 84 (6), 3033–3038. DOI: 10.1021/ac2033968.
  24. Su, Y.; Zhou, X.; Long, Y.; Li, W. Immobilization of Horseradish Peroxidase on Amino-Functionalized Carbon Dots for the Sensitive Detection of Hydrogen Peroxide. *Mikrochim. Acta* **2018**, 185 (2), 114. DOI: 10.1007/s00604-017-2629-x.
  25. Mollarasouli, F.; Asadpour-Zeynali, K.; Campuzano, S.; Yáñez-Sedeño, P.; Pingarrón, J. M. Non-enzymatic Hydrogen Peroxide Sensor Based on Graphene Quantum Dots-Chitosan/Methylene Blue Hybrid Nanostructures. *Electrochim. Acta* **2017**, 246, 303–314. DOI: 10.1016/j.electacta.2017.06.003.
  26. Yang, C.; Hu, L. W.; Zhu, H. Y.; Ling, Y.; Tao, J. H.; Xu, C. X. rGO Quantum Dots/ZnO Hybrid Nanofibers Fabricated Using Electrospun Polymer Templates and Applications in Drug Screening Involving an Intracellular H<sub>2</sub>O<sub>2</sub> Sensor. *J. Mater. Chem. B* **2015**, 3 (13), 2651–2659. DOI: 10.1039/c4tb02134g.
  27. Bai, J.; Sun, C.; Jiang, X. Carbon Dots-Decorated Multiwalled Carbon Nanotubes Nanocomposites as a High-Performance Electrochemical Sensor for Detection of H<sub>2</sub>O<sub>2</sub> in

- Living Cells. *Anal. Bioanal. Chem.* **2016**, *408* (17), 4705–4714. DOI: 10.1007/s00216-016-9554-4.
28. Razmi, H.; Mohammad-Rezaei, R. Graphene Quantum Dots as a New Substrate for Immobilization and Direct Electrochemistry of Glucose Oxidase: Application to Sensitive Glucose Determination. *Biosens. Bioelectron.* **2013**, *41*, 498–504. DOI: 10.1016/j.bios.2012.09.009.
29. Li, Y.; Zhong, Y.; Zhang, Y.; Weng, W.; Li, S. Carbon Quantum Dots/Octahedral Cu<sub>2</sub>O Nanocomposites for Non-enzymatic Glucose and Hydrogen Peroxide Amperometric Sensor. *Sens. Actuators B* **2015**, *206*, 735–743. DOI: 10.1016/j.snb.2014.09.016.
30. Sadhukhan, M.; Bhowmik, T.; Kundu, M. K.; Barman, S. Facile Synthesis of Carbon Quantum Dots and Thin Graphene Sheets for Non-enzymatic Sensing of Hydrogen Peroxide. *R.S.C. Adv.* **2014**, *4* (10), 4998–5005. DOI: 10.1039/c3ra46050a.
31. Jahanbakhshi, M.; Habibi, B. A Novel and Facile Synthesis of Carbon Quantum Dots via Salep Hydrothermal Treatment as the Silver Nanoparticles Support: Application to Electroanalytical Determination of H<sub>2</sub>O<sub>2</sub> in Fetal Bovine Serum. *Biosens. Bioelectron.* **2016**, *81*, 143–150. DOI: 10.1016/j.bios.2016.02.064.
32. Jiang, Y.; Li, Y.; Li, Y.; Li, S. A Sensitive Enzyme-Free Hydrogen Peroxide Sensor Based on a Chitosan–Graphene Quantum Dot/Silver Nanocube Nanocomposite Modified Electrode. *Anal. Methods* **2016**, *8* (11), 2448–2455. DOI: 10.1039/C5AY02976G.
33. Jiang, D.; Zhang, Y.; Huang, M.; Liu, J.; Wan, J.; Chu, H.; Chen, M. Carbon Nanodots as Reductant and Stabilizer for One-Pot Sonochemical Synthesis of Amorphous Carbon-Supported Silver Nanoparticles for Electrochemical Nonenzymatic H<sub>2</sub>O<sub>2</sub> Sensing. *J. Electroanal. Chem.* **2014**, *728*, 26–33. DOI: 10.1016/j.jelechem.2014.06.017.
34. Ju, J.; Chen, W. In Situ Growth of Surfactant-Free Gold Nanoparticles on Nitrogen-Doped Graphene Quantum Dots for Electrochemical Detection of Hydrogen Peroxide in Biological Environments. *Anal. Chem.* **2015**, *87* (3), 1903–1910. DOI: 10.1021/ac5041555.
35. Bai, J.; Sun, C.; Jiang, X. Carbon Dots-Decorated Multiwalled Carbon Nanotubes Nanocomposites as a High-Performance Electrochemical Sensor for Detection of H<sub>2</sub>O<sub>2</sub> in Living Cells. *Anal. Bioanal. Chem.* **2016**, *408* (17), 4705–4714. DOI: 10.1007/s00216-016-9554-4.
36. Sadhukhan, M.; Bhowmik, T.; Kundu, M. K.; Barman, S. Facile Synthesis of Carbon Quantum Dots and Thin Graphene Sheets for Non-enzymatic Sensing of Hydrogen Peroxide. *R.S.C. Adv.* **2014**, *4* (10), 4998–5005. DOI: 10.1039/c3ra46050a.
37. Li, Y.; Zhong, Y.; Zhang, Y.; Weng, W.; Li, S. Carbon Quantum Dots/Octahedral Cu<sub>2</sub>O Nanocomposites for Non-enzymatic Glucose and Hydrogen Peroxide Amperometric Sensor. *Sens. Actuators B* **2015**, *206*, 735–743. DOI: 10.1016/j.snb.2014.09.016.
38. Jiang, D.; Zhang, Y.; Huang, M.; Liu, J.; Wan, J.; Chu, H.; Chen, M. Carbon Nanodots as Reductant and Stabilizer for One-Pot Sonochemical Synthesis of Amorphous Carbon-Supported Silver Nanoparticles for Electrochemical Nonenzymatic H<sub>2</sub>O<sub>2</sub> Sensing. *J. Electroanal. Chem.* **2014**, *728*, 26–33. DOI: 10.1016/j.jelechem.2014.06.017.
39. Mollarasouli, F.; Asadpour-Zeynali, K.; Campuzano, S.; Yáñez-Sedeño, P.; Pingarrón, J. M. Non-enzymatic Hydrogen Peroxide Sensor Based on Graphene Quantum Dots-Chitosan/Methylene Blue Hybrid Nanostructures. *Electrochim. Acta* **2017**, *246*, 303–314. DOI: 10.1016/j.electacta.2017.06.003.

40. Yang, C.; Hu, L. W.; Zhu, H. Y.; Ling, Y.; Tao, J. H.; Xu, C. X. rGO Quantum Dots/ZnO Hybrid Nanofibers Fabricated Using Electrospun Polymer Templates and Applications in Drug Screening Involving an Intracellular H<sub>2</sub>O<sub>2</sub> Sensor. *J. Mater. Chem. B* **2015**, 3 (13), 2651–2659. DOI: 10.1039/c4tb02134g.
41. Qin, X.; Asiri, A. M.; Alamry, K. A.; Al-Youbi, A. O.; Sun, X. Carbon Nitride Dots Can Serve as an Effective Stabilizing Agent for Reduced Graphene Oxide and Help in Subsequent Assembly with Glucose Oxidase into Hybrids for Glucose Detection Application. *Electrochim. Acta* **2013**, 95, 260–267. DOI: 10.1016/j.electacta.2013.02.014.
42. Razmi, H.; Mohammad-Rezaei, R. Graphene Quantum Dots as a New Substrate for Immobilization and Direct Electrochemistry of Glucose Oxidase: Application to Sensitive Glucose Determination. *Biosens. Bioelectron.* **2013**, 41, 498–504. DOI: 10.1016/j.bios.2012.09.009.
43. Buk, V.; Pemble, M. E.; Twomey, K. Fabrication and Evaluation of a Carbon Quantum Dot/Gold Nanoparticle Nanohybrid Material Integrated onto Planar Micro Gold Electrodes for Potential Bioelectrochemical Sensing Applications. *Electrochim. Acta* **2019**, 293, 307–317. DOI: 10.1016/j.electacta.2018.10.038.
44. Gupta, S.; Smith, T.; Banaszak, A.; Boeckl, J. Graphene Quantum Dots Electrochemistry and Development of Ultrasensitive Enzymatic Glucose Sensor. *M.R.S. Adv.* **2018**, 3 (15–16), 831–847. DOI: 10.1557/adv.2018.324.
45. Akhtar, N.; El-Safy, S. A.; Abdelsalam, M. E.; Shenashen, M. A.; Kawarada, H. Radially Oriented Nanostrand Electrodes to Boost Glucose Sensing in Mammalian Blood. *Biosens. Bioelectron.* **2016**, 77, 656–665. DOI: 10.1016/j.bios.2015.10.023.
46. Samuei, S.; Fakkar, J.; Rezvani, Z.; Shomali, A.; Habibi, B. Synthesis, and Characterization of Graphene Quantum Dots/CoNiAl-Layered Double-Hydroxide Nanocomposite: Application as a Glucose Sensor. *Anal. Biochem.* **2017**, 521, 31–39. DOI: 10.1016/j.ab.2017.01.005.
47. Jiang, G.; Jiang, T.; Zhou, H.; Yao, J.; Kong, X. Preparation of N-Doped Carbon Quantum Dots for Highly Sensitive Detection of Dopamine by an Electrochemical Method. *R.S.C. Adv.* **2015**, 5 (12), 9064–9068. DOI: 10.1039/C4RA16773B.
48. Huang, Q.; Lin, X.; Lin, C.; Zhang, Y.; Hu, S.; Wei, C. A High Performance Electrochemical Biosensor Based on Cu<sub>2</sub>O–Carbon Dots for Selective and Sensitive Determination of Dopamine in Human Serum. *R.S.C. Adv.* **2015**, 5 (67), 54102–54108. DOI: 10.1039/C5RA05433H.
49. Zhang, H.; Dai, P.; Huang, L.; Huang, Y.; Huang, Q.; Zhang, W.; Wei, C.; Hu, S. A Nitrogen-Doped Carbon Dot/ferrocene@ $\beta$ -cyclodextrin Composite as an Enhanced Material for Sensitive and Selective Determination of Uric Acid. *Anal. Methods* **2014**, 6 (8), 2687–2691. DOI: 10.1039/C4AY00140K.
50. Zhang, Z.; Li, Y.; Xu, J.; Wen, Y. Electropolymerized Molecularly Imprinted Polypyrrole Decorated with Black Phosphorene Quantum Dots onto Poly (3, 4-Ethylenedioxythiophene) Nanorods and Its Voltammetric Sensing of Vitamin C. *J. Electroanal. Chem.* **2018**, 814, 153–160. DOI: 10.1016/j.jelechem.2018.02.059.
51. Pandey, I.; Jha, S. S. Molecularly Imprinted Polyaniline–Ferrocene–Sulfonic Acid–Carbon Dots Modified Pencil Graphite Electrodes for Chiral Selective Sensing of D-Ascorbic Acid and L-Ascorbic Acid: A Clinical Biomarker for Preeclampsia. *Electrochim. Acta* **2015**, 182, 917–928. DOI: 10.1016/j.electacta.2015.10.005.

52. Canevari, T. C.; Cincotto, F. H.; Gomes, D.; Landers, R.; Toma, H. E. Magnetite Nanoparticles Bonded Carbon Quantum Dots Magnetically Confined onto Screen Printed Carbon Electrodes and Their Performance as Electrochemical Sensor for NADH. *Electroanalysis* **2017**, *29* (8), 1968–1975. DOI: 10.1002/elan.201700167.
53. Punrat, E.; Maksuk, C.; Chuanuwatanakul, S.; Wonsawat, W.; Chailapakul, O. Polyaniline/Graphene Quantum Dot-Modified Screen-Printed Carbon Electrode for the Rapid Determination of Cr(VI) Using Stopped-Flow Analysis Coupled with Voltammetric Technique. *Talanta* **2016**, *150*, 198–205. DOI: 10.1016/j.talanta.2015.12.016.
54. Shao, X.; Gu, H.; Wang, Z.; Chai, X.; Tian, Y.; Shi, G. Highly Selective Electrochemical Strategy for Monitoring of Cerebral Cu<sup>2+</sup> Based on a Carbon Dot-TPEA Hybridized Surface. *Anal. Chem.* **2013**, *85* (1), 418–425. DOI: 10.1021/ac303113n.
55. Ahour, F.; Taheri, M. Anodic Stripping Voltammetric Determination of Copper (II) Ions at a Graphene Quantum Dot-Modified Pencil Graphite Electrode. *J. Iran. Chem. Soc.* **2018**, *15* (2), 343–350. DOI: 10.1007/s13738-017-1235-5.
56. Li, L.; Liu, D.; Shi, A.; You, T. Simultaneous Stripping Determination of Cadmium and Lead Ions Based on the N-Doped Carbon Quantum Dots-Graphene Oxide Hybrid. *Sens. Actuators B* **2018**, *255*, 1762–1770. DOI: 10.1016/j.snb.2017.08.190.
57. Rice, K. M.; Walker, E. M., Jr.; Wu, M.; Gillette, C.; Blough, E. R. Environmental Mercury and Its Toxic Effects. *J. Prev. Med. Public Health* **2014**, *47* (2), 74–83. DOI: 10.3961/jpmph.2014.47.2.74.
58. Ting, S. L.; Ee, S. J.; Ananthanarayanan, A.; Leong, K. C.; Chen, P. Graphene Quantum Dots Functionalized Gold Nanoparticles for Sensitive Electrochemical Detection of Heavy Metal Ions. *Electrochim. Acta* **2015**, *172*, 7–11. DOI: 10.1016/j.electacta.2015.01.026.
59. Punrat, E.; Maksuk, C.; Chuanuwatanakul, S.; Wonsawat, W.; Chailapakul, O. Polyaniline/Graphene Quantum Dot-Modified Screen-Printed Carbon Electrode for the Rapid Determination of Cr(VI) Using Stopped-Flow Analysis Coupled with Voltammetric Technique. *Talanta* **2016**, *150*, 198–205. DOI: 10.1016/j.talanta.2015.12.016.
60. Wen, J.; Li, M.; Xiao, J.; Liu, C.; Li, Z.; Xie, Y.; Ning, P.; Cao, H.; Zhang, Y. Novel Oxidative Cutting Graphene Oxide to Graphene Quantum Dots for Electrochemical Sensing Application. *Mater. Today Commun.* **2016**, *8*, 127–133. DOI: 10.1016/j.mtcomm.2016.07.006.
61. Li, L.; Liu, D.; Shi, A.; You, T. Simultaneous Stripping Determination of Cadmium and Lead Ions Based on the N-Doped Carbon Quantum Dots-Graphene Oxide Hybrid. *Sens. Actuators B* **2018**, *255*, 1762–1770. DOI: 10.1016/j.snb.2017.08.190.
62. Ou, J.; Tao, Y.; Ma, J.; Kong, Y. Well-Dispersed Chitosan-Graphene Quantum Dots Nanocomposites for Electrochemical Sensing Platform. *J. Electrochem. Soc.* **2015**, *162* (12), H884–H889. DOI: 10.1149/2.0421512jes.
63. Zhou, C.; Jiang, W.; Via, B. K. Facile Synthesis of Soluble Graphene Quantum Dots and Its Improved Property in Detecting Heavy Metal Ions. *Colloids Surf. B Biointerfaces* **2014**, *118*, 72–76. DOI: 10.1016/j.colsurfb.2014.03.038.
64. Wan, H.; Sun, Q.; Li, H.; Sun, F.; Hu, N.; Wang, P. Screen-Printed Gold Electrode with Gold Nanoparticles Modification for Simultaneous Electrochemical Determination of Lead and Copper. *Sens. Actuators B* **2015**, *209*, 336–342. DOI: 10.1016/j.snb.2014.11.127.

65. Wang, Y.; Zhao, S.; Li, M.; Li, W.; Zhao, Y.; Qi, J.; Cui, X. Graphene Quantum Dots Decorated Graphene as an Enhanced Sensing Platform for Sensitive and Selective Detection of Copper (II). *J. Electroanal. Chem.* **2017**, *797*, 113–120. DOI: 10.1016/j.jelechem.2017.05.031.
66. Lu, L.; Zhou, L.; Chen, J.; Yan, F.; Liu, J.; Dong, X.; Xi, F.; Chen, P. Nanochannel-Confined Graphene Quantum Dots for Ultrasensitive Electrochemical Analysis of Complex Samples. *ACS Nano* **2018**, *12* (12), 12673–12681. DOI: 10.1021/acsnano.8b07564.
67. Lu, L.; Zhou, L.; Chen, J.; Yan, F.; Liu, J.; Dong, X.; Xi, F.; Chen, P. Nanochannel-Confined Graphene Quantum Dots for Ultrasensitive Electrochemical Analysis of Complex Samples. *ACS Nano* **2018**, *12* (12), 12673–12681. DOI: 10.1021/acsnano.8b07564.
68. Ting, S. L.; Ee, S. J.; Ananthanarayanan, A.; Leong, K. C.; Chen, P. Graphene Quantum Dots Functionalized Gold Nanoparticles for Sensitive Electrochemical Detection of Heavy Metal Ions. *Electrochim. Acta* **2015**, *172*, 7–11. DOI: 10.1016/j.electacta.2015.01.026.
69. Ju, J.; Chen, W. Synthesis of Highly Fluorescent Nitrogen-Doped Graphene Quantum Dots for Sensitive, Label-Free Detection of Fe (III) in Aqueous Media. *Biosens. Bioelectron.* **2014**, *58*, 219–225. DOI: 10.1016/j.bios.2014.02.061.
70. Namdari, P.; Negahdari, B.; Eatemadi, A. Synthesis, Properties and Biomedical Applications of Carbon-Based Quantum Dots: An Updated Review. *Biomed. Pharmacother.* **2017**, *87*, 209–222. DOI: 10.1016/j.biopha.2016.12.108.
71. Tao, H.; Yang, K.; Ma, Z.; Wan, J.; Zhang, Y.; Kang, Z.; Liu, Z. In Vivo NIR Fluorescence Imaging, Biodistribution, and Toxicology of Photoluminescent Carbon Dots Produced from Carbon Nanotubes and Graphite. *Small* **2012**, *8* (2), 281–290. DOI: 10.1002/smll.201101706.
72. Lin, L.; Zhang, S. Creating High Yield Water Soluble Luminescent Graphene Quantum Dots via Exfoliating and Disintegrating Carbon Nanotubes and Graphite Flakes. *Chem. Commun. (Camb)* **2012**, *48* (82), 10177–10179. DOI: 10.1039/c2cc35559k.
73. Zhu, S.; Song, Y.; Zhao, X.; Shao, J.; Zhang, J.; Yang, B. The Photoluminescence Mechanism in Carbon Dots (Graphene Quantum Dots, Carbon Nanodots, and Polymer Dots): Current State and Future Perspective. *Nano Res.* **2015**, *8* (2), 355–381. DOI: 10.1007/s12274-014-0644-3.
74. Holá, K.; Sudolská, M.; Kalytchuk, S.; Nachtigallová, D.; Rogach, A. L.; Otyepka, M.; Zbořil, R. Graphitic Nitrogen Triggers Red Fluorescence in Carbon Dots. *ACS Nano* **2017**, *11* (12), 12402–12410. DOI: 10.1021/acsnano.7b06399.
75. Yuan, F.; Wang, Z.; Li, X.; Li, Y.; Tan, Z. A.; Fan, L.; Yang, S. Bright Multicolor Bandgap Fluorescent Carbon Quantum Dots for Electroluminescent Light-Emitting Diodes. *Adv. Mater.* **2017**, *29* (3), 1604436. DOI: 10.1002/adma.201604436.
76. Baker, S. N.; Baker, G. A. Luminescent Carbon Nanodots: Emergent Nanolights. *Angew. Chem. Int. Ed. Engl.* **2010**, *49* (38), 6726–6744. DOI: 10.1002/anie.200906623.
77. Shen, J.; Zhu, Y.; Yang, X.; Li, C. Graphene Quantum Dots: Emergent Nanolights for Bioimaging, Sensors, Catalysis and Photovoltaic Devices. *Chem. Commun. (Camb)* **2012**, *48* (31), 3686–3699. DOI: 10.1039/c2cc00110a.
78. Wu, X.; Tian, F.; Wang, W.; Chen, J.; Wu, M.; Zhao, J. X. Fabrication of Highly Fluorescent Graphene Quantum Dots Using L-glutamic Acid for In Vitro/In Vivo Imaging and Sensing. *J. Mater. Chem. C Mater.* **2013**, *1* (31), 4676–4684. DOI: 10.1039/C3TC30820K.

79. Torres Landa, S. D.; Reddy Bogireddy, N. K.; Kaur, I.; Batra, V.; Agarwal, V. Heavy Metal Ion Detection Using Green Precursor Derived Carbon Dots. *iScience* **2022**, 25 (2), 103816. DOI: 10.1016/j.isci.2022.103816.
80. Wei, W.; Huang, J.; Gao, W.; Lu, X.; Shi, X. Carbon Dots Fluorescence-Based Colorimetric Sensor for Sensitive Detection of Aluminum Ions with a Smartphone. *Chemosensors* **2021**, 9 (2), 25. DOI: 10.3390/chemosensors9020025.
81. Ju, J.; Chen, W. Synthesis of Highly Fluorescent Nitrogen-Doped Graphene Quantum Dots for Sensitive, Label-Free Detection of Fe (III) in Aqueous Media. *Biosens. Bioelectron.* **2014**, 58, 219–225. DOI: 10.1016/j.bios.2014.02.061.
82. Mohapatra, S.; Sahu, S.; Sinha, N.; Bhutia, S. K. Synthesis of a Carbon-Dot-Based Photoluminescent Probe for Selective and Ultrasensitive Detection of Hg<sup>2+</sup> in Water and Living Cells. *Analyst* **2015**, 140 (4), 1221–1228. DOI: 10.1039/c4an01386g.
83. Sun, H.; Gao, N.; Wu, L.; Ren, J.; Wei, W.; Qu, X. Highly Photoluminescent Amino-Functionalized Graphene Quantum Dots Used for Sensing Copper Ions. *Chemistry* **2013**, 19 (40), 13362–13368. DOI: 10.1002/chem.201302268.
84. Wang, L.; Li, B.; Xu, F.; Shi, X.; Feng, D.; Wei, D.; Li, Y.; Feng, Y.; Wang, Y.; Jia, D.; Zhou, Y. High-Yield Synthesis of Strong Photoluminescent N-Doped Carbon Nanodots Derived from Hydrosoluble Chitosan for Mercury Ion Sensing via Smartphone APP. *Biosens. Bioelectron.* **2016**, 79, 1–8. DOI: 10.1016/j.bios.2015.11.085.
85. Li, L.; Liu, D.; Shi, A.; You, T. Simultaneous Stripping Determination of Cadmium and Lead Ions Based on the N-Doped Carbon Quantum Dots-Graphene Oxide Hybrid. *Sens. Actuators B* **2018**, 255, 1762–1770. DOI: 10.1016/j.snb.2017.08.190.
86. Niu, W. J.; Shan, D.; Zhu, R. H.; Deng, S. Y.; Cosnier, S.; Zhang, X. J. Dumbbell-Shaped Carbon Quantum Dots/AuNCs Nanohybrid as an Efficient Ratiometric Fluorescent Probe for Sensing Cadmium (II) Ions and L-Ascorbic Acid. *Carbon* **2016**, 96, 1034–1042. DOI: 10.1016/j.carbon.2015.10.051.
87. Shellaiah, M.; Sun, K. W. Review on Carbon Dot-Based Fluorescent Detection of Biothiols. *Biosensors* **2023**, 13 (3), 335. DOI: 10.3390/bios13030335.
88. Khan, Z. G.; Patil, P. O. A Comprehensive Review on Carbon Dots and Graphene Quantum Dots Based Fluorescent Sensor for Biothiols. *Microchem. J.* **2020**, 157, 105011. DOI: 10.1016/j.microc.2020.105011.
89. Tuerhong, M.; Xu, Y.; Yin, X. Review on Carbon Dots and Their Applications. *Chin. J. Anal. Chem.* **2017**, 45 (1), 139–150. DOI: 10.1016/S1872-2040(16)60990-8.





# MARINE MOLECULES FROM ALGAE AND CYANOBACTERIA

Extraction, Purification, Toxicology and Applications

Edited by

Paz Otero Fuertes • Dakeshwar Kumar Verma



ELSEVIER

# Contents

List of contributors	xi
About the editors	xiii
Preface	xv
Acknowledgments	xvii

## Part I Marine molecules from Algae

### 1. Diversity of marine algae, cultivation techniques, and sources of natural products for biotechnological applications

*Antía Torres, Sabina Naz, Dakeshwar Kumar Verma and Paz Otero*

1.1 Introduction	3
1.2 Microalgae as a potential source for chemical compounds of interest	4
1.2.1 Dietary source	4
1.2.2 Pharmaceutical and medical interest	6
1.2.3 Livestock feed	7
1.2.4 Cosmetics	8
1.2.5 Biofuel products	8
1.3 Macroalgae as a potential source for chemical compounds of interest	9
1.3.1 Human food	9
1.3.2 Pharmaceutical and medical applications	11
1.3.3 Livestock and agriculture	12
1.3.4 Cosmetics	13
1.3.5 Biofuel products	13
1.4 Factors that influence the production of algae biocompounds	14
1.5 Challenges in production and use of algae compounds and conclusions	16
Conflict of interests	17
Acknowledgments	17
References	17

### 2. Extraction and purification of protein from algae (microalgae and seaweeds)

*Sabiha Naz and Arpita Mukherjee*

2.1 Introduction	25
2.2 Protein types in algae	26
2.3 Various applications of algal proteins	27
2.3.1 Human nutrition	27
2.3.2 Industrial applications	27
2.3.3 Meat for animals	28
2.3.4 Aquaculture	28
2.3.5 Bioactive peptides	28
2.4 Algae protein extraction methods	29
2.4.1 Solid–liquid extraction	30
2.4.2 Enzyme-assisted extraction	31
2.4.3 Pulse electric field – assisted extraction	31
2.4.4 High hydrostatic pressure extraction	32
2.4.5 Ultrasound-assisted extraction	32
2.4.6 Microwave-assisted extraction	33
2.5 Protein purification	33
2.5.1 Ultrafiltration	33
2.5.2 Ionic-exchange chromatography	33
2.5.3 Dialysis	34
2.6 Hydrolysis and peptide production	34
2.7 Conclusion and future prospective	36
References	36

### 3. Extraction and enrichment of fatty acids from marine microalgae

*Lavanyasri Rathinavel, Yuvaraj Ravikumar, Deepika Jothinathan, Sagaya John Paul J., Ashutosh Pandey and Chandan Mahata*

3.1 Introduction to marine microalgae fatty acids	41
---	----

# Diversity of marine algae, cultivation techniques, and sources of natural products for biotechnological applications

Antía Torres<sup>1</sup>, Sabina Naz<sup>2</sup>, Dakeshwar Kumar Verma<sup>3</sup> and Paz Otero<sup>1</sup>

<sup>1</sup>Nutrition and Bromatology Group, Department of Analytical Chemistry and Food Science, Faculty of Science, University de Vigo, Ourense, Spain,

<sup>2</sup>Department of Biotechnology, Bhilai Mahila Mahavidyalaya, Bhilai, Chhattisgarh, India, <sup>3</sup>Department of Chemistry, Govt. Digvijay Autonomous Postgraduate College, Rajnandgaon, Chhattisgarh, India

## 1.1 Introduction

The biological diversity in marine ecosystems offers an abundance of highly potent secondary metabolites for exploitation as bioactive compounds that might vary from the metabolites produced by terrestrial microorganisms. These compounds have evolved over millions of years as defense strategies to help marine organisms paralyze their preys (Pangestuti & Kim, 2011). From all marine organisms, algae have shown one of the major sources of new marine molecules providing unusual and unique chemical structures upon which molecular modeling and chemical synthesis of new nutraceuticals can be developed (Silva et al., 2021).

Marine algae can be divided into two main groups, macroalgae or seaweed and microalgae (Fig. 1.1). Microalgae are autotrophic microorganisms, which utilize light energy and inorganic nutrients (carbon dioxide, nitrogen, phosphorus, etc.) to synthesize valuable biomass compounds, such as lipids, proteins, carbohydrates, and pigments (Otero et al., 2017; Saha et al., 2020). They represent the largest and one of the most poorly understood groups of microorganisms on Earth. Microalgae thrive in harsh environmental conditions of high UV irradiance and photooxidation stresses due to their unique survival strategies (Browne et al., 2023). Growth rates, and thus the yields, of many microalgae are much higher than those of terrestrial crops (Mata et al., 2010), making them an appealing choice for natural biomolecule production. On the other hand, macroalgae or seaweed are multicellular plants that can reach sizes of up to 60 m in length. They are classified based on their pigmentation into three broad groups as brown seaweed (Phaeophyceae), red seaweed (Rhodophyceae), and green seaweed (Chlorophyceae) (El Gamal, 2010; Otero et al., 2018). Biodiversity within red, green, and brown macroalgae offers the possibility of finding a wide variety of bioactive natural compounds such as carotenoid pigments, phycosterols, peptides, polyunsaturated fatty acids (PUFA), betaines, taurine, polyphenols, minerals, and vitamins (Carreira-Casais et al., 2021; Otero, López-Martínez, & García-Risco, 2019; Pereira et al., 2021). Seaweeds accumulate a variety of phloroglucinol-based polyphenols known as phlorotannins involved in the protection of UV light-induced skin damage (Echave et al., 2022). Similarly, polysaccharides isolated from macroalgae such as fucoidan and laminarin of brown algae, carrageenan of red algae, and ulvan of green algae have anticoagulant, antioxidant, antiproliferative, antitumoral, antiinflammatory, antihyaluronidase, and antiviral activities (Otero, Carpena, et al., 2021).

The high content of bioactive in both micro and macroalgae allows their use for gastronomic, nutraceutical, and therapeutic purposes. Thus, notable efforts have been made to recover bioactive compounds from algae and use them as functional additives or drugs in the pharmaceutical, nutraceutical, and cosmetic industries. To obtain the maximum benefit from algae, it is necessary to extract and purify their active components, which is usually performed in the form of

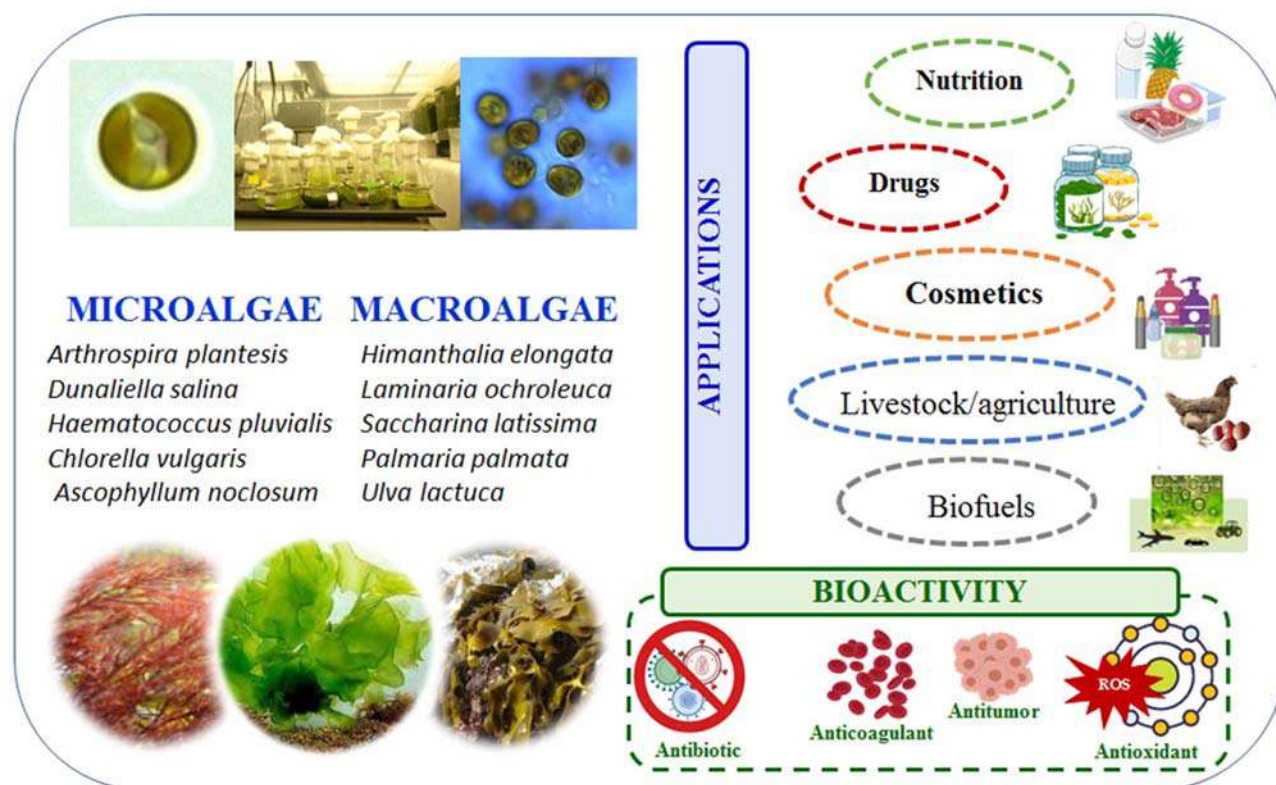


FIGURE 1.1 Some micro- and macroalgae for nutrition, pharmaceutical, cosmetic, livestock, agriculture, and biofuels production.

extracts. In this chapter, we introduced the main sources of micro- and macroalgae producing natural products of interest for nutraceuticals, pharmaceuticals, and cosmetic industry along with the main uses of these compounds in livestock feed, agriculture, and biofuel products.

## 1.2 Microalgae as a potential source for chemical compounds of interest

Microalgae have great potential in the nutritional and pharmaceutical and cosmetic industries due to their ability to synthesize a wide variety of bioactive compounds with therapeutic properties. Looking for new and sustainable energy alternatives, converting microalgae to biofuel is a sustainable energy alternative process to the use of fossil fuels. Table 1.1 collects information regarding innovative applications of microalgae as livestock feed, biofuel products as well as in their uses in the food, pharmaceutical, cosmetic industries, and they are deeply explained further.

### 1.2.1 Dietary source

The use of microalgae biomass in the production of food, feed ingredients, and nutraceuticals has been widely documented as an alternative source of traditional food (Otero, López-Martínez, & García-Risco, 2019). Today, its consumption has increased considerably during the last 20 years, due to our growing concern for health and nutrition (Rumin et al., 2020). In the food technology field, microalgae constitute a little-explored biological source of bioactive ingredients, which can be used in food fortification to develop functional foods (Barkia et al., 2019; Garcia-perez et al., 2023). Specifically, microalgae contain a high proportion of vitamins, which is essential for tissue growth and repair (Mahendran et al., 2021). On the other hand, the presence of healthy fats, such as omega-3 fatty acids, has been shown to improve human health and prevent diseases (for example, type 2 diabetes, cardiovascular disease, depression, or schizophrenia) (Rumin et al., 2020). Furthermore, despite macro- and microelements, they contain biopigments, such as chlorophyll and carotenoids, which give them powerful antioxidant potential and may help prevent cell damage and reduce the risk of diseases such as cancer (Mahendran et al., 2021).

**TABLE 1.1** Innovative applications of microalgae as livestock feed, biofuel products as well as in the food, pharmaceutical, cosmetic industries.

Microalgae	Analyte	Innovative application	Benefit	References
<i>Applications in the food industry as dietary source</i>				
<i>Porphyridium cruentum</i>	EPA	Antimicrobial and antiinflammatory effects	Nutraceutical; Baby and health food supplements	Mahendran et al. (2021)
<i>Chlorella vulgaris</i>	Proteins	Detoxify toxic metals and pesticides	Detoxifier	Mahendran et al. (2021)
<i>Haematococcus pluvialis</i>	Astaxanthin	Antiinflammatory and antidiabetic effects	Decreased glucose release in the production of whole foods	Mularczyk et al. (2020)
<i>Athrospira platensis</i>	GLA; Phycocyanin	Antiviral, anticancer, antioxidant, and antiinflammatory properties	High-quality protein source; Used as a food additive	Barkia et al. (2019)
<i>Applications in the pharmaceutical industry and medical interest</i>				
<i>H. pluvialis</i>	Astaxanthin	Anticancer	Increased levels of immune cells, natural killer cells and plasma $\gamma$ interferon in mice after astaxanthin treatment	Mularczyk et al. (2020)
<i>Dunaliella salina</i>	$\beta$ -carotene	Antioxidant and anticancer	Increased total number of T and B lymphocytes; increased cytotoxic activity of natural killer cells; reduced biomarkers of oxidative damage	Molino et al. (2018)
<i>A. platensis</i>	Phycocyanin	Antiviral effect	Downregulation of expression of inflammatory factor	Carbone et al. (2021)
<i>Euglena gracilis</i>	$\beta$ -glucan	Immunomodulatory effect	Activated NK cells and increased the levels of two proinflammatory mediators TFN $\alpha$ and IL-6	Riccio and Lauritano (2020)
<i>Applications as livestock feed</i>				
<i>Chlorella</i> sp.	$\beta$ -1,3-glucan	Antioxidant effect	Helps in lowering cholesterol levels in blood; Meat with a well-balanced lipid profile in pigs	Saadaoui et al. (2021)
<i>Nanochloropsis</i> sp.	PUFA	Improved quality	Improve the quality of milk in terms of useful fatty acids	Saadaoui et al. (2021)
<i>A. platensis</i>	PUFA- $\omega$ 3, EPA, DHA	Improved meat color; Antibiotic activity	Reduced risk of chronic disease, improved well-being	Camacho et al. (2019)
<i>Navicula</i> sp.	Oligosaccharides	Probiotic effects	Improved immune system and antioxidant activity in the feed	Camacho et al. (2019)
<i>Applications in cosmetic sector</i>				
<i>A. platensis</i>	GLA	Immunity booster	Maintains tissue integrity and delays aging	Mahendran et al. (2021)
<i>Chlorella</i> sp.	$\beta$ -1,3-glucan	Free-radicals collector; Immunomodulatory	Used in cosmetics for sensitive and reactive skin	Mourelle (2017)
<i>D. salina</i>	$\beta$ -cryptoxanthin	Antiinflammatory effect; antioxidant	Revitalize and hydrate the skin; rejuvenate tissues; protect against UV-rays	Mourelle (2017)
<i>Porphyridium</i>	Polysaccharides	Antiinflammatory effect	Inhibition of the movement of polymorphonuclear leukocytes; Inhibition of the development of erythema	Mohamed Abdoul-Jatif et al. (2021)
(Continued)				

**TABLE 1.1** (Continued)

Microalgae	Analyte	Innovative application	Benefit	References
<i>Applications as biofuel products</i>				
<i>Chlorococcum infusionum</i>	Glucose	Hydrolysis	Bioethanol production by biomass pretreatment	Simas-Rodrigues et al. (2015)
<i>Isochrysis galbana</i>	Fucoxanthin	Biorefinery	Obtaining biofuels from supercritical CO <sub>2</sub>	Gilbert-López et al. (2015)
<i>Nannochloropsis gaditana</i>	PUFA	Biorefinery	Biodiesel production	Koyande et al. (2019)
<i>Dunaliella tertiolecta</i>	Lipids; Fatty acids	Biorefinery	Obtain chair ad bio-oil from deffated biomass	Koyande et al. (2019)

Abbreviations: *DHA*, Docosahexaenoic acid; *EPA*, eicosapentaenoic acid; *GLA*,  $\gamma$ -linolenic-acid; *PUFAs*, polyunsaturated fatty acids.

From all microalgae susceptible to be used in human nutrition, just few species such as *Arthrospira plantensis*, *Haematococcus pluvialis*, *Dunaliella salina*, and *Chlorella vulgaris* are the most frequently used because of their relevant composition and bioactivities (Rumin et al., 2020). *A. plantensis* is a blue-green microalgae, also known as Spirulina, which is rich in protein, healthy fats, essential vitamins, and minerals and has antiviral, anticancer, antioxidant and antiinflammatory properties, among other beneficial effects (Mahendran et al., 2021). *C. vulgaris* has shown healthy properties such as cholesterol reduction, and antioxidant, antibacterial, and antitumoral activities (Mahendran et al., 2021). *H. pluvialis* is a green freshwater microalga, which contains a high concentration of astaxanthin (Otero et al., 2017) as well as an important antioxidant, antiinflammatory, antidiabetic, and anticancer activities (Mularczyk et al., 2020). *D. salina* habits very saline waters, accumulating large amount of beta-carotene with antioxidant and anticancer properties (Molino et al., 2018). *C. vulgaris* and *A. plantensis* are the most sought after in the global market due to their high protein content and their wide spectrum of minerals, vitamins, lipids, carbohydrates, pigments, and other trace elements (Cofrades et al., 2017). Similarly, other species, such as nori or wakame, are very popular in food, since they are used in the preparation of sushi, soups, and salads, standing out for high-value proteins, fibers, and essential minerals, such as iodine (Fraga-Corral et al., 2021).

Microalgae for human nutrition can be sold as food additives in a variety of food products (such as smoothies), in culinary dishes preparations, highly standardized in Asian countries, in drinks (such as juices), and in the form of supplements (either capsules or powders). However, to increase their acceptance, there are still some issues to be considered in their production and commercialization in regard to the bioactive compounds stability improvement, final product quality, and the risk assessment of an overconsumption (Barkia et al., 2019; Rumin et al., 2020).

### 1.2.2 Pharmaceutical and medical interest

Microalgae constitute an important source of bioactive compounds of natural origin, which have been a vital source of medicine for thousands of years. The characteristic chemical composition of microalgae gives them significant biological properties, which makes these microorganisms an important natural resource to be used in the prevention and treatment of certain diseases (Vieira et al., 2020).

Their applications in the pharmacological and medical field have grown exponentially in recent years due to their biological properties (Vieira et al., 2020). One of the most active and important research areas in this field is the use of microalgae due to their antioxidant potential, as the pharmacological industry increasingly considers these microorganisms for their antioxidant potential (Coulombie et al., 2021). Microalgae contain a wide variety of metabolites with great pharmacological relevance, such as carotenoids, polyphenols, fatty acids, or vitamins (Ferdous et al., 2021). These compounds can act as a defense against oxidative damage, by neutralizing free radicals, which prevents cell oxidative damage. For this reason, they can act in the prevention and treatment of diseases such as cancer or cardiovascular diseases, among others (Ferdous et al., 2021; Coulombie et al., 2021). One of the most studied species for its antioxidant

activity is *H. pluvialis*, specifically because of the biopigment astaxanthin, which is capable of protecting against various effects produced by oxidative stress (Vieira et al., 2020). Another studied activity is their immunomodulatory activity due to compounds such as sulfopolysaccharides or polyunsaturated fatty acids, capable of stimulating macrophage cells, T cells, or dendritic cells, in addition of being able to act as adjuvants or specific immune responses (Ricchio & Lauritano, 2020). Therefore, these compounds stimulate the immune system in human and murine models, so algae containing this bioactive compounds are promising drugs with potential applications to treat human pathologies (Ricchio & Lauritano, 2020). On the other hand, inflammation is a key component of the immune system's response to pathogens, toxic agents, or tissue damage, and microalgae have been studied because of their antiinflammatory effects. For example, the carotenoids have shown various beneficial effects in many inflammatory diseases, such as nonalcoholic fatty liver disease, type 2 diabetes mellitus, asthma, or psoriasis, among others (Ávila-Román et al., 2021). Next, hypertension is a disease that causes thousands of deaths worldwide and has shown an increasing trend in recent years as a serious noncommunicable disease. In this case, peptides from microalgae have great potential for the prevention and treatment of hypertension due to their biological properties, specifically acting as promising angiotensin-converting enzyme (ACE) inhibitors (Jiang et al., 2021). Finally, microalgae attract the attention of researchers in the search for new molecules with antiviral effects. Thus, the antiviral effect of compounds such as lectin, carotenoids, astaxanthin, or polysaccharides has been documented in infections caused by viruses, such as Hepatitis C, diseases caused by herpes viruses, HIV, or SARS-COV-2 (Carbone et al., 2021). However, despite the great potential of microalgae, its use in this field still needs more development. The environmental impact of large-scale production is also a concern, due to the use of natural resources and energy (Ahmad & Hassan, 2022). More research and efforts are needed to find ways to exploit the various properties of microalgae compounds, but in an environmentally friendly way, as well as optimizing culture conditions and reducing costs of production (Ahmad & Hassan, 2022).

### 1.2.3 Livestock feed

It is known that approximately 30% of the total world production of microalgae is used in animal applications (Pas et al., 2021). Thus, these microorganisms are considered as a very promising food or feed ingredient due to their nutritional characteristics, which vary according to the species of microalgae and the amount consumed in the diet of the animals (Camacho et al., 2019). One of the reasons of microalgae use in livestock feed is because they are of high quality and relatively cheap ingredients with good carbohydrates, carotenoids, vitamins, and lipoproteins nutritional profile, providing livestock benefits such as the stimulation of their immune system or the improvement of milk quality cow (Saadaoui et al., 2021).

Microalgae are a very important source of protein for livestock feed, some strains produce large amounts of protein, normally between 25% and 50% (Pas et al., 2021; Saadaoui et al., 2021), although others such as *A. plantensis* can contain up to 70% protein (Saadaoui et al., 2021). Some most used species for protein supplements are *Chlorella* and *Arthrospira* containing proteins such as methionine and lysine, which in high concentrations have been found to increase chicken breast and thigh muscles, as well as improve meat quality and quantity (Saadaoui et al., 2021). Lipids are also important nutrients found in microalgae and depending strain, they can produce up to 50% lipids by dry weight, and sometimes even more (Saadaoui et al., 2021). Among the lipids, it is worth highlighting arachidonic acid (AA), alpha-linolenic acid (ALA), and eicosapentaenoic acid (EPA), which have a variety of biological functions such as antioxidant and antiinflammatory activities (Otero et al., 2022; Otero, Garcia-Oliveira, et al., 2021). This makes the idea of using these lipids for the production of feed additives for cattle breeding very promising (Dolganyuk et al., 2020). In addition to proteins and lipids, microalgae can be considered a rich source of vitamins and minerals, which confers benefits to livestock in terms of meat quality and production when administered in feed. Some vitamins stand out in microalgae with vitamin A, folic acid (B9), biotin (B7), or thiamine (B1). Similarly, we can find minerals such as sodium, potassium, or iron (Saadaoui et al., 2021). As previously mentioned, microalgae have tremendous potential as animal feed due to their composition rich in essential biomolecules, which improve the nutritional quality of animal products, making these microorganisms considered a sustainable source of nutrition for cattle (Parmar et al., 2023; Saadaoui et al., 2021).

However, despite the many advantages of feeding microalgae to cattle, there are still some challenges that need to be addressed. For example, knowing the ideal dose to administer in animal feed is one of the objectives to be addressed in this field (Saadaoui et al., 2021). In addition, the high water and nutrient requirements, as well as the energy needed, make the technology used for the extraction and production of microalgae composites nowadays commercially unsustainable (Parmar et al., 2023). Moreover, it is important to consider that many species of microalgae are not safe for consumption by livestock or humans, since they produce toxic molecules with harmful effects on health

(Otero et al., 2020; Otero, Alfonso, Alfonso, et al., 2010; Otero, Alfonso, Vieytes, et al., 2010; Parmar et al., 2023). To address these challenges, efforts have to be made to develop new, more efficient, and cost-effective microalgae cultivation techniques, as well as study the microalgae species that are safe and beneficial for livestock. Some key research directions can be to figure out the risk assessment of produced biomass, development of cost-effective processes, and identification of microalgae strains with broad environmental adaptability (Parmar et al., 2023).

In summary, microalgae are a rich source of nutrients for livestock, including proteins, lipids, vitamins, and minerals, which can have an impact on the quality of meat and dairy products (Camacho et al., 2019). The inclusion of microalgae in the diet can have benefits on the health and welfare of animals and, consequently, on humans who consume the meat (Camacho et al., 2019; Pas et al., 2021). However, it is important to focus research in this field to understand how the consumption of microalgae impacts animal health and welfare, in addition to addressing challenges related to the cost of production and food safety (Parmar et al., 2023).

#### 1.2.4 Cosmetics

Microalgae are one of the most widely used products of plant origin in the cosmetics industry, due to their biological properties such as ultraviolet (UV) absorption, antiaging, or antistain properties, among others (Stoyneva-gärtner et al., 2022). There is a wide variety of cosmetic products on the market that are used for body, hair, and skin care, which is the largest category (Ferreira et al., 2021). As this area is constantly being renewed, the cosmetic industry increasingly explores derivatives of natural products, especially those of plant origin (Stoyneva-gärtner et al., 2022).

Microalgae are widely used in the production of skin care cosmetics, as they can be used in sunscreens, moisturizing agents, sunscreens, etc. (Martínez-Ruiz et al., 2022) or to prevent blemishes, repair skin damage, and inhibit the inflammation process (Mourelle, 2017). The most studied species in this field are *Arthrospira* and *C. vulgaris*, with well-established and reliable results (Ferreira et al., 2021). One of the most important problems facing the cosmetics industry today is sensitive skin, as it affects a large proportion of the world's population. In this sense, *C. vulgaris* is used as a therapeutic preventive agent for different inflammatory skin diseases, such as atopic dermatitis (AD). These microalgae have been studied due to their ability to synthesize sulfated polysaccharides, which prevent and protect from free radicals and reactive oxygen species (ROS) (Ferreira et al., 2021). Another concern is that population is slowing down the effects of skin aging. For this, the effect of the polysaccharide  $\beta$ -1, 3-glucan, produced by *C. vulgaris*, has been studied for its use in formulas for preventing external aging. In addition, the carotene  $\beta$ -cryptoxanthin, produced by *D. salina*, has the ability to induce the synthesis of hyaluronic acid, which hydrates and delays skin aging (Mourelle, 2017). Antioxidants derived from microalgae are also used in the cosmetic industry for skin care as moisturizers and sunscreens for the prevention of wrinkles from aging and the treatment of skin cancer (Martínez-Ruiz et al., 2022). Pigments produced by microalgae are also of great value to the cosmetics industry, due to their antioxidant properties and their use as natural colorants. One of the most widely used biopigments is  $\beta$ -carotene, produced by *D. salina*, which is used in decorative cosmetics to produce products such as lipsticks (Mourelle, 2017). On the other hand, astaxanthin is also widely used in the formulation of sun protection products, since it acts against photo-oxidation induced by UV rays as well as lycopene, which is also a promising agent in the formulation of antiaging skin products (Mourelle, 2017). Chlorophyll is another widely used biopigment with great relevance in the cosmetics industry, particularly, in the production of deodorants or toothpastes, due to its powerful ability to mask odors (Mourelle, 2017). In addition, microalgae are of relevance in hair care, usually associated with the formulation of products for scalp problems, such as the prevention of antimicrobial activity, and hair growth (Mohamed Abdoul-latif et al., 2021). Silva and colleagues studied the effect in hair fiber of the combination of *Arthrospira plantensis* and *Ascophyllum nodosum*, showing improvements in the hair mechanical properties and the fibers surface (Silva et al., 2019). However, the relationship between microalgae and hair care is not yet well documented, since the results are scarce. More studies are needed on the use of these microorganisms in hair care products, as it seems to be a very promising line of research.

#### 1.2.5 Biofuel products

The rapid growth of the world population continuously increases the demand for energy fuels, which leads to their intensive use and, consequently, a depletion of these resources (Khan et al., 2018). Biofuels are taking on great relevance today since they are an excellent alternative to fossil fuels. Biofuels are mainly produced from traditional crops such as soybeans or palm oil; however, these crops present significant environmental disadvantages, such as increased deforestation. In this context, renewable, clean, and sustainable energy sources are sought, where microalgae stand out mainly (Musa et al., 2019). Among the different types of biofuels from microalgae, biodiesel and bioethanol stand out,



which have proven to be an excellent alternative to common fuels. Each of these biofuels has its own characteristics, as well as advantages and disadvantages, which are discussed further.

Bioethanol is one of the most important and clean biofuels used worldwide produced by fermentation with fungi or bacteria from the microalgae biomass, specifically species such as *Chlorococcum* or *Chlorella*, or from polysaccharides such as starch (Simas-Rodrigues et al., 2015). It has many advantages over fossil fuels, such as the production of fewer greenhouse gases or its possible direct use, without modification, in the automotive industry. However, issues such as the maximization of microalgae biomass or the reduction of costs in their production and maintenance must still be tackled (Khan et al., 2018).

As mentioned earlier, biodiesel is also one of the most prominent biofuels today. This is also considered a good alternative to fossil fuels, since its resulting energy is renewable, sustainable, and carbon neutral (Yang et al., 2023). For the production of this compound, a selection of microalgae are used according to their lipid profile, since it is a determining factor, but it is not a problem since most microalgae species are favorable for the production of biodiesel (Khan et al., 2018; Yang et al., 2023). Despite these advantages, there are still limitations and challenges regarding the production of biodiesel from microalgae, such as high costs and low productivity, as well as the difficulty of its commercialization on a large scale (Khan et al., 2018). There is a need to find economic and sustainable techniques to stimulate the accumulation of lipids and thereby improve production and reduce costs (Yang et al., 2023).

Another biofuel that is not as widespread or studied is biogas. This can be produced by anaerobic digestion from the residues resulting from the production from microalgae of other biofuels, such as biodiesel. This could mean a reduction in production and maintenance costs, as well as in the energy required, but it is not yet fully demonstrated, so more studies are needed (Torres et al., 2021).

Summarizing, current living conditions make the demand for energy fuels continuously increase; therefore, to avoid their massive use, other alternatives such as biofuels have been developed. Biofuels, such as bioethanol, biodiesel, or biogas, are an excellent alternative to fossil fuels, since they are considered renewable, clean, and sustainable sources of energy. These products have countless advantages, such as the reduction of greenhouse gases, but also disadvantages such as costs or low production. Despite this, biofuels are a commitment to the future, so methods for obtaining them must continue to be studied, how to address the problems that affect them, and new sustainable energy alternatives.

### 1.3 Macroalgae as a potential source for chemical compounds of interest

Seaweed is the base of the marine food chain. They produce a myriad of compounds and have been used in various types of industries. The global seaweed market by 2024 will be 22.13 billion US dollars and is expected to grow 8.9% per year by 2050. Table 1.2 collects information regarding innovative applications of macroalgae as livestock feed, biofuel products as well as in their uses in the food, pharmaceutical, cosmetic industries, and they are deeply explained further.

#### 1.3.1 Human food

There has been a rise in the consumption of macroalgae in both Western and eastern nations. This trend can be linked to the excellent nutritional properties of food products that are manufactured from macroalgae as well as the bioactive capabilities that are attributed to macroalgae itself. Since ancient times, people have eaten a plain meal made from the algae *Codium tomentosum*, *Himantalia elongata*, *Laminaria ochroleuca*, *Saccharina latissima*, *Porphyra* sp., *Palmaria palmata*, and *Ulva lactuca* (Otero, López-Martínez, & García-risco, 2019). The addition of *Laminaria* to smoked cheese, yoghurt, and milk desserts improved not only the nutritional content but also the overall flavor and texture of these meals. Other examples include wakame (*Undaria pinnatifida*), kombu (*Saccharina japonica*), Irish moss (*Chondrus crispus*), and thongweed or sea spaghetti (*Himantalia elongate*) (Parniakov et al., 2015). These are all substances that contribute to the gelling, thickening, and stabilizing qualities of substances such as agar, alginate, and carrageenan (Cofrades et al., 2017). Because algae possess these characteristics, they are most frequently used in the food industry as hydrocolloids or as functional ingredients in a wide variety of fish and meat products (steaks, frankfurters, or sausages), milk-based and fermented products (Hamzaoui et al., 2020), or cereal-based products (flour, pasta, bread, and biscuits) (García-Vaquero et al., 2017). Also, these hydrocolloids made from algae are very important for creative areas of the food business, such as molecular gastronomy. This is because of the potential antibacterial and antioxidant abilities of algae such as wakame (*U. pinnatifida*) and kombu (*Laminaria japonica*), which are used to maintain product quality and enhance long shelf lives (Khan et al., 2018). In addition to these, the *H. elongata* brown alga used as a natural alternative for food preservative has a significant quantity of phenolics, tannins, and flavonoids and possesses

**TABLE 1.2** Innovative applications of macroalgae as livestock feed, biofuel products as well as in the food, pharmaceutical, cosmetic industries.

Microalgae	Analyte	Innovative application	Benefit	References
<i>Applications in the food industry as dietary source</i>				
<i>Gracilaria, Gelidium, Laminaria</i> and <i>Macrocystis</i> spp.	Agar, alginate, and carrageenan	Gelling, thickening, and stabilizing qualities of substances	Used as hydrocolloids or as functional ingredients in a wide variety of fish and meat products (steaks, frankfurters, or sausages), milk-based and fermented products	Cofrades et al. (2017), Hamzaoui et al. (2020)
<i>H. elongata</i>	Phenolics, tannins, and flavonoids	Antioxidant characteristics. Food preservative.	Prevent the growth of both food-spoiling microbes ( <i>Pseudomonas aeruginosa</i> and <i>Enterococcus faecalis</i> )	Cox et al. (2010).
<i>H. elongata</i>	Phenolics, tannins, and flavonoids	Antioxidant characteristics. Food preservative.	Improve the quality of the meat. Prevent the growth of food-poisoning microorganisms ( <i>Listeria monocytogenes</i> and <i>Salmonella abony</i> )	Bortoluzzi et al. (2016)
<i>Applications in the pharmaceutical industry and medical interest</i>				
<i>Punctaria plantaginea</i>	Chemically transformed branched xylofucans	Antithrombotic and anticoagulant effects	To be used as anticoagulant as the heparinoid Clexane (enoxaparin)	Bilan et al. (2014)
Macroalgae spp.	Xanthophyll carotenoid astaxanthin	Antiinflammatory, antiaging, and neuroprotective properties	therapeutic treatment or prevention of neurodegenerative disorders such as Alzheimer's and Parkinson's diseases	Barbosa et al. (2014)
<i>Ulva fasciata</i>	P	Anticancer activity. suppresses the proliferation of tumor cells in human colon cancer by 50%	To reduce the risk of developing cancer	Ryu et al. (2013)
<i>Gracilariopsis lemaneiformis</i>	P	Antitumor activity against human lung cancer cell line A549, the gastric cancer cell line MKN28, and the mouse melanoma cell line B16	Slowing the progression of existing tumors	Kang et al. (2017)
<i>Applications as livestock feed</i>				
<i>Ulva</i> spp., <i>Codium</i> spp., <i>Cladophora</i> spp., <i>Ascophyllum</i> spp., <i>Fucus</i> spp., <i>Laminaria</i> spp., <i>Undaria</i> spp., <i>Palmaria</i> spp.	Vitamin, mineral, soluble P, PUFAs	High nutritional quality	Seaweed meal for livestock	Craigie (2011)
<i>Laminaria digitata</i>	Phenolics	Antioxidant potential	Boost pork's ADG and feed efficiency	Costa et al. (2021)
red seaweed, <i>Asparagopsis taxiformis</i> (AT).	Bromoform	Promising candidate as a biotic methane mitigation strategy in the largest milk or beef producing	Reduce enteric methane emission from rumen fermentation	Choi et al. (2022), Roque et al. (2019)

(Continued)

**TABLE 1.2 (Continued)**

Microalgae	Analyte	Innovative application	Benefit	References
<i>Applications in cosmetic sector</i>				
<i>Ulva</i>	Rhamnosa (P)	Moisturizing properties	Hydration	Khan et al. (2009)
<i>L. digitata</i>	The alginates (P)	Thickening properties	Used as a gelling, viscosifying, or dispersion stabilizing agent	Fertah et al. (2017)
<i>Sargassum</i> spp. and <i>Fucus</i> spp.	Fucoidans (P)	Antihyaluronidase, anticoagulant, and antiinflammatory activities.	Incorporation in creams. Improve skin lightening, photoprotection	Medeiros et al. (2008), Wang et al. (2013), Yampakdee et al. (2019)
<i>Eisenia</i> spp., <i>Saccharina</i> spp., or <i>Laminaria</i> spp.	Laminarin (P)	The antioxidant and antimicrobial properties.	Laminarin applied topically could speed up the healing process and protect against oxidative and bacterial stress	Brandt et al. (2011), Hartmann et al. (2015)
Red macroalgae <i>Porphyra</i> spp.	Porphyran (P)	Anti-inflammatory effect	Reduce inflammation, prevent ulcers, and alleviate pain	Lomartire and Gonçalves (2022)
<i>Applications as biofuel products</i>				
<i>Laminaria hyperborean</i>	Whole algae cells	anaerobic digestion treatment	biomethane production of 70%	Hinks et al. (2013)
Abbreviations: P, Polysaccharide; PUFAs, polyunsaturated fatty acids.				

antioxidant characteristics. Its methanolic extract was shown to prevent the growth of both food-spoiling microbes (*Pseudomonas aeruginosa* and *Enterococcus faecalis*) (Cox et al., 2010) and food-poisoning microorganisms (*Listeria monocytogenes* and *Salmonella abony*) to improve the quality of the meat (Bortoluzzi et al., 2016). The use of natural scents has the potential to cut down on the number of incidents of this kind. Even though macroalgae have not been highlighted as a very common source of aromas, several authors have already conducted research on the volatile compounds that can be found in the green alga, *Capsosiphon fulvescens* (C. Agardh) Setchell, and the brown alga *Fucus serratus* L. (Eom et al., 2012).

### 1.3.2 Pharmaceutical and medical applications

Seaweeds are known to have a wide range of bioactive compounds. Many of these compounds have the potential to help prevent or treat a number of diseases. For example, sodium alginate led to a reduction in the blood glucose level in diabetes type II (Sharifuddin et al., 2015). The peptide obtained from *Porphyra yezoensis* reduces the amount of sugar in rats' and rabbits' blood and reduces their blood pressure (Qu et al., 2010). Chemically transformed branched xylofucans isolated from *Punctaria plantaginea* had antithrombotic and anticoagulant effects, as did the heparinoid Clexane (enoxaparin) (Bilan et al., 2014). *E. cava* is an excellent source of bioactive marine polyphenols, which have been shown to have antihyperglycemic, antihyperlipidemic, antiinflammatory, and antioxidant effects (Ustyuzhanina et al., 2016). Several studies have shown that the xanthophyll carotenoid astaxanthin, which is also found in macroalgae, has antiinflammatory and antiaging characteristics. Astaxanthin possesses neuroprotective properties, which points to the possibility of its application in the therapeutic treatment or prevention of neurodegenerative disorders such as Alzheimer's disease and Parkinson's disease (Barbosa et al., 2014). Seaweed has the potential to lower the chance of getting depressed during pregnancy (Miyake et al., 2014). Polysaccharides found in seaweed have been shown to have antifatigue effects (Shao et al., 2013).

*L. ochroleuca*, *P. palmata*, and *H. elongata* had significantly higher antifungal properties. Due to phycocyanins, phlorotannins, carotenoids, polysaccharides, polyunsaturated fatty acids, and phenolic components (curcumin, epigallocatechin gallate, and flavonoid) were shown to have considerable antiallergic activity (Biris-Dorhoi et al., 2020).

Fucoidan isolated from *U. pinnatifida* (Pimentel et al., 2019) and Porphyran isolated from *Porphyra tenera* and *P. yezoensis* contain antiallergic characteristics (Ishihara et al., 2005). Macroalgae have a role in reducing the risk of developing cancer, slowing the progression of existing tumors, and even aiding in the body's recovery after undergoing radiotherapy or chemotherapy (Pimentel et al., 2019). Several polysaccharides found in seaweed, such as alginate, laminaran, and fucoidan, have shown anticancer properties (Otero, Carpena, et al., 2021). *Sargassum latifolium* decreased the number of viable 1301 cells and induced apoptosis (Gamal-Eldeen et al., 2009). *Ulva fasciata* extract suppresses the proliferation of tumor cells in human colon cancer by 50% (Ryu et al., 2013). *Gracilariopsis lemaneiformis* has antitumor activity by causing apoptosis in several cancer cell lines, such as the human lung cancer cell line A549, the gastric cancer cell line MKN28, and the mouse melanoma cell line B16, and extracts of *Hydroclathrus clathratus* inhibit the growth of the ascitic Sarcoma 180 tumor (Kang et al., 2017).

### 1.3.3 Livestock and agriculture

The harsh competition that exists between the food, feed, and biofuel industries can be mitigated somewhat with the use of seaweeds as feed ingredients. Seaweeds are viable, sustainable alternatives to corn and soybeans. In addition to this, macroalgae can act as a barrier to eutrophication and contribute to bioremediation. In addition to its usage as feed, macroalgae are already being incorporated into other kinds of food as both a nutritious ingredient and a component of nutraceutical products. European countries such as Iceland, France, and Norway usually use seaweeds in animal husbandry to fill the deficiency in mineral pastures (Leandro et al., 2020). Seaweed meal, used principally as a vitamin, mineral supplement, including bioactive compounds, such as soluble polysaccharides, with some species being good sources of n-3 and n-6 polyunsaturated fatty acids. It is produced mainly from the *Ulva*, *Codium*, and *Cladophora* for green algae; kelps *Ascophyllum* spp., *Fucus* spp., *Laminaria* spp., *Macrocystis* spp. and *Undaria* spp., for brown algae; and *Pyropia*, *Chondrus*, and *Palmaria* for red algae (Craigie, 2011). *Ascophyllum nodosum* can increase average daily gain (ADG) in ruminant and pig mostly, enhances marbling score, color uniformity and redness, and can decrease saturated fatty acids in ruminant meats. The use of *Laminaria* species, specifically *Laminaria digitata*, has been shown to boost pork's ADG and feed efficiency, in addition to its antioxidant potential (Costa et al., 2021). It has been demonstrated that a mixture of *Ulva* sp. and *Codium* sp. can boost the growth of poultry by up to 10% when added to their feed. On the other hand, feeding seaweeds and macroalgal products has been shown to reduce enteric methane emission from rumen fermentation (Choi et al., 2022), which makes this type of feeding a promising candidate as a biotic methane mitigation strategy in the largest milk or beef production (Roque et al., 2019).

The commercial production and use of compounds that can be made from marine macroalgae and have interesting biotechnological uses. These compounds include microbicides, nematicides, insecticides, biofertilizers, biostimulators, and soil conditioners (Tuhy et al., 2013). Some pathogens that attack plants are thought to be killed by bioactive substances such as fatty acids, proteins (amino acids), bioflavonoids, sulfated polysaccharides, carotenoids, polyphenols, and carbohydrates. There are auxin-like compounds that have been found in some seaweed (Sangha et al., 2010). These compounds confer tolerance to freezing and resistance to biotic stresses, and they also increase the plant's capacity to absorb nutrients (Akila & Jeyadoss, 2010). Seaweeds and the compounds they produce can promote early seed germination, as well as root and plant growth.

At the moment, the brown seaweed *A. nodosum* is the most used species to make commercial extracts. Other species such as *Codium* spp., *Ulva intestinalis*, *U. lactuca*, (Chlorophyta), *C. crispus* and *Gelidium* spp., (Rhodophyta) *Durvillaea* spp., *Ecklonia maxima*, *Fucus* spp., *Laminaria* spp., *Saccorhiza* spp., and *Sargassum* spp. are also utilized (Craigie, 2011). Extracts from seaweeds, such as laminarin, can increase the natural defense responses in plants. Also, it has been established that certain higher plant species respond favorably to the growth-promoting effects that alginate oligomers possess (Khan et al., 2009).

Furthermore, seaweed extracts are implicated in the expression of genes that code for a variety of pathogenesis-related proteins that have antibacterial capabilities. The antimicrobial activity of extracts obtained from a wide variety of algae species, including *U. fasciata*, *Bryopsis plumosa*, *Chaetomorpha antennina*, *Acrosiphonia orientalis*, *Sargassum wightii*, *Grateloupia filicina*, *Hypnea pannosa*, *Gracilaria corticated*, *Portieria hornemannii*, *Cheilosporum spectabile*, *Centroceras clavulatum*, *Chnoospora bicanaliculata*, and *Padina tetrastromatica*.

Anthraquinones, coumarins, rutin, quercetin, cycloeuodesmol, laurinterol, and debromolaurinterol, and kaempferol and flavonoids were the major phenolic compounds that were isolated from marine algae with antimicrobial activity (Al-Saif et al., 2014; El Gamal, 2010). Fucoidan, alginate, and other similar substances are added to soil, they improve the soil's structure and aeration, which in turn stimulates microorganisms and root systems, which helps plants grow better (Deolu-Ajayi et al., 2022). Several crude algal extracts from *Caulerpa scalpelliformis* (Asimakis et al., 2022),

*Padina pavonica* (Sahayaraj & Jeeva, 2012), *Sargassum tenerrimum* (Sahayaraj et al., 2012), *U. fasciata*, and *U. lactuca* (Asimakis et al., 2022) were tested for their ability to kill the cotton insect pest *Dysdercus* spp. Both lectins from *Ulva pertusa* and kappa/beta-carrageenans isolated from *Tichocarpus crinitus* (Nagorskaya et al., 2008) have been shown to have antiTMV action. The brown saltwater algae known as *Dictyota ciliolata* have cytotoxic and antiviral properties, making it effective against certain plant viruses (Chen et al., 2018). By mixing powders of *Spatoglossum variable*, *Polycladia indica*, and *Melanothamnus afaqhusainii* into the soil, it was found that the root knot nematode (*Meloidogyne incognita*) infection was greatly reduced (Baloch et al., 2013).

### 1.3.4 Cosmetics

Nowadays, new cosmeceutical products have been developed using a combination of extracts based on macroalgal polysaccharides. Some species of interest include *Gigartina stellata* (Rhodophyceae), *H. elongata* (L.), *Monostroma nitidum* Wittrock, *Laminaria* spp., and *Ulva* spp. (Phaeophyceae and Chlorophyceae) respectively, which are used in the extraction of PS and PS derivatives. Agar is a gelatinous hydrocolloid found in hand lotions, deodorants, foundation, exfoliants, scrubs, cleanser, shaving cream, antiaging treatments, facial moisturizers and lotions, liquid soap, acne treatments, body washes, and facials for increasing the amount of moisture. Most commonly obtained are from red macroalgae such as *Gracilaria* spp. and *Gelidium* spp.

*Ulva* contains a significant amount of rhamnose, which is an essential component of a moisturizing PS (Khan et al., 2009). The alginates that are extracted from various brown macroalgae, such as *L. digitata* (Huds) J.V. Lamouroux, are used as a gelling, viscosifying, or dispersion stabilizing agent (Fertah et al., 2017). In the food (due to its protein content) and cosmetics industries, carrageenans are used as gelling, thickening, and stabilizing agents. Carrageenans are extracted from red macroalgae, which belong to the Rhodophyceae family. The gelatinous extracts of *C. crispus* white seaweed have been used as an additive as a vegan alternative to gelatin (Liao et al., 2021). Brown macroalgae from the genera *Sargassum* and *Fucus* can be used to get fucoidans. These fucoidans have been put to use in a variety of bioactivities, including those related to skin lightening and photoprotection (Yarnpakdee et al., 2019), antihyaluronidase activity (Wang et al., 2013), and anticoagulant and antiinflammatory activities (Medeiros et al., 2008).

Laminarin is a polysaccharide that dissolves in water and can be taken from *Eisenia* spp., *Saccharina* spp., or *Laminaria* spp. The antioxidant and antimicrobial properties of rich laminarin extracts have been proven (Hartmann et al., 2015). Laminarin applied topically could speed up the healing process and protect against oxidative and bacterial stress (Brandt et al., 2011). Porphyran is another sulfated PS that may be found in red macroalgae of the genus *Porphyra* having the potential to whiten the skin, reduce inflammation, prevent ulcers, and alleviate pain (Lomartire & Gonçalves, 2022). Some secondary metabolites include phenolic compounds, terpenes, halogen compounds, carotenoids, vitamins, and sulfur and nitrogen derivatives, which are also of great interest to the cosmetic industry (Lourenço-Lopes et al., 2020).

### 1.3.5 Biofuel products

In terms of third-generation biofuel yields, macroalgae can generate more with less resource input. Fig. 1.2 shows macroalgae species used to produce different biofuels. Moreover, macroalgae offer advantages such as rapid growth, high CO<sub>2</sub> collection, and ease cultivation even in desolate places, which have the ability to satisfy the demands of the current energy crisis. Algae are the most promising source of nonconsumable biofuel because it can grow quickly even in harsh environments, salty water, and salt. The biofuel made from algae is completely safe and compostable, and it does not contain any sulfur (Mat Aron et al., 2020). The growth rate of macroalgae is approximately 20–30 times faster than that of fodder crops, and the oil content that may be found in macroalgae is around 30 times higher than that of traditional feedstocks (Vergara-Fernández et al., 2008).

Numerous species of macroalgae have already been successfully mass-cultivated in Asia, including *L. japonica*, *Eucheuma* spp., *Kappaphycus salverezii*, *Pyropia yezoensis*, *U. pinnatifida*, and *Gracilaria verrucosa* (Fernand et al., 2017). Biodiesel can be made from *C. antennina* (Sharmila et al., 2012), *Gracilaria corticata* (Suganya et al., 2014), *Enteromorpha compressa* (Xu et al., 2014), and *Cladophora glomerata* (Borines et al., 2013). The generation of bioethanol from *Sargassum* spp. was accomplished at a conversion yield rate of 89% (Borines et al., 2013) and 0.43 g/g sugars from *Gracilaria verrucosa* (Asnaghi et al., 2017). *Ulva reticulata*, which yielded a bioethanol concentration of 0.37% v/v from 1 gramme of sample (Yoza & Masutani, 2013), and *Ulva intestinalis*, which recovered a yield of 0.081 g/g dry weight (Osman et al., 2020). The treatment of seaweed waste with saccharification and fermentation procedures resulted in a conversion yield of 90.9% for bioethanol (Tan & Lee, 2014), whereas 26.2% are from *P. palmata*

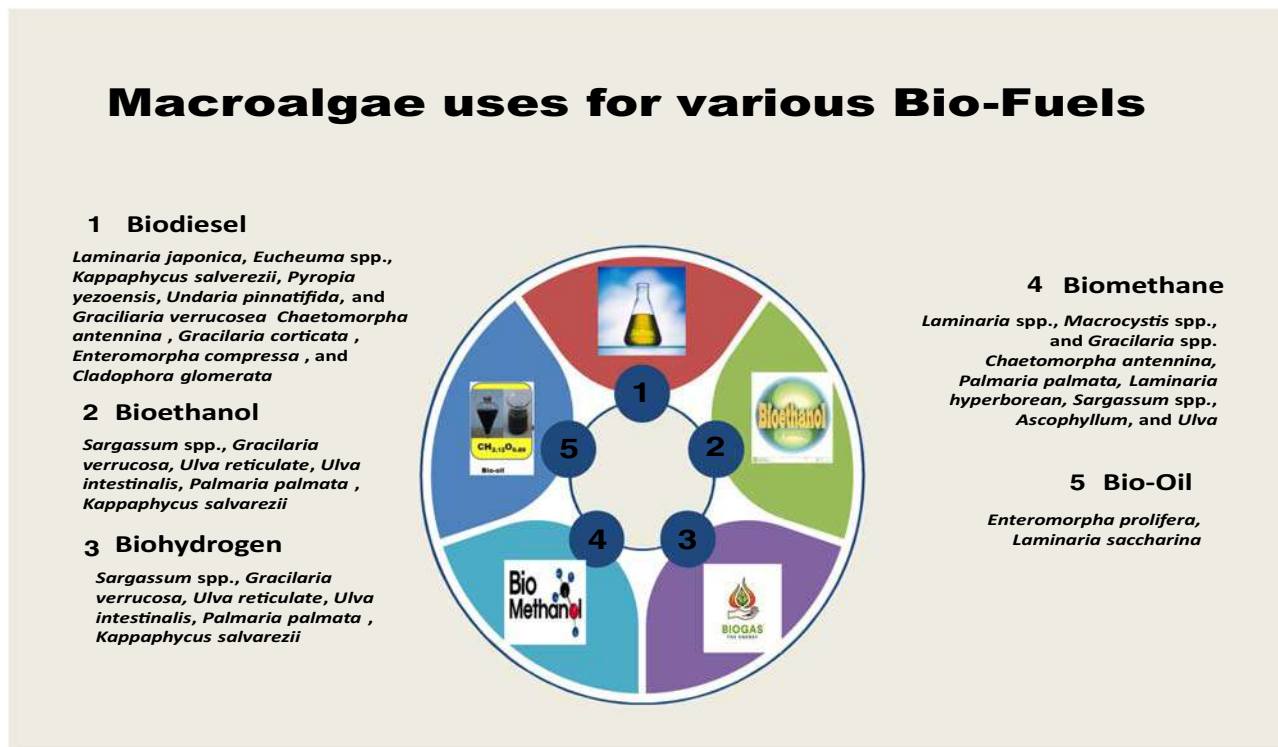


FIGURE 1.2 Various macroalgae uses to produce different biofuels.

(Torres et al., 2019) and 30.6% are from *Kappaphycus salvarezii* (Khambhaty et al., 2012). A high energy yield of 15.8 mL/g TS was achieved by biohydrogen synthesis in *L. japonica* (Yin et al., 2019), and *U. reticulata* of 45.5 mL by Kumar et al. (2018). According to the findings of several investigations, the amount of biomethane recovered from *Laminaria* spp., *Macrocystis* spp., and *Gracilaria* spp. ranges from 260 to 500 mL of methane per gramme of dry weight. The *C. antennina* algal biomass produces biomethane at a rate of 47.25 mL per gramme of COD (Tamilarasan et al., 2017). *P. palmata* achieved high biomethane production of  $308 \pm 9$  mL/g volatile solids (Jard et al., 2013). *Laminaria hyperborean* was treated with anaerobic digestion to attain biomethane production of 70% (Hinks et al., 2013). The biomethane yield of marine biomass has shown promise for stable methane production. Yields from green and brown algae genera, such as *Sargassum*, *Gracilaria*, *Laminaria*, *Ascophyllum*, and *Ulva*, were 179.35–256.28 mL/g of VS biomethane, respectively. The liquefaction of the green macroalgal species *Enteromorpha prolifera* with catalyst,  $\text{Na}_2\text{CO}_3$ , obtained 23.0% dw and *Laminaria saccharina* 19.3% without catalyst (Hyung et al., 2014) can directly produce bio-oil, which can then be used as a fuel. Bio-oil production from macroalgae was achieved by the use of a fixed-bed reactor and yielded 47% through the use of microwave treatment of 18.4% wt. (Wang et al., 2021).

### 1.4 Factors that influence the production of algae biocompounds

Researchers are working on making synthesis methods more efficient and finding ways to get the most useful biocompounds out of algae cells. The vast majority of algae are able to produce a wide variety of therapeutic compounds, including ash (8.4%–43.6%), high fiber (5.3%–52.3%), low protein (4.9%–37.8%), small amounts of fatty acids (0.92%–5.2%), and a wide variety of secondary metabolites (Rocha et al., 2018). Algal growth, the overall yield of biomass, and the production of therapeutic biocompounds such as lipids, proteins, polysaccharides, vitamins, pigments, and minerals are all affected by environmental factors such as the availability of nutrients (N, P, K, etc.), salinity, temperature, inorganic carbon, oxygen, light intensity,  $\text{CO}_2$ , pH of the seawater, and sampling season (Menaar et al., 2020) (Fig. 1.3). These factors can be found, and as a result, it is difficult to determine what the reference values should be for the polysaccharides, minerals, and trace elements that are available in algae. It has been shown that abiotic stress conditions can also have a deleterious impact on the growth of marine algae (Kaur et al., 2022).

The pH of the surrounding environment is a significant component that influences the growth of algae and plays a role in preventing contamination by other species or microbes (De Morais et al., 2015). Because it has such a direct

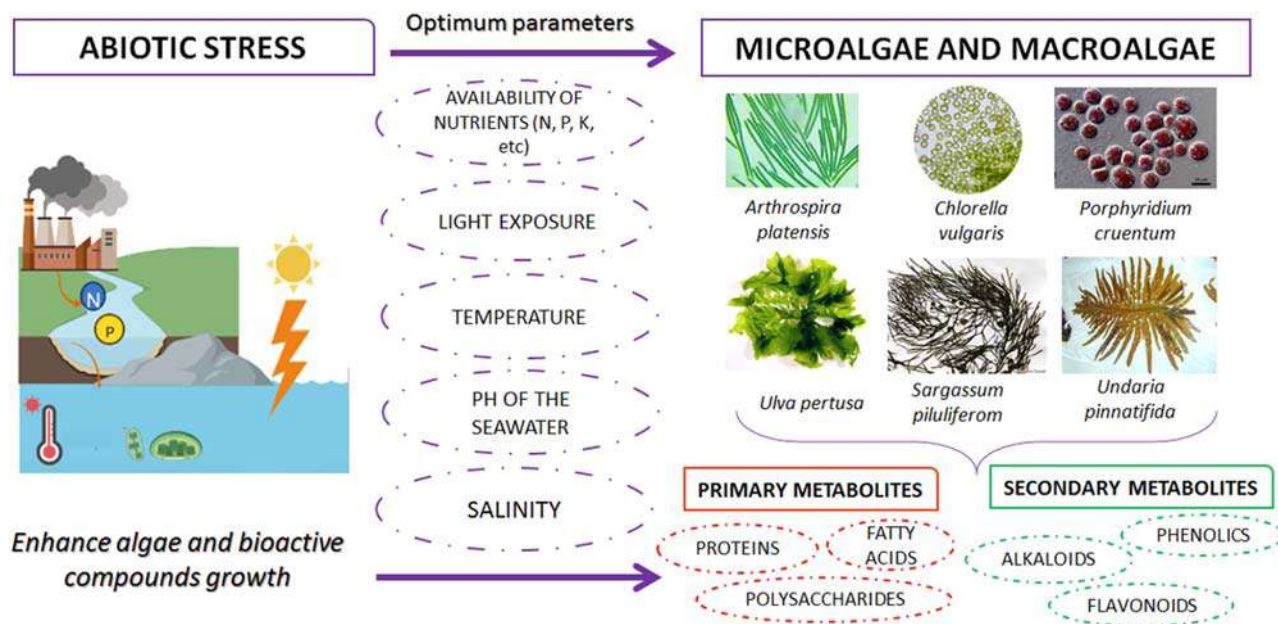


FIGURE 1.3 Factors that influence the production of micro and macroalgae.

influence on the bioavailability and stability of a wide variety of chemical elements, pH management is absolutely necessary for the efficient absorption of the components of the culture medium. Changes in pH have deleterious effects on algae cells (Kaur et al., 2022; Lavoie et al., 2012), and different species of algae have unique pH requirements for growth and nutrient uptake. Algae species also have varying pH requirements. For example, the green microalga *C. vulgaris* has the ability to thrive in a wide pH range; however, the optimal growth rate and biomass productivities were found at pH 9–10 (Kroeker et al., 2012). Furthermore, changes in the amount of nitrogen consumed by algae can affect their metabolic cycles, resulting in variations in the amounts of lipids or carbohydrates produced (Khan et al., 2018). The green seaweed *U. pertusa* made a lot of total FAs when it grew in a high-salinity environment (Peng et al., 2015).

The primary limiting parameters that have a significant impact on the biochemical content of microalgae and the amount of biomass produced are the length and intensity of the light exposure (Khan et al., 2009). Light makes it harder for cells to divide, which makes algal growth slower and less productive. The rate of photosynthesis goes up when there is more light, but photorespiration and photoinhibition keep the rate from going too high up to a certain point. Once this point is passed, the cell becomes upset (Jiménez-Escrig et al., 2011). The FA composition in algae is typically regulated by a variety of environmental variables, including the intensity of the light, the temperature, and the salinity of the seawater (Otero et al., 2017). This is because chloroplasts are mostly made of lipids, and because there is more light, there needs to be more chloroplast activity. There was an observed rise in the levels of the majority of saturated fatty acids (SFAs) (Vaz et al., 2016). But the amount of FAs in the green algae *U. pertusa* went up as the light got brighter, while almost all FAs in the brown algae *Sargassum piluliferum* went down (Peng et al., 2015). This suggests that the type of algae determines whether or not light induces the production of FAs.

Temperature is another important factor that affects algae growth, the production of biomass (such as proteins, lipids, and phenolic compounds), and the biochemical processes inside the cell (Uzair et al., 2020). A fall in temperature that is more than the appropriate level has an effect on photosynthesis by decreasing the activity of carbon assimilation, which will either slow down or stop the growth and activity of algae (Zozaya-valdés et al., 2016). In contrast, an increase in temperature that is higher than the optimal level causes a reduction in photosynthesis, cell size, and respiration. This, in turn, inactivates the proteins that are responsible for photosynthesis and throws off the equilibrium of energy within the cell. It has been shown that lower temperatures have an effect on the levels of FAs in a variety of species (Peng et al., 2015). In addition, photosynthesis and respiration are both affected by temperature, and the specific growth rate of microalgae is directly proportional to the gross rate of CO<sub>2</sub> fixation and O<sub>2</sub> production as well as the respiration rate (Smale & Wernberg, 2013). The brown seaweed *U. pinnatifida* (wakame) attained its maximum size of up to 4 m at the end of the summer when water temperatures averaged between 10.2°C and 11.4°C (Schaffelke & Hewitt, 2008). The brown seaweed *Egregia menziesii* had the highest total FA concentration in the spring (13.3 mg/g of dry

weight), whereas in the summer, it had the lowest total FA content (6.3 mg/g of dry weight) (Guerra-Rivas et al., 2011). FAs in algal cell membranes are temperature-sensitive, and when the temperature is low, the level of unsaturated FAs (UFAs) increases by raising the levels of polar lipids. FAs in algal cell membranes are temperature-sensitive.

This results in a decrease in melting temperatures and keeps lipids in a liquid state, both of which are necessary for normal protoplasmic viscosity. Also, the compositions of saturated fatty acids (SFA) are also affected by temperature, and temperature can also be used to change the amount of SFA (Khairy & El-shafay, 2013). The amount of (n-6) PUFA in *Phaeophyta Saccharina japonica* was highest when temperatures were high, while the amount of (n-3) PUFA was highest when temperatures were low (Schaffelke & Hewitt, 2008). For marine algae, *Rhodophyta Palmaria palmata* had higher levels of EPA at 11°C and AA at 15°C (Hamid et al., 2015).

The nutritional prerequisites change from one species of algae to another. Absorption of nutrients is species-specific; brown algae are rich in iodine and soluble fiber, whereas red and green species are rich in carbohydrates (Hamid et al., 2015).

Having said that, the fundamental needs are the same for all species. Indeed, nitrogen, phosphorus, and carbon make up the framework of algae (CH1.7 O0.4 N0.15 P0.0094) (Khan et al., 2018). Because these nutrients are involved in a number of enzymatic reactions that help algae grow, they could change the path algae take during biosynthesis, which would let them make and store a bioproduct of interest (De Moraes et al., 2015). The process through which algae take in nutrients involves a variety of distinct systems. Passive diffusion along the concentration gradient is used to take up uncharged molecules and gases such as CO<sub>2</sub>, O<sub>2</sub>, and NH<sub>3</sub>, whereas active transportation is used to take up inorganic elements such as nitrogen and phosphorous (Harrison & Hurd, 2001). Even when they grow in the same climate, come from the same place, and are harvested at the same time, the different families and genera of algae have a wide range of mineral and trace element concentrations. It's possible that the number of polysaccharides in algal cell walls, as well as their composition, contributes in different ways to the rates of biosorption of minerals and trace elements (Venugopal, 2019). The minerals and polysaccharides that are present in the cell walls of different microalgal genera and species can be found in a variety of different combinations (Peng et al., 2015). The protein and carbohydrate contents of the green algae *U. lactuca*, as well as the red algae *Jania rubens* and *Pterocladia capillacea*, which were taken from the western coast of Alexandria (Egypt), particularly from spring to autumn, were analyzed (Khairy & El-shafay, 2013). *P. capillacea* had the highest levels of both protein and carbohydrates, whereas *U. lactuca* had higher levels of both lipids and proline than the other two species combined. Also, *J. rubens* was found to have more total fatty acids, while *P. capillacea* was found to have more saturated fatty acids, mostly because it had more palmitic acid. Due to the dominance of DHA, the levels of PUFAs found in *J. rubens* were the highest. In a separate piece of research, it was shown that different algal species found in the north and south of Portugal during the summer had different amounts of polysaccharides in their cell walls because of how they reproduced during the different seasons (Serebryakova et al., 2018). It was discovered that temporal changes happened largely within the tip tissues and less within the basal blades, which may lead to a significant shift in the nutraceuticals of marine algae. These findings were made possible by the fact that temporal changes occurred within the tip tissues.

Algae contribute a substantial involvement to the primary production that occurs on a global scale. In addition, algae play an important role in the uptake of dissolved nutrients from the environment that surrounds them, the protection of coastal areas from dangerous waves, and possibly even the sequestration of carbon.

## 1.5 Challenges in production and use of algae compounds and conclusions

Microalgae have great potential in the medical and pharmaceutical field due to their ability to synthesize a wide variety of bioactive compounds with important biological activities (antioxidant, antiinflammatory, anticancer, and antiviral properties) and with great potential to be used as supplements for the prevention, management, and treatment of diseases (Barkia et al., 2019). However, more research and efforts are still needed to optimize production and reduce costs, as well as to find sustainable ways of production (Ahmad & Hassan, 2022). In addition, algae have excellent potential as animal feed due to their content of essential biomolecules such as amino acids, carotenoids, or vitamins, which improve the nutritional quality of animal products. Thus, including algae in livestock feed can be considered a promising strategy for improving the sustainability and efficiency of animal feed production. However, some challenges still need to be addressed, such as investigating the impact on animal health and welfare, in addition to addressing challenges related to the cost of production and food safety (Parmar et al., 2023). Parallely, the cosmetic industry is in constant renewal for exploring natural derivatives of vegetable origin. Algae are widely used in the formulation of skin care products, decorative cosmetics (makeup), or hair care products (Lourenço-Lopes et al., 2020), and in this sense, microalgae are one of the most used options in the production of cosmetics due to their biological properties such as



UV absorption or antiaging. Despite the advantages of using algae as source of biofuels, there are still limitations and challenges in the production of biodiesel from microalgae, such as high costs and low productivity, as well as the difficulty of its commercialization on a large scale (Khan et al., 2018). There is a need to find economic and sustainable techniques to stimulate the accumulation of lipids and thereby improve production and reduce costs (Yang et al., 2023).

Although microalgae can be an important source of nutrients for the human diet, there are still some considerations to be considered in their production, and commercialization such as the risks of misuse or overconsumption of these microorganisms as well as challenges in regard to the optimization of the cultivation processes, biomass production monitoring, and the improvement of bioactive compounds stability and the final quality of the products (Barkia et al., 2019; Rumin et al., 2020). A major bottleneck in industrial scale microalgal cultivation systems is the successful establishment of a balance between high biomass concentration because of maximum photosynthetic rate with adequate carbon dioxide supply and reduced oxygen production so as to avoid growth inhibition. Microalgae are generally cultivated in open or closed systems and require light, nutrients, and mixing while minimizing shear forces and high oxygen levels. Phototrophic microalgal production technologies have resulted in large accumulations of biomass with low yields of bioactive compounds. In open pond systems, water temperature and light intensity cannot be controlled and consequently lead to photo-inhibition and/or photo-saturation resulting in low productivity levels. Open pond growth systems are also susceptible to contamination from other contaminating and faster growing opportunistic microbes. Enclosed photo-bioreactor systems are also used in industrial scale for production of marine bioactives (astaxanthin production by *H. pluvialis*). Photo-bioreactor designs have to take into account not only the scale-up of single reactors but also the ability of individual photo-bioreactors to be assembled in repeat units into entire facilities of bioreactors (bioreactor farms). Online culture monitoring and bioreactor simulation will aid in reactor design optimization. Environmental control of growth conditions provides a cost effective and “nongenetic manipulation” method of optimizing and managing the bioactive characteristics of microalgae. Through manipulation of the growth environment of a species, it is possible to increase the abundance of bioactive compounds.

## Conflict of interests

Authors declared no conflict of interests.

## Acknowledgments

We would like to thank MICINN for supporting Ramón y Cajal’s grant for PazOtero (RYC2022-036690-I).

## References

- Ahmad, A., & Hassan, S. W. (2022). An overview of microalgae biomass as a sustainable aquaculture feed ingredient : Food security and circular economy. *Bioengineered*, 13(4), 9521–9547. Available from <https://doi.org/10.1080/21655979.2022.2061148>.
- Akila, N., & Jeyadoss, T. (2010). The potential of seaweed liquid fertilizer on the growth and antioxidant enhancement of *Helianthus annuus* L. *Oriental Journal of Chemistry*, 26(4), 1353–1360.
- Al-Saif, S. S. A. L., Abdel-Raouf, N., El-Wazanani, H. A., & Aref, I. A. (2014). Antibacterial substances from marine algae isolated from Jeddah coast of Red sea, Saudi Arabia. *Saudi Journal of Biological Sciences*, 21(1), 57–64. Available from <https://doi.org/10.1016/j.sjbs.2013.06.001>.
- Asimakis, E., Shehata, A. A., Eisenreich, W., Acheuk, F., Lasram, S., Basiouni, S., Emekci, M., Ntougias, S., Taner, G., May-Simera, H., Yilmaz, M., & Tsiamis, G. (2022). Algae and their metabolites as potential bio-pesticides. *Microorganisms*, 10(2). Available from <https://doi.org/10.3390/microorganisms10020307>.
- Asnaghi, V., Pecorino, D., Ottaviani, E., Pedroncini, A., Bertolotto, R. M., & Chiantore, M. (2017). A novel application of an adaptable modeling approach to the management of toxic microalgal bloom events in coastal areas. *Harmful Algae*, 63, 184–192. Available from <https://doi.org/10.1016/j.hal.2017.02.003>.
- Ávila-Román, J., García-Gil, S., Rodríguez-Luna, A., Motilva, V., & Talero, E. (2021). Anti-inflammatory and anticancer effects of microalgal carotenoids. *Marine Drugs*, 19, 531. Available from <https://doi.org/10.3390/md19100531>.
- Baloch, G. N., Tariq, S., Ehteshamul-Haque, S., Athar, M., Sultana, V., & Ara, J. (2013). Management of root diseases of eggplant and watermelon with the application of asafetida and seaweeds. *Journal of Applied Botany and Food Quality*, 86(1), 138–142. Available from <https://doi.org/10.5073/JABFQ.2013.086.019>.
- Barbosa, M., Valentão, P., & Andrade, P. B. (2014). Bioactive compounds from macroalgae in the new millennium: Implications for neurodegenerative diseases. *Marine Drugs*, 12(9), 4934–4972. Available from <https://doi.org/10.3390/md12094934>.
- Barkia, I., Saari, N., & Manning, S. R. (2019). Microalgae for high-value products towards human health and nutrition. *Marine Drugs*, 17(5), 1–29. Available from <https://doi.org/10.3390/md17050304>.

- Bilan, M. I., Shashkov, A. S., & Usov, A. I. (2014). Structure of a sulfated xylofucan from the brown alga *Punctaria*. *Carbohydrate Research*, 393, 1–8. Available from <https://doi.org/10.1016/j.carres.2014.04.022>.
- Biris-Dorhoi, E. S., Michiu, D., Pop, C. R., Rotar, A. M., Tofana, M., Pop, O. L., Socaci, S. A., & Farcas, A. C. (2020). Macroalgae—A sustainable source of chemical compounds with biological activities. *Nutrients*, 12(10), 1–23. Available from <https://doi.org/10.3390/nu12103085>.
- Borines, M. G., de Leon, R. L., & Cuello, J. L. (2013). Bioethanol production from the macroalgae *Sargassum* spp. *Bioresource Technology*, 138, 22–29. Available from <https://doi.org/10.1016/j.biortech.2013.03.108>.
- Bortoluzzi, C., Schmidt, J. M., Bordignon, H. L. F., Fülber, L. M., Layter, J. R., & Fernandes, J. I. M. (2016). Efficacy of yeast derived glucomannan or algae-based antioxidant or both as feed additives to ameliorate mycotoxicosis in heat stressed and unstressed broiler chickens. *Livestock Science*, 193(August), 20–25. Available from <https://doi.org/10.1016/j.livsci.2016.09.005>.
- Brandt, F. S., Cazzaniga, A., & Hann, M. (2011). Cosmeceuticals: Current trends and market analysis. *Seminars in Cutaneous Medicine and Surgery*, 30(3), 141–143. Available from <https://doi.org/10.1016/j.sder.2011.05.006>.
- Browne, N., Otero, P., Murray, P., & Saha, S. K. (2023). Rapid Screening for Mycosporine-like amino acids (MAAs) of Irish marine cyanobacteria and their antioxidant potential. *Sustainability (Switzerland)*, 15(4), 1–16. Available from <https://doi.org/10.3390/su15043792>.
- Camacho, F., Macedo, A., & Malcata, F. (2019). Potential industrial applications and commercialization of microalgae in the functional food and feed industries: A short review. *Marine Drugs*, 17(6), 312. Available from <https://doi.org/10.3390/md17060312>.
- Carbone, D. A., Pellone, P., Lubritto, C., & Ciniglia, C. (2021). Evaluation of microalgae antiviral activity and their bioactive compounds. *Antibiotics*, 10(6), 746. Available from <https://doi.org/10.3390/antibiotics10060746>.
- Carreira-Casais, A., Otero, P., Garcia-Perez, P., Garcia-Oliveira, P., Pereira, A. G., Carpena, M., Soria-Lopez, A., Simal-Gandara, J., & Prieto, M. A. (2021). Benefits and drawbacks of ultrasound-assisted extraction for the recovery of bioactive compounds from marine algae. *International Journal of Environmental Research and Public Health*, 18(17). Available from <https://doi.org/10.3390/ijerph18179153>.
- Chen, J., Li, H., Zhao, Z., Xia, X., Li, B., Zhang, J., & Yan, X. (2018). Diterpenes from the marine algae of the genus *Dictyota*. *Marine Drugs*, 16(5). Available from <https://doi.org/10.3390/md16050159>.
- Choi, Y., Lee, S. J., Kim, H. S., Eom, J. S., Jo, S. U., Guan, L. L., Park, T., Seo, J., Lee, Y., Bae, D., & Lee, S. S. (2022). Red seaweed extracts reduce methane production by altering rumen fermentation and microbial composition in vitro. *Frontiers in Veterinary Science*, 9. Available from <https://doi.org/10.3389/fvets.2022.985824>.
- Cofrades, S., Benedí, J., Garcimartin, A., Sánchez-Muniz, F. J., & Jimenez-Colmenero, F. (2017). A comprehensive approach to formulation of seaweed-enriched meat products: From technological development to assessment of healthy properties. *Food Research International*, 99, 1084–1094. Available from <https://doi.org/10.1016/j.foodres.2016.06.029>.
- Costa, M., Cardoso, C., Afonso, C., Bandarra, N. M., & Prates, J. A. M. (2021). Current knowledge and future perspectives of the use of seaweeds for livestock production and meat quality: A systematic review. *Journal of Animal Physiology and Animal Nutrition*, 105(6), 1075–1102. Available from <https://doi.org/10.1111/jpn.13509>.
- Coulombier, N., Jauffrais, T., & Lebouvier, N. (2021). Antioxidant compounds from microalgae: A review. *Marine Drugs*, 19, 549. Available from <https://doi.org/10.3390/md19100549>.
- Cox, S., Abu-Ghannam, N., & Gupta, S. (2010). An assessment of the antioxidant and antimicrobial activity of six species of edible Irish seaweeds. *International Food Research Journal*, 17(1), 205–220. Available from <https://doi.org/10.21427/D7HC92>.
- Craigie, J. S. (2011). Seaweed extract stimuli in plant science and agriculture. *Journal of Applied Phycology*, 23(3), 371–393. Available from <https://doi.org/10.1007/s10811-010-9560-4>.
- De Morais, M. G., Vaz, B. D. S., De Morais, E. G., & Costa, J. A. V. (2015). Biologically active metabolites synthesized by microalgae. *BioMed Research International*, 2015. Available from <https://doi.org/10.1155/2015/835761>.
- Deolu-Ajayi, A. O., van der Meer, I. M., van der Werf, A., & Karlova, R. (2022). The power of seaweeds as plant biostimulants to boost crop production under abiotic stress. *Plant Cell and Environment*, 45(9), 2537–2553. Available from <https://doi.org/10.1111/pce.14391>.
- Dolganyuk, V., Andreeva, A., Budenkova, E., Sukhikh, S., Babich, O., Ivanova, S., Prosekov, A., & Ulrikh, E. (2020). Study of morphological features and determination of the fatty acid composition of the microalgae lipid complex. *Biomolecules*, 10(1571). Available from <https://doi.org/10.3390/biom10111571>.
- Echave, J., Otero, P., Garcia-Oliveira, P., Munekata, P. E. S., Pateiro, M., Lorenzo, J. M., Simal-Gandara, J., & Prieto, M. A. (2022). Seaweed-derived proteins and peptides: Promising marine bioactives. *Antioxidants*, 11(Issue 1). Available from <https://doi.org/10.3390/antiox11010176>, MDPI.
- El Gamal, A. A. (2010). Biological importance of marine algae. *Saudi Pharmaceutical Journal*, 18(Issue 1), 1–25. Available from <https://doi.org/10.1016/j.jsps.2009.12.001>, King Saud University.
- Eom, S. H., Kim, Y. M., & Kim, S. K. (2012). Antimicrobial effect of phlorotannins from marine brown algae. *Food and Chemical Toxicology*, 50(9), 3251–3255. Available from <https://doi.org/10.1016/j.fct.2012.06.028>.
- Ferdous, U. T., Norhana, Z., & Yusof, B. (2021). Medicinal prospects of antioxidants from algal sources in cancer therapy. *Frontiers in Pharmacology*, 12(March), 1–22. Available from <https://doi.org/10.3389/fphar.2021.593116>.
- Fernand, F., Israel, A., Skjermo, J., Wichard, T., Timmermans, K. R., & Golberg, A. (2017). Offshore macroalgae biomass for bioenergy production: Environmental aspects, technological achievements and challenges. *Renewable and Sustainable Energy Reviews*, 75, 35–45. Available from <https://doi.org/10.1016/j.rser.2016.10.046>, January 2016.
- Ferreira, M. S., Resende, D. I. S. P., Lobo, J. M. S., Sousa, E., & Almeida, I. F. (2021). Marine ingredients for sensitive skin: Market overview. *Marine Drugs*, 19, 464. Available from <https://doi.org/10.3390/md19080464>.

- Fertah, M., Belfkira, A., Dahmane, E. M., Taourirte, M., & Brouillette, F. (2017). Extraction and characterization of sodium alginate from Moroccan *Laminaria digitata* brown seaweed. *Arabian Journal of Chemistry*, 10, S3707–S3714. Available from <https://doi.org/10.1016/j.arabjc.2014.05.003>.
- Fraga-Corral, M., Otero, P., Echave, J., Garcia-Oliveira, P., Carpena, M., Jarboui, A., Nuñez-Estevéz, B., Simal-Gandara, J., & Prieto, M. A. (2021). By-products of agri-food industry as tannin-rich sources: A review of tannins' biological activities and their potential for valorization. *Foods*, 10 (1). Available from <https://doi.org/10.3390/foods10010137>.
- Gamal-Eldeen, A. M., Ahmed, E. F., & Abo-Zeid, M. A. (2009). In vitro cancer chemopreventive properties of polysaccharide extract from the brown alga, *Sargassum latifolium*. *Food and Chemical Toxicology*, 47(6), 1378–1384. Available from <https://doi.org/10.1016/j.fct.2009.03.016>.
- García-perez, P., Cassani, L., Garcia-oliveira, P., Xiao, J., Simal-gandara, J., Prieto, M. A., & Lucini, L. (2023). Algal nutraceuticals : A perspective on metabolic diversity, current food applications, and prospects in the field of metabolomics. *Food Chemistry*, 409(December 2022), 135295. Available from <https://doi.org/10.1016/j.foodchem.2022.135295>.
- García-Vaquero, M., Rajauria, G., O'Doherty, J. V., & Sweeney, T. (2017). Polysaccharides from macroalgae: Recent advances, innovative technologies and challenges in extraction and purification. *Food Research International*, 99, 1011–1020. Available from <https://doi.org/10.1016/j.foodres.2016.11.016>.
- Gilbert-López, B., Mendiola, J. A., Fontecha, J., van den Broek, L. A., Sijtsma, L., Cifuentes, A., Herrero, M., & Ibáñez, E. (2015). Downstream processing of *Isochrysis galbana*: A step towards microalgal biorefinery. *Green Chemistry*, 17, 4599–4609. Available from <https://doi.org/10.1039/c5gc01256b>.
- Guerra-Rivas, G., Gómez-Gutiérrez, C. M., Alarcón-Arteaga, G., Soria-Mercado, I. E., & Ayala-Sánchez, N. E. (2011). Screening for anticoagulant activity in marine algae from the Northwest Mexican Pacific coast. *Journal of Applied Phycology*, 23(3), 495–503. Available from <https://doi.org/10.1007/s10811-010-9618-3>.
- Hamid, N., Ma, Q., Boulom, S., Liu, T., Zheng, Z., Balbas, J., & Robertson, J. (2015). *Seaweed minor constituents. Seaweed sustainability: Food and non-food applications* (pp. 193–242). Elsevier Inc. Available from <https://doi.org/10.1016/B978-0-12-418697-2.00008-8>.
- Hamzaoui, A., Ghariani, M., Sellem, I., Hamdi, M., Feki, A., Jaballi, I., Nasri, M., & Amara, I. B. (2020). Extraction, characterization and biological properties of polysaccharide derived from green seaweed “*Chaetomorpha linum*” and its potential application in Tunisian beef sausages. *International Journal of Biological Macromolecules*, 148, 1156–1168. Available from <https://doi.org/10.1016/j.ijbiomac.2020.01.009>.
- Harrison, P. J., & Hurd, C. L. (2001). Nutrient physiology of seaweeds: Application of concepts to aquaculture. *Cahiers de Biologie Marine*, 42, 71–82.
- Hartmann, A., Gostner, J., Fuchs, J. E., Chaita, E., Aliyannis, N., Skaltsounis, L., & Ganzera, M. (2015). Inhibition of collagenase by mycosporine-like amino acids from marine sources. *Planta Medica*, 81(10), 813–820. Available from <https://doi.org/10.1055/s-0035-1546105>.
- Hinks, J., Edwards, S., Sallis, P. J., & Caldwell, G. S. (2013). The steady state anaerobic digestion of *Laminaria hyperborea*—Effect of hydraulic residence on biogas production and bacterial community composition. *Bioresource Technology*, 143, 221–230. Available from <https://doi.org/10.1016/j.biortech.2013.05.124>.
- Hyung, J., Chul, H., & Jin, D. (2014). Pyrolysis of seaweeds for bio-oil and bio-char production. *Chemical Engineering Transactions*, 37, 121–126. Available from <https://doi.org/10.3303/CET1437021>.
- Ishihara, K., Oyamada, C., Matsushima, R., Murata, M., & Muraoka, T. (2005). Inhibitory effect of porphyran, prepared from dried “Nori,” on contact hypersensitivity in mice. *Bioscience, Biotechnology, and Biochemistry*, 69(10), 1824–1830. Available from <https://doi.org/10.1271/bbb.69.1824>.
- Jard, G., Dumas, C., Delgenes, J. P., Marfaing, H., Sialve, B., Steyer, J. P., & Carrère, H. (2013). Effect of thermochemical pretreatment on the solubilization and anaerobic biodegradability of the red macroalga *Palmaria palmata*. *Biochemical Engineering Journal*, 79, 253–258. Available from <https://doi.org/10.1016/j.bej.2013.08.011>.
- Javier, Á., Garc, S., Rodr, A., Motilva, V., & Talero, E. (2021). *Anti-Inflammatory and Anticancer Effects of Microalgal Carotenoids*. 1–49.
- Jiang, Q., Chen, Q., Zhang, T., Liu, M., Duan, S., & Sun, X. (2021). The antihypertensive effects and potential molecular mechanism of microalgal angiotensin I-converting enzyme inhibitor-like peptides: A mini review. *International Journal of Molecular Sciences*, 22, 4068. Available from <https://doi.org/10.3390/ijms22084068>.
- Jiménez-Escrig, A., Gómez-Ordóñez, E., & Rupérez, P. (2011). Seaweed as a source of novel nutraceuticals: Sulfated polysaccharides and peptides. *Advances in Food and Nutrition Research*, 64, 325–337. Available from <https://doi.org/10.1016/B978-0-12-387669-0.00026-0>.
- Kang, Y., Wang, Z. J., Xie, D., Sun, X., Yang, W., Zhao, X., & Xu, N. (2017). Characterization and potential antitumor activity of polysaccharide from *Gracilariopsis lemaneiformis*. *Marine Drugs*, 15(4), 1–14. Available from <https://doi.org/10.3390/md15040100>.
- Kaur, M., Saini, K. C., Ojah, H., Sahoo, R., Gupta, K., Kumar, A., & Bast, F. (2022). Abiotic stress in algae: Response, signaling and transgenic approaches. *Journal of Applied Phycology*, 34(4), 1843–1869. Available from <https://doi.org/10.1007/s10811-022-02746-7>.
- Khairy, H. M., & El-shafay, S. M. (2013). Seasonal variations in the biochemical composition of some common seaweed species from the coast of Abu Qir Bay, Alexandria, Egypt. *Oceanologia*, 55(2), 435–452. Available from <https://doi.org/10.5697/oc.55-2.435>.
- Khambhaty, Y., Mody, K., Gandhi, M. R., Thampy, S., Maiti, P., Brahmabhatt, H., Eswaran, K., & Ghosh, P. K. (2012). Bioresource technology *Kappaphycus alvarezii* as a source of bioethanol. *Bioresource Technology*, 103(1), 180–185. Available from <https://doi.org/10.1016/j.biortech.2011.10.015>.
- Khan, M. I., Shin, J. H., & Kim, J. D. (2018). The promising future of microalgae: Current status, challenges, and optimization of a sustainable and renewable industry for biofuels, feed, and other products. *Microbial Cell Factories*, 17(1), 1–21. Available from <https://doi.org/10.1186/s12934-018-0879-x>.

- Khan, W., Rayirath, U. P., Subramanian, S., Jithesh, M. N., Rayorath, P., Hodges, D. M., Critchley, A. T., Craigie, J. S., Norrie, J., & Prithiviraj, B. (2009). Seaweed extracts as biostimulants of plant growth and development. *Journal of Plant Growth Regulation*, 28(4), 386–399. Available from <https://doi.org/10.1007/s00344-009-9103-x>.
- Koyande, K. A., Show, P., Guo, R., Tang, B., Ogino, C., & Chang, J.-S. (2019). Bio-processing of algal bio-refinery : A review on current advances and future perspectives. *Bioengineered*, 10(1), 574–592. Available from <https://doi.org/10.1080/21655979.2019.1679697>.
- Kroeker, K. J., Micheli, F., & Gambi, M. C. (2012). Ocean acidification causes ecosystem shifts via altered competitive interactions. *Nature Climate Change*, 2(10), 1–4. Available from <https://doi.org/10.1038/nclimate1680>.
- Kumar, M. D., Tamilarasan, K., Kaliappan, S., Banu, J. R., Rajkumar, M., & Kim, S. H. (2018). Surfactant assisted disperser pretreatment on the liquefaction of *Ulva reticulata* and evaluation of biodegradability for energy efficient biofuel production through nonlinear regression modelling. *Bioresource Technology*, 255(January), 116–122. Available from <https://doi.org/10.1016/j.biortech.2018.01.116>.
- Lavoie, M., Le Faucheur, S., Boulléant, A., Fortin, C., & Campbell, P. G. C. (2012). The influence Of pH on algal cell membrane permeability and its implications for the uptake of lipophilic metal complexes. *Journal of Phycology*, 48(2), 293–302. Available from <https://doi.org/10.1111/j.1529-8817.2012.01126.x>.
- Leandro, A., Pereira, L., & Gonçalves, A. M. M. (2020). Diverse applications of marine macroalgae. *Marine Drugs*, 18(1), 1–15. Available from <https://doi.org/10.3390/md18010017>.
- Liao, Y. C., Chang, C. C., Nagarajan, D., Chen, C. Y., & Chang, J. S. (2021). Algae-derived hydrocolloids in foods: applications and health-related issues. *Bioengineered*, 12(1), 3787–3801. Available from <https://doi.org/10.1080/21655979.2021.1946359>.
- Lomartire, S., & Gonçalves, A. M. M. (2022). An overview of potential seaweed-derived bioactive compounds for pharmaceutical applications. *Marine Drugs*, 20(Issue 2). Available from <https://doi.org/10.3390/md20020141>.
- Lourenço-Lopes, C., Fraga-Corral, M., Jimenez-Lopez, C., Pereira, A. G., Garcia-Oliveira, P., Carpena, M., Prieto, M. A., & Simal-Gandara, J. (2020). Metabolites from macroalgae and its applications in the cosmetic industry: A circular economy approach. *Resources*, 9(9). Available from <https://doi.org/10.3390/RESOURCES9090101>.
- Mahendran, M. S., Dhanapal, A. C. T. A., Wong, L. S., Kasivelu, G., & Djearmane, S. (2021). Microalgae as a potential source of bioactive food compounds. *Current Research in Nutrition and Food Science Journal*, 9(3), 917–927. Available from <https://doi.org/10.12944/CRNFSJ.9.3.18>.
- Martínez-Ruiz, M., Martínez-González, C. A., Kim, D.-H., Santiesteban-Romero, B., Reyes-Pardo, H., Villaseñor-Zepeda, K. R., Meléndez-Sánchez, E. R., Ramírez-Gamboa, D., Díaz-Zamorano, A. L., Sosa-Hernández, J. E., Coronado-Apodaca, K. G., Gámez-Méndez, A. M., Iqbal, H. M. N., & Parra-Saldivar, R. (2022). Microalgae bioactive compounds to topical applications products-A review. *Molecules*, 27, 3512. Available from <https://doi.org/10.3390/molecules27113512>.
- Mat Aron, N. S., Khoo, K. S., Chew, K. W., Show, P. L., Chen, W. H., & Nguyen, T. H. P. (2020). Sustainability of the four generations of biofuels – A review. *International Journal of Energy Research*, 44(12), 9266–9282. Available from <https://doi.org/10.1002/er.5557>.
- Mata, T. M., Martins, A. A., & Caetano, N. S. (2010). Microalgae for biodiesel production and other applications: A review. *Renewable and Sustainable Energy Reviews*, 14(1), 217–232. Available from <https://doi.org/10.1016/j.rser.2009.07.020>.
- Medeiros, V. P., Queiroz, K. C., Cardoso, M. L., Monteiro, G. R., Oliveira, F. W., Chavante, S. F., Guimaraes, L. A., Rocha, H. A., & Leite, E. L. (2008). Sulfated galactofucan from *Lobophora variegata*: Anticoagulant and anti-inflammatory properties. *Biochemistry (Moscow)*, 73(9), 1018–1024. Available from <https://doi.org/10.1134/s0006297908090095>, PMID: 18976219.
- Mena, F., Wijesinghe, P. A. U. I., Thiripuranathar, G., Uzair, B., Iqbal, H., Khan, B. A., & Mena, B. (2020). Ecological and industrial implications of dynamic seaweed-associated microbiota interactions. *Marine Drugs*, 18(12), 1–25. Available from <https://doi.org/10.3390/md18120641>.
- Miyake, Y., Tanaka, K., Okubo, H., Sasaki, S., & Arakawa, M. (2014). Seaweed consumption and prevalence of depressive symptoms during pregnancy in Japan: Baseline data from the Kyushu Okinawa Maternal and Child Health Study. *BMC Pregnancy and Childbirth*, 14(1), 1–7. Available from <https://doi.org/10.1186/1471-2393-14-301>.
- Mohamed Abdoul-latif, F., Oumaskour, K., Boujaber, N., Ainane, A., Mohamed, J., & Ainane, T. (2021). Formulations of a cosmetic product for hair care based on extract of the microalga *Isochrysis galbana*: In vivo and in vitro activities. *Journal of Analytical Sciences and Applied Biotechnology*, 3(1), 15–19.
- Molino, A., Iovine, A., Casella, P., Mehariya, S., Chianese, S., Cerbone, A., Rimauro, J., & Musmarra, D. (2018). Microalgae characterization for consolidated and new application in human food, animal feed and nutraceuticals. *International Journal of Environmental Research and Public Health*, 1–21. Available from <https://doi.org/10.3390/ijerph15112436>.
- Mourelle, M. L. (2017). The potential use of marine microalgae and cyanobacteria in cosmetics and thalassotherapy. *Cosmetics*. Available from <https://doi.org/10.3390/cosmetics4040046>.
- Mularczyk, M., Michalak, I., & Marycz, K. (2020). Astaxanthin and other nutrients from *Haematococcus pluvialis*—Multifunctional applications. *Marine Drugs*, 18(Issue 9), 459. Available from <https://doi.org/10.3390/md18090459>, MDPI AG.
- Musa, M., Ayoko, G. A., Ward, A., Rösch, C., Brown, R. J., & Rainey, T. J. (2019). Factors affecting microalgae production for biofuels and the potentials of chemometric methods in assessing and optimizing productivity. *Cells*, 8(8). Available from <https://doi.org/10.3390/cells8080851>.
- Nagorskaya, V. P., Reunov, A. V., Lapshina, L. A., Yermak, I. M., & Barabanova, A. O. (2008). Influence of  $\kappa$ / $\beta$ -carrageenan from red alga *Tichocarpus crinitus* on development of local infection induced by tobacco mosaic virus in Xanthi-nc tobacco leaves. *Biology Bulletin*, 35(3), 310–314. Available from <https://doi.org/10.1134/S1062359008030126>.
- Osman, M. E. H., Abo-Shady, A. M., Elshobary, M. E., Abd El-Ghafar, M. O., & Abomohra, A. E. F. (2020). Screening of seaweeds for sustainable biofuel recovery through sequential biodiesel and bioethanol production. *Environmental Science and Pollution Research*, 27(26), 32481–32493. Available from <https://doi.org/10.1007/s11356-020-09534-1>.

- Otero, P., Alfonso, A., Alfonso, C., Vieytes, M. R., Louzao, M. C., Botana, A. M., & Botana, L. M. (2010). New protocol to obtain spiroclides from *Alexandrium ostenfeldii* cultures with high recovery and purity. *Biomedical Chromatography*, 24, 878–886.
- Otero, P., Alfonso, A., Vieytes, M. R., Cabado, A. G., Vieites, J. M., & Botana, L. M. (2010). Effects of environmental regimens on the toxin profile of *Alexandrium ostenfeldii*. *Environmental Toxicology and Chemistry*, 29(2), 301–310. Available from <https://doi.org/10.1002/etc.41>.
- Otero, P., Carpena, M., Fraga-Corral, M., Garcia-Oliveira, P., Soria-Lopez, A., Barba, F., Xiao, J. B., Simal-Gandara, J., & Prieto, M. (2022). Aquaculture and agriculture-by products as sustainable sources of omega-3 fatty acids in the food industry. *EFood*, 2(5), 209–233. Available from <https://doi.org/10.53365/efood.k/144603>.
- Otero, P., Carpena, M., Garcia-Oliveira, P., Echave, J., Soria-Lopez, A., Garcia-Perez, P., Fraga-Corral, M., Cao, H., Nie, S., Xiao, J., Simal-Gandara, J., & Prieto, M. A. (2021). Seaweed polysaccharides: Emerging extraction technologies, chemical modifications and bioactive properties. *Critical Reviews in Food Science and Nutrition*. Available from <https://doi.org/10.1080/10408398.2021.1969534>.
- Otero, P., Garcia-Oliveira, P., Carpena, M., Barral-Martinez, M., Chamorro, F., Echave, J., Garcia-Perez, P., Cao, H., Xiao, J., Simal-Gandara, J., & Prieto, M. A. (2021). Applications of by-products from the olive oil processing: Revalorization strategies based on target molecules and green extraction technologies. *Trends in Food Science and Technology*, 116, 1084–1104. Available from <https://doi.org/10.1016/j.tifs.2021.09.007>.
- Otero, P., López-Martínez, M. I., & García-risco, M. R. (2019). Application of pressurized liquid extraction (PLE) to obtain bioactive fatty acids and phenols from *Laminaria ochroleuca* collected in Galicia. *Journal of Pharmaceutical and Biomedical Analysis*, 164, 86–92. Available from <https://doi.org/10.1016/j.jpba.2018.09.057>.
- Otero, P., Quintana, S. E., Reglero, G., Fornari, T., & Garcia-Risco, M. (2018). Pressurized liquid extraction (PLE) as an innovative green technology for the effective enrichment of Galician algae extracts with high quality fatty acids and antimicrobial and antioxidant properties. *Marine Drugs*, 16(156). Available from <https://doi.org/10.3390/md16050156>.
- Otero, P., Saha, S. K., Gushin, J. M., Moane, S., Barron, J., & Murray, P. (2017). Identification of optimum fatty acid extraction methods for two different microalgae *Phaeodactylum tricorutum* and *Haematococcus pluvialis* for food and biodiesel applications. *Analytical and Bioanalytical Chemistry*, 409(December), 4659–4667. Available from <https://doi.org/10.1007/s00216-017-0412-9>.
- Otero, P., Vale, C., Boente-Juncal, A., Costas, C., Carmen Louzao, M., & Botana, L. M. (2020). Detection of cyclic imine toxins in dietary supplements of green lipped mussels (*Perna canaliculus*) and in shellfish mytilus chilensis. *Toxins*, 12(10), 1–16. Available from <https://doi.org/10.3390/toxins12100613>.
- Pangestuti, R., & Kim, S. K. (2011). Neuroprotective effects of marine algae. *Marine Drugs*, 9(5), 803–818. Available from <https://doi.org/10.3390/md9050803>.
- Parmar, P., Kumar, R., & Neha, Y. (2023). Microalgae as next generation plant growth additives : Functions, applications, challenges and circular bioeconomy based solutions. *Frontiers in Plant Science*, 14, 1–37. Available from <https://doi.org/10.3389/fpls.2023.1073546>.
- Parniakov, O., Barba, F. J., Grimi, N., Marchal, L., Jubeau, S., Lebovka, N., & Vorobiev, E. (2015). Pulsed electric field and pH assisted selective extraction of intracellular components from microalgae nannochloropsis. *Algal Research*, 8, 128–134. Available from <https://doi.org/10.1016/j.algal.2015.01.014>.
- Pas, M. F. W., Veldkamp, T., Haas, Y. D., Bannink, A., & Ellen, E. D. (2021). Adaptation of livestock to new diets using feed components without competition with human edible protein sources—A review of the possibilities and recommendations. *Animals*, 11, 2293.
- Peng, Y., Hu, J., Yang, B., Lin, X., Zhou, X., Yang, X., & Liu, Y. (2015). Chemical composition of seaweeds. In *Seaweed sustainability* (pp. 79–124). Elsevier Inc.
- Pereira, A.G., Otero, P., Echave, J., Carreira-Casas, A., Chamorro, F., Collazo, N., Jaboui, A., Lourenço-Lopes, C., Simal-Gandara, J., & Prieto, M.A. (2021). Xanthophylls from the sea: Algae as source of bioactive carotenoids. *Marine Drugs*, 19, 188. Available from <https://doi.org/10.3390/md19040188>.
- Pimentel, F. B., Alves, R. C., Harnedy, P. A., FitzGerald, R. J., & Oliveira, M. B. P. P. (2019). Macroalgal-derived protein hydrolysates and bioactive peptides: Enzymatic release and potential health enhancing properties. *Trends in Food Science and Technology*, 93(September), 106–124. Available from <https://doi.org/10.1016/j.tifs.2019.09.006>.
- Qu, W., Ma, H., Pan, Z., Luo, L., Wang, Z., & He, R. (2010). Preparation and antihypertensive activity of peptides from *Porphyra yezoensis*. *Food Chemistry*, 123(1), 14–20. Available from <https://doi.org/10.1016/j.foodchem.2010.03.091>.
- Riccio, G., & Lauritano, C. (2020). Microalgae with immunomodulatory activities. *Marine Drugs*, 18, 2.
- Rocha, D. H. A., Seca, A. M. L., & Pinto, D. C. G. A. (2018). Seaweed secondary metabolites in vitro and in vivo anticancer activity. *Marine Drugs*, 16(11), 1–27. Available from <https://doi.org/10.3390/md16110410>.
- Roque, B. M., Brooke, C. G., Ladau, J., Polley, T., Marsh, L. J., Najafi, N., Pandey, P., Singh, L., Kinley, R., Salwen, J. K., Eloë-Fadrosh, E., Kebreab, E., & Hess, M. (2019). Effect of the macroalgae *Asparagopsis taxiformis* on methane production and rumen microbiome assemblage. *Animal Microbiome*, 1(1), 1–14. Available from <https://doi.org/10.1186/s42523-019-0004-4>.
- Rumin, J., Nicolau, E., Gonçalves de Oliveira, R., Junior, D. O., Fuentes-Grünwald, C., & Picot, L. (2020). Analysis of scientific research driving microalgae market opportunities in Europe. *Marine Drug*, 18, 264. Available from <https://doi.org/10.3390/md18050264>.
- Ryu, M. J., Kim, A. D., Kang, K. A., Chung, H. S., Kim, H. S., Suh, I. S., Chang, W. Y., & Hyun, J. W. (2013). The green algae *Ulva fasciata* Delile extract induces apoptotic cell death in human colon cancer cells. *In Vitro Cellular and Developmental Biology - Animal*, 49(1), 74–81. Available from <https://doi.org/10.1007/s11626-012-9547-3>.
- Saadaoui, I., Rasheed, R., Aguilar, A., Cherif, M., Jabri, H., Al., Sayadi, S., & Manning, S. R. (2021). Microalgal-based feed : promising alternative feedstocks for livestock and poultry production. *Journal of Animal Science and Biotechnology*, 12(76), 1–15.
- Saha, S. K., Ermis, H., & Murray, P. (2020). Marine microalgae for potential lutein production. *Applied Sciences*, 10(18), 6457. Available from <https://doi.org/10.3390/APPI10186457>.

- Sahayaraj, K., Rajesh, S., Asha, A., & Rathi, J. (2012). Marine algae for the cotton pest and disease management. *Recent Trends in Agriculture, Water and Environment Research*, 49–60.
- Sahayaraj, K., & Jeeva, Y. M. (2012). Nymphicidal and ovipositional efficacy of seaweed *Sargassum tenerrimum* (J. Agardh) against *Dysdercus cingulatus* (Fab.) (Pyrrhocoridae). *Chilean Journal of Agricultural Research*, 72(1), 152–156. Available from <https://doi.org/10.4067/s0718-58392012000100024>.
- Sangha, J. S., Hobson, D., Hiltz, D., Critchley, A. T., & Prithiviraj, B. (2010). The use of commercial seaweed extracts as a means to alleviate abiotic stress in land plants: A review. *Algal Resources*, 3, 153–168.
- Schaffelke, B., & Hewitt, C. L. (2008). *Seaweed invasions: A synthesis of ecological, economic and legal imperatives. Impacts of introduced seaweeds* (pp. 77–97). De Gruyter.
- Serebryakova, A., Aires, T., Viard, F., Serrao, E. A., & Engelen, A. H. (2018). Summer shifts of bacterial communities associated with the invasive brown seaweed *Sargassum muticum* are location and tissue dependent. *PLOS ONE*, 13(12), e0206734. Available from <https://doi.org/10.6084/m9.figshare.7246949>. Funding.
- Shao, J. T., Wang, M. Y., & Zheng, L. B. (2013). Antifatigue effect of *Gracilaria eucheumoides* in mice. *Experimental and Therapeutic Medicine*, 6(6), 1512–1516. Available from <https://doi.org/10.3892/etm.2013.1346>.
- Sharifuddin, Y., Chin, Y. X., Lim, P. E., & Phang, S. M. (2015). Potential bioactive compounds from seaweed for diabetes management. *Marine Drugs*, 13(8), 5447–5491. Available from <https://doi.org/10.3390/md13085447>.
- Sharmila, S., Jeyanthi Rebecca, L., & Das, M. P. (2012). Production of biodiesel from *Chaetomorpha antennina* and *Gracilaria corticata*. *Journal of Chemical and Pharmaceutical Research*, 4(11), 4870–4874.
- Silva, L. N., Leite, M. G. A., Maria, P., & Gonçalves, B. (2019). Development of hair care formulations containing *Spirulina platensis* and *Ascophyllum nodosum* extracts. *International Journal of Phytocosmetics*, 6(13). Available from <https://doi.org/10.15171/ijpni.2019.13>.
- Silva, M., Seijas, P., & Otero, P. (2021). Exploitation of marine molecules to manage alzheimer's disease. *Marine Drugs*, 19(7), 1–26. Available from <https://doi.org/10.3390/md19070373>.
- Simas-Rodrigues, C., Villela, H. D. M., Martins, A. P., Marques, L. G., Colepicolo, P., & Tonon, A. P. (2015). Microalgae for economic applications: Advantages and perspectives for bioethanol. *Journal of Experimental Botany*, 66(14), 4097–4108. Available from <https://doi.org/10.1093/jxb/erv130>.
- Smale, D. A., & Wernberg, T. (2013). Extreme climatic event drives range contraction of a habitat-forming species. *Proceedings of the Royal Society B: Biological Sciences*, 280(1754). Available from <https://doi.org/10.1098/rspb.2012.2829>.
- Stoyneva-gärtner, M., Uzunov, B., & Gärtner, G. (2022). Aeroterrestrial and extremophilic microalgae as promising sources for lipids and lipid nanoparticles in dermal cosmetics. *Cosmetics*, 9(11). Available from <https://doi.org/10.3390/cosmetics9010011>.
- Suganya, T., Kasirajan, R., & Renganathan, S. (2014). Ultrasound-enhanced rapid in situ transesterification of marine macroalgae *Enteromorpha compressa* for biodiesel production. *Bioresource Technology*, 156, 283–290. Available from <https://doi.org/10.1016/j.biortech.2014.01.050>.
- Tamilarasan, K., Kavitha, S., Rajesh Banu, J., Arulazhagan, P., & Yeom, I. T. (2017). Energy-efficient methane production from macroalgal biomass through chemo disperser liquefaction. *Bioresource Technology*, 228, 156–163. Available from <https://doi.org/10.1016/j.biortech.2016.12.102>.
- Tan, I. S., & Lee, K. T. (2014). Enzymatic hydrolysis and fermentation of seaweed solid wastes for bioethanol production: An optimization study. *Energy*, 78, 53–62. Available from <https://doi.org/10.1016/j.energy.2014.04.080>.
- Torres, A., Padrino, S., Brito, A., & Díaz, L. (2021). Biogas production from anaerobic digestion of solid microalgae residues generated on different processes of microalgae-to-biofuel production. *Biomass Conversion and Biorefinery*, 4659–4672. Available from <https://doi.org/10.1007/s13399-021-01898-9>.
- Torres, M. D., Flórez-Fernández, N., & Domínguez, H. (2019). Integral utilization of red seaweed for bioactive production. *Marine Drugs*, 17(6). Available from <https://doi.org/10.3390/md17060314>.
- Tuhy, L., Chowanska, J., & Chojnacka, K. (2013). Seaweed extracts as biostimulants of plant growth: Review. *Chemik*, 67(7), 639–641.
- Ustyuzhanina, N. E., Bilan, M. I., Gerbst, A. G., Ushakova, N. A., Tsvetkova, E. A., Dmitrenok, A. S., Usov, A. I., & Nifantiev, N. E. (2016). Anticoagulant and antithrombotic activities of modified xylofucan sulfate from the brown alga *Punctaria plantaginea*. *Carbohydrate Polymers*, 136, 826–833. Available from <https://doi.org/10.1016/j.carbpol.2015.09.102>.
- Uzair, B., Liaqat, A., Iqbal, H., Menaa, B., & Razzaq, A. (2020). Green and cost-effective synthesis of metallic nanoparticles by algae: Safe methods for translational medicine. *Bioengineering*, 7, 129.
- Vaz, B., da, S., Moreira, J. B., Morais, M. G. D., & Costa, J. A. V. (2016). Microalgae as a new source of bioactive compounds in food supplements. *Current Opinion in Food Science*, 7, 73–77. Available from <https://doi.org/10.1016/j.cofs.2015.12.006>.
- Venugopal, V. (2019). Sulfated and non-sulfated polysaccharides from seaweeds and their uses: An overview. *EC Nutrition*, 14.2, 126–141.
- Vergara-Fernández, A., Vargas, G., Alarcón, N., & Velasco, A. (2008). Evaluation of marine algae as a source of biogas in a two-stage anaerobic reactor system. *Biomass and Bioenergy*, 32(4), 338–344. Available from <https://doi.org/10.1016/j.biombioe.2007.10.005>.
- Vieira, M. V., Pastrana, L. M., & Fuciños, P. (2020). Microalgae encapsulation systems for food, pharmaceutical and cosmetics applications. *Marine Drugs*, 18, 644. Available from <https://doi.org/10.3390/md18120644>.
- Wang, J., Jin, W., Hou, Y., Niu, X., Zhang, H., & Zhang, Q. (2013). Chemical composition and moisture-absorption/retention ability of polysaccharides extracted from five algae. *International Journal of Biological Macromolecules*, 57, 26–29. Available from <https://doi.org/10.1016/j.ijbiomac.2013.03.001>.
- Wang, X., Li, C., Chen, M., & Wang, J. (2021). Microwave-assisted pyrolysis of seaweed biomass for aromatics-containing bio-oil production. E3S Web of Conferences (ICEMEE 2021), 261, 02045. Available from <https://doi.org/10.1051/e3sconf/202126102045>.

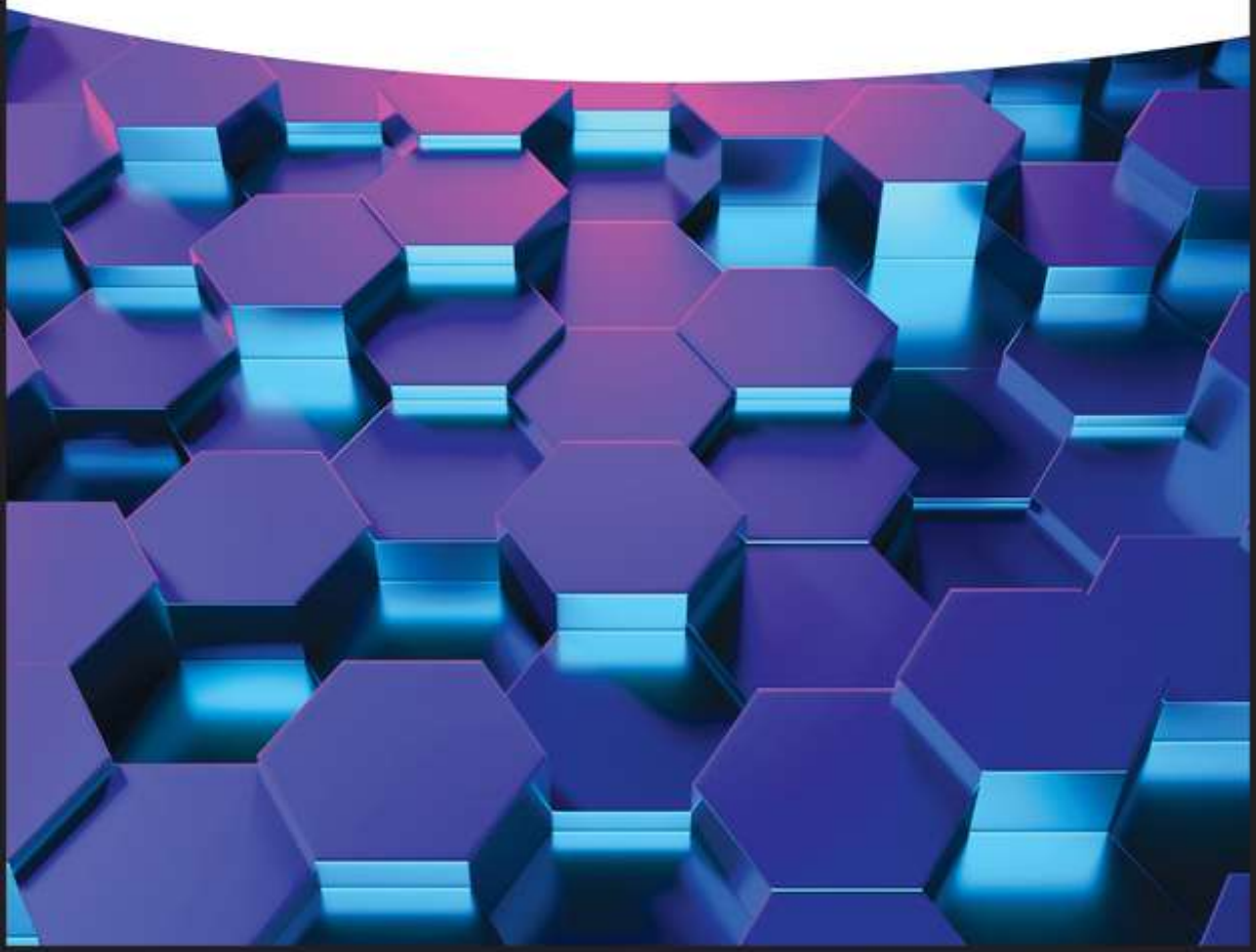
- Xu, X., Kim, J. Y., Oh, Y. R., & Park, J. M. (2014). Production of biodiesel from carbon sources of macroalgae, *Laminaria japonica*. *Bioresource Technology*, 169, 455–461. Available from <https://doi.org/10.1016/j.biortech.2014.07.015>.
- Yang, Y., Ge, S., Pan, Y., Qian, W., Wang, S., Zhang, J., & Zhuang, L. L. (2023). Screening of microalgae species and evaluation of algal-lipid stimulation strategies for biodiesel production. *Science of the Total Environment*, 857(August 2022), 159281. Available from <https://doi.org/10.1016/j.scitotenv.2022.159281>.
- Yarnpakdee, S., Benjakul, S., & Senphan, T. (2019). Antioxidant activity of the extracts from freshwater macroalgae (*Cladophora glomerata*) grown in Northern Thailand and its preventive effect against lipid oxidation of refrigerated eastern little tuna slice. *Turkish Journal of Fisheries and Aquatic Sciences*, 19(3), 209–219. Available from [https://doi.org/10.4194/1303-2712-v19\\_03\\_04](https://doi.org/10.4194/1303-2712-v19_03_04).
- Yin, Y., Hu, J., & Wang, J. (2019). Fermentative hydrogen production from macroalgae *Laminaria japonica* pretreated by microwave irradiation. *International Journal of Hydrogen Energy*, 44(21), 10398–10406. Available from <https://doi.org/10.1016/j.ijhydene.2019.03.034>.
- Yoza, B., & Masutani, E. (2013). The analysis of macroalgae biomass found around Hawaii for bioethanol production. *Environmental Technology*, 34(13–14), 1859–186756. Available from <https://shodhganga.inflibnet.ac.in/jspui/handle/10603/7385>.
- Zozaya-valdés, E., Roth-schulze, A. J., & Thomas, T. (2016). Effects of temperature stress and aquarium conditions on the red macroalga *Delisea pulchra* and its associated microbial community. *Frontiers in Microbiology*, 7(February), 1–10. Available from <https://doi.org/10.3389/fmicb.2016.00161>.

WILEY-VCH

Edited by Dakeshwar Kumar Verma and  
Jeenat Aslam

# Organometallic Compounds

Synthesis, Reactions, and Applications





## 3

## Classification of Organometallic Compounds

Mukesh K. Tyagi<sup>1</sup>, Gokul R. Nishad<sup>2</sup>, Dakeshwar Kumar Verma<sup>2</sup>, Lei Guo<sup>3</sup>, and Elyor Berdimurodov<sup>4</sup>

<sup>1</sup>Hemchand Yadav University, Atal Bihari Vajpai, Govt. College, Department of Chemistry, Pandatarai, Kabirdham 491559, India

<sup>2</sup>Hemchand Yadav University, Government Digvijay Autonomous Postgraduate College, Department of Chemistry, Rajnandgaon 491441, India

<sup>3</sup>Tongren University, School of Materials and Chemical Engineering, Tongren 554300, China

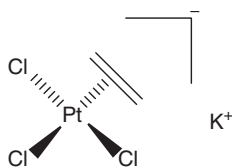
<sup>4</sup>National University of Uzbekistan, Faculty of Chemistry, Tashkent 100034, Uzbekistan

### 3.1 Introduction

Organometallic compounds are compounds in which at least one bond is found between metal and carbon, or in other words, those organic compounds which have direct linkage with one or more metal atoms of carbon. Alkaline metals and alkaline earth metals mediated organometallic compounds are common and very useful. Various metalloids such as selenium, silicon, and boron have been synthesized from organometallic compounds with various classes of organic compounds, but the most important organometallic compound has been synthesized from transition metals. Transition metal-mediated synthesized organometallic compounds are widely used and have numerous applications. Their applications include synthesis of catalysts, drugs, paints, metal organic framework (MOF), polymers, composites, adsorbents, supercapacitors, electrode materials, etc. Similarly, lanthanides and actinides metal-based organometallic materials have also come into existence and play a very vital role in different fields.

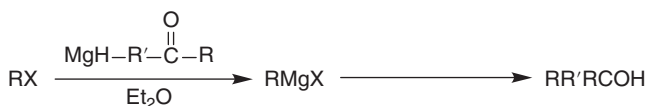
Overall, it can be said that organometallic mainly deals with the transformations of organic compounds by reacting metals of different groups like transition metals, s-block and p-block elements, lanthanides and actinides series. Organometallic chemistry in inorganic chemistry (EVM) is a part of coordination chemistry, which specifically studies M—C bonds, whereas coordination chemistry studies both metal elements and M—C bonds.

The discovery of Zeise's salts in the nineteenth century brought a revolution, which was mainly complex and containing platinum. The salt, which was discovered in 1827, is represented by  $[\text{PtCl}_3(\eta_2\text{-C}_2\text{H}_4)]$  [1] (Scheme 3.1).



Scheme 3.1

Similarly, in the twentieth century, French scientist Victor Grignard gave a new direction in the field of chemistry by discovering Grignard reagents in the field. They synthesized  $\text{RMgX}$  by reacting magnesium by oxidative addition of  $\text{RX}$ , whose key function was to alkylate carbonyl derivatives (Scheme 3.2) [2].



Where X = halogens (Cl, Br, I)

R = Alkyl, Aryl Compounds

Scheme 3.2

## 3.2 Classification of Organometallic Compound

### 3.2.1 Sigma-Bonded Organometallic Compound

A sigma-bonded organometallic compound is a two-centered, two-electron ( $2c-2e$ ) bond, in which the organic compound is bonded to the metal by a common covalent sigma bond. In sigma-bonded organometallic compounds, mainly metals having low electronegativity, form sigma bonds with nonmetallic elements, such as carbon atoms. Transition elements, alkali earth metals, and some main group elements form sigma-bonded organometallic compounds and are generally covalent in nature [3, 4].

For example,  $\text{W}(\text{CH}_3)_6$ ,  $\text{Mn}(\text{CO})_5$ ,  $\text{Ta}(\text{CH}_3)_5$ ,  $\text{Ph}(\text{CH}_3)_4$ ,  $\text{Al}(\text{CH}_3)_3$ ,  $\text{Si}(\text{CH}_3)_4$ ,  $\text{B}(\text{CH}_3)_3$ .

Figure 3.1 shows the classification of organometallic compounds.

Also, shapes of organometallic compounds depend on the hybridization of central metal ions.

Hybridization	Shape	Examples
$sp$	Linear	$\text{Be}(\text{CH}_3)_2$
$sp^2$	Triangular planner	$\text{Al}(\text{CH}_3)_3$ , $\text{B}(\text{CH}_3)_3$
$sp^3$	Tetrahedral	$\text{Pb}(\text{CH}_3)_4$ , $\text{Si}(\text{CH}_3)_4$
$sp^3d$	Trigonal bipyramidal	$\text{Ta}(\text{CH}_3)_5$
$sp^3d^2$	Octahedral	$\text{W}(\text{CH}_3)_6$ , $\text{Mn}(\text{CO})_5$

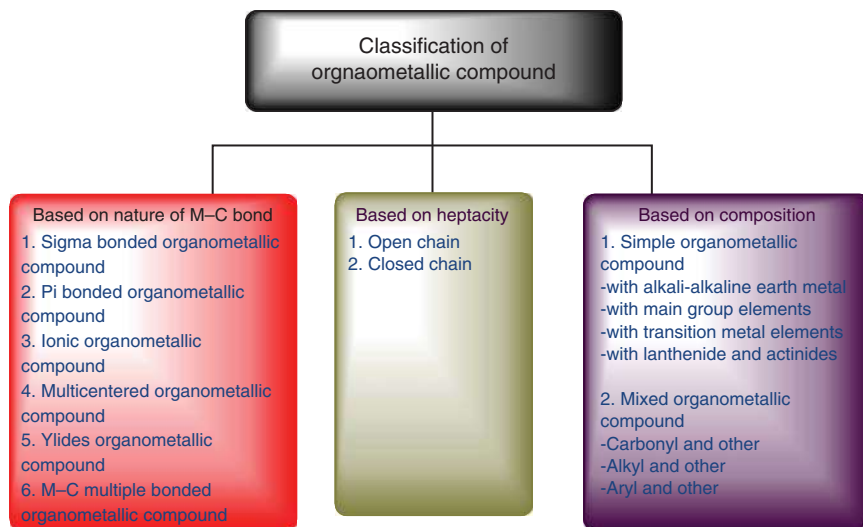
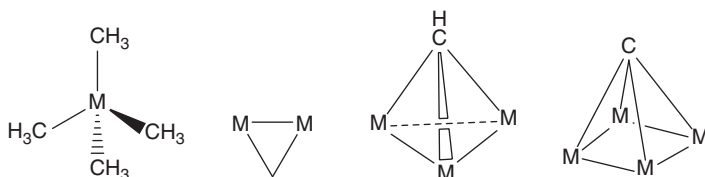


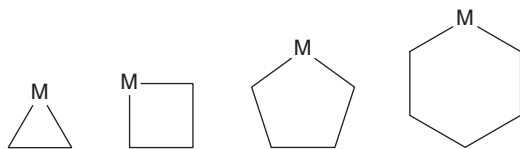
**Figure 3.1** Classification of organometallic compounds.

Transition metals and carbon-headedness are present in the coordinately sigma-bonded organometallic compound in the form of terminal metal-allyl complexes such as  $[\text{W}(\text{CH}_3)_6]$ . Similarly, tetrahedral compounds also form complexes in which they form various bridging complexes as shown in Scheme 3.3.



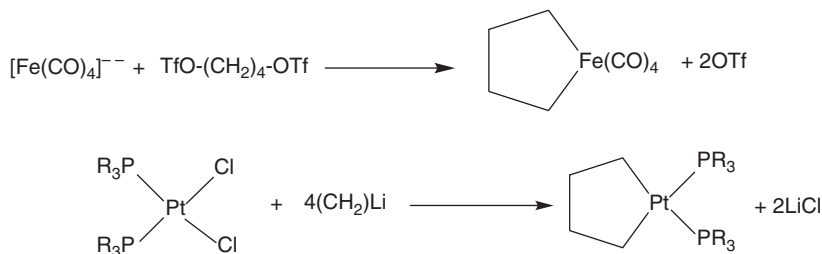
**Scheme 3.3**

**Metallocycles:** In this regard, metallocycles are a class of organometallic compound in which a metal ion is the ring atom (Scheme 3.4).



**Scheme 3.4**

These metallocycle organometallic compounds can be synthesized as given in Scheme 3.5.



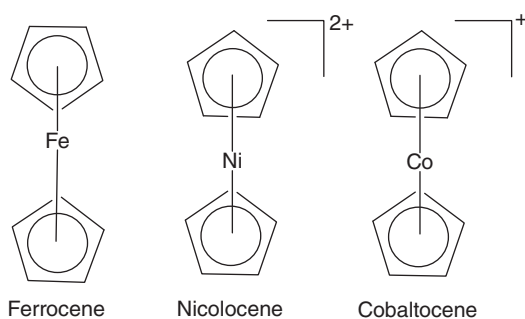
Scheme 3.5

Some common examples of bonded organometallic compounds are:

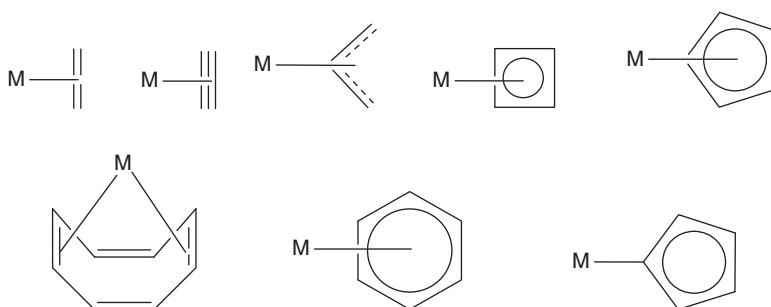
- i. *Group I and II compound*: These are covalent bonded compounds and mostly exist as tetrameric units. Similarly, berkelium and magnesium also exist in various polymeric forms.
- ii. *Grignard reagents*: It consist of magnesium and halogen (primarily Cl, Br, and I) and can covalent most aldehydes and ketones to alcohol. The general structure of Grignard reagents is  $\text{RMgX}$ , in which R = alkyl or aryl and X = Cl, Br, and I.
- iii. *Trimethyl aluminum and Tetra alkyl tri organometallic compound*:  $\text{Al}_2(\text{CH}_3)_6$  (trimetyhyl aluminum) exist in the dimer form in which alkyl group linked as bridge compound between the metals.  $\text{Al}_2(\text{CH}_3)_6$  formed 2-Al and 1 atom multicenter bond.  
Similarly, tetramethyl tin  $\text{Sn}(\text{CH}_3)_4$ , tetra ethyl tin,  $\text{Sn}(\text{Et})_4$ , and tetra methyl arsine ( $\text{As}(\text{CH}_3)_4$ ) are important classes of organometallic compounds.
- iv. *Diethylzinc ( $\text{Zn}(\text{C}_2\text{H}_5)_2$ )*: This zinc mediate compound is provide nucleophile form organic reaction.

### 3.2.2 $\pi$ -Bonded Organometallic Compounds

Generally, unsaturated compounds such as alkenes, alkynes, and other carbon-containing multiple bonds are electron-rich. When a metal with a vacant orbital or high oxidation state approaching the electron rich multiple bonded moiety, then they form a stable bond by approaches the electron rich center. Metal cation when it interacts with multiple carbon centers. It gets attached to all the carbon atoms linked by multiple bonds. Since all d-block transition elements have vacant d-orbital's, they readily interact with electron-rich  $\pi$  orbital's to form stable  $d\pi$ - $p\pi$  bonds. Unlike other metals such as alkali metals and alkali earth metals, the main group element lacks a vacant d-orbital, due to which it rarely forms stable bonds with unsaturated compounds. In this context, the credit for the discovery of the most stable and complex ferrocene goes to the scientist who discovered it in 1951. In ferrocene, there is a stable bond between iron and cyclopentadiene ions, and in this the center metal ion is equally attached to all the five carbon atoms through their nuclei, which are mainly covalent in nature [5, 6] (Scheme 3.6).

**Scheme 3.6**

Similarly, after a few decades, sandwich compounds such as nicolocene and cobaltocene were also synthesized (Scheme 3.6). A classic example of a pi-bonded organometallic compound is usually given as a metal with multiple covalent complexes (Scheme 3.7).

**Scheme 3.7**

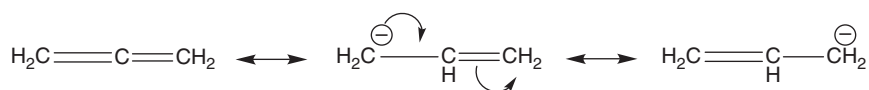
### 3.2.3 Ionic Bonded Organometallic Compounds

Bond formation in ionic bonded organometallic complexes occurs mainly by electrostatic bond formation between a metal cation and carbon having an electronegativity value lower than that of carbon. Earth metal cations are highly electropositive in character, with the shared electron being more localized toward the carbon atom. As a result, the metal ion becomes slightly positively charged and the carbon negatively charged. The alkali metals, alkaline earth metals, lanthanides, and actinide metals are slightly less electronegative and mostly form ionic bonds [7].

*Exceptions:* alkali and alkali earth metals, such as lithium, beryllium, and magnesium, which are relatively smaller in size and higher electronegative, resulting in mostly covalent bonds and being less reactive than other related organometallic compounds [8].

*Examples:* Sodium cyclopentadienide ( $C_5H_5^-Na^+$ ), phenyl sodium ( $Na^+C_6H_5$ ) and methyl potassium ( $CH_3^-K^+$ ) are well-known examples of organometallic compounds in this class. Their organic compounds are colorless, soluble in polar solvents and solids such as salts, and very reactive toward water and air [8].

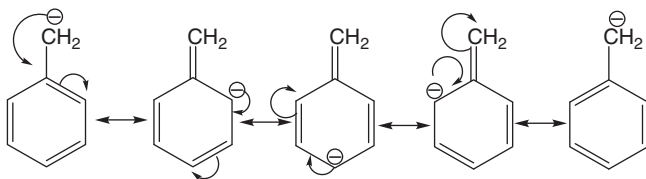
Generally the stability and reactivity of this class of compound depend on the organic anion. Extended conjugated alkenes containing organometallic compounds are more stable as compared to simple alkenes because in previous case, delocalization has taken place from one and two other ends, hence reactivity will be decreased (Scheme 3.8).



**Scheme 3.8**

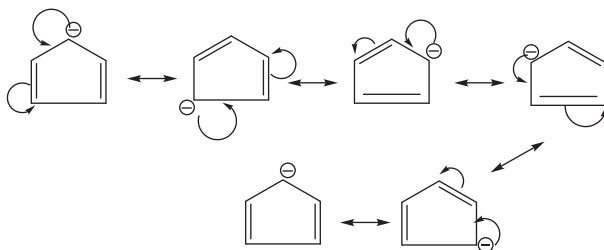
Because  $sp$  hybridized carbon atoms easily form carbanion due to the 50%–80%  $sp$  character of the carbon bond, electronegativity of alkyne carbon has been slightly increased and can easily remove attached proton by attracting shared paired electrons.

Similarly,  $\text{C}_6\text{H}_5\text{Na}$  and  $\text{C}_5\text{H}_5\text{CH}_2\text{Na}$  are both states of organometallic compounds. Compared to both,  $\text{C}_5\text{H}_5\text{CH}_2\text{Na}$  is more stable because the distributed negative charge is on all carbon atoms in the benzene ring and the nucleophilicity of the  $\text{CH}_2$  group is decreased. While in the case of  $\text{C}_6\text{H}_5^- \text{Na}^+$  the negatively charged delocalized are the  $sp^2$  hybridized carbon atoms. These are sigma type and hence unstable. Overall, due to the above effect,  $\text{C}_6\text{H}_5\text{Na}$  is more reactive toward electrophiles as a compound to  $\text{C}_5\text{H}_5\text{CH}^- \text{Na}^+$  (Scheme 3.9).



**Scheme 3.9**

Another example includes the nucleophilic comparison between  $\text{C}_5\text{H}_5^- \text{M}^+$  and  $\text{C}_5\text{H}_{11}^- \text{M}^+$ . In this case,  $\text{C}_5\text{H}_5^-$  is more stable as it follows the Huckel rule ( $4n+2\pi$ )  $e^-$  system and has a total  $6\pi$  electrons, whereas  $\text{C}_6\text{H}_4^-$  doesn't follow the Huckel rule and the negative charge localized only on one carbon atom (Scheme 3.10). Delocalization on  $\text{C}_6\text{H}_5^-$  ion:

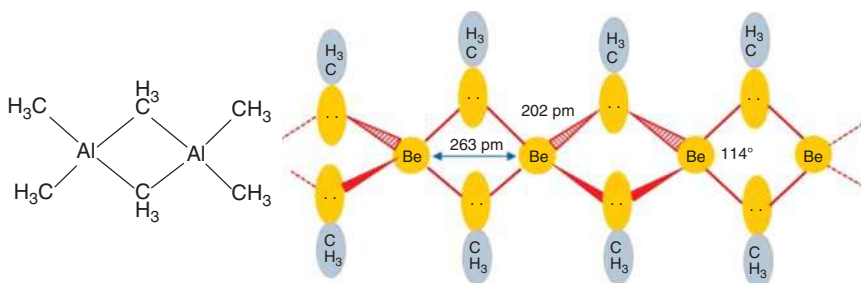


**Scheme 3.10**

### 3.2.4 Multicentered Bonded Organometallic Compounds

Elements such as Al, B, Mg, Be, and Li exhibited a higher tendency to make multicentered bonds with alkyls and aryl groups. In this case, alkyls and aryls acted as bridges between two HOMO-centered or hetero-centered metal ions. There, bridge compounds can be considered as intermediates between sigma-bonded and ionic organometallic compounds [9, 10].

Well-known examples of this class are dimeric trimethyl aluminum ( $\text{Al}_2(\text{CH}_3)_6$ ),  $[\text{Be}(\text{CH}_3)_2]_n$ , polymeric dimethyl-beryllium, dimeric triphenyl aluminum  $[\text{Al}_2(\text{C}_6\text{H}_5)_6]$ , etc. (Scheme 3.11).

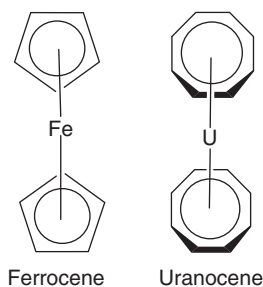


**Scheme 3.11**

5. Ylide: In this case, multiple bond, especially double bonded organometallic compounds, were extensively studied. Here the center metal ions bond with the carbon atom of the ligand. Transitional elements, such as Fe, W, Re, Mo, and Cr, primarily form double bonds with carbon atoms of ligands.

#### 3.2.4.1 Based on Heptacity ( $\eta 1$ to $\eta 8$ ):

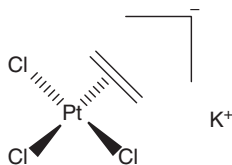
In organometallic chemistry, heptacity can be considered as the coordination of an unsaturated or multiple bond containing ligand (aliphatic or aryl) through a continuous and uninterrupted chain of atoms. Usually word heptacity has been described from Greece letter  $\eta$  form instand ita 4 demonstrated the coordination though, four contagious carbon atoms. In addition here are the examples of heptacity [11] (Scheme 3.12).



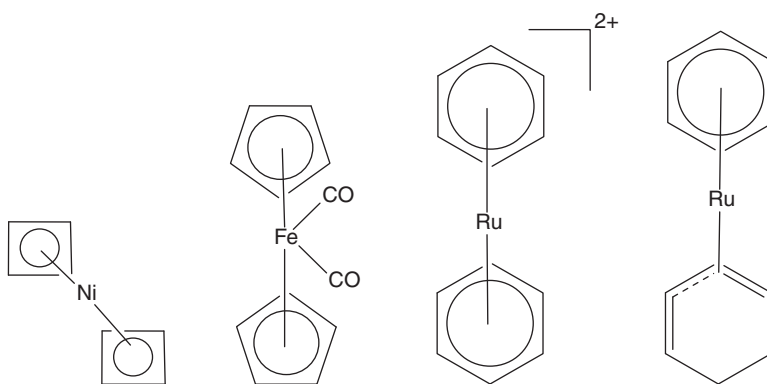
**Scheme 3.12**

Various and noteworthy contribution of hapticity in various forms:

- Side wise bonding of ligands containing multiple bond: Example – Zeise's Salt (Scheme 3.13)
- 18-electron rule applicable compound with hapticity (Scheme 3.14).



**Scheme 3.13**



**Scheme 3.14**

Additionally, Table 3.1 demonstrated the electron donation by unsaturated compound various hapticity.

### 3.3 Grignard Reagent (G.R.)

#### 3.3.1 Physical Properties

- Grignard reagents are colorless and nonvolatile crystalline solids.
- Grignard reagents are strong nucleophile.
- Grignard reagent should be kept in a dry environment (in dry ether). If moisture or water comes into contact with Grignard, Grignard is destroyed [12].

#### 3.3.2 Chemical Properties

##### 3.3.2.1 Alkanes

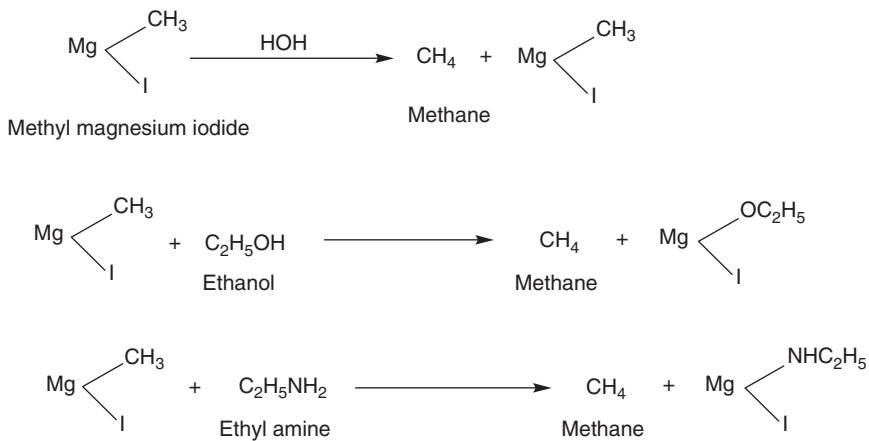
Alkanes can be obtained when Grignard reagent treated with water, alcohols and amines (Scheme 3.15) [13].



**Table 3.1** Electron donation by unsaturated compound various heptacity.

S. No.	Name and structure of ligands	Structure of compound	Number of electron which contributed
1	Allyl ligands: $\eta^1, \eta^3$		1 and 3
2	Alkene/Ethane: $\eta^2, \eta^2, \eta^4$		2, 2, and 4
3	Cyclopentadienyl: $\eta^1, \eta^3, \eta^5$		1, 3, and 5
4	Cyclohexane: $\eta^1, \eta^2, \eta^3, \eta^4, \eta^6$		1, 2, 3, 4, and 5
5	Polycyclic compound: $\eta^7, \eta^8$		7 and 8

Source: Adapted from Soto and Salcedo [11].

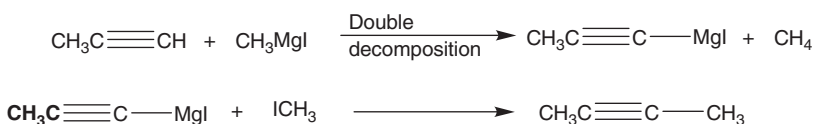
**Scheme 3.15**

**3.3.2.2 Alkenes**

These are obtained by the reaction of unsaturated halides on the Grignard reagent (Scheme 3.16).

**Scheme 3.16****3.3.2.3 Alkynes**

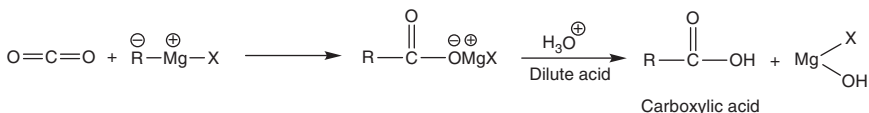
Grignard reagents react with unsaturated compound which possess active hydrogen (Scheme 3.17).

**Scheme 3.17****3.3.2.4 Ethers**

Higher ethers are prepared by the action of the Grignard reagent on a monochloroether (Scheme 3.18).

**Scheme 3.18****3.3.2.5 Reaction with carbon dioxide**

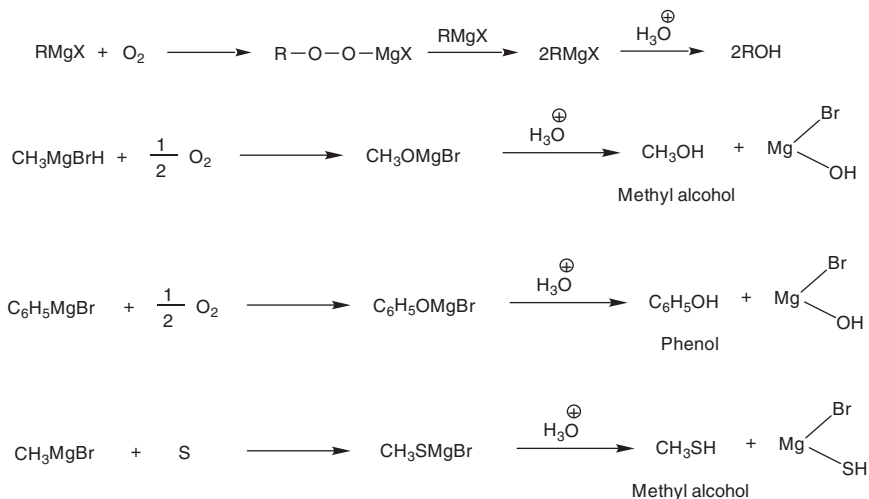
Grignard reagents when treated with solid carbon dioxide form nucleophilic addition products, which on treatment with dilute acid yield a monocarboxylic acid (Scheme 3.19) [14].

**Scheme 3.19****3.3.2.6 Insertion Reaction**

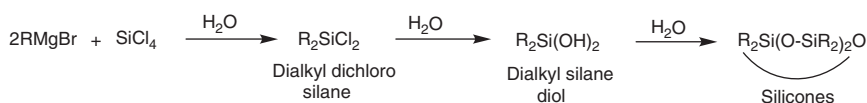
Oxygen, sulfur, and halogen react with Grignard reagents to form alcohols, thiols, and organic halides, respectively (Scheme 3.20) [14].

**3.3.2.7 Synthesis of Silicones**

Grignard reagent and silicone tetrachloride combine to form silicones, which are long-chain anhydrides. They are employed in the production of electrical insulators, silicone rubber, and premium lubricants (Scheme 3.21).



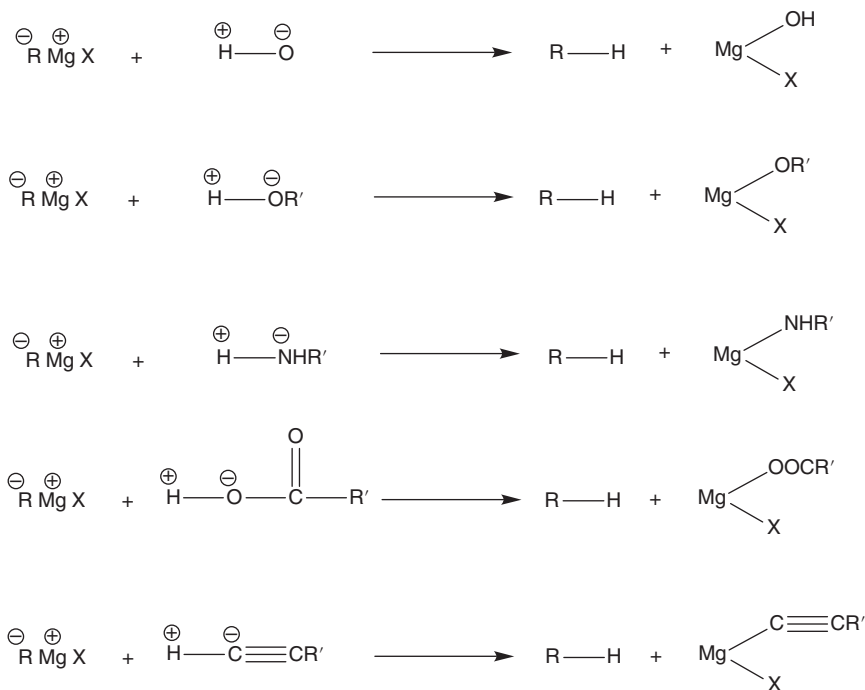
Scheme 3.20



Scheme 3.21

## 3.3.2.8 Nucleophilic Substitution

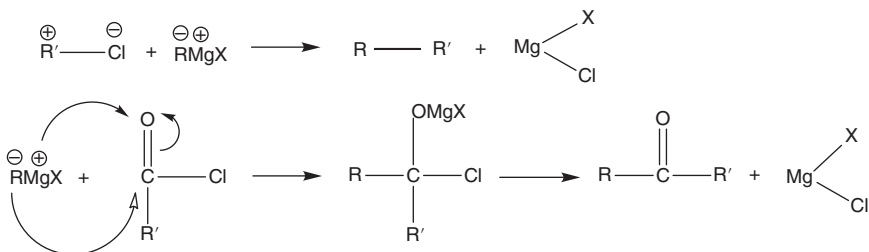
## 3.3.2.8.1 Grignard Reagent React with Active Hydrogen (Scheme 3.22) [15].



Scheme 3.22

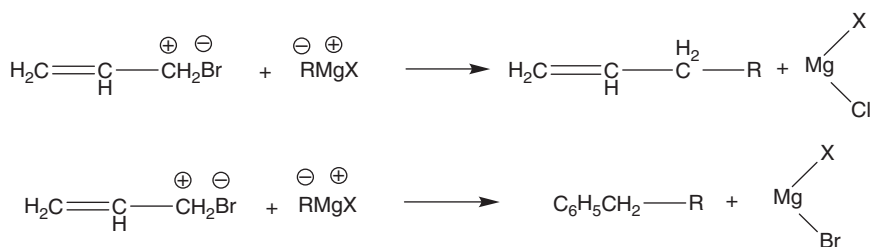
## 3.3.2.8.2 Grignard Reagents React with Halogen

(a) With alkyl and acyl halides- Grignard reagents reacts with alkyl halide to form alkanes (Scheme 3.23).



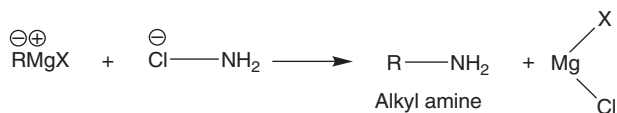
Scheme 3.23

(b) Grignard reagents when treated with allyl bromide and benzyl bromide, they produce 1-alkene and higher alkyl benzene (Scheme 3.24).



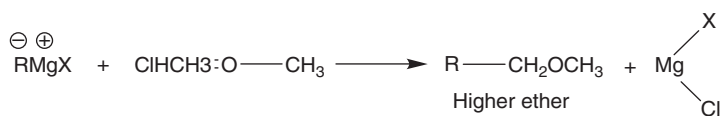
Scheme 3.24

(c) Grignard reagents when treated with chloramine it gives primary amines (Scheme 3.25):



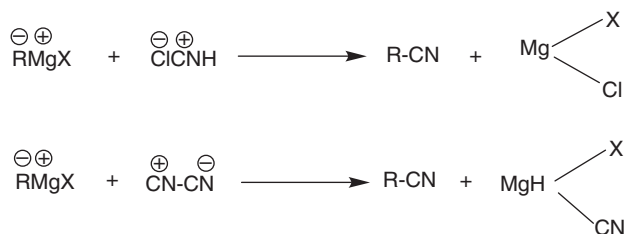
Scheme 3.25

(d) Grignard reagents on reaction with monochlorodimethyl ether gives higher ethers (Scheme 3.26).



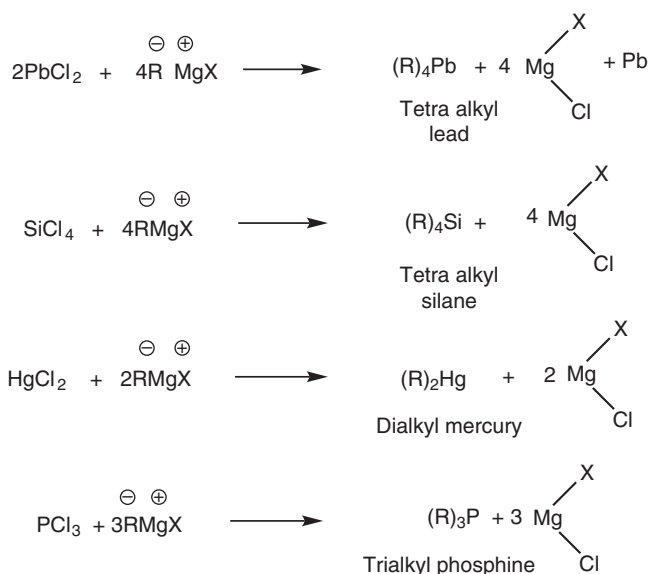
Scheme 3.26

(e) Alkyl cyanides are obtained with cyanogenchloride or even cyanogens (Scheme 3.27)



Scheme 3.27

(f) *With halide of certain metals and nonmetal:* Organometallic and organo non-metallic compound are formed (Scheme 3.28).



Scheme 3.28

## 3.4 Organozinc Compounds

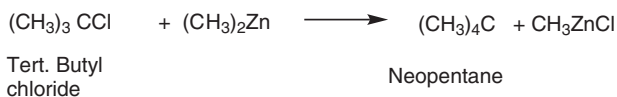
### 3.4.1 Physical Properties

Dialkyl zincs are colorless volatile liquids with unpleasant smells and low boiling points [(CH<sub>3</sub>)<sub>2</sub>Zn, 319 K; (C<sub>2</sub>H<sub>5</sub>)<sub>2</sub>Zn, 391 K]. They are spontaneously inflammable in the air [16].

### 3.4.2 Chemical Properties

Dialkyl zinc has been used in various synthetic reactions.

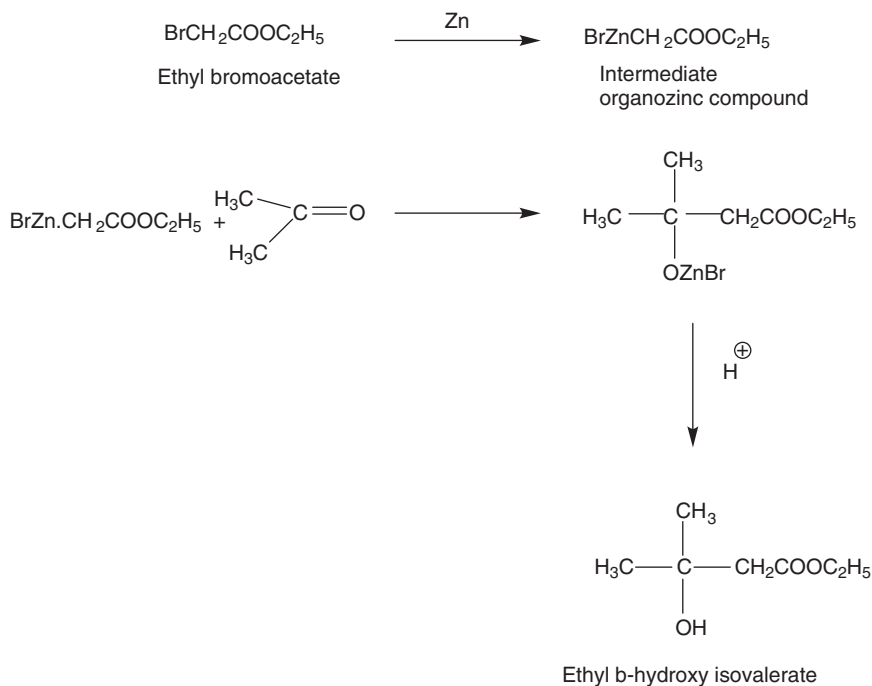
- (i) *Preparation of hydrocarbon containing quaternary carbon atom:* Dialkyl zinc reacts with tertiary butyl chloride to give neopentane (Scheme 3.29) [16].

**Scheme 3.29**

(ii) *Preparation of ketones:* When dialkyl zinc treated with acyl chloride it converts into ketones (Scheme 3.30) [17].

**Scheme 3.30**

(iii) *Reformatsky Reaction:* In this reaction between an  $\alpha$ -bromo ester and a carbonyl compound (aldehyde, ketone, or ester) in the presence of zinc using benzene as the solvent to yield  $\beta$ -hydroxy ester. Zinc is added to the mixture of bromoacid ester and the carbonyl compound in benzene and the mixture is then warmed. The  $\alpha$ -bromo ester and zinc react in benzene to yield an intermediate organozinc compound, which then adds to the carbonyl group of the aldehyde and ketone (Scheme 3.31) [18].

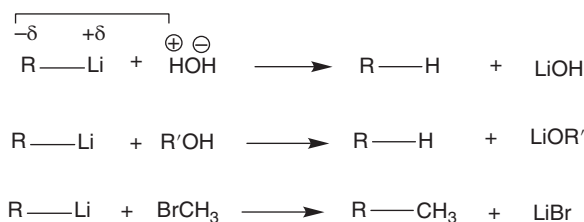
**Scheme 3.31**

## 3.5 Organolithium Compounds

Alkyl lithium is either liquid or low-melting solids. They are insoluble in water but soluble in nonpolar hydrocarbons as solvents. Organolithium compounds resemble Grignard reagents, but they are more reactive. The greater reactivity of organolithium compounds over Grignard reagents is due to greater ionic character of the C—Li bond in comparison to the C—Mg bond [19].

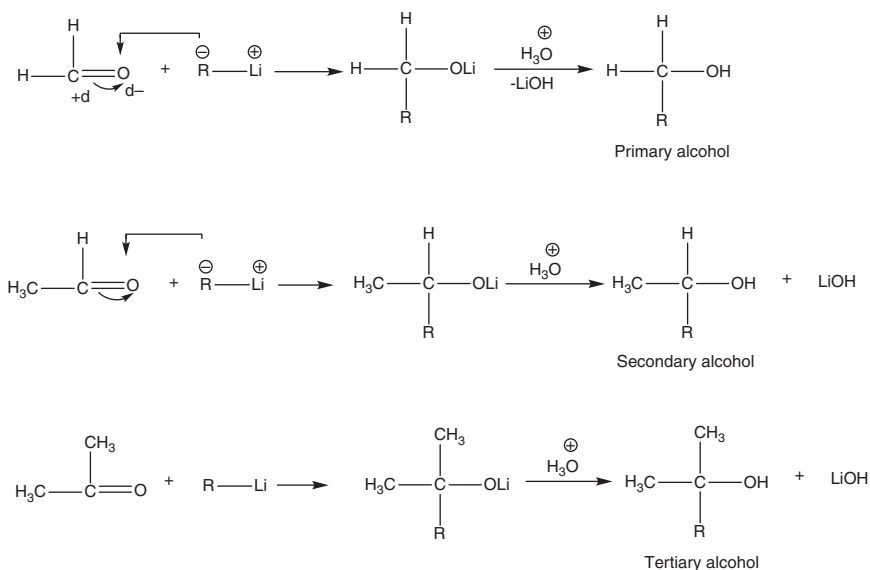
### 3.5.1 Reaction Resembling Grignard Reagents

(i) *Preparation of hydrocarbons:* Organolithium reagents react with active hydrogen-containing compounds (Scheme 3.32) [19].



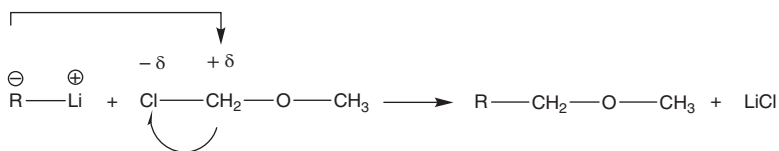
**Scheme 3.32**

(ii) *Preparation of alcohols:* Formaldehyde gives primary alcohol; other aldehydes give secondary alcohol while ketones give tertiary alcohol (Scheme 3.33).



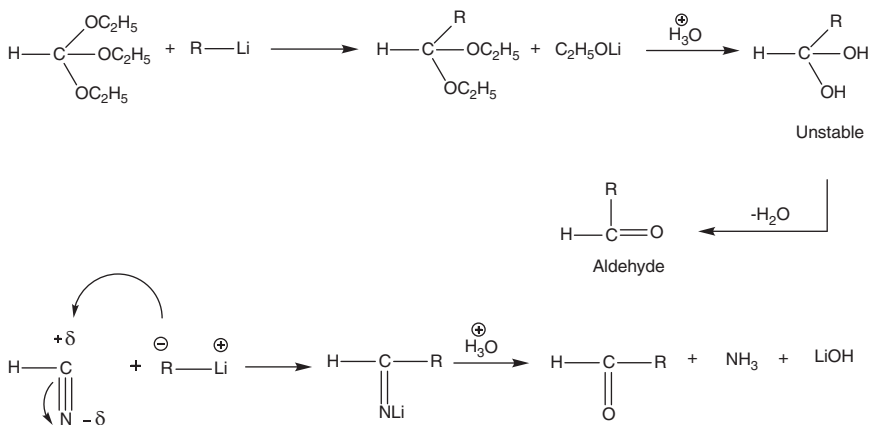
**Scheme 3.33**

(iii) *Preparation of higher ethers:* When treated with lower ether chloride it gives higher ether (Scheme 3.34).



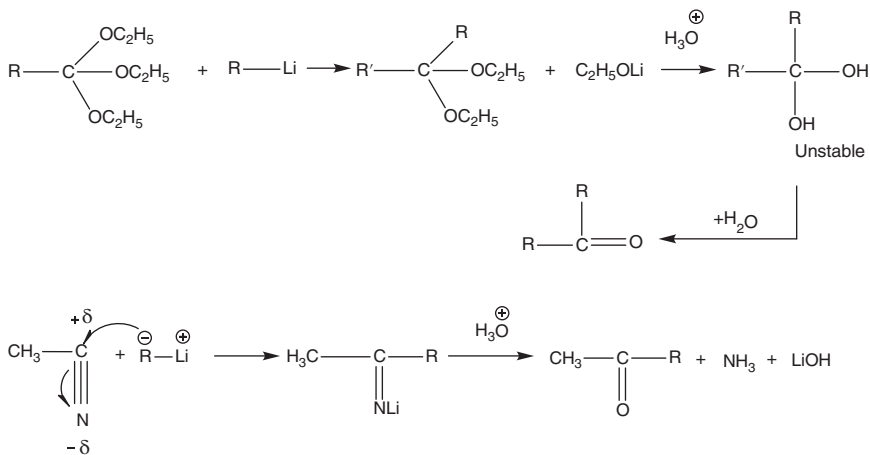
**Scheme 3.34**

(iv) *Preparation of aldehydes:* Organolithium compounds on reaction with ethyl orthoformate or hydrogen cyanide give aldehyde (Scheme 3.35).



**Scheme 3.35**

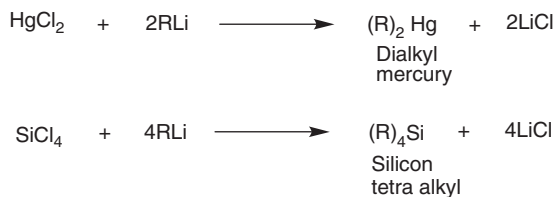
(v) *Preparation of ketones:* Ethyl ortho ester and alkyl cyanide give ketone (Scheme 3.36) [20].



**Scheme 3.36**



(vi) *Preparation of other metallic compounds:* When treated with other metal halides it gives organometallic compounds (Scheme 3.37).



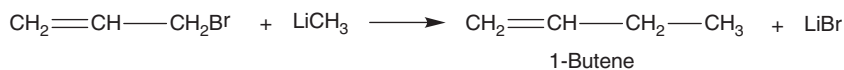
**Scheme 3.37**

(vii) *Preparations of amines:* It gives alkyl amines when react with amine chloride (Scheme 3.38).



**Scheme 3.38**

(viii) *Preparations of higher alkenes from allyl halide:* When it reacts with allyl bromide, it gives higher alkenes (Scheme 3.39).



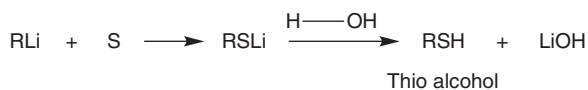
**Scheme 3.39**

(ix) *Preparations of alkyl cyanides:* When they react with halide cyanides (Scheme 3.40).



**Scheme 3.40**

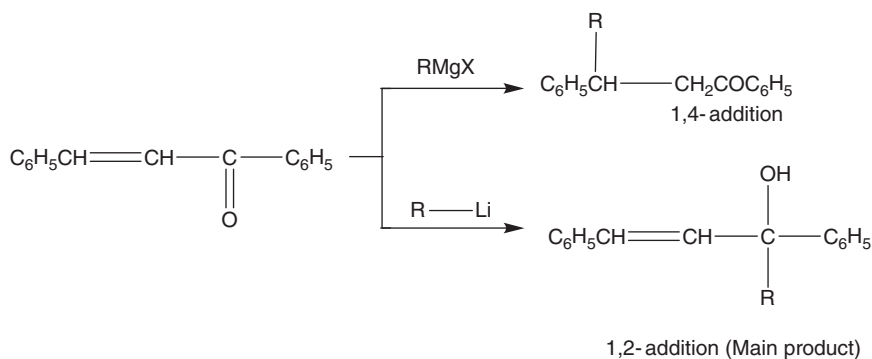
(x) *Preparations of thio-alcohols:* First alkyl lithium reacts with sulfur then the formed product reacts with water to give thio-alcohols (Scheme 3.41).



**Scheme 3.41**

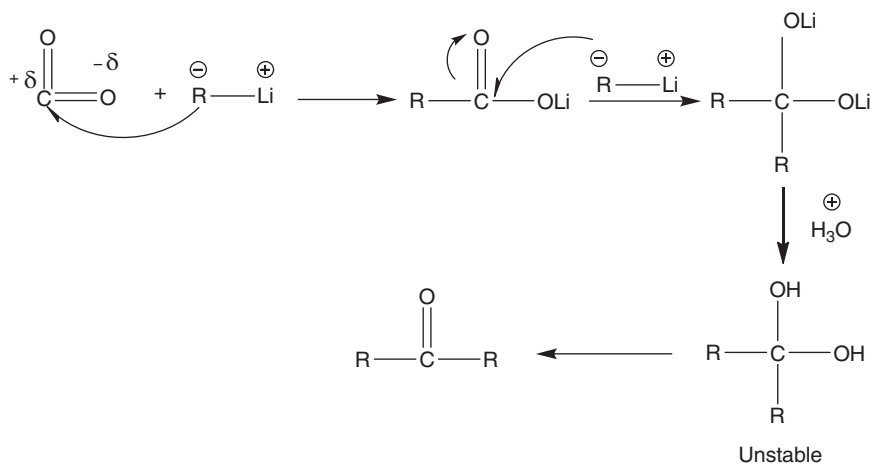
### 3.5.2 Reactions Different from Grignard Reagents

- (i) Grignard reagent with  $\alpha, \beta$ -unsaturated ketones gives a **1, 4-addition** product while organolithium compounds give a **1,2-adduct** (Scheme 3.42).



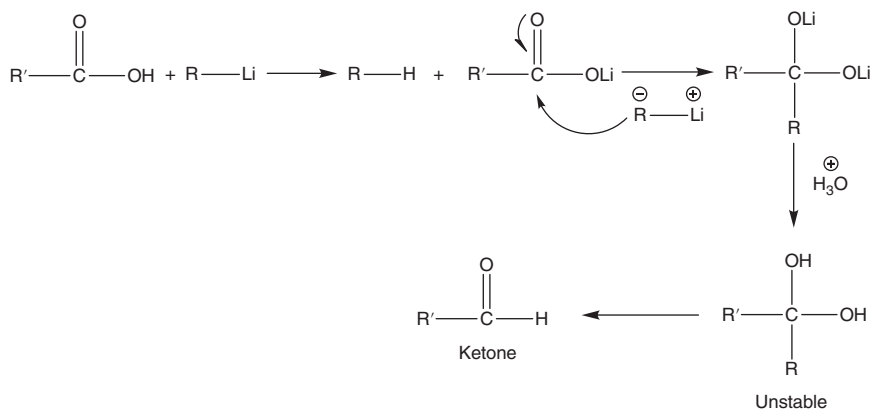
**Scheme 3.42**

- (ii) *Reaction with carbon dioxide:* Organolithium compounds gives ketone (Scheme 3.43).



**Scheme 3.43**

- Acid also gives a ketone when reacted with an organolithium compound (Scheme 3.44).



Scheme 3.44

## 3.6 Organosulfur Compounds

### 3.6.1 Physical Properties

- Methanethiol is a gas while higher homologues are volatile liquids having an extremely unpleasant odor. The boiling points of methanethiol is  $0^\circ$  and that of ethanethiol is  $37^\circ$ . Their disagreeable odor decreases with an increase in the molecular weight.
- The boiling points of thiols are much lower than corresponding alcohols, which is due to weaker intermolecular hydrogen bonding in thiols than alcohols. Due to lesser electronegativity of sulfur the character of sulfur hydrogen bond is much less ionic.
- Weak hydrogen bonding makes them less soluble in water as compared to alcohols. However they are readily soluble in organic solvents such as ether and alcohol [21].

### 3.6.2 Chemical Properties

- Reaction with alkali metals:* Thiols react with alkali metals like sodium, potassium, etc., to form mercaptides with the evolution of hydrogen (Scheme 3.45) [21].



Scheme 3.45

These mercaptides could be decomposed with water to give back thiols (Scheme 3.46).



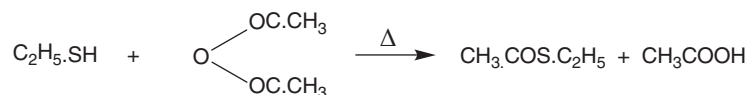
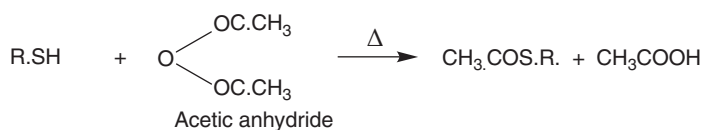
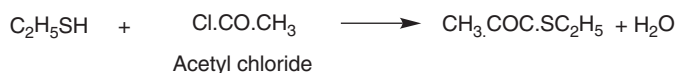
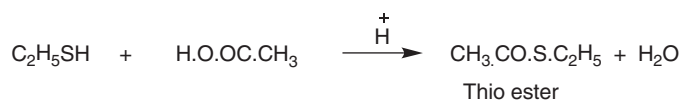
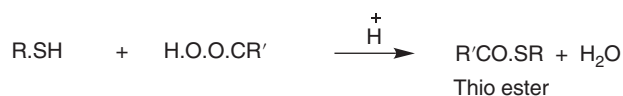
**Scheme 3.46**

Thiols also react with alkalis to form mercaptides (Scheme 3.47).



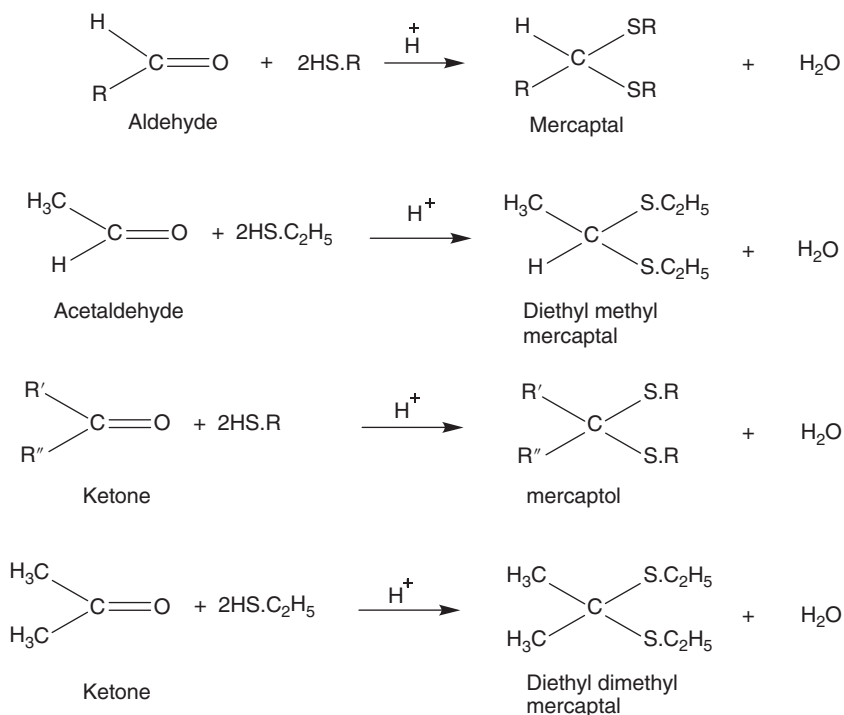
**Scheme 3.47**

b. *Reaction with acid and acid derivatives:* Like alcohol, thiols react with acid, acid chlorides, and acid anhydrides (Scheme 3.48).



**Scheme 3.48**

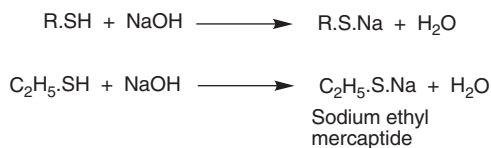
c. *Reaction with aldehyde and ketones:* Like alcohols, they react with aldehydes and ketones to form thioacetals or mercaptals and thioketals or mercaptals in the presence of hydrochloric acid (Scheme 3.49).



Scheme 3.49

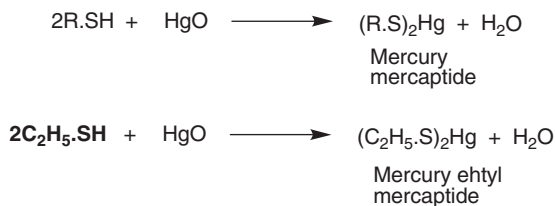
### 3.6.3 Properties Different from Alcohols

a. *Reaction with alkyls*: It gives sodium alkyl mercaptide (Scheme 3.50).

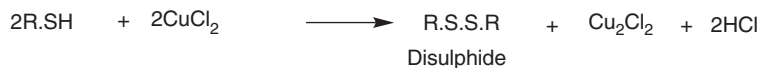


Scheme 3.50

b. *Reaction with metallic salts and metallic oxides*: It gives different mercaptide products (Scheme 3.51 and 3.52).

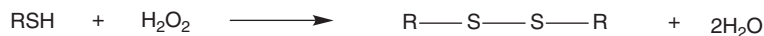


Scheme 3.51

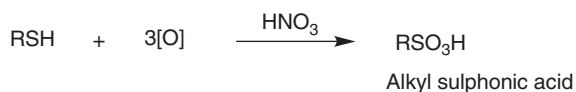
**Figure 3.51** (Continued)**Scheme 3.52**

c. *Oxidation*: Thiols differ significantly from alcohols in their behavior toward oxidizing agents

- (i) With mild oxidizing agents like air, hydrogen peroxide, cupric chloride, iodine, sodium hypochlorite, etc., thiols are oxidized to disulfides (Scheme 3.53).

**Scheme 3.53**

- (ii) With strong oxidizing agents like nitric acid and  $KMnO_4$  they are oxidized to sulphonic acids (Scheme 3.54).

**Scheme 3.54**

### 3.7 Conclusion

Organometallic compounds and their classification are mainly focused on the chemistry of s-block elements, p-block elements, transition elements, and lanthanide and actinide series with carbon-containing moieties. Here M—C bond is mainly formed, which is covalent in nature, through sometimes it behaves as an ionic character. Due to this polarity, these organometallic compounds play a vital role in various reactions.

### References

- 1 Thayer, J.S. (1969). Historical origins of organometallic chemistry. Part I, Zeise's salt. *J. Chem. Educ.* 46 (7): 442.
- 2 Gilman, H. and Schulze, F. (1925). A qualitative color test for the Grignard reagent. *J. Am. Chem. Soc.* 47 (7): 2002–2005.
- 3 Craig, P.J. and Jenkins, R. (2004). Organometallic compounds in the environment: an overview. In: *Organic Metal and Metalloid Species in the Environment; Analysis, Distribution, Processes and Toxicological Evaluation* (ed. A.V. Hirner and H. Emons), 1–15. Springer.
- 4 Mudi, S., Usman, M., and Ibrahim, S. (2015). Clinical and industrial application of organometallic compounds and complexes: a review. *Am. J. Chem. Appl.* 2 (6): 151–158.
- 5 Swope, W.C. and Schaefer, H.F. III, (1977). Model studies of  $\pi$ -bonded organometallic systems Mn-C<sub>2</sub>H<sub>2</sub> and Mn-C<sub>2</sub>H<sub>4</sub>. *Mol. Phys.* 34 (4): 1037–1048.
- 6 Rayón, V.M. and Frenking, G. (2003). Bis (benzene) chromium is a  $\delta$ -bonded molecule and ferrocene is a  $\pi$ -bonded molecule. *Organometallics* 22 (16): 3304–3308.
- 7 Gutmann, V. (1976). Solvent effects on the reactivities of organometallic compounds. *Coord. Chem. Rev.* 18 (2): 225–255.
- 8 Crabtree, R.H. (2009). *The Organometallic Chemistry of the Transition Metals*. Wiley.
- 9 Tang, J. and Zhao, L. (2020). Polynuclear organometallic clusters: synthesis, structure, and reactivity studies. *Chem. Commun.* 56 (13): 1915–1925.
- 10 Oliver, J.P. (1977). Rearrangements of organoaluminum compounds and their group III analogs. In: *Advances in Organometallic Chemistry*, vol. 16 (ed. F.G.A. Stone and R. West), 111–130. Elsevier.
- 11 Soto, D. and Salcedo, R. (2012). Coordination modes and different hapticities for fullerene organometallic complexes. *Molecules* 17 (6): 7151–7168.
- 12 Seyferth, D. (2009). *The Grignard Reagents*, 1598–1605. ACS Publications.
- 13 Tamura, M. and Kochi, J. (1971). Iron catalysis in the reaction of grignard reagents with alkyl halides. *J. Organomet. Chem.* 31 (3): 289–309.
- 14 Ashby, E. (1967). Grignard reagents. Compositions and mechanisms of reaction. *Q. Rev. Chem. Soc.* 21 (2): 259–285.

- 15 Ashby, E. (1980). A detailed description of the mechanism of reaction of Grignard reagents with ketones. *Pure Appl. Chem.* 52 (3): 545–569.
- 16 Knochel, P., Millot, N., Rodriguez, A.L., and Tucker, C.E. (2004). Preparation and applications of functionalized organozinc compounds. *Org. React.* 58: 417–759.
- 17 Furukawa, J. and Kawabata, N. (1974). Organozinc compounds in synthesis. In: *Advances in Organometallic Chemistry*, vol. 12 (ed. F.G.A. Stone and R. West), 83–134. Elsevier.
- 18 Fürstner, A. (1989). Recent advancements in the Reformatsky reaction. *Synthesis* 1989 (08): 571–590.
- 19 Wakefield, B.J. (2013). *The Chemistry of Organolithium Compounds*. Elsevier.
- 20 Gilman, H. and Cartledge, F.K. (1964). The analysis of organolithium compounds. *J. Organomet. Chem.* 2 (6): 447–454.
- 21 Block, E. (2013). *Reactions of Organosulfur Compounds: Organic Chemistry: A Series of Monographs*, vol. 37. Academic Press.



## 14

## Homogeneous and Heterogeneous Catalysis by Organometallic Complexes

Ratnakar D. Shukla<sup>1</sup>, Bhawna Jain<sup>2</sup>, Kuleshwar Patel<sup>3</sup>, Priyanka Singh<sup>3\*</sup>, Dakeshwar Kumar Verma<sup>3</sup>, Reema Sahu<sup>3</sup>, and Raghvendra K. Mishra<sup>4\*</sup>

<sup>1</sup>Pt. Deen Dayal Upadhyay Government College, Department of Chemistry, Bahua, Fatehpur, Uttar Pradesh, India

<sup>2</sup>Siddhachalam Laboratory, Raipur, Chhattisgarh, 493221, India

<sup>3</sup>Govt. Digvijay PG Autonomous College, Department of Chemistry, Rajnandgaon, Chhattisgarh, 491441, India

<sup>4</sup>IMDEA Materials, Madrid, Spain

### 14.1 Introduction

The concept of catalysis is very important in the field of chemistry and it is frequently used as a strategic tool in numerous areas such as life sciences, environmental sciences, energy, and industry [1]. Basically, catalysis, a molecular phenomenon, promotes chemical transformation. In fact, catalysis may be divided into two types heterogeneous or homogeneous, depending on the physical states of reactants and catalysts. In the current scenario, the connections between homogeneous catalysis and molecular organometallic chemistry are observed, whereas heterogeneous catalysis shows proximity towards solid-state chemistry and surface science [2]. In this chapter, the applications of organometallic compounds in homogeneous catalysis and several important chemical reactions catalyzed by them have been covered.

Homogeneous catalysis is regarded as one of the most successful applications of organometallic chemistry – a branch of chemistry that has combined organic and inorganic chemistry – to a remarkable degree [3, 4].

Here, the salient features of homogeneous catalysts are as follows:

- Dispersion of homogeneous catalysts “in the same phase” at molecular level.
- Simple, smooth, and reproducible synthesis and manufacturing.
- Easy characterization with the help of chemical and spectroscopic techniques.
- Substrate specific designing is based upon known principles of catalysis.

On the basis of divergent operating systems, previously heterogeneous and homogeneous catalysis were associated with different areas. Subsequently it was thought that both followed different mechanisms of catalysis in elementary steps.

\*Corresponding authors.

*Organometallic Compounds: Synthesis, Reactions, and Applications*, First Edition.

Edited by Dakeshwar Kumar Verma and Jeenat Aslam.

© 2023 WILEY-VCH GmbH. Published 2023 by WILEY-VCH GmbH.

Later, it was observed that both were approaching each other, and this connection was well studied in the field of organometallic surface chemistry.

The applications of organometallic compounds in the area of homogeneous catalysis have gone beyond the frontiers of industry to provide the small-scale synthesis of daily needs in a laboratory [5, 6]. The prominent example of such an application is alkene isomerization using transition metal organometallic complexes as a homogeneous catalyst. The conduction of hydrogenation reactions of substrates like alkene, arene, imine, and ketone is done using various types of transition metal organometallic catalysts. They also proceed via diverse mechanisms involving oxidative addition, homolytic, and heterolytic cleavages of the H—H bond.

In the current scenario, the study and exploration of organometallic compounds as homogeneous catalysts is highly demanding in the field of catalysis. The development of many novel organometallic catalysts accelerates the optimization and subsequent application of organometallic chemistry in homogeneous catalysis [7, 8]. The benefits of homogeneous organometallic catalysts have currently spread to all conceivable areas of chemical sciences, from the confines of industry for synthetic processes used on a daily basis to academics for organic synthesis. Presently, several developmental processes related to improving our daily lives have achieved their goals due to the incorporation of organometallic compounds in the field of homogeneous catalysis. Alkene metathesis is regarded as one of the important examples of the aforementioned target, which is executed with the help of homogeneous organometallic catalysts. The production of many novel chemical moieties has been achieved with the help of various homogeneous organometallic catalysts. Consequently, the library of novel synthesized chemical compounds is being explored in various fields of chemical sciences, including pharmaceutical chemistry.

## 14.2 Organometallic Compounds and Homogeneous Catalysis

When a metal or metalloid possesses at least one bond to a carbon atom directly, the resulting compound is regarded as an organometallic compound. Notably, the carbon metal bond may have either ionic or covalent characteristics. To expand the field of homogeneous transition-metal catalysis, exploitation of a diverse range of transition metal complexes has been done to check their catalytic efficacies. After the successful outcome, employment of homogeneous transition-metal catalysts has been examined for the synthesis of organic molecules [9].

In terms of selectivity of the reaction, it is observed that homogeneous catalysis works better in comparison to heterogeneous catalysis because homogeneous catalysis can be monitored with the incorporation of suitable ligands on the catalytic metal center [10]. One of the noticeable advantages of organometallic catalysis is the stepwise economic synthesis of organic compounds. In addition, conduction of enantioselective reactions employing homogeneous catalysts is done; consequently, high optical yields are obtained and this application has great importance in industry [11]. Furthermore, in homogeneous catalysis, smooth reaction conditions such as low temperature and pressure are frequently sufficient.

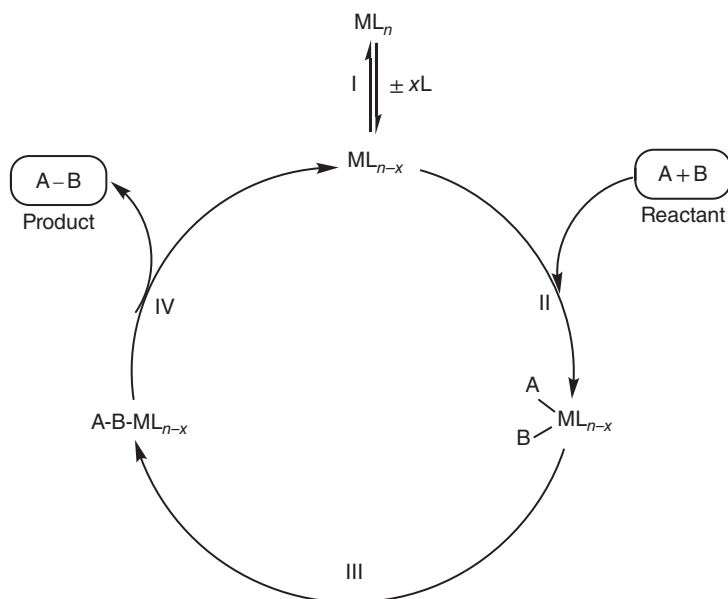
Due to the emergence of green and sustainable chemistry in the field of catalysis, the recovery of catalysts is highly desirable. In this context, numerous methods such as precipitation, immobilization on carrier materials, reverse osmosis, and reaction in two-phase liquid–liquid systems are available for catalyst recovery after the reaction [12–14]. Here, we will discuss some important organometallic homogeneous catalysis-driven chemical transformations one by one.

### 14.3 Catalytic Elementary Reactions

Basically, stepwise categorization of a catalytic cycle for a homogeneous catalyst can be done as follows [15–17]:

- I. Generation of the active species,
- II. coordination of metal center and the reactants,
- III. production of the product, and
- IV. elimination of the product with regeneration of the initial catalytically active species

The pictorial representation of the four aforementioned steps is well depicted below.



The first step is completed with the *in situ* conversion of starting complex  $ML_n$  to  $ML_{n-x}$  as a catalytically active species. The presence of vacant coordination sites in catalytically active species is the basic requirement for coordination of the reactants A and B. Often, the generation of active species is done after the dissociation of the ligand, i.e. by the elimination of Lewis bases like phosphines or Lewis acids such as protons.

The second step of the catalytic cycle is initiated with the binding of one or more reactants to the metal center. This step is completed either by oxidative addition, in which molecules like H-H, R-X, or H-X are cleaved and then the two fragments attach to the metal center via  $\sigma$ -bonds or by ligand association, i.e. addition of ligands such as carbon monoxide, alkenes or alkynes, to the metal center. Notably, in oxidative addition, the central metal observes an increase of two in both the oxidation state and coordination number.

The reactions of bond formation between the reactants associated with the metal center are observed in the third step. In addition, insertion reactions are often observed in this step.

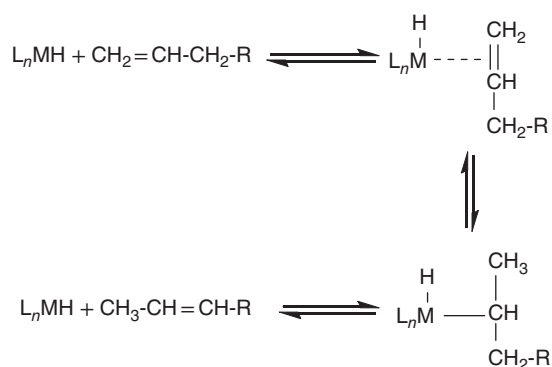
In the fourth step, the catalytic cycle is completed with the elimination of the product. Usually, the product is released via the mechanism of reductive elimination. Reductive elimination is just the reverse of oxidative addition.

### 14.3.1 Isomerization

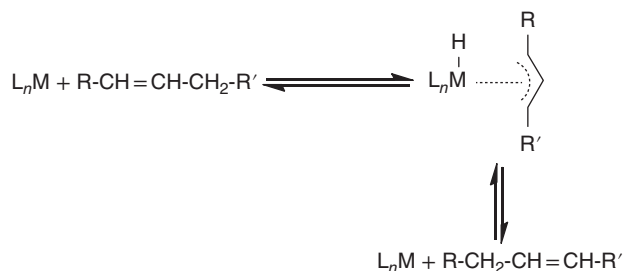
Mostly transition-metal complexes, particularly transition-metal hydride complexes having the general formula  $L_nMH$  (may also be generated *in situ* from  $ML_n$  and hydrogen), are explored as homogeneous catalysts for isomerization. In addition to the skeletal rearrangements of cyclic aliphatic compounds, the aforementioned homogeneous catalysts can also catalyze the isomerization of double-bond systems including alkenes, dienes, and allyl compounds [18–20].

The generation of thermodynamically more stable isomers is considered the driving force for the isomerization reaction. Isomerization strongly depends on reaction temperature, and this reaction is an example of an equilibrium reaction. At higher temperatures, it is also observed that the proportion of thermodynamically less stable isomers increases.

To understand the story of alkene isomerization, two mechanisms viz. the hydride mechanism and the allyl mechanism, are available. In the hydride mechanism, the addition of alkene to the transition-metal hydride to give an  $\eta^2$ -alkene complex takes place followed by generation of a  $\sigma$ -alkyl complex after rearrangement. Regeneration of the initial hydride complex occurs after the elimination of a product i.e. olefin.



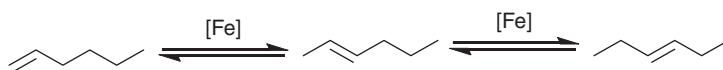
In the allyl mechanism,  $\eta^3$ -allyl complex is formed as an isomerization intermediate via the removal of a proton adjacent to the double bond in the presence of a transition metal.



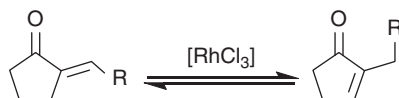
Several metal complexes of groups 6, 8, 9, and 10 can be exemplified as isomerization catalysts. Examples of the most common complexes which are frequently used as catalysts are iron carbonyls, rhodium chloride, rhodium chloro complexes, titanium, and palladium complexes.

### 14.3.2 Alkene Isomerization

The conversion of 1-hexene to 2- and 3-hexene can be achieved using iron carbonyls as a catalyst.

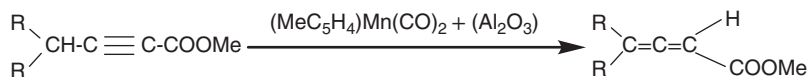


The transformation of exocyclic enones to endocyclic enones via isomerization reaction is done using rhodium(III) trichloride  $[RhCl_3]$ , which is a very suitable catalyst for this reaction. Subsequently 2-substituted cyclopentenones are synthesized.



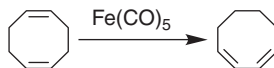
### 14.3.3 Alkyne Isomerization

Manganese complexes can conduct the conversion of alkynes to their corresponding allenes.



### 14.3.4 Diene Isomerization

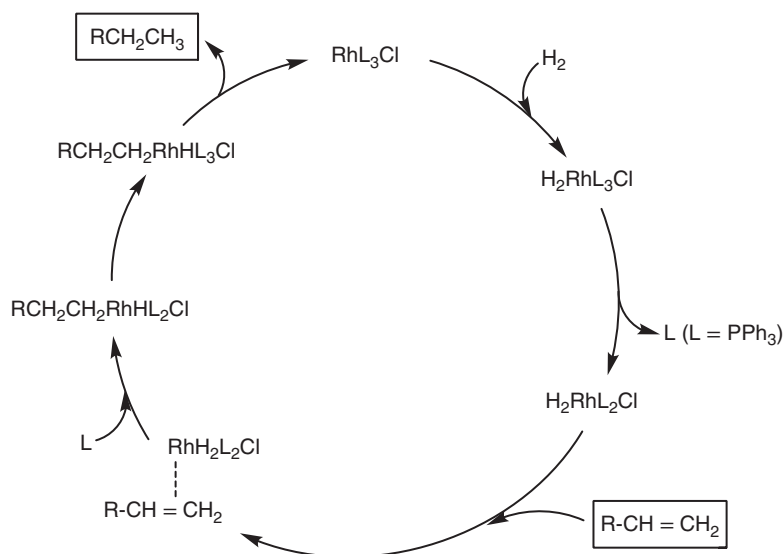
The conversion of thermodynamically more stable 1,3-isomer of cyclooctadiene from 1,5- is afforded in the presence of iron(0) pentacarbonyl [ $\text{Fe}(\text{CO})_5$ ]:



## 14.4 Hydrogenation

Numerous homogeneous transition-metal catalysts are used for the hydrogenation of alkenes, dienes, and alkynes [21–26].  $\text{H}_2\text{IrCl}_6$ ,  $[(\text{PPh}_3)_2\text{IrCl}(\text{CO})]$ ,  $[\text{HCo}(\text{CO})_4]$ , and  $[(\text{PPh}_3)_2(\text{CO})_2\text{RuCl}_2]$  are some typical examples of catalysts for hydrogenation. Wilkinson's catalyst  $[(\text{PPh}_3)_3\text{RhCl}]$  is one of the most commonly employed catalysts. In the presence of this catalyst, the hydrogenation is carried out under mild conditions. A simple reaction mechanism for hydrogenation reaction in the presence of Wilkinson's catalyst is clearly demonstrated below.

A dihydridorhodium(III) complex is obtained via oxidative addition of hydrogen, which after dissociating a phosphine ligand, creates a vacant coordination site for bonding of an alkene. A hydrido alkyl rhodium complex is obtained after the step of insertion. Then the desired product, an alkane, is obtained after elimination, and the starting complex is regenerated after complexation of the phosphine.

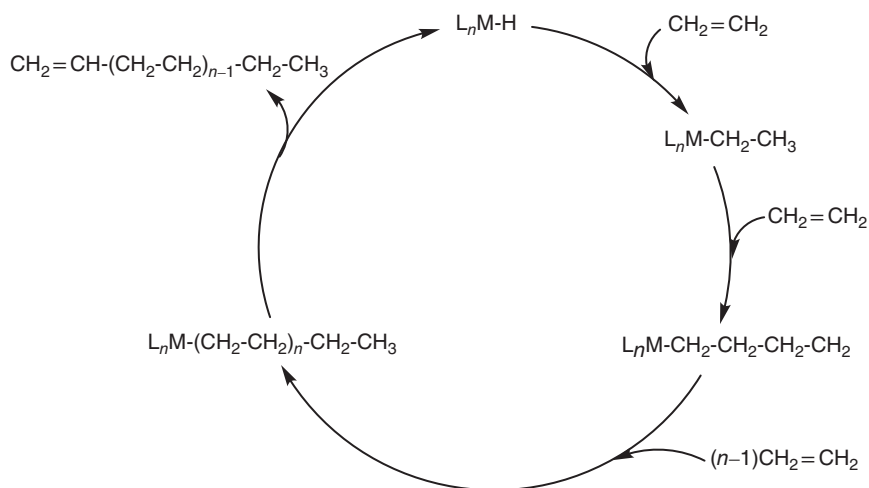


The hydrogenation of terminal and inner alkenes can be carried out by  $[(\text{PPh}_3)_3\text{RhCl}]$ , whereas the hydride complex i.e.  $[(\text{PPh}_3)_3\text{Rh}(\text{CO})\text{H}]$  hydrogenates

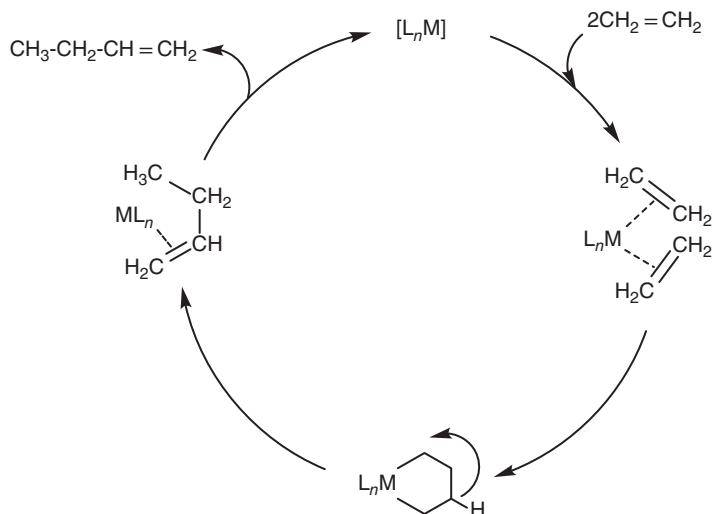
only terminal double bonds. It is also observed that this hydride complex is less reactive in comparison to Wilkinson's catalyst. The hydrogenation of ethene and propene is carried out by the carbonyl chloro complex *trans*-[(PPh<sub>3</sub>)<sub>3</sub>Rh(CO)Cl], but this catalyst hydrogenates in slow rates only. Furthermore, the hydrogenation reaction becomes fast in the presence of corresponding iridium complex *trans*-[(PPh<sub>3</sub>)<sub>3</sub>Ir(CO)Cl]. Notably, several cationic catalysts such as complexes of the type [L<sub>2</sub>Rh(THF)<sub>2</sub>]<sup>+</sup> shows high catalytic activity.

## 14.5 Carbon–Carbon Bond Formation

The processes of linear and cyclic oligomerization, telomerization, polymerization, and vinylogation are studied in this section [27–32]. The oligomerization of alkenes results in linear or branched high molecular mass alkenes. In the production of fine chemicals, plasticizers, and detergents, the linear or branched high molecular mass alkenes are used frequently. To understand the oligomerization of alkenes, two common mechanisms viz. the hydride mechanism and the metallacycle mechanism, are reported in the literature. In hydride mechanism, a metal hydride complex is considered as a catalytically active species and into the M—H bond of a metal hydride complex, the insertion of an alkene is observed. Next, due to the insertions of alkene molecules into the resulting metal–carbon (M—C) bond, the long-chain metal alkyls are generated. The β-hydrogen elimination terminates the reaction; consequently, the desired oligomer is liberated, followed by regeneration of the metal hydride.



Dimerization of ethene into butane is an example of the metallacycle mechanism. A bis(ethene) complex produces metallacyclopentane, which is then rearranged and hydrogen shifted to form a butene complex.



Development of several catalysts has been reported for ethene oligomerization. Ziegler–Natta catalyst is a prominent example of the aforementioned group. Ziegler–Natta catalysts are generated from an aluminum alkyl and a transition-metal component. Titanium, cobalt, nickel, and zirconium are the most common transition metals for these catalysts. Generally, titanium and zirconium are employed in the form of their halides or alkoxides, whereas nickel and cobalt are used as acetyl acetonates or allyl complexes. Adducts of the transition-metal complex and aluminum component are considered catalytically active species. When titanium tetrachloride and ethyl aluminum dichloride react, a complex is formed that has a free coordination site available for an olefin to bond to.

In addition to Ziegler–Natta catalysts, several other metal compounds have catalytic properties for the oligomerization of alkenes, in these cases; no activation by aluminum alkyls is required. Some of the important example of these type of catalysts are cobalt dinitrogen complex  $[CoH(N_2)(PPh_3)_3]$ , rhodium trichloride  $[RhCl_3]$ , ruthenium trichloride  $[RuCl_3]$ , and palladium dichloride  $[PdCl_2]$ .

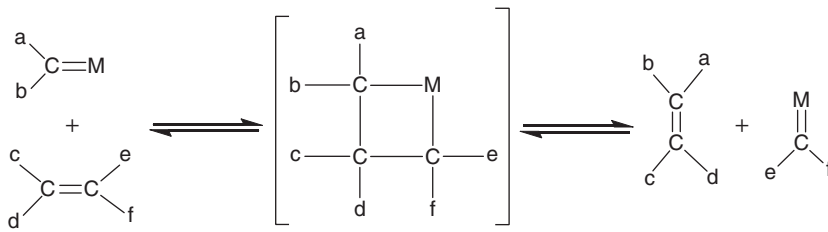
## 14.6 Metathesis

In general, metathesis is defined as the exchange of alkylidene groups between two alkenes [28–32].

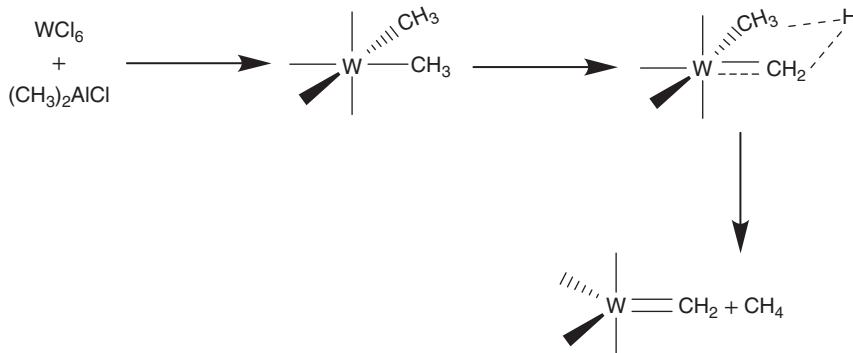


$WCl_6-EtOH-R_2AlCl$  is regarded as one of the most common homogeneous catalytic systems for metathesis. In fact, the reactive intermediates are commonly observed in the form of carbene complexes.





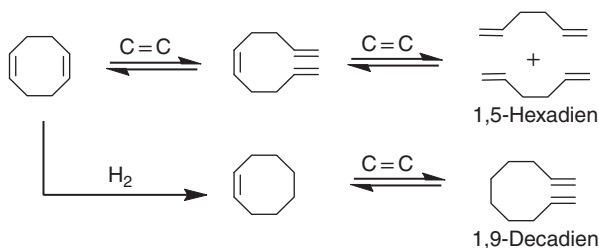
A detailed mechanism for the generation of metal from the catalytic system  $\text{WCl}_6\text{-Me}_2\text{AlCl}$  is depicted below.



Huls (1980) reported the generation of polyoctenamer from cyclooctene via metathesis. The trade name for the synthesized polyoctenamer is Vestenamer 8012.



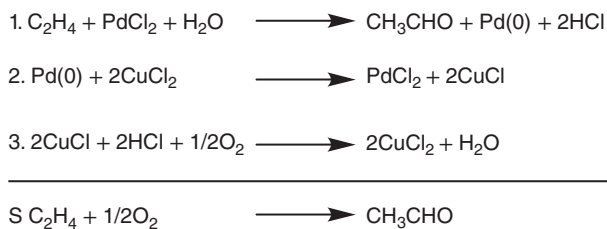
The conversion of  $\alpha,\omega$ -dienes from cycloolefins and ethane is studied as the Feast process. 1,5-cyclooctadiene, generated via cyclodimerization of butadiene, is explored as the starting material for the Feast process.



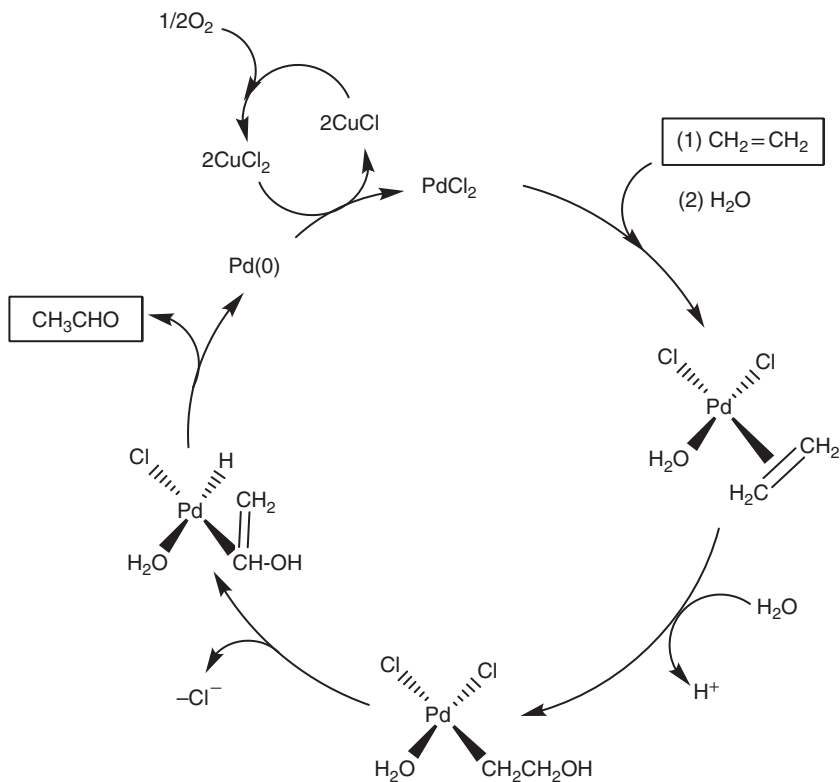
## 14.7 Oxidation

The Wacker-Hoechst process is a well-known process for oxidation. In this process, the decomposition of ethene chloro complexes of palladium(II) into acetaldehyde

and palladium(0) occurred in the presence of water. The use of air environment facilitates the oxidation of Pd(0) back to Pd(II), and the use of a Cu(I)/Cu(II) couple allows the reaction to be catalyzed. This process is completed in several steps, but the overall reaction of ethene and oxygen to give acetaldehyde can be written in one step, and the complete process is well depicted below [33–35].



Notably, when the terminal or inner alkenes is explored as substrates in this reaction, ketones are generated as ketones instead of aldehydes. For example, acetone is obtained from propene. The detailed mechanism of acetaldehyde generation via the Wacker–Hoechst process is being demonstrated. In the first step, the addition of ethene and water to the metal center takes place. In the next step, the hydroxyethyl complex is generated via oxypalladation. Finally, after rearranging into a hydridovinyl alcohol complex, acetaldehyde is obtained.

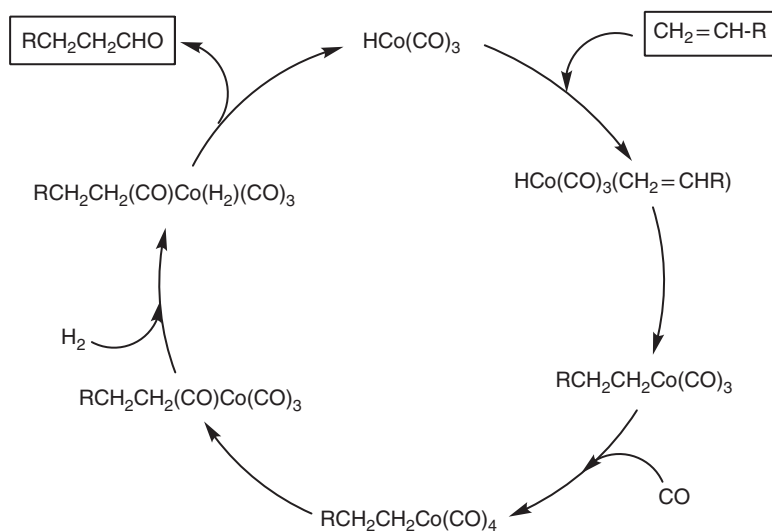


## 14.8 Reactions with Carbon Monoxide

In this section, transition-metal catalyzed reactions of carbon monoxide with hydrogen, alkenes, alkynes, and alcohols are discussed [36–39].

The substrate for the Fischer–Tropsch reaction is synthesis gas, which is generated from the reaction of carbon monoxide with hydrogen. Recently, Fischer–Tropsch chemistry research has primarily focused on controlling the formation of side products such as alcohols, short-chain olefins, and long-chain  $\alpha$ -olefins. Extensive investigations into the reactions of hydrogen and carbon monoxide in the presence of a homogeneous catalyst are highly explored. In this context, synthesis of ethylene glycol is afforded in presence of a rhodium catalyst [40, 41].

Roelenat Ruhrchemie reported the hydroformylation reaction, which is considered one of the most important reactions of carbon monoxide and alkenes [42].



In the hydroformylation reaction, propionaldehyde is obtained from ethane and synthesis gas using a cobalt carbonyl catalyst. In fact, aldehydes are the primary products of hydroformylation reactions, which are often transformed into other products, mostly alcohols. The mechanism of cobalt-catalyzed hydroformylation involves going through the formation of hydridocobalt carbonyl, which is regarded as a catalytically active species. An acyl complex is produced via the insertion of an olefin and carbon monoxide. Finally, aldehyde is produced followed by hydrogenation [43, 44].

## 14.9 Heterogenous Catalysis

Heterogeneous catalysis involves the use of solid or metallic catalysts. The reactants and/or products have different phases as compared to those of the catalyst. Phase difference stands for solid, liquid, or gaseous states along with immiscible mixtures as well as the presence of interfaces [45–47]. Table 14.1 enlists different

**Table 14.1** List of different heterogenous catalysis-based reactions.

S. No.	Reaction	Substrate	Catalyst	Product	References
1	Polymerization	Propene	MgCl <sub>2</sub> /TiCl <sub>4</sub>	Polypropylene	Cavallo and coworkers [48]
2	Hydrogenation	N <sub>2</sub>	Hydride-based complexes of Co, Fe, Ru, Rh, Ir, Mn, Mo, Ni, Ti, Ta	NH <sub>3</sub>	Kageyama and coworkers [49]
3	Hydrogenation	N <sub>2</sub>	Ru	NH <sub>3</sub>	Marakatti and Gaigneaux [50]
4	Hydrogenation	N <sub>2</sub>	Fe	NH <sub>3</sub>	Li and coworkers [51]
5	Dehydrogenation	Polyethylene glycol	Ni/ZrO <sub>2</sub>	H <sub>2</sub>	Wei and coworkers [52]
6	Oxidative coupling	Methane	Li/MgO	Ethane + ethylene	Tarr and coworkers [53]
7	Oxidation	Methane	Pt, Ni	CO + H <sub>2</sub> + formaldehyde	Tarr and coworkers [53]
8	Oxychloration	Ethylene + Cl <sub>2</sub>	CuPdCl	Vinyl chloride	Tarr and coworkers [53]
9	Oxychloration	Ethane + Cl <sub>2</sub>	AgMnCoO	Vinyl chloride	Tarr and coworkers [53]
10	Oxidation	Ethane	MoVNbO	Acetic acid	Tarr and coworkers [53]
11	Oxidation	<i>n</i> -Butane	(VO) <sub>2</sub> P <sub>2</sub> O <sub>7</sub>	Maleic anhydride	Tarr and coworkers [53]
12	Oxidation	Ethylene	Ag/Al <sub>2</sub> O <sub>3</sub>	Ethyl oxide, acetaldehyde, acetic acid	Tarr and coworkers [53]

heterogeneous catalysis-based reactions. The steps involved in heterogeneous catalysis (Figure 14.1) are:

- (i) *Diffusion of reactants toward the surface*: Concentration of the reactant and thickness of the surface affects the rate of diffusion.
- (ii) *Adsorption of reactants*: The adsorption of reactants on a surface can be through chemisorption or physisorption. In the case of chemisorption, bonds are formed between the reactant and the surface of the catalyst. The binding efficiency of a molecule or atom is known as the sticking coefficient, which is simply the percentage or proportion of molecules that remain bound to the surface.
- (iii) *Reaction*: Atoms and/or molecules bound to the catalyst surface react with each other, resulting in bond formation.
- (iv) *Desorption of product(s)*: Products are desorbed from the catalyst surface.
- (v) *Diffusion of product(s)*: The products diffuse away from the catalyst surface.

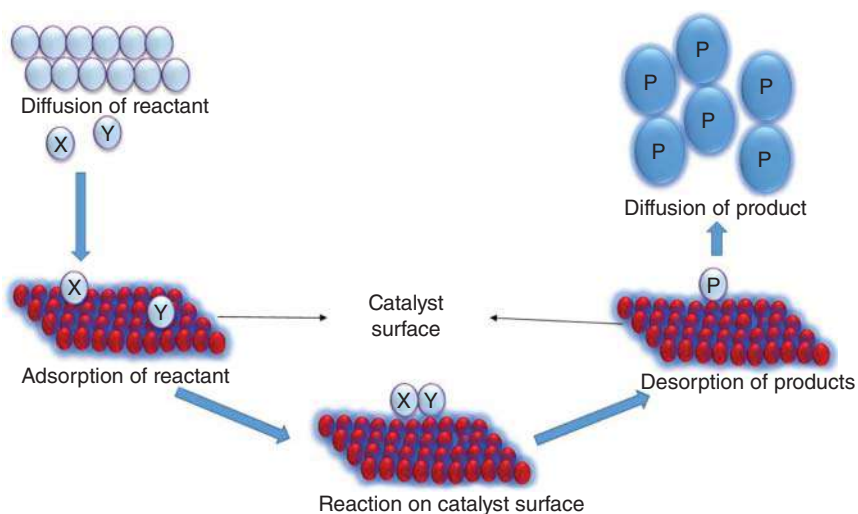


**Figure 14.1** Steps involved in heterogeneous catalysis.

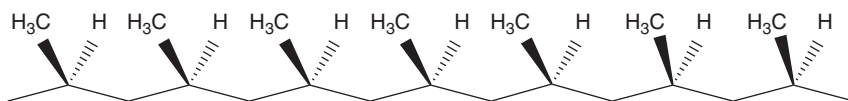
### 14.9.1 Ziegler–Natta Catalyst

Alkenes are polymerized in the presence of transition-metal complexes and aluminum alkyls. Ziegler et al. (1955) proposed the Ziegler–Natta polymerization of ethylene to give polyethylene in presence of  $\text{TiCl}_4$  and  $\text{Al}(\text{C}_2\text{H}_5)_3$  [46, 47, 49]. The noble prize (1963) in chemistry was shared by German chemist Karl Ziegler for the discovery of first Ti-based catalyst and Giulio Natta for preparation of stereoregular polymers by using this catalyst. Various polyolefins have been prepared commercially using the Ziegler–Natta catalyst; some of these include polyethylene, polypropylene, polycycloolefins, polyisoprene, polyacetylene, copolymers of ethylene, alkenes, etc.

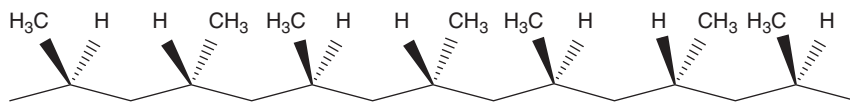
#### 14.9.1.1 Stereoregularity

Natta found that the polymers have a crystalline structure owing to stereoregularity. Polymers can have different tacticities depending on the orientation of alkyl groups in polymer chains having  $(-\text{CH}_2-\text{CH}_2-)_n$  units. The stereoregularity of polymers is dependent upon the type of catalyst, which is used to prepare it.

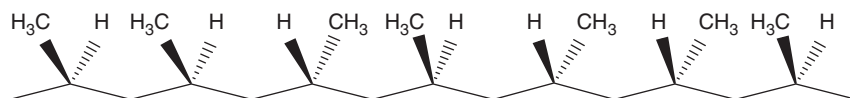
*Isotactic:* All the stereogenic (CHR) centers have same configuration. These polymers are crystalline.



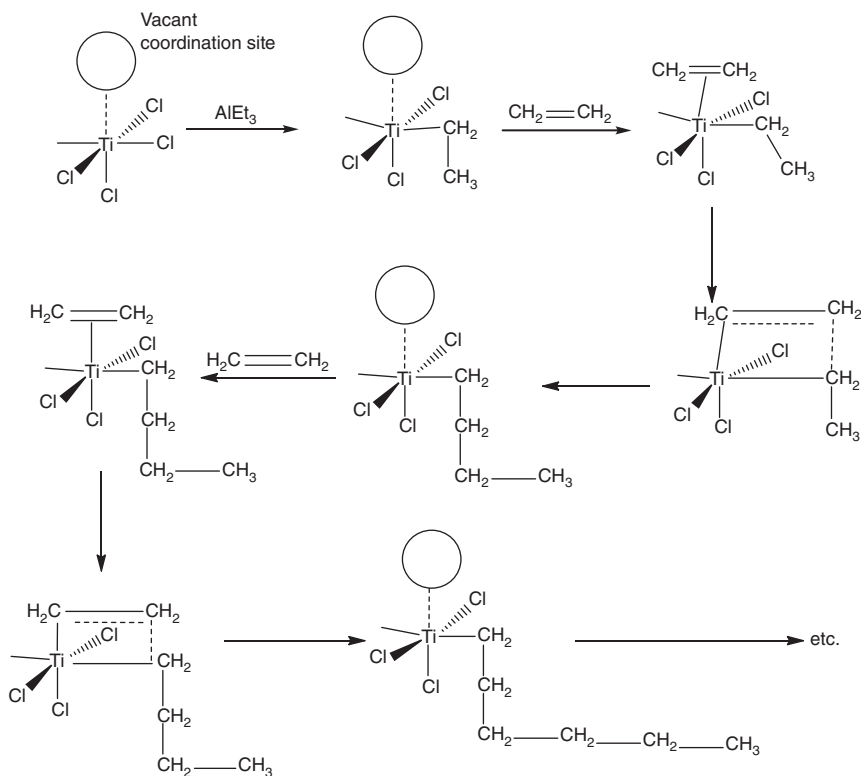
**Syndiotactic:** The stereogenic centers (CHR) have relatively alternate configuration. These polymers also show crystalline nature.



**Atactic:** These polymers do not have any regular arrangement of the alkyl substituents. These are amorphous in nature.



The mechanism proposed by Coscec and Arlman will be discussed here.  $\text{TiCl}_4$  reacts with  $\text{Al}(\text{C}_2\text{H}_5)_3$  to give  $\text{TiCl}_3$  [45, 46]. A titanium alkyl complex is obtained by the reaction between  $\text{TiCl}_3$  and  $\text{Al}(\text{C}_2\text{H}_5)_3$ . The alkene gets inserted into the  $\text{Ti}-\text{C}$  bond, resulting in the formation of a large alkyl complex. The chain length increases by further insertion of alkene.



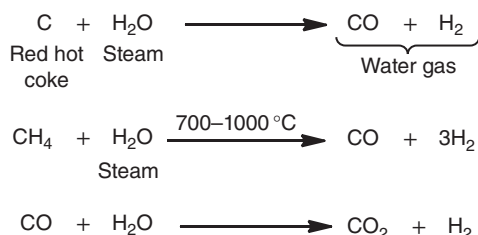
Gabe and coworkers (1985) have discussed the formation of a metallacyclobutane intermediate. According to this mechanism, the steps involved are

1. Alkylidene is obtained from metal alkyl complex.
2. Ethylene gets added to form metallacyclobutane.
3. Ethylene then gets added to the metal-carbon bond.

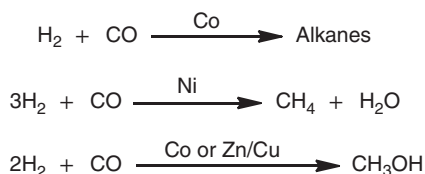
It's difficult to distinguish the mechanism being followed. But Cossec-Arlman mechanism is the commonly observed one for polymerization reactions. Green and coworkers have presented strong evidence in support of this mechanism [46].

### 14.9.2 Water Gas Reaction

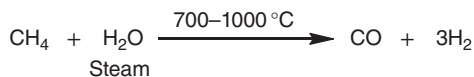
The reaction between steam (water) and a carbon source such as coke or coal at high temperature and pressure is known as the water-gas reaction [47].



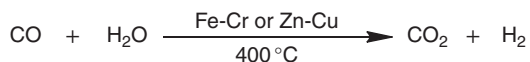
This reaction yields an equimolar mixture of hydrogen and carbon monoxide gases, also known as synthetic or syn gas. Some amounts of carbon dioxide gas might also be used in various other reactions. The Fischer-Tropsch process utilizes transition metals as catalysts to produce hydrocarbons, alcohols, alkanes, etc., from synthetic gas.



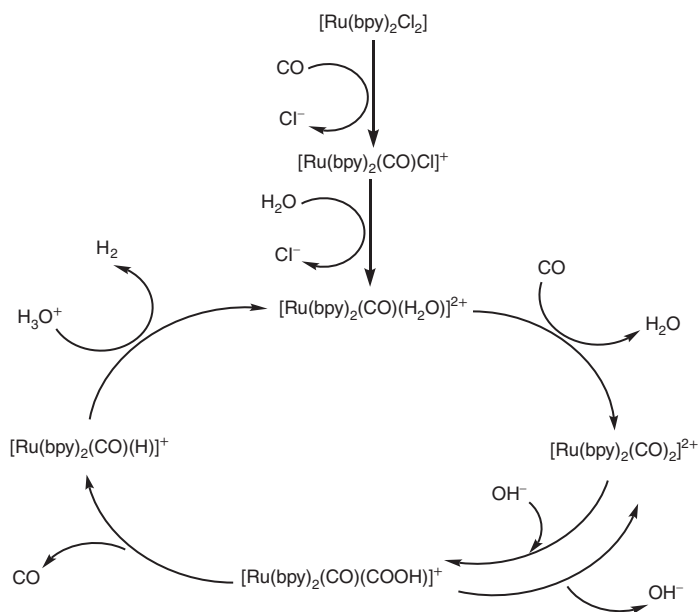
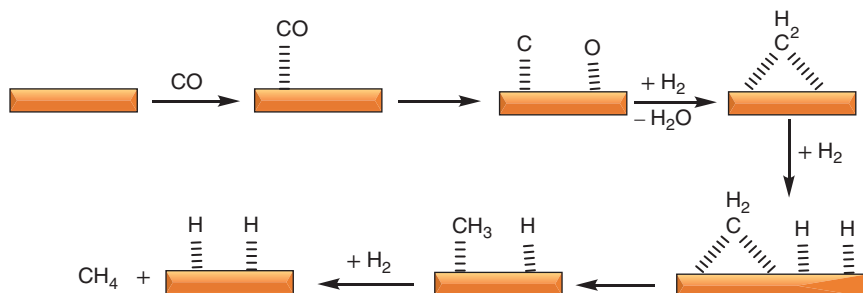
This process was used for the production of synthetic fuels in various countries during the Second World War. However, due to the high cost of obtaining H<sub>2</sub> and CO gases from coal or petroleum, all of these initiatives proved to be ineffective. Steam reforming involves the reaction between natural gas (methane) and steam at elevated temperatures and pressures to yield carbon monoxide and hydrogen.



This process is used for producing hydrogen gas on an industrial scale. Carbon monoxide obtained as a product can be recycled again to produce hydrogen gas.



This reaction is thermodynamically favorable and can yield 99% pure hydrogen gas, if  $\text{CO}_2$  is removed chemically.



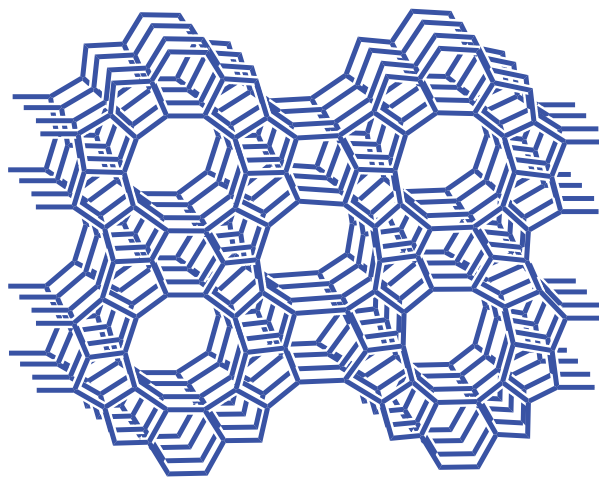
### 14.9.3 Zeolites

Zeolite is an aluminosilicate mineral that has a crystalline structure, silicon, aluminum, and oxygen. Its chemical formula is  $\text{M}_x\text{Al}_x\text{Si}_{1-x}\text{O}_2 \cdot y\text{H}_2\text{O}$ , where M is a metal ion.  $\text{AlO}_4$  and  $\text{SiO}_4$  have tetrahedral structures and form covalent networks



of zeolite. It consists of a frame of cavities and channels inside which cations, water and small molecules can exist due to the way zeolite is used as a molecular sieve. It is generally used as an adsorbent and catalyst. The term zeolite was coined by the mineralogist Axel Fredrik Kronstadt (Swedish) in 1756. Zeolites are produced industrially on a large scale but are also present in nature. More than 40 zeolites are known in nature.

Due to its porous nature, it can accommodate many cations such as  $\text{Na}^+$ ,  $\text{K}^+$ ,  $\text{Ca}^{2+}$ ,  $\text{Mg}^{2+}$ , and others. All these cations are easily replaced by another contact solution. Analcime, phillipsite, clinoptilolite, and heulandite are examples of common zeolites.  $\text{Na}_2\text{Al}_2\text{Si}_3\text{O}_{10}\cdot 2\text{H}_2\text{O}$  (natrolite) is a simple example of the mineral form of zeolites. Volcanic pillars and ash sheets treated with basic ground water are the natural sources of zeolites. Natural zeolites are frequently impure and polluted with other minerals, metals, or other zeolites. Its distinct porous assembly and adaptable acidity make it dynamic in various reactions. They are used for separation and trapping of molecules. They are extensively applied as ion-exchange coats in domestic as well as viable water softening and purification processes. Mesoporous zeolite materials are broadly applied as catalysts in the petrochemical industry for hydrocracking and liquid catalytic cracking. The acidic zeolites can ease many acid-catalyzed reaction like isomerization and alkylation. Zeolites have micro-porous nature to bind some ions of fission products from nuclear processes and to be detached from the waste permanently.



## 14.10 Conclusion

The use of organometallic chemistry in the field of catalysis has always been fascinating to researchers. Heterogeneous and homogeneous catalysis have been discussed in this chapter. Continuous research work is going on in this field. However, further research needs to be done in this field to explore the applicability of organometallic compounds in various reactions.

## References

- 1 Roduner, E. (2014). Understanding catalysis. *Chem. Soc. Rev.* 43: 8226–8239.
- 2 Speight, J.G. (2017). Heterogeneous catalysis and homogeneous catalysis. In *Rules of Thumb for Petroleum Engineers*, J.G. Speight (Ed.). <https://doi.org/10.1002/9781119403647.ch192>, Scrivener Publishing LLC.
- 3 Buckingham, J. (ed.) (1984). *Dictionary of Organometallic Chemistry*, vol. 1–3. London: Chapman and Hall.
- 4 Haiduc, I. and Zuckerman, J.J. (1985). *Basic Organometallic Chemistry*. Berlin: Walter de Gruyter.
- 5 Behr, A. (2005). *Organometallic Compounds and Homogeneous Catalysis*. Weinheim: Wiley-VCH Verlag GmbH & Co. KGaA.
- 6 Herrmann, W. (2022). Organometallic compounds for homogeneous catalysis. In: *Catalysis from A to Z* (ed. W. Herrmann, B. Cornils, H. Zanthoff and J.-H. Xu). <https://doi.org/10.1002/9783527809080.cataz11989>.
- 7 Blaser, H.-U., Indolese, A., and Schnyder, A. (2000). Applied homogeneous catalysis by organometallic complexes. *Curr. Sci.* 78 (11): 1336–1344.
- 8 Cadierno, V. (2021). Recent advances in organometallic chemistry and catalysis. *Catalysts* 11 (5): 646.
- 9 Denisov, E.T., Sarkisov, O.M., and Likhtenshtein, G.I. (2003). Catalysis by metal complexes, Chapter 17. In: *Chemical Kinetics: Fundamentals and New Developments*, 1e (ed. E.T. Denisov, O.M. Sarkisov and G.I. Likhtenshtein), 472–501. Amsterdam: Elsevier ISBN: 9780444509383.
- 10 Hagen, J. (2006). *Industrial Catalysis: A Practical Approach*, 1–14. Weinheim: Wiley-VCH.
- 11 Cheng, X., Lei, A., Mei, T.-S. et al. (2022). Recent applications of homogeneous catalysis in electrochemical organic synthesis. *CCS Chem.* 4: 1120–1152.
- 12 Kalck, P. and Monteil, F. (1992). Use of water-soluble ligands in homogeneous catalysis. *Adv. Organomet. Chem.* 34: 219–284.
- 13 Wache, S. (1995). Organometallic complex catalysis in water II. Water soluble organoruthenium (IV) catalysts for the emulsion polymerization of norbornene. *J. Organomet. Chem.* 494: 235–240.
- 14 Wan, K.T. and Davis, M.E. (1994). Design and synthesis of a heterogeneous asymmetric catalyst. *Nature* 370: 449–450.
- 15 Kochi, J.K. (1978). *Organometallic Mechanisms and Catalysis*. New York: Academic Press.
- 16 Parshall, G.W. (1978). Industrial applications of homogeneous catalysis. *J. Mol. Catal.* 4: 243–270.
- 17 Cornils, B. and Herrmann, W.A. (1996). *Applied Homogeneous Catalysis with Organometallic Compounds*, vol. 1, 2. Weinheim: Wiley-VCH Verlag.
- 18 Biellmann, J.F. and Jung, M.J. (1968). The mechanism of isomerization of an olefin and its possible relation to the mechanism of the catalytic hydrogenation with tris (triphenylphosphine) rhodium chloride. *J. Am. Chem. Soc.* 90: 1673.
- 19 Tani, K., Yamagata, T., Akutagawa, S. et al. (1984, 1984). Metal-assisted terpenoid synthesis. 7. Highly enantioselective isomerization of prochiral allylamines

- catalyzed by chiral diphosphine rhodium (I) complexes. Preparation of optically active enamines. *J. Am. Chem. Soc.* 106: 5208–5217.
- 20 Ma, W., Liu, B., Wang, D. et al. (2021). Catalytic isomerization of olefins and their derivatives: a brief overview. In: . <https://doi.org/10.5772/intechopen.99076>.
  - 21 Vaska, L. and Rhodes, R.E. (1965). Homogeneous catalytic hydrogenation of ethylene and acetylene with four-coordinated iridium and rhodium complexes. *J. Am. Chem. Soc.* 87: 4970.
  - 22 James, B.R. (1973). *Homogeneous Hydrogenation*. New York: Wiley-Interscience.
  - 23 McQuillin, F.J. (1976). *Homogeneous Hydrogenation in Organic Chemistry*. Dordrecht: Reidel Publ.
  - 24 Haack, K.-J. et al. (1997). Catalyst precursor, catalyst, and intermediate in the RuII-catalyzed asymmetric hydrogen transfer between alcohols and ketones. *Angew. Chem.* 109: 297–300.
  - 25 Struijk, J., Moene, R., van der Kamp, T., and Scholten, J.J.F. (1992). Partial liquid-phase hydrogenation of benzene to cyclohexene over ruthenium catalysts in the presence of an aqueous salt solution: II. Influence of various salts on the performance of the catalyst. *Appl. Catal. A* 89 (1): 77–102.
  - 26 James, B.R. (1997). Synthesis of chiral amines catalyzed homogeneously by metal complexes. *Catal. Today* 37: 209–221.
  - 27 Lefebvre, G. and Chauvin, Y. (1970). Aspects of homogeneous catalysis. In: *Carlo Manfredi (Milano)*, vol. 1 (ed. R. Ugo), 107.
  - 28 Komiya, S. and Yamamoto, A. (1972). Reactions of hydrido complexes of ruthenium and rhodium with carbon dioxide involving reversible insertion. *J. Organomet. Chem.* 46 (2): 58–60.
  - 29 Keim, W., Behr, A., and Röper, M. (1982). *Comprehensive Organometallic Chemistry*, vol. 8 (ed. G. Wilkinson), 371. Oxford: Pergamon Press.
  - 30 Strupinska, J. (1991). Oligomerization of  $\alpha$ -olefins to higher oligomers. *Chem. Rev.* 91: 613–648.
  - 31 Keim, W. and Maas, H. (1996). Copolymerization of ethylene and carbon monoxide. *J. Organomet. Chem.* 514: 271–276.
  - 32 Bianchi, M., Menchi, G., Matteoli, U., and Piacenti, F. (1996). Homo and co-oligomerization of C2-C5 olefins in the presence of cluster ruthenium complex. *J. Organomet. Chem.* 526: 33–41.
  - 33 Katz, T.J. (1977). The olefin metathesis reaction. *Adv. Organomet. Chem.* 16: 283.
  - 34 Grubbs, R.H. (1982). *Comprehensive Organometallic Chemistry*, vol. 8 (ed. G. Wilkinson), 499. Oxford: Pergamon Press.
  - 35 Ivin, K.J. (1983). *Olefin Metathesis*. London: Academic Press.
  - 36 Herrmann, W.A., Schattenmann, W.C., Nuyken, O., and Glander, S.C. (1996). Allylruthenium (IV) complexes as highly efficient ROMP catalysts. *Angew. Chem.* 108: 1169–1170.
  - 37 Eleuterio, H.S. (1991). Olefin metathesis: chance favors those minds that are best prepared. *J. Mol. Catal.* 65: 55–61.
  - 38 Bäckvall, J.E., Akermark, B., and Ljunggren, S.O. (1979). Stereochemistry and mechanism for the palladium (II)-catalyzed oxidation of ethene in water (the Wacker process). *J. Am. Chem. Soc.* 101: 2411.

- 39 Bäckvall, J.-E. (1983). Palladium in some selective oxidation reactions. *Acc. Chem. Res.* 16: 335–342.
- 40 Romano, A.M. and Ricci, M. (1997). New efficient catalysts for the aerobic oxidation of ethers. *J. Mol. Catal. A: Chem.* 120: 71–74.
- 41 Wender, J. and Pino, P. (ed.) (1968). *Organic Syntheses via Metal Carbonyls*, vol. 1 (1968), vol. 2 (1977). New York: Wiley-Interscience.
- 42 Pino, P. (1980). Hydroformylation of olefinic hydrocarbons with Rh and Co catalysts. *J. Organomet. Chem.* 200: 223–242.
- 43 Orchin, M. (1981).  $\text{HCo}(\text{CO})_4$ , the quintessential catalyst. *Acc. Chem. Res.* 14: 259–266.
- 44 Sneed, R.P.A. (1982). Organic syntheses where carbon monoxide is the unique source of carbon. In: *Comprehensive Organometallic Chemistry*, vol. 8 (ed. G. Wilkinson), 19. Oxford: Pergamon Press.
- 45 Housecroft, C.E. and Sharpe, A.G. (2018). *Inorganic Chemistry* (print and electronic), 5e. Pearson Education Limited.
- 46 Ivin, K.J., Rooney, J.J., Stewart, C.D., and Green, M.L.H. (1978). Mechanism for the stereospecific polymerization of olefins by Ziegler–Natta catalysts. *Chem. Commun.* 604–606.
- 47 Lee, J.D. (2021). *Concise Inorganic Chemistry*, 4e. Wiley India Pvt. Ltd.
- 48 Bahri-Laleh, N., Hanifpour, A., Mirmohammadi, S.A. et al. (2018). Computational modeling of heterogeneous Ziegler–Natta catalysts for olefins polymerization. *Prog. Polym. Sci.* 84: 89–114.
- 49 Kobayashi, Y., Tang, Y., Kageyama, T. et al. (2017). Titanium-based hydrides as heterogeneous catalysts for ammonia synthesis. *J. Am. Chem. Soc.* 139 (50): 18240–18246.
- 50 Marakatti, V.S. and Gagneaux, E.M. (2020). Recent advances in heterogeneous catalysis for ammonia synthesis. *ChemCatChem* 12 (23): 5838–5857.
- 51 Liu, J.C., Ma, X.L., Li, Y. et al. (2018). Heterogeneous  $\text{Fe}_3$  single-cluster catalyst for ammonia synthesis via an associative mechanism. *Nat. Commun.* 9 (1): 1–9.
- 52 Yan, B., Wu, J., Xie, C. et al. (2009). Supercritical water gasification with  $\text{Ni}/\text{ZrO}_2$  catalyst for hydrogen production from model wastewater of polyethylene glycol. *J. Supercrit. Fluids* 50 (2): 155–161.
- 53 Miessler, G.L., Fischer, P.J., and Tarr, D.A. (2014). *Inorganic Chemistry*, 5e. Pearson Education, Inc.

## 15

## Cluster Compounds: Boranes, Heteroboranes, and Metallaboranes

Elyor Berdimurodov<sup>1</sup>, Khasan Berdimuradov<sup>2</sup>, Abduvali Kholikov<sup>1</sup>, Khamdam Akbarov<sup>1</sup>, Omar Dagdag<sup>3</sup>, Brahim El Ibrahimy<sup>4</sup>, and Dakeshwar Kumar Verma<sup>5</sup>

<sup>1</sup>National University of Uzbekistan, Faculty of Chemistry, Tashkent, 100034, Uzbekistan

<sup>2</sup>Shahrisabz branch of Tashkent Institute of Chemical Technology, Faculty of Industrial Viticulture and Food Production Technology, Shahrisabz, 181306, Uzbekistan

<sup>3</sup>Centre for Materials Science, College of Science, Engineering and Technology, University of South Africa, Johannesburg 1710, South Africa

<sup>4</sup>Ibn Zohr University, Department of Applied Chemistry, Faculty of Applied Sciences, 86153, Morocco

<sup>5</sup>Government Digvijay Autonomous Postgraduate College, Department of Chemistry, Rajnandgaon, Chhattisgarh, 491441, India

### 15.1 Introduction

#### 15.1.1 Fundamentals of Cluster Compounds: Boranes, Heteroboranes, and Metallaboranes

The boranes, heteroboranes, and metallaboranes-based cluster compounds contained mainly 1–12 boron atoms. The general formulation of borane-based clusters is  $B_xH_y$ . These compounds were constructed with only borane and hydrogen atoms. They differ from hydrocarbon compounds in their molecular structure and molecular weight [1]. The heteroboranes-based cluster compounds contained heteroatoms such as nitrogen, phosphorous, and other nonmetal atoms. The heteroatoms influence the molecular properties of cluster compounds. Recently, the transition metal elements have been combined with the boranes-based cluster compounds to form the metallaboranes clusters. Figure 15.1 illustrates the representations of the molecular and electronic structures of  $B_xH_y$  [2]. Figure 15.2 shows the crystal structures and numbers of skeletal electron pairs for borane-based clusters [2]. It is clear from these illustrations that the  $B_xH_y$ -based clusters have inner and outer spheres. There are two types of B—H bonds: endo B—H bonds and exo B—H bonds. According to the electronic representations, the hybrid  $sp_z$  orbitals are the centroid of the cluster compounds while the tangential  $p_x$  and  $p_y$  orbitals are covered by the cluster centers [2]. Table 15.1 indicates the classifications in borane clusters [1]. The borane-based clusters are classified according to the number of borane atoms ( $n$ ).

The elements of boranes, heteroboranes, and metallaboranes-based cluster compounds are chemically linked together by the nonclassically bonded compounds. This is due to the fact that in these compounds there are enough electrons to form the

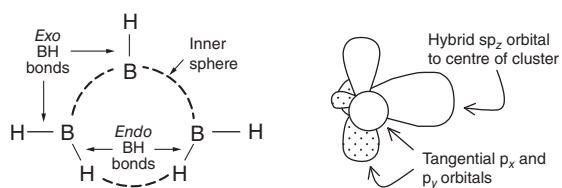


**Figure 15.1** Representations of molecular and electronic structures of  $B_xH_y$  [2].

<i>closo</i>	<i>nido</i>	<i>arachno</i>	SEP
5	4	3	<b>6</b>
6	5	4	<b>7</b>
7	6	5	<b>8</b>
8	7	6	<b>9</b>
9	8	7	<b>10</b>
10	9	8	<b>11</b>
11	10	9	<b>12</b>
12	11	10	<b>13</b>
13	12	11	<b>14</b>
14	13	12	<b>15</b>

**Figure 15.2** Crystal structures and numbers of skeletal electron pairs for borane-based clusters [2].

**Table 15.1** Classifications in borane clusters.

Cluster type	Chemical formula
<i>hypercloso-</i>	$B_nH_n$
<i>closo-</i>	$B_nH_n^{2-}$
<i>closo-</i>	$B_nH_n^{2-}$
<i>closo-</i>	$B_nH_n^{2-}$
<i>closo-</i>	$B_nH_n^{2-}$

**Table 15.2** Multi-cluster descriptors.

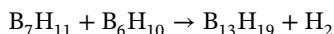
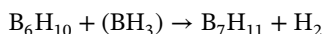
Prefix	Meaning
<i>megalo-</i>	Multiple conjoined clusters
<i>conjuncto-</i>	Conjoined clusters
<i>klado-</i>	Branched clusters

2-electron and 2-center bonds among the elements. William Lipscomb [3] described a new formulation for the bonding in borane-based clusters:

- 2-center 2-electron bonds (in B—B, B—H and BH<sub>2</sub>)
- 3-center 2-electron B—B—B bonds
- 3-center 2-electron B—H—B hydrogen bridges

This expression was extended by the lowest unoccupied orbitals and the highest occupied molecular orbital theories. For instance, the electrons of [B<sub>12</sub>H<sub>12</sub>]<sup>2-</sup> are equally distributed between 12 boron atoms [3].

The borane-based clusters have some multi-cluster boranes. Their molecular structure is different from the classical boranes. For instance, the BH<sub>3</sub> and B<sub>6</sub>H<sub>10</sub> compounds reacted with the simple borane clusters to form the *conjuncto*-borane clusters (Table 15.2). In these reactions, the borane cluster subunits are joined by the sharing of boron atoms [1].



On the other hand, the B—B bond is responsible for the subunit modifications. These clusters were formed by the PtBr<sub>2</sub> as a catalyst and ultraviolet irradiation of *nido*-boranes [4].

## 15.2 Main Part

### 15.2.1 Cluster Compounds of Boranes and Heteroboranes: Synthesis, Reactions, and Applications

#### 15.2.1.1 Basics

The cluster compounds of heteroboranes were synthesized by the formation of the B—S, B—P, B—N, and B—C bonds. These compounds are named sulfurboranes, phosphorboranes, nitroboranes, and carboranes. The cluster compounds of heteroboranes differ from each other related to their size, molecular structure, chemical or physical properties, and applications [5]. In another review, the Si, As, Se, Sb, and Te atoms also combined with the borane to form the B—Si, B—As, B—Se, B—Sb, and B—Te bonds [6].

#### 15.2.1.2 Synthesis

Joseph et al. [7] synthesized new S and Se-based heteroborane clusters according to the following reaction scheme (Figure 15.3). These reactions were carried out at high temperatures with the S and Se powders. The reaction was carried out in a toluene solvent. In the formed heteroborane cluster structure, the S and Se heteroatoms are directly linked with the borane atoms by the formation of the B—S and B—Se bonds.

Qiu [8] suggested the high thermal reaction for the synthesis of the carboranes (Figure 15.4). The reaction productivity was increased with the addition of Ag metal, in which the Ag acts as catalytic effects. The formed carboranes are stable in acidic and alcoholic solutions. These carboranes reactions were carried out at temperatures ranging from 600 to 700 °C.

Olejniczak et al. [9] synthesized some carboranes clusters (Figure 15.5) via solid support cleavage and deprotection, oxidation and capping, and coupling and detritylation modifications. All reactions were carried out by the B—H and C—H bonds.

#### 15.2.1.3 Reactions

Vrána et al. [10] studied some reactivity properties of cluster compounds of heteroboranes (Figure 15.6): *closo*-1,10-dicarbadeborane is referred to as para (p, green trace); *closo*-1,6-dicarbadeborane is referred to as meta (m, blue trace);

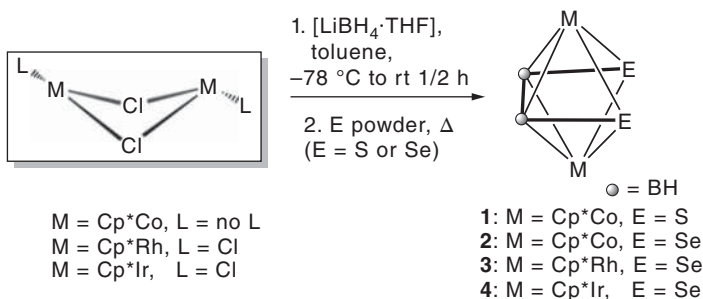
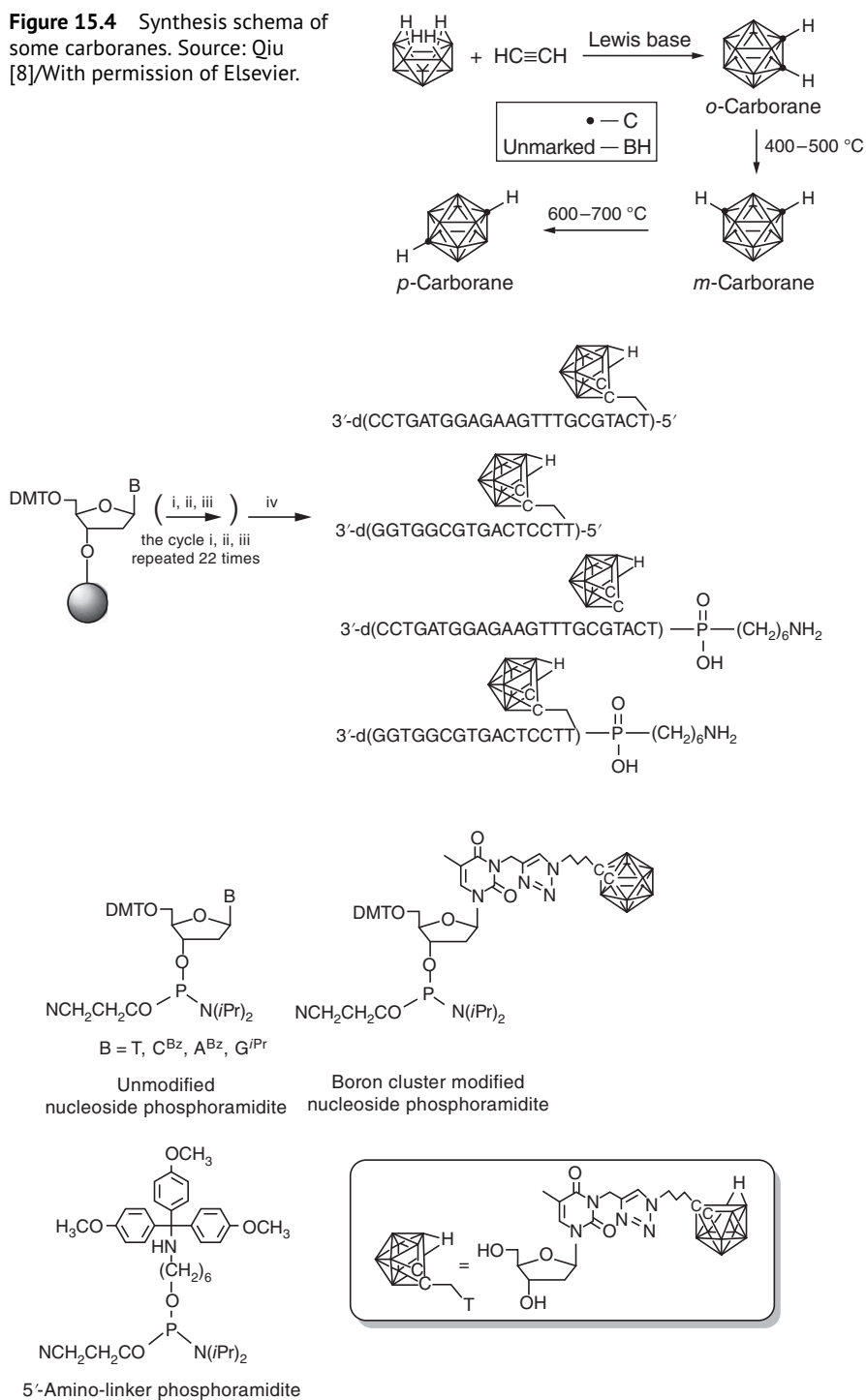


Figure 15.3 Synthetic procedure of S and Se-based heteroborane clusters [7].



**Figure 15.4** Synthesis schema of some carboranes. Source: Qiu [8]/With permission of Elsevier.



**Figure 15.5** Preparation of some carboranes clusters. Source: Olejniczak et al. [9]/MDPI/CC BY 4.0.

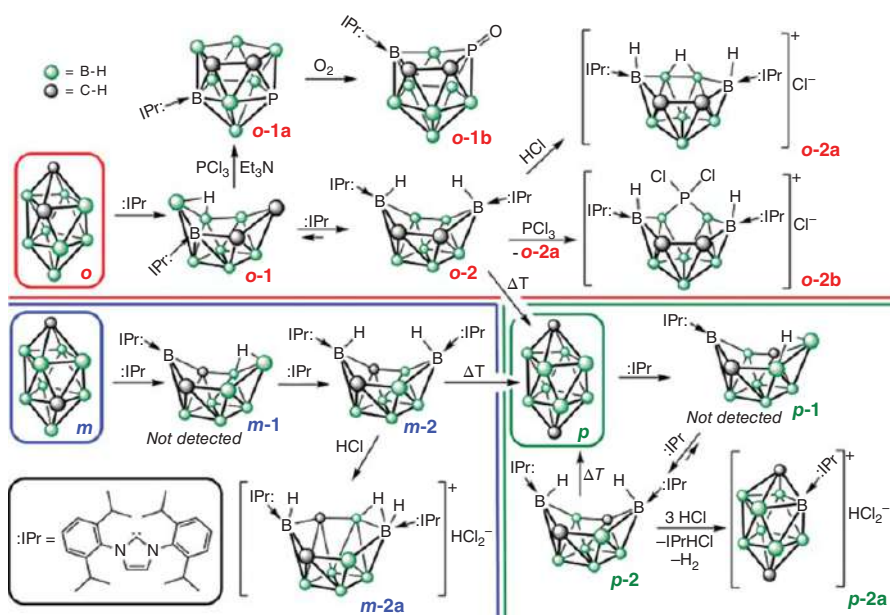


**Figure 15.6** Some reactivity properties of cluster compounds of heteroboranes: *closo*-1,10-dicarbadeborane is referred to as para (p, green trace); *closo*-1,6-dicarbadeborane is referred to as meta (m, blue trace); and *closo*-1,2-dicarbadeborane is referred to as ortho (o, red trace) [10].

*closo*-1,2-dicarbadekaborane is referred to as ortho (o, red trace). It is indicated that these compounds reacted with oxygen, hydrochloric acid, and  $\text{PCl}_3$  compounds.

Bakardjiev et al. [11] studied some nucleophilic reactions of heteroboranes (Figure 15.7). It was found that these cluster compounds have higher nucleophilic reaction ability. Almost all nucleophilic reactions are done by the B—H bonds. In this research work, the B—O bonds were formed by the nucleophilic reaction mechanisms.

#### 15.2.1.4 Applications

In modern times, carborane clusters are widely used in cancer therapy. They are modifying the cancer therapy drugs to enhance their effectiveness [12–14]. This is due to their excellent chemical and physical properties such as bioavailability, potency, and agent binding affinity. In breast cancer therapy, steroid estrogens play a significant role. The estrogen hormones have sensitive receptors, which support the interactions between the protein and DNA molecules. These hormones easily interacted with the DNA molecules, and as a result, gene transcription was carried out [12]. The heteroborane clusters are widely used to block the receptor part of hormones. Figure 15.8 shows the interactions of the carborane cluster with the estrogen receptors: estrogen receptor antagonist carborane derivatives (**11**, **12**); estrogen receptor agonist carborane derivatives (**10a–g**); hormone and  $\text{ER}\alpha$  antagonists (**7–9**).

The heteroboranes are modified with amino acids and proteins to create new bioactive peptides and unnatural amino acids. These compounds are used in medicine for various medicinal applications. On the other hand, the heteroboranes clusters are boron neutron capture therapy (BCNT), boron neutron capture synovectomy, and medical imaging [13, 15].

### 15.2.2 Cluster Compounds of Metallaboranes: Synthesis, Reactions, and Applications

#### 15.2.2.1 Basics

Metallaborane clusters compounds were mostly formed with the transition metals. The researchers devoted the metallaborane clusters into four categories related to the nature of interactions between the metal and borane atoms: transition metal complexes of boron; Me-complexes with boron-containing ligands; metallaboranes; and borides. The bonds between the borane and metal were built by nonclassical interactions: 2-center 2-electron bonds between boron and the metal center [16, 17].

#### 15.2.2.2 Synthesis

Bag et al. suggested a new synthesis methodology for metallaborane clusters (Figure 15.9) [18]. These synthetic reactions were done *in situ* models at low temperatures. Cr, Mo, and W  $(\text{CO})_4$  complexes were used. As a result, the previously reported compounds  $[\{\text{Cp}^*\text{W}(\text{CO})_2\}_2\text{B}_2\text{H}_2\text{M}(\text{CO})_4]$ , (M = Mo; W) [19], and  $[(\text{Cp}^*\text{W})_2\text{B}_5\text{H}_9]$  [20] were obtained, as well as the air and moisture-sensitive brown solids 1, 2, and 3.

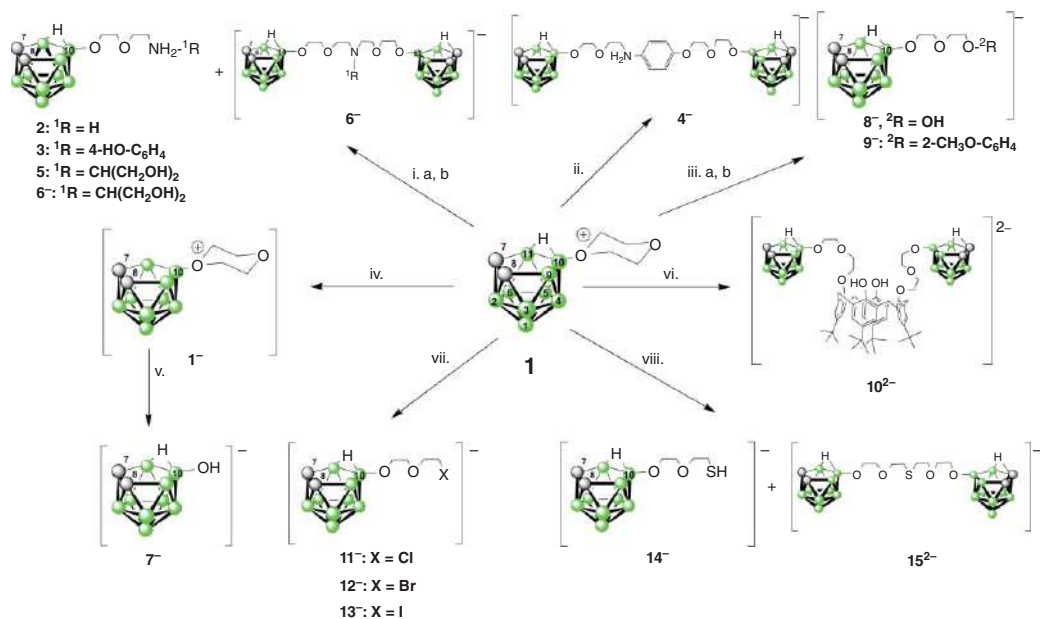


**Figure 15.7** Some nucleophilic reactions of heteroboranes. (b) for **9**<sup>-</sup>:  $\text{K}_2\text{CO}_3$ , 1-HO-2- $\text{CH}_3\text{O-C}_6\text{H}_4$  reflux; (iv) 2.5 M KOH rt; (v) 2.5 M KOH, reflux, (vi)  $\text{K}_2\text{CO}_3$ ,  $\text{CH}_3\text{CN}$ , *t*-Bu-calix[4]arene 0.5 equiv; (vii)  $\text{Bu}_4\text{NX}$ , 2 equiv ether, rt; (viii)  $\text{NaSH-H}_2\text{O}$  in excess, THF, rt (b) for **3**, THF rt; (ii) 1-HO- $\text{C}_6\text{H}_4$ -4- $\text{NH}_2$ ,  $\text{K}_2\text{CO}_3$  in  $\text{CH}_3\text{CN}$ , 80 °C; (iii) (a) for **8**<sup>-</sup>: KOH water-ether, rt (a) THF for **2**, ACE<sup>®</sup> pressure flask. Source: Bakardjiev et al. [11]/MDPI/CC BY 4.0.

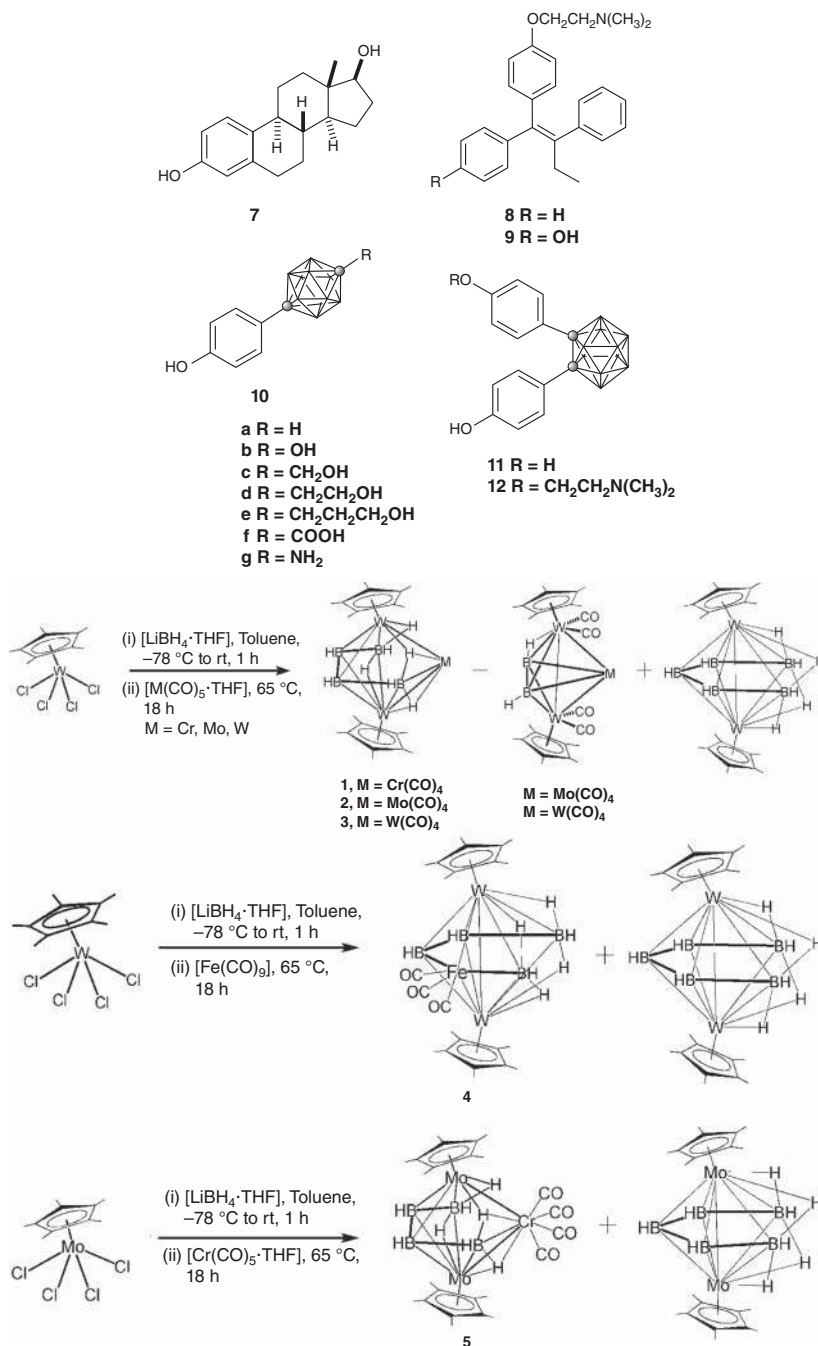


**Figure 15.8** The interactions of the carborane cluster with the estrogen receptors: estrogen receptor antagonist carborane derivatives (**11**, **12**); estrogen receptor agonist carborane derivatives (**10a–g**); and Hormone and ER $\alpha$  antagonists (**7–9**) [12].

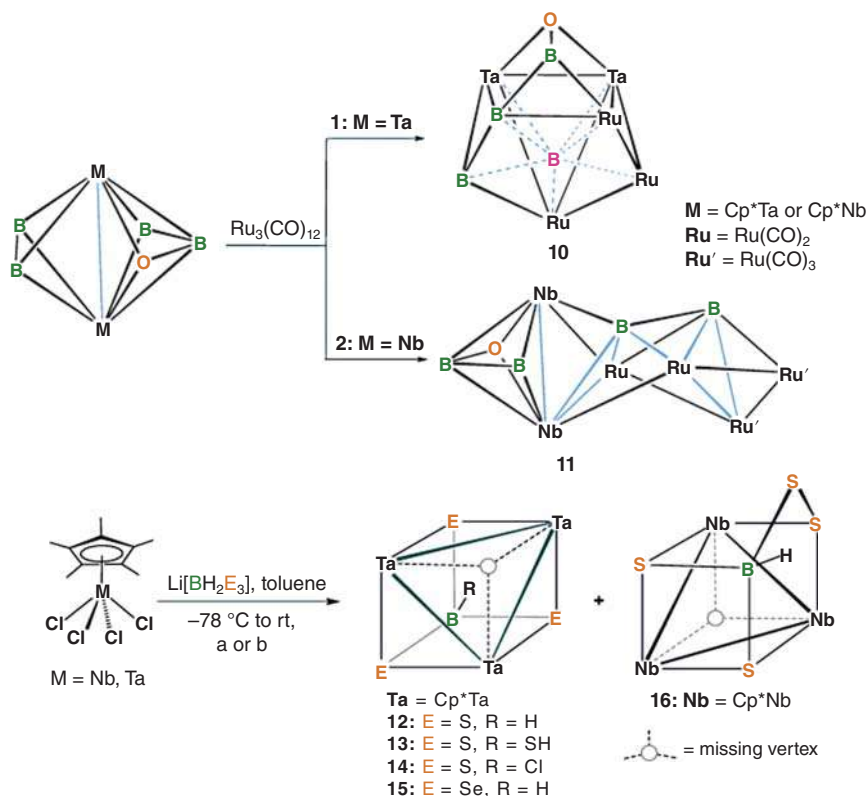


**Figure 15.9** Synthesis of some metallaborane clusters. Source: Bag et al. [18]/MDPI/CC BY 4.0.

Pathak et al. [21] synthesized the metallaborane clusters with Fe, Mo, Ta, Nb, Ru, and Co metals by the following reaction procedures (Figure 15.10). The Ru-based metallaborane clusters were prepared at room temperatures with a high reaction yield. The Nb-based metallaborane clusters were synthesized at very low ( $-78^\circ\text{C}$ ) temperatures. These reactions were carried out with the S and Se heteroborane clusters.

### 15.2.2.3 Reactions

Yuvaraj et al. [22] investigated some nucleophilic reactions (Figure 15.11). In these reactions, the nucleophilic agent of bromide chemically interacted with the borane atoms to form Br—B bonds. These reactions are done at higher temperatures. The chemical and physical properties of borane clusters were changed by the nucleophilic reactions.

### 15.2.2.4 Applications

The metallaborane clusters are mostly used in nanomedicine, targeted radiopharmaceuticals, medicinal imaging agents, cancer diagnostic agents, and BNCT of tumors

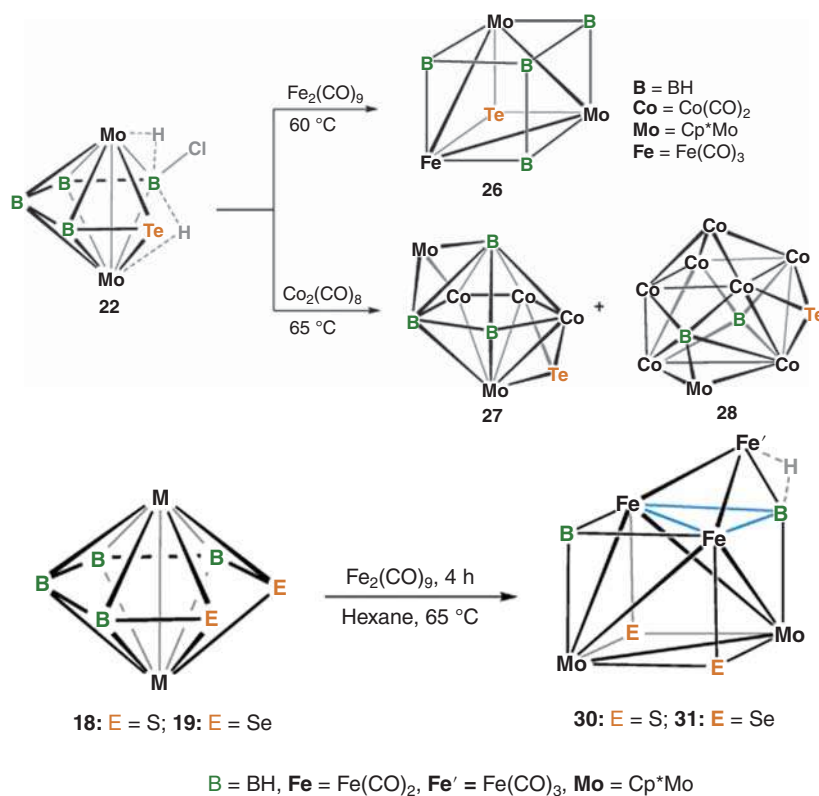


**Figure 15.10** Synthesis of some metallaborane clusters (Fe, Mo, Ta, Nb, Ru, and Co) [21].

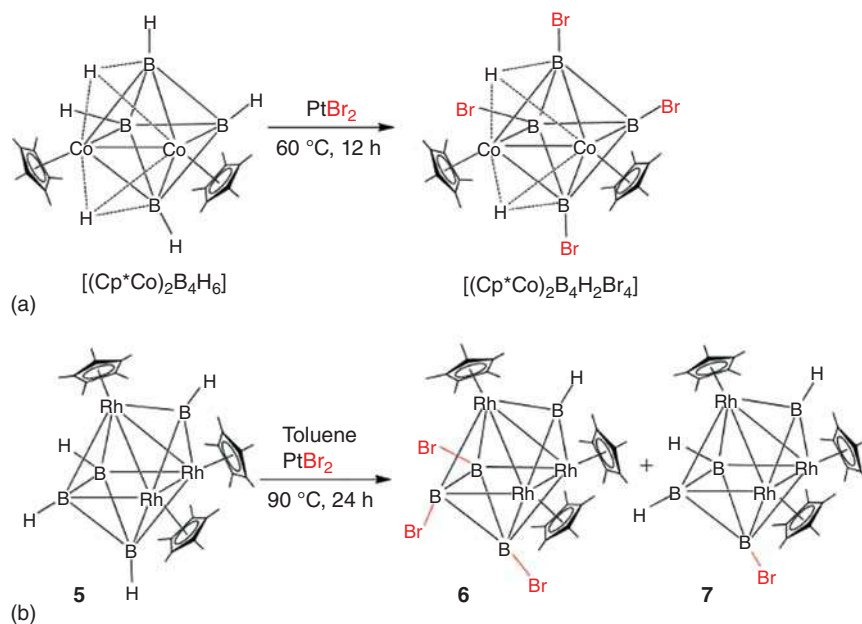


**Figure 15.11** Some reactions of metallaboranes [22].

[23–26]. The Rh-based metallacarboranes were performed to enhance molecular imaging.

### 15.3 Conclusion

In modern times, cluster compounds based on boranes, heteroboranes, and metallaboranes are widely used in cancer therapy. They are modifying cancer therapy drugs to enhance their effectiveness. This is due to their excellent chemical and physical properties such as bioavailability, potency, and agent binding affinity. In this chapter, the basics, synthesis procedures, reactions, chemical or physical properties, and applications of cluster compounds based on boranes, heteroboranes, and metallaboranes were reviewed and discussed with the relevant examples.

### References

- 1 Greenwood, N.N. and Earnshaw, A. (2012). *Chemistry of the Elements*. Elsevier.
- 2 Fox, M.A. and Wade, K. (2003). Evolving patterns in boron cluster chemistry. *Boron* 75 (9): 1315–1323.
- 3 Lipscomb, W.N. (1977). The boranes and their relatives. *Science* 196 (4294): 1047–1055.
- 4 Sneddon, L.G. (1987). Transition metal promoted reactions of polyhedral boranes and carboranes. *Pure Appl. Chem.* 59 (7): 837–846.
- 5 Olid, D., Nunez, R., Vinas, C., and Teixidor, F. (2013). Methods to produce B—C, B—P, B—N and B—S bonds in boron clusters. *Chem. Soc. Rev.* 42 (8): 3318–3336.
- 6 Schubert, D.M. (2000). Boron hydrides, heteroboranes, and their metall derivatives. In: *Kirk-Othmer Encyclopedia of Chemical Technology* (ed. C. Ley), 354. Wiley.
- 7 Joseph, B., Barik, S.K., Ramalakshmi, R. et al. (2018). Chemistry of triple-decker sandwich complexes containing four-membered open B<sub>2</sub>E<sub>2</sub> rings (E = S or Se). *Eur. J. Inorg. Chem.* 2018 (19): 2045–2053.
- 8 Qiu, Z. (2015). Recent advances in transition metal-mediated functionalization of *o*-carboranes. *Tetrahedron Lett.* 56 (8): 963–971.
- 9 Olejniczak, A.B., Nawrot, B., and Leśnikowski, Z.J. (2018). DNA modified with boron–metal cluster complexes [M(C<sub>2</sub>B<sub>9</sub>H<sub>11</sub>)<sub>2</sub>]<sup>+</sup>—synthesis, properties, and applications. *Int. J. Mol. Sci.* 19 (11): 3501.
- 10 Vrána, J., Holub, J., Samsonov, M.A. et al. (2021). Access to cationic polyhedral carboranes via dynamic cage surgery with N-heterocyclic carbenes. *Nat. Commun.* 12 (1): 1–7.
- 11 Bakardjiev, M., El Anwar, S., Baval, D. et al. (2020). Focus on chemistry of the 10-dioxane-*nido*-7,8-dicarba-undecahydrido undecaborate zwitterion; exceptionally easy abstraction of hydrogen bridge and double-action pathways observed in ring cleavage reactions with OH<sup>−</sup> as nucleophile. *Molecules* 25 (4): 814.



- 12 Zargham, E.O., Mason, C.A., and Lee, M.W. Jr., (2019). The use of carboranes in cancer drug development. *Int. J. Cancer Clin. Res.* 6: 110–113.
- 13 Armstrong, A.F. and Valliant, J.F. (2007). The bioinorganic and medicinal chemistry of carboranes: from new drug discovery to molecular imaging and therapy. *Dalton Trans.* 38: 4240–4251.
- 14 Issa, F., Kassiou, M., and Rendina, L.M. (2011). Boron in drug discovery: carboranes as unique pharmacophores in biologically active compounds. *Chem. Rev.* 111 (9): 5701–5722.
- 15 Valliant, J.F., Guenther, K.J., King, A.S. et al. (2002). The medicinal chemistry of carboranes. *Coord. Chem. Rev.* 232 (1–2): 173–230.
- 16 Braunschweig, H. and Colling, M. (2001). Transition metal complexes of boron – synthesis, structure and reactivity. *Coord. Chem. Rev.* 223 (1): 1–51.
- 17 Kennedy, J.D. (2016). Macropolyhedral metallaboranes – aspects of preparation, constitution and structure. *Coord. Chem. Rev.* 323: 71–86.
- 18 Bag, R., Saha, S., Borthakur, R. et al. (2019). Synthesis, structures and chemistry of the metallaboranes of group 4–9 with  $M_2B_5$  core having a cross cluster M—M bond. *Inorganics* 7 (3): 27.
- 19 Mondal, B., Bag, R., Ghorai, S. et al. (2018). Synthesis, structure, bonding, and reactivity of metal complexes comprising diborane (4) and diborene (2):  $\{[Cp^*Mo(CO)_2]_2\{\mu-\eta_2:\eta_2-B_2H_4\}\}$  and  $\{[Cp^*M(CO)_2]_2B_2H_2M(CO)_4\}$ , M = Mo, W. *Angew. Chem. Int. Ed.* 57 (27): 8079–8083.
- 20 Weller, A.S., Shang, M., and Fehlner, T.P. (1999). Synthesis of mono- and ditungstaboranes from reaction of  $Cp^*WCl_4$  and  $[Cp^*WCl_2]_2$  with  $BH_3 \cdot THF$  or  $LiBH_4$  ( $Cp^* = \eta_5-C_5Me_5$ ). Control of reaction pathway by choice of monoboron reagent and oxidation state of metal center. *Organometallics* 18 (1): 53–64.
- 21 Pathak, K., Nandi, C., and Ghosh, S. (2022). Metallaheteroboranes with group 16 elements: aspects of synthesis, framework and reactivity. *Coord. Chem. Rev.* 453: 214303.
- 22 Yuvaraj, K., Roy, D.K., Arivazhagan, C. et al. (2015). Chemistry of early and late transition metallaboranes: synthesis and structural characterization of periodinated dimolybdaborane  $[(Cp^*Mo)_2B_4H_3I_5]$ . *Pure Appl. Chem.* 87 (2): 195–204.
- 23 Ma, P., Pellizzeri, T.M.S., Zubieta, J., and Spencer, J.T. (2020). Synthesis and characterization of oxonium functionalized rhenium metallaborane. *J. Chem. Crystallogr.* 50 (1): 14–20.
- 24 El-Zaria, M.E., Janzen, N., and Valliant, J.F. (2012). Room-temperature synthesis of Re(I) and Tc(I) metallocarboranes. *Organometallics* 31 (16): 5940–5949.
- 25 Goszczyński, T.M., Kowalski, K., Leśnikowski, Z.J., and Boratyński, J. (2015). Solid state, thermal synthesis of site-specific protein–boron cluster conjugates and their physicochemical and biochemical properties. *Biochim. Biophys. Acta* 1850 (2): 411–418.
- 26 Laskova, J., Kozlova, A., Białek-Pietras, M. et al. (2016). Reactions of *closo*-dodecaborate amines. Towards novel bis(*closo*-dodecaborates) and *closo*-dodecaborate conjugates with lipids and non-natural nucleosides. *J. Organomet. Chem.* 807: 29–35.

## Contents

**Preface** *xix*

**About the Editors** *xxi*

<b>1</b>	<b>Organometallic Compounds: The Fundamental Aspects</b>	<b>1</b>
	<i>Geetha B. Markandeya and Srinivasa Budagumpi</i>	
1.1	Introduction	1
1.1.1	Organometallic Chemistry	1
1.1.2	Organometallic Compounds	1
1.1.3	Structure of Organometallic Compound	1
1.2	Milestones in Organometallic Compounds	2
1.2.1	Equation (1.1): Synthesis of First Organometallic Compound	2
1.2.2	Equation (1.2): Preparation of Zeise's Salt	2
1.2.3	Equations (1.3)–(1.5): Preparation of Organochlorosilane Compound	3
1.2.4	Equation (1.6): Synthesis of First Metal Carbonyl Compound	3
1.2.5	Equation (1.7): Synthesis of First Binary Metal Carbonyl Complex	3
1.2.6	Equation (1.8): Barbier Reaction	3
1.2.7	Equation (1.9): Synthesis of Organic Compound Using a Grignard Reagent	4
1.2.8	Equations (1.10) and (1.11): Synthesis of Alkyl lithium Compound	4
1.2.9	Equations (1.12) and (1.13): Synthesis of Organolithium Compound	4
1.2.10	Equation (1.14): Hydroformylation Reaction	4
1.2.11	Equation (1.15): Synthesis of Organochlorosilane Compound	4
1.2.12	Equation (1.16): Trimerization of Acetylene	5
1.2.13	Equation (1.17): Synthesis of Ferrocene	5
1.2.14	Equation (1.18): Asymmetric Catalysis Reaction	5
1.2.15	Equation (1.19): Palladium Catalyzed Suzuki Coupling Reaction	6
1.2.16	Equation (1.20): Synthesis of Bucky Ferrocene	6
1.3	Stability of Organometallic Compounds	9
1.4	Properties of Organometallic Compounds	9
1.5	Basic Concepts in Organometallic Compounds	9
1.5.1	18-Electron Rule	9
1.5.1.1	Statement of 18 Electron Rule	10
1.5.1.2	Examples	11

1.5.2	$\Pi$ –Back Bonding or Back Donation	12
1.5.3	Hapticity $\eta^x$	12
1.6	Hapticity of Ligands	12
1.7	Change in Hapticity	13
1.8	Hapticity Verses Denticity	14
1.9	Counting of Electrons and Finding out Metal–Metal Bonds	15
1.9.1	Calculating the Number of Metal–Metal Bonds	15
1.9.2	Writing the Probable Structure of Compound	15
1.9.3	How to Draw the Probable Structure of $\text{Ni}(\eta^1\text{-C}_3\text{H}_5)(\eta^3\text{-C}_3\text{H}_5)$	15
1.9.4	How to Draw the Probable Structure of $(\mu\text{-CO})\text{-}[\eta^5\text{-CpRh}]_3(\text{CO})$	15
1.10	Metals of Organometallic Compounds	16
1.10.1	Organometallic Compounds of Transition Metals	17
1.10.2	The Bonding and Structure in Different Metal complexes	17
1.10.2.1	Alkene Complexes	17
1.10.2.2	Allyl Complexes	17
1.10.2.3	Carbonyl Complexes	17
1.10.2.4	Metallocenes	18
1.10.2.5	Dihydrogen Complexes	18
1.10.2.6	Transition Metal Carbene Complex	18
1.11	Importance of Organometallic Compounds	19
1.11.1	Types of Organometallic Compounds	19
1.11.2	Uses of Organometallic Compounds	20
1.12	Conclusions	20
	References	21

## 2 Nomenclature of Organometallic Compounds 25

*Raj K. Rathore, Sadhucharan Mallick, and Bhavabhuti Prasad*

2.1	Introduction	25
2.2	Aim of the Nomenclature	26
2.3	Type of Nomenclature System	26
2.3.1	Binary Nomenclature	26
2.3.2	Substitutive Nomenclature	27
2.3.3	Additive Nomenclature or Coordination nomenclature	27
2.4	Concepts and Conventions	28
2.4.1	Oxidation Number	28
2.4.2	Coordination Number	29
2.4.3	Chelation	29
2.4.4	Ligands	29
2.4.5	Specifying Connectivity – The Kappa ( $\kappa$ ) Convention	30
2.4.6	Bridging Ligands – The Mu ( $\mu$ ) Convention	31
2.4.7	Hapticity – The Eta ( $\eta$ ) Convention	33
2.5	Regulations Concerning the Nomenclature of Transition Element Organometallic Compounds	36
	References	46

<b>3</b>	<b>Classification of Organometallic Compounds</b>	<b>47</b>
	<i>Mukesh K. Tyagi, Gokul R. Nishad, Dakeshwar Kumar Verma, Lei Guo, and Elyor Berdimurodov</i>	
3.1	Introduction	47
3.2	Classification of Organometallic Compound	48
3.2.1	Sigma-Bonded Organometallic Compound	48
3.2.2	$\pi$ -Bonded Organometallic Compounds	50
3.2.3	Ionic Bonded Organometallic Compounds	51
3.2.4	Multicentered Bonded Organometallic Compounds	53
3.2.4.1	Based on Hapticity ( $\eta_1$ to $\eta_8$ ):	53
3.3	Grignard Reagent (G.R.)	54
3.3.1	Physical Properties	54
3.3.2	Chemical Properties	54
3.3.2.1	Alkanes	54
3.3.2.2	Alkenes	56
3.3.2.3	Alkynes	56
3.3.2.4	Ethers	56
3.3.2.5	Reaction with carbon dioxide	56
3.3.2.6	Insertion Reaction	56
3.3.2.7	Synthesis of Silicones	56
3.3.2.8	Nucleophilic Substitution	57
3.4	Organozinc Compounds	59
3.4.1	Physical Properties	59
3.4.2	Chemical Properties	59
3.5	Organolithium Compounds	61
3.5.1	Reaction Resembling Grignard Reagents	61
3.5.2	Reactions Different from Grignard Reagents	64
3.6	Organosulfur Compounds	65
3.6.1	Physical Properties	65
3.6.2	Chemical Properties	65
3.6.3	Properties Different from Alcohols	67
3.7	Conclusion	69
	References	69
<b>4</b>	<b>Synthesis Methods of Organometallic Compounds</b>	<b>71</b>
	<i>Omar Dagdag, Rajesh Haldhar, Seong-Cheol Kim, Elyor Berdimurodov, Ekemini D. Akpan, and Eno E. Ebenso</i>	
4.1	Introduction	71
4.2	Synthesis Methods of Organometallic Compounds	72
4.2.1	Electrochemical Methods for the Synthesis of Organometallic Compounds	72
4.2.1.1	Synthesis of Cyano Cu(I) Complexes in the Electrochemical Cell	72
4.2.1.2	Synthesis of an Organorhenium Cyclopentadienyl Complex in the Electrochemical Cell	72

4.2.1.3	Synthesis of N-heterocyclic Carbene Complexes in the Electrochemical Cell	73
4.2.1.4	Synthesis of Organocopper (I) $\pi$ -Complexes in the Electrochemical Cell	73
4.2.1.5	Synthesis of Organonickel $\sigma$ -Complexes in the Electrochemical Cell	73
4.2.2	Synthesis of Organic Compounds in the Electrochemical Cell by Metal organic Catalysts	75
4.2.2.1	The Synthesis of Organic Compounds in the Electrochemical Cell by the Ni-Organic Catalysts	75
4.2.2.2	The Synthesis of Organic Compounds in the Electrochemical Cell by the Pd-Organic Catalysts	75
4.2.2.3	Synthesis of Organic Compounds in the Electrochemical Cell by the Sm-Organic Catalysts	78
4.2.3	Synthesis of Organometallic Nucleosides	79
4.2.3.1	A Category: Main Compounds	79
4.2.3.2	A1 Subcategory: Main Compounds	79
4.2.3.3	B Category: Main Compounds	80
4.2.3.4	C Category: Main Compounds	81
4.2.3.5	C1 Subcategory: Main Compounds	81
4.2.3.6	D Categories: Main Compounds	82
4.3	Conclusions	84
	Acknowledgment	84
	Authors Contributions	84
	Conflicts of Interest	84
	References	84
<b>5</b>	<b>Metal Carbonyls: Synthesis, Properties, and Structure</b>	<b>87</b>
	<i>Ramesh Rengan</i>	
5.1	Introduction	87
5.2	Classification of Metal Carbonyls	87
5.2.1	Classification Based on Coordinated Ligands	87
5.2.1.1	Homoleptic Carbonyls	88
5.2.1.2	Heteroleptic Carbonyls	88
5.2.2	Classification Based on Number of Metals and the Constitution of Carbonyls	88
5.2.2.1	Mononuclear Carbonyl Complexes	88
5.2.2.2	Polynuclear Carbonyl Complexes	89
5.3	Synthesis of Metal Carbonyls	90
5.3.1	Direct Reaction of Metal with Carbon Monoxide	90
5.3.2	Reductive Carbonylation	90
5.3.3	Photolysis and Thermolysis	91
5.3.4	Abstraction of CO from a Reactive Organic Carbonyl Compounds	91
5.4	Properties of Metal Carbonyls	92
5.4.1	Physical Properties	92
5.4.2	Chemical Properties	92

5.4.2.1	Ligand Substitution Reactions	92
5.4.2.2	Reaction with Sodium Metal	95
5.4.2.3	Reaction with Sodium Hydroxide	95
5.4.2.4	Reaction with Halogens	95
5.4.2.5	Reaction with Hydrogen	96
5.4.2.6	Reaction with Nitricoxide (NO)	96
5.4.2.7	Disproportionation	96
5.5	Structure of Metal Carbonyls	97
5.5.1	Structures of Some Mononuclear Carbonyl Complexes	97
5.5.2	Structures of Some Bi and Polynuclear Carbonyl Complexes	98
5.6	Bonding in Metal Carbonyls	99
5.6.1	Formation of Mixed Atomic Orbitals	99
5.7	Synergistic Effect	103
5.8	Conclusion	103
	Further Reading	104
	References	104
<b>6</b>	<b>Metal–Carbon Multiple Bonded Compounds</b>	<b>107</b>
	<i>Rakesh Kumar Sahu, Mukesh Kumar Tyagi, and Rajesh Haldhar</i>	
6.1	Introduction	107
6.2	Nomenclature	109
6.3	Classifications	111
6.3.1	Metal–alkylidene Complexes	111
6.3.2	Metal–alkylidyne Complexes	111
6.4	Structure	111
6.4.1	Alkylidene (Carbene)	111
6.4.2	Carbyne (Alkylidyne)	113
6.5	Preparation Methods	114
6.5.1	Metal–alkylidene Complexes	114
6.5.1.1	By Nucleophilic Carbene	115
6.5.1.2	By Electrophilic Alkylidenes	116
6.5.2	Metal–alkylidyne Complexes	118
6.6	Important Reactions	119
6.6.1	Reaction of Alkylidene Metathesis	119
6.6.2	Important Reaction of Alkylidyne Metathesis	124
6.7	Applications	125
	References	127
<b>7</b>	<b>Metallocene: Synthesis, Properties, and Structure</b>	<b>131</b>
	<i>Amarpreet K. Bhatia, Priyanka Singh, and Shippi Dewangan</i>	
7.1	Introduction	131
7.2	Structure of Metallocene	132
7.3	Synthesis of Metallocene	134
7.4	Chemical Properties of Metallocene	136
7.4.1	Ferrocene and Its Derivatives	136

7.4.2	Other Metallocene Sandwiches	138
7.4.3	Main-group Metallocene	139
7.4.4	Metal-bis-arene Sandwich Complexes	140
7.4.4.1	General View	140
7.4.4.2	Structure	142
7.4.4.3	Reactions	142
7.5	Conclusion	144
	References	144
<b>8</b>	<b><math>\sigma</math>-Complexes, <math>\pi</math>-Complexes, and <math>\eta^n</math>-C<sub>n</sub>R<sub>n</sub> Carbocyclic Polyenes-Based Organometallic Compounds</b>	<b>147</b>
	<i>Shippi Dewangan, Jeenat Aslam, and Amarpreet K. Bhatia</i>	
8.1	Introduction	147
8.2	$\sigma$ -Bond Containing Organometallic Compounds	148
8.2.1	Metal Carbonyl	148
8.2.1.1	General Overview	148
8.2.1.2	Syntheses of Metal Carbonyls	148
8.2.1.3	Structure of Metal Carbonyls	149
8.2.1.4	Reactions of Metal Carbonyls	150
8.2.2	Metal-Alkyl, -Vinyl, and -Hydride Complexes	150
8.2.2.1	Metal Alkyls	150
8.2.2.2	Metal Vinyls	152
8.2.2.3	Metal Hydrides	152
8.2.2.4	Metal-Carbene Complexes	154
8.3	$\pi$ -Bond Containing Organometallic Compounds	156
8.3.1	Metal-Olefin Complexes	156
8.3.1.1	General Overview	156
8.3.1.2	Syntheses of Metal-Olefin Complexes	157
8.3.1.3	Reactions of Metal-Olefin Complexes	157
8.3.2	Metal-Diene Complexes	157
8.3.3	Metal-Alkyne Complexes	158
8.3.4	$\pi$ -Allyl Complexes	158
8.3.4.1	Structure of $\pi$ -Allyl Complexes	158
8.3.4.2	Syntheses of $\pi$ -Allyl Complexes	159
8.3.4.3	Reactions of $\pi$ -Allyl Complexes	160
8.4	$\eta^n$ -C <sub>n</sub> R <sub>n</sub> Carbocyclic Polyenes Containing Organometallic Compounds	161
8.4.1	Cyclopropenyls, $\eta^3$ -C <sub>3</sub> R <sub>3</sub>	161
8.4.2	Cyclobutadienes, $\eta^4$ -C <sub>4</sub> R <sub>4</sub>	161
8.4.3	Cyclopentadienyls, $\eta^5$ -C <sub>5</sub> R <sub>5</sub>	162
8.4.3.1	General Overview	162
8.4.3.2	Structure of Metallocene	162
8.4.3.3	Syntheses of Metallocene	163
8.4.3.4	Chemical Properties of Metallocene	164
8.4.3.5	Applications of Metallocene	165

- 8.5 Conclusion 166  
References 166

## 9 Organometallic Complexes of the Lanthanides and Actinides 169

*Shippi Dewangan, Amarpreet K. Bhatia, and Priyanka Singh*

- 9.1 Introduction 169
- 9.2 Methods of Preparation 169
- 9.2.1 Salt Elimination 171
- 9.2.2 Metal Vapor Synthesis Method 173
- 9.2.3 Metathesis Reaction Method 174
- 9.2.4  $\sigma$ -Bond Metathesis 174
- 9.2.5 Acid-Base Method 175
- 9.3 Organometallic Compounds of Lanthanides 175
- 9.3.1 Types 175
- 9.3.1.1  $\sigma$ -Bonded Complexes 176
- 9.3.1.2  $\pi$ -Bonded Organometallic Compounds 177
- 9.4 Organometallic Compounds of Actinides 180
- 9.4.1 Types 180
- 9.4.2  $\sigma$ -Bonded Complexes 180
- 9.4.3  $\pi$ -Bonded Complexes 182
- 9.4.3.1 Cyclopentadienyl Derivatives 182
- 9.5 Stability 185
- 9.5.1 Maintaining Anhydrous and Anaerobic Conditions 185
- 9.5.2 Avoiding Elimination Reactions 186
- 9.5.3 Blocking the Coordination Sites 186
- 9.5.4 Donor-functionalized Chelating Pendant Donor Ligands 186
- 9.6 Properties 186
- 9.6.1 Thermodynamic and Kinetic Considerations 187
- 9.6.2 Solvation 187
- 9.6.3 Aggregation 187
- 9.6.4 Donor-Acceptor Interactions 187
- 9.6.5 Salt Occlusion or Ate Complexation 188
- 9.6.6 Neutral  $\pi$ -Donor Ligation 188
- 9.6.7 Agostic Interactions 189
- 9.6.8 Complex Agglomeration 189
- 9.6.9 Ligand Exchange and Redistribution Reactions 189
- 9.6.10 Insertion Reactions 190
- 9.6.11 Elimination Reactions 190
- 9.6.12 Redox Chemistry 191
- 9.6.13 Reaction Sequences – Catalytic Cycles 192
- 9.7 Applications of Organolanthanoids and Organoactinoids 193
- 9.7.1 Catalytic Applications 193
- 9.7.1.1 Catalysis of Polymerization 193
- 9.7.1.2 Catalysts and Reagents for Reduction Processes 193



9.7.1.3	Catalysts and Reagents for Oxidation Processes	195
9.7.2	Miscellaneous Applications	197
9.8	Conclusion	197
	Further Reading	197
<b>10</b>	<b>Bioorganometallic Chemistry</b>	<b>201</b>
	<i>Priyanka Tiwari</i>	
10.1	Introduction	201
10.2	Cobalamin: Vitamin B <sub>12</sub> -Coenzyme	202
10.2.1	Occurrence and Function	202
10.2.2	Structure	202
10.2.3	B <sub>12</sub> -dependent Enzymes	203
10.2.4	Occurrence	203
10.2.5	Function	203
10.3	Metalloproteins	204
10.3.1	Occurrence	204
10.3.2	Functions	204
10.3.3	Electron Transferases	204
10.3.3.1	Flavodoxins	205
10.3.3.2	Blue Copper Proteins	205
10.3.3.3	Iron–Sulfur Proteins	205
10.3.3.4	Cytochromes	207
10.4	Oxidoreductase	207
10.4.1	Iron–Porphyrin Complexes	208
10.4.2	Monoxygenases	208
10.5	Nitrogenases-catalyzing Nitrogen Fixation	209
10.6	Nickel Enzymes: CODH	211
10.7	Conclusion	212
	References	213
<b>11</b>	<b>Important Reactions of Organometallic Compounds</b>	<b>215</b>
	<i>Sandeep K. Vaishnav and Priyanka Singh</i>	
11.1	Introduction	215
11.2	Reactions Involving Gain or Loss of Ligands	215
11.2.1	Associative and Dissociative Substitution	216
11.2.1.1	Dissociation of Carbonyls	216
11.2.1.2	Dissociation of Nitrosyls	217
11.2.1.3	Dissociation of Phosphine	217
11.2.2	Oxidative Addition and C–H Bond Activation	218
11.2.2.1	Mechanism	219
11.2.2.2	Binuclear Oxidative Addition	221
11.2.2.3	Cyclometallations	222
11.2.2.4	Nucleophilic Displacement	222
11.3	Reductive Elimination and Pd-catalyzed Cross Coupling	223
11.3.1.1	Binuclear Reductive Elimination	224

- 11.4 Reactions Involving Modification of Ligands 225
    - 11.4.1 Insertion 225
      - 11.4.1.1 Carbonyl Insertion (Alkyl Migration) 226
      - 11.4.1.2 Olefin Insertion 230
      - 11.4.1.3 Other Insertion Reaction 232
    - 11.4.2 Hydride Elimination 233
      - 11.4.2.1 Avoidance of  $\beta$ -hydrogen Elimination 235
    - 11.4.3 Abstraction 236
      - 11.4.3.1 Nucleophilic Abstraction 237
  - 11.5 Conclusion 240
  - References 240
- 
- 12 Characterization Techniques of Organometallic Compounds 245**  
*Javad B. M. Parambath and Ahmed A. Mohamed*
    - 12.1 Introduction 245
    - 12.2 Conventional Methods 246
      - 12.2.1 Nuclear Magnetic Resonance (NMR) Spectroscopy 246
      - 12.2.2 Infrared and Raman Spectroscopy 248
      - 12.2.3 UV-Visible Spectroscopy 251
      - 12.2.4 X-Ray Crystallography 252
      - 12.2.5 Mass Spectroscopy 253
      - 12.2.6 Elemental Analysis 255
    - 12.3 Unconventional Methods 256
      - 12.3.1 Neutron Activation Analysis 256
      - 12.3.2 X-Ray Photoelectron Spectroscopy 256
      - 12.3.3 Electron Diffraction Crystallography and Microelectron Diffraction 258
      - 12.3.4 Mössbauer Spectroscopy 259
      - 12.3.5 Electroanalytical Methods 259
    - 12.4 Conclusion 260
    - References 261
- 
- 13 Organometallic Reagents 267**  
*Ranjan K. Basak and Ashish K. Asatkar*
    - 13.1 Organoboron Reagents 267
      - 13.1.1 Introduction 267
      - 13.1.2 Main Organoboron Reagents and Their Reactions 267
        - 13.1.2.1 Hydroboration and Subsequent Reactions 267
        - 13.1.2.2 Suzuki Coupling 273
        - 13.1.2.3 Acyltrifluoroborates 277
        - 13.1.2.4 Allylation 278
        - 13.1.2.5 Chan-Lam coupling 279
        - 13.1.2.6 Petasis Reaction 279
    - 13.2 Organocopper Reagents 280
      - 13.2.1 Introduction 280

- 13.2.2 Types of Organocuprates Reagents 281
  - 13.2.2.1 Gilman Reagent ( $R_2CuM$ ) 281
  - 13.2.2.2 Higher Order Organocuprates ( $R_2CuCNLi_2$ ) 282
  - 13.2.2.3 Grignard Copper(I) Reagents ( $RMgX \cdot CuY$ ) 282
- 13.2.3 Reactions of Organocuprates 283
  - 13.2.3.1 Increasing Chain Length of Alkyl halides 283
  - 13.2.3.2 Alkylation of the Allylic Halides 284
  - 13.2.3.3 Reaction with Vinyl Halides 284
  - 13.2.3.4 Alkylation of Acyl Halides 284
  - 13.2.3.5 Epoxide Opening 285
  - 13.2.3.6 Conjugate Additions 285
  - 13.2.3.7 Conjugate Addition in Presence of Lewis Acid and Electrophiles 286
  - 13.2.3.8 O-Trapping and C-Trapping Reaction 287
  - 13.2.3.9 Synthesis of Allenes 287
- 13.3 Organopalladium Reagents 288
  - 13.3.1 Introduction 288
  - 13.3.2 Types of C–C Cross-Coupling Reaction Catalyzed by Palladium Metal 289
    - 13.3.2.1 Heck Reaction 289
    - 13.3.2.2 Negishi Coupling 290
    - 13.3.2.3 Suzuki Coupling 291
    - 13.3.2.4 Stille Coupling 291
    - 13.3.2.5 Kumada Coupling 292
    - 13.3.2.6 Hiyama Coupling 293
    - 13.3.2.7 Sonogashira Coupling 293
    - 13.3.2.8 Butchwald–Hartwig Coupling 294
    - 13.3.2.9 Cyanation Reaction 294
    - 13.3.2.10 Carbonylation Reaction 295
- 13.4 Grignard Reagents 296
  - 13.4.1 Introduction 296
  - 13.4.2 Synthesis 296
  - 13.4.3 Reactivity 297
  - References 298

## 14 Homogeneous and Heterogeneous Catalysis by Organometallic Complexes 301

*Ratnakar D. Shukla, Bhawna Jain, Kuleshwar Patel, Priyanka Singh, Dakeshwar Kumar Verma, Reema Sahu, and Raghvendra K. Mishra*

- 14.1 Introduction 301
- 14.2 Organometallic Compounds and Homogeneous Catalysis 302
- 14.3 Catalytic Elementary Reactions 303
  - 14.3.1 Isomerization 304
    - 14.3.2 Alkene Isomerization 305
    - 14.3.3 Alkyne Isomerization 305
    - 14.3.4 Diene Isomerization 306

- 14.4 Hydrogenation 306
- 14.5 Carbon–Carbon Bond Formation 307
- 14.6 Metathesis 308
- 14.7 Oxidation 309
- 14.8 Reactions with Carbon Monoxide 311
- 14.9 Heterogenous Catalysis 311
  - 14.9.1 Ziegler–Natta Catalyst 313
    - 14.9.1.1 Stereoregularity 313
    - 14.9.2 Water Gas Reaction 315
    - 14.9.3 Zeolites 316
  - 14.10 Conclusion 317
  - References 318
  
- 15 Cluster Compounds: Boranes, Heteroboranes, and Metallaboranes 321**  
*Elyor Berdimurodov, Khasan Berdimuradov, Abduvali Kholikov, Khamdam Akbarov, Omar Dagdag, Brahim El Ibrahim, and Dakeshwar Kumar Verma*
  - 15.1 Introduction 321
    - 15.1.1 Fundamentals of Cluster Compounds: Boranes, Heteroboranes, and Metallaboranes 321
  - 15.2 Main Part 324
    - 15.2.1 Cluster Compounds of Boranes and Heteroboranes: Synthesis, Reactions, and Applications 324
      - 15.2.1.1 Basics 324
      - 15.2.1.2 Synthesis 324
      - 15.2.1.3 Reactions 324
      - 15.2.1.4 Applications 327
    - 15.2.2 Cluster Compounds of Metallaboranes: Synthesis, Reactions, and Applications 327
      - 15.2.2.1 Basics 327
      - 15.2.2.2 Synthesis 327
      - 15.2.2.3 Reactions 330
      - 15.2.2.4 Applications 330
  - 15.3 Conclusion 332
  - References 332
  
- 16 Applications of Organometallic Compounds for Carbon Dioxide Fixation, Reduction, Gas Adsorption, and Gas Purification 335**  
*Zhoveta Yhobu, Monica Vijayakumar, Nagaraju D. Hanumantharayudu, and Srinivasa Budagumpi*
  - 16.1 Organometallic Compounds for Fixation of CO<sub>2</sub> 335
  - 16.2 Organometallic Compounds in Reduction of CO<sub>2</sub> 336
    - 16.2.1 Nickel Complexes 338
    - 16.2.2 Iron and Manganese Complexes 339

- 16.2.3 Copper and Cobalt Complexes 341
- 16.2.4 Palladium Complexes 342
- 16.2.5 Ruthenium, Rhenium, and Rhodium Complexes 343
- 16.2.6 N-Heterocyclic Carbenes 344
- 16.3 Organometallic Compounds in Gas Adsorption and Purification 346
  - 16.3.1 Metal Organic Frameworks (MOFs) for Gas Adsorption 347
  - 16.3.2 Classification of MOFs as Adsorbents for Gas Separation 348
    - 16.3.2.1 Rigid MOFs as Adsorbents for Selective Gas Separation 348
    - 16.3.2.2 Flexible MOFs as Adsorbents for Gas Separation 349
  - 16.4 Gas Purification with MOFs 352
    - 16.4.1 Kinetic Separation 352
    - 16.4.2 Quantum Sieving Effect for H<sub>2</sub>/D<sub>2</sub> Separation 352
    - 16.4.3 Membrane-Based Gas Separation 353
  - References 353
- 17 Emerging Role of Organometallic Compounds for Drug Delivery, Renewable Energy, and Wastewater Treatment 357**  
*Shokoh Parham, Hadi Sarvari, Seyed-Shirin Parham, and Hadi Nur*
  - 17.1 Introduction 357
  - 17.2 Organometallic Compounds 359
  - 17.3 Organometallic Compounds for Drug Delivery 363
  - 17.4 Organometallic Compounds for Renewable Energy 364
  - 17.5 Organometallic Compounds for Wastewater Treatment 365
  - 17.6 Conclusion 366
  - 17.7 Outlook 366
  - Acknowledgment 367
  - References 367
- 18 Computational Approaches in Some Important Organometallic Catalysis Reaction 375**  
*Pratibha Gumasta, Naresh C. Deshmukh, Aseel A. Kadhem, Snehlata Katheria, Reena Rawat, and Bhawana Jain*
  - 18.1 Introduction 375
  - 18.2 Computational Method 376
    - 18.2.1 Geometry Calculation 377
    - 18.2.2 Energy 378
  - 18.3 Organometallic Catalysis Reactions 379
    - 18.3.1 Palladium 379
      - 18.3.1.1 C—H Bond Activation 380
      - 18.3.1.2 Coupling Reactions 382
    - 18.3.2 Nickel 386
      - 18.3.2.1 Coupling Reactions 386
      - 18.3.2.2 C—O Bond Activation 388
      - 18.3.2.3 Cyclization Reactions 389
      - 18.3.2.4 Olefin Functionalization 389

18.3.3	Rhodium	390
18.3.3.1	Hydrogenation	390
18.3.3.2	Olefin Functionalization	391
18.3.3.3	Reactions of Rh Carbenoids and Nitrenoids	391
18.3.4	Iridium	394
18.3.4.1	Hydrogenation	394
18.3.4.2	Other Bond Activations	396
18.4	Conclusion	396
	References	397
	<b>Index</b>	409

# Metal Organic Frameworks

Fundamentals to Advanced

Edited by  
Bhawana Jain  
Dakeshwar Kumar Verma  
Ajaya Kumar Singh  
Jai Singh



## CHAPTER 10

# Density functional theory–based molecular modeling for metal-organic frameworks

Swati Chandrawanshi<sup>1</sup>, Rakesh Kumar Sahu<sup>2</sup>, Sushama Sahu<sup>3</sup>,  
Dakeshwar Kumar Verma<sup>4</sup> and Reema Sahu<sup>4</sup>

<sup>1</sup>Department of Chemistry, Laxman Prasad Baidh Government Girls College Bemetara, Bemetara, Chhattisgarh, India

<sup>2</sup>Department of Chemistry, BCS Government PG College Dhamtari, Dhamtari, Chhattisgarh, India

<sup>3</sup>School of Studies in Chemistry, Pt. Ravishankar Shukla University, Raipur, Chhattisgarh, India

<sup>4</sup>Department of Chemistry, Government Digvijay Autonomous Postgraduate College, Rajnandgaon, Chhattisgarh, India

### 10.1 Introduction

Activated carbon, zeolite, covalent organic framework (COFs), and metal-organic frameworks (MOFs) are such amorphous or crystalline materials, which come under the category of mainly porous materials, which are mainly composed of coordination of metal and carbon-based material [1,2]. This type of porous material is formed by the reaction of organic molecules or inorganic materials with metal ions [3]. Due to their porous nature, their application is done in a very broad area, which is the demand of the present. Major applications include water absorption, biomedical remediation, toxic gas adsorption, toxic removal and energy application, chemical sensing energy applications, light harvesting, and catalysis [4,5]. Broad surface MOFs are eco-friendly, large variety in pore size, cost-effective, and are more energy efficient due to which they are being used as new advanced material for many different applications [6,7]. Recently more than ten thousand MOF materials have been synthesized and hole crystals in formation of above materials enlisted in Cambridge structural database (SD) [8]. For the structural study and their various reactions, both experimental and computational, that is, hypothetically, are equally important. Additionally, Fig. 10.1A and B represents the hypothetical and synthesized MOFs through cube and number of research paper based on only MOFs and MOFs with simulation, respectively [10,11]. Theoretical analysis has many advantages, which include less time-consuming, cost-effective, green nontoxic, and most importantly, there is no need for any sophisticated laboratory.



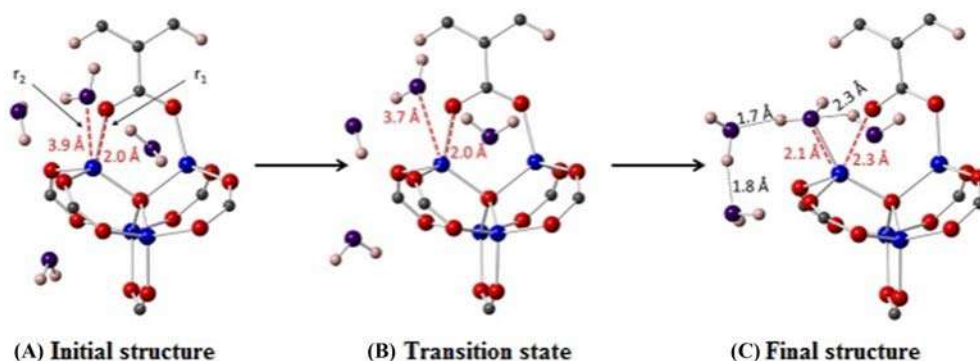


**Figure 10.1** MOF-5 water insertion method. (A) An enlarged view of the MOF-5 structure showing four water molecules attached close to the ZnO cluster. (B) Transition state as determined by the NEB calculations at  $T = 0$  K. (C) The final MOF-5 structure with a Zn-O bond that has been disrupted by the addition of a single water molecule [9]. *NEB*, Nudged elastic band.

## 10.2 Role of density functional theory in the development of metal-organic frameworks for water adsorption and separation applications

Water is everywhere. The molecule that separates life and death is water, more than half of the world will face a water shortage. Water is scarce in the desert areas. Due to a lack of rain, resources are scarce, and in those areas with more water, either a dearth of clean drinking water or a persistent concern about its purity continues to be a problem. The diminishing underground water resources in agricultural areas of the world, security concerns associated with the fact that 160 countries import their water, the increasing salinity of large bodies of water nearby desalination plants and the environmental effects of continued fossil fuel use on weather patterns are additional factors aggravating this “global water challenge.” There is additionally the growing demand for clean water as a result of the expanding global population and the negative health effects on societies where clean water is scarce [12]. Therefore, MOFs are a potential solution for water adsorption and separation applications [13]. MOFs are network-structured porous crystal coordination polymer materials that self-assemble from metal ions (or clusters) and organic ligands. These materials are referred to as porous coordination polymers (PCPs) because they self-assemble. MOFs as organic–inorganic hybrid materials have both inorganic and organic characteristics. They have different compositions and structures, specific surface area, and high porosity, and are simple to create. Due to their potential for use in gas storage, gas purification, gas separation, catalysis, sensors, and environmental remediation, MOFs have attracted a lot of research attention such as extensively and rapidly studied in the field of environmental remediation [14–16].

### 10.2.1 Role of density functional theory calculations

For MOF structure and complex architecture determination, property prediction and computational characterization, including large-scale screening and geometrical properties of MOFs, diffusion and adsorption processes in MOFs, density functional theory (DFT) was employed. To investigate chemical stability, mechanical, photophysical, optical, and magnetic properties, photoluminescence, porosity, and semiconductor or metallic nature, DFT calculations have been used in the MOF field. The development of MOF/polymer membranes, adsorbents for CO<sub>2</sub> uptake, separation of C<sub>2</sub>H<sub>2</sub>/CH<sub>4</sub>, C<sub>2</sub>H<sub>2</sub>/CO<sub>2</sub>, and inert gases, radionuclides sequestration, water adsorption, the prediction of MOF analogs with open-metal sites, studies of chemical bonding, the prediction of energies by quantum mechanics, and other promising advancements have been done [17]. Various MOFs have been studied for water adsorption applications. The kinetics and thermodynamics of water insertion and adsorption into the MOF-5 as a model compound at 0 and 300 K were predicted using the thermodynamic integration, transition-state finding methods, and van der Waals augmented DFT. Water adsorption processes were determined at different MOF-5 sites. The computations showed that the exothermic nature of H<sub>2</sub>O insertion into the MOF-5 structure only occurs when a significant number of water molecules were coadsorbed close to a Zn-O cluster (Fig. 10.1). Breaking the Zn-O bonds makes it simpler for water molecules to enter (the energy barrier is 0.04 eV at 300 K and 0.17 eV at 0 K) [9]. Zang et al. (2013) described copper-based MOFs for the water adsorption applying by DFT calculations. Water adsorption was examined in the CuMBTC (methyl-1,3,5-benzenetricarboxylate) and CuEBTC (ethyl-1,3,5-benzenetricarboxylate) on the basis of the 1200 DFT-D2 calculations with good agreement between calculated and experimental results [18]. Cr-doped UiO-66 was studied for water adsorption, and results showed that Cr-doped UiO-66 has higher pore volume and specific surface area than pure UiO-66. Cr doping improved the water adsorption performances of UiO-66. The water uptake of Cr-UiO-66 was 0.69 g g<sup>-1</sup> (at 25°C and p/p<sub>0</sub> = 0.9) [19].

### 10.2.2 Adsorption mechanisms

Three types of mechanisms were studied for water adsorption in MOFs: (1) chemisorption on open metal sites, (2) capillary condensation, and (3) cluster adsorption [20].

#### 10.2.2.1 Chemisorption on open metal sites

Zirconium (IV)-based metal-organic framework (Zr-MOF) membrane (i.e., UiO-66-Zr) contains Zr<sub>6</sub>O<sub>4</sub>(OH)<sub>4</sub> cores and bridged by 1,4-benzene dicarboxylate (BCD) linkers, which shows chemisorptions on open metal sites. On alumina hollow fibers, pure-phase Zr-MOF (also known as UiO-66) polycrystalline membranes were created using

an in situ solvothermal synthesis technique. The integrity and functionality of the membrane were verified through single-gas permeation and ion rejection experiments. Therefore, chemisorptions of the water in the secondary building units (SBUs) are totally reversible [21,22].

### 10.2.2.2 Capillary condensation

Capillary condensation occurs before water is adsorbed in pores with diameters greater than a critical number  $D_c$ . The adsorption branch never achieves thermodynamic balance, so there is always a hysteresis loop between the adsorption and desorption branches. Pores larger than 2.0 nm are predicted to exhibit capillary condensation behavior and adsorption-desorption hysteresis [23]. Kusgens et al. (2009) observed water physisorption properties and the water stability of the MOFs HKUST-1 ( $=(\text{Cu}_3(\text{BTC})_2)$  (BTC = benzene-1,3,5-tricarboxylate)), ZIF-8, MIL-101, MIL-100(Fe), and DUT-4 ( $=\text{Al}(\text{OH})(\text{NDC})$ ) (NDC = naphthalene-2,6-dicarboxylate). The water physisorption isotherms were compared to nitrogen physisorption isotherms, and the chemical stability after water adsorption was studied [24].

### 10.2.2.3 Cluster adsorption

Matériel Institut Lavoisier-53 (MIL-53) ( $M = \text{Cr}, \text{Fe}, \text{Al}, \text{and Ga}$ ) is made up of 1D channels that are connected by an unlimited number of rod-like SBUs using benzene-1,4-dicarboxylate (BDC) linkers. As demonstrated by functionalized MIL-53(Al)-OH, it exhibits a noticeable respiratory effect carried on by water molecules. In the initial MIL-53(Al), which is in its narrow pore form, only one water molecule is adsorbed on each metal unit at saturated vapor pressure. When the relative pressure is close to  $p/p_0 = 0.75$ , breathing is made feasible by the addition of OH groups on the BDC linkers. Pore filling takes place, and in the big pore phase of MIL-53(Al)-OH (free dimensions of  $1.7 \text{ nm} \times 1.2 \text{ nm}$ ), five water molecules are eventually adsorbed per metal unit. At a relative pressure of approximately  $p/p_0 = 0.47$  in the desorption branch, the structure transitions back to the narrow pore phase (free dimensions of  $1.9 \text{ nm} \times 0.8 \text{ nm}$ ), leaving a sizable hysteresis loop ascribed to the breathing behavior [25].

## 10.2.3 Applications involving water adsorption

### 10.2.3.1 Heat pump and chillers

MOFs or PCPs are inorganic-organic composite materials with a stable three-dimensional porous metal-ligand network. In terms of porosity and reversible guest exchange characteristics, PCPs or MOFs are the inorganic-organic equivalents of zeolites. Adsorption heat pumps (AHPs) or thermally driven adsorption chillers (TDCs) are two low-temperature heat transformation uses that are increasingly focusing on microporous water-stable PCPs with high water uptake capacities. TDCs or AHPs can greatly reduce primary energy consumption and greenhouse gas emissions produced

by industrial or domestic heating and cooling processes by using solar or waste heat as the operating energy. TDCs and AHPs are founded on the sequential adsorption and evaporation of coolant liquids, ideally water, under particular circumstances. The microporosity and hydrophilicity of the sorption substance were used to drive and regulate the process. The reversible evaporation and following adsorption of a working fluid have emerged as the most promising of several working principles. The fundamental procedure is depicted in Fig. 10.2 [26,27] (Fig. 10.3).

### 10.2.3.2 Proton conducting metal-organic frameworks

A proton exchange membrane fuel cell (PEMFC) is an attractive energy conversion device that generates power from clean renewable sources like hydrogen and air. A polymer electrolyte membrane (PEM) separates a porous anode from a porous cathode in a PEMFC. The anode receives hydrogen and is oxidized to create an electron and a proton. The proton exchange membrane carries protons to the cathode. Once at the cathode, arriving protons and electrons join with oxygen to form water. The electric circuit that the fuel cell is powering experiences a current movement as a result. The crystalline structure of MOFs makes it possible to precisely understand the structural changes that occur upon hydration, making them suitable candidates for applications involving water adsorption. They have received a lot of interest as PEM materials for PEMFCs because of these factors [28]. The “vehicle mechanism” and “Grotthus hopping” are the two most well-known explanations for proton conduction mechanism. The vehicle mechanism described by proton diffusion is occurring along with the diffusion of the vehicle (water molecule). Here, the proton is transported by counter-diffusion of unprotonated water. Water diffusion in the media is crucial for this kind of proton motion. The Grotthus process does not require the transport of water because proton motion is transferred from one water molecule to another via hydrogen bonding [29,30].

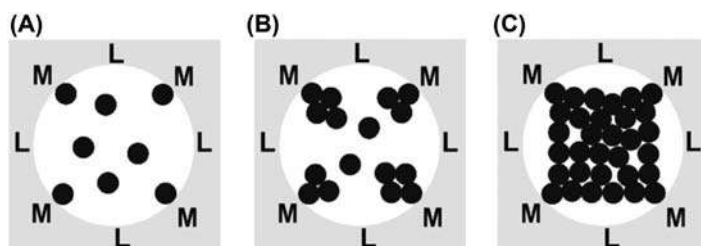


**Figure 10.2** Bridging effect: sketch of the formation of hydrogen bridging in the pores of the adsorbent and the resulting voids. (A) Adsorption of single water molecules to the hydrophilic centers. (B) Formation of water clusters due to hydrogen binding. (C) Filled pore with free voids between the water agglomerates. M and L denote the metal cluster and the organic linker, respectively. Black dots depict the water molecules [9]. Source: Reproduced with permission from Y. Ming, N. Kumar, D.J. Siegel, *Water adsorption and insertion in MOF-5*, *ACS Omega*, 2 (2017), 4921. 2009 @ ELSEVIER.

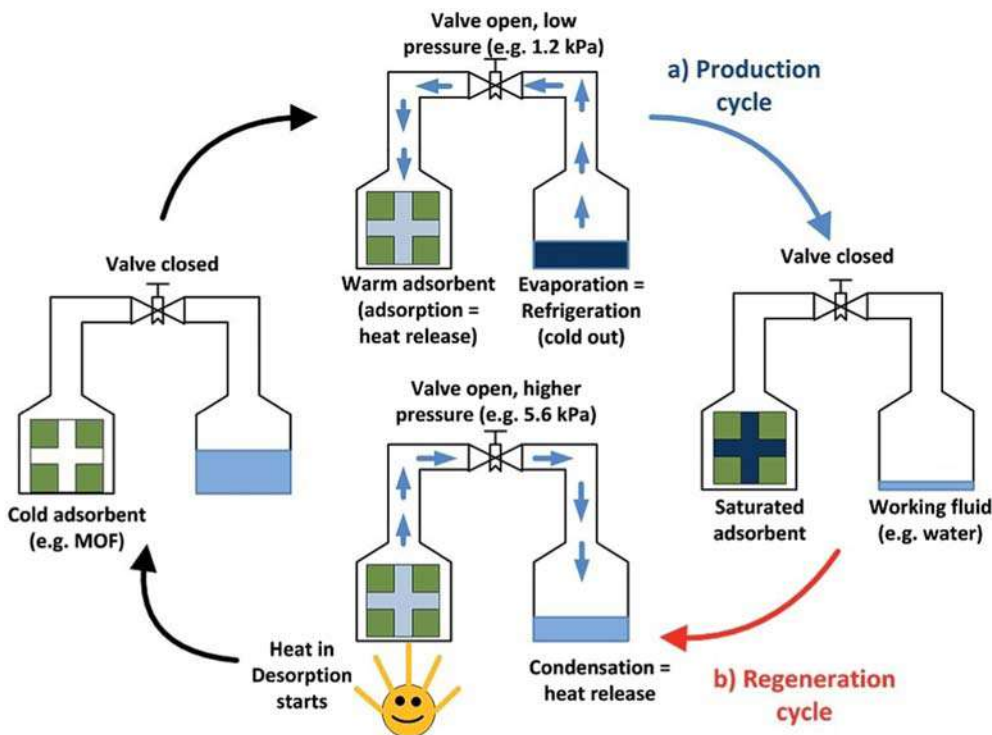


Figure 10.3 Illustration of the basic principle for adsorption chillers or heat pumps [26].

### 10.3 Role of density functional theory in the development of metal-organic frameworks for gas storage, adsorption, and separation

DFT is a computational method used to study the electronic properties of materials, including MOFs. MOFs are a class of porous materials that consist of metal ions or clusters linked by organic ligands. MOFs are known for their high surface area, tunable pore size, and high thermal and chemical stability. These properties make MOFs promising materials for gas storage, adsorption, and separation applications [31,32]. DFT has played a significant role in the development of MOFs for gas storage, adsorption, and separation. Specifically, DFT calculations can predict the properties of MOFs, such as their adsorption capacity and selectivity toward different gas molecules. DFT can also provide insights into the fundamental interactions between gas molecules and MOFs, such as the nature of the binding sites and the strength of the adsorption [3,33,34].

Using DFT, researchers can study the electronic structure of MOFs, including the distribution of electron density and the location of the metal ions and ligands. This information can help researchers design MOFs with specific properties that are

optimized for gas storage, adsorption, and separation applications [33–36]. DFT can also help researchers understand how MOFs can be synthesized and optimized. For example, DFT can predict the energy barriers associated with various synthesis routes, allowing researchers to identify the most efficient synthesis methods. DFT can also help researchers identify ways to modify existing MOFs to enhance their gas storage, adsorption, and separation properties [1,37–39].

For example, DFT can be used to predict the adsorption energy and selectivity of carbon dioxide ( $\text{CO}_2$ ) and methane ( $\text{CH}_4$ ) in different MOFs. These predictions can guide the selection of MOFs with high selectivity for  $\text{CO}_2$  over  $\text{CH}_4$ , which is important for the removal of  $\text{CO}_2$  from natural gas or flue gas streams. DFT can also be used to study the diffusion of gas molecules in MOFs, which is important for designing MOFs with high gas uptake and fast gas transport [40–42].

### 10.3.1 Modeling carbon dioxide ( $\text{CO}_2$ ) trap in metal-organic frameworks

Due to the industrial revolution and the growing use of fossil fuels,  $\text{CO}_2$  gas emissions have increased seriously in the last several decades. As a result, greenhouse effect, global warming, and climate change are clearly being observed. To deal with this warning, a number of researches have been conducted to trap  $\text{CO}_2$  and convert it into valuable gases. Among them, material-based storage for regeneration is a more efficient and less energy-consuming technology. There are many efforts to trap  $\text{CO}_2$  in MOFs, which can be used for further  $\text{CO}_2$  separation [43–45].

One of the key factors in modeling  $\text{CO}_2$  adsorption in MOFs is the choice of exchange–correlation functional. These functionals are used to describe the electronic interactions between the  $\text{CO}_2$  molecules and the MOF framework. However, there are many different functionals to choose from, each with its own strengths and weaknesses. To accurately model  $\text{CO}_2$  adsorption, it is important to benchmark these functionals against experimental data and choose the one that best reproduces the observed behavior [41,42,44].

Another important factor is the role of dispersive interactions, also known as van der Waals interactions, in estimating binding energy (BE). These interactions are attractive forces that arise from fluctuations in the electron density of the  $\text{CO}_2$  molecule and the MOF framework. They can play a significant role in determining the stability of the  $\text{CO}_2$ –MOF complex, but they are often neglected in traditional modeling approaches. Including these interactions requires more advanced computational methods, such as DFT with dispersion corrections or methods based on the random phase approximation [40,41,43,45].

Professor Donald J. Siegel and his research group have made significant contributions to the field of computational materials science, particularly in the area of MOFs. They have developed and applied a range of theoretical and computational tools to understand the behavior of MOFs, including molecular dynamics simulations, Monte Carlo simulations, and DFT calculations. The authors have compared the BE with respect to the

experimental enthalpies ( $\Delta H$ ) of CO<sub>2</sub> adsorption on four variants of M2(DOBDC) [46–48] (M = Mg, Ni, Co) and Cu-HKUST-1 [49] based on Vienna Ab initio Simulation Package code that has been used for the DFT calculations. To describe the interaction between core and valence electrons, the projector-augmented wave has been used [50,51]. Transition metals (i.e., Co, Ni, and Cu) containing MOFs and spin-polarized calculations have been performed. 500 eV has been set for plane-wave cutoff energy. The energy functional of eight different forms has been used for the energy of per CO<sub>2</sub> molecule adsorption. These include the Ceperley-Alder LDA [52], PBE GGA [53], Grimme's DFT-D2 method [54], and five vdW-DFs in which the exchange–correlation energy is given by one of optB86b–vdW [55], optB88–vdW [56], optPBE–vdW [56], revPBE–vdW [57], and the modified PW86 functional, referred to as rPW86–vdW [58].

#### 10.4 Density functional theory studies at catalytic activity of metal-organic frameworks and derivatives

MOFs and their derivatives are crystalline materials having extended frameworks in their structure. Therefore, DFT has been used to examine the proposed reaction mechanism for catalytic applications of MOFs and its derivatives. This shows the approximate reaction enthalpy at 0 K with a zero-point energy correction, which has been calculated using vibrational frequencies. While, either harmonic or anharmonic low-frequency modes could be applied for the calculation of entropy. Further, free energies of reaction mechanism are used to analyze the temperature-dependent equilibrium constants [59,60]. Thus, the calculations by DFT are convincing methods specifically in the area of localized catalytic reactions.

MOFs are constructed by different metal-containing clusters or ions through the inorganic building node and organic ligands as linkers. Sometimes, coordinatively unsaturated metal site shows catalytic effect in MOFs and derivatives. These sites are shown to be structurally identical and well separated. Accordingly, their truncated structures are used to examine the reaction mechanism by DFT method [60]. For instance, FeCo-PBA-derived bimetallic alloys with N-doped graphene layers encapsulation were given by Chen et al. [61]. The work reported that the linkers of cyanide group directly transformed into N-doped graphene throughout the annealing treatment, and the process does not need the addition of other carbon sources. Here, the presence of graphene layer prevents the agglomeration of FeCo alloys and corrosion of the alloy particles also, during the electrocatalysis process. In this work, DFT calculations indicated a decrease in the H adsorption free energy ( $\Delta G_{H^*}$ ) of N atoms in graphene and the formation of metal–graphene composites contribute to the high electrocatalytic activity.

## 10.5 Role of density functional theory in the structure exploration of metal-organic frameworks and derivatives

Nowadays, it is urge to develop more efficient renewable energy sources on the basis of electrocatalysis-based energy renovation and storage machineries [62,63]. However, most of these techniques are cost-effective and shortage of availability, such as iridium and ruthenium oxides ( $\text{IrO}_2$  and  $\text{RuO}_2$ ), thus cannot be taken for its large-scale applications [62,64,65]. Consequently, it is of great importance to develop competent electrocatalytic techniques by the use of economic resources. For this, MOFs have been constructed using metal ions and organic linkers with periodical arrangements. The MOFs show well-defined coordination environments with their flexible structure, which can easily be examined by DFT method. The DFT model is extensively used for the analysis of MOF pores, particularly if mesopores close to 2 nm in width or micropores ( $<2$  nm) are present [66]. In many experiments, DFT technique is used to figure out the nature of interaction also at the microscopic level.

The electron density of different molecules is dependent on the three spatial coordinates, while the many-body wave function depends on the entire spatial coordinates of all electrons in the system. Thus, the electron density is a computationally simpler object, where DFT vacates the many-particle electron [67,68]. DFT can easily examine the number of atoms present in the molecular species using modern computing infrastructures. It plays a key role as it precisely provides NMR spectra, vibrational analysis, molecular geometries, atomic charges, electronic energies, excited state molecules, etc. [69]. This also gives information about the catalytic centers inside the molecule. The fundamental principle of DFT is to study the structural information of many components in which the total energy of the system is a unique functional of the electron density [70]. Thus, it does not need to compute the wave function of the entire body. MOFs are also known as PCPs. These are linked by coordination bonds between metal-containing units in which a variety of organic moieties, such as imidazolates, carboxylates, pyridyl, and azolates, could be present and forms a crystalline framework [70–72].

A lot of research works have been presented using DFT to predict the structure of the active site in different components. Specifically, Lubitz et al. proposed comparative study of the experimental g tensor magnitudes and orientations for the Ni-C and Ni-L forms by DFT calculations [73]. The method provides better results between experimental and theoretical results in correspondence to Ni(III) species, while a hydride bridges between two metal atoms and to Ni(I) species with a vacant bridge position, respectively, are presented. In other work, Stein and Lubitz showed two H atoms are simultaneously coordinated to the Ni ion in the Ni-R form [74].



## 10.6 Conclusion

DFT could be containing different energy contributions, including the correlation contributions, which are directly associated with the behavior and mutual interactions between the electrons. Instead of them, several advantages of DFT for gas absorption, catalytic activity, and structure exploration are as follows: (1) DFT method possesses one-electron structure, thus, results can easily incorporate the correlation effects. (2) DFT studies of open-shell systems are equitable and known to enhance the importance of high-spin contributions. (3) On taking the different MOFs and derivatives for different spin, DFT results are observed to be near to the higher multiplicity contributions. Therefore, DFT wave functions are relatively close to a pure spin representation. (4) The method provides better results especially for molecular systems by characterizing near-degenerate states.

## Conflict of interest

Authors declared no conflict of interest.

## References

- [1] H. Demir, H. Daglar, H.C. Gulbalkan, G.O. Aksu, S. Keskin, Recent advances in computational modeling of MOFs: from molecular simulations to machine learning, *Coord. Chem. Rev.* 484 (2023) 215112.
- [2] R. Anderson, J. Rodgers, E. Argueta, A. Biong, D.A. Gómez-Gualdrón, Role of pore chemistry and topology in the CO<sub>2</sub> capture capabilities of MOFs: from molecular simulation to machine learning, *Chem. Mater.* 30 (18) (2018) 6325–6337.
- [3] R. Jose, G. Bangar, S. Pal, G. Rajaraman, Role of molecular modelling in the development of metal-organic framework for gas adsorption applications, *J. Chem. Sci.* 135 (2) (2023) 1–29.
- [4] L. Grajciar, O. Bludsky, P. Nachtigall, Water adsorption on coordinatively unsaturated sites in CuBTC MOF, *J. Phys. Chem. Lett.* 1 (23) (2010) 3354–3359.
- [5] Q. Yang, C. Zhong, Molecular simulation of carbon dioxide/methane/hydrogen mixture adsorption in metal-organic frameworks, *J. Phys. Chem. B* 110 (36) (2006) 17776–17783.
- [6] M. Fischer, J.R.B. Gomes, M. Jorge, Computational approaches to study adsorption in MOFs with unsaturated metal sites, *Mol. Simul.* 40 (7–9) (2014) 537–556.
- [7] G. Alonso, D. Bahamon, F. Keshavarz, X. Giménes, P. Gamallo, R. Sayós, Density functional theory-based adsorption isotherms for pure and flue gas mixtures on Mg-MOF-74. Application in CO<sub>2</sub> capture swing adsorption processes, *J. Phys. Chem. C* 122 (7) (2018) 3945–3957.
- [8] J.A. Gee, D.S. Sholl, Characterization of the thermodynamic stability of solvated metal-organic framework polymorphs using molecular simulations, *J. Phys. Chem. C* 117 (40) (2013) 20636–20642.
- [9] Y. Ming, N. Kumar, D.J. Siegel, Water adsorption and insertion in MOF-5, *ACS Omega* 2 (2017) 4921.
- [10] R. Babarao, M. Eddaoudi, J.W. Jiang, Highly porous ionic rhf metal – organic framework for H<sub>2</sub> and CO<sub>2</sub> storage and separation: a molecular simulation study, *Langmuir* 26 (13) (2010) 11196–11203.
- [11] Taku Watanabe, David S. Sholl, Accelerating applications of metal-organic frameworks for gas adsorption and separation by computational screening of materials, *Langmuir* 28 (40) (2012) 14114–14128.

- [12] A. Boretti, L. Rosa, Reassessing the projections of the world water development report, *npj Clean Water* 2 (2019) 15.
- [13] W. Xu, O.M. Yaghi, Metal-organic frameworks for water harvesting from air, anywhere, anytime, *ACS Cent. Sci.* 6 (2020) 1348–1354.
- [14] S. Keskin, T.M. Heest, D.S. Sholl, Metal-organic framework materials play a useful role in large-scale carbon dioxide separations, *ChemSusChem* 3 (2010) 879–891.
- [15] P.M. Schoenecker, C.G. Carson, K.S. Walton, Structural stability of metal organic frameworks under humid conditions, *Abstr. Pap. Am. Chem. Soc.* 242 (2011).
- [16] Z. Chen, P. Li, R. Anderson, X. Wang, X. Zhang, L. Robison, et al., Balancing volumetric and gravimetric uptake in highly porous materials for clean energy, *Science* 368 (2020) 297–303.
- [17] O.V. Kharissova, B.I. Kharisov, L.T. Gonzalez, Recent trends on density functional theory–assisted calculations of structures and properties of metal–organic frameworks and metal–organic frameworks–derived nanocarbons, *J. Mater. Res.* 109 (2020) 1–15.
- [18] J. Zang, S. Nair, D.S. Sholl, Prediction of water adsorption in copper-based metal-organic frameworks using force fields derived from dispersion-corrected DFT calculations, *J. Phys. Chem. C.* 117 (2013) 7519–7525.
- [19] G. Fu, P. Wu, J. Yang, S. Zhang, X. Huai, Cr-doped UiO-66 with enhanced water adsorption for adsorption heat transformation, *Microporous Mesoporous Mater.* 331 (2022) 111642.
- [20] X. Liu, X. Wang, F. Kapteijn, Water and metal-organic frameworks: from interaction toward utilization, *Chem. Rev.* (2019) 1–75.
- [21] J.H. Cavka, S. Jakobsen, U. Olsbye, N. Guillou, C. Lamberti, S. Bordiga, et al., A new zirconium inorganic building brick forming metal organic frameworks with exceptional stability, *J. Am. Chem. Soc.* 130 (2008) 13850–13851.
- [22] X. Liu, N.K. Demir, Z. Wu, K. Li, Highly water-stable zirconium metal-organic framework UiO-66 membranes supported on alumina hollow fibers for desalination, *J. Am. Chem. Soc.* 137 (2015) 6999–7002.
- [23] M. Thommes, K. Kaneko, A.V. Neimark, J.P. Olivier, F. Rodriguez-Reinoso, J. Rouquerol, et al., Physisorption of gases, with special reference to the evaluation of surface area and pore size distribution (IUPAC Technical Report), *Pure Appl. Chem.* 87 (2015) 1051–1069.
- [24] P. Kusgens, M. Rose, I. Senkovska, H. Frode, A. Henschel, S. Siegle, et al., Characterization of metal-organic frameworks by water adsorption, *Microporous Mesoporous Mater.* 120 (2009) 325–330.
- [25] A. Shigematsu, T. Yamada, H. Kitagawa, Wide control of proton conductivity in porous coordination polymers, *J. Am. Chem. Soc.* 133 (2011) 2034–2036.
- [26] S.K. Henninger, F. Jeremias, H. Kummer, C. Janiak, MOFs for use in adsorption heat pump processes, *Eur. J. Inorg. Chem.* (2011) 1–11.
- [27] C. Janiak, S.K. Henninger, Porous coordination polymers as novel sorption materials for heat transformation processes, *Chimia* 67 (2013) 419–424.
- [28] J.H. Wee, Applications of proton exchange membrane fuel cell systems, *Renew. Sustain. Energy Rev.* 11 (2007) 1720.
- [29] K.D. Kreuer, A. Rabenau, W. Weppner, Vehicle mechanism, a new model for the interpretation of the conductivity of fast proton conductors, *Angew. Chem. Int. Ed.* 21 (1982) 208.
- [30] K.D. Kreuer, Proton conductivity: materials and applications, *Chem. Mater.* 8 (1996) 610.
- [31] M.A. Abdelkareem, Q. Abbas, M. Mouselly, H. Alawadhi, A.G. Olabi, High-performance effective metal–organic frameworks for electrochemical applications, *J. Sci.-Adv. Mater. Dev.* 7 (3) (2022) 100465.
- [32] O.K. Farha, I. Eryazici, N. Cheon Jeong, B.G. Hauser, C.E. Wilmer, A.A. Sarjeant, et al., Metal–organic framework materials with ultrahigh surface areas: is the sky the limit? *J. Am. Chem. Soc.* 134 (36) (2012) 15016–15021.
- [33] H. Li, L. Li, R.-B. Lin, W. Zhou, Z. Zhang, S. Xiang, et al., Porous metal-organic frameworks for gas storage and separation: status and challenges, *EnergyChem* 1 (1) (2019) 100006.
- [34] A. Gulati, R. Kakkar, DFT studies on storage and adsorption capacities of gases on MOFs, *Phys. Sci. Rev.* 3 (8) (2018) 20170196.

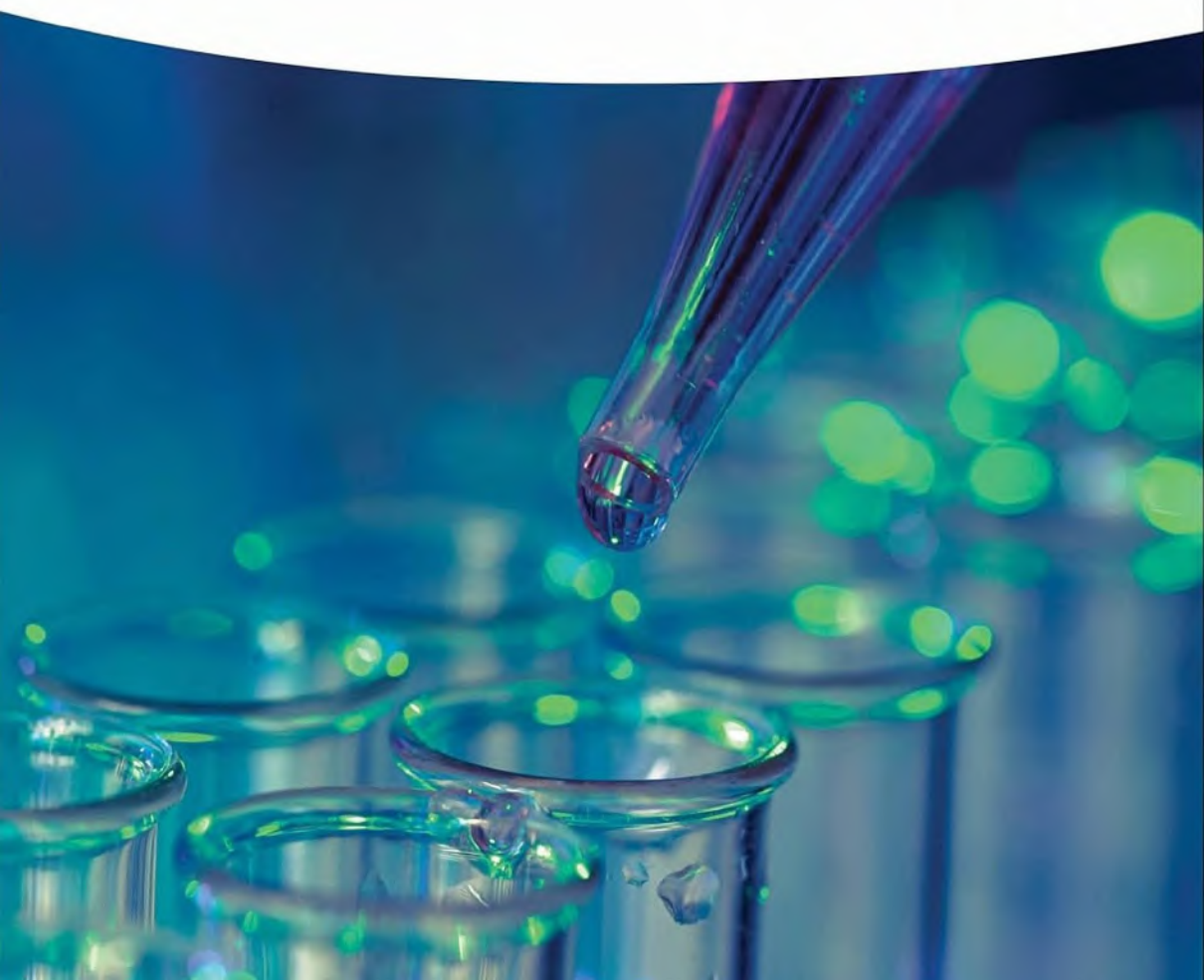
- [35] C. Altintas, O.F. Altundal, S. Keskin, R. Yildirim, Machine learning meets with metal organic frameworks for gas storage and separation, *J. Chem. Inf. Model.* 61 (5) (2021) 2131–2146.
- [36] E. Mahmoud, L. Ali, A. El Sayah, S.A. Alkhatib, H. Abdulsalam, M. Juma, et al., Implementing metal-organic frameworks for natural gas storage, *Crystals* 9 (2019) 406.
- [37] S. Siwaipram, S.A. Impeng, P. Bopp, et al., Density Functional Theory Studies of Catalytic Sites in Metal-Organic Frameworks', *IntechOpen*, 2019. 10.5772/intechopen.80698.
- [38] C.P. Raptopoulou, Metal-organic frameworks: synthetic methods and potential applications, *Materials (Basel)* 14 (2) (2021) 310.
- [39] N. Stock, S. Biswas, Synthesis of metal-organic frameworks (mofs): routes to various MOF topologies, morphologies, and composites, *Chem. Rev.* 112 (2) (2012) 933–969.
- [40] S. Denning, A.A. Majid, J.M. Lucero, J.M. Crawford, M.A. Carreon, C.A. Koh, Metal-organic framework HKUST-1 promotes methane hydrate formation for improved gas storage capacity, *ACS Appl. Mater. Interfaces* 12 (2020) 53510.
- [41] V.Y. Mao, P.J. Milner, J.H. Lee, A.C. Forse, E.J. Kim, R.L. Siegelman, Cooperative carbon dioxide adsorption in alcoholamine-and alkoxyalkylamine-functionalized metal-organic frameworks, *Angew. Chem. Int. Ed* 59 (2020) 19468.
- [42] A. Jaffe, M.E. Ziebel, D.M. Halat, N. Biggins, R.A. Murphy, K. Chakarawet, Selective, high-temperature O<sub>2</sub> adsorption in chemically reduced, redox-active iron-pyrazolate metal-organic frameworks, *J. Am. Chem. Soc.* 142 (2020) 14627.
- [43] E.J. Kim, R.L. Siegelman, H.Z. Jiang, A.C. Forse, J.H. Lee, J.D. Martell, Cooperative carbon capture and steam regeneration with tetraamine-appended metal-organic frameworks, *Science* 369 (2020) 392.
- [44] B.M. Connolly, D.G. Madden, A.E. Wheatley, D. Fairen-Jimenez, Shaping the future of fuel: monolithic metal-organic frameworks for high-density gas storage, *J. Am. Chem. Soc.* 142 (2020) 8541.
- [45] L. Morris, J.J. Hales, M.L. Trudeau, P. Georgiev, J.P. Embs, J. Eckert, A manganese hydride molecular sieve for practical hydrogen storage under ambient conditions, *Energy. Environ. Sci.* 12 (2019) 1580.
- [46] M.K. Rana, H.S. Koh, J. Hwang, D.J. Siegel, Comparing van der Waals density functionals for CO<sub>2</sub> adsorption in metal organic frameworks, *J. Phys. Chem. C.* 116 (2012) 16957.
- [47] S.R. Caskey, A.G. Wong-Foy, A.J. Matzger, Dramatic tuning of carbon dioxide uptake via metal substitution in a coordination polymer with cylindrical pores, *J. Am. Chem. Soc.* 130 (2008) 10870.
- [48] P.D. Dietzel, Y. Morita, R. Blom, H. Fjellvag, An in situ high-temperature single-crystal investigation of a dehydrated metal-organic framework compound and field-induced magnetization of one-dimensional metal-oxygen chains, *Angew. Chem. Int. Ed* 44 (2005) 6354.
- [49] S.S.Y. Chui, S.M.F. Lo, J.P. Charmant, A.G. Orpen, I.D. Williams, A chemically functionalizable nanoporous material [Cu<sub>3</sub>(TMA)<sub>2</sub>(H<sub>2</sub>O)<sub>3</sub>]<sub>n</sub>, *Science* 283 (1999) 1148.
- [50] A. Becke, Density-functional thermochemistry. III The role of exact exchange, *J. Chem. Phys.* 98 (1993) 564.
- [51] M. Asgari, S. Jawahery, E.D. Bloch, M.R. Hudson, R. Flacau, B. Vlasisavljevich, An experimental and computational study of CO<sub>2</sub> adsorption in the sodalite-type M-BTT (M = Cr, Mn, Fe, Cu) metal-organic frameworks featuring open metal sites, *Chem. Sci.* 9 (2018) 457.
- [52] G. Kresse, J. Hafner, Ab initio molecular dynamics for liquid metals, *Phys. Rev. B* 47 (1993) 558.
- [53] P. Giannozzi, S. Baroni, N. Bonini, M. Calandra, R. Car, C. Cavazzoni, QUANTUM ESPRESSO: a modular and open-source software project for quantum simulations of materials, *J. Phys. Condens* 21 (2009) 395502.
- [54] D.E. Jaramillo, D.A. Reed, H.Z. Jiang, J. Oktawiec, M.W. Mara, A.C. Forse, Selective nitrogen adsorption via backbonding in a metal-organic framework with exposed vanadium sites, *Nat. Mater.* 19 (2020) 517.
- [55] M. Dinca, A. Dailly, Y. Liu, C.M. Brown, D.A. Neumann, J.R. Long, Hydrogen storage in a microporous metal-organic framework with exposed Mn<sup>2+</sup> coordination sites, *J. Am. Chem. Soc.* 128 (2006) 16876.
- [56] S.S. Han, H. Furukawa, O.M. Yaghi, W.A. Goddard Iii, Covalent organic frameworks as exceptional hydrogen storage materials, *J. Am. Chem. Soc.* 130 (2008) 11580.

- [57] L. Liu, Z. Yao, Y. Ye, Y. Yang, Q. Lin, Z. Zhang, Integrating the pillared-layer strategy and pore-space partition method to construct multicomponent MOFs for  $C_2H_2/CO_2$  Separation, *J. Am. Chem. Soc.* 142 (2020) 9258.
- [58] M. Ernzerhof, G.E. Scuseria, Assessment of the Perdew–Burke–Ernzerhof exchange–correlation functional, *J. Chem. Phys.* 110 (1999) 5029.
- [59] S. Siwaipram, S. Impeng, P.A. Bopp, S. Bureekaew, Density functional theory studies of catalytic sites in metal-organic frameworks in: *Density Functional Theory*, 5 November 2018, IntechOpen.
- [60] H. Yang, X. Wang, Secondary-component incorporated hollow MOFs and derivatives for catalytic and energy-related applications, *Adv. Mater.* (2018) 1800743–1800760.
- [61] Y. Yang, Z. Lun, G. Xia, F. Zheng, M. He, Q. Chen, Non-precious alloy encapsulated in nitrogen-doped graphene layers derived from MOFs as an active and durable hydrogen evolution reaction catalyst, *Energy Environ. Sci.* 8 (2015) 3563.
- [62] F. Li, Y. Tian, S. Su, C. Wang, D.-S. Li, D. Cai, et al., Theoretical and experimental exploration of tri-metallic organic frameworks (t-MOFs) for efficient electrocatalytic oxygen evolution reaction, *Appl. Catal. B: Environ.* 299 (2021) 120665.
- [63] Z.W. Seh, J. Kibsgaard, C.F. Dickens, I. Chorkendorff, J.K. Nørskov, T.F. Jaramillo, Combining theory and experiment in electrocatalysis: insights into materials design, *Science* 355 (2017) 4998.
- [64] K.N. Dinh, Q. Liang, C.-F. Du, J. Zhao, A.I.Y. Tok, H. Mao, et al., Nanostructured metallic transition metal carbides, nitrides, phosphides, and borides for energy storage and conversion, *Nano Today* 25 (2019) 99–121.
- [65] M.A. Khan, H. Zhao, W. Zou, Z. Chen, W. Cao, J. Fang, et al., Recent progresses in electrocatalysts for water electrolysis, *Electrochim. Energy. Rev.* 1 (2018) 483–530.
- [66] A.J. Howarth, A.W. Peters, N.A. Vermeulen, T.C. Wang, J.T. Hupp, O.K. Farha, Best practices for the synthesis, activation, and characterization of metal – organic frameworks, *Chem. Mater.* 29 (2017) 26–39.
- [67] A. Suvitha, N.S. Venkataramanan, R. Sahara, Y. Kawazoe, A theoretical exploration of the intermolecular interactions between resveratrol and water: a DFT and AIM analysis, *J. Mol. Model.* 25 (2019) 56.
- [68] M.T. Lusk, A.E. Mattsson, High-performance computing for materials design to advance energy science, *MRS Bull.* 36 (2011) 169–174.
- [69] G.A. McCarver, T. Rajeshkumar, K.D. Vogiatzis, Computational catalysis for metal-organic frameworks: an overview, *Coord. Chem. Rev.* 436 (2021) 213777.
- [70] C.R. Chimie, Role of molecular simulations in the structure exploration of metal-organic frameworks: illustrations through recent advances in the field, *Adv. field* 19 (2016) 207–215.
- [71] H.C. Zhou, J.R. Long, O.M. Yaghi, Introduction to metal–organic frameworks, *Chem. Rev.* 112 (2012) 673.
- [72] M. Bruschi, G. Zampella, P. Fantucci, L.D. Gioia, DFT investigations of models related to the active site of [NiFe] and [Fe] hydrogenases, *Coord. Chem. Rev.* 249 (2005) 1620–1640.
- [73] M. Stein, W. Lubitz, Relativistic DFT calculation of the reaction cycle intermediates of [NiFe] hydrogenase: a contribution to understanding the enzymatic mechanism, *J. Inorg. Biochem* 98 (2004) 862.
- [74] F. Miyazaki, S. Foerster, M. Stein, M. Brecht, H. Ogata, Y. Higuchi, et al., Single crystal EPR studies of the reduced active site of [NiFe] hydrogenase from *Desulfovibrio vulgaris*, *Am. Chem. Soc.* 125 (1) (2003) 83–93.

9.4	Functioning of ion exchange in metal-organic frameworks	173
9.5	The use of computational models in ionic compounds	174
9.6	Conclusion	185
	References	185
<b>10.</b>	<b>Density functional theory–based molecular modeling for metal-organic frameworks</b>	<b>193</b>
	Swati Chandrawanshi, Rakesh Kumar Sahu, Sushama Sahu, Dakeshwar Kumar Verma and Reema Sahu	
10.1	Introduction	193
10.2	Role of density functional theory in the development of metal-organic frameworks for water adsorption and separation applications	194
10.3	Role of density functional theory in the development of metal-organic frameworks for gas storage, adsorption, and separation	198
10.4	Density functional theory studies at catalytic activity of metal-organic frameworks and derivatives	200
10.5	Role of density functional theory in the structure exploration of metal-organic frameworks and derivatives	201
10.6	Conclusion	202
	Conflict of interest	202
	References	202
 <b>Part 3 Significance and importance</b>		
<b>11.</b>	<b>Metal-organic frameworks based electrode materials for supercapacitor application</b>	<b>209</b>
	Rabia Ahmad, Naseem Iqbal, Usman Ali Khan, Maryam Raza, Iqra Shaukat and Tayyaba Noor	
11.1	Introduction	209
11.2	Metal-organic frameworks	213
11.3	Pristine metal-organic framework as electrode material for supercapacitors	214
11.4	Metal-organic framework-derived electrode materials for supercapacitors	219
11.5	Metal-organic framework composites as electrode material for supercapacitors	223
11.6	Future prospect	229
	References	230
<b>12.</b>	<b>Metal-organic frameworks for reasonable carbon dioxide fixation and electrocatalytic carbon dioxide reduction</b>	<b>235</b>
	Ganesh Gollavelli, Bakuru Vasudeva Rao and Ling Yong-Chien	
12.1	Introduction	235
12.2	CO <sub>2</sub> and metal-organic frameworks	236

Edited by Dakeshwar Kumar Verma,  
Chandrabhan Verma, and Paz Otero Fuertes

# Green Chemical Synthesis with Microwaves and Ultrasound



## Contents

**About the Editors** *xiii*

**Preface** *xv*

- 1      **Ultrasound Irradiation: Fundamental Theory, Electromagnetic Spectrum, Important Properties, and Physical Principles** 1**  
*Sumit Kumar, Amrutlal Prajapat, Sumit K. Panja, and Madhulata Shukla*
  - 1.1      Introduction 1
  - 1.2      Cavitation History 3
    - 1.2.1    Basics of Cavitation 3
    - 1.2.2    Types of Cavitation 5
  - 1.3      Application of Ultrasound Irradiation 7
    - 1.3.1    Sonoluminescence and Sonophotocatalysis 9
    - 1.3.2    Industrial Cleaning 10
    - 1.3.3    Material Processing 11
    - 1.3.4    Chemical and Biological Reactions 12
  - 1.4      Conclusion 14
  - Acknowledgments 15
  - References 15
  
- 2      **Fundamental Theory of Electromagnetic Spectrum, Dielectric and Magnetic Properties, Molecular Rotation, and the Green Chemistry of Microwave Heating Equipment** 21**  
*Raghvendra K. Mishra, Akshita Yadav, Vinayak Mishra, Satya N. Mishra, Deepa S. Singh, and Dakeshwar Kumar Verma*
  - 2.1      Introduction 21
    - 2.1.1    Historical Background 25
    - 2.1.2    Green Chemistry Principles for Sustainable System 28
  - 2.2      Fundamental Concepts of the Electromagnetic Spectrum Theory 35
  - 2.3      Electrical, Dielectric, and Magnetic Properties in Microwave Irradiation 38
  - 2.4      Microwave Irradiation Molecular Rotation 41
  - 2.5      Fundamentals of Electromagnetic Theory in Microwave Irradiation 42
    - 2.5.1    Electromagnetic Radiations and Microwave 43

- 2.5.2 Heating Mechanism of Microwave: Conventional Versus Microwave Heating 44
- 2.6 Physical Principles of Microwave Heating and Equipment 46
- 2.7 Green Chemistry Through Microwave Heating: Applications and Benefits 53
- 2.8 Conclusion 57
- References 57

### **3 Conventional Versus Green Chemical Transformation: MCRs, Solid Phase Reaction, Green Solvents, Microwave, and Ultrasound Irradiation 69**

*Shailendra Yadav, Dheeraj S. Chauhan, and Mumtaz A. Quraishi*

- 3.1 Introduction 69
- 3.2 A Brief Overview of Green Chemistry 69
  - 3.2.1 Definition and Historical Background 69
  - 3.2.2 Significance 70
- 3.3 Multicomponent Reactions 71
- 3.4 Solid Phase Reactions 73
- 3.5 Microwave Induced Synthesis 74
- 3.6 Ultrasound Induced Synthesis 75
- 3.7 Green Chemicals and Solvents 77
- 3.8 Conclusions and Outlook 78
- References 79

### **4 Metal-Catalyzed Reactions Under Microwave and Ultrasound Irradiation 83**

*Suresh Maddila, Immandhi S.S. Anantha, Pamerla Mulralidhar, Nagaraju Kerru, and Sudhakar Chintakula*

- 4.1 Ultrasonic Irradiation 83
  - 4.1.1 Iron-Based Catalysts 86
    - 4.1.1.1 Dihydropyrimidinones by Cu-Based Catalysts 91
    - 4.1.1.2 Dihydroquinazolinones by Cu-Based Catalysts 92
  - 4.1.2 Copper-Based Catalysts 89
    - 4.1.2.1 Misalliances Metal-Based Catalysts 94
- 4.2 Microwave-Assisted Reactions 97
  - 4.2.1 Solid Acid and Base Catalysts 98
    - 4.2.1.1 Condensation Reactions 98
    - 4.2.1.2 Cyclization Reactions 100
    - 4.2.1.3 Multi-component Reactions 104
    - 4.2.1.4 Friedel–Crafts Reactions 106
    - 4.2.1.5 Reaction Involving Catalysts of Biological Origin 107
    - 4.2.1.6 Reduction 109
    - 4.2.1.7 Oxidation 110
    - 4.2.1.8 Coupling Reactions 113
    - 4.2.1.9 Micelliances Reactions 121
    - 4.2.1.10 Click Chemistry 125



4.3	Conclusion	127
	Acknowledgments	128
	References	128
<b>5</b>	<b>Microwave- and Ultrasonic-Assisted Coupling Reactions</b>	<b>133</b>
	<i>Sandeep Yadav, Anirudh P.S. Raman, Kashmiri Lal, Pallavi Jain, and Prashant Singh</i>	
5.1	Introduction	133
5.2	Microwave	134
5.2.1	Microwave-Assisted Coupling Reactions	135
5.2.2	Ultrasound-Assisted Coupling Reactions	142
5.3	Conclusion	150
	References	151
<b>6</b>	<b>Synthesis of Heterocyclic Compounds Under Microwave Irradiation Using Name Reactions</b>	<b>157</b>
	<i>Sheryn Wong and Anton V. Dolzhenko</i>	
6.1	Introduction	157
6.2	Classical Methods for Heterocyclic Synthesis Under Microwave Irradiation	158
6.2.1	Piloty–Robinson Pyrrole Synthesis	158
6.2.2	Clauson–Kaas Pyrrole Synthesis	158
6.2.3	Paal–Knorr Pyrrole Synthesis	159
6.2.4	Paal–Knorr Furan Synthesis	160
6.2.5	Paal–Knorr Thiophene Synthesis	160
6.2.6	Gewald Reaction	161
6.2.7	Fischer Indole Synthesis	162
6.2.8	Bischler–Möhlau Indole Synthesis	162
6.2.9	Hemetsberger–Knittel Indole Synthesis	163
6.2.10	Leimgruber–Batcho Indole Synthesis	163
6.2.11	Cadogan–Sundberg Indole Synthesis	163
6.2.12	Pechmann Pyrazole Synthesis	164
6.2.13	Debus–Radziszewski Reaction	164
6.2.14	van Leusen Imidazole Synthesis	166
6.2.15	van Leusen Oxazole Synthesis	166
6.2.16	Robinson–Gabriel Reaction	167
6.2.17	Hantzsch Thiazole Synthesis	167
6.2.18	Einhorn–Brunner Reaction	168
6.2.19	Pellizzari Reaction	169
6.2.20	Huisgen Reaction	169
6.2.21	Finnegan Tetrazole Synthesis	171
6.2.22	Four-component Ugi-azide Reaction	172
6.2.23	Kröhnke Pyridine Synthesis	172
6.2.24	Bohlmann–Rahtz Pyridine Synthesis	173
6.2.25	Boger Reaction	174

## 2

## Fundamental Theory of Electromagnetic Spectrum, Dielectric and Magnetic Properties, Molecular Rotation, and the Green Chemistry of Microwave Heating Equipment

Raghvendra K. Mishra<sup>1</sup>, Akshita Yadav<sup>2</sup>, Vinayak Mishra<sup>3</sup>, Satya N. Mishra<sup>4</sup>, Deepa S. Singh<sup>5</sup>, and Dakeshwar Kumar Verma<sup>6</sup>

<sup>1</sup>Cranfield University, School of Aerospace, Transport and Manufacturing, College Rd, Wharley End, Bedford MK43 0AL, United Kingdom

<sup>2</sup>State University of New York at Buffalo, Department of Mechanical and Aerospace Engineering, Buffalo, NY 14260-4400, USA

<sup>3</sup>International Institute of Information Technology, Department of Computer Aided Structural Engineering, CR Roa Road, Telangana 500032, India

<sup>4</sup>Brahmanand PG College, Department of Mathematics, Mall Road, Kanpur, Uttar Pradesh 208011, India

<sup>5</sup>M.J.P. Rohilkhand University, Hindu College, Department of Zoology, Station Road, Moradabad, Uttar Pradesh 244001, India

<sup>6</sup>Govt. Digvijay Autonomous Postgraduate College, Department of Chemistry, Rajnandgaon, Chhattisgarh 491441, India

### 2.1 Introduction

The fundamental concept revolves around designing hybrid microwave-ultrasonication irradiation systems to enhance the efficiency and selectivity of green chemical reactions. These systems function by combining microwave and ultrasonic radiation to promote reactions while overcoming limitations like nonuniformity. This is significant for sustainable chemistry due to its potential to reduce energy consumption and harmful solvent usage. Applications are observed in various fields, motivating research in disciplines such as chemistry and materials science. Researchers work with materials that can focus and distribute radiation, aiming to optimize system efficiency. Ongoing research explores mechanisms and principles governing this technology, with implications for greener chemical synthesis [1]. The fundamental concept involves the design of a hybrid material for sustainable high-value chemical production in industrial settings. This material system combines to enhance reaction efficiency when interacting with electromagnetic radiation while minimizing its environmental impact. It functions by utilizing metamaterial-based applicators and pulsed radiation to focus and distribute energy effectively. Significantly, it offers scalable, cost-effective, and safe operation, motivating research in fields like materials science and engineering. Key materials include transparent reactors and durable applicators. Ongoing research explores sensor-based control systems for optimized production, marking the forefront of

current research in sustainable chemical synthesis [2]. The fundamental concept involves the utilization of green synthesis, specifically supercritical fluids, and biocatalysis, to enhance the production of high-value products with increased efficiency and sustainability. Supercritical fluids, operating above critical conditions, act as nontoxic and nonflammable solvents, reducing waste impact on surroundings, and finding applications in pharmaceuticals, nanomaterials, and food additives. Biocatalysis employs enzymes for selective reactions in mild conditions, minimizing the use of hazardous chemicals. Both technologies motivate research in materials science and engineering. Their significance lies in reducing cost, waste production, and energy consumption while providing sustainable alternatives to traditional methods [3]. Green chemistry is a scientific concept focused on designing and implementing chemical processes and products to minimize or eliminate hazardous substances, thereby reducing ecological disasters. It functions through principles such as waste prevention, maximizing atom economy, using safer chemicals and solvents, and designing products for easy degradation. Its significance lies in promoting sustainable and environmentally friendly chemical practices. Applications are employed in various industries, driven by the need to reduce environmental harm, improve efficiency, and create more eco-friendly products. This field engages principles of thermodynamics, kinetics, catalysis, and material science to develop greener chemical synthesis routes, offering the potential to transform the chemical industry and benefit the ecosystem [4]. Figure 2.1 visually represents the 12 fundamental principles of green chemistry, offering a comprehensive framework for sustainable chemical practices that prioritize waste reduction, safe solvents, and energy efficiency. These principles are put into practical applications, notably in pharmaceutical synthesis, where eco-friendly reactions align with the goals of green chemistry by minimizing waste. The Nobel Prize recognition underscores the significance of sustainable chemistry, with metathesis applications benefiting various fields by reducing waste and energy consumption. The emergence of green chemistry in the 1990s, coupled with Anastas and Warner's principles, has shifted chemical research toward proactive pollution prevention, leaving a lasting impact on academia. Moreover, extending these principles to encompass concepts like the circular economy, sustainability metrics, and global collaboration further enhances global sustainability efforts within chemical processes.

In 2012, Elevance Renewable Sciences earned the Presidential Green Chemistry Challenge Award for their pioneering use of metathesis to convert natural oils into eco-friendly chemicals, including concentrated cold-water detergents. This approach reduced waste and improved energy saving, showcasing green chemistry's impact across industries. Similarly, Los Alamos National Laboratory's use of supercritical carbon dioxide transformed computer chip manufacturing, reducing resource consumption, and aligning with sustainability principles. These examples illustrate how innovative technologies and green chemistry principles are reshaping industries, promoting eco-conscious solutions in line with academic research and scientific goals [6]. Richard Wool's innovative use of chicken feathers for keratin-based fibers has the potential to revolutionize printed circuit board technology, offering lightweight and durable solutions applicable to chip technology

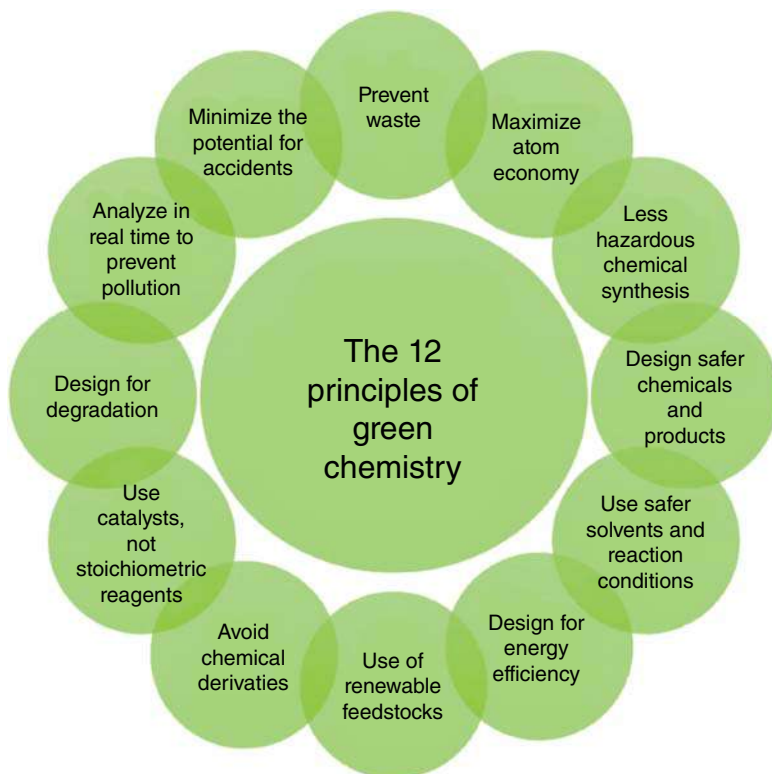


**Figure 2.1** Scheme of the 12 principles of green chemistry. Source: Trombino et al. [5]/MDPI/Public Domain/CC by 4.0.

and biofuel production, in line with sustainability principles. In the pharmaceutical sector, the collaboration between Merck and Codexis has led to a greener synthesis for sitagliptin, reducing waste, improving yield, and safety, and eliminating the need for metal catalysts. This approach promises more sustainable pharmaceutical manufacturing and safer medication products, emphasizing the significance of eco-conscious chemical routes in achieving safer and environmentally friendly outcomes [7]. Green chemistry finds extensive applications across various sectors, focusing on the development of environmentally friendly compounds and eco-conscious solvents, particularly in industries like paint and coatings. These applications prioritize sustainability through energy conservation, waste reduction, and the substitution of hazardous substances with safer alternatives. Green chemistry's alignment with academic research and scientific objectives underscores its vital role in advancing environmentally responsible chemical practices, contributing to a more sustainable and eco-conscious future across diverse domains [8].

Microwave-assisted chemistry represents a transformative approach to chemical synthesis, offering rapid reactions, improved yields, and higher purity while adhering to green chemistry principles. In pharmaceutical synthesis, it embodies biodegradable practices, promoting sustainability and shaping academic research

and scientific pursuits. Beyond its current applications, microwave chemistry holds promise in diverse fields such as materials science, environmental science, and food processing, signifying a shift toward environmentally responsible and resource-efficient chemical practices [9]. Microwave chemistry revolutionizes chemical reactions with dramatically shortened reaction times, leading to improved yields and minimizing by-product formation. This aligns with green chemistry's principles of energy conservation and waste reduction. Microwave synthesis has found success in applications such as pharmaceutical manufacturing, promoting faster and more environmentally friendly production processes, and reflecting a shift toward efficient and ecological practices at the industry level [10]. Nevertheless, the challenge of limited equipment accessibility for researchers persists. To overcome this hurdle, initiatives focused on affordable equipment, materials development, and hybrid approaches are necessary. These efforts can democratize the use of microwave technology, making it more widely available, and thereby promoting environment-friendly chemical implementations in scientific research while advancing sustainability goals in academia and industry [11]. Excessive microwave heating in chemical processes does pose risks, including potential harm to tissues and DNA due to radioactive decay and hazardous reactions. However, when used in conjunction with green chemistry principles, microwave exposure offers sustainable synthesis options. The effective management of these risks through safety measures and protocols enables researchers and industries to harness microwave irradiation for eco-conscious exercises, aligning with scientific research goals for a cleaner and safer future. Case studies further highlight the success of this synergy, showcasing advancements in eco-friendly chemistry practices operations [12]. Green chemistry plays a pivotal role by prioritizing environmentally responsible practices and biodegradable products. Microwave and ultrasonication irradiation techniques, based on electromagnetic principles, offer sustainability in various fields, including physics and medicinal chemistry. Their alignment with green chemistry's objectives promotes eco-friendly applications, driving progress in the research domain toward a cleaner and more sustainable future [13]. These technologies optimize chemical transformations, fostering sustainability across various aspects, as exemplified by real-world applications, effectively advancing sustainable goals in academic research as well as scientific exploration [14]. Microwave and vibrational irradiation methods exhibit remarkable versatility in addressing environmental concerns, effectively removing pollutants from soil and water without generating harmful waste products. These eco-friendly applications seamlessly align with green chemistry principles, emphasizing sustainable approaches to remediate polluted areas and restore ecosystems. Their capacity to tackle environmental issues underscores their significance in academic research and scientific endeavors, promoting cleaner and more sustainable practices for a greener future, and reflecting a commitment to eco-conscious chemistry practices with a strong focus on environmental stewardship [15]. Aligned with sustainability and environmental responsibility, these methods have diverse applications across industries, promoting cleaner and more sustainable chemical practices. In academic research and scientific exploration, they represent a pivotal step toward a

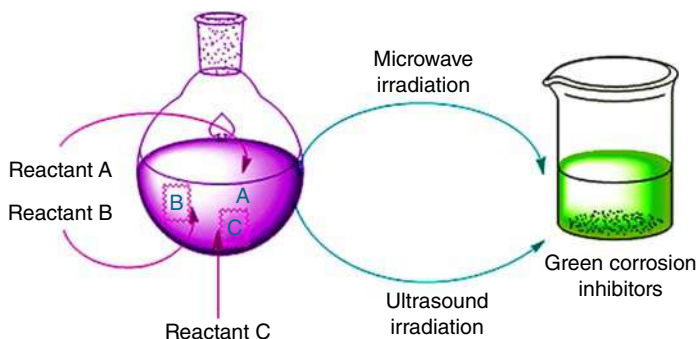


**Figure 2.2** Illustration showcasing the transformative impact of microwave and ultrasonication irradiation in green chemistry. Source: Verma et al. [18]/Elsevier.

greener and more innovative future, emphasizing a commitment to eco-conscious chemistry practices and a transformative shift in chemical processes toward a more sustainable and environmentally friendly direction [16]. In each context, they contribute to cleaner and more efficient processes while minimizing the ecological footprint of industrial activities [17]. Figure 2.2 illustrates the transformative impact of microwave and ultrasonication irradiation in green chemistry. These techniques align seamlessly with green chemistry principles, offering benefits such as rapid reaction times, improved product selectivity, and minimized environmental impact. They have become indispensable tools for sustainable chemical processes in various industries. In the following sections, we will delve deeper into the fundamental principles governing microwave and ultrasonication irradiation, highlighting how they optimize chemical reactions. Additionally, we will explore their advantages, including enhanced selectivity and reduced reaction times, and examine their applications in specific industries. Through this detailed examination, we aim to provide a comprehensive understanding of the transformative potential of these technologies in the realm of green chemistry and their pivotal role in shaping a more sustainable future.

### 2.1.1 Historical Background

The integration of microwave and ultrasonication methods into green chemistry practices is driven by the need to address environmental concerns and promote sustainable chemical processes. These methods offer rapid and efficient reactions, aligning with green chemistry's principles of energy efficiency and waste reduction. They find applications across diverse industries, from pharmaceuticals to materials science, exemplifying a transformative shift toward more sustainable and environmentally friendly chemical processes [19]. The integration of microwave and ultrasonication methods into green chemistry practices is driven by the imperative to uphold sustainability and environmental responsibility. This entails aligning chemical transformations with eco-conscious values and striving for cleaner and more resource-efficient processes. This transformative incorporation, exemplified

by the introduction of microwave irradiation in organic synthesis in the 1980s, has since catalyzed ongoing advancements in academia and research, fostering cleaner and more efficient chemical processes across diverse industries [19]. The historical underpinnings of microwave irradiation's integration into organic synthesis have paved the way for the continuous development of eco-friendly chemical transformations. These foundations, aligned with the unwavering pursuit of environmentally conscious and efficient processes, exemplify the field's commitment to innovation and ecological awareness. This evolution represents a persistent drive for progress within the realm of chemical science. Microwave irradiation's consistent expansion in utilization, driven by its effectiveness in reducing reaction times and increasing product yields, aligns seamlessly with academic research and scientific objectives [20]. Microwave irradiation technology accelerates chemical reactions by inducing molecular rotations, effectively enhancing reaction kinetics, and enabling precise control by selectively heating specific portions of the reaction mixture. Conversely, ultrasonication irradiation has a historical presence in the food industry, notably improving plant compound extraction and fat emulsification since the 1950s. Both techniques exemplify the multifaceted utility of innovative methods in optimizing chemical processes. Microwave irradiation finds applications in pharmaceutical synthesis, reducing reaction times and improving yields, aligning with academic research and scientific goals. Ultrasonication plays a pivotal role in food technology, enhancing flavor extraction and emulsion stability. These applications highlight their versatility and significance in academia and research, promoting efficiency and precision in chemical processes [21]. Ultrasonication irradiation gained recognition in the 1990s for its pivotal role in advancing environmentally responsible chemical methodologies. The concept of integrating microwave and ultrasonication irradiation for green chemical transformations emerged in the early 2000s, offering the promise of improved reaction efficiency and selectivity. This innovative approach embodies the ongoing pursuit of more sustainable and efficient chemical processes, aligning with the tenets of green chemistry. It signifies the evolution of techniques aimed at optimizing chemical reactions while reducing environmental impact. The combination of microwave and ultrasonication irradiation works synergistically to enhance desired chemical product yields while simultaneously minimizing the formation of undesired byproducts, meeting the objectives of academic exploration [22]. The strategy of integrating microwave and ultrasonication irradiation represents a pioneering approach dedicated to enhancing chemical processes, harmonizing perfectly with the core principles of green chemistry that prioritize sustainability and environmental conscientiousness. The collaboration between these two irradiation methods marks a noteworthy progression in the quest for more efficient and environmentally responsible chemical transformations. This evolution of green chemical transformation is a testament to the dynamic interplay between scientific principles and technological innovations, in alignment with the overarching ideas of academic and scientific findings, aimed at achieving both precision and environmental obligation in chemical processes [23]. The late 1990s marked a significant juncture in the consolidation of green chemistry principles within the scientific community. During this period, there was

a resounding recognition of the imperative for chemical processes to pivot toward renewable and environmental management, and economic viability. This pivotal era symbolized a deliberate commitment to bridging scientific principles with practical solutions, reflecting the ongoing pursuit of more sustainable chemical practices. It underscored the growing awareness of the need for environmentally conscious methodologies to address contemporary environmental and economic complexities, all in alignment with the overarching goals of academic as well as scientific study [3].

During the late 1990s, there was a concerted effort to reduce the use of hazardous chemicals, minimize waste generation, and enhance process efficiency, aligning with the principles of green chemistry. A pivotal development in this context was the introduction of microwave irradiation in the 1980s, revolutionizing organic synthesis. Its unique capability to induce molecular rotations facilitated rapid heating, resulting in significantly shorter reaction times. Furthermore, its precision in selectively heating specific components within a reaction mixture expanded its potential to improve reaction selectivity. This innovation epitomizes the fusion of scientific ingenuity with sustainability objectives, underscoring its profound impact on advancing eco-conscious chemistry practices, as emphasized in systematic exploration [24]. The historical context underscores a steadfast commitment to adopting environmentally conscious and efficient methodologies in chemical processes. Ultrasonication, originally utilized in the food industry in the 1950s for tasks like plant compound extraction and fat emulsification, gradually gained recognition within organic synthesis, particularly in the 1990s. However, a pivotal turning point emerged in the early 2000s with the conceptualization of combining microwave and ultrasonication irradiation methods. This marked a significant leap forward in the pursuit of sustainable and efficient chemical transformations, aligning seamlessly with the goals of academic research and scientific exploration, showcasing the evolving landscape of eco-conscious chemistry practices [25]. The innovative amalgamation of microwave and ultrasonication irradiation techniques represented a significant leap toward advancing the efficiency and sustainability of chemical processes. This collaborative integration harnessed the potent capabilities of both methods to optimize chemical reactions fundamentally. It stemmed from the recognition that their combined application had the potential to enhance product yield while concurrently reducing the generation of undesired by-products. The evolution of these techniques signifies a dynamic stride in the pursuit of more environmentally responsible and efficient chemical practices, illustrating their pivotal role in shaping the landscape of sustainable chemistry [26]. The innovative fusion of microwave and ultrasonication irradiation techniques represents a significant leap toward achieving rapid, efficient, and highly selective chemical transformations, all while eliminating the use of hazardous solvents and reagents. This approach signifies a substantial stride in realizing environmentally responsible and efficient chemical methodologies, underpinned by a historical trajectory reflecting an enduring commitment to advancing eco-conscious chemical practices. This merger in green chemical transformation exemplifies the transition from theoretical principles to practical application, marking a pivotal



advancement in developing more sustainable and eco-friendly chemical processes. It underscores the central themes of innovation and ecological responsibility in the field of chemistry, aligning seamlessly with academic research and scientific goals, embodying the transformative potential of eco-conscious chemistry practices [27]. The integration of microwave and ultrasonication irradiation techniques embodies a resolute commitment to bridging the chasm between scientific ideals and practical applications, propelling the evolution of more sustainable and efficient chemical methodologies. This journey epitomizes an unwavering pursuit of ecological responsibility and heightened efficiency in chemical processes, with innovation and adaptability at its core. It underscores the transformative potential of eco-conscious chemistry practices, symbolizing a determined endeavor toward a more environmentally aware and efficient future in the domain of chemistry, a journey of profound significance embraced by academia and scientific exploration. It reflects a commitment to continuously explore and implement advanced methodologies that align with sustainability principles. This drive for innovation is central to addressing environmental challenges and optimizing chemical processes for a greener and more sustainable tomorrow.

### **2.1.2 Green Chemistry Principles for Sustainable System**

Green chemistry is a transformative paradigm emphasizing sustainability and reduced environmental impact in chemical products and processes. It significantly advances scientific knowledge by promoting innovation in ethical and sustainable chemical methodologies. For instance, it can replace hazardous solvents with water, develop greener pharmaceutical synthesis, and catalyze reactions to minimize waste. In research grant peer reviews, projects tackling issues like wastewater treatment with environmentally friendly catalysts exemplify its potential impact in building a cleaner, more sustainable future [28]. In the realm of drug delivery systems, the paramount focus is on selecting solvents with low toxicity, biodegradability, and minimal harm to human health, aligning with green chemistry principles. Ionic liquids (ILs), known for their unique properties and ability to remain in a liquid state at lower temperatures, stand out as attractive solvents. Recycling ILs emerges as a pivotal facet, reducing waste generation and meeting the ongoing demand for these chemicals. This approach underscores a commitment to eco-conscious pharmaceutical research, aligning with academic research and scientific objectives where safety and environmental responsibility are paramount. ILs offer advantages in improving drug solubility, stability, and bioavailability while adhering to sustainable practices, making them a noteworthy choice in advancing drug delivery systems [29]. Green chemistry is a transformative approach that prioritizes environmentally responsible chemical products and processes, aligning with sustainability principles by minimizing the use and production of harmful substances. ILs, chosen for their low toxicity and biodegradability, exemplify eco-conscious solvent selection. Recycling ILs is integral to sustainability, reducing waste, and production demands. This approach mirrors the commitment to eco-conscious pharmaceutical research, emphasizing safety and environmental

stewardship. The “cradle-to-cradle” design philosophy underscores the importance of minimizing environmental impact throughout a product’s lifecycle. Green chemistry plays a pivotal role in addressing global challenges, offering a path toward a more sustainable and eco-friendly future [30]. Green chemistry principles play a pivotal role in the development of drug delivery systems that offer precise and controlled drug release, thereby reducing waste and potential adverse effects. For instance, biodegradable polymers, such as poly(lactic-co-glycolic acid) (PLGA), are used to encapsulate drugs and slowly release them over time, improving patient adherence by eliminating the need for frequent dosing. This aligns with academic research and scientific objectives that prioritize eco-conscious pharmaceutical solutions. By minimizing the use of harmful substances and optimizing drug release, green chemistry not only enhances patient outcomes but also contributes to environmental stewardship. This approach underscores the broader commitment to sustainable healthcare practices, emphasizing safety and effectiveness while minimizing ecological impact [31]. In the realm of green drug delivery systems, material selection plays a pivotal role in ensuring both safety and environmental sustainability. Biocompatible substances like chitosan and hyaluronic acid (HA) are favored choices due to their compatibility with biological systems, minimizing the risk of adverse reactions. This aligns with the core principles of green chemistry, which aims to reduce the generation of harmful by-products in chemical processes. For instance, when considering chitosan-based drug delivery, its natural origin and biodegradability exemplify green chemistry in action. Chitosan’s ability to encapsulate and release drugs in a controlled manner not only enhances therapeutic outcomes but also reduces the environmental burden associated with drug manufacturing and disposal [32]. ILs are a promising class of solvents for drug delivery. They have a number of unique properties that make them attractive for this application, including low volatility, nonflammability, and high solvation capabilities. ILs can be used to design greener drug delivery systems by reducing the use of hazardous solvents and reagents and by creating more targeted drug delivery systems. ILs have the potential to make drug delivery safer, more effective, and more environmentally friendly [33]. Chitosan-based hydrogels and nanoparticles are promising materials for drug delivery due to their biocompatibility, tunable properties, and ability to encapsulate and control the release of drugs. These materials are being used to develop new and more effective treatments for a variety of diseases, including diabetes, cancer, and infectious diseases. For example, chitosan-based hydrogels can be implanted under the skin to release insulin in a controlled manner, improving blood sugar control in patients with diabetes. Chitosan-based nanoparticles can be targeted at tumors to deliver cancer drugs more effectively and reduce side effects. The development of chitosan-based hydrogels and nanoparticles for drug delivery is a significant scientific advancement with the potential to revolutionize the field of pharmaceutical science. These materials offer the promise of safer, more effective, and more targeted drug delivery [34]. Click chemistry is a group of chemical reactions that are highly efficient and specific, making them ideal for use in drug delivery. It can be used to functionalize and crosslink drug delivery carriers in a variety of ways. Targeting ligands are molecules that bind

to specific cells or tissues, and they can be used to direct drug delivery carriers to specific sites in the body. This can improve the efficacy of treatment and reduce side effects. Crosslinking involves linking two or more drug delivery carriers together to form a network. This can improve the stability of the drug delivery system in the body and extend its release profile. Click chemistry is being used to develop new and more effective drug delivery systems for a variety of diseases, including cancer, infectious diseases, and chronic diseases. For example, click chemistry is being used to develop targeted nanoparticles for the delivery of cancer drugs, crosslinked hydrogels for the delivery of proteins and other biological drugs, and new types of drug delivery systems, such as micelles and vesicles [35]. Polymer grafting and environmentally friendly processes can be combined to design more effective and sustainable drug delivery systems. This approach has the potential to improve the treatment of diseases and make drug delivery more accessible to people around the world. Specific examples of this approach include water-soluble nanoparticles for cancer drug delivery, hydrogels for the sustained release of proteins, and other biological drugs, and new types of drug delivery systems, such as micelles and vesicles [36]. Chitosan-based hydrogels and stabilized metal nanoparticles are promising materials for drug delivery. Chitosan-based hydrogels can encapsulate and release drugs in a controlled manner. Stabilized metal nanoparticles can target drugs to specific cells or tissues. Combining these technologies can lead to more effective and precise drug delivery systems. Examples of applications include controlled delivery of chemotherapy drugs and targeted delivery of cancer drugs. These technologies have the potential to revolutionize drug delivery for a wide range of diseases [37]. HA-based hydrogels, known for their biocompatibility, have garnered attention across diverse biomedical fields, including tissue regeneration, diagnostics, and drug delivery. HA-based hydrogels are promising materials for therapeutic and diagnostic applications. HA-based hydrogels are biocompatible, tunable, and versatile. HA-based hydrogels can be used to deliver drugs to specific cells or tissues. HA-based hydrogels can also be used to deliver proteins and other biological drugs to specific tissues. HA-based hydrogels can also be used to support tissue regeneration. HA-based hydrogels are being developed as biosensors and imaging contrast agents [38]. Targeting ligands and crosslinkers are promising tools for designing more effective and targeted drug delivery systems. Targeting ligands can be used to guide drugs to specific cells or tissues, improving the efficacy of treatment and reducing side effects. Crosslinkers can be used to create stable drug delivery systems for controlled drug release. Targeting ligands and crosslinkers are being used to develop new drug delivery systems for a variety of diseases. These technologies have the potential to revolutionize the field of medicine and make it possible to develop more effective and personalized treatments for a wide range of diseases [39]. IEDDA click reaction-based HA hydrogels are promising materials for targeted drug delivery. These hydrogels are catalyst-free, stimuli-responsive, and can be targeted to specific cells or tissues by attaching targeting ligands. IEDDA click reaction-based HA hydrogels are formed by the reaction of tetrazine and trans-cyclooctene groups, which is a catalyst-free and stimuli-responsive reaction. These hydrogels can be targeted to specific cells or tissues by attaching targeting

ligands to the hydrogel surface. IEDDA click reaction-based HA hydrogels are being used to develop new drug delivery systems for a variety of diseases, including cancer, infectious diseases, and cardiovascular diseases. For example, researchers are developing IEDDA click reaction-based HA hydrogels to deliver chemotherapy drugs to cancer cells. The hydrogels are targeted at cancer cells by attaching folic acid to the hydrogel surface. The hydrogels are also designed to be pH-responsive so that the drugs are released in the tumor microenvironment. These hydrogels have the potential to revolutionize the field of medicine and make it possible to develop more effective and personalized treatments for a wide range of diseases [40]. Starch-based materials (SHs) are a promising new class of materials with a wide range of potential applications. They are derived from starch, a renewable and abundant resource. SHs are biodegradable, compostable, nontoxic, and versatile. SHs can be used to develop sustainable materials and solutions for a variety of global challenges, such as climate change, food insecurity, and plastic pollution. For example, SHs can be used to produce biofuels, sustainable packaging materials, biodegradable food packaging materials, edible films and coatings, biodegradable straws, utensils, food packaging materials, and bio-based plastics. By understanding the unique properties of SHs and developing new ways to use them, we can create new and innovative ways to reduce our environmental impact and create a more sustainable future [41]. SHs are a promising class of materials for sustainable development. They are derived from renewable resources, exhibit properties that make them versatile for various sectors and can be used to develop sustainable solutions for global challenges. SHs are aligned with green chemistry principles and can be used to develop a wide range of products, including packaging materials, food additives, textiles, and drug delivery systems. SHs can also be used to develop sustainable solutions for global challenges, such as climate change, food insecurity, and plastic pollution. Some specific examples of SH-based products that are currently available or under development – edible films and coatings, biodegradable straws, utensils, food packaging materials, bio-based plastics, and SH-based drug delivery systems. As research on SHs continues, we can expect to see even more innovative and sustainable products made from these materials in the future [42]. SHs are a promising class of sustainable materials derived from starch, a renewable and abundant resource. SHs are biodegradable, compostable, nontoxic, and versatile. SHs can be used to develop sustainable packaging materials, food additives, textiles, drug delivery systems, and solutions for global challenges, such as climate change, food insecurity, and plastic pollution. It is important to consider the ethical and social implications of using SHs, such as their impact on food security and the environment. By carefully weighing the benefits and drawbacks, we can ensure that SHs are used in a responsible and sustainable manner [43]. Starch's molecular arrangement, defined by amylose and amylopectin, plays a vital role in its properties. Understanding this structure is essential for developing sustainable materials and enhanced functionality in food science, biotechnology, and material engineering. Interdisciplinary research focuses on optimizing amylose and amylopectin components to achieve desired properties [44]. Amylose and amylopectin are the two major components of starch, with amylopectin being the dominant

one. The relative composition of these two components varies depending on the source of starch, such as corn, wheat, potato, and rice. This variation in composition also affects the physical properties of starch, such as its amorphous-crystalline balance, digestibility, viscosity, and texture. Interdisciplinary research is ongoing to leverage the diversity of starch and its components to develop tailored materials with functional and sustainable properties. For example, researchers are developing starch-based bioplastics, food additives, textiles, and drug delivery systems with enhanced properties by manipulating the amylose and amylopectin components [45]. By understanding the role of amylose and amylopectin in the crystallinity and biodegradability of starch, researchers can design starch-based bioplastics with tailored properties for specific applications. Starch-based food additives, such as thickeners, emulsifiers, and stabilizers, are widely used in the food industry. Researchers can leverage the unique properties of amylose and amylopectin to develop starch-based food additives with improved functionality and reduced environmental impact. Amylose and amylopectin can be used to engineer starch-based drug delivery systems with controlled release of drugs [46]. Native starch has limitations in dimensional stability, mechanical properties, and processing efficiency. To address these challenges, researchers are developing cutting-edge approaches to modify starch properties using green chemical methods, composite materials, and scalable processing methods. These new materials offer eco-friendly alternatives with tailored functionalities for diverse applications [47]. Researchers employ green chemistry principles to modify starch for diverse applications, driven by sustainability concerns. This approach aims to enhance starch performance while reducing environmental impact. Interdisciplinary collaboration in materials science and chemistry is essential to explore innovative materials and compositions. Ongoing cutting-edge research focuses on sustainable starch-based solutions for global challenges [48]. Radiation-based modifications of starch offer a promising approach to developing sustainable materials with enhanced properties for diverse applications. This green chemistry-inspired method allows precise and eco-friendly alterations to starch's properties, promoting sustainability. Interdisciplinary efforts involving materials science and radiation physics are essential to advance this technique, with ongoing research aimed at optimizing radiation-based modifications for various applications [17]. Green chemistry-inspired radiation-based modification of starch is a promising approach to developing sustainable materials with enhanced properties for diverse applications. This method allows precise and eco-friendly alterations to starch properties while ensuring safety. Interdisciplinary efforts encompassing radiation physics and materials science are essential to advance this technique. Researchers are exploring sustainable techniques to further enhance performance and reduce environmental impact, such as using natural crosslinkers [49]. Starch citrate, a sustainable and versatile material with natural antibacterial properties, can be further enhanced through green chemistry-inspired radiation-based modification. This approach allows precise and eco-friendly alterations to starch citrate's properties, tailoring its performance for specific applications. Interdisciplinary efforts encompassing radiation physics, materials science, and microbiology are essential to advance this technique [50].

Green chemistry-inspired radiation-based modification of starch citrate and lignin is a promising approach to developing sustainable materials with enhanced antimicrobial properties and improved performance for diverse applications. This technique offers precise and eco-friendly alterations to material properties, enabling tailoring to specific needs. Interdisciplinary collaboration and optimization are essential to advance this field. Lignin-based innovations are gaining traction as researchers seek to address environmental challenges and create more sustainable materials. Larraneta et al. [51] introduced an eco-friendly approach to preparing these materials by combining LIG with poly(ethylene glycol) and poly(methyl vinyl ether-co malic acid) through an esterification reaction, significantly accelerating the process using microwave (MW) radiation. Microwave-assisted modification of starch citrate and lignin is a promising green chemistry-inspired approach to developing sustainable materials with enhanced properties and performance for diverse applications. This method allows precise and eco-friendly alterations to material properties, enabling tailoring to specific needs. Interdisciplinary collaboration and optimization are essential to advance this field. Microwave technology offers numerous advantages, such as reduced production time, energy consumption, and costs, making it a particularly valuable tool for industries seeking more efficient and eco-friendly manufacturing [52]. Sustainable drug delivery systems based on starch citrate, lignin, and inulin offer a promising green chemistry-inspired approach to developing innovative and eco-friendly materials for targeted and controlled drug delivery. These systems have the potential to address the limitations of traditional drug delivery systems, such as systemic side effects and poor drug bioavailability. Interdisciplinary collaboration and optimization are essential to advance this field and bring these systems to fruition [53]. Researchers could design a sustainable and scalable green chemistry-inspired drug delivery system based on linseed mucilage for the controlled release of an oral insulin formulation. The pH-responsive hydrogel would release insulin in the acidic environment of the stomach, ensuring direct delivery to the bloodstream. The system would be biocompatible, biodegradable, and adaptable for use with other drugs and delivery routes. This example demonstrates the potential of linseed mucilage-based materials in developing sustainable and innovative drug delivery systems [54].

Green chemistry-inspired synthesis of Ag-NPs is a promising approach to developing sustainable and effective antimicrobial materials. These Ag-NPs possess antioxidant and antimicrobial properties, making them promising candidates for a variety of applications beyond biomedicine, including environmental remediation and food packaging [55]. Gellan gum (GG) stands out as a sustainable biopolymer, boasting biocompatibility, hydrophilicity, and gelling properties. Its applications span agriculture, where GG-based formulations control pesticide and fertilizer release, mitigating environmental concerns. In food technology, GG's gelling prowess elevates textures and prolongs product shelf life, reducing food waste. Moreover, GG's potential in biomedicine encompasses drug delivery and tissue engineering. GG's versatility and eco-friendliness make it a key player in crafting innovative and sustainable solutions across these diverse fields [56]. Electro-stimulated drug release devices (EDRDs) are innovative medical tools

designed to respond to electrical signals, offering precise and adaptable controlled substance release. Notably, they hold immense promise in the realm of insulin delivery for diabetes management. These devices are characterized by their precision, ensuring patients receive the correct insulin dose when needed, enhancing safety through biocompatible materials, and adaptability to individual insulin requirements. For instance, researchers envision an EDRD comprising an implantable device equipped with a reservoir for insulin and a microfluidic network. It can be powered by a battery, rechargeable with an external transmitter, and programmed to adjust insulin release based on real time blood sugar monitoring. Such EDRDs, typically constructed from durable materials like silicone and titanium, offer improved blood sugar control, reduced diabetes-related complications, and an enhanced quality of life for individuals with diabetes [57]. Genipin-based crosslinked materials represent a sustainable avenue for creating controlled release systems in agriculture, benefiting both the environment and crop health. Genipin, a natural and biodegradable crosslinking agent, serves as an eco-friendly choice. An example of such a system is the biodegradable capsule, which combines pesticides, nutrients, and genipin to ensure prolonged chemical release near plant roots. By adjusting capsule attributes and genipin concentration, this approach can be tailored to meet specific crop needs, reducing environmental impact, enhancing crop efficiency, and maintaining nutrient consistency [58]. Genipin-crosslinked materials, leveraging the natural and biodegradable properties of genipin, offer a sustainable solution for wastewater treatment. They excel in pollutant removal, including heavy metals, due to their tailored affinity. These materials enhance water quality, reduce environmental impacts, and protect public health, exemplifying their versatile applications in improving wastewater treatment systems [59]. Green chemistry principles are driving the development of sustainable and scalable nanomaterial synthesis methods, particularly for applications in consumer electronics and renewable energy. These approaches prioritize eco-friendliness by minimizing hazardous chemicals and waste production. Examples include using natural materials like cellulose nanofibers, silver nanowire synthesis, and employing aqueous solutions and mild conditions for silicon nanocrystal production. Furthermore, continuous flow reactors facilitate large-scale nanomaterial production. These advancements are crucial for integrating nanotechnology into consumer electronics and renewable energy solutions [60]. Green composites are ushering in a transformation in the transportation sector, particularly in lightweight auto parts and aerospace applications. These composites, crafted from renewable and recyclable materials like plant fibers and bio-based resins, offer substantial environmental advantages compared to petroleum-based counterparts. Notable examples include natural fiber-reinforced polymer (NFRP) composites for lightweight auto parts and carbon fiber-reinforced bioresin (CFRB) composites for aerospace applications. These innovations hold the potential to revolutionize the industry, making vehicles more fuel-efficient, lighter, and eco-friendly [61]. Sustainable food packaging materials are emerging as a pivotal solution to address global food waste issues, enhancing food security and reducing the environmental footprint of the food industry. Two notable examples include edible coatings, which preserve product freshness by reducing moisture

loss and inhibiting microbial growth, and active packaging materials, designed to interact with food or the environment to extend shelf life. These innovations hold the potential to revolutionize the food industry by ensuring safer, fresher, and more sustainable food products [62]. Academic sustainable chemistry programs educate future scientists on eco-friendly practices. Research institutions prioritize sustainability, advancing green technologies globally. Sustainable materials and green chemistry foster an environmentally responsible future, addressing global challenges while promoting harmony with the planet.

## 2.2 Fundamental Concepts of the Electromagnetic Spectrum Theory

The electromagnetic spectrum theory is a foundational concept in physics, describing the behavior of electromagnetic waves characterized by oscillating electric and magnetic fields propagating through space at the speed of light. This theory plays a pivotal role in numerous scientific and technological domains, including communication, imaging, and scientific research, spanning radio waves to gamma rays. Some key principles include the transverse nature of electromagnetic waves, their constant speed in a vacuum, and the inverse relationship between frequency and wavelength. One challenging application is the design of an early stage cancer cell detection system utilizing electromagnetic waves. To accomplish this, researchers would need to determine the most suitable type of electromagnetic waves for precise imaging, establish methods to differentiate between cancerous and healthy cells, enhance sensitivity for early detection, and ensure the system's safety and affordability [63]. The electromagnetic spectrum encompasses a wide range of electromagnetic radiation, from long radio waves to short gamma rays, capable of traveling through various mediums, even vacuum. Frequency, measured in Hertz (Hz), denotes the number of wave cycles within a unit of time, while wavelength represents the spatial length of one complete cycle, inversely related to frequency. The speed of light ( $c$ ) in a medium is the product of frequency and wavelength, as expressed in the equation  $c = f\lambda$ , highlighting their fundamental interdependence. For instance, visible light spans a frequency range of 400–700 THz, with corresponding wavelengths of 400–700 nm. In a vacuum, light travels at a constant speed of approximately 300 000 km/s, where the inverse relationship between frequency and wavelength holds true, distinguishing colors like red and blue based on their frequencies and wavelengths. A challenging task related to this topic involves designing an electromagnetic wave-based imaging system to detect cancer cells in their early stages. This challenge demands a profound understanding of electromagnetic theory to select the appropriate waves, devise mechanisms for cancer cell differentiation, enhance sensitivity for early detection, and ensure safety and affordability for patients [64]. In the realm of electromagnetic waves and energy harvesting, it is crucial to understand that the energy of these waves corresponds directly to their frequency. The electromagnetic spectrum covers an extensive range of frequencies, from extremely low to extremely high, each with its unique



applications across various fields, including telecommunications, medical imaging, and more. Energy harvesting, on the other hand, involves converting environmental energy into electrical power, and electromagnetic wave-based systems offer the potential to harness energy from any part of the spectrum. An illustrative example introduces a broadband electromagnetic energy harvester capable of converting a wide spectrum of frequencies into electricity [65]. This innovative technology holds promise for powering wireless sensor nodes and small electronic devices, albeit with the ongoing challenge of achieving cost-effective and efficient energy harvesting across a broader range of applications. Potential applications for electromagnetic wave-based energy harvesting are diverse, ranging from powering environmental sensors and small electronics to providing energy solutions in remote or off-grid areas, including disaster zones. Furthermore, this technology can play a role in sustainable energy generation from renewable sources like solar and wind. However, several challenges must be addressed, including refining the efficiency and cost-effectiveness of energy harvesting systems, ensuring they can harness energy across a wide frequency range, enhancing their durability and reliability, and integrating them effectively with existing energy grids [66].

The utilization of electromagnetic waves in the quest to detect and identify exoplanets presents promising opportunities. Different approaches involve designing devices to detect how exoplanets interact with electromagnetic waves, either by absorbing or reflecting them. Additionally, the unique spectral signatures of exoplanets, shaped by their composition and atmosphere, offer another avenue for identification. A recent example in this field highlights the potential of using radio waves to detect exoplanets, particularly smaller and fainter ones, through reflection [67]. Nonetheless, challenges persist, including the need for highly sensitive and affordable devices, as well as the distinction between exoplanets and other celestial objects. Despite these challenges, the development of electromagnetic wave-based devices for exoplanet detection is a vibrant research area with the potential to revolutionize exoplanetary astronomy and expand our search for extraterrestrial life [68].

The wave-particle duality of electromagnetic radiation, inherent in the quantum nature of photons, has profound implications for various scientific and technological applications. Notably, this duality plays a pivotal role in the functionality of devices harnessing electromagnetic waves. Quantum devices, capitalizing on the unique properties of quantum systems, offer capabilities beyond classical counterparts. Quantum computers, for instance, leverage the superposition and entanglement of quantum particles, enabling computations unattainable by classical computers. Similarly, quantum cryptography devices exploit the quantum properties of light to establish unhackable communication channels. A pertinent example from research explores the potential of using photons to construct quantum computers, shedding light on the advantages and challenges of this approach [69]. These quantum devices hold promise in diverse fields, including materials science, secure communication, high-precision sensing, and advanced imaging. However, their development requires meticulous control of quantum systems and addressing sensitivity to external disturbances. Despite these challenges, ongoing research in quantum devices stands poised to usher in transformative technologies with

far-reaching implications [70]. Microwaves are a type of electromagnetic radiation with wavelengths ranging from approximately 1 mm to 30 cm. They have a variety of applications, including cooking, communication, and medical imaging. One of the potential applications of microwaves is in the noninvasive detection and identification of tumors. Microwaves can interact with matter in a variety of ways, depending on the dielectric properties of the material. Dielectric properties are the electrical properties of a material, and they can vary depending on the composition of the material. Tumors typically have different dielectric properties than healthy tissue, so it may be possible to use microwaves to detect the presence of tumors. There are a number of different approaches to designing microwave-based devices for detecting and identifying tumors. One approach is to design a device that can detect the difference in dielectric properties between tumors and healthy tissue. Another approach is to design a device that can detect the metabolic activity of tumors. Tumors typically have higher metabolic activity than healthy tissue, so it may be possible to use microwaves to detect the increased metabolic activity of tumors [71].

Microwaves, with their unique interaction capabilities based on material dielectric properties, are at the forefront of material property control. Their applications span multiple domains, from enhancing the conductivity of semiconductors to crafting patterns in materials and guiding crystal growth. Notably, microwave-assisted synthesis of nanomaterials offers significant promise, as highlighted in research on nanomaterial production. Challenges encompass the need for precise, scalable, and cost-effective control devices, as well as deeper insights into fundamental microwave-material interactions. Nevertheless, ongoing research in this dynamic field is poised to revolutionize various industries, leading to improved material properties, more efficient manufacturing processes, and the creation of novel nanomaterials. This burgeoning area of microwave-based material control holds the potential to transform industries and drive innovation across multiple sectors [72].

Microwave cooking, a popular and convenient method, harnesses electromagnetic radiation with wavelengths from 1 mm to 30 cm. It relies on the interaction of microwaves with polar molecules, which possess positive and negative ends. When exposed to microwaves, these molecules rotate and generate heat. The heat generated depends on microwave frequency and the material's dielectric properties, which vary with its composition. This cooking technique exploits the high dielectric properties of water, a key component in most foods. As microwaves interact with water molecules in the food, they induce molecular rotation, resulting in heat generation and food cooking. Beyond culinary applications, microwave heating finds utility in scientific realms like food processing, chemical synthesis, and materials science, facilitating quick and efficient drying, pasteurization, chemical synthesis, and annealing of materials. Understanding the fundamental interaction between microwaves and polar molecules is crucial for mastering microwave cooking and optimizing its application in scientific research. It plays a pivotal role in food preparation, from cooking diverse foods to defrosting, reheating, and even making popcorn. In the scientific domain, microwave technology has enabled advances in food processing, chemical synthesis, and materials science, enhancing efficiency and enabling innovative research [73]. Electromagnetic

radiation comprises oscillating electric and magnetic fields traveling at the speed of light, guided by Maxwell's equations. Microwave irradiation's efficacy lies in its selective interaction with molecules like water, inducing their rotation and generating heat. This principle finds applications in various fields, including science and cooking, emphasizing the importance of understanding these interactions [74]. Understanding these principles elucidates microwave heating mechanisms, crucial for efficient cooking as microwaves penetrate and heat food from within. Beyond cooking, microwaves are applied in diverse fields, including chemistry and materials research, due to their selective interaction with specific materials. This fundamental understanding is vital for optimizing microwave applications in various disciplines [75]. Microwave selectivity facilitates precise manipulation and research in scientific and industrial sectors. This versatility highlights its value in diverse contexts, from chemistry to materials research, enhancing efficiency and precision. Understanding this capability is fundamental for optimizing microwave applications across disciplines [76]. A profound understanding of the electromagnetic spectrum and MW principles reveals their wide-ranging applications in daily life, science, and industry. Microwaves, as a part of the spectrum, are harnessed for tasks like cooking and scientific research. Understanding wave-particle duality, wavelength-frequency relationships, and microwave-material interactions is crucial for effective utilization in diverse applications, laying the foundation for comprehending their significance in various fields.

### **2.3 Electrical, Dielectric, and Magnetic Properties in Microwave Irradiation**

Microwave irradiation employs electromagnetic waves within the microwave frequency range (300 MHz to 300 GHz) to induce dielectric and magnetic properties in materials, facilitating various scientific and industrial applications. These interactions are crucial for fields such as chemistry, materials research, and communication technologies. Understanding these principles is fundamental for harnessing microwave irradiation's potential in diverse contexts [77]. Understanding microwave-material interactions, driven by dielectric characteristics and polarization, is essential for the effective utilization of this technology. Its broad applications encompass materials science, chemistry, and communication, underscoring its importance in diverse scientific and practical realms. Researchers explore novel materials and compositions, advancing current understanding and pushing the boundaries of microwave-based research in various disciplines [78]. The dielectric constant, or relative permittivity, characterizes a material's ability to store electrical energy under an electric field, influencing electromagnetic wave propagation. This property is crucial in optimizing microwave-material interactions, particularly in materials science and communication. Materials with higher dielectric constants exhibit greater microwave absorption, impacting various scientific and industrial applications [79]. Dielectric loss ( $\tan \delta$ ) quantifies energy dissipation as heat in response to an electric field's polarization phase angle. Materials with higher  $\tan \delta$

absorb more microwave energy, vital for controlled heating in applications like cooking and scientific research. Understanding and manipulating  $\tan \delta$  in various materials are significant for optimizing microwave-based processes [80]. Magnetic permeability is vital for materials' interaction with magnetic components of electromagnetic waves, especially microwaves. High magnetic permeability enhances this interaction, impacting microwave-based processes. This knowledge is critical in fields like materials science and electromagnetic applications, where precise control of materials' magnetic response is significant for optimizing performance [81]. Understanding these properties is crucial for optimizing material behavior in various applications. Materials with dielectric losses can be heated using microwaves and applied in industrial processes like curing and medical hyperthermia for cancer treatment. This knowledge is relevant in materials science, engineering, and medical disciplines for efficient energy absorption and controlled heating [82]. Microwave irradiation is versatile, used in polymerization, chemical synthesis, and nanoparticle production. Knowledge of dielectric and magnetic properties is crucial for antenna and radar system design, but these properties can vary with material composition and conditions. Microwave technology has diverse applications in both scientific and industrial domains. A comprehensive understanding of material properties is essential for optimizing microwave applications in diverse fields, enabling tailored and enhanced performance in scientific and industrial settings. Conductive polymer composites (CPCs) are integral in applications involving microwave irradiation due to their critical electrical, dielectric, and magnetic properties. These properties are essential for applications like electromagnetic interference (EMI) shielding, capacitors, and integrated circuits when exposed to MW. CPCs offer versatility in materials and compositions, driving ongoing cutting-edge research across multiple disciplines to optimize their performance in various scientific and industrial contexts [83]. In the realm of microwave irradiation, optimizing CPCs demands a balance between achieving favorable electrical and dielectric properties while mitigating challenges related to high nanofiller content. This balance is crucial for applications like EMI shielding and integrated circuits. Interdisciplinary research focuses on reducing the percolation threshold, enhancing electrical conductivity, and addressing processing complexities to improve CPC performance in diverse scientific and industrial contexts [84]. In the context of microwave applications, the "segregated network" strategy involves selectively dispersing nanofillers at composite interfaces and impacting electrical and dielectric properties. This approach is relevant for applications like EMI shielding but may pose challenges related to polymeric molecule diffusion and structural integrity. Achieving the right balance in electrical conductivity is crucial, driving interdisciplinary research in materials science and engineering to optimize CPC performance in diverse contexts [85]. In microwave applications, CPCs with electrical conductivity below  $1 \text{ S m}^{-1}$  are sought for effective EMI shielding, but achieving both low conductivity and microwave transparency is challenging. Commercially, EMI shielding effectiveness targets are often below 20 dB. Carbon-based nanofillers such as multi-walled carbon nanotubes (MWCNTs), graphene nanoplatelets, and carbon nanofibers, known for high aspect ratios and electrical conductivity, are favored for reinforcing CPCs in microwave

scenarios, driving interdisciplinary research in materials science and engineering for improved performance [86]. Research on CPCs for microwave applications focuses on unraveling structure-property relationships. This entails investigating how nanofiller distribution, concentration, and type influence CPCs' electrical, dielectric, and magnetic characteristics under microwave irradiation. Achieving the right balance of these properties is vital for optimizing CPCs in applications requiring EMI shielding and microwave transparency, driving interdisciplinary research in materials science and engineering for enhanced CPC performance [87]. Studying dielectric constants in microwave irradiation is essential for optimizing the materials' microwave absorption. This property impacts various scientific and industrial applications, especially in microwave heating. Materials with higher dielectric constants absorb more microwave energy, making them valuable for processes like cooking and materials processing. This research contributes to understanding and harnessing microwave energy for diverse purposes, involving materials science and engineering disciplines [87]. Microwave irradiation can enhance the electrical conductivity of materials by promoting ion mobility. This phenomenon is relevant in material processing and chemical reactions, where increased conductivity can accelerate processes. The interdisciplinary field involves materials science and chemistry, aiming to optimize conductivity for various industrial applications. Understanding these mechanisms contributes to more efficient processes and innovative technologies [88]. The dielectric loss factor ( $\tan \delta$ ) signifies a material's ability to convert microwave energy into heat. Materials with higher  $\tan \delta$  values absorb and dissipate microwave energy efficiently. This phenomenon, known as dielectric relaxation, involves rapid dipole oscillation and is crucial for optimizing microwave heating processes in various scientific and industrial applications. Research in this field explores how different materials and compositions impact dielectric behavior, contributing to improved microwave-based technologies [89]. Magnetic permeability characterizes a material's response to a magnetic field, influencing its interaction with electromagnetic waves during microwave irradiation. High magnetic permeability materials can significantly affect heating behavior in microwave applications, making their study important in optimizing such processes. Research in this area explores how material compositions impact magnetic properties, contributing to advancements in microwave technology and applications [90]. Research into materials like iron-based compounds explores their strong magnetic responses to microwaves, enabling applications like induction heating. This research delves into how these properties vary with factors like frequency and temperature, providing insights into energy absorption mechanisms. It is crucial for optimizing microwave-based heating processes in various fields, from metallurgy to materials science [91]. Research in tailoring materials and processes for electrical, dielectric, and magnetic responses to microwave irradiation has wide-ranging applications, spanning from food processing to environmental remediation. It promises enhanced energy efficiency and product quality across industries. This interdisciplinary field involves materials science, engineering, and physics, focusing on optimizing energy absorption mechanisms for diverse industrial and scientific purposes.

## 2.4 Microwave Irradiation Molecular Rotation

Microwave irradiation employs microwave electromagnetic waves to induce molecular rotation in materials. This technique is vital in scientific research, chemistry, and various industrial applications. Researchers from disciplines such as chemistry, physics, and materials science study this process to optimize microwave-related outcomes, such as heating and material processing, across a spectrum of materials and compositions. Understanding these principles contributes to advancements in energy-efficient technologies and diverse scientific domains [92, 93]. Understanding molecular rotation induced by MW is pivotal for optimizing its applications in scientific research and industrial processes. This phenomenon occurs in polar molecules due to the interaction between their electric dipole moments and microwave electromagnetic fields. Researchers across disciplines such as chemistry, physics, and engineering investigate these processes, contributing to advancements in diverse fields and the development of energy-efficient technologies [94]. Molecular rotation induced by microwave energy is essential for diverse applications in chemistry, materials science, and communication. It involves polar molecules absorbing microwave energy and causing transitions between rotational states. Researchers from various disciplines investigate these processes, advancing scientific knowledge and technological innovations across industries [78]. Microwave ovens utilize molecular rotation of water molecules to efficiently heat food through MW absorption, causing friction and generating heat. This process is fundamental in cooking and has broad applications in scientific contexts. Understanding this heating mechanism is crucial for efficient microwave technology utilization in various fields, involving interdisciplinary research and practical significance [95]. Microwave irradiation's role in molecular rotation is pivotal for accelerating chemical reactions, particularly in organic synthesis, where it offers precision and speed. This technique finds application in diverse scientific and industrial contexts, enhancing reaction efficiency. Understanding these mechanisms is essential for optimizing microwave irradiation across various disciplines, involving material-specific applications and ongoing research into reaction kinetics [96]. Microwave irradiation, operating in the 300 MHz to 300 GHz frequency range, has diverse applications in materials science and medical chemistry. Nonpolar molecules do not undergo molecular rotation in response to MW, distinguishing their behavior from polar molecules. This understanding of microwave characteristics is vital for its application and significance across scientific disciplines and industrial domains [97]. Molecular responses to MW are pivotal in materials science and medical chemistry. Microwaves induce rotations in molecules with a dipole moment, altering their energy levels, impacting diverse applications. This knowledge is pivotal for precise molecular control in scientific and industrial contexts [98]. Microwave technology, utilized in applications like microwave ovens and chemical synthesis, selectively excites water molecules, inducing molecular rotation and heat generation. This accelerates chemical reactions, particularly in chemistry and materials research, enhancing precision and efficiency. Understanding these principles is crucial for advancing scientific and industrial processes reliant on controlled molecular interactions [99]. Microwave

irradiation enhances process efficiency and precision in scientific and industrial applications. Tailored utilization of this technology relies on understanding molecular response to microwaves, considering factors like structure and dipole moment. This knowledge informs applications in various disciplines, optimizing processes dependent on controlled molecular behavior [100]. Microwave irradiation, with limitations, is employed for selective heating of polar molecules, particularly in materials like water. Its application is constrained by the need for compatible materials and specific frequency and wavelength ranges. Microwave irradiation, despite limitations, is a versatile tool for scientific and industrial applications. Its impact on molecular rotation informs tailored approaches in various domains, emphasizing precision in controlling molecular behavior. A profound understanding of these principles underpins its valuable real-world applications.

## **2.5 Fundamentals of Electromagnetic Theory in Microwave Irradiation**

Chemical reactions are initiated using diverse energy sources, such as heat, light, pressure, plasma, ultrasound, and microwaves. These methods enable bond breaking and formation, vital for reactions across chemistry, materials science, and industry. Their application varies, optimizing processes in different fields, and ongoing research explores their mechanisms and significance in precision-controlled reactions [101]. Microwave heating, also called dielectric heating, is an efficient method using electromagnetic waves to induce rapid and precise heating in materials, replacing traditional conductive heating. Its significance lies in its speed and precision, finding applications in chemistry, materials synthesis, and industry. Ongoing research explores its mechanisms and potential for controlled heating processes [102]. Microwave heating is often referred to as dielectric heating because it primarily relies on the dielectric properties of materials to generate heat when exposed to MW. Dielectric heating occurs due to the interaction between the alternating electric field of microwaves and polar molecules within the material. The rapid changes in the electric field cause the polar molecules to continuously reorient themselves, generating heat through friction and molecular movement. This dielectric heating mechanism is the fundamental principle behind how microwave ovens and other microwave heating applications work. Microwave heating harnesses the ability of materials, both liquids and solids, to convert MW into internal heat. This method is pivotal in various scientific and industrial processes, offering rapid and precise heating capabilities. Its applications span chemistry, materials synthesis, and product testing, where efficiency and controlled heating are essential for enhancing process outcomes and productivity. Researchers in disciplines like chemistry and materials science continue to explore innovative applications and mechanisms to optimize microwave heating for diverse purposes [103].

### 2.5.1 Electromagnetic Radiations and Microwave

Researchers are advancing electromagnetic radiation-based devices to finely manipulate atomic and molecular-level properties of materials, offering transformative impacts across industries such as manufacturing, medicine, and electronics. These devices encompass lasers, microwaves, and terahertz radiation, enabling precise control over chemical reactions, material properties, and even molecular rotation. Challenges include controlled manipulation, affordability, and integration with existing processes, making this field of research highly promising for revolutionizing various industries and enhancing material properties, manufacturing efficiency, and medical applications, as shown in Figure 2.3a [104]. Electromagnetic radiation-based devices for detecting and identifying exoplanets are crucial for exploring distant worlds beyond our solar system. They tackle the challenge of detecting faint exoplanets in the presence of bright stars. Two primary devices are transit photometers, which observe the dimming of a star when an exoplanet passes in front of it, revealing the exoplanet's size and orbit, and radial velocity spectrometers, which measure the star's Doppler shift caused by the gravitational pull of an orbiting exoplanet, allowing for the determination of its mass. These devices offer profound implications, from discovering potentially habitable exoplanets to studying their atmospheres for signs of life and furthering our knowledge of exoplanetary system formation and evolution. The interdisciplinary nature of this field involves astronomy, physics, engineering, and materials science, pushing the boundaries of our understanding of exoplanets and the cosmos [105]. Microwave-based energy harvesting devices harness MW to generate electricity, offering a clean and renewable energy source. They can convert MW into electrical power, primarily through devices like rectennas and thermoelectric converters. Microwaves are abundant in the environment, originating from various sources, including the sun and human-made devices. Research in this field aims to develop efficient and affordable devices that can power a wide range of applications, from smartphones to remote sensors, and even utilize waste heat for energy harvesting. Interdisciplinary research spanning engineering, physics, and materials science drives innovation, with a focus on improving efficiency and compatibility with existing energy systems, thus potentially reducing reliance on fossil fuels and advancing sustainable energy solutions, as shown in Figure 2.3b. Microwave-based devices in chemical reactions aim to enhance efficiency and safety. By utilizing MW, these devices heat reactants rapidly and uniformly, as seen in microwave synthesis reactors, leading to shorter reaction times and increased yields. Additionally, microwave plasma reactors can create plasmas to accelerate various chemical reactions. Safety is improved by decomposing hazardous chemicals through microwave heating or radiation exposure with catalysts. Research spans various disciplines, including chemistry and materials science, aiming to design cost-effective devices compatible with existing equipment and scale up reactions from labs to industry. This innovation holds the potential to revolutionize chemical, pharmaceutical,



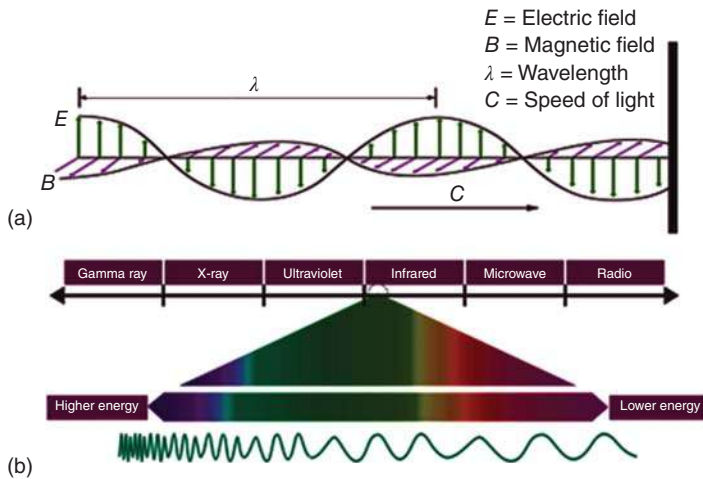


**Figure 2.3** (a) Electromagnetic radiation and (b) electromagnetic spectrum.

and materials industries, promoting environmental sustainability and creating enhanced products [106].

### 2.5.2 Heating Mechanism of Microwave: Conventional Versus Microwave Heating

Microwave-based devices for heating materials offer efficient and controlled heating in industrial and scientific applications. They utilize MW to heat materials rapidly and uniformly, reducing processing times and enhancing product quality. Examples include microwave volumetric heaters and flow-through reactors, which minimize heat loss and support continuous processing. Challenges include designing precise and compatible devices while ensuring affordability and scalability. Advancements in this field have the potential to revolutionize manufacturing, food processing, and medical devices, offering improved efficiency and innovation in various industries [107]. The dominant role of the electric field component of MW in heating polar molecules arises from the tendency of polar molecules to align with the electric field, leading to rapid molecular rotation and heat generation through collisions. This principle is harnessed in various innovative microwave-based devices. This phenomenon is crucial for microwave ovens, microwave plasma reactors, and medical devices that selectively heat cells, with applications spanning food processing, chemical reactions, and medical treatments. Challenges include device efficiency, affordability, and safety [108]. The fundamental concept involves designing microwave-based devices to precisely control microwave-matter interactions at the nanoscale for synthesizing unique nanomaterials. MW offers advantages such as rapid, uniform heating and acceleration of chemical reactions, revolutionizing nanomaterial synthesis. This research addresses the challenge of precise control over nanomaterial properties, aiming to impact industries such as electronics, energy, and healthcare. Interdisciplinary efforts encompass chemistry, materials

science, and engineering. The forefront involves combining microwave volumetric heating and plasma synthesis for nanomaterial design, with potential implications for advanced technologies [108]. Microwave-based technologies hold the potential to address major challenges in materials processing, food science, medical devices, and scientific research. By enabling rapid and uniform heating, they facilitate the synthesis of novel materials, energy-efficient food processing, minimally invasive medical procedures, and advanced scientific instrumentation, revolutionizing these fields. Interdisciplinary engagement spanning materials science, engineering, and biomedical sciences is essential to harness microwave-based innovations, ushering in a new era of efficient and impactful solutions [109]. The fundamental concept of microwave-based heating in science and engineering is based on the interaction of MW with polar molecules and ions in materials. Microwaves cause rapid dipolar rotation and ionic conduction, generating heat within the material. This technology is significant for its ability to provide efficient and precise heating, finding applications in materials processing, such as sintering ceramics and drying materials. Its study is motivated by the pursuit of energy-efficient heating methods. Academic disciplines engaged include materials science, electrical engineering, chemistry, and physics. Researchers explore advanced microwave technologies, control systems, and novel materials. The field's forefront involves refining microwave heating methods and understanding complex microwave-matter interactions, with implications spanning improved materials processing and scientific research tools, contributing significantly to advancements in science and engineering. The fundamental concept here is harnessing dipolar rotation and ionic conduction through MW to create new microwave-based devices for efficient and precise material heating. These devices function by applying microwaves to polar molecules and ions in materials, inducing rapid rotation and conduction, thereby generating heat. This concept holds significance in various applications, including materials processing, medical devices, and scientific research, where precise heating is crucial. The process involves controlled microwave-matter interactions for targeted heating. This area of study is motivated by the pursuit of energy-efficient and precise heating methods, driving research toward innovative device designs, control systems, and materials utilization. Dipolar rotation involves the movement of polar molecules aligning with electric fields, generating heat in microwave heating. Ionic conduction is the movement of charged ions responding to electric fields, contributing to heat generation in materials. These mechanisms underlie efficient microwave-based heating in various applications, including materials processing and medical devices [110]. Microwave technology, a field of significant scientific and engineering importance, revolves around the utilization of electromagnetic waves in the microwave frequency range for various applications. Fundamentally, microwaves interact with materials at a molecular level, causing dipolar rotation and ionic conduction, generating heat. This concept is significant as it offers rapid, uniform, and efficient heating, impacting diverse areas such as materials processing, medical devices, and scientific research. Applications include microwave ovens, medical hyperthermia treatments, and materials synthesis. Researchers across science and engineering disciplines collaborate to optimize this technology, exploring novel

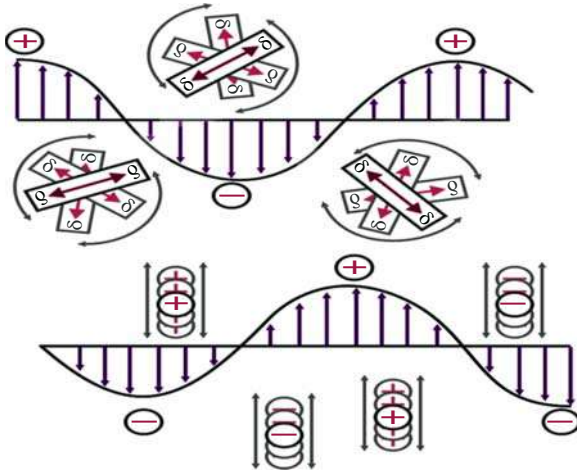


**Figure 2.4** Translational motions with changing electric field.

materials, control methods, sensors, and energy harvesting devices. Governing principles involve electromagnetic wave propagation and material interactions, with implications spanning improved industrial processes, medical treatments, and advanced materials development, as shown in Figure 2.4.

## 2.6 Physical Principles of Microwave Heating and Equipment

The fundamental concept involves using MW to accelerate and control chemical reactions for the synthesis of new materials. MW rapidly heats materials through dipolar rotation and ionic conduction, enabling precise control over reaction conditions. This is significant because it offers a more efficient and uniform method for synthesizing materials with unique properties. Applications are observed in various fields, motivating interdisciplinary research. Materials and compositions can vary widely, from nanomaterials to polymers. Current research focuses on designing microwave-based devices that provide precise control over reaction parameters and scalability for industrial production. Principles of electromagnetic wave interaction with matter govern this technology, with implications spanning materials science, electronics, energy, and catalysis. The pivotal scientific implications include the potential to revolutionize materials synthesis processes across industries [111]. The fundamental concept involves using metamaterials and nano-optics to design a microwave-based device that selectively and precisely heats materials. Metamaterials are engineered materials with specific electromagnetic properties, allowing for the creation of devices that can selectively heat materials or regions of a material. Nano-optics, on the other hand, deals with the precise interaction of light with matter at the nanoscale, enabling the focused application of MW with high precision. This concept is significant because it offers a novel approach to tailored material processing and chemical synthesis, potentially leading to improved product quality,

reduced waste, and the development of new materials. Applications are observed in various fields, motivating interdisciplinary research, and the materials used can vary depending on the specific application. Current research focuses on designing effective metamaterial structures and refining nano-optical techniques for precise microwave heating [112]. The fundamental concept involves using metamaterials and nano-optics to design a microwave-based device capable of highly selective and precise material heating. Metamaterials, engineered for specific electromagnetic properties, enable the creation of devices, selectively heating materials or regions within them. Nano-optics, dealing with nanoscale light-matter interactions, provides the means to focus MW with extraordinary precision. Combining these techniques leads to a device with applications in tailored material processing and chemical synthesis. Research challenges include designing metamaterials with desired electromagnetic properties, developing precise nano-optical techniques, and integrating these into existing equipment. The successful development of such microwave-based devices holds the potential to revolutionize various industries, enhancing material properties, and enabling more efficient chemical synthesis methods, ultimately impacting fields like manufacturing and chemistry [113]. Metamaterials are engineered materials designed at the micro or nanoscale with unique electromagnetic properties not found in nature. They can manipulate electromagnetic waves, enabling effects like negative refraction and invisibility cloaking. Their applications span optics, telecommunications, radar, and materials science, with the potential for revolutionary advances in technology. One innovative approach to designing a new microwave-safe container or utensil involves the integration of microwave-transparent and microwave-absorbing materials in its construction. This concept aims to achieve uniform and controlled microwave heating by allowing the container to absorb and evenly distribute MW while shielding the contents from overheating. Another promising avenue is the incorporation of sensors and feedback mechanisms within the container to monitor and regulate the heating process. These sensors can assess the temperature of the material being heated and adjust the microwave power output, accordingly, ensuring precise and even heating. This research area holds significance in various applications, including culinary arts, scientific research, and industrial processes, as it can enhance safety, precision, and convenience in microwave heating procedures, ultimately reducing waste, and improving outcomes across diverse sectors [114]. One innovative approach to enhancing microwave oven safety features involves the integration of artificial intelligence (AI) and advanced sensor technologies. AI can monitor the oven's operation and identify potential hazards, such as the presence of non-microwavable objects, overheating of food or materials, or incomplete oven door closure. When hazards are detected, the AI system can automatically deactivate the oven or initiate corrective actions. Additionally, advanced sensors can measure internal temperatures, detect gases like steam indicating overheating, and ensure proper door closure, providing critical data for hazard assessment and control. This research area holds significant promise for reducing accidents and injuries associated with microwave oven use, fostering user safety, mitigating product liability concerns, and bolstering consumer trust in microwave oven products [24]. Metamaterials are

engineered to focus MW with high precision, reducing uneven heating and the risk of superheating. Nano-optics further refine heating precision by focusing radiation at the nanoscale. Smart sensors monitor material temperature and moisture content, enabling real time feedback control of microwave power output to ensure even heating without damage [24]. Microwaves, falling within the gigahertz (GHz) frequency range and characterized by their relatively short wavelengths, are a subset of electromagnetic waves with extensive scientific and engineering significance. Their generation relies on specialized vacuum tube technologies, including klystrons, magnetrons, and Gunn diodes. Klystrons utilize the principle of electron bunching and velocity modulation within a resonant cavity to produce microwaves, while magnetrons generate microwaves through the interaction of electrons with a magnetic field within a vacuum. Gunn diodes exploit the Gunn effect in semiconductor materials for microwave generation. Understanding the frequency and wavelength properties of microwaves is fundamental for their diverse applications, encompassing communication, scientific research (spectroscopy, material characterization, cosmic microwave background study), and efficient microwave heating, such as in microwave ovens. Ongoing cutting-edge research is dedicated to enhancing microwave technology, including the development of metamaterials for innovative electromagnetic control and the exploration of quantum phenomena in the microwave realm, with the potential to revolutionize quantum computing and communication [115]. Designing a microwave oven that can uniformly and efficiently heat food while minimizing radiation exposure entails several scientific and engineering principles. One fundamental concept involves using advanced materials, such as metamaterials, with unique electromagnetic properties that enable the controlled manipulation and focusing of MW. This allows for more even penetration and heating of food, addressing the challenge of uneven cooking. Additionally, optimizing microwave oven designs, such as incorporating multiple emitters or reflectors to distribute microwaves evenly, contributes to efficient cooking. Moreover, enhancing shielding technologies with innovative materials and cavity designs can significantly reduce MW leakage, thus improving safety. This interdisciplinary field involves physics, materials science, and engineering, with applications in household appliances and commercial [10]. To design a microwave oven that heats food evenly and efficiently while minimizing radiation exposure using the latest advances in materials science, nanotechnology, and quantum physics, several fundamental concepts and principles come into play. Materials science enables the development of advanced materials like metamaterials that possess unique electromagnetic properties, allowing precise manipulation and focusing of MW to ensure even heating. Nanotechnology contributes by offering nanomaterials that can enhance microwave absorption and create highly reflective materials for improved shielding. Additionally, quantum physics plays a role in developing novel microwave generation and detection technologies, as well as materials with high dielectric constants for stronger interactions with MW. These interdisciplinary approaches hold significant potential for creating microwave ovens with reduced cooking time, improved food quality, enhanced safety, and decreased energy consumption, making them valuable innovations for households

and commercial kitchens [116]. Designing a new type of microwave device that harnesses the wave behaviors of microwaves, including reflection, transmission, refraction, diffraction, and interference, offers significant technological possibilities. Understanding these behaviors is crucial in creating innovative applications. For instance, microwave imaging utilizes microwaves to produce images for medical diagnostics, security screening, and nondestructive testing. Microwave communications encompass satellite communication, cellular networks, and radar systems. Microwave heating, as exemplified by microwave ovens, is integral to both household and industrial processes like material drying and adhesive curing. Additionally, microwave weapons employ microwaves to disrupt or destroy electronic equipment. Recent research in this field has explored advanced materials like metamaterials to enhance microwave focusing and interference for applications such as cloaking devices, with implications for military and stealth technology [117]. Designing a novel microwave device to harness the unique properties of microwaves, such as their ability to penetrate certain materials and reflect off metal surfaces, presents a formidable challenge. One concept involves a microwave device capable of inspecting the interiors of objects by exploiting microwaves' penetrating properties. Such a device could find applications in security screening, nondestructive testing, and medical imaging. Alternatively, it could be used to create an advanced communication system by capitalizing on microwaves' ability to reflect off metal surfaces, benefiting satellite communication, radar technology, and cellular networks. Another avenue explores using microwaves for industrial processes, harnessing their heating capabilities for tasks like material drying, adhesive curing, and material synthesis [78]. Designing a novel microwave heating device that achieves precise and efficient heating of materials with minimal energy consumption and environmental impact is a multifaceted challenge. One critical issue is addressing uneven heating, which can result in hot spots and cold spots, affecting various applications. To mitigate this, metamaterials, engineered with specific electromagnetic properties, offer a promising solution by enabling more precise and efficient MW control. Additionally, optimizing microwave heating devices to operate at lower frequencies can reduce interference with electronic equipment and potentially improve heating efficiency. Moreover, the integration of AI algorithms can further enhance heating precision and efficiency by dynamically controlling power and frequency. These innovations in microwave heating technologies have the potential to revolutionize various fields, including manufacturing, food processing, and medicine, by minimizing energy consumption and environmental impact while ensuring precise and uniform heating. Examples of ongoing research in this domain include studies on metamaterial-based microwave heating devices, as demonstrated, and the application of AI for optimizing microwave food processing [118]. These advancements underscore the significance of microwave heating technology in addressing efficiency and precision challenges across diverse applications [119]. Designing innovative materials and microwave heating devices to harness the fundamental mechanism of dielectric heating is pivotal for achieving precise and energy-efficient material heating with reduced environmental impact. Dielectric heating relies on the interaction between microwave energy

and polar molecules within materials, inducing molecular oscillations and generating frictional heat. Additionally, advanced microwave heating devices, such as those employing metamaterials, can focus MW, ensuring more uniform and efficient heating. The integration of AI algorithms further optimizes the process, allowing precise control of power and frequency to minimize energy consumption [120]. These advancements have far-reaching implications across industries, from enhancing food processing to medical applications and manufacturing [99]. In microwave heating applications, a profound comprehension of penetration depth is indispensable for precise control over heating depth. This attribute significantly influences the effectiveness and controllability of microwave heating processes. The essential components of a microwave heating system encompass a microwave generator, such as a magnetron, a waveguide for directing microwaves, and an applicator designed for focusing microwaves on the target material. Diverse applicator configurations, such as cavity, multimode, and single-mode designs, are tailored to meet specific heating requirements [121]. These components collaboratively orchestrate precise and controlled microwave heating across diverse applications. The selection of an applicator design is meticulously tailored to the specific heating process and the unique characteristics of the material in question. For instance, in household microwave ovens, cavity applicators are commonly utilized, reflecting the continued relevance and development of microwave heating methods in modern times [16]. Designing an innovative microwave heating device that efficiently utilizes the fundamental principle of dielectric heating while ensuring safety and environmental responsibility is a complex task. Dielectric heating relies on the interaction between microwaves and polar molecules within materials, causing molecular oscillations and generating heat through friction. To address the challenges and enhance precision, efficiency, and safety, various approaches can be pursued. Developing materials with high dielectric constants and low thermal conductivity is essential. Redesigning microwave heating devices using multiple emitters, reflectors, or metamaterials to focus MW can result in more even and efficient heating. A 2023 study on ResearchGate demonstrated the superior efficiency of a metamaterial-based microwave heating device. Ensuring user and environmental safety is paramount. Incorporating safety features, such as improved shielding materials, robust door seals, and fail-safe mechanisms, can prevent microwave leakage and mitigate potential hazards [122]. Exploiting microwave interaction with substances allows for the development of innovative technologies across diverse fields. Microwave-assisted drying (MAD) enhances food processing, preserving nutrients and flavor. In medicine, microwave ablation efficiently treats tumors with minimal side effects. Manufacturing benefits from microwave sintering for improved material properties, exemplified by titanium nitride coatings. Microwave-assisted synthesis in materials science yields high-purity nanoparticles like graphene. Understanding these principles drives advancements, involving physics, chemistry, engineering, and materials science, with applications in food, medicine, manufacturing, and materials synthesis. These technologies have profound implications, improving processes and products in various industries, and impacting human lives positively. Fundamentally, microwave interactions induce

molecular oscillations, generating heat, and enabling precise and efficient heating in diverse applications. These innovations address industry needs, motivate interdisciplinary research, and continually advance scientific understanding and technological capabilities [123]. Addressing the challenges of microwave heating involves innovating materials, devices, and AI algorithms. New materials with elevated dielectric constants and reduced thermal conductivity enhance heating efficiency, even for highly conductive substances. Innovative microwave heating devices employing metamaterials or multiple emitters/reflections distribute radiation evenly, mitigating issues related to penetration depth and nonpolar materials. Furthermore, controlling microwave polarization through metamaterials improves heating precision. Harnessing AI optimizes heating processes, adjusting power, frequency, and polarization for various material properties. These advancements transcend fields, enhancing heating efficiency and expanding the applicability of microwaves. Fundamentally, microwave heating relies on dielectric loss mechanisms and electromagnetic wave interactions. Innovations motivate multidisciplinary research, encompassing physics, materials science, engineering, and AI. These advancements have far-reaching implications, improving processes and products in various industries while minimizing energy consumption and environmental impact [124]. The fundamental concept underlying the design of new microwave heating technologies is the interaction of microwaves with substances. Microwaves are electromagnetic waves that induce molecular vibrations and generate heat within materials containing polar molecules. This principle is significant because it enables rapid and efficient heating with minimal energy consumption, making microwaves valuable in various applications. Current research focuses on using metamaterials to distribute microwaves evenly, nanotechnology to enhance material properties, and AI to optimize heating processes. These innovations transcend disciplines, involving physics, materials science, engineering, and AI. Fundamentally, microwave heating relies on dielectric loss mechanisms and electromagnetic wave interactions. Innovations motivate multidisciplinary research, encompassing physics, materials science, engineering, and AI. These advancements have far-reaching implications, improving processes and products in various industries while minimizing energy consumption and environmental impact [125]. The fundamental concept underlying the design of a new microwave heating device based on standing waves is the phenomenon of constructive and destructive interference between incident and reflected microwaves. Standing waves are formed when these interference patterns result in regions of high and low microwave intensity within the heating chamber. This concept is significant as it can be harnessed to achieve precise and efficient heating of materials by controlling the distribution of standing waves. Applications of this phenomenon are observed in various fields, including food processing, materials science, and medical treatments, where controlled heating is essential. Multidisciplinary research encompassing physics, engineering, materials science, and safety engineering is engaged to develop innovative devices. Safety precautions, such as effective shielding, fail-safe mechanisms, and user education, ensure the safe operation of these devices. Research in this area is at the forefront of optimizing standing wave-based microwave heating



for diverse applications, with implications for enhanced efficiency and safety across industries [126]. The fundamental concept underlying the design of a new microwave heating device based on dielectric heating principles is the interaction between MW and polar molecules within materials. Dielectric heating relies on the phenomenon of polar molecules aligning with the alternating electric field of microwaves, leading to molecular motion and frictional heat generation. This concept is significant because it enables precise and efficient heating of materials, finding applications in various fields like food processing, medicine, manufacturing, and materials science. To improve dielectric heating, approaches involve metamaterials for better microwave distribution, advanced control of microwave beams, development of materials with tailored dielectric properties, and the integration of AI for optimization. Safety measures include shielding, fail-safe mechanisms, and user education. Ongoing research aims to enhance dielectric heating efficiency and overcome its challenges for broader applications [127].

The fundamental concept in designing a microwave heating device lies in the interaction of microwaves with materials. Microwaves, with their specific frequency range, induce molecular motion by interacting with polar molecules within materials, generating frictional heat through dielectric loss. This concept is significant for achieving precise and efficient material heating, with applications spanning various fields. Research focuses on innovative approaches such as metamaterials to control microwave distribution, AI optimization, and tailored materials with enhanced dielectric properties. Ensuring user and environmental safety involves shielding, fail-safe mechanisms, and user education. By addressing microwave heating challenges and safety, novel technologies can transform industries such as food processing, medicine, manufacturing, and materials science, improving global living standards [128].

The fundamental concept involves optimizing MW for precise and efficient heating in microwave ovens. This is achieved through innovations like metamaterials to control radiation distribution, and improved dielectric materials. It is significant for revolutionizing cooking and food processing, finding applications in diverse settings. Research motives include enhancing cooking efficiency and safety. Materials utilized include metamaterials and high-dielectric materials [129]. Microwave heating finds extensive applications in industrial settings for various processes such as drying, sintering, sterilization, and thawing. Industrial microwave systems often employ specialized applicators to ensure uniform heating by efficiently delivering microwaves into the material undergoing processing [129].

The fundamental concept involves optimizing microwave plasma heating for PECVD to achieve precise and efficient thin film deposition while reducing environmental impact. This is achieved by utilizing metamaterials to control radiation distribution and pulsed MW for improved efficiency. It is significant for enhancing thin film manufacturing for various applications. Research motives include improving efficiency and sustainability. The fundamental idea is to improve microwave plasma heating for accurate deposition of thin films in PECVD processes, aiming to boost manufacturing efficiency while minimizing environmental effects. This concept involves the use of metamaterials and draws from engineering, materials science, and environmental science [130]. Safety is a paramount consideration in microwave heating due to the potential for burns and injuries. Proper equipment design and

maintenance are crucial to prevent microwave leakage and ensure safe operation [131]. Adhering to the manufacturer's instructions and using only microwave-safe materials is essential for safe microwave heating. Microwave technology offers rapid and effective heating for various applications, including food preparation, material synthesis, and industrial processes. Proper usage and safety precautions are vital to ensure efficient heating and prevent accidents [132]. Microwave heating relies on the rapid rotation and oscillation of polar molecules in response to electromagnetic fields, generating heat within the material. Careful design of microwave heating equipment, including applicators and safety measures, is crucial to ensure effective and controlled heating in various applications [14, 132]. In summary, microwave heating harnesses the dielectric properties of materials to generate heat efficiently. It is employed across various fields and serves as a valuable tool in both household and industrial applications. However, it is essential to prioritize safety precautions when utilizing microwave technology.

## 2.7 Green Chemistry Through Microwave Heating: Applications and Benefits

In recent years, the field of green chemistry has gained significant attention due to its focus on developing sustainable and environmentally friendly chemical processes. One innovative approach that has emerged as a powerful tool in advancing green chemistry is the utilization of microwave heating. Microwave-assisted reactions offer a range of advantages, such as reduced environmental impact, cost-effectiveness, shorter reaction times, and enhanced yields [133]. This two-page write-up explores the applications of microwave heating in the context of green chemistry and its profound benefits. Microwave heating facilitates energy-efficient chemical reactions by directly delivering energy to reactants. This focused energy transfer reduces heat loss to the surroundings, making reactions more energy-efficient and environmentally friendly. Microwave-assisted reactions often require less solvent or even allow for solvent-free processes [12]. This reduction in solvent usage aligns with green chemistry principles, minimizing the generation of hazardous waste. Microwave heating can enhance the catalytic activity of substances, leading to more efficient reactions. This can reduce the need for large quantities of catalysts, which is in line with the principle of minimizing resource consumption. Precise control of temperature during microwave-assisted reactions can improve the selectivity of chemical transformations [2]. This can lead to fewer byproducts and a higher yield of the desired product. Microwave heating significantly accelerates reaction kinetics, reducing reaction times from hours to minutes or even seconds. This not only conserves energy but also increases laboratory productivity. Microwave-assisted reactions often require lower quantities of reagents and solvents. Additionally, the reduced reaction times translate into cost savings, making it an economically viable choice. The decreased solvent usage and energy consumption in microwave-assisted reactions contribute to a smaller environmental footprint. This aligns with the green chemistry goal of minimizing environmental impact [10]. The unique energy absorption and propagation characteristics of microwave irradiation have opened

up new avenues for research in synthetic chemistry. Researchers can explore novel reaction pathways and discover more sustainable synthetic routes. The improved selectivity and reduced byproduct formation in microwave-assisted reactions lead to less waste generation. This is crucial in adhering to the green chemistry principle of waste minimization. Microwave heating can enhance safety in chemical laboratories [134]. Shorter reaction times reduce the exposure of researchers to potentially hazardous materials, contributing to a safer working environment. Microwave heating can be applied to reactions involving renewable feedstocks, supporting the use of sustainable resources in chemical synthesis. Microwave-assisted synthesis has found extensive applications in pharmaceutical and fine chemical industries, where precise control of reaction conditions is crucial for product quality [12], as shown in Figure 2.5. Figure 2.5 highlights the integration of microwave heating with green chemistry principles, emphasizing its applications and the advantages it offers in promoting environmentally friendly and sustainable chemical processes.

Thiazolidin-4-one, a potent moiety found in various approved medications, holds a significant place in contemporary antimicrobial and antiviral chemotherapy. Its broad spectrum and potent activity have made it a focal point of research in the field. Medicinal chemists have been drawn to the diverse medicinal properties exhibited by thiazolidin-4-one-related drugs, motivating them to synthesize an array of novel medicinal substances. MW, an alternative to traditional heating, directly energizes reactions, sparking innovative concepts in synthetic chemistry, particularly in the synthesis of thiazolidin-4-one analogs. It also explores the antiviral and antimicrobial properties of these compounds, offering insights into potential pharmaceutical applications, as shown in Figure 2.6. This evolution

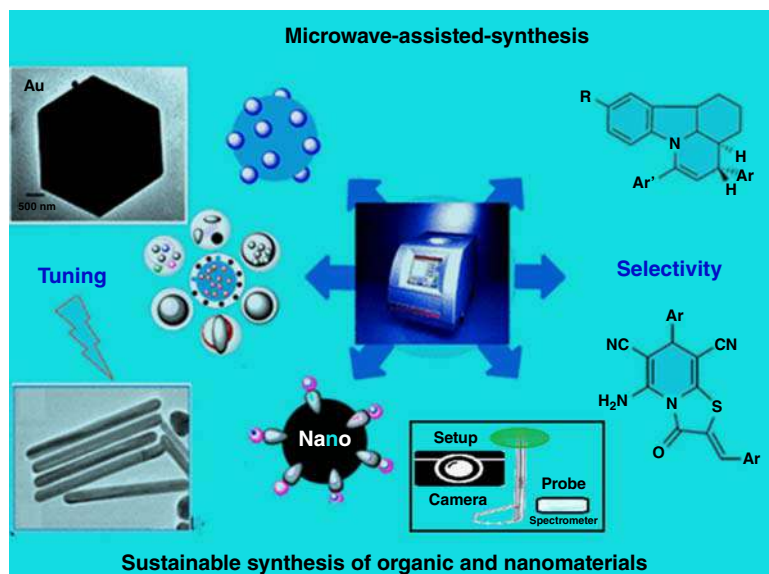


**Figure 2.5** Microwave heating with green chemistry in environmentally friendly and sustainable chemical processes. Source: Verma et al. [18]/American Chemical Society.

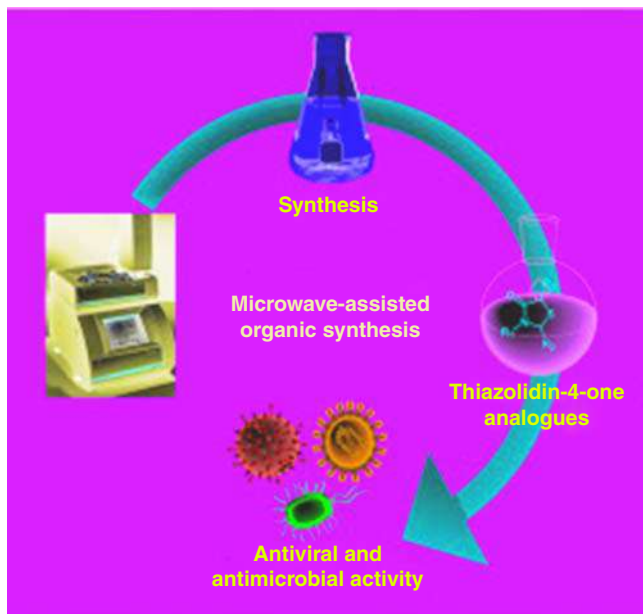


**Figure 2.6** Microwave irradiation -based synthetic routes of various thiazolidin-4-one derivatives.

has brought the principles of green chemistry to the forefront in recent years. Microwave heating has emerged as a green protocol in organic synthesis, aligning with these principles. Its advantages encompass a straightforward experimental setup, production of high-purity compounds with excellent yields, solvent-free reactions, reduced reaction times, minimized side product formation, and decreased by-product rates. Heterocyclic compounds, particularly nitrogen-containing ones, hold immense significance not only due to their presence in natural products but also their extensive applications in the pharmaceutical industry.

The multifaceted role of microwaves in heterogeneous catalytic systems is elegantly dissected into four distinct categories, as thoughtfully summarized in Figure 2.7. These categories provide a holistic perspective on the applications of microwave chemistry – First, the operational mode of microwave chemistry is highlighted, where microwaves serve as the direct heat source for substances. This approach offers the potential for automated, robot-assisted chemical synthesis, reminiscent of microwave heating in household ovens. Second, microwaves find a significant niche in green chemistry applications. They remarkably reduce reaction times, even in processes devoid of solvents and catalysts. This environmentally friendly aspect underscores the greener side of microwave-assisted chemistry. The third facet delves into chemical reaction applications. Microwaves are shown to be catalysts themselves, enhancing the kinetics of various chemical reactions. The ability to manipulate microwave frequency and other related phenomena opens new doors for optimizing chemical processes. Lastly, specific heating emerges as a unique application. Microwaves are not just heat sources; they actively contribute to the creation of novel materials [92].

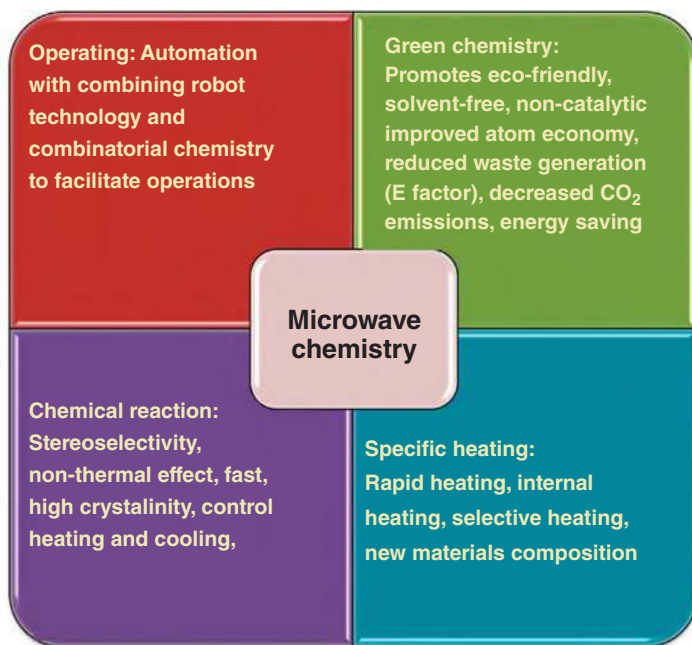


**Figure 2.7** The role of microwave radiation in microwave chemistry. Source: Palma et al. [92]/MDPI/Public Domain/CC by 4.0.

The N-heterocycles are integral components of numerous biologically active molecules such as microwave-mediated synthesis of biologically crucial N-heterocycles, highlighting their relevance in contemporary organic synthesis, as shown in Figure 2.8. This application emphasizes the precision and targeted nature of microwave-induced heating. It is essential to acknowledge that while

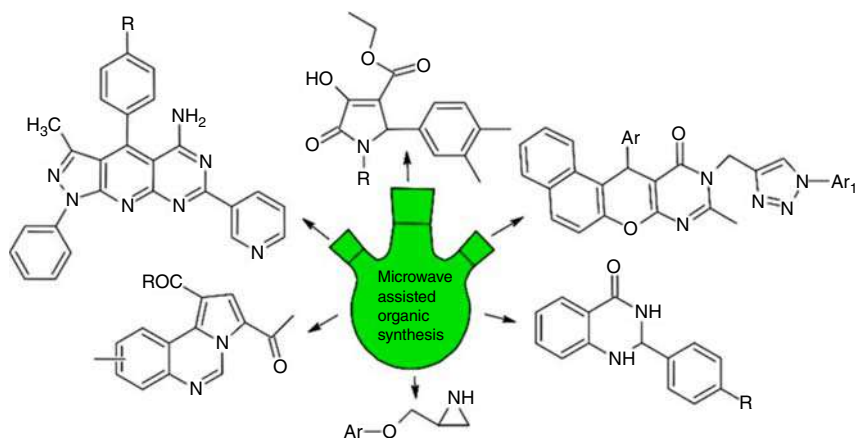


**Figure 2.8** Microwave-promoted synthesis of N-based heterocycles. Source: Dinodia [135]/Bentham Science Publishers.

this classification offers a comprehensive framework, the versatility of microwaves in chemistry and catalysis may extend beyond these categories. Understanding the nuanced differences between microwave and classical heating methods is paramount, and the study of electric and magnetic radiation fields in microwave heating holds significant promise. While many studies employ microwaves as a heat source in chemical reactions, a deeper exploration of MW characteristics remains an intriguing avenue for further research.

## 2.8 Conclusion

In conclusion, this review chapter has provided a comprehensive examination of the fundamental principles underlying microwave irradiation and its far-reaching implications across various domains. The incorporation of microwave and ultrasonication irradiation within the framework of green chemistry highlights its potential as a revolutionary approach for achieving sustainable chemical processes. By adhering to green chemistry principles and minimizing the use of hazardous substances, this technology has the potential to reshape the chemical industry, promoting greater environmental responsibility. Dielectric and magnetic properties, molecular rotation, and the physical principles of microwave heating have shed light on the intricate mechanisms driving the effectiveness of microwave irradiation. This knowledge serves as the foundation for optimizing interactions in fields ranging from materials science to medical chemistry. The synergy between microwave and ultrasonication irradiation offers a versatile toolkit, enabling a wide range of applications from organic synthesis to environmental remediation. As the field of microwave irradiation continues to advance, its capacity to revolutionize chemical processes while upholding sustainability principles becomes increasingly evident. The fusion of science, innovation, and ethical responsibility underscores its significance in shaping a greener future for the chemical industry. By continually enhancing our comprehension of the foundational principles of microwave irradiation and its alignment with the tenets of green chemistry, we are poised to harness its transformative potential and contribute to a more sustainable and responsible scientific landscape.

## References

- 1 Kumar Mishra, R., Thomas, S., and Karikal, N. (2017). *Micro and Nano Fibrillar Composites (MFCs and NFCs) from Polymer Blends*. Elsevier. <https://doi.org/10.1016/B978-0-08-101991-7.09989-1>.
- 2 DeVierno Kreuder, A., House-Knight, T., Whitford, J. et al. (2017). A method for assessing greener alternatives between chemical products following the 12 principles of green chemistry. *ACS Sustainable Chem. Eng.* 5: 2927–2935. <https://doi.org/10.1021/acssuschemeng.6b02399>.

- 3 de Marco, B.A., Rechelo, B.S., Tótolí, E.G. et al. (2019). Evolution of green chemistry and its multidimensional impacts: a review. *Saudi Pharm. J.* 27: 1–8. <https://doi.org/10.1016/j.jpsps.2018.07.011>.
- 4 Anastas, J.C. and Warner, P.T. (1998, Encyclopedia of Toxicology, 1998). *Green Chemistry: Theory and Practice*. New York: Oxford University Press.
- 5 Trombino, S., Sole, R., Di Gioia, M.L. et al. (2023). Green chemistry principles for nano- and micro-sized hydrogel synthesis. *Molecules* 28: 2107. <https://doi.org/10.3390/molecules28052107>.
- 6 Cheng, L. and Ye, X.P. (2010). Recent progress in converting biomass to biofuels and renewable chemicals in sub- or supercritical water. *Biofuels* 1 (1): 109–128. <https://doi.org/10.4155/bfs.09.3>.
- 7 Hernandez, A.L.M. and Santos, C.V. (2012). Keratin fibers from chicken-feathers: structure and advances in polymer composites. In: *Keratin Structure, Properties and Applications* (ed. R. Dullaart et al.), 149–211. Nova Science Publishers.
- 8 Chirayil, C.J., Mishra, R.K., and Thomas, S. (2019). Materials recovery, direct reuse and incineration of PET bottles. In: *Recycling of Polyethylene Terephthalate Bottles*, 37–60. Elsevier. <https://doi.org/10.1016/B978-0-12-811361-5.00003-1>.
- 9 Nayak, J., Devi, C., and Vidyapeeth, L. (2016). Microwave assisted synthesis : a green chemistry approach. *Int. Res. J. Pharm. Appl. Sci.* 3: 278–285.
- 10 Krishnan, R., Shibu, S.N., Poelman, D. et al. (2022). Recent advances in microwave synthesis for photoluminescence and photocatalysis. *Mater. Today Commun.* 32: 103890. <https://doi.org/10.1016/j.mtcomm.2022.103890>.
- 11 Dąbrowska, S., Chudoba, T., Wojnarowicz, J., and Łojkowski, W. (2018). Current trends in the development of microwave reactors for the synthesis of nanomaterials in laboratories and industries: a review. *Crystals (Basel)*. 8: 379. <https://doi.org/10.3390/cryst8100379>.
- 12 Tiwari, S. and Talreja, S. (2022). Green chemistry and microwave irradiation technique: a review. *J. Pharm. Res. Int.* 74–79. <https://doi.org/10.9734/jpri/2022/v34i39A36240>.
- 13 Escobedo, R., Miranda, R., and Martínez, J. (2016). Infrared irradiation: toward green chemistry, a review. *Int. J. Mol. Sci.* 17: 453. <https://doi.org/10.3390/ijms17040453>.
- 14 Pawełczyk, A., Sowa-Kasprzak, K., Olender, D., and Zaprutko, L. (2018). Microwave (MW), ultrasound (US) and combined synergic MW-US strategies for rapid functionalization of pharmaceutical use phenols. *Molecules* 23: 2360. <https://doi.org/10.3390/molecules23092360>.
- 15 Bradu, P., Biswas, A., Nair, C. et al. (2022). Recent advances in green technology and Industrial Revolution 4.0 for a sustainable future. *Environ. Sci. Pollut. Res.* <https://doi.org/10.1007/s11356-022-20024-4>.
- 16 Chatel, G. and Varma, R.S. (2019). Ultrasound and microwave irradiation: contributions of alternative physicochemical activation methods to Green Chemistry. *Green Chem.* 21: 6043–6050. <https://doi.org/10.1039/C9GC02534K>.

- 17 Raghvendrakumar, M. (2017). Chitosan as promising materials for biomedical application: review. *Res. Dev. Mater. Sci.* 2. <https://doi.org/10.31031/RDMS.2017.02.000543>.
- 18 Verma, C., Quraishi, M.A., and Ebenso, E.E. (2018). Microwave and ultrasound irradiations for the synthesis of environmentally sustainable corrosion inhibitors: an overview. *Sustainable Chem. Pharm.* 10: 134–147. <https://doi.org/10.1016/j.scp.2018.11.001>.
- 19 Landers, R., Pfister, A., Hübner, U. et al. (2002). Fabrication of soft tissue engineering scaffolds by means of rapid prototyping techniques. *J. Mater. Sci.* 37: 3107–3116. <https://doi.org/10.1023/A:1016189724389>.
- 20 Segura-Salazar, J. and Tavares, L. (2018). Sustainability in the minerals industry: seeking a consensus on its meaning. *Sustainability* 10: 1429. <https://doi.org/10.3390/su10051429>.
- 21 Taylor, C.J., Pomberger, A., Felton, K.C. et al. (2023). A brief introduction to chemical reaction optimization. *Chem. Rev.* 123: 3089–3126. <https://doi.org/10.1021/acs.chemrev.2c00798>.
- 22 Baig, R.B.N. and Varma, R.S. (2012). Alternative energy input: mechanochemical, microwave and ultrasound-assisted organic synthesis. *Chem. Soc. Rev.* 41: 1559–1584. <https://doi.org/10.1039/C1CS15204A>.
- 23 Hernández Fernández, F.J. and de los Ríos, A.P. (2021). Special Issue: Green sustainable chemical processes. *Processes* 9: 1097. <https://doi.org/10.3390/pr9071097>.
- 24 Jha, A. (2021). Microwave assisted synthesis of organic compounds and nanomaterials. In: *Nanofibers – Synthesis, Properties and Applications*. IntechOpen. <https://doi.org/10.5772/intechopen.98224>.
- 25 Bhargava, N., Mor, R.S., Kumar, K., and Sharanagat, V.S. (2021). Advances in application of ultrasound in food processing: a review. *Ultrason. Sonochem.* 70: 105293. <https://doi.org/10.1016/j.ultsonch.2020.105293>.
- 26 Wysokowski, M., Luu, R.K., Arevalo, S. et al. (2023). Untapped potential of deep eutectic solvents for the synthesis of bioinspired inorganic–organic materials. *Chem. Mater.* <https://doi.org/10.1021/acs.chemmater.3c00847>.
- 27 Martínez-Huitle, C.A., Rodrigo, M.A., Sirés, I., and Scialdone, O. (2023). A critical review on latest innovations and future challenges of electrochemical technology for the abatement of organics in water. *Appl. Catal. B.* 328: 122430. <https://doi.org/10.1016/j.apcatb.2023.122430>.
- 28 Anastas, P.T., Kirchhoff, M.M., and Williamson, T.C. (2001). Catalysis as a foundational pillar of green chemistry. *Appl. Catal., A* 221: 3–13. [https://doi.org/10.1016/S0926-860X\(01\)00793-1](https://doi.org/10.1016/S0926-860X(01)00793-1).
- 29 Pedro, S.N., Freire, C.S.R., Silvestre, A.J.D., and Freire, M.G. (2020). The role of ionic liquids in the pharmaceutical field: an overview of relevant applications. *Int. J. Mol. Sci.* 21: 8298. <https://doi.org/10.3390/ijms21218298>.
- 30 Verma, D.K., Dewangan, Y., Singh, A.K. et al. (2022). Ionic liquids as green and smart lubricant application: an overview. *Ionics (Kiel)*. 28. <https://doi.org/10.1007/s11581-022-04699-w>.



- 31 Patra, J.K., Das, G., Fraceto, L.F. et al. (2018). Nano based drug delivery systems: recent developments and future prospects. *J. Nanobiotechnol.* 16: 71. <https://doi.org/10.1186/s12951-018-0392-8>.
- 32 Mikušová, V. and Mikuš, P. (2021). Advances in chitosan-based nanoparticles for drug delivery. *Int. J. Mol. Sci.* 22: 9652. <https://doi.org/10.3390/ijms22179652>.
- 33 Coelho, J.F., Ferreira, P.C., Alves, P. et al. (2010). Drug delivery systems: advanced technologies potentially applicable in personalized treatments. *EPMA J.* 1: 164–209. <https://doi.org/10.1007/s13167-010-0001-x>.
- 34 Jiménez-Gómez, C.P. and Cecilia, J.A. (2020). Chitosan: a natural biopolymer with a wide and varied range of applications. *Molecules.* 25: 3981. <https://doi.org/10.3390/molecules25173981>.
- 35 Hein, C.D., Liu, X.-M., and Wang, D. (2008). Click chemistry, a powerful tool for pharmaceutical sciences. *Pharm. Res.* 25: 2216–2230. <https://doi.org/10.1007/s11095-008-9616-1>.
- 36 Purohit, P., Bhatt, A., Mittal, R.K. et al. (2023). Polymer Grafting and its chemical reactions. *Front. Bioeng. Biotechnol.* 10. <https://doi.org/10.3389/fbioe.2022.1044927>.
- 37 Rajendran, R.A., Gudimalla, A.P., Mishra, R.A. et al. (2019). Electrospinning as a novel delivery vehicle for bioactive compounds in food. In: *Innovative Food Science and Emerging Technologies*, 1e (ed. S. Thomas, R. Rajakumari, A. George, and N. Kalarikkal), 426–453. New York: Apple Academic Press.
- 38 Mishra, R.K. and Kumar, A. (2021). Advanced biopolymer-based composites: an introduction and fracture modeling. In: *Sustainable Biopolymer Composites: Biocompatibility, Self-Healing, Modeling, Repair and Recyclability*, A Volume in Woodhead Publishing Series in Composites Science and Engineering. <https://doi.org/10.1016/B978-0-12-822291-1.00001-4>.
- 39 Mohapatra, S.S., Ranjan, S., Dasgupta, N. et al. (2018). *Applications of Targeted Nano Drugs and Delivery Systems: Nanoscience and Nanotechnology in Drug Delivery*. Elsevier. <https://doi.org/10.1016/B978-0-12-814029-1.01001-2>.
- 40 Parveen, F. and Kumar Mishra, R. (2019). Different fabrication techniques of aerogels and its applications. In: *Advanced Polymeric Materials for Sustainability and Innovations*. <https://doi.org/10.1201/b22326-14>.
- 41 Kumar, A., Mishra, R.K., Verma, K. et al. (2023). A comprehensive review of various biopolymer composites and their applications: from biocompatibility to self-healing. *Mater. Today Sustainability*. <https://doi.org/10.1016/j.mtsust.2023.100431>.
- 42 Raghvendra, K.M. (2018). Nanostructured biomimetic, bioresponsive, and bioactive biomaterials. In: *Fundamental Biomaterials: Metals*, 35–65. Elsevier. <https://doi.org/10.1016/B978-0-08-102205-4.00002-7>.
- 43 Mishra, R.K. and Rajakumari, R. (2019). Nanobiosensors for biomedical application. In: *Characterization and Biology of Nanomaterials for Drug Delivery*, 1–23. Elsevier. <https://doi.org/10.1016/B978-0-12-814031-4.00001-5>.
- 44 Buléon, A., Colonna, P., Planchot, V., and Ball, S. (1998). Starch granules: structure and biosynthesis. *Int. J. Biol. Macromol.* 23: 85–112. [https://doi.org/10.1016/S0141-8130\(98\)00040-3](https://doi.org/10.1016/S0141-8130(98)00040-3).

- 45 Domene-López, D., García-Quesada, J.C., Martín-Gullón, I., and Montalbán, M.G. (2019). Influence of starch composition and molecular weight on physicochemical properties of biodegradable films. *Polymers (Basel)*. 11: 1084. <https://doi.org/10.3390/polym11071084>.
- 46 Sajilata, M.G., Singhal, R.S., and Kulkarni, P.R. (2006). Resistant starch – a review. *Compr. Rev. Food Sci. Food Saf.* 5: 1–17. <https://doi.org/10.1111/j.1541-4337.2006.tb00076.x>.
- 47 Peidayesh, H., Ahmadi, Z., Khonakdar, H.A. et al. (2020). Baked hydrogel from corn starch and chitosan blends cross-linked by citric acid: preparation and properties. *Polym. Adv. Technol.* 31: 1256–1269. <https://doi.org/10.1002/pat.4855>.
- 48 Fan, Y. and Picchioni, F. (2020). Modification of starch: a review on the application of “green” solvents and controlled functionalization. *Carbohydr. Polym.* 241: 116350. <https://doi.org/10.1016/j.carbpol.2020.116350>.
- 49 Chin, S.F., Romainor, A.N.B., Pang, S.C., and Lihan, S. (2019). Antimicrobial starch-citrate hydrogel for potential applications as drug delivery carriers. *J. Drug Delivery Sci. Technol.* 54: 101239. <https://doi.org/10.1016/j.jddst.2019.101239>.
- 50 Ma, C., Gerhard, E., Lu, D., and Yang, J. (2018). Citrate chemistry and biology for biomaterials design. *Biomaterials* 178: 383–400. <https://doi.org/10.1016/j.biomaterials.2018.05.003>.
- 51 Larrañeta, E., Imízcoz, M., Toh, J.X. et al. (2018). Synthesis and characterization of lignin hydrogels for potential applications as drug eluting antimicrobial coatings for medical materials. *ACS Sustainable Chem. Eng.* 6: 9037–9046. <https://doi.org/10.1021/acssuschemeng.8b01371>.
- 52 Larrañeta, E., Lutton, R.E.M., Brady, A.J. et al. (2015). Microwave-assisted preparation of hydrogel-forming microneedle arrays for transdermal drug delivery applications. *Macromol. Mater. Eng.* 300: 586–595. <https://doi.org/10.1002/mame.201500016>.
- 53 Afinjuomo, F., Fouladian, P., Parikh, A. et al. (2019). Preparation and characterization of oxidized inulin hydrogel for controlled drug delivery. *Pharmaceutics* 11: 356. <https://doi.org/10.3390/pharmaceutics11070356>.
- 54 Imran, M., Hussain, S., Mehmood, K. et al. (2021). Optimization of ecofriendly synthesis of Ag nanoparticles by *Linum usitatissimum* hydrogel using response surface methodology and its biological applications. *Mater. Today Commun.* 29: 102789. <https://doi.org/10.1016/j.mtcomm.2021.102789>.
- 55 Hsueh, Y.-H., Lin, K.-S., Ke, W.-J. et al. (2015). The antimicrobial properties of silver nanoparticles in *Bacillus subtilis* are mediated by released Ag<sup>+</sup> ions. *PLoS One* 10: e0144306. <https://doi.org/10.1371/journal.pone.0144306>.
- 56 Muthukumar, T., Song, J.E., and Khang, G. (2019). Biological role of gellan gum in improving scaffold drug delivery, cell adhesion properties for tissue engineering applications. *Molecules* 24: 4514. <https://doi.org/10.3390/molecules24244514>.
- 57 Yi, Y.T., Sun, J.Y., Lu, Y.W., and Liao, Y.C. (2015). Programmable and on-demand drug release using electrical stimulation. *Biomicrofluidics* 9. <https://doi.org/10.1063/1.4915607>.

- 58 Yadav, A., Yadav, K., Ahmad, R., and Abd-Elsalam, K.A. (2023). Emerging frontiers in nanotechnology for precision agriculture: advancements, hurdles and prospects. *Agrochemicals* 2: 220–256. <https://doi.org/10.3390/agrochemicals2020016>.
- 59 Bercea, M. (2022). Bioinspired hydrogels as platforms for life-science applications: challenges and opportunities. *Polymers (Basel)*. 14: 2365. <https://doi.org/10.3390/polym14122365>.
- 60 Fuku, X., Dyosiba, X., and Iftikhar, F.J. (2023). Green prepared nanomaterials from various biodegradable wastes and their application in energy. *Nano-Struct. Nano-Objects* 35: 100997. <https://doi.org/10.1016/j.nanoso.2023.100997>.
- 61 Sarfraz, M.S., Hong, H., and Kim, S.S. (2021). Recent developments in the manufacturing technologies of composite components and their cost-effectiveness in the automotive industry: A review study. *Compos. Struct.* 266: 113864. <https://doi.org/10.1016/j.compstruct.2021.113864>.
- 62 Marsh, K. and Bugusu, B. (2007). Food packaging? roles, materials, and environmental issues. *J. Food Sci.* 72: R39–R55. <https://doi.org/10.1111/j.1750-3841.2007.00301.x>.
- 63 Luo, X. (2015). Principles of electromagnetic waves in metasurfaces. *Sci. China Phys., Mech. Astron.* 58: 594201. <https://doi.org/10.1007/s11433-015-5688-1>.
- 64 Pfeifer, R.N.C., Nieminen, T.A., Heckenberg, N.R., and Rubinsztein-Dunlop, H. (2007). Colloquium: momentum of an electromagnetic wave in dielectric media. *Rev. Mod. Phys.* 79. <https://doi.org/10.1103/RevModPhys.79.1197>.
- 65 Tofighi, M.R. and Chiao, J.C. (2012). IEEE transactions on microwave theory and techniques. *IEEE Trans. Microwave Theory Tech.* 60. <https://doi.org/10.1109/TMTT.2012.2205624>.
- 66 Zhou, X., Jia, Z., Feng, A. et al. (2020). Dependency of tunable electromagnetic wave absorption performance on morphology-controlled 3D porous carbon fabricated by biomass. *Compos. Commun.* 21: 100404. <https://doi.org/10.1016/j.coco.2020.100404>.
- 67 Erkaev, N.V., Weber, C., Griebmeier, J.-M. et al. (2022). Can radio emission escape from the magnetosphere of  $\upsilon$  Andromedae b – a new method to constrain the minimum mass of Hot Jupiters. *Mon. Not. R. Astron. Soc.* 512: 4869–4876. <https://doi.org/10.1093/mnras/stac767>.
- 68 Liu, Y., Yuan, Z., Wang, J. et al. (2019). Simulation of EM wave propagation along a femtosecond laser plasma filament. *Results Phys.* 14. <https://doi.org/10.1016/j.rinp.2019.102359>.
- 69 Sen Zhong, H., Wang, H., Deng, Y.H. et al. (2020). Quantum computational advantage using photons. *Science* (1979): 370. <https://doi.org/10.1126/science.abe8770>.
- 70 Sheng, W., Yucel, A.C., Liu, Y. et al. (2023). A Domain-decomposition-based surface integral equation simulator for characterizing em wave propagation in mine environments. *IEEE Trans. Antennas Propag.* 71. <https://doi.org/10.1109/TAP.2023.3256579>.

- 71 Yang, X., Wei, B., and Yin, W. (2017). Analysis on the characteristics of em waves propagation in the plasma sheath surrounding a hypersonic vehicle. *IEEE Trans. Plasma Sci.* 45. <https://doi.org/10.1109/TPS.2017.2755723>.
- 72 Yang, X., Wei, B., and Yin, W. (2017). A new method to analyze the EM wave propagation characteristics in the hypersonic sheath. *Optik (Stuttg)*. 148. <https://doi.org/10.1016/j.ijleo.2017.08.117>.
- 73 Nguyen, B.T., Samimi, A., Vergara, S.E.W. et al. (2019). Analysis of electromagnetic wave propagation in variable magnetized plasma via polynomial chaos expansion. *IEEE Trans. Antennas Propag.* 67. <https://doi.org/10.1109/TAP.2018.2879676>.
- 74 Vendik, I., Vendik, O., Pleskachev, V. et al. (2021). Wireless monitoring of biological objects at microwaves. *Electronics (Switzerland)*. 10. <https://doi.org/10.3390/electronics10111288>.
- 75 Javandel, V., Akbari, A., Ardebili, M., and Werle, P. (2022). Simulation of negative and positive corona discharges in air for investigation of electromagnetic waves propagation. *IEEE Trans. Plasma Sci.* 50. <https://doi.org/10.1109/TPS.2022.3194836>.
- 76 Cheng, J., Zhang, H., Xiong, Y. et al. (2021). Construction of multiple interfaces and dielectric/magnetic heterostructures in electromagnetic wave absorbers with enhanced absorption performance: a review. *J. Materiomics* 7. <https://doi.org/10.1016/j.jmat.2021.02.017>.
- 77 Zamorano Ulloa, R., Santiago, M.G.H., and Rueda, V.L.V. (2019). The interaction of microwaves with materials of different properties. In: *Electromagnetic Fields and Waves*. IntechOpen. <https://doi.org/10.5772/intechopen.83675>.
- 78 Sun, J., Wang, W., and Yue, Q. (2016). Review on microwave-matter interaction fundamentals and efficient microwave-associated heating strategies. *Materials* 9: 231. <https://doi.org/10.3390/ma9040231>.
- 79 Parodi, F. (1989). Physics and chemistry of microwave processing. In: *Comprehensive Polymer Science and Supplements*, 669–728. Elsevier. <https://doi.org/10.1016/B978-0-08-096701-1.00258-5>.
- 80 Psarras, G.C. (2018). Fundamentals of dielectric theories. In: *Dielectric Polymer Materials for High-Density Energy Storage*, 11–57. Elsevier. <https://doi.org/10.1016/B978-0-12-813215-9.00002-6>.
- 81 Mishra, R.R. and Sharma, A.K. (2016). Microwave–material interaction phenomena: heating mechanisms, challenges and opportunities in material processing. *Compos. Part A Appl. Sci. Manuf.* 81: 78–97. <https://doi.org/10.1016/j.compositesa.2015.10.035>.
- 82 Angela, A. and dAmore, M. (2012). Relevance of dielectric properties in microwave assisted processes. In: *Microwave Materials Characterization*. InTech. <https://doi.org/10.5772/51098>.
- 83 Mishra, R.K., Dutta, A., Mishra, P., and Thomas, S. (2018). Recent progress in electromagnetic absorbing materials. *Adv. Mater. Electromag. Shiel.* <https://doi.org/10.1002/9781119128625.ch7>.

- 84 Feller, J.F., Bruzaud, S., and Grohens, Y. (2004). Influence of clay nanofiller on electrical and rheological properties of conductive polymer composite. *Mater. Lett.* 58: 739–745. <https://doi.org/10.1016/j.matlet.2003.07.010>.
- 85 Zhai, W., Zhao, S., Wang, Y. et al. (2018). Segregated conductive polymer composite with synergistically electrical and mechanical properties. *Compos. Part A Appl. Sci. Manuf.* 105: 68–77. <https://doi.org/10.1016/j.compositesa.2017.11.008>.
- 86 Yaragalla, S., Thomas, S., Maria, H.J. et al. (2019). *Carbon-based Nanofiller and Their Rubber Nanocomposites*. Elsevier. <https://doi.org/10.1016/C2018-0-02522-0>.
- 87 Jayalakshmy, M.S. and Mishra, R.K. (2019). Applications of carbon-based nanofiller-incorporated rubber composites in the fields of tire engineering, flexible electronics and EMI shielding. In: *Carbon-Based Nanofillers and Their Rubber Nanocomposites*. <https://doi.org/10.1016/B978-0-12-817342-8.00014-7>.
- 88 S. Yaragalla, R. Mishra, S. Thomas, N. Kalarikkal, H.J. Maria, *Carbon-based nanofillers and their rubber nanocomposites*, 2018. <https://doi.org/10.1016/C2016-0-03648-3>.
- 89 Loharkar, P.K., Ingle, A., and Jhavar, S. (2019). Parametric review of microwave-based materials processing and its applications. *J. Mater. Res. Technol.* 8: 3306–3326. <https://doi.org/10.1016/j.jmrt.2019.04.004>.
- 90 Mishra, R.K., Thomas, M.G., Abraham, J. et al. (2018). Electromagnetic interference shielding materials for aerospace application. In: *Advanced Materials for Electromagnetic Shielding*, 327–365. Wiley. <https://doi.org/10.1002/9781119128625.ch15>.
- 91 Li, K., Xu, J., Li, P., and Fan, Y. (2022). A review of magnetic ordered materials in biomedical field: constructions, applications and prospects. *Compos. B Eng.* 228: 109401. <https://doi.org/10.1016/j.compositesb.2021.109401>.
- 92 Palma, V., Barba, D., Cortese, M. et al. (2020). Microwaves and heterogeneous catalysis: a review on selected catalytic processes. *Catalysts* 10. <https://doi.org/10.3390/catal10020246>.
- 93 Li, S., Li, C., and Shao, Z. (2022). Microwave pyrolysis of sludge: a review. *Sustainable Environ. Res.* 32. <https://doi.org/10.1186/s42834-022-00132-z>.
- 94 Hu, Q., He, Y., Wang, F. et al. (2021). Microwave technology: a novel approach to the transformation of natural metabolites. *Chin. Med.* 16: 87. <https://doi.org/10.1186/s13020-021-00500-8>.
- 95 Michalak, J., Czarnowska-Kujawska, M., Klepacka, J., and Gujska, E. (2020). Effect of microwave heating on the acrylamide formation in foods. *Molecules*. 25: 4140. <https://doi.org/10.3390/molecules25184140>.
- 96 Albuquerque, H.M.T., Pinto, D.C.G.A., and Silva, A.M.S. (2021). Microwave irradiation: alternative heating process for the synthesis of biologically applicable chromones, Quinolones, and Their Precursors. *Molecules* 26: 6293. <https://doi.org/10.3390/molecules26206293>.
- 97 Gawande, M.B., Shelke, S.N., Zboril, R., and Varma, R.S. (2014). Microwave-assisted chemistry: synthetic applications for rapid assembly of nanomaterials and organics. *Acc. Chem. Res.* 47: 1338–1348. <https://doi.org/10.1021/ar400309b>.

- 98 Mitev, D.P., Townsend, A.T., Paull, B., and Nesterenko, P.N. (2014). Microwave-assisted purification of detonation nanodiamond. *Diamond Relat. Mater.* 48: 37–46. <https://doi.org/10.1016/j.diamond.2014.06.007>.
- 99 de Medeiros, T.V., Manioudakis, J., Noun, F. et al. (2019). Microwave-assisted synthesis of carbon dots and their applications. *J. Mater. Chem. C Mater.* 7: 7175–7195. <https://doi.org/10.1039/C9TC01640F>.
- 100 Giri, S.K. and Prasad, S. (2007). Drying kinetics and rehydration characteristics of microwave-vacuum and convective hot-air dried mushrooms. *J. Food Eng.* 78: 512–521. <https://doi.org/10.1016/j.jfoodeng.2005.10.021>.
- 101 Hwang, J., Bae, C., Park, J. et al. (2016). Microwave-assisted plasma ignition in a constant volume combustion chamber. *Combust. Flame* 167: 86–96. <https://doi.org/10.1016/j.combustflame.2016.02.023>.
- 102 Mehedi, H.A., Achard, J., Rats, D. et al. (2014). Low temperature and large area deposition of nanocrystalline diamond films with distributed antenna array microwave-plasma reactor. *Diamond Relat. Mater.* 47: 58–65. <https://doi.org/10.1016/j.diamond.2014.05.004>.
- 103 Singh, R.K., Kumar, R., Singh, D.P. et al. (2019). Progress in microwave-assisted synthesis of quantum dots (graphene/carbon/semiconducting) for bioapplications: a review. *Mater. Today Chem.* 12. <https://doi.org/10.1016/j.mtchem.2019.03.001>.
- 104 Jiang, Y., Wang, B., Meng, F. et al. (2015). Microwave-assisted preparation of N-doped carbon dots as a biosensor for electrochemical dopamine detection. *J. Colloid Interface Sci.* 452: 199–202. <https://doi.org/10.1016/j.jcis.2015.04.016>.
- 105 Xu, Z., Wang, C., Jiang, K. et al. (2015). Microwave-assisted rapid synthesis of amphibious yellow fluorescent carbon dots as a colorimetric nanosensor for Cr(VI). *Part. Part. Syst. Char.* 32: 1058–1062. <https://doi.org/10.1002/ppsc.201500172>.
- 106 Menéndez-Flores, V.M. and Ohno, T. (2014). High visible-light active Ir-doped-TiO<sub>2</sub> brookite photocatalyst synthesized by hydrothermal microwave-assisted process. *Catal. Today* 230: 214–220. <https://doi.org/10.1016/j.cattod.2014.01.032>.
- 107 Xu, Y., Li, H., Wang, B. et al. (2018). Microwave-assisted synthesis of carbon dots for “turn-on” fluorometric determination of Hg(II) via aggregation-induced emission. *Microchim. Acta* 185: 252. <https://doi.org/10.1007/s00604-018-2781-y>.
- 108 Sharma, B., Thakur, S., Trache, D. et al. (2020). Microwave-assisted rapid synthesis of reduced graphene oxide-based gum tragacanth hydrogel nanocomposite for heavy metal ions adsorption. *Nanomaterials* 10: 1616. <https://doi.org/10.3390/nano10081616>.
- 109 Qin, X., Lu, W., Asiri, A.M. et al. (2013). Microwave-assisted rapid green synthesis of photoluminescent carbon nanodots from flour and their applications for sensitive and selective detection of mercury(II) ions. *Sens. Actuators, B* 184: 156–162. <https://doi.org/10.1016/j.snb.2013.04.079>.
- 110 Show, Y., Swope, V.M., and Swain, G.M. (2009). The effect of the CH<sub>4</sub> level on the morphology, microstructure, phase purity and electrochemical properties of carbon films deposited by microwave-assisted CVD from Ar-rich source

- gas mixtures. *Diamond Relat. Mater.* 18: 1426–1434. <https://doi.org/10.1016/j.diamond.2009.09.011>.
- 111** Vicente, I., Salagre, P., Cesteros, Y. et al. (2009). Fast microwave synthesis of hectorite. *Appl. Clay Sci.* 43: 103–107. <https://doi.org/10.1016/j.clay.2008.07.012>.
- 112** Das, S., Mukhopadhyay, A.K., Datta, S., and Basu, D. (2009). Prospects of microwave processing: an overview. *Bull. Mater. Sci.* 32: 1–13. <https://doi.org/10.1007/s12034-009-0001-4>.
- 113** Sharan, N. (2009). Microwave sintering of zirconia and alumina. *Int. J.* 1: 1–4.
- 114** Li, Z., Yao, Y., Lin, Z. et al. (2010). Ultrafast, dry microwave synthesis of graphene sheets. *J. Mater. Chem.* 20: 4781. <https://doi.org/10.1039/c0jm00168f>.
- 115** Mitra, S., Chandra, S., Kundu, T. et al. (2012). Rapid microwave synthesis of fluorescent hydrophobic carbon dots. *RSC Adv.* 2: 12129. <https://doi.org/10.1039/c2ra21048g>.
- 116** Zhu, H., Wang, X., Li, Y. et al. (2009). Microwave synthesis of fluorescent carbon nanoparticles with electrochemiluminescence properties. *Chem. Commun.* 5118. <https://doi.org/10.1039/b907612c>.
- 117** Mishra, R.K., Loganathan, S., Jacob, J. et al. (2018). Progress in polymer nanocomposites for electromagnetic shielding application. In: *Modern Physical Chemistry: Engineering Models, Materials, and Methods with Applications*, 1e (ed. R.K. Haghi, E. Besalu, M. Jaroszewski, et al.), 198–237. New York: Apple Academic Press.
- 118** Yang, R. and Chen, J. (2021). Mechanistic and machine learning modeling of microwave heating process in domestic ovens: a review. *Foods* 10: 2029. <https://doi.org/10.3390/foods10092029>.
- 119** Zhao, H., Cai, K., Ma, Z. et al. (2018). Synthesis of molybdenum carbide superconducting compounds by microwave-plasma chemical vapor deposition. *J. Appl. Phys.* 123: 053301. <https://doi.org/10.1063/1.5010101>.
- 120** Khan, T. (2020). An intelligent microwave oven with thermal imaging and temperature recommendation using deep learning. *Appl. Sys. Innov.* 3: 13. <https://doi.org/10.3390/asi3010013>.
- 121** Zhang, Y.M., Wang, P., Han, N., and Lei, H.F. (2007). Microwave irradiation: a novel method for rapid synthesis of D,L-lactide. *Macromol. Rapid Commun.* 28: 417–421. <https://doi.org/10.1002/marc.200600668>.
- 122** Voiry, D., Yang, J., Kupferberg, J. et al. (1979). High-quality graphene via microwave reduction of solution-exfoliated graphene oxide. *Science* 353 (2016): 1413–1416. <https://doi.org/10.1126/science.aah3398>.
- 123** Chen, W., Lu, X., Yang, Q. et al. (2006). Effects of gas flow rate on diamond deposition in a microwave plasma reactor. *Thin Solid Films* 515: 1970–1975. <https://doi.org/10.1016/j.tsf.2006.08.007>.
- 124** Narayanan, T.N., Sunny, V., Shaijumon, M.M. et al. (2009). Enhanced microwave absorption in nickel-filled multiwall carbon nanotubes in the S band. *Electrochem. Solid-State Lett.* 12: K21. <https://doi.org/10.1149/1.3065992>.
- 125** Dora, T.L., Owhal, A., Roy, T. et al. (2023). Thermo-physical characteristics of 3C-SiC structure subjected to microwave exposure: a molecular dynamics

- study. *Mater. Today Commun.* 35: 105693. <https://doi.org/10.1016/j.mtcomm.2023.105693>.
- 126** Liu, X., Li, T., Hou, Y. et al. (2016). Microwave synthesis of carbon dots with multi-response using denatured proteins as carbon source. *RSC Adv.* 6: 11711–11718. <https://doi.org/10.1039/C5RA23081K>.
- 127** Shakir, M.F., Abdul Rashid, I., Tariq, A. et al. (2020). EMI shielding characteristics of electrically conductive polymer blends of PS/PANI in microwave and IR region. *J. Electron. Mater.* 49. <https://doi.org/10.1007/s11664-019-07631-7>.
- 128** Tsugawa, K., Ishihara, M., Kim, J. et al. (2006). Large-area and low-temperature nanodiamond coating by microwave plasma chemical vapor deposition. *New Diamond Front. Carbon Technol.* 16: 337–346.
- 129** Wang, X.J. and Yan, C.L. (2010). Synthesis of nano-sized NaY zeolite composite from metakaolin by ionothermal method with microwave assisted. *Inorg. Mater.* <https://doi.org/10.1134/S0020168510050146>.
- 130** Marciano, F.R., Bonetti, L.F., Santos, L.V. et al. (2009). Antibacterial activity of DLC and Ag-DLC films produced by PECVD technique. *Diamond Relat. Mater.* 18: 1010–1014. <https://doi.org/10.1016/j.diamond.2009.02.014>.
- 131** Zhou, K., Ke, P., Li, X. et al. (2015). Microstructure and electrochemical properties of nitrogen-doped DLC films deposited by PECVD technique. *Appl. Surf. Sci.* 329: 281–286. <https://doi.org/10.1016/j.apsusc.2014.12.162>.
- 132** Aldosari, M.A., Othman, A.A., and Alsharaeh, E.H. (2013). Synthesis and characterization of the in situ bulk polymerization of PMMA containing graphene sheets using microwave irradiation. *Molecules* 18: 3152–3167. <https://doi.org/10.3390/molecules18033152>.
- 133** Kumar, A., Kuang, Y., Liang, Z., and Sun, X. (2020). Microwave chemistry, recent advancements, and eco-friendly microwave-assisted synthesis of nanoarchitectures and their applications: a review. *Mater. Today Nano* 11: 100076. <https://doi.org/10.1016/j.mtnano.2020.100076>.
- 134** Prielcel, P. and Lopez-Sanchez, J.A. (2019). Advantages and Limitations of Microwave Reactors: From Chemical Synthesis to the Catalytic Valorization of Biobased Chemicals. *ACS Sustainable Chem. Eng.* 7: 3–21. <https://doi.org/10.1021/acssuschemeng.8b03286>.
- 135** Dinodia, M. (2023). Microwave-promoted synthesis of novel bioactive N-based heterocycles. *Mini-Rev. Org. Chem.* 20: 136–155. <https://doi.org/10.2174/1570193X19666220420133723>.



EMERGING MATERIALS AND TECHNOLOGIES

# Biosorbents

Diversity, Bioprocessing,  
and Applications

Edited by

**PRAMOD KUMAR MAHISH,  
DAKESHWAR KUMAR VERMA,  
and SHAILESH KUMAR JADHAV**



**CRC Press**  
Taylor & Francis Group

<b>Chapter 14</b>	Application of Biosorbents in Separation of Radionuclides .....	218
	<i>Elyor Berdimurodov, Khasan Berdimuradov, Ilyos Eliboyev, Dakeshwar Kumar Verma, and Omar Dagdag</i>	
14.1	Introduction .....	218
14.2	Chitosan-Based Biosorbents in the Separation of Radionuclides .....	220
14.3	Other Biosorbents in the Separation of Radionuclides .....	222
14.4	Conclusion .....	225
	References .....	225
<b>Chapter 15</b>	Biosorption of Volatile Organic Compounds .....	228
	<i>Godwin Anywar, Jane Namukobe, Patience Tugume, Jamilu Ssenku, Moses Okol, and Julius Mulindwa</i>	
15.1	What Are Volatile Organic Compounds? .....	228
15.2	Biosorption of Organic Volatile Compounds .....	230
15.3	Biosorption of Volatile Organic Compounds Using Microorganisms .....	231
15.4	Biosorption of Volatile Organic Compounds by Food Waste Materials .....	235
15.5	Synthetic Biosorbents and Their Efficacy in Removing Volatile Organic Compound .....	236
15.6	Nanoadsorbents and Nanocomposite Adsorbents .....	237
	References .....	239
<b>Chapter 16</b>	Nano-biosorbents and Their Applications in Electrochemical Sensing and Adsorptive Removal of Environmental Pollutants .....	249
	<i>Shreanshi Agrahari, Ankit Kumar Singh, Ravindra Kumar Gautam, and Ida Tiwari</i>	
16.1	Introduction .....	249
16.2	Nano-Biosorbents .....	251
16.3	Various Types of Immobilized Nano-Biosorbents .....	254
16.4	Conventional Techniques for the Removal of Environmental Contaminants .....	258
16.5	Various Electrochemical Techniques Using Nano-biosorbents for the Detection of Environmental Contaminants .....	259
16.6	Challenges in the Analysis of Environmental Pollutants Using Nano-biosorbent .....	261
16.7	Conclusions and Future Aspects .....	261
	Acknowledgments .....	262
	References .....	262
	Index .....	267

---

# 14 Application of Biosorbents in Separation of Radionuclides

*Elyor Berdimurodov, Khasan Berdimuradov,  
Ilyos Eliboyev, Dakeshwar Kumar Verma,  
and Omar Dagdag*

## 14.1 INTRODUCTION

### 14.1.1 SEPARATION OF RADIONUCLIDES

The radionuclides are dangerous elements for human and animal health. The radionuclides are not stable, causing serious cancer illness. The spread of radionuclides has occurred from the nuclear processes [1]. The degree of radioactivity is an important factor for radioecology monitoring [2–4]. The high level of radioactivity is a crucial factor in the human body. Therefore, the separation of radionuclides from the wastewater, atmosphere and other environmental samples is important task in materials science. For example, the  $^{125}\text{Sb}$ ,  $^{54}\text{Mn}$ ,  $^{60}\text{Co}$ ,  $^{155}\text{Eu}$ ,  $^{154}\text{Eu}$ ,  $^{137}\text{Cs}$  and  $^{134}\text{Cs}$  were most dangerous radionuclides. Their gamma-emitting level is much higher in the wastewater, atmosphere and other environmental samples [5, 6].

The various separation methods for Cm, Am, Pu, Np, U, Th, Tc, Sr and Cs were used in the separation science. Before the separation of radionuclides, various analytical methods were used to determine the amounts of radionuclides [7, 8]. Thermal ionisation mass spectrometry inductively coupled plasma mass spectrometry, mass spectrometry,  $\gamma$ -spectrometry, liquid scintillation, low background beta counting,  $\beta$ -spectrometry and  $\alpha$ -spectrometry were the most used methods in the determination of radionuclides. The extraction chromatography, ion exchange, membrane separation, liquid-liquid extraction and separation approaches including precipitation methods were used in the separation of radionuclides [9].

Ion-exchange chromatography, solid-phase extraction and other extraction chromatographic methods can separate the radionuclides related to the ion-exchange processes, in which the metal ions (radionuclides) were exchanged with the corresponding anions on the surface or matrix of ion exchange. As a result, the radionuclides were chemically or physically linked to the surface or matrix of the polymer ion exchanger. For example, ion-selective resins were used to separate the lanthanides and actinides-based radionuclides. The ion exchange is the next important technique for the separation of radionuclides. The ion exchangers are categorised into anion- and cation-exchange resins [10, 11]. The following functional groups are functionalised

to anion ion exchangers:  $-\text{N}(\text{CH}_3)_2\text{OH}$ ,  $-\text{N}(\text{CH}_3)_3\text{OH}$ , while the cation exchanger contained the  $-\text{COOH}$  and  $-\text{SO}_3\text{H}$ . The separation of radionuclides is linked to the following factors: solution temperature, pH and other ions (Figure 14.1). The radionuclides were separated from the wastewater using membrane-based separation. For example, reverse osmosis, nanofiltration, ultrafiltration and microfiltration methods

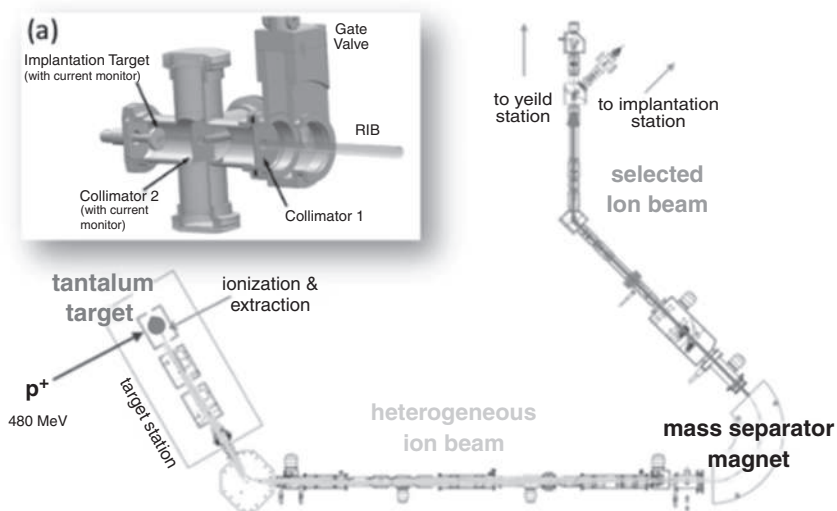
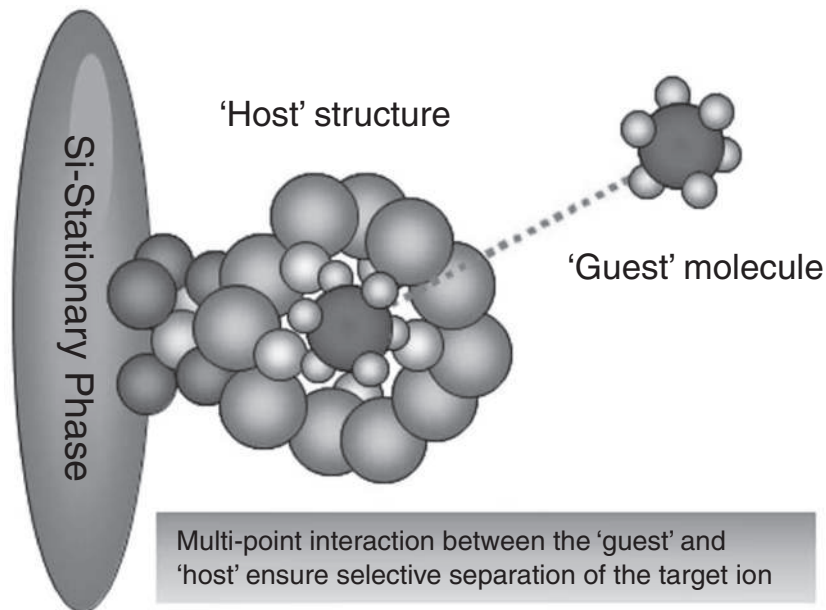


**FIGURE 14.1** (a) Separation technique [12], (b) TRIUMF ISOL method for radionuclides separation [13]

are membrane-based methods. The selective membrane must be more porosity material, because the radionuclides are separated related to the size of the pore. Therefore, porosity is an important fact for membrane-based separation [12, 13].

## 14.2 CHITOSAN-BASED BIOSORBENTS IN THE SEPARATION OF RADIONUCLIDES

The radionuclides were serious pollutants for the environment. In recent times, various methods were used to separate the radionuclides from the environmental samples. Chitosan-based biosorbents were new and green technology in the separation of radionuclides. These types of biosorbents were more efficient and low-cost materials in the separation of radionuclides [14, 15]. The preparation methods of chitosan-based materials were easy and did not require high-degree technologies. Chitosan is a natural product and green polymer. There are many research works related to the separation of radionuclides from wastewater and other environmental samples. The adsorption of radionuclides depends on the following main properties: biosorption mechanisms, isotherm and kinetics models, desorbing agents, pH and contact time, and the influence of the intrinsic nature of metal ions and metal sorption capacities. The cobalt (Co-60), caesium (Cs-137), strontium (Sr-90), polonium (Po), radium (Ra), thorium (Th) and uranium (U) were separated effectively by the chitosan-based biosorbents in the various biological, physical and chemical methods: electrochemical methods, flotation, coagulation and flocculation, membrane filtration, adsorption, ion exchange and chemical precipitation. The radionuclide separation by biological methods is classified into the following categories [1, 16, 17]:

- i. The biological processes were used to separate the radionuclides, such as constructed wetlands, flocculation and biosorption. In these biological processes, the enrichment mechanisms, accumulation and adsorption of radionuclides were used.
- ii. The evaporation, electro dialysis, reverse osmosis, ion exchange, extraction and active carbon adsorption were used to separate the radionuclides by the separation, enrichment and sorption processes.
- iii. The targeted radionuclides were separated by chemical reactions, such as electrolysis, chemical reduction and chemical precipitation.

Zemskova et al. [18, 19] introduced the M (M—Cu, Ni) potassium ferrocyanide chitosan-based biosorbents for the caesium and cerium radionuclide. This material can then separate the caesium radionuclide from the alkaline solution by co-precipitation methods. This radioactive metal is effectively adsorbed on the polymer matrix of chitosan. The Cu and Ni ions on the chitosan matrix promote the biosorbent performance of the suggested material. In this enhancement, the structural performance and chemical performances of chitosan biopolymer were changed. As a result, the adsorption performance of this material for radioactive metal was enhanced considerably (Figure 14.2).

In this research work [20], the chitosan-based biosorbents are classified into the following categories related to the metal-sorbent interactions: halogenated derivatives,

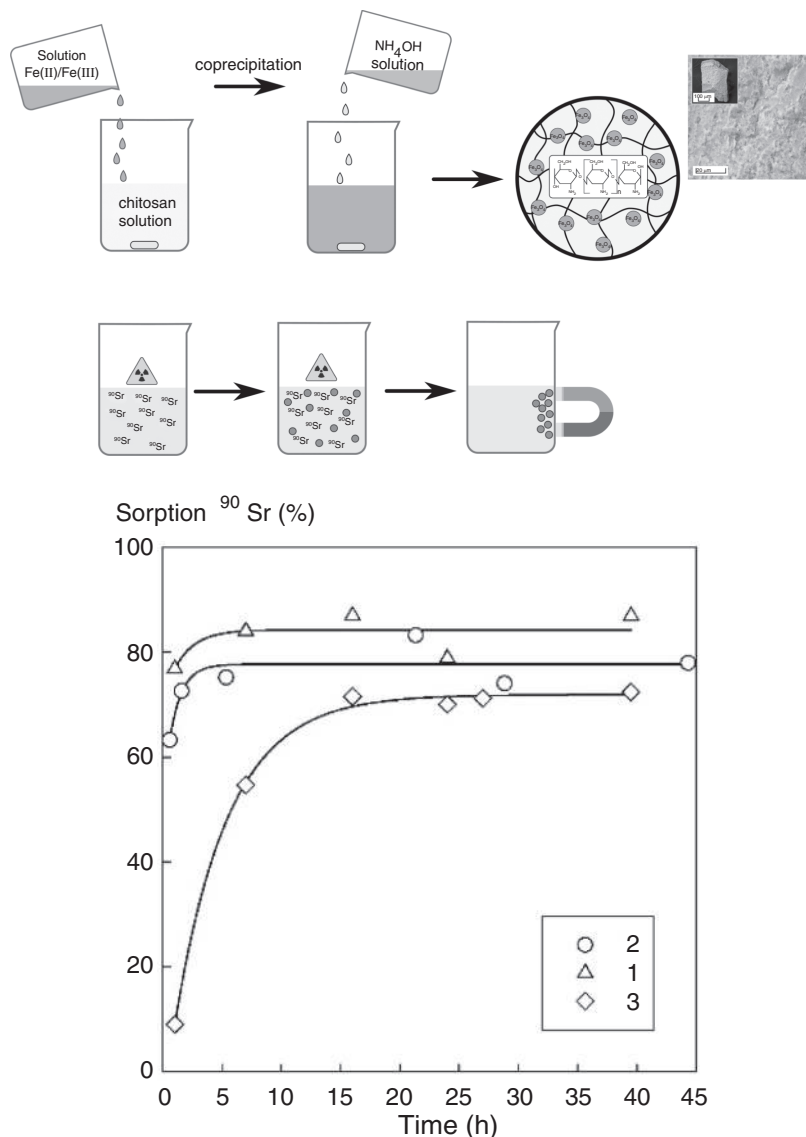


**FIGURE 14.2** (a) Caesium and cerium radionuclides separation processes and (b) sorption kinetics of radionuclide on the surface of chitosan biosorbents [19]

chitosan-cyclodextrin conjugates, derivatives with 1,3 dicarbonyl compounds, chitosan graft sugars, chitosan graft copolymers, chitosan Ethylenediaminetetraacetic acid (EDTA)/ Diethylenetriaminepentaacetic acid (DTPA) complexes, chitosan crown ethers, derivatives of chitosan containing N, P and S as the heteroatom, templated chitosan and crosslinked chitosan (Figure 14.3). Ngh et al. [21] suggested several types of chitosan derivatives as biosorbents: bentonite modification, calcium

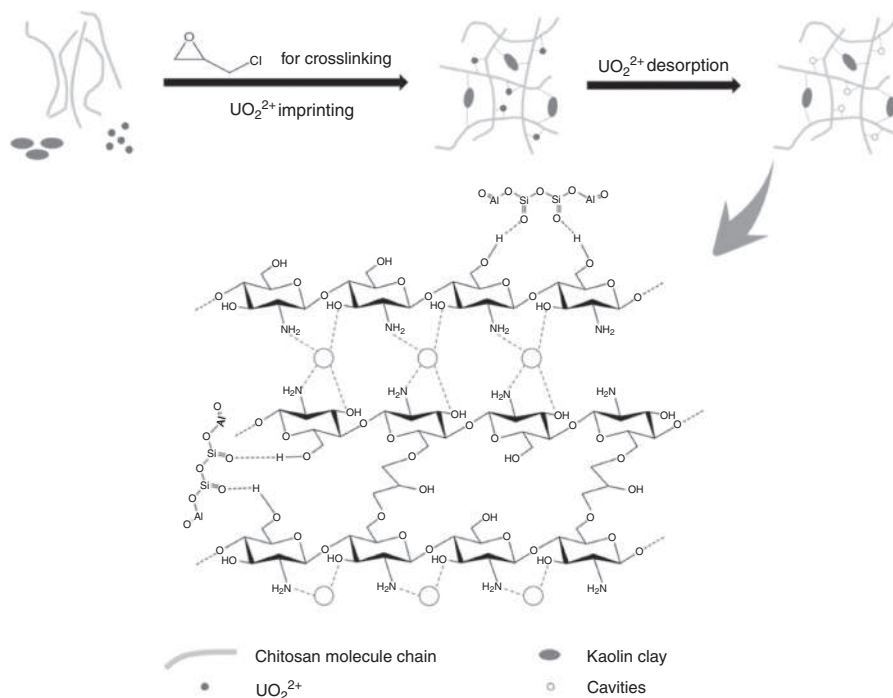


FIGURE 14.3 Separation of uranium by chitosan/kaolin clay composite foams [23]

alginate modification, polyvinyl chloride modification, polyvinyl alcohol modification, montmorillonite modification, cellulose modification, sand modification, cotton fibre modification, magnetite modification, oil palm ash modification and ceramic alumina modification [22].

### 14.3 OTHER BIOSORBENTS IN THE SEPARATION OF RADIONUCLIDES

The effective natural polymer-based biosorbents contained the following good characteristics [1, 24, 25]:

- i. The natural polymer-based biosorbents have good mechanical, chemical, physical, diffusion, porosity and adsorption performances.
- ii. These materials are easily recycled and regenerated materials after the biosorption of radionuclides with a strong alkaline and acidic medium.
- iii. They can separate the radionuclides from the wastewater and other environmental examples at a high rate and effectively.
- iv. The selectivity of these materials for the separation of radionuclides was high.
- v. The sorption capacitance for radionuclides was relatively higher than the traditional methods.

- vi. The sorption performance is very high and more stable in aggressive conditions: acidic, alkaline, hydraulic shock, high temperature, pH and low temperature.

Žukauskaitė et al. [26] suggested the new biosorbents named oak sawdust (*Quercus robur*) and moss (*Ptilium crista – castrensis*) for the separation of  $^{137}\text{Cs}$  and plutonium isotopes from the aquatic system. It was found that

- i. The rise of active functional groups is mainly responsible for the enhancement in the sorption capacitance of  $^{137}\text{Cs}$  and plutonium isotopes. The hydroxyl and carboxyl groups are mainly responsible for the sorption of  $^{137}\text{Cs}$  and plutonium isotopes on the surface and pore of oak sawdust (*Quercus robur*) and moss (*Ptilium crista – castrensis*). In this action, the radionuclides chemically or physically interacted with the functional groups (Figure 14.4).
- ii. The increase in values of anion and cation on the sorbent promotes the sorption capacitance of this material.
- iii. The pore value and area of the surface are important factors in the rise of sorption of capacitance.
- iv. The sorption efficiency was over 80% for  $^{137}\text{Cs}$  and plutonium isotopes, which means that over 80% of radionuclides in the wastewater solution were effectively removed from the examples.
- v. The oak sawdust (*Quercus robur*) and moss (*Ptilium crista – castrensis*) biosorbents can be easily regenerated. Additionally, these biosorbents can remove radionuclides from aquatic systems in dynamic conditions.

Dulanská et al. [27] suggested an efficient biosorbent based on the wood-decay fungus *Fomes fomentarius* for the caesium radionuclides from the wastewater solution. It is reported that the sorption processes depend on the pH level and ionic strength. The suggested methodology was used in the Water Research Institute in Bratislava for the sorption of  $^{137}\text{Cs}$ . The maximum adsorption capacitance of this biosorbent was 66 mg/g for caesium radionuclides.

El-khalafawy et al. [28] suggested the phalaris seeds peel powder (PSP) for the sorption of Cs(I) and Eu(III). This suggested biosorbents are low-cost and economically effective. In the sorption analysis of this biosorbent, the interference ions on the sorption of Eu(III) and Cs(I), the effect of media pH, initial metal concentration and contact time were investigated by the various spectroscopic, surface and theoretical methods. The obtained results suggested (Figure 14.5) that

- i. The adsorption of  $\text{Eu}^{3+}$  and  $\text{Cs}^+$  on the surface of the biosorbent is endothermic, indicating that the adsorption of  $\text{Eu}^{3+}$  and  $\text{Cs}^+$  required additional energy. Additionally, their adsorption is spontaneously processed.
- ii. The selectivity for the  $\text{Eu}^{3+}$  is higher than  $\text{Cs}^+$ .
- iii. The separation indicator is lower than 1, confirming that the PSP is more effective for the sorption of Cs(I) and Eu(III).



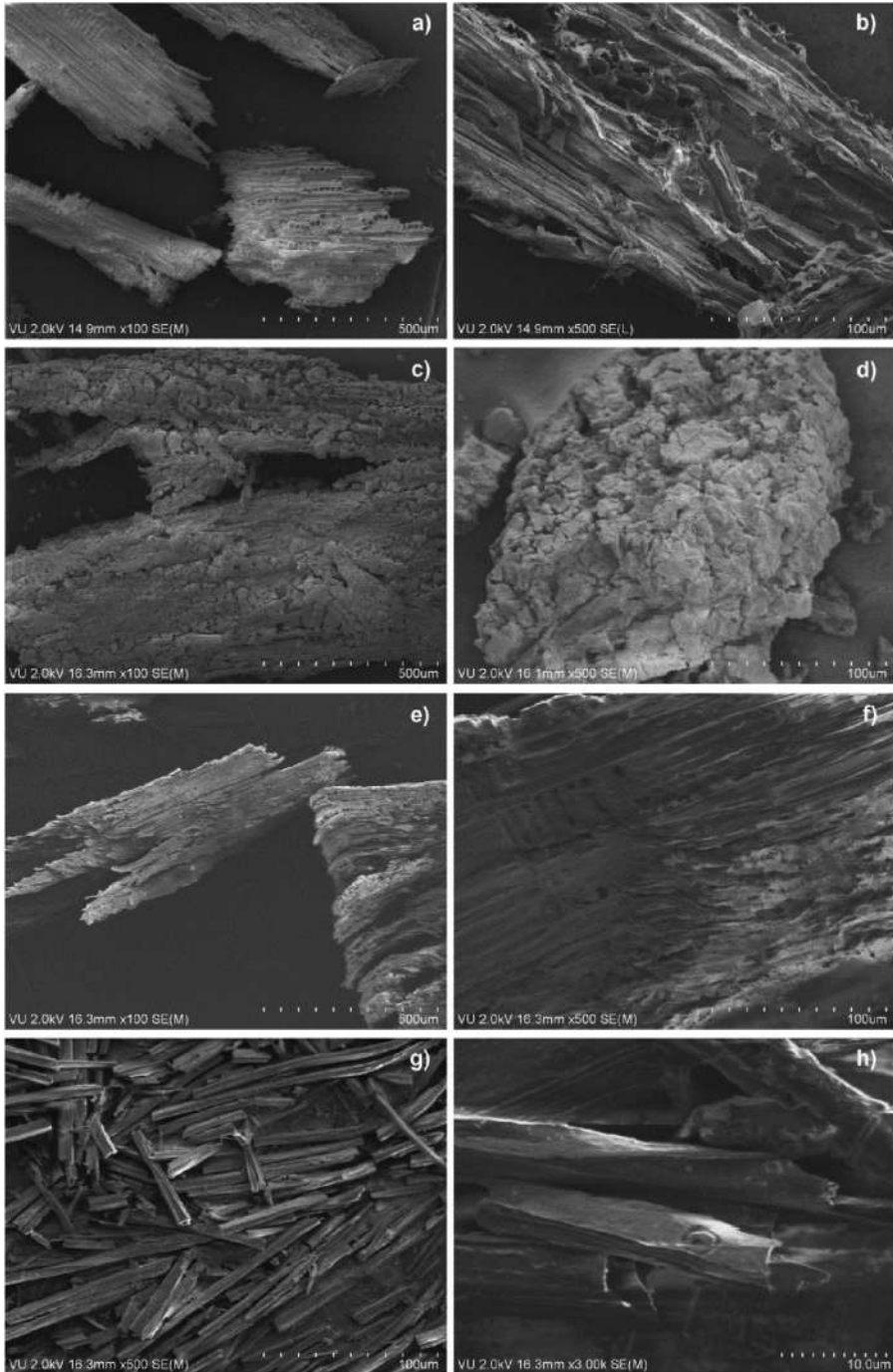


**FIGURE 14.4** Scanning electron pictures before  $\times 100$  (a),  $\times 500$  (b) and after the functionalised with iron hydroxide  $\times 100$  (c),  $\times 500$  (d), after the carbonisation of sawdust  $\times 100$  (e),  $\times 500$  (f), additionally, carbonised sawdust functionalised with HCl  $\times 500$  (g),  $\times 3000$  (h) [26]

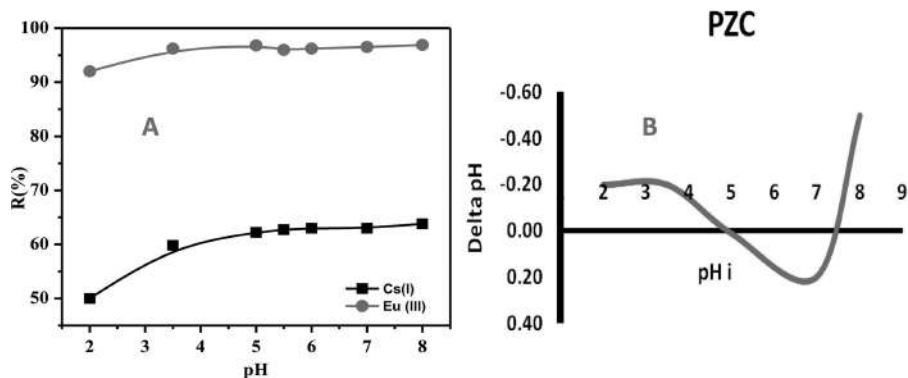


**FIGURE 14.5** (a) Effectiveness of PSP for the sorption of Cs(I) and Eu(III) and (b) point of zero charge analysis [28]

## 14.4 CONCLUSION

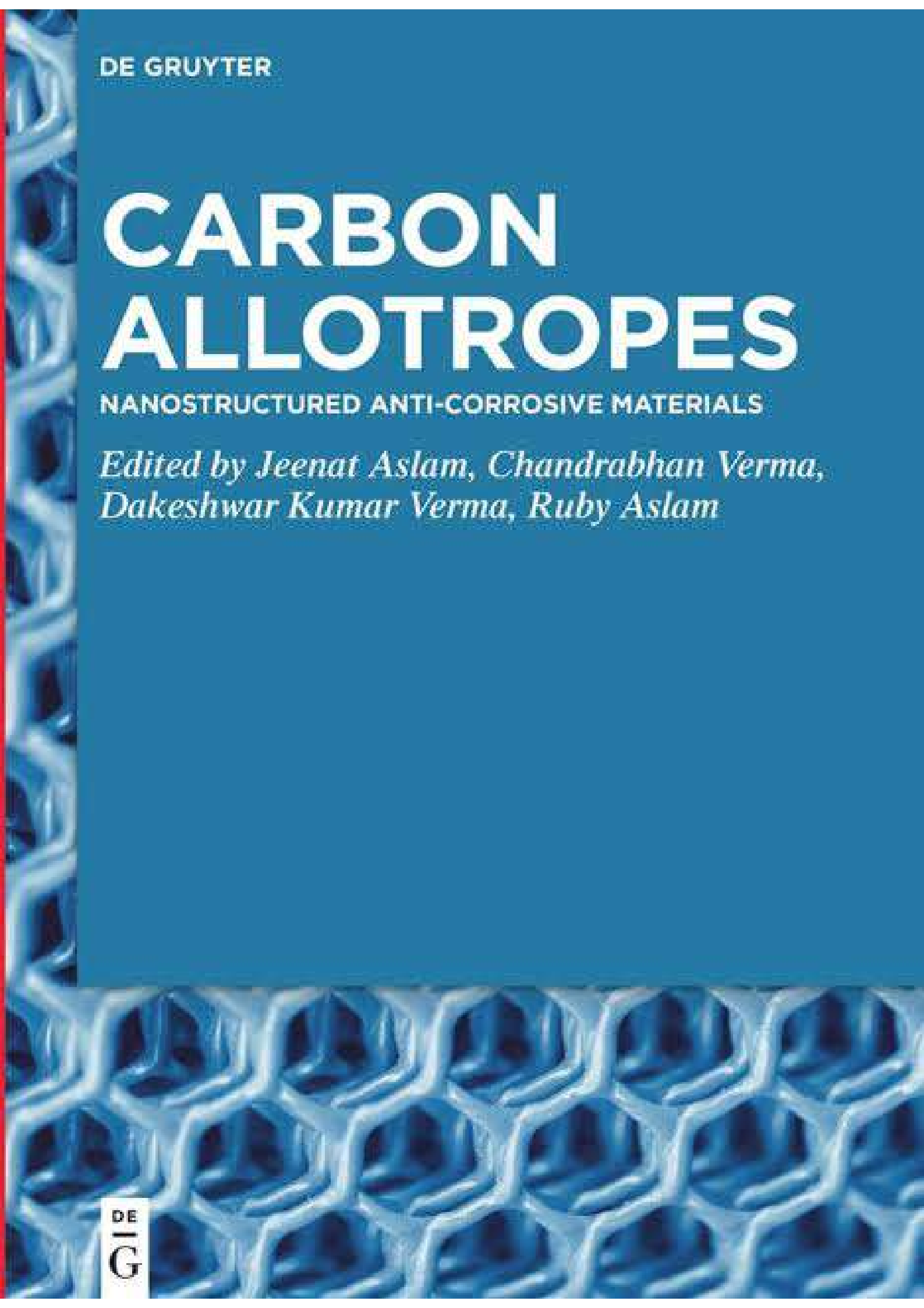
In this book chapter, the application of biosorbents in the separation of radionuclides was reviewed and discussed with modern examples. Currently, the separation of radionuclides from environmental examples is an urgent task in modern engineering sciences. Chitosan-based biosorbents were new and green technology in the separation of radionuclides. These types of biosorbents were more efficient and low-cost materials in the separation of radionuclides. The preparation methods of chitosan-based materials were easy and did not require high-degree technologies. Chitosan is a natural product and green polymer. There are many research works related to the separation of radionuclides from wastewater and other environmental samples. In addition to this, the animal organ, plant parts, and algal, fungal and bacterial biosorbents were suggested as effective in the separation of radionuclides [29].

## REFERENCES

1. Wang, J. and C. Chen, Chitosan-based biosorbents: Modification and application for biosorption of heavy metals and radionuclides. *Bioresource Technology*, 2014. **160**: p. 129–141.
2. Maksoud, M.I.A.A., et al., Insight on water remediation application using magnetic nanomaterials and biosorbents. *Coordination Chemistry Reviews*, 2020. **403**: p. 213096.
3. Kılınc, E., et al., A new method for the preconcentrations of U (VI) and Th (IV) by magnetized thermophilic bacteria as a novel biosorbent. *Analytical and Bioanalytical Chemistry*, 2021. **413**(4): p. 1107–1116.
4. Datta S, K. Radhapyari, N. Saha, S.K. Samanta, Recent trends in the application of biowaste for hazardous radioactive waste treatment, in *Environmental Sustainability and Industries*. 2022, Elsevier. p. 159–192.
5. Heidari, F., et al., Isolation of an efficient biosorbent of radionuclides ( $^{226}\text{Ra}$ ,  $^{238}\text{U}$ ): Green algae from high-background radiation areas in Iran. *Journal of Applied Phycology*, 2017. **29**(6): p. 2887–2898.
6. Wang, J. and S. Zhuang, Removal of cesium ions from aqueous solutions using various separation technologies. *Reviews in Environmental Science and Bio/Technology*, 2019. **18**(2): p. 231–269.

7. Gupta, N.K., et al., Biosorption-an alternative method for nuclear waste management: A critical. *Journal of Environmental Chemical Engineering*, 2018. **6**: p. 2159–2175.
8. Shutova, V.V., et al., Levant from *Azotobacter vinelandii* as a Component of Biosorbents for Heavy Metals and Radionuclides. *Applied Biochemistry and Microbiology*, 2021. **57**(1): p. 102–109.
9. Varala, S., et al., Desorption studies for the recovery of radionuclides (Th and Zr) and optimization using Taguchi mixed design L18 (2132)—A regeneration step for loaded biosorbent, general mathematical model for multistage operation. *Journal of Environmental Chemical Engineering*, 2017. **5**(6): p. 5396–5405.
10. Dai, Y., et al., Macroporous ion-imprinted chitosan foams for the selective biosorption of U (VI) from aqueous solution. *International Journal of Biological Macromolecules*, 2020. **164**: p. 4155–4164.
11. Zhuang, S. and J. Wang, Removal of cesium ions using nickel hexacyanoferrates-loaded bacterial cellulose membrane as an effective adsorbent. *Journal of Molecular Liquids*, 2019. **294**: p. 111682.
12. Alam, M.F., et al., Selective separation of radionuclides from environmental matrices using proprietary solid-phase extraction systems: A review. *Microchemical Journal*, 2022. **181**: p. 107637.
13. Fiaccabrino, D.E., P. Kunz, and V. Radchenko, Potential for production of medical radionuclides with on-line isotope separation at the ISAC facility at TRIUMF and particular discussion of the examples of <sup>165</sup>Er and <sup>155</sup>Tb. *Nuclear Medicine and Biology*, 2021. **94–95**: p. 81–91.
14. Kapashi E., M. Kapnisti, A. Dafnomili, F. Noli, Aloe Vera as an effective biosorbent for the removal of thorium and barium from aqueous solutions. *Journal of Radioanalytical and Nuclear Chemistry*. 2019 Jul 15. **321**: pp. 217–226.
15. Gamal, R., N.M. Sami, and H.S. Hassan, Assessment of modified *Salvadora Persica* for removal of <sup>134</sup>Cs and <sup>152+154</sup>Eu radionuclides from aqueous solution. *Environmental Science and Pollution Research*, 2022. **29**(2): p. 3072–3090.
16. Yin, Y., et al., Removal of strontium ions by immobilized *Saccharomyces cerevisiae* in magnetic chitosan microspheres. *Nuclear Engineering and Technology*, 2017. **49**(1): p. 172–177.
17. Wani, A.A., et al., Recent advances and future perspectives of polymer-based magnetic nanomaterials for detection and removal of radionuclides: A review. *Journal of Molecular Liquids*, 2022. **365**: p. 119976.
18. Zemskova, L., et al., Chitosan-based biosorbents: immobilization of metal hexacyanoferrates and application for removal of cesium radionuclide from aqueous solutions. *Journal of Sol-Gel Science and Technology*, 2019. **92**(2): p. 459–466.
19. Zemskova, L., et al., New chitosan/iron oxide composites: Fabrication and application for removal of Sr<sup>2+</sup> radionuclide from aqueous solutions. *Biomimetics*, 2018. **3**(4): p. 39.
20. Varma, A.J., S.V. Deshpande, and J.F. Kennedy, Metal complexation by chitosan and its derivatives: A review. *Carbohydrate Polymers*, 2004. **55**(1): p. 77–93.
21. Ngah, W.S.W., L.C. Teong, and M.A.K.M. Hanafiah, Adsorption of dyes and heavy metal ions by chitosan composites: A review. *Carbohydrate Polymers*, 2011. **83**(4): p. 1446–1456.
22. Attia, L.A., M.A. Youssef, and O.A. Abdel Moamen, Feasibility of radioactive cesium and europium sorption using valorized *punica granatum* peel: Kinetic and equilibrium aspects. *Separation Science and Technology*, 2021. **56**(2): p. 217–232.
23. Yu, H., et al., Selective biosorption of U(VI) from aqueous solution by ion-imprinted honeycomb-like chitosan/kaolin clay composite foams. *International Journal of Biological Macromolecules*, 2022. **206**: p. 409–421.
24. Zhuang, S., et al., Adsorption of Co<sup>2+</sup> and Sr<sup>2+</sup> in aqueous solution by a novel fibrous chitosan biosorbent. *Science of the Total Environment*, 2022. **825**: p. 153998.

25. Gök, C., S. Aytas, and H. Sezer, Modeling uranium biosorption by *Cystoseira* sp. and application studies. *Separation Science and Technology*, 2017. **52**(5): p. 792–803.
26. Žukauskaitė, Z., et al., Separation of anthropogenic radionuclides from aqueous environment using raw and modified biosorbents. *Journal of Environmental Radioactivity*, 2022. **244–245**: p. 106829.
27. Dulanská, S., et al., Modified biosorbent wood-decay fungus *Fomes fomentarius* for pre-concentration of  $^{137}\text{Cs}$  in water samples. *Journal of Radioanalytical and Nuclear Chemistry*, 2018. **318**(3): p. 2493–2500.
28. El-khalafawy, A., D.M. Imam, and M.A. Youssef, Enhanced biosorption of europium and cesium ions from aqueous solution onto phalaris seed peel as environmental friendly biosorbent: Equilibrium and kinetic studies. *Applied Radiation and Isotopes*, 2022. **190**: p. 110498.
29. Gupta, N.K., et al., Biosorption-an alternative method for nuclear waste management: A critical review. *Journal of Environmental Chemical Engineering*, 2018. **6**(2): p. 2159–2175.



DE GRUYTER

# CARBON ALLOTROPES

NANOSTRUCTURED ANTI-CORROSIVE MATERIALS

*Edited by Jeenat Aslam, Chandrabhan Verma,  
Dakeshwar Kumar Verma, Ruby Aslam*

DE  
G

# Contents

About the editors — V

Preface — VII

Bhawana Jain, Reena Rawat, Daniel Amoako Darko

**Chapter 1**

**Carbon allotropes: properties and applications – state of the art — 1**

Alimorad Rashidi, Maryam Sirati Gohari, Seyed Ali Rezaei

**Chapter 2**

**Carbon allotropes: synthesis and characterization — 33**

Sourav Kr. Saha, Namhyun Kang

**Chapter 3**

**Corrosion: basics, economic adverse effects, and its mitigation — 67**

Maryam Sirati Gohari, Seyed Ali Rezaei, Alimorad Rashidi

**Chapter 4**

**Carbon allotropes for anticorrosive applications, challenges, and opportunities — 89**

Gokul Ram Nishad, Ashwani Kumar Sharma, Dakeshwar Kumar Verma

**Chapter 5**

**Carbon allotropes: mechanism of corrosion prevention and control — 117**

Omar Dagdag, Rajesh Haldhar, Seong-Cheol Kim, Elyor Berdimurodov, Chandrabhan Verma, Ekemini D. Akpan, Eno E. Ebenso

**Chapter 6**

**Graphene and graphene oxide as nanostructured corrosion inhibitors — 133**

Sanjukta Zamindar, Manilal Murmu, Naresh Chandra Murmu, Priyabrata Banerjee

**Chapter 7**

**Chemically modified graphene and graphene oxides as corrosion inhibitors — 149**

Manilal Murmu, Sanjukta Zamindar, Naresh Chandra Murmu,  
Priyabrata Banerjee

**Chapter 8**

**Polymer composites of graphene and graphene oxides as  
corrosion inhibitors — 175**

Seyed Ali Rezaei, Maryam Sirati Gohari, Alimorad Rashidi

**Chapter 9**

**Carbon nanotubes (CNTs) and their composites as nanostructured  
corrosion inhibitors — 201**

Avni Berisha

**Chapter 10**

**Chemically modified CNTs as corrosion inhibitors — 227**

Roli Jain, Daniel Amoako Darko, Bhawana Jain, Ruchi Sharma, Reena Rawat

**Chapter 11**

**Carbon quantum dots (CQDS), carbon nanorods (CNRS), and their composites  
as nanostructured corrosion inhibitors — 241**

Seyyed Arash Haddadi, Saeed Ghaderi,

Mohammad Ebrahim Haji Naghi Tehrani, Bahram Ramezanzadeh

**Chapter 12**

**Recent advances in carbon allotropes nanostructured as anticorrosive  
coatings — 271**

Taiwo W. Quadri, Lukman O. Olasunkanmi, Omolola E. Fayemi, Eno E. Ebenso

**Chapter 13**

**Industrial corrosion inhibitors: nanostructured carbon allotropes as  
ideal substitutes — 327**

Navid Hosseinabadi

**Chapter 14**

**Carbon allotropes-based materials as ideal substitutes for industrially useful  
self-healing coatings: recent advancements and future proponents — 355**

Gokul Ram Nishad\*, Ashwani Kumar Sharma,  
Dakeshwar Kumar Verma

## Chapter 5

# Carbon allotropes: mechanism of corrosion prevention and control

**Abstract:** Many methods are used to protect the corrosion occurring in metallic materials, out of which the corrosion inhibitors are mainly used at present. In addition to the traditionally used inhibitors for corrosion inhibition, the practice of smart coating materials has increased in the last few decades, in which carbon allotropes and their composites are being used mainly at present. Some of their characteristics, such as thermal stability and stable protective layer formation, resist to corrosive attack and keep them in the category of special type of corrosion inhibitor. In the present work, description has been given about carbon allotropes-based materials and their corrosion inhibition mechanism and experimental techniques.

**Keywords:** corrosion inhibitor, adsorption, carbon allotropes, metallic materials, electrochemical analysis, computational calculations

## 5.1 Introduction

Corrosion is a natural phenomenon in which metallic materials convert into their most stable forms such as oxides, chlorides and sulphates etc. due to environmental conditions. Metallic materials such as steel, aluminum, copper, zinc, and its alloys are mainly used in industries such as construction, petroleum, power plants, nuclear power plants, and aerospace [1–3]. Before use, these metals undergo a process like acid picking and descaling to remove the accumulated rust or scull, in which hydrochloric acid, sulphuric acid, nitric acid, etc. are prominently used as acidic solutions [4, 5]. After removing the rust that has accumulated on the metal surface, this corrosive solution starts consuming by attacking the base metal surface. To prevent this loss, a small amount of substance is added to the electrolytic medium, which is called corrosion inhibitor, because it damages the metal surface. By depositing above, they

---

\*Corresponding author: Gokul Ram Nishad, Department of Chemistry, Govt. Digvijay Autonomous Postgraduate College, Rajnandgaon, Chhattisgarh 491441, India, e-mail: nishadgokul505@gmail.com  
Ashwani Kumar Sharma, Dakeshwar Kumar Verma, Department of Chemistry, Govt. Digvijay Autonomous Postgraduate College, Rajnandgaon, Chhattisgarh 491441, India



protect them from further corrosion [6, 7]. imidazole derivatives [8], thioglycoluril derivatives [9, 10] supramolecule derivatives [11, 12], and drug molecules [13].

Due to their long synthesis process and environmental threats, there is a need for such inhibitors which are green and stable. Graphene, graphene oxide, graphene composites, carbon nanotubes (CNTs), fullerene, and carbon quantum dots (CQDs) are mainly used [14, 15]. All these allotropes behave like smart anticorrosive material, and being stable even in an aggressive environment, forming a protective layer on the metal surface protects the metallic surface from further corrosion. Mainly experimental tools, surface study, and theoretical calculation are predominant for corrosion monitoring techniques. The present review work is mainly focused on the corrosion inhibition mechanism of carbon allotropes. Additionally Fig. 5.1 demonstrated the key characteristics of carbon allotropes.

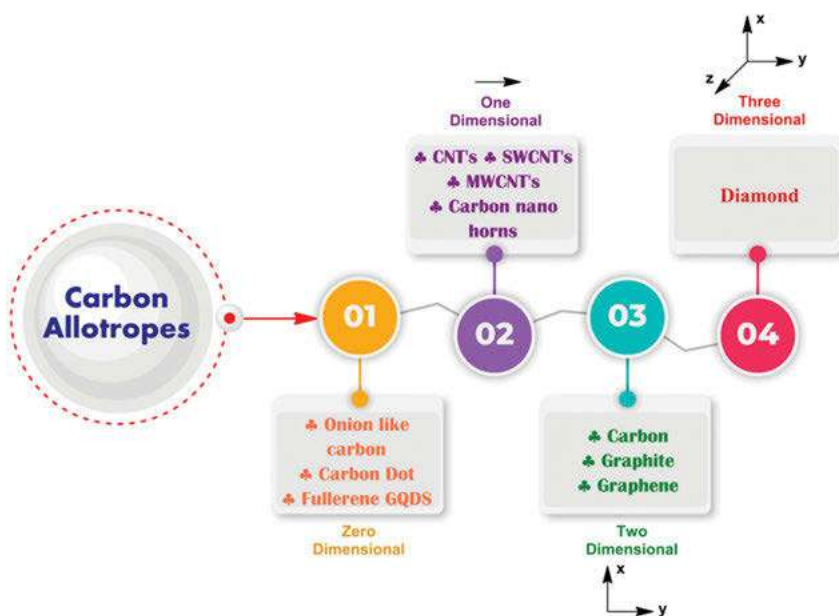


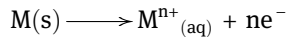
Fig. 5.1: Important characteristics of carbon allotropes [14].

## 5.2 General corrosion reaction mechanism

### – Electrochemical reactions

Corrosion on metal surface considered as electrochemical process which involved two half cell reactions i.e. cathodic and anodic. Usually in the oxidation reaction electron has been produced while in reduction reaction electron is involved as reactant. There are mainly two types of electrochemical reactions:

- i) *Anodic reaction*: Anodic reaction is also considered as oxidation reaction as it involves the increase in oxidation state of metal ion by losing electron(s) i.e. electron can be produced during the reaction, for example:



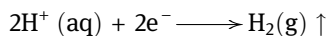
where M = Fe, Al, Zn, Cu

N = 0, 1, 2, 3, 4, etc.

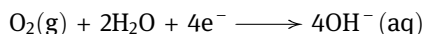
Anodic reaction in metal complexes:



- ii) *Cathodic reaction*: In this reaction oxidation number of species decreases due to gain electrons i.e. it can be considered as reduction reaction. Here species gain electron at cathodic side, and this reaction is termed as hydrogen evolution reaction. If the electrolytic solution is acidic, for example:



Cathodic reactions also exist in neutral or basic solution. In this case dissolved oxygen is reduced to hydroxyl ions as given below:



– *Overall electrochemical process*

In acidic electrolytic medium, both anodic and cathodic reactions take together at coupled manner on metal surface.

Formation of potential difference on the metal surface can be considered as the driving force for the course of corrosion. Additionally, Fig. 5.2 shows the coupled reaction on metal surface. Overall process can be representation as follows:

– *Electrochemical analysis*

Corrosion is electrochemical phenomenon, which is generated due to the potential difference in metallic surface. The analysis of corrosion behavior and corrosion rates is done by electrochemical studies. Mainly three electrode cell assembly uses for electrochemical analysis i.e. working electrode, reference electrode, and counter electrode. As working electrode, that metal is taken for which corrosion study is done, such as iron, aluminum, copper, and zinc electrode. Calomel electrode is mainly used for reference electrode, and platinum electrode is mainly used for counter electrode. Electrochemical impedance spectroscopy (EIS) and potentiodynamic polarization are studied under electrochemical techniques.

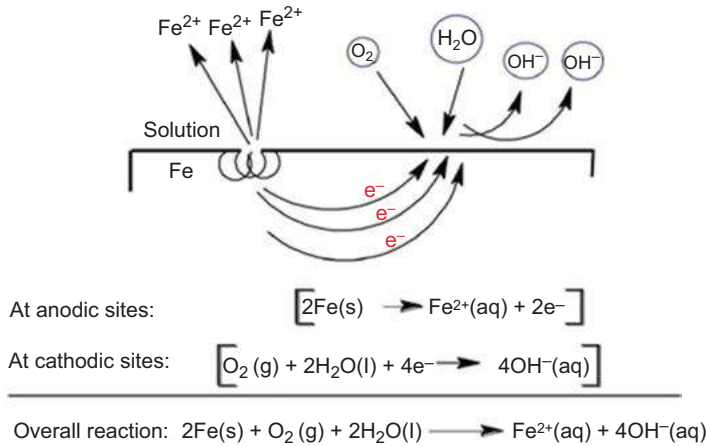


**Fig. 5.2:** Coupled reactions occurring on metal surface at different electrolytic medium [16].

– *Open circuit potential*

Open circuit potential (OCP) is a passive technique, also known as rest potential, open circuit voltage, equilibrium potential, corrosion potential, and zero potential. It is mainly used to determine the resting potential of the system from which further experiments depend on. Mainly with EIS the potential is set against the OCP, not against the reference electrode. The resting potential between the working electrode and the reference electrode is measured by OCP.

Information about the stability of the electrochemical system in the electrolytic medium is also obtained through the OCP. Overall it can be considered that OCP is simply the potential difference between reference electrode and working electrode.

$$E_{\text{OCP}} = E_{\text{working}} - E_{\text{ref}}$$

Hence the potential can be used as normal voltmeter to measure the potential difference between two difference sites or points.

– *Electrochemical impedance spectroscopy*

EIS techniques are used to explain the effect of the corrosion process on surface inhomogeneity. Electrochemical AC and DC techniques are used for performing electrochemical processes in a method to determine corrosion rates.

## 5.3 Corrosion inhibitors: Past to present perspective

Generally good corrosion inhibitors should have the following properties [17]:

- i) Inhibiting molecules having functional group containing different heteroatoms and electron-rich unsaturated bond is present.
- ii) Highly water soluble.
- iii) Eco-friendly, zero-toxic, and should be cost-effective.
- iv) Stable in electrolytic solution.
- v) From the methods of making it to the application in it, the process is zero dangerous.

### 5.3.1 Inorganic corrosion inhibitors

Inorganic inhibitors, such as chromate, phosphate, and silicate, were mainly used as inhibitors a few decades ago, based on the above properties of inhibitors. But due to the ill-effects of living beings, their use started to decrease. A few decades ago, organic corrosion inhibitors were mainly used as replacements for inorganic corrosion inhibitors. Most of the effective inorganic corrosion inhibitors are chromate, phosphate, sulphate, nitrite, and silicates salts of various metals like zinc, copper, and nickel. The inorganic salts mentioned here react with the metal cations present on the surface, and this further gets deposited on the metal surface in the form of a protective layer that prohibits further corrosion [18, 19]. Chromate salts especially  $\text{SrCrO}_4$  have shown effective inhibition properties by forming a thin stable protective film on the metal surface even without depending upon the environmental parameters like the presence of  $\text{O}_2$  and pH [20].

A. I. Munoz and his coworkers examined the copper, nickel, and two copper-nickel ( $\text{Cu}_{90}/\text{Ni}_{10}$ ,  $\text{Cu}_{70}/\text{Ni}_{30}$ ) alloys in 850 g/L LiBr solution in the absence and presence of chromate ( $\text{CrO}_4^{2-}$ ), molybdate ( $\text{MoO}_4^{2-}$ ), and tetraborate ( $\text{B}_4\text{O}_7^{2-}$ ) inhibitors. The efficiency was measured using potentiodynamic and cyclic voltametry, and they found that chromate is the most effective inhibitor among the three [21].

B. Ramezanzadeh, E. Ghasemi, F. Askari, and Mahadavian analyzed corrosion-inhibitive pigments based on zinc acetate/benzotriazole in 3.5 wt% NaCl solution on mild steel samples by polarization test and EIS. They found that the zinc acetate/benzotriazole is a good inhibitor, and it also decreases the dissolution rate of steel [22].

Q. H. Zhang and his coworkers have studied the corrosion inhibition properties of combined corrosion inhibitors LHD + PT made by mixing amino acid (L-histidine) and 1-phenylthiourea and a modified inhibitor PT-HD (phenylcarbamothioylhistidine) for the corrosion of carbon steel in  $\text{CO}_2$ -saturated formation water. Experimental data prove that PT-HD is better inhibitor as compared to LHD + PT (inhibition efficiency of 99.2% for 0.4 mM LHD + PT and 99.3% for 0.4 mM PT-HD).

### 5.3.2 Organic corrosion inhibitors

Organic corrosion inhibitors mainly functional groups of diffusion present electron-rich centers by which they interact with the metal surface. The use of organic corrosion inhibitors has several advantages over inorganic inhibitors such as electron-rich center, less hazardous, green in nature, highly soluble, nontoxic, and eco-friendly. [23, 24]. Molecules are mainly used as organic corrosion inhibitors in aliphatic, aromatic, heterocyclic, carbocyclic, ionic liquids, etc. Organic corrosion inhibitors mainly pharmaceutical molecules, imidazole derivatives [25], indole derivatives [26], thiophene derivatives [27], pyrazine derivatives [28], benzothiazole derivatives [29], etc. have been mainly used by the former researchers. But due to the complex process ranging from synthesis methods to applications of organic corrosion inhibitors, it has also attracted the attention of scientific and researchers toward biomass-based materials in search of alternative inhibitors. Ahmed and coworkers (2022) studied nonanedioic acid toward anticorrosive material for mild steel in 1 M HCl aggressive solution. They reported maximum inhibition efficiency of 97% according to experimental technique at temperature ranging from 303 to 333 K [30]. Due to the toxic, harmful behavior toward the environment, the use of inorganic inhibitors is being reduced. Heteroatoms like S, N, O, and P are present in organic inhibitors. Their two properties viz. higher basicity and electron-donor abilities make them center for absorption on a metal surface.

Palaniappan N. and team members have successfully examined the 4,5-diphenyl-imidazole-functionalized CNTs in 1 M H<sub>2</sub>SO<sub>4</sub> as a corrosion-inhibiting barrier layer on nickel alloy surfaces [31]. Abrishami, Naderi, and Ramezanzadeh have synthesized many organic/inorganic using zinc acetylacetonate and organic compounds such as *Urtica Dioica* leave extracts (ZnAA-U.D). They have examined the synthesized pigments in corrosion control in 3.5 wt.% NaCl solutions and found that the synthesized pigments showed excellent corrosion inhibition properties at pH = 4 [32].

Yujie Qiang and his team have studied corrosion inhibition properties of indazole (IA) and 5-aminoindazole (AIA) for copper in NaCl solution, and they found these compounds very effective corrosion inhibitors with inhibition efficiency order AIA > IA [33].

### 5.3.3 Biomass materials

Biomass-based corrosion inhibitor I mainly comes across from algae, fungi, bacteria, plant extracts, etc. Materials based on plant extracts include various parts such as bark, root, leaves, flower, fruit, and seed rind, which are currently being used as green rust inhibitors. Plant extract mainly contains a variety of phytoconstituents such as flavonoids, terpenoids, alkaloids, and cholesterol. All these phytoconstituents are electron rich with different diffusion function groups. Plants extract corrosion-resistant, cost-effective, environment-friendly, and are nonhazardous [34, 35].

Biomasses specially extracted from plants have also shown excellent corrosion inhibition properties. The corrosion inhibition potential of the green inhibitors depends upon the structure of the active ingredient. The use of naturally occurring substances as green corrosion inhibitors has been successfully reported in both the acidic as well as basic medium by many researchers.

O. K. Abiola and his coworkers have studied the corrosion inhibition properties of aluminum in hydrochloric acid solutions of *Delonix regia* extract in hydrochloric acid solutions [36], and rosemary leaves were examined by M. Kliskic et al. as corrosion inhibitor for the Al + 2.5 Mg alloy in a 3% NaCl solution at 25 °C [37]. Honey [38] and opuntia extracts [39] were examined by El-Etre as a corrosion inhibitor for copper and aluminum, respectively.

The corrosion inhibition activity of *R. communis* extract against reinforcing steel corrosion in concrete in 3.5% NaCl media has been studied successfully by S. P. Palanisamy et al. The layer of *R. communis* on reinforcing steel in concrete also increases the compressive strength and splitting tensile strength [40]. Xin Lai et al. have examined chitosan derivatives for corrosion inhibition properties on aluminum alloy. The corrosion inhibition activities were checked at different concentrations. The maximum inhibition efficiency of chitosan derivatives reaches 94.5% at 200 PPM after being immersed in 3.5 wt% NaCl solution for 72 h [41]. Watermelon extract:Zn complex has been studied in a 3.5% NaCl solution on mild steel (MS) and found that it controls 96% of MS corrosion [42].

## 5.4 Carbon allotropes as anticorrosive materials

The revolution of materials science facilitates the development of a new generation of effective materials for applications. Compared to other anticorrosive materials, carbon allotropes are among the most preferred materials in the field of corrosion protection due to their characteristics such as large surface area, excellent mechanical properties, light weight and easy synthesis process, and other synergistic behavior.

### 5.4.1 Graphene, graphene oxide (GO), and its composites as anticorrosive materials

Prasai et al. [43] reported graphene coating on various metals such as Zn and Ni as a protective coating that prevents corrosion. They used electrochemical methods to study the corrosion inhibition of copper and nickel by growing graphene on either of these metals. They found that the graphene coating effectively suppresses metal oxidation and oxygen reduction by cyclic voltammetry measurements. Their EIS measurements showed that while graphene itself is not damaged, the metal beneath

it corrodes over cracks in the graphene film. They reported using chemical vapor deposition (CVD) for graphene coating the corrosion rate of copper films is seven times slower in aerated  $\text{Na}_2\text{SO}_4$  solution than in bare copper. They reported that nickel with multilayer graphene film corrosives is 20 times slower than nickel surface coated with four layers of mechanically transferred graphene, i.e. four times slower than bare nickel. They were ultimately found to establish graphene as the thinnest known corrosion-protecting coating [43]. Zhang et al. [44] proposed graphene as a biocompatible protective film for metal with potential for biomedical applications and also confirmed that graphene effectively protects Cu surface from corrosion in various biological aqueous environment stops. Their various tests showed that graphene greatly reduces the toxicity of Cu by inhibiting corrosion and reducing the concentration of  $\text{Cu}^{2+}$  ions produced. They demonstrated that additional thiol derivatives assembled on graphene-coated Cu surface can significantly enhance the stability of the only graphene protection limited by defects in the graphene film [44]. Necolau et al. [45] explained the most recent progress in the field of anticorrosive coatings based on graphene oxide nanostructures as an active filler. With regard to graphene-based coatings, synthesis methods, protective functions, anticorrosion mechanisms, feasibility problems, and some ways to improve the overall properties were highlighted. With regard to the contribution of nanostructures to be used to improve the material's capability, the synergistic effect of graphene is demonstrated primarily with the oxide-refining effect of graphene as being functional with other compounds [45]. Mostly scientists explain that all the revolutionary material can be used in the synthesis of advanced composite coatings by combining the capability of restricting the permeability of water and aggressive species with other extraordinary features of polymeric materials. There is a considerable number of published works on GO polymer composites for anticorrosive applications, and the recent ones focused on the possibility of tailoring and modifying the surface features of graphene oxide in order to obtain advanced materials by various strategies, most of them based on both chemical and physical interactions [46–49].

Graphene oxide has the capability of ensuring the coatings when used as filler with hydrophobic features and can also diminish the adsorption and migration of corrosive media, which effectively improve the corrosion resistance of the composite coating. Ramezanzadeh et al. (2020) developed a nanoplatform with superior anticorrosive action built up through a one-pot synthesis method of zeoliticimidazolate framework-8 (ZIF-8) on the graphene oxide sheets. The particles applied on a steel sample showed a corrosion inhibition efficiency of about 79% when immersed in an NaCl solution by polarization tests. Zhu et al. [50] synthesized functionalized graphene oxide (GO-PPy) by in-situ process to grow polypyrrole (PPy) film on GO surface as shown in Fig. 5.3. This nanocomposites were characterized by FI-TR, XRD, Raman, and FESEM techniques. They also explained that  $\text{GP}_0.05\%$  coating showed the best impermeable and corrosion protection performance compared to other coatings according to EIS (Fig. 5.4) [50].



Fig. 5.3: Schematic representation of synthesis of graphene oxide-polypyrrole [50].

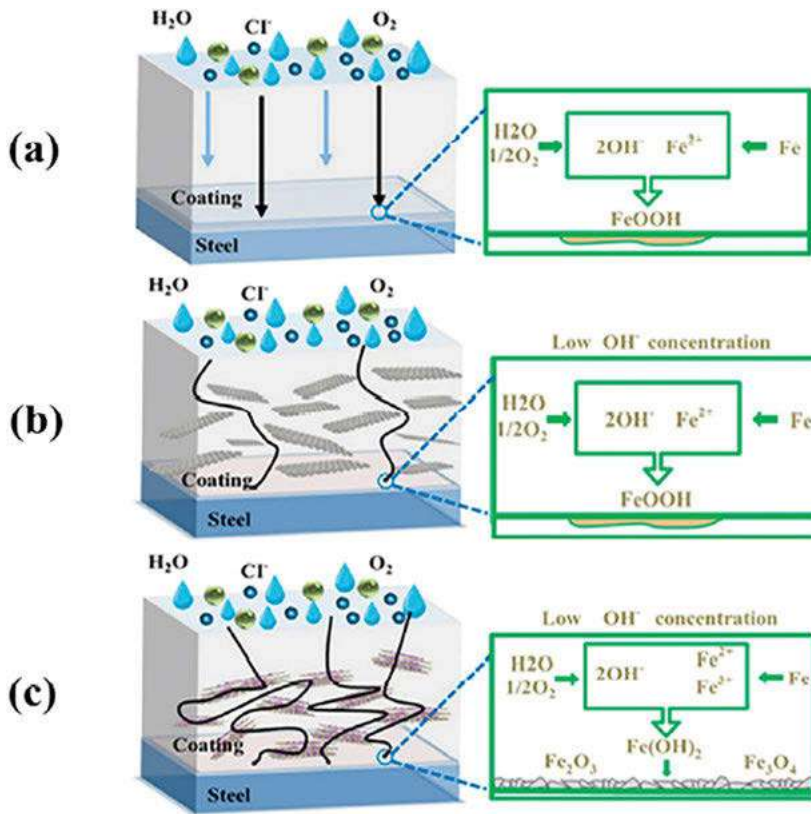


Fig. 5.4: The protective mechanism of graphene oxide-polypyrrole in corrosion protection formulations [50].



## 5.4.2 Carbon dots, carbon quantum dots, and their composites as anticorrosive materials

The unique properties of carbon dots (CDs) such as rapid solubility in water, biocompatibility, low toxicity, excellent anti-bacterial agent, chemically stable, and high thermal and nonflammable establish it as a versatile material at present, that the corrosion of metal materials in aggressive acidic, saline, CO<sub>2</sub>-saturated saline, and microbiological solutions continues in the oil, gas, and other organic chemical industry. Which is in quick need of corrosion protection, for which the use of CDs and their derivatives is an ecological and environmentally efficient method? It contains more pyrrole-like-N, pyridine-N, graphitic N atoms, and O atoms, in which lone electron pairs promote CDs that become efficient corrosion inhibitors.

Saraswat et al. [51] prepared CQDs CD1 and CD2 anticorrosive material for MS in 15% HCl aggressive solution. They reported the maximum protection degree 96.4% and 90%, respectively, according to experimental techniques [51]. Cui et al. [52] synthesized nitrogen-doped CDs (NCDs) toward anticorrosive material for Q235 carbon steel in 0.1 M HCl aggressive solution by microwave synthesis. They reported maximum protection degree 89.98% at 500 ppm according to various experimental techniques and characterized by spectroscopic method [52].

Continuously Cen et al. [53] also synthesized N and S co-doped CDs as effective corrosion inhibitors for 5,052 aluminium alloy in 0.1 M HCl anticorrosive solution. They explained their maximum protection degree 89.9%5 mg/L by experimental techniques. Also Fig. 5.5 demonstrated the 2D and 3D AFM images of inhibitor on metallic surface [53]. p-CDs and o-CDs novel nitrogen-doped CDs corrosion inhibitors are prepared by Cui and coworkers (2018) for Q235 carbon steel in 1 M HCl aggressive solution. The maximum protection degree of this material found 97% by various experimental techniques and characterized by spectroscopic method [54]. Ye et al.

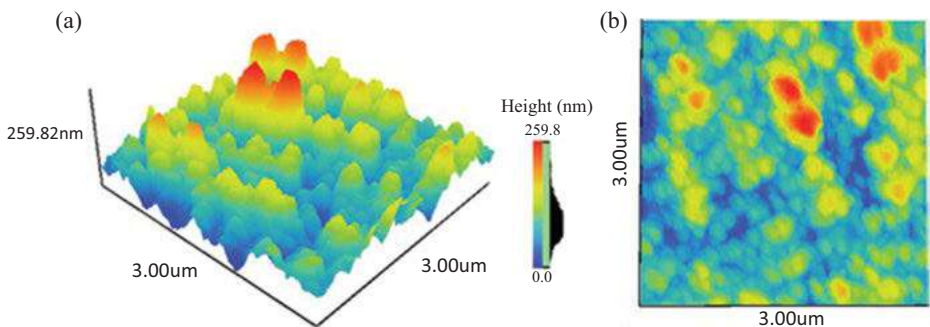


**Fig. 5.5:** Surface morphology of Al-alloy after immersion with 5 mg L<sup>-1</sup> N, S-CDs for (a) 3D AFM image and (b) 2D AFM image.

[55] prepared green and effective corrosion inhibitor of functionalized CDs for Q235 steel in 1 M HCl aggressive solution. They reported maximum protection degree 90% at 100 mg/L according to the experimental techniques [55].

## 5.5 Carbon nanotubes and its composites as anticorrosive materials

CNTs and its derivative are very useful at present due to its specific properties i.e. good conductors of heat and electricity, including high dispersibility, excellent mechanical strength, good mechanical property, high thermal and chemical resistance, high surface-to-volume ratio, and excellent ability to interact with metal surfaces. Along with their corrosion inhibition properties, CNTs and their derivatives are successfully applied as catalysts. Salvetat et al. [58] prepared CNTs from various methods including CVD, thermal synthesis process, and arc discharge evaporation [56–59]. Additionally, Fig. 5.6 shows the SEM and TEM microphotographs of carbon allotropes with their composites on metallic surface.

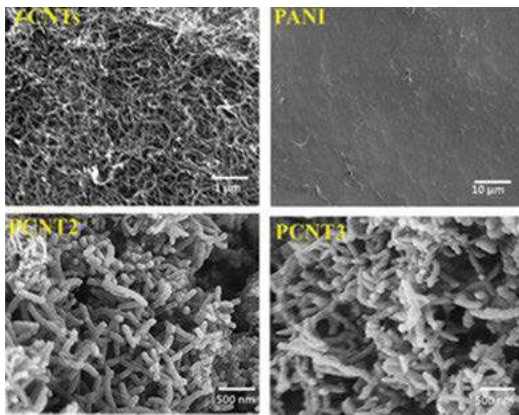


**Fig. 5.6:** SEM and TEM microphotographs of carbon allotropes with their composites on metallic surface [60].

Ionita et al. [61] explained the mechanical properties of (PPy)/polyaminobenzene-sulfonic acid-functionalized single-walled CNT-(PABS) and PPy/carboxylic acid-functionalized single-walled CNT-(CA) using molecular mechanics and molecular dynamics approaches [61]. In another study they found that the PPy film, CNT-PABS, and CNT-CA were used as anticorrosive composite coatings for carbon steel (OL 48–50) alloys in 3.5% NaCl. Potentiodynamic polarization, SEM, and TEM techniques were used to measure the anticorrosive effect of various formulations [62].

## 5.6 Corrosion inhibition mechanism

In general, corrosion inhibition is acid-base interaction chemistry, in which the inhibitor molecules act as Lewis bases. Whereas metal/alloy surface behaves like Lewis acid. Corrosion inhibitors generally contain various types of hetero-atoms such as O, S, N, P, and pi-electrons as functional groups, which are generally rich in electrons. Whereas on the metal surface, the metal cations generally reside above in the form of  $M^{n+}$ , which behave as electron acceptors [12, 63, 64]. Electron-rich centers are present in carbon-based materials and many composites. These molecules are highly stable, blocking the metal surface and protecting the metal surface from further corrosion. Corrosion inhibitors are deposited on the surface of the metal mainly through chemisorption and physisorption mechanisms, with chemisorption being stronger because there is a direct interaction between the metal surface and the inhibitor molecule [65–67]. Additionally, Fig. 5.7 demonstrates the interaction mechanism of CDs on the steel surface.

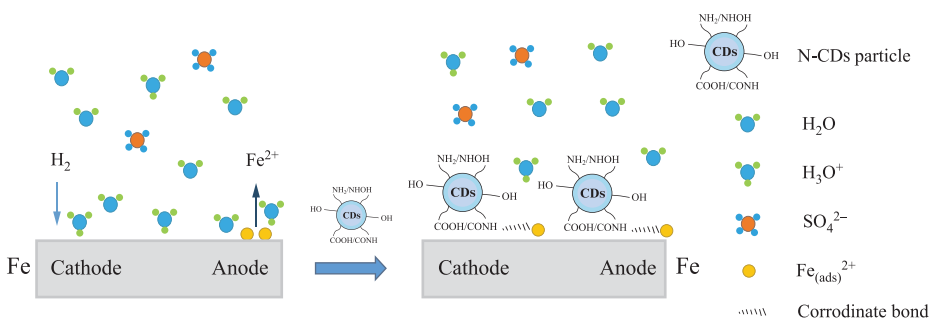


Fig. 5.7: Demonstrated the interaction mechanism of carbon dots on the steel surface [15].

## 5.7 Conclusion

Carbon allotropes namely graphene, GOs, CNTs, carbon nanorods, fullerenes, and their composite materials with polymers and nanomaterials exhibited broad applications in various fields. Their some unique properties such as small size, large surface area, hydrophobic nature, nano-filler, high temperature stability, and resistance to corrosive environment make them suitable for multiple applications. In this regards, carbon allotropes are used widely as smart anticorrosive materials toward metallic materials in various aggressive electrolytic media. Carbon allotropes are very stable towards corrosive environment to protect metallic surface from further attack. Since the nature of carbon-based materials are very stable and rigid, it can enhance the protection property. Because of their polymeric nature, these materials are associated with

huge intermolecular (Van der Waals) force of attraction they readily undergo agglomeration inside the polymer matrix that adversely affect their uniform distribution and ultimately their corrosion inhibition performance. Recently various reports are published in which covalently and non-covalently modified carbon allotropes have been evaluated as corrosion inhibitors.

## References

- [1] Jawad, A.Q., et al. Synthesis, characterization, and corrosion inhibition potential of novel thiosemicarbazone on mild steel in sulfuric acid environment. *Coatings* 2019, 9(11), 729.
- [2] Abbaszadegan, A., et al. The effect of charge at the surface of silver nanoparticles on antimicrobial activity against gram-positive and gram-negative bacteria: A preliminary study. *J. Nanomater.* 2015, 2015.
- [3] Haldhar, R., et al. Corrosion inhibitors: Industrial applications and commercialization. In: *Sustainable corrosion inhibitors II: Synthesis, design, and practical applications*, ACS Publications, 2021, 219–235.
- [4] Verma, D., et al. Inhibition performance of Glycine max, *Cuscuta reflexa* and *Spirogyra* extracts for mild steel dissolution in acidic medium: Density functional theory and experimental studies. *Results Phys.* 2018, 10, 665–674.
- [5] Abd El-Lateef, H.M.; Abdallah, Z.A.; Ahmed, M.S.M. Solvent-free synthesis and corrosion inhibition performance of Ethyl 2-(1, 2, 3, 6-tetrahydro-6-oxo-2-thioxopyrimidin-4-yl) ethanoate on carbon steel in pickling acids: Experimental, quantum chemical and Monte Carlo simulation studies. *J. Mol. Liq.* 2019, 296, 111800.
- [6] Verma, D.K.; Khan, F. Corrosion inhibition of mild steel in hydrochloric acid using extract of glycine max leaves. *Res. Chem. Intermed.* 2016, 42(4), 3489–3506.
- [7] Verma, D.K., et al. Gravimetric, electrochemical surface and density functional theory study of acetohydroxamic and benzohydroxamic acids as corrosion inhibitors for copper in 1 M HCl. *Results Phys.* 2019, 13, 102194.
- [8] Berdimurodov, E., et al. New and green corrosion inhibitor based on new imidazole derivate for carbon steel in 1 M HCl medium: Experimental and theoretical analyses. *Int. J. Eng. Res. Afr.* 2022. *Trans Tech Publ.*
- [9] Berdimurodov, E., et al. Thioglycoluril derivative as a new and effective corrosion inhibitor for low carbon steel in a 1 M HCl medium: Experimental and theoretical investigation. *J. Mol. Struct.* 2021, 1234, 130165.
- [10] Berdimurodov, E.T., et al. Novel glycoluril pharmaceutically active compound as a green corrosion inhibitor for the oil and gas industry. Available at SSRN 3951074.
- [11] Berdimurodov, E., et al. Novel cucurbit [6] uril-based [3] rotaxane supramolecular ionic liquid as a green and excellent corrosion inhibitor for the chemical industry. *Colloids Surf. A Physicochem. Eng. Asp.* 2022, 633, 127837.
- [12] Berdimurodov, E., et al. Novel bromide–cucurbit [7] uril supramolecular ionic liquid as a green corrosion inhibitor for the oil and gas industry. *J. Electroanal. Chem.* 2021, 901, 115794.
- [13] Verma, D.K., et al. Experimental and theoretical studies on mild steel corrosion inhibition by the grieseofulvin in 1 M HCl. *Eur. Chem. Bull.* 2017, 6(1), 21–30.
- [14] Berdimurodov, E., et al. The recent development of carbon dots as powerful green corrosion inhibitors: A prospective review. *J. Mol. Liq.* 2021, 118124.

- [15] Cao, S., et al. Nitrogen-doped carbon dots as high-effective inhibitors for carbon steel in acidic medium. *Colloids Surf. A Physicochem. Eng. Asp.* 2021, 616, 126280.
- [16] Verma, D.K. Density functional theory (DFT) as a powerful tool for designing corrosion inhibitors in aqueous phase. *Adv. Eng. Test.* 2018, 87.
- [17] Verma, D.K., et al. Heteroatom-based compounds as sustainable corrosion inhibitors: An overview. *J. Bio-Tribo-Corros.* 2021, 7(1), 1–18.
- [18] Deyab, M., et al. Experimental evaluation of new inorganic phosphites as corrosion inhibitors for carbon steel in saline water from oil source wells. *Desalination* 2016, 383, 38–45.
- [19] Raja, P.B., et al. Reviews on corrosion inhibitors: A short view. *Chem. Eng. Commun.* 2016, 203(9), 1145–1156.
- [20] Sinko, J. Challenges of chromate inhibitor pigments replacement in organic coatings. *Prog. Organ. Coat.* 2001, 42(3–4), 267–282.
- [21] Muñoz, A.I., et al. Inhibition effect of chromate on the passivation and pitting corrosion of a duplex stainless steel in LiBr solutions using electrochemical techniques. *Corros. Sci.* 2007, 49(8), 3200–3225.
- [22] Ramezanzadeh, B., et al. Synthesis and characterization of a new generation of inhibitive pigment based on zinc acetate/benzotriazole: Solution phase and coating phase studies. *Dyes Pigm.* 2015, 122, 331–345.
- [23] Brycki, B.E., et al. Organic corrosion inhibitors. *Corros. Inhibit. Principles Recent Appl.* 2018, 3, 33.
- [24] Verma, C., et al. Adsorption behavior of glucosamine-based, pyrimidine-fused heterocycles as green corrosion inhibitors for mild steel: Experimental and theoretical studies. *J. Phys. Chem. C* 2016, 120(21), 11598–11611.
- [25] Kumar, D.; Jain, V.; Rai, B. Imidazole derivatives as corrosion inhibitors for copper: A DFT and reactive force field study. *Corros. Sci.* 2020, 171, 108724.
- [26] Lebrini, M., et al. Electrochemical and quantum chemical studies of some indole derivatives as corrosion inhibitors for C38 steel in molar hydrochloric acid. *Corros. Sci.* 2010, 52(10), 3367–3376.
- [27] Arrousse, N., et al. Thiophene derivatives as corrosion inhibitors for 2024-T3 aluminum alloy in hydrochloric acid medium. *RSC Adv.* 2022, 12(17), 10321–10335.
- [28] Li, X.; Deng, S.; Fu, H. Three pyrazine derivatives as corrosion inhibitors for steel in 1.0 M H<sub>2</sub>SO<sub>4</sub> solution. *Corros. Sci.* 2011, 53(10), 3241–3247.
- [29] Fouda, A., et al. Benzothiazole derivatives as corrosion inhibitors for carbon steel in 1 M phosphoric acid (H<sub>3</sub>PO<sub>4</sub>) solution. *Afr. J. Pure Appl. Chem.* 2013, 7(2), 67–78.
- [30] Al-Amiery, A.A., et al. Experimental and theoretical study on the corrosion inhibition of mild steel by nonanedioic acid derivative in hydrochloric acid solution. *Sci. Rep.* 2022, 12(1), 1–21.
- [31] Palaniappan, N., et al. Experimental and DFT studies of carbon nanotubes covalently functionalized with an imidazole derivative for electrochemical stability and green corrosion inhibition as a barrier layer on the nickel alloy surface in a sulphuric acidic medium. *RSC Adv.* 2019, 9(66), 38677–38686.
- [32] Abrishami, S.; Naderi, R.; Ramezanzadeh, B. Fabrication and characterization of zinc acetylacetonate/Urtica Dioica leaves extract complex as an effective organic/inorganic hybrid corrosion inhibitive pigment for mild steel protection in chloride solution. *Appl. Surf. Sci.* 2018, 457, 487–496.
- [33] Qiang, Y., et al. Experimental and theoretical studies on the corrosion inhibition of copper by two indazole derivatives in 3.0% NaCl solution. *J. Colloid Interface Sci.* 2016, 472, 52–59.
- [34] Verma, C., et al. An overview on plant extracts as environmental sustainable and green corrosion inhibitors for metals and alloys in aggressive corrosive media. *J. Mol. Liq.* 2018, 266, 577–590.

- [35] Zucchi, F.; Omar, I.H. Plant extracts as corrosion inhibitors of mild steel in HCl solutions. *Surf. Technol.* 1985, 24(4), 391–399.
- [36] Abiola, O., et al. Eco-friendly corrosion inhibitors: The inhibitive action of Delonix Regia extract for the corrosion of aluminium in acidic media. *Anti-Corros. Methods Mater.* 2007.
- [37] Kliškić, M., et al. Aqueous extract of *Rosmarinus officinalis* L. as inhibitor of Al–Mg alloy corrosion in chloride solution. *J. Appl. Electrochem.* 2000, 30(7), 823–830.
- [38] El-Etre, A.; Abdallah, M. Natural honey as corrosion inhibitor for metals and alloys II. C-steel in high saline water. *Corros. Sci.* 2000, 42(4), 731–738.
- [39] El-Etre, A. Inhibition of aluminum corrosion using *Opuntia* extract. *Corros. Sci.* 2003, 45(11), 2485–2495.
- [40] Annaamalai, M., et al. Investigation of corrosion inhibition of welan gum and Neem gum on reinforcing steel embedded in concrete. *Int. J. Electrochem. Sci.* 2018, 13, 9981–9998.
- [41] Lai, X., et al. Chitosan derivative corrosion inhibitor for aluminum alloy in sodium chloride solution: A green organic/inorganic hybrid. *Carbohydr. Polym.* 2021, 265, 118074.
- [42] Mofidabadi, A.H.J.; Dehghani, A.; Ramezanzadeh, B. Investigating the effectiveness of Watermelon extract-zinc ions for steel alloy corrosion mitigation in sodium chloride solution. *J. Mol. Liq.* 2022, 346, 117086.
- [43] Prasai, D., et al. Graphene: Corrosion-inhibiting coating. *ACS Nano* 2012, 6(2), 1102–1108.
- [44] Zhang, W., et al. Use of graphene as protection film in biological environments. *Sci. Rep.* 2014, 4(1), 1–8.
- [45] Necolau, M.-I.; Pandele, A.-M. Recent advances in graphene oxide-based anticorrosive coatings: An overview. *Coatings* 2020, 10(12), 1149.
- [46] Calovi, M., et al. Effect of functionalized graphene oxide concentration on the corrosion resistance properties provided by cathaphoretic acrylic coatings. *Mater. Chem. Phys.* 2020, 239, 121984.
- [47] Nayak, S.R.; Mohana, K.N.; Hegde, M.B. Anticorrosion performance of 4-fluoro phenol functionalized graphene oxide nanocomposite coating on mild steel. *J. Fluor. Chem.* 2019, 228, 109392.
- [48] Zhang, F., et al. The effect of functional graphene oxide nanoparticles on corrosion resistance of waterborne polyurethane. *Colloids Surf. A Physicochem. Eng. Asp.* 2020, 591, 124565.
- [49] Zhao, Z., et al. Polydopamine functionalized graphene oxide nanocomposites reinforced the corrosion protection and adhesion properties of waterborne polyurethane coatings. *Eur. Polym. J.* 2019, 120, 109249.
- [50] Zhu, Q., et al. Epoxy coating with in-situ synthesis of polypyrrole functionalized graphene oxide for enhanced anticorrosive performance. *Prog. Organ. Coat.* 2020, 140, 105488.
- [51] Saraswat, V.; Yadav, M. Carbon dots as green corrosion inhibitor for mild steel in HCl solution. *ChemistrySelect* 2020, 5(25), 7347–7357.
- [52] Cui, M., et al. Microwave synthesis of eco-friendly nitrogen doped carbon dots for the corrosion inhibition of Q235 carbon steel in 0.1 M HCl. *Int. J. Electrochem. Sci.* 2021, 16, 151019.
- [53] Cen, H., et al. Carbon dots as effective corrosion inhibitor for 5052 aluminium alloy in 0.1 M HCl solution. *Corros. Sci.* 2019, 161, 108197.
- [54] Cui, M.; Li, X. Nitrogen and sulfur Co-doped carbon dots as ecofriendly and effective corrosion inhibitors for Q235 carbon steel in 1 M HCl solution. *RSC Adv.* 2021, 11(35), 21607–21621.
- [55] Ye, Y.; Yang, D.; Chen, H. A green and effective corrosion inhibitor of functionalized carbon dots. *J. Mater. Sci. Technol.* 2019, 35(10), 2243–2253.
- [56] Peng, Y.G., et al. Preparation of poly (m-phenylenediamine)/ZnO composites and their photocatalytic activities for degradation of Cl acid red 249 under UV and visible light irradiations. *Environ. Prog. Sustain. Energy* 2014, 33(1), 123–130.

- [57] Olad, A.; Rashidzadeh, A.; Amini, M. Preparation of polypyrrole nanocomposites with organophilic and hydrophilic montmorillonite and investigation of their corrosion protection on iron. *Adv. Polym. Technol.* 2013, 32(2).
- [58] Salvetat, J.-P., et al. Mechanical properties of carbon nanotubes. *Appl. Phys. A* 1999, 69(3), 255–260.
- [59] Lu, J.P. Elastic properties of carbon nanotubes and nanoropes. *Phys. Rev. Lett.* 1997, 79(7), 1297.
- [60] Kumar, A.M.; Gasem, Z.M. In situ electrochemical synthesis of polyaniline/f-MWCNT nanocomposite coatings on mild steel for corrosion protection in 3.5% NaCl solution. *Prog. Organ. Coat.* 2015, 78, 387–394.
- [61] Ioniță, M.; Prună, A. Polypyrrole/carbon nanotube composites: Molecular modeling and experimental investigation as anti-corrosive coating. *Prog. Organ. Coat.* 2011, 72(4), 647–652.
- [62] Ganash, A. Electrochemical synthesis and corrosion behaviour of polypyrrole and polypyrrole/carbon nanotube nanocomposite films. *J. Compos. Mater.* 2014, 48(18), 2215–2225.
- [63] Dewangan, Y.; Dewangan, A.K.; Verma, D.K. Carbon nanotubes as corrosion inhibitors. *Org. Corros. Inhib.* 2021, 371–385.
- [64] Dewangan, A.K., et al. Synthetic environment-friendly corrosion inhibitors. In: *Environmentally sustainable corrosion inhibitors*, Elsevier, 2022, 71–95.
- [65] Dewangan, A.; Dewangan, Y.; Verma, D. Pyrazine derivatives as green corrosion inhibitors. *Theory Appl. Green Corros. Inhib.* 2021, 86, 161–182.
- [66] Dewangan, Y., et al. Ionic liquids as green corrosion inhibitors. In: *Environmentally sustainable corrosion inhibitors*, Elsevier, 2022, 219–244.
- [67] Aslam, R., et al. Corrosion inhibition of steel using different families of organic compounds: Past and present progress. *J. Mol. Liq.* 2021, 118373.

# CORROSION PREVENTION NANOSCIENCE

NANOENGINEERING MATERIALS AND TECHNOLOGIES

*Edited by Berdimurodov Elyor Tukhlievich  
and Chandrabhan Verma*

DE  
—  
G



Scanned with OKEN Scanner



Dheeraj Singh Chauhan

**Chapter 7**

**Graphene (Gr)/graphene oxide (GO) and functionalized Gr/GO in corrosion prevention — 99**

Dakeshwar kumar Verma, Reema Sahu, Santosh Bahadur Singh, Bharti Yarda, Vikas Kumar Jain, Shailendra Yadav, Vikash Kande, Sharad Tiwari, Gokul Ram Nishad, Younus Raza Beg, Vandana Mishra, Durgesh Sinha

**Chapter 8**

**Carbon dots (CDs) and heteroatom-doped CDs in corrosion prevention — 121**

Muhammed Safa Çelik, Hüseyin Fatih Çetinkaya, Serap Çetinkaya, Gamze Tüzün, Burak Tüzün

**Chapter 9**

**Polymeric nanoparticles and their composites in corrosion inhibition — 135**

Amir Hossein Jafari Mofidabadi, Nariman Alipanah, Ali Dehghani

**Chapter 10**

**Organic–inorganic hybrid nanostructured materials in corrosion prevention — 147**

Manash Protim Mudoi, Rhythm Katyal, Khushi Bhatt, Vidushi Singh, Asmita Choudhary, Sanskriti Gupta

**Chapter 11**

**Ceramic nanomaterials in corrosion prevention — 165**

Khasan Berdimuradov, Elyor Berdimurodov, Ilyos Eliboev, Nurbek Umirov, Bakhtiyor Borikhonov, Abduvali Kholikov, Khamdam Akbarov

**Chapter 12**

**Smart-hybrid nanomaterials in corrosion prevention — 181**

**Index — 195**

Dakeshwar kumar Verma\*, Reema Sahu, Santosh Bahadur Singh\*,  
Bharti Yarda, Vikas Kumar Jain, Shailendra Yadav, Vikash Kande,  
Sharad Tiwari, Gokul Ram Nishad, Younus Raza Beg, Vandana Mishra,  
Durgesh Sinha

## Chapter 8

# Carbon dots (CDs) and heteroatom-doped CDs in corrosion prevention

**Abstract:** With diameters about 10–100 nm, carbon dots (CDs) and heteroatom-doped CDs are intriguing types of carbon nanoparticles. Low toxicity, photo-induced electron transfer, chemical inertness, good biocompatibility and highly controllable photoluminescence behavior are some special qualities of CDs and heteroatom-doped CDs. Due to their affordability, environmental friendliness and ability to reduce waste generation, sustainable raw materials are frequently employed in the production of CDs and heteroatom-doped CDs. Laser ablation, electrochemical oxidation, hydrothermal reaction, microwave irradiation, reflux technique and ultrasonication can all be used to synthesize CDs and heteroatom-doped CDs. Additionally, it has highly desirable characteristics like semiconductor nanoparticles and oxygen-based functional groups. As a result, CDs are promising nanomaterials for applications such as photo-catalysis, ion sensing, biological imaging, heavy metal detection, adsorption treatment, supercapacitor, membrane construction and water pollution control. The physical and chemical characteristics of CDs, the raw materials and processes employed in their production, their stability and their

---

**Acknowledgments:** The authors thank Dr. K. L. Tandekar, Principal, Govt Digvijay Autonomous PG College, Rajnandgaon, Chhattisgarh, for providing basic facilities.

---

\***Corresponding author: Dakeshwar kumar Verma**, Department of Chemistry, Government Digvijay Autonomous Postgraduate College, Rajnandgaon 491441, Chhattisgarh, India,  
e-mail: dakeshwarverma@gmail.com

\***Corresponding author: Santosh Bahadur Singh**, Department of Chemistry, University of Allahabad, Prayagraj 211002, Uttar Pradesh, India, e-mail: singhsbau2012@gmail.com

**Reema Sahu, Bharti Yarda, Vikash Kande, Sharad Tiwari, Gokul Ram Nishad, Younus Raza Beg, Vandana Mishra**, Department of Chemistry, Government Digvijay Autonomous Postgraduate College, Rajnandgaon 491441, Chhattisgarh, India

**Vikas Kumar Jain**, Department of Technical Education Indravati Bhawan, Nava Raipur, Atal Nagar, Raipur 492002, Chhattisgarh, India

**Shailendra Yadav**, Department of Chemistry, AKS University, Satna, Madhya Pradesh, India

**Durgesh Sinha**, Department of Chemistry, Gurughasidas Central University, Bilaspur, Chhattisgarh, India



prospective uses in the prevention of corrosion of metals in various acidic conditions will all be covered in this review.

**Keywords:** Carbon dots, corrosion inhibition, mild steel, acidic solution, electrochemical study, SEM-EDS, DFT

## 8.1 Introduction

Corrosion-induced metal deterioration can lead to significant financial loss and compromised life safety. Acidification of oil wells, chemical cleaning and processing, pickling and so on include the use of common acid-aggressive media including sulfuric acid, hydrochloric acid, phosphoric acid and hydrofluoric acid [1, 2]. The metal substrate's protective approach is crucial during the aforementioned operations. The use of corrosion inhibitors is one of many anticorrosion techniques that is thought to be a successful, easy-to-use and inexpensive tactic for delaying or reducing the corrosion of the steel substrate. The structural properties of an inhibitor, the type of metal surface, the harsh environment and so on affect how effective it is at inhibition [3]. Some conventional high-efficiency corrosion inhibitors, like chromate and compounds containing phosphorus, are hazardous to some extent and have a difficult time degrading in the environment [4]. In the accelerated growth of industrial technology, which affects numerous national production domains, metal corrosion has been a global issue [5]. According to study corrosion costs the world economy up to 3% of GDP annually and results in the loss of roughly one-third of the steel produced [6]. As a result, the industry has developed a variety of methods for protecting against metal corrosion. One of the simplest ways to prevent metals from corroding in corrosive environments is to use a corrosion inhibitor. As a result, the use of organic corrosion inhibitors is becoming increasingly important in industrial areas. As effective corrosion inhibitors for metals in aggressive environments, organic compounds having N, O, P and S as well as an aromatic ring and a long alkyl chain in their structural component have been reported [7, 8]. These corrosion inhibitors provide effective inhibition, but some of them are toxic and bad for the environment and human health. The demand for environmentally friendly pickling corrosion inhibitors with high corrosion inhibition efficiency and low price has increased as a result of people's heightened awareness of the environment [9, 10]. Nanosized semiconductor crystals, such as carbon dots (CDs) and heteroatom-doped CDs, are typically organic in origin. Due to the fact that poisonous heavy metals are primarily used in their production, inorganic quantum dots are subject to numerous safety and toxicity problems. Due to the fact that they are both organic and inorganic in nature and are widely employed as anticorrosion materials, the recently produced CDs and heteroatom-doped CDs can solve this drawback. Additionally Table 8.1 reveals the global GDP decline caused by the corrosion and Table 8.2 shows the development of corrosion inhibitors for aqueous electrolytes.

**Table 8.1:** The global GDP decline brought caused by rust (source: <http://impact.nace.org/economic-impact.aspx>).

Monetary region	Agri CoC (\$ billion)	Industry CoC (\$ billion)	Services CoC (\$ billion)	Total CoC (\$ billion)	Total GDP (\$ billion)	CoC % GDP
Arab World	13.3	34.2	92.6	140.1	2,789	5.0%
China	56.2	192.5	146.2	394.9	9,330	4.2%
European region	3.5	401	297	701.5	18,331	3.8%
India	17.7	20.3	32.3	70.3	1,670	4.2%
Japan	0.6	45.9	5.1	51.6	5,002	1.0%
Russia	5.4	37.2	41.9	84.5	2,113	4.0%
USA	2.0	303.2	146.0	451.3	16,720	2.7%
Other part of the globe	52.4	382.5	117.6	552.5	16,057	3.4%
<b>Global</b>	<b>152.7</b>	<b>1,446.7</b>	<b>906.0</b>	<b>2,505.4</b>	<b>74,314</b>	<b>3.4%</b>

**Table 8.2:** Corrosion inhibitors for aqueous electrolytes are being developed [11].

Time edge	Need	Examples (inhibitor type)
Before 1960	Protection efficiency	Borates, silicates, phosphates, borates, chromates, zinc salts and phosphates
Between 1960 and 1980	Economy	Phosphono acids, molybdates, polyphosphates, chelate molecules, carboxylates, gluconates, soluble oils, cations and polyacrylates are some examples of chemical compounds
Between 1980 and 1995	Ecology	Inhibitors found in nature including vitamins, biopolymers and tannins
From 1995 to present	Green and sustainability	REM, synergistic organic/inorganic compounds, inhibitor encapsulation and polyfunctional organic molecules

## 8.2 CDs and heteroatom-doped CDs: preparative methods, properties, and recent applications

The pyrolysis approach was used to produce citric acid-based CDs in the study at various reaction temperatures. The major goal was to investigate the connections between reaction temperature, microstructure and the capacity of as-obtained N-CDs to suppress corrosion in a 1 M HCl environment. Meanwhile, the corrosion inhibition mechanism of the as-obtained N-CDs was thoroughly analyzed using molecular dynamics and quantum chemical simulation calculations. In the recent years, we have seen a rise in interest in CDs (CDs), a type of carbon-based fluorescent (FL) nanomaterial with minimal cytotoxicity, high water solubility and exceptional corrosion inhibition

capabilities. Different natural carbon sources including orange juice [12], citric acid [13], bananas [14] and red chillies [15] have all been used to create CDs. Hydrothermal carbonization, arc discharge, electrochemical synthesis, microwave approach and laser ablation have all been used to prepare CDs [16–18]. Inorganic nutrients and hazardous metals may taint CDs made from natural sources. Spice-derived CDs do not display cytotoxicity, making them suitable for application in the development of cancer therapy protocols or drug delivery management techniques [15]. Researchers study on the behavior and mechanism of N-doped CDs for metal in acid environments. These N-CDs' inhibitive efficacy in this instance was greater than 90%. Calculations revealed that the as-prepared N-CDs' standard adsorption free energies were  $-25.99$ ,  $-26.94$  and  $-25.78$  kJ/mol, indicating that both chemisorption and physisorption were engaged in the adsorption film [19]. In addition, Figure 8.1 exhibits the synthesis method of NCDs.

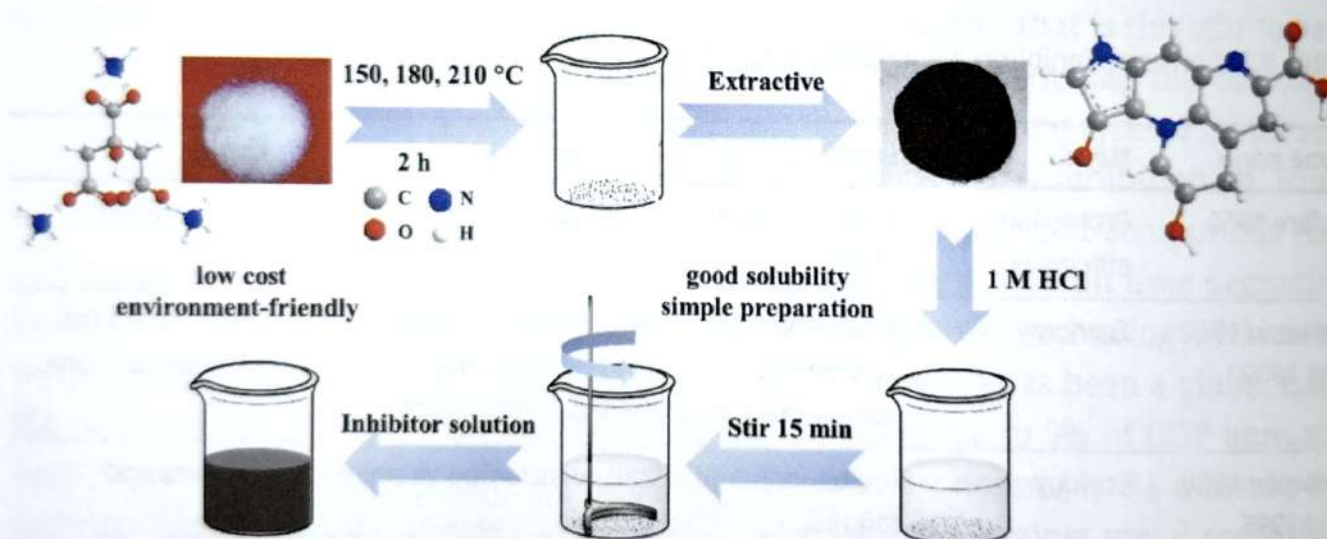


Figure 8.1: Synthesis methods of NCDs [19].

Before being placed into polytetrafluoroethylene autoclaves and heated to high temperature for long time, 4-aminosalicylic acid (ASA) was first dissolved in known amount of ethanol while being stirred. After cooling to ambient temperature, dark brown solutions were obtained. The obtained solution was purified for one day using dialysis bags to get rid of nonreactive molecules. After rotary evaporation and drying under vacuum, N-CDs were eventually obtained as a black solid and have greater solubility in ethanol. DI water should be replaced every 3 h [20].

### 8.3 CDs and heteroatom-doped CDs as advanced anticorrosive materials: experimental and computational approaches

It is discovered that CDs, a novel family of nanomaterials, are effective inhibitors. Given that there is no precise mechanical explanation in the literature for how CDs prevent carbon steel from corroding in an aggressive environment. Eco-friendly CDs and nitrogen-doped functionalized carbon dots (N-CDs) were easily made by reacting citric acid and urea, two inexpensive raw materials with several functional groups, in a single hydrothermal step. Electrochemical techniques and surface analysis were used to carefully explore their corrosion inhibition characteristics. For carbon steel in an acidic solution, the resulting CDs and N-CDs were found to be an efficient corrosion inhibitor. The Langmuir adsorption model and the N-doped CDs' 94% inhibitory efficacy at 200 mg/L show that the N-doped CDs under investigation are mixed type [21]. At 200 mg/L, N-CDs had the highest inhibition efficiency (96.13%), followed by the Langmuir model [22]. At 200 mg/L, CDs had an IE of over 90.9%, the inhibitor displayed the Langmuir adsorption model and the steel/solution interface underwent both chemical and physical adsorptions [23]. The %IE for *p*-CDs and *o*-CDs was more than 97% and changed gradually as immersion duration increased. The absorption of the *p*-CDs and *o*-CDs involved both chemisorption and physisorption according to the Langmuir adsorption isotherm [24]. At N-CDs 298 K at 30 mg/L, a percentage inhibition efficiency of 97.8% was obtained. Various adsorption models were looked at, and it was discovered that both physical and chemical adsorption took place at the steel/solution interface [25]. In a similar approach the % IE of N, S-CDs achieved 85.9% at 5 mg/L [26]. N, S-CDs is a mixed-type inhibitor, more obviously blocking the anodic reaction, with % IE of 93% at 50 mg/L [27]. The Langmuir adsorption model, in which physical contact was predominate, was used, and the % IE of N-doped CDs was 88.96% at 200 mg/L [28]. The physicochemical interaction at the steel/solution interface was exploited as the adsorption mechanism, and the % IE of FCDs was above 90% at 100 mg/L [29]. Additionally, Table 8.3 demonstrates the CDs-mediated corrosion inhibitor, electrolyte and metal sample, techniques applied and outcomes of CDs and doped materials as anticorrosion materials.

Despite the addition of various quantities of N, S-CDs, the capacitive loops grew during the first 3 h and then gradually shrank as immersion duration increased as seen in Figure 8.3(c–f). Additionally, the difference between the impedance spectra measured at various immersion periods is inversely proportional to the inhibitor concentrations, with the least change occurring at 5 mg/L N, S-CDs. The numerous inductive loops are responsible for the Bode plots' low-frequency display of various time constants in the blank condition (Figure 8.2) [26].

Via ASA as a precursor, the N-CDs were produced using a solvothermal process. According to scanning probe microscopy and transmission electron microscopy, N-CDs

**Table 8.3:** CD-mediated corrosion inhibitor, electrolyte and metal sample, techniques applied, and outcomes of CDs and doped materials as anticorrosion materials.

CDs-mediated corrosion inhibitor	Electrolyte and metal sample	Techniques applied	Outcomes	Reference
N-doped carbon dots	1 M HCl/steel	FTIR, UV-vis, XPS, EIS and WL	The Langmuir adsorption model and the N-doped carbon dots' (CDs') 94% inhibitory efficacy at 200 mg/L show that the N-doped CDs under investigation are mixed type	[21]
N-doped carbon dots (NCDs)	0.1 M HCl/Q235 steel	FTIR, UV-vis, XRF, XPS, OCP, Tafel, EIS analysis and MD simulation	At 200 mg/L, N-CDs had the highest inhibition efficiency (96.13%), followed by the Langmuir model	[22]
N-doped carbon dots (CDs)	1 M HCl/Q235 steel	FTIR, UV-vis, XPS, TEM, SPM, OCP, EIS, WL and zeta potential analysis	At 200 mg/L, CDs had an IE of over 90.9%, the inhibitor displayed the Langmuir adsorption model, and the steel/solution interface underwent both chemical and physical adsorptions	[23]
p-CDs and o-CDs	1 M HCl Q235/ carbon steel	PDP, EIS, SEM and EDX	The % IE for p-CDs and o-CDs was more than 97% and changed gradually as immersion duration increased. The absorption of the p-CDs and o-CDs involved both chemisorption and physisorption according to the Langmuir adsorption isotherm.	[24]
Nitrogen-doped functionalized carbon dots (NCDs)	0.5 M H <sub>2</sub> SO <sub>4</sub> / carbon steel	FTIR, UV-vis, XRD, TEM, EIS, PDP, AFM, SEM and XPS	At N-CDs 298 K at 30 mg/L, a percentage inhibition efficiency of 97.8% was obtained. Various adsorption models were looked at, and it was discovered that both physical and chemical adsorption took place at the steel/solution interface	[25]
N and S codoped carbon dots (N, SCDs)	0.1 M HCl/5,052 Al alloy	XPS, WL, OCP, PDP, SEM, IFM, FTIR, AFM, weight	% IE of N, S-CDs achieved 85.9% at 5 mg/L	[26]

N and S-codoped carbon dots (N, S-CDs)	CO <sub>2</sub> -saturated 3% NaCl/carbon steel	WL, XPS, SEM, AFM, contact angle, OCP, PDP and EIS	N, S-CDs is a mixed-type inhibitor, more obviously blocking the anodic reaction, with % IE of 93% at 50 mg/L	[27]
N-doped carbon dots	3.5% NaCl/carbon steel	EIS, WL, and corrosion morphology	The Langmuir adsorption model, in which physical contact was predominate, was used, and the % IE of N-doped carbon dots was 88.96% at 200 mg/L	[28]
Functionalized carbon dots (FCDs)	1 M HCl Q235/steel	OCP, EIS, Tafel, SVET and corrosion morphology analysis	The physicochemical interaction at the steel/solution interface was exploited as the adsorption mechanism, and the % IE of FCDs was above 90% at 100 mg/L	[29]



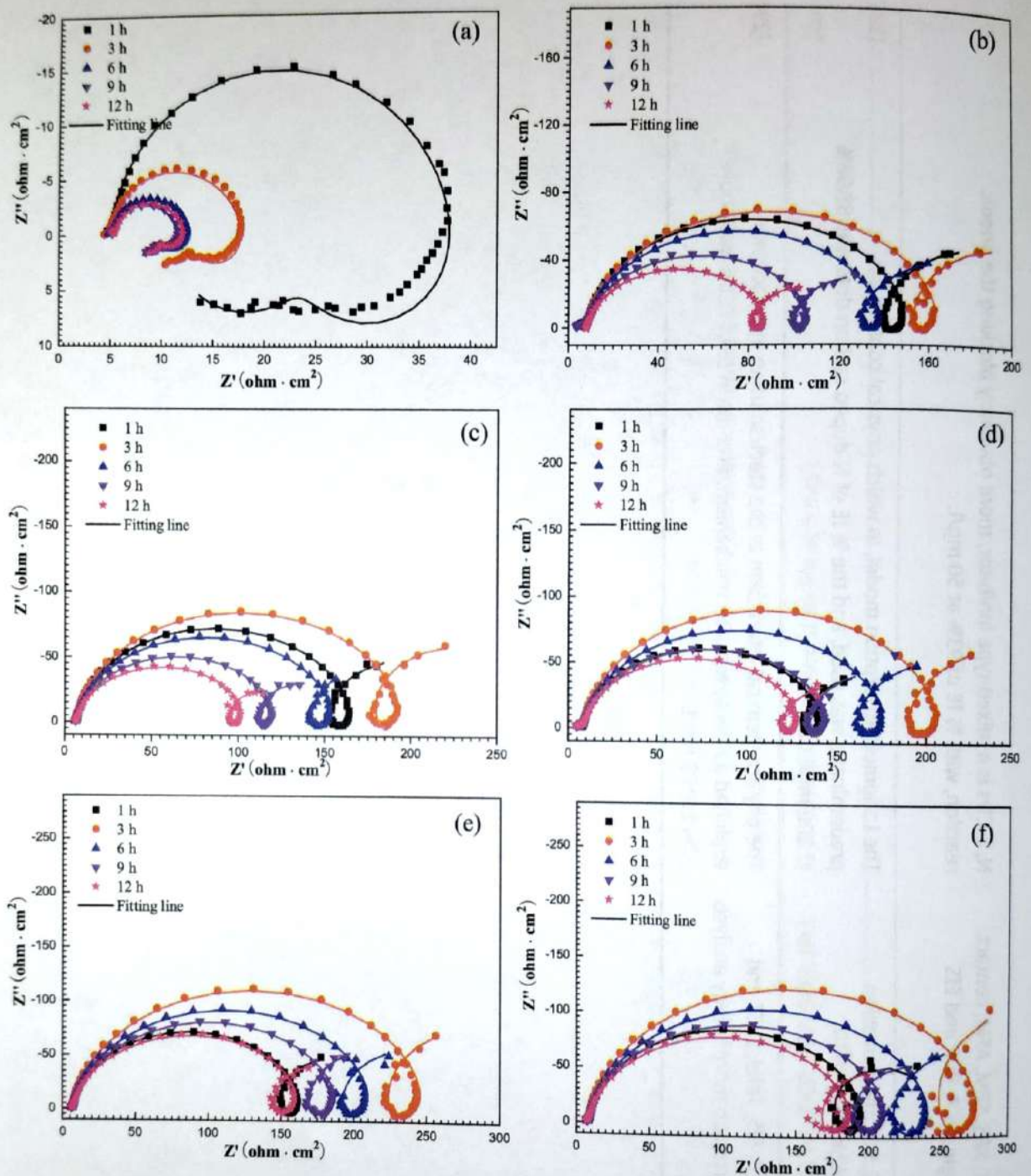


**Figure 8.2:** Nyquist plots for aluminum alloy measured in various immersion time with different concentrations of N, S-CDs for (a) blank, (b) 1 mg/L, (c) 2 mg/L, (d) 3 mg/L, (e) 4 mg/L and (f) 5 mg/L [26].

have a diameter and height of 3–5 nm. EIS is used to analyze the corrosion resistance performance of the coatings without and with N-CDs after 70 days of immersion in 3.5 wt% aqueous NaCl. The findings suggest that the bond interactions between N-CDs and polymer chains, the defect-repairing properties of N-CDs on iron surface coatings with 0.5 wt% N-CDs their better anticorrosive performance [26]. In addition, Figure 8.4 exhibits the SEM microphotographs of inhibitor at various concentrations.

An easy-to-use tool AFM is preferred to characterize the adsorbate with 3D distribution at metal/solution interfaces in corrosion processes. It is utilized to observe the

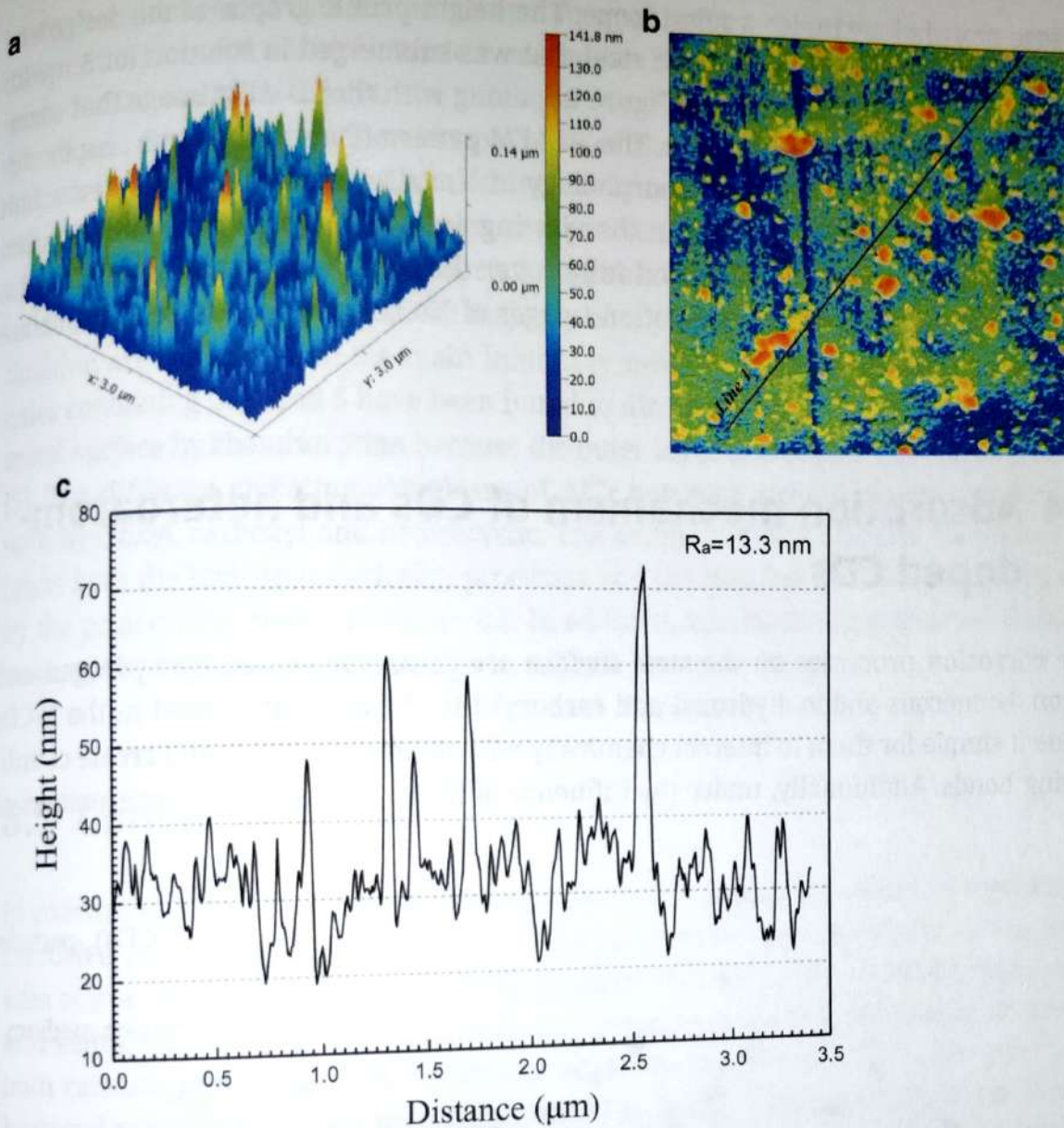


**Figure 8.3:** The surface morphology of carbon steel immersed with 50 mg/L N, S-CDs for (a) 3D AFM image, (b) 2D AFM image and (c) corresponding height profile graphs of Line 1 indicated in 2D image for 5 h at 50 °C [27].

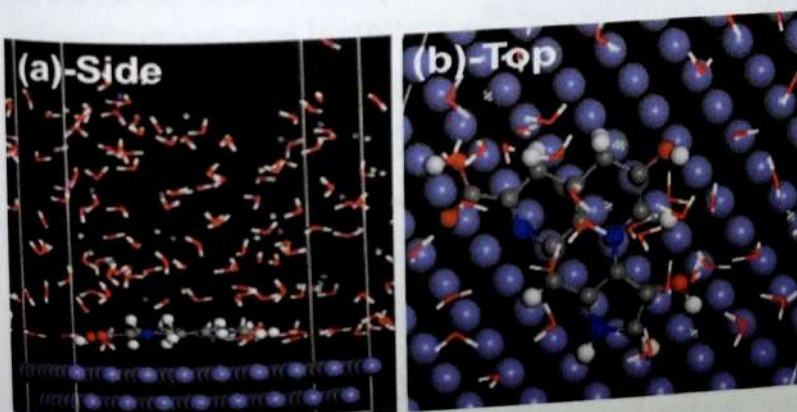


**Figure 8.4:** Equilibrium adsorption configurations of as-obtained N-CDs molecule on Fe (110) surface: (a) side and (b) top [27].

surface morphology under a microscope. The height profile graphs of the designated region in the 2D picture for carbon steel that was submerged in solution for 5 h with 50 mg/L of N, S-CDs are shown in Figure 8.5, along with the 2D AFM image that corresponds to the 3D-distributed image. The 3D AFM pattern (Figure 8.3) of the coupon displays the distribution and micromorphology of N, S-CDs, which formed a dense film with particles as tall as 141.8 nm in the viewing area. As a result, the inhibitory film made of N, S-CDs can efficiently and fully cover the surface of carbon steel [27]. Also Figure 8.4 exhibited the MD simulation images of N-CDs molecule on Fe (110) surface rom top and flat orientation.

## 8.4 Adsorption mechanism of CDs and heteroatom-doped CDs

The corrosion processes on the steel surface are primarily caused by hydrogen and anion. Numerous amino, hydroxyl and carboxyl functional groups found in the N-CDs made it simple for them to interact chemically with the metal surface and create coordinating bonds. Additionally, under the influence of hydrogen ions, some heteroatoms of

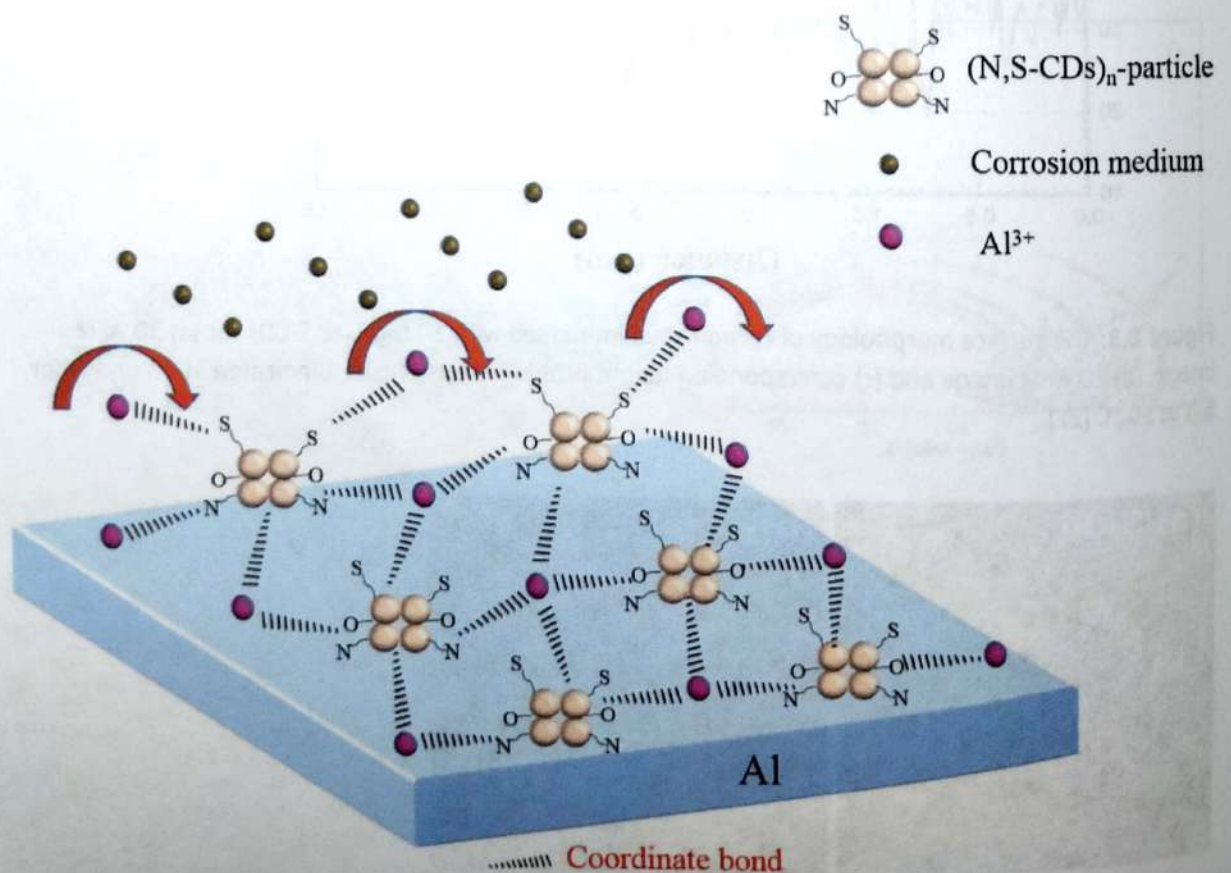


**Figure 8.5:** Schematic illustration of inhibition mechanism on aluminum surface for N, S-CDs in solution [26].

N-CDs were converted into the protonated form of N-CDs, which interacted electrostatically with the metal surface. Physical adsorption is a type of adsorption that can promote N-CDs' ability to inhibit. The inhibitor contains graphitic N, pyridine-N, pyrrole-like N and O atoms. The lone electron pairs of the pyrrole-like N and the pyridine-N help the corrosion inhibitor's chemical interactions. In order to create covalent connections and deposit inhibitor molecules as a protective layer on the metal surface, electron pairs are shared with iron's open 3d orbitals. This prevents additional aggressive anionic acid solution attack. For the majority of organic inhibitors, adsorption and coordination are thought to be the main inhibitory mechanisms. Only a few organic molecules containing O, N and S have been found to directly establish covalent bonds on the metal surface by chemisorption because the outer layer of aluminum lacks the d orbital [5]. The different chelating complexes of  $Al^{3+}$ , however, exhibit simple coordination with hydroxyl, carboxyl and heterocyclic. The addition of N, S-CDs and the catalyst inhibits both the hydrogen evolution processes and the dissolution of aluminum, as seen by the polarization curves in Figure 8.2. In addition, schematic illustration of inhibition mechanism on aluminum surface for N, S-CDs is shown in Figure 8.5.

## 8.5 Conclusion

In conclusion, CDs and heteroatom-doped CDs work wonders at preventing corrosion in corrosive solutions on metals. The electrochemical results demonstrated that the active sites at iron reduction were significantly hindered in the presence of inhibitors in acidic and saline media, demonstrating that the advanced materials effectively controlled both cathodic and anodic electrochemical reactions. Additionally, CDs offer great antibacterial capabilities, strong biocompatibility, low toxicity, chemical stability, high thermal activity and nonflammability. With these characteristics, CD-mediated inhibitors may soon dominate the corrosion inhibitor market. The endothermic nature of adsorption and inhibition was demonstrated by the standard enthalpy, whereas CD adsorption on the metal surface was spontaneous. According to Langmuir isotherms, the CDs were primarily mixed-type inhibitors.

**Conflicts of interest:** Authors declare no conflict of interests.

## References

- [1] Laadam, G., El Faydy, M., Benhiba, F., Titi, A., Amegroud, H., Al-Gorair, A.S., Hawsawi, H., Touzani, R., Warad, I., Bellaouchou, A., Outstanding anti-corrosion performance of two pyrazole derivatives on carbon steel in acidic medium: Experimental and quantum-chemical examinations, *Journal of Molecular Liquids*, 2023, 121268.

- [2] Verma, D.K., Kazi, M., Alqahtani, M.S., Syed, R., Berdimurodov, E., Kaya, S., Salim, R., Asatkar, A., Haldhar, R., N-hydroxybenzothioamide derivatives as green and efficient corrosion inhibitors for mild steel: Experimental, DFT and MC simulation approach, *Journal of Molecular Structure*, 2021, 1241, 130648.
- [3] Qiang, Y., Guo, L., Li, H., Lan, X., Fabrication of environmentally friendly Losartan potassium film for corrosion inhibition of mild steel in HCl medium, *Chemical Engineering Journal*, 2021, 406, 126863.
- [4] Verma, D.K., Ebenso, E.E., Quraishi, M., Verma, C., Gravimetric, electrochemical surface and density functional theory study of acetohydroxamic and benzohydroxamic acids as corrosion inhibitors for copper in 1 M HCl, *Results in Physics*, 2019, 13, 102194.
- [5] Nofrizal, S., Rahim, A.A., Saad, B., Bothi Raja, P., Shah, A.M., Yahya, S., Elucidation of the corrosion inhibition of mild steel in 1.0 M HCl by catechin monomers from commercial green tea extracts, *Metallurgical and Materials Transactions A*, 2012, 43, 1382–1393.
- [6] Verma, D.K., Aslam, R., Aslam, J., Quraishi, M., Ebenso, E.E., Verma, C., Computational modeling: Theoretical predictive tools for designing of potential organic corrosion inhibitors, *Journal of Molecular Structure*, 2021, 1236, 130294.
- [7] Cao, S., Liu, D., Ding, H., Wang, J., Lu, H., Gui, J., Task-specific ionic liquids as corrosion inhibitors on carbon steel in 0.5 M HCl solution: An experimental and theoretical study, *Corrosion Science*, 2019, 153, 301–313.
- [8] Chaouiki, A., Lgaz, H., Chung, I.-M., Ali, I., Gaonkar, S.L., Bhat, K., Salghi, R., Oudda, H., Khan, M., Understanding corrosion inhibition of mild steel in acid medium by new benzonitriles: Insights from experimental and computational studies, *Journal of Molecular Liquids*, 2018, 266, 603–616.
- [9] Chong, A.L., Mardel, J.I., MacFarlane, D.R., Forsyth, M., Somers, A.E., Synergistic corrosion inhibition of mild steel in aqueous chloride solutions by an imidazolium carboxylate salt, *ACS Sustainable Chemistry & Engineering*, 2016, 4, 1746–1755.
- [10] Verma, C., Verma, D.K., Ebenso, E.E., Quraishi, M.A., Sulfur and phosphorus heteroatom-containing compounds as corrosion inhibitors: An overview, *Heteroatom Chemistry*, 2018, 29, e21437.
- [11] KaHlmaHn, E., Routes to the development of low toxicity corrosion inhibitors for use in neutral solutions, A= Orking Party Report on Corrosion Inhibitors, 1994, 12.
- [12] Sahu, S., Behera, B., Maiti, T.K., Mohapatra, S., Simple one-step synthesis of highly luminescent carbon dots from orange juice: Application as excellent bio-imaging agents, *Chemical Communications*, 2012, 48, 8835–8837.
- [13] Dhenadhayalan, N., Lin, K.-C., Suresh, R., Ramamurthy, P., Unravelling the multiple emissive states in citric-acid-derived carbon dots, *The Journal of Physical Chemistry C*, 2016, 120, 1252–1261.
- [14] De, B., Karak, N., A green and facile approach for the synthesis of water soluble fluorescent carbon dots from banana juice, *Rsc Advances*, 2013, 3, 8286–8290.
- [15] Vasimalai, N., Vilas-Boas, V., Gallo, J., De Fátima Cerqueira, M., Menéndez-Miranda, M., Costa-Fernández, J.M., Diéguez, L., Espiña, B., Fernández-Argüelles, M.T., Green synthesis of fluorescent carbon dots from spices for in vitro imaging and tumour cell growth inhibition, *Beilstein Journal of Nanotechnology*, 2018, 9, 530–544.
- [16] Zhang, J., Yu, S.-H., Carbon dots: Large-scale synthesis, sensing and bioimaging, *Materials Today*, 2016, 19, 382–393.
- [17] Wang, F., Pang, S., Wang, L., Li, Q., Kreiter, M., Liu, C.-Y., One-step synthesis of highly luminescent carbon dots in noncoordinating solvents, *Chemistry of Materials*, 2010, 22, 4528–4530.
- [18] Zheng, X.T., Ananthanarayanan, A., Luo, K.Q., Chen, P., Glowing graphene quantum dots and carbon dots: Properties, syntheses, and biological applications, *Small*, 2015, 11, 1620–1636.
- [19] Liu, Z., Ye, Y., Chen, H., Corrosion inhibition behavior and mechanism of N-doped carbon dots for metal in acid environment, *Journal of Cleaner Production*, 2020, 270, 122458.
- [20] Wang, J., Du, P., Zhao, H., Pu, J., Yu, C., Novel nitrogen doped carbon dots enhancing the anticorrosive performance of waterborne epoxy coatings, *Nanoscale Advances*, 2019, 1, 3443–3451.

- [21] Luo, J., Cheng, X., Zhong, C., Chen, X., Ye, Y., Zhao, H., Chen, H., Effect of reaction parameters on the corrosion inhibition behavior of N-doped carbon dots for metal in 1 M HCl solution, *Journal of Molecular Liquids*, 2021, 338, 116783.
- [22] Ye, Y., Zhang, D., Zou, Y., Zhao, H., Chen, H., A feasible method to improve the protection ability of metal by functionalized carbon dots as environment-friendly corrosion inhibitor, *Journal of Cleaner Production*, 2020, 264, 121682.
- [23] Ye, Y., Yang, D., Chen, H., Guo, S., Yang, Q., Chen, L., Zhao, H., Wang, L., A high-efficiency corrosion inhibitor of N-doped citric acid-based carbon dots for mild steel in hydrochloric acid environment, *Journal of Hazardous Materials*, 2020, 381, 121019.
- [24] Cui, M., Ren, S., Zhao, H., Wang, L., Xue, Q., Novel nitrogen doped carbon dots for corrosion inhibition of carbon steel in 1 M HCl solution, *Applied Surface Science*, 2018, 443, 145–156.
- [25] Cao, S., Liu, D., Wang, T., Ma, A., Liu, C., Zhuang, X., Ding, H., Mamba, B.B., Gui, J., Nitrogen-doped carbon dots as high-effective inhibitors for carbon steel in acidic medium, *Colloids and Surfaces A, Physicochemical and Engineering Aspects*, 2021, 616, 126280.
- [26] Cen, H., Zhang, X., Zhao, L., Chen, Z., Guo, X., Carbon dots as effective corrosion inhibitor for 5052 aluminium alloy in 0.1 M HCl solution, *Corrosion Science*, 2019, 161, 108197.
- [27] Cen, H., Chen, Z., Guo, X., N, S co-doped carbon dots as effective corrosion inhibitor for carbon steel in CO<sub>2</sub>-saturated 3.5% NaCl solution, *Journal of the Taiwan Institute of Chemical Engineers*, 2019, 99, 224–238.
- [28] Ye, Y., Jiang, Z., Zou, Y., Chen, H., Guo, S., Yang, Q., Chen, L., Evaluation of the inhibition behavior of carbon dots on carbon steel in HCl and NaCl solutions, *Journal of Materials Science & Technology*, 2020, 43, 144–153.
- [29] Ye, Y., Yang, D., Chen, H., A green and effective corrosion inhibitor of functionalized carbon dots, *Journal of Materials Science & Technology*, 2019, 35, 2243–2253.

# Electrochemical and DFT Studies of the *Pistacia Integerrima* Gall Extract: An Eco-friendly Approach towards the Corrosion of Steel in Acidic Medium

Jasdeep Kaur, Hamad Almujibah, Mohammad Mahtab Alam, Abha Singh, Akhil Saxena,\*  
Dakeshwar Kumar Verma, and Elyor Berdimurodov



Cite This: *ACS Omega* 2024, 9, 7643–7657



Read Online

ACCESS |



Metrics & More

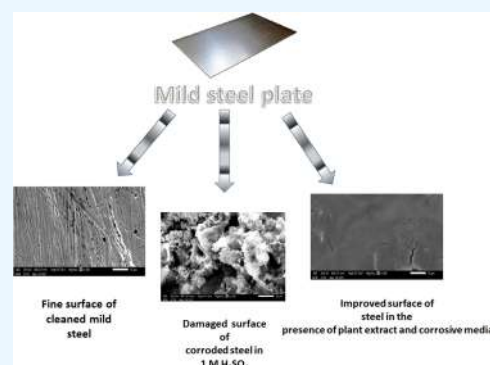


Article Recommendations



Supporting Information

**ABSTRACT:** A novel application of the *Pistacia integerrima* gall extract as an environmentally friendly corrosion inhibitor is reported in this study. The major phytochemicals present in the gall extract, namely pistagremic acid,  $\beta$ -sitosterol, pistiphlorogluciny ether, pistaciaphenyl ester, naringenin, and 5,7-dihydroxy-2-(4-hydroxyphenyl)-2,3-dihydrochromen-4-one, play key roles in its anticorrosive behavior on steel in aggressive media. Several approaches were used to study the corrosion prevention activity of steel in 1 M  $H_2SO_4$ , including weight loss analysis, scanning electron microscopy (SEM), electrochemical impedance spectroscopy (EIS), potentiodynamic polarization (PDP), and density functional theory (DFT). At 2000  $mg\ L^{-1}$ , the highest efficiency of 92.19% was observed in 1 M  $H_2SO_4$ . An SEM study was conducted to validate the surface coverage of the metal surface. DFT studies revealed several nucleophilic regions present in the phytochemicals of the inhibitor, which supported the favorable nucleophilicity. Corrosion studies have not been performed on this sample. Phytochemicals make it an effective corrosion inhibitor, and its extraction process utilizes distilled water, making it better than other inhibitors. It has been proven that the obtained values of  $\Delta E_{Inh}^{DFT}$  for pistiphlorogluciny ether, pistaciaphenyl ether, and naringenin organic compounds were very low, confirming the high reactivity of these corrosion inhibitors. The order of the values of  $\Delta E_{Inh}^{DFT}$  is as follows: pistaciaphenyl ether > pistiphlorogluciny ether > naringenin organic compound; this suggests that pistaciaphenyl ether is more reactive than the other compounds. In this study, *P. integerrima* gall extract emerges as a novel and highly effective corrosion resistance agent in 1 M  $H_2SO_4$ , chosen for its relevance to acid pickling and cleaning processes.



## 1. INTRODUCTION

The powerful mechanical strength of mild steel makes it a popular choice in many industries. However, the corrosion of mild steel happens due to the interaction between steel and aggressive materials such as  $H_2SO_4$  and HCl, which are commonly used for pickling and descaling. Pipelines, bridges, and buildings, as well as vehicles, wastewater systems, and even home appliances, can all be damaged by corrosion.<sup>1</sup> A study found that iron rust absorbs arsenic easily and contaminates the environment.<sup>2</sup> The presence of iron rust can also speed up the growth of Legionella bacteria in water. The growth rate may be increased by  $10^3$ – $10^5$  fold by ferric oxide.<sup>3</sup> A variety of strategies are employed to prevent corrosion, including design, material selection, and protection by electrochemical methods and inhibitor application. The application of a corrosion inhibitor is regarded as an especially cost-effective and simple method of minimizing corrosion among the listed strategies. Corrosion is controlled by a variety of chemical inhibitors, including synthetic compounds that can be harmful to humans and the environment.<sup>2</sup> The best way to reduce this problem is to use natural and biodegradable corrosion inhibitors that are nontoxic and affordable.<sup>3–5</sup>

Several plants with different phytochemicals have been reported in the literature,<sup>6–13</sup> which show excellent inhibition efficiency. Phytochemicals contain heteroatoms that may enhance the effectiveness of green inhibitors.<sup>14–20</sup> According to Bhawsar et al.,<sup>21</sup> *Nicotiana tabacum* extract inhibits steel in 2 M sulfuric acid with 94% efficiency at 1 g/L concentration. The alkaloids perakine and tetrahydroalstonine in *Rauwolfia macrophylla* provide corrosion protection in both HCl and  $H_2SO_4$ .<sup>22</sup> Applying this extract to mild steel surfaces can suppress or prevent corrosion. Various plant parts have plenty of phytochemicals that are effective corrosion inhibitors.<sup>23–37</sup> Plants, being ecologically friendly and plentiful, provide an affordable alternative to hazardous, chemical-based inhibitors.<sup>38–40</sup> In industries, there is a high probability of metals

Received: September 8, 2023

Revised: December 30, 2023

Accepted: January 22, 2024

Published: February 8, 2024



getting corroded when they come in contact with a highly corrosive environment due to acid cleaning or pickling of metal surfaces. The utility of this work is that the studied plant extract of the gall of "*Pistacia integerrima*" can be used as a pickling agent in industries wherever acidic corrosion occurs, and this reduces the corrosion rate of metal by creating a protective layer on the metal surface. This study evaluates *P. integerrima* gall extracts as eco-friendly corrosion inhibitors for steel in 1 M sulfuric acid solution using weight loss analysis, potentiodynamic polarization techniques, and electrochemical impedance spectroscopy. Following the immersion of steel samples in aggressive solutions, UV–visible spectroscopy was basically used to examine the mechanism. Additionally, scanning electron microscopy analysis was performed on steel samples to examine their surface morphology. DFT studies were also used for theoretical calculations to determine the adsorbing capacity of the phytochemicals. Kakar singhi is another name for *P. integerrima*, which belongs to the Anacardiaceae family. This plant grows at elevations between 2438 and 3657 m. *P. integerrima* is utilized as a treatment for a variety of diseases, including hepatitis, liver disorders, and inflammatory diseases, although its corrosion properties have not yet been explored. Based on the literature, the *P. integerrima* extract contains a variety of phytochemicals such as pistiphlorogluciny, pistacia-phenyl ethers, and naringenin, which make it suitable for use as a corrosion inhibitor, and distilled water is used as a solvent for the extraction process, which in turn makes it superior to other inhibitors.

The main objective of this study is to determine the corrosion resistance capacity of the gall extract of *P. integerrima* on steel in 1 M H<sub>2</sub>SO<sub>4</sub> using electrochemical methods, weight loss, and adsorption studies. Surface morphological studies are performed by scanning electron microscopy and atomic force microscopy.

## 2. EXPERIMENTAL STUDIES

**2.1. Preparation of the Specimen of Steel.** The metal (mild steel) composition employed in the research is as follows: the major component is iron (99.2%); other elements are silicon, carbon, manganese, sulfur, and phosphorus present in the proportion of 0.120, 0.105, 0.378, 0.079, and 0.0795% respectively. Steel samples have a surface area of 1 cm<sup>2</sup>. In order to examine corrosion on steel coupons, several sandpapers were used to clean them.

**2.2. Preparation of an Inhibitor from the Sample.** The *P. integerrima* gall was purchased from Sirhind, Punjab. A thorough cleaning was conducted to remove dust and sand, followed by washing with double-distilled water and then drying in the shade for 3 days. The dried plant sample was then crushed to a coarse powder. Then, the crushed material (100 g) was refluxed with 250 mL of distilled water for 48 h by utilizing a Soxhlet apparatus. Afterward, the final solution was filtered to remove impurities. The extract was then dried in a hot water bath and rotatory evaporator, which was then used for further studies.

**2.3. Preparation of the Corrosive Media.** Loba Chemie AR grade concentrated H<sub>2</sub>SO<sub>4</sub> was used to prepare 1 M H<sub>2</sub>SO<sub>4</sub> in double-distilled water. We prepared solutions of different concentrations (800, 1000, 1500, and 2000 mg L<sup>-1</sup>) by dissolving particular amounts of the prepared extract in 1 M H<sub>2</sub>SO<sub>4</sub>. In 1 M H<sub>2</sub>SO<sub>4</sub>, the plant extract was soluble, and the maximum solubility of the *P. integerrima* gall extract in 1 M H<sub>2</sub>SO<sub>4</sub> was 2000 mg L<sup>-1</sup>.

**2.4. Weight-Loss Measurements.** For each weight loss study, 100 mL of an aggressive medium was used. A 1 cm<sup>2</sup> steel coupon was polished with various grades of emery paper before every corrosion study. Following weighing, the steel coupons were immersed in aggressive media of 1 M H<sub>2</sub>SO<sub>4</sub> for 24 h with various inhibitor concentrations (800, 1000, 1500, and 2000 mg L<sup>-1</sup>). The weight loss measurements were performed at temperatures of 298, 308, and 318 K using the following equations after the coupons were rinsed with acetone and dried:<sup>41</sup>

$$\eta\% = \frac{W_0 - W_i}{W_0} \times 100 \quad (1)$$

$$\theta = \frac{W_0 - W_i}{W_0}$$

$$W_0 - W_i = \Delta W \quad (2)$$

Here,  $\Delta W$  represents the weight loss (gm),  $W_0$  and  $W_i$  denote the loss of weight without the plant extract and with the involvement of the extract, respectively, and  $\theta$  is the surface coverage.

**2.5. Langmuir Adsorption Isotherm.** The weight loss data can be applied to investigate the adsorption behavior of the extract. Equation 3 can be used to calculate the adsorption equilibrium constant<sup>40</sup> by plotting  $C/\theta$  vs  $\log C$ <sup>7</sup>

$$\frac{C}{\theta} = \frac{1}{K_{\text{ads}}} + C \quad (3)$$

Here, the surface coverage is denoted by  $\theta$ , the extract concentration is denoted by  $C$ , and  $K_{\text{ads}}$  represents the adsorption equilibrium constant. Inhibitors are assumed to strictly follow the Langmuir adsorption isotherm if the slope of the graph and the coefficient of correlation of the straight line produced by plotting a graph of  $C/\theta$  versus  $C$  are close to 1.

**2.6. Analyses of Electrochemical Studies.** A PGSTAT-204 Metrohm Auto lab electrochemical analyzer was used to conduct electrochemical analysis on steel coupons at 298 K.<sup>42,43</sup> In the corrosion cell, three electrodes were connected: the working electrode (steel), the reference electrode (calomel), and the counter electrode (platinum). A 1 cm<sup>2</sup> portion of the steel surface was exposed for reaction after being coated with Araldite resin. The Tafel curves were recorded in the current range of 100 nA to 1 mA in the potential range of -0.1–0.1 V. The scan rate of PDP analysis was 0.001 V/s. From the plot of the potential against the logarithm of current, the corrosion potential ( $E_{\text{corr}}$ ), corrosion current ( $I_{\text{corr}}$ ), and Tafel slope for the cathodic ( $\beta_c$ ) and anodic ( $\beta_a$ ) reactions were estimated.<sup>44</sup> Triplicate experiments were performed for each concentration to assess the reproducibility.

PDP data are used to calculate the efficiency using the following relationship<sup>45</sup>

$$\eta\% = \frac{I_{0\text{corr}} - I_{\text{icorr}}}{I_{0\text{corr}}} \times 100 \quad (4)$$

Here,  $I_{\text{icorr}}$  and  $I_{0\text{corr}}$  are the corrosion current density values with and without *P. integerrima* gall extract, respectively. An electrochemical workstation similar to that used for PDP analysis was used for EIS. The EIS studies were performed in the frequency range of 100,000–0.1 Hz with 10 frequencies per decade using an amplitude of 0.01 V. A 45 min immersion in an acidic medium was required to set the OCP electrode.



**Table 1. Data of Inhibition Efficiency, Surface Coverage, and Corrosion Rate of *P. integerrima* in 1 M H<sub>2</sub>SO<sub>4</sub>**

corrosive medium	inhibition conc. (mg L <sup>-1</sup> )	inhibition efficiency (%) of extract at 298 K	inhibition efficiency (%) of extract at 308 K	inhibition efficiency (%) of extract at 318 K	surface coverage ( $\theta$ )	CR (mm/Y)
1 M H <sub>2</sub> SO <sub>4</sub>	0					396.95
	800	76.80	72.19	69.89	0.768	91.72
	1000	81.86	79.18	75.15	0.818	71.98
	1500	87.62	82.15	80.12	0.876	49.11
	2000	90.46	85.02	82.10	0.904	37.84

Equation 5 was used to evaluate the effectiveness of the inhibitor

$$\eta\% = \frac{R_{ct} - R_{ct}^0}{R_{ct}} \times 100 \quad (5)$$

$R_{ct}^0$  and  $R_{ct}$  represent the charge-transfer resistance in the absence and presence of the plant inhibitor, respectively.

**2.7. Phytochemical Testing.** The *P. integerrima* aqueous extract was examined for alkaloids, flavonoids, saponins, quinones, coumarin, and sugar. 0.30 g of the concentrate was dissolved in 50 mL of distilled water, and then the solution was used for phytochemical analysis to determine which heterocyclic compounds might be present in the extract. Various tests, such as the Wagner test, Mayer test, conc. HCl test, sulfuric test, Fehling solution test, etc., were carried out as discussed below:

**2.7.1. Investigation of Alkaloids.** The Mayer reagent test was performed on the solution to determine its alkaloid content. A yellow color in the solution indicates the presence of alkaloids.<sup>46</sup>

The *P. integerrima* aqueous extract was also treated with the Wagner reagent. Brownish-reddish precipitates indicate the presence of alkaloids.<sup>46</sup>

**2.7.2. Investigation of Flavonoids.** A small amount of the *P. integerrima* aqueous extract was mixed with concentrated hydrochloric acid. A red color was a quick indicator of flavonoids.<sup>47</sup>

**2.7.3. Investigation of Saponins.** The filtrate and water were vigorously mixed. Saponins are evident by the formation of foam.<sup>48</sup>

**2.7.4. Investigation for Quinones.** In order to verify the presence of quinones, 1 mL of the extract was added to H<sub>2</sub>SO<sub>4</sub>, resulting in a color change.<sup>49</sup>

**2.7.5. Test for Coumarin.** 3–4 drops of alcoholic sodium hydroxide solution were mixed with the extract. A yellow coloration indicated the presence of coumarin.<sup>49</sup>

**2.7.6. Fehling Solution Test for Sugars.** Fehling solutions A and B were combined in a 1:1 ratio and boiled for 1 min. In the water bath, 1 mL of the extract was heated for 5–10 min. The presence of carbohydrates is indicated by yellowish or brick-red precipitates.

**2.8. Examination for UV–Visible Spectra.** An extract of *P. integerrima* in 1 M H<sub>2</sub>SO<sub>4</sub> was also analyzed by using a UV–visible spectrophotometer. We conducted UV–visible analyses on solutions in which steel specimens were dipped for 24 h as well as on solutions in which steel specimens were not dipped, to examine the adsorption and desorption of the *P. integerrima* extract. It was necessary to examine both spectra to comprehend the inhibitory mechanism.<sup>50</sup>

**2.9. Surface Inspection.** The corrosion protection process was also estimated by performing SEM and AFM on steel. Specimens that were cleaned and dipped in an acid solution for 24 h without and with an inhibitor were examined through their SEM and AFM images.

**2.10. DFT-Based Theoretical Investigations.** Modern molecular modeling techniques, such as molecular dynamics simulations, have become powerful tools for designing and studying the mechanisms of inhibition. The importance of these calculations lies in understanding atom-scale details, the interpretation of experimental results, and the testing of corrosion inhibitors. A DFT-based theoretical investigation is performed to explore the relation between corrosion inhibition and molecular structures at the atomic scale. This is because it is difficult to gain a deep understanding of corrosion inhibition at the atomic scale by experimental investigations.<sup>51,52</sup> Various submethods of DFT-based theoretical studies were utilized to access the theoretical basis of corrosion inhibition by selected organic compounds.<sup>53,54</sup> The GAMESS-US<sup>55</sup> with the 6-21G basis sets,<sup>56</sup> density functional theory (DFT), and B3LYP<sup>57</sup> methods were chosen to perform the DFT-based theoretical investigations of pistiphloglucinyll, pistaciaphenyl ether, and naringenin corrosion inhibitors. wxMacMolPlt<sup>58</sup> and Avogadro<sup>59</sup> were employed for analysis and visualization.

### 3. RESULTS AND DISCUSSION

**3.1. Measurements of Weight Reduction.** Weight loss values are recorded at temperatures of 298, 308, and 318 K, which are depicted in Table 1, at different concentrations of the *P. integerrima* gall extract, and mild steel surface coverage and inhibition efficiency were calculated. According to the information in Table 1, on moving toward higher concentrations of the inhibitor, more area of the surface is occupied by the inhibitor molecules, and the corrosion process on the steel surface is reduced as the inhibitor molecule creates a barrier by forming a protective layer on the steel surface, and hence, the corrosion inhibition efficiency increases with each inhibitor concentration.

This increase is possible only if heteroatoms with lone pairs are absorbable on the metal surface and delay the pace of metal corrosion in the abrasive medium. As the concentration of inhibitors increases, the corrosion rate declines.

**3.2. Langmuir Adsorption Isotherm Study.** The Langmuir adsorption study provided the theoretical description of the adsorption of the inhibitor molecule on the surface of mild steel. Here, the data obtained from the weight loss were fitted in the Langmuir adsorption isotherm, and the effectiveness of the inhibitor was observed. The graph of concentration ( $C$ ) of the *P. integerrima* gall extract against  $C/\theta$  is shown in Figure 1. The adsorption equilibrium constant ( $K_{ads}$ ), the slope of the line, and the intercept were calculated. If the slope of the line is close to about 1, it is considered that the inhibitor adsorbs on the surface of the mild steel properly.<sup>60</sup> Here, the obtained line is linear, with a slope value of 0.97848; hence, this confirms the proper adsorption of the inhibitor. The calculated value of  $K_{ads}$  was 0.0470 L/mg at a temperature of 298 K.

The obtained  $K_{ads}$  value was used to determine the standard free energy of adsorption ( $G_{ads}^0$ ) according to eq 6

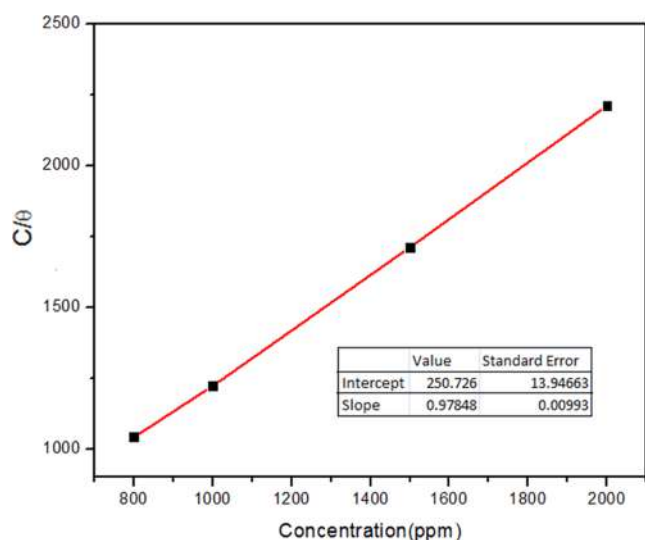


**Figure 1.** Adsorption isotherm study for *P. integerrima* on steel in 1 M  $\text{H}_2\text{SO}_4$ .

$$\Delta G_{\text{ads}}^0 = -RT \ln (55.5 \times K_{\text{ads}}) \quad (6)$$

where  $\Delta G_{\text{ads}}^0$  is the standard free energy of adsorption, the molar concentration of water = 55.5,  $R$  is the gas constant, and  $T$  is the absolute temperature.

Physisorption bonding of an inhibitor is indicated by a value of  $\Delta G_{\text{ads}}^0$  equal to or more positive than  $-20 \text{ kJ mol}^{-1}$ , while its chemisorption on a mild steel surface is indicated by a value equal to or more negative than  $-40 \text{ kJ mol}^{-1}$ .<sup>60</sup> Based on eq 6,  $\Delta G_{\text{ads}}^0$  is  $-2.37 \text{ kJ mol}^{-1}$  at 298 K, which indicates surface physisorption on the metal. A corrosion inhibitor is considered effective due to the possibility of interaction between the above-mentioned phytochemicals and metal surfaces. Coatings prevent corrosion on mild steel surfaces by blocking the active sites.

**3.2.1. Activation Parameter.** As shown in Figure 2, it is possible to calculate the activation energy  $E_a$  by relating the  $\log(\text{CR})$  and  $1000/T$  (at temperatures of 298, 308, and 318 K). The Arrhenius law states that  $E_a$  varies with temperature, which

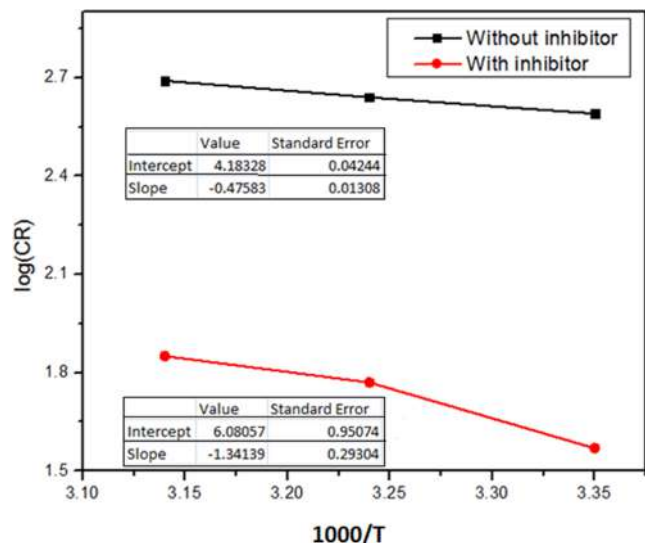


**Figure 2.** Plot showing the log of the corrosion rate for metal dissolutions with and without the plant extract against  $1000/T$ .

accelerates the corrosion of metals, and  $E_a$  can be calculated according to eq 7.

$$E_a = -\text{slope} \times 2.303 \times 8.314 \quad (7)$$

On increasing the amount of the inhibitor in the corrosive solution, the activation energy values increased.<sup>61</sup> The calculated value of the activation energy for the blank solution ( $0 \text{ mg L}^{-1}$ ) is  $9.09 \text{ kJ mol}^{-1}$ ; this value was increased to  $50.31 \text{ kJ mol}^{-1}$  at  $2000 \text{ mg L}^{-1}$  inhibitor concentration.

**3.2.2. Adsorption Parameters.** Adsorption entropy and enthalpy were calculated using the following equation

$$\log \left\{ \frac{\text{CR}}{T} \right\} = \log \left\{ \frac{R}{N_a h} \right\} + \frac{\Delta S_a}{2.303R} - \frac{\Delta H_a}{2.303 RT} \quad (8)$$

In this formula,  $N_a$ ,  $h$ ,  $\Delta S_a$ , and  $\Delta H_a$  represent the Avogadro number, Planck constant, standard activation entropy, and standard activation enthalpy, respectively.

As illustrated in Figure 3, a graph of  $\log(\text{CR}/T)$  against  $1000/T$  is plotted to determine the  $\Delta H_a$  and  $\Delta S_a$  parameters shown in

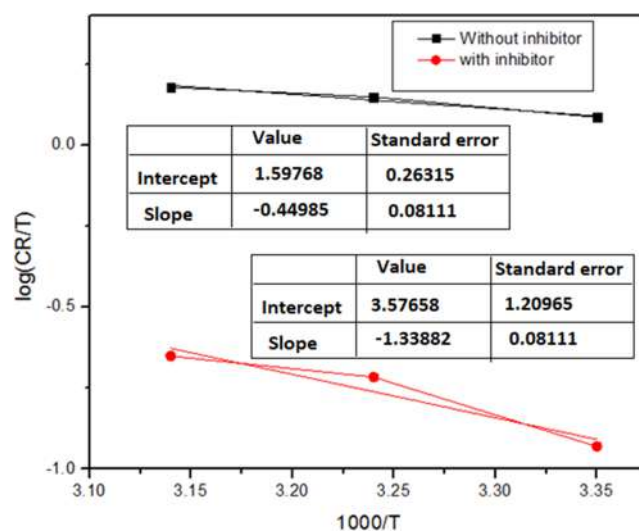


**Figure 3.** Graph of  $\log(\text{CR}/T)$  versus  $1000/T$  regarding the dissolution of the metal both without and with the gall extract.

**Table 2.** Different Parameters for Steel Both in the Presence and in the Absence of the Gall Extract in 1 M  $\text{H}_2\text{SO}_4$

plant extract	extract concentration in ( $\text{mg L}^{-1}$ )	$\Delta H_a$ ( $\text{kJ mol}^{-1}$ )	$\Delta S_a$ ( $\text{J mol}^{-1} \text{K}^{-1}$ )
<i>P. integerrima</i>	0	8.59	20.12
gall extract	2000	25.46	58.03

Table 2. As a result of the corrosion-preventing energy barrier maintained by the inhibitor, the metal is very well protected, as demonstrated by the fact that  $\Delta H_a$  is higher when the inhibitor is present ( $25.46 \text{ kJ mol}^{-1}$ ) compared to that when the inhibitor is not present ( $8.59 \text{ kJ mol}^{-1}$ ). The adsorption of the plant inhibitor increases the enthalpy of the corrosion reaction. An entropy value of  $58.03 \text{ J mol}^{-1} \text{K}^{-1}$  was obtained with the inhibitor as compared to  $20.12 \text{ J mol}^{-1} \text{K}^{-1}$  with the blank.

**3.3. Electrochemical Studies.** **3.3.1. Potentiodynamic Polarization Study (PDP).** In the aggressive solvent with

different extract concentrations, Figure 4 shows the cathodic as well as anodic polarization study of mild steel coupons, and

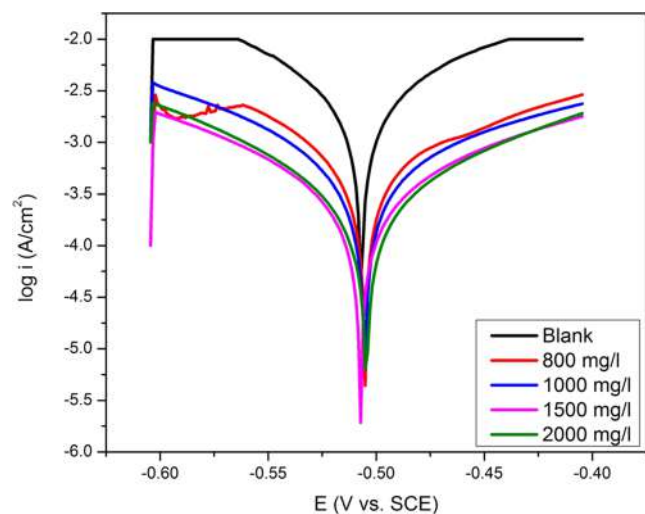


**Figure 4.** Tafel polarization curves in 1 M H<sub>2</sub>SO<sub>4</sub> in the absence and presence of the gall extract.

Table 3 presents the related corrosion measurements and inhibition efficiencies at 298 K. Using the PDP study, the values of the corrosion current density ( $I_{\text{corr}}$ ) and the corrosion potential ( $E_{\text{corr}}$ ) are calculated by extrapolating the linear parts of cathodic and anodic curves. The cathodic and anodic sections of current density decrease in the presence of the *P. integerrima* extract according to the Tafel curves. This behavior demonstrates that the inhibitor may stop cathodic H<sub>2</sub> gas formation as well as metal oxidation.<sup>62</sup> Tafel graphs of the anodic and cathodic reactions changed with certain concentrations of the *P. integerrima* extract, demonstrating that the inhibitor affects the cathode H<sub>2</sub> gas evolution and interferes with the Fe-dissolving process. Consequently, the *P. integerrima* extract prevents cathodic and anodic corrosion reactions in 1 M H<sub>2</sub>SO<sub>4</sub>. As a result, adding more *P. integerrima* extract should prevent mild steel corrosion.<sup>63</sup> The *P. integerrima* extract concentration reduces the corrosion current density, as shown in Table 3. The calculated value of the corrosion current density for the blank solution (0 mg L<sup>-1</sup>) is  $2.9 \times 10^{-3}$  A/cm<sup>2</sup>; this value increased for each increase in the concentration of the inhibitor, and at the final concentration, i.e., at a concentration of 2000 mg L<sup>-1</sup>, its value was  $2.7 \times 10^{-3}$  A/cm<sup>2</sup>. Accordingly, we conclude that the values of inhibition efficiency increase with increasing inhibitor concentration. The highest inhibition efficiency was observed to be 90.68%. A decline in the corrosion rate (CR) is also shown in Table 3. This can be attributed to the extract adsorbing onto the surface of the metal, which reduces metal dissolution through the formation of a protective layer.

3.3.2. Electrochemical Impedance Spectroscopy Study. The Nyquist and Bode diagrams are shown in Figure 5a,b, and

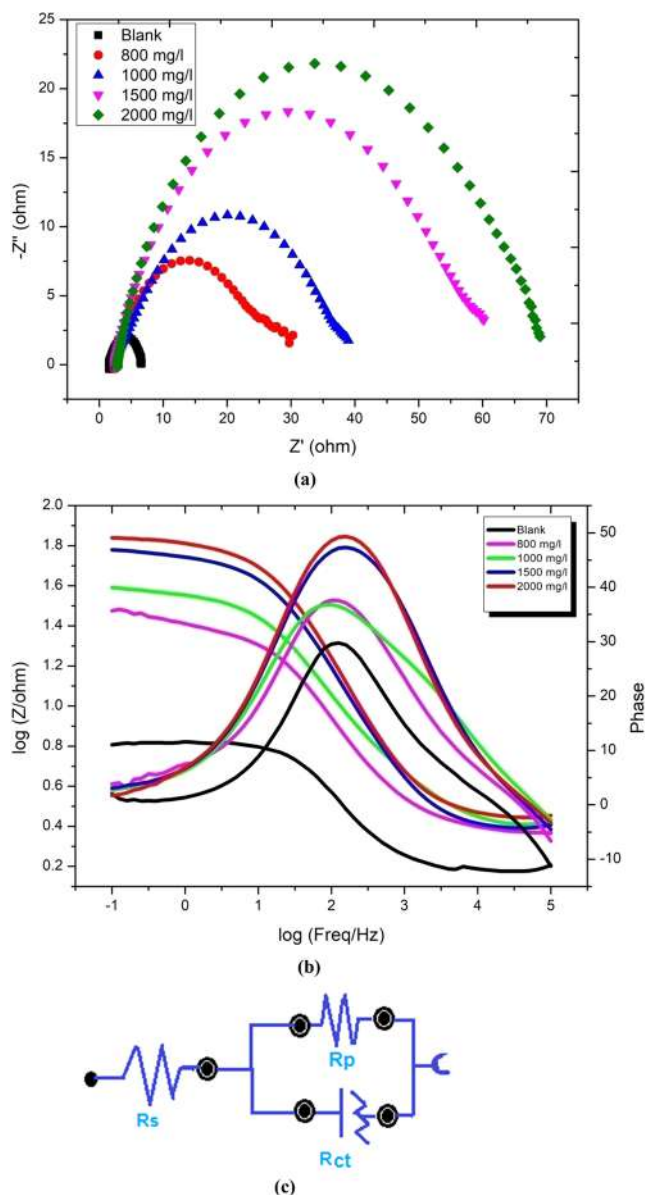


**Figure 5.** Nyquist (a) and Bode (b) plots and the constant phase element circuit (c) for steel in 1 M H<sub>2</sub>SO<sub>4</sub> with and without the *P. integerrima* extract at 298 K.

the results are depicted in Table 4. Figure 5c represents the circuit used in this study. It is clear from Figure 5a that the diameter of the capacitive loops increased when the extract was present as compared to when the extract was not added, indicating that this addition of the inhibitor significantly

**Table 3. Polarization Parameters Both with and without the Gall Extract at Various Concentrations**

extract concentration (mg L <sup>-1</sup> )	$E_{\text{corr}}$ (V vs SCE)	$I_{\text{corr}}$ (A cm <sup>-2</sup> )	$\beta_a$ (V/dec)	$-\beta_c$ (V/dec)	corrosion rate	efficiency ( $\eta$ %)
0	-0.506	$2.9 \times 10^{-3}$	0.09527	0.06263	34.03	0
800	-0.696	$6.37 \times 10^{-4}$	0.1582	0.0916	7.40	78.03
1000	-0.547	$3.59 \times 10^{-4}$	0.0996	0.07838	4.18	87.62
1500	-0.525	$3.0 \times 10^{-4}$	0.1291	0.1084	3.49	89.65
2000	-0.526	$2.7 \times 10^{-3}$	0.1200	0.0973	3.23	90.68

**Table 4. Polarization Measurements for Steel in 1 M H<sub>2</sub>SO<sub>4</sub> with and without a Plant Extract**

acid solution used in study	concentration of inhibitor (mg L <sup>-1</sup> )	R <sub>s</sub> (solution resistance) (Ω)	R <sub>ct</sub> (charge transfer resistance) (Ω)	constant phase element (CPE) (μFcm <sup>-2</sup> )	n	efficiency (%)
1 M H <sub>2</sub> SO <sub>4</sub>	0	1.482	5.22	5.19 × 10 <sup>-4</sup>	0.83	
	800	2.415	24.32	2.76 × 10 <sup>-4</sup>	0.71	78.53
	1000	2.545	36.09	2.34 × 10 <sup>-4</sup>	0.68	85.53
	1500	2.451	56.92	1.53 × 10 <sup>-4</sup>	0.72	90.82
	2000	2.850	66.87	1.30 × 10 <sup>-4</sup>	0.73	92.19

decreased the dissolution of mild steel. The deviation of the semicircles obtained in the Nyquist plot is because of corrosion-induced inhomogeneity and roughness of the working electrode (steel). In the circuit obtained by fitting the EIS data, the parameters of solution resistance (R<sub>s</sub>), constant phase element (CPE), and charge-transfer resistance (R<sub>ct</sub>) were considered. CPE can be introduced to compensate for the inhomogeneity and surface roughness of the working electrode. The outcomes shown in Table 4 indicate that increasing the amount of inhibitor will increase the value of R<sub>ct</sub> as well as the inhibition efficiency.

Based on the Bode angle diagram, the presence of a protective layer on the surface just after the introduction of the inhibitor causes the curves to widen and move to the left (toward lower frequencies). This study, in particular, found that R<sub>ct</sub> values increase with an increase in inhibitor concentrations, which indicates that the extract from *P. integerrima* is easily absorbable on the surface of mild steel with the highest efficiency of 92.19% at 2000 mg L<sup>-1</sup> and at 298 K. The slightly flattened semicircles are an indication of nonideal capacitors caused by electrode flaws and/or surface reactions. Variations in the capacitor behavior are represented by values of 0 < n < 1 (n = 1 represents a pure capacitor). In this study, n was found to be around 0.8, as shown in Table 4.<sup>60</sup>

**3.4. Analyses of Phytochemicals.** Plants are reservoirs of phytochemicals. Various tests were performed to confirm the existence of different phytochemicals in the *P. integerrima* gall extract, which helped understand the relation between the plant extract and the corrosion inhibition efficiency of the gall extract. The higher the extent of phytochemicals, the greater the efficiency of that plant.

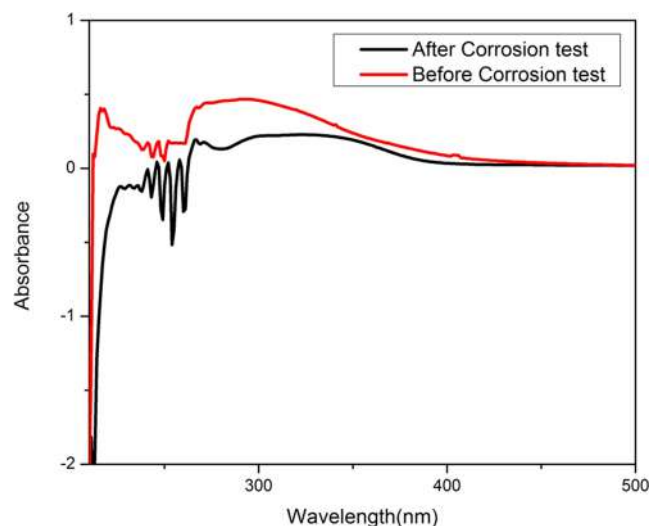
The phytochemicals present in the *P. integerrima* extract are presented in Table 5.

**Table 5. Phytochemical-Related Outcomes of *Pistacia integerrima***

S. No.	phytochemicals tested	various tests performed	results
1.	alkaloids	Wagner's test	++
		Mayer's Test	++
2.	flavonoids	Conc. HCl test	--
3.	quinones	Concentrated H <sub>2</sub> SO <sub>4</sub> test	++
4.	coumarins	Alcoholic sodium hydroxide test	++
5.	sugar	Fehling solutions test	--
6.	saponins	Froth test	++

Based on the phytochemical analysis of the *P. integerrima* gall extract, it is clear that phytochemicals such as alkaloids, quinones, coumarin, and saponins are present, while flavonoids and sugar were reported to be absent. Therefore, alkaloids, quinones, coumarin, and saponins are the key phytochemicals that will be majorly adsorbed on the mild steel surface by forming a coordinate with the metal surface.

**3.5. UV–Visible Spectroscopy.** The UV spectra of the 1 M H<sub>2</sub>SO<sub>4</sub> corrosive solutions at 2000 mg L<sup>-1</sup> inhibitor concentration were obtained in two different experimental conditions. First of all, we recorded the UV spectra for 1 M H<sub>2</sub>SO<sub>4</sub> at 2000 mg L<sup>-1</sup> without dipping the mild steel coupons. Second, we immersed the steel coupon in the same solution for a time period of 24 h. Then, both of these UV spectra were compared to analyze their absorbance values. The UV spectra after dipping the mild steel coupons in the corrosive solution (after the corrosion test) showed lower values of absorbance than the spectra of the uninhibited solution before the corrosion test, as shown in Figure 6. This is because of the adsorption of

**Figure 6.** UV Spectrum of the solution both before and after corrosion inhibition.

the active constituents of the *P. integerrima* gall extract on the surface of mild steel, which yields lower values of absorbance. This clearly indicates the formation of a protective coating on the metal surface.<sup>64</sup>

**3.6. Surface Examination.** **3.6.1. Scanning Electron Microscopy (SEM).** Using a scanning electron microscope, the surface morphology of the mild steel coupons was determined. Here, the SEM micrographs of the coupons were obtained under three different conditions. First of all, the SEM image of the cleaned steel surface appeared to be absolutely fine, as shown in Figure 7a. Second, the same steel coupon was immersed in 1 M H<sub>2</sub>SO<sub>4</sub> without the inhibitor for 24 h. Then, the SEM image was obtained and compared to the SEM image in Figure 7a. Now, the SEM image shows a highly damaged surface; this is because of the acidic corrosion taking place on the metal surface. At last, the steel coupons were dipped in 1 M H<sub>2</sub>SO<sub>4</sub> with 2000 mg L<sup>-1</sup> of the *P. integerrima* gall extract. Figure 7c shows that there is a significant improvement in the surface morphology of the steel. This is because of the adsorption of the *P. integerrima* gall extract

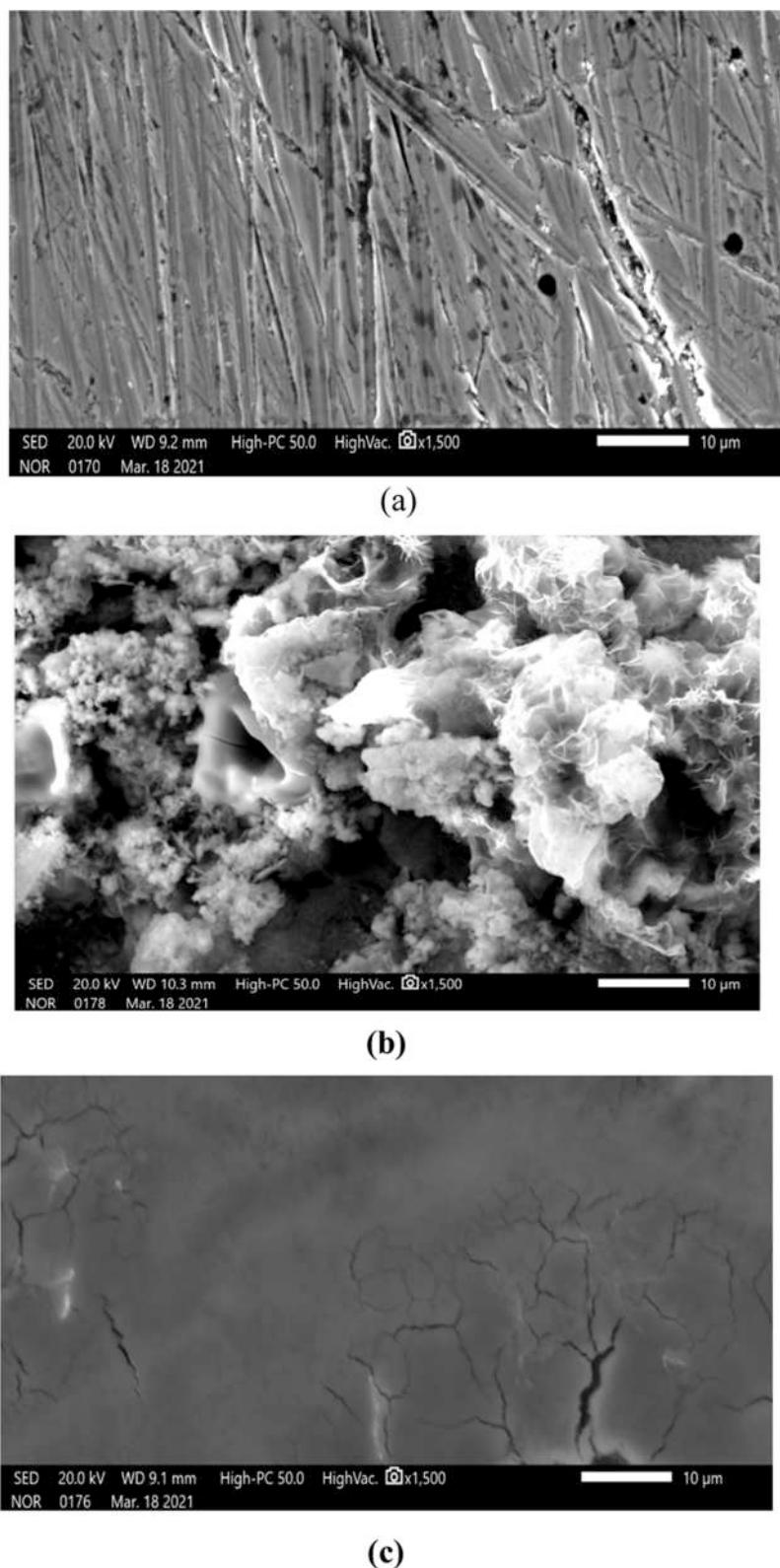


**Figure 7.** Images of the surface of the (a) cleaned mild steel coupon, (b) steel coupon corroded in 1 M H<sub>2</sub>SO<sub>4</sub>, and (c) steel coupon inhibited by 2000 mg L<sup>-1</sup> extract.

on the metal surface, which forms a protective layer, creates a barrier to the acid attack, and reduces the corrosion rate.<sup>65,66</sup>

**3.6.2. Atomic Force Microscopy (AFM).** AFM images of cleaned, uninhibited, and protected steel in 1 M H<sub>2</sub>SO<sub>4</sub> with the *P. integerrima* gall extract are shown in Figure 8a–c. A polished

and cleaned steel surface had a roughness value of 2.08 nm. Because steel was dissolved in the acidic solution without the *P. integerrima* gall extract, its surface was extensively corroded, and its average surface roughness was recorded at 145.75 nm in this condition. The surface roughness was 25.67 nm when the *P.*

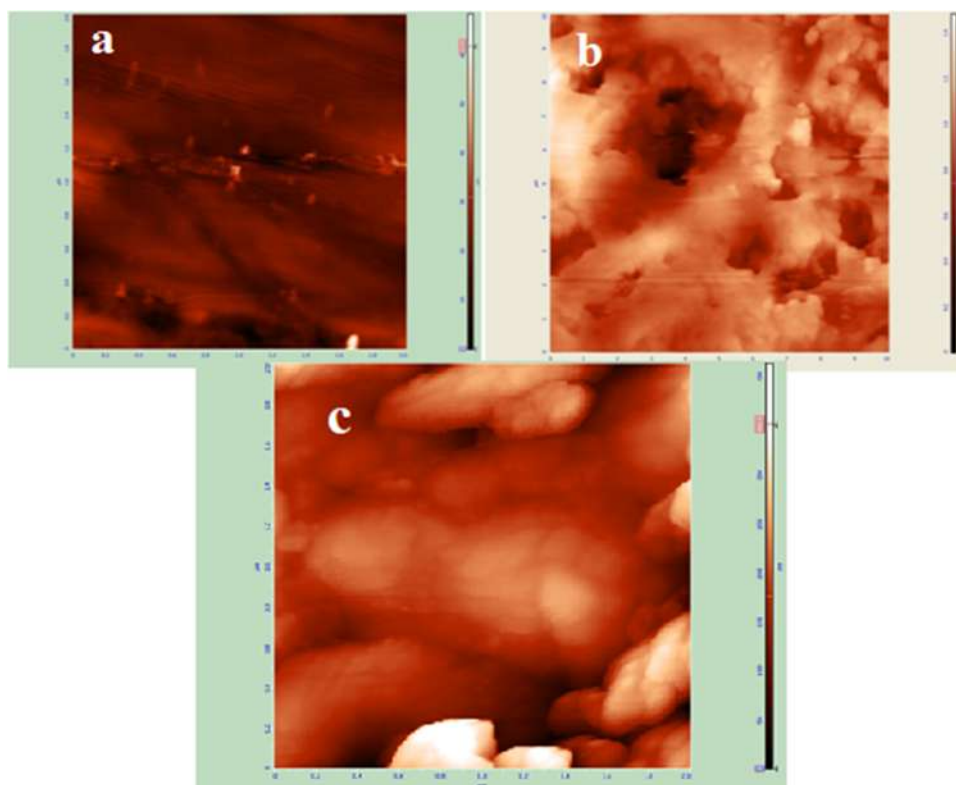


**Figure 8.** AFM images of (a) cleaned mild steel coupon, (b) steel coupon corroded in 1 M H<sub>2</sub>SO<sub>4</sub>, and (c) steel coupon inhibited by 2000 mg L<sup>-1</sup> extract.

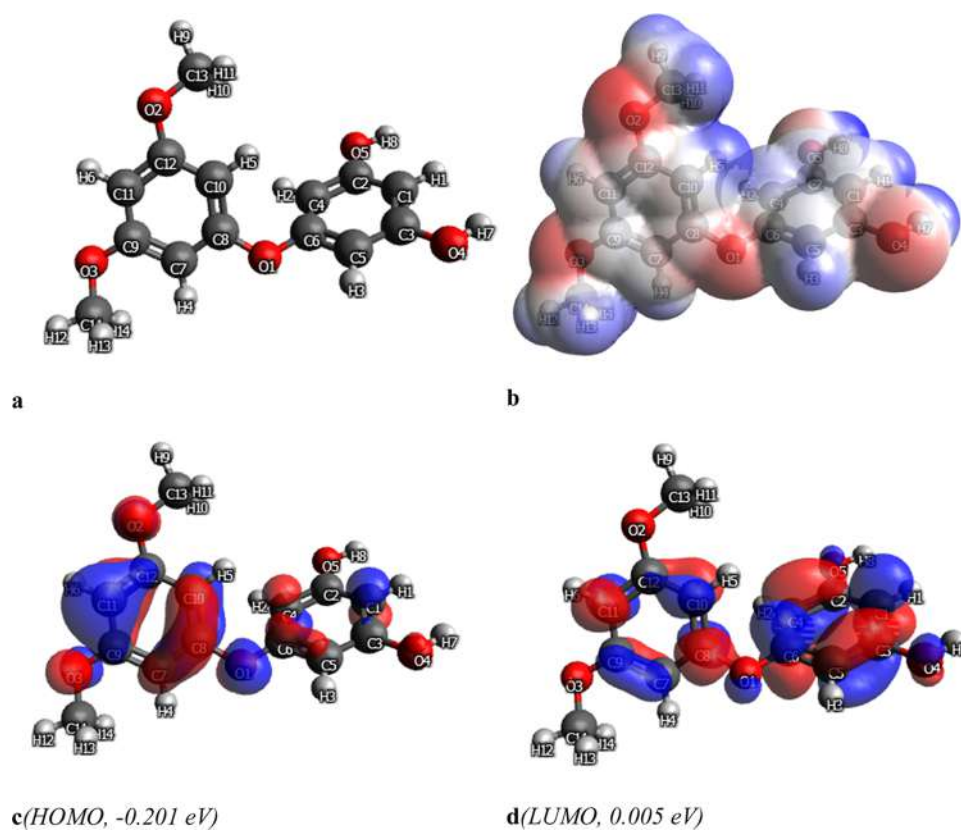


**Figure 9.** (a) Optimized structure and (b) MEP, (c) HOMO, and (d) LUMO structures of pistiphloroglucynyl ether.

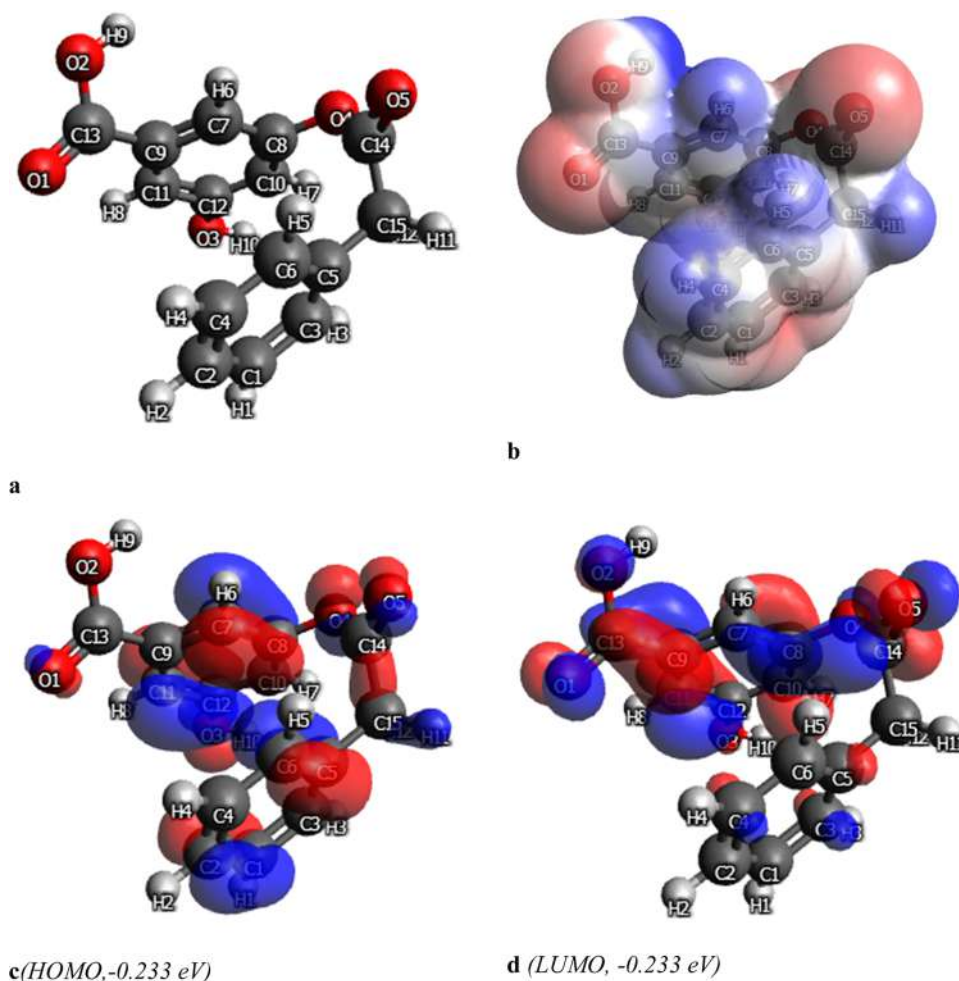


**Figure 10.** (a) Optimized structure and (b) MEP, (c) HOMO, and (d) LUMO structures of pistaciaphenyl ester.

*integerrima* gall extract was used. As can be seen from the roughening values, the metal surface has developed a protective layer.

**3.7. DFT-Based Theoretical Investigations.** **3.7.1. Optimization Investigations.** The corrosion inhibition effectiveness of pistiphlorogluciny, pistaciaphenyl ether, and naringenin corrosion inhibitors depends on their nature of optimization. In this research work, the optimization analysis of the selected corrosion was performed based on the DFT calculations. The resulting optimized structures of pistiphlorogluciny, pistaciaphenyl ether, and naringenin organic compounds are represented in Figures 9a, 10a, and 11a, respectively. Overall, what is remarkable about the findings is that the optimized structures of pistiphlorogluciny, pistaciaphenyl ether, and naringenin corrosion inhibitors show highly polarized molecules. The values of the polarization index were also very high for all selected compounds. These results confirmed the following:

- (i) The pistiphlorogluciny, pistaciaphenyl ether, and naringenin corrosion inhibitors have a high polarization index.
- (ii) Their highly polar nature promotes their good solubility in aquatic solutions.
- (iii) The adsorption performance of the studied corrosion inhibitors is supported by their highly polar nature.

- (iv) The benzoyl rings are polar centers in the optimized structures of pistiphlorogluciny, pistaciaphenyl ether, and naringenin corrosion inhibitors.
- (v) The oxygen of the hydroxyl functional groups and heteroatoms of the ether group promote an increase in the polarization index of the obtained molecular structures.
- (vi) The transfer of delocalized  $\pi$ -electrons between the benzoyl rings and nonequivalent positions of active functional groups is also an additional factor for the high polarity.

**3.7.2. Charge Distribution Investigations.** The charge distribution is the next part of the DFT-based theoretical investigations. As observed, the charge values of the elements changed slowly. The theoretical charge values of elements were simultaneously changed in the molecular structures due to various effects, such as the stereochemical, chemical, physical, or planar nature of functional groups, heteroatoms, and the  $\pi$ -system. Additionally, it has been discovered that hydroxyl oxygen atoms have a stronger negative charge than others, confirming that the pistiphlorogluciny, pistaciaphenyl ether, and naringenin inhibitors adsorbed on the steel coupons by the more negative oxygen atoms as adsorption centers.<sup>67–69</sup>

**3.7.3. Investigations of the Molecular Electrostatic Potential (MEP).** The MEP analysis shows available electrophilic and nucleophilic areas.<sup>70–72</sup> The resulting MEPs of pistiphlor-

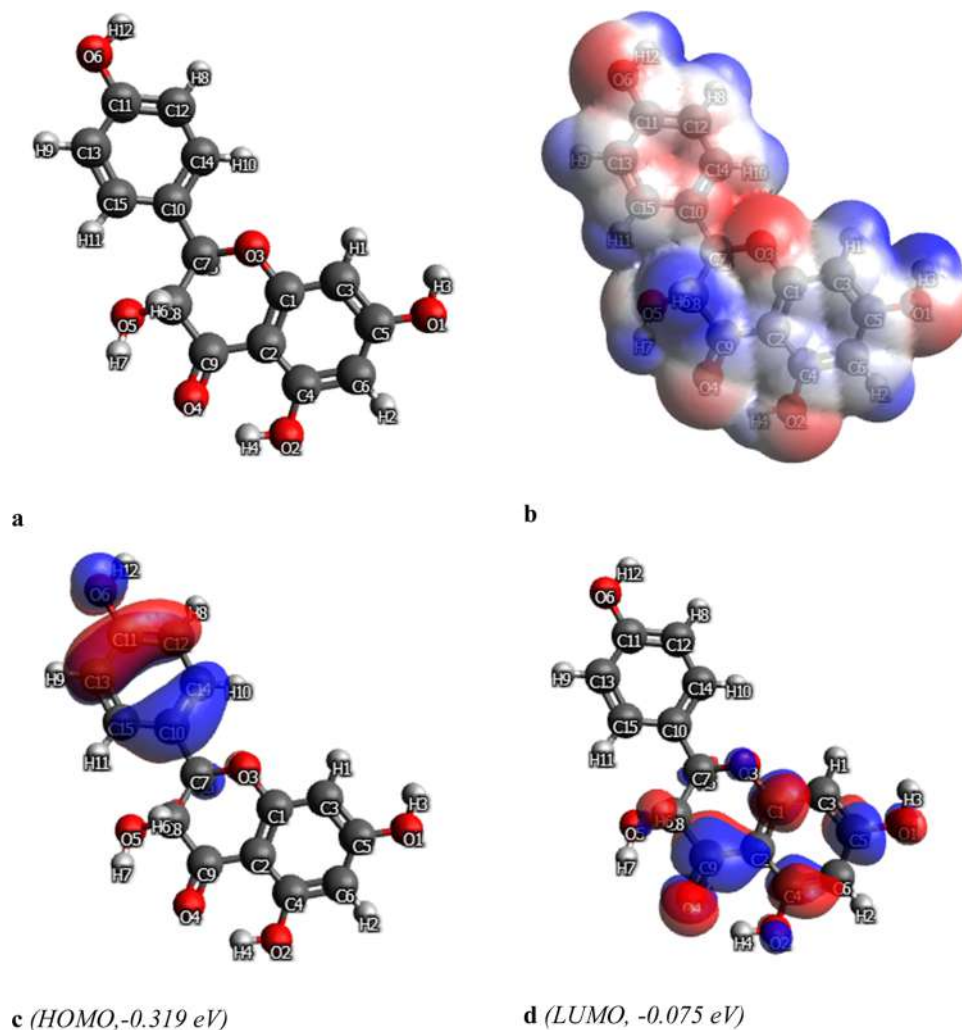


**Figure 11.** (a) Optimized structure and (b) MEP, (c) HOMO, and (d) LUMO structures of naringenin.

ogluconyl, pistaciaphenyl ether, and naringenin organic compounds are represented in Figures 9b, 10b, and 11b, respectively. The electrophilic and nucleophilic regions are indicated on these maps by the colors red and blue, respectively. This makes it generally clear that the pistiphlorogluconyl, pistaciaphenyl ether, and naringenin organic inhibitors contained many nucleophilic areas, confirming their favorable nucleophilic nature. The inhibition performances of pistiphlorogluconyl, pistaciaphenyl ethers, and naringenin increased in many nucleophilic regions. This is because the nucleophilic portions of the inhibitors have been adsorbed onto the steel surface. The aromatic rings and functional groups are centers of MEP regions.

**3.7.4. Frontier Molecular Orbital (FMO) Investigations.** FMO analysis estimated the electron distribution in HOMO and LUMO areas.<sup>73–75</sup> The resulting HOMOs of pistiphlorogluconyl, pistaciaphenyl ether, and naringenin organic compounds are represented in Figures 9c, 10c, and 11c, respectively. The results and discussion found are given below:

- (i) The HOMO regions are mainly cited around C5–C11=C12 for pistiphlorogluconyl ether, C2–C1, C7–C8–C10, and C6–C5 for pistaciaphenyl ether, and C13–C11=C12 and C15–C10=C14 for naringenin organic compounds.
- (ii) The electrons mainly occupied the HOMO regions, and as a result, the molecules are negatively charged.

- (iii) The energies of HOMO orbitals for the selected compounds are as follows: pistaciaphenyl ether > pistiphlorogluconyl ether > naringenin organic compound. When compared to other corrosion inhibitors, pistaciaphenyl ether is more effective.
- (iv) The bonding orbitals adsorb corrosion inhibitors on the steel surface.
- (v) As a consequence of electrons being transferred to the unoccupied d-orbitals of Fe on the metal surface, this corrosion inhibitor can interact effectively with the metal surface, preventing corrosion.

On the other hand, LUMO regions were also found. The resulting LUMOs of pistiphlorogluconyl, pistaciaphenyl ethers, and naringenin organic compounds are represented in Figures 9d, 10d, and 11d, respectively. The results and discussion found are as follows:

- (i) The LUMO areas show antibonding orbitals, which are more suitable for accepting electrons.
- (ii) Some filled d-orbitals of Fe donate free electrons to antibonding orbitals of corrosion inhibitors (LUMO regions). Therefore, the LUMO regions promote chemical bond formation between the corrosion inhibitor and steel.<sup>76,77</sup>



**3.7.5. Molecular Reactivity Investigations.** The reactivity criteria of molecules of pistiphloroglucinyll, pistaciaphenyl ether, and naringenin organic compounds were evaluated by utilizing the energy difference ( $\Delta E_{\text{Inh}}^{\text{DFT}}$ ) between the HOMO ( $E_{\text{HOMO}(\text{Inh})}^{\text{DFT}}$ ) and LUMO ( $E_{\text{LUMO}(\text{Inh})}^{\text{DFT}}$ ) according to eqs 9–18.<sup>78–82</sup> Table 6 presents the outcomes that were obtained.

**Table 6. Theoretical Measurements of Corrosion Inhibitors (DFT, B3LYP, and 6-31G basis sets)**

parameters	values (eV), pistiphloroglucinyll ether	values (eV), pistaciaphenyl ether	values (eV), naringenin
$E_{\text{HOMO}(\text{Inh})}^{\text{DFT}}$	-0.201	-0.233	-0.319
$E_{\text{LUMO}(\text{Inh})}^{\text{DFT}}$	0.005	-0.043	0.075
$\Delta E_{\text{Inh}}^{\text{DFT}}$	0.206	0.19	0.394
$\sigma_{\text{Inh}}^{\text{DFT}}$	9.4786	10.526	5.076
$\omega_{\text{Inh}}^{\text{DFT}}$	0.0478	0.1	0.0377
$\eta_{\text{Inh}}^{\text{DFT}}$	0.1055	0.095	0.197
$\chi_{\text{Inh}}^{\text{DFT}}$	0.1005	0.138	0.122
$I_{\text{Inh}}^{\text{DFT}}$	0.201	0.233	0.319
$A_{\text{Inh}}^{\text{DFT}}$	-0.005	0.043	-0.075
$\mu_{\text{Inh}}^{\text{DFT}}$	-0.1005	-0.138	-0.122
$\epsilon_{\text{Inh}}^{\text{DFT}}$	20.92	10	26.52
$\Delta N_{\text{Inh}}^{\text{DFT}}$	32.7	36.1	17.45
$\psi_{\text{Inh}}^{\text{DFT}}$	16.35	18.06	8.72

As explored, the following main findings and discussions were found:

- (i) The energy distinction between HOMO and LUMO demonstrates the nature of reactivity of inhibitors. It should be stressed that the obtained values of  $\Delta E_{\text{Inh}}^{\text{DFT}}$  for pistiphloroglucinyll, pistaciaphenyl ether, and naringenin organic compounds were very low, confirming the high reactivity of these corrosion inhibitors. The order of values of  $\Delta E_{\text{Inh}}^{\text{DFT}}$  is as follows: pistaciaphenyl ether > pistiphloroglucinyll ether > naringenin organic compound; this suggests that the pistaciaphenyl ether was more reactive than others. The main reason for this is the

carboxyl functional groups and aromatic rings that promote the high reactivity of pistaciaphenyl ether. These results also confirm that molecules with higher reactivity are good corrosion inhibitors. Therefore, pistaciaphenyl ether is a better corrosion inhibitor than others.

- (ii) The resulting values of chemical softness ( $\sigma_{\text{Inh}}^{\text{DFT}}$ ) and chemical hardness ( $\eta_{\text{Inh}}^{\text{DFT}}$ ) confirmed that the pistiphloroglucinyll, pistaciaphenyl ether, and naringenin organic compounds exhibit high chemical softness and lower hardness. Molecules with high chemical softness serve as good corrosion inhibitors. This means that the electrons are easily shared from the soft molecule to the metal surface.
- (iii) The possible values of electronic nucleophilicity ( $\epsilon_{\text{Inh}}^{\text{DFT}}$ ), electron affinity ( $A_{\text{Inh}}^{\text{DFT}}$ ), global electrophilicity index ( $\omega_{\text{Inh}}^{\text{DFT}}$ ), chemical potential ( $\mu_{\text{Inh}}^{\text{DFT}}$ ), electronic negativity ( $\chi_{\text{Inh}}^{\text{DFT}}$ ), and molecular ionization potential ( $I_{\text{Inh}}^{\text{DFT}}$ ) suggest that the pistiphloroglucinyll, pistaciaphenyl ether, and naringenin organic compounds are effective corrosion inhibitors.
- (iv) Values of the electron fraction transfer ( $\Delta N_{\text{Inh}}^{\text{DFT}}$ ) (connected to Koopmans's theory) and the electronic fraction ( $\psi_{\text{Inh}}^{\text{DFT}}$ ) revealed that the adsorption of pistiphloroglucinyll, pistaciaphenyl ether, and naringenin organic compounds onto the metal occur chemically by the transfer of the electrons.

$$\Delta E_{\text{Inh}} = E_{\text{LUMO}(\text{Inh})} - E_{\text{HOMO}(\text{Inh})} \quad (9)$$

$$I_{\text{Inh}} = -E_{\text{HOMO}(\text{Inh})} \quad (10)$$

$$A_{\text{Inh}} = -E_{\text{LUMO}(\text{Inh})} \quad (11)$$

$$\eta_{\text{Inh}} = \frac{1}{2(I_{\text{Inh}} - A_{\text{Inh}})} \quad (12)$$

$$\epsilon_{\text{Inh}} = \frac{1}{\omega_{\text{Inh}}} \quad (13)$$

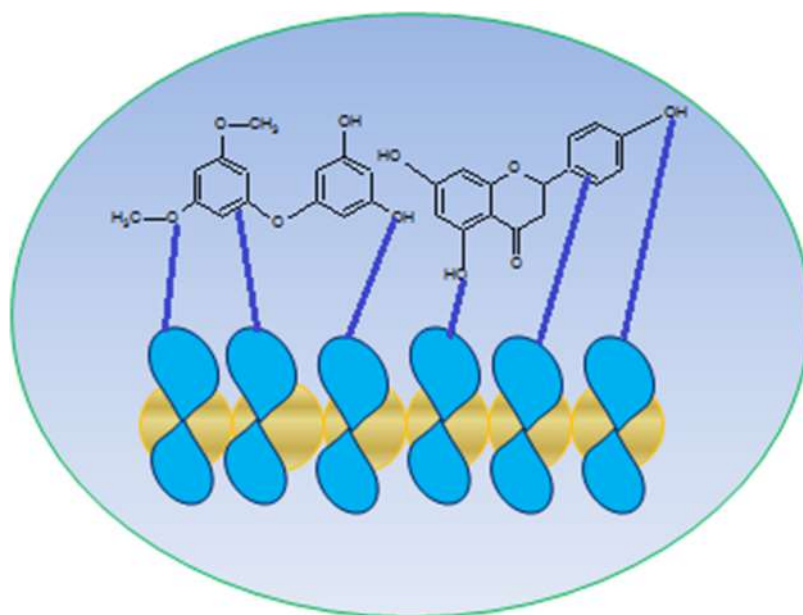


**Figure 12.** Phytochemical adsorption of *P. integerrima* on steel to form a protective coating.

$$-\mu_{\text{Inh}} = \chi_{\text{Inh}} = \frac{1}{2(I_{\text{Inh}} + A_{\text{Inh}})} \quad (14)$$

$$\omega_{\text{Inh}} = \frac{(\chi_{\text{Inh}})^2}{2\eta_{\text{Inh}}} \quad (15)$$

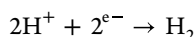
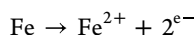
$$\sigma_{\text{Inh}} = \frac{1}{\eta} \quad (16)$$

$$\Delta N_{\text{Inh}} = \frac{(\chi_{\text{Fe}} - \chi_{\text{Inh}})}{2(\eta_{\text{Fe}} + \eta_{\text{Inh}})} \quad (17)$$

$$\psi_{\text{Inh}} = \frac{(\chi_{\text{Fe}} - \chi_{\text{Inh}})}{4(\eta_{\text{Fe}} + \eta_{\text{Inh}})} \quad (18)$$

where  $\eta_{\text{Fe}} = 0 \text{ eV mol}^{-1}$  and  $\chi_{\text{Fe}} = 7 \text{ eV mol}^{-1}$ .

**3.8. Mechanism of Corrosion Inhibition by the *P. integerrima* Gall Extract on Mild Steel.** During corrosion, oxidation takes place on the anode, and reduction takes place on the cathode.



A coordinate bond is formed when heteroatoms donate electrons to the metal orbital. The phytochemicals present in the *P. integerrima* extract can be used to reduce steel corrosion in 1 M sulfuric acid. In addition to double bonds, these phytochemicals have carbonyl, hydroxyl, and carboxylic acid functional groups. According to Figure 12, electrons in heteroatoms and multiple bonds in phytochemicals form coordinate bonds. Plant extracts block the active site by acting as inhibitors on the metal surface. As per the adsorption parameters, the value of  $\Delta G_{\text{ads}}^{\circ}$  indicates that the adsorption of the *P. integerrima* gall extract on the mild steel surface is physical in nature. Meanwhile, using DFT studies, it is observed that the *P. integerrima* gall extract is an inhibitor that adsorbs onto the metal surface by forming chemical bonds. In general, it can be concluded that both physical and chemical adsorption take place, and therefore, the extract can be considered to be a mixed-type corrosion inhibitor.

## 5. CONCLUSIONS

Many studies have been performed to assess the anticorrosive properties of the *P. integerrima* extract. The corrosion inhibition efficiency of the *P. integerrima* extract is determined by performing weight loss and electrochemical studies. According to EIS studies, we determined the maximum inhibition efficiency of 92.19% at an inhibitor concentration of 2000 mg L<sup>-1</sup>. The obtained inhibition efficiency at various concentrations indicates that on increasing the inhibitor concentration, the corrosion rate decreases and inhibition efficiency increases. Surface morphological studies are in favor of the formation of a protective layer on the metal surface. Different phytochemicals found in the extract affect the potency of the inhibitor. The obtained results of DFT-based theoretical calculations confirmed that the order of values of corrosion efficiency is as follows: pistaciaphenyl ether > pistiphlorogluciny ether > naringenin organic compound; this suggests that pistaciaphenyl ether was a more favored corrosion inhibitor than others. The reason for this is that the carboxyl functional groups as well as

aromatic rings primarily promote the high reactivity of the pistaciaphenyl ether.

## ■ ASSOCIATED CONTENT

### Supporting Information

The Supporting Information is available free of charge at <https://pubs.acs.org/doi/10.1021/acsomega.3c06824>.

Figure S1: Plant parts having different kinds of phytochemicals; Figure S2: Establishment of a protective layer on a steel surface in the presence of an inhibitor; Table S1: Different phytochemicals in plants; Table S2: Ability of some plants to suppress corrosion; Table S3: Phytochemicals of the *P. integerrima* gall extract (PDF)

## ■ AUTHOR INFORMATION

### Corresponding Author

Akhil Saxena – Department of Chemistry, Chandigarh University Mohali, Sahibzada Ajit Singh Nagar, Punjab 140413, India; [orcid.org/0000-0003-2501-5244](https://orcid.org/0000-0003-2501-5244); Email: [akhil.uis@cumail.in](mailto:akhil.uis@cumail.in)

### Authors

Jasdeep Kaur – Department of Chemistry, Chandigarh University Mohali, Sahibzada Ajit Singh Nagar, Punjab 140413, India

Hamad Almujiab – Department of Civil Engineering, College of Engineering, Taif University, Taif City 21974, Saudi Arabia

Mohammad Mahtab Alam – Department of Basic Medical Sciences, College of Applied Medical Science, King Khalid University, Abha 61421, Saudi Arabia

Abha Singh – Department of Basic Sciences, College of Science and Theoretical Studies, Dammam-branch, Saudi Electronic University, Riyadh 11673, Saudi Arabia

Dakeshwar Kumar Verma – Department of Chemistry, Government Digvijay Autonomous Postgraduate College, Chhattisgarh 491441, India

Elyor Berdimurodov – New Uzbekistan University, Tashkent 100007, Uzbekistan; Medical School, Central Asian University, Tashkent 111221, Uzbekistan; Faculty of Chemistry, National University of Uzbekistan, Tashkent 100034, Uzbekistan

Complete contact information is available at:

<https://pubs.acs.org/doi/10.1021/acsomega.3c06824>

### Notes

The authors declare no competing financial interest.

## ■ ACKNOWLEDGMENTS

The authors express their gratitude to the Deanship of Scientific Research at King Khalid University for funding this work through the Large Research Groups Project under Grant No. RGP.2-504-44.

## ■ REFERENCES

- (1) Schmitt, G.; Schütze, M.; Hays, G. F.; Burns, W.; Han, E.; Pourbaix, A.; Jacobson, G. *Global Needs for Knowledge Development in Materials Deterioration and Corrosion Control*, in cooperation with, Fed. Highw. Adm. FHWA-RD-01, 2009, pp 1-44.
- (2) El-Hashemy, M. A.; Sallam, A. The inhibitive action of *Calendula officinalis* flower heads extract for mild steel corrosion in 1 M HCl solution. *J. Mater. Res. Technol.* **2020**, *9*, 13509–13523.
- (3) Chung, I. M.; Malathy, R.; Priyadarshini, R.; Hemapriya, V.; Kim, S.; Prabakaran, M. Inhibition of mild steel corrosion using *Magnolia*

*kobus* extract in sulphuric acid medium. *Mater. Today Commun.* **2020**, *25*, No. 101687.

(4) Ahanotu, C. C.; Onyechu, I. B.; Solomon, M. M.; Chikwe, I. S.; Chikwe, O. B.; Eziukwu, C. A. *Pterocarpus santalinoides* leaves extract as a sustainable and potent inhibitor for low carbon steel in a simulated pickling medium. *Sustainable Chem. Pharm.* **2020**, *15*, No. 100196.

(5) Saxena, A.; Thakura, K. K.; Bhardwaj, N. Electrochemilgical studies and surface examination of low carbon steel by applying the extract of *Musa acuminata*. *Surf. Interfaces* **2020**, *18*, No. 100436.

(6) Zakaria, K.; Abbas, M.; Bedair, M. Herbal expired drug bearing glycosides and polysaccharides moieties as green and cost-effective oilfield corrosion inhibitor: Electrochemical and computational studies. *J. Mol. Liq.* **2022**, *352*, No. 118689.

(7) Haldhar, R.; Kim, S.; Prasad, D.; Bedair, M.; Bahadur, I.; Kaya, S.; Dagdag, O.; Guo, L. Papaver somniferum as an efficient corrosion inhibitor for iron alloy in acidic condition: DFT, MC simulation, LCMS and electrochemical studies. *J. Mol. Struct.* **2021**, *1242*, No. 130822.

(8) Parthipan, P.; Elumalai, P.; Narenkumar, J.; Machuca, L.; Murugan, K.; Karthikeyan, O.; Rajasekar, A. *Allium sativum* (garlic extract) as a green corrosion inhibitor with biocidal properties for the control of MIC in carbon steel and stainless steel in oilfield environments. *Int. Biodeterior. Biodegrad.* **2018**, *132*, 66–73.

(9) Saxena, A.; Prasad, D.; Haldhar, R.; Singh, G.; Kumar, A. Use of *Sida cordifolia* Extract as Green Inhibitor for Mild Steel in 0.5M H<sub>2</sub>SO<sub>4</sub>. *J. Environ. Chem. Eng.* **2018**, *6*, 694–700.

(10) Saxena, A.; Prasad, D.; Haldhar, R.; Singh, G.; Kumar, A. Use of *Saraca ashoka* extract as green corrosion inhibitor for mild steel in 0.5 M H<sub>2</sub>SO<sub>4</sub>. *J. Mol. Liq.* **2018**, *258*, 89–97.

(11) Saxena, A.; Prasad, D.; Haldhar, R. Investigation of corrosion inhibition effect and adsorption activities of *Cuscuta reflexa* extract for mild steel in 0.5 M H<sub>2</sub>SO<sub>4</sub>. *Bioelectrochemistry* **2018**, *124*, 156–16.

(12) Haldhar, R.; Prasad, D.; Saxena, A. *Armoracia rusticana* as sustainable and eco-friendly corrosion inhibitor for mild steel in 0.5M sulphuric acid: Experimental and theoretical investigations. *J. Environ. Chem. Eng.* **2018**, *6*, 5230–5238.

(13) Haldhar, R.; Prasad, D.; Saxena, A. *Myristica fragrans* extract as an eco-friendly corrosion inhibitor for mild steel in 0.5 M H<sub>2</sub>SO<sub>4</sub> solution. *J. Environ. Chem. Eng.* **2018**, *6*, 2290–2301.

(14) Alibakhshi, E.; Ramezanzadeh, M.; Bahlakeh, G.; Ramezanzadeh, B.; Mahdavian, M.; Motamedi, M. *Glycyrrhiza glabra* leaves extract as a green corrosion inhibitor for mild steel in 1 M hydrochloric acid solution: Experimental, molecular dynamics, Monte Carlo and quantum mechanics study. *J. Mol. Liq.* **2018**, *255*, 185–198.

(15) Satapathy, A.; Gunasekaran, G.; Sahoo, S.; Amit, K.; Rodrigues, P. Corrosion inhibition by *Justicia gendarussa* plant extract in hydrochloric acid solution. *Corros. Sci.* **2009**, *51*, 2848–2856.

(16) Chauhan, L.; Gunasekaran, G. Corrosion inhibition of mild steel by plant extract in dilute HCl medium. *Corros. Sci.* **2007**, *49*, 1143–1161.

(17) El-Etre, A. Khillah extract as inhibitor for acid corrosion of SX 316 steel. *Appl. Surf. Sci.* **2006**, *252*, 8521–8525.

(18) Oguzie, E. E. Studies on the inhibitive effect of *Occimum viridis* extract on the acid corrosion of mild steel. *Mater. Chem. Phys.* **2006**, *99*, 441–446.

(19) El-Etre, A.; Abdallah, M.; El-Tantawy, Z. Corrosion inhibition of some metals using lawsonia extract. *corros. Sci.* **2005**, *47* (X), 385–395.

(20) Lebrini, M.; Robert, F.; Lecante, A.; Roos. Corrosion inhibition of C38 steel in 1 M hydrochloric acid medium by alkaloids extract from *Oxandra asbeckii* plant. *Corros. Sci.* **2011**, *53*, 687–695.

(21) Bhawsar, J.; Ain, Pk.; Jain, P. Experimental and computational studies of *Nicotiana tabacum* leaves extract as green corrosion inhibitor for mild steel in acidic medium. *Alexandria Eng. J.* **2015**, *54*, 769–774.

(22) Ngouné, B.; Pengou, M.; Nouteza, A.; Nanseu-Njiki, C.; Ngameni, E. Performances of Alkaloid Extract from *Rauvolfia macropphylla* Stapf toward Corrosion Inhibition of C38 Steel in Acidic Media. *ACS Omega* **2019**, *4*, 9081–9091.

(23) Prabakaran, M.; Hemapriya, S.; Kim, V.; Chung, I. Evaluation of polyphenol composition and anti-corrosion properties of *Cryptostegia*

*grandiflora* plant extract on mild steel in acidic medium. *J. Indust. Eng. Chem.* **2016**, *37*, 2016.

(24) Hassan, K. H.; Khadom, A. A.; Kursheed, N. *Citrus aurantium* leaves extracts as a sustainable corrosion inhibitor of mild steel in sulfuric acid. *S. Afr. J. Chem. Eng.* **2016**, *22*, 1–5.

(25) Dehghani, A.; Bahlakeha, G.; Ramezanzadeh, B. A detailed electrochemical/theoretical exploration of the aqueous *Chinese gooseberry* fruit shell extract as a green and cheap corrosion inhibitor for mild steel in acidic solution. *J. Mol. Liq.* **2019**, *282*, 366–384.

(26) Dehghani, A.; Bahlakeha, G.; Ramezanzadehb, B.; Ramezanzadeh, M. Potential of *Borage* flower aqueous extract as an environmentally sustainable corrosion inhibitor for acid corrosion of mild steel: Electrochemical and theoretical studies. *J. Mol. Liq.* **2019**, *277*, 895–911.

(27) Benarioua, M.; Mihi, A.; Bouzeghaia, N.; Naoun. Mild steel corrosion inhibition by Parsley (*Petroselinum Sativum*) extract in acidic media. *Egypt. J. Pet.* **2019**, *28*, 155–159.

(28) Muthukrishnan, P.; Jeyaprabha, B.; Prakash, P. Adsorption and corrosion inhibiting behavior of *Lannea coromandelica* leaf extract on mild steel corrosion. *Arabian J. Chem.* **2013**, *S2343–S2354*.

(29) Mehdipour, M.; Ramezanzadeh, B.; Arman, S. Electrochemical noise investigation of Aloe plant extract as green inhibitor on the corrosion of stainless steel in 1 M H<sub>2</sub>SO<sub>4</sub>. *J. Indust. Eng. Chem.* **2015**, *21*, 318–327.

(30) Uwah, I.; Okafor, P.; Ebikepe, V. Inhibitive action of ethanol extracts from *Nauclea latifolia* on the corrosion of mild steel in H<sub>2</sub>SO<sub>4</sub> solutions and their adsorption characteristics. *Arabian J. Chem.* **2013**, *6*, 253–352.

(31) Bagga, M. K.; Gadi, R.; Yadav, O.; Kumar, R.; Chopra, R.; Singh, G. Investigation of phytochemical components and corrosion inhibition property of *Ficus racemosa* stem extract on mild steel in H<sub>2</sub>SO<sub>4</sub> medium. *J. Environ. Chem. Eng.* **2016**, *4*, 4699–4707.

(32) Haldhar, R.; Prasad, D.; Mandal, N.; Benhiba, F.; Bahadur, I.; Dagdag, O. Anticorrosive properties of a green and sustainable inhibitor from leaves extract of *Cannabis sativa* plant: Experimental and theoretical approach. *Colloids Surf, A* **2021**, *614*, No. 126211.

(33) Patel, N.; Šnita, D. Ethanol extracts of *Hemidesmus indicus* leaves as eco-friendly inhibitor of mild steel corrosion in H<sub>2</sub>SO<sub>4</sub> medium. **2014**, 1747 1754.

(34) Umoren, S.; Obot, I.; Israel, A.; Asuquo, P.; Solomon, M.; Eduok, U.; Udoh, A. Inhibition of mild steel corrosion in acidic medium using coconut coir dust extracted from water and methanol as solvents. *J. Ind. Eng. Chem.* **2014**, *20*, 3612–3622.

(35) Singh, M. A green Approach: A corrosion inhibition of mild steel by adhatoda vasica plant extract in 0.5 M H<sub>2</sub>SO<sub>4</sub>. *J. Mater. Environ. Sci.* **2013**, *4*, 119–126.

(36) Dehghani, A.; Bahlakeh, G.; Ramezanzadeh, B.; Ramezanzadeh, M. A combined experimental and theoretical study of green corrosion inhibition of mild steel in HCl solution by aqueous *Citrullus lanatus* fruit (CLF) extract. *J. Mol. Liq.* **2019**, *279*, 603–624.

(37) Dehghani, A.; Bahlakeh, G.; Ramezanzadeh, B. Green Eucalyptus leaf extract: A potent source of bio-active corrosion inhibitors for mild steel. *Bioelectrochemistry* **2019**, *130*, No. 107339.

(38) Wang, Y.; Qiang, Y.; Zhi, H.; Ran, B.; Zhang, D. Evaluating the synergistic effect of maple leaves extract and iodide ions on corrosion inhibition of Q235 steel in H<sub>2</sub>SO<sub>4</sub> solution. *J. Ind. Eng. Chem.* **2023**, *117*, 422–33.

(39) Yao, X.; Qiang, Y.; Guo, L.; Xu, Q.; Wen, L.; Jin, Y. Renewable low-cost brassica rapa subsp. Extract for protection of Q235 steel in H<sub>2</sub>SO<sub>4</sub> medium: Experimental and modeling studies. *J. Ind. Eng. Chem.* **2022**, *114*, 427–37.

(40) Bedair, M.; Metwally, M.; Soliman, S.; Al-Sabagh, A.; Salem, A.; Mohamed, T. EXTRACTS OF MINT AND TEA AS GREEN CORROSION INHIBITORS FOR MILD STEEL IN HYDROCHLORIC ACID SOLUTION. *Al-Azhar Bull. Sci.* **2015**, *26*, 1–14.

(41) Hassan, A.; Heakal, B.; Younis, A.; Bedair, M.; El - Billy, M.; Mohamed, M. Synthesis of some triazole Schiff base derivatives and their metal complexes under Microwave irradiation and evaluation of their corrosion inhibition and biological activity. *Egypt. J. Chem.* **2019**.

- (42) Raja, P. B.; Qureshi, A.; Rahim, A.; Osman, H.; Awang, K. Neolamarckia cadamba alkaloids as eco-friendly corrosion inhibitors for mild steel in 1M HCl media. *Corros. Sci.* **2013**, *69*, 292–301.
- (43) Lgaz, H.; Salghi, R.; Jodeh, S.; Hammouti, B. Effect of clozapine on inhibition of mild steel corrosion in 1.0 M HCl medium. *J. Mol. Liq.* **2017**, *225*, 271–280.
- (44) Majeed, M.; Yousif, Q.; Bedair, M. Study of the Corrosion of Nickel–Chromium Alloy in an Acidic Solution Protected by Nickel Nanoparticles. *ACS Omega* **2022**, 729850–29857.
- (45) Elaryian, H. M.; Bedair, M.; Bedair, A.; Aboushabha, R.; Fouda, A. Synthesis, characterization of novel coumarin dyes as corrosion inhibitors for mild steel in acidic environment: Experimental, theoretical, and biological studies. *J. Mol. Liq.* **2022**, *346*, No. 118310.
- (46) Ismail, A. M.; Mohamed, E.; Marghany, M.; Motaal, V.; Abdel-Farid, V. I.; Sayed, M. E. Preliminary phytochemical screening, plant growth inhibition and antimicrobial activity studies of *Faidherbia albida* legume extracts. *J. Saudi Soc. Agric. Sci.* **2016**, *15*, 112–117.
- (47) Alqethami, A.; Aldhebani, A. Medicinal plants used in Jeddah, Saudi Arabia: Phytochemical screening. *Saudi J. Biol. Sci.* **2021**, *28*, 805–812.
- (48) Kumar, J.; Kaur, A.; Narang, P. Phytochemical screening and metal binding studies on floral extract of *Solanum nigrum*. *Mater. Today: Proc.* **2020**, *26*, 3332–3336.
- (49) El-Sabbah, M.; Bedair, M.; Abbas, M.; Fahmy, A.; Hassaballa, S.; Moustafa, A. Synergistic Effect between Natural Honey and 0.1 M KI as Green Corrosion Inhibitor for Steel in Acid Medium. *Zeitsch. Phys. Chem.* **2019**, *233*, 627–649.
- (50) Dewangan, Y.; Verma, D.; Berdimurodov, E.; Haldhar, R.; Dagdag, O.; Tripathi, M.; Mishra, V.; Kumar, P. N-hydroxypyrazine-2-carboxamide as a new and green corrosion inhibitor for mild steel in acidic medium: experimental, surface morphological and theoretical approach. *J. Adhes. Sci. Technol.* **2022**, *36*, 1–21.
- (51) Berdimurodov, E.; Kholikov, A.; Akbarov, K.; Guo, L.; Kaya, S.; Verma, D. K.; Rbaa, M.; Dagdag, O. Novel glycoluril pharmaceutically active compound as a green corrosion inhibitor for the oil and gas industry. *J. Electroanal. Chem.* **2022**, *907*, No. 116055.
- (52) Dagdag, O.; Haldhar, R.; Kim, S.-C.; Guo, L.; El Gouri, M.; Berdimurodov, E.; Hamed, O.; Jodeh, S.; Akpan, E. D.; Ebenso, E. E. Recent progress in epoxy resins as corrosion inhibitors: design and performance. *J. Adhes. Sci. Technol.* **2022**, 1–22.
- (53) Berdimurodov, E.; Kholikov, A.; Akbarov, K.; Guo, L.; Abdullah, A. M.; Elik, M. A gossypol derivative as an efficient corrosion inhibitor for St2 steel in 1 M HCl + 1 M KCl: An experimental and theoretical investigation. *J. Mol. Liq.* **2021**, *328*, No. 115475.
- (54) Barca, G. M. J.; Bertoni, C.; Carrington, L.; Datta, D.; De Silva, N.; Deustua, J. E.; Fedorov, D. G.; Gour, J. R.; Gunina, A. O.; Guidez, E.; et al. Recent developments in the general atomic and molecular electronic structure system. *J. Chem. Phys.* **2020**, *152*, No. 154102.
- (55) Schmidt, M. W.; Baldrige, K. K.; Boatz, J. A.; Elbert, S. T.; Gordon, M. S.; Jensen, J. H.; Koseki, S.; Matsunaga, N.; Nguyen, K. A.; Su, S.; et al. General atomic and molecular electronic structure system. *J. Comput. Chem.* **1993**, *14*, 1347–1363.
- (56) Becke, A. D. Density-functional thermochemistry. III. The role of exact exchange. *J. Chem. Phys.* **1993**, *98* (n.d.), 5648.
- (57) Lee, C.; Yang, W.; Parr, R. G. Development of the Colle-Salvetti correlation-energy formula into a functional of the electron density. *Phys. Rev. B* **1988**, *37*, 785.
- (58) Hanwell, M. D.; Curtis, D. E.; Lonie, D. C.; Vandermeersch, T.; Zurek, E.; Hutchison, G. R. Avogadro: an advanced semantic chemical editor, visualization, and analysis platform. *J. Cheminform.* **2012**, *4*, 1–17.
- (59) A. an open-source molecular builder and visualization tool. V. 1. X. <http://avogadro.cc/>.
- (60) Bedair, M.; Alosaimi, E.; Melhi, S. A study of the inhibitive effect for corrosion of steel in 1.0 M HCl using a new nonionic surfactant based on coumarin moiety: chemical, electrochemical and quantum mechanics calculations. *J. Adhes. Sci. Technol.* **2021**, 1–31.
- (61) Abdelsalam, M. M.; Bedair, M.; Hassan, A.; Heikal, B.; Younis, A.; Elbially, Z.; Badawy, M.; Fawzy, H.; Fareed, S. Green synthesis, electrochemical, and DFT studies on the corrosion inhibition of steel by some novel triazole Schiff base derivatives in hydrochloric acid solution. *Arab. J. Chem.* **2022**, *15*, No. 103491.
- (62) Shabani-Nooshabadi, M.; Ghandchi, M. Santolina chamaecyparissus extract as a natural source inhibitor for 304 stainless steel corrosion in 3.5% NaCl. *J. Ind. Eng. Chem.* **2015**, *31*, 231–237.
- (63) Ferreira, E.; Giacomelli, C.; Giacomelli, F.; Spinelli, A. Evaluation of the inhibitor effect of L-ascorbic acid on the corrosion of low alloy steel. *Mater. Chem. Phys.* **2004**, *83*, 129–134.
- (64) Gebril, M. A.; Bedair, M.; Soliman, S.; Bakr, F.; Mohamed M, M. Experimental and computational studies of the influence of non-ionic surfactants with coumarin moiety as corrosion inhibitors for carbon steel in 1.0 M HCl. *J. Mol. Liq.* **2022**, *349*, No. 118445.
- (65) Mostafa, M.; Ashmawy, A.; Reheim, M.; Bedair, M.; Abuelela, A. Molecular structure aspects and molecular reactivity of some triazole derivatives for corrosion inhibition of aluminum in 1 M HCl solution. *J. Mol. Struct.* **2021**, *1236*, No. 130292.
- (66) Berdimurodov, E.; Kholikov, A.; Akbarov, K.; Guo, L. Experimental and theoretical assessment of new and eco-friendly thioglycoluril derivative as an effective corrosion inhibitor of St2 steel in the aggressive hydrochloric acid with sulfate ions. *J. Mol. Liq.* **2021**, *335*, No. 116168.
- (67) Shahmoradi, A.; Ranjbarghanei, M.; Javidparvar, A.; Guo, L.; Berdimurodov, E.; Ramezanzadeh, B. Theoretical and surface/electrochemical investigations of walnut fruit green husk extract as effective inhibitor for mild-steel corrosion in 1M HCl electrolyte. *J. Mol. Liq.* **2021**, *338*, No. 116550.
- (68) Haldhar, R.; Kim, S.; Berdimurodov, E.; Verma, D.; Hussain, C. (2021) Corrosion Inhibitors: Industrial Applications and Commercialization, in: *Sustain. Corros. Inhib. II Synth. Des. Pract. Appl.*; American Chemical Society, 210–219.
- (69) Dagdag, O.; Berisha, A.; Mehmeti, V.; Haldhar, R.; Berdimurodov, E.; Hamed, O.; Jodeh, S.; Lgaz, H.; Sherif, E.; Ebenso, E. Epoxy coating as effective anti-corrosive polymeric material for aluminum alloys: Formulation, electrochemical and computational approaches. *J. Mol. Liq.* **2022**, *346*, No. 117886.
- (70) Berdimurodov, E.; Kholikov, A.; Akbarov, K.; Guo, L.; Kaya, S.; Katin, K.; Verma, D.; Rbaa, M.; Dagdag, O. Novel cucurbit[6]uril-based [3]rotaxane supramolecular ionic liquid as a green and excellent corrosion inhibitor for the chemical industry. *Colloids Surf., A* **2022**, *633*, No. 127837.
- (71) Berdimurodov, E.; Kholikov, A.; Akbarov, K.; Guo, L.; Kaya, S.; Verma, D.; Rbaa, M.; O Dagdag, O. New and Green Corrosion Inhibitor Based on New Imidazole Derivate for Carbon Steel in 1 M Hcl Medium: Experimental and Theoretical Analyses. *Int. J. Eng. Res. Africa* **2022**, *58*, 11–44.
- (72) Berdimurodov, E.; Guo, L.; Kholikov, A.; Akbarov, K.; Zhu, M. MOFs-Based Corrosion Inhibitors. *Supramol. Chem. Corros. Biofouling Prot.*, CRC Press: 2022; pp 287–305.
- (73) Bahgat Radwan, A.; Mannah, C.; Sliem, M.; Al-Qahtani, N.; Okonkwo, P.; Berdimurodov, E.; Mohamed, A.; Abdullah, A. Electrospun highly corrosion-resistant polystyrene–nickel oxide superhydrophobic nanocomposite coating. *J. Appl. Electrochem.* **2021**, *51*, 1605–1618.
- (74) Berdimurodov, E.; Kholikov, A.; Akbarov, K.; Guo, L.; Kaya, S.; Katin, K.; Verma, D.; Rbaa, M.; Dagdag, O.; Haldhar, R. Novel bromide–cucurbit[7]uril supramolecular ionic liquid as a green corrosion inhibitor for the oil and gas industry. *J. Electroanal. Chem.* **2021**, *901*, No. 115794.
- (75) Berdimurodov, E.; Verma, C.; Berdimurodov, K.; Quraishi, M.; Kholikov, A.; Akbarov, K.; Umirov, N.; Borikhonov, B. 8–Hydroxyquinoline is key to the development of corrosion inhibitors: An advanced review. *Inorg. Chem. Commun.* **2022**, *144*, No. 109839.
- (76) Berdimurodov, E.; Eliboyev, I.; Berdimurodov, K.; Kholikov, A.; Akbarov, K.; Dagdag, O.; Rbaa, M.; El Ibrahimy, B.; Ibrahimy, B.; Verma, D.; Haldhar, R. Green  $\beta$ -cyclodextrin-based corrosion inhibitors: Recent developments, innovations and future opportunities. *Carbohydr. Polym.* **2022**, *292*, No. 119719.

(77) Zhu, M.; Guo, L.; He, Z.; Z Marzouki, H.; Marzouki, R.; Zhang, R.; Zhang, R.; Berdimurodov, E. Insights into the newly synthesized N-doped carbon dots for Q235 steel corrosion retardation in acidizing media: A detailed multidimensional study. *J. Colloid Interface Sci.* **2022**, *608*, 2039–2049.

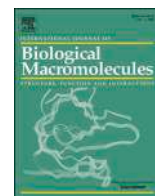
(78) Berdimurodov, E.; Verma, D. K.; Kholikov, A.; Akbarov, K.; Guo, L. The recent development of carbon dots as powerful green corrosion inhibitors: A prospective review. *J. Mol. Liq.* **2022**, *349*, No. 118124.

(79) Verma, D. K.; Kazi, M.; Alqahtani, M. S.; Syed, R.; Berdimurodov, E.; Kaya, S.; Salim, R.; Asatkar, A.; Haldhar, R. N-hydroxybenzothioamide derivatives as green and efficient corrosion inhibitors for mild steel: Experimental, DFT and MC simulation approach. *J. Mol. Struct.* **2021**, *1241*, No. 130648.

(80) Vashishth, P.; Bairagi, H.; Narang, R.; Shukla, S.; Mangla, B. Thermodynamic and electrochemical investigation of inhibition efficiency of green corrosion inhibitor and its comparison with synthetic dyes on MS in acidic medium. *J. Mol. Liq.* **2022**, *365*, No. 120042.

(81) Qiang, Y.; Zhi, H.; Guo, L.; Fu, A.; Xiang, T.; Jin, Y. Experimental and molecular modeling studies of multi-active tetrazole derivative bearing sulfur linker for protecting steel from corrosion. *J. Mol. Liq.* **2022**, *351*, No. 118638.

(82) Qiang, Y.; Guo, L.; Li, H.; Lan, X. Fabrication of environmentally friendly Losartan potassium film for corrosion inhibition of mild steel in HCl medium. *Chem. Eng. J.* **2021**, *406*, No. 126863.



# Integrating experimental and theoretical studies in the development of a novel alginate-based bio-composite for copper anticorrosion in 3.5 % NaCl environments

Mohamed El Mahamdi <sup>a,1</sup>, Walid Daoudi <sup>b,\*</sup>, Omar Dagdag <sup>c,1</sup>, Hansang Kim <sup>c,\*</sup>, Firdaouss Eddaoudy <sup>b</sup>, Dakeshwar Kumar Verma <sup>d</sup>, Sangeeta Gupta <sup>e</sup>, Avni Berisha <sup>f</sup>, Mohamed Loutou <sup>b</sup>, Benchat Nouredine <sup>a</sup>, Abdelmalik El Aatiaoui <sup>b</sup>

<sup>a</sup> Laboratory of Applied Chemistry and Environment (LCAE-URAC18), Department of Chemistry, Faculty of Sciences, University Mohamed I, Po. Box 717, 60000 Oujda, Morocco

<sup>b</sup> Laboratory of Molecular Chemistry, Materials and Environment (LCM2E), Department of Chemistry, Multidisciplinary Faculty of Nador, University Mohamed I, 60700 Nador, Morocco

<sup>c</sup> Department of Mechanical Engineering, Gachon University, Seongnam 13120, Republic of Korea

<sup>d</sup> Department of Chemistry, Govt. Dignvijay Autonomous Postgraduate College, Rajnandgaon, Chhattisgarh 491441, India

<sup>e</sup> Department of Chemistry, Govt. Shivnath Science College, Rajnandgaon, Chhattisgarh 491441, India

<sup>f</sup> Department of Chemistry, Faculty of Natural and Mathematics Science, University of Prishtina, 10000 Prishtina, Kosovo

## ARTICLE INFO

### Keywords:

Biopolymer  
Coating  
Nanocomposite  
Nanoparticle SrTiO<sub>3</sub>  
Corrosion and computational approaches

## ABSTRACT

The development of new coatings based on a biopolymer, epichlorohydrin-modified alginate, and alginate-epichlorohydrin-SrTiO<sub>3</sub> nanocomposites incorporating SrTiO<sub>3</sub> (STO) nanoparticles in the alginate (Alg) matrix (Alg-Ep-STO), has been addressed in this study. Various characterization techniques were employed to analyze the prepared compounds, including X-ray diffraction spectroscopy (XRD), Fourier-transform infrared spectroscopy (FTIR), as well as surface analysis methods such as Scanning electron microscopy coupled with energy-dispersive X-ray spectroscopy (SEM-EDX). Furthermore, electrochemical impedance spectroscopy (EIS) and potentiodynamic polarisation (PDP) methods were used to evaluate corrosion inhibition and protection durability. The results demonstrate that the incorporation of STO nanoparticles into the alginate matrix with epichlorohydrin significantly improved the metal's resistance to corrosion. The experimental findings received reinforcement from various computational methods, including density functional theory (DFT), Molecular Dynamics (MD) and Monte Carlo (MC) simulations, which were employed to investigate the interactions between the Alg-Ep-STO nanocomposite and the copper surface. The computational outcomes revealed that the Alg-Ep-STO nanocomposite exhibits robust adhesion to the copper surface, maintaining a flat orientation, with its alignment being notably influenced by the presence of STO nanoparticles.

## 1. Introduction

The corrosion problem persists globally, causing significant economic losses in the metals industry and posing substantial risks to the environment and the health of living [1–3]. Copper and its alloys are widely appreciated in various industrial applications due to their natural resistance to corrosion, excellent mechanical properties, high thermal and electrical conductivity, and ease of weldability [4,5]. These materials find utility in areas such as heat exchangers [6], electronics [7],

construction, and marine applications [8]. However, in the presence of aggressive environments containing corrosive substances such as oxygen [9], water, chloride ions [10], and sulfates [11], forms of degradation, such as pitting corrosion, are frequently observed on this metal [12,13]. A great deal of research has been devoted to protecting copper against corrosion in artificial marine environments by adding organic or inorganic inhibitors [14,15]. These inhibitors protect copper by various adsorption mechanisms such as physisorption and chemisorption [16]. In this respect, Jianjia Shen et al. [17] studied the inhibitory effect of

\* Corresponding authors.

E-mail addresses: [walid.daoudi@ump.ac.ma](mailto:walid.daoudi@ump.ac.ma) (W. Daoudi), [hskim70@gachon.ac.kr](mailto:hskim70@gachon.ac.kr) (H. Kim).

<sup>1</sup> These authors contributed equally to this work.

two neonicotinoid derivatives, 1-[(2-Chloro-5-thiazolyl)-methyl]-4, 5-dihydro-N-nitro-1H-imidazol-2-amine and (2E)-1-[(6-Chloro-pyridin-3-yl)-methyl]-N-nitro-imidazolidin-2-imine, on copper corrosion in a 3.5 % NaCl medium using various analytical techniques. They demonstrated that the two inhibitors are of mixed types and that the adsorption mechanism involves the coexistence of physical adsorption and chemical adsorption, with chemical adsorption predominating. In addition, they confirmed that the preferred electrophilic site in both molecules is the N connected to  $-\text{NO}_2$ , prone to provide free double electrons the  $\pi$  electrons to co-ordinate with the unoccupied d orbital of copper. Also, Zining Liu et al. [18] assembled two benzothiazole derivatives, namely 2-mercaptobenzothiazole (MBT) and 2-aminobenzothiazole (ABT), separately with cyclodextrin ( $\beta$ -CD) to form CD-M and CD-A, two inhibitors of copper corrosion in saline environments. The electrochemical studies carried out showed that the two assemblies could be considered as mixed-type corrosion inhibitors with a predominantly cathodic effect. The inhibition efficiency of CD-M was insensitive to increasing temperature, while the passive layer was damaged, accompanied by severe desorption of the inhibitors in the system inhibited by CD-A with increasing temperature. In addition, the Cu—S binding donor-acceptor pair and the electrostatic attraction between the anionic thione form of MBT and the Cu (I)/(II) species preformed on the copper surface were the driving force behind the controllable release and spontaneous adsorption of metastable metals. The release of ABT was attributed to Cu—N bonding, which was less than the above physicochemical synergy. Nevertheless, the limitations of using corrosion inhibitors to protect copper in marine environments, such as durability, environmental impact and the need for continuous monitoring, are prompting researchers to develop new methods of corrosion protection. The most commonly used on an industrial scale being coating protection [19,20]. This approach involves isolating the metal from the aggressive environment by applying a continuous, adherent, and impermeable coating layer [19,21]. With this in mind, Fatma Masmoudi et al. [22] developed a coating based on SEBS (a polystyrene-*block*-poly(ethylene-*ran*-butylene)-*block*-polystyrene copolymer) and SEBS-CB (SEBS-Carbon Black nanoparticles) for protecting copper against corrosion in saline environments. The study carried out on the performance of this type of coating showed that increasing the SEBS ratio improved the anti-corrosion characteristics of Cu-SEBS and Cu-SEBS-CB, indicating a reduction in the accessibility of aggressive species to the copper surface. The use of CB nanoparticles slightly improved the corrosion protection performance of SEBS films due to the existence of  $\pi$ - $\pi$  stacking in the aromatic rings of SEBS and CB. The adsorption mechanism was of the mixed type. In another instance, Le Bo et al. [23] employed the electrophoretic deposition (EPD) method to develop a graphene coating on a copper substrate aimed at inhibiting copper corrosion in a NaCl solution. Electrochemical assessments conducted on the copper with the coating revealed that the open circuit potential (OCP) of the coated sample ( $-0.107$  V) exceeded that of the substrate ( $-0.199$  V) by approximately 0.1 V, and the corrosion current density ( $i_{\text{corr}}$ ) reduced significantly by an order of magnitude. Moreover, an excessive deposition time or elevated deposition voltage resulted in defects in the deposited coating, contributing to a decline in corrosion resistance. Furthermore, Vinod Kumar et al. [24] designed novel nanoclay composite coatings based on epoxy resin (EP) and montmorillonite (MMT) for copper. They evaluated the coating effectiveness against electrochemical impedance spectroscopy (EIS) and potentiodynamic polarisation (PDP) in a 0.5 M NaCl solution. Their findings indicated that the EPMC coating incorporating nanoclays exhibited superior performance compared to the EPMC coating alone. They concluded that the EPMC coating containing 5 % nano-MMT clay emerged as the optimal choice among those tested for preventing copper corrosion. The prevention of copper corrosion was attributed to the insulating properties of MMT and the enhanced surface coverage of copper facilitated by MMT nanoclays.

Recently, natural biopolymers meet environmental requirements for corrosion protection applications with an extremely low or even zero

risk of pollution. The use of biopolymers such as cellulose such as cellulose [25–28], starch [25,29,30], alginate [31–33], and chitosan [34–37], which are biodegradable and environmentally friendly macromolecules, possess corrosion inhibition properties and are therefore viable alternatives. In this context, alginate is an anionic biopolymer, more abundant in the composition of brown algae, composed of  $\beta$ -D-mannuronate and  $\alpha$ -L-guluronate linked by 1  $\rightarrow$  4 glycosidic bonds. It contains two reactive functional groups, hydroxyl and carboxylate, making it chemically modifiable to tailor the polymer's final properties for various corrosion inhibitory applications across different metals and environments [38,39]. Over the past two decades, the incorporation of inorganic nanoparticles (NPs) into polymer matrices has proved to be a catalyst for improving the properties of these materials [40], considerably broadening their fields of application, including medical, electronic, construction, etc. [41,42]. Various inorganic nanomaterials, including metals, metal oxides and ceramics [43], have been used in polymer-inorganic nanocomposites, demonstrating improvements in physicochemical properties [44–46]. The development of alginate-based nanocomposite coatings for corrosion inhibition is less common compared to other biopolymers [47]. One significant reason for incorporating inorganic particles into polymers is to enhance their mechanical properties for practical applications.  $\text{SrTiO}_3$  nanoparticles are widely used as ceramic materials in electronic applications [48].

In this study, our primary aim is to develop a new environmentally friendly bio-nanocomposite coating, exhibiting significant durability and inhibitory efficiency for the protection of copper in an artificial marine environment. Initially, we modified alginate with epichlorohydrin (Ep), serving as a cross-linking agent to enhance the mechanical resistance of the coating by facilitating the bonding between constituent molecules [49]. Subsequently, we incorporated 10 %  $\text{SrTiO}_3$  (STO) nanoparticles into the alginate matrix (Alg) to create a novel biocompatible nanocomposite. This nanocomposite was used to formulate adhesive coatings on a copper metal substrate through the dip-coating technique to shield it from corrosion phenomena in a 3.5 % NaCl weight solution. The first section is dedicated to the characterization of this nanocomposite using XRD to confirm the presence of STO nanoparticles in the alginate matrix, FTIR to demonstrate the chemical modification of alginate (Alg) by epichlorohydrin, as well as the interaction of alginate-epichlorohydrin (Alg-Ep) with STO nanoparticles. SEM-EDX is employed to examine the dispersion of STO nanoparticles in the Alg-Ep matrix and the elemental distribution of the Alg-Ep-STO coating. Finally, EIS and PDP are used to assess inhibitory performance, durability, and the protective mechanism. The second section delves into the examination of the adhesion of the Alg-Ep-STO nanocomposite coating on copper, employing computational methods. This study involves MD and MC simulations to investigate the adhesion. Furthermore, electronic properties of the Alg-Ep-STO nanocomposite contributing to its interaction with copper were assessed through ab initio quantum mechanics using the DFT approach.

## 2. Materials and methods

### 2.1. Materials

The reagents employed in this study were procured from a local supplier, specifically Sigma Aldrich, and were utilized without requiring additional purification. Commercial copper plates, mainly composed of copper (at least 99.85 %) and oxygen (0.013–0.050 %), with impurity levels not exceeding 0.06 %, were supplied by a local supplier. These plates, measuring 495 mm  $\times$  195 mm  $\times$  1 mm, were then cut into disks with a surface area of  $S = 0.9$  mm<sup>2</sup> for coating purposes. To ensure the reliability of our results, a working electrode undergoes systematic pretreatment before each test. This pretreatment involves mechanical polishing using various grades of silicon carbide abrasive paper to achieve smooth and mirror-like surfaces.

## 2.2. Methods

### 2.2.1. Dip-coating process

The dip-coating process involved immersing the copper plate into the appropriate solutions and then lifting it at a specific rate. Subsequently, the plate was dried at a temperature of 60 °C for 3 h [50]. This process was repeated to obtain two coated plates, each with a different coating: One plate with Alg-Ep and the other with Alg-Ep-STO (Fig. 1).

### 2.2.2. Preparation of alginate-epichlorohydrin (Alg-Ep)

For the Alg-Ep solution, 0.5 g of alginate was carefully dissolved in a minimal amount of distilled water, requiring approximately 20 ml. The solution was stirred until all the solid matter was completely dissolved. Next, 2 % epichlorohydrin was added, followed by a few drops of 1 N NaOH solution. The mixture was stirred continuously for 4 h. Part of this solution was used to prepare Alg-Ep coatings, while the remainder was used to prepare thin films for subsequent characterization (Fig. 2).

### 2.2.3. Preparation of the nanocomposite (Alg-Ep-STO)

For the Alg-Ep-STO solution, 0.5 g of alginate was dissolved in the same way in a minimal quantity of distilled water (approximately 20 ml), stirred until complete dissolution. Next, 10 % SrTiO<sub>3</sub> was added to the solution, which was stirred and heated to 40 °C for 20 min. The mixture was then placed in an ultrasonic bath for 15 min, followed by stirring and heating for 24 h. Finally, 2 % epichlorohydrin and a few drops of 1 N NaOH solution were added and the mixture was left to stir for 4 h. Part of this solution was used to make Alg-Ep-STO coatings, while the rest was used to prepare thin films for later characterization.

### 2.2.4. X-ray diffraction (XRD)

The X-ray diffraction (XRD) patterns of the samples were obtained using a Shimadzu XRD-6000 X-ray diffractometer. The use of XRD enables the identification of different crystalline phases present in a sample, as well as the determination of the material's structure, including lattice parameters and atomic positions. This technique provides detailed information about the arrangement and nature of atoms within the crystalline material under investigation.

### 2.2.5. Fourier transform infrared (FTIR)

FTIR enables the acquisition of detailed infrared spectra that provide information about the functional groups present in molecules, facilitating their identification and characterization. In this study, infrared spectra were recorded using an FT/IR-4700 spectrophotometer. The absorption bands are reported in cm<sup>-1</sup>.

### 2.2.6. Scanning electron microscopy (SEM-EDX)

The SEM micrographs of the specimens were captured using a BRUKER SEM NANOANALYSIS instrument. SEM stands out as one of the most versatile and accessible techniques for surface analysis, facilitating the imaging of a sample's surface and the analysis of its microstructure



Fig. 1. Coated copper plates.

morphology. The surface morphology of bare copper and copper with various coatings was investigated through scanning electron microscopy (SEM) following immersion in a 3.5 % by weight NaCl solution for 72 h.

### 2.2.7. Electrochemical tests

In general, PDP and EIS techniques are commonly used to study the reaction mechanisms and characterise the surface layers or protective films during the corrosion of copper in the presence of a 3.5 % NaCl solution. These methods make it possible to understand the protection mechanism and to analyze the electrochemical reactions occurring at the interface between the copper and the saline solution, as well as in the inter-electrode space, encompassing phenomena such as charge transfer, adsorption, mass transport and diffusion. Potential-current curves were obtained by PDP, recorded in the range between -100 mV and -800 mV/ESC, with a scan speed of 100 mV/min. EIS was recorded in the frequency range from 10 MHz to 100 kHz while applying a 5 mV signal perturbation to generate an electrical impedance response. Electrochemical measurements were conducted using a BioLogic SP300 potentiostat, equipped with three electrodes: a working electrode (WE), a saturated calomel reference electrode, and a Pt counter-electrode.

### 2.2.8. Quantum calculation method

The DFT calculations were performed using the Dmol3 module integrated within the Biovia Materials Studio software [51,52]. Generalized Gradient Approximation [53] employing the pbe [54,55] and the DND [56] were used for geometry optimizations. The investigation and comprehension of interactions between Alg-Ep-STO matrix with the Copper surface were conducted through MC and MD simulations. These simulations are commonly utilized to explore multiple adsorption configurations and the interaction system between the Alg-Ep-STO matrix and the Cu (111) surface. The Materials Studio 8.0 software was employed for performing MC and MD simulations [57-59]. Geometry optimization and energy parameters of Alg-Ep-STO are shown in Fig. 3.

## 3. Results and discussion

### 3.1. Characterization of samples: pure alginate, Alg-STO film, and STO nanoparticles

The XRD patterns of the STO, Alg and Alg-Ep and Alg-Ep-STO nanoparticles films are shown in Fig. 4. XRD analysis of SrTiO<sub>3</sub> nanopowder (STO) reveals a distinct pattern of characteristic crystalline peaks, highlighting the crystalline nature of these particles (Fig. 4a). The angular positions of the diffraction peaks are observed at angles of 22.78°, 32.42°, 39.98°, 46.48°, 52.35°, 57.79°, 67.80°, 72.54°, and 77.17°. These peaks correspond, respectively, to the crystallographic planes (100), (110), (111), (200), (210), (211), (220), (300), and (310) of the SrTiO<sub>3</sub> crystalline lattice. The presence of these well-defined peaks serves as clear evidence of the regularity of the crystalline structure of SrTiO<sub>3</sub> nanoparticles, thus confirming their high purity and structural integrity. Fig. 4 (b, c) shows the XRD pattern of the STO nanopowder and the XRD patterns of Alg, Alg-Ep and Alg-Ep-STO films. In the case of the Alg and Alg-Ep pure alginate films, an amorphous blister is observed in the corners of the 10° to 30° region for both samples, indicating that neither sample has a crystalline proportion, both samples being totally amorphous. However, when the Alg-Ep-STO hybrid film is analyzed, there is a significant shift in the main crystalline peaks appearing at angles of 22.6°, 32.3°, 39.9°, 46.4°, 57.7°, 67.8° and 77.16°. It should be noted that the peaks characteristic of the pure alginate structure are still present with some shifts in the Alg-Ep-STO matrix. These observations suggest that significant changes have occurred in the molecular structure of the Alg-Ep-STO films compared to pure alginate. It is plausible that the breaking of numerous hydrogen bonds involving COOH, -C-O- and OH groups in the polymer chain has contributed to these changes. This structural reconfiguration is an important aspect to consider in the context of the use of Alg-Ep-STO



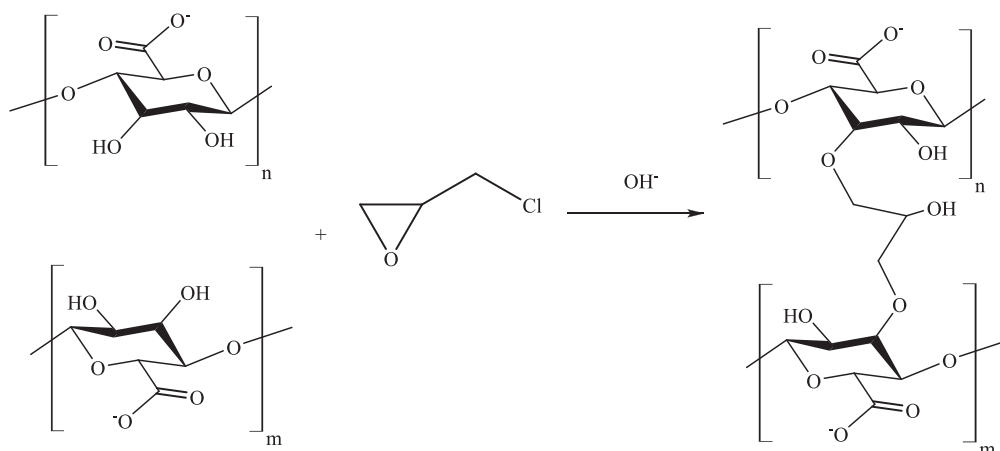


Fig. 2. Cross-linking reaction of alginate with epichlorohydrin.

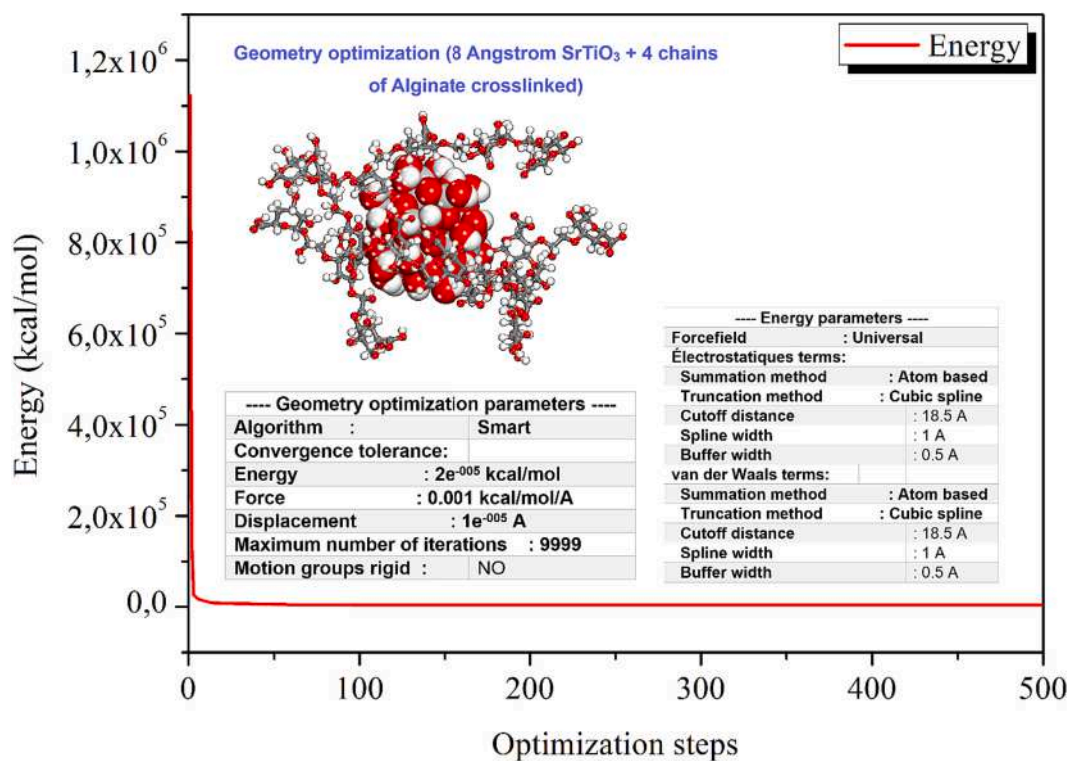


Fig. 3. Geometry optimization and energy parameters of Alg-Ep-STO matrix.

films, as it may influence their physical and chemical properties, which will be explored in more detail in the next part of this study.

Fig. 5 shows the FTIR spectra of STO, Alg, Alg-Ep and Alg-Ep-STO. The FTIR analysis provides further evidence of the consistency and quality of the nanoparticles used in this study. The FTIR spectrum indicates the presence of a strong and broad peak in the spectral region of  $496\text{--}680\text{ cm}^{-1}$ , attributed to the characteristic vibration of the Ti-O-Ti bonds within the nanoparticle structure. The FTIR spectrum of sodium alginate presented above reveals the presence of important characteristic bonds linked to the hydroxyl, carboxylate and ether groups:

A broad absorption band appearing in the range  $[3200\text{--}3292\text{ cm}^{-1}]$  is attributed to the valence vibration mode of the O-H bond in the hydroxyl groups. Vibrations of aliphatic C-H bonds are observed at  $2930\text{ cm}^{-1}$ . The bands at  $1600\text{ cm}^{-1}$  and  $1407\text{ cm}^{-1}$  are attributed to the stretching vibrations of asymmetric and symmetric alginate carboxylates ( $\text{COO}^-$ ) respectively. The band at  $1024\text{ cm}^{-1}$  is attributed to the

valence vibration of the C-O-C bond of the ether group. After modification and cross-linking, the alginate-specific primary bands appear in all the spectra of the prepared samples (Alg-Ep and Alg-Ep-STO). In the FTIR spectra of alginate chemically cross-linked with epichlorohydrin (Alg-Ep) and nanocomposite (Alg-Ep-STO), a decrease in the intensity of the band in the range  $[3200\text{--}3292\text{ cm}^{-1}]$  corresponding to hydroxyl groups, as well as an increase in the intensity of the  $1024\text{ cm}^{-1}$  band attributed to the C-O-C group, were observed. In addition, a very small band appeared at  $2960\text{ cm}^{-1}$  for both samples. The decrease in the intensity of the absorption band characteristic of -OH hydroxyl groups is probably due to the number of hydroxyl groups that reacted during the cross-linking process to form new C-O-C ether groups, which was confirmed by the increase in the intensity of the absorption band characteristic of C-O-C ether groups in Alg-Ep and Alg-Ep-STO. The appearance of a small band around  $2960\text{ cm}^{-1}$  in the Alg-Ep and Alg-Ep-STO samples is attributed to the  $\text{CH}_2$  of the cross-linking chain.

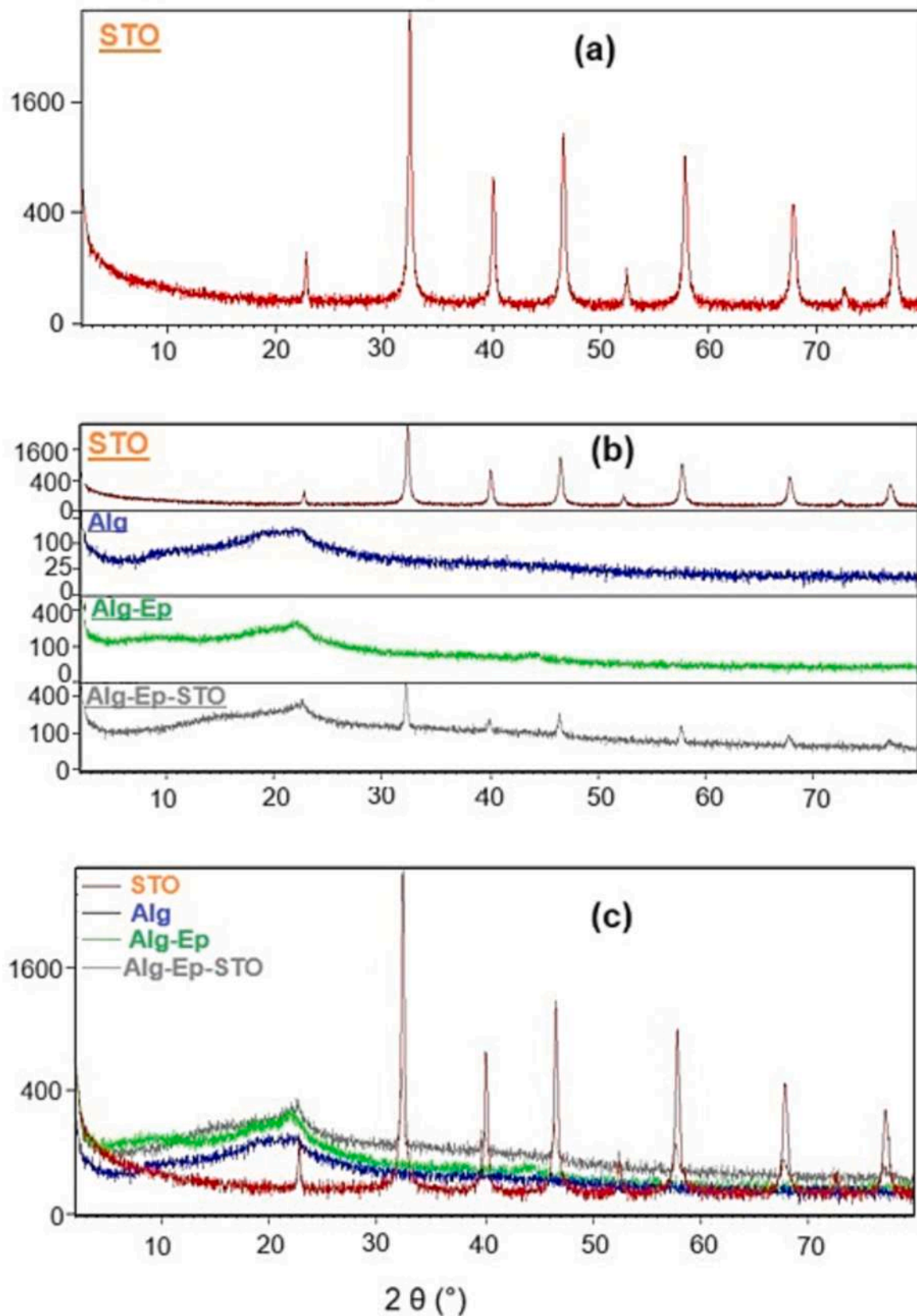


Fig. 4. XRD patterns of STO, Alg, Alg-Ep and Alg-Ep-STO films.

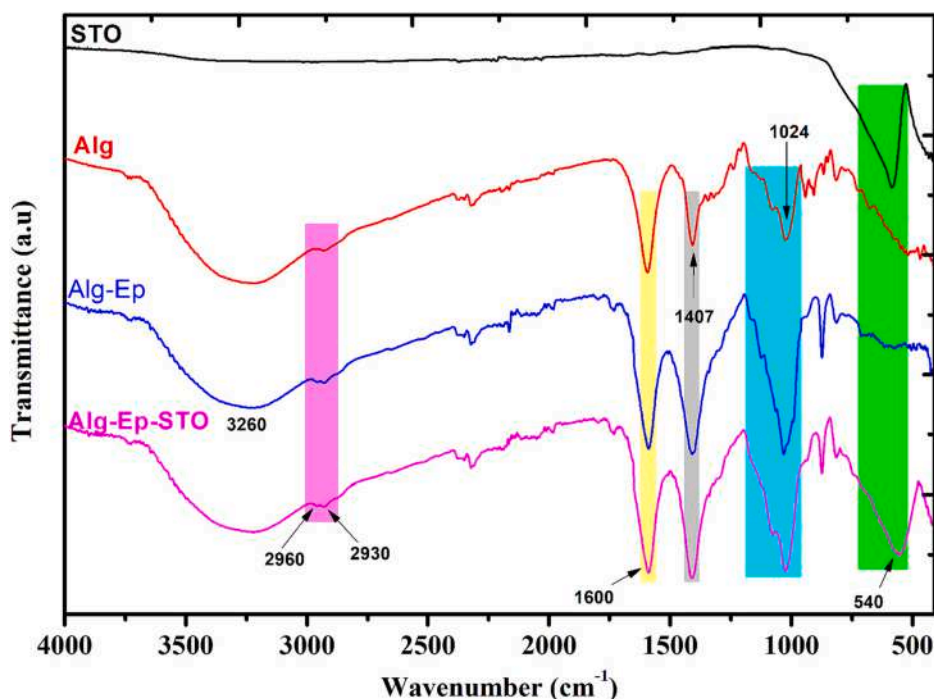


Fig. 5. FTIR spectra of STO, Alg, Alg-Ep and Alg-Ep-STO.

Comparison of the FTIR spectra of Alg-Ep-STO and Alg-Ep reveals similar absorption bands for alginate cross-linked with epichlorohydrin. However, the main distinction lies in the appearance of a new absorption band around  $540\text{ cm}^{-1}$ , which is attributed to the vibration of the Ti-O-Ti groups [60]. In addition, comparison of the FTIR spectra of Alg-Ep-STO and STO shows a slight shift in the band of the Ti-O-Ti group in Alg-Ep-STO compared with STO. This slight shift could be attributed to a weak van der Waals-type interaction between the groups characteristic of the polymer chain and  $\text{SrTiO}_3$ .

SEM images of STO nanopowder and Alg-Ep-STO film at different magnifications are shown in Fig. 6. The image obtained through SEM of the STO nanoparticles revealed the presence of relatively uniform and well-defined particles characterized by average dimensions of less than  $1\ \mu\text{m}$ . However, it is important to note that the SEM analysis also confirmed the significant presence of aggregates or agglomerates within the sample. This observation indicates a tendency of the nanoparticles to aggregate. For the Alg-Ep-STO film at different magnifications it is observed that the nanoparticles are uniformly dispersed within the alginate matrix, likely due to the prior use of ultrasound before the formation of the nanocomposite film. The morphology displayed reveals the presence of agglomerates of spherical-shaped grains; however, these grains exhibit varying sizes. This size variability can be attributed to potential differences in the nanoparticle formation times, warranting further in-depth analysis.

The EDX analysis was used to examine the composition of the Alg-Ep-STO film is shown in Fig. 7. Furthermore, EDX analysis reveals significant results. Peaks of elements such as titanium (at 0.5 keV, 4.5 keV, and 4.99 keV), strontium (at 1.8 keV), sodium (at 1 keV), oxygen (at 0.5 keV), and carbon (at 0.25 keV) are clearly identified on the Alg-Ep-STO film. These observations confirm the presence and composition of the constituent elements of the nanocomposite film.

### 3.2. Assessment of anticorrosion coating performance PDP and EIS

The behaviour and anticorrosive performance of Alg, Alg-Ep and Alg-Ep-STO coatings for the protection of copper against corrosion in a medium containing 3.5 wt% NaCl were studied using the PDP and EIS methods. Tafel potentiodynamic polarisation curves for the dissociation

of bare copper, Alg-coated copper, Alg-Ep-coated copper and Alg-Ep-STO-coated copper are shown in Fig. 8. The results obtained show a reduction in the corrosion current density for the three coatings Alg, Alg-Ep and Alg-Ep-STO, highlighting the anticorrosive effectiveness of this type of coating for copper in a 3.5 % NaCl solution. Comparison of the Tafel curves shows that the Alg, Alg-Ep and Alg-Ep-STO coatings modify the shape of the anodic and cathodic polarisation curves, reflecting the adverse effect of these three coatings on the anodic and cathodic reactions. The Tafel polarisation parameters obtained by the extrapolation methods are presented in Table 1. These parameters show a shift in corrosion potential ( $E_{\text{corr}}$ ) values in the positive direction for all coatings, particularly for the Alg-Ep-STO coating, implying that all three coatings are mixed-type corrosion inhibitors with a predominance of anodic. The corrosion protection performance demonstrated by the Tafel polarisation parameters shows the superiority of the Alg-Ep-STO coating over the Alg and Alg-Ep coatings, which could be due to the occupation of the pores present in the Alg-Ep matrix by the STO nanoparticles, preventing the penetration of aggressive species such as water molecules, chloride ions and sodium ions.

In Fig. 9, Nyquist plots are shown, illustrating the protective effect of Alginate coating (Alg), alginate-epichlorohydrin coating (Alg-Ep), and alginate-epichlorohydrin- $\text{SrTiO}_3$  nanocomposite coating (Alg-Ep-STO) on copper immersed for 30 min in a medium containing 3.5 % NaCl. It's worth noting that the loops obtained in the Nyquist representation do not exhibit a perfect semi-circular shape. To better interpret information regarding the barrier properties of the coating and the corrosion of the metal surface, modeling using equivalent electrical circuits of the EIS spectra is necessary, as shown in Fig. 10. Indeed, the increase in the diameter of the half-circle in the Nyquist diagrams is generally correlated with an improvement in the corrosion resistance of the protective film. This in-depth analysis of the EIS spectra will allow for a better evaluation of the effectiveness of the coatings and the identification of the one that offers the best corrosion protection, depending on the specific applications envisioned [24,61].

The impedance diagrams obtained are fitted using the equivalent circuit presented in Fig. 10. The values of EIS and the resulting efficiency for each protective coating (Alg, Alg-Ep and Alg-Ep-STO) are listed in the Table 2.

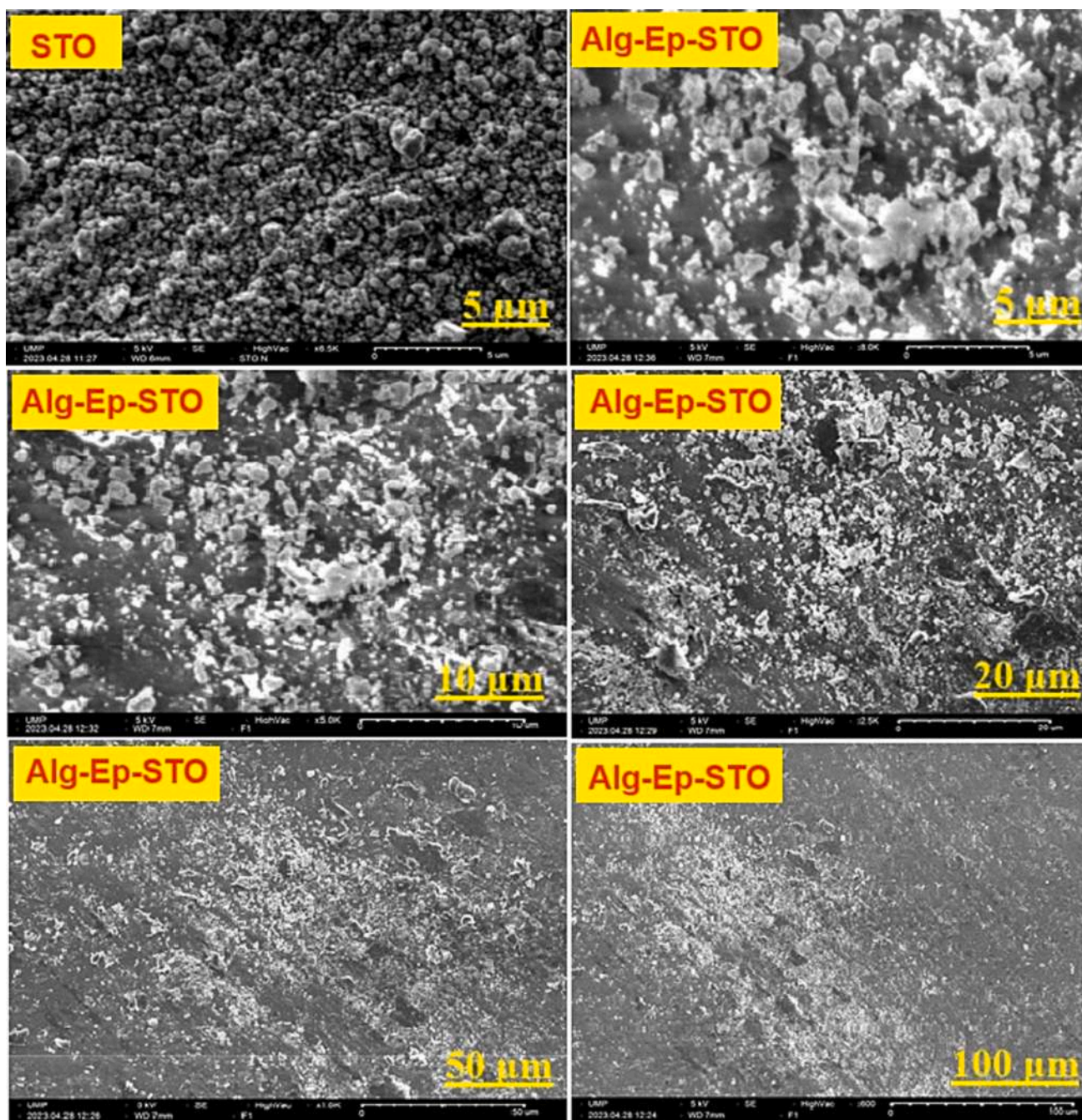


Fig. 6. SEM images of STO nanopowder and Alg-Ep-STO film at different magnifications.

It should be noted that the incorporation of STO nanoparticles into the alginate matrix provides a high level of protective efficacy compared with the Alg-Ep coating. This observation suggests that Alg-Ep-STO, once added to the interface, acts proactively by actively blocking corrosive sites. It thus forms a thin protective layer on the copper surface, resulting in a significant improvement in the coating's barrier properties. This enhanced performance confirms the promising potential of Alg-Ep-STO as an effective anticorrosion coating in corrosive environments containing NaCl.

The durability of the protective effectiveness of the Alg-Ep-STO coating against copper corrosion in a solution containing 3.5 % NaCl was studied by PDP and EIS after immersion for 24 h, 48 h and 72 h. Fig. 11 shows the copper potentiodynamic polarisation (Tafel) curves, with and without the Alg-Ep-STO coating, after immersion for 24, 48 and 72 h in a 3.5 % NaCl solution. During immersion, the Tafel curves

show little change, indicating that the protection mechanisms of this coating are not influenced by the duration of immersion in the corrosive medium containing 3.5 % NaCl.

The potentiodynamic polarisation parameters of bare copper and copper with Alg-Ep-STO coating after 24, 48 and 72 h of immersion in a 3.5 % NaCl environment, grouped in Table 3, reveal, in the case of copper bare, an insignificant change in corrosion potential ( $E_{\text{corr}}$ ) and an increase in corrosion current ( $i_{\text{corr}}$ ) as the immersion time increases, indicating that the immersion time promotes the corrosion process. On the other hand, in the case of copper coated with Alg-Ep-STO, a slightly perceptible change in the  $E_{\text{corr}}$  in the negative direction and a slight increase in the  $i_{\text{corr}}$  is observed. This observation can be attributed to the weakening of the adhesion force of the Alg-Ep-STO coating to the copper surface with the immersion time.

The Nyquist plots of copper without and with Alg-Ep-STO coating in

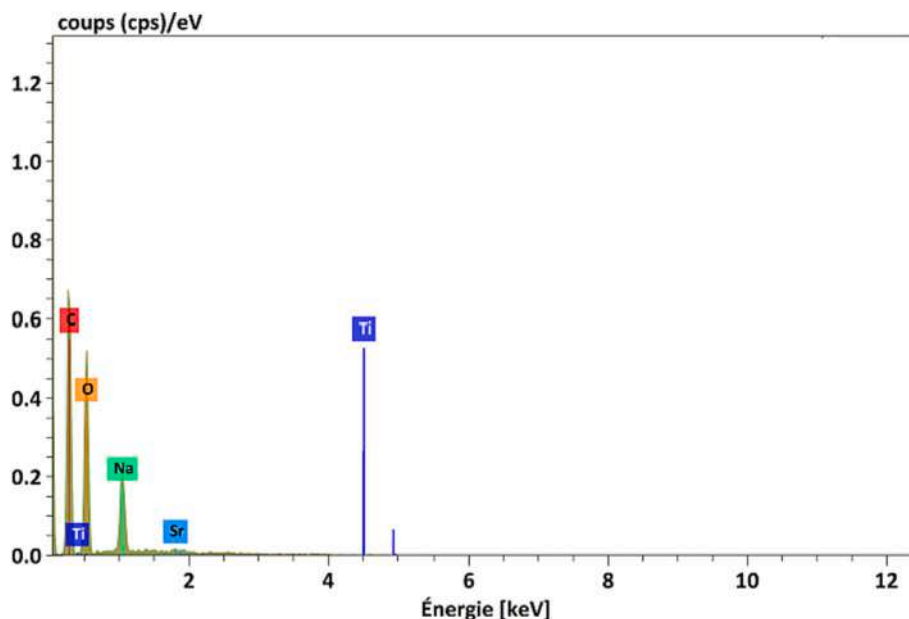


Fig. 7. EDX spectrum of Alg-Ep-STO film.

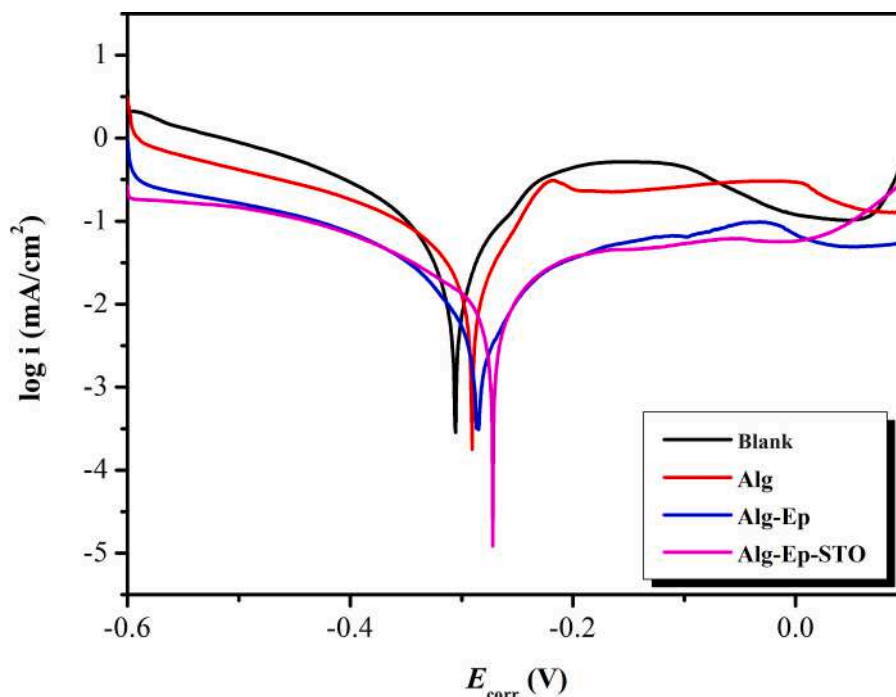


Fig. 8. Tafel PDP curves for bare copper and copper coated with Alg, Alg-Ep and Alg-Ep-STO in a 3.5 % NaCl environment.

**Table 1**  
Potentiodynamic polarisation parameters for copper corrosion in a 3.5 % NaCl solution without and with different coatings.

Comp	$-E_{corr}$ (mV/ECS)	$i_{corr}$ ( $\mu\text{A}/\text{cm}^2$ )	$-\beta_c$ (mV)	$\beta_a$ (mV)
Blank	-290.40	260.04	557.00	-
Alg	-285.59	52.75	254.60	52.30
Alg-Ep	-264.24	19.75	313.90	207.10
Alg-Ep-STO	-226.13	8.63	346.28	42.23

3.5 % NaCl medium of different immersion times (24, 48 and 72 h) are shown in Fig. 12. For bare copper immersed in the NaCl solution, the Nyquist spectra show capacitive loops of the same shape with a decrease in loop diameter with increasing immersion time, indicating attenuation of the charge transfer barrier. In the case of copper coated with Alg-Ep-STO for different immersion times in 3.5 % NaCl solution, the loops show a similar shape with a slight difference in diameter between the loops, suggesting that immersion time does not alter the corrosion protection process of copper in 3.5 % NaCl solution.

The EIS values obtained by adjustment using the equivalent circuit in Fig. 10 are grouped in Table 4. In the case of bare copper, the values of  $R_{ct}$  and  $R_{coat}$  decrease as the immersion time increases, manifesting the

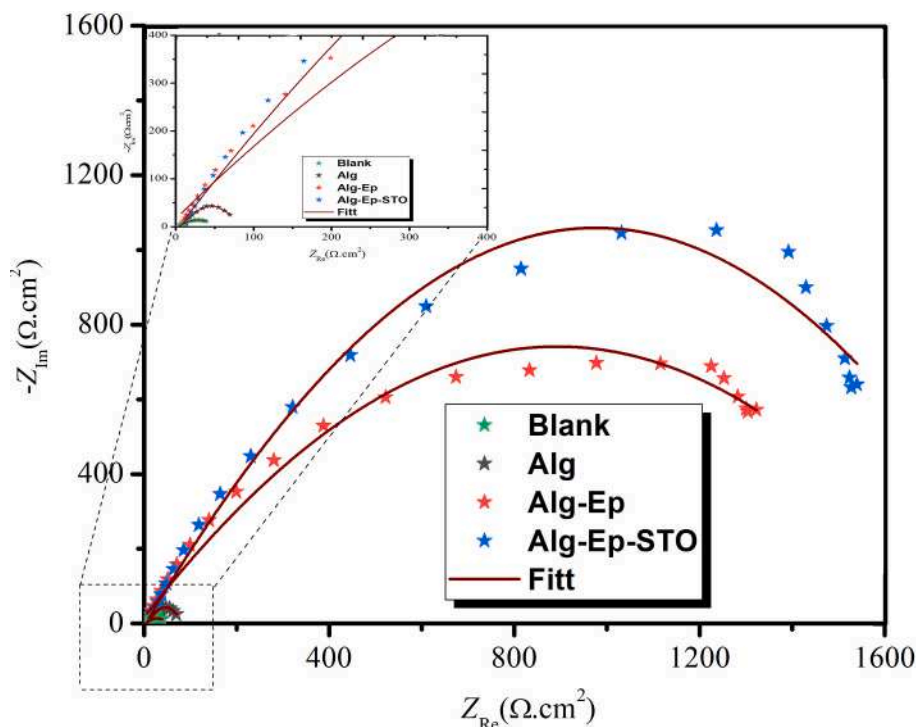


Fig. 9. Nyquist plot for copper coated with Alg, Alg-Ep and Alg-Ep-STO in a 3.5 % NaCl environment.

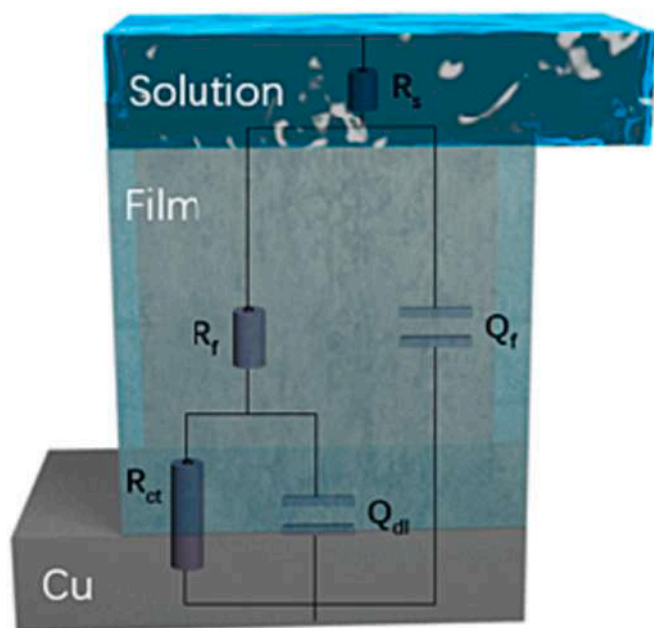


Fig. 10. Proposed equivalent circuit for fitting impedance spectra obtained in the presence of coating on copper in 3.5 % NaCl solution.

Table 2  
Impedance parameters in a 3.5 % NaCl solution for copper coated with Alg, Alg-Ep and Alg-Ep-STO.

Comp.	$R_{ct}$ ( $\Omega.cm^2$ )	$n_1$	$R_{coat}$ ( $\Omega.cm^2$ )	$n_2$	$C_{dl}$ ( $\mu F/cm^2$ )
Blank	59.44	0.13	7.73	0.79	25.27
Alg	100	0.8	10	0.6	17.13
Alg-Ep	1298	0.79	136.7	0.9	14.6
Alg-Ep-STO	1562	0.76	670	0.86	6.7

diffusion of corrosive species and the destruction of surface passivation of copper. An increase in the capacitive characteristic ( $C_{dl}$ ) is also observed with the increase in the immersion time, this increase being due to the adsorption of corrosive species on the copper surface. However, in the case of copper coated with Alg-Ep-STO, a decrease in the  $R_{ct}$  value is observed with the increase in the immersion time due to the weakening of the adhesion force of the Alg-Ep-STO coating on the copper surface. This confirms the results obtained by the PDP. In addition, slight decreases in the  $R_{coat}$  value over time suggest a low penetration of corrosive ions in the coating, as well as an increase in the capacitive characteristic  $C_{dl}$ , interpreted as the adsorption of corrosive species to the surface of the coating.

### 3.3. Surface study

In order to evaluate the protective power of the Alg, Alg-Ep and Alg-Ep-STO coatings against copper corrosion in a solution containing 3.5 % NaCl, a morphological analysis of the copper surface was carried out by taking SEM images of the copper surface after its immersion in a 3.5 % NaCl solution for 72 h, followed by the removal of the various coatings.

SEM images of the surface of bare copper (blank) and copper protected by different coatings (Alg, Alg-Ep and Alg-Ep-STO) after immersion for 72 h in a 3.5 % NaCl solution (Fig. 13), show a clear and visible difference between the surface of bare copper, the surface of copper protected by Alg coating, the surface of copper protected by Alg-Ep coating and the surface of copper protected by Alg-Ep-STO coating. It seems obvious that the bare copper surface is damaged by the appearance of bumps, suggesting the formation of copper oxides and copper salts. The surface of the Alg-protected copper showed pores and the formation of a small number of bumps. On the other hand, the surface of the copper protected by the Alg-Ep coating is less damaged and only has a few pits. However, the surface of the copper protected by the Alg-Ep-STO coating appears to be smooth without any damage. These results confirm the conclusions obtained by electrochemical methods.

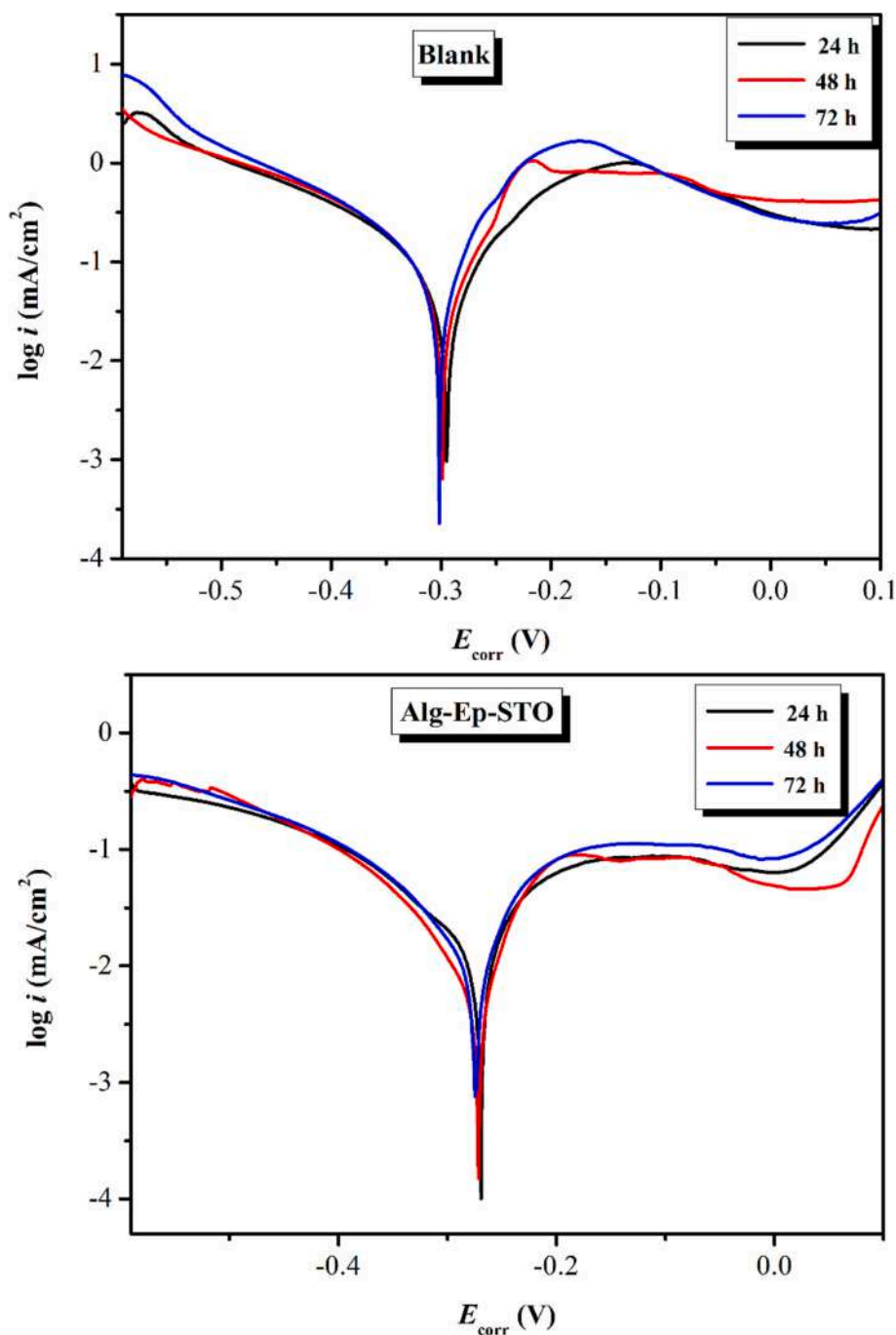


Fig. 11. Tafel PDP curves for copper without and with Alg-Ep-STO coating after 24, 48 and 72 h of immersion in a 3.5 % NaCl environment.

Table 3

Potentiodynamic polarisation parameters for copper without and with Alg-Ep-STO coating after 24, 48 and 72 h of immersion in a 3.5 % NaCl environment.

Comp	Immersion time (hours)	$-E_{corr}$ (mV/ECS)	$i_{corr}$ ( $\mu\text{A}/\text{cm}^2$ )	$-\beta_c$ (mV)	$\beta_a$ (mV)
Blank	24	-292.12	232.32	548.1	35.4
	48	-298.96	246.49	279.5	281
	72	-301.64	281.12	230.7	220.1
Alg-Ep-STO	24	-213.56	10.99	367.12	78.89
	48	-271.64	33.68	238.8	348.7
	72	-274.20	61.18	484.3	736.2

### 3.4. Theoretical analysis

#### 3.4.1. DFT results

DFT is one of the most frequently used computational techniques to study metal-coating interactions in terms of several theoretical indices such as molecular frontier orbital energies ( $E_{LUMO}$  and  $E_{HOMO}$ ), energetic band gap ( $\Delta E_{gap}$ ), electronegativity ( $\chi$ ), hardness ( $\eta$ ), softness ( $\sigma$ ), electron transfer fraction ( $\Delta N$ ), ionization potential (I) and electronic affinity (A) [62,63]. The numerous DFT parameters derived for Alg-Ep are presented in Table 5.

Chemical reactivity descriptors are important clues in the DFT study for interpreting the anticorrosive performance of organic molecules during the coating process. Molecular frontier orbitals (FMOs) play a fundamental role in chemistry, helping to assess the chemical reactivity

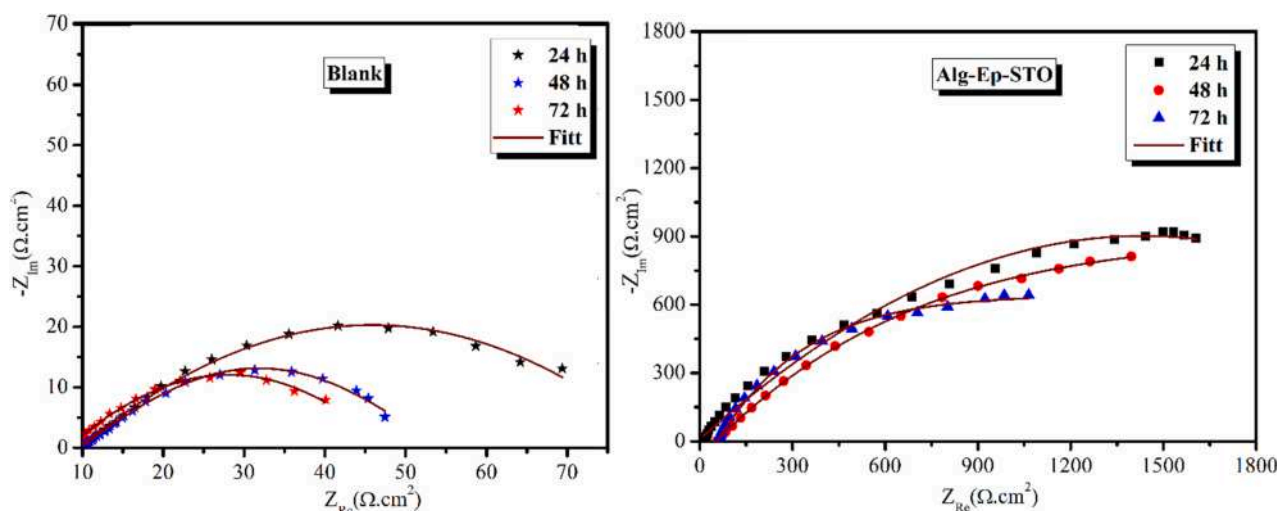


Fig. 12. Nyquist plots for copper without and with Alg-Ep-STO coating after 24, 48 and 72 h of immersion in a 3.5 % NaCl environment.

Table 4

Impedance parameters for copper without and with Alg-Ep-STO coating after 24, 48 and 72 h of immersion in a 3.5 % NaCl environment.

Comp	Immersion time (hours)	$R_{ct}$ ( $\Omega \cdot \text{cm}^2$ )	$n_1$	$R_{coat}$ ( $\Omega \cdot \text{cm}^2$ )	$n_2$	$C_{dl}$ ( $\mu\text{F}/\text{cm}^2$ )
Blank	24	49.43	0.61	6.12	0.97	65.33
	48	42.95	0.58	5.14	0.86	81.09
	72	40.26	0.45	4.4	0.67	104.7
Alg-Ep-STO	24	2062	0.88	10.57	0.71	8.39
	48	1687	0.67	10.21	0.50	9.67
	72	773.80	0.79	6.51	0.98	11.2

of molecules responsible for adsorption on the copper surface. In this work, we carried out an optimization of the Alg-Ep compound geometry, to determine the values of the  $E_{\text{HOMO}}$  and  $E_{\text{LUMO}}$  boundary orbital energies, the ESP and the Gap. A high  $E_{\text{HOMO}}$  value indicates the compound's capacity to donate electrons to the unoccupied d orbital of the copper metal surface, while a lower  $E_{\text{LUMO}}$  value signifies its ability to accept electrons from the metal surface [57,64].

Fig. 14 displays 3D plots of the optimized structure, HOMO, LUMO, and ESP representations for the Alg-Ep molecule under examination.

Upon examining the results, it becomes evident that the HOMO primarily resides over one of the alginate moieties, signifying that this segment of the Alg-Ep molecule possesses a high electron density and is prone to acting as an electron donor in interactions with metals. Conversely, the LUMO is predominantly localized on the alcolate and -C-O- groups of the Alg-Ep molecule, suggesting that this portion is more inclined to act as an electron acceptor in metal-(Alg-Ep) interactions. It is a well-established fact that organic coatings engage with metallic surfaces through donor-acceptor interactions. Elevated  $E_{\text{HOMO}}$  values coupled with diminished  $E_{\text{LUMO}}$  values are indicative of robust interactions between the metal and the coating. In the current scenario, Alg-Ep exhibits relatively high  $E_{\text{HOMO}}$  and low  $E_{\text{LUMO}}$  values, underscoring its potent capacity to react with and adsorb onto metallic surfaces. Likewise, a reduced  $\Delta E$  value corresponds to heightened reactivity and enhanced coating effectiveness. The smaller  $\Delta E$  value observed for Alg-Ep points to its heightened reactivity and its role as a potent adsorbent on metallic surfaces. Reduced electronegativity and hardness values further suggest that Alg-Ep is a highly reactive molecule, capable of both electron donation and acceptance in its interactions with metal-Alg-Ep systems.

Moreover, the negative value of  $\Delta E_{\text{back-donation}}$  indicates that electron charge transfer to the molecule and subsequent back-donation of electrons from the molecule are energetically favorable processes. In order

to pinpoint locations suitable for electrophilic and nucleophilic reactions, we employed ESP mapping technique, as illustrated in Fig. 14, to delineate electron density regions on the optimized Alg-Ep geometry. The ESP map shows that electrophilic zones are represented by the red and yellow colors, while the light blue and blue colors indicate active nucleophilic ranges. The Alg-Ep compound exhibits electron-rich regions around heteroatoms (oxygen) and double bonds, which serve as the active sites for nucleophilic reactions during the anticorrosive coating process.

#### 3.4.2. MC and MD simulations

MC and MD simulations are frequently employed for exploring and gaining insight into the interactions between the Alg-Ep-STO coating and the Cu(111) surface within a NaCl medium. The adsorption equilibrium configurations of the Alg-Ep-STO coating on the metal surface are illustrated in Fig. 15. It can be observed that the Alg-Ep-STO coating is adsorbed on the Cu(111) surface in a position that is nearly parallel to the rigid structure of the coating concerning the metal surface, as shown in Fig. 15. It is important to note that Alg-Ep-STO demonstrates effective adsorption when interacting with heteroatoms. Furthermore, the adsorption capability of Alg-Ep-STO is enhanced, particularly with the inclusion of oxygen (O) heteroatoms especially alcolate, -C-O-, hydroxyl groups and SrTiO<sub>3</sub>. This observation validates that Alg-Ep-STO is inclined to adhere to the metal surface, creating a compact and hydrophobic barrier that significantly hinders the penetration of chloride ions. The nearest O atom (of the alginate chain to surface is 3.74 Angstrom). This discovery aligns well with the outcomes obtained from DFT investigations. To quantitatively assess the energy associated with the adsorption of the Alg-Ep-STO composite on the Cu (111) surface, calculations were performed using the following relationship [65]:

$$E_{\text{ads}} = E_{\text{total}} - (E_{\text{surf+solu}} + E_{\text{coat+solu}}) + E_{\text{sol}}$$

In general, a more negative  $E_{\text{ads}}$  value indicates a stronger adsorption affinity between a matrix and a metal surface. The computed  $E_{\text{ads}}$  value for the adsorption of Alg-Ep-STO on the metallic surface is  $-380.28$  kcal/mol, as depicted in Fig. 16. The negative value of  $E_{\text{ads}}$  suggests spontaneous nature of Alg-Ep-STO composite adsorption on Cu (111) surface. This outcome demonstrates that the examined matrix serves as an effective anti-corrosive material, and the inclusion of SrTiO<sub>3</sub> in the Alg-Ep composite significantly contributes to its successful adsorption.



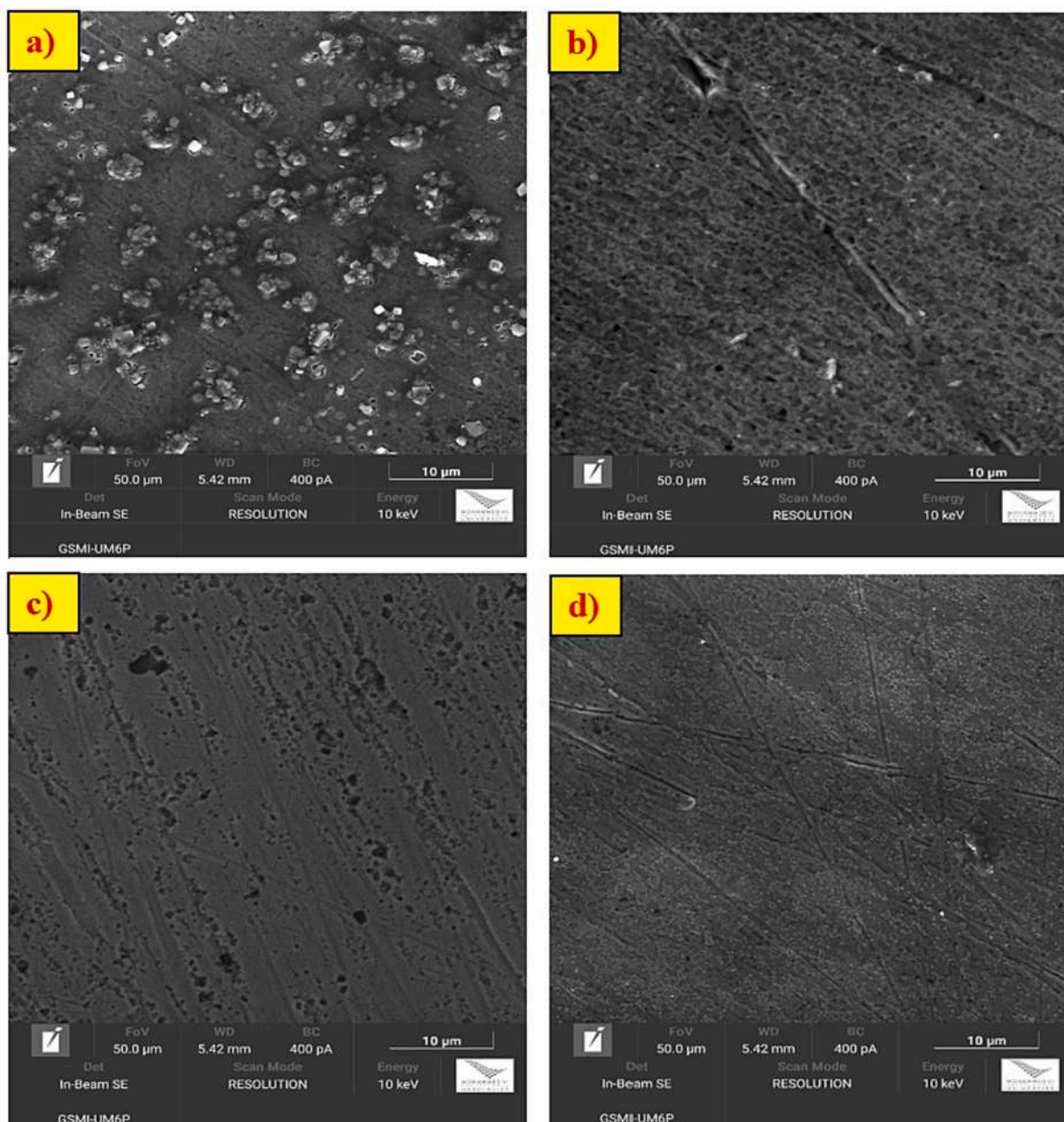


Fig. 13. SEM images of the copper surface after immersion for 72 h in the 3.5 % NaCl solution, a) Bare copper, b) Copper protected by Alg, c) Copper protected by Alg-Ep and d) Copper protected by Alg-Ep-STO.

Table 5

Calculated theoretical parameters of Alg-Ep structure.

Descriptor	Alg-Ep
HOMO	-5.591
LUMO	-1.916
$\Delta E_{(HOMO-LUMO)}$	3.675
I	5.591
A	1.916
$\chi$	3.753
$\eta$	1.837
$\sigma$	0.544
$\Delta N$	0.290
$\Delta E$ back-donation	-0.460

### 3.5. Comparison study

Table 6 summarizes the main results of the EIS study for anticorrosive coatings applied to different substrates and exposed to various environments. The data were collected after a one-day immersion. The Alg-Ep-STO coating, based on alginate, provides highly effective anticorrosion protection in environments containing NaCl, even after extended immersion, surpassing other tested coatings. The biocompatible nature, ease of application, and adhesion of the Alg-Ep-STO coating to metallic substrates create a robust barrier that ensures prolonged durability against corrosive conditions. This combination makes it a promising choice, both practical and environmentally friendly, compared to other works found in the literature.

### 4. Conclusion

The utilization of alginate and its derivatives as anticorrosive

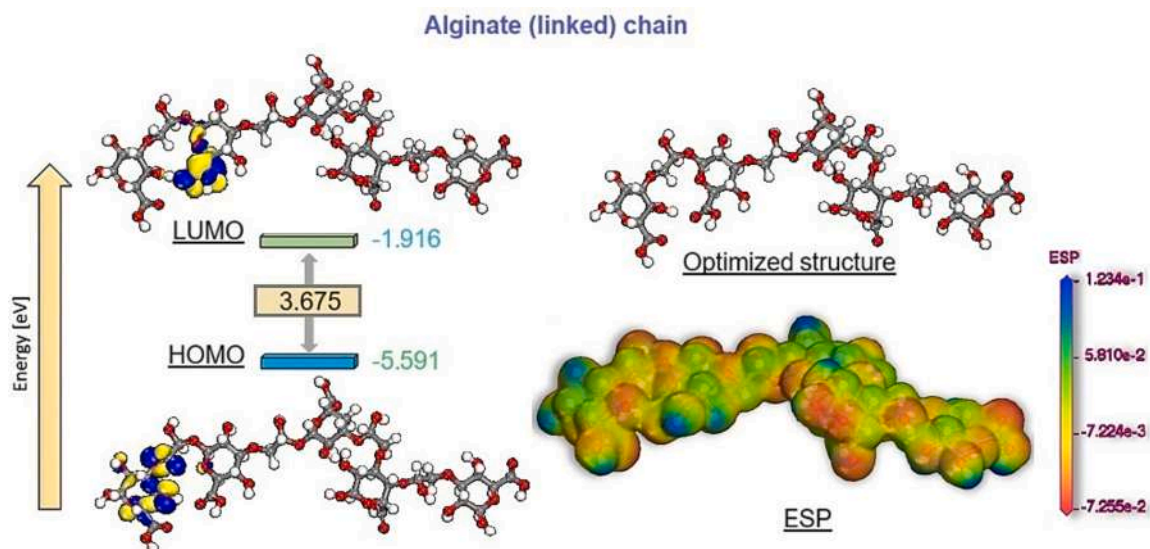


Fig. 14. Optimized structures, FMO and ESP surfaces of the Alg-Ep structure.

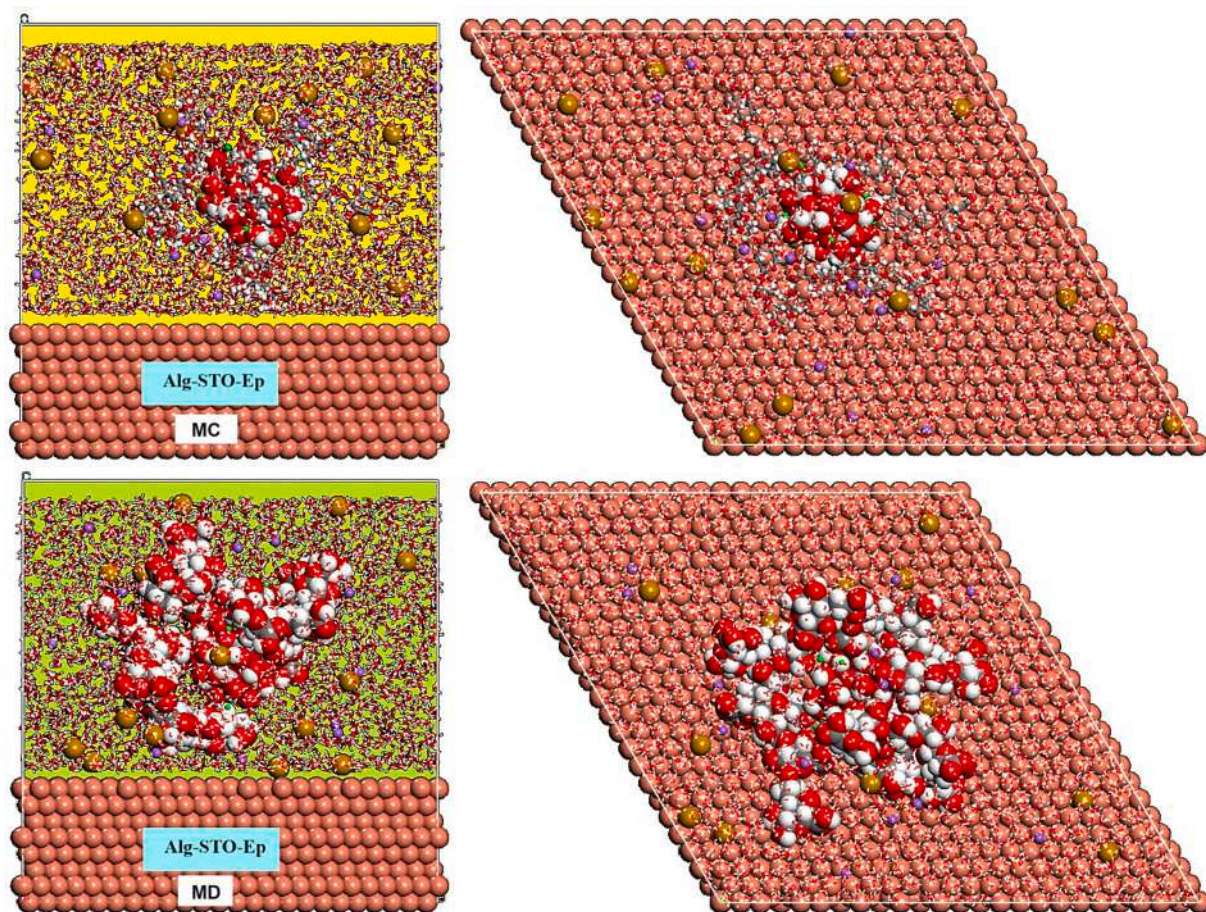


Fig. 15. Top and side perspectives of the most stable, low-energy configurations for the adsorption onto Cu (111)/Alg-STO-Ep + 3000H<sub>2</sub>O + 15Na<sup>+</sup> and 15Cl<sup>-</sup> ions system obtained using MC and MD simulations.

coatings in solution, mainly due to the presence of hydroxyl and carboxylic acid groups which confer certain anti-corrosion properties. However, it is recognized that these properties are often insufficient to ensure effective and long-lasting protection of metals against corrosion, mainly due to the physicochemical characteristics of alginate. In this study, the modification of alginate by epichlorohydrin, as well as the

incorporation of 10 % SrTiO<sub>3</sub> nanoparticles into the alginate matrix, were explored to enhance the anticorrosive properties of alginate. This approach has shown promise in protecting metal surfaces against corrosion, thanks to the unique crystalline structure of the nanoparticles and their successful integration into the alginate matrix. XRD analysis confirmed the effective encapsulation of STO nanoparticles in the

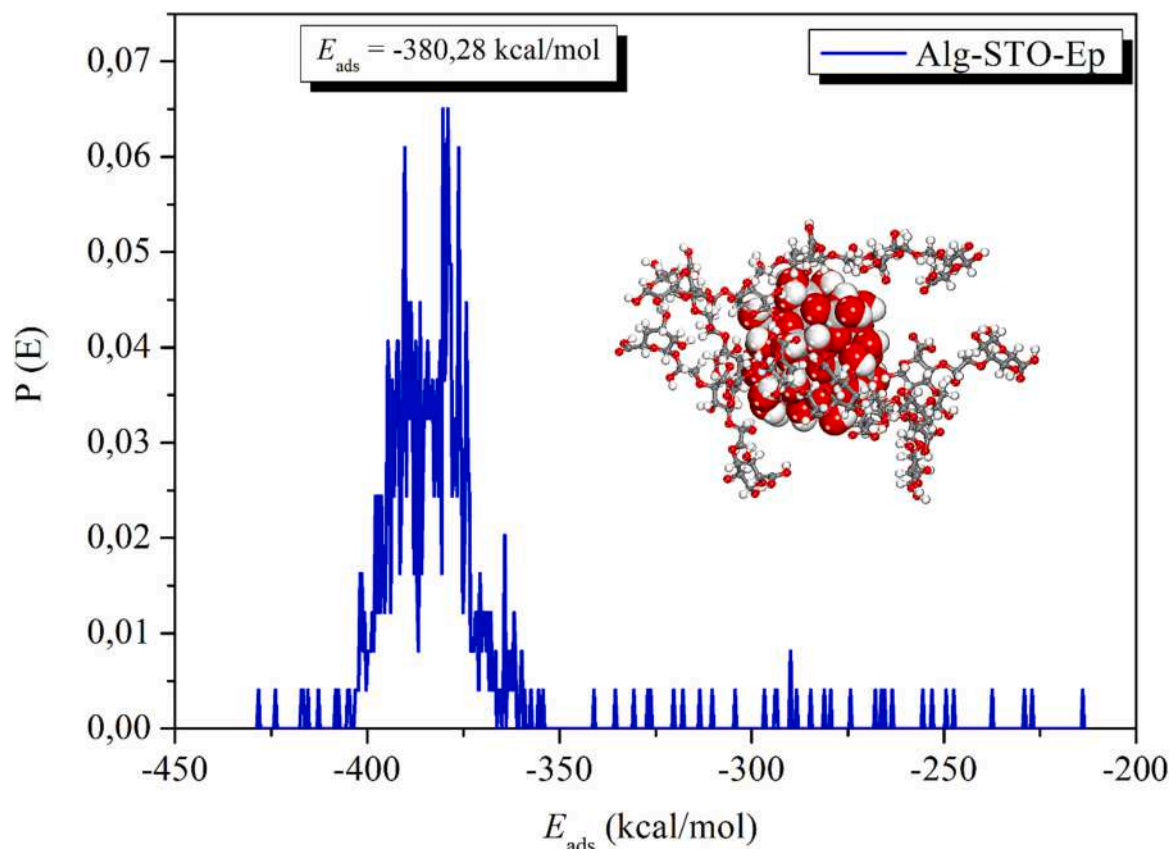


Fig. 16. Distribution of the  $E_{ads}$  of Alg-STO-Ep on the Cu (111) surface.

Table 6

Comparative table between the efficiencies of different coatings of several metal substrates after immersion for 1 day in an environment containing NaCl.

Coating	Substrate	Medium	Polarisation resistance $R_p$ ( $k\Omega.cm^2$ )		Efficiency (%)	Ref.
			Blank	Coating		
PNEA-10Si	Copper	3.5 % NaCl	39.990	321.120	87.54	[66]
PNMA-5P	Copper	3.5 % NaCl	0.599	21.611	97.22	[67]
PSC2	Steel	4 % NaCl	4.886	5.739	14.86	[68]
Pc	Steel	3.5 % NaCl	110	590	81.35	[69]
Zn-GO <sub>3</sub>	Zinc	3.5 % NaCl	0.139	0.334	58.38	[70]
Nano ZnO-phosphate	Zinc	3.5 % NaCl	0.269	6.085	91.11	[71]
Alg-Ep-STO	Copper	3.5 % NaCl	0.055	2.072	97.32	In this study

alginate matrix, imparting a crystalline structure to the film. The protective efficiency of copper plates in a 3.5 % NaCl solution was evaluated using the dip-coating method and analyzed through EIS. The results demonstrated that the Alg-Ep-STO coating exhibited significantly higher protection efficiency compared to the Alg-Ep coating. In summary, this study opens interesting prospects for the development of more effective anticorrosion coatings by combining the intrinsic properties of alginate with the advantages offered by SrTiO<sub>3</sub> nanoparticles, thereby providing enhanced protection against corrosion of metal surfaces. These advancements have the potential to find applications in various sectors where corrosion protection is crucial. The computational findings suggest that the Alg-Ep-STO coating exhibits robust and planar adsorption onto the alcolate, -C-O-, hydroxyl groups, and SrTiO<sub>3</sub>. Moreover, the results indicate a strong adhesion of Alg-Ep-STO to the Cu (111) surface, with an adsorption energy of  $-380.28$  kcal/mol.

#### CRedit authorship contribution statement

Mohamed El mahamdi and Walid Daoudi: Conceptualization,

Data curation, Investigation. **Omar Dagdag**: Investigation, Methodology, Writing – original draft. **Hansang Kim**: Supervision, Validation. **Firdaouss Eddaoudy**: Writing – review & editing. **Dakeshwar Kumar Verma**: Supervision, Validation. **Sangeeta Gupta**: Writing – review & editing. **Avni Berisha**: Software. **Mohamed Loutou and Benchat Noureddine**: Writing – review & editing. **Abdelmalik El Aatiaoui**: Visualization.

#### Declaration of competing interest

The authors declare that there is no conflict of interest.

#### Data availability

Data will be made available on request.

#### Acknowledgements

This research is a research project supported by the “Renewable

Energy Core Technology Development Project” of the Ministry of Trade, Industry and Energy (MOTIE) and the Korea Institute of Energy Technology Evaluation and Planning (KETEP). (NO. 2022303004020A). In addition, this work was also supported by the “Automotive Industry Technology Development Project” of the Ministry of Trade, Industry and Energy (MOTIE) and the Korea Institute of Industrial Technology (KEIT). (NO. 20015346). The authors also would like to express their sincere gratitude to the members of the Department of Chemistry of Oujda, and to Mr. Abdelmonaem TALHAOUI for their assistance in conducting some of the experimental studies.

## References

- [1] L.K. Kimbell, Y. Wang, P.J. McNamara, The impact of metal pipe materials, corrosion products, and corrosion inhibitors on antibiotic resistance in drinking water distribution systems, *Appl. Microbiol. Biotechnol.* 104 (2020) 7673–7688, <https://doi.org/10.1007/s00253-020-10777-8>.
- [2] R.F. Wright, P. Lu, J. Devkota, F. Lu, M. Ziomek-Moroz, P.R. Ohodnicki, Corrosion sensors for structural health monitoring of oil and natural gas infrastructure: a review, *Sensors* 19 (2019) 3964, <https://doi.org/10.3390/s19183964>.
- [3] T. Kirchgorg, I. Weinberg, M. Hörnig, R. Baier, M.J. Schmid, B. Brockmeyer, Emissions from corrosion protection systems of offshore wind farms: evaluation of the potential impact on the marine environment, *Mar. Pollut. Bull.* 136 (2018) 257–268, <https://doi.org/10.1016/j.marpolbul.2018.08.058>.
- [4] B. Lu, W.J. Meng, F. Mei, Experimental investigation of Cu-based, double-layered, microchannel heat exchangers, *J. Micromechanics Microengineering*. 23 (2013), 035017, <https://doi.org/10.1088/0960-1317/23/3/035017>.
- [5] A. Armanious, K. Johannsen, Alternative methods for copper corrosion studies in household plumbing systems, *Mater. Corros.* 63 (2012) 438–444, <https://doi.org/10.1002/maco.201005796>.
- [6] S. Chupradit, A.T. Jalil, Y. Enina, D.A. Neganov, M.S. Alhassan, S. Aravindhan, A. Davarpanah, Use of organic and copper-based nanoparticles on the Turbulator installment in a Shell tube heat exchanger: a CFD-based simulation approach by using Nanofluids, *J. Nanomater.* 2021 (2021) 1–7, <https://doi.org/10.1155/2021/3250058>.
- [7] Z. Li, S. Khuje, A. Chivate, Y. Huang, Y. Hu, L. An, Z. Shao, J. Wang, S. Chang, S. Ren, Printable copper sensor electronics for high temperature, *ACS Appl. Electron. Mater.* 2 (2020) 1867–1873, <https://doi.org/10.1021/acsaem.0c00358>.
- [8] L. Yan, B. Zhang, J. Zhu, Y. Li, P. Tsiakaras, P. Kang Shen, Electronic modulation of cobalt phosphide nanosheet arrays via copper doping for highly efficient neutral-pH overall water splitting, *Appl. Catal. Environ.* 265 (2020), 118555, <https://doi.org/10.1016/j.apcatb.2019.118555>.
- [9] Q. Zhou, W. Zhang, M. Qiu, Y. Yu, Role of oxygen in copper-based catalysts for carbon dioxide electrochemical reduction, *Mater. Today Phys.* 20 (2021), 100443, <https://doi.org/10.1016/j.mtphys.2021.100443>.
- [10] A. Fateh, M. Aliofkhaazraei, A.R. Rezvanian, Review of corrosive environments for copper and its corrosion inhibitors, *Arab. J. Chem.* 13 (2020) 481–544, <https://doi.org/10.1016/j.arabjc.2017.05.021>.
- [11] T. Wu, Z. Zhou, S. Xu, Y. Xie, L. Huang, F. Yin, A corrosion failure analysis of copper wires used in outdoor terminal boxes in substation, *Eng. Fail. Anal.* 98 (2019) 83–94, <https://doi.org/10.1016/j.engfailanal.2019.01.070>.
- [12] M.N. El-Haddad, Chitosan as a green inhibitor for copper corrosion in acidic medium, *Int. J. Biol. Macromol.* 55 (2013) 142–149, <https://doi.org/10.1016/j.ijbiomac.2012.12.044>.
- [13] K.W. Shinato, A.A. Zewde, Y. Jin, Corrosion protection of copper and copper alloys in different corrosive medium using environmentally friendly corrosion inhibitors, *Corrosion Rev.* 38 (2020) 101–109, <https://doi.org/10.1515/corrrev-2019-0105>.
- [14] A.M. Abdel-karim, H.M. Hussien, S. Shahen, O.A.A. El-Shamy, I.M. Ghayad, N. M. Saleh, N.E.A.A. El-Sattar, Green synthesis of novel bis structure of (Carbamothioyl) oxalamide derivatives as corrosion inhibitors for copper in 3.5% NaCl; experimental and theoretical investigation, *J. Mol. Struct.* 1295 (2024), 136597, <https://doi.org/10.1016/j.molstruc.2023.136597>.
- [15] A.H. Noorbakhsh Nezhad, A. Davoodi, E. Mohammadi Zahrani, R. Arefinia, The effects of an inorganic corrosion inhibitor on the electrochemical behavior of superhydrophobic micro-nano structured Ni films in 3.5% NaCl solution, *Surf. Coat. Technol.* 395 (2020), 125946, <https://doi.org/10.1016/j.surfcoat.2020.125946>.
- [16] L. Tan, Y. Sun, J. Li, S. Han, X. Zhou, Y. Tang, X. Zeng, Interfacial adsorption and corrosion inhibition behavior of environmentally friendly imidazole derivatives for copper in the marine environment, *Langmuir* 39 (2023) 2579–2588, <https://doi.org/10.1021/acs.langmuir.2c02843>.
- [17] J. Shen, D. Yang, L. Ma, Z. Gao, A. Yan, Q. Liao, Exploration of neonicotinoids as novel corrosion inhibitors for copper in a NaCl solution: experimental and theoretical studies, *Colloids Surf. A Physicochem. Eng. Asp.* 636 (2022), 128058, <https://doi.org/10.1016/j.colsurfa.2021.128058>.
- [18] Z. Liu, B. Fan, J. Zhao, B. Yang, X. Zheng, Benzothiazole derivatives-based supramolecular assemblies as efficient corrosion inhibitors for copper in artificial seawater: formation, interfacial release and protective mechanisms, *Corros. Sci.* 212 (2023), 110957, <https://doi.org/10.1016/j.corsci.2022.110957>.
- [19] A.A. Farag, Applications of nanomaterials in corrosion protection coatings and inhibitors, *Corrosion Rev.* 38 (2020) 67–86, <https://doi.org/10.1515/corrrev-2019-0011>.
- [20] S. Akula, P. Kalaiselvi, A.K. Sahu, S. Chellammal, Electrodeposition of conductive PAMT/PPY bilayer composite coatings on 316L stainless steel plate for PEMFC application, *Int. J. Hydrogen Energy* 46 (2021) 17909–17921, <https://doi.org/10.1016/j.ijhydene.2021.02.196>.
- [21] F. Zhong, Y. He, P. Wang, C. Chen, Y. Wu, Novel pH-responsive self-healing anti-corrosion coating with high barrier and corrosion inhibitor loading based on reduced graphene oxide loaded zeolite imidazole framework, *Colloids Surf. A Physicochem. Eng. Asp.* 642 (2022), 128641, <https://doi.org/10.1016/j.colsurfa.2022.128641>.
- [22] F. Masmoudi, I. Jedidi, Y.B. Amor, M. Masmoudi, Corrosion protection evaluation of copper coated with a block copolymer and block copolymer/carbon black nanoparticles in 3 wt% NaCl solution, *ChemistrySelect* 8 (2023), e202202608, <https://doi.org/10.1002/slct.202202608>.
- [23] L. Bo, X. Liu, D. Wang, Electrophoretic deposition of graphene coating as a corrosion inhibitor for copper in NaCl solution, *Results Surf. Interfaces.* 8 (2022), 100077, <https://doi.org/10.1016/j.rsufri.2022.100077>.
- [24] V. Kumar, N. Kumar Arya, A.V. Ullas, G. Ji, Coating of epoxy resin and MMT clay nano-composite on copper and examination of their corrosion behaviours in NaCl, *Mater. Today Proc.* (2023), <https://doi.org/10.1016/j.matpr.2023.02.172>.
- [25] L. Huang, W.-Q. Chen, S.-S. Wang, Q. Zhao, H.-J. Li, Y.-C. Wu, Starch, cellulose and plant extracts as green inhibitors of metal corrosion: a review, *Environ. Chem. Lett.* 20 (2022) 3235–3264, <https://doi.org/10.1007/s10311-022-01400-5>.
- [26] A. Farhadian, S. Assar Kashani, A. Rahimi, E.E. Oguzie, A.A. Javidparvar, S. C. Nwanonyeni, S. Yousefzadeh, M.R. Nabid, Modified hydroxyethyl cellulose as a highly efficient eco-friendly inhibitor for suppression of mild steel corrosion in a 15% HCl solution at elevated temperatures, *J. Mol. Liq.* 338 (2021), 116607, <https://doi.org/10.1016/j.molliq.2021.116607>.
- [27] M.S. Hasanin, S.A. Al Kiey, Environmentally benign corrosion inhibitors based on cellulose niacin nano-composite for corrosion of copper in sodium chloride solutions, *Int. J. Biol. Macromol.* 161 (2020) 345–354, <https://doi.org/10.1016/j.ijbiomac.2020.06.040>.
- [28] S.A. Al Kiey, M.S. Hasanin, S. Dacrorry, Potential anticorrosive performance of green and sustainable inhibitor based on cellulose derivatives for carbon steel, *J. Mol. Liq.* 338 (2021), 116604, <https://doi.org/10.1016/j.molliq.2021.116604>.
- [29] X. Li, S. Deng, T. Lin, X. Xie, G. Du, Cassava starch ternary graft copolymer as a corrosion inhibitor for steel in HCl solution, *J. Mater. Res. Technol.* 9 (2020) 2196–2207, <https://doi.org/10.1016/j.jmrt.2019.12.050>.
- [30] S. Deng, X. Li, G. Du, An efficient corrosion inhibitor of cassava starch graft copolymer for aluminum in phosphoric acid, *Chin. J. Chem. Eng.* 37 (2021) 222–231, <https://doi.org/10.1016/j.cjche.2020.08.013>.
- [31] I. Nadi, Z. Belatmania, B. Sabour, A. Reani, A. Sahibed-dine, C. Jama, F. Bentiss, Sargassum muticum extract based on alginate biopolymer as a new efficient biological corrosion inhibitor for carbon steel in hydrochloric acid pickling environment: gravimetric, electrochemical and surface studies, *Int. J. Biol. Macromol.* 141 (2019) 137–149, <https://doi.org/10.1016/j.ijbiomac.2019.08.253>.
- [32] P. Kesari, G. Udayabhanu, A. Roy, S. Pal, Biopolymer sodium alginate based titania and magnetite nanocomposites as natural corrosion inhibitors for mild steel in acidic medium, *J. Ind. Eng. Chem.* 122 (2023) 303–325, <https://doi.org/10.1016/j.jiec.2023.02.031>.
- [33] W. Zhang, B. Nie, H.-J. Li, Q. Li, C. Li, Y.-C. Wu, Inhibition of mild steel corrosion in 1 M HCl by chondroitin sulfate and its synergistic effect with sodium alginate, *Carbohydr. Polym.* 260 (2021), 117842, <https://doi.org/10.1016/j.carbpol.2021.117842>.
- [34] C. Verma, M.A. Quraishi, A. Alfantazi, K.Y. Rhee, Corrosion inhibition potential of chitosan based Schiff bases: design, performance and applications, *Int. J. Biol. Macromol.* 184 (2021) 135–143, <https://doi.org/10.1016/j.ijbiomac.2021.06.049>.
- [35] M. Rbaa, M. Ouakki, M. Galai, A. Berisha, B. Lakhri, C. Jama, I. Warad, A. Zarrouk, Simple preparation and characterization of novel 8-Hydroxyquinoline derivatives as effective acid corrosion inhibitor for mild steel: experimental and theoretical studies, *Colloids Surf. A Physicochem. Eng. Asp.* 602 (2020), 125094, <https://doi.org/10.1016/j.colsurfa.2020.125094>.
- [36] K.R. Ansari, D.S. Chauhan, M.A. Quraishi, M.A.J. Mazumder, A. Singh, Chitosan Schiff base: an environmentally benign biological macromolecule as a new corrosion inhibitor for oil & gas industries, *Int. J. Biol. Macromol.* 144 (2020) 305–315, <https://doi.org/10.1016/j.ijbiomac.2019.12.106>.
- [37] Q. Zhao, J. Guo, G. Cui, T. Han, Y. Wu, Chitosan derivatives as green corrosion inhibitors for P110 steel in a carbon dioxide environment, *Colloids Surf. B Biointerfaces* 194 (2020), 111150, <https://doi.org/10.1016/j.colsurfb.2020.111150>.
- [38] M. Fardoui, M. Rbaa, F. Benhiba, M. Galai, T. Guedira, B. Lakhri, I. Warad, A. Zarrouk, Bio-active corrosion inhibitor based on 8-hydroxyquinoline-grafted-alginate: experimental and computational approaches, *J. Mol. Liq.* 323 (2021), 114615, <https://doi.org/10.1016/j.molliq.2020.114615>.
- [39] Y. Wang, X. Ren, X. Ma, W. Su, Y. Zhang, X. Sun, X. Li, Alginate-intervened hydrothermal synthesis of hydroxyapatite nanocrystals with Nanopores, *Cryst. Growth Des.* 15 (2015) 1949–1956, <https://doi.org/10.1021/acs.cgd.5b00113>.
- [40] P.N. Dave, P.M. Macwan, B. Kamaliya, Synthesis and rheological investigations of gum-ghatti-cl-poly(NIPAm-co-AA)-graphene oxide based hydrogels, *Mater. Adv.* 4 (2023) 2971–2980, <https://doi.org/10.1039/D3MA00092C>.
- [41] P.N. Dave, P.M. Macwan, B. Kamaliya, Biodegradable gg-cl-poly(NIPAm-co-AA)/-o-MWCNT based hydrogel for combined drug delivery system of metformin and sodium diclofenac: in vitro studies, *RSC Adv.* 13 (2023) 22875–22885, <https://doi.org/10.1039/D3RA04728H>.
- [42] P.N. Dave, P.M. Macwan, B. Kamaliya, Synthesis and characterization of biodegradable gum ghatti-cl-poly(AA-co-NIPAm)/GO based hydrogel for metformin and sodium diclofenac combined drug delivery system, *Colloids Surf. A*

- Physicochem. Eng. Asp. 673 (2023), 131815, <https://doi.org/10.1016/j.colsurfa.2023.131815>.
- [43] B.P. Kamaliya, P.N. Dave, L.V. Chopda, Synthesis of GG-g-P(NIPAM-co-AA)/GO and evaluation of adsorption activity for the diclofenac and metformin, *J. Environ. Health Sci. Eng.* 21 (2023) 403–416, <https://doi.org/10.1007/s40201-023-00867-w>.
- [44] M. Abdollahi, M. Alboofetileh, M. Rezaei, R. Behrooz, Comparing physico-mechanical and thermal properties of alginate nanocomposite films reinforced with organic and/or inorganic nanofillers, *Food Hydrocoll.* 32 (2013) 416–424, <https://doi.org/10.1016/j.foodhyd.2013.02.006>.
- [45] L.V. Trandafilović, D.K. Božanić, S. Dimitrijević-Branković, A.S. Luyt, V. Djoković, Fabrication and antibacterial properties of ZnO–alginate nanocomposites, *Carbohydr. Polym.* 88 (2012) 263–269, <https://doi.org/10.1016/j.carbpol.2011.12.005>.
- [46] M. Alboofetileh, M. Rezaei, H. Hosseini, M. Abdollahi, Effect of montmorillonite clay and biopolymer concentration on the physical and mechanical properties of alginate nanocomposite films, *J. Food Eng.* 117 (2013) 26–33, <https://doi.org/10.1016/j.jfoodeng.2013.01.042>.
- [47] B. Kolathupalayam Shanmugam, S. Rangaraj, K. Subramani, S. Srinivasan, W. K. Aicher, R. Venkatachalam, Biomimetic TiO<sub>2</sub>-chitosan/sodium alginate blended nanocomposite scaffolds for tissue engineering applications, *Mater. Sci. Eng. C* 110 (2020), 110710, <https://doi.org/10.1016/j.msec.2020.110710>.
- [48] S. Zhang, J. Liu, Y. Han, B. Chen, X. Li, Formation mechanisms of SrTiO<sub>3</sub> nanoparticles under hydrothermal conditions, *Mater. Sci. Eng. B* 110 (2004) 11–17, <https://doi.org/10.1016/j.mseb.2004.01.017>.
- [49] P.N. Dave, P.M. Macwan, B. Kamaliya, Preparation and enhancing properties of pH-sensitive hydrogel in light of gum Ghatti-cl-poly(acrylic acid)/-o-MWCNT for sodium diclofenac drug release, *Macromol. Chem. Phys.* 224 (2023), <https://doi.org/10.1002/macp.202300038>, 2300038.
- [50] C. Coquery, *Fonctionnalisation du chitosane : vers un nouveau revêtement biosourcé pour la protection des métaux contre la corrosion*, phdthesis, Ecole nationale supérieure de chimie, Montpellier, 2018 <https://theses.hal.science/tel-03623530> (accessed November 19, 2023).
- [51] R.A. Yukna, D.P. Callan, J.T. Krauser, G.H. Evans, M.E. Aichelmann-Reidy, K. Moore, R. Cruz, J.B. Scott, Multi-center clinical evaluation of combination Anorganic bovine-derived hydroxyapatite matrix (ABM)/cell binding peptide (P-15) as a bone replacement graft material in human periodontal osseous defects. 6-month results, *J. Periodontol.* 69 (1998) 655–663, <https://doi.org/10.1902/jop.1998.69.6.655>.
- [52] J. Andzelm, R.D. King-Smith, G. Fitzgerald, Geometry optimization of solids using delocalized internal coordinates, *Chem. Phys. Lett.* 335 (2001) 321–326, [https://doi.org/10.1016/S0009-2614\(01\)00030-6](https://doi.org/10.1016/S0009-2614(01)00030-6).
- [53] A. Berisha, Interactions between the Aryldiazonium cations and graphene oxide: a DFT study, *J. Chem.* 2019 (2019), e5126071, <https://doi.org/10.1155/2019/5126071>.
- [54] R. Peverati, D.G. Truhlar, Performance of the M11 and M11-L density functionals for calculations of electronic excitation energies by adiabatic time-dependent density functional theory, *Phys. Chem. Chem. Phys.* 14 (2012) 11363–11370, <https://doi.org/10.1039/C2CP41295K>.
- [55] L. Goerigk, S. Grimme, A thorough benchmark of density functional methods for general main group thermochemistry, kinetics, and noncovalent interactions, *Phys. Chem. Chem. Phys.* 13 (2011) 6670–6688, <https://doi.org/10.1039/C0CP02984J>.
- [56] Y. Inada, H. Orita, Efficiency of numerical basis sets for predicting the binding energies of hydrogen bonded complexes: evidence of small basis set superposition error compared to Gaussian basis sets, *J. Comput. Chem.* 29 (2008) 225–232, <https://doi.org/10.1002/jcc.20782>.
- [57] S. Lamghafri, W. Daoudi, A. El Aatiaoui, O. Dagdag, A. Berisha, A. Barrahi, W. B. Wan Nik, A. Zarrouk, A. Lamhamdi, Comparative study of the performance and inhibitory efficiency of two new organic heterocyclic in the chemical industry, *Mater. Sci. Eng. B* 297 (2023), 116779, <https://doi.org/10.1016/j.mseb.2023.116779>.
- [58] W. Daoudi, B. El Ibrahim, O. Dagdag, E. Berdimurodov, L. Guo, E.E. Ebenso, A. Oussaid, A. El Aatiaoui, New chlorophenyl-imidazole derivative as a novel corrosion inhibitor in the gas and oil industry, *J. Phys. Chem. Solid* 179 (2023), 111409, <https://doi.org/10.1016/j.jpcs.2023.111409>.
- [59] S.K. Gupta, R.K. Mehta, M. Yadav, O. Dagdag, V. Mehmeti, A. Berisha, E.E. Ebenso, Diazenyl derivatives as efficient corrosion inhibitors for mild steel in HCl medium: gravimetric, electrochemical and computational approach, *J. Mol. Liq.* 382 (2023), 121976, <https://doi.org/10.1016/j.molliq.2023.121976>.
- [60] S. Shahabuddin, N. Muhamad Sarih, S. Mohamad, J. Joon Ching, SrTiO<sub>3</sub> Nanocube-doped polyaniline nanocomposites with enhanced photocatalytic degradation of methylene blue under visible light, *Polymers* 8 (2016) 27, <https://doi.org/10.3390/polym8020027>.
- [61] S.A. Al Kiey, M.S. Hasanin, F.E.-T. Heakal, Green and sustainable chitosan–gum Arabic nanocomposites as efficient anticorrosive coatings for mild steel in saline media, *Sci. Rep.* 12 (2022) 13209, <https://doi.org/10.1038/s41598-022-17386-7>.
- [62] Z. Zhou, X. Min, S. Wan, J. Liu, B. Liao, X. Guo, A novel green corrosion inhibitor extracted from waste feverfew root for carbon steel in H<sub>2</sub>SO<sub>4</sub> solution, *Results Eng.* 17 (2023), 100971, <https://doi.org/10.1016/j.rineng.2023.100971>.
- [63] O. Dagdag, R. Hsissou, A. El Harfi, A. Berisha, Z. Safi, C. Verma, E.E. Ebenso, M. Ebn Touhami, M. El Gouri, Fabrication of polymer based epoxy resin as effective anti-corrosive coating for steel: computational modeling reinforced experimental studies, *Surf. Interfaces* 18 (2020), 100454, <https://doi.org/10.1016/j.surfin.2020.100454>.
- [64] S.K. Gupta, R.K. Mitra, M. Yadav, O. Dagdag, A. Berisha, B.B. Mamba, T.T. I. Nkambule, E.E. Ebenso, S.K. Singh, Electrochemical, surface morphological and computational evaluation on carbonyldiazide Schiff bases as corrosion inhibitor for mild steel in acidic medium, *Sci. Rep.* 13 (2023) 15108, <https://doi.org/10.1038/s41598-023-41975-9>.
- [65] O. Dagdag, R. Hsissou, A. El Harfi, Z. Safi, A. Berisha, C. Verma, E.E. Ebenso, M. A. Quraishi, N. Wazzan, S. Jodeh, M. El Gouri, Epoxy resins and their zinc composites as novel anti-corrosive materials for copper in 3% sodium chloride solution: experimental and computational studies, *J. Mol. Liq.* 315 (2020), 113757, <https://doi.org/10.1016/j.molliq.2020.113757>.
- [66] H. Liu, B. Fan, G. Fan, Y. Ma, H. Hao, W. Zhang, Anti-corrosive mechanism of poly(N-ethylamine)/sodium silicate electrochemical composites for copper: correlated experimental and in-silico studies, *J. Mater. Sci. Technol.* 72 (2021) 202–216, <https://doi.org/10.1016/j.jmst.2020.08.064>.
- [67] H. Liu, B. Fan, G. Fan, X. Zhao, Z. Liu, H. Hao, B. Yang, Long-term protective mechanism of poly(N-methylamine)/phosphate one-step electropolymerized coatings for copper in 3.5% NaCl solution, *J. Alloys Compd.* 872 (2021), 159752, <https://doi.org/10.1016/j.jallcom.2021.159752>.
- [68] E.-S.M. Sherif, M.M. El Rayes, H.S. Abdo, WC-co and WC-co-Cr coatings for the protection of API pipeline steel from corrosion in 4% NaCl solution, *Coatings* 10 (2020) 275, <https://doi.org/10.3390/coatings10030275>.
- [69] A. Liyanage, D.J. Karunaratne, S. Nasrazadani, F. D'Souza, H.R. Siller, T. D. Golden, Polyphthalocyanine coatings for corrosion protection on additive manufactured steel materials, *Prog. Org. Coat.* 170 (2022), 106990, <https://doi.org/10.1016/j.porgcoat.2022.106990>.
- [70] M.M. Karimi Azar, H. Shoostari Gugtaph, M. Rezaei, Evaluation of corrosion protection performance of electroplated zinc and zinc-graphene oxide nanocomposite coatings in air saturated 3.5 wt. % NaCl solution, *Colloids Surf. Physicochem. Eng. Asp.* 601 (2020), 125051, <https://doi.org/10.1016/j.colsurfa.2020.125051>.
- [71] V.S. Kathavate, D.N. Pawar, N.S. Bagal, P.P. Deshpande, Role of nano ZnO particles in the electrodeposition and growth mechanism of phosphate coatings for enhancing the anti-corrosive performance of low carbon steel in 3.5% NaCl aqueous solution, *J. Alloys Compd.* 823 (2020), 153812, <https://doi.org/10.1016/j.jallcom.2020.153812>.

## CRITICAL REVIEW



Cite this: DOI: 10.1039/d3gc05207a

# Principles and theories of green chemistry for corrosion science and engineering: design and application

Chandrabhan Verma,<sup>ID</sup>\*<sup>a</sup> Dheeraj Singh Chauhan,<sup>ID</sup><sup>j</sup> Ruby Aslam,<sup>c</sup>  
Priyabrata Banerjee,<sup>ID</sup><sup>d</sup> Jeenat Aslam,<sup>e</sup> Taiwo W. Quadri,<sup>ID</sup><sup>f</sup> Saman Zehra,<sup>ID</sup><sup>g</sup>  
Dakeshwar Kumar Verma,<sup>ID</sup><sup>h</sup> Mumtaz A. Quraishi,<sup>ID</sup><sup>b</sup> Shikha Dubey,<sup>i</sup>  
Akram Alfantazi<sup>a</sup> and Tahir Rasheed<sup>b</sup>

Given the high toxicity of inorganic inhibitors, organic substances, primarily heterocycles, have been proven to be one of the most efficient, cost-effective, and practical alternatives. Severe limitations in the application of organic corrosion inhibitors, particularly their environmental toxicity, have greatly accelerated the investigation of eco-friendly and sustainable alternatives. Corrosion control has made significant use of green chemistry ideas in recent years. This involves using different sustainable materials, techniques and strategies for corrosion control. Bio-based materials, including plant extracts, natural polymers, gums, waste, amino acids, and carbohydrates, are widely employed as sustainable materials. They are considered the best eco-friendly substitutes owing to their natural origin, biodegradability, and non-accumulation. Recently, several green synthetic techniques have been used to create green synthetic inhibitors, including microwave (MW) and ultrasonic (US) irradiation, particularly in conjunction with one-step multicomponent reactions (MCRs). Besides being green and sustainable, compounds derived from MW and US irradiation are more effective inhibitors than those obtained via traditional synthesis. Synthetic inhibitors derived using sustainable chemicals, solvents, and catalysts are also regarded as green alternatives. Inhibitors synthesized using natural substrates such as AAs and carbohydrates are semisynthetic alternatives. Recently, self-healing and synergism have emerged as additional environmentally friendly corrosion prevention methods. Computational modeling and simulations such as density functional theory (DFT), molecular dynamics (MD), and Monte Carlo (MC) simulations save money and resources by minimizing the number of experimental trials. Herein, we discuss the current research on using various eco-friendly and sustainable materials, technologies, and strategies for corrosion prevention together with their challenges and opportunities.

Received 31st December 2023,

Accepted 16th February 2024

DOI: 10.1039/d3gc05207a

rsc.li/greenchem

## 1. Introduction

### 1.1. Corrosion and corrosion inhibition: a shift from inorganic (toxic) to green corrosion inhibitors

Metallic materials are extensively employed in various fields, including building supplies, particularly in the petroleum, oil,

and gas industries.<sup>1</sup> Unfortunately, most metals rapidly succumb to corrosive degradation due to the reactivity of environmental elements as they are thermodynamically unstable in their pure form. Corrosion is a natural phenomenon that impacts the economy, public safety, and environment. Numerous industrial processes employ extremely aggres-

<sup>a</sup>Department of Chemical Engineering, Khalifa University of Science and Technology, P.O. Box 127788, Abu Dhabi, United Arab Emirates.

E-mail: chandraverma.rs.apc@itbhu.ac.in

<sup>b</sup>Interdisciplinary Research Center for Advanced Materials, King Fahd University of Petroleum and Minerals, Dhahran 31261, Saudi Arabia.

E-mail: maquraishi.apc@itbhu.ac.in, tahir.rasheed@hotmail.com

<sup>c</sup>School of Civil Engineering and Architecture, Chongqing University of Science and Technology, Chongqing, China. E-mail: drrubyaslam@gmail.com

<sup>d</sup>Electric Mobility and Tribology Research Group, CSIR-Central Mechanical Engineering Research Institute, Mahatma Gandhi Avenue, Durgapur 713209, India.

E-mail: pr\_banerjee@cmeri.res.in

<sup>e</sup>Department of Chemistry, College of Science, Taibah University, Yanbu 30799, Al-Madina, Saudi Arabia. E-mail: drjeenataslam@outlook.com

<sup>f</sup>Institute for Nanotechnology and Water Sustainability, College of Science, Engineering and Technology, University of South Africa, Johannesburg 1710, South Africa. E-mail: taiwoquadri27@gmail.com

<sup>g</sup>Corrosion Research Laboratory, Department of Applied Chemistry, Faculty of Engineering and Technology, Aligarh Muslim University, Aligarh 202002, India. E-mail: samanzechra2050@gmail.com

<sup>h</sup>Department of Chemistry, Government Dignvijay Autonomous Postgraduate College, Rajnandgaon, Chhattisgarh 491441, India. E-mail: dakeshwarverma@gmail.com

<sup>i</sup>Department of Chemistry, School of Sciences, Hemvati Nandan Bahuguna Garhwal University, Srinagar 246174, Garhwal, India. E-mail: dubey.shikha.bhu@gmail.com

<sup>j</sup>Modern National Chemicals, Second Industrial City, Dammam 31421, Saudi Arabia. E-mail: dheerajchauhan.rs.apc@itbhu.ac.in

sive electrolytes, which disintegrate metallic components and undesirable surface contaminants. The National Association of Corrosion Engineers (NACE) estimation predicts that the global cost of corrosion is about 3.4% (US \$2.5 trillion) of the world's gross domestic product (GDP).<sup>2,3</sup> Fortunately, existing techniques can reduce the expense of corrosion by 15% (US \$375 billion) to 35% (US \$875 billion).<sup>4,5</sup> Before 1965, the efficiency of corrosion inhibitors was the primary factor in their selection, regardless of their effect on the environment. The first line of protection was utilizing inorganic species such as chromates, nitrates, nitrites, phosphates, molybdates, and tungstates because of their great potential at relatively low concentrations. These species are called passivators because they shield metal surfaces from corrosion by generating a passive covering. Chromates, nitrates, and nitrites are oxidizing anions or oxygen-free passivators as they passivate metal surfaces without oxygen.<sup>6,7</sup> In contrast, phosphates, molybdates, and tungstates passivate metal surfaces only in the presence of oxygen; therefore, they are referred to as oxygen-dependent passivators or non-oxidizing anions.<sup>8</sup> However, because of their toxicity and bioaccumulative nature, less expensive and more practical substitutes gradually replaced them (Fig. 1). Economic factors came into play between 1965 and 1978, and corrosion engineers and scientists created and used some affordable substitutes. Following that (1980–1995), rising ecological consciousness compelled scientists and engineers to

employ comparatively eco-friendly substitutes. However, recent (from 1995) corrosion science and engineering studies have cast doubt on the creation of reasonably priced ecologically suitable substitutes. Among them, organic compounds remain the top options given that they are well-established as one of the most efficient, cost-effective, and profitable means of corrosion protection.<sup>9–11</sup>

The use of numerous materials with natural and manmade origins in green corrosion protection has recently increased.<sup>9–11</sup> Natural green corrosion inhibitors, including plant extracts, have been extensively researched and tested. Because of their plant-based origin, they are the best environmentally friendly, commercially viable, bio-degradable, bio-tolerable, and non-bioaccumulative substitutes for hazardous corrosion inhibitors.<sup>12–14</sup> Each extract contains a variety of phytochemicals, ranging from simple to complex, which are joined by frequent conjugation to form polar functional groups and aromatic rings. In addition to other natural substances, such as carbohydrates, bio-surfactants, biopolymers, amino acids, and pharmaceuticals (chemical medications), green corrosion inhibition has attracted significant attention.<sup>15–19</sup> The term “green substitute” can also be used to describe synthetic inhibitors made utilizing green starting materials (e.g. carbohydrates, amino acids, and natural resources), green solvents (e.g. water, supercritical carbon dioxide and deep eutectic solvent), and green (bio-based) cata-



**Chandrabhan Verma**

*Chandrabhan Verma works at the Department of Chemical Engineering, Khalifa University of Science and Technology, Abu Dhabi, United Arab Emirates. Dr Verma obtained his B.Sc. and M.Sc. degrees from Udai Pratap Autonomous College, Varanasi (UP), India. He received his PhD from the Department of Chemistry, Indian Institute of Technology (Banaras Hindu University) Varanasi, under the supervision of Prof. Mumtaz A.*

*Quraishi in Corrosion Science and Engineering. He is a reviewer and editorial board member of various internationally recognized ACS, RSC, Elsevier, Wiley, and Springer platforms. Dr Verma published numerous research and review articles in different areas of science and engineering at ACS, Elsevier, RSC, Wiley, Springer, etc. He has a total citation of more than 12 200 with an h-index of 61 and an i-10 index of 157. His current research focuses on designing and developing industrially applicable corrosion inhibitors. Dr Verma has edited/authored over 40 books for ACS, Elsevier, RSC, Springer, and Wiley. He has received several awards for his academic achievements, including a gold medal in M.Sc. (Organic Chemistry; 2010) and Best Publication awards from the Global Alumni Association of IIT-BHU (second prize 2013).*



**D. S. Chauhan**

*Dr Dheeraj Singh Chauhan is Corrosion Specialist at the Modern National Chemicals in Dammam, Saudi Arabia. He received his BSc (Hons) (2002) and MSc (2004) degrees from Banaras Hindu University (BHU), India, and his PhD (2012) from the Indian Institute of Technology (IIT, BHU). Soon after, he joined Nanjing University of Science and Technology, China, as a post-doctoral research fellow*

*(2013–2015). After that, Dr Chauhan worked as Post-Doctoral Research Fellow at the Center of Research Excellence in Corrosion, King Fahd University of Petroleum and Minerals, Saudi Arabia (2018–2020). He is currently working on developing corrosion inhibitors for the oil and gas industry. Dr Chauhan has over 90 publications with over 5300 citations, an H-index of 46, and an i-10 index of 72.*

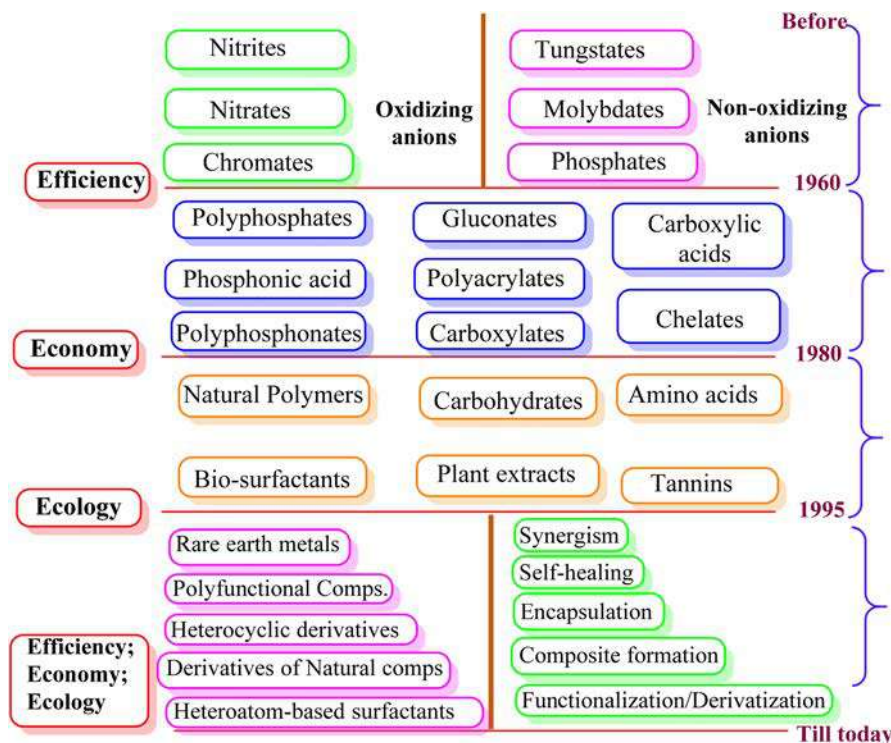


Fig. 1 Chronological growth in the development of green corrosion inhibitors (a journey to effectivity) (1960–1980; economy to ecology) (1980–present) [self-illustration, copyright permission not required].



R. Aslam

Ruby Aslam, PhD, is a postdoctoral fellow in the School of Civil Engineering and Architecture at Chongqing University of Science and Technology, Chongqing, China. She received her M.Sc., M. Phil., and PhD from Aligarh Muslim University, India. She has authored/co-authored more than 80 research articles in international peer-reviewed journals, including critical reviews and book chapters. She has edited more than ten books.



P. Banerjee

Priyabrata Banerjee is a Principal Scientist and Associate Professor (AcSIR) at the Electric Mobility & Tribology Research Group, CSIR-CMERI, India. He received his PhD from IACS, Jadavpur, Kolkata, India, in 2007. He did his Post-Doctoral research at the Max Planck Institute for Bio-Inorganic Chemistry, Mülheim, Germany. He was a Visiting Fellow at HTW Dresden, Germany, and presently, he has been selected as a CSIR-Raman Research Fellow at Ghent University, Belgium. He has published 177 research papers (8812 citations, *h*-index: 50, *i*-index: 157) in several international SCI journals, 36 book chapters, and 15 magazines. He is Editor of *Advances in Materials and Processing Technologies*, Taylor & Francis Online, and Guest Editor of *Frontiers in Chemistry and Molecules*, MDPI. His current research interest broadly covers selective bio-relevant cation–anion detection, corrosion chemistry, solid waste management, wastewater treatment, metal-mediated C–heteroatom bond fusion, metal–organic complexes and their unexplored radical chemistry development, and electrochemical energy conversion.



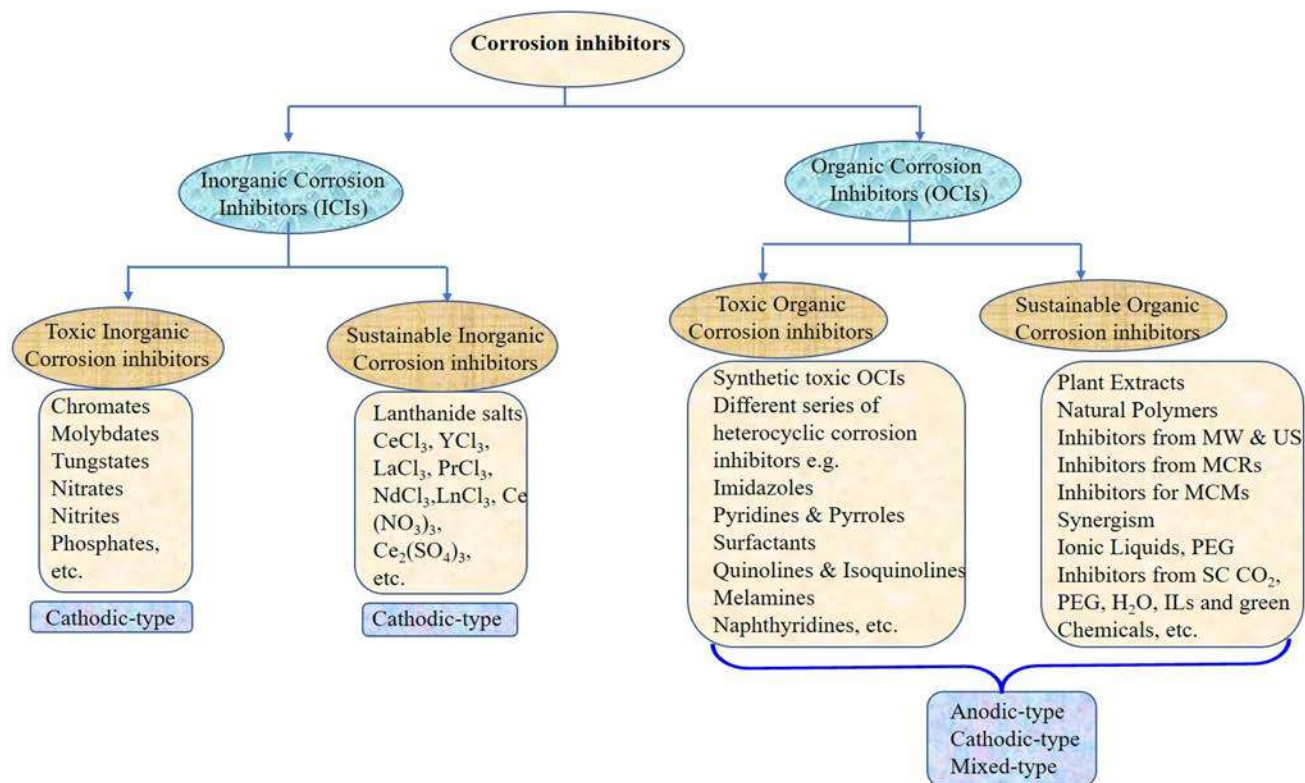


Fig. 2 Common examples of toxic and sustainable inorganic and organic corrosion inhibitors and examples of their toxic and sustainable alternatives [self-illustration, copyright permission not required].

lysts. Additionally, multicomponent reactions (MCRs) have several advantages over traditional synthetic processes, making them “green”.<sup>20</sup> Fig. 2 illustrates common examples of

toxic and sustainable organic and inorganic corrosion inhibitors. Accordingly, corrosion inhibitors prepared *via* MCRs, particularly applying microwave and ultrasound irradiation, can



J. Aslam

Dr Jeenat Aslam, Ph.D., currently serves as an Associate Professor in the Department of Chemistry at the College of Science, Taibah University, Yanbu, Al-Madina, Saudi Arabia. She obtained her M.Sc. and PhD in Chemistry from Aligarh Muslim University, Aligarh, India. Her research primarily focuses on materials, corrosion, nanotechnology, and surface chemistry. Dr Jeenat has contributed significantly to her field, publishing numerous

research and review articles in peer-reviewed international journals, including ACS, Wiley, Elsevier, Springer, Taylor & Francis, and Bentham Science. In addition, she has authored over forty book chapters and edited over thirty books for prestigious publishers such as the American Chemical Society, Elsevier, the Royal Society of Chemistry, Springer, Wiley, De Gruyter, and Taylor & Francis.



T. W. Quadri

Taiwo W. Quadri is currently a postdoctoral fellow at the Centre for Materials Science, College of Science, Engineering and Technology, University of South Africa. He obtained his BSc. degree in Chemical Engineering from the University of Lagos, Akoka, Nigeria. He completed his MSc. and PhD studies in Chemistry from the North-West University, South Africa under the supervision of Prof. Eno E. Ebenso. His research focuses on

the discovery, design and development of novel, effective and environmentally friendly compounds for metallic corrosion protection. He has published more than 25 research articles and book chapters in peer-reviewed international journals and books.

also be referred to as green alternatives.<sup>21,22</sup> Herein, we offer a thorough and historical overview of the developments in green corrosion inhibition. Green chemistry principles and theories are emphasized in the design, development, and use of green corrosion inhibitors and green inhibition. The advantages, challenges, and prospects of each series of green alternatives have been explored using the action and behavior of industrial-based electrolytes.

Corrosion science and engineering have made significant strides in recent years, focusing on the design, synthesis, and implementation of environmentally friendly alternatives to conventional toxic inhibitors in response to growing public awareness of environmental issues and strict ecological policies.<sup>23,24</sup> Examining the bioaccumulation potential, biodegradability, and environmental toxicity of a chemical species is a straightforward way to ascertain whether it is environmentally friendly as a corrosion inhibitor.<sup>25,26</sup> These factors are evaluated by international organizations such as the Oslo and Paris Commission (OSPAR) and the Registration, Evaluation, Authorization, and Restriction of Chemicals (REACH). REACH, a regulation of the European Union (EU), was adopted on December 18, 2006, and became effective on June 7, 2007.<sup>27</sup> The 849-page EU regulation discusses the design, development, and use of chemicals and their effects on the natural world and human health. The Oslo Convention against Dumping of Wastes at Sea, signed in 1972, and the Paris Convention on Marine Pollution from Land-Based Sources, signed in 1974, were combined and updated to become OSPAR on September 22, 1992.<sup>28–30</sup> The bioaccumulation, biodegradability and toxicity of chemical compounds and their effects

on the environment and human health can all be evaluated using the recommendations and indices established by these commissions. The effective and lethal concentrations of a chemical compound, which are denoted as  $EC_{50}$  and  $LC_{50}$ , respectively, can be used to evaluate the toxicity of the compound before it is utilized as a corrosion inhibitor.<sup>31,32</sup>  $EC_{50}$  indicates the chemical concentration that negatively impacts the growth of the living population, while  $LC_{50}$  suggests the concentration of a substance that results in the death of 50% of the population. A lower  $LC_{50}/EC_{50}$  ratio indicates more significant sensitive toxicity and *vice versa*. Alternatively, a substance is considered harmless if its  $LC_{50}/EC_{50}$  value exceeds  $10 \text{ mg kg}^{-1}$ .<sup>33,34</sup>

Microorganisms known as decomposers spontaneously break down most chemicals, albeit the process is quite sluggish and can take days, months, or even years.<sup>35</sup> If a chemical breaks down by 60% or more in 28 days, it can be considered environmentally benign.<sup>36</sup> The ability of a chemical to accumulate in a living thing when its only supply is water is known as bioaccumulation.<sup>37,38</sup> Usually, the partition coefficient, which is abbreviated as  $\log K_{OW}$  or  $D^{OW}$ , is used to measure it. In general,  $K_{OW}$  or  $D^{OW}$  denotes the ratio of a concentration of a compound in a mixture of two immiscible solvents at equilibrium. The measurement in an octanol and water mixture is called bioaccumulation. An environmentally friendly compound should have a  $K_{OW}$  or  $D^{OW}$  value of three or less.<sup>39</sup> Sustainable technology development depends on addressing the problem of toxicological data (*i.e.* toxicity ( $LC_{50}/EC_{50}$ ), biodegradability and bioaccumulation ( $K_{OW}$  or  $D^{OW}$ ) and the environment and human health) in corrosion inhibition



**S. Zehra**

*Dr Saman Zehra, PhD, works at the Women Scientist Program (WOS-A) of DST, New Delhi, in the Department of Applied Chemistry of Aligarh Muslim University, Aligarh, India. Her area of research broadly covers stimulus-responsive smart, functional anti-corrosion coatings and corrosion inhibitors. She received her Ph.D. and M.Sc. from the same university. She has published several articles in international peer-reviewed journals,*

*including reviews and book chapters. She has also presented her research work at national and international conferences.*



**D. K. Verma**

*Dr Dakeshwar Kumar Verma, who holds a Ph.D., is Assistant Professor of Chemistry at Govt. Digvijay Autonomous Postgraduate College in Rajnandgaon, Chhattisgarh, India. A profound passion for scientific exploration drives him and his research focuses primarily on preparing and designing organic compounds for diverse applications. With an impressive track record, Dr Verma has authored more than 100 research*

*articles, review articles, and book chapters that have found their places in esteemed peer-reviewed international journals, including those published by ACS, RSC, Wiley, Elsevier, Springer, and Taylor & Francis, among others. Dr Verma has taken on editorial/authored responsibilities for various published and upcoming books slated to be published by renowned publishers. With a cumulative citation count of more than 1800, an h-index of 25, and an i-10 index of 34, Dr Verma's impact is evident through the recognition and relevance of his work in the scientific community.*

investigations.<sup>40,41</sup> The utilization of toxicology data is essential to guaranteeing that the corrosion inhibitors employed in different industries are appropriate for human health, the environment, and corrosion prevention.<sup>42,43</sup> To reduce any possible impact on ecosystems and human health, researchers and developers can make well-informed decisions by evaluating the toxicity of corrosion inhibitors.<sup>44</sup> This proactive strategy helps ensure that the market accepts these innovations and they remain viable over the long run, while also in agreement with ethical and environmental concerns. The foundation for responsible innovation is laid by highlighting the significance of toxicity data in the early phases of corrosion inhibitor research.<sup>40,41</sup> It represents a dedication to developing technology that addresses the direct problems associated with corrosion, while also advancing ecological responsibility and sustainability in the long run.

### 1.2. Green corrosion inhibition: practices and applications

Green corrosion inhibition has emerged as a sustainable and environmentally conscious method to safeguard metal structures against the detrimental impacts of corrosion.<sup>45</sup> These techniques aim to mitigate the ecological footprint associated with conventional corrosion inhibitors by utilizing inhibitors derived from renewable sources. These inhibitors create a protective layer on the metal surface, preventing corrosive sub-

stances from infiltrating and deteriorating the metal through film formation, adsorption, and passivation. Numerous alternatives of natural and synthetic origins have been developed to protect against metallic corrosion in industrial environments (Fig. 3). Among them, corrosion inhibitors made from plants and animals, such as biological extracts, biopolymers (such as polysaccharides), and amino acids, are common. These alternatives undoubtedly contain a variety of molecules known as biochemicals and phytochemicals, which are obtained from animals and plants, respectively (Fig. 3), aiding in their absorption and function as efficient inhibitors.<sup>46</sup> However, the degradation of the inhibitors obtained from biological systems at high temperatures limits their utility. Thus, synthetic alternatives are still the best option because they are considerably more stable, efficient, and cost-effective, particularly at high solution temperatures and with aggressive electrolytes. The use of green corrosion inhibitors offers several advantages. Firstly, minimizing reliance on non-renewable resources and restricting the release of dangerous substances into the environment help preserve the ecosystem. Green inhibitors are also frequently biodegradable, ensuring their safe disposal without endangering the ecosystem in the long term.<sup>47,48</sup> Additionally, they exhibit lower toxicity levels than their traditional counterparts, enhancing the safety of those involved in their application and handling. Another notable advantage of green inhibitors is their cost-effective-



**M. A. Quraishi**

*Prof. Mumtaz A. Quraishi is Chair Professor at the Interdisciplinary Center for Research in Advanced Materials at King Fahd University of Petroleum and Minerals (KFUPM), Saudi Arabia. He obtained his Ph.D. in Synthetic Organic Chemistry in 1986 from Kurukshetra University. He was awarded a D.Sc. 2004 from Aligarh Muslim University Aligarh in Corrosion Inhibition of Industrial Metals and Alloys.*

*Before joining KFUPM, he was Full Professor at IIT BHU Varanasi, India. He also served as Head (Chairman) of the Department of Chemistry at IIT BHU. He has more than 35 years of teaching experience. He has received several national and international awards. Dr Quraishi is Associate Editor of Current Material Science Bentham and a member of the Editorial Board of more than 30 international journals. Dr Quraishi is a Fellow of the Royal Society of Chemistry UK and a member of the American Chemical Society. He has published over 400 papers in peer-reviewed journals with an h-index of 108 and citations of more than 37 900. His global status is one regarding the h-index in corrosion inhibitors. He has authored the book Heterocyclic Organic Corrosion Inhibitors Principles and Applications, Elsevier 2020.*



**Shikha Dubey**

*Dr Shikha Dubey is currently serving as Assistant Professor (Analytical Chemistry) at the Department of Chemistry, Hemvati Nandan Bahuguna Garhwal University, Srinagar, Garhwal, Uttarakhand. Dr Dubey obtained her Bachelor's (B.Sc. Hons.) and Master's degree (M.Sc. Analytical Chemistry) from the Department of Chemistry, Institute of Science, Banaras Hindu University, Varanasi. After quali-*

*fying for the CSIR-NET exam, she joined the Department of Chemistry, Indian Institute of Technology (BHU). She has synthesized various nanomaterials via simple precipitation and green routes to treat metal-laden water and wastewater. Her research interest involves nano-biomaterial synthesis and characterization, development of low-cost adsorbents/nano adsorbents/magnetic nano-sorbents for water remediation and green-synthesis of materials, characterization and application in environmental remediation, photocatalytic degradation of organic and inorganic pollutants, etc. Dr Dubey has attended several international and national conferences and delivered expert talks. She also has attended several workshops.*

ness, given that they can be produced at competitive prices due to the availability of renewable resources and scalable manufacturing processes.

Various industries including oil and gas refineries, power generation, pharmaceutical utilities, and metal and mining, have adopted green corrosion inhibition practices.<sup>49</sup> The demand and market size for corrosion inhibitors that are oil-based, solvent-based, and water-based are rapidly increasing due to the rising industrialization. During the period 2022–2029, the corrosion inhibitor business is projected to grow at an astounding compound annual growth rate (CAGR) of 4.7%. The worldwide market for corrosion inhibitors is expected to grow from US \$7.5 billion in 2021 to US \$11.33 billion by 2029. Because of its large reserves of petroleum and natural gas and increased R&D efforts, Asia–Pacific now holds a monopoly on the corrosion inhibitors market. Green inhibitors are employed in bridges, buildings, and pipelines in the construction and infrastructure sector to prevent corrosion, extend their lifespan, and reduce maintenance costs.<sup>50</sup> The automotive and transportation industries enhance the corrosion resistance of their vehicles and prolong their service life by incorporating green inhibitors into coatings, fuel systems, and cooling systems. Furthermore, energy and power generation systems, such as power plants, wind turbines, and solar panels, benefit from green inhibitors to ensure the efficiency and durability of these renewable energy sources. Green corrosion inhibitors play a pivotal role in safeguarding ships, offshore platforms, and underwater structures from corrosion, given that they are constantly exposed to harsh marine and offshore environments, which can be detrimental to these systems.<sup>51</sup> In manufacturing and industrial processes such as metalworking, oil and gas refining, and chemical processing, green inhibitors are essential for preventing equipment and component corrosion, thereby maintaining operational

efficiency and minimizing downtime. The successful implementation of green corrosion inhibition practices necessitates the optimization of formulations, appropriate surface preparation, and practical application methods. Real-world examples underscore the effectiveness and cost-efficiency of green inhibitors across various industries, showcasing their potential to revolutionize corrosion prevention, while promoting environmentally responsible practices.<sup>52</sup>

### 1.3. Green chemistry and green chemistry principles in service of corrosion science

The term “green chemistry”, which is also referred to as clean chemistry or benign and sustainable chemistry, encompasses the fabrication of chemicals and the development of processes aimed at reducing risks to human health and minimizing environmental pollution. The fundamental objective of green chemistry solutions is mitigating or eradicating the harmful impacts of chemicals throughout their life cycle. The inception of green chemistry dates back to 1991, which was marked by the launch of the Alternative Synthetic Pathways for Pollution Prevention research program by the U.S. Environmental Protection Agency (EPA). This program emerged under the umbrella of the Pollution Prevention Act of 1990. It substantially shifted from previous EPA endeavours by emphasizing reducing or eliminating hazardous substance production. This approach is different from the conventional management of chemicals after manufacturing and their release into the environment. Over time, this research initiative expanded to encompass the exploration of more environmentally friendly solvents and safer chemicals. In 1996, “green chemistry” was officially embraced to include these principles.<sup>53,54</sup> Since then, green chemistry has emerged as a promising avenue of exploration regarding metallic material degradation.



**Akram Alfantazi**

*Akram Alfantazi is a Professor in the Department of Chemical Engineering and Theme Lead (Materials and Chemistry) at the Nuclear Technology Center at Khalifa University in Abu Dhabi. Dr Alfantazi obtained his PhD in Metallurgical Engineering from Queen's University, Canada, in 1994. His research areas are corrosion and environmental degradation of materials, electrochemical processes in materials science and engineering,*

*chemical and extractive metallurgy, and failure analysis. Dr Alfantazi has over 350 publications, including about 250 refereed journal publications.*



**T. Rasheed**

*Dr Tahir Rasheed is a researcher at the Interdisciplinary Research Center for Advanced Materials, King Fahd University of Petroleum and Minerals, Saudi Arabia. He completed his Ph.D. and postdoctoral research in Polymer Chemistry at the School of Chemistry and Chemical Engineering, Shanghai Jiao Tong University, China. His research interests focus on multiple disciplines, including controllable synthesis, characterization and*

*self-assembly of polymeric materials, polymer-based composites, nanomaterials and nanocomposites, and advanced functional materials, with particular emphasis on their potential applications in the field of sensing, electrocatalysis, degradation of various emerging pollutants, and energy storage devices.*

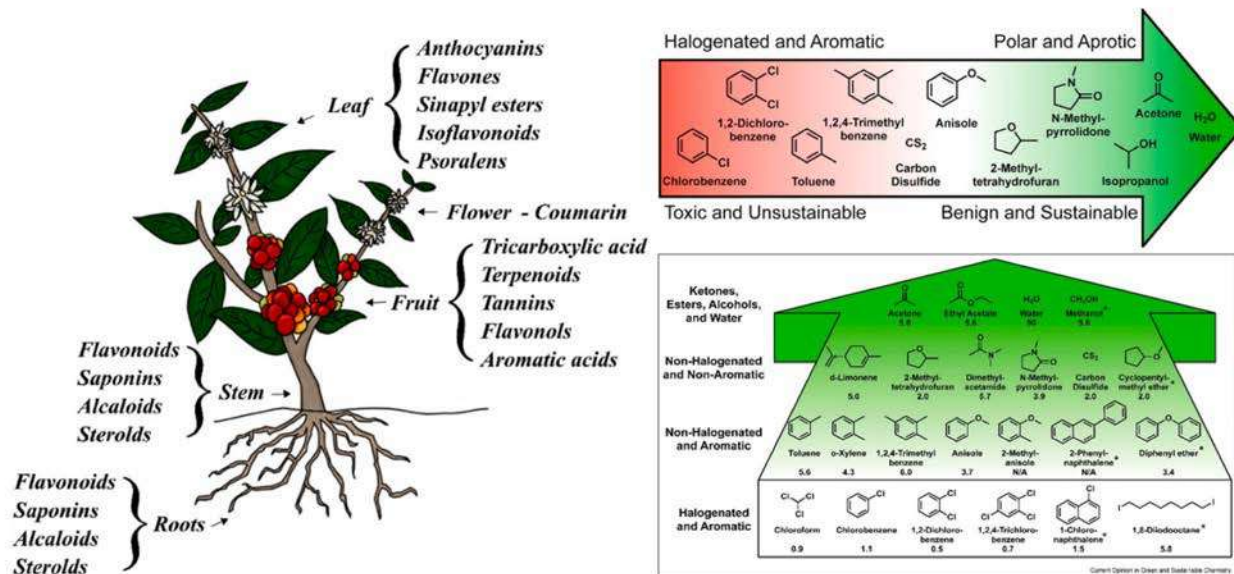
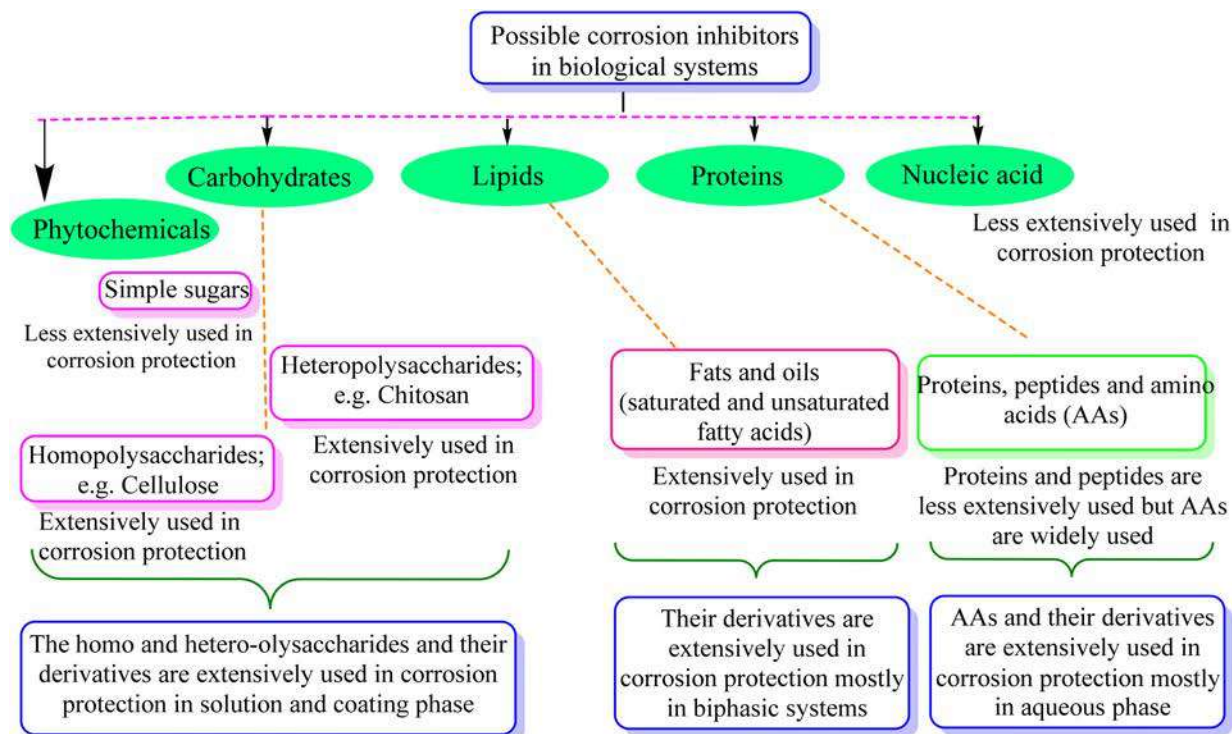


Fig. 3 Schematic illustration of some major classes of natural (animal and plant derived) corrosion inhibitors and their peculiar examples (upper) and different phytochemicals or constituents present in extracts that can serve as corrosion inhibitors (lower)<sup>46</sup> [the lower portion was reproduced from ref. 46 and appropriate permission has been obtained, Copyright, Elsevier, 2017].

Specifically, employing inhibitors is a strategic approach for pre-empting, managing, or retarding metal corrosion. Traditional corrosion inhibitors often involve toxic or environmentally harmful substances, leading to unintended consequences. In contrast, green chemistry techniques seek to design effective inhibitors against corrosion and are environmentally friendly throughout their life cycle. Green chemistry presents a promising approach for preventing, managing, and

mitigating corrosion. In recent years, the focus of green chemistry has shifted towards safeguarding both the environment and human well-being through economically advantageous means, aiming to eliminate toxins and curtail waste. In the realm of metallic material degradation, which is an area often confronted with the use of harmful substances, “green chemistry” has emerged as a thriving domain of research. The use of inhibitors is a well-established strategy when combatting

metal corrosion through prevention, control, or deceleration. Conventional corrosion inhibitors have been demonstrated to be effective but are associated with significant drawbacks, including environmental ramifications, toxicity concerns, and adherence to regulatory stipulations.

However, as the emphasis on environmental impact grows, the demand for more sustainable alternatives is increasing accordingly. In this case, “green chemicals” or environmentally friendly compounds offer a novel and promising avenue for addressing corrosion issues. Within the realm of corrosion science, green chemistry frequently involves the deployment of inhibitors, which are substances designed to reduce the corrosion rate. These inhibitors are meticulously engineered to exhibit biodegradability, renewability, and reduced toxicity. They can be derived from natural sources such as plants, biopolymers, and amino acids, which contain organic compounds capable of forming protective films on metal surfaces. Additionally, embracing green methodologies for corrosion resistance may involve substituting solvent-based coatings with water-based counterparts. The endeavours in green chemistry all share a common goal, *i.e.*, to diminish the environmental footprint, while effectively safeguarding materials from corrosion. This contribution to corrosion inhibition stems from the commitment of green chemistry to developing environmentally friendly and sustainable inhibitors. These inhibitors are meticulously designed to reduce the reliance on toxic chemicals and minimize waste generation.

The theories and concepts of green chemistry offer a fresh perspective on corrosion science and engineering by emphasizing the creation of environmentally friendly materials and processes with the fewest detrimental effects on the environment.<sup>20,55</sup> Essentially, green chemistry encourages the development of intrinsically safe protective coatings and corrosion inhibitors by reducing or eliminating the hazardous chemicals commonly employed in corrosion control practices. Green chemistry connects corrosion research with broader sustainability goals by highlighting the creation of environmentally friendly solutions, such as bio-based inhibitors derived from renewable resources and using energy-efficient electrochemical processes that produce fewer toxic byproducts. The lifetime and integrity of materials are guaranteed by this integration, which also promotes a comprehensive approach where environmental stewardship and material preservation principles come together to drive innovation and responsible practices in corrosion research and engineering. The twelve principles of green chemistry reinforce creating and using environmentally friendly materials and processes.<sup>56–58</sup> Regarding green corrosion inhibitors, these principles direct the creation and application of materials that meet standards such as waste avoidance, safer chemical design, and the utilization of renewable feedstocks. Green corrosion inhibitors reduce environmental pollution by ensuring that their application produces few or no harmful by-products, which is consistent with waste prevention principles.<sup>59,60</sup> Furthermore, these inhibitors place a high priority on creating non-toxic compounds and protecting ecosystems. The synthesis of these

materials using renewable resources is consistent with the concepts of sustainability and resource efficiency. In addition, adding these inhibitors lessens operations that consume a large amount of energy, which is an example of energy efficiency. Generally, green corrosion inhibitors promote safe, effective, and sustainable corrosion prevention methods, while reducing harmful environmental effects, embodying the twelve principles.

Reducing toxicity, limiting environmental effects, and utilizing plant extracts, amino acids, and carbohydrates as corrosion inhibitors are examples of various green chemistry principles.<sup>3,14,15</sup> This is because they provide non-toxic and biodegradable solutions, being composed of natural substances and can be considered environmentally benign substitutes for synthetic inhibitors. Furthermore, applying plant extracts, amino acids, and carbohydrates can lessen the requirement for energy-intensive procedures to create synthetic inhibitors, which is consistent with the energy efficiency principle. More environmentally friendly compounds that inhibit corrosion with less adverse effects on human health and the environment include biodegradable polymers, polyethylene glycol (PEG), and ionic liquids (ILs).<sup>3,20</sup> These materials are prime examples of green chemistry. These substances adhere to the synthesis of less dangerous chemicals by reducing their volatility and toxicity, while offering efficient corrosion prevention. Biodegradable polymers fulfil the crucial requirement of designing for breakdown by guaranteeing that the inhibitors decompose into innocuous chemicals.

The solvent-free strategy adheres to the waste prevention concept by minimizing environmental damage related to solvent use by avoiding the requirement for solvents.<sup>61,62</sup> Additionally, the solvent-free approach promotes atom economy by combining all reactants in the finished product and maximizing the resource efficiency. It lowers health and safety hazards, which is consistent with creating safer chemicals. By giving preference to environmentally friendly solutions, corrosion inhibitors developed from green solvents exemplify multiple green chemistry concepts.<sup>63–65</sup> The successful application of green chemistry principles to environmental responsibility and corrosion avoidance is exemplified by corrosion inhibitors derived from green solvents. Green chemistry principles are best shown by MW (microwave)- and ultrasonic-derived corrosion inhibitors, which promote efficient synthesis methods that reduce energy consumption and waste production.<sup>22</sup> Faster reaction times, energy savings, and improved process efficiency are common outcomes of MW and US irradiation.<sup>66</sup> Furthermore, consistent with the idea of creating cleaner chemicals, these techniques frequently require little or no harmful solvents. The environmental factor, sometimes known as the *E*-factor, is a metric to assess how a chemical process affects the environment. Eqn (1) can be used to determine the *E*-factor by dividing the entire amount of waste generated during a procedure by the mass of the intended product.<sup>67</sup> A method with a lower *E*-factor produces less waste, and therefore is more environmentally friendly. The environmental impact of a process is influenced by several variables,

such as raw material selection, energy use, and waste production. However, information regarding the *E*-factor of corrosion inhibitors is scarce. Our research team synthesized three glucose derivatives, namely ethylenediamine-modified glucose (EMG), tetramethylenediamine-modified glucose (TMG), and hexamethylenediamine-modified glucose (HMG), and investigated their ability to inhibit mild steel corrosion in 1 M HCl.<sup>68</sup> The results showed that for every kg of product (EMG, TMG, and HMG), 1–2 kg of waste was produced, which is acceptable considering the application of corrosion inhibition.<sup>69,70</sup> A subsequent investigation indicated that the *E*-factors of zwitterionic corrosion inhibitors derived from amino acids were 2.592 and 4.854, respectively.<sup>71</sup>

$$E\text{-factor} = \frac{\text{Total mass of waste generated}}{\text{Mass of desired product}} \quad (1)$$

### 1.3.1. Mechanism of action of green corrosion inhibitors.

Green corrosion inhibitors are chemicals or compounds that are environmentally friendly and designed to protect metals and alloys from corrosion in a corrosive environment.<sup>13,72</sup> They are considered “green” because they aim to minimize or eliminate the harmful effects on the environment and human health, often by being biodegradable, non-toxic, and less hazardous compared to traditional corrosion inhibitors. These inhibitors are used in various industries, including oil and gas, manufacturing, marine applications, and transportation,

where metal corrosion can lead to significant economic losses and safety hazards. The common types of green corrosion inhibitors include, drugs, organic compounds, plant extracts, polysaccharides, nanoparticles, amino acids, dyes and green salts.<sup>73,74</sup> Green or sustainable corrosion inhibition is a relatively new and rapidly growing field to explore and develop new environmentally friendly alternatives for toxic alternatives. The goal is to reduce the environmental impact associated with corrosion protection, while maintaining high-performance standards.<sup>75,76</sup> The primary selection criteria of a sustainable corrosion inhibitor are illustrated in Fig. 4.

Similar to traditional inhibitors, sustainable corrosion inhibitors of natural and biological origin become effective by forming a corrosion inhibitive film through their adsorption. The adsorption may be purely chemical, physical or physico-chemical type. Generally, the adsorption of the inhibitor begins with physisorption and is established as chemisorption. Physisorption involves weak electrostatic interactions, while chemisorption involves stronger chemical bonds. Fig. 5 represents the physisorption and chemisorption of an organic inhibitor in an acidic electrolyte. Certain green corrosion inhibitors participate in redox reactions, donating or accepting electrons from the metal surface. This electron transfer process alters the electrochemical reactions during corrosion, reducing its rate.<sup>77,78</sup> The combined action of multiple inhibitors can lead to a more significant reduction in the corrosion rate. The enhanced inhibitive effect of using two or more cor-

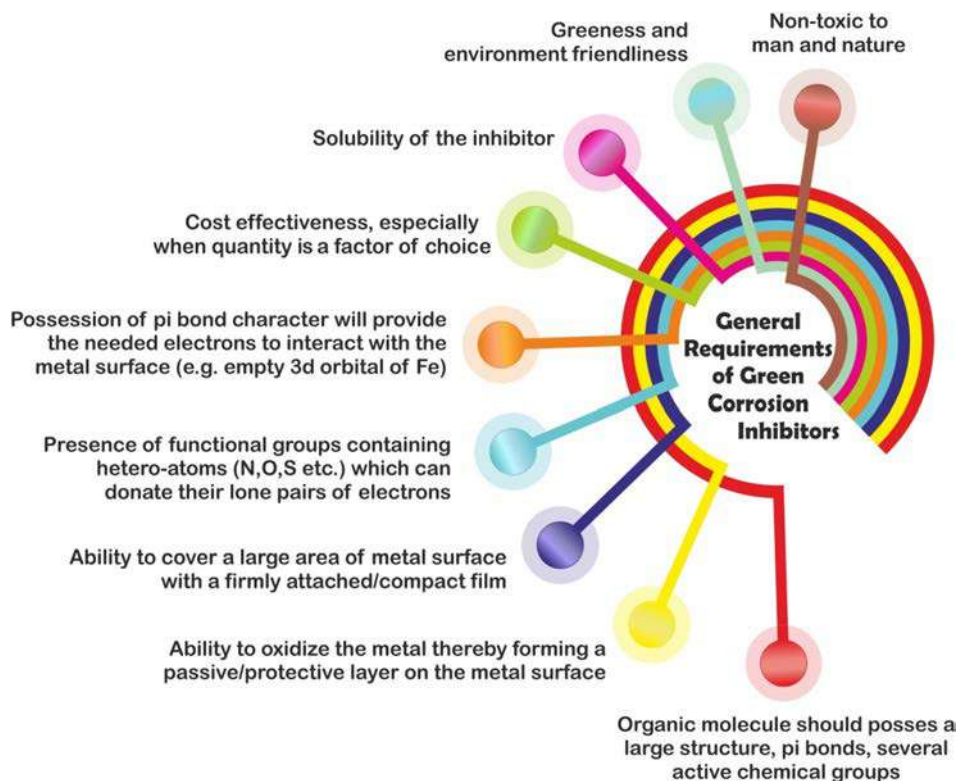
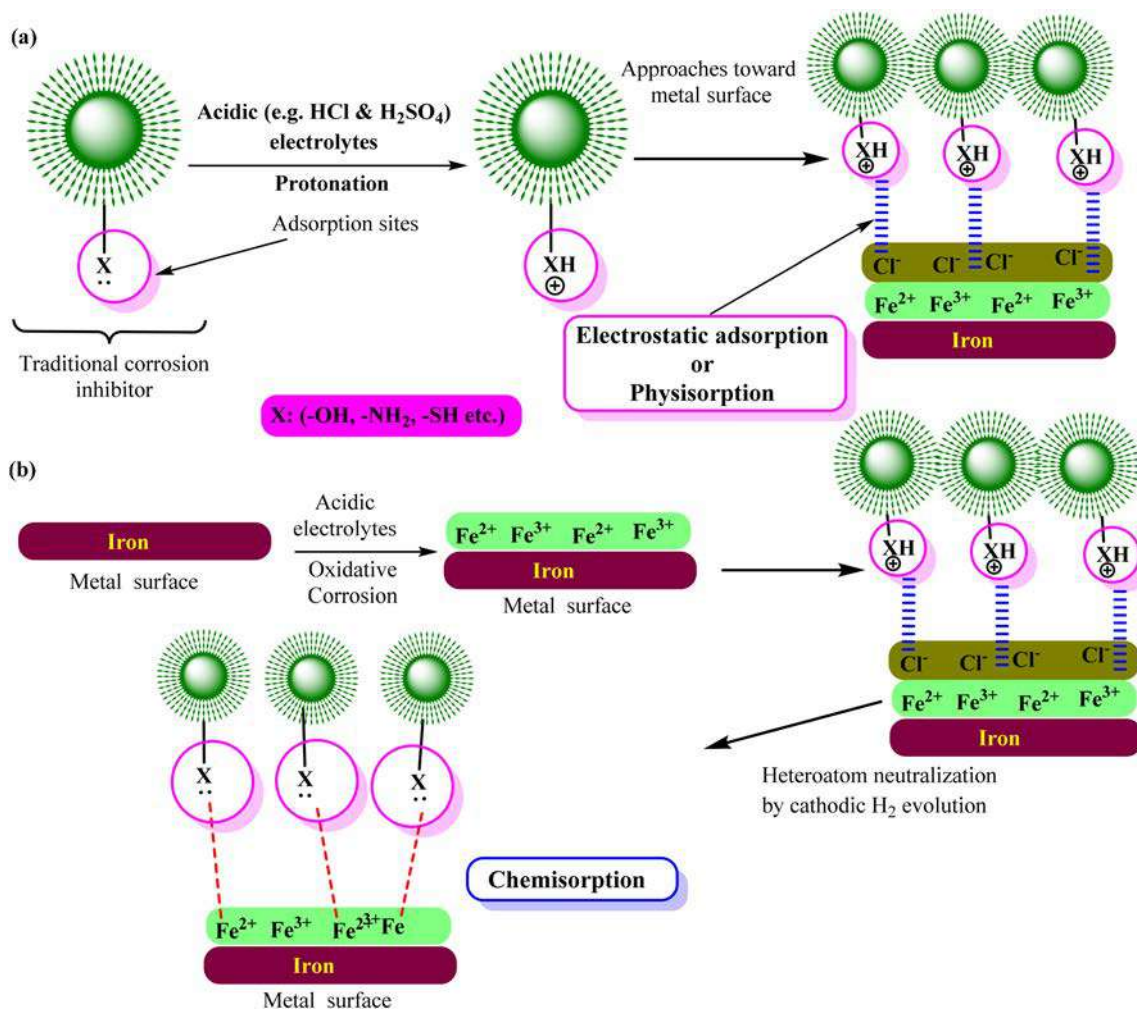


Fig. 4 Schematic illustration of the general requirements of a compound to be used as a corrosion inhibitor [self-illustration, copyright permission not required].



**Fig. 5** Schematic presentation of the adsorption of a corrosion inhibitor having an amino (–NH<sub>2</sub>) substituent on steel surface in acidic (HCl, H<sub>2</sub>SO<sub>4</sub>, etc.) and the mode of physisorption and chemisorption [self-illustration, copyright permission not required].

rosion inhibitors in combination, where their combined effect is more efficient than the sum of their individual effects, is known as the synergistic mechanism of corrosion inhibition.<sup>79,80</sup> It can result in corrosion protection, which is more effective and economical. In organic inhibitors, halide ions (I<sup>-</sup>, Br<sup>-</sup> and Cl<sup>-</sup>) frequently work in concert with corrosion inhibitors.<sup>81,82</sup> Increasing the adsorption of organic inhibitors on metal surfaces can strengthen the corrosion prevention. Furthermore, Zn<sup>2+</sup>, Cu<sup>2+</sup>, and Sn<sup>2+</sup> are the primary metal cations that can work together to form a more stable protective film on the metal surface. For instance, zinc ions are frequently employed in conjunction with organic inhibitors as synergists.<sup>79,83–85</sup>

Surfactants and polymeric compounds are also used in corrosion protection as synergists. Some inorganic anions (NO<sub>3</sub><sup>-</sup>, SO<sub>4</sub><sup>2-</sup> and PO<sub>4</sub><sup>3-</sup>) can influence the electrochemical processes at the metal interface, thereby acting as synergists.<sup>86,87</sup> They can alter the kinetics of corrosion and enhance the overall efficacy of the process in inhibiting corrosion. The type of metal being protected, the particular corrosion environment

and the type of corrosion inhibitor used all influence the choice of synergists. Synergistic pairings are frequently customized to meet the unique requirements of a specific corrosion situation. Noticeably, the inhibition potential of inhibitors depends on many factors, including their electronic structure, nature of the metal and electrolytes, operating temperature and presence of additives.<sup>88–90</sup> After getting adsorbed, green corrosion inhibitors retard both anodic and cathodic reactions, although in some cases, slight cathodic or anodic predominance has also been reported.

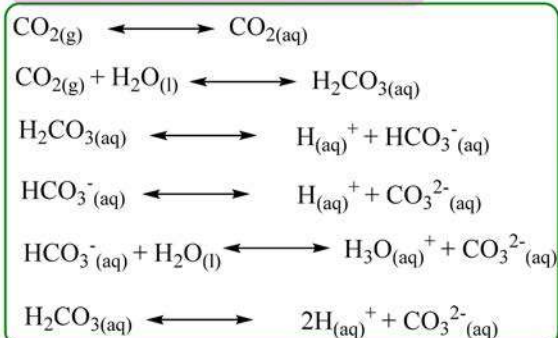
The corrosion protective film of inhibitors acts as a barrier between the metal and the corrosive environment.<sup>91,92</sup> The inhibitor film may be monolayered or polylayered depending on the nature of the metal, electrolyte and inhibitors. Its specific functional groups can strongly bond with the metal surface, creating a well-organized and tightly packed film. In some circumstances, it can undergo chemical reactions on the metal surface, forming protective precipitates. Also, corrosion products provide some protection from further dissolution by serving as a barrier between the metal and the environment.



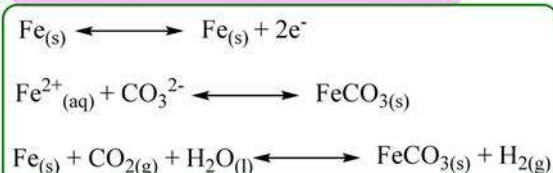
### Mechanism of formation of carbonate and sulfide precipitates

#### Carbonate formation/ CO<sub>2</sub> corrosion

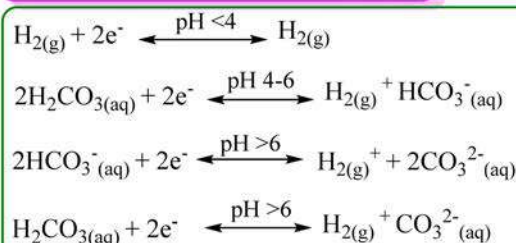
##### Formation and dissolution of H<sub>2</sub>CO<sub>3</sub>



##### Overall mechanism of FeCO<sub>3</sub> formation



##### The effect of pH on H<sub>2</sub>CO<sub>3</sub> dissolution



##### Sulfide (mackinawite) formation/ H<sub>2</sub>S corrosion

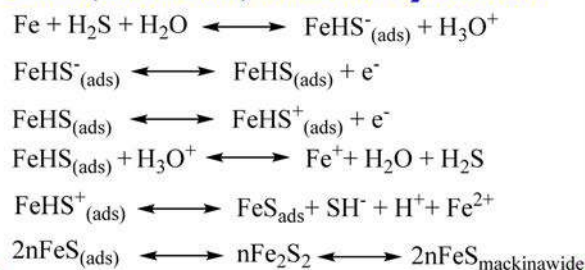


Fig. 6 Schematic presentation of the formation of H<sub>2</sub>CO<sub>3</sub> and FeCO<sub>3</sub> at different pH in CO<sub>2</sub>-rich (sweet) environment and mackinawite (nFeS) in H<sub>2</sub>S-rich (sour) environment [self-illustration, copyright permission not required].

The formation of carbonates and sulfides in the presence of CO<sub>2</sub> and H<sub>2</sub>S is a common example of corrosion protection *via* precipitates.<sup>93,94</sup> The formation of precipitates occurs under certain conditions, *e.g.*, the formation of FeCO<sub>3</sub> occurs preferably below pH 6 and temperature of 90 °C.<sup>95</sup> The dissolution of CO<sub>2</sub> in H<sub>2</sub>O and the formation of FeCO<sub>3</sub> are presented in Fig. 6.

The most efficient organic inhibitors have polar functional groups in their chemical structures.<sup>9-11,96</sup> The substituents substantially impact the coordination proficiency of organic inhibitors by altering the electron density at the donor sites, which are also known as adsorption or coordination sites. The polar substituents at the *p*-position that produce resonance effects include -OCH<sub>3</sub>, -OH, -NMe<sub>2</sub>, -NH<sub>2</sub>, -NO<sub>2</sub>, -CN, and -COOH. The corrosion inhibition efficiency (%IE) may occasionally be increased by *e*-withdrawing polar substituents at the *o*-position due to the potential chelation and substituent effects of polar substituents at the *o*-position.<sup>11</sup> Due to their -*R*-effect, *e*-withdrawing substituents such as -NO<sub>2</sub>, -CN, and -COOH, often harm the inhibition potential. Alternatively, macromolecules (polymers) may be beneficial for the %IE by increasing the solubility of the inhibitor.<sup>97-99</sup> These substituents affect the electron density at donor sites due to their ±*R*-effect (Taft substituent constant) and ±*R*-effect (Hammett substituent constant). The effect of some common substituents on the inhibition potential of some heterocyclic inhibitors is schematically presented in Fig. 7.

#### 1.4. Greenness of corrosion inhibitors: toxicity, solubility control, and degradation aspects

Corrosion inhibitors are classified as “green” based on three main criteria, *i.e.*, toxicity, solubility control, and degradation. These factors are critical when determining and guaranteeing the environmental friendliness of corrosion inhibitors. The utilization of green corrosion inhibitors exemplifies how the reduction of toxicity can significantly enhance the principles of sustainable development. This multifaceted approach can be elucidated through various key facets. Firstly, addressing human health and safety is pivotal. Conventional corrosion inhibitors frequently incorporate toxic elements such as heavy metals and hazardous organic compounds.<sup>100</sup> These substances pose substantial threats to the well-being of humans throughout their lifecycle, from production to disposal. Those engaged in the manufacturing and application of these inhibitors encounter potential exposure to perilous chemicals. Thus, the shift towards green corrosion inhibitors, distinguished by lower toxicity levels, effectively mitigates these health risks, fostering safer working environments. Furthermore, environmental protection becomes paramount, given that the harmful inherent components in conventional corrosion inhibitors have the potential to infiltrate the environment during both their application and disposal phases.<sup>101</sup> This pollution, with far-reaching consequences for soil, water, and air quality, threatens ecosystems and potentially contaminates the food chain.

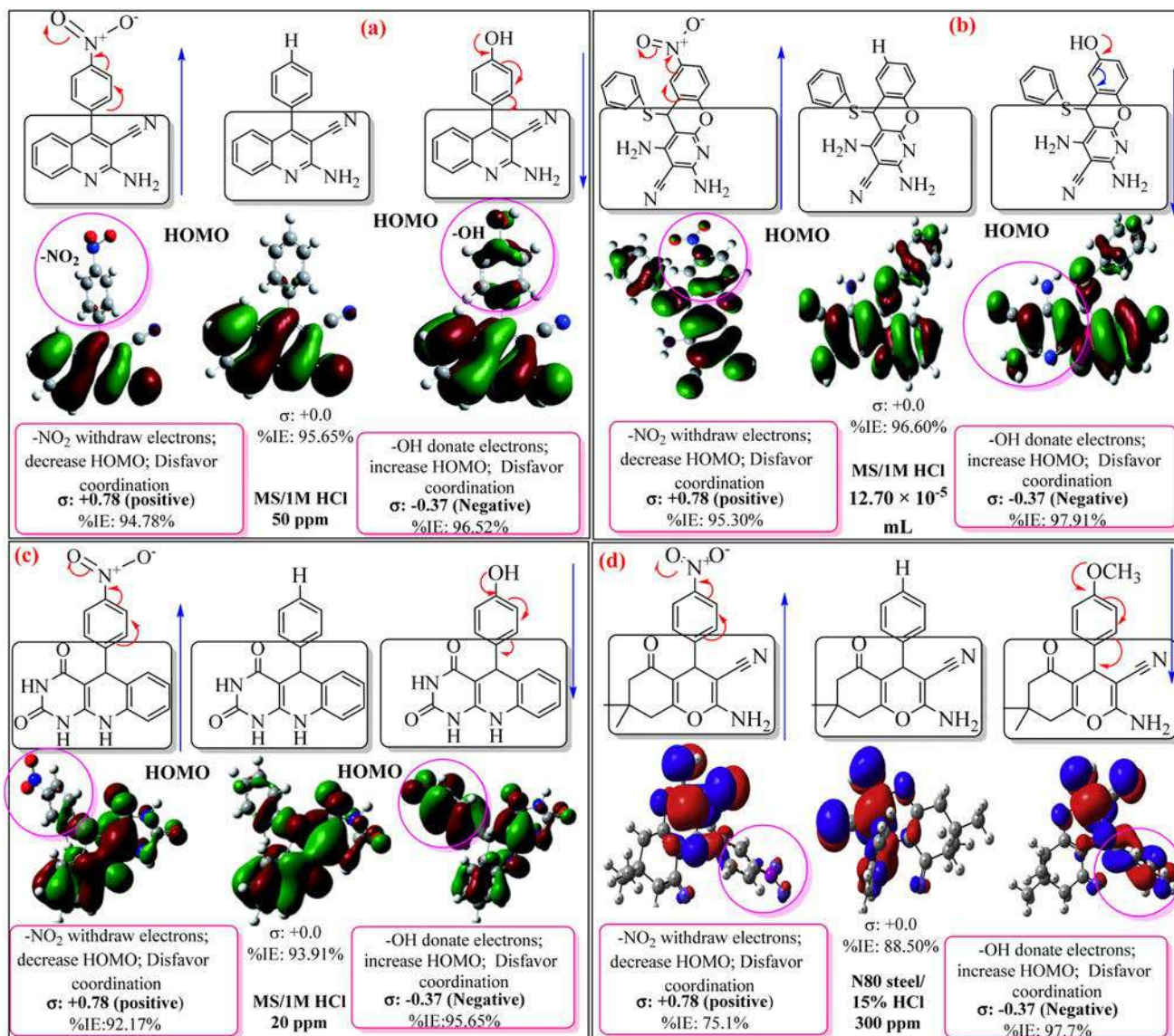


Fig. 7 Schematic illustration of the effect of some common substituents on the inhibition potential of some representative series of organic inhibitors.<sup>11</sup> [Reproduced from ref. 11 with permission, Copyright, Elsevier, 2023.]

Green corrosion inhibitors are formulated with a keen awareness of minimizing environmental harm. By curtailing the discharge of toxic substances, these alternatives play a pivotal role in shielding natural resources and maintaining the ecological equilibrium.<sup>102</sup> Sustainable manufacturing, as a pivotal tenet, is equally underscored. Green corrosion inhibitors are frequently composed of natural extracts,<sup>103,104</sup> biopolymers,<sup>16</sup> and ecologically-friendly compounds. These materials are marked by their renewability and sustainable attributes compared to the less sustainable toxic alternatives. This shift towards greener materials harmonizes the manufacturing process with sustainable paradigms, thereby curbing resource depletion and energy usage. The significance of waste reduction is also accentuated. The reduced toxicity of green corrosion inhibitors makes managing waste generated from

their production and use considerably less complex. In contrast, toxic waste disposal requires specialized handling and treatment, inevitably exacerbating the environmental consequences. Adopting green inhibitors eliminates the need for specialized waste management, thus easing the burden on waste management systems.<sup>59</sup> The pivotal aspect of regulatory compliance has to be considered. Given the stringent regulations governing the employment and disposal of toxic substances in various regions, integrating green corrosion inhibitors inherently facilitates adherence to these mandates. This proactive approach not only averts potential penalties but also averts legal entanglements associated with the use of toxic materials. Ultimately, the pursuit of long-term sustainability takes center stage. As industries shift towards sustainable practices, incorporating green corrosion inhibitors merges seam-

lessly with overarching sustainable development objectives. The abatement of toxicity curtails adverse impacts on both human society and the environment and contributes to the realization of a more harmonious and sustainable future.

Solubility control is a fundamental concept that is crucial in advancing sustainable development, particularly in green corrosion inhibitors. This principle is based on the intricate balance between two critical aspects, *i.e.*, the solubility of the inhibitor and its effectiveness in preventing corrosion. Within this complex interplay, the solubility characteristics of an inhibitor can significantly impact both its performance and environmental impact.<sup>20</sup> Corrosion inhibitors with high solubility carry the inherent risk of potentially leaching into the surrounding environment. When these highly soluble inhibitors are employed, they are more likely to extend beyond their designated application areas. This can result in unintended environmental consequences, such as the contamination of soil, water bodies, and ecosystems. Furthermore, the release of these inhibitors into the environment can disrupt the delicate ecological balance and adversely affect the flora, fauna, and human health. Thus, solubility control is pivotal in mitigating these undesirable outcomes. Alternatively, inhibitors with low solubility may face challenges in providing adequate corrosion protection. If an inhibitor has limited solubility, it may struggle to disperse and interact with the metal surface to form a protective layer. This can compromise the ability of the inhibitor to prevent corrosion effectively. Consequently, there should be a trade-off between the solubility of an inhibitor and its capacity to deliver reliable corrosion resistance. The essence of green corrosion inhibitors lies in their endeavor to strike an optimal balance in solubility. The goal is to identify and formulate inhibitors that achieve an ideal solubility threshold. This equilibrium ensures that the inhibitor dissolves sufficiently, allowing it to interact with the metal surface and inhibit corrosion. Simultaneously, the solubility of the inhibitor is controlled to prevent its excessive leaching into the environment. By attaining this equilibrium, green corrosion inhibitors simultaneously address corrosion prevention and environmental impact. The controlled solubility ensures that the inhibitor effectively serves its intended purpose, while minimizing the potential for harm to the ecosystem and human health.<sup>105</sup> This harmonious alignment of effectiveness and environmental consideration exemplifies a fundamental principle of sustainable development, namely the capability to harmonize technological progress with the responsible management of natural resources.

Degradation represents a pivotal and multifaceted aspect that significantly contributes to the advancement of sustainable development, especially within the domain of green corrosion inhibitors. This principle is based on the inherent capacity of these inhibitors to undergo breakdown or degradation over time. The underlying objective of degradation is to ensure that inhibitors do not persist in the environment, curtailing their potential for long-term and adverse ecological effects. By integrating degradation as a central consideration, green corrosion inhibitors underscore their commitment to

effective corrosion prevention and environmental responsibility.<sup>106</sup> Biodegradability is a cornerstone of green corrosion inhibitors and pivotal in orchestrating their compatibility with sustainable principles.<sup>13</sup> This intrinsic quality empowers these inhibitors to be naturally dismantled by microorganisms or other environmental processes, ultimately forming non-toxic byproducts. This natural degradation pathway serves as a counterbalance to the persistence of traditional inhibitors that can endure and accumulate in the environment, potentially inducing negative ramifications. The propensity of green corrosion inhibitors to biodegrade enhances their sustainability quotient by preventing the undue accumulation of inhibitors in the ecosystem and natural systems.<sup>59</sup> Incorporating biodegradable materials takes precedence to effectively facilitate degradation and curtail the ecological footprint of green corrosion inhibitors. Bio-based polymers<sup>107</sup> and natural compounds<sup>108</sup> are prime examples of materials that align with the principles of sustainable development. These materials, marked by their capacity to undergo natural degradation processes, further amplify the environmental compatibility of green inhibitors. Integrating these materials not only fosters the breakdown of inhibitors but also minimizes their potential to disrupt the ecological balance, thus bolstering their credentials as environmentally friendly solutions.

The holistic perspective on green corrosion inhibitors reveals that their sustainability exceeds their mere efficacy in corrosion prevention. Their foundational principles include low toxicity, solubility control, and crucially, degradation. This comprehensive approach underscores the overarching commitment to curbing the adverse impacts on human well-being and the environment throughout their lifecycle. By adhering to these principles, green inhibitors seamlessly align with the core tenets of sustainable chemistry, effectively advocating for the adoption of corrosion prevention practices that are effective and environmentally conscientious.<sup>109</sup> It is important to recognize that the evolution of green corrosion inhibitors is an ongoing process marked by continuous research and development endeavors. The perpetual quest to refine these inhibitors and enhance their green credentials remains imperative. As science and technology progress, the endeavors to further optimize the degradation characteristics of these inhibitors remain paramount, bolstering the efficacy of sustainable approaches in corrosion control. This commitment to innovation resonates strongly with the overarching goals of sustainable development, *i.e.*, harmonious coexistence between technological advancement and environmental stewardship.

In conclusion, transitioning from traditional hazardous corrosion inhibitors to their green alternatives offers numerous advantages. This paradigm shift protects the environment and human health. It significantly contributes to sustainable development by promoting safer workplaces, reducing environmental pollution, supporting sustainable manufacturing, and ensuring compliance with legal requirements. Controlling solubility is pivotal in sustainable development, especially regarding eco-friendly corrosion inhibitors. Striking the right balance between functional efficacy and environmental

responsibility is essential, given that the solubility and ability of an inhibitor to prevent corrosion are intricately linked. Pursuing optimal solubility thresholds is at the heart of green corrosion inhibitors, embodying their commitment to aligning with the principles of sustainable development. Sustainable progress in green corrosion inhibitors significantly hinges on the aspect of degradation. These inhibitors prioritize minimal environmental impact and limited persistence in ecosystems by emphasizing their inherent capacity to break down over time. Achieving this objective involves integrating biodegradable materials and practices, which aligns seamlessly with the principles of sustainable development. The amalgamation of degradation, alongside other environmentally conscious attributes, signifies the evolution of green corrosion inhibitors towards more responsible and effective corrosion prevention methodologies.<sup>110</sup>

### 1.5. Green metallic materials: pursuit of sustainable corrosion inhibition

Metallic materials, especially steel alloys are the most commonly used metallic alloys for building materials across various industries, including infrastructure development, because of their high mechanical strength, extended lifespan, versatility, and low cost.<sup>111,112</sup> The annual steel output already exceeds 2 billion tons; by 2050, it is projected to increase by 33%.<sup>113,114</sup> In the oil-gas and petroleum sectors, these alloys have also been used widely for building transport pipes, storage tanks, distillation and purification towers, *etc.* Iron is recovered from two types of ore, *i.e.*, magnetite ( $\text{Fe}_3\text{O}_4$ ) and hematite ( $\text{Fe}_2\text{O}_3$ ), using a blast furnace and a significant amount of coke or coal. However, steel production releases considerable  $\text{CO}_2$ , a greenhouse gas (GHG) contributing 7–11% of global GHG emissions.<sup>115,116</sup> To maintain global warming (GW) at 1.5 °C, the United Nations (UN) advises that

industry GHG emissions must be drastically decreased.<sup>117,118</sup> To accomplish this goal, the steel industry and other sectors must reduce their GHG emissions by 93% by 2050 (IEA; International Energy Agency). The steel industry is one of the largest  $\text{CO}_2$  producers. In the UK, 25% of all industrial GHG emissions are related to the manufacturing of steel.<sup>119</sup> Fig. 8 depicts the amount of energy used by significant UK industries together with their greenhouse gas emissions.<sup>119,120</sup>

A literature examination revealed that a ton of steel ore heated in a blast furnace emits 1710–1714 kg  $\text{CO}_2$ .<sup>119,120</sup> Coke production and sintering are responsible for almost 90% of the  $\text{CO}_2$  emissions from blast furnaces. Alternatively, renewable energy sources, electrification, and hydrogen are often used as fuel to produce green carbon steel. Recently, to reduce  $\text{CO}_2$  emissions and limit local warming, many European countries, including the UK, have started restricting steel production using conventional methods. The two most practical and efficient strategies to minimize GHG emissions are electrification and hydrogen as a fuel, but they are also likely to be expensive. The cost of steel produced through direct reduction utilizing electricity and hydrogen would reportedly be 20–30% costlier than steel generated through conventional steel building. The fact that hydrogen is a low- or zero-carbon energy source should be emphasized. However, roughly 70% of steel is created using blast furnace heating. Alternatively, in Sweden, the United States, and Europe in particular, where GHG emissions have decreased by 95%, 20%, and 40%, respectively, hydrogen-based steelmaking has made significant achievements.

Techniques and procedures to address socioeconomic and environmental problems are in great demand due to the increased ecological concerns about green chemistry and sustainable development. Due to urbanization and industrialization, carbon steel is one of the most often used metal-based

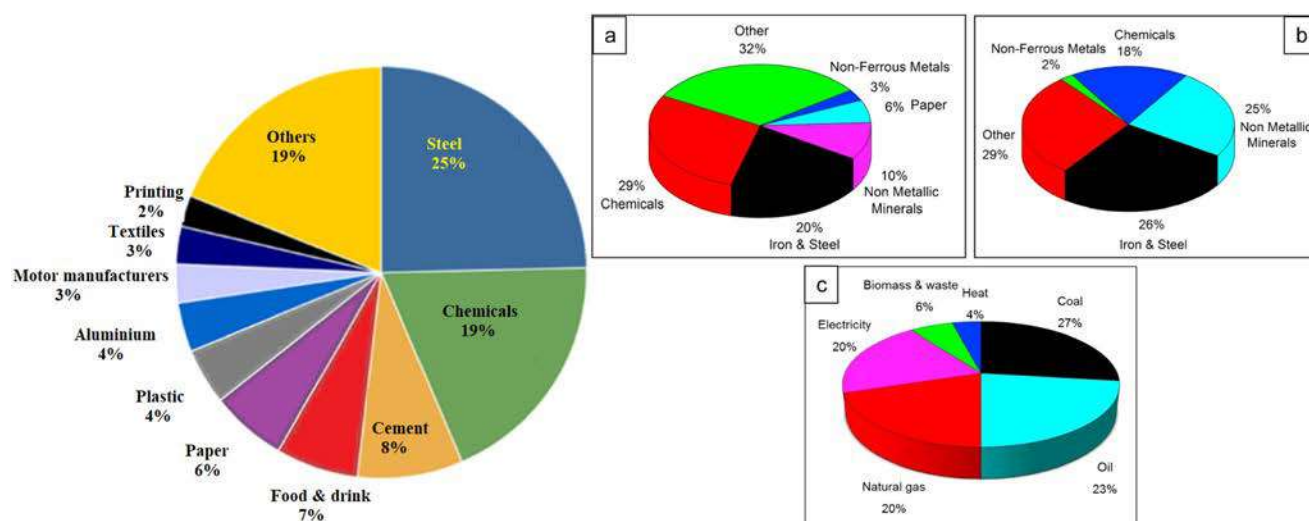


Fig. 8 (Left) Greenhouse gas (GHG) emissions from the UK industry.<sup>119</sup> [Reproduced from ref. 119 with permission, Copyright, Elsevier, 2021.] (Right) (a) Share of energy consumption in the industrial sector; (b)  $\text{CO}_2$  emissions and (c) final energy use in the industrial sector by fuel type.<sup>120</sup> [Reproduced from ref. 120 with permission, Copyright, Elsevier, 2021.]

construction materials, and its use and production are both predicted to increase. Thus, steel industry experts and authorities are searching for ways to develop efficient and sustainable steelmaking processes that have the potential to reduce the global CO<sub>2</sub> emissions to almost zero to lessen the impact of GHG emissions. Compared to conventional blast furnace steelmaking, it is thought that the global CO<sub>2</sub> emissions from the production of green carbon steel can be reduced by 95%. Notably, the release of about two tons of CO<sub>2</sub> into the environment is correlated with the production of one ton of steel. Currently, there is a two billion-ton annual demand for steel worldwide. Thus, the production and marketing of green carbon are necessary for its advancement. Since 1975, up to a 50% reduction in GHG emissions has been achieved due to efforts such as carbon capture and storage (CCS), using bioenergy instead of coal for heating, electrification, and using hydrogen as an energy carrier. However, despite the substantial improvements in the creation of green carbon steel, around 75% of steel manufacturing is still heated using fossil fuels. Nevertheless, many nations, notably those in Europe, aim to address this issue, where Sweden is currently leading globally.<sup>121</sup> Projections show that 31% of global steelmaking companies heat their facilities without the use of fossil fuels.

A Swedish company estimated that the cost of green carbon steel will be 20–30% higher than carbon steel made from fossil fuels. This method requires 144 000 tons of hydrogen to produce the two million tons of green steel. Fortunately, the use of green carbon steel may not impact the overall cost of the finished goods. For instance, the value of a middle-size vehicle would only increase by 0.3% to 0.7%, or not more than €250, if traditional carbon steel was converted to green carbon steel at a rate of 100%. Engine cars contribute roughly 23% of GHG emissions. Similarly, steel contributes approximately 25% of appliance carbon emissions. However, switching entirely from traditional to green carbon steel would only add about 2–4% to the price of the appliance, or about €12. Notably, the use of fossil-free heating reduces GHG emissions and coal pollutants. Nevertheless, heavy metal and chemical impurities related to iron ores remain, and thus may need particular treatments before discharge.

## 2. Green corrosion inhibition: current advancements and future directions

### 2.1. Green corrosion inhibition by selection: replacement of toxic alternatives

Sustainable chemistry or “green chemistry” is a relatively new and expanding field of chemistry and chemical engineering that focuses on developing goods and procedures that utilize less harmful materials and produce less waste. Recently, the manufacture and use of risky conventional volatile corrosion-inhibiting substances have been prohibited by regulations related to the environment and the global growing ecological consciousness. Therefore, improving synthetic and engineering chemistry using environmentally benign starting materials

or carefully planning synthesis employing non-classical energy sources such as ultrasound and microwave heating is imperative. One of the best alternative synthetic methodologies for “green synthesis” is the use of MCRs in conjunction with ultrasonic (sonochemical) and microwave irradiation. Green corrosion inhibition refers to the use of environmentally friendly and non-toxic substances to prevent or reduce the corrosion of metals. The goal is to replace traditional corrosion inhibitors that may be toxic or harmful to the environment and human health. This approach is aligned with sustainable practices and is gaining increasing attention as industries seek to reduce their environmental impact.<sup>122,123</sup>

To achieve green corrosion inhibition, researchers and industries are focused on finding alternative corrosion inhibitors that meet the following criteria:

a. *Non-toxic*: The selected inhibitors should not pose risks to human health or the environment during production, application, or disposal.

b. *Biodegradable*: The inhibitors should be easily broken down by natural processes, reducing their environmental persistence.

c. *Renewable*: Preferably, the inhibitors should be derived from renewable resources, which ensures a continuous supply without depleting finite resources.

d. *High performance*: The selected inhibitors should effectively protect metals from corrosion, maintaining or surpassing the performance of traditional toxic inhibitors.

e. *Cost-effective*: The inhibitors should be economically viable and comparable in cost to conventional inhibitors to encourage their widespread adoption.

f. *Minimal side effects*: The inhibitors should not adversely affect the properties or performance of the metal substrate.

g. *Compatibility*: The chosen inhibitors should be compatible with existing corrosion protection methods and coatings.<sup>124,125</sup>

The selection of a suitable green corrosion inhibitor depends on various factors, such as the metal to be protected, the environment in which it will be used, and the specific corrosion challenges it needs to address. Extensive research and testing are necessary to identify and optimize the most effective and environmentally friendly option for a particular application. Replacing toxic alternatives with green corrosion inhibitors is a step toward sustainable and responsible corrosion protection practices, contributing to preserving human health and the environment.<sup>126</sup> Researchers are exploring various green corrosion inhibition strategies, such as using plant extracts, naturally occurring compounds, green synthesis of nanoparticles, and bio-based polymers. These substances have shown promising results in laboratory studies as corrosion inhibitors for different metals. However, although progress is being made in this field, it is important to note that developing effective green corrosion inhibitors may require further research and testing before they can be widely adopted in industrial applications. The choice of the most suitable inhibitor may also vary depending on the specific metal, environment, and intended application. The movement

towards green corrosion inhibition reflects a broader trend in seeking sustainable and environmentally responsible solutions across various industries. In this regard, Goni *et al.* (2019), Shehata *et al.* (2018) and Verma *et al.* (2018) demonstrated the application of green corrosion inhibitors such as plant extracts, ionic liquids, heterocyclic organic compounds, nano-materials, drug molecules, and carbon allotropes, and their advantages and future outlook.<sup>102</sup> Promoting the replacement of toxic alternatives contributes to the overall goal of reducing the impact of human activities on the planet.<sup>127,128</sup>

There are several other approaches to achieving green corrosion inhibition, as follows:

**Bio-based inhibitors:** These are derived from natural sources, such as plant extracts, essential oils, and biodegradable polymers. They offer adequate corrosion protection, while being non-toxic and eco-friendly. **Green synthesized inhibitors:** These are compounds synthesized using green chemistry principles, which aim to minimize the use of hazardous substances and reduce waste generation. **Nanotechnology-based inhibitors:** Nanostructured materials can be corrosion inhibitors due to their unique properties. Some nanomaterials have shown excellent corrosion inhibition performance, while being relatively environmentally safe. **Passivation techniques:** Instead of chemical inhibitors, passivation methods can form a protective layer on the metal surface, preventing corrosion. Passivation often involves the use of non-toxic substances. **Hybrid inhibitors:** These are combinations of different non-toxic substances or methods to provide enhanced corrosion protection.

Researchers and industries are actively exploring green corrosion inhibitors to promote sustainability and reduce their environmental impact. These inhibitors are designed to be as effective as their traditional counterparts but without the negative environmental consequences. The selection and replacement of toxic alternatives involve finding suitable green corrosion inhibitors to replace those currently in use. This process involves the following: **Identifying non-toxic compounds:** Researchers are searching for compounds that have inhibitive properties but are non-toxic to humans and the environment. Natural compounds, plant extracts, and biodegradable materials are often considered for this purpose. **Screening and testing:** Once potential green corrosion inhibitors are identified, they undergo rigorous screening and testing. Various parameters, such as corrosion rate, inhibition efficiency, and compatibility with the metal surface, are evaluated to determine their effectiveness. **Performance comparison:** The selected green corrosion inhibitors are compared with traditional toxic ones to ensure they provide similar levels of corrosion protection. **Application feasibility:** Besides corrosion inhibition efficiency, practical aspects such as cost-effectiveness, ease of application, and long-term stability are considered to ensure that green inhibitors are viable alternatives. **Implementing and promoting green practices:** After successful identification and testing, industries and end-users are encouraged to adopt green corrosion inhibitors and replace toxic alternatives. Khanari *et al.* reviewed green corrosion inhibitors for aluminium and its alloys. In the same vein, different literature

reviews have shown that phytochemicals can act as green corrosion inhibitors in various corrosive conditions.<sup>129–132</sup> By adopting green corrosion inhibitors, industries can reduce their environmental footprint and contribute to sustainable practices. Additionally, choosing non-toxic alternatives can lead to safer working conditions for employees and improved environmental protection. Thus, the transition to green corrosion inhibition is essential to a more sustainable and eco-friendly future.

Gravimetric analysis and electrochemical investigations are performed to learn about the basic properties of corrosion inhibitors, for example, adsorption nature, corrosion potential, inhibition efficiency, and adsorption types on the surface of metals by the inhibitor. In general, this can be performed in the lab *via* weight loss (WL) measurement, which does not require complicated or expensive tools. Electrochemical systems are typically three-electrode systems in which the metal to be inhibited is employed as the working electrode. Electrochemical tests often involve open circuit potential (OCP), linear polarization resistance (LPR), electrochemical impedance spectroscopy (EIS) and potentiodynamic polarization (PDP) studies. El Ibrahim (2020) used experimental methodologies in which WL and EIS demonstrated that the correct sequence of %IE follows the order of MPBD > PBD > DMBD, which can be attributed to the presence of electron-donating groups.<sup>133</sup> Alaoui (2018) extensively examined triazepine carboxylate derivatives such as Cl–Me–CO<sub>2</sub>Et, Me–CN, and Cl–Me–CN, with Cl–Me–CN having a %IE of 99% at a concentration of 10<sup>−3</sup> M.<sup>134</sup> Mo (2017) used a Schiff base, *N*-isonicotinamido-3-methoxy-4-hydroxybenzalaldehyde (IM), to create vanillin and isoniazid green corrosion inhibitors, which demonstrated outstanding inhibition effectiveness according to the EIS analysis.<sup>135</sup> Abdallah (2016) utilized phenyl sulphonyl ethanone derivatives (PSED) compound-1 and compound-2 with reported values of 85.5% and 83.5% at 5 × 10<sup>−4</sup> M, respectively.<sup>136</sup> According to Yadav *et al.* (2016), EIS analysis indicated %IE values of 95.7% for BIHT and 91.9% for MIHT. Their increased value is related to the presence of heteroatoms (N, O, S) and aromatic rings from the inhibitors, which significantly interact with the surface of Fe (110).<sup>137</sup>

Experimental approaches help determine corrosion mitigation on metals and alloys in harsh media. Therefore, many experimental techniques such as gravimetric and electrochemical analyses are widely used. These approaches are also used for determining the primary effectiveness of inhibitors in corrosion inhibition. 2-mercaptobenzothiazole (MBT)-functionalized ILs are used to prevent corrosion. EIS and PDP studies demonstrated that MBT-functionalized inhibitors inhibited corrosion in bronze significantly more than the standard IL [BMIM][BF<sub>4</sub>].<sup>138</sup> The two new green ILs [VAIM][PF<sub>6</sub>] and [VAIM][BF<sub>4</sub>] displayed effective corrosion inhibition for carbon steel in 1.0 M HCl solution, with [VAIM][PF<sub>6</sub>] performing better than [VAIM][BF<sub>4</sub>].<sup>139</sup> Two ammonium-derived ILs, *N*-trioctyl-*N*-methyl ammonium (TMA) methyl sulphate and *N*-tetradecyl-*N*-trimethyl ammonium (TTA) methylsulfate, were applied as corrosion inhibitors for API-X52 steel (1 M HCl), in which TMA

showed 85% inhibition efficiency. In contrast, TTA exhibited 68% %IE according to the electrochemical analysis at the optimum concentration of 0.209 mM and 0.272 mM, respectively.<sup>140</sup> Three pyrazine derivatives, HMIMI, BMIMI, and MPIMI, were used as corrosion inhibitors for mild steel (1 M HCl), and their inhibition efficiencies were determined to be 93.1%, 87.8%, and 80.4%, respectively, according to EIS measurements at their optimum concentration of  $1 \times 10^{-3}$  M.<sup>141</sup> At low temperatures, [BsMIM][HSO<sub>4</sub>] and [BsMIM][BF<sub>4</sub>] showed strong corrosion inhibition characteristics in hostile medium (1 M H<sub>2</sub>SO<sub>4</sub> solution). The inhibitory efficiency of [BsMIM][BF<sub>4</sub>] and [BsMIM][HSO<sub>4</sub>] is quite comparable.

Traditional approaches are widely used in experiments to assess corrosion and its process in metallic materials such as metals and alloys. Cao *et al.* (2020) investigated the effect of N-doped carbon dots on carbon steel corrosion in sulphuric acid media. They evaluated N-doped CDs as corrosion inhibitors for carbon steel using X-ray diffraction spectroscopy (XRD), Fourier transform infrared spectroscopy (FTIR), transmission electron microscopy (TEM), and electrochemical methods. According to the PDP study, they reported 97.8% percentage inhibition efficiency at a concentration of 30 mg L<sup>-1</sup> N-CDs. They also observed that as the concentration of inhibitor increased, the values of anodic Tafel slope ( $\beta_a$ ) and cathodic Tafel slope ( $\beta_c$ ) decreased gradually. The PDP results demonstrated their good corrosion inhibition ability.<sup>142</sup> Saraswat and Yadav (2020) published similar results, in which they employed S, N co-doped CDs as a possible corrosion inhibitor for mild steel in 1 M HCl. The WL and electrochemical techniques were used in their investigation. CD1 and CD2 had inhibitory efficiencies of 94.4% and 90.8%, respectively, at their optimal concentrations, according to the EIS measurements.<sup>143</sup> Surface characterization methods, such as FTIR, XRD, scanning electron microscopy (SEM), energy dispersive X-ray spectroscopy (EDS), atomic force microscopy (AFM), and X-ray photoelectron spectroscopy (XPS), were used to determine their inhibitory efficiency, adsorptive property, and interaction with metal surfaces. The morphological changes in the metal surface in the presence of an acidic solution were examined using these techniques before and after using the inhibitors. The chemistry of the metal surface was investigated using EDS. The AFM and XPS methods were used to describe the changes in the bonding energy between the 3D metal surface and inhibitor.

Yuwei *et al.* (2020) also investigated the inhibitory performance of N-doped citric acid-based CDs on the surface of mild steel in 1 M HCl electrolyte.<sup>144</sup> They described a variety of methodologies for determining the inhibitory performance of the CD materials, including electrochemical measurement, FTIR, XPS, SEM, and AFM. The results of the surface characterization demonstrated great agreement with the other applied techniques.<sup>144</sup> Organic compounds containing heteroatoms (O, P, N, S) have been widely explored as mild steel corrosion inhibitors. Jia *et al.* (2011) studied the inhibitory characteristics of L-cysteine derivatives such as NASHCYS, NACYS, NASBCYS, and CYS in mild steel corrosive solutions contain-

ing 1 M HCl. Their study included the density functional theory (DFT), molecular dynamics (MD) simulation, PDP, and WL techniques. NASBCYS was shown to be the most effective corrosion inhibitor among the inhibitors tested.<sup>145</sup> Muthukrishna *et al.* (2014) used AC impedance, PDP, and WL methods to assess the %IE of CDHBAP against mild steel in a corrosive solution of 1 M H<sub>2</sub>SO<sub>4</sub>.<sup>146</sup> The results showed that CDHBAP has 99% %IE at 100 ppm concentration. The creation of a protective barrier over the metal surface was verified by SEM and FTIR.<sup>146</sup> Ousslim *et al.* (2009) evaluated the mild steel corrosion inhibition efficiency of two piperazine derivatives in an aggressive solution of 3.9 M HCl through the PDP and WL methods.<sup>147</sup> Mohamed (2006) investigated quinine as a corrosion inhibitor for low carbon steel in HCl solution using the PDP and EIS methodologies, reporting an inhibition efficacy of 96% at a concentration of 0.48 mM.<sup>148</sup> Rajeswarie *et al.* (2013) investigated the inhibition activity of three Schiff bases on cast iron using aqueous solutions of NaCl, NaOH, NH<sub>4</sub>Cl, and HCl.<sup>149</sup> The additive impact of KI synergism was investigated. Electrochemical measurements and the WL technique were employed for this aim. The results showed that at low temperatures, the inhibitory efficiency was reduced with an increase in concentration. Also, it was discovered that the adsorption of Schiff base obeyed the Langmuir adsorption isotherm with and without KI.<sup>149</sup> At the optimal concentration (303 K), Inh III (R = -OCH<sub>3</sub>) demonstrated an inhibition efficacy of 90.5%.<sup>150</sup> At high concentrations, Gemini surfactant had an %IE of 94.2%.<sup>151</sup>

## 2.2. Green corrosion inhibition using natural products (plant extracts, amino acids, carbohydrates, etc.)

The use of green corrosion inhibitors generated from natural sources presents a possible route towards a more sustainable and corrosion-resistant future for metal-based infrastructure and applications, as society increasingly values sustainability and environmental responsibility. Recent years have seen a substantial increase in interest in using natural ingredients as green corrosion inhibitors as part of a larger commitment to environmentally benign and long-lasting corrosion prevention techniques. The concepts, processes, and use of these eco-friendly inhibitors are highlighted in this section, which examines the developing topic of "green corrosion inhibition using natural products". The intrinsic corrosion inhibition capabilities of natural products, including plant extracts, essential oils, and bio-based compounds, are thoroughly examined. Compared to conventional chemical inhibitors, these inhibitors have a lower environmental effect due to their emphasis on eco-friendliness and biodegradability. Natural products have the potential to change corrosion protection tactics in a variety of sectors, while also shedding light on current research initiatives and difficulties in the industry.

Substances originating from plants, animals, or other naturally occurring sources are referred to as natural products. They are often employed in several fields, including medicine, cosmetics, and even corrosion inhibition. Natural goods are prized for their possible medicinal benefits, low environ-

mental impact, and environmentally friendly manufacturing processes.<sup>152</sup> Plant extracts, essential oils, proteins, polysaccharides, and other substances can all be included. These organic components are more environmentally friendly than synthetic compounds and are well-known for their wide range of uses.<sup>153</sup> Although several synthetic chemicals have shown effective anticorrosive properties, the majority are very harmful to both humans and the environment. Industry use of corrosion inhibitors has long raised safety and environmental concerns on a worldwide scale. These inhibitors may harm organ systems, such as the kidneys and liver, either temporarily or permanently, or they may interfere with biochemical processes or enzyme systems at a specific location inside the body.<sup>154</sup> The toxicity may manifest either during the synthesis of the compound or its applications. Thus, natural anticorrosion products, which are safe for the environment and non-toxic, are now often used as a result of these hazardous consequences. Fig. 9 depicts how natural products can be used to inhibit green corrosion. The suitability of several natural compounds that have been investigated as corrosion inhibitors is described in the following sections.

**2.2.1. Plant extracts.** Due to the rising demand for green chemistry in science and technology, the development of green corrosion inhibitors and green inhibition techniques has recently been in high demand. The last few decades have witnessed a substantial increase in interest in using plant extracts as inhibitors of metallic corrosion. Plant materials are excellent eco-friendly replacements for conventional harmful corrosion inhibitors. Also, plant extracts are a good alternative to the pricy and hazardous conventional synthetic corrosion inhibitors because of their lower environmental risk, lower

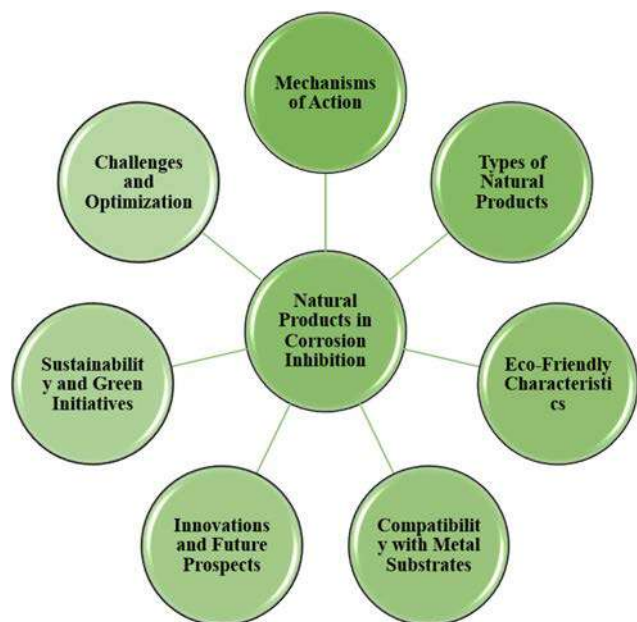


**Fig. 9** Schematic presentation of different aspects of using natural products in corrosion protection [self-illustration, copyright permission not required].

cost, wide availability, and strong corrosion inhibition efficiency. A review of the literature suggests that various extracts, including leaf, root, stem, bark, pulp, and fruit, have been used successfully as long-lasting inhibitors of corrosion for various metals and alloys.<sup>155</sup> The non-nutritive components of plants that give them their flavor, fragrance, and color are known as phytochemicals. The phytochemicals obtained from different parts of the plants are shown in Fig. 10A. There are various groups of phytochemicals that may be divided, including terpenoids, polyphenols, and organic acids.

The electronic structures of phytochemicals frequently resemble conventional synthetic organic corrosion inhibitors. Consequently, it is understood that different compounds can provide corrosion resistance under varying corrosive circumstances.<sup>13</sup> Since the majority of plants and their extracts are non-toxic, they are a great alternative to toxic organic inhibitors. Fig. 10B displays several inhibitors obtained from various plant sections. They are especially appealing because of how quickly they can be disposed of due to their biodegradable nature. Additionally, their extraction process is very simple and inexpensive. Extracting ecologically friendly corrosion inhibitors from a range of plant parts, such as fruit, leaves, bark, roots, seeds, or peels, is conceivable. The inhibitory effects of a plant extract are frequently caused by a combination of phytochemicals with various functional groups capable of sticking to the surface of metals. However, the intricate makeup of biomass extracts has prevented a thorough understanding of their mechanism for inhibiting corrosion. Analyzing each of the distinct and/or combined interactions of organic species on the metal surface is difficult without first isolating the active elements of any biomass extract. Plant extracts can be seen as eco-friendly and sustainable resources as inhibitors for metals and alloy corrosion in hostile media, such as HCl, H<sub>2</sub>SO<sub>4</sub>, H<sub>3</sub>PO<sub>4</sub>, and HNO<sub>3</sub>.<sup>128</sup> This is due to their biological and natural origins, as well as their eco-friendly extraction. Plant extracts were obtained using a variety of techniques in the literature. However, the scope of the current review does not allow a thorough discussion of these techniques. Fig. 11 illustrates an outline of the extraction procedure.<sup>20</sup>

Celandine (*Chelidonium majus*) and the dried stems, leaves, and seeds of other plants were employed as plant extracts in the 1930s in H<sub>2</sub>SO<sub>4</sub> pickling baths. A corrosion-controlling additive called ZH-1 was created, which was made of finely divided oil cake, a by-product in the production of phytin. According to Saleh *et al.*,<sup>156</sup> steel is well protected by *Opuntia* extract, *Aloe eru* leaves, orange peels and mango peels in 5% and 10% HCl at 25 °C and 40 °C, respectively. According to Srivastav,<sup>157</sup> lignin, castor oil seeds, acacia gum, black pepper, tobacco, and black pepper all work well as steel inhibitors in an acidic environment. The effectiveness of caffeine<sup>158</sup> and nicotine<sup>159</sup> in preventing metallic corrosion was investigated. The use of herbs (such as anise, hibiscus, garden cress, coriander, and black cumin) as a new form of green inhibitors for the acidic corrosion of steel was demonstrated by Khamis *et al.*<sup>160</sup> El-etre<sup>161</sup> researched the use of natural honey as a



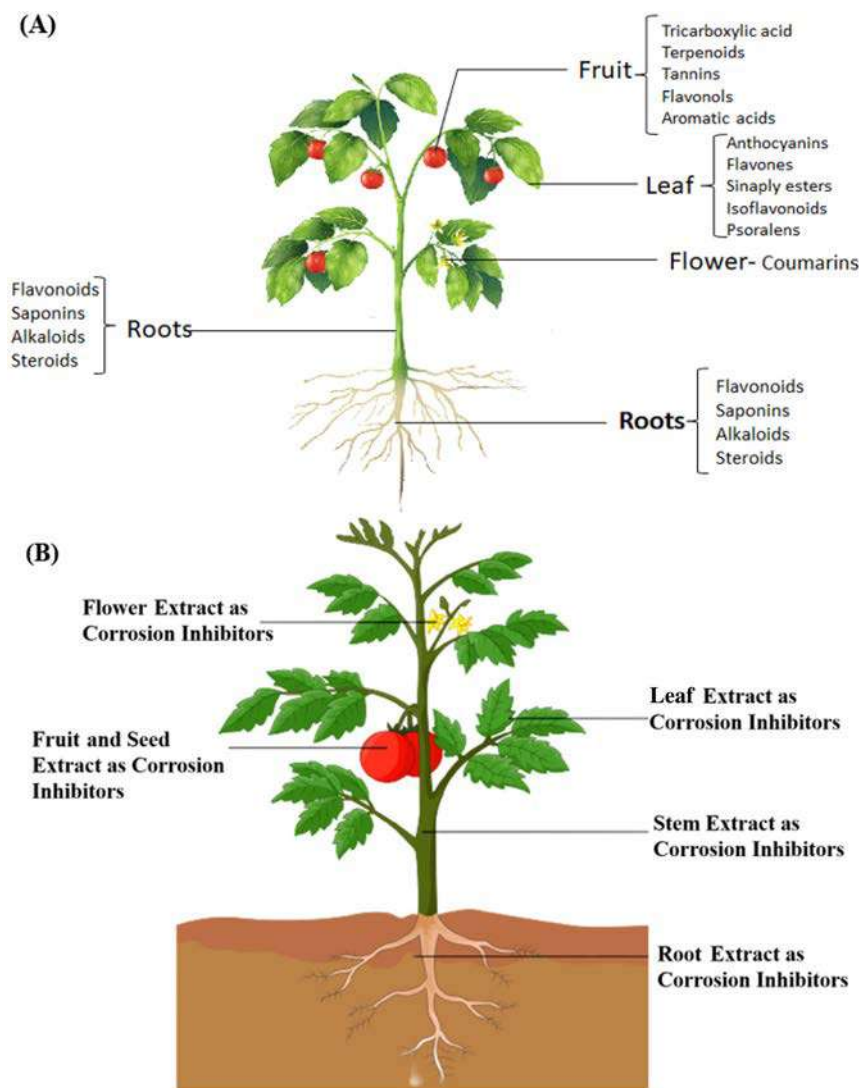


**Fig. 10** (A) Outline of the phytochemicals obtained from different parts of the plant and (B) parts of the plant utilized as corrosion inhibitors [self-illustration, copyright permission not required].

copper aqueous solution corrosion inhibitor. Carbon steel has also been the subject of a similar investigation.<sup>162</sup> Sathiyathan *et al.*<sup>163</sup> investigated the effects of an ethanolic extract of *Ricinus communis* leaves on the prevention of mild steel from corroding in acid medium. The anticorrosion activity of henna<sup>164</sup> and thyme<sup>165</sup> extracts was examined. Pomegranate peel<sup>166–169</sup> and beet root<sup>170</sup> were investigated as corrosion inhibitors in different corrosive environments. *Emblica officinalis*,<sup>171</sup> *Terminalia chebula*,<sup>172–174</sup> *Terminalia bel-lirica*,<sup>175</sup> and *Acacia concinna*<sup>176</sup> have all been studied for their anticorrosion properties.

For steel in acid medium, corrosion prevention studies have also been conducted using extracts of *Eucalyptus* leaves, *Carica papaya*, *Annona squamosa*, *Swertia angustifolia*, *Pongamia glabra*, *Azadirachta indica*, *Eugenia jambolans*, *Accacia Arabica*, and *Vernonia amygdalina*.<sup>177</sup> Tea wastes<sup>178</sup> and *Andrographis*

*paniculata*<sup>179</sup> have both been found to have anticorrosive properties. *Rosmarinus officinalis* aqueous extract was examined by Kliškić *et al.*<sup>180</sup> as an aluminium alloy corrosion inhibitor in a chloride solution. Abdallah *et al.*<sup>181</sup> examined the anticorrosion properties of guar gum. Martinez and Štern<sup>182</sup> conducted research on the Mimosa tannin-induced inhibition of low carbon steel corrosion in H<sub>2</sub>SO<sub>4</sub> medium. In both HCl and H<sub>2</sub>SO<sub>4</sub> medium, Oguzie looked into the effectiveness of *Telfairia occidentalis* extract as a corrosion inhibitor.<sup>183</sup> Awiri and colleagues investigated the ability of *Vernonia amygdalina* to prevent the corrosion of aluminium alloys in HCl and HNO<sub>3</sub>.<sup>184</sup> Gunasekaran *et al.*<sup>185</sup> investigated the inhibition of mild steel corrosion by *Zanthoxylum alatum* extract in aqueous orthophosphonic acid. The leaves of *Nypa fruticans wurmb*<sup>186</sup> were investigated for their ability to prevent mild steel from corroding in HCl solution. The impact of saccharides, specifi-

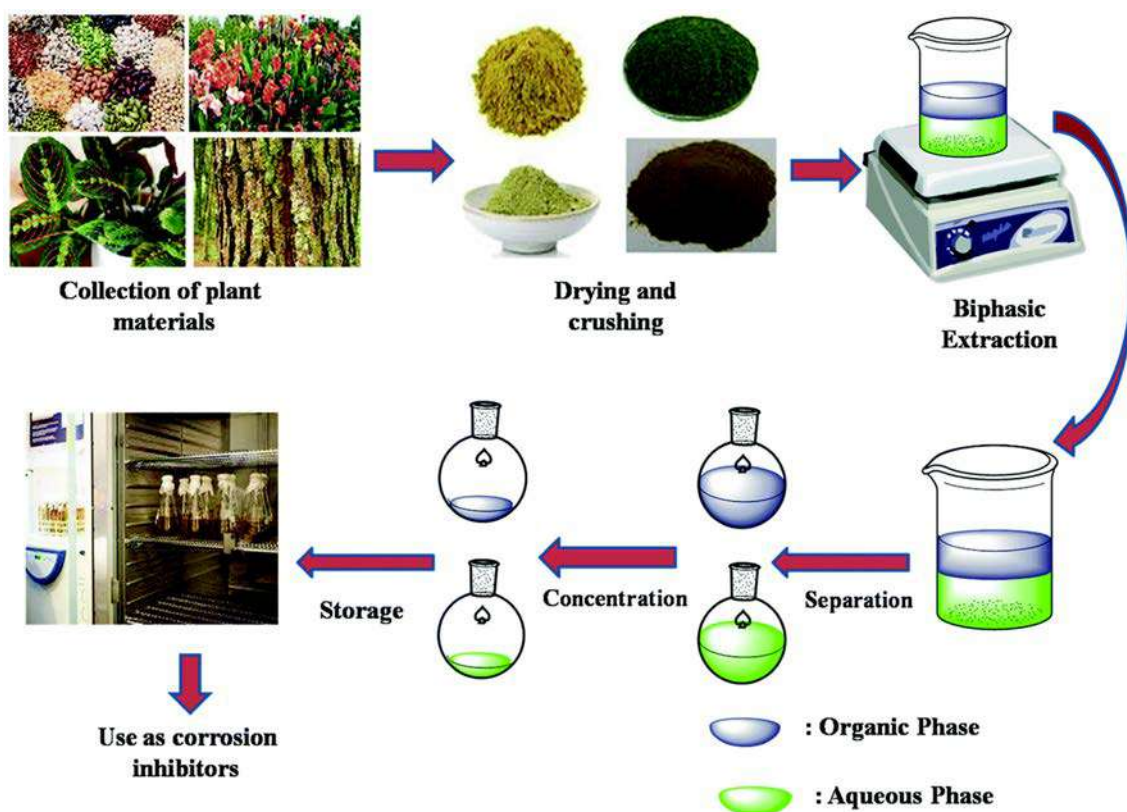


Fig. 11 Schematic diagram of extraction procedure of phytochemicals.<sup>20</sup> [Reproduced from ref. 20, RSC publication, copyright permission is required.]

cally reducing sugars like mannose and fructose, on the dissolution of zinc and aluminum in alkaline conditions was studied by Müller.<sup>187</sup>

Hammouti *et al.* investigated the extracts of ginger,<sup>188</sup> jojoba oil,<sup>189,190</sup> eugenol, and acetyl-eugenol<sup>191</sup> for the purpose of preventing the corrosion of steel in acidic environments. Oguzie investigated the inhibitory effects of *Sansevieria trifasciata* extract<sup>192</sup> and *Ocimum viridis* extract<sup>193</sup> on the acid and alkaline corrosion of aluminium alloy. El-Etre *et al.*<sup>194</sup> investigated the effects of Lawsonia extract against the acid-induced corrosion of metals, khillah extract<sup>195</sup> for the inhibition of SX 316 steel corrosion in acid media, *Opuntia* extract<sup>196</sup> for the inhibition of aluminium corrosion in acid medium, and vanillin<sup>197</sup> for the inhibition of mild steel corrosion in acid media. Li *et al.*<sup>198</sup> investigated the anticorrosion properties of berberine, an alkaloid isolated from *Coptis*, for mild steel corrosion in H<sub>2</sub>SO<sub>4</sub> medium. *Cassia occidentalis*, *Carica papaya*, *Delonix regia*, and *Datura stramonium* as well as *Azadiracta indica*, *Calotropis procera*, and *Auforpio turkiale* sap, have all been reported to be effective as inhibitors of acid corrosion by Zucchi and Omar.<sup>199</sup> Awad<sup>200</sup> investigated the anticorrosive properties of quinine on carbon steel in 1 M HCl.

Numerous of these plant extracts exhibit corrosion inhibitory action, which may be caused by the presence of heterocyclic components such as alkaloids and flavonoids. Even the presence of cellulose, tannins, or polycyclic chemicals tends to

increase the number of layers that form over the metal surface, which promotes corrosion inhibition. Thus, according to the current debate, it may be inferred that plant extracts are the best candidates to replace the conventionally used, costly, and hazardous inorganic and synthetic organic corrosion inhibitors. Numerous phytochemicals and other compounds found in plant extracts have excellent adsorption and corrosion-inhibiting properties. As efficient corrosion-control agents for aluminium, steel, and other metallic materials in acidic (HNO<sub>3</sub>, H<sub>2</sub>SO<sub>4</sub>, H<sub>3</sub>PO<sub>4</sub> and HCl), basic (NaOH), and neutral (NaCl) conditions, a wide variety of extracts, including leaves, roots, stems, and other extracts, have been investigated. It has been noted that the leaf is the part of the plant that contains the most phytochemicals, which is where they are produced.

**2.2.2. Essential oils.** Hydrophobic liquids (concentrated) generated from plants are called essential oils. Volatile oils, etherolea, and ethereal oils are other names for essential oils. Generally, essential oils encapsulate the essence of the source ingredients from which they are extracted.<sup>201</sup> Since they are biocompatible with the natural world, these oils are also regarded as “green” or eco-friendly inhibitors. The use of affordable, potent materials with little to no environmental harm is the primary goal of research into environmentally friendly corrosion inhibitors. Additionally, the potent anticorrosion, antibacterial, biodegradable, and readily available properties of essential oils have made them particularly appealing

for use in large-scale applications. The idea behind using essential oils as corrosion inhibitors is that they can create a shield on the surface of metals, which slows down the corrosion process. By acting as a physical barrier, this shield keeps corrosive substances such as oxygen and moisture from coming into contact with the metal surface. Also, the organic substances present in essential oils, such as terpenes and phenols, naturally have anti-corrosive characteristics. These substances may adhere to metal surfaces when applied, forming a coating that prevents the electrochemical processes that lead to corrosion. In addition, essential oils are preferred for preventing corrosion given that they are non-toxic and safe for the environment, making them a better option than conventional chemical inhibitors. The idea of employing essential oils as corrosion inhibitors is consistent with the quest of sustainable and environmentally friendly corrosion protection techniques for various metals, although the research in this field is still ongoing.

The effective use of a variety of essential oils to prevent metal corrosion in both acidic and alkaline environments has been covered in numerous reports. Essential oils, including jojoba oil,<sup>189,190</sup> rosemary oil,<sup>202–204</sup> *Artemisia* oil,<sup>205</sup> and *Eucalyptus* oil,<sup>206</sup> have been evaluated as effective inhibitors against corrosion. Additionally, it has been discovered that essential oils obtained from various sources work well as anticorrosion agents for a variety of metals in a variety of hostile conditions (e.g., HCl, H<sub>2</sub>SO<sub>4</sub>, and NaCl). According to the results, oil adheres to the metal surface and slows corrosion. Znini *et al.*<sup>207–209</sup> observed that essential oils such as *Mentha spicata* and *Warionia sahara* prevent the corrosion of steel in acidic environments. Also, the use of Moroccan *Ammodaucus leucotrichus* fruit-derived essential oils, *Limbarda crithmoides*,<sup>210</sup> and *Verbena officinalis*<sup>211</sup> to prevent mild steel corrosion in HCl medium has been studied.

The possible use of green inhibitors based on essential oils has attracted increasing interest in recent years. Numerous investigations have been conducted to define a variety of essential oils and assess how well they prevent metal corrosion brought on by chemical assault. However, there are few published findings on the effectiveness of essential oils for inhibiting microbial-induced corrosion.<sup>212</sup> Additionally, to date, there are no published studies on the anticorrosion properties of commercially available ultra-pure essential oils such as cinnamon, clove, basil, and oregano against harsh environments. This may be due to the fact that although they show significant technological promise, ultra-pure commercial essential oils are very expensive, resulting in a lack of interest in employing them as corrosion inhibitors. Alternatively, essential oils have strong antibacterial properties.<sup>213</sup> López *et al.*<sup>214</sup> assessed the antimicrobial activity of essential oils of *Rosmarinus officinalis*, *Syzygium aromaticum*, *basillicum*, *Anethum graveolens*, *Origanum vulgare*, *Zingiber officinalis* *Thymus vulgaris* and *Cinnamon zeylanicum* against a group of food-borne bacteria (e.g., yeast, *A. flavus*, *P. islandicum*, and *C. albicans*). Ağaoğlu *et al.*<sup>215</sup> reported that a few dietary additives, such as essential oils (red crushed pepper, anise, cumin, cloves, poppy, cardamom,

ginger, fennel, and cinnamon), exhibited antibacterial action against certain microorganisms (*M. luteus*, *P. aeruginosa*, *K. pneumoniae*, *E. faecalis*, *E. coli*, *S. aureus*, and *C. albicans*). With the exception of *M. luteus*, cinnamon was determined to be the most effective antibacterial agent. The essential oils of cloves, cinnamon, cumin, and fennel had less antibacterial action against these bacteria.

A literature survey also revealed that various other essential oils such as *Artemisia herba-alba*,<sup>216–220</sup> *Artemisia mesatlantica*,<sup>221,222</sup> *Artemisia abrotanum*,<sup>223,224</sup> *Rosmarinus officinalis*,<sup>225–227</sup> *Eucalyptus globulus*,<sup>228–231</sup> *Foeniculum vulgare*,<sup>232</sup> *Syzygium aromaticum* (Clove),<sup>233</sup> *Carum carvi*<sup>234</sup> have been applied for the protection of various metals and alloys in different corrosive environments. As corrosion inhibitors for different metals, essential oils have demonstrated remarkable promise. They are a desirable replacement for conventional chemical inhibitors due to their natural and environmentally benign qualities as well as their capacity to create protective barriers on metal surfaces. However, to completely comprehend their operations and maximize their efficiency in various metal corrosion conditions, more studies are necessary. The continued study of essential oils as corrosion inhibitors highlights their significance as ecologically benign and sustainable solutions in the field of metal corrosion prevention.

**2.2.3. Amino acids.** Amino acids are organic compounds that play a fundamental role as the basic components of proteins in living organisms. They consist of an amino group (–NH<sub>2</sub>), carboxyl group (–COOH), and side chain that varies in structure.<sup>235</sup> Amino acids have gained attention as potential corrosion inhibitors for metals, including copper, bronze, zinc, aluminum, tin, and their alloys. Their availability, non-toxic nature, and ease of production make them attractive candidates for corrosion inhibition.<sup>236</sup> Additionally, amino acids have shown capability to adsorb onto metal surfaces through their nitrogen atom, which is an important aspect of their corrosion inhibition mechanism. Thus, amino acids have emerged as promising corrosion inhibitors due to their ability to slow down the corrosion process. Organic compounds that contain heteroatoms, multiple bonds, and certain functional groups are known to be efficient corrosion inhibitors. Amino acids, with their diverse structure and functional groups such as –OH, –COOH, and –NH<sub>2</sub> possess the necessary characteristics to be considered excellent corrosion inhibitors, particularly in acidic media. They can control corrosion by attacking cathodic activity, inhibiting the reduction of oxygen to hydroxyl ions. Furthermore, amino alcohols, a subclass of amino acids, have been found to be effective corrosion inhibitors by displacing chloride ions and blocking the sites where oxygen picks up electrons, further inhibiting corrosion.

Given the environmental concerns associated with conventional corrosion inhibitors, the use of amino acids as corrosion inhibitors provides a sustainable alternative. Amino acids are non-toxic and readily available compounds that can replace biohazardous inhibitors such as nitrites, benzoates, phosphonates, and quaternary ammonium salts. Their easy production and non-toxic nature make amino acids an attrac-

tive choice for corrosion inhibition in various industries. Furthermore, amino acids exhibit an adsorption mechanism on metal surfaces, which allows them to act as natural corrosion inhibitors. This adsorption mechanism involves binding to the metal surface *via* the nitrogen atom of the amino acid molecule. This adsorption process facilitates the formation of a protective layer on the metal surface, effectively slowing down the corrosion rate. In addition to their effectiveness as corrosion inhibitors, amino acids also meet the increasing requirements of environmental regulations.

The biodegradability of amino acids ensures that they do not contribute to environmental pollution, aligning with the principles of green chemistry and sustainable development. Amino acids have emerged as promising corrosion inhibitors due to their ability to prevent or slow down the corrosion process. The use of amino acids as corrosion inhibitors is of great importance in various industries. For example, in the oil and gas industry, where corrosion poses a significant threat to equipment and infrastructure, the use of amino acids as corrosion inhibitors can significantly reduce the economic and environmental costs associated with corrosion. Furthermore, amino acids have been found to be particularly effective in acidic media, where the corrosion rates are typically higher.

Zhang *et al.*<sup>18</sup> tested amino acids such as glycine, cysteine, glutamic acid and their derivative glutathione as copper corrosion inhibitors. In aerated 0.5 M HCl solution, Zhang *et al.*<sup>237</sup> conducted a comparative study among benzotriazole (BTA), alanine and cysteine by performing WL, PDP and EIS. de Matos *et al.*<sup>238</sup> observed that cysteine exhibited inhibitory effects at higher concentrations ( $10^{-3}$  and  $10^{-2}$  M) in de-aerated sulfuric media. This was attributed to the formation of a Cu(I)-cysteine complex and the subsequent film formation on the copper surface. The influence of pH of a 0.5 M Na<sub>2</sub>SO<sub>4</sub> solution on the corrosion protection properties of cysteine for copper was investigated by Petrović *et al.*<sup>239</sup> and Simonović *et al.*<sup>240</sup> A summary of some of the work reported in this field is presented in Table 1. According to the available data, it can be concluded that in a variety of industrial applications, amino acids have demonstrated great promise as corrosion inhibitors. They are a feasible substitute for conventional chemical inhibitors due to their capacity to create protective layers on metal surfaces and the fact that they are sustainable and environmentally friendly. However, to maximize their efficiency, comprehend their processes of action in more detail, and investigate their suitability with various metals and corrosive conditions, additional research and development are required. Amino acids show significant promise for influencing the future of corrosion inhibition technology as we continue to search for greener and more effective corrosion prevention solutions. However, despite the numerous benefits of amino acids as corrosion inhibitors, such as their eco-friendliness and film-forming ability, when determining whether they are appropriate for a given corrosion protection application, it is important to consider their limitations in terms of effectiveness, compatibility, and cost. Thus, scientists and businesses are devoting their efforts to overcoming these restrictions and

realizing the full potential of amino acids in corrosion prevention.

**2.2.4. Polysaccharides and biopolymers.** Biopolymers are natural polymers derived from renewable sources such as plants, animals, and microorganisms.<sup>263</sup> Due to their distinctive qualities and commitment to the environment, they have attracted attention. Chitosan, alginate, lignin, starch, and cellulose are examples of common biopolymer types. Due to their capacity to create protective layers on metal surfaces and prevent the entry of corrosive chemicals, these biopolymers can be employed in a variety of applications, including corrosion inhibition. They offer sustainable and effective alternatives to traditional corrosion inhibitors.<sup>264</sup> Because of their capacity to adhere to metal surfaces and produce protective layers that hinder the electrochemical processes that cause corrosion, biopolymers are good corrosion inhibitors.<sup>265</sup> The adsorption process is influenced by factors such as pH, temperature, polymer concentration, and surface charge.<sup>266</sup> By interacting with metal surfaces through electrostatic forces, hydrogen bonds, and other molecular interactions, biopolymers can prevent corrosive substances from penetrating the surface. Due to their distinct chemical makeup, some biopolymers also have inherent corrosion-inhibiting qualities. For instance, the biopolymer chitosan, which is derived from chitin, has amino and hydroxyl functional groups that help metal surfaces develop a passivation layer.<sup>267</sup> For example, exopolysaccharides produced by bacteria provide localized protection by capturing corrosive ions and inhibiting their migration to the metal surface.<sup>268,269</sup>

Some of the many metal substrates that biopolymers may be used to prevent their corrosion include iron, aluminium, copper, and their alloys. Studies have shown that biopolymers exhibit excellent performances in preventing both general and localized corrosion. For instance, xanthan gum, a polysaccharide produced by bacterial fermentation, demonstrated encouraging outcomes in preventing mild steel corrosion.<sup>270</sup> Similarly, polysaccharides extracted from plant sources have exhibited corrosion inhibition on several metallic surfaces.<sup>271</sup> The type of metal substrate, the surrounding environment, and the particular biopolymer utilized all have an impact on how well biopolymers work. To achieve the best corrosion protection, biopolymer formulations must be specifically matched to the characteristics of the metal substrate and the corrosive environment. Sustainability is one of the most important benefits of using biopolymers to reduce corrosion. Because biopolymers are made from renewable resources, they have a lower impact on the environment than synthetic corrosion inhibitors manufacture and disposal. Furthermore, this lessens our reliance on fossil fuels. Unlike certain synthetic equivalents, biopolymers do not remain in the environment because of their biodegradability. Utilizing biopolymers supports the development of ecologically friendly corrosion mitigation techniques and is consistent with the concepts of green chemistry. Their use can result in a decrease in the production of hazardous waste and the overall carbon footprint of corrosion control techniques. However, despite their great

**Table 1** Summary of some major reports on the corrosion inhibition potential of amino acids

S. no.	Metal/medium	Amino acids	Findings	Ref.
1	Iron/1 M HCl	Cysteine, cystine, methionine, valine, omithine, glutamine, serine, threonine, glutamic acid, aspartic acid, leucine, asparagine, alanine, arginine, glycine	All tested amino acids behaved as cathodic inhibitors. Cystine, methionine and cysteine gave the highest surface protection due to the presence of sulfur atoms in their molecular structure	241
2	Iron/0.1 M H <sub>2</sub> SO <sub>4</sub>	Glutamic acid derivatives	<i>N</i> -Phthaloyl-L-glutamic acid (66.89%) < <i>N</i> -benzoyl-L-glutamic acid (64.03%) < <i>N</i> -(1-oxooctadecyl)-L-glutamic acid (60.04%). Formation of protective layers	242
3	Iron/9 g L <sup>-1</sup> NaCl	Methionine and some amino esters: methionine ethyl ester and methionine methyl ester	%IE: B (80%) > A (40%) > methionine (28%) at 10 <sup>-2</sup> M. The sulfur atom improves the adsorption, whose electronegativity is improved by the ethyl moiety, an electron donor in the structure of B. The adherence of B aligns with the Frumkin isotherm	243
4	Carbon steel/0.5 M H <sub>2</sub> SO <sub>4</sub>	Polyaspartic acid	Polyaspartic acid acted as a predominant anodic inhibitor. %IE = 80% at 10 °C. Formation of shielding layer. Freundlich adsorption isotherm	244
5	Low alloy steel/0.2 M ammoniated	Glutamic acid	%IE: glutamic acid (81.5%). A stable chelate was formed on to aluminum surface. Acted as a mixed-type inhibitor. Hill-de Boer isotherm. Chemical adsorption	245
6	Al/0.1 M HCl	Glutamic acid	%IE: glutamic acid (66.67%). Physisorption. Frumkin, Langmuir, Flory-Huggins, El-Awady adsorption isotherms and kinetic and thermodynamic	246
7	Al/0.2–1 M HCl	Alanine, valine, methionine, proline, and tryptophan	%IE: alanine (56.3%), valine (58.2%), leucine (62.4%), proline (63.3%), methionine (81.0%), and tryptophan (90.0%). Acted as mixed-type inhibitors. Adherence of these inhibitors on the aluminum surface aligns with the Frumkin and Langmuir isotherms. The SEM images validate the surface protection of aluminum in mixed acid solutions by amino acids	247
8	Al/1 M HCl + 1 M H <sub>2</sub> SO <sub>4</sub>	Glycine, glutamic acid, alanine, valine, aspartic acid, phenylalanine	Chemisorption and physisorption play a crucial role in the inhibition of pitting corrosion.	248
9	Aluminum alloy AA7075/0.05 M NaCl	Glycine	Behaved as a mixed-type inhibitor. %IE of 87.4% at 500 ppm Gly + 100 ppm KI. S <sup>2-</sup> ions increase the SCC of alloy: Gly successfully inhibited Cu10Ni alloy corrosion	249
10	Cu10Ni/3.5% NaCl + 20 ppm Na <sup>2</sup> S	Cysteine, <i>N</i> -acetylcysteine, and methionine	%IE: cysteine (96%) > <i>N</i> -acetylcysteine (88%) > methionine (77%) at 6.0 mM. Langmuir adsorption isotherm. Strong physisorption	250
11	Cu10Al 5Ni/neutral 3.5% NaCl	Methionine	Acted as a mixed-type inhibitor; %IE increases with decreasing MET concentration; physical adsorption	251
12	Cu/3.5% NaCl	Methionine, asparagine, serine, glutamine, cysteine, and arginine,	%IE: Arg > Gln > Asn > Met > Cys > Ser at 10 <sup>-2</sup> M; Arg was mainly a cathodic inhibitor. However, Cys, Met, Asn, Gln, Ser behaved as mixed-type inhibitors	252
13	Cu/0.1 M H <sub>2</sub> SO <sub>4</sub>	Cysteine	Cysteine acted as a good inhibitor for Cu corrosion; Physical adsorption	253
14	Cu/3.5% NaCl	Phenylalanine	Phenylalanine with Ce <sup>4+</sup> ions gave a robust synergistic effect by forming Phe/Ce <sup>4+</sup> complex film on the Cu surface; IE = 72% for 5 mM Phe + 2 mM Ce <sup>4+</sup>	254
15	Cu/0.5 M HCl	Proline, glycine, alanine, phenylalanine, histidine and cysteine	Physical adsorption. Phenylalanine, cysteine and histidine gave the highest %IE. The theoretical studies corroborated the experimental observations	255
16	Cu/8 M H <sub>3</sub> PO <sub>4</sub>	Cysteine	Mixed-type inhibitor; mixed adsorption	256
17	Cu/2 M HNO <sub>3</sub>	Cysteine, glutamic acid, glycine, and its derivative (glutathione)	Physical adsorption; %IE increases in the following order: glutathione > Cys > Cys + Glu-A + Gly > Glu-A > Gly	257
18	Cu/0.5 M HCl	Methionine	MET behaved as a cathodic inhibitor; the mixed CTAB/MET has a better synergistic influence compared with the mixed CPB/methionine; stronger electrostatic interaction	258
19	Cu/0.5 M HCl	Glycine, phenylalanine, threonine, and glutamic acid	Mainly cathodic inhibitors (except phenylalanine); Glutamic acid exhibited the strongest protective effect (%IE = 53.6%)	259
20	Cu/0.5 M HCl	Glycine, tyrosine, valine, and alanine,	Behaved as mixed-type inhibitors. %IE depends on the chemical structure of amino acids. %IE: valine = alanine ≪ glycine < tyrosine	260

Table 1 (Contd.)

S. no.	Metal/medium	Amino acids	Findings	Ref.
21	Cu/0.5 M H <sub>2</sub> SO <sub>4</sub> in O <sup>2-</sup> -saturated solution	Methionine	Methionine demonstrated limited surface protection properties; physisorption; synergic effect between methionine and Zn <sup>2+</sup> ions	261
22	Cu/0.5 M HCl	Serine, threonine, and glutamic acid	Cathodic inhibitors; %IE: glutamic acid (90.4%) > threonine > serine (54.7%) at 1 mM; chemical adsorption	237
23	Cu/0.5 M HCl	Cysteine	Mainly cathodic inhibitor; physical adsorption. In the presence of Cu <sup>2+</sup> ions, the %IE increases	262

promise, several issues need to be resolved before biopolymers can be widely used to limit corrosion. Performance irregularities may result from variations in biopolymer composition, supply, and extraction techniques. Thus, to achieve accurate and repeatable findings, biopolymer formulations and testing procedures must be standardized. Furthermore, for the practical use of biopolymer-based coatings and inhibitors, it is essential to comprehend their long-term stability and endurance. Additional study is required to determine how well biopolymers operate in various environmental settings and how well they work with various coating techniques.

**2.2.4.1. Chitosan.** Through several processes, including its capacity to create barrier coatings on metal surfaces, chitosan shows corrosion prevention. The amino and hydroxyl groups in chitosan interact with metal ions to produce a film on the surface of metals. This adsorption of chitosan is responsible for the formation of a film. This adsorption slows the corrosion process by blocking electrochemical reactions and preventing the migration of corrosive substances.<sup>272</sup> Furthermore, the inherent biocidal properties of chitosan can suppress microbial-induced corrosion (MIC) by inhibiting the growth of corrosive microorganisms on metal surfaces.<sup>273</sup> Its multifaceted inhibitive mechanisms contribute to its effectiveness under different corrosive conditions. Also, the corrosion inhibition performance of chitosan has been investigated across a wide range of metal substrates, including carbon steel,<sup>274–283</sup> aluminum alloys,<sup>284,285</sup> and copper.<sup>286–288</sup>

Several variables, including pH, temperature, concentration, and exposure period, may affect the effectiveness of chitosan. Because of its amphoteric nature, studies have indicated that the inhibitory impact of chitosan is more evident under neutral to acidic environments.<sup>272</sup> Because different metal substrates exhibit varying electrochemical behaviours and surface qualities, chitosan performs differently with each type of metal substrate. Thus, to realize the best corrosion protection, chitosan formulations must be specifically matched to the characteristics of each metal given that their interaction with the metal surface determines the creation of protective layers. To increase the robustness and endurance of corrosion protection, recent research has concentrated on creating coatings and inhibitors based on chitosan. The inhibitive qualities of chitosan can be enhanced by combining it with other substances, such as nanoparticles, to optimize its effectiveness for certain purposes. Green corrosion prevention is based on the

same principles as chitosan, which is environmentally beneficial. Chitosan, which is derived from natural sources and has biodegradable properties, provides a sustainable substitute for synthetic corrosion inhibitors. Its ability to prevent microbial-induced corrosion as well as general and localised corrosion makes it a vital tool in the creation of environmentally friendly corrosion control methods.

**2.2.4.2. Alginates.** Due to its biodegradability and low toxicity, alginate, a natural biopolymer derived from seaweed, offers a sustainable and environmentally benign alternative for corrosion inhibition. Its importance in corrosion control techniques are highlighted by its mechanisms of inhibition, compatibility with different metal substrates, and alignment with green chemistry concepts.<sup>289</sup> As research progresses, alginate-based corrosion inhibitors are poised to play a crucial role in promoting both environmental sustainability and corrosion protection. Alginate exhibits corrosion inhibition properties through several mechanisms,<sup>290</sup> as follows: (a) *Film Formation*: Alginate molecules adhere to metal surfaces to form a shielding coating, which serves as a physical barrier against corrosive substances. Corrosive ions cannot spread as easily through this coating, which prevents them from reaching the metal surface. (b) *Passivation*: Alginate molecules adhere to metal surfaces to form a shielding coating, which serves as a physical barrier against corrosive substances. Corrosive ions cannot spread as easily through this coating, which prevents them from reaching the metal surface. (c) *Complexation*: Alginate can complex with metal cations, reducing their reactivity and preventing them from participating in corrosive processes.

The corrosion inhibition effectiveness of alginate has been investigated on various metal substrates, including steel, aluminum, and copper.<sup>15,289–295</sup> The type of metal and the surrounding environment can have an impact on how well it performs. Alginate has demonstrated great promise in preventing corrosion on aluminium surfaces, making it applicable in fields such as aerospace and automotive where aluminium alloys are often utilized. The ability of alginate to inhibit corrosion can be affected by variables such as pH, temperature, concentration, and exposure duration. Thus, achieving the best corrosion protection requires optimizing these characteristics. However, although alginate has potential as a green corrosion inhibitor, it is still associated with certain difficulties. For example, inconsistent outcomes may be caused by variations in the alginate content, extraction techniques, and per-

formance under various circumstances. Thus, to achieve accurate and repeatable results, the testing procedures and formulas must be standardized. Alginate-based coatings should be optimized for certain metal substrates in future studies, and its compatibility with other coating systems should also be investigated. Furthermore, the creation of alginate-based smart coatings that adapt to shifting environmental conditions may pave the way for cutting-edge methods of corrosion prevention.

**2.2.4.3. Lignin.** In recent years, researchers have explored the use of lignin, a complex natural polymer found in plant cell walls,<sup>296</sup> as an eco-friendly corrosion inhibitor. Lignin offers corrosion inhibition through several mechanisms,<sup>297</sup> as follows: (a) *Adsorption*: Lignin molecules can adhere to metal surfaces and provide a shielding layer. This coating serves as a physical barrier, preventing corrosive substances such as oxygen and moisture from coming into contact with the metal. (b) *Complexation*: Lignin has functional groups that can interact with metal ions during the corrosion process, such as phenolic hydroxyls. As a result of these interactions, fewer metal ions are available for corrosion processes, resulting in stable complexes. (c) *Passivation*: On metal surfaces, lignin can encourage the development of passive layers. These layers inhibit further corrosion by blocking electron transfer at the metal–electrolyte interface. The effectiveness of lignin as a corrosion inhibitor has been assessed on a variety of metal substrates, including steel, aluminium, and copper.<sup>297–301</sup> The efficacy of lignin-based inhibitors may vary with environmental factors such as pH, temperature, and exposure time. Lignin-based corrosion inhibitors are positioned to play a crucial role in advancing environmental sustainability and efficient corrosion prevention as research continues to improve and overcome obstacles.

**2.2.4.4. Polysaccharides.** Among the natural substances investigated for corrosion inhibition, polysaccharides, which are composed of glucose units such as cellulose and starch, have demonstrated promise. Polysaccharides demonstrate the ability to prevent corrosion through several processes, as follows: (a) *Barrier effect*: When used as coatings or additives, cellulose and starch form a physical barrier on the metal surface. This barrier protects the metal from corrosive substances including ions, oxygen, and moisture. Thus, by limiting the direct interaction between the metal and these corrosive elements, the rate of corrosion is reduced significantly. (b) *Adsorption*: The surface of the metal can adsorb molecules of cellulose and starch. The interactions between the metal atoms and the hydroxyl groups found in these polysaccharides during this adsorption are both physical and chemical. Consequently, a shielding layer develops, further preventing corrosive species from reaching the metal substrate. (c) *Complex formation*: Starch and cellulose both have hydroxyl groups that can interact with the metal cations in the corrosive environment. Complexes are created as a result of this interaction and are less reactive than the free metal ions. Hence, the metal is vulnerable to corrosion.

Cellulose and starch have demonstrated corrosion inhibition efficacy on a variety of metal substrates such as steel,

aluminum, and copper.<sup>302</sup> A potential and environmentally acceptable option for corrosion inhibition is provided by cellulose and starch. Their importance in corrosion control techniques is highlighted by their numerous modes of inhibition, compatibility with a range of metal substrates, and agreement with green chemistry principles. Cellulose and starch-based corrosion inhibitors are positioned to play a crucial role in advancing environmental sustainability and efficient corrosion prevention as research advances and obstacles are overcome. However, although biopolymers-based corrosion inhibitors show promise, several challenges and areas for future research exist, as follows: *Variability*: Inconsistent outcomes may be caused by variations in composition, extraction techniques, and performance under various circumstances. Thus, to achieve accurate results, testing procedures and formulas must be standardized. *Optimization*: To improve formulations for certain metal substrates and ambient circumstances, more studies are required. Also, it is crucial to customize these inhibitors to meet certain requirements. *Innovation*: Corrosion prevention may be revolutionized by investigating novel strategies such as intelligent coatings and sophisticated materials that contain cellulose and starch, such as self-healing coatings and sensitive materials that adjust to shifting environmental circumstances.

### 2.3. Green corrosion inhibition using energy-efficient synthesis

Green chemistry, also known as sustainable chemistry, has emphasized the value of safeguarding the environment and human health over the last few decades. This fast-growing approach in the overall realm of corrosion inhibition-related science and technology entails reducing or eliminating the use and manufacturing of hazardous inhibitor compounds by appropriate target-specific innovation, aligned design, and user-friendly application. Additionally, the as-required materials should have energy-efficient synthetic routes.<sup>55</sup> The mass level of environmental awareness and rigorous environmental regulations worldwide have strictly prohibited the synthesis and utilization of conventional hazardous corrosion inhibitors. In this perspective, designed engineering and subsequent development of synthetic inhibitors must be ameliorated by employing ecologically benign starting precursor materials or unconventional energy sources such as microwave and ultrasonic (*i.e.*, sonochemical) heating in the contemporary domain. More specifically, microwave and ultrasonic heating have numerous advantages, including immediate interior heating, excellent temperature uniformity, and high selectivity, which are attributed to their benefits in the development of inhibitors *via* unconventional heating techniques. Green synthesis can be accomplished using multicomponent reactions, *e.g.*, microwave and ultrasonic irradiation. It is worthwhile to mention that implementing multicomponent reactions has attracted significant attention because of their superior features such as easy operational protocols, less time consuming nature, less laborious, high reaction yield, and significantly lower quantities of waste production.<sup>303</sup> Moreover,

organic synthesis in the solid phase often correlates with a greater reaction yield, shorter reaction times, and significantly avoids the use of hazardous solvents and metal catalysts, providing another reason for green synthesis.

**2.3.1. Microwave-assisted synthesis.** In the current scenario, microwave-assisted synthesis has emerged as a new era in synthetic chemistry. After a vast literature survey on green corrosion inhibitors, several recent works have monitored and focused on the microwave-assisted synthetic procedure. It can be two-component and multicomponent multi-step reactions facilitated by microwave-assisted reactions.

The corrosion retardance effectiveness of six thiaziazole derivatives with various alkyl chain lengths, *e.g.*, ethyl (for IC-2), *n*-propyl (for IC-3), *n*-pentyl (for IC-5), heptyl (for IC-7), undecyl (for IC-11) and tridecyl (for IC-13), was assessed for the steel surface in 1 M H<sub>2</sub>SO<sub>4</sub>.<sup>304</sup> Both conventional and green microwave heating approaches were employed to develop the targeted inhibitors. As the reaction rate was expedited with marginally larger yields, the inhibitor molecules were produced more effectively by employing the microwave irradiation approach, as depicted in Fig. 12(a). The required acid, concentrated sulfuric acid, and thiosemicarbazide were mixed in a flask placed within a closed vessel. The mixture was magnetically stirred in a microwave reactor at 80–90 °C (20 W) for one hour. Once the reaction was finished, the mixture was chilled in cold water and neutralized with ammonia solution. EIS and SEM were utilized to comprehend the corrosion inhi-

bition effectiveness of the six compounds. It was observed that all the as-synthesized inhibitors could reduce the double-layer capacitance compared to that of the blank owing to the variations in the thickness of the as-formed protective layer of the inhibitors. As more surface coverage was achieved, the inhibition efficiency increased from IC-2 to IC-11 with an increase in the alkyl chain length. Surprisingly, the inhibition efficiency decreased for IC-13, indicating that the alkyl chain of IC13 is no longer straight but twisted into a loop-like shape. Consequently, less surface coverage was associated with IC-13, although it possessed the longest chain length. The Langmuir adsorption isotherm further confirmed the chemisorption tendency of the inhibitors.

In 2018, Singh *et al.* reported the use of 2-amino-*N'*-((thiophen-2-yl)methylene)benzohydrazide (ATMBH) as an excellent corrosion inhibitor for the protection of mild steel in the presence of 0.5 M H<sub>2</sub>SO<sub>4</sub>.<sup>305</sup> ATMBH was synthesized *via* a solvent-free microwave-assisted methodology, as shown in Fig. 12(b). Thiophene-2-carboxaldehyde was first reacted with *ortho*-amino benzoylhydrazide in the presence of a catalytic amount of acid clay in a microwave reactor. The targeted product was formed in 91% yield within 4 min of reaction. The significance of this green synthesis protocol was highlighted by its added environmental benignity, high yield of the as-synthesized corrosion inhibitor, diminished energy consumption, and shorter reaction time than other conventional synthetic procedures. Gravimetric analysis and electrochemical investigations were

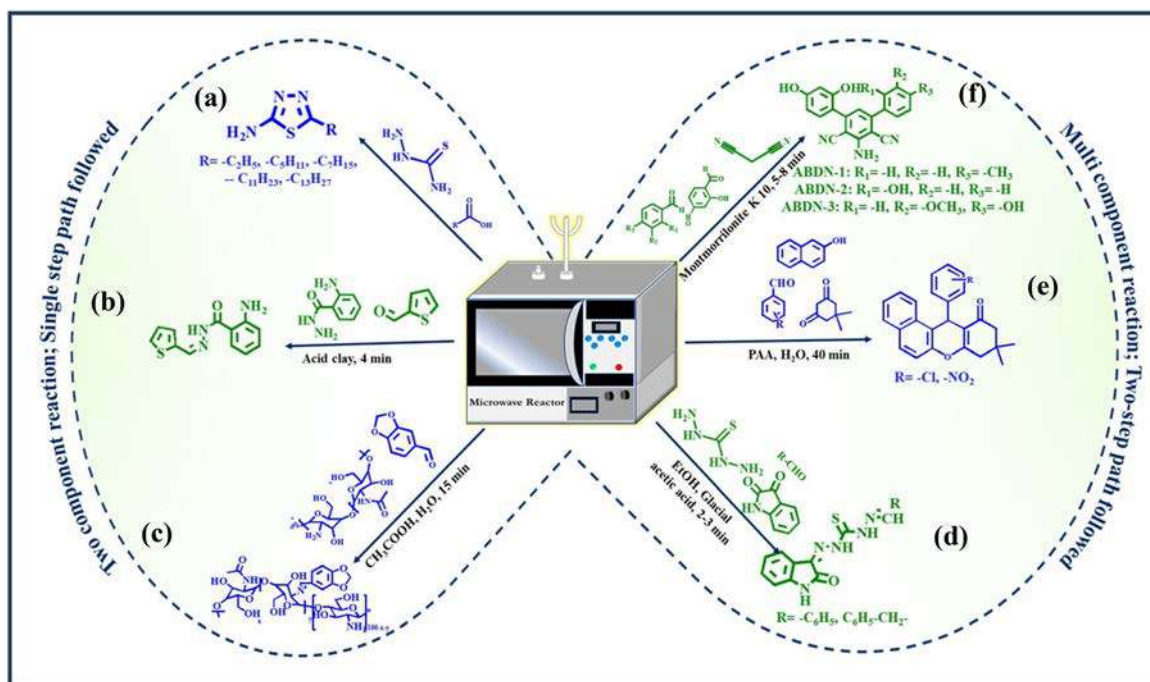


**Fig. 12** Schematic presentation of the green synthetic pathways for corrosion inhibitors *via* microwave irradiation for (a) thiaziazole derivatives<sup>304</sup> [reproduced from ref. 304 with permission; Copyright, Elsevier, 2012], (b) ATMBH<sup>305</sup> [reproduced from ref. 305 with permission; Copyright, RSC, 2018], (c) piperonal-chitosan (Pip-Cht)<sup>306</sup> [reproduced from ref. 306 with permission; Copyright, ACS, 2014], (d) thiosemicarbazone derivative<sup>307</sup> [reproduced from ref. 307 with permission; Copyright, Elsevier, 2015], (e) xanthone derivative<sup>308</sup> [reproduced from ref. 308 with permission; Copyright, Elsevier, 2023], and (f) ABDN derivative<sup>309</sup> [reproduced from ref. 309 with permission; Copyright, Elsevier, 2015].



used to investigate the corrosion inhibition efficiency of the inhibitors. It was observed that the corrosion inhibition efficiency of ATMBH increased with an increase in its concentration in the electrolyte solvent. SEM and AFM further validated these inhibition efficiency analyses results. The inhibition efficiency of ATMBH is attributed to the blockage of the active sites (specifically, the cathodic sites) through its physisorption and chemisorption on the mild steel surface, which followed the Langmuir adsorption isotherm. The contact angle measurement revealed the reduced hydrophilicity towards the aqueous acid solution in the presence of a higher concentration of inhibitor.

Similarly, this group reported the microwave-assisted synthesis of thiophene hydrazone derivatives, namely, acetyl thiophene benzohydrazide (ATBH), propanoyl thiophene amino benzohydrazide (PTABH), propanoyl thiophene benzohydrazide (PTBH) and acetyl thiophene amino benzohydrazide (ATABH).<sup>310</sup> It was observed that the conventional reflux method in the presence of ethanol and acetic acid took 3–5 h, while the microwave-assisted technique helped in acquiring the as-required products within 3–5 min. Aoun *et al.* reported the use of 1-(3-bromopropyl)-4-(dimethylamino)pyridinium bromide (DPB) IL as a preferable contender for the corrosion mitigation of carbon steel in an HCl environment.<sup>311</sup> EIS and LPR studies indicated an increase in the %IE with an increase in concentration. Alternatively, the thermodynamic studies revealed a discernible drop in %IE with an increase in temperature, indicating the physisorption of the inhibitor molecules under the current working circumstances. The Langmuir isotherm well fitted the physisorption nature of the inhibitor.

Piperonal-chitosan (Pip-Cht), a novel Schiff base of chitosan, was synthesized using microwave irradiation and characterized by spectroscopic methods. Gravimetric and electrochemical methods were used to analyze its corrosion-suppressing ability in carbon steel in 15% HCl media.<sup>312</sup> Pip-Cht was synthesized by mixing chitosan with glacial acetic acid, distilled water and ethanolic piperonal solution, as shown in Fig. 12(c). The temperature of the microwave irradiation was ramped to 60 °C for 15 min. The effectiveness of the Pip-Cht was significantly increased by the addition of KI as a synergistic agent. Even at a high temperature of 65 °C, the inhibitor showed a substantial action that inhibited corrosion. The AFM study confirmed the adhesion of the inhibitor to the metallic surface and the development of a barrier film, which resulted in a reduction in the surface roughness of the metal. The presence of KI promoted the inhibitor adsorption, where the SEM study showed a smoother morphology of the steel surface in the presence of the inhibitor. DFT-based quantum chemical calculations showed that the Pip-Cht inhibitor exhibited improved adsorption behavior compared to the chitosan and piperonal parent molecules.

Three chitosan Schiff bases, namely, benzaldehyde (CSB-1), 4-(dimethylamino)benzaldehyde (CSB-2), and 4-hydroxy-3-methoxybenzaldehyde (CSB-3), as corrosion inhibitors were synthesized *via* the microwave-assisted pathway and their effective corrosion inhibition was analyzed on mild steel in the

presence of 1 N HCl medium.<sup>313</sup> After adding chitosan to distilled water, glacial acetic acid was mixed at room temperature. The as-required aldehydes were dissolved in ethanol. Subsequently, the aldehyde solution was added dropwise, while stirring continuously for 30 min at 303 K in the chitosan solution flask. The reaction mixture was subjected to 600 W microwave irradiation in a microwave-assisted reactor. Then, the sample temperature was raised gradually to 60 °C and maintained for 15–20 min until the completion of the reaction.

In another work, two isatin-thiosemicarbazone derivatives, namely, 1-benzylidene-5-(2-oxoindoline-3-ylidene) thiocarbohydrazone (TZ-1) and 1-(4-methylbenzylidene)-5-(2-oxoindolin-3-ylidene) thiocarbohydrazone (TZ-2), were synthesized. Their protective nature towards mitigating the corrosion of mild steel in the presence of 20% H<sub>2</sub>SO<sub>4</sub> was assessed by employing experimental and computational analytical techniques.<sup>307</sup> The synthetic procedure is schematically presented in Fig. 12(d). In the first step of the synthesis, thiocarbohydrazide was allowed to react with aldehyde in the presence of ethanol and glacial acetic acid. Herein, isatin was added to the mixture with the above-mentioned solvents under microwave irradiation for 2–3 min. The outcomes demonstrated that both inhibitors functioned as mixed-type inhibitors and that their adsorption on the metallic surface complied with the Langmuir isotherm model. Computational analyses were performed to validate the experimental findings. Later, Singh *et al.* reported the synthesis of two xanthone derivatives, namely 12-(4-chlorophenyl)-9,9-dimethyl-8,9,10,12-tetrahydro-11*H*-benzo[*a*]xanthen-11-one (BX-Cl) and 9,9-dimethyl-12-(4-nitrophenyl)-8,9,10,12-tetrahydro-11*H*-benzo[*a*]xanthen-11-one (BX-NO<sub>2</sub>), utilizing microwave-assisted technology, as presented in Fig. 12(e).<sup>308</sup> An equimolar ratio of 2-naphthol, dimidone, and 4-chloroaldehyde/4-nitroaldehyde was added to an aqueous solution of polyacrylic acid. Subsequently, the resultant combination was subjected to 40 min of microwave irradiation (560 W). These two derivatives were used to protect P110 steel in the presence of a 15% HCl solution. The incorporation of KI enhanced the corrosion inhibition and mitigation abilities of BX-Cl and BX-NO<sub>2</sub>. The WL studies showed that increasing the concentration of BX-Cl and BX-NO<sub>2</sub> from 50 to 200 mg L<sup>-1</sup> enhanced the corrosion inhibition efficiency from 62.10% to 92.21% and 47.36% to 84.21%, respectively. As calculated from the EIS data, the charge transfer resistance value reached 644.8 Ω cm<sup>2</sup> for BX-Cl. This observation revealed the strong adsorption of the xanthone derivatives on the metal surface. However, the impedance decreased with an increase in temperature, which suggests that the increase in temperature led to the desorption of the adsorbed inhibitors from the metal surface.

Furthermore, the DFT and MD simulation results nicely corroborated the experimental findings. Three 2-aminobenzene-1,3-dicarbonitrile derivatives (ABDNs), namely, 5-amino-2,4-dihydroxy-4-methyl-1,1:3,1-terphenyl-4,6-dicarbonitrile (ABDN-1), 5-amino-2,2,4-trihydroxy-1,1:3,1-terphenyl-4,6-dicarbonitrile (ABDN-2) and 5-amino-2,3,4-trihydroxy-1,3-methoxy-1,1:3,1-terphenyl-4,6-dicarbonitrile (ABDN-3), were synthesized and evaluated for their ability to

suppress mild steel deterioration in 1 M HCl utilizing WLand electrochemical methods.<sup>309</sup> The synthesis was performed using a microwave-assisted protocol involving a two-step process, as presented in Fig. 12(f). According to the electrochemical, morphological, and theoretical investigations, the corrosion inhibition effectiveness followed the order of ABDN-3 > ABDN-2 > ABDN-1, which was explained by the different substituents found in the aromatic ring. The electron-donation ability of -OH in ABDN-1 is somehow reduced by resonance, while the electron-donation ability of the -CH<sub>3</sub> of ABDN-2 is facilitated by a positive inductive effect. Additionally, the strong electron-donating group, *i.e.*, -OCH<sub>3</sub> group, in ABDN-3 results in the better adsorption of ABDN-3. Accordingly, ABDN-3 acts as a better corrosion inhibitor than ABDN-2, followed by ABDN-1. The quantum chemical calculation investigation supported the WL, electrochemical, and surface analysis. This research group further utilized these inhibitors to analyze their corrosion inhibition effectivity on aluminum in the presence of 0.5 M NaOH solution.<sup>314</sup>

**2.3.2. Sonochemical synthesis.** “Sonochemistry” involves the use of ultrasound irradiation for diverse chemical synthesis, which has emerged as a revolutionary and interesting area in green and energy-efficient synthesis. Ultrasonic-assisted synthesis in a circular economy plays a pivotal role because of the accelerated rate of chemical transformation in homogeneous and heterogeneous systems. Thus, this technique is widely used as an alternative to synthesizing organic materials for several applications. It was observed that the corrosion rate retardation ability increased with the concentration

of the inhibitor solution in the study by Singh *et al.*, where three chalcones, *i.e.*, (*E*)-3-(4-hydroxyphenyl)-*N*-phenylacrylamide (INH-1), (*E*)-3-(4-(dimethylamino)phenyl)-*N*-phenylacrylamide (INH-2) and (*E*)-3-(4-hydroxy-3-methoxyphenyl)-*N*-phenylacrylamide (INH-3), were successfully synthesized *via* the ultrasonic irradiation technique (Fig. 13(a)).<sup>315</sup> The synthesized chalcones were examined for their ability to restrain dissolution of mild steel using electrochemical and WL techniques in the presence of 1 M HCl. The findings demonstrated that all the as-synthesized chalcones acted as effective corrosion inhibitors. Similarly, 2-hydroxy-*N'*-((thiophene-2-yl)methylene)-benzohydrazide (HTMBH), an organic Schiff base molecule, was synthesized *via* a conventional method and an ultra-sonochemical technique *via* the reaction of 2-hydroxybenzoylhydrazide and thiophene-2-carboxaldehyde in the presence of ethanol as the solvent.<sup>316</sup> The ultrasonic-assisted synthesis method is depicted in Fig. 13(b). In the second method, the product yield significantly increased (from 78% in the conventional approach to 95% in the ultrasound-assisted method), and the reaction time was reduced (from 3 h to only 4 min). Compared to the conventional approach, it offers a quicker and more efficient process for synthesizing the investigated chemical HTMBH.

Recently, not only in chemical synthesis protocols but also several sonochemical-assisted extractions of phytochemicals have been reported in the literature. For example, Khanra *et al.* reported the utilization of *Scenedesmus sp.*, a microalga, to extract unsaturated fatty acids for the protection purpose of

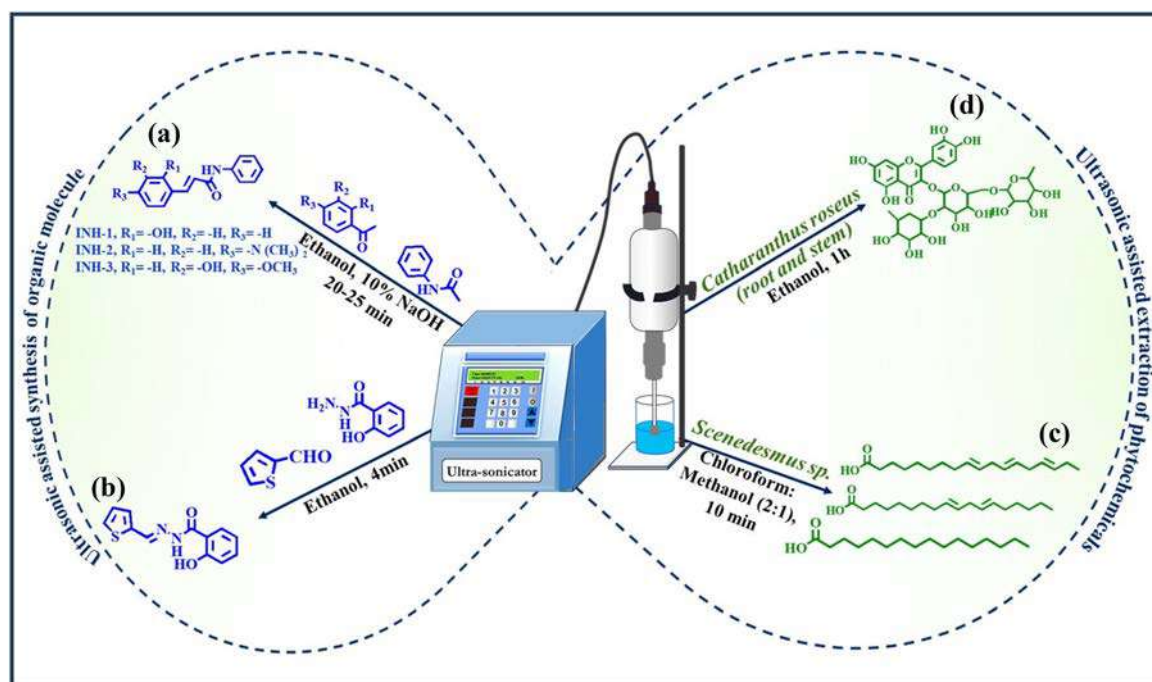


**Fig. 13** Schematic presentation of the green synthetic pathways for corrosion inhibitors *via* the ultrasound-assisted protocol for (a) INH-1, INH-2, and INH-3<sup>315</sup> [reproduced from ref. 315 with permission; Copyright, Elsevier, 2014]; (b) HTMBH<sup>316</sup> [reproduced from ref. 316 with permission; Copyright, ACS, 2018]; (c) *Scenedesmus sp.* extract<sup>317</sup> [reproduced from ref. 317 with permission; Copyright, ACS, 2018]; and (d) *Catharanthus roseus* extract<sup>318</sup> [reproduced from ref. 318 with permission; Copyright, RSC, 2020].

mild steel in the presence of 1 M HCl solution.<sup>317</sup> The cell pellets were centrifuged, dried, and then the fatty acids extracted using a 1 : 2 mixture of methanol and chloroform. After being ultrasonically treated for 10 min, the mixture was shaken for a whole night at 130 rpm in an orbital shaker (Fig. 13(c)). In the next step, the supernatant liquid was collected *via* further centrifugation. After phase separation, the lower organic phase was recovered and dried in a rotary evaporator. The *Scenedesmus* sp. fatty acid (SFA)-containing organic phase was used as an inhibitor. It was found that 9,12,15-octadecatrienoic acid (C18:3), 9,12-octadecadienoic acid (C18:2), and hexadecanoic acid (C16:0) constituted the majority of fatty acids, as analyzed by gas chromatography-mass spectrometry (GC-MS). The EIS study revealed that 95.1% corrosion inhibition efficiency was achieved for 36 ppm of inhibitor solution. The hydrogen gas evolution reaction (HER) also supported the decreased HER rate in the presence of SFA, *i.e.*, there was less corrosion reaction in the presence of SFA. The ability of SFA to suppress the rate of corrosion followed the order of C18:3 > C18:2 > C16:0. The SEM, AFM and theoretical studies such as DFT nicely agreed with the electrochemical observations. Similarly, in 2020, ethanolic extracts of the roots and stems of *Catharanthus roseus* were obtained through ultrasonic energy, as schematically presented in Fig. 13(d).<sup>318</sup> This extract was further used for the corrosion inhibition study of mild steel in a sea-water-like saline environment (*i.e.*, 3.5 wt% NaCl). UV-vis spectroscopy (UV-vis), FTIR, Raman spectroscopy, gravimetric analysis, and electrochemical investigations (OCP, EIS and Tafel) were performed to investigate the corrosion inhibition efficiency. Around 70% corrosion inhibition efficacy was achieved from these phytochemicals. According to the outcomes of the quantum chemical analysis, the *C. roseus* extract was significantly adsorbed on the surface of mild steel.

Similarly, Luo and coworkers demonstrated a highly effective enzyme-based ultrasound-assisted tannin extraction technique from acorns at a fixed pH of ~5.0.<sup>319</sup> The response surface methodology was implemented to further optimize the extraction conditions, including the four factors of temperature, ultrasonic power, ultrasonic time, and cellulose concentration. Firstly, the optimum ranges of the four significant factors were obtained through fundamental single-factor experiments. The experimental results were adequately explained using the second-order polynomial model. Consequently, the most suitable parameters used for extraction were as follows: 2.51 h, ultrasonic power of 97.92 W, temperature of 38 °C, and 3.44 g L<sup>-1</sup> of cellulose.

**2.3.3. Other green approaches.** Other energy-efficient green synthetic pathways exist besides the microwave- and ultrasonic-assisted syntheses. To prepare a carbon dot-based pickling solution on a large scale, a green, *in situ* acid oxidation technique was employed by He *et al.*<sup>320</sup> Carbon dots have been used as a revolutionary and green corrosion inhibitor owing to their inexpensive precursors, straightforward synthetic techniques, nontoxicity, excellent dispersibility, ideal water solubility, and low cost.<sup>321–323</sup> Fructose solution was used as a green precursor of carbon dots. In a study, H<sub>2</sub>SO<sub>4</sub> and DI water were

used for synthetic purposes, and stirring with a glass rod at room temperature was the only mechanical force applied. Excitingly, the strong oxidizing nature of H<sub>2</sub>SO<sub>4</sub> and the heat produced during the exothermic reaction between H<sub>2</sub>SO<sub>4</sub> and DI were the main accelerating factors for this reaction. Eventually, it only took 3 min to obtain the as-required carbon dots. The WL test, EIS, and PDP measurements supported that the *in situ*-synthesized carbon dots effectively prevented corrosion (with corrosion inhibition efficiency of ~95%) in Q235 carbon steel in 0.5 M H<sub>2</sub>SO<sub>4</sub> at a minute concentration of 0.26%.<sup>320</sup> Another study reported the grinding of an equimolar mixture of malononitrile, phenyl hydrazine, and aromatic aldehydes for 2 to 5 min in a mortar and pestle to obtain the as-desired products, namely, 5-amino-1,3-diphenyl-2,3-dihydro-1H-pyrazole-4-carbonitrile (AHPC), 5-amino-3-(4-nitrophenyl)-1-phenyl-2,3-dihydro-1H-pyrazole-4-carbonitrile (ANPC) and 5-amino-3-(4-methoxyphenyl)-1-phenyl-2,3-dihydro-1H-pyrazole-4-carbonitrile (AMPC).<sup>324</sup> The 3-aminopyrazole carbonitrile derivatives (AHPC, ANPC, and AMPC) were demonstrated to be good corrosion inhibitors for mild steel in 1 M HCl. At a concentration of 7.69 × 10<sup>-4</sup> M, AHPC, ANPC, and AMPC exhibited corrosion inhibition efficiencies of 90.34%, 92.04%, and 95.45%, respectively.

## 2.4. Green corrosion inhibition using mechanochemical and one-step syntheses

**2.4.1. Solid-phase reactions.** A great Greek philosopher once stated, “No Coopora nisi Fluida”, meaning “No reaction occurs in the absence of solvent”. This philosophy greatly influenced the development of modern science in Europe and provided a historical reason why most organic syntheses are carried out and studied in solution. Alternatively, it has been established mechanistically that molecules can move relatively freely in the solid state and even enantioselectively.<sup>325</sup> It has also been proven that organic reactions can proceed by mixing powdered reactants and reagents in the absence of solvent and with the efficient collection of the reaction products. In some cases, organic reactions can also be performed under solvent-free conditions throughout the reaction process as well as product isolation. This technique offers several advantages including reduced pollution, cost-effectiveness, simple approach and handling.<sup>326,327</sup> These factors are critical in different industrial practices. In the early 20th century, W. Nernst categorized various branches of chemistry based on the energy source supplied to the system: electrochemistry, thermochemistry, and photochemistry. Mechanochemistry was introduced to describe reactions induced by mechanical energy, with tribochemistry applied to reactions caused by friction during the milling of solid reagents.<sup>328,329</sup>

The mechanical grinding of solids involves numerous processes, including:

- Breaking of particles to diminutive sizes.
- Creating larger, newly exposed surfaces.
- Forming dislocations and point defects in the crystalline structure.

(d) Inducing phase transformations in polymorphic materials.

(e) Chemical reactions including ionic exchange, decomposition, oxidation–reduction, complex and adduct formation.

The International Union of Pure and Applied Chemistry (IUPAC) defines a mechanochemical reaction as “a chemical reaction induced by the direct absorption of mechanical energy”.<sup>330</sup> However, this area can be further divided into (i) mechanical activation of solids, (ii) mechanical alloying, and (iii) reactive milling of solids.<sup>331–333</sup> The grinding of two solid substances leads to intricate series of transformations. The mechanical energy disrupts the order of the crystalline structure, creating cracks and exposing new surfaces. Deformation and potential melting occur at the edge collision points, forming hot spots where molecules experience high vibrational excitation, leading to bond breakage. Ultimately, the energy stored in the defects of the crystalline structure can facilitate slower chemical processes. Nowadays, milling under controlled temperature, light irradiation, sound agitation, or electrical impulses in newly developed experimental setups has led to reactions not achievable *via* conventional mechanochemical processing.<sup>326</sup> Consequently, thermo-mechanochemistry, sono-mechanochemistry, electro-mechanochemistry and photo-mechanochemistry represent notable advances in modern mechanochemistry and herald a new level of solid-state reactivity of mechanochemistry 2.0 (Fig. 14).

Mechanical milling using a mixer mill or planetary mill has been fruitfully utilized in organic synthesis under solvent-free conditions. In the literature, mechanical milling is sometimes called grinding, which may cause confusion. Thus, to differentiate these two mechanochemical techniques, it is strongly rec-

ommended that grinding is defined as a process in a mortar and pestle and the like, such as a Retsch RM100 mortar grinder. In contrast, milling should only refer to that performed in a mixer/shaker mill or a planetary mill.<sup>334,335</sup> A mechanochemical process may involve carbon–carbon and carbon–heteroatom covalent bonds, metal–ligand coordination bonds, non-covalent interactions such as hydrogen bonds, halogen bonds or  $\pi$ – $\pi$  arene stacking interactions. Alternatively, ball milling is a mechanical method broadly used to granulate minerals into very fine particles and prepare or alter inorganic solids. However, its use in organic synthesis is relatively uncommon.<sup>336,337</sup>

Milling can be conducted in various ways. The simplest method involves using a laboratory mortar and pestle. This manual milling process can induce many mechanochemical reactions that do not require overcoming a high energy barrier. Alternatively, ball mills are employed when higher energy levels are needed and when milling times extend to hours or even days. Laboratory vibrators, such as those of the Wiggle-Bug type, are highly efficient for milling small samples. For prolonged high-energy milling, such as in mechanical alloying or the amorphization of hard crystalline solids, very high energy vibrators like high-speed attritors or high-impact stainless steel ball mills (such as Spex type) are used.<sup>328,329</sup> Ultrasonication can also be employed as a method of mechanochemical processing.<sup>338,339</sup> Fig. 15 shows a brief timeline of the development of mechanochemistry and direct mechanocatalysis. The solid-state synthesis can easily be monitored by measurement of the IR or UV spectrum as a Nujol mull. Solid-state NMR can be beneficial, and Mossbauer spectroscopy is most valuable with Fe and Sn compounds. Other techniques,

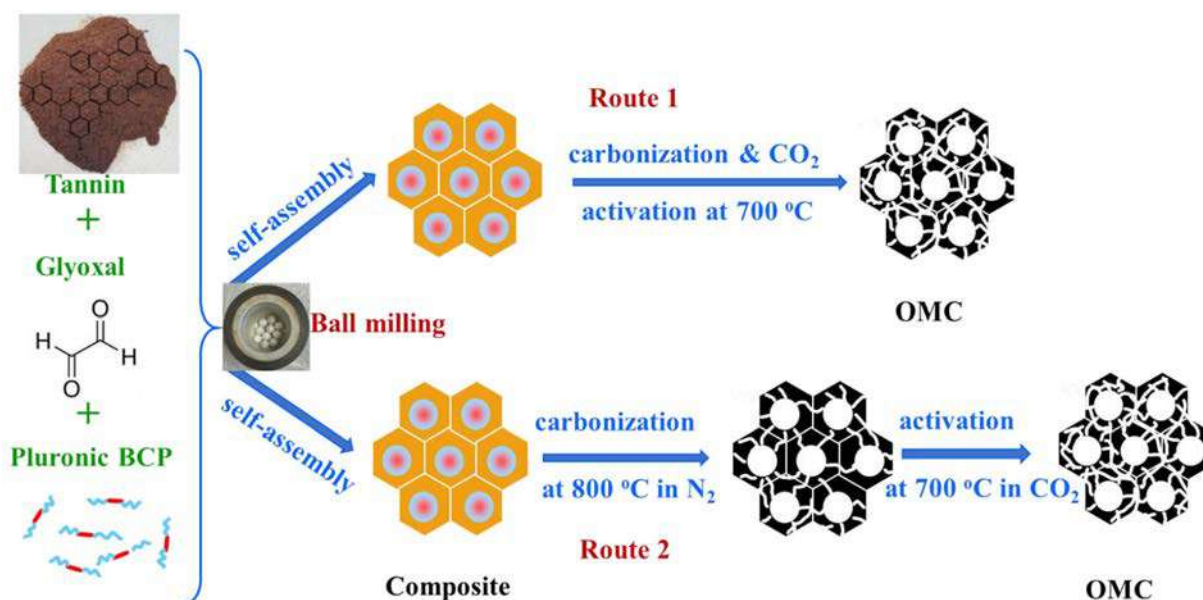


Fig. 14 Diagrammatic representation of the two processes used in the mechanochemical synthesis of OMCs: carbonization under N<sub>2</sub> and subsequent CO<sub>2</sub> activation (route 2); one-step carbonization and CO<sub>2</sub> activation (route 1) utilizing tannin, glyoxal, and block copolymer<sup>327</sup> [reproduced from ref. 327; open access article, copyright permission is not required].

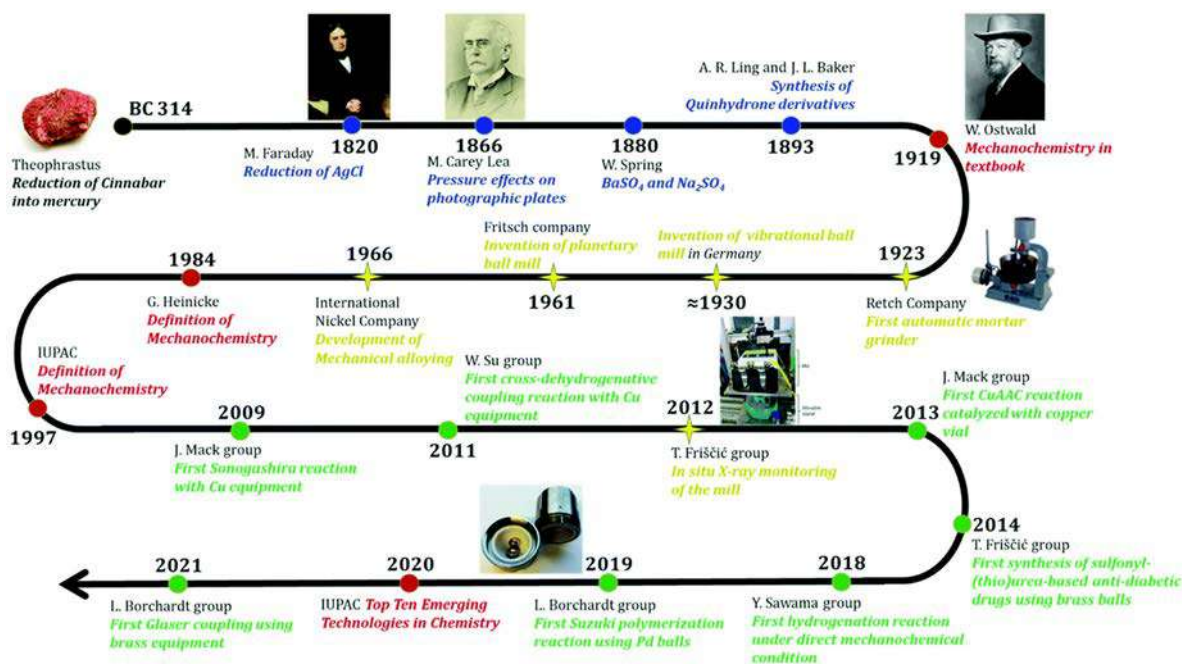


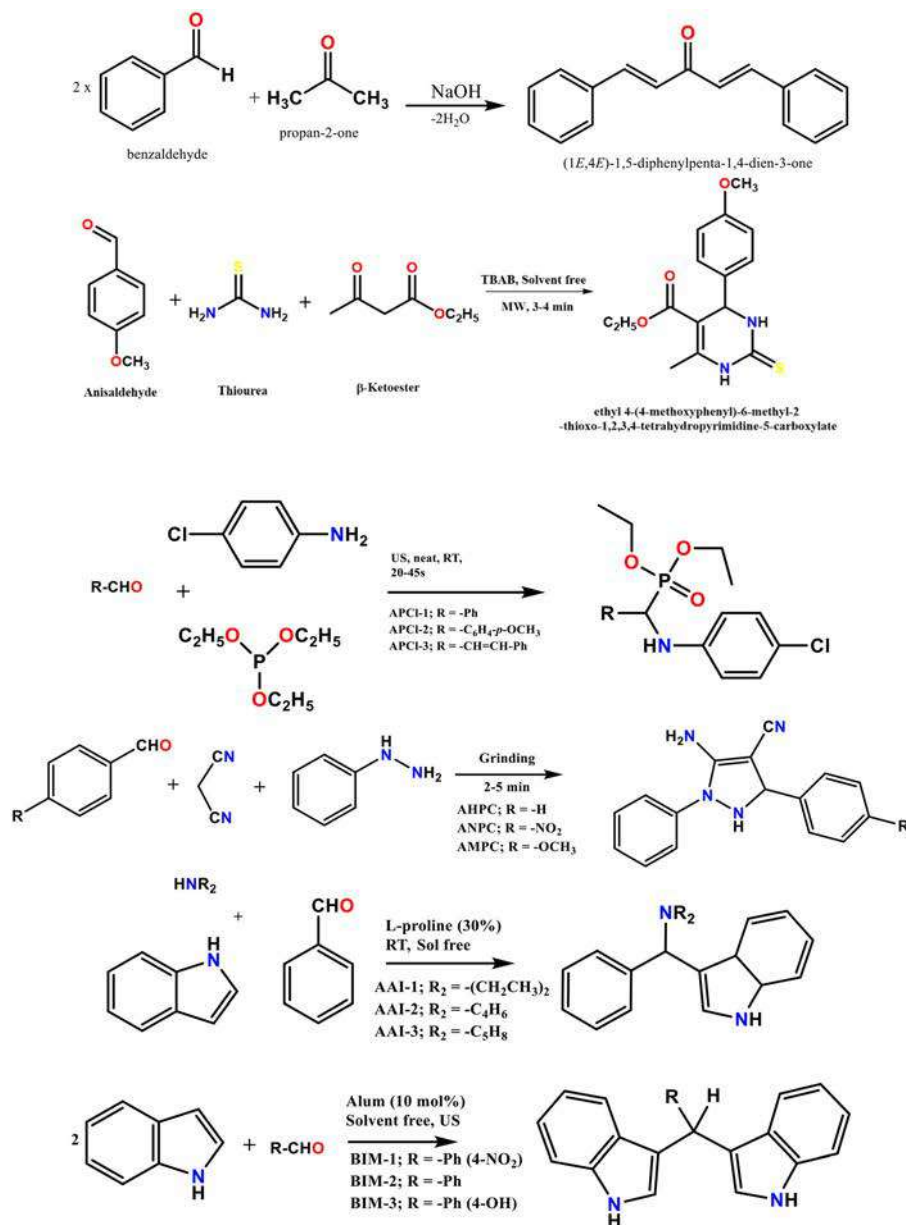
Fig. 15 Timeline of mechanochemistry and "direct mechanocatalysis"<sup>342</sup> [reproduced from ref. 342, RSC publication, copyright permission is not required].

such as high-resolution electron microscopy (HREM), electron cyclotron resonance (ECR) and extended X-ray absorption fine structure (EXAFS) spectroscopy, have been utilized to analyze new surfaces.<sup>328,340</sup> Mass spectrometry (MS) can also be used to determine gaseous products, such as in the decomposition of bromates and nitrates.<sup>341</sup>

Several corrosion inhibitors have been synthesized using solid-state or solvent-less synthesis procedures, as shown in Scheme 1. Some of the schemes are given below for the preparation of condensation products,<sup>343,344</sup> pyrimidine derivatives,<sup>345</sup> phosphonates,<sup>346</sup> pyrazoles,<sup>324</sup> indole derivatives,<sup>347,348</sup> *etc.* Considering the requirement for diverse industrial practices, the production of corrosion inhibitors is required (i) to be cost-effective, (ii) on a large scale, (iii) consume less time, and (iv) to be environmentally friendly. It can be shown in the given examples that the production of inhibitors, employing a solvent-free mechanochemical approach could result in their synthesis *via* simple stirring<sup>343,344</sup> or grinding<sup>324</sup> within the span of a few minutes and even at room temperature. In some cases, the synthesis also involves the use of greener catalysts such as nano-metal oxides<sup>348</sup> and amino acids.<sup>347</sup> Further, to enhance solvent-free synthesis, modern methods such as microwave irradiation<sup>345</sup> and ultrasonic irradiation-induced<sup>346</sup> synthesis can be used, as presented in some examples. According to the above discussion, and the shared schemes, it is obvious that corrosion inhibitors can be produced using the mechanochemical approach in a simple synthetic procedure within significantly less time. This approach minimizes the production of waste and avoids the cumbersome isolation and purification steps

required for conventional organic synthesis. This is incredibly convenient for the large-scale production of organic molecules to be used in various industries as corrosion inhibitors. Therefore, this methodology can prevent unnecessary waste, realize atom economy, lower-hazard chemical reactions due to the absence of toxic chemicals and reagents, and minimize the energy consumption. Considering the development of corrosion inhibitors using solid-phase preparation, this approach can be, in general, a cheaper, simple, cost-effective, and less time-consuming process, and therefore practically applicable for industrial purposes.

**2.4.2. One-step multi-component reactions.** The conventional synthesis procedures require long steps, with isolation and purification in each step leading to the considerable loss of reagents and colossal expenditure. One-step MCRs (Fig. 16a), or in other words, multicomponent assembly processes (MCAPs), are the term given to the chemical synthesis process wherein three or more reactive molecules are converted to the product following a single-step reaction.<sup>349–352</sup> MCRs represent an attractive green strategy as a fruitful alternative to the conventionally utilized multiple-step synthesis procedure.<sup>353,354</sup> They are especially useful for developing green chemicals for industrial and biological applications. The salient features of MCRs include short reaction times, high yields, high chemical selectivity, low operating cost, and low number of purification steps. Their other benefits are less consumption of toxic solvents and purification reagents that can harm the environment.<sup>97,355</sup> Some of the salient features of MCRs are presented in Fig. 16b. In a green MCR, most of the atoms in the reagents should be converted to the product.



**Scheme 1** Solid-phase synthesis of (a) dibenzalacetone,<sup>343,344</sup> (b) pyrimidine derivatives,<sup>345</sup> (c) phosphonates,<sup>346</sup> (d) pyrazoles,<sup>324</sup> (e) 3-aminoalkylated indoles,<sup>347</sup> and (f) bis(indolyl) methanes<sup>348</sup> [the synthetic schemes were reproduced and suitable copyright permissions have been obtained].

Also, water is usually the major by-product of such green MCR reactions.<sup>349</sup> An astonishing feature of MCRs is that independent of the preferred reaction pathway, all mechanisms lead to the same final product. MCRs allow direct and elegant access to bioactive compound libraries and fulfil the requirement for biologically active compound syntheses and discovery.

The Strecker synthesis of  $\alpha$ -amino cyanides developed in 1850 is considered the first documented MCR. Currently, metal-catalyzed MCRs, isocyanide-based MCRs, organoboron-based MCRs, and free radical-facilitated MCRs are the most reported one-step MCRs for developing novel organic molecules, including corrosion inhibitors. The synthesis of organic

compounds having application in various industrial practices using one-step MCRs agrees with the principles of “green chemistry”. Thus, MCRs are frequently utilized for various chemical transformations, including Biginelli reaction, alkyne trimerization, Gewald reaction, Bucherer–Bergs reaction, Hantzsch pyridine synthesis, Kabachnik–Fields reaction, Grieco three-component coupling, Passerini reaction, Mannich reaction, Petasis reaction, Strecker amino acid synthesis, Ugi reaction, Asinger reaction, A3 coupling reaction and Pauson–Khand reaction.<sup>122,303,357–359</sup> An increasing number of applications of MCRs has been reported in medicinal chemistry and drug discovery programs, combinatorial chemistry,

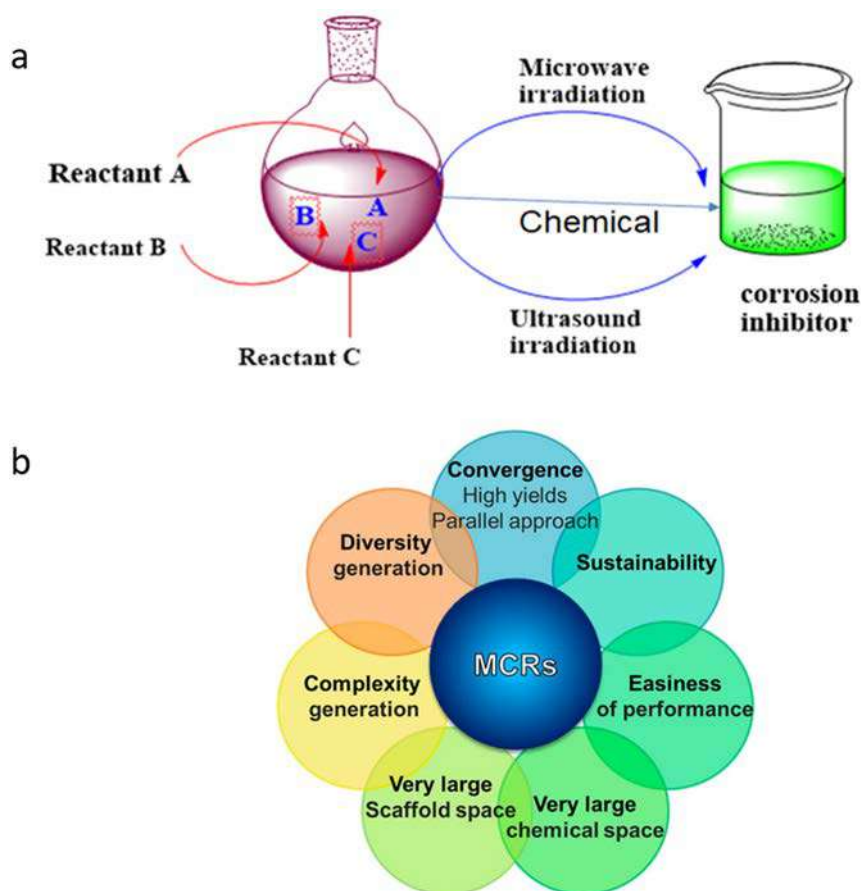


**Fig. 16** (a) Schematic of MCRs facilitated using microwave and ultrasound irradiation and (b) basic characteristics of MCRs<sup>356</sup> [reproduced from ref. 356; open access article, copyright permission is not required].

natural product synthesis, agrochemistry, and polymer chemistry.<sup>303</sup> A brief timeline of the development of MCRs is shown in Fig. 17.

In a green MCR, most of the atoms in the reagents should be converted to the product. Water is usually the major by-product of such green MCR reactions.<sup>349</sup> Noticeably, compared to the conventional tedious synthesis of corrosion inhibitors, MCRs show synthetic advantages regarding simplicity, efficiency, selectivity, convergence, and atom economy. Ideally, all or most of the steps during multicomponent reactions (MCRs) would reach reversible equilibrium, with the last step being irreversible, leading to the final products. In this case, the products can precipitate from the reaction mixture, which enables purification by filtration and washing without chromatography or recrystallization. A survey of the literature showed that most of the research on corrosion inhibitors has been undertaken on the effect of electron-donating/withdrawing substituents and their influence on the corrosion inhibition efficiency.<sup>11,18,19</sup> Hence, a thorough review of the literature is required to consider the crucial structural features of organic corrosion inhibitors such as (i) the carbon chain length, (ii) the nature of heteroatoms, (iii) the effect of stereochemistry, (iv) the effect of the ring size, and (v) influence of substituents

on the corrosion inhibition performance. In this context, the MCR protocol has led to the development of a series of libraries consisting of heterocycles established for quantitative structure activity-relationship (QSAR) studies on corrosion inhibition. Thus, multicomponent reactions represent valuable tools in the repertoire of sustainable synthetic methods for developing environmentally benign corrosion inhibitors and their synergistic utilization with other green technologies, which can bring organic chemists closer to the ideal synthesis.

As discussed above, the requirement for efficient corrosion inhibitors based on organic molecules also attempts to address the ease of synthesis and cost-effectiveness of the synthesized products and overall environmentally safer procedures. MCRs have been recognized as one of the greenest alternatives for developing green chemicals with numerous industrial and biological applications. In this context, MCRs have several advantages such as ease of performance, lower number of steps, high selectivity, facile automation, unique product, high atom economy, simple purification of the product, high synthetic efficiency, and low waste production because of the reduction in the number of work-up steps, thus saving time and resources.

Several corrosion inhibitors have been synthesized following the MCR approach, as shown in Scheme 2.<sup>360–365</sup> Although

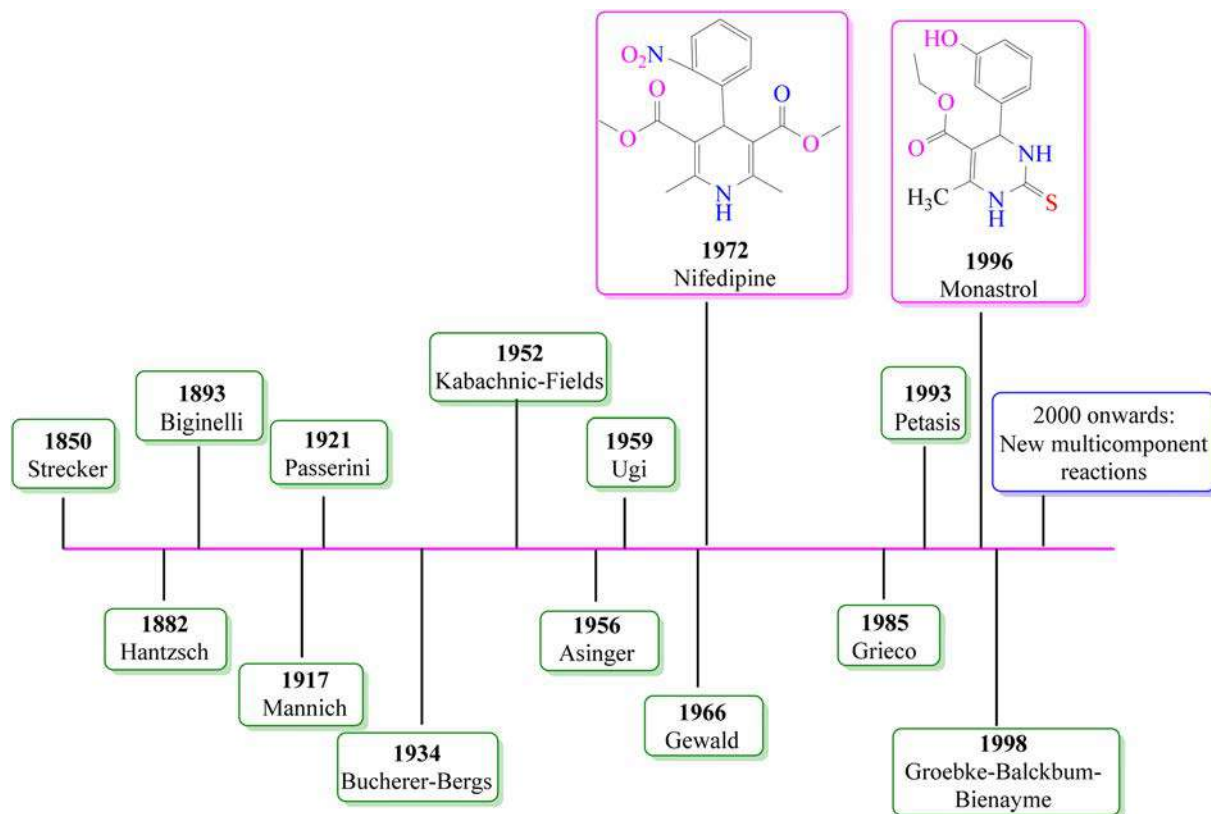


Fig. 17 Timeline of multicomponent reactions (1850–2000) [self-illustration, copyright permission is not required].

corrosion inhibitors are derived using one-step MCRs, which deliver several synthetic benefits, MCRs suffer from several challenges. One of the biggest challenges of MCRs is the possibility of side reactions during the reaction progress, reducing the overall yield and efficiency of the synthesis. The side reactions not only decrease the result of the reaction but also cause the release of enormous amounts of environmentally harmful solvents and chemicals that adversely affect the surrounding environments. Also, the possibilities of bimolecular side reactions become greater under harsh reaction conditions. Therefore, it is recommended that the synthesis of corrosion inhibitors using MCRs should be carried out under comparatively milder conditions. Further, most of the corrosion inhibitors were synthesized using MCRs; therefore, exploring the synthesis of the corrosion inhibitors using three- and four-component reactions is also recommended. Generally, the corrosion inhibitors derived from MCRs are associated with high inhibition efficiency, which is attributed to several polar functional groups. The polar functional groups act as adsorption centers for metal-inhibitor interactions. The polar functional groups not only facilitate the adsorption of the corrosion inhibitors but also enhance their solubility in polar electrolytic media, such as  $\text{H}_2\text{O}$  and  $\text{HCl}$ . The combination of MCRs with non-traditional irradiation further improves their synthetic efficiency. Therefore, it is recommended that MCRs be carried out in association with

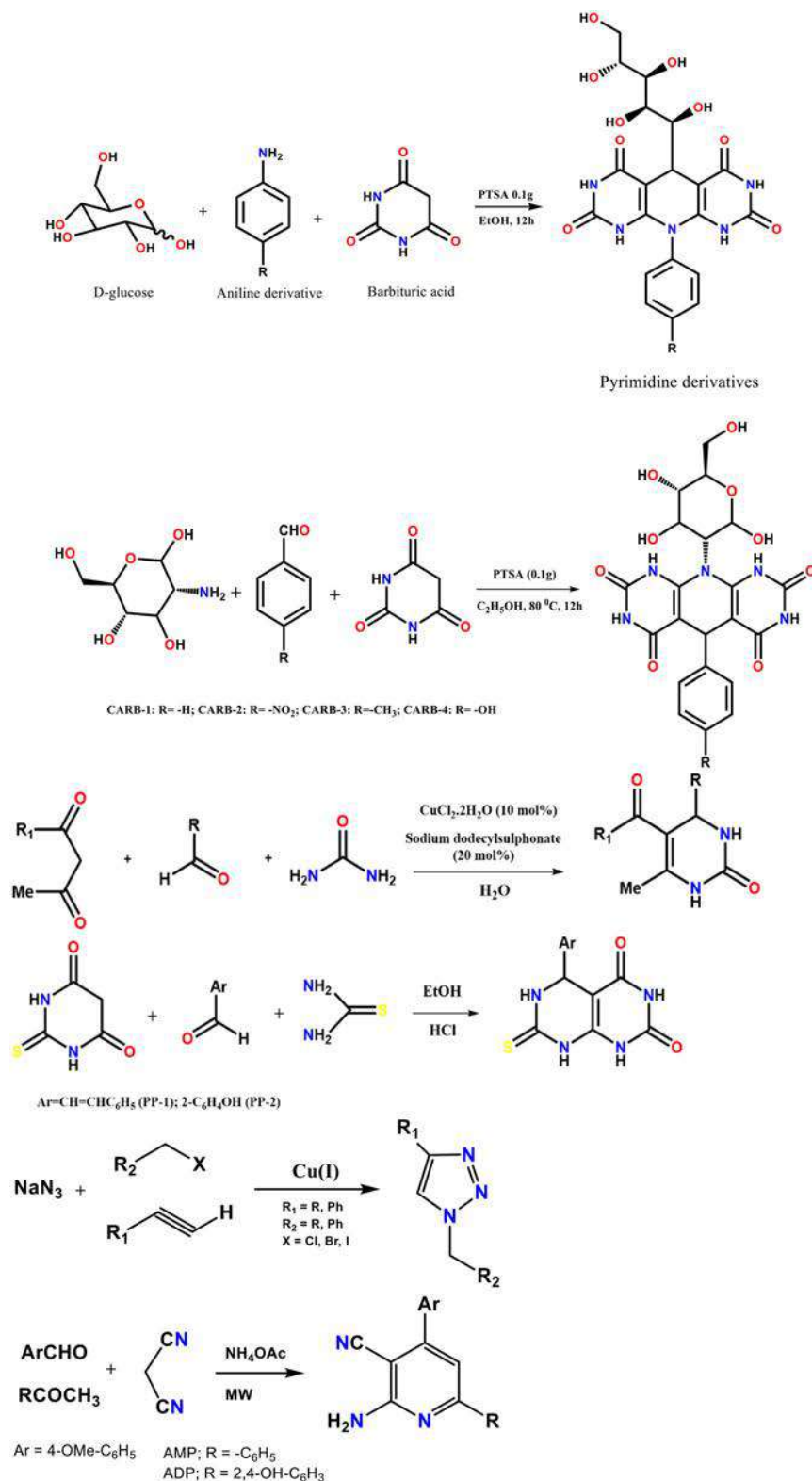
microwave and ultrasound irradiation. Insertion of polar functional groups should be enhanced as much as possible. The inhibition characteristics of the corrosion inhibitors derived from MCRs have been investigated mainly for ferrous alloys. Therefore, their use should be explored for non-ferrous metallic alloys. According to the ongoing discussion, it is also clear that corrosion inhibitors derived from MCRs are regarded as environmentally benign because of their association with several synthetic efficiencies, including higher reaction yield and lower reaction time. Thus, MCRs, in combination with non-conventional microwave and ultrasound irradiation, offer one of the greenest and most efficient protocols for developing and designing environmentally benign corrosion inhibitors.

## 2.5. Green corrosion inhibition using benign solvents, chemicals and catalysts

### 2.5.1. Water as a green solvent for the synthesis of inhibitors.

Sustainable organic methodologies are in high demand in various industrial applications for producing multiple organic scaffolds, such as fine chemicals, medicinal and pharmaceutical agents, and agrochemicals.<sup>366,367</sup> Scientists are advocating the use of water as a solvent due to its environmentally friendly nature, cost-effectiveness, non-flammability, and abundant availability. Water as a solvent promotes the activation of functional groups *via* hydrogen bond formation. Owing to the high surface tension and hydrophobicity,<sup>368</sup> the





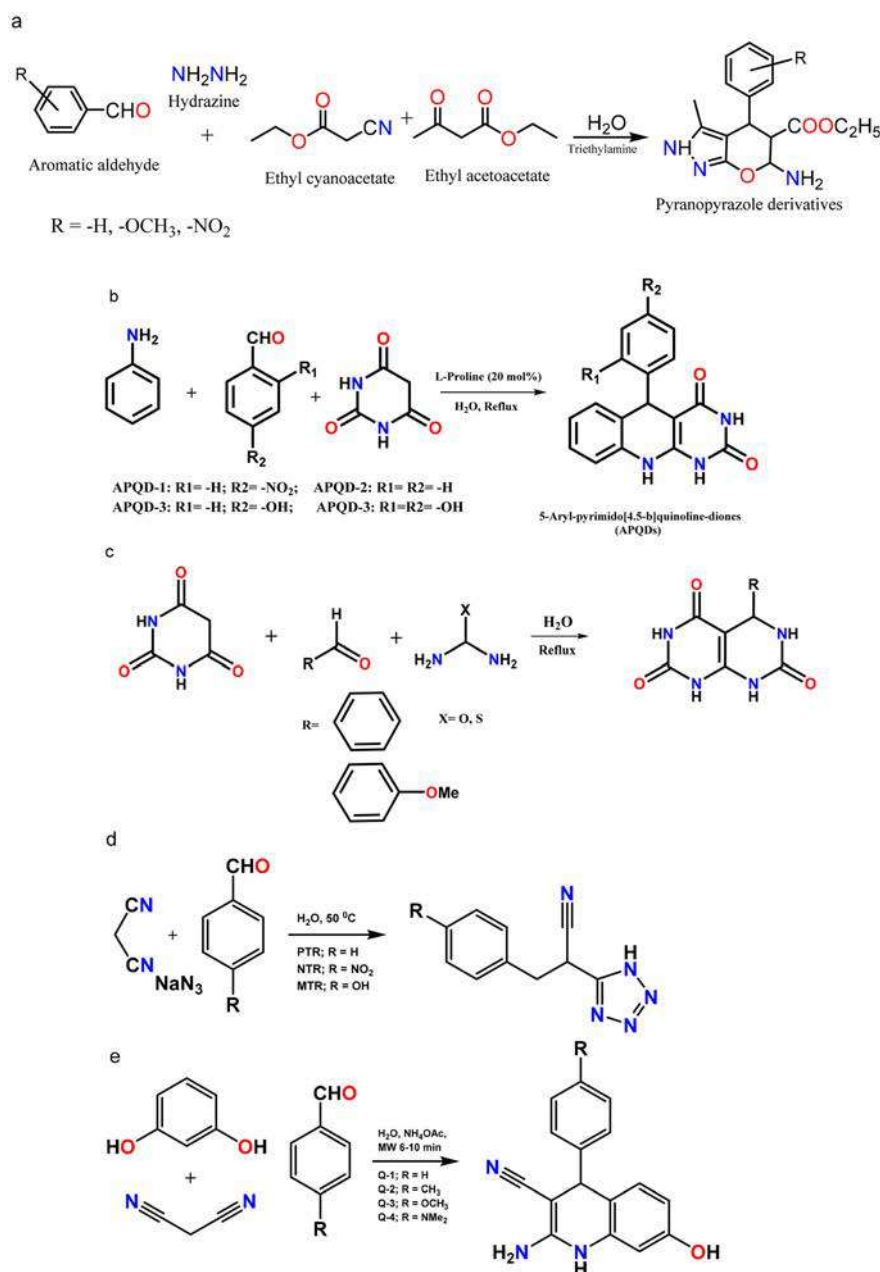
**Scheme 2** Examples of MCR-based synthesis of corrosion inhibitors (a),<sup>360</sup> (b),<sup>361</sup> (c),<sup>362</sup> (d),<sup>363</sup> (e),<sup>364</sup> and (f)<sup>365</sup> [the synthetic schemes were reproduced and suitable copyright permissions have been obtained].

reactants in an aqueous environment are bound to form aggregates to reduce the exposed organic surface area,<sup>369,370</sup> increasing the reaction rate. Therefore, a “strong collaboration”

between US and aqueous reaction media is essential to develop environmentally sustainable synthesis protocols. Further, solvent-less or solid phase synthesis or synthesis in

aqueous medium is in general preferred considering the non-flammable nature, high dielectric constant, abundant availability, ease of handling, low cost, *etc.* of water.<sup>371,372</sup> These beneficial aspects in terms of sustainability have motivated scientists and researchers to explore organic synthesis in aqueous media. Moreover, modern techniques such as MS and US have facilitated organic synthesis to be carried out in aqueous media.<sup>339,373–375</sup> Considering the requirement of large-scale production of corrosion inhibitors, the use of an aqueous medium significantly reduces the high cost required for conventional organic solvents. Moreover, using water as a

solvent is also a greener and cleaner approach. Some methods for preparing organic corrosion inhibitors in aqueous medium are presented in Scheme 3. It can be noticed that several organic molecule-based corrosion inhibitors have been synthesized using water as the reaction solvent.<sup>376–380</sup> Considering the requirement of large-scale synthesis, preference for the MCR approach and overall greenness of the synthesis protocol, water becomes an obvious choice as the synthesis medium for preparing organic corrosion inhibitors. In most cases, in water as the reaction medium, single-step reactions are carried out to afford high yield and minimize the iso-



**Scheme 3** Scheme for the synthesis of corrosion inhibitors based on (a) pyranopyrazoles,<sup>376</sup> (b) pyrimidoquinolines,<sup>377</sup> (c) pyrimidine derivatives,<sup>378</sup> (d) tetrazoles,<sup>379</sup> and (e) quinoline derivatives<sup>380</sup> in an aqueous medium [the synthetic schemes were reproduced and suitable copyright permissions have been obtained].

lation/purification steps. Simple reflux methods are used for synthesis, although MW and US-facilitated synthesis of organic inhibitors has also been reported.

### 2.5.2. Other green solvents for the synthesis of inhibitors.

Green analytical chemistry describes the contribution of analytical chemists towards sustainable development. The specialists attempt to introduce sustainability attributes to their activities and specific fields of expertise. It is important to establish good disposal practices to develop greener corrosion inhibitors, especially for solvent waste. Solvent distillation *vs.* incineration was compared *via* a life cycle analysis (LCA).<sup>381</sup> Spent solvents widely applied in analytical chemistry, such as acetonitrile, tetrahydrofuran, acetone, acetic acid, cyclohexane and toluene, should be recycled *via* distillation. Analytical solvent waste originating from methanol, ethanol, pentane, hexane or heptane applications should be treated by incineration. Accordingly, the trend in solvent application in analytical chemistry is to apply new types of solvents, such as bio-based solvents,<sup>382</sup> deep eutectic solvents<sup>383</sup> and ILs.<sup>384</sup> Similar to ionic liquids, bio-based solvents are considered green alternatives to more traditional ones. The typical solvents used in laboratories, such as methanol and acetone, can be derived from the lignocellulose feedstock.

Another aspect of analytical reagents for testing corrosion inhibitors is the application of acids and bases for digestion<sup>385</sup> and as various auxiliary chemicals. Due to their different chemical properties, acids and bases require the application of slightly different parameters during their greenness assessment.<sup>386</sup> The assessment systems are based on environmental, safety and health issues and problems with hazardous by-products or disposal problems. Fig. 18 lists some of the commonly used green solvents, including water.

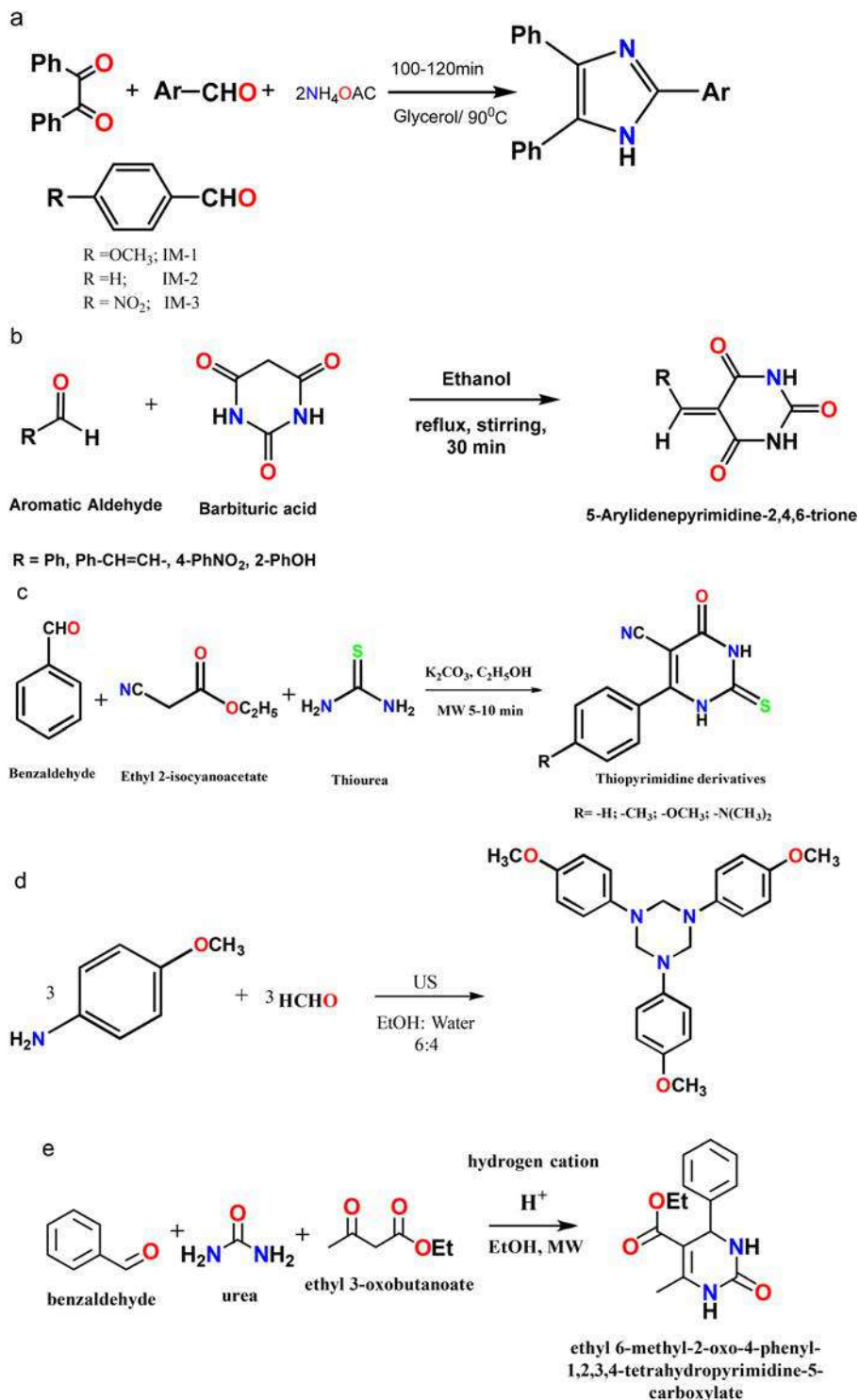


Fig. 18 Different types of green solvents [self-illustration, copyright permission is not required].

In addition to water, several organic solvents have been recognized as green solvents for organic synthesis, including “fluorous” solvents such as perfluorinated alkanes, dialkyl ethers, and trialkyl amines.<sup>63</sup> These perfluorinated liquids have useful and attractive properties for organic synthesis, such as chemical inertness, high thermal stability, nonflammability, extreme nonpolar character and small intermolecular attraction.<sup>387</sup> ILs<sup>388–390</sup> serve as solvents for reaction media for many separation or catalytic processes because there is a wide range of organic, inorganic and polymeric molecules that is well soluble in ionic liquids.<sup>391,392</sup> The solvating properties of ionic liquids depend on their smaller anions and larger organic cations. Organic carbonates represent esters of carbonic acids and are a class of compounds with a broad field of application due to their unusual properties. They are readily available in large amounts, inexpensive, low (eco)toxic, and entirely biodegradable. Organic carbonates are widely used for extraction, pharmaceutical and medical applications, and batteries. At room temperature, carbon dioxide exists as a liquid with excellent wetting properties and very low viscosity. Above its critical temperature and pressure (31 °C and 73.8 bar, respectively) CO<sub>2</sub> exists in the supercritical state,<sup>388,393</sup> featuring gas-like viscosities and liquid-like densities. Also, carbon dioxide is renewable, nontoxic, nonflammable, readily evaporates and chemically inert towards many substances, and thus features outstanding characteristics for utilization in green chemistry. Biosolvents have been developed as an alternative to volatile organic compounds (VOC), which are usually harmful to the environment and human health. The most important chemical classes of biosolvents are esters of naturally occurring acids and fatty acids, bioethanol, terpenic compounds, isosorbide, glycerol, and glycerol derivatives.<sup>394,395</sup> These compounds offer the advantage of being produced from renewable sources such as vegetable, animal or mineral raw materials by chemical and physical processes without consuming fossil resources. The objective of a green solvent is to minimize the environmental impact of the consumption of solvents in chemical production. Thus, the effective utilization of green solvents such as water, supercritical fluids, liquid polymers, and ILs can help reduce environmental pollution. The properties of novel green solvent or biosolvents include low toxicity, phase behavior, favourable chemical kinetics and thermodynamics, biodegradability, and non-flammability. Schemes for synthesizing corrosion inhibitors in greener solvents are shown in Scheme 4. The commonly used green solvents for preparing organic corrosion inhibitors include glycerol, methanol, and ethanol.<sup>396–400</sup> This simplifies the synthesis protocol and reduces the overall cost of synthesis.

### 2.5.3. Greener catalysts for the synthesis of inhibitors.

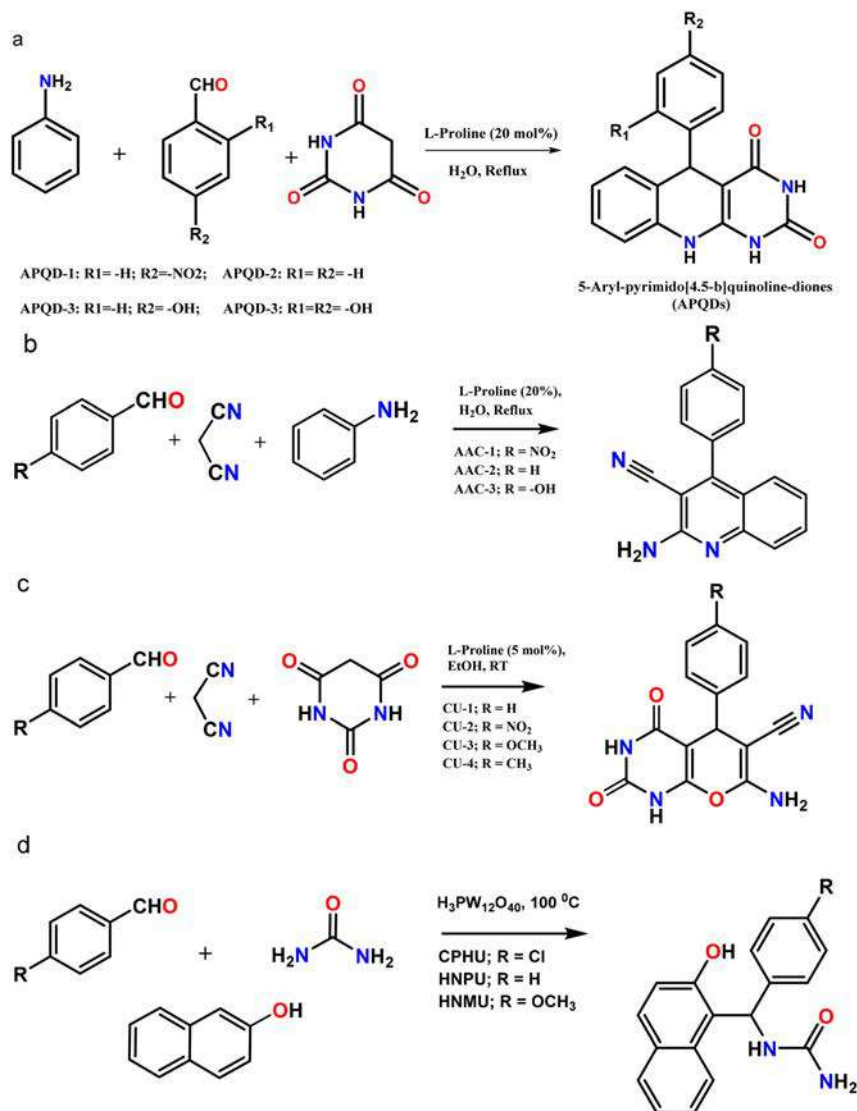
Greener catalysis means moving from stoichiometric processes to homogenous and heterogeneous catalytic reactions using organic, organometallic, inorganic and biological catalysts.<sup>401,402</sup> Amino acids and enzymes can be classified as nontoxic, renewable, and natural catalysts, which are usually metal free. In addition to their high reaction selectivity, the catalytic activity of enzymes is very high, even *in vitro*.



**Scheme 4** Scheme for the synthesis of corrosion inhibitors based on (a) imidazole derivatives<sup>396</sup> [reproduced from ref. 396, open access publication, copyright permission is not required], (b) barbiturates<sup>397</sup> [reproduced from ref. 397, open access publication, copyright permission is not required], (c) thiopyrimidines<sup>398</sup> [reproduced from ref. 398 with permission, Copyright, Elsevier, 2016], (d) triazine derivatives<sup>399</sup> [reproduced from ref. 399, copyright permission is not required], and (e) dihydropyrimidinones<sup>400</sup> [reproduced from ref. 400 with permission, Copyright, Elsevier, 2020] in environmentally benign solvents.

Moreover, green catalysts include magnetic nanoparticles, zeolites, natural food additives, and noble metal nanoparticles. Schemes for synthesizing corrosion inhibitors using greener

catalysts are shown in Scheme 5. L-Proline is commonly reported as a green catalyst for synthesizing organic corrosion inhibitors.<sup>403-406</sup> In addition, metal oxides<sup>407</sup> have also been



**Scheme 5** Schemes for the synthesis of corrosion inhibitors based on (a) pyrimidoquinolines,<sup>403,404</sup> (b) quinoline derivatives,<sup>405</sup> (c) condensed uracils,<sup>406</sup> and (d) urea derivatives<sup>407</sup> using environmentally safer catalysts [the synthetic schemes were reproduced and suitable copyright permissions have been obtained].

reported as catalysts for synthesizing corrosion inhibitors. By using trace amounts of green catalysts in single-step transformations, efficient corrosion inhibitor molecules with high yield and purity can be obtained.

**2.5.4. Green chemicals as corrosion inhibitors.** In addition to the abovementioned modern techniques for green synthesis, several precursor molecules can be classified as green and environmentally safe. Their application in the synthesis agrees with several green chemistry principles of ecologically benign and low toxicity reagents, renewable raw materials, and minimizing waste production.<sup>56,408</sup> The major categories include (i) extracts from plants and tree parts<sup>409</sup> such as roots, stems, leaves, bark, shells, seeds, and flowers. These parts contain several phytochemicals that are complex compositions of naturally occurring chemicals and are environmentally safe.

(ii) Carbohydrates<sup>286,410</sup> such as glucose, chitin, chitosan, cellulose, starch, and pectin. These large molecular weight chemicals contain abundant surface functional groups, which allow considerable prospects of reactivity. (iii) Amino acids<sup>50</sup> such as glycine, proline, and histidine in the essential amino acid category, providing reactivity, solubility, and prospects for chemical functionalization. In addition, polyamino acids such as polyaspartic acid and proteins such as soy, gluten, casein, and gelatin have also found diverse applications. It is understood that the abovementioned categories are of natural origin and have considerable biocompatibility. Other classes include (iv) heterocyclic biomolecules<sup>411</sup> such as vitamins and hormones; (v) pharmaceutical products, *i.e.*, drugs, and (vi) ILs (Fig. 19).<sup>411</sup> These types of chemicals are abundant, environmentally safe, and cheap. The guidelines for the classification

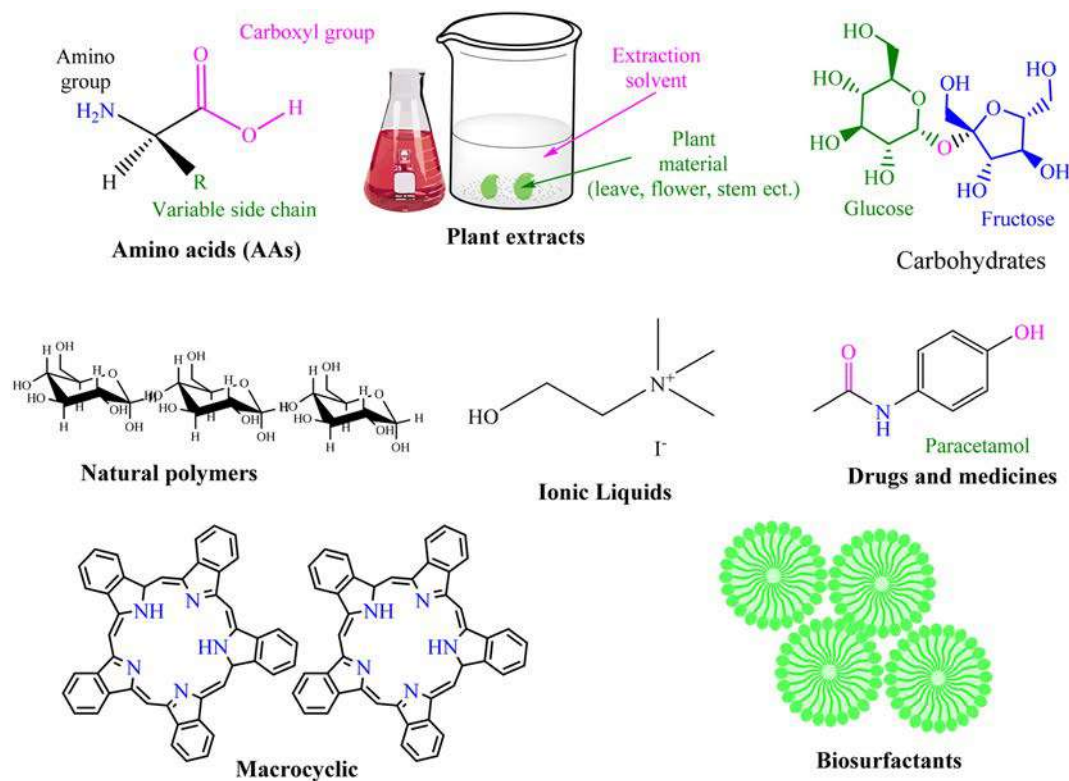


Fig. 19 Some of the greener chemicals for the development of corrosion inhibitors [self-illustration, copyright permission is not required].

Table 5 Classification criteria of green corrosion inhibitors [self-illustration, copyright permission is not required]<sup>a</sup>

Category	LD <sub>50</sub> value (mg kg <sup>-1</sup> )	Identification	Symbol
1	5	Fatal if swallowed	
2	50	Fatal if swallowed	
3	300	Toxic if swallowed	
4	>300 ≤ 2000	Environmentally benign	
5	>2000 ≤ 5000	green inhibitors	

Key: green inhibitors belong to category 4 and 5. <sup>a</sup> International standard for chemical safety, globally harmonized system of classification and labelling of chemicals (GHS), United Nations Institute for Training and Research Program Advisory Group.

of green corrosion inhibitors are based on the following criteria (Table 5):<sup>412–415</sup>

(i) Toxicity: The LD<sub>50</sub> value should be >500 mg kg<sup>-1</sup> weight of a rat.

(ii) Biodegradation: The biodegradability should be 60% in 28 days.

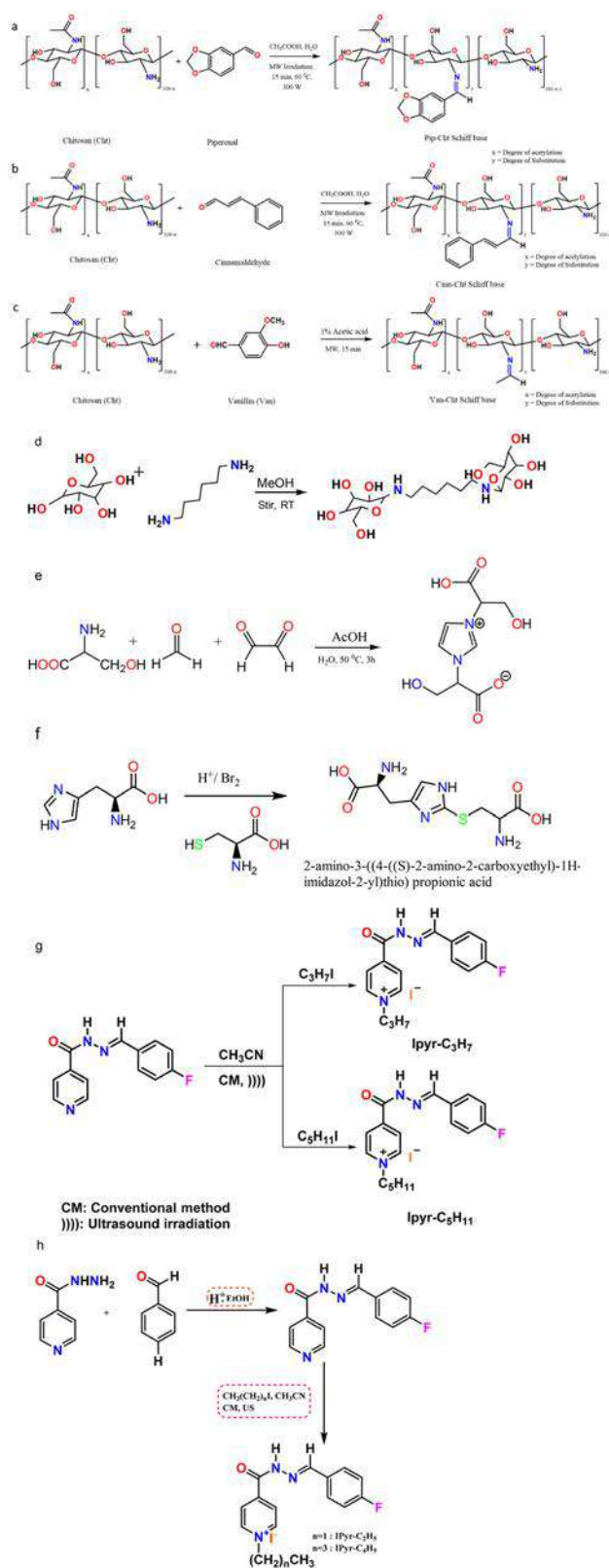
(iii) Bioaccumulation: The capability of a chemical to accumulate in living organisms can be computed employing the partition coefficient ( $\log P_{o/w}$ ), where  $\log P_{o/w}$  limit < 3.0.

A wide range of heterocyclic compounds has been reported as corrosion inhibitors, including pyridines,<sup>416</sup> pyrimidines,<sup>417</sup> pyrazole,<sup>418</sup> imidazoles,<sup>419</sup> triazoles,<sup>420</sup> tetrazoles,<sup>421</sup> indoles,<sup>347</sup> thiazoles,<sup>422,423</sup> oxadiazoles,<sup>424</sup> benzotriazoles,<sup>425,426</sup> benzimidazoles,<sup>427,428</sup> and macrocyclic compounds,<sup>429,430</sup> and biomolecules. Previously, conventional research in corrosion inhibition was limited to small molecules, such as benzotriazole and other simple compounds, with little or no attention to biological and macromolecules. However, recently, scientists and researchers have focused on exploring novel inhibition chemistries that can be effective, easier to obtain/synthesize, and environmentally suitable. Their application in the synthesis agrees with several provisos of green chemistry principles of environmentally benign and low toxicity reagents, renewable raw materials, and minimising waste production.<sup>56,408</sup> The major categories of green corrosion inhibitors include (i) the extracts from plants and tree parts<sup>409</sup> such as roots, stems, leaves, bark, shells, seeds, flowers, and seeds. These parts contain several phytochemicals that are complex compositions of naturally occurring chemicals and are environmentally safe; (ii) carbohydrates<sup>286,410</sup> such as glucose, chitin, chitosan, cellulose, starch, pectin, *etc.* These large molecular weight chemicals contain abundant surface functional groups that allow considerable prospects of reactivity; (iii) amino acids<sup>431</sup> such as glycine, proline, histidine, and

others are among the essential amino acid member categories. These provide reactivity, solubility, and prospects for chemical functionalization. In addition, polyamino acids such as polyaspartic acid and proteins such as soy, gluten, casein, gelatin, *etc.* have also found diverse applications. It is understood that the abovementioned categories are of natural origin and have considerable biocompatibility. Other classes include (iv) heterocyclic biomolecules<sup>411</sup> such as vitamins, hormones *etc.*; (v) pharmaceutical products, *viz.* drugs, and (vi) ILS (Table 5).<sup>411</sup> These types of chemicals are abundant, are environmentally safe, and afford cheap costs. Notably, some of the green chemicals presented in Table 5 can find applications as environmentally safer corrosion inhibitors. In addition, some methods are proposed to develop novel derivatives of such greener chemicals to obtain greener corrosion inhibitors. These biomolecules have been reported for their environmentally benign nature and considerable corrosion inhibition efficiency in aggressive aqueous media. Further, to achieve an improvement in corrosion inhibition performance, different chemical functionalization methods have been explored.

Polymers have found wide applications in corrosion inhibition due to their high molecular surface area, which can afford superior adsorption. Additionally, the presence of abundant available sites for adsorption allows excellent interaction with the metallic substrate. Naturally derived polymers such as chitosan, carboxymethyl cellulose, dextran, maltodextrin, and starch have been reported to exhibit significant inhibition behaviour.<sup>432–434</sup> These polymers can be extracted from natural sources or synthesized from living organisms.<sup>432</sup> The diverse applications of these biological polymers originate from their intrinsic biodegradability combined with excellent properties such as non-toxic nature, biocompatibility, renewability, barrier action, low cost, and demonstrated potential application in corrosion inhibition. Several natural polymers, such as chitosan,<sup>410,435–437</sup> cellulose,<sup>438,439</sup> dextrans,<sup>440,441</sup> and starch,<sup>442,443</sup> have been utilized as corrosion inhibitors. Exudate gums, such as xanthan gum and Gum Arabic, have also been reported. Further, considering their interesting inhibition and protection performance, researchers have also attempted the chemical modification of several natural polymers and reported their performance as corrosion inhibitors. Recently, several polymeric nanoparticles<sup>443</sup> and nanobiocomposites<sup>444,445</sup> derived from naturally occurring polymers have also been reported as environmentally friendly corrosion inhibitors. Schemes for the synthesis of organic molecule-based corrosion inhibitors using chitosan Schiff bases, amino acids, and ionic liquids are presented in Scheme 6. Other carbohydrate derivatives have also been reported as inhibitors.<sup>446,447</sup>

Amino acids are organic molecules composed of nitrogen, oxygen, and hydrogen, which are the building blocks of proteins.<sup>452</sup> Amino acid molecules contain an  $-NH_2$  group,  $-COOH$  group, and a side chain (aliphatic/aromatic) specific to each amino acid molecule. These functional groups can adsorb on a desired metallic substrate, thereby promoting the corrosion protection by amino acids. Amino acids exist in



**Scheme 6** Schemes for the synthesis of corrosion inhibitors using environmentally safer reagents such as (a–c) chitosan,<sup>410,435–437</sup> (d) glucose,<sup>446,447</sup> (e and f) amino acids,<sup>448,449</sup> and (g and h) ionic liquids<sup>450,451</sup> [the synthetic schemes are reproduced from their respective publications with permission and copyright permissions have been obtained].

aqueous solutions as zwitterions, *i.e.*, containing separate positively ( $-\text{NH}_3^+$ ) and negatively charged ( $-\text{COOH}^-$ ) groups, imparting high solubility. Moreover, amino acids are naturally occurring, biodegradable, cost-effective, and present as alternatives to commercially used toxic corrosion inhibitors.<sup>448,449</sup> Several reports have emerged in the literature on the application of amino acids as corrosion inhibitors.<sup>18,431</sup> The chemical modification of amino acids *via* functionalization strategies to develop amino acid derivative-based corrosion inhibitors has also been reported.

Natural extracts derived from plants present one of the leading categories of green corrosion inhibitors. Due to their natural origin, these extracts are considered green, and their application in corrosion inhibition agrees with environmental regulations. Extracts from almost all plant parts, *e.g.*, leaves, fruits (including pulp, skin, shells, and seeds), stem, bark, flowers, and roots, are useful as corrosion inhibitors.<sup>128</sup> The different sections of a plant are composed of various phytochemicals such as alkaloids, terpenoids, flavonoids, catechins, and co-enzymes, including carbohydrates, amino acids, vitamins, and proteins. Accordingly, plant extract-based corrosion inhibitors have been utilized in various corrosive media on different metal surfaces.<sup>128,409</sup> Pharmaceutical products are organic compounds composed of heteroatoms (N, S, O, and P), functional groups, heterocyclic rings, phenyl rings,  $\pi$ -bonds, *etc.* in their molecular structure. Given that they are produced for human consumption, these products are green and environmentally friendly.

Besides, medicines can be easily solubilized by water and oils. Several research articles have been published on the use of drugs or chemical medicines as corrosion inhibitors.<sup>453,454</sup> Almost all types of drugs, *e.g.*, antimalarial, antibacterial, antifungal, antiviral, antihypertensive, and anticancer, have been utilized as corrosion inhibitors. Considering the cost of medicines, several expired pharmaceutical products have recently been reported as corrosion inhibitors.<sup>455–459</sup> The use of oleochemicals in various applications aligns with the green chemistry principles and promotes the use of renewable, sustainable, and bio-based chemicals.<sup>460,461</sup> Oleochemicals, which are fats and oils extracted from plant and animal sources, also represent this category. Due to their natural origin, oleochemicals are environmentally benign. Oleochemicals bear the structure of long-chain fatty acids, which aid in the effective adsorption on the target metal surfaces. Furthermore, the presence of other surface functionalities, in the form of polar functional groups, heteroatoms, heterocycles and/or phenyl rings  $\pi$ -bonds, facilitate their adsorption. Due to their ready availability, low toxicity, and biodegradable properties, oleochemicals present a major category of environmentally benign corrosion inhibitors.

Recently, the use of biosurfactants in corrosion protection has been gaining particular attention. It is important to note that generally, surfactants have found application together with conventional inhibitors, wherein these molecules aid in the dissolution of the inhibitors in corrosive media. However, a literature survey indicated that numerous cationic-, non-

ionic-, Gemini- and ionic liquid-based surfactants have been widely reported as corrosion inhibitors.<sup>462,463</sup> It also showed that ionic liquids are effective by adsorbing on metallic surfaces.<sup>464,465</sup> Through their adsorption, ionic liquids block the active sites of metal surfaces responsible for corrosive damage. Similar to traditional organic corrosion inhibitors, the adsorption of ILs may follow the physisorption, chemisorption or physiochemisorption mechanism. Ionic liquids are also widely used as corrosion inhibitors for various metal/electrolyte systems.<sup>450,451</sup> Macrocylic compounds refer to large molecular structures similar to that commonly found in calixarenes, crown ethers, cyclodextrins, porphyrin rings, phthalocyanines, crown ethers, *etc.*<sup>466</sup> Several antibiotics are based on macrocylic compounds. These compounds can form highly stable chelates and complexes with transition metals and lanthanides. Their higher molecular weight affords them high metallic surface coverage. A greater number of heteroatom  $\pi$ -bonds, conjugation, additional phenyl rings, and heterocycles is favorable for surface adsorption on metallic substrates.<sup>353</sup> Several studies by the authors are available on the effect of ring size and heteroatoms of macrocylic compounds on their inhibition performance.<sup>429,466–470</sup>

## 2.6. Green corrosion inhibition using bio-based materials

The control of metallic corrosion using biobased compounds has gained significant momentum in response to the global campaign against the use and discharge of toxic chemicals into the environment. Various biobased compounds have captured keen interest from corrosion experts in recent years. This section provides a concise overview of the pertinent literature on biobased compounds, such as pharmaceutical drugs and essential oils, subjected to empirical testing for their anticorrosive activities. According to the literature, pharmaceutical drugs, which are known for their diverse clinical applications, including antihypertensive, anticonvulsant, antiviral, and antidepressant properties, represent biobased chemicals with substantial anticorrosion potential.<sup>471</sup> These pharmaceutical drugs exhibit structural attributes similar to conventional organic inhibitors, thus prompting researchers to scrutinize their performance as corrosion inhibitors. Their key features such as conjugated multiple bonds, polar functional groups, planar structures, and heteroatoms contribute significantly to their inhibitory capabilities against corrosion. These attributes enable drug molecules to adsorb onto metal surfaces, forming a protective barrier against corrosive agents. Furthermore, pharmaceutical drugs possess the advantages of water-solubility, non-toxicity, ecofriendliness, cost-effectiveness and biodegradability. In this case, expired drugs are preferable as metallic corrosion inhibitors due to their environmental and economic benefits compared to fresh drugs.<sup>472,473</sup>

The effectiveness of fresh and expired pharmaceutical drugs in inhibiting corrosion reactions has been extensively documented in the literature.<sup>471–475</sup> In two distinct reports, investigations were carried out on the inhibition performance of azithromycin for stainless steel 316L in KOH<sup>476</sup> and mild steel in 2 M HCl.<sup>477</sup> These investigations employed electro-



chemical and surface analytical methods and revealed the ability of azithromycin to significantly reduce the corrosion rate even at minimal doses, functioning as a mixed inhibitor. The proposed inhibition mechanism for both cases involved physical adsorption, with the Freundlich isotherm governing the inhibition process in SS 316L/KOH and the Langmuir isotherm in MS/2 M HCl. Table 2 provides an overview of the significant research publications in 2023 pertaining to the utilization of pharmaceutical drugs as corrosion inhibitors.

Recent reports highlight the growing interest in hybrid systems, combining at least one type of drug with synergistic agents such as other drugs, halide ions, nanoparticles and natural gums to enhance the corrosion resistance of metallic materials. For instance, incorporating cyclodextrin into piroxicam resulted in outstanding resistance in a steel/1 M HCl system, achieving an impressive 98.65% inhibition at a concentration as low as 0.4 mM. This synergistic inhibitor exhibited a significantly superior performance to several individual drugs tested as corrosion inhibitors.<sup>502</sup> Nevertheless, it remains crucial to determine the optimal dosage ratio of the inhibitor components to maximize the protection performance of these hybrid systems. Recent research efforts have focused on uncovering the remarkable inhibitory effects of drug-based hybrid inhibitors in investigating the corrosion behaviour of diverse metal/electrolyte systems.<sup>503–508</sup>

In the realm of employing computational tools to elucidate the inhibition mechanisms of drug molecules, Mrani *et al.*<sup>509</sup> conducted comprehensive computational studies on seven sulfa drugs as inhibitors of steel corrosion. These investigations combined *in silico* toxicity assessments with DFT and MC simulation. The findings demonstrated that the tested

drug compounds can be classified as non-toxic and highly effective steel corrosion inhibitors. A QSAR model was developed in a separate study to predict the inhibition performance of 250 commercial drugs employing an autoregressive with exogenous input (ARX) approach. This model utilized hard-soft acid-base (HSAB) descriptors derived from third-order DFTB. Its reliability was assessed through a five-fold cross validation process, and subsequently subjected to external validation, yielding exceptionally favorable results. To substantiate the credibility of the developed model, the authors further validated it by assessing newly synthesized lidocaine using electrochemical methods, achieving an impressive peak %IE of 92.5% (EIS) and 87.51% (PDP) at a concentration of 100 ppm. Remarkably, these experimental results are closely aligned with the predicted %IE of 87.51% obtained from the ARX model.<sup>510</sup> Similarly, a recent report by Abeng and Anadebe harnessed the capability of artificial neural network (ANN) and adaptive neuro-fuzzy inference system (ANFIS) models to evaluate the protective performance of the doxorubicin drug. These modelling assessments were performed alongside well-established experimental and theoretical techniques. Both models showed remarkable agreement between the experimental and predicted inhibition performances of doxorubicin in a 0.5 M H<sub>2</sub>SO<sub>4</sub> solution. Conclusively, the ANFIS model exhibited superior accuracy to the ANN model.<sup>511</sup>

Essential oils are natural, biobased and volatile liquids extracted from plants, which are well-known for their versatile applications across various domains, including cosmetics and medicine. These oils are distinguished by their purity and natural origin, natural abundance, high volatility with pronounced fragrances, liquid state at room temperature and

**Table 2** Summary of recent significant works on pharmaceutical drugs as corrosion inhibitors

S. no.	Drug	Metal	Medium	Conc.	Max %IE (%)	Inhibitor category	Ref.
1	Mebendazole	5Cr pipeline steel	1 M HCl	5 mM	94.40	Mixed/LAI	478
2	Ribavirin	Q235 steel	1 M HCl	10 mM	97.70	Mixed/LAI	479
3	Ibuprofen	Copper	0.5 M H <sub>2</sub> SO <sub>4</sub>	5 × 10 <sup>-3</sup> M	95.25	LAI	480
4	Ampicillin	Mild steel	5% HCl	20 mM	96.70	Mixed/LAI	481
5	Aspirin	Aluminium	0.5 M H <sub>2</sub> SO <sub>4</sub>	300 ppm	96.98	LAI	482
6	Aspirin	Carbon steel XC48	1 M HCl	5 × 10 <sup>-3</sup> M	96.50	LAI	483
7	Bifonazole	Carbon steel	1 M HCl	375 mg L <sup>-1</sup>	92.08	Mixed/LAI	484
8	Terconazole	Carbon steel	1 M HCl	375 mg L <sup>-1</sup>	94.19	Mixed/LAI	484
9	Thiamazole	Copper	3% NaCl	10 <sup>-4</sup> M	97.00	Mixed/LAI	485
10	Gabapentin	Mild steel	1 M HCl	400 ppm	90.30	Mixed/LAI	486
11	Gabapentin	Zinc	0.1 M HCl	400 mg L <sup>-1</sup>	84.90	Mixed/LAI	487
12	Vildagliptin	Mild steel	1 M HCl	1 mM	97.50	Mixed	488
13	Ethambutol hydrochloride	Mild steel	0.5 M H <sub>2</sub> SO <sub>4</sub>	1000 ppm	92.78	Mixed/LAI	489
14	Vilazodone	Aluminium	1 M HCl	150 ppm	95.00	Mixed/LAI	490
15	Omeprazole	Al-Mg-Si alloy	0.5 M H <sub>2</sub> SO <sub>4</sub>	1.5 g L <sup>-1</sup>	90.50	Mixed/LAI	491
16	Clonazepam	Mild steel	3.5% NaCl	500 ppm	91.40	Mixed/LAI	492
17	Linagliptin	Mild steel	1 M HCl	7.5 × 10 <sup>-3</sup> M	96.30	Mixed/LAI	493
18	Chlorpheniramine	Mild steel	2 M HCl	800 mg L <sup>-1</sup>	95.10	Mixed/LAI	494
19	Furosemide	Carbon steel	1 M HCl	300 ppm	90.50	Mixed/LAI	495
20	Tizanidine	E24 carbon steel	10% HCl	7 × 10 <sup>-3</sup> M	97.10	Mixed/LAI	496
21	Pipotiazine	Mild steel	1 M HCl	1000 ppm	73.59	Mixed/LAI	497
22	Famciclovir	Carbon steel	1 M HCl	1 mM	96.87	Mixed/LAI	498
23	Ebastine	Carbon steel	1 M HCl	17.03 × 10 <sup>-5</sup> M	95.81	Mixed/LAI	499
24	Fucoidan	304 stainless steel	3.5% NaCl	200 ppm	81.70	Mixed/LAI	500
25	Favipiravir	Aluminium alloy	1 M HCl	100 ppm	96.45	Mixed/LAI	501

lower density than water. In terms of their anticorrosive properties, essential oils stand out due to their natural abundance, non-toxicity, zero/minimal environmental impact, affordability, excellent biodegradability and outstanding adsorption capabilities.<sup>512</sup> Most essential oils contain a rich assortment of chemical constituents, including monoterpene phenols, ketones, alcohols, hydrocarbons, and esters, many of which contribute to their anticorrosive abilities.<sup>513</sup> These extracts are often derived from various parts of plants, with leaves being a common source.<sup>514,515</sup> However, essential oils can also be obtained from seeds/nuts, flowers and fruits.<sup>516</sup> The primary method employed in extracting essential oils, as frequently reported in the literature, is hydrodistillation, although other techniques, such as hydro-extractive steam distillation are also used.<sup>517</sup> The choice of extraction method typically depends on the nature of the plant materials and the physicochemical characteristics of the essential oil being extracted.<sup>516</sup> To identify the chemical constituents of essential oils, researchers often employ analytical tools such as FTIR, gas chromatography with flame ionization detection (GC-FID), GC and GC-MS.<sup>518</sup>

In assessing the protective performances of essential oils, gravimetric and electrochemical methods such as WL, OCP, LPR, PDP and EIS are commonly utilized.<sup>519</sup> Using these techniques, the corrosion behaviour of a metallic specimen in the presence and absence of the essential oils is evaluated. For instance, using PDP and EIS methods, the inhibition performance of essential oils derived from the needles of black pine (*Pinus nigra*) was found to be 97% and 96%, respectively, at a concentration of 200 ppm.<sup>520</sup> Furthermore, modern analytical instruments such as FTIR, UV-vis, SEM-EDX, AFM, XPS, XRD, contact angle tests, and Raman spectroscopy are increasingly employed to investigate the structural and morphological changes on metal surfaces in the presence and absence of essential oils.<sup>517,521</sup> For instance, the morphological assessment of the anticorrosion performance of essential oils derived from *Elettaria cardamomum* (ECPE).<sup>522</sup> The study revealed that the addition of 250 ppm ECPE reduced the average surface roughness and the contact angle of MS from 316.73 (blank) to 297.8 nm (ECPE) and 124.9° (blank) to 74.0° (ECPE), respectively, indicating their efficacy.

As a complement to experimental assessments, quantum chemistry approaches such as DFT and DFTB are now being explored to gain insights into the anticorrosive mechanism of essential oils by elucidating the electronic properties of their primary constituents. Beniaich *et al.*<sup>523</sup> utilized the DFT method to study the adsorption of *Artemisia herba-alba* essential oils on metal surfaces, providing spatial distributions in the aqueous phase (Fig. 20). Molecular simulations are also employed to investigate the interactions between the essential oil components and metal surfaces, yielding critical parameters such as binding energy, stable adsorption configuration and diffusion behaviour.<sup>524–526</sup> Moreover, recent studies have introduced response surface modelling (RSM) using a quadratic model to optimize the interactive effects of concentration, exposure time and temperature on the maximum inhi-

tion performance of essential oils. For instance, Ansari *et al.*<sup>527</sup> employed RSM and achieved a peak %IE of 88.10% for *Ocimum basilicum* essential oil on C38 steel in sulfuric acid under the optimal conditions. Similarly, Loto *et al.* employed statistical analysis, demonstrating the outstanding protection performances of essential oils from ginger, grapefruit and tea trees against steel corrosion in sulfuric acid. This study reported peak %IE of 99.56%, 98.32% and 98.17% for ginger, grapefruit and tea tree essential oils, respectively.<sup>528</sup>

Several studies have also explored the effect of combining various essential oils on the corrosion characteristics of metals.<sup>521,529,530</sup> These synergistic actions have demonstrated enhanced resistance against the infiltration of corrosion ions into metal surfaces. The mechanism by which essential oils inhibit corrosion entails an electrocatalytic effect, active site blocking effect and geometric blocking effect. Most essential oils combine these actions, engaging with the metal surface through physical and chemical adsorption. The abundance of  $\pi$ -electrons in double and triple bonds and the presence of heteroatoms in essential oil molecules play a vital role in their anticorrosive properties. Furthermore, the efficacy of essential oils has been investigated across various metal types and corrosive environments. Studies have shown the effectiveness of essential oil to inhibit copper corrosion in 0.5 M HCl,<sup>518,531</sup> aluminium alloy corrosion in 3.5% NaCl,<sup>532</sup> and Cu-Zn alloy corrosion in 3% NaCl.<sup>533</sup> In addition, other biobased compounds such as protein extracts, biodiesels and glycerol have been documented as effective, efficient and environmentally benign inhibitors of metallic corrosion.<sup>534–542</sup>

However, despite the recorded success in utilizing biobased chemicals as green corrosion inhibitors, there is still the need for the further exploration of the potential of synergistic/hybrid systems in controlling corrosion control for different types of metal/medium systems. In addition, integrating modern machine learning tools for modelling inhibition behaviour and predicting the performance of these biobased chemicals is crucial to reducing costs, saving time, and minimising extensive experimental trials. In industrial applications of pharmaceutical drugs such as green corrosion inhibitors, addressing the high procurement costs is essential, and comprehensive investigations into their toxicity assessment and environmental concerns are imperative. Emerging studies revealed that the chemical functionalization of existent drugs offers a promising prospect for achieving effective and sustainable control of metallic degradation on a large scale.<sup>543</sup>

## 2.7. Green corrosion inhibition using efficiency enhancement (synergism, self-healing, etc.)

Synergism has attracted significant interest in corrosion inhibitors due to its potential to enhance the effectiveness of many organic compounds that typically exhibit low to moderate inhibition capabilities. This has led to corrosion experts exploring synergistic opportunities across diverse corrosive environments. This section delves into the concept of “efficiency enhancement” as a fresh approach to elevating the performance of environmentally friendly corrosion inhibitors.

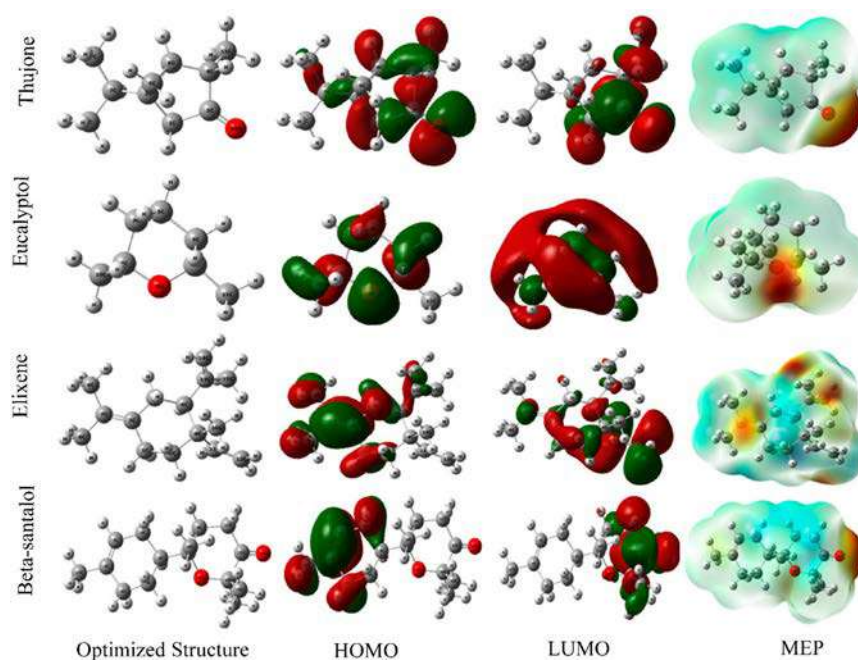


**Fig. 20** Spatial distributions of *Artemisia herba-alba* compounds in an aqueous medium<sup>523</sup> [reproduced from ref. 523, open access publication, copyright permission not required].

The research aims to enhance the corrosion inhibition efficiency of various green inhibitors, including plant extracts and biodegradable polymers, by employing innovative techniques such as nanostructuring, surface modification, and synergistic combinations. The discoveries from these studies offer promising insights into sustainable corrosion prevention methods, significantly contributing to developing eco-conscious solutions for industries grappling with corrosion-related challenges.

The concept of “green corrosion inhibition” addresses the dual objectives of safeguarding assets from corrosion, while minimizing the adverse environmental repercussions of corrosion prevention methods. This paradigm shift has led to innovative strategies that leverage the forces of nature, biodegradable materials, and sustainable chemistry to combat corrosion effectively. However, in this pursuit, a crucial question arises: How can the effectiveness of green corrosion inhibitors be heightened without compromising their environmentally friendly attributes? This section explores this pivotal question by delving into the novel “efficiency enhancement” concept within the context of green corrosion inhibition. It seeks to bridge the gap between sustainable corrosion prevention and optimal performance, offering a pathway towards corrosion mitigation solutions that are both efficacious and environmentally conscious. To accomplish this goal, studies should focus on various green corrosion inhibitors, such as plant extracts, biodegradable polymers, and amino acids, while investigating innovative techniques such as nanostructuring, surface modification, and synergistic combinations to elevate their corrosion inhibition efficiency.

Furthermore, the synergistic combinations of multiple inhibitors can enhance their effectiveness. These combinations of corrosion inhibitors collaborate to offer multiple layers of protection and target different aspects of the corrosion process. This can lead to improved inhibition effectiveness compared to a single inhibitor. Combinations such as organic corrosion inhibitors with their inorganic counterparts or mixtures of various organic inhibitors can be employed to enhance the synergistic effect of corrosion inhibitors. In the subsequent sections, we delve into the methodology, findings, and implications of the approaches used to improve the corrosion inhibition capabilities of these inhibitors. This will shed light on the promising advancements in green corrosion inhibition.

**2.7.1. Efficiency enhancement by nanostructuring.** Efficiency enhancement by nanostructuring is a technique used to improve the performance of materials or systems by manipulating their structure at the nanoscale, potentially reducing the amount of inhibitor needed, while increasing its effectiveness. Nanostructuring involves altering the arrangement, size, or morphology of materials at dimensions ranging from 1 to 100 nanometers. This manipulation at such a small scale can significantly improve the various properties of materials, including their efficiency in specific applications such as corrosion inhibition. In corrosion inhibition, efficiency enhancement by nanostructuring typically involves the principles shown in Fig. 21.

Basheer *et al.*<sup>54</sup> developed a novel  $\text{TiO}_2 \cdot \text{B}_2\text{O}_3$  [TBID] nanocomposite as a corrosion inhibitor. They assessed its impact on carbon steel at concentrations in the range of 100 to

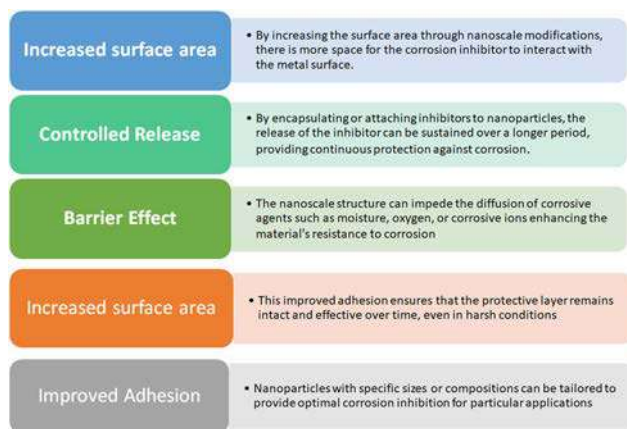


Fig. 21 Effect of nanostructure on the efficiency enhancement [self-illustration, copyright permission not required].

500 ppm in a 1 M HCl solution at 35 °C. The highest observed inhibition efficiency (IE%) was 99.91% at a 100 ppm concentration of the  $\text{TiO}_2 \cdot \text{B}_2\text{O}_3$ -[TBID] inhibitor in an acidic medium. In a separate investigation,<sup>544</sup> researchers examined the efficacy of an olive leaf extract-mediated chitosan (CHT)-CuO nanocomposite as a corrosion inhibitor for X60 carbon steel exposed to a 5% HCl solution. The corrosion inhibition performance displayed the following trend: CHT1.0-CuO nanocomposite (90.35%) exhibited a superior performance compared to CHT0.5-CuO (90.16%) and CHT2.0-CuO (89.52%). These nanocomposites substantially reduced the corrosion rate of X60 steel when immersed in a 5% HCl solution, which was particularly evident at a temperature of 25 °C, as illustrated in Fig. 22. However, as the temperature increased from 40 °C to 60 °C, the corrosion rates escalated in both the presence and absence of nanocomposites, peaking at 60 °C.

In their study, Al-Mhyawi and colleagues<sup>545</sup> synthesized silver nanoparticles using tobacco leaf extract at 3, 5, and 10 mM concentrations to investigate their corrosion inhibition properties on carbon steel exposed to 1.0 N HCl. They employed various chemical, electrochemical, and analytical techniques to assess the impact of concentration (ranging from 50 to 200 ppm) and temperature (ranging from 303 to 333 K) on the ability of the material to inhibit corrosion. Their findings indicated that as the temperature increased, the inhibitory effectiveness decreased, while higher concentrations resulted in increased inhibition. The most significant inhibition effectiveness, achieving a remarkable 98%, was obtained when utilizing 200 ppm of the nanomaterials. This outcome was attributed to the formation of a safeguarding barrier film, which acts as a shield, guarding the metal against corrosive elements. Also, the adsorption and bonding of the nanomaterial inhibitor to the metal surface contributed to this result.

In their study,<sup>546</sup> Aslam and colleagues explored the inhibitory characteristics of a graphene/ $\text{Fe}_3\text{O}_4$  nanocomposite functionalized with glycine called Gr/Fe@Gly NC. The objective was to assess its ability to reduce corrosion in mild steel when exposed to acidic environments. Gr/Fe@Gly NC exhibited remarkable effectiveness and stability, maintaining its inhibitory properties even at temperatures as high as 60 °C. The most effective concentration of 50 ppm resulted in an impressive inhibition efficiency of 98.28%. An analysis of the adsorption isotherm revealed that the inhibitor closely conformed to the Langmuir isotherm, indicating a strong preference for chemical adsorption. Furthermore, Aslam and colleagues<sup>547</sup> introduced a novel nanocomposite called  $\text{ZrO}_2$ -glycine, also called  $\text{ZrO}_2$ -Gly NC. To evaluate its potential for inhibiting corrosion, they conducted WL and electrochemical tests using different concentrations of  $\text{ZrO}_2$ -Gly NC on mild steel immersed in a 1 M HCl solution in the temperature range of

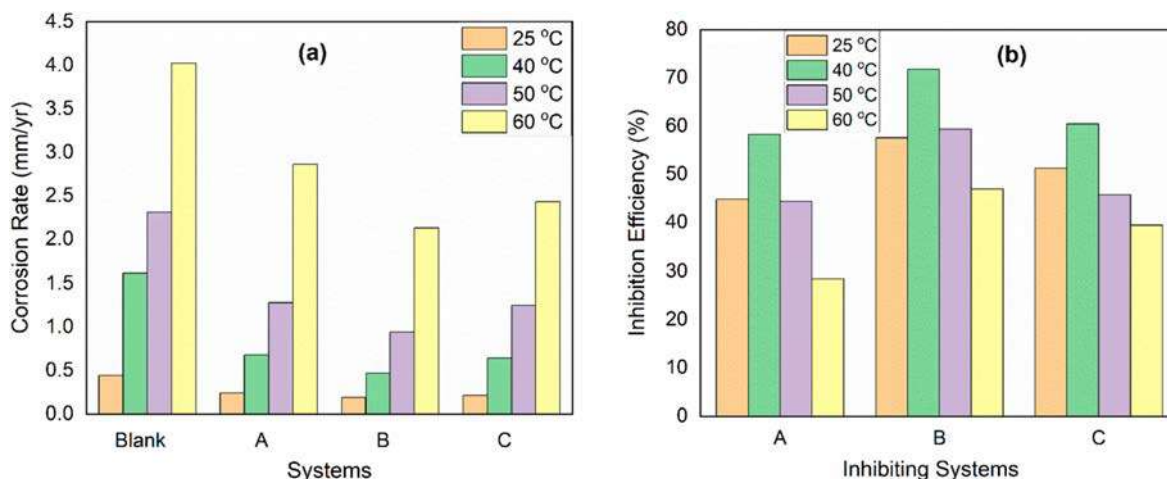


Fig. 22 Plots of (a) corrosion rate and (b) inhibition efficiency for X60 steel in 5% HCl without and with (A) 0.5% of CHT0.5-CuO, (B) CHT1.0-CuO, and (C) CHT2.0-CuO nanocomposites at different temperatures [reproduced from ref. 544, open access publication, copyright permission not required].

40–80 °C. With an increase in the concentration and temperature, the percentage inhibition efficiency of ZrO<sub>2</sub>-Gly NC demonstrated an upward trend, reaching its peak of approximately 81.01% at 500 ppm and 70 °C, with a slight decrease observed at 80 °C, where it exhibited a 73.5% inhibition efficiency. Based on polarization measurements, it was determined that ZrO<sub>2</sub>-Gly NC predominantly acted as a mixed-type inhibitor, with a primary focus on suppressing the cathodic process.

### 2.7.2. Efficiency enhancement by synergistic combinations

#### 2.7.2.1. Combinations of organic and inorganic inhibitors.

Incorporating organic and inorganic inhibitors is applicable across various industries such as oil and gas, automotive, aerospace, and infrastructure. This combination of organic and inorganic inhibitors presents a promising and well-established strategy. As industries continually adapt to increasingly challenging corrosion environments, the collaboration between these two types of inhibitors offers a versatile and adaptable solution to effectively combat the relentless forces of corrosion, ultimately contributing to economic sustainability and safety. The introduction of inorganic salts and rare earth metals in organic compounds has demonstrated a synergistic effect, leading to improved inhibition efficiency.<sup>81,548–550</sup> When salts are added to organic inhibitors, the primary objective is to enhance their adsorption capacity, while minimizing the concentration of the inhibitor in the aqueous phase. Researchers have also explored the influence of various metal ions on the inhibitory effect of organic compounds.<sup>79</sup>

A study<sup>551</sup> focused on exploring the synergistic inhibitory effect of Ce<sup>4+</sup> and melamine on the corrosion of aluminum alloy 2024 (AA2024) in a 3.5% NaCl solution. The combination of melamine and Ce<sup>4+</sup> exhibited a significantly higher inhibition efficiency than the sum of their individual inhibitory effects. The highest inhibition efficiency, measured at 90.4% ± 1.8%, was achieved when a mixture containing 5 ppm Ce<sup>4+</sup> and 5 ppm melamine was employed. The cooperative inhibitory effect of Ce<sup>4+</sup> combined with 3,4-dihydroxybenzaldehyde on cold-rolled steel exposed both in sulfuric acid and hydrochloric acid solutions was investigated by Li *et al.*<sup>552</sup> It should be noted that although this idea relied on the capacity of Ce<sup>4+</sup> to form complexes using its open orbitals (4f, 5d, and 6s), no chemical study was done to verify the chemical composition of the complex. El-Lateef<sup>553</sup> investigated the effects of a combination of Ce<sup>4+</sup> and polyethylene glycols (PEG) on reducing corrosion in carbon steel exposed to diluted sulfuric acid solution. The author hypothesized that a complex between Ce<sup>4+</sup> and PEG may be responsible for the increased corrosion resistance. However, it is crucial to stress that no additional research was done to support this theory.

Mohammed *et al.*<sup>554</sup> conducted a study to assess the inhibitory impact of a non-ionic surfactant, specifically nonylphenoxy poly(ethyleneoxy) ethanol (NPPE), on the corrosion of carbon steel in oilfield formation water. Interestingly, they found that adding halide ions (KCl, KBr, and KI) to the inhibitor enhanced the inhibition efficiency of NPPE. In a separate investigation, Hu *et al.*<sup>555</sup> examined the corrosion inhibition

performance of a magnesium alloy (GW103) containing Mg-10Gd-3Y in corrosive water, according to the ASTM D1384-87 standards. They studied the combined effects of organic sodium aminopropyltriethoxysilicate (APTS-Na) and inorganic zinc nitrate on corrosion using electrochemical techniques and immersion tests. It was observed that a combination of 0.5 mM APTS-Na<sup>+</sup> and 0.1 mM Zn(NO<sub>3</sub>)<sub>2</sub> exhibited a high inhibition efficiency of 92%, significantly surpassing its individual components, which showed a weaker inhibition performance (65% for 0.5 mM APTS-Na<sup>+</sup> and 60% for 0.1 mM Zn(NO<sub>3</sub>)<sub>2</sub>). This enhanced inhibition efficiency was attributed to the deposition of protective films comprised of Mg(OH)<sub>2</sub> and Zn(Mg) silicates, resulting in a compact and protective layer on GW103.

Li *et al.*<sup>556</sup> disclosed the impact of chloride ions on the inhibitory effectiveness of cetyltrimethylammonium bromide (CTAB) in solutions of 1.0–4.0 M H<sub>3</sub>PO<sub>4</sub> for carbon steel (cold-rolled steel). Their findings indicated that the chloride ions acted synergistically to enhance the %IE of CTAB in various acid concentrations. In a different investigation,<sup>557</sup> researchers explored the impact of halide salts, specifically NaCl, NaBr, and NaI, on the corrosion inhibition properties of a cationic Gemini surfactant known as 1,3-butan-bis-(dimethyl dodecyl ammonium bromide), referred to as 12-4-12, when applied to low carbon steel immersed in a 1 M HCl solution at a temperature of 20 ± 1 °C. The introduction of halide salts in the surfactant solution led to synergistic effects, enhancing the inhibition efficiency of the surfactant. For instance, at a concentration of 10<sup>-6</sup> M, the surfactant alone exhibited an %IE of 62%. However, in the presence of 10<sup>-6</sup> M surfactant and 0.1 M of NaI, NaBr, and NaCl, the %IE increased to 90%, 77.3%, and 84.4%, respectively. Additionally, adjusting the solution pH from 0 to 3 reduced the corrosion rate.

Mobin *et al.*<sup>549</sup> investigated the influence of 0.01 M sodium iodide (NaI) and sodium salicylate (NaSal) on the corrosion inhibition properties of *m*-E2-*m*-type surfactants in an acidic environment for mild steel corrosion using WL measurements. The addition of NaSal exhibited a synergistic effect on the inhibition efficiency of the *m*-E2-*m* surfactants, as evidenced by the synergism parameter of greater than 1. This higher effect of NaSal can be attributed to its more significant reduction in the critical micelle concentration (CMC) compared to Γ<sup>-</sup>. Additionally, the interaction between organic anions (Sal<sup>-</sup>) and the positively charged surfactant, Gemini surfactant (GS) through cation-π interactions, as depicted in Fig. 23, likely contributed to the further decrease in the CMC. Consequently, aromatic counter ions such as Sal<sup>-</sup> have a more remarkable ability to penetrate the head group region of the surfactants, promoting micellar growth at lower concentrations, unlike the less penetrating inorganic counter ions (Γ<sup>-</sup>).

In a separate investigation, Aslam and coworkers<sup>558</sup> examined the impact of sodium tosylate (NaTos) on the corrosion inhibitory impact of 1,2-bis(*N*-hexadecyl-*N,N*-dimethylammonium) ethane dibromide, denoted as 16-2-16. The experimental results showcased an increase in the %IE of the 16-2-16 surfactant from 77% to 90.8% in the presence of

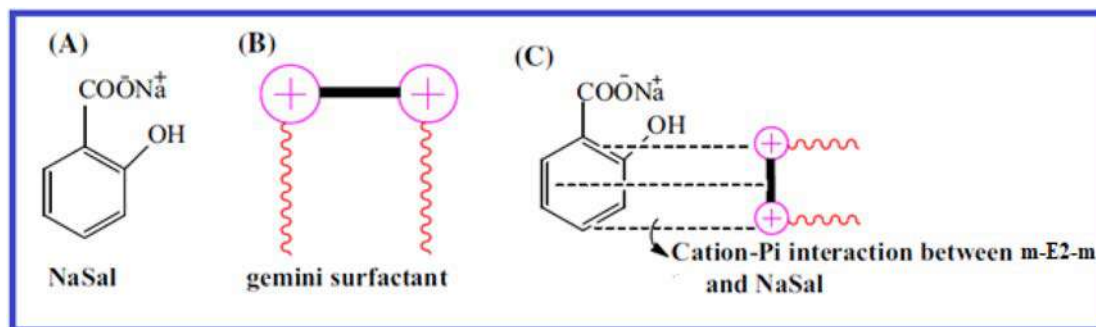


Fig. 23 Structure of NaSal (a), gemini surfactant (b) and various interactions existing between the *m*-E2-*m* and the NaSal mixture (c) [reproduced from ref. 549, copyright permission not required].

50 ppm of sodium tosylate (NaTos). The addition of the salt effectively elevated the ionic strength, which consequently reduced the electrostatic repulsion between the ionic heads of the surfactant and promoted its more significant adsorption on the steel surface. In a study by Khamis *et al.*,<sup>559</sup> they investigated the corrosion inhibition of mild steel in a 0.5 M H<sub>2</sub>SO<sub>4</sub> solution using cetyltrimethylammonium bromide (CTAB) in combination with various salts (NaCl, NaBr, and NaI). Their findings revealed a synergistic effect in the adsorption and inhibition action against acid corrosion of mild steel when CTAB was combined with different halides.

**2.7.2.2. Mixtures of organic inhibitors.** Studies have examined the impact of various organic additives, such as alcohols and surfactants, on the corrosion inhibition efficacy of environmentally friendly organic inhibitors such as polymers, amino acids, and plant extracts. The objective was to enhance the %IE of inhibitors, such as amino acids and polymers, through synergistic interactions, while preserving their environmentally friendly attributes. Asefi *et al.*<sup>560</sup> combined a cationic Gemini surfactant, 1,3-butan-bis(dodecyl dimethyl ammonium bromide) (12-4-12), with non-ionic co-surfactants (C<sub>7</sub>H<sub>16</sub>O, C<sub>12</sub>H<sub>26</sub>O, and C<sub>5</sub>H<sub>12</sub>O) to inhibit corrosion on low carbon steel in an acidic environment. The results indicated that the corrosion rates decreased with an increase in surfactant concentration. Moreover, when the chain length difference between the surfactant and co-surfactant was lower, it resulted in better compatibility and improved inhibition efficiency behaviour of the surfactant and co-surfactant mixture. Among the mixtures studied, C<sub>12</sub>H<sub>26</sub>O + gemini surfactant exhibited the highest increase in %IE (84.5%) (which was 74.9% for C<sub>7</sub>H<sub>16</sub>O + gemini surfactant and 77.5% for C<sub>5</sub>H<sub>12</sub>O + gemini surfactant).

In a separate investigation conducted by Mobin *et al.*,<sup>561</sup> they examined the anti-corrosive properties of Gemini surfactants, namely 1,2-ethane bis(dimethyl alkyl ammonium bromide) referred to as C<sub>*m*</sub>H<sub>2*m*+1</sub>, *m*-2-*m*, where *m* = 10 and 12, number of carbon in the hydrophobic chain. However, their focus in this study was on enhancing the %IE of these compounds using butanol. The %IE of the compounds varied with the inhibitor concentration and immersion time. The effectiveness of C<sub>4</sub>H<sub>9</sub>OH in increasing %IE values followed the order of

12-2-12 (95.4%) > 10-2-10 (90.8%). Mobin *et al.*<sup>562</sup> investigated the corrosion inhibition performance of L-cysteine (CYS) in 1 M HCl solution for mild steel. They studied the impact of adding small concentrations of three surfactants, *i.e.*, Triton X-100 (TX), SDS, and CPC (cetylpyridinium chloride). Among them, Cys + TX (97.76%) exhibited the highest inhibition performance compared to Cys + SDS (95.09%) > Cys + CPC (91.99%) > Cys (85.62%).

In the study by Zehra *et al.*,<sup>563</sup> they examined the corrosion inhibition properties of the glycine derivative *N*-benzylidene-2-((2-oxo-2-(10*H*-phenothiazine-10*yl*)ethyl)amino)acetohydrazide (BPAA) in 1 M HCl solution for mild steel. This study also considered the addition of surfactant additives such as SDS and CPC. It was found that the corrosion inhibition efficiency of the inhibitor was synergistically enhanced in the presence of the surfactant additives, SDS and CPC at lower concentrations. In another study conducted by Mobin *et al.*,<sup>564</sup> they investigated the impact of SDS and CTAB on the corrosion inhibition behavior of L-methionine (LMT) for mild steel in a 0.1 M H<sub>2</sub>SO<sub>4</sub> solution. When LMT was combined with surfactants, the corrosion rates of MS were further reduced compared to LMT alone. This observation suggested a synergistic effect between LMT and surfactants, with the mixture of LMT + CTAB exhibiting a higher inhibitory effect on steel corrosion than the combination of LMT + SDS.

In the study by Parveen and colleagues,<sup>565</sup> they examined the impact of SDS and CPC on the corrosion inhibition capabilities of L-tyrosine (Tyr) for mild steel corrosion in a 1 M HCl environment at temperatures ranging from 30 °C to 60 °C. The findings indicated a substantial enhancement in the inhibition efficiency percentage of Tyr when SDS or CPC was introduced at different concentrations. Regardless of whether used independently or in conjunction with SDS or CPC, Tyr demonstrated mixed-type inhibition characteristics. Mobin and Parveen observed the effect of SDS and CTAB on L-cystine (LCY),<sup>566</sup> L-histidine (LHS),<sup>567</sup> and L-tryptophan<sup>568</sup> for mild steel in a 0.1 M H<sub>2</sub>SO<sub>4</sub>. The findings revealed that the corrosion performance of L-histidine was significantly improved in the presence of surfactants. Mobin and Khan<sup>569</sup> researched the corrosion inhibition properties of polyvinyl alcohol (PVA) in a 0.1 M H<sub>2</sub>SO<sub>4</sub> environment for mild steel. This study

further explored the impact of SDS and CPC surfactants. It was observed that the inhibitory effect of PVA was significantly enhanced when a very small quantity of surfactants was added. The calculated synergism parameter exceeded one, indicating that the increased inhibition efficiency of PVA resulting from the surfactant addition was due to synergism.

In another report, Mobin *et al.*<sup>570</sup> investigated the corrosion inhibition of mild steel in a sulfuric acid solution in the presence of starch. Starch exhibited moderate inhibition of mild steel corrosion in the tested medium, although this inhibition decreased as the temperature increased from 30 °C to 60 °C. Notably, the %IE of starch was significantly enhanced when both SDS and CTAB were added, and this enhancement was found to be synergistic. In a separate study, Mobin and Khan<sup>571</sup> reported the adsorption and corrosion inhibition effects of gum acacia (GA), both alone and in the presence of SDBS and CTAB surfactants, for MS in a 0.1 M H<sub>2</sub>SO<sub>4</sub> environment. The inhibitory action of GA was synergistically improved with the addition of a small amount of surfactants. Furthermore, the Freundlich adsorption model was applicable in describing the corrosion inhibition mechanism for GA alone and in combination with SDBS and CTAB on the surfaces of the mild steel at all the studied temperatures.

Mobin and Rizvi<sup>572</sup> researched the inhibitory effect of xanthan gum (XG) in conjunction with synergistic surfactant additives, namely SDS, CPC, and TX, for mitigating mild steel corrosion in a 1 M HCl solution. The inhibitory action of XG was significantly enhanced with the addition of small amounts of surfactants, following the order of XG + SDS (83.17%) > XG + Triton X (82.31%) > XG + CPC (75.89%) > XG alone (74.24%). In a related study, Mobin and Rizvi<sup>573</sup> further investigated the inhibitory effect of hydroxyethyl cellulose (HEC) in the presence of CPC and SDS for controlling A1020 carbon steel corrosion in a 1 M HCl solution employing various techniques. They observed that combining HEC and surfactants increased the inhibition efficiency more than either HEC or surfactants, indicating a synergistic effect between HEC and surfactants.

Aslam *et al.*<sup>574</sup> conducted a study on the synergistic effect between Rhodamine blue (RhB) dye and a GS, namely 1,2-ethanediy-bis(dimethyldecylammonium bromide), referred to as 10-2-10, for mitigating mild steel corrosion in a 1 M HCl medium. Although individual RhB and 10-2-10 GS exhibited a low inhibition efficiency, the inhibitory efficacy of RhB significantly increased when combined with a low concentration of 10-2-10 GS. In another investigation, Aslam *et al.*<sup>575</sup> further explored the anti-corrosion performance of a polymer, the sodium salt of carboxymethyl cellulose (NaCMC), in combination with surfactants, specifically green cationic di-ester-bonded gemini surfactants known as ethane-1,2-diylbis(*N,N*-dimethyl-*N*-alkylammoniumacetoxyl)dichloride, denoted as *m*-E2-*m*, where *m* = 12, 14, 16, for MS corrosion in a 1 M HCl solution. According to the experimental results, the inhibition efficiency and surface coverage values followed the order of NaCMC < NaCMC/12-E2-12 < NaCMC/14-E2-14 < NaCMC/16-E2-16. The maximum %IE (90.1%) was achieved with NaCMC/16-E2-16 at 30 °C, while the minimum (57.3%) was

observed for NaCMC alone at the same temperature. The inhibitory characteristics of CPC in the presence of a copolymer of vinyl pyrrolidone and vinyl acetate were investigated for the corrosion of carbon steel in cyclohexane propionic acid (CHPA) using polarization, conductivity, and EIS measurements.<sup>576</sup> This study also examined the influence of KCl on the %IE of the CPC/polymer system. The results revealed that CPC exhibited mixed-type inhibition behaviour, particularly when the copolymer was added (at pH > 4 or in the presence of Cl<sup>-</sup> ions).

Parveen *et al.*<sup>577</sup> reported on the inhibitory effect of *L*-proline (LPr) and a combination of LPr with sodium benzoate (LPr + NaBenz) for mitigating mild steel corrosion in a 1 M HCl solution at temperatures of 30 °C, 40 °C, 50 °C, and 60 °C. The analysis of the polarization parameters indicated that both LPr and LPr + NaBenz acted as mixed-type inhibitors, with a more pronounced influence on the cathodic reaction. In another investigation, they<sup>565</sup> presented findings regarding the inhibitory impact of *L*-tyrosine (Tyr) in combination with sodium dodecyl sulphate (Tyr + SDS) or cetylpyridinium chloride (Tyr + CPC) on the corrosion of mild steel in 1 M HCl in the temperature range of 30 °C to 60 °C. The results showed that Tyr, whether on its own or in combination with SDS or CPC, acted as a mixed-type inhibitor and adhered to the surface of mild steel following the Langmuir adsorption isotherm. Elsewhere, Mobin *et al.*<sup>578</sup> explored the influence of adding minute amounts of SDS, CPC, and Triton X-100 on the corrosion inhibition performance of *L*-cysteine (CYS) for mild steel in aerated and unstirred 1 M HCl solution in the temperature range of 30–60 °C. Their findings indicated a substantial increase in the inhibition efficiency of CYS in the presence of all three surfactants.

**2.7.3. Surface modification by grafting or polymerization.** To enhance the water solubility of natural starch, Deng *et al.*<sup>579</sup> synthesized a cassava starch-acrylamide graft copolymer (CS-AAGC) through the grafting of cassava starch with acrylamide, utilizing (NH<sub>4</sub>)<sub>2</sub>S<sub>2</sub>O<sub>8</sub> and NaHSO<sub>3</sub> as initiators. Their research, employing WL and electrochemical analysis, uncovered that CS-AAGC functioned as a hybrid inhibitor for aluminum in 1 M H<sub>3</sub>PO<sub>4</sub>. This copolymer significantly inhibited the anodic reaction, achieving a maximum %IE of 90.6%. Hou *et al.*<sup>580</sup> embarked on starch modification by grafting it with acrylic acid (AA). They explored its corrosion inhibition performance on Q235 carbon steel exposed to an HCl environment, assessing the effects through WL and electrochemical methods. Their findings indicated that a concentration of 200 ppm of this terpolymer exhibited an inhibition efficiency of up to 90.1% at 30 °C. Li *et al.*<sup>581</sup> initiated the grafting of acrylamide (AA) on cassava starch (CS) and examined its corrosion inhibition effect on aluminum in 1 M HNO<sub>3</sub>. Through WL measurements and electrochemical analysis, they observed that the acrylamide-grafted starch demonstrated superior anti-corrosion performance compared to the unmodified starch. Although the maximum inhibition efficiency remained below 30% for CS and reached 50% for AA, the grafted derivatives exhibited an efficiency exceeding 90%. The inhibition process followed the Langmuir isotherm, with CSGC acting as a mixed-type inhibitor, primarily retarding anodic corrosion. The study

conducted by Wang and colleagues<sup>582</sup> demonstrated that acrylamide (AM)-grafted starch can effectively act as an inhibitor to protect zinc in a 1 M HCl environment, exhibiting a remarkable inhibition efficiency of up to 92.2%. Li *et al.*<sup>583</sup> also conducted research involving grafting sodium allyl sulfonate and acrylamide to tapioca starch in a separate investigation. Their findings revealed that this terpolymer displayed exceptional anti-corrosion properties when applied to cold-rolled steel. Specifically, it achieved remarkable inhibition efficiencies of 97.2% in 1 M HCl and 90% in 1 M H<sub>2</sub>SO<sub>4</sub>. The SEM and AFM images provided (Fig. 24) visual evidence of the effective inhibition of the cold-rolled steel surface by CS-SAS-AAGC, forming a hydrophobic film in the inhibited system.

## 2.8. Green corrosion inhibition using computational modelings (reduction in trials)

The advancement in the implementation of computational chemistry as a burgeoning field has substantially emerged as a new era in the design and development of next-generation 'green' and sustainable corrosion inhibitors.<sup>584–586</sup>

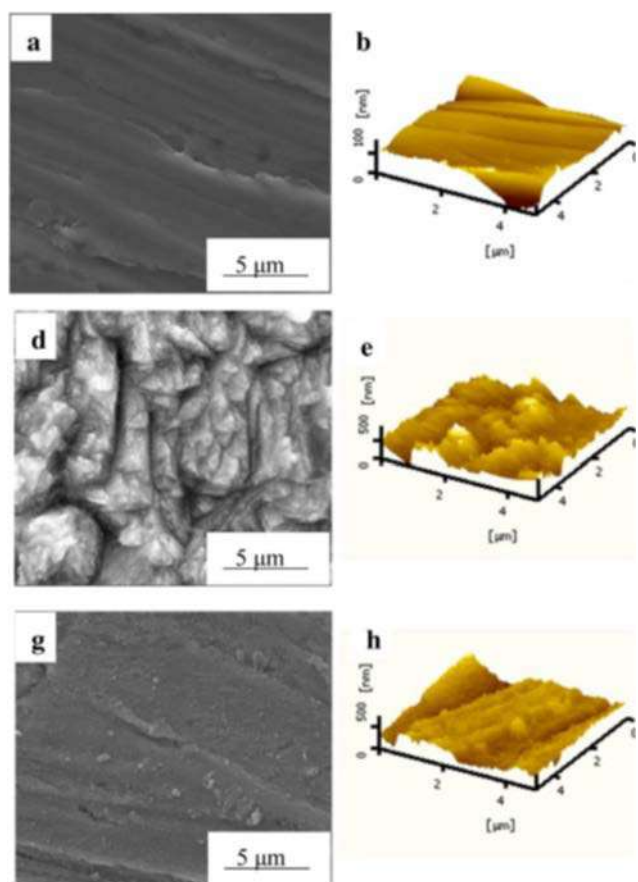


**Fig. 24** SEM (a, d, and g), AFM (b, e, and h), and contact angle images (c, f, and i) of CRS surfaces: (a–c) before immersion; (d–f) after 6 h of immersion at 20 °C in 1.0 M HCl solution; (g–i) after 6 h of immersion at 20 °C in 50 mg L<sup>-1</sup> CS-SAS-AAGC + 1.0 M HCl solution [reproduced from ref. 583, open access publication, copyright permission is not required].

Considering time, finances, and ecological constraints, as well as sometimes the inability to perform experimental approaches at every juncture to produce significant mechanistic insight into the interaction of metal surfaces and inhibitors, computational techniques are becoming more prevalent and straightforward approaches for researchers in the contemporary domain. Furthermore, computational modeling can be implemented as a substantial prediction tool for the 'cherry picking' of corrosion inhibitor scaffolds. For example, DFT can be used as an essential module to screen inhibitor molecules before their wet laboratory synthesis.<sup>584–586</sup> Another positive aspect of computational modeling is its ability to anticipate the most suitable spatial orientation of organic compounds in the context of the inhibitory approach and in determining the tentative active sites responsible for interactions with metallic surfaces. Computational modeling techniques, specifically DFT-based quantum chemical calculations, molecular dynamics (MD), and Monte Carlo (MC) simulations, have recently been introduced as revolutionary and greener approaches to studying the adsorption behavior of aqueous phase corrosion inhibitors.<sup>585,587</sup>

**2.8.1. DFT as a green computational technique.** The utilization of DFT is highly significant given that it provides information regarding the electronic descriptors, *e.g.*, electron density distribution in the frontier molecular orbitals (FMO), the energy of the highest occupied molecular orbital ( $E_{\text{HOMO}}$ ) and lowest unoccupied molecular orbital ( $E_{\text{LUMO}}$ ), their energy gap ( $\Delta E$ ), ionization potential ( $I$ ), electronegativity value ( $A$ ), electronegativity ( $\chi$ ), global softness ( $\sigma$ ), hardness ( $\eta$ ), and dipole moment, within shorter time-span. The fraction of electrons transferred between molecules and metal ( $\Delta N$ ) can also be obtained from DFT. Generally, the equations used to calculate the electronic parameters are presented in Fig. 25.

These parameters further help to comprehend the electron-donating and accepting (D–A) ability of green corrosion inhibitors to the metal surface. The adsorption property of molecules is highly reliant on their D–A capability. When inhibitors are added to the electrolytic solution, they are first adsorbed on the metal surface. Better surface coverage will result in greater inhibitory effectiveness. Accordingly, DFT analysis helps in screening the inhibitory function of molecules.  $E_{\text{HOMO}}$  represents the ability of a molecule to donate electrons, whereas  $E_{\text{LUMO}}$  signifies its ability to accept back-donated electrons. A higher  $E_{\text{HOMO}}$  value often denotes the propensity of an inhibitor molecule to transfer electrons to an empty metal d-orbital. Additionally, a lower  $E_{\text{LUMO}}$  value suggests a more effortless flow of electrons from the metallic matrix to the inhibitors. A lower value of  $\Delta E$  reflects the higher tendency of electron donation and acceptance by inhibitors. Shao *et al.* reported the use of an amide derivative, namely *N*-[2-(3-indolyl)ethyl]-cinnamamide (IA) as a green corrosion inhibitor for Q235 steel in 0.5 M HCl medium.<sup>588</sup> The DFT study showed that IA has greater  $E_{\text{HOMO}}$  and lower  $\Delta E$  value than tryptamine (TA), the precursor of IA. The geometry-optimized structures, HOMO, and LUMO, are presented in Fig. 26. To further comprehend the electrostatic potential (ESP) distribution of inhibitor mole-



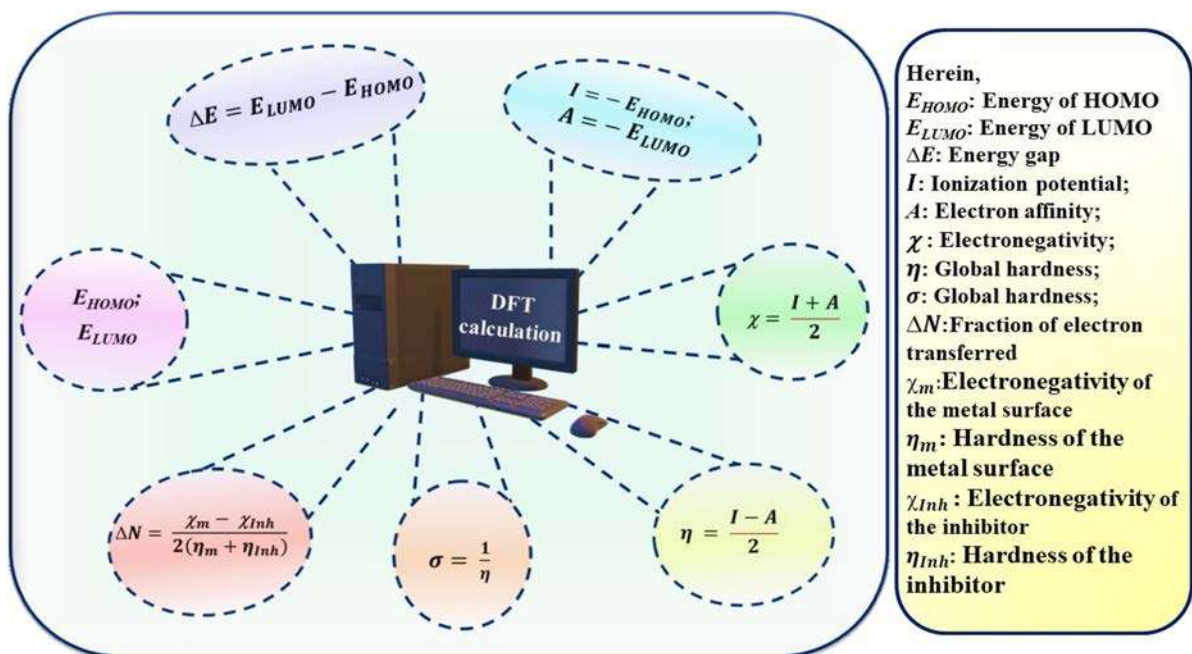


Fig. 25 General equations used in DFT to calculate the electronic parameters [self-illustration, copyright permission is not required].

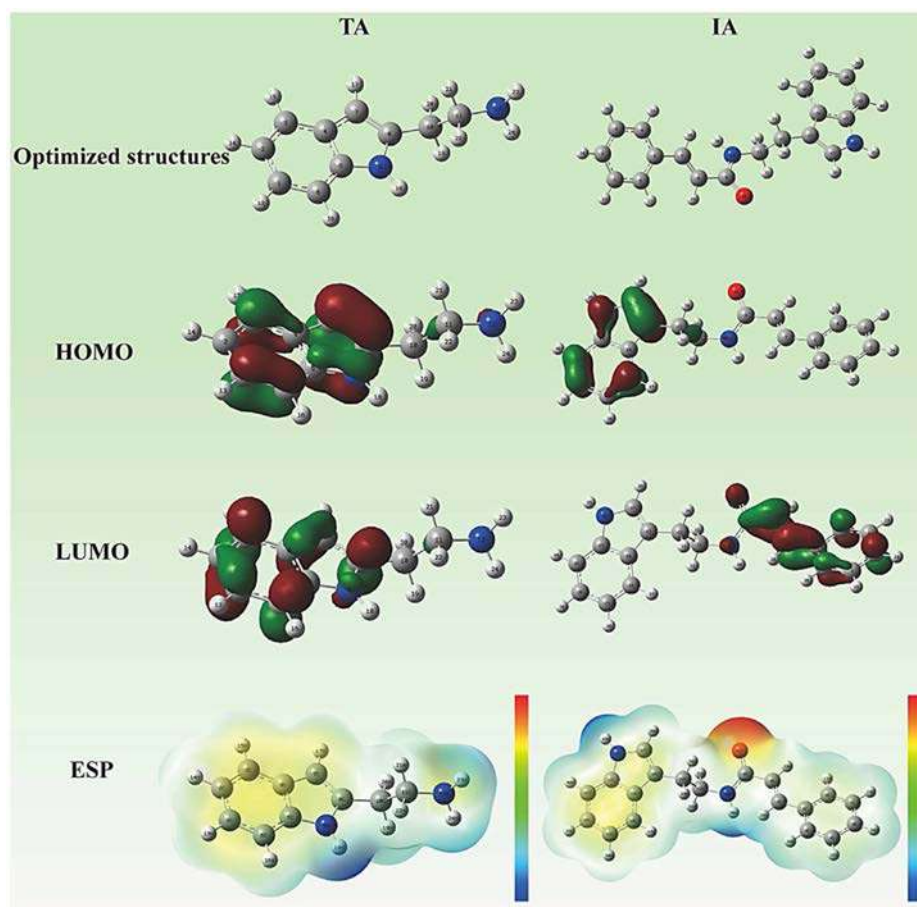


Fig. 26 Geometry-optimized structures, density distributions in HOMO–LUMO, and electrostatic potential (ESP) distributions of TA and IA<sup>588</sup> [reproduced from ref. 588, open access publication, copyright permission not required].

cules, the ESP distributions of TA and IA were further investigated (Fig. 26). The arrows in the picture shown in green and blue denote the positive and negative electrostatic potential, respectively. It was observed that the electron-rich sites are situated mainly on the heteroatoms such as N and O.

A recent study reported the use of garlic peel as a green corrosion inhibitor for protecting AISI 1020 mild steel.<sup>589</sup> The electrochemical analysis was conducted in 0.5 M HCl, 0.5 M NaOH and 0.5 M NaCl to understand the corrosion suppression ability of the green inhibitor at different pH. WL tests, electrochemical investigations (EIS and PDP) and morphological analysis (SEM) were performed to investigate the corrosion inhibition ability of the two main components of garlic peel extract, alliin (ALL) and allicin (ALC) molecules, and computational analysis was performed to validate the experimental findings. Since there is only one amine group, it gets protonated and becomes positively charged (ALL<sup>+</sup>) at acidic pH levels. Alternatively at neutral pH, one protonated amine group and one deprotonated carboxyl group result in zero total charge (ALL<sup>+/-</sup>). A negatively charged deprotonated carboxyl group is present in ALL at basic pH, leading to the formation of ALL<sup>-</sup>. The electronic parameters derived from the theoretical study assisted in explaining the correlation between the molecules and their inhibitory effects with respect to the pH level. The inhibitor response at different pH levels was presented with quantum chemical calculations, which showed that the number of active and adsorbable species increases at basic pH.

Similarly, the corrosion inhibition effectiveness of bispyrazolopyrazoles, namely, 4,4'-(1,4-phenylene)bis(6-amino-3-methyl-2,4-dihydropyran[2,3-*c*]pyrazole-5-carbonitrile) (BP-1) and 4,4'-(1,4-phenylene)bis(6-amino-3-methyl-1-phenyl-1,4-dihydropyran[2,3-*c*]pyrazole-5-carbonitrile) (BP-2) was perceived *via* both experiments and DFT approach.<sup>590</sup> All the quantum chemical parameters were calculated for the neutral and protonated BP-1 and BP-2. The higher energy value of HOMO, lower energy gap, higher fraction of electrons transferred, and higher global softness value for BP-2 than that of BP-1 strongly imply that BP-2 binds to the Fe metal *via* strong bonds given that BP-2 exhibits higher inhibition effectiveness (98.01%) than BP-1 (96.02%). Also, 93.13% corrosion inhibition efficiency was achieved from petals of *B. glabra* for mild steel in 0.5 M H<sub>2</sub>SO<sub>4</sub>.<sup>591</sup> The potentiodynamic study, EIS, and gravimetric techniques were utilised to evaluate the surface protective nature of petals of *B. glabra* with varying concentrations (93.13% corrosion inhibition efficiency at 250 ppm) and varying temperatures (up to 40 °C). Metallurgical microscopy and SEM analysis were employed for the surface assessment. Furthermore, a DFT study was performed to support the experimental data. Gallic acid, quercetin, ascorbic acid, betalain, and peltogynoid molecules were found to be present in the *B. glabra* petal extract, as confirmed by the spectroscopic analyses such as UV-vis, FTIR, and nuclear magnetic resonance (NMR) studies. The DFT calculation was carried out for the three main components. To investigate the electron distribution in the HOMO and LUMO, chemical potential, elec-

tron affinity, electron density distribution per atom, van der Waals surfaces, DFT and adsorption locator investigations were carried out.

Several DFT-based local descriptors can be obtained through Fukui indices ( $f_k$ ). Frontier electron theory has a strong foundation on the  $f_k$ . The following reactive sites for nucleophilic, electrophilic, and radical attacks can be obtained using Mulliken population analysis. The first derivative of electron density,  $\rho(\vec{r})$ , with respect to the number of electrons,  $N$ , at a fixed external potential,  $v(\vec{r})$ , is commonly used to formulate  $f_k$ , according to eqn (2).

$$f_k = \left( \frac{\partial \rho(\vec{r})}{\partial N} \right)_{v(\vec{r})} \quad (2)$$

where  $f_k^+$  represents the Fukui function for nucleophilic attack and  $f_k^-$  for electrophilic assault, as mentioned in eqn (3) and (4).<sup>584,592</sup> Alternatively, the availability for the radical attack is governed by  $f_k^0$ , as shown by eqn (5).<sup>585</sup>

$$f_k^+ = q_k(N+1) - q_k(N) \quad (3)$$

$$f_k^- = q_k(N) - q_k(N-1) \quad (4)$$

$$f_k^0 = \frac{q_k(N+1) - q_k(N-1)}{2} \quad (5)$$

where  $q_k$  denotes the gross charge of the K<sup>th</sup> atom in the cationic ( $N+1$ ), neutral ( $N$ ), or anionic ( $N-1$ ) form of the molecule. High  $f_k^+$  values imply that the site is best suited for nucleophilic attack. In contrast, high  $f_k^-$  values suggest that the site is particularly accessible to electrophilic attack. Fukui analysis was performed to determine the reactive sites in the neutral and protonated forms of luteolin, citral, rosmarinic acid, chlorogenic acid, germacrene, and caryophyllene, which are the main ingredients of *Lemon Balm* extract, as reported by Asadi *et al.*<sup>593</sup> It was found that the double bonds in neutral caryophyllene were susceptible to the electrophilic attack because of its high values for the  $f_k^-$  function on the carbon atoms (C4 and C5). The double-bond C atoms were the target of the nucleophilic attack, which had  $f_k^+$  values of 0.113 and 0.178 on the C1 and C13 atoms and 0.054 and 0.050 on the C4 and C5 sites, respectively. The electrophilic and nucleophilic nature of protonated caryophyllene are primarily comparable to that in neutral caryophyllene, with the difference that the nucleophilic attack only occurs in the protonated area. In another work, the analysis of the Fukui indices revealed the presence of reactive sites in *Glycyrrhiza glabra* leaf extract, which are responsible for the adsorption of its organic components, such as liquiritigenin (LTG), licochalcone E (LCE), glycyrrhizin (GL), glabridin (GLD), 18 $\beta$ -glycyrrhetic acid (GA), and licochalcone A (LCA), on the active sites of mild steel. It can be observed in Fig. 27 that in protonated licochalcones A and licochalcones E, the aromatic ring, methoxy and carbonyl oxygen, and C-C double bond exhibited electrophilic behavior, which is in agreement with the corresponding DFT results, further demonstrating their propensity for electron donation to the unoccupied d orbitals of the surface atoms of iron.<sup>594</sup>

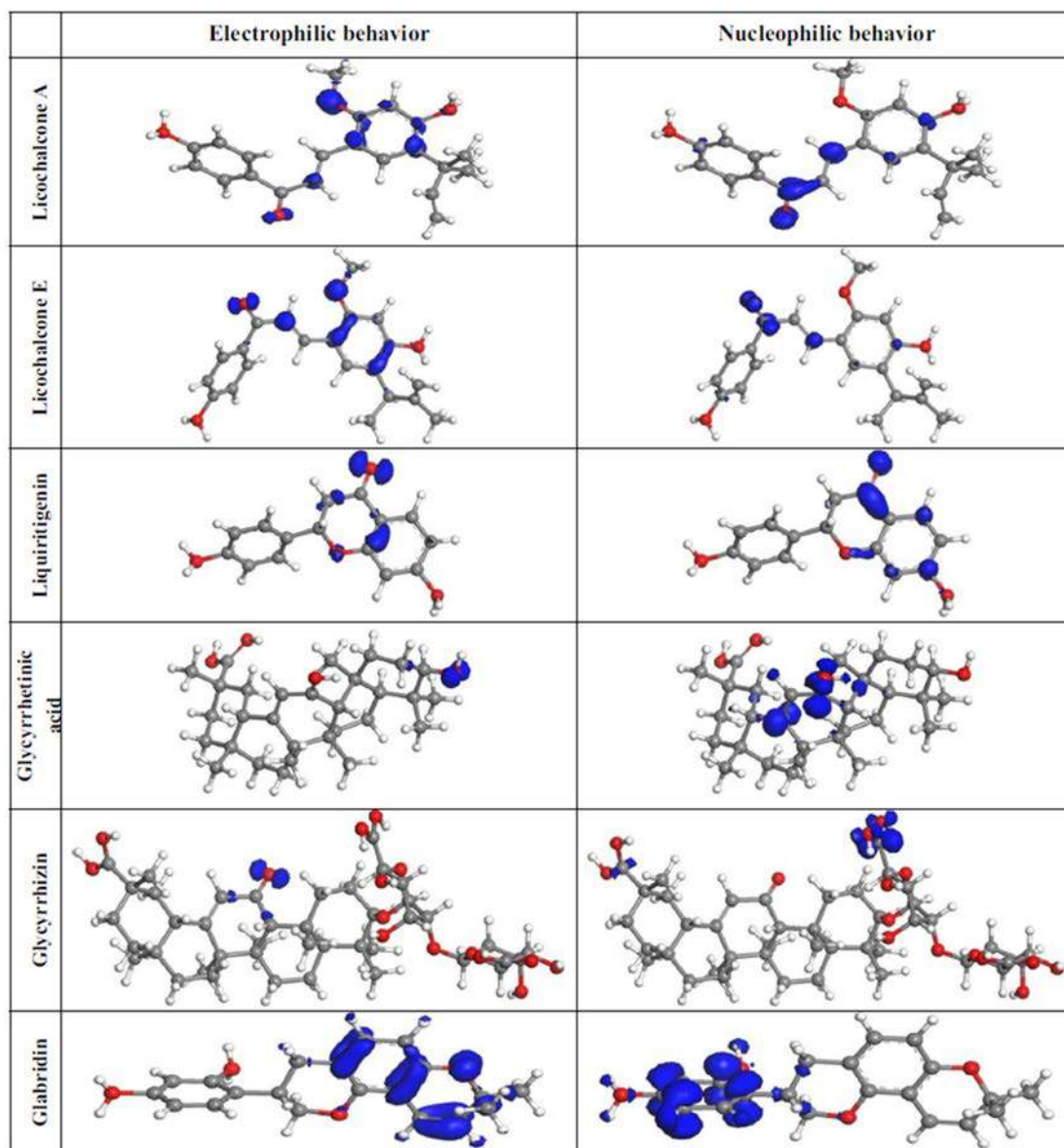


Fig. 27 Fukui index calculation for protonated licochalcone A, licochalcone E, liquiritigenin, 18 $\beta$ -glycyrrhetic acid, glycyrrhizin, and glabridin present in *Glycyrrhiza glabra* leaf extract<sup>594</sup> [reproduced from ref. 594 with permission, Copyright, Elsevier, 2018].

**2.8.2. Molecular-level simulation techniques.** In the current scenario, molecular-level simulation techniques such as molecular dynamics (MD) simulation and MC simulation are gaining high-level traction in the scientific community because of their meaningful molecular-level insight through a comparatively less time-consuming, less laborious, cost-effective and greener approach. The MD simulation study provides details on the interaction energy ( $E_{\text{int}}$ ), binding energy ( $E_{\text{bind}}$ ), and molecular orientation on the metal surface, as calculated as follows (eqn (6) and (7)):<sup>595–597</sup>

$$E_{\text{int}} = E_{\text{T}} - (E_{\text{m+sol}} + E_{\text{Inh}}) \quad (6)$$

$$E_{\text{bind}} = -E_{\text{int}} \quad (7)$$

where  $E_{\text{T}}$  is the total energy of the simulation system;  $E_{\text{m+sol}}$  and  $E_{\text{Inh}}$  denote the energy of the metal together with the corrosive solution and the energy of the inhibitor molecule, respectively. The more negative the value of  $E_{\text{bind}}$ , the more significant the interaction of the inhibitor molecule with the investigated surface. This indicates the better surface protection ability of the inhibitor in terms of higher adsorption and better interaction. In the literature, several studies are based on computational modelling as an efficient technique for successfully understanding the corrosion inhibition mechanism. A glimpse into the usefulness of MD and MC simulation approaches in the province of green corrosion inhibition is presented here.

The inhibitory effect of pectin-amino acid derivatives, namely pectin-glycine (P-Gly) and pectin-lysine (P-Lys), on N80

carbon steel in the presence of CO<sub>2</sub>-saturated groundwater was explored.<sup>598</sup> P-AAs exhibited good corrosion inhibition efficiencies at a low concentration of 800 mg L<sup>-1</sup>, where P-Gly (99.01%) and P-Lys (99.36%) showed sustained outstanding adsorption stability for 120 h, as observed from electrochemical and gravimetric experiments. DFT and MD simulation studies were performed for theoretical corroboration. The Fe (110) surface was selected as a representative of N80 carbon steel on which the studied molecules could be adsorbed in a corrosive medium (herein, water). These molecules got adsorbed on the metal plane in a planar fashion, as visualized in Fig. 28. The  $E_{\text{ads}}$  followed the order of P-Lys ( $-799.957 \text{ kJ mol}^{-1}$ ) > P-Gly ( $-635.425 \text{ kJ mol}^{-1}$ ) > pectin ( $-536.251 \text{ kJ mol}^{-1}$ ), which indicates the better adsorption of P-Lys compared to P-Gly and pectin. P-Lys can get adsorbed more significantly due to its higher negative binding energy. Accordingly, this outcome is consistent with the aforementioned experimental findings.

In a recent work, two environmentally friendly corrosion inhibitors with heteroatoms of phosphorous (PEG-6 isotridecyl phosphate) and nitrogen (PEG-2 oleamide) were used to reduce the tribo-corrosion assault on 1018 carbon steel in

water-based emulsion drilling fluids (WBEs).<sup>599</sup> Using a pin-on-disk tribometer connected to an electrochemical workstation, the effects of the corrosion inhibitors on the tribo-corrosion behavior of steel samples submerged in the manufactured WBEs with and without inhibitors at varied sliding speeds were assessed. Employing a 3D optical profilometer, potentiostatic and potentiodynamic measurement, it was possible to analyze the effect of corrosion inhibitors on improving the anti-tribo-corrosion properties of steel and to calculate the volume losses brought on by wear, corrosion, and wear-corrosion synergy. SEM-EDS and XPS studies were performed to investigate the shape and chemical makeup of the wear tracks, respectively. First-principles calculations and MD simulations were conducted to better comprehend the underlying mechanism for the performance disparity between the PEG-6 isotridecyl phosphate and PEG-2 oleamide corrosion inhibitors. In the MD simulation study, the COMPASS-II forcefield was applied under the NVT ensemble, maintaining a temperature of 300 K for 100 ps. The driving force on the N-containing molecular fragment is primarily responsible for grabbing the PEG-2 oleamide molecule to the iron surface. In contrast, the PEG-6 isotridecyl phosphate molecule gets attracted to the iron

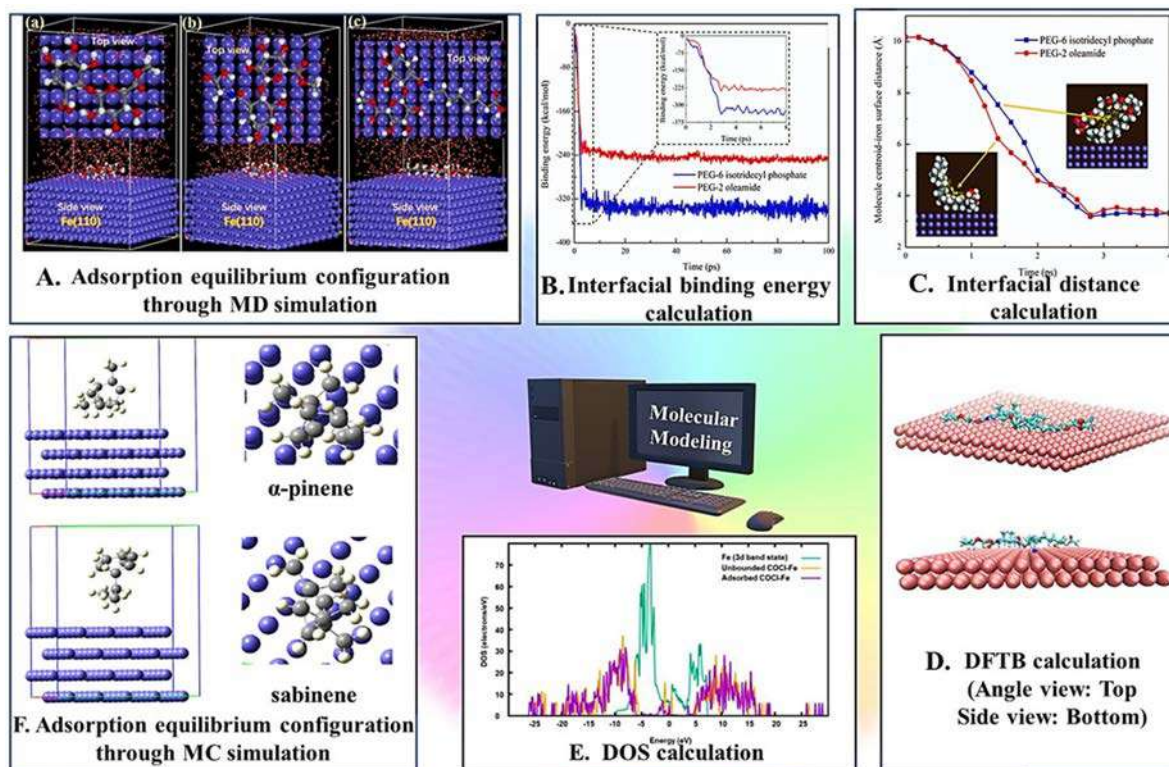


**Fig. 28** A. Equilibrium adsorption configurations of (a) pectin, (b) P-Gly, and (b) P-Lys on the Fe (110) surface<sup>598</sup> [reprinted with permission, Copyright, Elsevier, 2022]; B. change in interfacial binding energies during a simulated physisorption process<sup>599</sup> [reprinted with permission, Copyright, Elsevier, 2023]; C. relative distances of two corrosion inhibitors from the iron surface during simulated physisorption process<sup>599</sup> [reprinted with permission, Copyright, Elsevier, 2023]; D. DFTB calculation for the interaction between COCl and Fe (110) surface<sup>600</sup> [reprinted with permission, Copyright, Elsevier, 2020]; E. change in density of states (DOS)<sup>600</sup> [reprinted with permission, Copyright, Elsevier, 2020]; and F. adsorption equilibrium configuration of on the Fe (110) surface obtained from MC simulation<sup>78</sup> [reprinted with permission, Copyright, Elsevier, 2021].

surface. This is mainly attributed to the driving force on the C–H chain tail and is consistent with the electrostatic potential distribution of each molecule.

Fig. 28(B) depicts the changes in interfacial binding energies throughout the physisorption process for the two species. It is clear from this figure that the PEG-6 isotridecyl phosphate molecule binds to the iron surface much more strongly than the PEG-2 oleamide molecule through physisorption. The relative distances of the two corrosion inhibitors from the iron surface during the physisorption process are shown in Fig. 28 (C). It can be observed from the comparison that the speeds of the two molecules approaching the iron surface are relatively similar. However, the interfacial distance of PEG-6 isotridecyl phosphate is much greater because of its larger size. The density-functional tight-binding (DFTB) method is another important theoretical approach for better understanding the anticorrosive process and to get a qualitative description of these adsorption systems. Self-consistent charge density-functional tight-binding (SCC-DFTB) based on the DFT-derived second-order expansion of the total energy estimated around a reference density was used to predict the interaction of castor oil-based corrosion inhibitor (COCI) and Fe (110) surface (Fig. 28(D)).<sup>600</sup>

Furthermore, the projected density of states (PDOS), another important tool in computational modeling, was utilized to vividly illustrate the COCI–Fe (110) interaction before and after their adsorption. According to Fig. 28(D), COCI has several distinct bands close to the Fermi energy state of the iron surface (between –7 and 2 eV) before it interacts with the Fe surface, and their peak notably decreases after the interaction. This data implies that an electron transition from the inhibitor to the Fe 3d band state occurs in the COCI–Fe (110) surface interaction. Adsorption typically refers to an exothermic process in which energy gets released in the form of heat. Employing the computational approach, the scale and corrosion inhibition aptitudes of green polyaspartic acid (PASP), polyepoxysuccinic acid (PESA), oxidized starch (OS) and carboxymethyl cellulose (CMC) were examined. With and without water, the relationship between the inhibitor and the surfaces of CaCO<sub>3</sub> (110), CaCO<sub>3</sub> (104), CaSO<sub>4</sub> (020), and Fe (110) was explored using DFT, MD and radial distribution function (RDF) analysis.<sup>601</sup> The RDF, also known as the pair correlation function, is the possibility that another particle will be scattered in space once the location of the center atom has been established. RDF analysis was adopted to ascertain the interaction between the oxygen atoms of the carboxyl group of the inhibitors with the metal and metal oxide crystal surfaces. In general,  $r = 3.5 \text{ \AA}$  indicates chemical bond formation between the adsorbate and the adsorbent, *i.e.*, chemisorption occurs.

Similarly, a non-bonded interaction is facilitated throughout the  $3.5 \text{ \AA} < r < 5.0 \text{ \AA}$  range. Accordingly, physisorption occurs.<sup>602,603</sup> Herein, Fig. 29 depicts the RDF plot of the inhibitors and calcite. The bond length between the Ca and O atoms is 2.39, with a noticeable peak at about 2.36. This demonstrates that the inhibitor may be associated with the CaCO<sub>3</sub> surface through chemisorption given that at this point, the

oxygen atom of the inhibitor and Ca-atom form an ionic bond. The peak value in the presence of water is lower than the highest value in the absence of water. This observation illustrates that the interaction between the inhibitor and the calcite surface is weakened with an increase in the number of water molecules. The peak values of the four inhibitors follow the order of PESA > PASP > OS > CMC (Fig. 29), which corresponds to the earlier binding energy results obtained from MD.

The energy and other parameters may be estimated due to the interaction and adsorption of the concerned inhibitor species at the atomic and molecular levels using MC simulation, which is a vital corrosion inhibition monitoring tool. The crucial variables such as  $E_T$ ,  $E_{\text{int}}$ , deformation energy ( $E_{\text{def}}$ ), adsorption energy ( $E_{\text{ads}}$ ), rigid adsorption energy ( $E_{\text{rigid}}$ ) and metal–inhibitor configuration energy ( $dE_{\text{ads}}/dN_i$ ) of the system can potentially be determined with the assistance of MC simulation.  $E_T$  and  $E_{\text{ads}}$  can be calculated as follows (eqn (8) and (9), respectively):<sup>584,602,604</sup>

$$E_T = E_{\text{inh}} + E_{\text{rigid}} + E_{\text{def}} \quad (8)$$

$$E_{\text{ads}} = E_{\text{rigid}} + E_{\text{def}} \quad (9)$$

MC simulation was carried out for nutmeg oil on the Fe (110) surface.<sup>78</sup> The obtained binding energies over the Fe surface follow the order of  $\beta$ -pinene < limonene <  $\alpha$ -pinene < sabinene, which suggests that sabinene and  $\alpha$ -pinene get adsorbed readily over the Fe surface. Using experimental and theoretical investigations, the ability of three naphthyridine derivatives (*viz.*, 5-amino-9-hydroxy-2-phenylchromeno[4,3,2-*de*][1,6]-naphthyridine-4-carbonitrile abbreviated as N-1, 5-amino-9-hydroxy-2-(*p*-tolyl) chromeno[4,3,2-*de*][1,6]-naphthyridine-4-carbonitrile abbreviated as N-2, and 5-amino-9-hydroxy-2-(4-methoxyphenyl)chromeno[4,3,2-*de*][1,6]-naphthyridine-4-carbonitrile abbreviated as N-3) to suppress mild steel corrosion in a 1 M HCl solution was thoroughly investigated. The MC simulation findings revealed that the naphthyridine derivatives adhere to Fe (110) surfaces in a nearly horizontal orientation. The binding energies for N-1, N-2, and N-3 were, 8.024 kcal mol<sup>–1</sup>, 8.376 kcal mol<sup>–1</sup>, 8.469 kcal mol<sup>–1</sup>, respectively, which are consistent with the experimentally determined trend of inhibitory efficiency, *i.e.*, N-1 < N-2 < N-3. Not only for iron surfaces, but there are also several significant applications of MD and MC simulations to comprehend the interaction of inhibitor molecules on other non-ferrous metal surfaces. An MC simulation study was successfully applied for understanding the interaction phenomena between the Cu (111) surface and the inhibitors (juzube shell extract) in the presence of H<sub>2</sub>O (55 no), H<sub>3</sub>O<sup>+</sup> (2 no) and Cl<sup>–</sup> (2 no) ions to mimic the 1 M HCl environment.<sup>43</sup> The computation of the adsorption energy provided by the MC simulation explained the spontaneity of the adsorption of ascorbic acid (AA) linoleic acid (LA), oleanolic acid (OA), and triterpenic acid (TA) present in juzube shell extract on the copper surface.

## 2.9. Green corrosion inhibition using waste materials (economy)

Green chemistry underscores the critical need to safeguard the environment and well-being of humans within a challenging

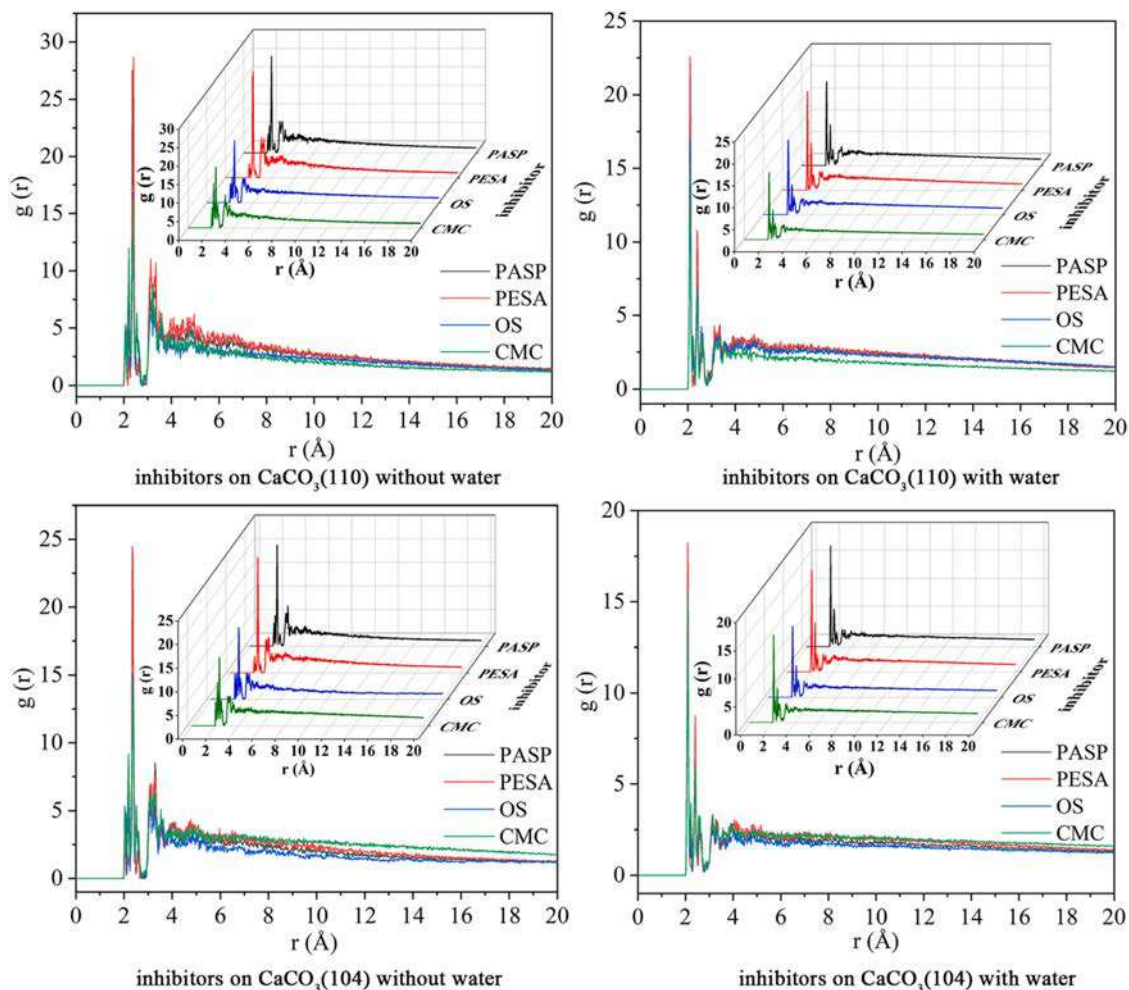


Fig. 29 Radial distribution function plot for the distance between the oxygen atom of inhibitors and the Ca-atom of calcite crystal surface<sup>601</sup> [reprinted with permission, Copyright, Elsevier, 2021].

economic landscape, which can be achieved by eliminating toxic elements and reducing waste *via* valorization. Green corrosion inhibition using waste materials is an innovative and environmentally conscious approach to tackle corrosion challenges in various industries. Traditional corrosion inhibitors often involve toxic or harmful chemicals, negatively impacting human health and the ecosystem. However, utilizing waste materials as corrosion inhibitors presents a sustainable alternative. Ongoing research delves into developing and applying these green corrosion inhibitors, simultaneously mitigating corrosion-related issues, while minimizing environmental harm, which appears increasingly promising, heralding a more sustainable future for corrosion protection. By repurposing waste substances such as agricultural byproducts, discarded plant matter, and industrial residues,<sup>544,545</sup> researchers aim to create effective corrosion inhibitors that efficiently protect metals and alloys and contribute to waste reduction and resource optimization. Research indicates that household-generated food waste comprised of fresh fruits and vegetables accounts for nearly half of this type of waste.<sup>546</sup>

According to the Food and Agriculture Organization (FAO), fruits and vegetables exhibit the highest rates of losses and waste compared to other food categories, with potential levels of wastage reaching up to 60%. The processes involved in fruit and vegetable production generate considerable by-products, constituting around 25% to 30% of the total volume within this commodity group.<sup>547</sup> This residual material primarily includes seeds, peels, juice, leaves, and stems, which contain a variety of bioactive compounds with potential value. These compounds inherently possess antioxidant and anti-corrosion attributes, effectively inhibiting corrosion and extending the lifespan of metal structures.<sup>548</sup> Furthermore, using waste as a corrosion inhibitor presents a series of merits, including formidable anti-corrosion efficacy, accessibility, renewability, cost-effectiveness, minimal environmental risks, and the ability to form protective layers on metal surfaces.<sup>79,551</sup> This approach serves not only to address corrosion control but also contributes to waste reduction and aligns with the principles of a circular economy. Also, this approach is consistent with the principles of green chemistry, promoting the transform-

ation of waste into valuable assets. By establishing a nexus between waste management and corrosion control, this section endeavours to showcase the feasibility of utilizing fruit, vegetable, industrial, and agricultural waste as efficient and environmentally friendly corrosion inhibitors.

**2.9.1. Agro-industrial waste.** Agro-residual compounds are attracting increasing attention as a sustainable and environmentally friendly substitute for synthetic inhibitors in safeguarding metals and alloys from corrosion across diverse industries. Adopting agricultural waste, such as rice husk, sugarcane bagasse, wheat straw, and various other abundant resources, has demonstrated efficacy in mitigating the corrosive deterioration of metal surfaces. These materials harbor a wealth of natural compounds such as lignin, cellulose, and hemicellulose, which are endowed with intrinsic inhibitory properties. The United Nations<sup>605</sup> defines agricultural waste as the byproduct of diverse agricultural activities. It includes manure and waste from farms, poultry establishments, and slaughterhouses; residual material from harvesting; fertilizer runoff from fields; pesticides infiltrating water, air, or soil; and salts and silts from fields. Agricultural waste constitutes the remains of plants used in agriculture. These residues primarily originate from cultivated land and horticulture. Agricultural waste includes the portion of crops not suitable for human or animal consumption. Crop residues are predominantly comprised of stalks, branches, and leaves.<sup>605</sup> It has been observed that approximately 80% of plant matter qualifies as agricultural waste.<sup>553</sup> Sugarcane, maize, cereals, and rice are among the most extensively cultivated crops worldwide.<sup>554</sup> The composition of agricultural waste can be summarized based on the origin of the residue, where rice crop waste includes husk and bran, while wheat-derived waste includes bran and straw. Maize waste is comprised of stover, husk, trimmings, and cobs. Sugarcane waste contains sugarcane tops, bagasse, and molasses.

In recent years, numerous endeavours have been undertaken to enhance the utilization of agro-waste biomass across diverse domains. However, estimating the precise quantity of agrowaste remains challenging, and due to its relatively low market value, this residue often yields economic returns that are outpaced by the costs associated with its collection, transportation, and processing for beneficial applications. Annually, a staggering amount of nearly one billion tons of this waste is generated,<sup>555–557</sup> with this volume steadily rising. A substantial 80% of the total solid waste found on agricultural lands is constituted by organic waste. Although agrowaste was once indiscriminately incinerated on fields, technological advancements have transformed this material into valuable resources for numerous applications.<sup>548,549,558</sup> Harnessing agricultural waste for corrosion inhibition boasts multiple merits, representing a sustainable and ecologically sound solution to address corrosion issues.

By repurposing agricultural waste, which is materials that would otherwise be discarded or left to decompose, we can alleviate the burden on landfills and reduce the environmental repercussions of waste disposal. Furthermore, the abundance

and cost-effective nature of agricultural waste make it an appealing choice for corrosion inhibition, particularly in regions or countries with constrained resources. Various agricultural waste types have been explored for their potential as corrosion inhibitors. For instance, residues such as straw, husks, and stalks, which are rich in polyphenolic compounds, lignin, cellulose, and other bioactive constituents, exhibit excellent corrosion inhibition potential. These compounds intrinsically possess antioxidative and metal-chelating attributes, enabling them to effectively curtail corrosion rates and hinder the formation of rust on metal surfaces.<sup>606</sup> Other forms of agricultural waste, including fruit peels, seed coats, and oil-cakes, also display corrosion inhibition potential due to their distinct chemical compositions. To assess the efficacy of agricultural waste as corrosion inhibitors, researchers have employed diverse experimental techniques, including electrochemical tests, surface analysis, and corrosion rate assessments.<sup>560</sup> The upcoming section will delve into the outcomes of a literature survey, aiming to enhance our comprehension of the corrosion performance provided by agricultural waste and its operational mechanisms.

Sanni and colleagues conducted a study<sup>607</sup> investigating the adsorption and corrosion inhibitory performance of palm kernel shell extract (PKSE) as an eco-friendly corrosion inhibitor on stainless steel (SS) within a simulated seawater environment. The findings of this study indicated that the corrosion inhibition efficiency of PKSE was notably effective, surpassing 90% inhibition efficiency. PKSE acts as a dual-mode inhibitor, demonstrating chemical and physical adsorption on the stainless-steel surface by the Langmuir adsorption model. Furthermore, a closer examination of the surface morphology by SEM revealed that PKSE forms a protective film on the stainless-steel surface, exhibiting firm attachment. Similarly, Oyewole and co-authors explored the efficacy of palm kernel leaf extract (PKLE)<sup>608</sup> using central composite design (CCD). This investigation involved conducting a phytochemical analysis of the extract. The process variables were optimized, including the extract concentration (ranging from 0.5 to 1.5 g L<sup>-1</sup>), duration (3 to 5 days), and temperature (30 °C to 50 °C). The optimal conditions were determined as inhibitor concentration (1.500 g L<sup>-1</sup>), temperature (30 °C), and time (3 days), leading to an inhibition efficiency of 96.74%. The PKLE extract derived from the agricultural waste of *Elaeis guineensis* was proven to be an effective inhibitor. Additionally, the lignin polymer obtained from this waste source was modified for use as a green corrosion inhibitor,<sup>300</sup> involving the incorporation of aromatic scavengers (2-naphthol: AHN EOL and 1,8-dihydroxyanthraquinone: AHD EOL).

Bhardwaj and co-researchers conducted an assessment<sup>609</sup> of the corrosion inhibition characteristics of *Phyllanthus emblica* seed extract (PESE), which was derived from discarded seeds, within a 15% HCl medium on stainless steel (SS-410). EIS unveiled a remarkable 92.43% corrosion inhibition efficiency when employing 4 g L<sup>-1</sup> of PESE. Further analysis through SEM, AFM and XRD confirmed the adsorption of PESE on the SS-410 surface. The adherence of PESE to the

Langmuir adsorption isotherm corroborated the formation of a PESE monolayer on the SS-410 surface. The theoretical investigation confirmed that 3,4,8,9,10-pentahydroxy-dibenzo[*b,d*]pyran-6-one played a pivotal role as the key phytochemical responsible for the anti-corrosive effect. Another instance involving seed extract pertains to the research conducted by Fernine and colleagues<sup>610</sup> on *Ocimum basilicum* seed extract (OBSE) as a green corrosion inhibitor for mild steel in a 1 M HCl solution. This study entailed varying the concentration of OBSE. The polarization results indicated the mixed adsorption behavior of the inhibitor on the mild steel surface in the corrosive environment of 1 M HCl. At an inhibitor concentration of 1.0 g L<sup>-1</sup> and a temperature of 298 K, OBSE demonstrated an inhibition efficiency of 95.12%. Surface morphology examination utilizing SEM facilitated the identification of a protective thin film on the external surface of mild steel, guarding it against HCl. Notably, the mild steel samples retained a smooth appearance after 6 h of immersion in a 1 M HCl solution with 1 g L<sup>-1</sup> of the extract, reducing the dissolution of iron. Theoretical calculations based on the chemical quantum and MC methodologies unequivocally demonstrated the adsorption of most molecules on the metal surface.

Shahmoradi *et al.*<sup>611</sup> explored the use of pistachio nut shell extracts containing eco-friendly compounds such as cellulose and lignin as organic inhibitors for steel corrosion in 1 M HCl solution. Using 800 ppm of the inhibitor, they achieved a 92% inhibition efficiency within 6 h through EIS testing. The inhibitor exhibited mixed-type action in polarization tests. Adsorption of the compounds followed the Langmuir isotherm, involving both chemical and physical processes.

Wu and colleagues<sup>612</sup> investigated the efficacy of walnut green husk extract (WGHE) as a corrosion inhibitor for magnesium alloys in a NaCl solution. Electrochemical assessments unveiled an optimal inhibition efficiency of merely 44.8% with 1.0 g L<sup>-1</sup> WGHE. Interestingly, elevating the WGHE concentration failed to enhance this efficiency further. However, immersing magnesium alloy samples in a 1.0 g L<sup>-1</sup> WGHE solution for 48 h remarkably elevated the inhibition efficiency to 92.5% under the same corrosive conditions. Notably, menadione, a component in WGHE, emerged as the key contributor to the enhanced corrosion resistance. El-Deeb *et al.*<sup>613</sup> extracted lignin from wheat straw agricultural waste through soda pulping, subsequently modifying and characterizing it using spectroscopic and thermal analysis. The investigation focused on two modified lignin compounds, LG-OH and LG-COOH, as corrosion inhibitors for aluminum in 1 M NaOH, comparing their performance to unmodified lignin (LG). PDP measurements and morphological analysis were employed. The findings revealed that the modified lignin compounds shifted the corrosion of aluminium and open circuit potentials toward more noble values. Moreover, they reduced the corrosion current density compared to the blank solution. Among the compounds, LG-COOH exhibited the highest inhibition efficiency, followed by LG-OH and LG. This difference can be attributed to the more significant number of active adsorption sites in LG-COOH. The Langmuir adsorption isotherm with a

physical nature provided the best fit, and the thermodynamic parameters indicated the endothermic nature of the corrosion process with more organized activated complexes in the presence of lignin compounds. Kaban *et al.*<sup>28</sup> investigated the anti-corrosion behaviour of liquid smoke derived from rice husk ash in a 1 M HCl solution in a separate study. The corrosion tests revealed that the inhibitor acted as a mixed-type inhibitor, achieving the optimal inhibition at 80 ppm and 323 K, displaying an impressive 99% inhibition efficiency. AFM analysis demonstrated a smoother surface with a lower skewness parameter of -0.5190 nm on the treated mild steel. Employing an ANN model showcased the reduced overfitting on inhibited steel, a higher prediction accuracy of 81.08%, and a lower loss rate of 0.6001. This neural network successfully modelled the correlation between EIS and PDP and the development of the passive layer on treated mild steel.

Asra *et al.*<sup>614</sup> explored the potential of nanosilicate extracts from rice husk ash (RHA) as a corrosion inhibitor for carbon steel in distilled water. The nanosilicates were extracted through wet chemical methods, resulting in a powder form with particle sizes in the range of 5 to 10 nm. This size range was verified using TEM and zeta size analysis. Remarkably, corrosion measurements exhibited a high %IE of up to 98% with the nanosilicate extract. The adsorption behavior of the inhibitor on the carbon steel surface was found to align with the Temkin isotherm. The potentiodynamic polarization outcomes of this study indicated that the inhibitors functioned as mixed type. The EIS results showcased increased charge transfer resistance and inhibition efficiency percentage with an increase in the nanosilicate concentration. Moreover, the surface analysis revealed that the specimens treated with nanosilicate exhibited smoother surfaces with fewer corrosion products than the untreated specimens. In a study conducted by Matos *et al.*<sup>615</sup> the potential of barley agro-industrial waste (AW) extract as a corrosion inhibitor for AISI 304 stainless steel in H<sub>2</sub>SO<sub>4</sub> was explored. The inhibitor demonstrated an impressive inhibition efficiency of 97%. However, the investigation needed to assess the stability and long-term durability of the inhibitor. Similarly, Raghavendra *et al.*<sup>616</sup> delved into the effectiveness of a yellow color ripe (YCR) husk extract when applied to aluminum surfaces and exposed to a 0.5 M HCl solution. The researchers evaluated the performance of the extract using EIS and WL measurements. A direct relationship was observed between the inhibitor concentration and corrosion inhibition efficiency.

Shahmoradi and coauthors<sup>617</sup> harnessed the extract from the green peel of walnut fruit as a corrosion inhibitor in a 1 M HCl solution. Their approach involved a straightforward, environmentally friendly water-based extraction method to isolate the chemical compounds from the walnut green husk. The presence of organic compounds and the inhibitory agent juglone in the green husk were validated through XPS, FT-IR, and DFT assessments. Their study strongly supported the formation of effective organic-inorganic complexes between the juglone molecules and metal cations, resulting in corrosion inhibition. This assertion was substantiated by the remarkable



95% inhibition efficiency observed in this study. Lin *et al.*<sup>618</sup> studied the inhibitory capabilities of pomelo peel extract in a 1 M  $\text{H}_3\text{PO}_4$  solution. The EIS test revealed a corrosion inhibition efficiency of 92.8% after 224 h. Additionally, surface analysis using field emission scanning electron microscopy (FE-SEM) indicated a smooth, corrosion-free metal surface in the presence of  $5.0 \text{ g L}^{-1}$  of pomelo peel extract. This observation suggests the successful adsorption of pomelo peel extract on the mild steel surface, contributing to effectively mitigating corrosion. In their research, Paul and co-researchers<sup>619</sup> utilized papaya seed extract to evaluate its corrosion-inhibiting potential on carbon steel. The adsorption analysis indicated that the inhibition mechanism aligns with the Temkin isotherm adsorption model, which is likely attributed to the physical adsorption of the benzyl isothiocyanate molecule present in papaya seed. Additionally, both EIS and polarization tests yielded significant results, showcasing a remarkable 90% inhibition efficiency upon exposure to a papaya extract concentration of 1500 ppm.

**2.9.2. Food waste as corrosion inhibitors.** Besides agricultural waste, an inventive approach to tackling corrosion involves harnessing waste food as an inhibitor source. Waste food, a substantial byproduct of the food industry, presents an opportunity for a cost-effective and sustainable solution across various corrosive settings. Examples such as fruit peels, tea leaves, and coffee grounds have demonstrated effective inhibition, showcasing the diverse potential of waste food as an inhibitor source.<sup>620–622</sup> Exploring waste food as an inhibitor holds promise, offering circular and environmentally conscious solutions to a prevalent challenge. Simultaneously, it opens avenues for revenue generation within the food industry. Furthermore, this approach can substantially reduce corrosion prevention expenses and mitigate environmental waste.<sup>59,60,623–625</sup> Fruits and vegetables are recognized sources of diverse bioactive elements such as polyphenols, carotenoids, and terpenes. Extracting these beneficial biomolecules from residual products holds potential. Various extraction methods are available to obtain waste food materials for use as corrosion inhibitors, including solvent extraction, ultrasound-assisted extraction, microwave-assisted extraction, and supercritical fluid extraction. Characterization techniques play a significant role in understanding the composition and attributes of waste food materials. FTIR, GC-MS, and high-performance liquid chromatography (HPLC) are commonly utilized for chemical analysis. Additional techniques such as SEM, AFM, XRD, and thermogravimetric analysis (TGA) aid in characterizing the morphology, crystal structure, and thermal stability of waste food materials.

Larissa Aparecida Corrêa Matos *et al.*<sup>626</sup> employed barley agro-industrial waste (AW) as an environmentally friendly source to minimize corrosion phenomena. Their approach involved utilizing AW extract to inhibit corrosion in a sulfuric acid environment on AISI 304 stainless steel. The extract showcased an impressive inhibition efficiency of up to 97%, which was attributed to the physical bonds formed between the adsorbed extract components and the steel surface. Fig. 30

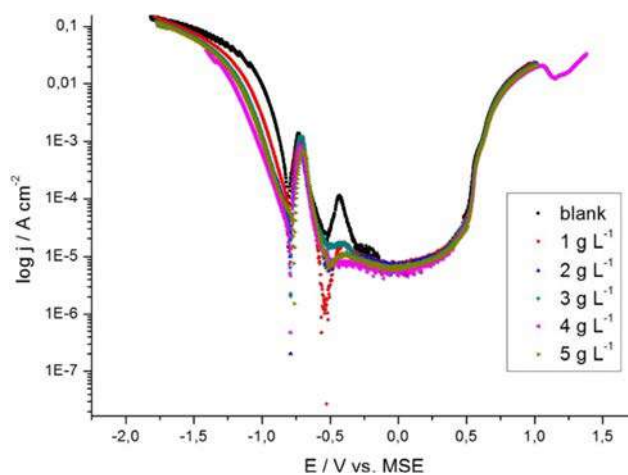


**Fig. 30** Tafel plots obtained for AISI 304 stainless steel in  $1.5 \text{ mol L}^{-1}$   $\text{H}_2\text{SO}_4$  with and without the AW acid extract at a  $1 \text{ mV s}^{-1}$  scanning rate<sup>626</sup> [reproduced for ref. 626, open access publication, copyright permission is not required].

shows that the addition of the AW acid extract to the reaction medium promoted a decrease in the corrosion current density and increased the polarization resistance of the stainless-steel samples, suggesting that the extract inhibits the corrosion process.

The SEM images also revealed that the presence of the extract curtailed metal oxidation reactions (Fig. 31). Furthermore, this study reported a shift in the cathodic mechanism reaction on the inhibitor-free surface, indicating the alteration in the adsorption mechanism of the AW extract.

Gusti and colleagues<sup>627</sup> explored coffee bean husk waste as a corrosion inhibitor for mild steel in a  $0.75 \text{ M H}_2\text{SO}_4$  environment. This waste contained chemical compounds such as tannins and flavonoids that augment adsorption, providing a broad surface area. Using the WL methodology, the addition of  $10 \text{ g L}^{-1}$  of coffee bean husk waste achieved an inhibition efficiency of approximately 80%. Over 72 h, this efficiency climbed to 97.5%, causing the authors to recommend coffee bean husk waste as an effective inhibitor under the tested conditions. Ayoola *et al.*<sup>628</sup> investigated the inhibition potential of waste citrus limonum peel extract for A36 mild steel in a  $0.5 \text{ M}$  sulfuric acid environment. This study employed various techniques, demonstrating that a concentration of  $0.4 \text{ w/v}\%$  of citrus limonum led to a remarkable 94% inhibition at temperatures ranging from  $18 \text{ }^\circ\text{C}$  to  $28 \text{ }^\circ\text{C}$ . The efficiency only decreased by 2% at higher temperatures up to  $45 \text{ }^\circ\text{C}$ , illustrating the robust reactivity of the extract as an eco-friendly corrosion inhibitor across a wide temperature range. The SEM/EDX analysis further supported the efficient adsorption of the inhibitor, requiring only a small quantity.

Salinas-Solano *et al.*<sup>629</sup> explored the eco-friendly corrosion inhibition potential of rice bran oil-based agro-industrial waste. The process involved extracting and filtering rice bran oil using the Soxhlet method with hexane as the solvent. Their investigation applied various electrochemical techniques to

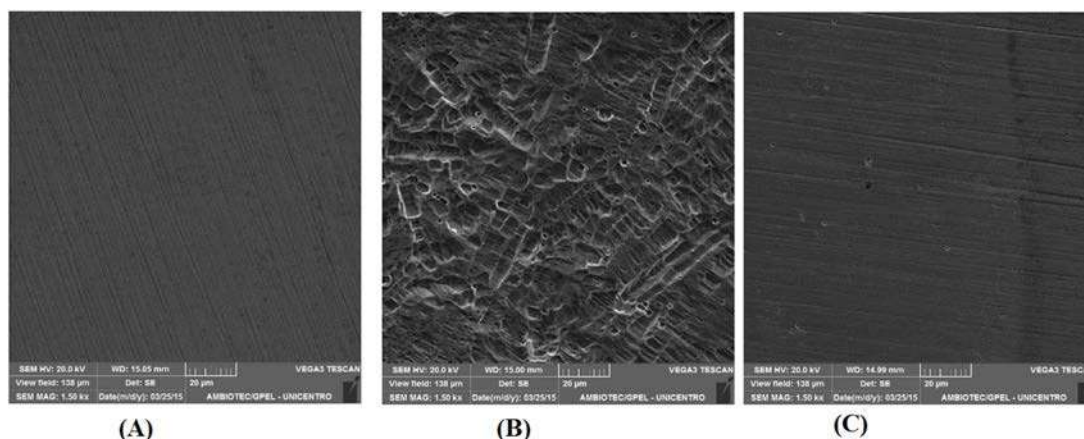


**Fig. 31** SEM images of AISI 304 stainless steel: (A) before immersion, (B) after immersion in  $\text{H}_2\text{SO}_4$ , and (C) after immersion in  $\text{H}_2\text{SO}_4$  containing  $5 \text{ g L}^{-1}$  of AW acid extract (1500X increase). [reproduced for ref. 626, open access publication, copyright permission is not required].

examine the corrosion inhibition on 1018 steel. The addition of 25 ppm of the inhibitor remarkably elevated the inhibition process, achieving over 99% inhibition. This enhancement was attributed to the formation of a protective barrier film on the metal surface, as confirmed by the EIS spectra and adsorption isotherm modeling. This thin film increased the charge-transfer resistance of the metallic material. Vera *et al.*<sup>630</sup> evaluated the corrosion-inhibiting potential of an extract from Fuji apple (*Malus Domestica*) skin collected in Chile's Valparaiso region. Their study involved carbon steel immersed in a saline medium. WL measurements, impedance measurements, and polarization curves were utilized to estimate the inhibitory performance, which reached 90% efficiency at a concentration of 1000 ppm of the extract. In 2019, Cruz-Zabalegui *et al.* employed a Gemini-surfactant synthesized from waste avocado oil as a  $\text{CO}_2$  corrosion inhibitor for X-52 steel.<sup>631</sup> This inhibitor exhibited effective mixed-type corrosion inhibition, achieving an impressive 94% efficiency at a concentration of just 10 ppm. It reduced the corrosion rate by forming a thin film due to the adsorption of inhibitor components on the steel interface, forming a physical bond, according to the Langmuir adsorption isotherm.

Halambek *et al.*<sup>632</sup> investigated tomato peel waste-derived pectin (TPP) as a tin corrosion inhibitor. They aimed to promote natural inhibitors over synthetic ones and enhance the biopolymer production. Electrochemical evaluations revealed an inhibition efficiency of 62.19% for CAP and 65.48% for TPP at a pectin concentration of  $4 \text{ g L}^{-1}$ . Microscopic analysis indicated that pectins prevented the degradation of tin surfaces in aggressive media. Kusumaningrum *et al.*<sup>633</sup> assessed *Artocarpus heterophyllus* peel extract as a non-toxic fruit waste inhibitor. The extract effectively reduced the corrosion rates and protected pure copper in contact with  $1 \text{ M HNO}_3$ . The highest efficiency reached 98% at an optimal concentration of 800 ppm, confirming the potential of this extract for tin corrosion protection.

Bhardwaj *et al.*<sup>634</sup> undertook a study to explore the viability of *Beta vulgaris* peel (BVP) waste material as a green corrosion inhibitor for SS 410 in a 15% HCl solution. The PDP analysis revealed that a concentration of  $4 \text{ g L}^{-1}$  of BVP extract exhibited the highest %IE of 90.17% in the HCl solution. The experimental findings were consistent with the Langmuir adsorption isotherm, confirming the creation of a monolayer on the SS 410 surface due to the peel extract. The anti-corrosive effect was primarily attributed to vitexin, as supported by the theoretical and computational analyses of the phytochemical composition. Molecular simulation techniques were used to explore the interactions of vitexin with SS 410. Additionally, the study revealed that the *B. vulgaris* peels acted as anodic inhibitors. The peel extract components adsorbed on the metal surfaces, forming a protective layer, which effectively reduced the corrosion rates due to its protective properties.

Fekri *et al.*<sup>635</sup> introduced turnip peel extract (TPE) as an innovative, eco-friendly, and cost-effective solution for inhibiting copper corrosion in a 3.5 wt% NaCl solution. This study demonstrated that increasing TPE concentration enhanced the inhibition efficiency, reaching an impressive maximum %IE of 91.2%. Furthermore, it assessed the impact of temperature variations (298–338 K) on the performance of TPE as a corrosion inhibitor, indicating a gradual decline in IE with an increase in temperature. Nonetheless, even at 338 K, the %IE remained acceptably high at approximately 64%. A comprehensive analysis revealed that the TPE molecules primarily underwent physical adsorption on the copper surface. The positive  $\Delta H$  value and the agreement between the experimental data and the Langmuir isotherm model supported this conclusion. Notably, the investigation of the TPE components revealed the presence of heteroatoms (S, O, and N) in their molecular structures, playing a crucial role in forming a protective film on the copper surface and effectively inhibiting the corrosion processes. Radi *et al.*<sup>636</sup> investigated the corrosion inhibitory potential of pumpkin seeds for the 7075-T6 aluminum alloy in a 3.5% NaCl solution using electrochemical,

surface, and theoretical analyses. This study revealed an impressive inhibition efficiency of 95% at 298 K and  $1 \text{ g L}^{-1}$  concentration. The Tafel polarization analysis suggested that the pumpkin seeds function as cathodic inhibitors. The adsorption of the pumpkin seeds on the aluminum alloy surface followed the Langmuir adsorption isotherm. However, longer immersion times led to a decrease in the protection efficiency.

## 2.10. Green corrosion inhibition using material design

Material design offers a promising pathway to green corrosion inhibition by combining sustainable principles with innovative techniques. The cutting-edge field of green corrosion prevention through material design is examined in this section. Developing effective and environmentally friendly inhibitors is essential to address corrosion challenges, while minimizing ecological impacts. We explore the production of intelligent coatings, use of nanotechnology, and development of sustainable materials. The discussion includes predictive modelling methods, AI-driven optimization, and green manufacturing procedures. The emphasis is on collaborative research initiatives and regulatory assistance as change agents. The research alludes to a future where environmentally friendly corrosion inhibition protects crucial infrastructure and fosters environmental sustainability by adhering to these standards. As research advances, material design will play a pivotal role in shaping the future of green corrosion protection.

As already mentioned, corrosion tremendously impacts metal structures in various sectors, resulting in substantial financial losses, environmental issues, and safety risks.<sup>637</sup> Traditional corrosion inhibitors frequently use hazardous chemicals, which raises concerns for the environment and human health. In response, designing materials according to green principles has become a potential strategy for creating efficient and environmentally friendly corrosion inhibitors. The intriguing “green corrosion inhibition through material design” method focuses on successfully developing materials with specific features to fight corrosion, while reducing their environmental impact.<sup>13</sup> One of these tactics is designing materials to build a protective film on the metal surface. This layer acts as a barrier to prevent corrosive substances from directly touching the metal, delaying the corrosion process.<sup>638,639</sup> These substances are frequently called corrosion inhibitors. Several elements are considered when creating these materials to provide green corrosion inhibition.

Toxic or harmful components should not be used, and the materials should be eco-friendly. This ensures that no harmful compounds are released into the environment during the corrosion inhibition process. Additionally, the materials must successfully halt corrosion, while remaining stable over time. They should have qualities such as strong adherence to the metal surface, decent resistance to deterioration, and the capacity to repair themselves after being harmed. This guarantees that the metal structure will be protected longer.<sup>529,640</sup>

Academics and industry professionals use different material design strategies to achieve green corrosion inhibition. These

strategies involve using organic substances, polymers, nano-materials, and bioinspired materials. These materials may be tuned for certain corrosion avoidance applications by adjusting their composition, structure, and surface qualities. Overall, green corrosion inhibition *via* material design is a novel and sustainable method for preventing corrosion, while reducing its adverse environmental effects. It has enormous potential to increase the toughness and longevity of metal structures across a range of industries, from manufacturing and infrastructure to transportation and infrastructure. This section emphasizes the significant ideas, approaches, and most recent developments in this area, emphasizing using materials design tactics to develop green corrosion inhibitors.

**2.10.1. Importance of material selection in inhibitor design.** Green corrosion inhibition aims to provide corrosion-prevention strategies that are sustainable and kind to the environment. In this context, the choice of materials for inhibitor design is of particular importance given that it directly affects the efficacy, safety, and environmental impact of corrosion inhibition tactics.<sup>641–643</sup> In conclusion, careful material selection is a key component of the design of green corrosion inhibitors. Design professionals may produce corrosion inhibition solutions that are efficient and sustainable, improving both industrial processes and the health of the world by considering the environment, human health, performance, and regulatory factors (Fig. 32). Here, we provide a more thorough explanation of why choosing suitable materials is essential when developing green corrosion inhibitors.

(i) *Environmental sustainability*: The minimal negative effects on the environment are the core of green corrosion inhibition.<sup>644–646</sup> In line with the sustainability tenets, materials made from renewable resources or biodegradable should be used. These materials support a healthy ecosystem by lowering the production of toxic waste.

(ii) *Non-toxic nature*: Corrosion inhibitors should be safe for humans and the environment. Through careful material selection, the inhibitors are made safe for users, consumers, and ecosystems by preventing the release of toxic compounds into the environment.<sup>640</sup>

(iii) *Reduced carbon footprint*: Climate change may be mitigated by choosing materials with a smaller carbon footprint during manufacturing and use. Choosing materials involving less energy-intensive manufacturing processes or emissions can reduce the environmental effect.

(iv) *Biocompatibility*: The chosen inhibitors must be biocompatible when the protected materials interact with live species, such as in agricultural or marine applications.<sup>647</sup> This guarantees that the inhibitors will not hurt aquatic, terrestrial, or plant life.

(v) *Renewable resources*: Utilizing renewable resources lessens the reliance on finite resources and supports sustainable practices. Examples of these materials are plant extracts,<sup>13,648,649</sup> natural polymers,<sup>15,650,651</sup> and waste byproducts.<sup>178,652,653</sup>

(vi) *Integration into existing processes*: Green corrosion inhibitors must be easily incorporated into current industrial

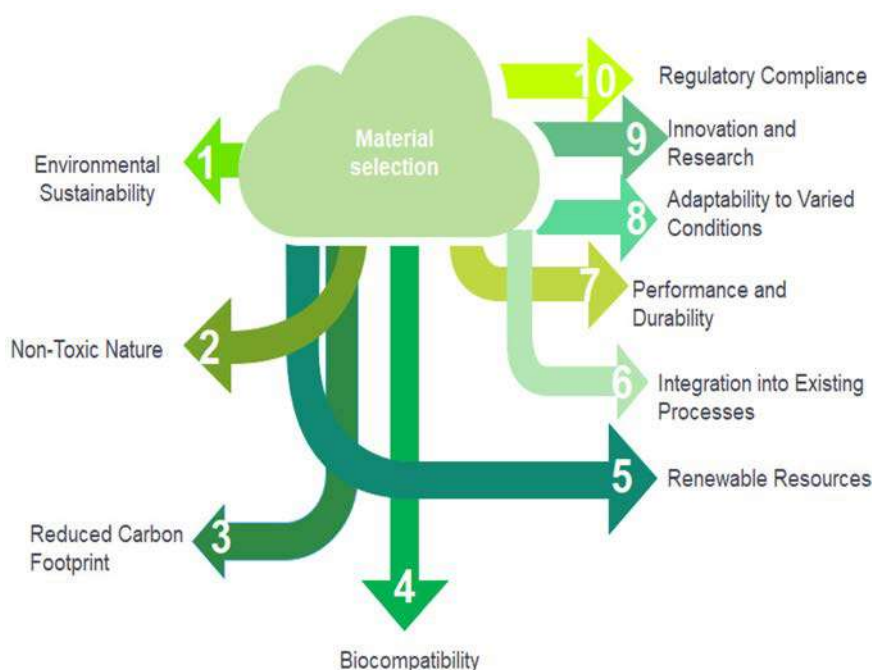


Fig. 32 General depiction of the importance of material selection in inhibitor design [self-illustration, copyright permission is not required].

processes without requiring substantial changes. Implementing green corrosion inhibition techniques across sectors is facilitated by selecting materials compatible with existing production processes.

(vii) *Performance and durability*: The chosen materials must have corrosion inhibition capabilities that are comparable with or better than conventional inhibitors. They should also continue to work well over time, providing materials with long-lasting protection.

(viii) *Adaptability to varied conditions*: Corrosion protection that can adjust to changing circumstances is needed for various locations and applications. The materials should be adaptable in multiple environments without sacrificing their inhibitory qualities.<sup>306</sup>

(ix) *Innovation and research*: Innovation in creating green corrosion inhibitors is made possible by investigating innovative materials and combinations. Researchers can create composite materials with improved performance and little environmental effect or find novel chemicals.

(x) *Regulatory compliance*: Standards and regulations that control the use of chemicals and materials apply to many different sectors. Implementing green corrosion inhibitors will go more smoothly using products that adhere to these requirements.

**2.10.2. Design principles for eco-friendly corrosion inhibitors.** The design of environmentally friendly corrosion inhibitors has gained popularity, placing greater emphasis on sustainability and diminished environmental impact.<sup>645,652</sup> Some of the major design principles for green corrosion inhibition are shown in Fig. 33. An outline of this principle is explained here.

(i) *Renewable resource utilization*: Environmentally friendly corrosion inhibitors must utilise organic materials, biopolymers, and plant extracts as renewable resources. The inherent biodegradability of these materials prevents the accumulation of potentially harmful residues. For instance, employing plant compounds conserves non-renewable resources and provides a sustainable alternative to conventional inhibitors.

(ii) *Non-toxic nature*: The selection of materials that are safe for the environment and human health is strongly encouraged by design guidelines. This idea agrees with the principles of green chemistry and ensures that inhibitors do not introduce dangerous substances into ecosystems. Using non-toxic inhibitors makes it possible to handle, store, and dispose of dangers more safely.

(iii) *Molecular compatibility*: Design standards strongly recommend using materials safe for the environment and human health. This notion guarantees that inhibitors do not introduce harmful compounds into ecosystems and is consistent with the principles of green chemistry. Handling, storing, and disposing of risks more securely when non-toxic inhibitors are used are feasible.

(iv) *Biodegradability and low persistence*: Natural biodegradable eco-friendly inhibitors should eventually break down into harmless components. Biodegradability reduces the persistence of inhibitor residues in the environment, minimising their long-term effects. Furthermore, it promotes the broad aims of environmental stewardship.

(v) *Reduced energy consumption in synthesis*: Green inhibitor design encourages using less energy-intensive and less-byproduct-producing processes. Employing energy-efficient synthesis techniques may significantly reduce the environmental

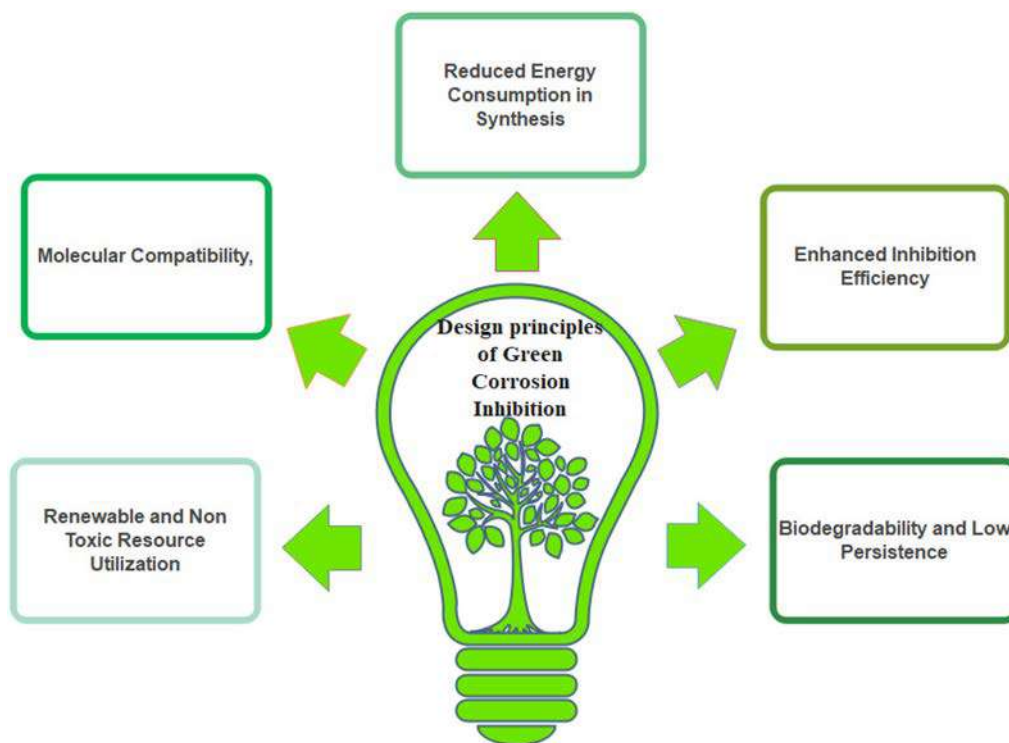


Fig. 33 Outline of the major design principles for green corrosion inhibition [self-illustration, copyright permission is not required].

effect of manufacturing inhibitors. This idea promotes the overall sustainability of the manufacture of inhibitors.

(vi) *Enhanced inhibition efficiency*: The effectiveness of the corrosion prevention by an inhibitor should not be hampered by its environmental friendliness. To maximize the inhibitory performance, design concepts emphasize striking a balance among molecular interactions, film-forming ability, and long-term stability. This ensures that environmentally friendly inhibitors are both effective material protectors and safe for the environment.

### 2.11. Green corrosion inhibition using safer chemicals (ILs, biodegradable polymers, surfactants and dyes)

The nexus between chemical and environmental sciences has necessitated the development of chemical substances that are viable for numerous industrial applications and eco-friendly. A solution-focused approach to the challenges of chemical production has prompted the design and development of safer chemicals to replace toxic traditional chemicals.<sup>654</sup> Safer chemicals, now widely known as green chemicals, reduce or eliminate adverse impacts on human health and the environment. These chemical substances are tailored to minimize or have zero environmental impact in their production, use and disposal, while still serving their intended purpose. Some main characteristics of safer chemicals include potency, efficiency, low cost, facile synthesis, non-toxicity, biodegradability, tolerability and non-bioaccumulative properties.<sup>655</sup> In recent years, the stringent campaigns and regulations for using safer chemicals in various industries have led to the

advancement of green chemistry initiatives. The field of corrosion science has also embraced the progressive view of utilizing safer chemicals to develop highly effective metallic inhibitors. This section overviews the use of prominent, safer chemicals such as ILs, biodegradable polymers, biosurfactants and dyes as effective, efficient and environmental benign inhibitors.

**2.11.1. Ionic liquids.** ILs represent a category of molten salts characterized by their remarkable property of having a melting point temperature below 100 °C.<sup>656</sup> The process of designing ILs involves the precise combination of organic cations, including imidazolium, pyridinium, phosphonium, and ammonium, with inorganic anions such as acetates, halides, phosphates, and sulfonates. This exceptional flexibility in designing ILs, coupled with their array of fascinating properties, such as non-toxicity, low volatility, high solubility, remarkable surface activity, superior conductivity, robust thermal stability, and outstanding chemical stability, has propelled their extensive range of applications.<sup>88,657</sup> Given these distinctive properties, ILs have found valuable utility across various scientific disciplines, including electrochemistry, analytical science, catalysis, biology, and chemistry.<sup>658</sup>

Due to their exceptional biocompatibility, solubility, and adsorption capacity, ILs have emerged as promising eco-friendly alternatives to traditional corrosion inhibitors. Recent advancements in corrosion science, engineering, and technology have showcased the viability of employing ILs for inhibiting metallic corrosion. Over the past decade, the adoption of ILs as environmentally friendly corrosion inhibitors has

witnessed a significant upsurge in research activity.<sup>659,660</sup> ILs possess the necessary attributes of high-performance inhibitors, featuring multiple heteroatoms,  $\pi$ -electrons, varying alkyl chain lengths, and numerous reactive centers, which facilitate their robust adsorption onto metal surfaces.<sup>659,661</sup> Their inhibition capabilities are remarkable, with numerous studies reporting impressive %IE ranging from 90% to 99% at low concentrations. In most instances, ILs often display a mixed-type effect and become effective by adhering to the metal substrate, aligning with the Langmuir adsorption isotherm. The mechanism of action has been widely observed to be both physical and chemical adherence to the metal surface.

Among the diverse classes of ILs explored, imidazolium-based ILs (Im-ILs) have garnered the most attention in the literature. These ILs, similar to others, predominantly inhibit metallic degradation through a mechanism in which their polar hydrophilic groups attach to the metal substrate. Simultaneously, their nonpolar hydrocarbon segments interact with the solution end. For instance, in the study by Haldhar *et al.*,<sup>662</sup> they illustrated the hydrophilic and hydrophobic interactions of three Im-ILs in an HCl environment, specifically for applications in oil and gas pipelines (Fig. 34). In a general context, several critical parameters have been identified as influential factors in determining the inhibitive properties of ILs. These factors include inhibitor concentration, immersion time, temperature, electrolyte composition, alkyl chain length, nature of the alkyl group, effect of synergism, and the type of anion/cation. Extensive research has been

devoted to investigating the impact of these variables on the effectiveness of ILs as corrosion inhibitors.<sup>392,663–667</sup> Extending present knowledge on the relationship between the structural attributes of ILs and their inhibition behaviour, several authors have constructed quantitative structure–activity relationship (QSAR) models.<sup>668–670</sup> The outstanding inhibition behaviour of ILs derived from lignin,<sup>671</sup> pyridinium,<sup>672,673</sup> pyrrolidinium,<sup>674,675</sup> polymers,<sup>676,677</sup> and amino acids<sup>77,678</sup> has also been recently reported. These reports have demonstrated the inhibiting capability of different ILs to suppress corrosion in different metal/electrolyte system. Table 3 presents a summary of recent reports on the inhibition of different metals using ILs.

A notable achievement in corrosion control in the chemical and oil industry has recently emerged with the development and evaluation of innovative and environmentally friendly supramolecular ILs.<sup>689,690</sup> In these pioneering studies, Berdimurodov *et al.* introduced two distinct types of supramolecular ILs, namely bromide–cucurbit[7]uril supramolecular ILs (BrCU)<sup>689</sup> and cucurbit[6]uril-based[3]rotaxane supramolecular ILs (CB6),<sup>690</sup> both designed to mitigate the corrosion of CS. These ILs were investigated in two distinct corrosive environments, namely NaCl saturated with H<sub>2</sub>S and CO<sub>2</sub> in a NaCl medium and the other in a 1 M OH<sup>−</sup> + 1 M Cl<sup>−</sup> solution. To assess the inhibitive performance of these supramolecular ILs, a comprehensive array of test methods was employed, including cyclic voltammetry (CV), electrochemical noise (EN), EIS, PDP, SEM, EDX, DFT, and MD simulation. Remarkably,

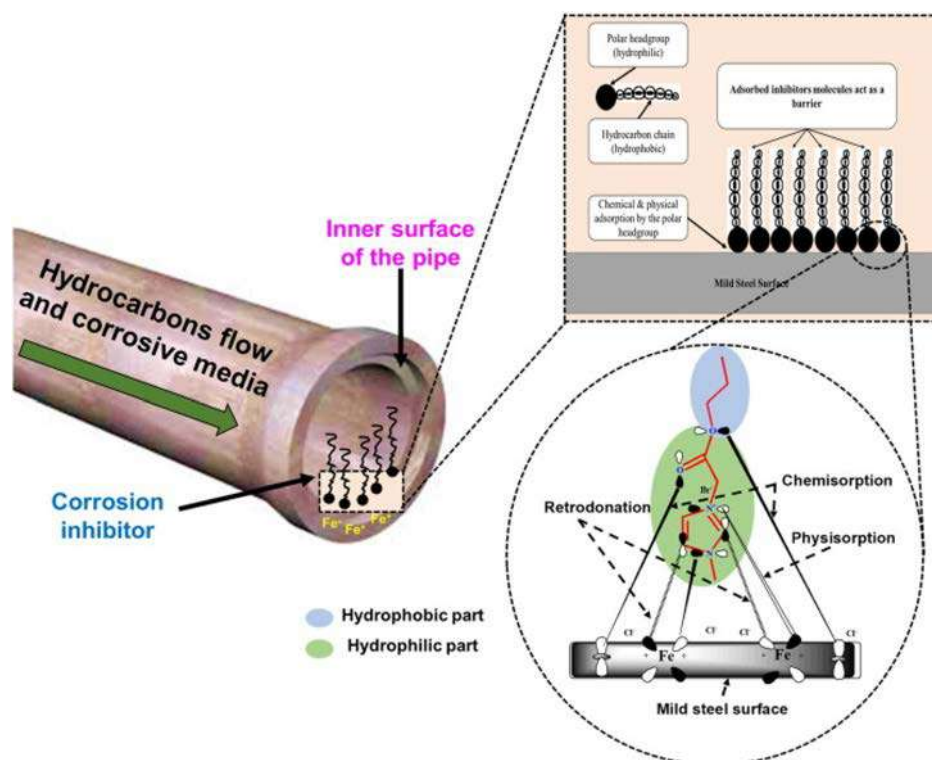
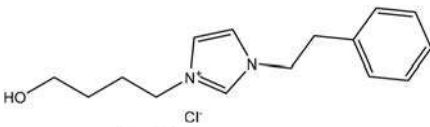
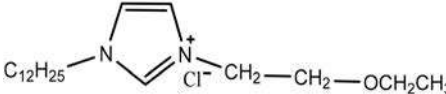
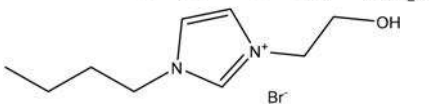
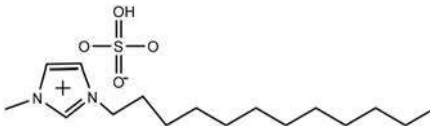
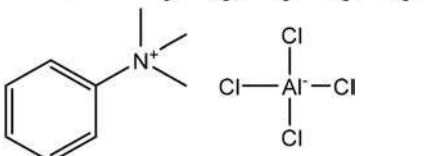
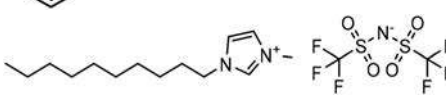
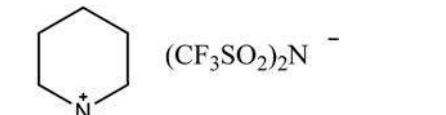
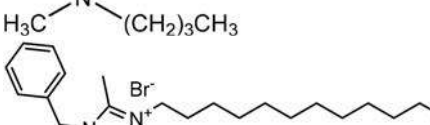
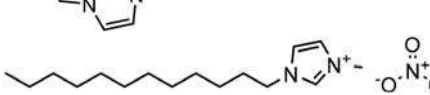
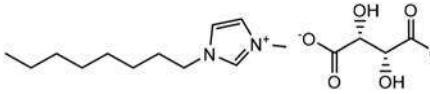


Fig. 34 Mechanism of action of Im-ILs in 1 M HCl<sup>662</sup> [reproduced from ref. 662 with permission, Copyright, Elsevier, 2023].

**Table 3** Recent applications of ionic liquids for different metal types in various media

Ionic liquid	Substrate	Medium	Max %IE	Ref.
	Mild steel	1 M HCl	96.20%	679
	Stainless steel	2 M HCl	95.40%	680
	Carbon steel	0.3 M NaCl	88.90%	681
	Carbon steel	CO <sub>2</sub> -saturated NaCl brine	94.46%	682
	Carbon steel	1 N HCl	96.00%	683
	AZ31B magnesium	0.5 wt% NaCl	93.91%	684
	Q235 steel	1 M HCl	95.80%	685
	Aluminium	1 M HCl	80.90%	686
	Copper	0.5 M H <sub>2</sub> SO <sub>4</sub>	96.60%	687
	Copper	3.5% NaCl	95.00%	688

the results demonstrated that the inclusion of merely 100 mg L<sup>-1</sup> of BrCU and CB6 yielded an outstanding %IE of 97.54% and 97.97%, respectively, at a temperature of 303 K. The analysis of the Tafel plots indicated that both supramolecular ILs acted as mixed-type inhibitors, predominantly influencing the anodic corrosion process. Subsequent investigations unveiled that these ILs shielded the metal substrate from corrosive ions through physical and chemical interactions. The exceptional corrosion inhibition exhibited by these novel ILs can be attributed to several key factors, including their heightened solubility, substantial planar structure featuring numerous heteroatoms, and the presence of delocalized pi-electrons. This innovative approach marks a significant leap forward in the quest for green and effective corrosion control strategies, promising sustainable solutions for the chemical and oil industry.

**2.11.2. Biopolymers.** Biodegradable polymers form a distinct class of polymeric materials with the inherent capability to undergo decomposition. Depending on their origin, these polymers can be categorized as natural or synthetic. Notably, natural polymers, often called biopolymers, exhibit unique characteristics such as biodegradability, biocompatibility, biotolerance, and non-bioaccumulative properties, which are attributes frequently constrained in synthetic polymers.<sup>644,691</sup> The natural sourcing of biodegradable polymers makes them environmentally friendly substitutes, making them an integral part of the family of green corrosion inhibitors due to their biocompatibility, biodegradability, biotolerance, and non-bioaccumulative nature. Consequently, they find diverse applications across various industrial sectors. Furthermore, extensive research has been undertaken to investigate their inhibitive be-

havior in the context of corrosion control. These compounds have demonstrated exceptional potential in safeguarding metal surfaces, which is primarily attributed to their substantial surface area, complexation capabilities, and numerous binding centers.<sup>692,693</sup> This section provides a concise overview of some biopolymers that have undergone evaluation as corrosion inhibitors.

Cellulose and starch are the most encountered plant polysaccharides, which are celebrated for their widespread applications across various industries. Cellulose is regarded as the most abundant biopolymer on Earth.<sup>302</sup> The appeal of cellulose and starch appeal lies in their affordability, biocompatibility, and favorable physicochemical characteristics. However, in the case of employing them as corrosion inhibitors, especially in their unaltered native forms, their utility is somewhat constrained due to various associated challenges.<sup>570,694,695</sup> These challenges are intimately linked to their source, concentration, composition, and solubility, collectively contributing to their suboptimal inhibitive effects. For instance, irrespective of its source, starch is inherently insoluble and necessitates a substantial dosage exceeding 700 mg L<sup>-1</sup> to achieve an inhibition performance comparable to traditional inhibitors administered at a mere 50 mg L<sup>-1</sup>.<sup>302</sup> Nevertheless, modifying starch and cellulose has emerged as a transformative approach, effectively mitigating these limitations. When exposed to corrosive environments, modified starch and cellulose derivatives exhibit improved solubility and enhanced adsorption capacities.

In a series of extensive studies on grafted cassava starch conducted by the Chinese research group led by Prof. Li, it was conclusively demonstrated that physical and chemical modification enhanced its water solubility in the test medium and significantly reinforced its corrosion resistance. One of these studies showcased the protective capabilities of cassava starch graft copolymers synthesized from the grafting of acryl amide using gravimetric, electrochemical techniques and surface imaging tools. This study offered a promising avenue for corrosion protection of 90.6% with 1 g L<sup>-1</sup> at 293 K for Al in H<sub>3</sub>PO<sub>4</sub>.<sup>579</sup> Water-soluble moieties such as -OH and C=O groups in the inhibitor were found to bond and interact with the metal surface coordinatively. The modification of cellulose with the introduction of hydroxyl propyl<sup>696</sup> and carboxymethyl<sup>697</sup> showed that functionalized cellulose can lower the metal corrosion rate in given media.

Lignin is the second most prevailing biopolymer on Earth after cellulose. It is a phenolic macromolecule with many functional groups, including hydroxyl, carboxyl, methoxy, aldehyde, and phenolic moieties. These diverse functional groups serve as potential centers for adhesion to metallic surfaces. Notably, these functional groups contain double bonds and electron pairs on oxygen atoms, endowing lignin with the remarkable capability to adhere to metal surfaces effectively. This adhesion mechanism facilitates the formation of a protective barrier in the metal/electrolyte system. The recent study conducted by Rahayu *et al.* carried out lignin extraction from sugarcane bagasse, and subsequently utilized it as a corrosion

inhibitor with noteworthy results. The authors reported a peak performance of 80.79% when employing a concentration of 10 g L<sup>-1</sup> after a 6 h exposure period.<sup>698</sup>

Natural gums derived from plants have emerged as exceptional adsorption agents, primarily owing to their remarkable complexation capabilities facilitated by functional groups, extensive surface coverage on metal substrates, and the presence of heteroatoms that serve as centers for adsorption. These natural gums are often composed of polysaccharides, contributing to their robust inhibitory potential. Numerous studies have been conducted to elucidate the inhibitory properties of natural gums and their modified forms.<sup>699,700</sup> A case study used Gum Arabic variants from Mauritania, Senegal, and Morocco as effective anticorrosive agents. These variants were rigorously tested for their anticorrosive efficacy against mild steel in a highly corrosive environment of 1 M HCl. The investigation included various electrochemical, surface analytical, and computational analyses. Remarkably, the study yielded promising results, with all three Gum Arabic variants demonstrating inhibition efficiencies ranging from 94% to 96%. The inhibitory mechanism for these variants was elucidated by applying the Langmuir single-layer model. Furthermore, advanced techniques such as AFM and XPS conclusively established a protective layer on the steel sample. To further enhance the understanding of the inhibitory process, a QSAR model was developed. The final model revealed a consistent influence of lipophilicity on the inhibition process, with a commendable *R*<sup>2</sup> value exceeding 0.7.<sup>701</sup> These findings underscore the significant potential of natural gums as effective and environmentally friendly corrosion inhibitors, paving the way for sustainable corrosion control solutions. Table 4 portrays other popular natural gums reported as corrosion inhibitors of metals in different electrolytic media.

Chitosan is widely recognized as a linear polysaccharide characterized by numerous functional moieties along its polymer chain. These functional groups play a pivotal role in enhancing the solubility and facilitating robust adhesion to metallic surfaces. Chitosan-based biopolymers have attracted significant attention due to their diverse industrial, environmental, and biological applications.<sup>711</sup> Their appeal stems from their exceptional biological tolerance, non-toxicity, minimal environmental footprint, and inherent biodegradability.

**Table 4** Protection of metals using natural gums as ecofriendly anticorrosive materials

Natural gums	Substrate	Medium	Max %IE	Ref.
Gum Arabic	Mild steel	1 M HCl	94.00%	702
Locust bean	Stainless steel	0.15 M NaCl	99.99%	703
Guar gum	Aluminium	1 M HCl	82.85%	704
Exudate gum	N80 carbon steel	1 M HCl	95.50%	705
Alginate	Copper	1 M HCl	83.00%	706
Pectin	Carbon steel	0.5 M HCl	89.50%	707
Dextrin	Reinforced steel	1 M HCl	85.00%	708
Inulin	Reinforced steel	1 M HCl	93.00%	708
Xanthan gum	X80 steel	1 M H <sub>2</sub> SO <sub>4</sub>	94.85%	709
Almond gum	Mild steel	1 M HCl	96.37%	710



ity.<sup>712</sup> As integral components of the green corrosion inhibitors family, chitosan and its derivatives excel in their capacity to effectively bind to metallic substrates, thereby preventing the infiltration of corrosive ions. Multiple research studies have provided compelling evidence of the anti-corrosive capabilities of chitosan, particularly in safeguarding mild steel and various other metal types.<sup>713,714</sup> Research into the functionalization of chitosan has unveiled a remarkable enhancement in its anti-corrosive properties. Chitosan derivatives have undergone comprehensive examination as aqueous corrosion inhibitors across various solutions and for diverse metal types, consistently demonstrating exceptional %IE values that outweigh its pure forms.<sup>715</sup> Several studies have demonstrated the ability of chitosan derivatives to adhere to metal surfaces to deter the invasion of corrosive ions under different experimental conditions.<sup>715-717</sup>

Green synthetic biopolymers have also been reported as effective and eco-friendly metallic inhibitors under different environments. Among these synthetic biopolymers, PEG is prominent, which is characterized by its high molecular weight, ranging from 200 to several tens of thousands.<sup>691</sup> PEG has earned recognition for its exceptional properties, including high solubility, strong adhesive characteristics, effective dispersion, cost-effectiveness, and environmentally friendly attributes. Its applications span a broad spectrum, encompassing food science, biology, pharmaceuticals, and chemistry. According to a comprehensive review of the existing literature, it becomes evident that the inhibitory capabilities of PEG are dependent on its molecular weight. Lower molecular weight PEG variants are associated with diminished %IE, implying that the effectiveness of PEG as a corrosion inhibitor is intricately linked to its specific molecular characteristics. A literature review also showed that a host of biodegradable polymers including poly(vinyl alcohol),<sup>718</sup> poly(lactic acid), poly(acrylic-maleic acid),<sup>719</sup> and polyvinyl pyrrolidone<sup>720</sup> are capable of acting as sustainable anticorrosive agents.

**2.11.3. Surfactants.** Green surfactants represent a unique and noteworthy category within the framework of green corrosion inhibitors, garnering recent attention for their corrosion inhibition capabilities. Surfactants, also known as surface-active agents, are dipolar organic compounds derived from various chemical processes, including esterification, amination of haloalkanes, epoxide and alcohol reactions, as well as sulfonation of long-chain hydrocarbons and benzene derivatives.<sup>19</sup> Within the realm of corrosion protection, particular focus has been directed towards environmentally friendly biosurfactants sourced from plants and microorganisms. Biosurfactants have garnered significant interest due to their advantages, including ease of synthesis, non-toxicity, biodegradability, and high compatibility with ecological considerations.<sup>721</sup> Based on the polar head groups of surfactants they can be classed as non-ionic surfactants, ionic surfactants, dimeric surfactants, and bolaamphiphile surfactants, which have been tested as environmentally benign chemical additives across various environmental conditions. These surfactants offer compelling advantages, including being readily syn-

thesized, non-toxic, cost-effective, and consistently exhibiting to robust inhibition performance. However, despite their considerable potential, there remains a lack of comprehensive reports on using surfactants for corrosion prevention across various electrolytes, warranting further exploration in this promising domain. The latest research has been conducted on the inhibition potential of novel cationic Gemini surfactants,<sup>722-725</sup> zwitterionic surfactants,<sup>726</sup> tera-cationic surfactants,<sup>727</sup> and Quaternium-22<sup>728</sup> for metallic materials in different media using different advanced testing techniques.

**2.11.4. Dyes.** Dyes are essential colorants with extensive medical, food, and textile applications. They have been utilized since ancient times due to their affordability, solubility, and aesthetic appeal. Moreover, dyes have been explored as environmentally friendly materials with potential as anticorrosive agents. In the study by Bedair *et al.*,<sup>729</sup> newly synthesized coumarin dyes were characterized using FTIR, <sup>1</sup>H NMR and mass spectral studies. Furthermore, the PDP and EIS techniques were implemented to investigate their anticorrosive activity for mild steel in a highly corrosive environment of 1 M HCl. The analysis of the Tafel plots revealed the simultaneous retardation of the anodic and cathodic reactions, leading to an impressive %IE of 93.01% for the best dye (azo acetyl coumarin) when employing a concentration of  $7.50 \times 10^{-4}$  M. The inhibition mechanism of the tested dye was found to align closely with the Langmuir isotherm model, shedding light on its mode of action. Furthermore, the SEM analysis yielded compelling visual evidence depicting the protective effect of the dye on the metal surface, resulting in a notably smoother and safeguarded surface. To further enhance the depth of understanding, the study was enriched by applying MD simulation and DFT studies, which provided valuable insights into the molecular interactions in this innovative corrosion inhibition approach. The optimized structures, HOMO and LUMO as well as the ESP of the tested dyes are presented in Fig. 35. The literature is replete with studies on the inhibition behaviour of dyes under different empirical conditions.<sup>729-731</sup>

## 2.12. Green corrosion inhibition in industry (oil-well, petrochemicals, acidization, etc.)

Several factors require careful consideration when addressing corrosion issues within the oil and gas sector. These factors encompass the composition of reservoir rocks, the use of acids for stimulation, the selection of tubing and casings in oil well operations, and the prevailing operational conditions. Among these variables, oxygen stands out as a critical element. It is typically absent in productive formations but introduced during the drilling phase when oxygen-contaminated fluids appear, significantly influencing the corrosive potential. Thus, mismanagement of drilling mud can damage well casings, drilling equipment, pipelines, and mud-handling apparatus. Furthermore, whether naturally occurring or introduced for secondary recovery, water and carbon dioxide can induce substantial corrosion in oil well steels. Moreover, it is worth noting that the acids employed for scale removal can readily corrode metal and dealing with hydrogen sulfide (H<sub>2</sub>S) intro-

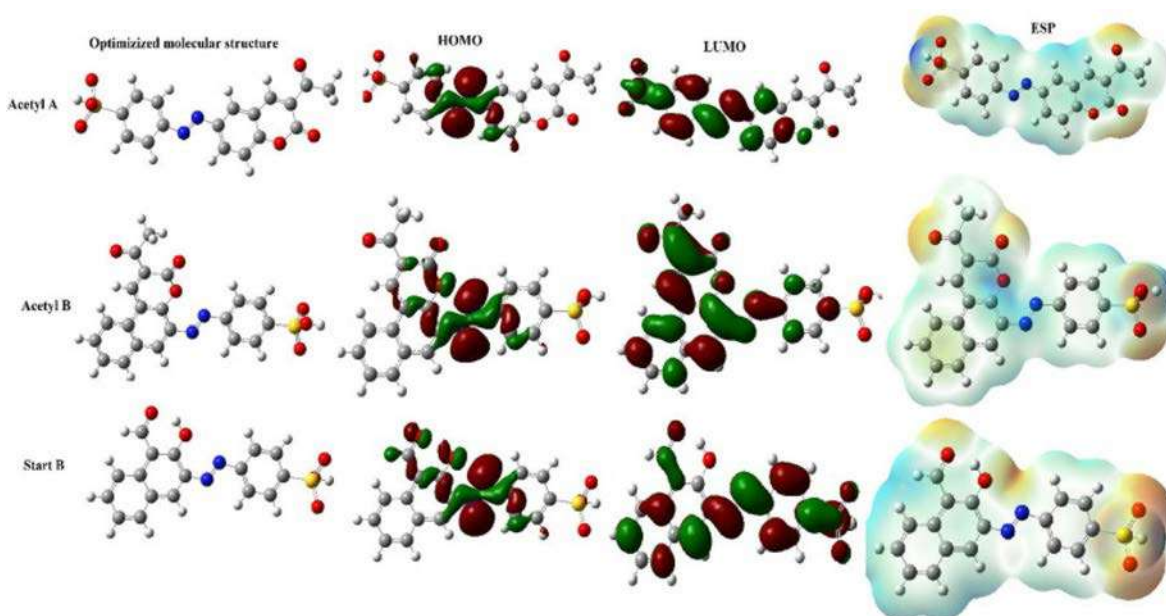
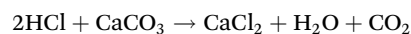


Fig. 35 Optimized, HOMO, LUMO, and ESP representations of the tested dyes as corrosion inhibitors<sup>730</sup> [reproduced from ref. 730, with permission, Copyright, Elsevier, 2022].

duces challenges. Thus, successfully navigating these diverse corrosion scenarios necessitates the expertise of a corrosion engineer, particularly given the demanding conditions of high temperatures, pressures, and stresses prevalent in drilling and production. The role of corrosion engineers is progressively gaining significance.<sup>732</sup> The primary culprits behind oil and gas production corrosion are the combination of carbon dioxide (CO<sub>2</sub>) and H<sub>2</sub>S gases with water. Additionally, this industry commonly employs water flooding techniques to enhance oil recovery, while simultaneously reinjecting production water into the reservoir to maintain the pressure and stability. As oilfields age, the proportion of water in the produced fluids increases significantly, often surpassing 95%, exacerbating corrosion challenges.<sup>733</sup> Consequently, extensive efforts have been dedicated to enhancing their corrosion resistance.<sup>734</sup> In scenarios where environmental conditions prove to be excessively harsh for uncoated carbon steels, using inhibitors or corrosion-resistant alloys presents two viable alternatives for mitigating corrosion issues.<sup>735</sup> Heating HCl solutions to stimulate oil wells can lead to considerable corrosion issues affecting production tubing, downhole equipment, and casing.<sup>736,737</sup> Oil well stimulation is an overarching term encompassing various procedures conducted on a well to enhance its productivity.

Matrix acidization is a carefully controlled technique employed to address the production challenges within the wellbore without inducing fractures or harming the reservoir. It introduces acid into the wellbore at specific rates and pressures.<sup>738</sup> Typically, hydrofluoric acid (HF) acid is chosen for addressing issues related to sandstone or silica, while HCl or CH<sub>3</sub>COOH (acetic acid) is preferred for problems associated with limestone or carbonate formations. Matrix acidization

primarily mitigates damage caused by factors such as drilling, completion, work-over fluids, and the accumulation of deposits from produced water. Indeed, in carbonate reservoirs, fracture acidization is an alternative strategy to the conventional hydraulic fracturing and propping methods. This technique begins with hydraulic fracturing, followed by the application of acid to etch the fracture surfaces, generating linear flow channels that facilitate the flow of fluids to the wellbore.<sup>739</sup> Fractures are initiated by injecting fluid into the well, thereby increasing the pressure and causing pre-existing fractures within the formation to expand and open. Propping agents such as glass beads, sand, epoxy, and silica sand are commonly employed to maintain the newly created fractures and keep them open. The acid reaction can be expressed using the following equations.<sup>740</sup>



Inhibitor additives are introduced into completed wells to prevent acid-induced corrosion of the steel casing and maintain the structural integrity of the well.<sup>741</sup> Various well-stimulation techniques combine inorganic, organic, and surfactant acids. In conventional acidizing treatments, a range of acids is commonly used, with the following acids being among the most prevalent: HCl, HF, CH<sub>3</sub>COOH, HCOOH (formic acid), H<sub>2</sub>NSO<sub>3</sub>H (sulfamic acid), and ClCH<sub>2</sub>COOH (chloroacetic acid).<sup>740,742</sup> These acids are often applied individually or in specific formulations tailored to the particular application. Typically, the weight concentration of HCl utilized in the field is 15%. However, its concentration can vary from 5% to approximately 35%.<sup>743</sup> HCl has been proven to be highly

effective in dissolving carbonates such as limestone and dolomite. Conversely, acetic acid (HAc) is a slowly reacting, weakly ionized acid. Although the cost of using acetic acid to dissolve a given weight of limestone is higher compared to HCl, there are notable advantages associated with its use.<sup>744</sup> These include the ease of inhibiting corrosion, maintaining prolonged contact with the tubing or casing without significant corrosion risk, and natural sequestration properties that prevent iron precipitation. The use of surfactants is imperative in acidization techniques to reduce the surface and interfacial tension, prevent the formation of emulsions, and promote the wetting of the formation. These surfactants play a pivotal role in enhancing the efficiency of the acid treatment.<sup>745</sup> Suspending agents, typically composed of polymers or surfactants, prevent insoluble particles from settling and forming bridges, which can lead to blockages in the formed pores or fractures. In addition to their emulsion-preventing properties, certain suspending particles aid in improving the formation wetting by reducing the surface tension of the fresh and spent acid.<sup>744,746</sup>

Sequestering agents play a vital role in acidization by complexing ions present in iron and other metallic salts, thereby preventing their precipitation. Allowing the precipitation of insoluble iron complexes, such as ferric hydroxide, during acidizing can result in the redeposition of these complexes near the wellbore, leading to persistent clogging issues. During the use of HCl, HAc is employed to maintain a low pH, while citric acid is a valuable chelating agent, which is particularly effective when dealing with higher iron concentrations. Sequestered HCl acid is commonly applied to treat injection and disposal wells.<sup>747</sup> Anti-sludge chemicals are used when specific crude oils, particularly heavy asphaltic crudes, encounter acid to prevent the formation of insoluble sludge. Sludge is typically comprised of components such as asphaltenes, resins, paraffin waxes, high molecular weight hydrocarbons, and fine materials or clays from the formation.<sup>748</sup> Certain surfactants can prevent sludge formation by maintaining the dispersion of colloidal materials. Moreover, these surfactants that prevent sludge formation often act as emulsion inhibitors. Managing sludge can be challenging, especially when using potent acids.<sup>749</sup>

Inhibitors in the oil and gas industry are chemical substances employed to safeguard the surfaces of metals from corrosion.<sup>750</sup> They achieve this protection by either bonding with the metals or reacting with environmental impurities that may lead to pollution. These inhibitors are applied to metals as a solution, subsequently creating a thin layer or film over the metal surface, effectively shielding it. By altering the anodic and cathodic polarization behaviors, inhibitors deter and reduce the diffusion of ions onto the metallic surface. They also contribute to developing electrical resistance across the metal surface. Several factors must be considered before utilizing a corrosion inhibitor in the oil and gas sector, including its toxicity, environmental compatibility, availability, and cost.<sup>751</sup> Corrosion inhibitors employed in this context can be categorized into various types based on their modes of oper-

ation, including vapor phase, cathodic, anodic, passivating, film forming, neutralizing, and reactive inhibitors.<sup>751</sup>

Employing acid treatment on wells is a prevalent technique for boosting oil and gas extraction. Acidization improves the permeability of geological layers and facilitates the movement of oil and gas towards the wellbore.<sup>752</sup> Its application extends to well testing and preparation, as well as the cleansing of oil and gas conduits and water transmission lines. This process eliminates salt deposits from the inner metal surfaces.<sup>753</sup> Utilizing a concentrated HCl solution to stimulate oil and gas wells is crucial in enhancing the production and mitigating formation damage.<sup>754</sup> The acids employed during this procedure engage with acid-sensitive substances within the well due to their heightened chemical reactivity. Consequently, unless controlled, the acid may be expended before achieving a satisfactory penetration depth within the formation. Thus, several approaches have been suggested to curtail the rapid reaction of these acids, including the utilization of aqueous acid emulsions within oil-rich settings or dissolving the acids within non-aqueous solutions.<sup>755</sup> The tubing near the surface encounters acids at lower temperatures throughout the acid treatment procedure, while the bottom of the well comes into contact with hotter acids. Additionally, the microstructure of the inner tubing is uneven, even when employing alloys of the same API grade throughout the well.<sup>754</sup> Consequently, corrosion-related challenges arise with the acid treatment process. Thus, to mitigate the effect of these highly corrosive acids, inhibitors are added.<sup>756,757</sup> Choosing appropriate inhibitors for these conditions involves evaluating factors such as the acid type, fluid temperature, and flow velocity.<sup>758</sup> The inhibitors frequently employed include alkenyl phenones, aromatic aldehydes, acetylenic alcohols, quaternary salts, nitrogen-containing heterocycles, and condensation products of carbonyls and amines. Nevertheless, these inhibitors have drawbacks, primarily their reliance on high concentrations and their adverse environmental impact due to their toxicity. Hence, there is a pressing need to explore innovative environmentally-friendly corrosion inhibitors that are both efficient and safe for application in oil well steel, particularly N80 steel, in 15% HCl systems.

Corrosion prevention in the oil and gas industry is complex, requiring specialized inhibitors designed for specific applications such as refineries, wells, recovery units, and pipelines. Corrosive gases such as H<sub>2</sub>S, CO<sub>2</sub>, and organic acids further compound the challenge of inhibiting corrosion in wells. Passivating, neutralizing, or adsorption-type inhibitors are commonly employed to mitigate wet corrosion in refineries. Slag inhibitors are employed in conjunction with corrosion inhibitors to reduce deposit formation. Both oil- and water-soluble inhibitors are used in pipelines, with adsorption-type inhibitors being a popular choice to prevent internal corrosion in pipelines transporting refined petroleum products. In environments with elevated operating temperatures and/or higher acid concentrations, using a relatively higher quantity of corrosion inhibitor is typically necessary. To ensure that the inhibitor establishes a protective coating on metal sur-

faces, introducing the inhibitor at a higher dosage rate is often recommended, normally ranging from 2000 to 5000 ppm. Once this protective layer has been formed, the dosage can be reduced to a maintenance level, typically ranging from 10 to 100 ppm. It is worth noting that nitrogen-based corrosion inhibitors tend to be less effective in high-temperature settings. Additionally, phosphorus substances may hinder the performance of various catalysts used to treat crude oil.<sup>752</sup>

**2.12.1. Previous research on green corrosion inhibitors for oil well steels.** The oil industry grapples with a substantial corrosion issue, incurring annual costs far exceeding that of many other businesses, amounting to millions of dollars. Acid formulations, including HCl, HF, CH<sub>3</sub>COOH, HCOOH, and chloroacetic acid, are employed in acidizing treatments. HCl is often favored due to its cost-effectiveness and absence of insoluble reaction by-products, making it the primary component in acidic solutions to mitigate wellbore obstructions and enhance petroleum production. The model systems for laboratory-based inhibitor testing typically include tubular steels such as N80, L80, J55, and P110 in the presence of 15–28% HCl together with elevated temperatures. As discussed in the aforementioned sections, several green inhibitor chemistries, namely, biopolymers, natural extracts, and gums together with synergistic agents have been reported in the acidizing procedures with promising results. A further discussion on the specific inhibitor types reported in this area is provided later. In recent times, efforts have been made to integrate eco-friendly inhibitors into industrial applications. The heightened societal expectations and regulations imposed by relevant institutions have spurred extensive research into the sourcing, performance evaluation, and potential incorporation of green inhibitors in an industrial context.<sup>759</sup> As a trustee, the Paris Commission has stipulated three criteria for assessment: bioaccumulation, biodegradation, and toxicity.<sup>55</sup> The eco-friendly inhibitors being explored in line with these criteria include natural oils,<sup>760</sup> plant extracts,<sup>761</sup> drugs,<sup>762</sup> amino acids,<sup>763</sup> natural polymers<sup>651</sup> and ionic liquids.<sup>77</sup> These environmentally conscious corrosion inhibitors have found application in managing the corrosion of downhole tubing. In the subsequent sections, we will present a succinct overview of the current research gap related to environmentally friendly corrosion inhibitors, specifically in an industrial context. Zhang *et al.*<sup>75</sup> conducted a comprehensive study introducing two newly developed amino acid-modified dextran derivatives (LDT and S-LDT) as effective and eco-friendly corrosion inhibitors for carbon steel within CO<sub>2</sub>-rich oilfield-produced water. Meticulous electrochemical measurements showed that S-LDT exhibited exceptional inhibitory properties, showcasing a noteworthy inhibition efficiency and consistent stability (99.7% after 72 h of immersion). Loto *et al.*<sup>764</sup> reported that a mixture consisting of clove essential oil extract, basil oil, and atlas cedar oil showed significant corrosion inhibition properties when applied to low-carbon steel samples exposed to diluted solutions of H<sub>2</sub>SO<sub>4</sub> and HCl. This combined treatment exhibited corrosion inhibition efficiencies surpassing 80% across various inhibitor concentrations in both acidic solutions.

Recently, a blend containing extracts of rosemary and *Cinnamomum cassia* essential oils demonstrated remarkable effectiveness in mitigating the deterioration of mild steel when subjected to diluted solutions of H<sub>2</sub>SO<sub>4</sub> and HCl. This approach yielded exceptional inhibition outcomes, consistently exceeding 90% inhibition efficiency across all concentrations tested.<sup>765</sup> A similar inhibition efficiency was observed for pipeline steel in the presence of Gum Arabic.<sup>766</sup> Aribó *et al.*<sup>757</sup> employed extracts from *Tridax procumbens* and *Chromolaena odorata* to protect super austenitic stainless steel in a corrosive environment consisting of a 1 : 1 mixture of 4 M HCl and a CO<sub>2</sub>-saturated 3.5% NaCl solution. The researchers achieved inhibition efficiencies exceeding 90%. Furtado *et al.*<sup>767</sup> presented a novel green inhibitor using cashew nutshell liquid. They found that combining cardanol residue with butyl glycol and acetylenic alcohol produced a synergistic outcome, resulting in an impressive inhibition efficiency of 99.47% for API P110 carbon steel when exposed to 15% HCl.

Quraishi *et al.*<sup>768</sup> conducted a study on environmentally friendly vanillin-modified chitosan, which displayed noteworthy corrosion inhibition characteristics when employed on carbon steel specimens exposed to diluted solutions of 15% HCl. The findings demonstrated a remarkable corrosion inhibition efficiency of 92%. Palimi *et al.*<sup>769</sup> conducted an extensive investigation aimed at assessing the effects of three environmentally conscious inhibitors, which were derived from fatty acids, *i.e.*, polyethylene glycol-2 oleamide, glycerol myristate, and glycerol linoleate, within drilling fluids based on emulsions. The central objective of this research was to address the specific issue of corrosion associated with 1018 carbon steel in environments saturated with CO<sub>2</sub> and KCl. The findings of this study highlighted the substantial efficacy of these environmentally friendly inhibitors. Notably, polyethylene glycol-2 oleamide emerged as an exceptional performer, achieving an impressive inhibition efficiency of 99.7%.

The inhibition of API grade N80 steel in a 15% HCl solution was studied using two environmentally friendly compounds, namely 2-amino-*N*-octadecylacetamide (AOA) and 2-amino-*N*-octadecyl-3-(4-hydroxyphenyl) propionamide (AOHP). Various concentrations of these synthesized inhibitors were added to the test solution, and their inhibitory effectiveness was evaluated through mass loss, PDP and EIS. At a concentration of 150 ppm, the optimal inhibition performance was observed for both AOA and AOHP. In the WL tests, AOA achieved an efficiency of 90.04%, while AOHP demonstrated an even higher efficiency of 94.97%. This superiority of AOHP over AOA across all test parameters can be attributed to the more significant number of active centers and larger molecular size of AOHP compared to AOA. Electrochemical assessments, FTIR and SEM analyses determined that these inhibitors exhibit a hybrid nature. The inhibition mechanism of these compounds predominantly involves their absorption on the surface of the N80 steel alloy.<sup>770</sup>

An extensive research study assessed the effectiveness of 2-(2-pyridyl) benzimidazole, an environmentally friendly corrosion inhibitor, in mitigating CO<sub>2</sub>-induced corrosion. This

meticulous investigation was conducted under particular conditions of turbulent fluid dynamics within a non-corrosive environment. Notably, the inhibitor demonstrated exceptional efficacy, achieving a remarkable 90% effectiveness rate during carefully executed experimental trials, all conducted at a consistent rotational speed of 2000 rpm.<sup>771</sup> Moreover, their findings revealed an efficiency of at least 86% at 4000 rpm after 12 h. The subsequent introduction of thiobarbituric acid further heightened the effectiveness, resulting in an enhanced efficiency of 95.6% following a 12 h immersion period.<sup>771</sup>

In the context of corrosion inhibition, one proposed compound is the amalgamation of zinc sulfate and calcium gluconate. Moreover, investigations delving into the collaborative influence of aspartates and alkyl polyglucosides as both environmentally friendly and efficacious inhibitors have underscored the essential requirement for an optimal alkyl chain length to facilitate the creation of a corrosion protection film. These inhibitors demonstrated robust compatibility with fluids and equipment employed in oil fields. Nonetheless, achieving heightened effectiveness demands introducing more significant quantities of these inhibitors than their traditional counterparts.<sup>772</sup> However, although the literature highlights the notable inhibition efficiency of various components, uncertainties continue to linger. For instance, the precise mechanism through which molecules present in plant extracts impede corrosion and the specific constituents responsible for this phenomenon remain elusive. Furthermore, crucial factors such as toxicity, biodegradation, and bioaccumulation necessitate consideration, although these parameters are frequently omitted from studies. Elaborate documentation regarding the extraction procedures of inhibitors from their sources needs to be presented, given that it is a pivotal facet for gauging the feasibility and economic viability of mass-producing these inhibitors. Ultimately, an imperative need persists for further research, encompassing authentic downhole scenarios and real-world environments, to effectively establish a hierarchy among environmentally friendly inhibitors, positioning them as potential substitutes for their current counterparts.

### 3. Conclusion, challenges and opportunities

The ongoing debate demonstrates that corrosion inhibition has extensively used green chemistry concepts and principles, especially in the last several decades. Considering the toxicity of inorganic inhibitors, organic compounds, primarily heterocycles, have emerged as one of the most effective, economical, and valuable substitutes. The development of environmentally benign and sustainable alternatives has advanced significantly due to the drawbacks of utilizing organic corrosion inhibitors, particularly their extreme environmental toxicity. This entails using various eco-friendly corrosion protection methods, materials, and procedures. Toxicology, bioaccumulation, and biodegradability are three indicators of the sustainability of a chemical. Thus, to evaluate the sustainability indices, OSPAR

and REACH have established some standards. The lethal concentration ( $LD_{50}$ ) and effective concentration ( $EC_{50}$ ), which represent the concentration of a species that adversely affects the growth of 50% of the living population and kills 50% of the living population, respectively, are two ways to quantify the toxicity of a species. A chemical species may be considered green or harmless if its  $LC_{50}/EC_{50}$  value is  $10 \text{ mg kg}^{-1}$  (oral, rat) or higher. The natural degradability of the impacted species is a further sustainability factor. If a chemical species dissolves 60% or more in 28 days, it can be considered eco-friendly according to the OSPAR and REACH regulations. The partition coefficient ( $\log K_{OW}$  or  $D^{OW}$ ) is the primary metric to measure bioaccumulation.  $\log K_{OW}$  or  $D^{OW}$  is typically calculated using a water and octanol mixture, which should be less than 3 for a non-bioaccumulative species.

Among the natural green corrosion inhibitors, various bio-based resources are used as sustainable building materials, including plant extracts, natural polymers, gums, waste, amino acids, and carbohydrates. They are the most excellent eco-friendly alternatives given their natural nature, biodegradability, and lack of accumulation. However, their industrial usage is restricted because of their sensitivity to deterioration at high temperatures. Furthermore, obtaining, processing, and preparing extracts often requires significant work, time, and money. Consequently, the preparation and application of bio-based materials cannot be considered a cost-effective method, especially for extracts from species and decorative plants with a specific distribution. However, semi-synthetic substances such as carbohydrates (chitosan, cellulose, *etc.*) and amino acids derivatives that have undergone chemical modification have significantly improved long-term and effective corrosion inhibition. The development and application of organic compounds resulting from MW and US irradiation with and without the addition of MCRs have been widely studied. Future research on the usage of semi-synthetic chemicals, particularly those produced by MW and US irradiation in conjunction with MCRs, is warranted, given their many positive green attributes. Sustainable corrosion protection has also made tremendous progress using relatively safer chemicals such as ionic liquids and biodegradable synthetic polymers. Poly(vinyl alcohol) (PVA), poly(amino acids) (PAA), poly(lactic acid) (PLA), poly(caprolactone) (PCL), poly(malic acid) (PMA) and poly(ethylene glycol) (PEG) are among the biodegradable synthetic polymers (BDSPs) that are widely employed in corrosion prevention. However, there are drawbacks to using them as well. These materials are expensive and not advised for further research because of the increased cost of using costly catalysts, solvents, and chemicals.

In long-term corrosion prevention, the synergism (efficiency improvement) and self-healing (efficiency and durability improvement) have also significantly increased. Urea and thiourea are two hazardous chemical compounds employed to increase the corrosion inhibition potential of other metal cations and toxic organic compounds. However, only a small number of studies examined the impact of environmentally friendly synergists such as amino acids on the ability of

organic inhibitors to stop corrosion. This calls for further research. Computational modeling and simulations have recently been recognized as potent, successful, economical, and environmentally friendly methods for evaluating the potential inhibition of organic inhibitors. Before being synthesized, the potential of a compound as an inhibitor can be assessed based on its effectiveness, solubility, toxicity, adsorption potential, additive effects, orientation on the metallic surface, charge-sharing molecular sites, etc. Although computational modeling and simulations are frequently used in assessing inhibition potential and supporting the experimental %IE, they occasionally need to improve their ability to forecast the features of the actual environment.

## Author contributions

Conception: Mumtaz A. Quraishi, Priyabrata Banerjee and Akram AlFantazi; Writing first draft: Chandrabhan Verma, Ruby Aslam, Dheeraj Singh Chauhan, Jeenat Aslam, Taiwo W. Quadri, Saman Zehra and Dakeshwar Kumar Verma. Editing: Shikha Dubey, Tahir Rasheed and Chandrabhan Verma. Submission and correspondence: Chandrabhan Verma.

## Conflicts of interest

There are no conflicts to declare.

## References

- 1 M. Uerdingen, C. Treber, M. Balsler, G. Schmitt and C. Werner, *Green Chem.*, 2005, **7**, 321–325.
- 2 G. Koch, *Trends in oil and gas corrosion research and technologies*, 2017, pp. 3–30.
- 3 C. Verma, *Handbook of science & engineering of green corrosion inhibitors: modern theory, fundamentals & practical applications*, Elsevier, 2021.
- 4 R. Ganjoo, S. Sharma, C. Verma, M. Quraishi and A. Kumar, *Int. J. Biol. Macromol.*, 2023, 123571.
- 5 R. Ganjoo, C. Verma, A. Kumar and M. Quraishi, *Adv. Colloid Interface Sci.*, 2022, 102832.
- 6 M. Stranick, *Corrosion*, 1984, **40**, 296–302.
- 7 J. Godinez-Alvarez, J. L. Mora-Mendoza, E. Rodriguez-Betancourt, G. Zavala-Olivares and M. A. Gonzalez-Nunez, NACE CORROSION, NACE-04412, NACE, 2004.
- 8 M. A. A. Ali, *Inhibition of mild steel corrosion in cooling systems by low and non toxic corrosion inhibitors* (Doctoral Dissertation), The University of Manchester, United Kingdom, 2017.
- 9 C. Verma, A. Thakur, R. Ganjoo, S. Sharma, H. Assad, A. Kumar, M. Quraishi and A. Alfantazi, *Coord. Chem. Rev.*, 2023, **488**, 215177.
- 10 E. D. Akpan, O. Dagdag and E. E. Ebenso, *Coord. Chem. Rev.*, 2023, **489**, 215207.
- 11 C. Verma, A. Alfantazi, M. Quraishi and K. Y. Rhee, *Coord. Chem. Rev.*, 2023, **495**, 215385.
- 12 A. Miralrio and A. Espinoza Vázquez, *Processes*, 2020, **8**, 942.
- 13 A. Zakeri, E. Bahmani and A. S. R. Aghdam, *Corros. Commun.*, 2022, **5**, 25–38.
- 14 S. H. Alrefaee, K. Y. Rhee, C. Verma, M. Quraishi and E. E. Ebenso, *J. Mol. Liq.*, 2021, **321**, 114666.
- 15 S. A. Umoren and U. M. Eduok, *Carbohydr. Polym.*, 2016, **140**, 314–341.
- 16 M. Shahini, B. Ramezanzadeh and H. E. Mohammadloo, *J. Mol. Liq.*, 2021, **325**, 115110.
- 17 L. Hamadi, S. Mansouri, K. Oulmi and A. Kareche, *Egypt. J. Pet.*, 2018, **27**, 1157–1165.
- 18 D. Zhang, B. Xie, L. X. Gao, Q. Cai, H. G. Joo and K. Y. Lee, *Thin Solid Films*, 2011, **520**, 356–361.
- 19 C. Verma, C. M. Hussain, M. Quraishi and A. Alfantazi, *Adv. Colloid Interface Sci.*, 2022, 102822.
- 20 C. Verma, E. E. Ebenso, M. Quraishi and C. M. Hussain, *Mater. Adv.*, 2021, **2**, 3806–3850.
- 21 C. Verma, J. Haque, M. Quraishi and E. E. Ebenso, *J. Mol. Liq.*, 2019, **275**, 18–40.
- 22 C. Verma, M. Quraishi and E. E. Ebenso, *Sustainable Chem. Pharm.*, 2018, **10**, 134–147.
- 23 S. M. Powell, H. McMurray and D. Worsley, *Corrosion*, 1999, **55**, 1040–1051.
- 24 H. Wang and J. Zheng, *Corros. Sci. Prot. Technol.*, 2002, **14**, 275–279.
- 25 A. N. Kabra, M.-K. Ji, J. Choi, J. R. Kim, S. P. Govindwar and B.-H. Jeon, *Environ. Sci. Pollut. Res.*, 2014, **21**, 12270–12278.
- 26 M. Sun, H. Lin, W. Guo, F. Zhao and J. Li, *J. Ocean Univ. China*, 2017, **16**, 1167–1174.
- 27 J. Greenwood, *Br. J. Political Sci.*, 2007, **37**, 333–357.
- 28 A. Kaban, W. Mayangsari, M. Anwar, A. Maksun, T. Adityawarman, J. W. Soedarsono and A. Ridhova, *East-Eur. J. Enterp. Technol.*, 2022, **5**, 119.
- 29 W. P. Dinter, *Federal Agency for Nature Conservation*, Bonn, Germany, 2001, vol. 167.
- 30 P. Heslenfeld and E. L. Enserink, *ICES J. Mar. Sci.*, 2008, **65**, 1392–1397.
- 31 A. Castano, M. Cantarino, P. Castillo and J. Tarazona, *Chemosphere*, 1996, **32**, 2141–2157.
- 32 J. Hermens, H. Canton, N. Steyger and R. Wegman, *Aquat. Toxicol.*, 1984, **5**, 315–322.
- 33 A. L. Parra, R. S. Yhebra, I. G. Sardiñas and L. I. Buela, *Phytomedicine*, 2001, **8**, 395–400.
- 34 A. Zakari and D. Kubmarawa, *Nat. Prod. Chem. Res.*, 2016, **4**, 2.
- 35 M. D. Summers, S. L. Blunk and B. M. Jenkins, *Ecological Building Network*, 2003.
- 36 R. Wedmann, I. Ivanovic-Burmazovic and M. R. Filipovic, *Interface Focus*, 2017, **7**, 20160139.
- 37 J. M. Conder, R. A. Hoke, W. d. Wolf, M. H. Russell and R. C. Buck, *Environ. Sci. Technol.*, 2008, **42**, 995–1003.

- 38 S. A. van der Heijden and M. T. Jonker, *Environ. Sci. Technol.*, 2009, **43**, 8854–8859.
- 39 W. M. Meylan, P. H. Howard, R. S. Boethling, D. Aronson, H. Printup and S. Gouchie, *Environ. Toxicol. Chem.*, 1999, **18**, 664–672.
- 40 A. Thakur and A. Kumar, *J. Bio-Tribo-Corros.*, 2021, **7**, 1–48.
- 41 M. Lavanya and A. A. Machado, *Sci. Total Environ.*, 2023, 168407.
- 42 J. Panchal, D. Shah, R. Patel, S. Shah, M. Prajapati and M. Shah, *J. Bio-Tribo-Corros.*, 2021, **7**, 107.
- 43 A. Jmiai, A. Tara, S. El Issami, M. Hilali, O. Jbara and L. Bazzi, *J. Mol. Liq.*, 2021, **322**, 114509.
- 44 P. van Gelder, P. Klaassen, B. Taebi, B. Walhout, R. van Ommen, I. van de Poel, Z. Robaey, L. Asveld, R. Balkenende and F. Hollmann, *Int. J. Environ. Res. Public Health*, 2021, **18**, 6329.
- 45 M. Damej, S. Skal, J. Aslam, M. Zouarhi, H. Erramli, A. A. Alrashdi, H.-S. Lee and H. Lgaz, *Colloids Surf., A*, 2022, **643**, 128745.
- 46 C. Verma, A. Alfantazi, M. A. Quraishi and K. Y. Rhee, *Sustainable Chem. Pharm.*, 2023, **31**, 100943.
- 47 J. Aslam, M. Mobin, Huda, A. Aslam and R. Aslam, *Int. J. Environ. Sci. Technol.*, 2023, **20**, 2441–2454.
- 48 D. Darling and R. Rakshpal, CORROSION NACE, NACE, 1998.
- 49 N. Chaubey, A. Qurashi, D. S. Chauhan and M. Quraishi, *J. Mol. Liq.*, 2021, **321**, 114385.
- 50 G. Koch, in *Trends in Oil and Gas Corrosion Research and Technologies*, ed. A. M. El-Sherik, Woodhead Publishing, Boston, 2017, pp. 3–30. DOI: [10.1016/B978-0-08-101105-8.00001-2](https://doi.org/10.1016/B978-0-08-101105-8.00001-2).
- 51 G. R. Meira, C. Andrade, C. Alonso, I. Padaratz and z. J. Borba, *Corros. Sci.*, 2008, **50**, 2724–2731.
- 52 B. A. Al Jahdaly, Y. R. Maghraby, A. H. Ibrahim, K. R. Shouier, A. M. Alturki and R. M. El-Shabasy, *Mater. Today Sustainability*, 2022, **20**, 100242.
- 53 M. M. Khalaf, A. H. Tantawy, K. A. Soliman and H. M. Abd El-Lateef, *J. Mol. Struct.*, 2020, **1203**, 127442.
- 54 N. A. Basheer, A. A. Ali, R. H. Allawi and A. A. Mashaf, *Chem. Pap.*, 2023, **77**, 1655–1667.
- 55 V. S. Sastri, *Green corrosion inhibitors: theory and practice*, John Wiley & Sons, 2012.
- 56 P. Anastas and N. Eghbali, *Chem. Soc. Rev.*, 2010, **39**, 301–312.
- 57 R. A. Sheldon, *Green Chem.*, 2014, **16**, 950–963.
- 58 A. Gałuszka, Z. Migaszewski and J. Namieśnik, *TrAC, Trends Anal. Chem.*, 2013, **50**, 78–84.
- 59 S. Marzorati, L. Verotta and S. P. Trasatti, *Molecules*, 2018, **24**, 48.
- 60 A. Thakur, S. Sharma, R. Ganjoo, H. Assad and A. Kumar, *Mater. Today: Proc.*, 2022, **66**, 609–621.
- 61 N. Winterton, *Clean Technol. Environ. Policy*, 2021, **23**, 2499–2522.
- 62 J. H. Clark, A. Hunt, C. Topi, G. Paggiola and J. Sherwood, *Sustainable Solvents: Perspectives from Research, Business and International Policy*, Royal Society of Chemistry, 2017.
- 63 V. Hessel, N. N. Tran, M. R. Asrami, Q. D. Tran, N. V. D. Long, M. Escribà-Gelonch, J. O. Tejada, S. Linke and K. Sundmacher, *Green Chem.*, 2022, **24**, 410–437.
- 64 F. A. Etzkorn, *Green chemistry: Principles and case studies*, Royal Society of Chemistry, 2019.
- 65 W. Carroll, S. A. Green, H. Plaumann, M. Straka, L. Putman, L. Kolopajlo, M. Mio and M. Kerr, *Sustainable Green Chemistry*, Walter de Gruyter GmbH & Co KG, 2017.
- 66 B. Borah, K. D. Dwivedi, B. Kumar and L. R. Chowhan, *Arabian J. Chem.*, 2022, **15**, 103654.
- 67 R. A. Sheldon, *Green Chem.*, 2017, **19**, 18–43.
- 68 J. Haque, V. Srivastava, D. S. Chauhan, M. Quraishi, A. M. Kumar and H. Lgaz, *Sustainable Chem. Pharm.*, 2020, **16**, 100260.
- 69 R. A. Sheldon, *Chem. Soc. Rev.*, 2012, **41**, 1437–1451.
- 70 R. D. Rogers and K. R. Seddon, *Ionic liquids: industrial applications for green chemistry*, ACS Publications, 2002.
- 71 J. Haque, V. Srivastava, M. A. Quraishi, D. S. Chauhan, H. Lgaz and I.-M. Chung, *Corros. Sci.*, 2020, **172**, 108665.
- 72 A. Badawi and I. Fahim, *Int. J. Corros. Scale Inhib.*, 2021, **10**, 1385–1406.
- 73 D. Wang, Y. Li, B. Chen and L. Zhang, *Chem. Eng. J.*, 2020, **402**, 126219.
- 74 R. Farahati, S. M. Mousavi-Khoshdel, A. Ghaffarinejad and H. Behzadi, *Prog. Org. Coat.*, 2020, **142**, 105567.
- 75 Q. Zhang, B. Hou, Y. Li, G. Zhu, Y. Lei, X. Wang, H. Liu and G. Zhang, *Chem. Eng. J.*, 2021, **424**, 130519.
- 76 O. Ogunleye, A. Arinkoola, O. Eletta, O. Agbede, Y. Osho, A. Morakinyo and J. Hamed, *Heliyon*, 2020, **6**, e03205.
- 77 R. Aslam, M. Mobin, I. B. Obot and A. H. Alamri, *J. Mol. Liq.*, 2020, **318**, 113982.
- 78 M. Abdallah, H. Altass, A. S. Al-Gorair, J. H. Al-Fahemi, B. Jahdaly and K. Soliman, *J. Mol. Liq.*, 2021, **323**, 115036.
- 79 S. A. Umoren and M. M. Solomon, *J. Environ. Chem. Eng.*, 2017, **5**, 246–273.
- 80 Y. Zhu, Q. Sun, Y. Wang, J. Tang, Y. Wang and H. Wang, *Corros. Sci.*, 2021, **185**, 109414.
- 81 S. Umoren and M. Solomon, *J. Ind. Eng. Chem.*, 2015, **21**, 81–100.
- 82 M. Djellab, H. Bentrach, A. Chala and H. Taoui, *Mater. Corros.*, 2019, **70**, 149–160.
- 83 G. K. Shamnamol, J. M. Jacob, P. Rugma and J. R. Anoop Raj, *J. Adhes. Sci. Technol.*, 2021, **35**, 133–163.
- 84 C. Verma, E. E. Ebenso and M. Quraishi, *J. Mol. Liq.*, 2017, **248**, 927–942.
- 85 F. Zhang, P. Ju, M. Pan, D. Zhang, Y. Huang, G. Li and X. Li, *Corros. Sci.*, 2018, **144**, 74–88.
- 86 L. Veleva, *Paint and Coating Testing Manual*, 2012, pp. 282–299.
- 87 N. A. Awang, W. N. Wan Salleh, F. Aziz, N. Yusof and A. F. Ismail, *J. Chem. Technol. Biotechnol.*, 2023, **98**, 22–44.
- 88 Y. L. Kobzar and K. Fatyeyeva, *Chem. Eng. J.*, 2021, **425**, 131480.
- 89 S. Z. Salleh, A. H. Yusoff, S. K. Zakaria, M. A. A. Taib, A. A. Seman, M. N. Masri, M. Mohamad, S. Mamat, S. A. Sobri and A. Ali, *J. Cleaner Prod.*, 2021, **304**, 127030.

- 90 M. Ramezanzadeh, G. Bahlakeh, B. Ramezanzadeh and Z. Sanaei, *J. Ind. Eng. Chem.*, 2019, **77**, 323–343.
- 91 A. M. Vaysburd and P. H. Emmons, *Cem. Concr. Compos.*, 2004, **26**, 255–263.
- 92 G. Palanisamy, *Corrosion inhibitors*, 2019, pp. 1–24.
- 93 R. B. Rebak and T. E. Perez, NACE CORROSION, 2017, NACE-2017-8933.
- 94 M. Asadian, M. Sabzi and S. M. Anijdan, *Int. J. Press. Vessels Pip.*, 2019, **171**, 184–193.
- 95 I. B. Obot, A. A. Sorour, C. Verma, T. A. Al-Khaldi and A. S. Rushaid, *Eng. Fail. Anal.*, 2022, 107008.
- 96 C. Verma and M. Quraishi, *Coord. Chem. Rev.*, 2021, **446**, 214105.
- 97 C. Verma, L. O. Olasunkanmi, E. E. Ebenso, M. A. Quraishi and I. B. Obot, *J. Phys. Chem. C*, 2016, **120**, 11598–11611.
- 98 C. Verma, E. E. Ebenso and M. Quraishi, *J. Mol. Liq.*, 2020, **316**, 113874.
- 99 D. S. Chauhan, C. Verma and M. Quraishi, *J. Mol. Struct.*, 2021, **1227**, 129374.
- 100 A. A. Al-Amiery, W. N. R. W. Isahak and W. K. Al-Azzawi, *Lubricants*, 2023, **11**, 174.
- 101 W. R. de Souza Morais, J. S. da Silva, N. M. P. Queiroz, C. L. de Paiva e Silva Zanta, A. S. Ribeiro and J. Tonholo, *Appl. Sci.*, 2023, **13**, 7482.
- 102 K. M. O. G. Lipiar and A. J. M. Mohammad, in *Corrosion Inhibitors*, ed. S. Ambrish, IntechOpen, Rijeka, 2019, p. 5. DOI: [10.5772/intechopen.81376](https://doi.org/10.5772/intechopen.81376).
- 103 K. M. S. Newaz, W. J. Basirun, H. B. M. Ali, F. L. Faraj and G. M. Khan, *Int. J. Electrochem. Sci.*, 2015, **10**, 6120–6134.
- 104 A. Peter, I. Obot and S. K. Sharma, *Int. J. Ind. Chem.*, 2015, **6**, 153–164.
- 105 S. K. Sharma, A. Mudhoo, E. K. E. Khamis and G. Jain, *J. Corros. Sci. Eng.*, 2008, **11**, 1–14.
- 106 A. Rajasekar, S. Maruthamuthu, N. Palaniswamy and A. Rajendran, *Microbiol. Res.*, 2007, **162**, 355–368.
- 107 M. Mobin, M. Rizvi, L. O. Olasunkanmi and E. E. Ebenso, *ACS Omega*, 2017, **2**, 3997–4008.
- 108 D. S. Chauhan, M. A. Quraishi, H. Al-Qahtani and M. A. Jafar Mazumder, *Polymeric Corrosion Inhibitors for Greening the Chemical and Petrochemical Industry*, 2022, pp. 1–22.
- 109 M. A. A. Khan, O. M. Irfan, F. Djavaanroodi and M. Asad, *Sustainability*, 2022, **14**, 9502.
- 110 N. Al Otaibi and H. H. Hammud, *Molecules*, 2021, **26**, 7024.
- 111 F. Luborsky, *Amorphous metallic alloys*, 1983, vol. 1.
- 112 L. E. Shoemaker, *Superalloys*, 2005, **718**, 409–418.
- 113 Y. Sun, S. Tian, P. Ciaisi, Z. Zeng, J. Meng and Z. Zhang, *Nat. Commun.*, 2022, **13**, 297.
- 114 W. Chen, X. Yin and D. Ma, *Appl. Energy*, 2014, **136**, 1174–1183.
- 115 Z. Liu, Y. Geng, S. Lindner and D. Guan, *Energy*, 2012, **45**, 1059–1068.
- 116 G. Q. Chen and B. Zhang, *Energy Policy*, 2010, **38**, 6180–6193.
- 117 R. Clémençon, *J. Environ. Dev.*, 2016, **25**, 3–24.
- 118 R. Kumar and A. K. Sharma, *Uttar Pradesh J. Zool.*, 2020, **41**, 1–8.
- 119 P. W. Griffin and G. P. Hammond, *Glob Transit.*, 2021, **3**, 72–86.
- 120 E. Mousa, C. Wang, J. Riesbeck and M. Larsson, *Renewable Sustainable Energy Rev.*, 2016, **65**, 1247–1266.
- 121 H. Musleman, X. Liang, K. Kaesehage, F. Ascui and J. Wilson, *J. Cleaner Prod.*, 2021, **315**, 128127.
- 122 A. Dömling, *Chem. Rev.*, 2006, **106**, 17–89.
- 123 M. S. Singh and S. Chowdhury, *RSC Adv.*, 2012, **2**, 4547–4592.
- 124 R. C. Cioc, E. Ruijter and R. V. A. Orru, *Green Chem.*, 2014, **16**, 2958–2975.
- 125 C. Capello, U. Fischer and K. Hungerbühler, *Green Chem.*, 2007, **9**, 927–934.
- 126 D. K. Verma, S. Kaya, E. Ech-chihbi, F. El-Hajjaji, M. M. Phukan and H. M. Alnashiri, *J. Mol. Liq.*, 2021, **329**, 115531.
- 127 O. S. Shehata, L. A. Korshed and A. Attia, *Corrosion inhibitors, principles and recent applications*, 2018, vol. 121.
- 128 C. Verma, E. E. Ebenso, I. Bahadur and M. A. Quraishi, *J. Mol. Liq.*, 2018, **266**, 577–590.
- 129 K. Khanari, M. Finšgar, M. K. Hrnčič, U. Maver, Ž. Knez and B. Seiti, *RSC Adv.*, 2017, **7**, 27299–27330.
- 130 J. Buchweishaija, *Tanz. J. Sci.*, 2009, **35**, 77–92.
- 131 S. Ghareba and S. Omanovic, *Corros. Sci.*, 2010, **52**, 2104–2113.
- 132 Z. Shang and J. Zhu, *J. Mater. Res. Technol.*, 2021, **15**, 5078–5094.
- 133 B. El Ibrahim, *Colloid Interface Sci. Commun.*, 2020, **37**, 100279.
- 134 K. Alaoui, M. Ouakki, A. S. Abousalem, H. Serrar, M. Galai, S. Derbali, K. Nouneh, S. Boukhris, M. E. Touhami and Y. El Kacimi, *J. Bio-Tribo-Corros.*, 2018, **5**, 1.
- 135 S. Mo, L. J. Li, H. Q. Luo and N. B. Li, *J. Mol. Liq.*, 2017, **242**, 822–830.
- 136 Y. M. Abdallah, *J. Mol. Liq.*, 2016, **219**, 709–719.
- 137 M. Yadav, T. K. Sarkar and I. B. Obot, *RSC Adv.*, 2016, **6**, 110053–110069.
- 138 Y. Li, S. Zhang, Q. Ding, D. Feng, B. Qin and L. Hu, *Tribol. Int.*, 2017, **114**, 121–131.
- 139 Y. Guo, B. Xu, Y. Liu, W. Yang, X. Yin, Y. Chen, J. Le and Z. Chen, *J. Ind. Eng. Chem.*, 2017, **56**, 234–247.
- 140 P. Arellanes-Lozada, O. Olivares-Xometl, N. V. Likhanova, I. V. Lijanova, J. R. Vargas-García and R. E. Hernández-Ramírez, *J. Mol. Liq.*, 2018, **265**, 151–163.
- 141 F. A. Azeez, O. A. Al-Rashed and A. A. Nazeer, *J. Mol. Liq.*, 2018, **265**, 654–663.
- 142 S. Cao, D. Liu, T. Wang, A. Ma, C. Liu, X. Zhuang, H. Ding, B. B. Mamba and J. Gui, *Colloids Surf., A*, 2021, **616**, 126280.
- 143 V. Saraswat and M. Yadav, *ChemistrySelect*, 2020, **5**, 7347–7357.
- 144 Y. Ye, D. Yang, H. Chen, S. Guo, Q. Yang, L. Chen, H. Zhao and L. Wang, *J. Hazard. Mater.*, 2020, **381**, 121019.



- 145 J.-j. Fu, S.-n. Li, Y. Wang, X.-d. Liu and L.-D. Lu, *J. Mater. Sci.*, 2011, **46**, 3550–3559.
- 146 P. Muthukrishnan, B. Jeyaprabha, P. Tharmaraj and P. Prakash, *Res. Chem. Intermed.*, 2015, **41**, 5961–5984.
- 147 A. Ousslim, K. Bekkouch, B. Hammouti, A. Elidrissi and A. Aouniti, *J. Appl. Electrochem.*, 2009, **39**, 1075–1079.
- 148 M. I. Awad, *J. Appl. Electrochem.*, 2006, **36**, 1163–1168.
- 149 V. Rajeswari, D. Kesavan, M. Gopiraman and P. Viswanathamurthi, *J. Surfactants Deterg.*, 2013, **16**, 571–580.
- 150 M. Yadav, D. Behera, S. Kumar and R. R. Sinha, *Ind. Eng. Chem. Res.*, 2013, **52**, 6318–6328.
- 151 R. Aslam, M. Mobin, S. Zehra, I. B. Obot and E. E. Ebenso, *ACS Omega*, 2017, **2**, 5691–5707.
- 152 P. Ekins and D. Zenghelis, *Sustainability Sci.*, 2021, **16**, 949–965.
- 153 P. Bolouri, R. Salami, S. Kouhi, M. Kordi, B. Asgari Lajayer, J. Hadian and T. Astatkie, *Molecules*, 2022, **27**(24), 8999.
- 154 X. Li, S. Deng and H. Fu, *Prog. Org. Coat.*, 2010, **67**, 420–426.
- 155 N. Hossain, M. Aminul Islam and M. Asaduzzaman Chowdhury, *Results Chem.*, 2023, **5**, 100883.
- 156 R. M. Saleh, A. A. Ismail and A. A. El Hosary, *Br. Corros. J.*, 1982, **17**, 131–135.
- 157 K. Srivastav and P. Srivastava, *Br. Corros. J.*, 1981, **16**, 221–223.
- 158 F. S. de Souza, C. Giacomelli, R. S. Gonçalves and A. Spinelli, *Mater. Sci. Eng., C*, 2012, **32**, 2436–2444.
- 159 H. Wang, M. Gao, Y. Guo, Y. Yang and R. Hu, *Desalination*, 2016, **398**, 198–207.
- 160 E. Khamis and N. AlAndis, *Mater. Werkst.*, 2002, **33**, 550–554.
- 161 A. Y. El-etre, *Corros. Sci.*, 1998, **40**, 1845–1850.
- 162 A. Y. El-Etre and M. Abdallah, *Corros. Sci.*, 2000, **42**, 731–738.
- 163 R. A. L. Sathiyathan, S. Maruthamuthu, M. Selvanayagam, S. Mohanan and N. Palaniswamy, *Indian J. Chem. Technol.*, 2005, **12**, 356–360.
- 164 A. Hamdy and N. S. El-Gendy, *Egypt. J. Pet.*, 2013, **22**, 17–25.
- 165 T. Ibrahim, H. Alayan and Y. A. Mowaqet, *Prog. Org. Coat.*, 2012, **75**, 456–462.
- 166 A. Ait Aghzzaf, D. Veys-Renaux and E. Rocca, *Mater. Corros.*, 2020, **71**, 148–154.
- 167 H. Ashassi-Sorkhabi, S. Mirzaee, T. Rostamikia and R. Bagheri, *Int. J. Corros.*, 2015, **2015**, 197587.
- 168 A. Harouat, A. Bezzar and L. Sail, *Eur. J. Environ. Civ. Eng.*, 2023, 1–34, DOI: [10.1080/19648189.2023.2220788](https://doi.org/10.1080/19648189.2023.2220788).
- 169 A. Buyuksagis, M. Dilek and M. Kargioglul, *Prot. Met. Phys. Chem. Surf.*, 2015, **51**, 861–872.
- 170 H. Nazari Mehdi, J. Yu and X. Shi, *J. Mater. Civ. Eng.*, 2020, **32**, 04020281.
- 171 R. Saratha and V. G. Vasudha, *E-J. Chem.*, 2010, **7**, 162375.
- 172 A. Saxena, K. K. Thakur, K. K. Saxena, S. Chambyal and A. Sharma, *Mater. Today: Proc.*, 2020, **26**, 1360–1367.
- 173 D. Prabhu, P. R. Prabhu and P. Rao, *Chem. Pap.*, 2021, **75**, 653–667.
- 174 E. E. Oguzie, M. A. Chidiebere, K. L. Oguzie, C. B. Adindu and H. Momoh-Yahaya, *Chem. Eng. Commun.*, 2014, **201**, 790–803.
- 175 S. Sutthiruangwong, C. Wongpaiboon, N. Sritha and N. Anukulkich, *Metals*, 2023, **13**, 262.
- 176 R. Haldhar, D. Prasad and N. Bhardwaj, *Arab. J. Sci. Eng.*, 2020, **45**, 131–141.
- 177 P. B. Raja and M. G. Sethuraman, *Mater. Lett.*, 2008, **62**, 113–116.
- 178 A. Pal and C. Das, *Ind. Crops Prod.*, 2020, **151**, 112468.
- 179 A. Singh, V. K. Singh and M. A. Quraishi, *Int. J. Corros.*, 2010, **2010**, 275983.
- 180 M. Kliškić, J. Radošević, S. Gudić and V. Katalinić, *J. Appl. Electrochem.*, 2000, **30**, 823–830.
- 181 M. Abdallah, *Port. Electrochim. Acta*, 2004, **22**, 161–175.
- 182 S. Martinez and I. Štern, *J. Appl. Electrochem.*, 2001, **31**, 973–978.
- 183 E. E. Oguzie, *Pigm. Resin Technol.*, 2005, **34**, 321–326.
- 184 G. O. Awwiri and F. O. Igho, *Mater Lett.*, 2003, **57**, 3705–3711.
- 185 L. R. Chauhan and G. Gunasekaran, *Corros. Sci.*, 2007, **49**, 1143–1161.
- 186 K. O. Orubite and N. C. Oforka, *Mater. Lett.*, 2004, **58**, 1768–1772.
- 187 B. Müller, *Corros. Sci.*, 2002, **44**, 1583–1591.
- 188 A. Bouyanzer, B. Hammouti and L. Majidi, *Mater. Lett.*, 2006, **60**, 2840–2843.
- 189 A. Chetouani, B. Hammouti and M. Benkaddour, *Pigm. Resin Technol.*, 2004, **33**, 26–31.
- 190 R. T. Loto and O. Olowoyo, *Procedia Manuf.*, 2019, **35**, 310–314.
- 191 E. Chaieb, A. Bouyanzer, B. Hammouti and M. Benkaddour, *Appl. Surf. Sci.*, 2005, **246**, 199–206.
- 192 E. E. Oguzie, *Corros. Sci.*, 2007, **49**, 1527–1539.
- 193 E. E. Oguzie, *Mater. Chem. Phys.*, 2006, **99**, 441–446.
- 194 A. Y. El-Etre, M. Abdallah and Z. E. El-Tantawy, *Corros. Sci.*, 2005, **47**, 385–395.
- 195 A. Y. El-Etre, *Appl. Surf. Sci.*, 2006, **252**, 8521–8525.
- 196 A. Y. El-Etre, *Corros. Sci.*, 2003, **45**, 2485–2495.
- 197 A. Y. El-Etre, *Corros. Sci.*, 2001, **43**, 1031–1039.
- 198 Y. Li, P. Zhao, Q. Liang and B. Hou, *Appl. Surf. Sci.*, 2005, **252**, 1245–1253.
- 199 F. Zucchi and I. H. Omar, *Surf. Technol.*, 1985, **24**, 391–399.
- 200 M. I. Awad, *J. Appl. Electrochem.*, 2006, **36**, 1163–1168.
- 201 B. Monica and S. Ioan, *J. Biotechnol. Biomed. Sci.*, 2018, **1**, 35–43.
- 202 R. T. Loto and A. Busari, *IOP Conf. Ser.: Mater. Sci. Eng.*, 2020, **770**, 012046.
- 203 M. Bendahou, M. Benabdellah and B. Hammouti, *Pigm. Resin Technol.*, 2006, **35**, 95–100.
- 204 I. Dhoubi, F. Masmoudi, M. Bouaziz and M. Masmoudi, *Arabian J. Chem.*, 2021, **14**, 102961.

- 205 K. Boumhara, H. Harhar, M. Tabyaoui, A. Bellaouchou, A. Guenbour and A. Zarrouk, *J. Bio-Tribo-Corros.*, 2018, **5**, 8.
- 206 N. Al-Akhras and Y. Mashaqbeh, *J. Build. Eng.*, 2021, **35**, 101848.
- 207 M. Znini, L. Majidi, A. Bouyanzer, J. Paolini, J. M. Desjobert, J. Costa and B. Hammouti, *Arabian J. Chem.*, 2012, **5**, 467–474.
- 208 M. Znini, G. Cristofari, L. Majidi, A. Ansari, A. Bouyanzer, J. Paolini, J. Costa and B. Hammouti, *Int. J. Electrochem. Sci.*, 2012, **7**, 3959–3981.
- 209 M. Mansouri, Y. El Ouadi, M. Znini, J. Costa, A. Bouyanzer, J. M. Desjobert and L. Majidi, *J. Mater. Environ. Sci.*, 2015, **6**, 631–646.
- 210 S. Andreani, M.-C. De Cian, J. Paolini, J.-M. Desjobert, J. Costa and A. Muselli, *Chem. Biodiversity*, 2013, **10**, 2061–2077.
- 211 D. B. Hmamou, R. Salghi, A. Zarrouk, H. Zarrouk, M. Errami, B. Hammouti, L. Afia, L. Bazzi and L. Bazzi, *Res. Chem. Intermed.*, 2013, **39**, 973–989.
- 212 T. Benabbouha, M. Siniti, H. El Attari, K. Chefira, F. Chibi, R. Nmila and H. Rchid, *J. Bio-Tribo-Corros.*, 2018, **4**, 39.
- 213 J. K. Patra and K.-H. Baek, *Molecules*, 2016, **21**(3), 388.
- 214 P. López, C. Sánchez, R. Batlle and C. Nerín, *J. Agric. Food Chem.*, 2007, **55**, 4348–4356.
- 215 S. Ağaoğlu, N. Dostbil and S. Alemdar, *Bull. Vet. Inst. Pulawy*, 2007, **51**, 53–57.
- 216 M. Boudalia, R. M. Fernández-Domene, M. Tabyaoui, A. Bellaouchou, A. Guenbour and J. García-Antón, *J. Mater. Res. Technol.*, 2019, **8**, 5763–5773.
- 217 O. Ouachikh, A. Bouyanzer, M. Bouklah, J. M. Desjobert, J. Costa, B. Hammouti and L. Majidi, *Surf. Rev. Lett.*, 2009, **16**, 49–54.
- 218 N. Hechiche, D. Boughrara, A. Kadri, N. Dahmani and N. Benbrahim, *Anal. Bioanal. Electrochem.*, 2019, **11**, 1129–1147.
- 219 W. Daoudi, A. El Aatiaoui, O. Dagdag, K. Zaidi, R. Haldhar, S.-C. Kim, A. Oussaid, A. Aouinti, A. Berisha, F. Benhiba, E. E. Ebenso and A. Oussaid, *Coatings*, 2023, **13**, 611.
- 220 M. Benabdellah, M. Benkaddour, B. Hammouti, M. Bendahhou and A. Aouniti, *Appl. Surf. Sci.*, 2006, **252**, 6212–6217.
- 221 K. Boumhara, F. Bentiss, M. Tabyaoui, J. Costa, J. M. Desjobert, A. Bellaouchou, A. Guenbour, B. Hammouti and S. S. Al-Deyab, *Int. J. Electrochem. Sci.*, 2014, **9**, 1187–1206.
- 222 K. Boumhara, M. Tabyaoui, C. Jama and F. Bentiss, *J. Ind. Eng. Chem.*, 2015, **29**, 146–155.
- 223 A. Hbika, A. Bouyanzer, M. Jalal, N. Setti, E. Loukili, A. Aouniti, Y. Kerroum, I. Warad, B. Hammouti and A. M. Zarrouk, *Anal. Bioanal. Electrochem.*, 2023, **15**, 17–35.
- 224 M. Ali, B. Kim, K. D. Belfield, D. Norman, M. Brennan and G. S. Ali, *Mater. Sci. Eng., C*, 2016, **58**, 359–365.
- 225 A. Belakhdar, H. Ferkous, S. Djellali, R. Sahraoui, H. Lahbib, Y. B. Amor, A. Erto, M. Balsamo and Y. Benguerba, *Colloids Surf., A*, 2020, **606**, 125458.
- 226 B. A. Al Jahdaly, *Arabian J. Chem.*, 2023, **16**, 104411.
- 227 R. T. Loto, *Results Phys.*, 2018, **8**, 172–179.
- 228 M. Tezeghdenti, L. Dhoubi and N. Etteyeb, *J. Bio-Tribo-Corros.*, 2015, **1**, 16.
- 229 R. Haldhar and D. Prasad, *J. Bio-Tribo-Corros.*, 2020, **6**, 48.
- 230 A. M. Abdel-Gaber, H. T. Rahal and F. T. Beqai, *Int. J. Ind. Chem.*, 2020, **11**, 123–132.
- 231 S. M. Z. Hossain, S. A. Razzak and M. M. Hossain, *Arab. J. Sci. Eng.*, 2020, **45**, 7137–7159.
- 232 A. Bouoidina, M. Chaouch, A. Abdellaoui, A. Lahkimi, B. Hammouti, F. El-Hajjaji, M. Taleb and A. Nahle, *Anti-Corros. Methods Mater.*, 2017, **64**, 563–572.
- 233 P. Parthipan, M. S. AlSalhi, S. Devanesan and A. Rajasekar, *Bioprocess Biosyst. Eng.*, 2021, **44**, 1441–1452.
- 234 L. El Hattabi, A. A. Guenbour, A. Ballaouchou and M. Tabyaoui, *Mor. J. Chem.*, 2016, **2016**, 4.
- 235 S. Maloy, in *Brenner's Encyclopedia of Genetics*, ed. S. Maloy and K. Hughes, Academic Press, San Diego, 2nd edn, 2013, pp. 108–110. DOI: [10.1016/B978-0-12-374984-0.00051-6](https://doi.org/10.1016/B978-0-12-374984-0.00051-6).
- 236 R. Malak, in *Introduction to Corrosion*, ed. S. Ambrish, IntechOpen, Rijeka, 2023, p. 3. DOI: [10.5772/intechopen.109816](https://doi.org/10.5772/intechopen.109816).
- 237 D.-Q. Zhang, Q.-R. Cai, L.-X. Gao and K. Y. Lee, *Corros. Sci.*, 2008, **50**, 3615–3621.
- 238 D. G. de Matos and C. C. Furnus, *Theriogenology*, 2000, **53**, 761–771.
- 239 M. B. Petrović, M. B. Radovanović, A. T. Simonović, S. M. Milić and M. M. Antonijević, *Int. J. Electrochem. Sci.*, 2012, **7**, 9043–9057.
- 240 A. T. Simonović, M. B. Petrović, M. B. Radovanović, S. M. Milić and M. M. Antonijević, *Chem. Pap.*, 2014, **68**, 362–371.
- 241 A. Aouniti, K. F. Khaled and B. Hammouti, *Int. J. Electrochem. Sci.*, 2013, **8**, 5925–5943.
- 242 Z. Zhang, G. Yan and L. Ruan, *Adv. Mater. Res.*, 2012, **415–417**, 964–967.
- 243 D. Bouzidi, A. Chetouani, B. Hammouti, S. Kertit, M. Taleb and S. S. Al-Deyab, *Int. J. Electrochem. Sci.*, 2012, **7**, 2334–2348.
- 244 R. Cui, N. Gu and C. Li, *Mater. Corros.*, 2011, **62**, 362–369.
- 245 A. D. Zapata-Loría and M. A. Pech-Canul, *Chem. Eng. Commun.*, 2014, **201**, 855–869.
- 246 A. A. Muhammad, A. Uzairu, J. F. Iyun and H. Abba, *IOSR J. Appl. Chem.*, 2014, **7**, 50–62.
- 247 H. Ashassi-Sorkhabi, Z. Ghasemi and D. Seifzadeh, *Appl. Surf. Sci.*, 2005, **249**, 408–418.
- 248 A. Yurt, G. Bereket and C. Ogretir, *J. Mol. Struct.: THEOCHEM*, 2005, **725**, 215–221.
- 249 A. Abdel Nazeer, N. K. Allam, G. I. Youssef and E. A. Ashour, *Ind. Eng. Chem. Res.*, 2011, **50**, 8796–8802.
- 250 G. M. A. El-Hafez and W. A. Badawy, *Electrochim. Acta*, 2013, **108**, 860–866.

- 251 G. Kılınççeker and H. Demir, *Prot. Met. Phys. Chem. Surf.*, 2013, **49**, 788–797.
- 252 D.-Q. Zhang, Q.-R. Cai, X.-M. He, L.-X. Gao and G.-D. Zhou, *Mater. Chem. Phys.*, 2008, **112**, 353–358.
- 253 G. Kılınççeker and H. Demir, *Anti-Corros. Methods Mater.*, 2013, **60**, 134–142.
- 254 D.-Q. Zhang, H. Wu and L.-X. Gao, *Mater. Chem. Phys.*, 2012, **133**, 981–986.
- 255 H. A. Rahman, A. Moustafa and M. Awad, *Int. J. Electrochem. Sci.*, 2012, **7**, 1266–1287.
- 256 M. Kuruvilla, S. John and A. Joseph, *Res. Chem. Intermed.*, 2013, **39**, 3531–3543.
- 257 D.-Q. Zhang, B. Xie, L.-X. Gao, Q.-R. Cai, H. G. Joo and K. Y. Lee, *Thin Solid Films*, 2011, **520**, 356–361.
- 258 L. Wang, X. Yin, W. Wang, L. Jin and Z. Li, *Int. J. Electrochem. Sci.*, 2014, **9**, 6088–6102.
- 259 N. V. Makarenko, U. V. Kharchenko and L. A. Zemnukhova, *Russ. J. Appl. Chem.*, 2011, **84**, 1362–1365.
- 260 M. A. Amin and K. Khaled, *Corros. Sci.*, 2010, **52**, 1194–1204.
- 261 D.-Q. Zhang, Q.-R. Cai, X.-M. He, L.-X. Gao and G. S. Kim, *Mater. Chem. Phys.*, 2009, **114**, 612–617.
- 262 K. M. Ismail, *Electrochim. Acta*, 2007, **52**, 7811–7819.
- 263 E. A. MacGregor, in *Encyclopedia of Physical Science and Technology*, ed. R. A. Meyers, Academic Press, New York, 3rd edn, 2003, pp. 207–245. DOI: [10.1016/B0-12-227410-5/00064-8](https://doi.org/10.1016/B0-12-227410-5/00064-8).
- 264 D. S. Chauhan, M. A. Quraishi, H. Al-Qahtani and M. A. Jafar Mazumder, in *Polymeric Corrosion Inhibitors for Greening the Chemical and Petrochemical Industry*, 2022, pp. 1–22. DOI: [10.1002/9783527835621.ch1](https://doi.org/10.1002/9783527835621.ch1).
- 265 M. H. Shahini, B. Ramezanzadeh and H. E. Mohammadloo, *J. Mol. Liq.*, 2021, **325**, 115110.
- 266 A. Toghan and A. Fawzy, *Polymers*, 2023, **15**(14), 3144.
- 267 C. P. Jiménez-Gómez and J. A. Cecilia, *Molecules*, 2020, **25**, 3981.
- 268 J. Scheerder, R. Breur, T. Slaghek, W. Holtman, M. Vennik and G. Ferrari, *Prog. Org. Coat.*, 2012, **75**, 224–230.
- 269 M. Moradi, Z. Song and T. Xiao, *J. Mater. Sci. Technol.*, 2018, **34**, 2447–2457.
- 270 M. Mobin and M. Rizvi, *Carbohydr. Polym.*, 2016, **136**, 384–393.
- 271 P. I. Murungi, A. A. Sulaimon, O. Ssembatya and P. Nwankwo, *SPE Nigeria Annual International Conference and Exhibition*, SPE, 2022, D021S007R003.
- 272 H. Ashassi-Sorkhabi and A. Kazempour, *Carbohydr. Polym.*, 2020, **237**, 116110.
- 273 P. A. Rasheed, A. Alfantazi, K. A. Jabbar and K. A. Mahmoud, *J. Bio-Tribo-Corros.*, 2021, **7**, 103.
- 274 Q. H. Zhang, N. Xu, Z. N. Jiang, H. F. Liu and G. A. Zhang, *J. Colloid Interface Sci.*, 2023, **640**, 1052–1067.
- 275 D. S. Chauhan, M. A. Quraishi, A. A. Sorour, S. K. Saha and P. Banerjee, *RSC Adv.*, 2019, **9**, 14990–15003.
- 276 N. K. Gupta, P. G. Joshi, V. Srivastava and M. A. Quraishi, *Int. J. Biol. Macromol.*, 2018, **106**, 704–711.
- 277 M. Srivastava, S. K. Srivastava, G. J. Nikhil and R. Prakash, *Int. J. Biol. Macromol.*, 2019, **140**, 177–187.
- 278 P. Kong, H. Feng, N. Chen, Y. Lu, S. Li and P. Wang, *RSC Adv.*, 2019, **9**, 9211–9217.
- 279 R. Menaka and S. Subhashini, *Polym. Int.*, 2017, **66**, 349–358.
- 280 S. A. Umoren, M. J. Banera, T. Alonso-Garcia, C. A. Gervasi and M. V. Mirifico, *Cellulose*, 2013, **20**, 2529–2545.
- 281 S. N. Dalhatu, K. A. Modu, A. A. Mahmoud, Z. U. Zango, A. B. Umar, F. Usman, J. O. Dennis, A. Alsadig, K. H. Ibrnaouf and O. A. Aldaghri, *Polymers*, 2023, **15**, 398.
- 282 M. A. Quraishi, K. R. Ansari, D. S. Chauhan, S. A. Umoren and M. A. J. Mazumder, *Cellulose*, 2020, **27**, 6425–6443.
- 283 W. Zhang, Y. Zhang, B. Li, H. Guo, X. Dou, K. Lu and Y. Feng, *Bioelectrochemistry*, 2023, **150**, 108330.
- 284 O. S. I. Fayomi, I. G. Akande and A. P. I. Popoola, *J. Bio-Tribo-Corros.*, 2018, **4**, 73.
- 285 I. G. Arwati, E. H. Majlan, S. Alva and W. Muhammad, *Energies*, 2022, **15**, 8511.
- 286 K. El Mouaden, B. El Ibrahim, R. Oukhrib, L. Bazzi, B. Hammouti, O. Jbara, A. Tara, D. S. Chauhan and M. A. Quraishi, *Int. J. Biol. Macromol.*, 2018, **119**, 1311–1323.
- 287 A. Jmiai, B. El Ibrahim, A. Tara, R. Oukhrib, S. El Issami, O. Jbara, L. Bazzi and M. Hilali, *Cellulose*, 2017, **24**, 3843–3867.
- 288 M. N. El-Haddad, *Int. J. Biol. Macromol.*, 2013, **55**, 142–149.
- 289 A. Jmiai, B. El Ibrahim, A. Tara, S. El Issami, O. Jbara and L. Bazzi, *J. Mol. Struct.*, 2018, **1157**, 408–417.
- 290 S. A. Umoren, M. M. Solomon and V. S. Saji, in *Polymeric Materials in Corrosion Inhibition*, ed. S. A. Umoren, M. M. Solomon and V. S. Saji, Elsevier, 2022, pp. 271–286. DOI: [10.1016/B978-0-12-823854-7.00014-X](https://doi.org/10.1016/B978-0-12-823854-7.00014-X).
- 291 P. Kesari, G. Udayabhanu, A. Roy and S. pal, *J. Ind. Eng. Chem.*, 2023, **122**, 303–325.
- 292 S. M. Tawfik, *RSC Adv.*, 2015, **5**, 104535–104550.
- 293 W. Zhang, B. Nie, H.-J. Li, Q. Li, C. Li and Y.-C. Wu, *Carbohydr. Polym.*, 2021, **260**, 117842.
- 294 I. B. Obot, I. B. Onyeachu and A. M. Kumar, *Carbohydr. Polym.*, 2017, **178**, 200–208.
- 295 M. Fardioui, M. Rbaa, F. Benhiba, M. Galai, T. Guedira, B. Lakhrissi, I. Warad and A. Zarrouk, *J. Mol. Liq.*, 2021, **323**, 114615.
- 296 M. Mariana, T. Alfatah, H. P. S. Abdul Khalil, E. B. Yahya, N. G. Olaiya, A. Nuryawan, E. M. Mistar, C. K. Abdullah, S. N. Abdulmadjid and H. Ismail, *J. Mater. Res. Technol.*, 2021, **15**, 2287–2316.
- 297 C. Gao, X. Zhao, P. Fatehi, X. Dong, K. Liu, S. Chen, S. Wang and F. Kong, *Ind. Crops Prod.*, 2021, **168**, 113585.
- 298 M. H. Hussin, A. A. Rahim, M. N. Mohamad Ibrahim and N. Brosse, *Measurement*, 2016, **78**, 90–103.
- 299 Y. Ren, Y. Luo, K. Zhang, G. Zhu and X. Tan, *Corros. Sci.*, 2008, **50**, 3147–3153.
- 300 M. H. Hussin, A. A. Rahim, M. N. Mohamad Ibrahim and N. Brosse, *Mater. Chem. Phys.*, 2015, **163**, 201–212.

- 301 J. J. Liao, N. H. A. Latif, D. Trache, N. Brosse and M. H. Hussin, *Int. J. Biol. Macromol.*, 2020, **162**, 985–1024.
- 302 L. Huang, W.-Q. Chen, S.-S. Wang, Q. Zhao, H.-J. Li and Y.-C. Wu, *Environ. Chem. Lett.*, 2022, **20**, 3235–3264.
- 303 R. C. Cioc, E. Ruijter and R. V. Orru, *Green Chem.*, 2014, **16**, 2958–2975.
- 304 M. Palomar-Pardavé, M. Romero-Romo, H. Herrera-Hernández, M. Abreu-Quijano, N. V. Likhanova, J. Uruchurtu and J. Juárez-García, *Corros. Sci.*, 2012, **54**, 231–243.
- 305 A. Singh, S. Thakur, B. Pani and G. Singh, *New J. Chem.*, 2018, **42**, 2113–2124.
- 306 J. Haque, V. Srivastava, D. S. Chauhan, H. Lgaz and M. A. Quraishi, *ACS Omega*, 2018, **3**, 5654–5668.
- 307 K. Ansari, M. Quraishi and A. Singh, *Corros. Sci.*, 2015, **95**, 62–70.
- 308 A. Singh, K. Ansari, P. Bedi, T. Pramanik, I. H. Ali, Y. Lin, P. Banerjee and S. Zamindar, *J. Phys. Chem. Solids*, 2023, **172**, 111064.
- 309 C. B. Verma, M. Quraishi and A. Singh, *J. Taiwan Inst. Chem. Eng.*, 2015, **49**, 229–239.
- 310 A. Singh, S. Thakur, B. Pani, B. Chugh, H. Lgaz, I.-M. Chung, P. Chaubey, A. Pandey and J. Singh, *J. Mol. Liq.*, 2019, **283**, 788–803.
- 311 S. B. Aoun and M. Messali, *Int. J. Electrochem. Sci.*, 2018, **13**, 3757–3776.
- 312 D. S. Chauhan, M. J. Mazumder, M. Quraishi, K. Ansari and R. Suleiman, *Int. J. Biol. Macromol.*, 2020, **158**, 231–243.
- 313 J. Haque, V. Srivastava, D. Chauhan, H. Lgaz and M. Quraishi, *ACS Omega*, 2018, **3**(5), 5654–5668.
- 314 C. Verma, P. Singh, I. Bahadur, E. Ebenso and M. Quraishi, *J. Mol. Liq.*, 2015, **209**, 767–778.
- 315 P. Singh, M. Quraishi, E. Ebenso and C. B. Verma, *Int. J. Electrochem. Sci.*, 2014, **9**, 7446–7459.
- 316 A. K. Singh, S. Thakur, B. Pani, E. E. Ebenso, M. A. Quraishi and A. K. Pandey, *ACS Omega*, 2018, **3**, 4695–4705.
- 317 A. Khanra, M. Srivastava, M. P. Rai and R. Prakash, *ACS Omega*, 2018, **3**, 12369–12382.
- 318 N. Palaniappan, I. Cole, F. Caballero-Briones, S. Manickam, K. J. Thomas and D. Santos, *RSC Adv.*, 2020, **10**, 5399–5411.
- 319 X. Luo, R. Bai, D. Zhen, Z. Yang, D. Huang, H. Mao, X. Li, H. Zou, Y. Xiang and K. Liu, *Ind. Crops Prod.*, 2019, **129**, 405–413.
- 320 C. He, X.-Q. Li, G.-L. Feng and W.-J. Long, *Green Chem.*, 2022, **24**, 5842–5855.
- 321 B. A. Al Jahdaly, M. F. Elsadek, B. M. Ahmed, M. F. Farahat, M. M. Taher and A. M. Khalil, *Sustainability*, 2021, **13**, 2127.
- 322 Y. Ye, D. Zhang, Y. Zou, H. Zhao and H. Chen, *J. Cleaner Prod.*, 2020, **264**, 121682.
- 323 Z. Xu, Y. Gan, J. Zeng, J. Chen, A. Fu, X. Zheng and W. Li, *Chem. Eng. J.*, 2023, 144425.
- 324 A. Mishra, C. Verma, S. Chauhan, M. Quraishi, E. E. Ebenso and V. Srivastava, *J. Bio-Tribo-Corros.*, 2018, **4**, 1–15.
- 325 K. Tanaka, *Solvent-free organic synthesis*, John Wiley & Sons, 2009.
- 326 K. Tanaka and F. Toda, *Chem. Rev.*, 2000, **100**, 1025–1074.
- 327 R. Dubadi and M. Jaroniec, *Nanomaterials*, 2023, **13**, 2262.
- 328 J. F. Fernandez-Bertran, *Pure Appl. Chem.*, 1999, **71**, 581–586.
- 329 K. Tkáčová, *Mechanical activation of minerals*, Elsevier, Amsterdam, Tokyo New York, NY, 1989.
- 330 A. D. McNaught and A. Wilkinson, *Compendium of Chemical Terminology: IUPAC Recommendations, IUPAC Chemical Data Series*, 1997.
- 331 S. L. James and T. Friščić, *Chem. Soc. Rev.*, 2013, **42**, 7494–7496.
- 332 T. Friščić, C. Mottillo and H. M. Titi, *Angew. Chem.*, 2020, **132**, 1030–1041.
- 333 J.-L. Do and T. Friščić, *ACS Cent. Sci.*, 2017, **3**, 13–19.
- 334 A. Stolle, T. Szuppa, S. E. Leonhardt and B. Ondruschka, *Chem. Soc. Rev.*, 2011, **40**, 2317–2329.
- 335 V. Martinez, T. Stolar, B. Karadeniz, I. Brekalo and K. Užarević, *Nat. Rev. Chem.*, 2023, **7**, 51–65.
- 336 R. R. Bolt, J. A. Leitch, A. C. Jones, W. I. Nicholson and D. L. Browne, *Chem. Soc. Rev.*, 2022, **51**, 4243–4260.
- 337 R. Laskar, T. Pal, T. Bhattacharya, S. Maiti, M. Akita and D. Maiti, *Green Chem.*, 2022, **24**, 2296–2320.
- 338 F. Penteado, B. Monti, L. Sancineto, G. Perin, R. G. Jacob, C. Santi and E. J. Lenardão, *Asian J. Org. Chem.*, 2018, **7**, 2368–2385.
- 339 T. Kimura, in *Sonochemistry and the Acoustic Bubble*, Elsevier, 2015, ch. 171, pp. 171–186.
- 340 D. C. Martin, J. Chen, J. Yang, L. F. Drummy and C. Kübel, *J. Polym. Sci., Part B: Polym. Phys.*, 2005, **43**, 1749–1778.
- 341 A. Tiusanen, J. Ruiz-Jimenez, K. Hartonen and S. K. Wiedmer, *Environ. Sci.: Process. Impacts*, 2023, **25**, 1263–1287.
- 342 S. Hwang, S. Grätz and L. Borchardt, *Chem. Commun.*, 2022, **58**, 1661–1671.
- 343 K. Vanchinathan, G. Bhagavannarayana, K. Muthu and S. Meenakshisundaram, *Phys. B*, 2011, **406**, 4195–4199.
- 344 A. I. Vogel, *Practical Organic Chemistry*, 5th edn, 1956.
- 345 B. Ahmed, R. A. Khan and M. Keshari, *Tetrahedron Lett.*, 2009, **50**, 2889–2892.
- 346 N. K. Gupta, C. Verma, R. Salghi, H. Lgaz, A. Mukherjee and M. Quraishi, *New J. Chem.*, 2017, **41**, 13114–13129.
- 347 C. Verma, M. Quraishi, E. Ebenso, I. Obot and A. El Assyry, *J. Mol. Liq.*, 2016, **219**, 647–660.
- 348 C. Verma, P. Singh and M. Quraishi, *J. Assoc. Arab Univ. Basic Appl. Sci.*, 2016, **21**, 24–30.
- 349 H. G. Alvim, E. N. da Silva Junior and B. A. Neto, *RSC Adv.*, 2014, **4**, 54282–54299.
- 350 M. Puripat, R. Ranzani, M. Hatanaka, W. Parasuk, V. Parasuk and K. Morokuma, *J. Org. Chem.*, 2015, **80**, 6959–6967.

- 351 A. Stadler and C. O. Kappe, *J. Comb. Chem.*, 2001, **3**, 624–630.
- 352 C. Verma, J. Haque, M. A. Quraishi and E. E. Ebenso, *J. Mol. Liq.*, 2018, **275**, 18–40.
- 353 M. A. Quraishi, D. S. Chauhan and V. S. Saji, *Heterocyclic Organic Corrosion Inhibitors: Principles and Applications*, Elsevier Inc., Amsterdam, 2020.
- 354 C. Verma, M. A. Quraishi and D. S. Chauhan, *Green Corrosion Inhibition: Fundamentals, Design, Synthesis and Applications*, Royal Society of Chemistry, 2022.
- 355 P. Singh, E. E. Ebenso, L. O. Olasunkanmi, I. Obot and M. A. Quraishi, *J. Phys. Chem. C*, 2016, **120**, 3408–3419.
- 356 C. G. Neochoritis, T. Zarganes-Tzitzikas, K. Katsampoxaki-Hodgetts and A. Dömling, *J. Chem. Educ.*, 2020, **97**, 3739–3745.
- 357 N. Isambert, M. d. M. S. Duque, J.-C. Plaquevent, Y. Genisson, J. Rodriguez and T. Constantieux, *Chem. Soc. Rev.*, 2011, **40**, 1347–1357.
- 358 S. Vidyacharan, A. H. Shinde, B. Satpathi and D. S. Sharada, *Green Chem.*, 2014, **16**, 1168–1175.
- 359 C. S. Graebin, F. V. Ribeiro, K. R. Rogério and A. E. Kümmerle, *Curr. Org. Synth.*, 2019, **16**, 855–899.
- 360 C. Verma, M. Quraishi, K. Kluza, M. Makowska-Janusik, L. O. Olasunkanmi and E. E. Ebenso, *Sci. Rep.*, 2017, **7**, 44432.
- 361 C. Verma, L. O. Olasunkanmi, E. E. Ebenso, M. A. Quraishi and I. Obot, *J. Phys. Chem. C*, 2016, **120**, 11598–11611.
- 362 D. K. Yadav, B. Maiti and M. A. Quraishi, *Corros. Sci.*, 2010, **52**, 3586–3598.
- 363 J. Haque, K. Ansari, V. Srivastava, M. A. Quraishi and I. Obot, *J. Ind. Eng. Chem.*, 2017, **49**, 176–188.
- 364 R. González-Olvera, V. Román-Rodríguez, G. E. Negrón-Silva, A. Espinoza-Vázquez, F. J. Rodríguez-Gómez and R. Santillan, *Molecules*, 2016, **21**, 250.
- 365 K. R. Ansari, M. A. Quraishi and A. Singh, *Measurement*, 2015, **76**, 136–147.
- 366 T. Kitanosono, K. Masuda, P. Xu and S. Kobayashi, *Chem. Rev.*, 2018, **118**, 679–746.
- 367 R. A. Sheldon and D. Brady, *ChemSusChem*, 2019, **12**, 2859–2881.
- 368 B. H. Lipshutz, S. Ghorai and M. Cortes-Clerget, *Chem. – Eur. J.*, 2018, **24**, 6672–6695.
- 369 T. Kitanosono and S. Kobayashi, *Chem. – Eur. J.*, 2020, **26**, 9408–9429.
- 370 F. Zhou, Z. Hearne and C.-J. Li, *Curr. Opin. Green Sustain. Chem.*, 2019, **18**, 118–123.
- 371 T. Sahoo, J. Panda, J. Sahu, D. Sarangi, S. K. Sahoo, B. Nanda and R. Sahu, *Curr. Org. Synth.*, 2020, **17**, 426–439.
- 372 E. Breynaert, M. Houllberghs, S. Radhakrishnan, G. Grübel, F. Taulelle and J. A. Martens, *Chem. Soc. Rev.*, 2020, **49**, 2557–2569.
- 373 C. O. Kappe, *Angew. Chem., Int. Ed.*, 2004, **43**, 6250–6284.
- 374 C. O. Kappe, *Chem. Soc. Rev.*, 2008, **37**, 1127–1139.
- 375 C. Verma, M. A. Quraishi and E. E. Ebenso, *Sustainable Chem. Pharm.*, 2018, **10**, 134–147.
- 376 P. Dohare, K. Ansari, M. Quraishi and I. Obot, *J. Ind. Eng. Chem.*, 2017, **52**, 197–210.
- 377 C. Verma, L. Olasunkanmi, I. Obot, E. E. Ebenso and M. A. Quraishi, *RSC Adv.*, 2016, **6**, 15639–15654.
- 378 K. R. Ansari, Sudheer, A. Singh and M. A. Quraishi, *J. Dispersion Sci. Technol.*, 2015, **36**, 908–917.
- 379 C. Verma, M. A. Quraishi and A. Singh, *J. Taibah Univ. Sci.*, 2016, **10**, 718–733.
- 380 P. Singh, V. Srivastava and M. A. Quraishi, *J. Mol. Liq.*, 2016, **216**, 164–173.
- 381 M. Tobiszewski, *Anal. Methods*, 2016, **8**, 2993–2999.
- 382 F. Pena-Pereira, A. Kloskowski and J. Namieśnik, *Green Chem.*, 2015, **17**, 3687–3705.
- 383 T. Khezeli, A. Daneshfar and R. Sahraei, *Talanta*, 2016, **150**, 577–585.
- 384 Ł. Marcinkowski, F. Pena-Pereira, A. Kloskowski and J. Namieśnik, *TrAC, Trends Anal. Chem.*, 2015, **72**, 153–168.
- 385 D. L. Rocha, A. D. Batista, F. R. Rocha, G. L. Donati and J. A. Nobrega, *TrAC, Trends Anal. Chem.*, 2013, **45**, 79–92.
- 386 R. K. Henderson, A. P. Hill, A. M. Redman and H. F. Sneddon, *Green Chem.*, 2015, **17**, 945–949.
- 387 T. R. Sekharan, R. M. Chandira, S. Tamilvanan, S. Rajesh and B. Venkateswarlu, *Biointerface Res. Appl. Chem.*, 2022, **12**, 847–860.
- 388 S. V. Dzyuba and R. A. Bartsch, *Angew. Chem., Int. Ed.*, 2003, **42**, 148–150.
- 389 H. Zhao, S. Xia and P. Ma, *J. Chem. Technol. Biotechnol.*, 2005, **80**, 1089–1096.
- 390 C. G. Yoo, Y. Pu and A. J. Ragauskas, *Curr. Opin. Green Sustain. Chem.*, 2017, **5**, 5–11.
- 391 D. S. Chauhan, F. El-Hajjaji and M. Quraishi, in *Ionic Liquid-Based Technologies for Environmental Sustainability*, 2022, ch. 18, pp. 279–294. DOI: [10.1016/B978-0-12-824545-3.00018-0](https://doi.org/10.1016/B978-0-12-824545-3.00018-0).
- 392 X. Zeng, X. Zheng, L. Guo, Q. Xu, H. Huang and B. Tan, *J. Mol. Liq.*, 2021, **324**, 115063.
- 393 D. Lozowski, *Chem. Eng.*, 2010, **117**, 15.
- 394 X. Meng, Y. Wang, A. J. Conte, S. Zhang, J. Ryu, J. J. Wie, Y. Pu, B. H. Davison, C. G. Yoo and A. J. Ragauskas, *Bioresour. Technol.*, 2022, **368**, 128280.
- 395 S. Dahiya, A. N. Kumar, J. S. Sravan, S. Chatterjee, O. Sarkar and S. V. Mohan, *Bioresour. Technol.*, 2018, **248**, 2–12.
- 396 F. Nemati, M. M. Hosseini and H. Kiani, *J. Saudi Chem. Soc.*, 2016, **20**, S503–S508.
- 397 M. A. Quraishi, K. R. Ansari, D. K. Yadav and E. E. Ebenso, *Int. J. Electrochem. Sci.*, 2012, **7**, 12301–12315.
- 398 P. Singh, A. Singh and M. A. Quraishi, *J. Taiwan Inst. Chem. Eng.*, 2016, **60**, 588–601.
- 399 I. B. Onyeachu, D. S. Chauhan, M. Quraishi and I. Obot, *Corros. Eng., Sci. Technol.*, 2020, **56**, 154–161.
- 400 P. Singh, D. S. Chauhan, S. S. Chauhan, G. Singh and M. A. Quraishi, *J. Mol. Liq.*, 2019, **298**, 112051.

- 401 M. Vafaezadeh and H. Alinezhad, *J. Mol. Liq.*, 2016, **218**, 95–105.
- 402 R. A. Sheldon, *J. Mol. Catal. A: Chem.*, 2016, **422**, 3–12.
- 403 C. Verma, L. Olasunkanmi, I. B. Obot, E. E. Ebenso and M. A. Quraishi, *RSC Adv.*, 2016, **6**, 15639–15654.
- 404 M. Quraishi and R. Sardar, *Corrosion*, 2002, **58**, 748–755.
- 405 C. Verma, M. A. Quraishi, L. Olasunkanmi and E. E. Ebenso, *RSC Adv.*, 2015, **5**, 85417–85430.
- 406 D. K. Yadav and M. A. Quraishi, *Ind. Eng. Chem. Res.*, 2012, **51**, 14966–14979.
- 407 M. Bahrami, S. Hosseini and P. Pilvar, *Corros. Sci.*, 2010, **52**, 2793–2803.
- 408 M. Kurian and A. Paul, *Carbon Trends*, 2021, **3**, 100032.
- 409 N. Chaubey, A. Qurashi, D. S. Chauhan and M. Quraishi, *J. Mol. Liq.*, 2020, 114385, DOI: [10.1016/j.molliq.2020.114385](https://doi.org/10.1016/j.molliq.2020.114385).
- 410 K. E. Mouaden, D. S. Chauhan, M. Quraishi, L. Bazzi and M. Hilali, *Int. J. Biol. Macromol.*, 2020, **164**, 3709–3717.
- 411 M. A. Quraishi, D. S. Chauhan and V. S. Saji, *J. Mol. Liq.*, 2021, **341**, 117265.
- 412 OECD, Test No. 301: Ready Biodegradability, OECD Guidelines for the Testing of Chemicals, Section 3, 1992, DOI: [10.1787/9789264070349-en](https://doi.org/10.1787/9789264070349-en).
- 413 OECD, Guidance Document on Acute Oral Toxicity Testing, Organization for Economic Cooperation and Development, Paris, France, 1987, DOI: [10.1787/20777876](https://doi.org/10.1787/20777876).
- 414 OECD, Test No. 117: Partition Coefficient (n-octanol/water), HPLC Method, 2004, DOI: [10.1787/9789264069824-en](https://doi.org/10.1787/9789264069824-en).
- 415 D. S. Chauhan, M. Quraishi and A. Qurashi, *J. Mol. Liq.*, 2021, **326**, 115117.
- 416 C. T. Ser, P. Žuvela and M. W. Wong, *Appl. Surf. Sci.*, 2020, **512**, 145612.
- 417 K. Rasheeda, D. Vijaya, P. Krishnaprasad and S. Samshuddin, *Int. J. Corros. Scale Inhib.*, 2018, **7**, 48–61.
- 418 M. Yadav, R. R. Sinha, T. K. Sarkar and N. Tiwari, *J. Adhes. Sci. Technol.*, 2015, **29**, 1690–1713.
- 419 M. B. P. Mihajlović, M. B. Radovanović, Ž. Tasić and M. M. Antonijević, *J. Mol. Liq.*, 2017, **225**, 127–136.
- 420 M. ElBelghiti, Y. Karzazi, A. Dafali, B. Hammouti, F. Bentiss, I. Obot, I. Bahadur and E.-E. Ebenso, *J. Mol. Liq.*, 2016, **218**, 281–293.
- 421 J. Seetharaman, E. A. Reny, D. A. Johnson, K. B. Sawant and V. Sivaswamy, *Google Patents*, 2021.
- 422 M. A. Quraishi, W. Khan and M. Ajmal, *J. Electrochem. Soc. India*, 1997, **46**, 133–138.
- 423 M. A. Quraishi, W. Khan, M. Ajmal, S. Muralidharan and S. V. Iyer, *J. Appl. Electrochem.*, 1996, **26**, 1253–1258.
- 424 M. Quraishi and F. A. Ansari, *J. Appl. Electrochem.*, 2006, **36**, 309–314.
- 425 M. Albini, P. Letardi, L. Mathys, L. Brambilla, J. Schröter, P. Junier and E. Joseph, *Corros. Sci.*, 2018, **143**, 84–92.
- 426 C. Gattinoni and A. Michaelides, *Faraday Discuss.*, 2015, **180**, 439–458.
- 427 I. Obot and U. M. Edouk, *J. Mol. Liq.*, 2017, **246**, 66–90.
- 428 I. Obot, A. Madhankumar, S. Umoren and Z. Gasem, *J. Adhes. Sci. Technol.*, 2015, **29**, 2130–2152.
- 429 K. R. Ansari, S. Ramkumar, D. S. Chauhan, M. Salman, D. Nalini, V. Srivastava and M. A. Quraishi, *Int. J. Corros. Scale Inhib.*, 2018, **7**, 443–459.
- 430 S. Hadisaputra, S. Hamdiani, M. A. Kurniawan and N. Nuryono, *Indones. J. Chem.*, 2017, **17**, 431–438.
- 431 D. S. Chauhan, M. Quraishi, V. Srivastava, J. Haque and B. El Ibrahimy, *J. Mol. Struct.*, 2021, **1226**, 129259.
- 432 A. Jha and A. Kumar, *Bioprocess Biosyst. Eng.*, 2019, **42**, 1893–1901.
- 433 S. A. Umoren, M. M. Solomon, A. Madhankumar and I. B. Obot, *Carbohydr. Polym.*, 2020, **230**, 115466.
- 434 S. A. Umoren and M. M. Solomon, *Prog. Mater. Sci.*, 2019, **104**, 380–450.
- 435 D. S. Chauhan, M. J. Mazumder, M. A. Quraishi, K. Ansari and R. Suleiman, *Int. J. Biol. Macromol.*, 2020, **158**, 231–243.
- 436 D. S. Chauhan, M. J. Mazumder, M. A. Quraishi and K. Ansari, *Int. J. Biol. Macromol.*, 2020, **158**, 127–138.
- 437 M. A. Quraishi, K. R. Ansari, D. S. Chauhan, S. A. Umoren and M. A. J. Mazumder, *Cellulose*, 2020, **27**, 6425–6443.
- 438 S. A. Al Kiey, M. S. Hasanin and S. Dacrory, *J. Mol. Liq.*, 2021, **338**, 116604.
- 439 H. M. Abd El-Lateef, W. Albokheet and M. Gouda, *Cellulose*, 2020, **27**, 8039–8057.
- 440 C. Wang, C. Zou and Y. Cao, *J. Mol. Struct.*, 2021, **1228**, 129737.
- 441 A. Altin, M. Krzywiecki, A. Sarfraz, C. Toparli, C. Laska, P. Kerger, A. Zeradhan, K. J. Mayrhofer, M. Rohwerder and A. Erbe, *Beilstein J. Nanotechnol.*, 2018, **9**, 936–944.
- 442 L. Sihem, B. Abderrahim, B. Brahim, M. Asma, T. Lahcene and S. Marzorati, *Appl. Sci.*, 2019, **9**, 4684.
- 443 E. D. Paul, A. F. Egbuniwe and P. A. Ekwumemgbor, *ATBU J. Sci., Technol. Educ.*, 2018, **6**, 176–182.
- 444 M. M. Solomon, H. Gerengi and S. A. Umoren, *ACS Appl. Mater. Interfaces*, 2017, **9**, 6376–6389.
- 445 M. M. Solomon, H. Gerengi, T. Kaya and S. A. Umoren, *ACS Sustainable Chem. Eng.*, 2016, **5**, 809–820.
- 446 D. S. Chauhan, A. M. Kumar and M. A. Quraishi, *Chem. Eng. Res. Des.*, 2019, **150**, 99–115.
- 447 I. B. Onyeachu, D. S. Chauhan, K. R. Ansari, I. Obot, M. A. Quraishi and A. H. Alamri, *New J. Chem.*, 2019, **43**, 7282–7293.
- 448 J. Haque, V. Srivastava, M. A. Quraishi, D. S. Chauhan, H. Lgaz and I.-M. Chung, *Corros. Sci.*, 2020, **172**, 108665.
- 449 J. Haque, V. Srivastava, C. Verma and M. A. Quraishi, *J. Mol. Liq.*, 2017, **225**, 848–855.
- 450 F. El-Hajjaji, R. Salim, M. Taleb, F. Benhiba, N. Rezki, D. S. Chauhan and M. Quraishi, *Surf. Interfaces*, 2021, **22**, 100881.
- 451 F. El-Hajjaji, E. Ech-chihbi, N. Rezki, F. Benhiba, M. Taleb, D. S. Chauhan and M. Quraishi, *J. Mol. Liq.*, 2020, **314**, 113737.
- 452 M. Fisher, in *Lehninger Principles of Biochemistry*, ed. D. L. Nelson and M. M. Cox, 2001.
- 453 G. Gece, *Corros. Sci.*, 2011, **53**, 3873–3898.

- 454 C. Verma, D. S. Chauhan and M. A. Quraishi, *J. Mater. Environ. Sci.*, 2017, **8**, 4040–4051.
- 455 P. Dohare, D. S. Chauhan, A. A. Sorour and M. A. Quraishi, *Mater. Discovery*, 2017, **9**, 30–41.
- 456 P. Dohare, D. S. Chauhan, B. Hammouti and M. A. Quraishi, *Anal. Bioanal. Electrochem.*, 2017, **9**, 762.
- 457 P. Singh, D. S. Chauhan, K. Srivastava, V. Srivastava and M. A. Quraishi, *Int. J. Ind. Chem.*, 2017, **8**, 363–372.
- 458 P. Dohare, D. S. Chauhan and M. A. Quraishi, *Int. J. Corros. Scale Inhib.*, 2018, **7**, 25–37.
- 459 N. Vaszilcsin, V. Ordodi and A. Borza, *Int. J. Pharm.*, 2012, **431**, 241–244.
- 460 J. Salimon, N. Salih and E. Yousif, *Arabian J. Chem.*, 2012, **5**, 135–145.
- 461 P. Gallezot, *Chem. Soc. Rev.*, 2012, **41**, 1538–1558.
- 462 R. Aslam, M. Mobin, J. Aslam, A. Aslam, S. Zehra and S. Masroor, *Adv. Colloid Interface Sci.*, 2021, 102481.
- 463 Y. Zhu, M. L. Free, R. Woollam and W. Durnie, *Prog. Mater. Sci.*, 2017, **90**, 159–223.
- 464 M. Deyab, *J. Mol. Liq.*, 2020, **309**, 113107.
- 465 S. Gurjar, S. K. Sharma, A. Sharma and S. Ratnani, *Appl. Surf. Sci. Adv.*, 2021, **6**, 100170.
- 466 M. A. Quraishi and J. Rawat, *Corros. Rev.*, 2001, **19**, 273–299.
- 467 M. Ajmal, J. Rawat and M. A. Quraishi, *Anti-Corros. Methods Mater.*, 1998, **45**, 419–425.
- 468 A. Singh, Y. Lin, I. Obot, E. E. Ebenso, K. Ansari and M. A. Quraishi, *Appl. Surf. Sci.*, 2015, **356**, 341–347.
- 469 F. Bentiss, M. Lebrini, H. Vezin, F. Chai, M. Traisnel and M. Lagrené, *Corros. Sci.*, 2009, **51**, 2165–2173.
- 470 M. Lebrini, M. Lagrenée, H. Vezin, M. Traisnel and F. Bentiss, *Corros. Sci.*, 2007, **49**, 2254–2269.
- 471 A. M. El-Shamy and S. M. Mouneir, *J. Bio-Tribo-Corros.*, 2023, **9**, 3.
- 472 N. Vaszilcsin, A. Kellenberger, M. L. Dan, D. A. Duca and V. L. Ordodi, *Materials*, 2023, **16**, 5555.
- 473 S. Tanwer and S. K. Shukla, *Curr. Res. Green Sustainable Chem.*, 2022, **5**, 100227.
- 474 C. N. Njoku, T. U. Maduoma, W. Emori, R. E. Odey, B. M. Unimke, E. Yakubu, C. C. Anorundu, D. I. Uduwua, O. C. Njoku and K. B. Oyoh, *Pigm. Resin Technol.*, 2023, DOI: [10.1108/PRT-07-2023-0063](https://doi.org/10.1108/PRT-07-2023-0063).
- 475 S. Sharma, R. Ganjoo, S. Kumar and A. Kumar, *International Conference on Chemical, Bio and Environmental Engineering, Chm*: Springer International Publishing, 2021, pp. 1071–1082.
- 476 M. Ajiriyanto, S. Yudanto and F. Susetyo, *Int. J. Corros. Scale Inhib.*, 2023, **12**, 258–274.
- 477 A. I. Ikeuba, J. E. Ntibi, P. C. Okafor, B. I. Ita, A. U. Agobi, F. C. Asogwa, B. J. Omang, E. A. Eno, H. Loius and S. A. Adalikwu, *Results Chem.*, 2023, **5**, 100909.
- 478 F. Han, Z. Gong, R. Wang and S. Dang, *Int. J. Electrochem. Sci.*, 2023, **18**, 100319.
- 479 H. Dong, L. Ding, B. Ran, Y. Song, R. Wang, L. Zhao and Y. Niu, *Int. J. Electrochem. Sci.*, 2023, 100250.
- 480 S. El Harrari, S. Ayoub, D. Takky and Y. Naimi, *J. Electrochem. Sci. Eng.*, 2023, DOI: [10.5599/jese.1867](https://doi.org/10.5599/jese.1867).
- 481 K. A. Alamry, A. Khan, J. Aslam, M. A. Hussein and R. Aslam, *Sci. Rep.*, 2023, **13**, 6724.
- 482 A. N. Abd and E. S. Nasif, *AIP Conf. Proc.*, 2023, 2475, 1.
- 483 C. Merimi, B. Hammouti, K. Zaidi, B. Hafez, H. Elmsellem, R. Touzani and S. Kaya, *J. Mol. Struct.*, 2023, **1278**, 134883.
- 484 M. Abdallah, K. A. Soliman, M. Alfakeer, H. Hawsawi, A. M. Al-bonayan, S. S. Al-Juaid, S. Abd El Wanees and M. S. Motawea, *ACS Omega*, 2023, **8**(38), 34516–34533.
- 485 M. Hammi, C. Lazrak, Y. Ziat, O. Ifguis and H. Belkhanchi, *S. Afr. J. Chem. Eng.*, 2023, **44**, 265–275.
- 486 G. Swetha and H. Sachin, *Inorg. Chem. Commun.*, 2023, **155**, 111082.
- 487 G. Swetha, H. Sachin and J. R. Choudhuri, *Emergent Mater.*, 2023, 1–20.
- 488 L. C. Isaiah and N. B. Iroha, *World Sci. News*, 2023, **177**, 51–67.
- 489 R. Narang, P. Vashishth, H. Bairagi, S. K. Shukla and B. Mangla, *J. Mol. Liq.*, 2023, **384**, 122277.
- 490 M. M. Motawea and S. Melhi, *J. Indian Chem. Soc.*, 2023, **100**, 101013.
- 491 A. Belafhaili, M. El Hawary, A. Bellaouchou, A. Guenbour, I. Warad and A. M. Zarrouk, *Anal. Bioanal. Electrochem.*, 2023, **15**, 118–136.
- 492 F. Abeng, B. Ita, V. Anadebe, V. Chukwuike, K. Etiowo, P. Nkom, O. Ekerenam, N. Iroha and I. Ikot, *Results Eng.*, 2023, **17**, 100924.
- 493 N. B. Iroha, V. C. Anadebe, N. J. Maduelosi, L. A. Nnanna, L. C. Isaiah, O. Dagdag, A. Berisha and E. E. Ebenso, *Colloids Surf., A*, 2023, **660**, 130885.
- 494 A. I. Ikeuba, A. U. Agobi, L. Hitler, B. J. Omang, F. C. Asogwa, I. Benjamin, T. Unimuke and M. C. Udoinyang, *Chem. Afr.*, 2023, **6**, 983–997.
- 495 S. Abd El Maksoud, A. el Aziz Fouda, and H. Badawy, 2023, DOI: [10.21203/rs.3.rs-3306604/v1](https://doi.org/10.21203/rs.3.rs-3306604/v1).
- 496 N. B. Iroha, N. J. Maduelosi and L. A. Nnanna, *Emergent Mater.*, 2023, **6**, 137–146.
- 497 S. Sharma, R. Ganjoo, A. Thakur, H. Assad, S. Kaya and A. Kumar, *AIP Conf. Proc.*, 2023, **2800**, 020024.
- 498 L. Huang, W. Liu, J. Shen and Q. Liao, *Thin Solid Films*, 2023, **782**, 140005.
- 499 S. Eid, K. A. Soliman, A. El-Etre, E. Gad and H. Nady, *J. Bio-Tribo-Corros.*, 2023, **9**, 61.
- 500 A. A. Keshk, N. H. Elsayed, F. M. Almutairi, M. Al-Anazi, S. Said, H. M. Althurwi, R. K. Albalawi and M. El-Aassar, *Biomass Convers. Biorefin.*, 2023, 1–14.
- 501 M. Deyab, O. A. El-Shamy, H. K. Thabet and A. M. Ashmawy, *Sci. Rep.*, 2023, **13**, 8680.
- 502 B. Nie, J. Yan, S. Shi, L.-J. Wang, Y.-C. Wu and H.-J. Li, *J. Mater. Res. Technol.*, 2023, **23**, 3665–3675.
- 503 R. S. A. Hameed, S. Obeidat, M. Qureshi, S. Al-Mhyawi, E. H. Aljuhani and M. Abdallah, *J. Mater. Res. Technol.*, 2022, **21**, 2743–2756.
- 504 R. Abdel Hameed, M. Faride, M. Othman, B. Huwaimel, S. Al-Mhyawi, A. Shamroukh, F. Alshammary, E. Aljuhani and M. Abdallah, *Green Chem. Lett. Rev.*, 2022, **15**, 847–862.

- 505 R. K. Mehta and M. Yadav, *Mater. Sci. Eng., B*, 2023, **295**, 116566.
- 506 L. Feng, S. Zhang, Y. Zhou, R. Pan, H. Du, F. Liu and Y. Yang, *Crystals*, 2023, **13**, 205.
- 507 I. Martinović, Z. Pilić, G. Zlatić, V. Soldo and M. Šego, *Int. J. Electrochem. Sci.*, 2023, 100238.
- 508 M. R. Barrodi, A. Mirzaee, A. Kafashan, S. Zahedifard, H. J. Majidi, A. Davoodi and S. Hosseinpour, *Mater. Today Commun.*, 2023, **34**, 105390.
- 509 S. A. Mrani, N. Arrousse, R. Haldhar, A. A. Lahcen, A. Amine, T. Saffaj, S.-C. Kim and M. Taleb, *Lubricants*, 2022, **10**, 43.
- 510 C. Beltran-Perez, A. A. Serrano, G. Solís-Rosas, A. Martínez-Jiménez, R. Orozco-Cruz, A. Espinoza-Vázquez and A. Miralrio, *Int. J. Mol. Sci.*, 2022, **23**, 5086.
- 511 F. E. Abeng and V. C. Anadebe, *Comput. Theor. Chem.*, 2023, 114334.
- 512 A. Ehsani and E. Kamali Ardakani, *J. Bio-Tribo-Corros.*, 2022, **8**, 93.
- 513 S. Hossain, S. Razzak and M. Hossain, *Arab. J. Sci. Eng.*, 2020, **45**, 7137–7159.
- 514 A. Hamdouch, A. Anejjar, L. Bijla, S. Gharby, A. Asdadi, B. Chebli, R. Salghi and L. I. Hassani, *Mor. J. Chem.*, 2023, **11**(1), 105–118.
- 515 M. Kemel, D. Zama, S. Benayache, J.-C. Chalchat, G. Figueredo, P. Chalard and F. Benayache, *Chem. Afr.*, 2022, **5**, 1015–1025.
- 516 S. Cherrad, A. A. Alrashdi, H.-S. Lee, H. Lgaz, B. Satrani, M. Ghanmi and A. Chaouch, *Arabian J. Chem.*, 2022, **15**, 103849.
- 517 F. Simescu-Lazar, S. Slaoui, M. Essahli, F. Bohr, A. Lamiri, L. Vanoye and J. P. Chopart, *Lubricants*, 2023, **11**, 56.
- 518 K. Dahmani, M. Galai, A. Ech-chebab, M. Ouakki, L. Kadiri, A. Elgendy, R. Ez-Zriouli and M. Cherkaoui, *J. Appl. Electrochem.*, 2022, **52**, 1629–1646.
- 519 L. Koursaoui, Y. Kerroum, M. Tabyaoui, A. Guenbour, A. Bellaouchou, A. M. Zarrouk, I. Warad, B. Satrani, M. Ghanmi and E. Aouane, *Anal. Bioanal. Electrochem.*, 2023, **15**, 198–213.
- 520 A. R. Simović, B. N. Grgur, J. Novaković, P. Janačković and J. Bajat, *Metals*, 2023, **13**, 508.
- 521 R. T. Loto, O. Osamudiamé, A. C. Nissi, O. O. Oluwakayode, U. V. Oghoho, O. C. Daniel, I. P. Smart, P.-A. C. Lemuel and O. R. Nwabeze, *J. Bio-Tribo-Corros.*, 2023, **9**, 19.
- 522 R. Shanmugapriya, M. Ravi, S. Ravi, M. Ramasamy and A. Maruthapillai, *Inorg. Chem. Commun.*, 2023, **154**, 110958.
- 523 G. Beniaich, M. Beniken, R. Salim, N. Arrousse, E. Ech-chihbi, Z. Rais, A. Sadiq, H.-A. Nafidi, Y. A. Bin Jordan and M. Bourhia, *Separations*, 2023, **10**, 396.
- 524 M. Damej, S. Skal, J. Aslam, M. Zouarhi, H. Erramli, A. A. Alrashdi, H.-S. Lee, Y. El aoufir and H. Lgaz, *Colloids Surf., A*, 2022, **643**, 128745.
- 525 W. Daoudi, A. El Aatiaoui, N. Falil, M. Azzouzi, A. Berisha, L. O. Olasunkanmi, O. Dagdag, E. E. Ebenso, M. Koudad and A. Aouinti, *J. Mol. Liq.*, 2022, **363**, 119839.
- 526 R. Ihamdane, M. Tiskar, B. Outemsaa, L. Zelmat, O. Dagdag, A. Berisha, E. Berdimurodov, E. E. Ebenso and A. Chaouch, *Arab. J. Sci. Eng.*, 2023, 1–17.
- 527 A. Ansari, O. Ou-Ani, L. Oucheikh, Y. Youssefi, D. Chebabe, A. Oubair and M. Znini, *Chem. Afr.*, 2022, 1–19.
- 528 R. T. Loto, E. Alagbe and A. Busari, *Mater. Today: Proc.*, 2023, **80**, 1408–1412.
- 529 R. T. Loto and M. M. Solomon, *Sci. Afr.*, 2023, **19**, e01489.
- 530 F. Laihemdi, A. Barhoumi, M. Zarri, M. Tahiri and M. Chafi, *Environ. Sci. Pollut. Res.*, 2023, 1–27.
- 531 K. Dahmani, M. Galai, M. Ouakki, A. Elgendy, R. Ez-Zriouli, R. Lachhab, S. Briche and M. Cherkaoui, *J. Mol. Liq.*, 2022, **347**, 117982.
- 532 O. Sanni, S. A. Iwarere and M. O. Daramola, *ACS Omega*, 2022, **7**, 40740–40749.
- 533 A. Chraka, N. B. Seddik, I. Raissouni, J. Kassout, M. Choukairi, M. Ezzaki, O. Zazaali, H. Belcadi, F. Janoub and A. I. Mansour, *J. Mol. Liq.*, 2023, **387**, 122715.
- 534 Q. Wang, Q. Zhang, H. Zheng, L. Liu, X. Wu, C. Zhao, X. Zhou, Y. Sun, Z. Yan and X. Li, *Sustainable Chem. Pharm.*, 2023, **34**, 101177.
- 535 A. M. El-Azaly, *Int. J. Electrochem. Sci.*, 2019, **14**, 2714–2731.
- 536 B. Liao, S. Ma, S. Zhang, X. Li, R. Quan, S. Wan and X. Guo, *Int. J. Biol. Macromol.*, 2023, **239**, 124358.
- 537 M. Zunita, D. Wahyuningrum, I. G. Wenten and R. Boopathy, *Bioresour. Technol. Rep.*, 2022, **17**, 100973.
- 538 K. Carla de Santana de Lima, V. Magno Paiva, M. Gustavo Araujo Schwarz, N. Martins Bomfim Barreto, D. Perrone and E. D'Elia, *Sustainable Chem. Pharm.*, 2023, **35**, 101174.
- 539 O. Khlopyk, S. Korniy, I. Zin and M. Holovchuk, *Chem. Eng. Commun.*, 2024, **211**(1), 124–132.
- 540 M. El Hawary, M. Khachani, F. Benhiba, G. Kaichouh, I. Warad, A. Guenbour, A. Zarrouk and A. Bellaouchou, *Chem. Data Coll.*, 2022, **40**, 100870.
- 541 L. Cai, H.-R. Guo, Y.-Q. Zhu, F.-S. Du, J.-T. Qi, L.-Y. Cui, C.-B. Liu and R.-C. Zeng, *Smart Mater. Manuf.*, 2023, **1**, 100014.
- 542 K. C. d. S. d. Lima, V. M. Paiva, D. Perrone, B. Ripper, G. Simões, M. L. M. Rocco, A. G. d. Veiga and E. D'Elia, *J. Mater. Res. Technol.*, 2020, **9**, 12756–12772.
- 543 M. Quraishi and D. S. Chauhan, in *Sustainable Corrosion Inhibitors II: Synthesis, Design, and Practical Applications*, ACS Publications, 2021, pp. 1–17.
- 544 P. S. Umoren, D. Kavaz and S. A. Umoren, *Sustainability*, 2022, **14**, 7981.
- 545 S. R. Al-Mhyawi, *Int. J. Electrochem. Sci.*, 2023, 100210.
- 546 R. Aslam, M. Mobin, M. Shoeb, M. Parveen, S. Zehra and J. Aslam, *Arab. J. Sci. Eng.*, 2021, **46**, 5489–5503.
- 547 R. Aslam, M. Mobin, M. Shoeb and J. Aslam, *Sci. Rep.*, 2022, **12**, 9274.
- 548 M. Mobin, R. Aslam, S. Zehra and M. Ahmad, *J. Surfactants Deterg.*, 2017, **20**, 57–74.
- 549 M. Mobin, R. Aslam and J. Aslam, *Mater. Chem. Phys.*, 2017, **191**, 151–167.



- 550 M. Parveen, M. Mobin, S. Zehra and R. Aslam, *Sci. Rep.*, 2018, **8**, 7489.
- 551 M. Gobara, A. Baraka, R. Akid and M. Zorainy, *RSC Adv.*, 2020, **10**, 2227–2240.
- 552 X. Li, S. Deng, H. Fu and G. Mu, *Corros. Sci.*, 2009, **51**, 2639–2651.
- 553 H. M. Abd El-Lateef, *Res. Chem. Intermed.*, 2016, **42**, 3219–3240.
- 554 K. Mohammed, A. Hamdy, A. Abdel-Wahab and N. Farid, *Life Sci. J.*, 2012, **9**, 424–434.
- 555 J. Hu, D. Huang, G.-L. Song and X. Guo, *Corros. Sci.*, 2011, **53**, 4093–4101.
- 556 X. Li, L. Tang, H. Liu, G. Mu and G. Liu, *Mater. Lett.*, 2008, **62**, 2321–2324.
- 557 A. Fouda, S. A. Abd El-Maksoud, A. El-Habab and A. R. Ibrahim, *Biointerface Res. Appl. Chem.*, 2021, **11**, 9382.
- 558 J. Aslam, *J. Adhes. Sci. Technol.*, 2019, **33**, 1989–2009.
- 559 A. Khamis, M. M. Saleh, M. I. Awad and B. El-Anadoulis, *J. Adv. Res.*, 2014, **5**, 637–646.
- 560 D. Asefi, N. M. Mahmoodi and M. Arami, *Colloids Surf., A*, 2010, **355**, 183–186.
- 561 M. Mobin, R. Aslam and J. Aslam, *Mater. Chem. Phys.*, 2019, **223**, 623–633.
- 562 M. Mobin, S. Zehra and M. Parveen, *J. Mol. Liq.*, 2016, **216**, 598–607.
- 563 S. Zehra, M. Mobin, J. Aslam and M. Parveen, *J. Adhes. Sci. Technol.*, 2018, **32**, 317–342.
- 564 M. Mobin, M. Parveen and M. Rafiquee, *Arabian J. Chem.*, 2017, **10**, S1364–S1372.
- 565 M. Parveen, M. Mobin and S. Zehra, *RSC Adv.*, 2016, **6**, 61235–61248.
- 566 M. Mobin and M. Parveen, *J. Dispersion Sci. Technol.*, 2014, **35**, 29–37.
- 567 M. Mobin, M. Parveen and M. Rafiquee, *J. Mater. Eng. Perform.*, 2013, **22**, 548–556.
- 568 M. Motamedi, A. R. Tehrani-Bagha and M. Mahdavian, *Electrochim. Acta*, 2011, **58**, 488–496.
- 569 M. Mobin and M. A. Khan, *Chem. Eng. Commun.*, 2013, **200**, 1149–1169.
- 570 M. Mobin, M. Khan and M. Parveen, *J. Appl. Polym. Sci.*, 2011, **121**, 1558–1565.
- 571 M. Mobin and M. A. Khan, *J. Dispersion Sci. Technol.*, 2013, **34**, 1496–1506.
- 572 M. Mobin and M. Rizvi, *Carbohydr. Polym.*, 2016, **136**, 384–393.
- 573 M. Mobin and M. Rizvi, *Carbohydr. Polym.*, 2017, **156**, 202–214.
- 574 R. Aslam, M. Mobin, J. Aslam, H. Igaz, I.-M. Chung and S. Zehra, *J. Mol. Struct.*, 2021, **1228**, 129751.
- 575 R. Aslam, M. Mobin, J. Aslam, H. Igaz and I.-M. Chung, *J. Mater. Res. Technol.*, 2019, **8**, 4521–4533.
- 576 M. A. Deyab and S. S. A. El-Rehim, *Int. J. Electrochem. Sci.*, 2013, **8**, 12613–12627.
- 577 M. Parveen, M. Mobin, S. Zehra and R. Aslam, *Sci. Rep.*, 2018, **8**, 7489.
- 578 M. Mobin, S. Zehra and M. Parveen, *J. Mol. Liq.*, 2016, **216**, 598–607.
- 579 S. Deng, X. Li and G. Du, *Chin. J. Chem. Eng.*, 2021, **37**, 222–231.
- 580 D. Hou, W. Yang and S. Dong, *Chem. Ind. Eng.*, 2022, **39**, 100–107.
- 581 X. Li, S. Deng, T. Lin and X. Xie, *J. Mol. Liq.*, 2019, **282**, 499–514.
- 582 Y. Wang, K. Wang, P. Gao, R. Liu, D. Zhao, I. Zhai and G. Qu, *J. Chin. Soc. Corros. Prot.*, 2021, **41**, 131–138.
- 583 X. Li, S. Deng, T. Lin, X. Xie and G. Du, *J. Mater. Res. Technol.*, 2020, **9**, 2196–2207.
- 584 D. K. Verma, R. Aslam, J. Aslam, M. Quraishi, E. E. Ebenso and C. Verma, *J. Mol. Struct.*, 2021, **1236**, 130294.
- 585 E. E. Ebenso, C. Verma, L. O. Olasunkanmi, E. D. Akpan, D. K. Verma, H. Igaz, L. Guo, S. Kaya and M. A. Quraishi, *Phys. Chem. Chem. Phys.*, 2021, **23**, 19987–20027.
- 586 I. Obot, D. Macdonald and Z. Gasem, *Corros. Sci.*, 2015, **99**, 1–30.
- 587 C. Verma, H. Igaz, D. Verma, E. E. Ebenso, I. Bahadur and M. Quraishi, *J. Mol. Liq.*, 2018, **260**, 99–120.
- 588 H. Shao, X. Yin, K. Zhang, W. Yang, Y. Chen and Y. Liu, *J. Mater. Res. Technol.*, 2022, **20**, 916–933.
- 589 C. A. R. Maestro, A. M. de Sousa Malafaia, C. F. Silva, C. S. Nascimento Jr., K. B. Borges, T. A. Simões, V. R. Capelossi and A. H. S. Bueno, *Mater. Chem. Phys.*, 2023, **305**, 127971.
- 590 X. Wang, H. Zhao, L. Chang, Z. Yu, Z. Xiao, S. Tang, C. Huang, J. Fan and S. Yang, *ACS Omega*, 2022, **7**, 39169–39180.
- 591 H. Kumar, P. Yadav, R. Kumari, R. Sharma, S. Sharma, D. Singh, H. Dahiya, P. Kumar, S. Bhardwaj and P. Kaur, *Colloids Surf., A*, 2023, **675**, 132039.
- 592 S. Mandal, S. Zamindar, S. Sarkar, M. Murmu, L. Guo, S. Kaya, H. Hirani and P. Banerjee, *J. Adhes. Sci. Technol.*, 2023, **37**, 1649–1665.
- 593 N. Asadi, M. Ramezanzadeh, G. Bahlakeh and B. Ramezanzadeh, *J. Taiwan Inst. Chem. Eng.*, 2019, **95**, 252–272.
- 594 E. Alibakhshi, M. Ramezanzadeh, G. Bahlakeh, B. Ramezanzadeh, M. Mahdavian and M. Motamedi, *J. Mol. Liq.*, 2018, **255**, 185–198.
- 595 S. K. Saha, M. Murmu, N. C. Murmu and P. Banerjee, *J. Mol. Liq.*, 2022, **364**, 120033.
- 596 S. Mandal, S. Bej and P. Banerjee, *J. Mol. Liq.*, 2023, **381**, 121789.
- 597 M. Mobin, S. Zamindar and P. Banerjee, *J. Mol. Liq.*, 2023, 122403.
- 598 D.-Y. Wang, J.-H. Wang, H.-J. Li and Y.-C. Wu, *Ind. Crops Prod.*, 2022, **189**, 115866.
- 599 M. Palimi, Y. Tang, S. Mousavi, W. Chen, V. Alvarez, E. Kuru and D. Li, *Tribol. Int.*, 2023, **187**, 108728.
- 600 A. Farhadian, A. Rahimi, N. Safaei, A. Shaabani, M. Abdouss and A. Alavi, *Corros. Sci.*, 2020, **175**, 108871.

- 601 X. Chen, Y. Chen, J. Cui, Y. Li, Y. Liang and G. Cao, *Comput. Mater. Sci.*, 2021, **188**, 110229.
- 602 S. Sengupta, M. Murmu, S. Mandal, H. Hirani and P. Banerjee, *Colloids Surf., A*, 2021, **617**, 126314.
- 603 S. Sengupta, M. Murmu, N. C. Murmu and P. Banerjee, *J. Mol. Liq.*, 2021, **326**, 115215.
- 604 O. Dagdag, Z. Safi, H. Erramli, N. Wazzan, I. Obot, E. Akpan, C. Verma, E. Ebenso, O. Hamed and A. El Harfi, *J. Mol. Liq.*, 2019, **287**, 110977.
- 605 X. Li, S. Deng, H. Fu and G. Mu, *Corros. Sci.*, 2010, **52**, 1167–1178.
- 606 A. Khamis, M. M. Saleh, M. I. Awad and B. E. El-Anadouli, *J. Adv. Res.*, 2014, **5**, 637–646.
- 607 O. Sanni, A. P. I. Popoola and O. S. I. Fayomi, *Mater. Today: Proc.*, 2021, **43**, 2215–2221.
- 608 O. Oyewole, J. B. Adeoye, V. C. Udoh and T. A. Oshin, *Egypt. J. Pet.*, 2023, **32**, 41–46.
- 609 N. Bhardwaj, P. Sharma, K. Singh, D. Rana and V. Kumar, *Chem. Phys. Impact*, 2021, **3**, 100038.
- 610 Y. Fernine, R. Salim, N. Arrousse, R. Haldhar, F. El Hajjaji, S.-C. Kim, M. E. Touhami and M. Taleb, *J. Mol. Liq.*, 2022, **355**, 118867.
- 611 A. Shahmoradi, N. Talebibahmanbigloo, A. Javidparvar, G. Bahlakeh and B. Ramezanzadeh, *J. Mol. Liq.*, 2020, **304**, 112751.
- 612 Y. Wu, Y. Zhang, Y. Jiang, N. Li, Y. Zhang, L. Wang and J. Zhang, *Colloids Surf., A*, 2021, **626**, 126969.
- 613 M. M. El-Deeb, E. N. Ads and J. R. Humaidi, *Int. J. Electrochem. Sci.*, 2018, **13**, 4123–4138.
- 614 D. Asra, N. K. Othman and Z. Dasuki, *AIP Conf. Proc.*, 2017, 1838.
- 615 L. A. C. Matos, M. C. Taborda, G. J. T. Alves, M. T. da Cunha, E. do Prado Banczek, M. de Fátima Oliveira, E. D'Elia and P. R. P. Rodrigues, *Int. J. Electrochem. Sci.*, 2018, **13**, 1577–1593.
- 616 N. Raghavendra and J. Ishwara Bhat, *J. Bio- Tribo-Corros.*, 2018, **4**, 44.
- 617 A. R. Shahmoradi, M. Ranjbarghanei, A. A. Javidparvar, L. Guo, E. Berdimurodov and B. Ramezanzadeh, *J. Mol. Liq.*, 2021, **338**, 116550.
- 618 B.-l. Lin, J.-j. Shao, Y.-y. Xu, Y.-m. Lai and Z.-n. Zhao, *Arabian J. Chem.*, 2021, **14**, 103114.
- 619 S. Paul and I. Koley, *J. Bio- Tribo-Corros.*, 2016, **2**, 6.
- 620 M. Sahraoui, M. Boulkroune, A. Chibani, Y. Larbah and A. Abdessemed, *J. Bio- Tribo-Corros.*, 2022, **8**, 54.
- 621 M. A. Chowdhury, M. M. S. Ahmed, N. Hossain, M. A. Islam, S. Islam and M. M. Rana, *Results Eng.*, 2023, **17**, 100996.
- 622 F. Bouhlal, N. Labjar, F. Abdoun, A. Mazkour, M. Serghini-Idrissi, M. El Mahi, E. M. Lotfi and S. El Hajjaji, *Int. J. Corros.*, 2020, **2020**, 1–14.
- 623 N. A. Reza, N. H. Akhmal, N. A. Fadil and M. F. M. Taib, *Metals*, 2021, **11**, 1062.
- 624 A. A. Farag, A. S. Ismail and M. Migahed, *Egypt. J. Pet.*, 2018, **27**, 1187–1194.
- 625 C. M. Fernandes, P. C. de Oliveira, V. G. Pina, B. S. Peixoto, F. F. Massante, M. C. Veloso, G. A. Romeiro, M. C. de Moraes and E. A. Ponzio, *Sustainable Chem. Pharm.*, 2022, **29**, 100751.
- 626 M. C. T. Larissa Aparecida Corrêa Matos, G. J. T. Alves, M. T. da Cunha, E. do Prado Banczek, M. d. F. Oliveira, E. D'Elia and P. R. P. Rodrigues, *Int. J. Electrochem. Sci.*, 2018, **13**, 1577–1593.
- 627 D. Gusti, I. Lestari, E. Permana and R. Anggraini, *IOP Conf. Ser: Earth Environ. Sci.*, 2020, 483.
- 628 A. Ayoola, R. Babalola, B. Durodola, E. Alagbe, O. Agboola and E. Adegbile, *Results Eng.*, 2022, **15**, 100490.
- 629 G. Salinas-Solano, J. Porcayo-Calderon, L. M. de la Escalera, J. Canto, M. Casales-Diaz, O. Sotelo-Mazon, J. Henao and L. Martinez-Gomez, *Ind. Crops Prod.*, 2018, **119**, 111–124.
- 630 R. Vera, F. Figueredo, A. Díaz-Gómez and A. Molinari, *Int. J. Electrochem. Sci.*, 2018, **13**, 4139–4159.
- 631 A. Cruz-Zabalegui, E. Vazquez-Velez, G. Galicia-Aguilar, M. Casales-Diaz, R. Lopez-Sesenes, J. Gonzalez-Rodriguez and L. Martinez-Gomez, *Ind. Crops Prod.*, 2019, **133**, 203–211.
- 632 J. Halambek, I. Cindrić and A. Ninčević Grassino, *Carbohydr. Polym.*, 2020, **234**, 115940.
- 633 I. Kusumaningrum, R. Soenoko, E. Siswanto and F. Gapsari, *Case Stud. Chem. Environ. Eng.*, 2022, **6**, 100223.
- 634 N. Bhardwaj, P. Sharma and V. Kumar, *Corros. Rev.*, 2021, **39**, 27–41.
- 635 M. H. Fekri, F. Omidali, M. M. Alemnezhad and A. Ghaffarinejad, *Mater. Chem. Phys.*, 2022, **286**, 126150.
- 636 M. Radi, R. Melian, M. Galai, N. Dkhirche, M. Makha, C. Verma, C. Fernandez and M. EbnTouhami, *J. Mol. Liq.*, 2021, **337**, 116547.
- 637 D. Payra, M. Naito, Y. Fujii, N. L. Yamada, S. Hiromoto and A. Singh, *RSC Adv.*, 2015, **5**, 15977–15984.
- 638 S. Zehra, M. Mobin and R. Aslam, in *Environmentally Sustainable Corrosion Inhibitors*, ed. C. M. Hussain, C. Verma and J. Aslam, Elsevier, 2022, pp. 47–67. DOI: [10.1016/B978-0-323-85405-4.00022-7](https://doi.org/10.1016/B978-0-323-85405-4.00022-7).
- 639 A. A. Al-Amiery, W. N. R. W. Isahak and W. K. Al-Azzawi, *Lubricants*, 2023, **11**, 174.
- 640 M. Rbaa, M. Galai, O. Dagdag, L. Guo, B. Tüzün, E. Berdimurodov, A. Zarrouk and B. Lakhrissi, in *Eco-Friendly Corrosion Inhibitors*, ed. L. Guo, C. Verma and D. Zhang, Elsevier, 2022, pp. 27–42. DOI: [10.1016/B978-0-323-91176-4.00026-X](https://doi.org/10.1016/B978-0-323-91176-4.00026-X).
- 641 M. A. Quraishi and D. S. Chauhan, in *Sustainable Corrosion Inhibitors II: Synthesis, Design, and Practical Applications*, American Chemical Society, 2021, vol. 1404, ch. 1, pp. 1–17.
- 642 C. Verma, M. A. Quraishi and K. Y. Rhee, *J. Mol. Liq.*, 2022, **348**, 118387.
- 643 R. Bender, D. Féron, D. Mills, S. Ritter, R. Bäßler, D. Bettge, I. De Graeve, A. Dugstad, S. Grassini, T. Hack,

- M. Halama, E.-H. Han, T. Harder, G. Hinds, J. Kittel, R. Krieg, C. Leygraf, L. Martinelli, A. Mol, D. Neff, J.-O. Nilsson, I. Odnevall, S. Paterson, S. Paul, T. Prošek, M. Raupach, R. I. Revilla, F. Ropital, H. Schweigart, E. Szala, H. Terryn, J. Tidblad, S. Virtanen, P. Volovitch, D. Watkinson, M. Wilms, G. Winning and M. Zheludkevich, *Mater. Corros.*, 2022, **73**, 1730–1751.
- 644 C. Verma, E. E. Ebenso, M. A. Quraishi and C. M. Hussain, *Mater. Adv.*, 2021, **2**, 3806–3850.
- 645 H. Wei, B. Heidarshenas, L. Zhou, G. Hussain, Q. Li and K. K. Ostrikov, *Mater. Today Sustainability*, 2020, **10**, 100044.
- 646 A. Thakur, S. Sharma, R. Ganjoo, H. Assad and A. Kumar, *J. Phys.: Conf. Ser.*, 2022, **2267**, 012079.
- 647 C. Verma, A. Alfantazi and M. A. Quraishi, *J. Mol. Liq.*, 2021, **343**, 117648.
- 648 B. R. Fazal, T. Becker, B. Kinsella and K. Lepkova, *npj Mater. Degrad.*, 2022, **6**, 5.
- 649 M. Alimohammadi, M. Ghaderi, A. Ramazani, S. A. and M. Mahdavian, *Sci. Rep.*, 2023, **13**, 3737.
- 650 M. Rizvi, in *Organic Corrosion Inhibitors*, 2021, pp. 411–434. DOI: [10.1002/9781119794516.ch18](https://doi.org/10.1002/9781119794516.ch18).
- 651 S. A. Umoren, M. M. Solomon, A. Madhankumar and I. B. Obot, *Carbohydr. Polym.*, 2020, **230**, 115466.
- 652 S. Marzorati, L. Verotta and S. P. Trasatti, *Molecules*, 2019, **24**, 48.
- 653 A. N. Grassino, J. Halambek, S. Djaković, S. Rimac Brnčić, M. Dent and Z. Grabarić, *Food Hydrocolloids*, 2016, **52**, 265–274.
- 654 K. Geiser, in *Sustainability Science and Engineering*, Elsevier, 2006, vol. 1, pp. 161–175.
- 655 S. C. DeVito, *Green Chem.*, 2016, **18**, 4332–4347.
- 656 C. Verma, S. H. Alrefae, M. Quraishi, E. E. Ebenso and C. M. Hussain, *J. Mol. Liq.*, 2021, **321**, 114484.
- 657 M. A. Usmani, I. Khan, A. Hasnat and A. Moheman, in *Advanced Applications of Ionic Liquids*, Elsevier, 2023, pp. 185–196.
- 658 K. Ghandi, *Green Sustainable Chem.*, 2014, **4**, 44–53.
- 659 L. Souza, E. Pereira, L. Matlakhova, V. A. Nicolin, S. N. Monteiro and A. R. de Azevedo, *J. Mater. Res. Technol.*, 2022, DOI: [10.1016/j.jmrt.2022.12.066](https://doi.org/10.1016/j.jmrt.2022.12.066).
- 660 J. Ye, R. Huang, X. Wang, Q. Bao, J. Mu, K. Pan, W. Ji, Z. Wei and H. Liu, *Ind. Eng. Chem. Res.*, 2023, **62**(36), 14427–14440.
- 661 E. K. Ardakani, E. Kowsari, A. Ehsani and S. Ramakrishna, *Microchem. J.*, 2021, **165**, 106049.
- 662 R. Haldhar, C. J. Raorane, V. Mishra, T. Periyasamy, A. Berisha and S.-C. Kim, *J. Mol. Liq.*, 2023, **372**, 121168.
- 663 O. A. Al-Rashed and A. A. Nazeer, *J. Mol. Liq.*, 2019, **288**, 111015.
- 664 C. Verma and M. A. Quraishi, *e-Prime Advances in Electrical Engineering, Electronics and Energy*, 2022, **2**, 100070.
- 665 Y. Shi, Y. Fu, H. Huang, H. Li, S. Zhang, W. Li and F. Gao, *J. Environ. Chem. Eng.*, 2021, **9**, 106679.
- 666 P. Singh, D. Singh Chauhan, S. Singh Chauhan, M. Ahmad Quraishi and S. Swarupa Tripathy, *ChemistrySelect*, 2021, **6**, 11417–11430.
- 667 M. Goyal, S. Kumar, L. Guo, S. H. Alrefae and C. Verma, *J. Taiwan Inst. Chem. Eng.*, 2021, **123**, 21–33.
- 668 T. W. Quadri, L. O. Olasunkanmi, O. E. Fayemi, E. D. Akpan, H.-S. Lee, H. Lgaz, C. Verma, L. Guo, S. Kaya and E. E. Ebenso, *Comput. Mater. Sci.*, 2022, **214**, 111753.
- 669 R. Huang, H. Liu, Z. Wei, Y. Jiang, K. Pan, X. Wang and J. Kong, *Environ. Sci. Pollut. Res.*, 2023, 1–23.
- 670 A. Rathore, S. Sharma, A. Sharma and S. K. Sharma, *J. Dispersion Sci. Technol.*, 2023, 1–13.
- 671 S. Monaci, D. Minudri, L. Guazzelli, A. Mezzetta, D. Mecerreyes, M. Forsyth and A. Somers, *Molecules*, 2023, **28**, 5568.
- 672 F. E. Hajjaji, R. Salim, M. Taleb, F. Benhiba, N. Rezki, D. S. Chauhan and M. Quraishi, *Surf. Interfaces*, 2021, **22**, 100881.
- 673 A. Singh, K. Ansari, I. H. Ali, Y. Lin, M. Murmu and P. Banerjee, *J. Mol. Liq.*, 2023, **376**, 121408.
- 674 O. Al-Rashed and A. Abdel Nazeer, *Materials*, 2022, **15**, 2326.
- 675 E. E. El-Katori and A. S. Abousalem, *RSC Adv.*, 2019, **9**, 20760–20777.
- 676 G. Gómez-Sánchez, O. Olivares-Xometl, P. Arellanes-Lozada, N. V. Likhanova, I. V. Lijanova, J. Arriola-Morales, V. Díaz-Jiménez and J. López-Rodríguez, *Int. J. Mol. Sci.*, 2023, **24**, 6291.
- 677 E. K. Ardakani, E. Kowsari and A. Ehsani, *Colloids Surf., A*, 2020, **586**, 124195.
- 678 E. Li, Y. Li, S. Liu and P. Yao, *Colloids Surf., A*, 2023, **657**, 130541.
- 679 A. Nahlé, R. Salim, F. E. Hajjaji, E. Ech-chihbi, A. Titi, M. Messali, S. Kaya, B. El Ibrahimy and M. Taleb, *Arabian J. Chem.*, 2022, **15**, 103967.
- 680 E. E. El-Katori, M. Nessim, M. Deyab and K. Shalabi, *J. Mol. Liq.*, 2021, **337**, 116467.
- 681 J. Cai, J. Liu, S. Mu, J. Liu, J. Hong, X. Zhou, Q. Ma and L. Shi, *Int. J. Electrochem. Sci.*, 2020, **15**, 1287–1301.
- 682 Y. Guo, J. Xue, J. Zhang, Q. Chen, L. Fan, C. Tang, K. Ren, A. Fu and Q. Bi, *Colloids Surf., A*, 2022, 129135.
- 683 P. Kannan, A. Varghese, K. Palanisamy and A. S. Abousalem, *Appl. Surf. Sci. Adv.*, 2021, **6**, 100150.
- 684 Y. Jiang, Y. Liu, S. Gao, X. Guo and J. Zhang, *J. Mol. Liq.*, 2022, **345**, 116998.
- 685 A. Singh, K. Ansari, P. Banerjee, M. Murmu, M. Quraishi and Y. Lin, *Colloids Surf., A*, 2021, **623**, 126708.
- 686 N. Kedimar, P. Rao and S. A. Rao, *J. Appl. Electrochem.*, 2023, 1–17.
- 687 S. Xu, Z. Luo, J. Zhang, B. Tan, S. Zhang and W. Li, *J. Mol. Liq.*, 2021, **340**, 117189.
- 688 H. Huang, B. Li, X. Zheng, J. Fan and M. Gong, *Int. J. Electrochem. Sci.*, 2022, **17**, 220344.
- 689 E. Berdimurodov, A. Kholikov, K. Akbarov, L. Guo, S. Kaya, K. P. Katin, D. K. Verma, M. Rbaa, O. Dagdag and R. Haldhar, *J. Electroanal. Chem.*, 2021, **901**, 115794.

- 690 E. Berdimurodov, A. Kholikov, K. Akbarov, L. Guo, S. Kaya, K. P. Katin, D. K. Verma, M. Rbaa and O. Dagdag, *Colloids Surf., A*, 2022, **633**, 127837.
- 691 C. Verma, M. A. Quraishi, A. Alfantazi and K. Y. Rhee, *Adv. Ind. Eng. Polym. Res.*, 2023, **6**(4), 407–435.
- 692 S. Umoren and M. Solomon, *The Open Mater. Sci. J.*, 2014, **8**, 39–54.
- 693 M. A. Quraishi, D. S. Chauhan and V. S. Saji, *J. Mol. Liq.*, 2021, **341**, 117265.
- 694 S. Nwanonenyi, I. Madufor, P. Uzoma and I. Chukwujike, *Int. Res. J. Pure Appl. Chem.*, 2016, 1–15.
- 695 T. W. Quadri, L. O. Olasunkanmi, O. E. Fayemi and E. E. Ebenso, *Grafted Biopolymers as Corrosion Inhibitors: Safety, Sustainability, and Efficiency*, 2023.
- 696 S. Nwanonenyi, H. Obasi and I. Eze, *Chem. Afr.*, 2019, **2**, 471–482.
- 697 Y. Lu, H. Feng, H. Xia and W. H. Xia, *Int. J. Electrochem. Sci.*, 2022, **17**, 221180.
- 698 P. P. Rahayu, C. D. D. Sundari and I. Farida, *IOP Conf. Ser.: Mater. Sci. Eng.*, 2018, **434**, 012087.
- 699 A. Peter, I. Obot and S. K. Sharma, *Int. J. Ind. Chem.*, 2015, **6**, 153–164.
- 700 N. R. Vaidya, P. Aklujkar and A. R. Rao, *J. Coat. Technol. Res.*, 2022, **19**, 223–239.
- 701 M. El Azzouzi, K. Azzaoui, I. Warad, B. Hammouti, S. Shityakov, R. Sabbahi, S. Saoiabi, M. Youssoufi, N. Akartasse and S. Jodeh, *J. Mol. Liq.*, 2022, **347**, 118354.
- 702 C. Shen, V. Alvarez, J. D. Koenig and J.-L. Luo, *Corros. Eng., Sci. Technol.*, 2019, **54**, 444–454.
- 703 A. Büyüksağış, A. Baydır and M. Dilek, *Prot. Met. Phys. Chem. Surf.*, 2021, **57**, 211–221.
- 704 G. Palumbo, K. Berent, E. Proniewicz and J. Banaś, *Materials*, 2019, **12**, 2620.
- 705 N. B. Iroha and O. Akaranta, *SN Appl. Sci.*, 2020, **2**, 1514.
- 706 A. Jmiai, B. El Ibrahimy, A. Tara, S. El Issami, O. Jbara and L. Bazzi, *J. Mol. Struct.*, 2018, **1157**, 408–417.
- 707 K. Shamsheera, A. R. Prasad, M. Arshad and A. Joseph, *J. Indian Chem. Soc.*, 2022, **99**, 100271.
- 708 A. Toghan and A. Fawzy, *Polymer*, 2023, **15**, 3144.
- 709 Y. Cao, C. Zou, C. Wang, W. Chen, H. Liang and S. Lin, *J. Mol. Liq.*, 2021, **341**, 117391.
- 710 M. Mobin, I. Ahmad, M. Basik, M. Murmu and P. Banerjee, *Sustainable Chem. Pharm.*, 2020, **18**, 100337.
- 711 N. K. Gupta, P. Joshi, V. Srivastava and M. Quraishi, *Int. J. Biol. Macromol.*, 2018, **106**, 704–711.
- 712 M. Srivastava, S. Srivastava, G. Ji and R. Prakash, *Int. J. Biol. Macromol.*, 2019, **140**, 177–187.
- 713 A. Fawzy, A. Toghan, N. Alqarni, M. Morad, M. E. Zaki, M. M. Sanad, A. I. Alakhras and A. A. Farag, *Polymers*, 2023, **15**, 891.
- 714 M. Erna, H. Herdini and D. Futra, *Int. J. Chem. Eng.*, 2019, **2019**, 8514132.
- 715 Q. Zhang, N. Xu, Z. Jiang, H. Liu and G. Zhang, *J. Colloid Interface Sci.*, 2023, **640**, 1052–1067.
- 716 P. Kesari, G. Udayabhanu, A. Roy and S. Pal, *Int. J. Biol. Macromol.*, 2023, **225**, 1323–1349.
- 717 A. Sun, G. Cui and Q. Liu, *Colloids Surf., A*, 2023, **664**, 131106.
- 718 W. Song, X. Zhao, Z. Jin, L. Fan, X. Ji, J. Deng and J. Duan, *J. Cleaner Prod.*, 2023, 136390.
- 719 T. A. Saleh, K. Haruna, M. M. Nur and B. Alharbi, *Prog. Org. Coat.*, 2022, **170**, 106974.
- 720 N. Talat, A. Dahadha, M. Abunuwar, A. Hussien and W. a. Odeh, *Int. J. Corros. Scale Inhib.*, 2023, **12**, 215–243.
- 721 A. Fawzy, A. Al Bahir, N. Alqarni, A. Toghan, M. Khider, I. M. Ibrahim, H. H. Abulreesh and K. Elbanna, *Sci. Rep.*, 2023, **13**, 2585.
- 722 X. Wang and W. Ding, *J. Dispersion Sci. Technol.*, 2023, **44**, 1288–1295.
- 723 A. Yousefi, S. Javadian, M. Sharifi, N. Dalir and A. Motae, *J. Bio-Tribo-Corros.*, 2019, **5**, 1–15.
- 724 S. Abd El-Maksoud, F. El-Dossoki, M. Abd-Elhamed and A. A. Farag, *J. Bio-Tribo-Corros.*, 2023, **9**, 1–16.
- 725 A. Elaraby, A. Elgendy, M. Abd-El-Raouf, M. Migahed, A. El-Tabei, A. M. Abdullah, N. H. Al-Qahtani, S. M. Alharbi, S. M. Shaban and D. H. Kim, *Colloids Surf., A*, 2023, **659**, 130687.
- 726 S. H. Shafek, E. A. Ghiaty, N. M. El Basiony, E. A. Badr and S. M. Shaban, *Z. Phys. Chem.*, 2023, **237**, 1–33.
- 727 A. Elaraby, S. A. El-samad, E. A. Khamis and E. Zaki, *Sci. Rep.*, 2023, **13**, 942.
- 728 R. Jalab, M. A. Saad, M. H. Sliem, A. M. Abdullah and I. A. Hussein, *Molecules*, 2022, **27**, 6414.
- 729 M. A. Bedair, H. M. Elaryian, A. H. Bedair, R. M. Aboushahba and A. E.-A. S. Fouda, *Inorg. Chem. Commun.*, 2023, **148**, 110304.
- 730 H. M. Elaryian, M. A. Bedair, A. H. Bedair, R. M. Aboushahba and A. E.-A. S. Fouda, *J. Mol. Liq.*, 2022, **346**, 118310.
- 731 A. M. Younis, T. H. Rakha, M. M. El-Gamil and G. M. A. El-Reash, *J. Inorg. Organomet. Polym. Mater.*, 2022, 1–17.
- 732 A. Groysman, *Koroze Ochr. Mater.*, 2017, **61**, 100–117.
- 733 D. Lopez, T. Perez and S. Simison, *Mater. Des.*, 2003, **24**, 561–575.
- 734 J. Sun, C. Sun, X. Lin, X. Cheng and H. Liu, *Materials*, 2016, **9**, 200.
- 735 J. Jiang, N. Li, Q. Li, Z. Jiang, B. Wang, Y. He, F. Liu and C. Liu, *Metals*, 2023, **13**, 826.
- 736 J. Feder, *J. Pet. Technol.*, 2020, **72**, 56–57.
- 737 J. Ning, Y. Yoon, H. Li and S. Srinivasan, NACE CORROSION, 2019, NACE-2019-13400.
- 738 S. A. Ali, L. J. Kalfayan and C. T. Montgomery, *Acid Stimulation*, Society of Petroleum Engineers, Richardson, Texas, 2016.
- 739 B. Williams and D. Nierode, *J. Pet. Technol.*, 1972, **24**, 849–859.
- 740 P. Rajeev, A. Surendranathan and C. S. Murthy, *J. Mater. Environ. Sci.*, 2012, **3**, 856–869.

- 741 P. Okafor, M. E. Ikpi, I. Uwah, E. Ebenso, U. Ekpe and S. Umoren, *Corros. Sci.*, 2008, **50**, 2310–2317.
- 742 M. Finšgar and J. Jackson, *Corros. Sci.*, 2014, **86**, 17–41.
- 743 C. F. Smith, F. E. Dollarhide and N. J. Byth, *J. Pet. Technol.*, 1978, **30**, 737–746.
- 744 O. A. Thomas and A. P. Roberts, *Production operations, Well completions, Work over and stimulation*, 2007.
- 745 H. A. Nasr-El-Din, S. A. Ali, L. Kalfayan and C. T. Montgomery, in *Acid Stimulation*, Society of Petroleum Engineers, 2016, DOI: [10.2118/9781613994269-09](https://doi.org/10.2118/9781613994269-09).
- 746 H. A. Nasr-El-Din, A. H. Al-Ghamdi, A. A. Al-Qahtani and M. M. Samuel, *SPE J.*, 2008, **13**, 35–47.
- 747 S. D. Harms, J. M. Smith, G. E. King and K. Posey, *Permian Basin Oil and Gas Recovery Conference*, SPE, 1988.
- 748 D. Hill, *Civil Engineering Magazine Archive*, 2014, **84**(1), 40–41.
- 749 H. Asaadian, P. Ahmadi, M. Z. Khormizi, S. Mohammadi, B. S. Soulgani, S. Baghersaei and B. Mokhtari, *J. Pet. Sci. Eng.*, 2022, **218**, 111009.
- 750 N. Hossain, M. A. Islam and M. A. Chowdhury, *Results Chem.*, 2023, **5**, 100883.
- 751 U. Bharatiya, P. Gal, A. Agrawal, M. Shah and A. Sircar, *J. Bio-Tribo-Corros.*, 2019, **5**, 1–12.
- 752 M. Ghommem, W. Zhao, S. Dyer, X. Qiu and D. Brady, *J. Pet. Sci. Eng.*, 2015, **131**, 18–33.
- 753 A. Shein and A. Denisova, *Prot. Met.*, 2006, **42**, 34–37.
- 754 W. Frenier, F. Growcock and V. Lopp, *SPE Prod. Eng.*, 1988, **3**, 584–590.
- 755 A. Singh and M. A. Quraishi, *J. Mater. Environ. Sci.*, 2015, **6**, 224–235.
- 756 K. Ansari, M. Quraishi and A. Singh, *J. Assoc. Arab Univ. Basic Appl. Sci.*, 2017, **22**, 45–54.
- 757 S. Aribio, S. J. Olusegun, L. J. Ibhadiyi, A. Oyetunji and D. O. Folorunso, *J. Assoc. Arab Univ. Basic Appl. Sci.*, 2017, **24**, 34–38.
- 758 E. Ghali, V. S. Sastri and M. Elboudjaini, *Corrosion prevention and protection: practical solutions*, John Wiley & Sons, 2007.
- 759 A. Marciales, T. Haile, B. Ahvazi, T.-D. Ngo and J. Wolodko, *Corros. Rev.*, 2018, **36**, 239–266.
- 760 M. Abdallah, I. Zaafarany, K. Khairou and Y. Emad, *Chem. Technol. Fuels Oils*, 2012, **48**, 234–245.
- 761 A. Fouda, A. Emam, R. Refat and M. Nageeb, *Surf. Eng. Appl. Electrochem.*, 2019, **55**, 294–303.
- 762 K. Haruna, T. A. Saleh and M. Quraishi, *J. Mol. Liq.*, 2020, **315**, 113716.
- 763 D. S. Chauhan, M. Quraishi, V. Srivastava and J. Haque, *J. Mol. Struct.*, 2021, **1226**, 129259.
- 764 R. T. Loto, E. Okorie and T. Olukeye, *S. Afr. J. Chem. Eng.*, 2019, **30**, 28–41.
- 765 R. T. Loto, *Sustainable Chem. Pharm.*, 2020, **17**, 100298.
- 766 G. Palumbo, M. Gorny and J. Banaś, *J. Mater. Eng. Perform.*, 2019, **28**, 6458–6470.
- 767 L. B. Furtado, R. Nascimento, P. R. Seidl, M. J. O. Guimarães, L. M. Costa, J. Rocha and J. Ponciano, *J. Mol. Liq.*, 2019, **284**, 393–404.
- 768 M. Quraishi, K. Ansari, D. S. Chauhan, S. A. Umoren and M. Mazumder, *Cellulose*, 2020, **27**, 6425–6443.
- 769 M. Palimi, Y. Tang, V. Alvarez, E. Kuru and D. Li, *Mater. Chem. Phys.*, 2022, **288**, 126406.
- 770 M. Yadav, S. Kumar and D. Sharma, *Anti-Corros. Methods Mater.*, 2014, **61**, 129–138.
- 771 I. B. Onyeachu, I. B. Obot, A. A. Sorour and M. I. Abdul-Rashid, *Corros. Sci.*, 2019, **150**, 183–193.
- 772 H. A. Craddock, S. Caird, H. Wilkinson and M. Guzmán, *SPE Proj., Fac. Const.*, 2007, **2**, 1–8.



## Review article



# Various synthesis and biological evaluation of some tri-tetra-substituted imidazoles derivatives: A review

Abdeljalil Hamdi<sup>a</sup>, Walid Daoudi<sup>b,\*</sup>, Mohamed Aaddouz<sup>c</sup>, Mohamed Azzouzi<sup>b</sup>, Hassan Amhamdi<sup>a</sup>, Abdellah Elyoussfi<sup>c</sup>, Abdelmalik El Aatiaoui<sup>b</sup>, Dakeshwar Kumar Verma<sup>d</sup>, Mohamed Abboud<sup>e,\*\*</sup>, M'hamed Ahari<sup>a</sup>

<sup>a</sup> Applied Chemistry Research Unit, FSTH, Abdelmalek Essaâdi University, AL Hoceïma, Tetouan, Morocco

<sup>b</sup> Laboratory of Molecular Chemistry, Materials and Environment (LCM2E), Departement of Chemistry, Multidisciplinary Faculty of Nador, University Mohamed I, 60700 Nador, Morocco

<sup>c</sup> Laboratoire de chimie analytique appliquée, matériaux et environnement (LC2AME), Faculté des Sciences, B.P. 717, 60000 Oujda, Morocco

<sup>d</sup> Department of Chemistry, Government Dignvijay Autonomous Postgraduate College, Rajnandgaon, Chhattisgarh-491441, India

<sup>e</sup> Catalysis Research Group (CRG), Department of Chemistry, College of Science, King Khalid University, Abha 61413, Saudi Arabia

## ARTICLE INFO

## Keywords:

Tri-tetra-substituted imidazole  
Radziszewski reaction  
Preclinical approaches  
Pharmacological applications

## ABSTRACT

The imidazole nucleus represents a significant group of heterocyclic molecules with diverse significance in the modern world due to its exploration potential and various pharmacological applications. The relevance of imidazole and its derivatives has gained popularity in recent years, especially in the production of commercial drugs and the treatment of various conditions. The imidazole nucleus is present in many natural compounds and widely distributed in essential amino acids, such as L-histidine, whose derivatives exhibit powerful pharmacological properties. In this review, we delve into the historical timeline and development of synthetic pathways for tri- and tetra-substituted imidazoles used in the renowned Radziszewski reaction. Furthermore, we explore various bacteriological applications documented in the literature, as well as current advances in preclinical approaches to imidazole-based drug discovery. Tri- or tetra-substituted imidazole derivatives show strong potential for new synthesis methods, such as reflux or microwave, as well as various biological activities.

## 1. Introduction

Imidazole is a planar five-membered heterocycle with the typical chemical formula  $(CH)_2N(NH)CH$ , containing two double bonds, two nitrogen atoms, three carbon atoms, and four hydrogen atoms. It is a colorless solid that dissolves in water and other polar solvents. In chemistry, it is classified as an aromatic heterocycle belonging to the diazole and alkaloid families. Imidazole is amphoteric, meaning it can act as both a base and an acid [1–3]. The molecule is considered aromatic due to the existence of a sextet of  $\pi$  electrons, comprised of a protonated nitrogen atom sharing a pair of electrons with one electron from each of the other four atoms in the ring. Heterocyclic structures play a crucial role in organic chemistry research and development, with millions of them having been discovered, each possessing unique characteristics and biological importance. Imidazole has been deliberately chosen from a range of

\* Corresponding author.

\*\* Corresponding author.

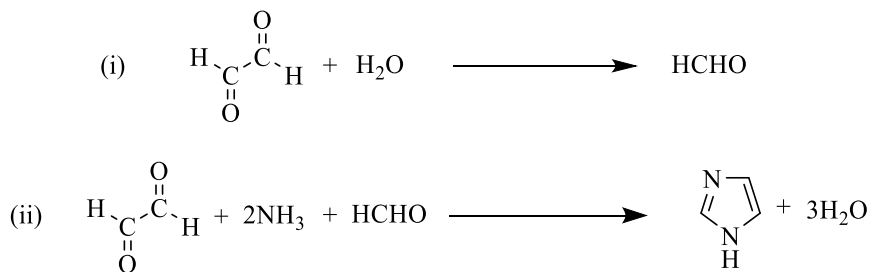
E-mail addresses: [walid.daoudi@ump.ac.ma](mailto:walid.daoudi@ump.ac.ma) (W. Daoudi), [mabboud@kku.edu.sa](mailto:mabboud@kku.edu.sa) (M. Abboud).

<https://doi.org/10.1016/j.heliyon.2024.e31253>

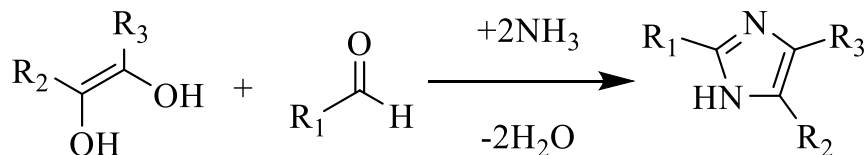
Received 9 November 2023; Received in revised form 20 April 2024; Accepted 13 May 2024

Available online 16 May 2024

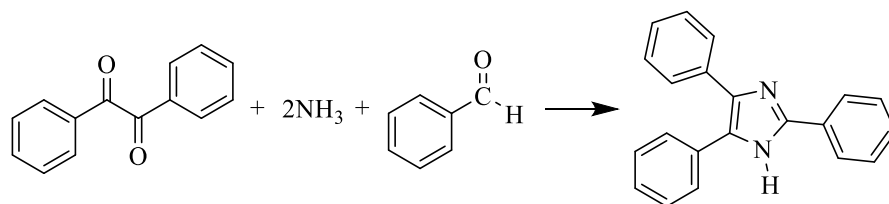
2405-8440/© 2024 The Authors. Published by Elsevier Ltd. This is an open access article under the CC BY license (<http://creativecommons.org/licenses/by/4.0/>).



Scheme 1.



Scheme 2.



Scheme 3.

chemicals due to its interesting biomedical activity and ability to form complexes with certain dyes [4–8]. For instance, Al-Adilee et al. [6] synthesized metal complexes for Pd(II) and Pt (IV) ions with an imidazole core for antioxidant and therapeutic applications. Their study demonstrated that the anticancer activity of imidazole complexes against breast cancer receptors was associated with their interaction with BCL-2 and a BAX BH3 peptide. Similarly, another study focused on preparing a series of metal complexes of imidazoles with the Ag(I) ion for biological applications [9]. The authors found that antimicrobial tests revealed significantly higher activity of Ag (I) complexes against fungi compared to bacterial species, highlighting the significant importance of imidazole metal complexes in the pharmacological field. It is conceivable that isomeric versions of imidazole, with a free imino hydrogen and a substituent in positions 4 and 5, or with two different substituents in these locations, may exist. The position of the imino hydrogen, which can be attached to either one of the two positively charged nitrogen atoms or both depending on the shape of the tautomer, varies [10]. Imidazole has emerged as a key component in the development of novel pharmaceutical medications. Heterocyclic imidazole derivatives exhibit a multitude of biological activities, including antibacterial properties [11], anti-inflammatory effects [12], antimycobacterial, anti-allergic, antitumor [13], antidiabetic [14], antiviral [15], antioxidant [16], antimalarial [17], anthelmintic, antifungal, and ulcerogenic activities [18].

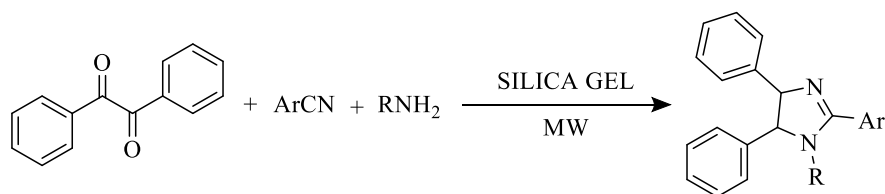
This review encompasses various synthesis pathways for tri- and tetra-substituted imidazoles, starting from benzyl, 9,10-phenanthrenequinone, isatin, acenaphthenequinone, and tracing their synthesis from discovery to the final product. The review then highlights different synthetic methodologies documented in the literature. One such method involves reacting ammonia with glyoxal to produce imidazole. However, the mechanism of this reaction has remained unknown, although one theory suggests that one molecule of glyoxal degrades into formic acid and formaldehyde. The latter then reacts as illustrated in Scheme 1 [19].

## 2. Major synthetic procedures

Heinrich Debus et al. have synthesized imidazole for the first time in 1858 [20], by ammonia combining glyoxal and formaldehyde, to form imidazole as indicated in the diagram below (Scheme 2).

Radiszewski et al. have identified triphenyl imidazole from condensation of benzyl such as di-carbonyl or glyoxal compound with benzaldehyde,  $\alpha$ -keto aldehyde in the presence two ammonia molecules, almost after a one hundred years (Scheme 3) [21].

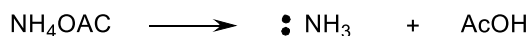
However, Bourissou et al. [22] synthesized the 1-substituted, 2-aryl, 4,5-phenylimidazole using benzyl, benzonitrile, and primary



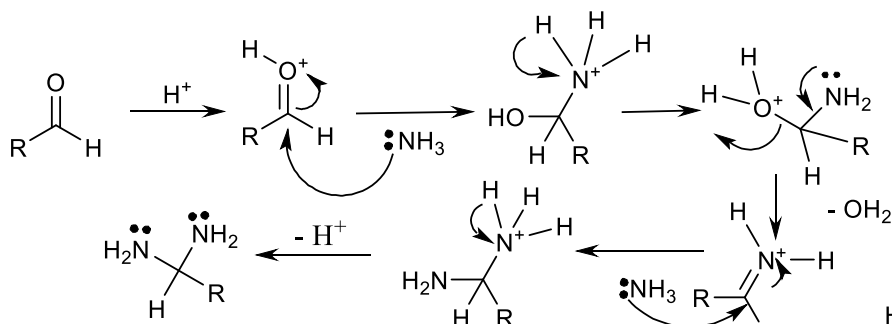
Ar = C<sub>6</sub>H<sub>5</sub>, 4-ClC<sub>6</sub>H<sub>4</sub>, 4-HOC<sub>6</sub>H<sub>4</sub>, 4-CH<sub>3</sub>C<sub>6</sub>H<sub>4</sub>, 4-NO<sub>2</sub>C<sub>6</sub>H<sub>4</sub> ; R = C<sub>6</sub>H<sub>5</sub>

Scheme 4.

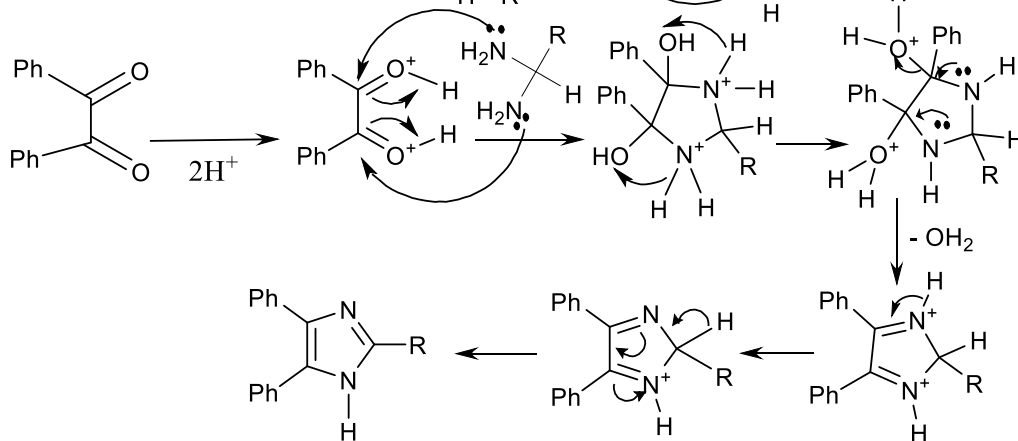
Step 1:



Step 2:



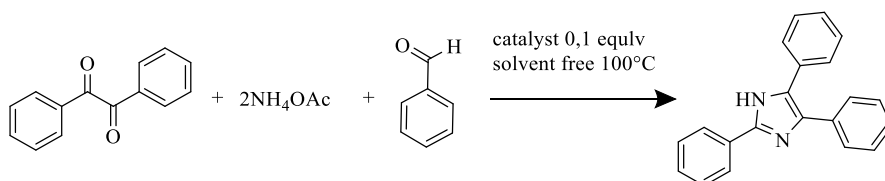
Step 3:



Scheme 5.

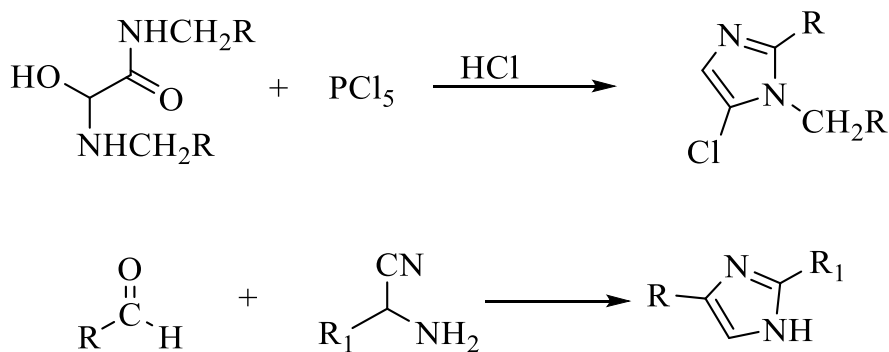
amines on the surface of silica gel under solvent-free conditions with microwave irradiation, yielding moderate efficiencies (Scheme 4).

The mechanism of the *Debus-Radziszewski* reaction for the synthesis of 2,4,5-trisubstituted imidazole is provided in Scheme 5 [23]. Safari et al. [24] obtained trisubstituted imidazoles in 80 % yields using the condensation of benzyl, various aldehydes and NH<sub>4</sub>OAc

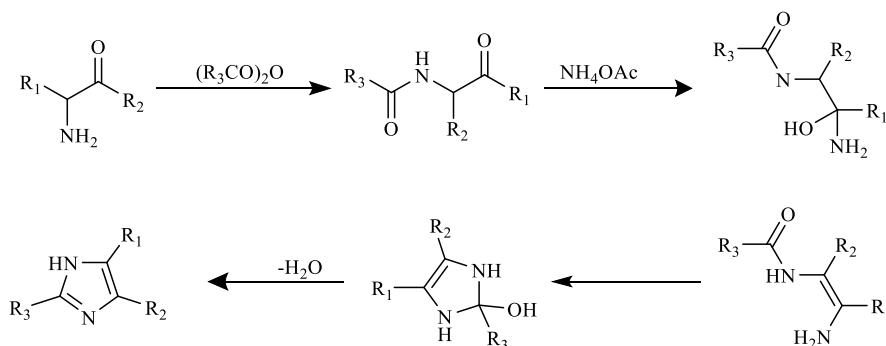


Scheme 6.

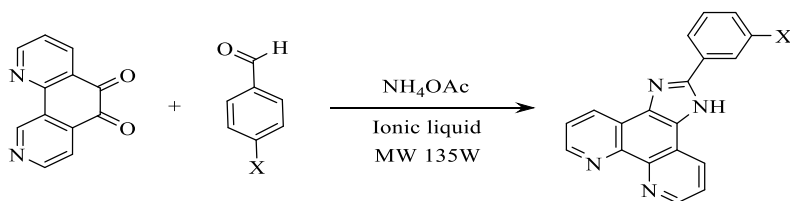




Scheme 7.



Scheme 8.



X = H ; 4-Cl; 4-F; 2-NO<sub>2</sub>; 3-NO<sub>2</sub>; 4-NO<sub>2</sub>; 2-OH; 4-OH; 4-OMe; 2,4,6-OMe; 4-CN; 4-N(Me)<sub>2</sub>

Scheme 9.

under microwave irradiation, under solvent-free conditions. The effective catalyst employed was (NH<sub>4</sub>)<sub>6</sub>Mo<sub>7</sub>O<sub>24</sub>·4H<sub>2</sub>O (Scheme 6).

Wallach et al. [25] have reported the reaction of N, N-dimethyl oxamide with phosphorus pentachloride PCl<sub>5</sub> as a convenient method of obtaining 5-chloro-substituted chlorinated imidazole in extremely moderate yields. Imidazole can be obtained by reacting aldehydes and aminonitrile derivatives (Scheme 7).

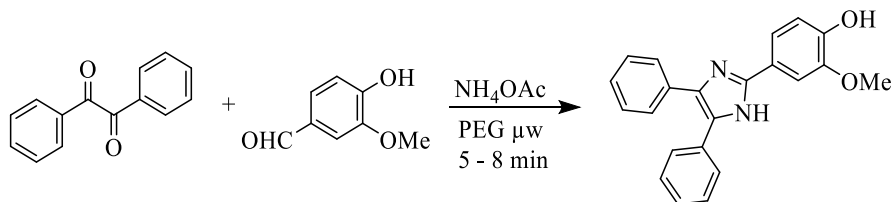
Moreover, cyclization of α-acylamino ketones in the presence of ammonium anhydride and acetate leads to the formation of imidazole in excellent yields (Scheme 8) [26].

### 3. The development of derivatives tri- or tetra imidazole, via microwave processes

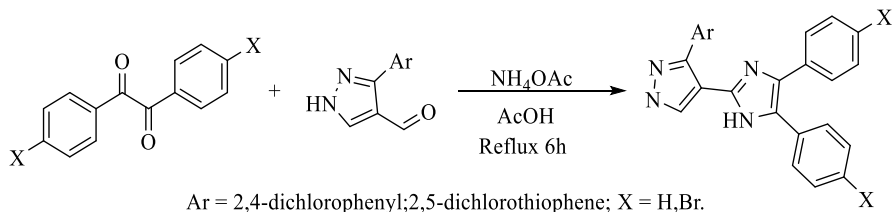
Qasim et al. [27] conducted the synthesis of 2-phenylimidazo [4,5-f], [1,10]phenanthrolines in a single step from three components: 1,10-phenanthroline-5,6-dione, various aldehydes, and NH<sub>4</sub>OAc, using SnCl<sub>2</sub>·2H<sub>2</sub>O as a cost-effective and non-hazardous catalyst. This reaction was carried out at room temperature, resulting in an excellent yield of 85 %, as illustrated in Scheme 9.

In 2010, Nalage et al. [28] carried out the synthesis of triaryl-imidazole in the presence of polyethylene glycol using benzyl, 3-methoxy-4-hydroxybenzaldehyde, and ammonium acetate under microwave irradiation for 5 min, achieving yields of up to 71 % (Scheme 10).

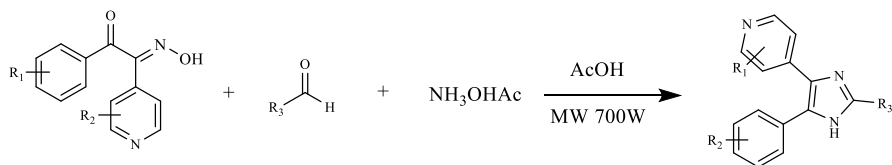
However, Wahyuningrum et al. [29] conducted the synthesis of 4,5-disubstituted imidazoles in the presence of MAOS by reacting a



Scheme 10.



Scheme 11.



Scheme 12.

diketone with various aldehydes or ketones, using  $\text{NH}_4\text{OAc}$  in glacial  $\text{AcOH}$  assisted by microwave irradiation for 5–7 min, achieving yields exceeding 84 % (Scheme 11).

Furthermore, Sparks et al. [30] synthesized the tri-substituted imidazole using keto-oxime and aldehyde with  $\text{NH}_4\text{OAc}$  in  $\text{AcOH}$  under microwave irradiation, with yields not exceeding 70 % during the cyclization of N-hydroxy imidazole at around 200 °C for 20 min (Scheme 12).

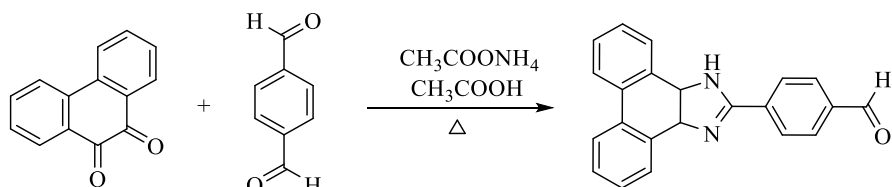
#### 4. Other techniques for synthesizing tri or tetra - imidazole include

This section of the review aims to explore alternative methods for synthesizing 2,4,5-substituted imidazoles, as well as 1,2,4,5-tetrasubstituted imidazoles. Consequently, several research groups have dedicated themselves to the synthesis of imidazole and the investigation of its numerous pharmacological properties. Steck and Day et al. synthesized 4-(1H-phenanthro [9,10-d]-imidazole-2-yl)-benzaldehyde from 9,10-phenanthroquinone with terephthalaldehyde and  $\text{NH}_4\text{OAc}$  in glacial  $\text{AcOH}$ , achieving excellent yields exceeding 70 % (Scheme 13) [31].

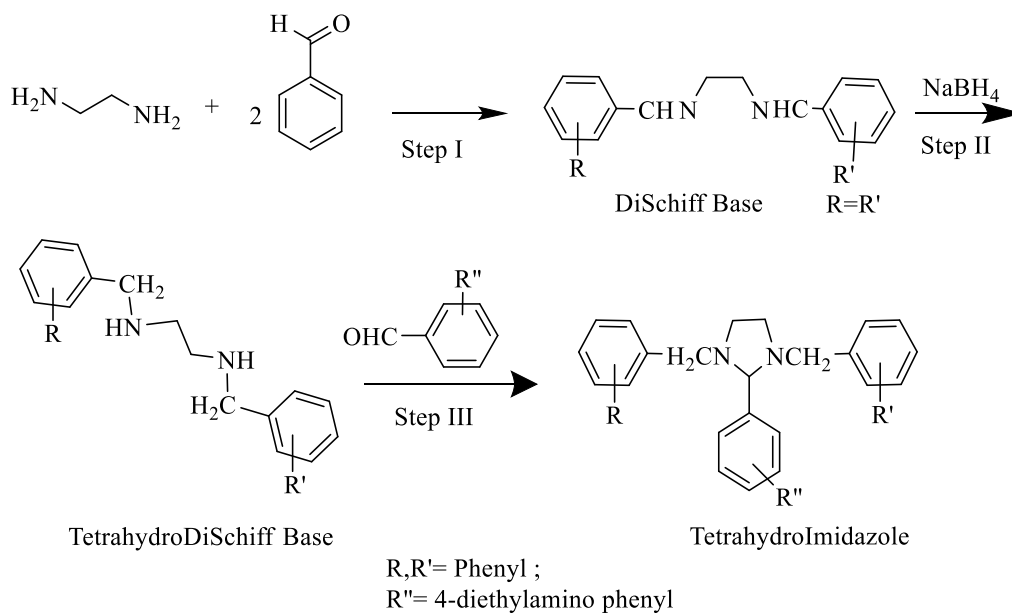
In 2001, Sharma et al. [32] synthesized their respective Schiff bases from aromatic aldehydes using ethylenediamine. These new compounds were then reduced to obtain tetrahydrodi Schiff bases. Finally, these derivatives were prepared with various aromatic aldehydes to yield tetrahydroimidazoles with yields exceeding 80 % (Scheme 14).

In 2007, Heravi et al. [33] synthesized triphenyl-imidazole with yields exceeding 92 % by condensing benzyl acetate and ammonium with aldehydes, in the presence of  $\text{NiCl}_2 \cdot 6\text{H}_2\text{O}$  as a catalyst in refluxing ethanol (Scheme 15).

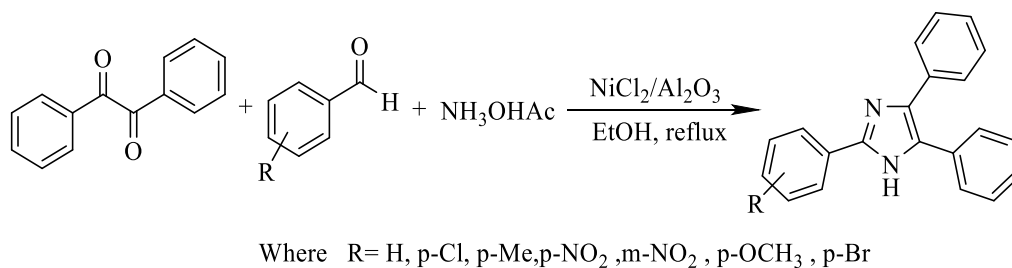
The same year, they developed and improved an efficient procedure for the synthesis of a tetrasubstituted imidazole, using Keggin-



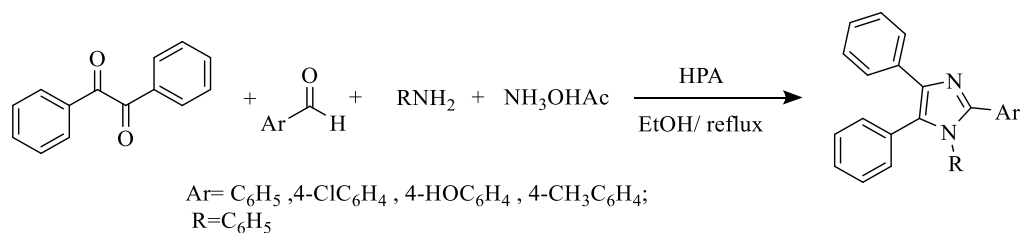
Scheme 13.



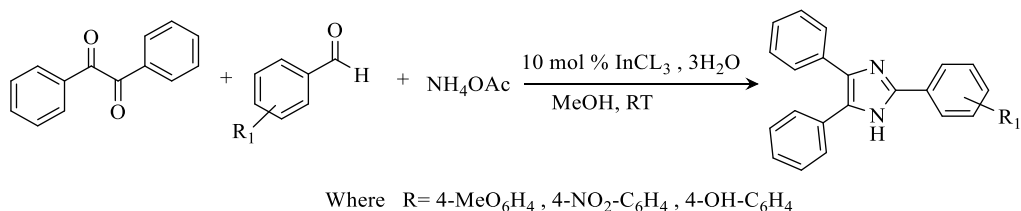
Scheme 14.



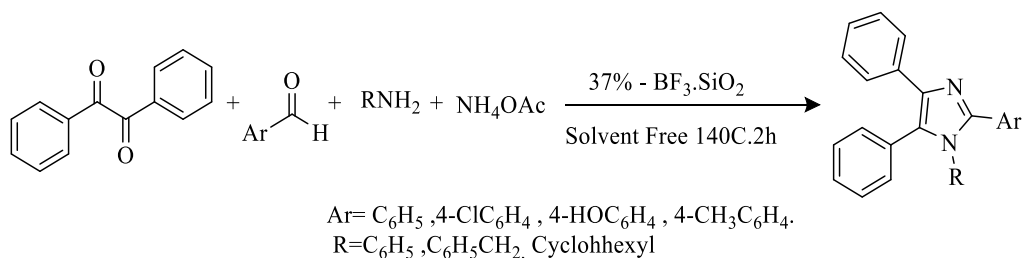
Scheme 15.



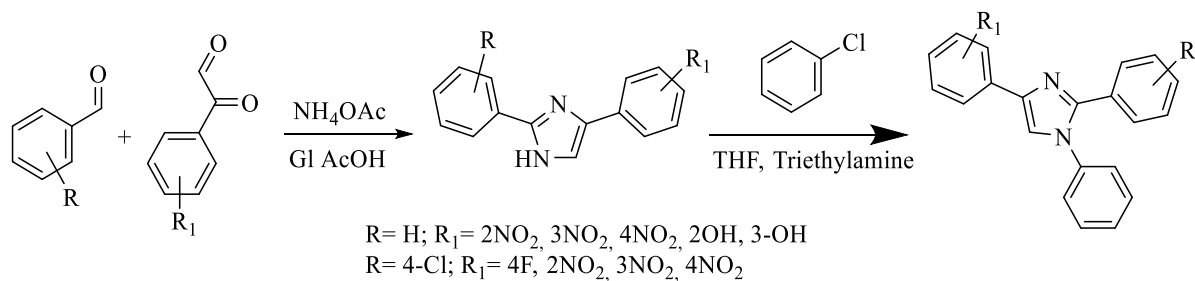
Scheme 16.



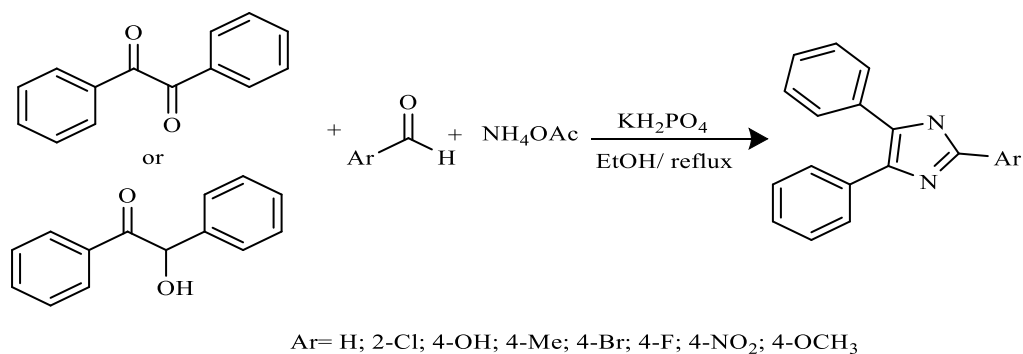
Scheme 17.



Scheme 18.



Scheme 19.



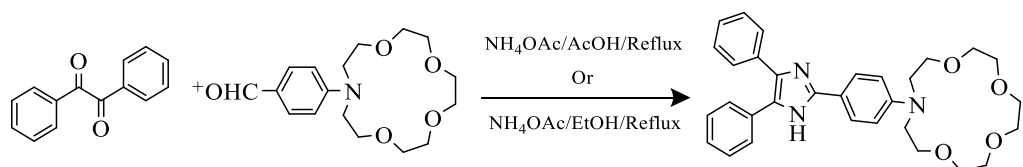
Scheme 20.

type heteropolytungstic acid (HPA) as a catalyst in refluxing ethanol (Scheme 16).

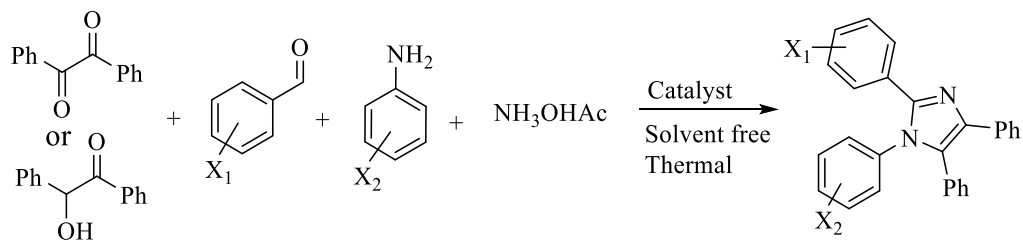
In 2008, Sharma et al. [34] accomplished the one-step synthesis of tri-substituted or tetra-substituted imidazoles with yields reaching 82 % at room temperature. This synthesis was carried out using benzyl, NH<sub>4</sub>OAc in the presence of InCl<sub>3</sub>.3H<sub>2</sub>O as a catalyst, and benzaldehyde (Scheme 17).

That year, Sadeghi et al. [35] synthesized 1,2,4,5-tetra-substituted imidazole using silica-supported boron trifluoride (BF<sub>3</sub>, SiO<sub>2</sub>) as a catalyst, a reusable and cost-effective material, in reaction with benzyl, aromatic aldehyde, amine, and NH<sub>4</sub>OAc. This one-step reaction is very simple, rapid, efficient, and yields a very high yield, reaching 96 % (Scheme 18).

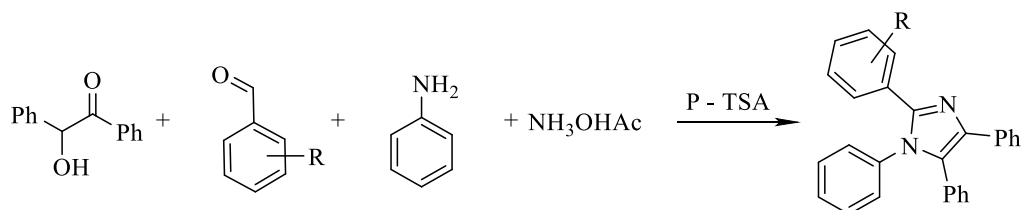
In 2009, Husain et al. [36] synthesized disubstituted imidazole using aromatic aldehydes, phenylglyoxal, ammonium acetate, and acetic acid. Subsequently, by mixing the 1,2,4-disubstituted imidazoles with chlorobenzene in the presence of triethylamine and



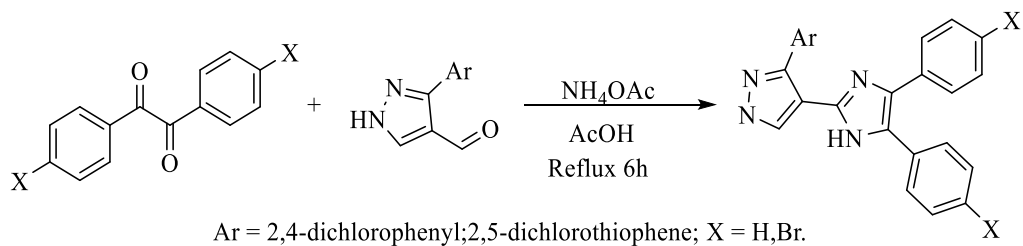
Scheme 21.



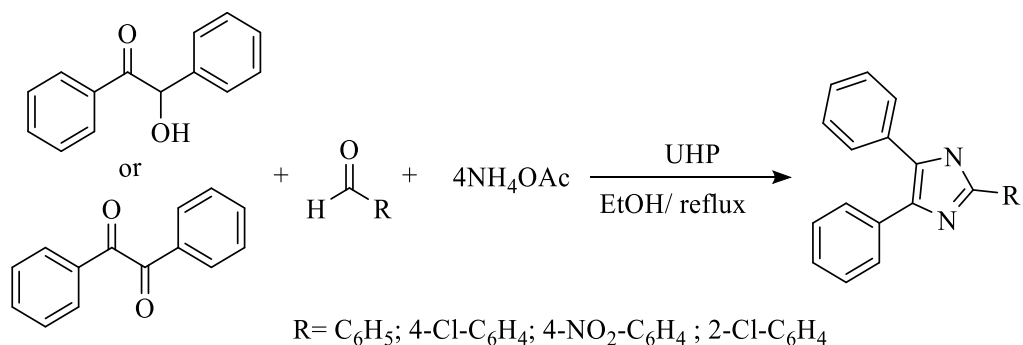
Scheme 22.



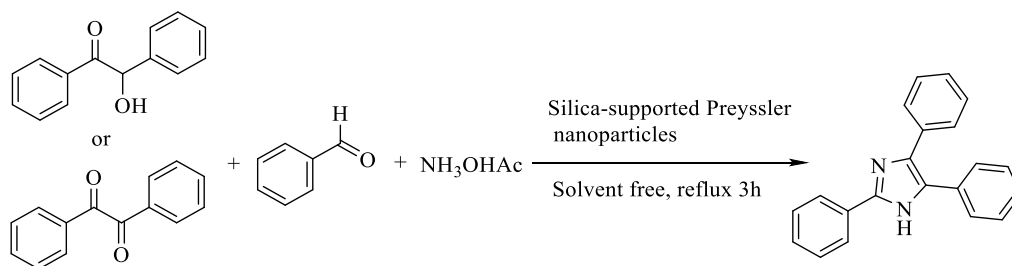
Scheme 23.



Scheme 24.



Scheme 25.



Scheme 26.

tetrahydrofuran (THF), the new product was obtained with a yield of 74 % (Scheme 19).

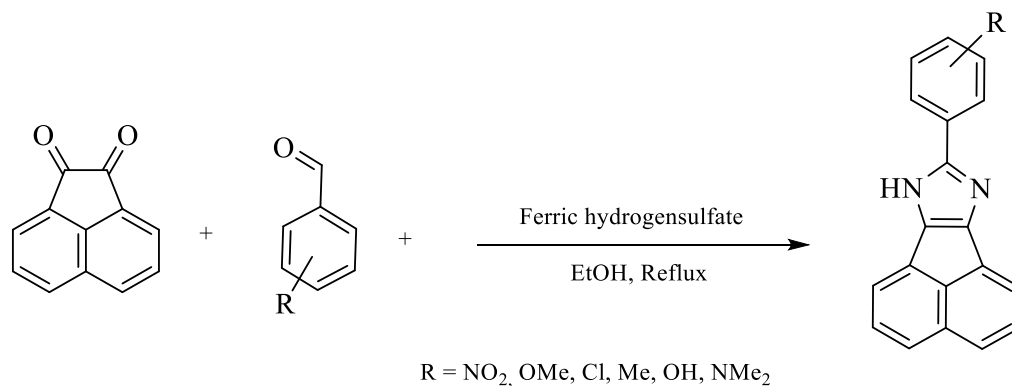
In 2010, Joshi et al. [37] synthesized 2-aryl, 4,5-diphenylimidazole by refluxing it in ethanol for 40–90 min under mild reaction conditions. They employed benzyl/benzoin with various aldehydes and ammonium acetate. This method, conducted in the presence of potassium dihydrogen phosphate ( $\text{KH}_2\text{PO}_4$ ), is simple, effective, and resulted in excellent yields reaching 93 % (Scheme 20).

In the same year, Oliveira et al. [38] prepared a new family of Diphenyl-imidazole-2-yl-phenyl-tetraoxa7-azacyclopentadecane from the formyl azacrown ether with  $\text{NH}_4\text{OAc}$  in glacial AcOH or ethanol for 12 h at reflux. This straightforward reaction resulted in a good to excellent yield, exceeding 64 % (Scheme 21).

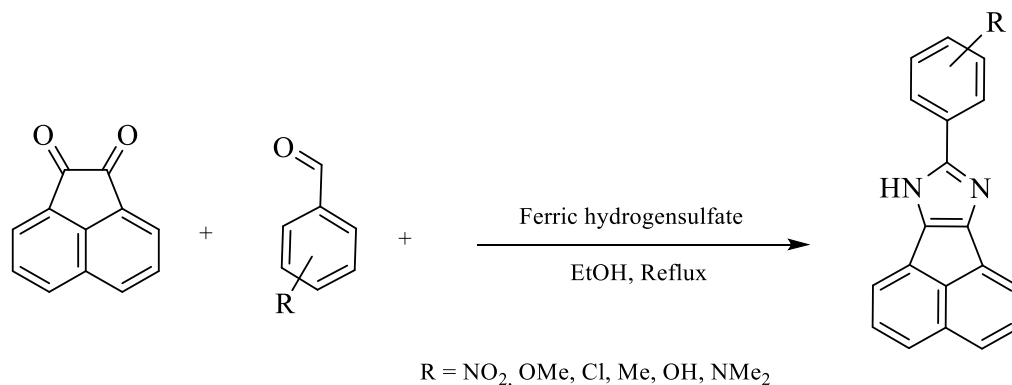
In 2011, Shaterian and Runge et al. [39] achieved the synthesis of 2,4,5-substituted imidazoles, as well as 1,2,4,5-tetrasubstituted imidazoles, using a solvent-free ionic liquid and a catalyst containing a Brønsted acid, namely triphenyl (propyl-3-sulfonyl) phosphonium toluene sulfonate, at a temperature of 100 °C. This method yielded excellent yields surpassing 96 % (Scheme 22).

In the same year, Pasha et al. [40] developed the synthesis of 1,4,5-phenyl,2-substituted imidazoles by condensing benzoin, aniline,  $\text{NH}_4\text{OAc}$ , and araldehydes with a simple catalyst, *p*-toluenesulfonic acid, in ethanol as a solvent under reflux. This method is straightforward, rapid, and resulted in yields of up to 92 % (Scheme 23).

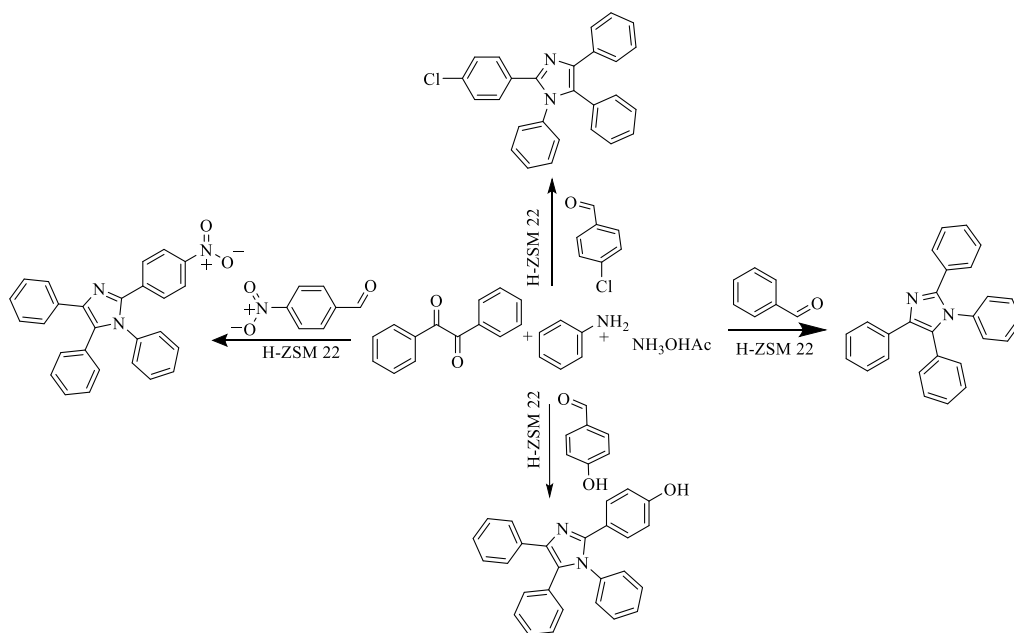
Furthermore, Vijesh et al. [41] synthesized 2,4,5-trisubstituted compounds by reacting 3-aryl-1H-pyrazole-4-carbaldehyde and



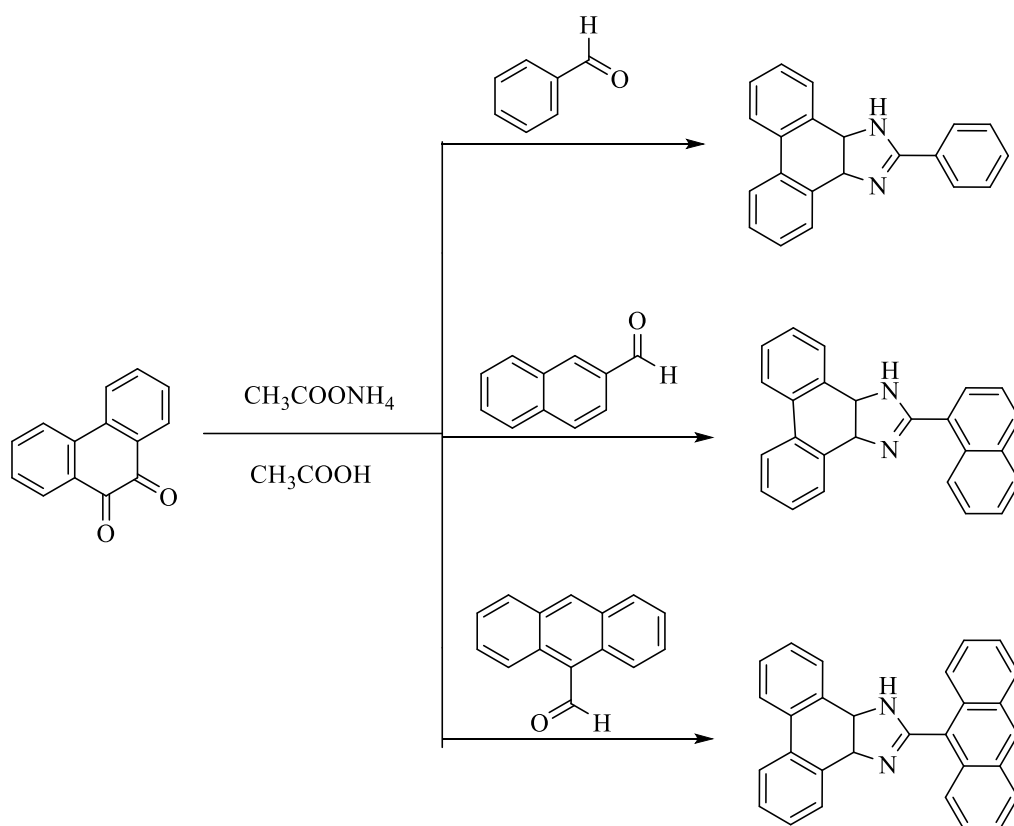
Scheme 27.



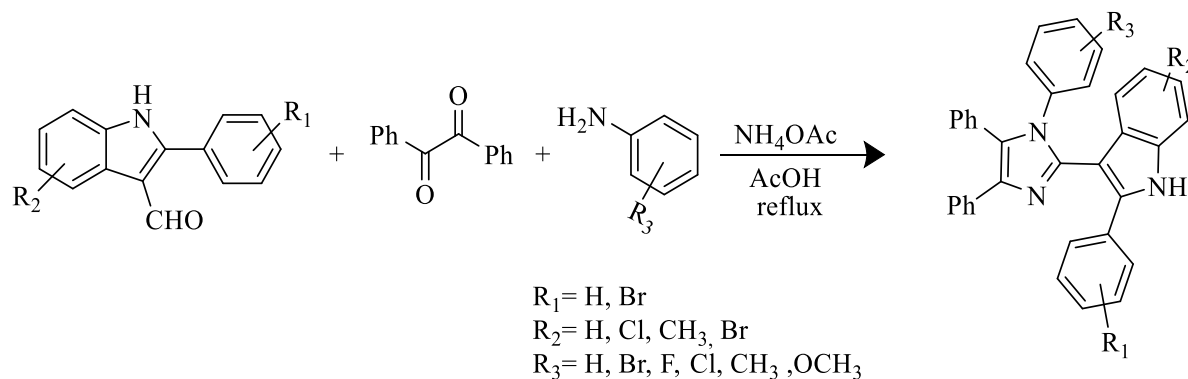
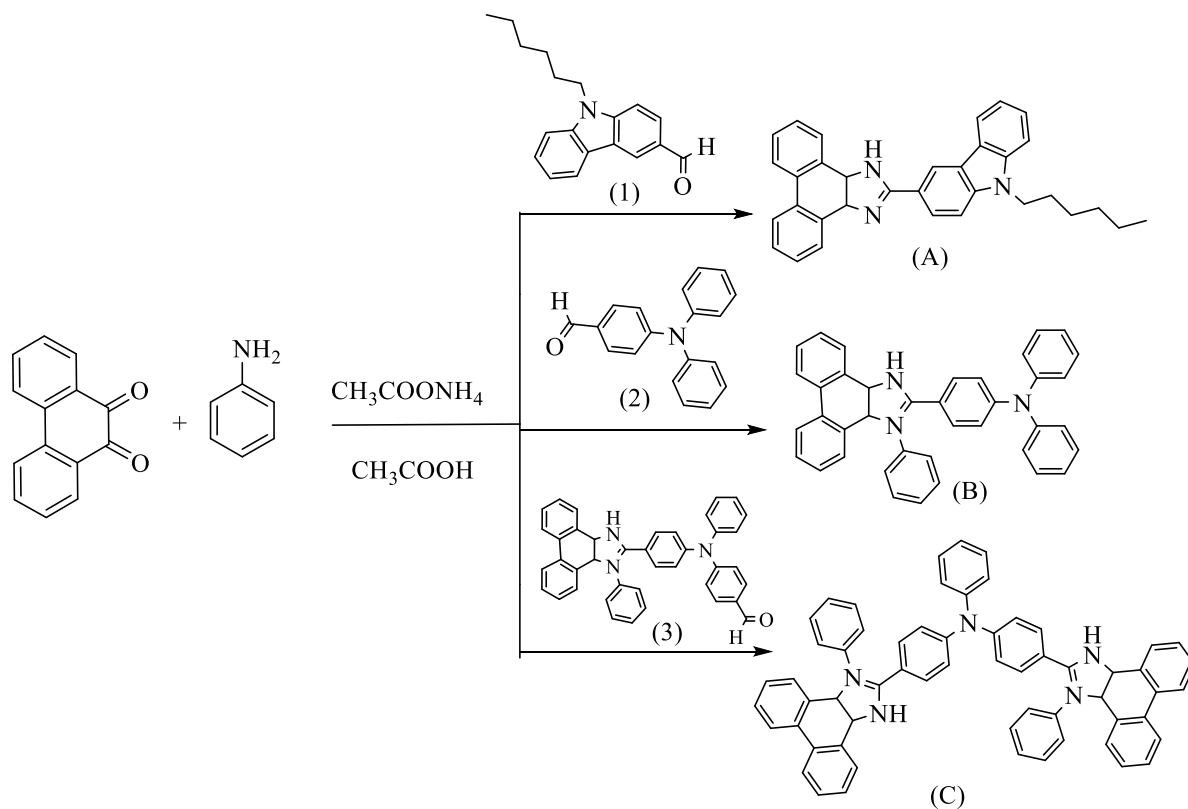
Scheme 28.



Scheme 29.



Scheme 30.



2-diketones with  $\text{NH}_4\text{OAc}$  in the presence of glacial acetic acid under reflux, achieving reasonably high yields up to 86 % (Scheme 24).

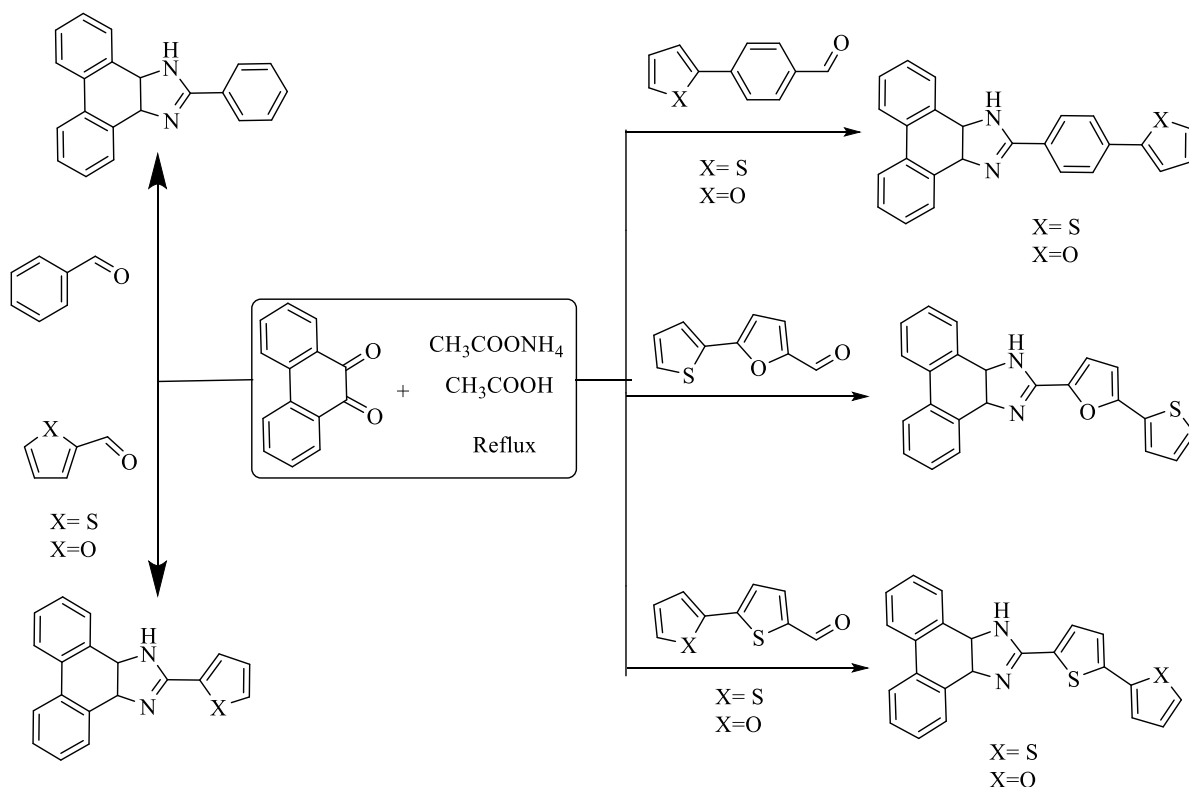
In 2013, Maleki et al. [42] synthesized 2-substituted 4,5-diphenylimidazole using benzyl or benzoil,  $\text{NH}_4\text{OAc}$ , and aldehydes, with hydrogen peroxide (UHP) as the catalyst, in ethanol under reflux. This reaction resulted in a yield of 88 %, as illustrated in Scheme 25.

In 2014, Gharib et al. [43] accomplished the multicomponent synthesis of 2,4,5- and 1,2,4,5-tetrasubstituted -1H-imidazole derivatives through the condensation of benzyl/benzoil,  $\text{NH}_4\text{OAc}$ , and aldehydes in the presence of silica-supported heteropolytungstic acid as a catalyst, with reflux, resulting in an excellent yield exceeding 94 % (Scheme 26).

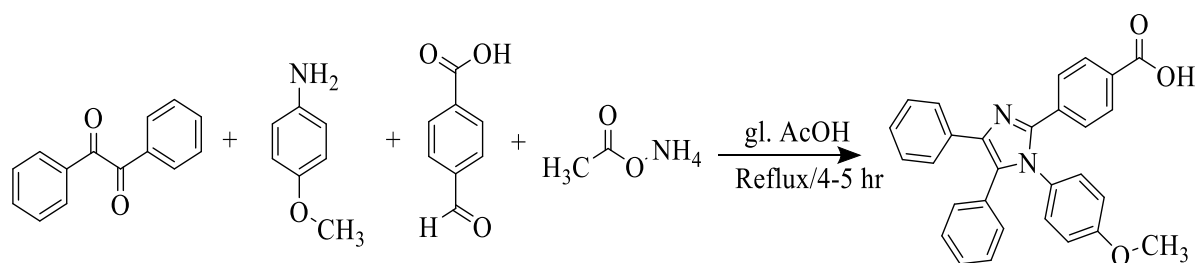
In the same year, Sandroos et al. [44] developed an innovative and efficient method for the synthesis of 8-aryl-7H-acenaphtho [1, 2-d]imidazole, resulting in excellent yields of 93 % under reflux. This approach involved the use of acenaphthylene-1,2-dione, substituted aldehydes,  $\text{NH}_4\text{OAc}$ , and ericinium hydrogen sulfate in ethanol (Scheme 27).

In 2015, Subeesh et al. [45] synthesized 2-(pyren-1-yl)-1H-phenanthro [9,10-d]imidazole with a yield of 60 %. This synthesis was carried out using phenanthrene-9,10-dione and pyrene-1-carbaldehyde with  $\text{NH}_4\text{OAc}$  in the presence of glacial AcOH under a nitrogen





Scheme 33.



Scheme 34.

atmosphere, during a 12-h reflux (Scheme 28).

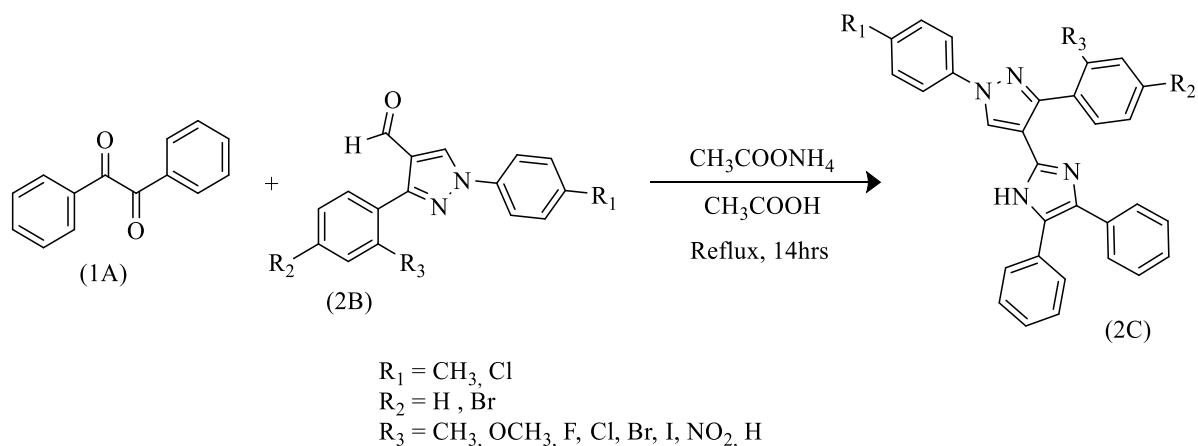
In 2016, Bha et al. [46] synthesized tetra-substituted imidazoles using various aldehyde derivatives in this reaction, with benzyl amines, and  $\text{NH}_4\text{OAc}$  in the presence of H-ZSM-22 as a catalyst, achieving a good yield of 86 % under solvent conditions (Scheme 29).

In the same year, Wang et al. [47] synthesized and characterized three ligands: 2-phenyl-1H-imidazo [4,5-f], [1,10]phenanthroline from benzaldehyde (1), 2-(2-naphthyl)1H-imidazo [4,5-f]phenanthroline from 2-naphthaldehyde (2), and 2-(2-anthryl)-1H-imidazo [4,5-f]phenanthroline from 9-anthrylaldehyde (3). These syntheses were carried out in the presence of ammonium acetate and AcOH for 4 h under reflux, with yields ranging from 45 to 68 % (Scheme 30).

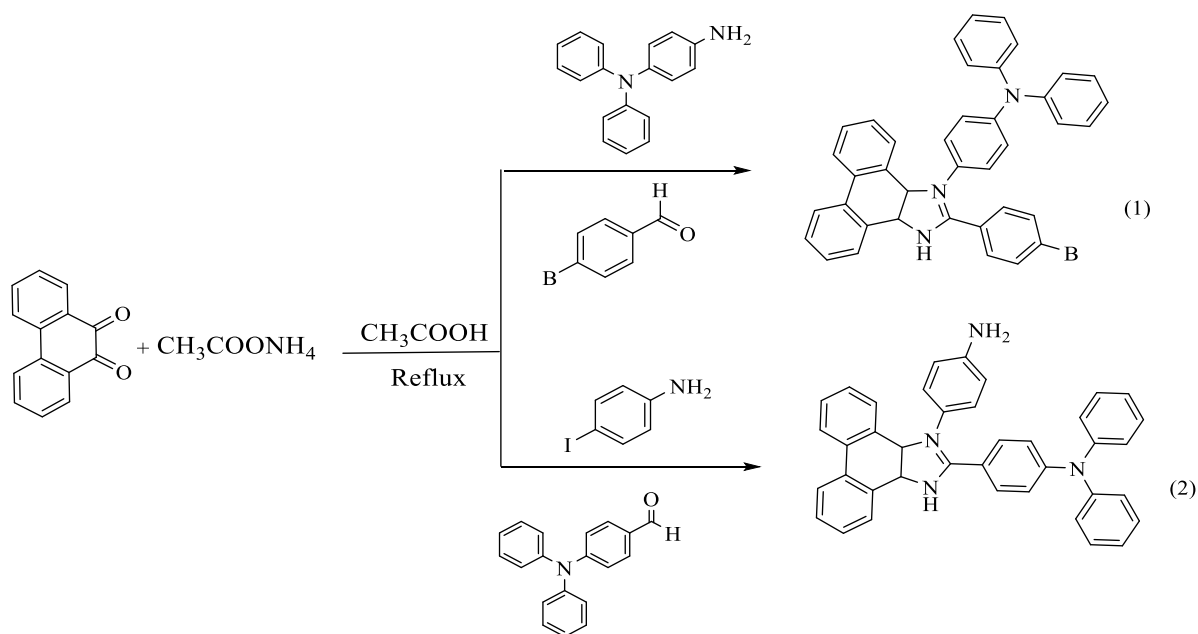
Additionally, Tavgeniene et al. [48] described three new derivatives, namely 2-(9-hexylcarbazoyl-3-yl)-1-phenylphenanthro [9,10-d]imidazole (A), 2-[4-(N,N-diphenylamino)phenyl]-1-phenylphenanthro [9,10-d]imidazole (B), and bis [4-(1-phenylphenanthro [9,10-d]imidazole-2-yl)phenyl]-N-phenylamine (C). These compounds were obtained using an excess of phenanthro [9,10-d]imidazole and 3-formyl-9-hexylcarbazole (1), 4-(diphenylamino)benzaldehyde (2), and diformyltriphenylamine (3), with  $\text{NH}_4\text{OAc}$  and aniline in AcOH, resulting in yields ranging from 64 to 44 % (Scheme 31).

In 2017, Naureen et al. [49] synthesized tetra-arylimidazole based on indole by refluxing, using 2-arylimidole-3-carbaldehydes, benzyl, anilines, and  $\text{NH}_4\text{OAc}$  in the presence of AcOH (Scheme 32).

In the same year, Ferreira et al. [50] synthesized phenanthroimidazole ligands using the Radziszewski method, employing various synthetic methodologies involving the precursors 9,10-phenanthrene-9,10-dione and formaldehyde with  $\text{NH}_4\text{OAc}$  in glacial AcOH. This



Scheme 35.



Scheme 36.

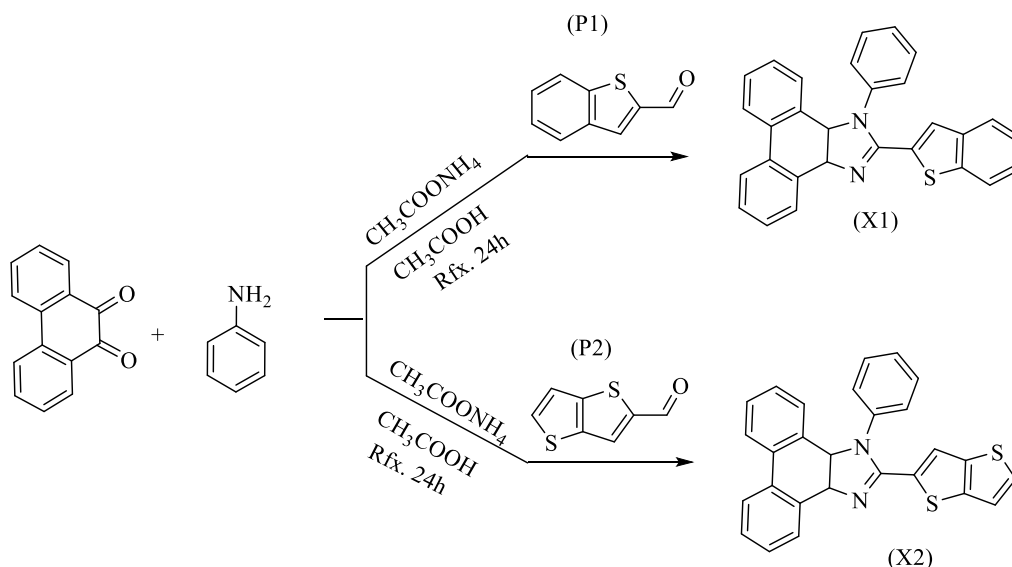
synthesis was carried out with moderate to excellent yields, ranging from 54 to 89 %, by refluxing for 8 h (Scheme 33).

In 2018, Ravindra et al. [51] synthesized a new compound, 4-(1-(4-methoxyphenyl)-4,5-diphenyl-1H-imidazole-2-yl)phenyl carboxylic acid, from 4-methoxyaniline, benzyl,  $\text{NH}_4\text{OAc}$ , and 4-formyl-benzoic acid, using glacial acetic acid as a solvent and a catalytic amount of concentrated sulfuric acid, under reflux, yielding 70 % (Scheme 34).

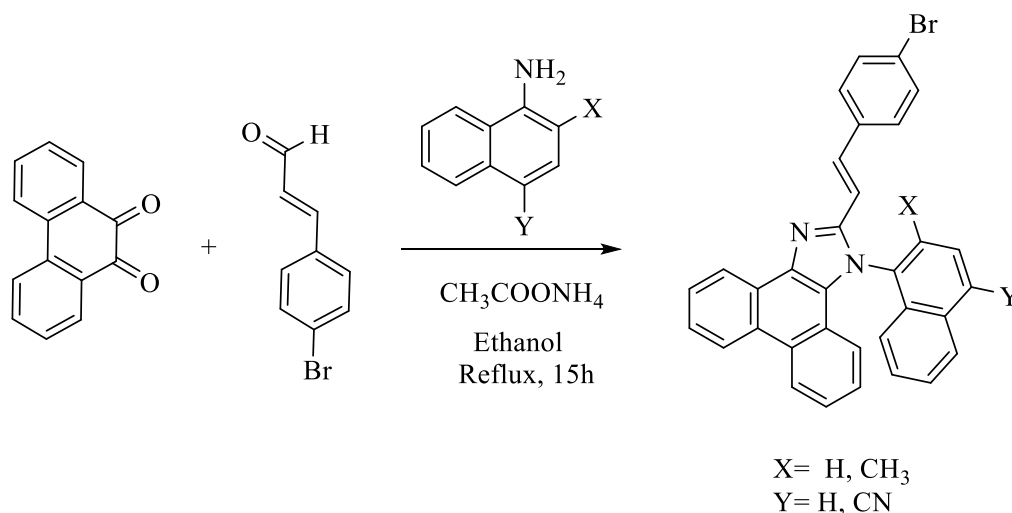
In the same year, Harshad et al. [52] prepared new tri-substituted imidazole derivatives (2C) using the well-known Radziszewski reaction. This synthesis was based on different derivatives of 1H-pyrazole-4-carbaldehyde (2B), with benzyl (1A) and  $\text{NH}_4\text{OAc}$  in glacial acetic acid, achieving good to excellent yields under reflux conditions (Scheme 35).

Similarly, Anupama et al. [53] developed a compound (1) synthesized from 9,10-phenanthrenequinone with bromobenzaldehyde and N1,N1-diphenylbenzene-1,4-diamine. For compound (2), it was prepared from 9,10-phenanthrenequinone with (diphenylamino)benzaldehyde and 4-iodoaniline. In both cases, the mixture with  $\text{NH}_4\text{OAc}$  in the presence of glacial AcOH for 4 h at reflux resulted in respective yields of 68 % and 76 % (Scheme 36).

Additionally, Kula et al. [54] synthesized a new compound, phenanthro [9,10-d]imidazole, with an excellent yield ranging from 76 % to 72 %. This cost-effective synthesis was achieved through an efficient method, the Debus Radziszewski reaction, by combining benzo [b]thiophene-2-carbaldehyde (P1) or thieno [3,2-b]thiophene-2-carbaldehyde (P2) with phenanthrenequinone, aniline, and  $\text{NH}_4\text{OAc}$  in the presence of acetic acid to obtain the new compound 2-(benzo[b]thiophene-2-yl)-1-phenyl-1H-phenanthro [9,10-d]



Scheme 37.



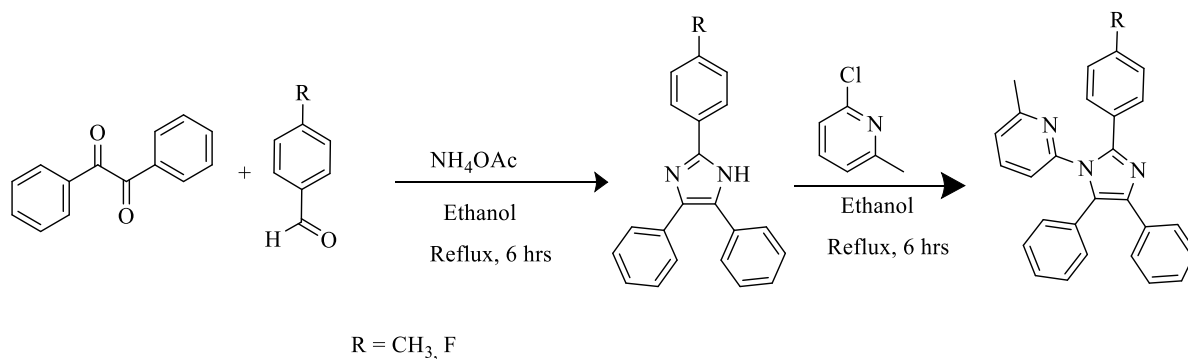
Scheme 38.

imidazole (X1) or 2-(thieno [3,2-b]thiophene-2-yl)-1-phenyl-1H-phenanthro [9,10-d]imidazole (X2) (Scheme 37).

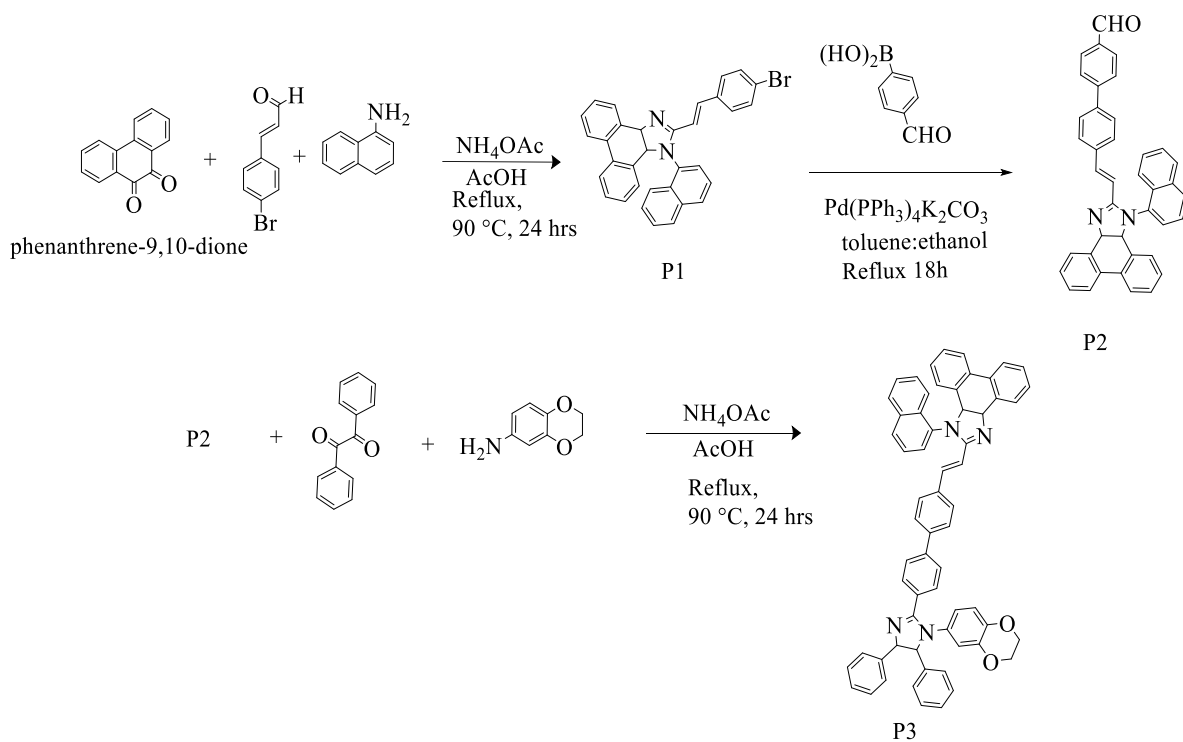
However, Jayaraman et al. [55] synthesized 2-(4-bromostyryl)-1-(naphthalen-1-yl)-1H-phenanthro [9,10-d]imidazole using phenanthrene-9,10-dione, 4-bromo-1-cinnamaldehyde, 1-naphthylamine, and  $\text{NH}_4\text{OAc}$  in AcOH or ethanol, refluxing for approximately 15 h, and achieving yields ranging from 58 % to 68 % (Scheme 38).

In 2019, Amala et al. [56] utilized the Radziszewski reaction as the foundation for the synthesis of derivatives of 2,4,5-triphenyl-1H-imidazole-1-(2-chloro)-6-methylpyridine. They carried out this synthesis in the presence of ethanol as the solvent, with anhydrous potassium carbonate and 2-chloro-6-methylpyridine, stirred at cold temperatures for 6 h, achieving a good yield ranging between 87 and 90 % (Scheme 39).

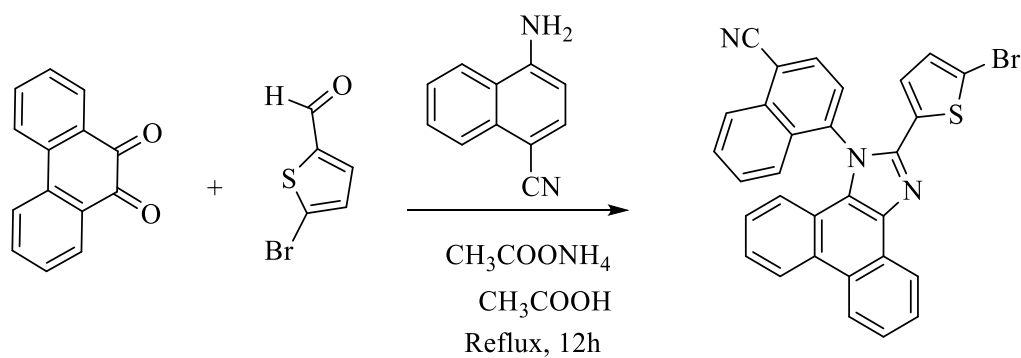
In the same year, Jayabharathi et al. [57] described a new protocol for the synthesis of compound (P1) with a yield of 75 %. This compound was synthesized from 9,10-phenanthrenequinone, naphthalene-1-amine, and (E)-3-(4-bromophenyl)acrylaldehyde in the presence of ammonium acetate in acetic acid under a nitrogen atmosphere. Then, by mixing the obtained product with 4-formylphenylboronic acid, aqueous  $\text{K}_2\text{CO}_3$  in a toluene:ethanol mixture, using  $\text{Pd}(\text{PPh}_3)_4$  as a catalyst, the product was obtained with a yield of 73 %. For the resulting compound (P2), a mixture with 2,3-dihydrobenzo [b] [1,4]dioxine-6-amine and benzyl in acetic acid in the presence of ammonium acetate was refluxed, resulting in the final product (P3) with a good yield ranging between 62 and 78 % (Scheme 40).



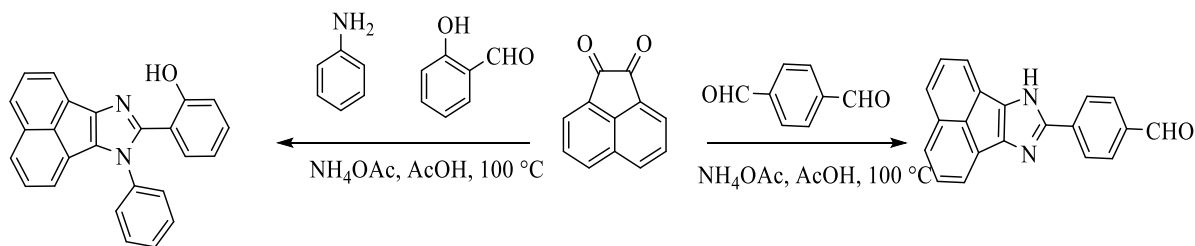
Scheme 39.



Scheme 40.



Scheme 41.



Scheme 42.

However, Jayaraman et al. [58] have synthesized new compound of the imidazole [4-(2-(5-bromothiophen-2-yl)-1H-phenanthro[9,10-d]imidazole-1-yl)naphthalene-1-carbonitrile] with good yield 65–70 % by using 5-bromothiophene-2-carbaldehyde, 4-amino-naphthalene-1-carbonitrile, and  $\text{NH}_4\text{OAc}$  in  $\text{AcOH}$  at reflux about 12h (Scheme 41).

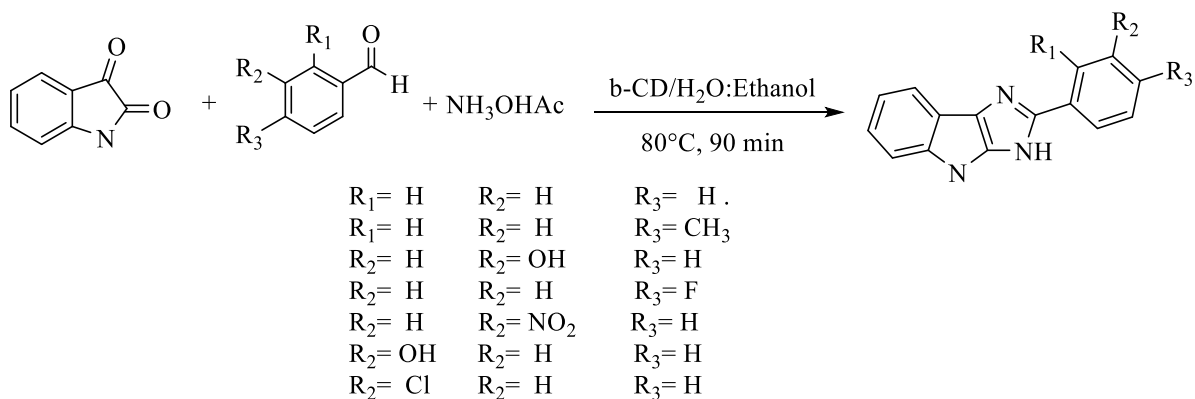
On the other hand, Singh et al. [59] prepared the products 2-(7-phenyl-7H-acenaphtho [1,2-d]imidazole-8-yl)phenol (A) and 4-(7H-acenaphtho [1,2-d]imidazole-8-yl)benzaldehyde (B) in 52–64 % yield from the condensation of acenaphthoquinone and aniline, salicylaldehyde for compound (A), but terephthalaldehyde for compound (B), all reagents being used with  $\text{NH}_4\text{OAc}$  in glacial  $\text{AcOH}$  (Scheme 42).

In 2020, Nipate et al. [60] synthesized 1,8-dihydroimidazo [2,3-b]indoles with yields of 79 % using  $\beta$ -cyclodextrin ( $\beta$ -CD) as an efficient, biodegradable, and recyclable catalyst. The reaction was carried out with isatin and three aldehyde compounds in the presence of  $\text{NH}_4\text{OAc}$  in a  $\text{H}_2\text{O}$ – $\text{EtOH}$  mixture under reflux. This method exhibited high yield, short reaction time, cost-effective starting material, non-toxicity, environmental friendliness, and easy availability (Scheme 43).

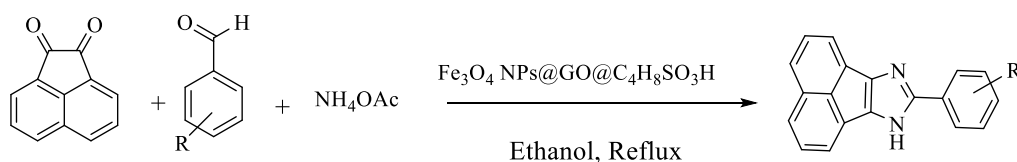
In the same year, Hasanzadeh et al. [61] prepared 8-aryl-7H-acenaphtho [1,2-d]imidazole using  $\text{Fe}_3\text{O}_4$  NPs@ $\text{GO}$ @ $\text{C}_4\text{H}_8\text{SO}_3\text{H}$  nanoparticles as a magnetic nanocatalyst, with acenaphthenequinone and ammonium acetate in ethanol under reflux, achieving a high yield ranging between 84 and 95 % (Scheme 44).

However, Peng et al. [62] prepared a new product (R-PPIM-TPA), where R represents Me, Cl,  $\text{C}(\text{CH}_3)_3$ , by combining a solution of 9, 10-phenanthrenequinone, 4-(diphenylamino)benzaldehyde, substituted aniline, and  $\text{NH}_4\text{OAc}$  in ethanol at 100 °C for 8 h, obtaining yields ranging from 51 to 63 % (Scheme 45).

In 2021, Burungale et al. [63] synthesized 1-substituted 2,4,5-triphenylimidazoles using acid chloride and triphenylimidazole in pyridine as a catalyst, with benzene as the solvent, under reflux for 4–5 h. The resulting new compound was isolated with a good yield

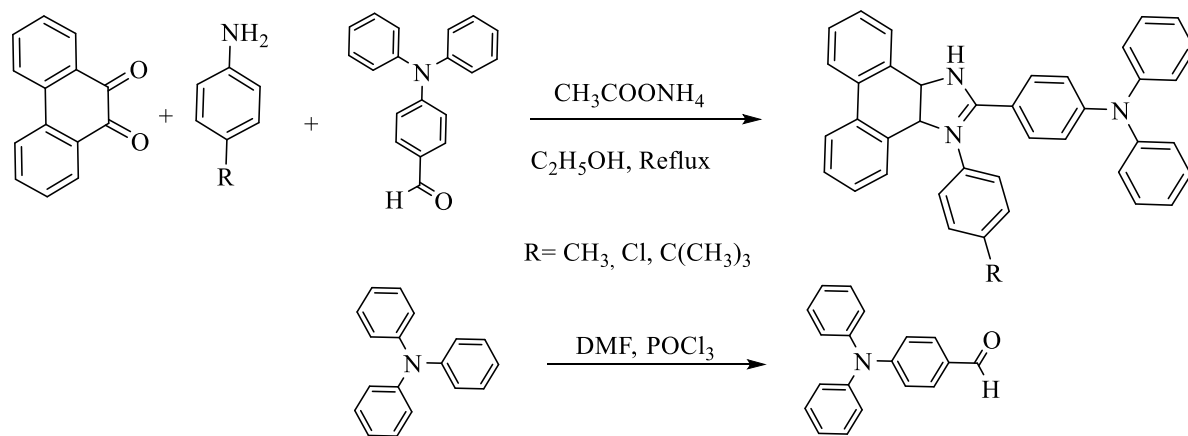


Scheme 43.

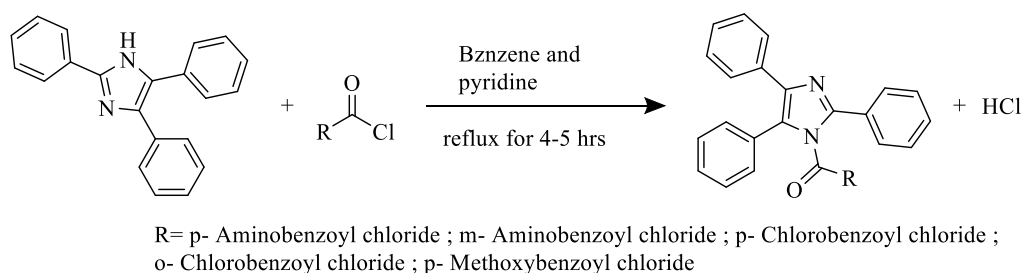


$\text{R} = 3\text{-NO}_2, 3\text{-OH}, 4\text{-Me}, 4\text{-Br}, 4\text{-F}, \text{H}, 2\text{-OH}, 2\text{-OH-3-OMe}, 2\text{-OMe}, 2,6\text{-Cl}_2$ .

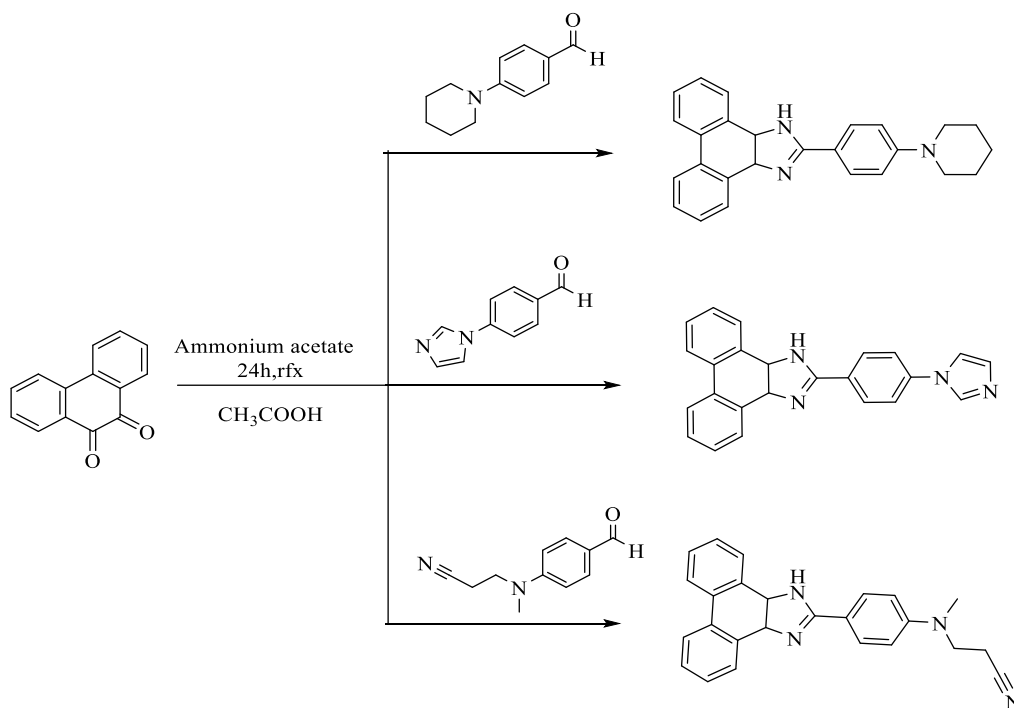
Scheme 44.



Scheme 45.

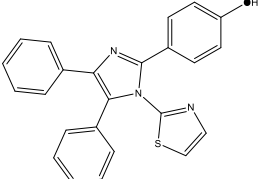
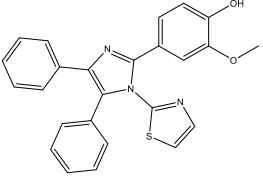
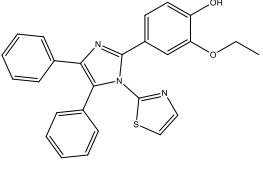
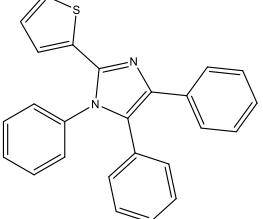
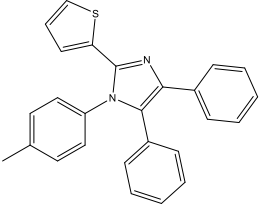
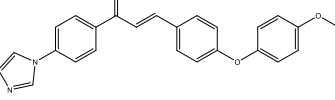
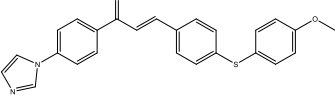
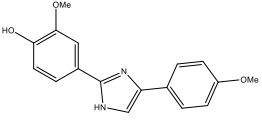


Scheme 46.



Scheme 47.

**Table 1**  
Antifungal activities of certain imidazole derivatives against three phytopathogenic fungi.

Compounds	bacterial strain	IC <sub>50</sub> (μg/ml)	Ref.
	<i>Fusarium oxysporum</i> <i>Candida albicans</i> <i>Aspergillus niger</i>	35 0.3 45	[74]
	<i>Fusarium oxysporum</i> <i>Candida albicans</i> <i>Aspergillus niger</i>	20 0.25 40	[74]
	<i>Fusarium oxysporum</i> <i>Candida albicans</i> <i>Aspergillus niger</i>	20 0.2 40	[74]
	<i>Fusarium oxysporum</i>	13	[75]
	<i>Fusarium oxysporum</i>	12	[76]
	<i>Candida albicans</i>	3.125	[77]
	<i>Candida albicans</i>	1.56	[77]
	<i>Candida albicans</i> <i>Aspergillus niger</i>	12.5 25	[78]

(continued on next page)

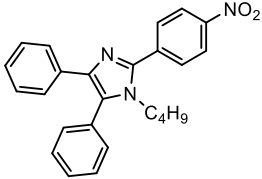
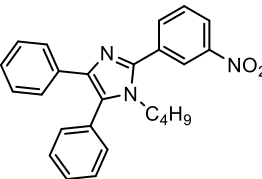
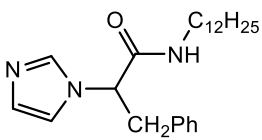
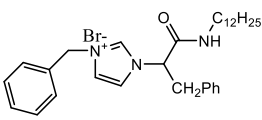
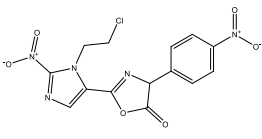
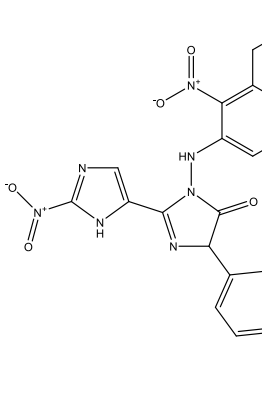




extremely high antifungal activity against *C. albicans*, *F. oxysporum*, and *A. niger* strains, compared to standard imidazole-based medications (Fig. 1). Nikalje et al. [74] observed that imidazole-thiazole compounds act by inhibiting ergosterol biosynthesis in *C. albicans*. Similarly, Husain et al. [78] revealed that imidazole derivatives exhibit excellent antifungal activity against *C. albicans* and *A. niger* strains with lower gastrointestinal irritation, especially compounds with methoxy (-OCH<sub>3</sub>) and nitro (-NO<sub>2</sub>) groups in the para position.

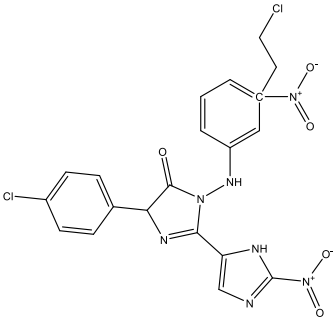
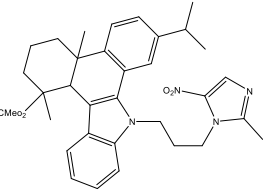
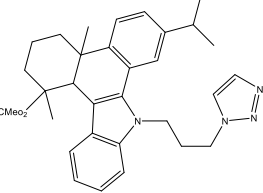
However, Ghorbani-Vaghei et al. [76] endeavored to investigate novel antifungal agents through in vitro susceptibility tests to establish guidelines for the potential clinical application of these new compounds against the *Fusarium oxysporum* strain. Both tested

**Table 2**  
The effect of various imidazole derivatives on two antibacterial strains.

Compounds	IC <sub>50</sub> (µg/ml)		Ref.
	E. coli	S. aureus	
	50	50	[80]
	50	50	[80]
	1000	16	[81]
	32	4	[81]
	50	50	[82]
	50	50	[82]

(continued on next page)

Table 2 (continued)

Compounds	IC <sub>50</sub> (µg/ml)		Ref.
	E. coli	S. aureus	
	50	50	[82]
	7.8	1.9	[83]
	15.6	31.2	[83]

compounds exhibited antifungal activity against *Fusarium oxysporum*, especially the one containing an alkyl group in the para position. Consequently, they can be regarded as promising antifungal agents.

### 5.1.2. Antibacterial activity

The antibacterial properties of imidazole as a compound are well-known. However, its direct use is often restricted due to its toxicity. To enhance both effectiveness and tolerance, modifications are frequently made to imidazole derivatives. Although imidazoles are primarily recognized for their antifungal properties, their antibacterial activity can vary depending on the specific compound and the class of targeted organisms. Table 2 presents some imidazole derivatives and their antibacterial activities against two strains, *Escherichia coli* (*E. coli*) and *Staphylococcus aureus* (*S. aureus*).

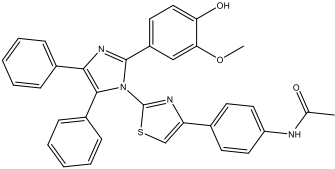
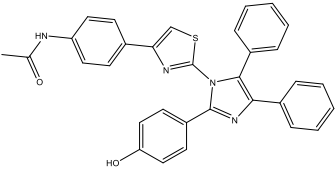
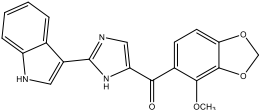
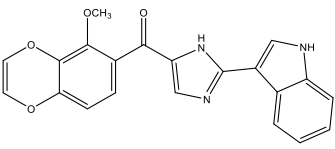
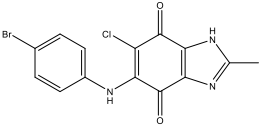
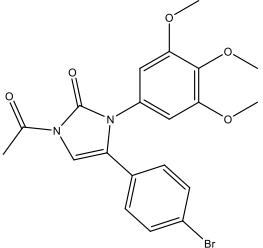
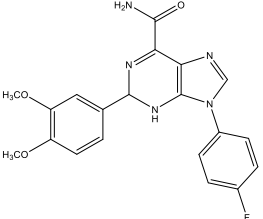
The results from Table 2 highlight that most derivatives of the imidazole core exhibit promising antibacterial activities, particularly against *E. coli* and *S. aureus* strains. Indeed, the presence of the nitro group (-NO<sub>2</sub>) in the compounds listed in Table 2 shows high activity against the studied bacterial strains. This is explained by the formation of hydrogen bonds with the active centers of cellular constituents, disrupting the normal cell structure and causing bacterial death [84]. On the other hand, Wen et al.'s research [83] tested various imidazole derivatives for their antibacterial activities and showed that compounds carrying a smaller alkyl amine motif exhibit moderate antibacterial activities. This is explained by the fact that the lipophilicity and size of the side chain of these derivatives play a crucial role in their antimicrobial activities.

### 5.1.3. Anticancer activities

Studies on imidazole compounds as anticancer agents have shown that some of these derivatives may exhibit antiproliferative properties and induce apoptosis in cancer cells. However, it is important to note that the anticancer efficacy can depend on various factors, such as the specific chemical structure of the derivative, the specific cell line, and the underlying molecular mechanisms. Table 3 summarizes certain imidazole derivatives along with their anticancer activities.

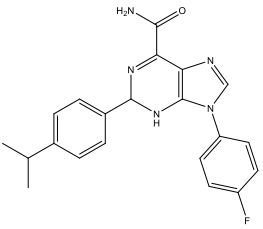
The imidazole derivatives listed in Table 3 exhibit significant anticancer activities against various cancer cell lines. Indeed, imidazole has the potential to overcome the limitations of current clinical drugs such as methotrexate, etoposide, and paclitaxel, which are used as chemotherapeutic agents. Therefore, the imidazole core could be utilized as a chemical structure for new anticancer agents with multiple potential mechanisms of action. In this regard, Sharma et al. [85] studied several imidazole derivatives that showed potent activity with a notable half-maximal inhibitory concentration (IC<sub>50</sub>). The presence of a phenolic group in imidazole compounds significantly affects activity due to their binding capability to cytoplasmic hormone receptors. Furthermore, in the search for more

**Table 3**  
Effect of various imidazole derivatives on certain anticancer cell lines.

Compounds	Cell Line	IC <sub>50</sub> (μM)	Mechanism	Ref.		
	Lymphoma Ascites (DLA)	138.50	Not determined	[85]		
	Erich's Ascites Carcinoma (EAC)	31.25	Not determined			
	Lymphoma Ascites (DLA)	102.86	Not determined	[85]		
	Erich's Ascites Carcinoma (EAC)	31.25	Not determined			
	Human melanoma cell lines (A375)	3.5	Anti-proliferative	[86]		
	Human melanoma cell lines (M14)	5.6				
	Human melanoma cell lines (RPMI7951)	5.6				
	Human melanoma cell lines (A375)	1.1	Anti-proliferative	[86]		
	Human melanoma cell lines (M14)	1.2				
	Human melanoma cell lines (RPMI7951)	3.3				
	Human umbilical vein endothelial cells (HUVECs)	0.4	Selective inhibitor for the HUVECs.	[87]		
	Smooth muscle cells (SMCs)	5.5	Activation of p38 signaling pathway.			
	Human myeloid leukemia cells (HL-60)	0.2	Exhibited excellent inhibitory activity on tumor growth in vivo	[88]		
	Human myeloid leukemia cells (K562)	1				
	Human myeloid leukemia cells (K562R)	0.9				
	Human prostate carcinoma cells (PC-3)	3.1				
	Human breast carcinoma cells (MCF-7)	10.6				
	Human esophageal carcinoma cells (ECA-109)	3.8				
	Human hepatocarcinoma cells (BEL-7402)	1.2				
	human non-small lung cancer cells (A549)	1.3				
	Human breast cancer cell line (MDA-MB-231)	6.76			Anti-proliferative	[89]
	Human breast cancer cell line (T47D)	9.96				
Human breast carcinoma cells (MCF-7)	5.71					
	Human lung cancer cell line (A549)	2.29	Anti-proliferative	[89]		
	Human colon adenocarcinoma cell line (HT-29)	3.29				

(continued on next page)

Table 3 (continued)

Compounds	Cell Line	IC <sub>50</sub> (μM)	Mechanism	Ref.
	Human breast cancer cell line (MDA-MB-231)	2.29	Anti-proliferative	[89]
	Human breast cancer cell line (T47D)	5.35		
	Human breast carcinoma cells (MCF-7)	3.46		
	Human lung cancer cell line (A549)	10.6		
	Human colon adenocarcinoma cell line (HT-29)	11.02		

potent and less toxic anticancer agents, several imidazole compounds were synthesized by Xue et al. [88] and tested in vitro. Among them, the compound mentioned in Table 3 exhibited higher activity against breast cancer cells (MCF-7) with an IC<sub>50</sub> of 10.6 μM compared to doxorubicin. This compound also demonstrated potent anticancer activity, with an IC<sub>50</sub> of 1.3 μM, against lung cancer cells (A549), and the authors concluded that these derivatives mediate anticancer activity by inducing apoptosis and suppressing cancer cell proliferation. Using in vitro experiments, Kalra et al. [89] investigated twenty-two compounds for their cytotoxicity, and the two compounds mentioned in Table 3 showed cytotoxic activity equal or more potent than docetaxel in a dose-dependent manner.

#### 5.1.4. Advances in preclinical approaches to imidazole-based drug discovery

The imidazole ring represents one of the most important nitrogen heterocycles, widely studied and exploited by the pharmaceutical industry in the search for new drugs. Due to their distinctive structural features and rich electronic environment, drugs containing imidazole rings interact with a variety of therapeutic targets, manifesting a diversity of biological activities. Numerous imidazole-based drugs are commonly used clinically to treat a variety of conditions, presenting significant therapeutic potential. Given their considerable medicinal value, the research and development of drugs containing the imidazole motif remains a dynamic and attractive area of medicinal chemistry. Currently, a substantial number of imidazole-motif compounds are in various stages of clinical trials, all of which have passed extensive preclinical evaluations. Details of parameters such as pharmacokinetics (PK), pharmacodynamics (PD) for each drug class, as well as the IUPAC names of selected drugs, are listed in Table 4.

Within a broad range of compounds screened through a structure-activity relationship (SAR) study, a robust and selective inhibitor of TGFβR1 named BMS-986260 emerged from a lead compound containing both an imidazole. The primary objective of the mentioned SAR studies was to enhance the efficacy, pharmacokinetic (PK) profile, and solubility profile of the drug candidate, as indicated in Table 4. BMS-986260 proved effective orally in the MC38 mouse tumor model when administered in combination with an anti-programmed cell death protein 1 (anti-PD-1) antibody. However, the drug was found to induce cardiovascular toxicities in preclinical studies due to continuous dosing intervals. To reduce these toxicities, a dose interruption schedule was explored and proved effective. An intermittent dosing schedule every two days for one week in a month provided comparable efficacy. Additionally, BMS-986260 is currently under evaluation as a clinical candidate in immuno-oncology for the treatment of various cancer types [90]. Furthermore, Blomgren et al. [93] revealed GS-9973 (entospletinib) as a selective SYK inhibitor currently undergoing clinical evaluation for hematologic malignancies. GS-9876 (lanraplenib), characterized by human pharmacokinetic properties suitable for once-daily administration and devoid of interactions with proton pump inhibitors (PPIs), is presently undergoing clinical evaluation in multiple autoimmune indications. In 2022, Smith et al. [92] targeted a new synthetic imidazole drug for treating cancers with MTAP gene deletion. Their discovery, the novel candidate drug MRTX1719, acts as a potent and selective binder to the PRMT5•MTA complex, selectively inhibiting PRMT5 activity in cells with MTAP deletion compared to wild-type MTAP cells.

## 6. Conclusion

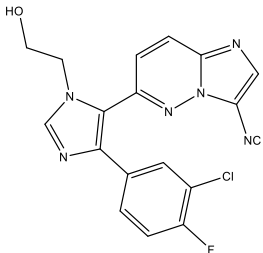
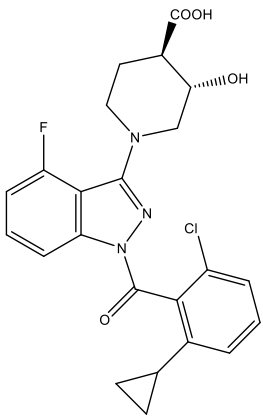
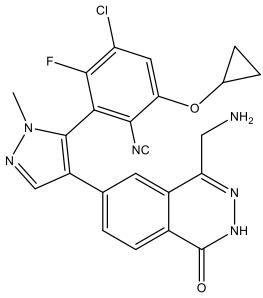
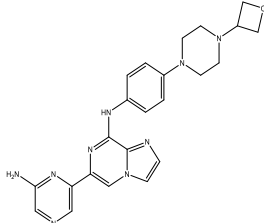
Tri-substituted and tetra-substituted imidazole constitute an essential heterocyclic system known for their numerous biological activities. On the other hand, they are widely used as a crucial synthesis for the production of biologically active compounds. Various strategies and techniques have been applied to achieve the condensation of these molecules. This review delves into the techniques and development of several synthetic routes for 2,4,5 and 1,2,4,5-imidazole tri or tetra-substituted synthesis, along with various analyses of pharmacological activities (antibacterial, antifungal, anticancer, antimicrobial). In conclusion, it has been observed that tri or tetra-substituted imidazoles demonstrate significant efficiency with a strong potential for new syntheses (by reflux or microwave) and can exhibit various biological activities, necessitating further in-depth research.

## Disclosure statement

A conflict of interest has not been reported, according to the authors.

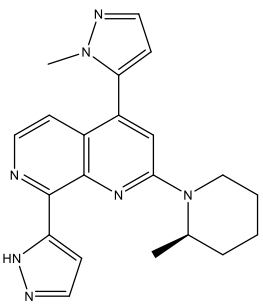
**Table 4**

Presents the structures, IUPAC names, mode of drug action, study models, Pharmacokinetic (PK) profile, Pharmacodynamic (PD) profile, and the targeted diseases.

Compound structure	IUPAC names	Nature of drug action and target receptor	Study model (s)	Pharmacokinetic (PK) parameters	Targeted Disease (s)	Ref.
	BMS-986260	Potent and selective inhibitor of TGFβR1	Mouse MC38 tumor model	Dose (mg/kg) iv/po = 5/10 Cmax (μM) po = 12.7 T½ (h) iv = 5.7 CL (mL/min/kg) iv = 5.6 Vss (L/kg) iv = 2.4	Clinical candidate as Immuno-oncology agent for the treatment of different types of cancers	[90]
	-	Allosteric inhibitor of RORγt	Acute PD model	CL (mL/min/kg) = 13 T1/2 (h) = 3.7 Vd (L/kg) = 0.6 F % = 35 %	Under clinical investigation for the treatment of autoimmune diseases	[91]
	MRTX1719	Lethal Inhibitor of the PRMT5•MTA Complex	CD-1 mouse model Beagle dog model	Dose (mg/kg) iv/po = 3/30 F % = 80 T½ (h) iv = 1.5 CL (mL/min/kg) iv = 83 Vss (L/kg) iv = 6.3	MTAP deleted Cancers	[92]
	Lanraplenib (GS9876)	Spleen tyrosine kinase Inhibitor	Spontaneous lupus efficacy model	Dose (mg/kg) iv = 1.0 Dose (mg/kg) po = 5.0 CL (L/h/kg) = 1.77 Vss (L/kg) = 2.5 T1/2 (h) = 3.7 F % = 60	Currently under clinical evaluation for the treatment of different autoimmune diseases such as systemic lupus erythematosus (SLE) and Lupus Nephritis (LN)	[93]

(continued on next page)

Table 4 (continued)

Compound structure	IUPAC names	Nature of drug action and target receptor	Study model (s)	Pharmacokinetic (PK) parameters	Targeted Disease (s)	Ref.
	BAY 1895344	Potent, Highly Selective, Orally Available ATR Inhibitor	Rat cancer xenograft model	Dose (mg/kg) = CLbiliary (mL/min/kg) = 1.2 F % = 87 Vss (L/kg) = 1.7 T1/2 (h) = 1.3	Solid tumors and Lymphomas	[94]

**Abbreviations:** CL (Clearance),  $T_{1/2}$  (Half Life), PK (Pharmacokinetics), Vss (Steady state volume), F (Bioavailability), TGF $\beta$ R1 (Transforming growth factor beta receptor 1), ROR $\gamma$ t (Retinoic acid-related orphan receptor gamma-t).

### Data availability statement

Data used to produce this article are available and listed in the references section.

### CRediT authorship contribution statement

**Abdeljalil Hamdi:** Writing – original draft, Investigation, Formal analysis. **Walid Daoudi:** Writing – review & editing, Validation, Software, Formal analysis. **Mohamed Aaddouz:** Investigation, Formal analysis. **Mohamed Azzouzi:** Investigation, Formal analysis. **Hassan Amhamdi:** Supervision, Resources, Project administration. **Abdellah Elyoussfi:** Validation, Methodology. **Abdelmalik EL Aatiaoui:** Writing – review & editing, Validation, Supervision, Formal analysis. **Dakeshwar Kumar Verma:** Writing – review & editing, Supervision, Resources. **Mohamed Abboud:** Validation, Supervision, Project administration, Funding acquisition. **M'hamed Ahari:** Validation, Supervision.

### Declaration of competing interest

The authors declare that they have no known competing financial interests or personal relationships that could have appeared to influence the work reported in this paper.

### Acknowledgement

The authors extend their appreciation to the Deanship of Scientific Research at King Khalid University for funding this work through Large Groups Project under grant number RGP.2/390/44.

### References

- [1] B. Liu, H. Chen, J. Cao, X. Chen, J. Xie, Y. Shu, F. Yan, W. Huang, T. Qin, Imidazole derivative assisted crystallization for high-efficiency mixed Sn–Pb perovskite solar cells, *Adv. Funct. Mater.* 34 (2024) 2310828, <https://doi.org/10.1002/adfm.202310828>.
- [2] W.-B. Xu, S. Li, C.-J. Zheng, Y.-X. Yang, C. Zhang, C.-H. Jin, Synthesis and evaluation of imidazole derivatives bearing imidazo[2,1-b][1,3,4]thiadiazole moiety as antibacterial agents, *Med. Chem.* 20 (2024) 40–51, <https://doi.org/10.2174/0115734064248204230919074743>.
- [3] M.S. Nasrollahzadeh, V. Eskandarpour, M.F. Maleki, F. Eivsand, M. Mashreghi, F. Hadizadeh, Z. Tayarani-Najaran, R. Ghodsi, Design, synthesis and biological evaluation of novel imidazole-based benzamide and hydroxamic acid derivatives as potent histone deacetylase inhibitors and anticancer agents, *J. Mol. Struct.* 1297 (2024) 136951, <https://doi.org/10.1016/j.molstruc.2023.136951>.
- [4] D. Chaudhury, J. Banerjee, N. Sharma, N. Shrestha, Routes of synthesis and biological significances of Imidazole derivatives, *World Journal of Pharmaceutical Sciences* (2015) 1668–1681.
- [5] R.S. Ahmed, R.A. Ali, L.S. Ahamed, Synthesis of new 2, 4, 5-triphenyl imidazole derivatives derived from benzoic acid and studying their biological activity, *Journal of Global Pharma Technology* 11 (2009). [https://www.researchgate.net/profile/Luma-Sami-2/publication/337076196\\_Journal\\_of\\_Global\\_Pharma\\_Technology\\_Synthesis\\_of\\_New\\_2\\_4\\_5-triphenyl\\_imidazole\\_Derivatives\\_Derived\\_from\\_benzoic\\_acid\\_and\\_Studying\\_their\\_Biological\\_Activity/links/60804af72fb9097e0cfdcafe/Journal-of-Global-Pharma-Technology-Synthesis-of-New-2-4-5-triphenyl-imidazole-Derivatives-Derived-from-benzoic-acid-and-Studying-their-Biological-Activity.pdf](https://www.researchgate.net/profile/Luma-Sami-2/publication/337076196_Journal_of_Global_Pharma_Technology_Synthesis_of_New_2_4_5-triphenyl_imidazole_Derivatives_Derived_from_benzoic_acid_and_Studying_their_Biological_Activity/links/60804af72fb9097e0cfdcafe/Journal-of-Global-Pharma-Technology-Synthesis-of-New-2-4-5-triphenyl-imidazole-Derivatives-Derived-from-benzoic-acid-and-Studying-their-Biological-Activity.pdf). (Accessed 20 January 2024).
- [6] K.J. Al-Adilee, S.H. Jawad, H.A.K. Kyhoiesh, H.M. Hassan, Synthesis, characterization, biological applications, and molecular docking studies of some transition metal complexes with azo dye ligand derived from 5-methyl imidazole, *J. Mol. Struct.* 1295 (2024) 136695, <https://doi.org/10.1016/j.molstruc.2023.136695>.
- [7] K. Al-Adilee, H.A.K. Kyhoiesh, Preparation and identification of some metal complexes with new heterocyclic azo dye ligand 2-[2--(1-Hydroxy-4-Chloro phenyl) azo]-imidazole and their spectral and thermal studies, *J. Mol. Struct.* 1137 (2017) 160–178, <https://doi.org/10.1016/j.molstruc.2017.01.054>.
- [8] A. Mahmoud, A. Mostafa, A.A. Al-Karmalawy, A. Zidan, H.S. Abulkhair, S.H. Mahmoud, M. Shehata, M.M. Elhefnawi, M.A. Ali, Telaprevir is a potential drug for repurposing against SARS-CoV-2: computational and in vitro studies, *Heliyon* 7 (2021) e07962. [https://www.cell.com/heliyon/pdf/S2405-8440\(21\)02065-X.pdf](https://www.cell.com/heliyon/pdf/S2405-8440(21)02065-X.pdf). (Accessed 5 March 2024).

- [9] M. McCann, R. Curran, M. Ben-Shoshan, V. McKee, M. Devereux, K. Kavanagh, A. Kellett, Synthesis, structure and biological activity of silver(I) complexes of substituted imidazoles, *Polyhedron* 56 (2013) 180–188, <https://doi.org/10.1016/j.poly.2013.03.057>.
- [10] T. Eicher, S. Hauptmann, A. Speicher, *The Chemistry of Heterocycles: Structures, Reactions, Synthesis, and Applications*, John Wiley & Sons, 2013.
- [11] Nidhi Rani, Trisubstituted Imidazole Synthesis: A Review - Google Scholar, (n.d.). [https://scholar.google.com/scholar?hl=fr&as\\_sdt=0%2C5&q=Trisubstituted+Imidazole+Synthesis%3A+A+Review&btnG=](https://scholar.google.com/scholar?hl=fr&as_sdt=0%2C5&q=Trisubstituted+Imidazole+Synthesis%3A+A+Review&btnG=) (accessed February 14, 2021).
- [12] G. Mohammadi Ziarani, Z. Dashtianeh, M. Shakiba Nahad, A. Badiie, One-pot synthesis of 1,2,4,5-tetra substituted imidazoles using sulfonic acid functionalized silica (SiO<sub>2</sub>-Pr-SO<sub>3</sub>H), *Arab. J. Chem.* 8 (2015) 692–697, <https://doi.org/10.1016/j.arabjc.2013.11.020>.
- [13] J. Chen, Z. Wang, Y. Lu, J.T. Dalton, D.D. Miller, W. Li, Synthesis and antiproliferative activity of imidazole and imidazoline analogs for melanoma, *Bioorg. Med. Chem. Lett* 18 (2008) 3183–3187, <https://doi.org/10.1016/j.bmcl.2008.04.073>.
- [14] S.J. Dominianni, T.T. Yen, *Oral Hypoglycemic Agents. Discovery and Structure-Activity Relationships of Phenacylimidazolium Halides*, ACS Publications, 2002, <https://doi.org/10.1021/jm00130a013>.
- [15] T.-C. Hung, C.-C. Huang, P.-J. Meng, A. Chuang, S.-J. Wu, Heavy metals in fish tissues and different species of fish from the southern coast of taiwan, *Chem. Ecol.* 16 (1999) 283–296, <https://doi.org/10.1080/02757549908037653>.
- [16] Y. Soujanya, G. Narahari Sastry, Theoretical elucidation of the antioxidant mechanism of 1,3-dihydro-1-methyl-2H-imidazole-2-selenol (MSeI), *Tetrahedron Lett.* 48 (2007) 2109–2112, <https://doi.org/10.1016/j.tetlet.2007.01.131>.
- [17] R. Jain, S. Vangapandu, M. Jain, N. Kaur, S. Singh, P.P. Singh, Antimalarial activities of ring-substituted bioimidazoles, *Bioorg. Med. Chem. Lett* 12 (2002) 1701–1704.
- [18] Y. Niwano, A. Seo, K. Kanai, H. Hamaguchi, K. Uchida, H. Yamaguchi, Therapeutic efficacy of Ianoconazole, a new imidazole antimycotic agent, for experimental cutaneous candidiasis in Guinea pigs, *Antimicrob. Agents Chemother.* 38 (1994) 2204–2206.
- [19] *Il Finar Organic Chemistry - AbeBooks*, (n.d.). [https://www.abebooks.com/book-search/kw/il-finar-organic-chemistry/\(accessed November 25, 2022\).](https://www.abebooks.com/book-search/kw/il-finar-organic-chemistry/(accessed November 25, 2022).) (Volume 2).
- [20] H. Debus, Ueber die Einwirkung des Ammoniaks auf Glyoxal, *Justus Liebigs Ann. Chem.* 107 (1858) 199–208. <https://doi.org/10.1002/jlac.18581070209..>
- [21] B. Radziszewski, Ueber die Constitution des Lophins und verwandter Verbindungen, *Ber. Dtsch. Chem. Ges.* 15 (1882) 1493–1496..
- [22] D. Bourissou, O. Guerret, F.P. Gabbaï, G. Bertrand, Stable carbenes, *Chem. Rev.* 100 (2000) 39–92, <https://doi.org/10.1021/cr940472u>.
- [23] J. Banothu, R. Gali, R. Velpula, R. Bavantula, Brønsted acidic ionic liquid catalyzed an efficient and eco-friendly protocol for the synthesis of 2, 4, 5-trisubstituted-1H-imidazoles under solvent-free conditions, *Arab. J. Chem.* 10 (2017) S2754–S2761.
- [24] J. Safari, S.D. Khalili, S.H. Banitaba, A novel and an efficient catalyst for one-pot synthesis of 2, 4, 5-trisubstituted imidazoles by using microwave irradiation under solvent-free conditions, *J. Chem. Sci.* 122 (2010) 437–441.
- [25] V.M. Abbasov, A.A. Marzouk, A.M. Mammadov, S.Z. Kazimova, A.H. Talybov, Imidazole derivatives, synthesis and biological activity, *Processes of Petrochemistry and Oil-Refining* 13 (2012) 52.
- [26] *Free Download Organic Chemistry Vol 2 By I L Finar Third Edition - ChemistryDocs.Com*, (n.d.). [https://chemistrydocs.com/organic-chemistry-vol-2-by-i-l-finar/\(accessed November 26, 2022\)..](https://chemistrydocs.com/organic-chemistry-vol-2-by-i-l-finar/(accessed November 26, 2022)..)
- [27] S.S. Qasim, S.S. Ali, S.K. Ahmed, *Research Journal of Pharmaceutical, Biological and Chemical Sciences*, (n.d.).
- [28] S.V. Nalage, M.B. Kalyankar, V.S. Patil, S.V. Bhosale, S.U. Deshmukh, R.P. Pawar, An efficient noncatalytic protocol for the synthesis of trisubstituted imidazole in polyethylene glycol using microwaves, *Open Catal. J.* 3 (2010).
- [29] S. Mala, PhD Thesis, in: *Design, Synthesis, Characterization and Biological Evaluation of Some Novel Anti Tubercular Agents Targeting L, D-Transpeptidase-2*, College of Pharmacy, Madras Medical College, Chennai, 2016.
- [30] R.B. Sparks, A.P. Combs, Microwave-assisted synthesis of 2,4,5-Triaryl-imidazole; A novel thermally induced N-hydroxyimidazole N–O bond cleavage, *Org. Lett.* 6 (2004) 2473–2475, <https://doi.org/10.1021/ol049124x>.
- [31] E.A. Steck, A.R. Day, Reactions of Phenanthraquinone and Retenequinone with Aldehydes and Ammonium Acetate in Acetic Acid Solution 1, ACS Publications, 2002, <https://doi.org/10.1021/ja01243a043>.
- [32] V. Sharma, M.S.Y. Khan, Synthesis of novel tetrahydroimidazole derivatives and studies for their biological properties, *Eur. J. Med. Chem.* 36 (2001) 651–658, [https://doi.org/10.1016/S0223-5234\(01\)01256-9](https://doi.org/10.1016/S0223-5234(01)01256-9).
- [33] M.M. Heravi, K. Bakhtiari, H.A. Oskooie, S. Taheri, Synthesis of 2,4,5-triaryl-imidazoles catalyzed by NiCl<sub>2</sub>·6H<sub>2</sub>O under heterogeneous system, *J. Mol. Catal. Chem.* 263 (2007) 279–281, <https://doi.org/10.1016/j.molcata.2006.08.070>.
- [34] S.D. Sharma, P. Hazarika, D. Konwar, An efficient and one-pot synthesis of 2, 4, 5-trisubstituted and 1, 2, 4, 5-tetrasubstituted imidazoles catalyzed by InCl<sub>3</sub>·3H<sub>2</sub>O, *Tetrahedron Lett.* 49 (2008) 2216–2220.
- [35] B. Sadeghi, B.B.F. Mirjalili, M.M. Hashemi, BF<sub>3</sub>·SiO<sub>2</sub>: an efficient reagent system for the one-pot synthesis of 1,2,4,5-tetrasubstituted imidazoles, *Tetrahedron Lett.* 49 (2008) 2575–2577, <https://doi.org/10.1016/j.tetlet.2008.02.100>.
- [36] A. Husain, S. Drabu, N. Kumar, Synthesis and biological screening of di-and trisubstituted imidazoles, *Acta Pol. Pharm.* 66 (2009) 243–248.
- [37] R.S. Joshi, P.G. Mandhane, M.U. Shaikh, R.P. Kale, C.H. Gill, Potassium dihydrogen phosphate catalyzed one-pot synthesis of 2,4,5-triaryl-1H-imidazoles, *Chin. Chem. Lett.* 21 (2010) 429–432, <https://doi.org/10.1016/j.ccl.2009.11.012>.
- [38] E. Oliveira, R.M.F. Baptista, S.P.G. Costa, M.M.M. Raposo, C. Lodeiro, Exploring the emissive properties of new azacrown compounds bearing aryl, furyl, or thienyl moieties: a special case of chelation enhancement of fluorescence upon interaction with Ca<sup>2+</sup>, Cu<sup>2+</sup>, or Ni<sup>2+</sup>, *Inorg. Chem.* 49 (2010) 10847–10857, <https://doi.org/10.1021/ic101095y>.
- [39] H.R. Shaterian, M. Ranjbar, An environmental friendly approach for the synthesis of highly substituted imidazoles using Brønsted acidic ionic liquid, N-methyl-2-pyrrolidonium hydrogen sulfate, as reusable catalyst, *J. Mol. Liq.* 160 (2011) 40–49, <https://doi.org/10.1016/j.molliq.2011.02.012>.
- [40] M.A. Pasha, A. Nizam, p-TSA catalysed efficient synthesis of 1,2,4,5-tetraaryl-imidazoles, *J. Saudi Chem. Soc.* 15 (2011) 55–58, <https://doi.org/10.1016/j.jscs.2010.10.009>.
- [41] A.M. Vijesh, A.M. Isloor, S. Telkar, S.K. Peethambar, S. Rai, N. Isloor, Synthesis, characterization and antimicrobial studies of some new pyrazole incorporated imidazole derivatives, *Eur. J. Med. Chem.* 46 (2011) 3531–3536, <https://doi.org/10.1016/j.ejmech.2011.05.005>.
- [42] A. Maleki, Z. Alirezvani, N. Ghamari, UHP as a mild and efficient catalyst for the synthesis of substituted imidazoles via multicomponent condensation strategy, in: *The 17th International Electronic Conference on Synthetic Organic Chemistry*, 2013, p. 3390. Doi.
- [43] A. Gharib, BrH. Khorasani, M. Jahangir, M. Roshani, L. Bakhtiari, S. Mohadeszadeh, Synthesis of 2, 4, 5-trisubstituted and 1, 2, 4, 5-tetrasubstituted-1H-imidazole derivatives and or 2, 4, 5-triaryloxazoles using of silica-supported preysler nanoparticles, *Bulg. Chem. Commun.* 46 (2014) 165–174.
- [44] R. Sndarous, S. Damavandi, Synthesis of 8-aryl-7H-acenaphtho[1,2-d]imidazoles by multicomponent reaction of acenaphthylene-1,2-dione and aromatic aldehydes with ammonium acetate catalyzed by ferric hydrogensulfate, *Res. Chem. Intermed.* 40 (2014) 2681–2687, <https://doi.org/10.1007/s11164-013-1121-4>.
- [45] M.S. Subeesh, K. Shanmugasundaram, C.D. Sunesh, Y.S. Won, Y. Choe, Utilization of a phenanthroimidazole based fluorophore in light-emitting electrochemical cells, *J. Mater. Chem. C* 3 (2015) 4683–4687.
- [46] S.U. Bhat, R.A. Naikoo, R. Tomar, One pot synthesis of tetra-substituted imidazole derivatives by condensation reaction using zeolite H-ZSM 22 as a heterogeneous solid acid catalyst, *Int. Res. J. Pure Appl. Chem.* (2016) 1–10.
- [47] J. Wang, S. Xu, F. Zhao, H. Xia, Y. Wang, Computational and spectroscopic studies of the imidazole-fused phenanthroline derivatives containing phenyl, naphthyl, and anthryl groups, *J. Mol. Struct.* 1108 (2016) 46–53, <https://doi.org/10.1016/j.molstruc.2015.11.082>.
- [48] D. Tavgeniene, G. Krucaitė, U. Baranaukyte, J.-Z. Wu, H.-Y. Su, C.-W. Huang, C.-H. Chang, S. Grigalevičius, Phenanthro[9,10-d]imidazole based new host materials for efficient red phosphorescent OLEDs, *Dyes Pigments* 137 (2017) 615–621, <https://doi.org/10.1016/j.dyepig.2016.11.003>.
- [49] S. Naureen, F. Ijaz, M.A. Munawar, N. Asif, F. Chaudhry, M. Ashraf, M.A. Khan, S. Naureen, F. Ijaz, M.A. Munawar, N. Asif, F. Chaudhry, M. Ashraf, M.A. Khan, Synthesis of TETRASUBSTITUTED imidazoles containing indole and their ANTIUREASE and antioxidant activities, *J. Chil. Chem. Soc.* 62 (2017) 3583–3587, <https://doi.org/10.4067/s0717-97072017000303583>.

- [50] R.C.M. Ferreira, S.P. Costa, H. Gonçalves, M. Belsley, M.M.M. Raposo, Fluorescent phenanthroimidazoles functionalized with heterocyclic spacers: synthesis, optical chemosensory ability and two-photon absorption (TPA) properties, *New J. Chem.* 41 (2017) 12866–12878.
- [51] M.K. Ravindra, K. Kumara, K.M. Mahadevan, H.B. Naik, K. Reddy, N.K. Lokanath, S. Naveen, Synthesis, characterization, crystal structure and hirshfeld surface analysis of 4-(1-(4-methoxyphenyl)-4, 5-diphenyl-1H-imidazole-2-yl) phenyl carboxylic acid monohydrate, *J. Applicable Chem* 7 (2018) 513–520.
- [52] H. Brahmabhatt, M. Molnar, V. Pavić, Pyrazole nucleus fused tri-substituted imidazole derivatives as antioxidant and antibacterial agents, *Karbala International Journal of Modern Science* 4 (2018) 200–206, <https://doi.org/10.1016/j.kijoms.2018.01.006>.
- [53] A. Ekbote, S.H. Han, T. Jadhav, S.M. Mobin, J.Y. Lee, R. Misra, Stimuli responsive AIE active positional isomers of phenanthroimidazole as non-doped emitters in OLEDs, *J. Mater. Chem. C* 6 (2018) 2077–2087.
- [54] S. Kula, A. Szlapa-Kula, S. Kotowicz, M. Filapek, K. Bujak, M. Siwy, H. Janeczek, S. Maćkowski, E. Schab-Balcerzak, Phenanthro[9,10-d]imidazole with thiophene rings toward OLEDs application, *Dyes Pigments* 159 (2018) 646–654, <https://doi.org/10.1016/j.dyepig.2018.07.014>.
- [55] J. Jayabharathi, S. Panimozhi, V. Thanikachalam, Hot exciton transition for organic light-emitting diodes: tailoring excited-state properties and electroluminescence performances of donor-spacer-acceptor molecules, *RSC Adv.* 8 (2018) 37324–37338, <https://doi.org/10.1039/C8RA07891B>.
- [56] S. Amala, G. Rajarajan, E. Dhineshkumar, M.A. Doss, M. Seenivasan, Design synthesis and characterization of 2-(4,5-dihydro-2,4,5-triphenylimidazol-1-yl)-6-methylpyridine:FT-IR, NMR, and computational investigation, *AIP Conf. Proc.* 2177 (2019) 020001, <https://doi.org/10.1063/1.5135176>.
- [57] J. Jayabharathi, G. Goperundevi, V. Thanikachalam, S. Panimozhi, Regulation of singlet and triplet excitons in a single emission layer: efficient fluorescent/phosphorescent hybrid white organic light-emitting diodes, *ACS Omega* 4 (2019) 15030–15042, <https://doi.org/10.1021/acsomega.9b01815>.
- [58] J. Jayabharathi, P. Nethaji, V. Thanikachalam, R. Ramya, Derivatives of cyanonaphthyl-substituted phenanthroimidazole as blue emitters for nondoped organic light-emitting diodes, *ACS Omega* 4 (2019) 4553–4570, <https://doi.org/10.1021/acsomega.8b03617>.
- [59] I. Singh, R. Rani, V. Luxami, K. Paul, Synthesis of 5-(4-(1H-phenanthro[9,10-d]imidazole-2-yl)benzylidene)thiazolidine-2,4-dione as promising DNA and serum albumin-binding agents and evaluation of antitumor activity, *Eur. J. Med. Chem.* 166 (2019) 267–280, <https://doi.org/10.1016/j.ejmech.2019.01.053>.
- [60] A.S. Nipate, C.K. Jadhav, A.V. Chate, K.S. Taur, C.H. Gill,  $\beta$ -Cyclodextrin catalyzed access to fused 1,8-dihydroimidazo[2,3-b]indoles via one-pot multicomponent cascade in aqueous ethanol: supramolecular approach toward sustainability, *J. Heterocycl. Chem.* 57 (2020) 820–829, <https://doi.org/10.1002/jhet.3828>.
- [61] F. Hasanazadeh, F.K. Behbahani, Synthesis of 8-aryl-7H-acenaphtho[1,2-d]imidazoles using Fe<sub>3</sub>O<sub>4</sub> NPs@GO@C<sub>4</sub>H<sub>8</sub>SO<sub>3</sub>H as a green and recyclable magnetic nanocatalyst, *Russ. J. Org. Chem.* 56 (2020) 1070–1076, <https://doi.org/10.1134/S1070428020060160>.
- [62] H. Peng, Z. Wei, L. Wu, X. Li, Efficient non-doped blue fluorescent OLEDs based on bipolar phenanthroimidazole-triphenylamine derivatives, *Opt. Mater.* 101 (2020) 109726, <https://doi.org/10.1016/j.optmat.2020.109726>.
- [63] D. Swati, Burungale, Synthesis of 2, 4, 5- triphenyl imidazole derivatives and biological evaluation for their antibacterial and anti-inflammatory activity, *Int. J. Pharmaceut. Sci. Res.* (2013) 4051–4057, <https://ijpsr.com/bft-article/synthesis-of-2-4-5-triphenyl-imidazole-derivatives-and-biological-evaluation-for-their-antibacterial-and-anti-inflammatory-activity/>.
- [64] S. Kula, P. Krawczyk, M. Filapek, A.M. Maron, Influence of N-donor substituents on physicochemical properties of phenanthro[9,10-d]imidazole derivatives, *J. Lumin.* 233 (2021) 117910, <https://doi.org/10.1016/j.jlumin.2021.117910>.
- [65] E. Lunt, C.G. Newton, C. Smith, G.P. Stevens, M.F. Stevens, C.G. Straw, R.J. Walsh, P.J. Warren, C. Fizames, F. Lavelle, *J. Med. Chem.* 30 (2) (Feb., 1987) 357–366. Recherche Google, (n.d.), [https://www.google.com/search?q=E.+Lunt+%2CC.G.+Newton+%2CC.+Smith+%2CC.G.P.+Stevens+%2CM.F.Stevens+%2CC.G.+Straw+%2CR.J.+Walsh+%2CP.J.Warren+%2CC.+Fizames+%2CF.+Lavelle+%2CJ.+Med.+Chem.%2C+1987%2C+30+\(2\)%2C+357+66.&aq=E.+Lunt+%2CC.G.+Newton+%2CC.+Smith+%2CC.P.+Stevens+%2CM.F.Stevens+%2CC.G.+Straw+%2CR.J.+Walsh+%2C+P.J.Warren+%2CC.+Fizames+%2CF.+Lavelle+%2C+J.+Med.+Chem.%2C+Feb.%2C+1987%2C+30+\(2\)%2C+357+66.&sourceid=chrome&ie=UTF-8](https://www.google.com/search?q=E.+Lunt+%2CC.G.+Newton+%2CC.+Smith+%2CC.G.P.+Stevens+%2CM.F.Stevens+%2CC.G.+Straw+%2CR.J.+Walsh+%2CP.J.Warren+%2CC.+Fizames+%2CF.+Lavelle+%2CJ.+Med.+Chem.%2C+1987%2C+30+(2)%2C+357+66.&aq=E.+Lunt+%2CC.G.+Newton+%2CC.+Smith+%2CC.P.+Stevens+%2CM.F.Stevens+%2CC.G.+Straw+%2CR.J.+Walsh+%2C+P.J.Warren+%2CC.+Fizames+%2CF.+Lavelle+%2C+J.+Med.+Chem.%2C+Feb.%2C+1987%2C+30+(2)%2C+357+66.&sourceid=chrome&ie=UTF-8). (Accessed 21 November 2022).
- [66] A. Bhatnagar, P.K. Sharma, N. Kumar, A review on “Imidazoles”: their chemistry and pharmacological potentials, *Int J PharmTech Res* 3 (2011) 268–282.
- [67] F. Suzuki, T. Kuroda, T. Tamura, S. Sato, K. Ohmori, S. Ichikawa, New Antiinflammatory Agents. 2. 5-Phenyl-3h-Imidazo[4,5-C][1,8]naphthyridin-4(5h)-Ones: a New Class of Nonsteroidal Antiinflammatory Agents with Potent Activity like Glucocorticoids, ACS Publications, 2002, <https://doi.org/10.1021/jm00093a020>.
- [68] R.A. Johnson, S.-M. Huong, E.-S. Huang, Inhibitory effect of 4-(4-fluorophenyl)-2-(4-hydroxyphenyl)-5-(4-pyridyl)1H-imidazole on HCMV DNA replication and permissive infection, *Antivir. Res.* 41 (1999) 101–111, [https://doi.org/10.1016/S0166-3542\(99\)00002-9](https://doi.org/10.1016/S0166-3542(99)00002-9).
- [69] M.D. Brewer, R.J.J. Dorgan, B.R. Manger, P. Mamalis, R.A.B. Webster, Isothiourea Derivatives of 6-Phenyl-2,3,5,6-Tetrahydroimidazo[2,1-B]thiazole with Broad-Spectrum Anthelmintic Activity, ACS Publications, 2002, <https://doi.org/10.1021/jm00393a028>.
- [70] S. Sumarsiha, M.D. Pratiwi, I.N. Ainna, H.R. Sinatriyaa, S. Soegijantob, T.H. Suciptob, H. Setyawatia, The influence of metal on the performance of 2, 4, 5- triphenylimidazole as an inhibitor of dengue virus replication, *Asia Pac. J. Mol. Biol. Biotechnol.* 28 (2020) 113–121.
- [71] J. Soni, A. Sethiya, N. Sahiba, D.K. Agarwal, S. Agarwal, Contemporary progress in the synthetic strategies of imidazole and its biological activities, *Curr. Org. Synth.* 16 (2019) 1078–1104, <https://doi.org/10.2174/1570179416666191007092548>.
- [72] A. Puratchikody, M. Doble, Antinociceptive and antiinflammatory activities and QSAR studies on 2-substituted-4,5-diphenyl-1H-imidazoles, *Bioorg. Med. Chem.* 15 (2007) 1083–1090, <https://doi.org/10.1016/j.bmc.2006.10.025>.
- [73] Y. Tanigawara, N. Aoyama, T. Kita, K. Shirakawa, F. Komada, M. Kasuga, K. Okumura, CYP2C19 genotype-related efficacy of omeprazole for the treatment of infection caused by *Helicobacter pylori*, *Clinical Pharmacology & Therapeutics* 66 (1999) 528–534, [https://doi.org/10.1016/S0009-9236\(99\)70017-2](https://doi.org/10.1016/S0009-9236(99)70017-2).
- [74] A.P.G. Nikalje, S.V. Tiwari, A.P. Sarkate, K.S. Karnik, Imidazole-thiazole coupled derivatives as novel lanosterol 14- $\alpha$  demethylase inhibitors: ionic liquid mediated synthesis, biological evaluation and molecular docking study, *Med. Chem. Res.* 27 (2018) 592–606, <https://doi.org/10.1007/s00044-017-2085-5>.
- [75] M. Kidwai, P. Mothra, A one-pot synthesis of 1,2,4,5-tetraarylimidazoles using molecular iodine as an efficient catalyst, *Tetrahedron Lett.* 47 (2006) 5029–5031, <https://doi.org/10.1016/j.tetlet.2006.05.097>.
- [76] R. Ghorbani-Vaghei, V. Izadkhah, J. Mahmoodi, R. Karamian, M. Ahmadi Khoei, The synthesis of imidazoles and evaluation of their antioxidant and antifungal activities, *Monatsh. Chem.* 149 (2018) 1447–1452, <https://doi.org/10.1007/s00706-018-2167-1>.
- [77] D. Osmaniye, B. Kaya Cavusoglu, B.N. Saglik, S. Levent, U. Acar Cevik, O. Atli, Y. Ozkay, Z.A. Kaplancikli, Synthesis and anticandidal activity of new imidazole-chalcones, *Molecules* 23 (2018) 831, <https://doi.org/10.3390/molecules23040831>.
- [78] A. Husain, S. Drabu, N. Kumar, M.M. Alam, S. Bawa, Synthesis and biological evaluation of di-and tri-substituted imidazoles as safer anti-inflammatory-antifungal agents, *J. Pharm. BioAllied Sci.* 5 (2013) 154.
- [79] D.S. Zinad, A. Mahal, O.A. Shareef, Antifungal activity and theoretical study of synthesized pyrazole-imidazole hybrids, *IOP Conf. Ser. Mater. Sci. Eng.* 770 (2020) 012053, <https://doi.org/10.1088/1757-899X/770/1/012053>.
- [80] A.K. Abhishek K Jain, V. Ravichandran, M. Sisodiya, R. Agrawal, Synthesis and antibacterial evaluation of 2-substituted-4,5-diphenyl-N-alkyl imidazole derivatives, *Asian Pac. J. Tropical Med.* 3 (2010) 471–474, [https://doi.org/10.1016/S1995-7645\(10\)60113-7](https://doi.org/10.1016/S1995-7645(10)60113-7).
- [81] A. Walls, J.J. Andreu, E. Falomir, S.V. Luis, E. Atrián-Blasco, S.G. Mitchell, B. Altava, Imidazole and imidazolium antibacterial drugs derived from amino acids, *Pharmaceuticals* 13 (2020) 482, <https://doi.org/10.3390/ph13120482>.
- [82] A.J.K. Atia, Synthesis and antibacterial activities of new metronidazole and imidazole derivatives, *Molecules* 14 (2009) 2431–2446, <https://doi.org/10.3390/molecules14072431>.
- [83] W. Gu, C. Qiao, S.-F. Wang, Y. Hao, T.-T. Miao, Synthesis and biological evaluation of novel N-substituted 1H-dibenzo[a,c]carbazole derivatives of dehydroabietic acid as potential antimicrobial agents, *Bioorg. Med. Chem. Lett.* 24 (2014) 328–331, <https://doi.org/10.1016/j.bmcl.2013.11.009>.
- [84] F.R. Japp, H.H. Robinson, Constitution des Lophins und des Amarins, *Ber. Dtsch. Chem. Ges.* 15 (1882) 1268–1270, <https://doi.org/10.1002/cber.188201501272>.
- [85] G.K. Sharma, S. Kumar, D. Pathak, Synthesis, antibacterial and anticancer activities of some novel imidazoles, *Der Pharm. Lett.* 2 (2010) 223–230.



- [86] Q. Wang, K.E. Arnst, Y. Wang, G. Kumar, D. Ma, H. Chen, Z. Wu, J. Yang, S.W. White, D.D. Miller, W. Li, Structural modification of the 3,4,5-trimethoxyphenyl moiety in the tubulin inhibitor VERU-111 leads to improved antiproliferative activities, *J. Med. Chem.* 61 (2018) 7877–7891, <https://doi.org/10.1021/acs.jmedchem.8b00827>.
- [87] K.-H. Chung, S.-Y. Hong, H.-J. You, R.-E. Park, C.-K. Ryu, Synthesis and biological evaluation of 5-arylamino-1H-benzo[d]imidazole-4,7-diones as inhibitor of endothelial cell proliferation, *Bioorg. Med. Chem.* 14 (2006) 5795–5801, <https://doi.org/10.1016/j.bmc.2006.05.059>.
- [88] N. Xue, X. Yang, R. Wu, J. Chen, Q. He, B. Yang, X. Lu, Y. Hu, Synthesis and biological evaluation of imidazole-2-one derivatives as potential antitumor agents, *Bioorg. Med. Chem.* 16 (2008) 2550–2557, <https://doi.org/10.1016/j.bmc.2007.11.048>.
- [89] S. Kalra, G. Joshi, M. Kumar, S. Arora, H. Kaur, S. Singh, A. Munshi, R. Kumar, Anticancer potential of some imidazole and fused imidazole derivatives: exploring the mechanism via epidermal growth factor receptor (EGFR) inhibition, *RSC Med. Chem.* 11 (2020) 923–939, <https://doi.org/10.1039/D0MD00146E>.
- [90] U. Velaparthi, C.P. Darne, J. Warriar, P. Liu, H. Rahaman, K. Augustine-Rauch, K. Parrish, Z. Yang, J. Swanson, J. Brown, G. Dhar, A. Anandam, V. K. Holenarsipur, K. Palanisamy, B.S. Wautlet, M.P. Fereshteh, J. Lippy, A.J. Tebben, S. Sheriff, M. Ruzanov, C. Yan, A. Gupta, A.K. Gupta, M. Vetrichelvan, A. Mathur, M. Gelman, R. Singh, T. Kinsella, A. Murtaza, J. Fargnoli, G. Vite, R.M. Borzilleri, Discovery of BMS-986260, a potent, selective, and orally bioavailable TGF $\beta$ R1 inhibitor as an immuno-oncology agent, *ACS Med. Chem. Lett.* 11 (2020) 172–178, <https://doi.org/10.1021/acsmchemlett.9b00552>.
- [91] H. Zhang, B.T. Lapointe, N. Anthony, R. Azevedo, J. Cals, C.C. Correll, M. Daniels, S. Deshmukh, H. van Eenenaam, H. Ferguson, L.G. Hegde, W.J. Karstens, J. Maclean, J.R. Miller, L.Y. Moy, V. Simov, S. Nagpal, A. Oubrie, R.L. Palte, G. Parthasarathy, N. Sciammetta, M. van der Stelt, J.D. Woodhouse, B.W. Trotter, K. Barr, Discovery of N-(Indazol-3-yl)piperidine-4-carboxylic acids as ROR $\gamma$ t allosteric inhibitors for autoimmune diseases, *ACS Med. Chem. Lett.* 11 (2020) 114–119, <https://doi.org/10.1021/acsmchemlett.9b00431>.
- [92] C.R. Smith, R. Aranda, T.P. Bobinski, D.M. Briere, A.C. Burns, J.G. Christensen, J. Clarine, L.D. Engstrom, R.J. Gunn, A. Ivetac, R. Jean-Baptiste, J.M. Ketcham, M. Kobayashi, J. Kuehler, S. Kulyk, J.D. Lawson, K. Moya, P. Olson, L. Rahbaek, N.C. Thomas, X. Wang, L.M. Waters, M.A. Marx, Fragment-based discovery of MRTX1719, a synthetic lethal inhibitor of the PRMT5•MTA complex for the treatment of MTAP-deleted cancers, *J. Med. Chem.* 65 (2022) 1749–1766, <https://doi.org/10.1021/acs.jmedchem.1c01900>.
- [93] P. Blomgren, J. Chandrasekhar, J.A. Di Paolo, W. Fung, G. Geng, C. Ip, R. Jones, J.E. Kropf, E.B. Lansdon, S. Lee, J.R. Lo, S.A. Mitchell, B. Murray, C. Pohlmeier, A. Schmitt, K. Sukawa-Pirrone, S. Wise, J.-M. Xiong, J. Xu, H. Yu, Z. Zhao, K.S. Currie, Discovery of lanraplenib (GS-9876): a once-daily spleen tyrosine kinase inhibitor for autoimmune diseases, *ACS Med. Chem. Lett.* 11 (2020) 506–513, <https://doi.org/10.1021/acsmchemlett.9b00621>.
- [94] U. Lücking, L. Wortmann, A.M. Wengner, J. Lefranc, P. Lienau, H. Briem, G. Siemeister, U. Bömer, K. Denner, M. Schäfer, M. Koppitz, K. Eis, F. Bartels, B. Bader, W. Bone, D. Moosmayer, S.J. Holton, U. Eberspächer, J. Grudzinska-Goebel, C. Schatz, G. Deeg, D. Mumberg, F. von Nussbaum, Damage incorporated: discovery of the potent, highly selective, orally available ATR inhibitor BAY 1895344 with favorable pharmacokinetic properties and promising efficacy in monotherapy and in combination treatments in preclinical tumor models, *J. Med. Chem.* 63 (2020) 7293–7325, <https://doi.org/10.1021/acs.jmedchem.0c00369>.

RESEARCH

Open Access



# Phytochemical profiling, antioxidant and antimicrobial investigations on *Viburnum simonsii* Hook. f. & Thoms, an unexplored ethnomedicinal plant of Meghalaya, India

Samson Rosly Sangma<sup>1</sup>, Mayur Mausoom Phukan<sup>1\*</sup> , Vahshi Chongloi<sup>1</sup>, Dakeshwar Kumar Verma<sup>2</sup>, Plaban Bora<sup>3</sup>, Sony Kumari<sup>4</sup> and Pranay Punj Pankaj<sup>5</sup>

## Abstract

**Background** *Viburnum simonsii* Hook. f. & Thoms is one of the 17 *Viburnum* species reported from India. *Viburnum* species such as *Viburnum opulus* and *Viburnum grandiflorum* have been used since time immemorial to treat various ailments and their therapeutic claims have been scientifically validated. However, the species under investigation despite having a long traditional usage history for the treatment of various illnesses in Meghalaya, India has grossly remained unexplored to date. No scientific report validating its therapeutic claim has been reported thus far. Therefore, the present study was mainly focused on investigating the antioxidant and antimicrobial properties of *V. simonsii* and its phytochemical profile.

**Result** Preliminary phytocompound assessment revealed the presence of alkaloids, phenolics, steroids, glycoside and terpenoids. The fruit extract displayed good antioxidant activity with phenolic and flavonoid content of  $250.20 \pm 8.12$  mgGAE/g and  $40.65 \pm 1.31$  mgQE/g respectively, and  $IC_{50}$  value of  $131.35 \pm 1.71$   $\mu$ g/ml. In antimicrobial assay, inhibitory activity was observed against gram-positive bacteria (*Staphylococcus aureus* and *Bacillus cereus*) with  $17.80 \pm 0.80$  mm and  $15.78 \pm 2.62$  mm zone of inhibition respectively. However, no activity was observed against gram-negative bacteria (*Escherichia coli* and *Salmonella enterica*) as well as fungus (*Candida albicans*). The absorption bands in the FTIR spectra of the sample corresponded to the presence of primary and secondary alcohols, alkanes, amines, aliphatic ethers, etc. Further, the GC–MS analysis revealed the presence of phytocompounds such as neophytadiene,  $\beta$ -sitosterol,  $\alpha$ -amyrin, lupeol, etc., which have bioactivity especially anticancer, antimicrobial, antioxidant and anti-inflammatory activities.

**Conclusions** The findings of the present study demonstrated that *V. simonsii* possessed appreciable antioxidant and antimicrobial activity and may be a potential target for pharmaceutical research.

**Keywords** Ethnomedicine, *Viburnum simonsii*, Meghalaya, Antioxidant, FTIR, GC–MS, Antimicrobial

\*Correspondence:

Mayur Mausoom Phukan  
mayur\_101@yahoo.com

Full list of author information is available at the end of the article



© The Author(s) 2023. **Open Access** This article is licensed under a Creative Commons Attribution 4.0 International License, which permits use, sharing, adaptation, distribution and reproduction in any medium or format, as long as you give appropriate credit to the original author(s) and the source, provide a link to the Creative Commons licence, and indicate if changes were made. The images or other third party material in this article are included in the article's Creative Commons licence, unless indicated otherwise in a credit line to the material. If material is not included in the article's Creative Commons licence and your intended use is not permitted by statutory regulation or exceeds the permitted use, you will need to obtain permission directly from the copyright holder. To view a copy of this licence, visit <http://creativecommons.org/licenses/by/4.0/>.

## Background

Mankind's reliance on plants predates recorded history. In addition to basic human needs such as food, clothing, shelter etc. plants are also an important source of medicines. Medicinal plants have been used to prevent and treat various diseases since time immemorial and their therapeutic usages have been passed on to subsequent generations among human communities [26]. Currently, 80% of the world's population depends on medicinal plants for therapeutic purposes [79]. It can be attributed to their extensive geographical availability and lesser adverse effects compared to synthetic drugs. Traditional medicinal plants have an exquisite impact on the evolution of the human health care system [79], since nearly 70% of all the presently available prescribed pharmaceutical drugs are made of plant-origin compounds [32].

Currently, concerns regarding the harmful impacts on health are intensifying as a result of industrial synthetic product use. Certain artificial antioxidants, such as butylated hydroxyanisole and dibutyl hydroxytoluene, have been demonstrated to stimulate carcinogenic activity [9, 65]. While naturally occurring, phenolic antioxidants have been proven to exhibit a range of health-beneficial biological actions [9, 12]. Recently, there has been a lot of attention focused on natural plant-based compounds including terpenoids, alkaloids, and flavonoids because of their numerous pharmacological qualities, which include antibacterial, antioxidant, and anticancer effects [2]. Enough dietary antioxidant consumption can strengthen the body's defences against free radicals since natural antioxidants derived from plants can scavenge harmful free radicals produced by the body. Furthermore, eating a diet high in antioxidant-rich foods is thought to be crucial in preventing or delaying the beginning of degenerative illness [29]. Additionally, multidrug-resistant (MDR) bacteria are also posing a serious threat to global health. This has prompted scientific research activities to prioritise the development of novel antibacterial drugs capable of combating antibiotic-resistant microorganisms [15, 17]. In this regard, naturally occurring bioactive compounds specifically derived from plants have surfaced as promising prospective medicinal agents [2].

With increase in health-related issues, there has been a scientific resurgence in medicinal plant research, mostly as a source of herbal medicine. Among the medicinal plants, the plants of the Genus *Viburnum* (family Adoxaceae) are considered very important for their ornamental as well as therapeutic potential [13]. *Viburnum*, a genus from Adoxaceae family (formerly Caprifoliaceae) comprises more than 230 species [62]. This genus is naturally predominant in temperate regions of the northern hemisphere and subtropical regions of Asia and Latin America [1]. The Eastern Himalayas harbour the majority

of the species from this genus, as this range has all the elements for their comfortable accommodation. Majority of these species are endemic [1, 82]. They are primarily used in folk medicines for the treatment of diseases, such as splenic asthenia, rheumatic arthritis, diabetes mellitus, cough, diarrhoea, tumefaction, kidney cramps and swelling [27, 75]. For instance, *V. opulus* and *V. prunifolium* (popularly known as cramp bark and black haw) have a long history of therapeutic usage for pregnancy issues within the Native American tribes [73]. The other *Viburnum* species which showed potential therapeutic properties were *V. lantana*, *V. macrocephalum*, *V. grandiflorum*, *V. odoratissimum*, *V. dilatatum*, etc., [73]. The therapeutic properties they exhibit include; antioxidant, antimicrobial, antidiabetic, antimalarial, hepato-protective, anti-inflammatory, anticancer, etc., [63, 73].

Phytochemically, diterpenes, triterpenes, monoterpenes, sesquiterpenes, flavonoids, phenols, iridoids, lignans, coumarins and alkaloids are the major chemical compounds found in the *Viburnum* plants [64]. Vibsane-type diterpenes are the characteristic chemical compounds of this genus. Owing to their limited distribution (found in *Viburnum* plants only), they are considered to be rare natural products. In terms of pharmacological interest, vibsane-type diterpenes possess neurotrophic activity, anti-inflammatory, antileukemic and anticancer properties [64, 83].

Literature review confirms that species such as *V. awabuki* [34], *V. dilatatum* [77], *V. fordiae* [13], *V. odoratissimum* [81], and *V. opulus* [27] have a maximum quantity of bioactive compounds in comparison to other species of the genus. It is also reported that fruits of *Viburnum* plants are rich in polyphenols, ascorbic acid, malic acid, oxalic acid and vitamin C [10]. Further, some in vitro and in vivo studies have revealed the antimicrobial, antifungal, anti-inflammatory, antioxidant, anticancer and neuroprotective properties of some species from this genus [27, 59, 81]. For such diverse chemical components and biological activities across the genus, the study of *Viburnum simonsii* Hook. f. & Thoms (synonym *Viburnum odoratissimum* var. *odoratissimum*) is of scientific curiosity pertaining to novel drug discovery and as a source for nutraceutical product development. *Viburnum simonsii* Hook. f. & Thoms is a small tree with a height of up to 40 ft, thin greyish bark, leaves are oppositely arranged, elliptic, distantly cuspidate, dentate and glabrous with lateral nerves of 5–8. Flowers are white or tinged red and sweet-scented. Fruits are 0.4–0.8 cm in diameter with bright red colour. Figure 1 shows the tree, flower, fruits and leaf of *Viburnum simonsii* Hook. f. & Thoms. Flowering time is between March–June, whereas fruiting time is July–October [23, 28]. It is endemic to the



**Fig. 1** Tree, flower, fruit and leaf of *V. simonsii*

Eastern Himalayan range. In India, the distribution is limited only to the state Meghalaya [42, 72]. The Khasi people (local tribe of Meghalaya) locally call it *Soh-lang-eit-ksew*. Traditionally the fruits of this species are used as tonic and anti-spasms [41]. Besides, the species is neglected and unexplored, which is evident with the declining population graph in the state.

Interestingly, the species under investigation is closely related to *V. odoratissimum* (possess diverse biological activities and a high number of phytochemicals) [58]. It is quite arguable to expect that the species under investigation (*Viburnum simonsii* Hook. f. & Thoms) will have diverse biological activities owing to the likely presence of varied phytochemicals. The local tribes of Meghalaya have been using and claiming the therapeutic value of this species [41], and this prompted to undertake the present investigation pertaining to scientific validation. In addition, no scientific reports concerning the biological and pharmacological activities of this species have been reported so far. Therefore, the current investigation aims to highlight *Viburnum simonsii* Hook. f. & Thoms as a potential medicinal plant with unexplored therapeutic potential. The investigation attempts to highlight the biological activities of *V. simonsii* and validate its biochemical attributes specifically emphasizing on its phytochemical, antioxidant and antimicrobial aspects.

## Methods

### Plant materials

The fresh leaves and fruits of the plant *V. simonsii* Hook. f. & Thoms. were collected from Cherrapunjee [25°14'42.1''N, 91°43'28.4''E], East Khasi Hills, Meghalaya. The plant species was identified by referring to the existing literatures [23, 24, 28] and authenticated by comparing the prepared herbarium specimen to the existing herbarium specimen of the species under investigation (Reference accession no: 90420) present in the Botanical Survey of India (BSI), Eastern Regional Centre, Shillong, Meghalaya, India.

### Chemicals and reagents

DPPH, TPTZ, Folin-Ciocalteu reagent, Anthrone and Gallic acid were purchased from SRL, India. Ascorbic acid, Bovine serum albumin (BSA), Quercetin and Ferric chloride were obtained from LOBA Chemie, India. Whereas, DMSO, Methanol, Sodium acetate, Aluminum Chloride and Mueller Hinton Agar (MHA) were procured from Merck Lifesciences and Himedia, India, respectively.

### Extract preparation

The collected leaves and fruits were washed well, shade dried and powdered with an electric grinder. The extract

preparation was carried out following the procedure described in the previous work [54] with slight modifications. Soxhlet extraction was performed at 65 °C using 80% CH<sub>3</sub>OH (Methanol) as the extraction solvent. The solvent following collection was cooled and subjected to rotary vacuum evaporation (Equitron Roteva 66 series – 8766.V0). The final concentrated extracts were methanolic leaf (MEVL) and fruit (MEVF) extracts. The extract was further subjected to lyophilization. These extracts were finally stored at 4 °C for further analysis.

#### Qualitative phytochemical screening

The qualitative phytochemical screening was carried out to determine the presence of different phytochemicals in the *V. simonsii* extracts. Phytochemicals such as alkaloids (Mayer's test), phenols and tannin (Ferric chloride test), flavonoid (Shinoda test), terpenoids (Saldowski test), glycoside (Liebermann's test), cardiac glycoside (Keller-Kilani test), saponins, steroids and anthraquinone were screened following the standard methods [22].

#### Carbohydrate content

The carbohydrate content was determined following the Anthrone's method [80]. Briefly, the powdered plant sample was acid hydrolyzed with HCl (2.5N) for 3 h and filtered. 1 ml of filtrate was mixed with 4 ml of Anthrone reagent and kept in a water bath (100 °C) for 10 min. Absorbances were recorded at 620 nm. Glucose of various concentrations (20–100 µg/ml) was used to plot a standard calibration curve graph. The carbohydrate content of the sample was calculated from the calibration curve graph and expressed as mg glucose equivalent/g of sample. The assay was carried out in triplicates and only the mean values are reported.

#### Protein content

The protein content of the samples was determined following Lowry's method [39]. The protein from the powdered sample was extracted using phosphate buffer as a solvent and filtered. The alkaline reagent was prepared by mixing reagent A (2% Na<sub>2</sub>CO<sub>3</sub> in 0.1N of NaOH) and reagent B (0.5% CuSO<sub>4</sub> and 1% potassium sodium tartrate in distilled water) at a ratio of 50:1. To 1 ml of filtrate, 4 ml of alkaline reagent and 0.5 ml Folin-Ciocalteu reagent was added and incubated for 30 min at 37 °C. The absorbances were recorded at 660 nm. Bovine serum albumin (BSA) was used to plot a standard calibration curve graph. Protein content of the sample was expressed as mg BSA equivalent/g of the sample. The assay was carried out in triplicates and only the mean values are reported.

#### Total phenolic content

The total phenolic content (TPC) of the methanolic extracts of *V. simonsii* leaf and fruit was carried out by the method described by Neupane and Lamichhane [44] with slight modification. To 100 µl of methanolic extract, 0.5 ml of Folin-Ciocalteu and 1.5 ml of Na<sub>2</sub>CO<sub>3</sub> (7.5%) were added and incubated at 37 °C for 2 h. The absorbances of the mixture were taken at 750 nm. A standard calibration curve graph was obtained using gallic acid as a standard. The TPC was calculated from the standard calibration curve graph and expressed in mg gallic acid equivalent (GAE)/g of dried extract. The assays were carried out in triplicates and only the mean values are reported.

#### Total flavonoid content

The total flavonoid content (TFC) of the methanolic extracts of the samples was estimated by the Aluminum Chloride method [44]. Briefly, to 1 ml of methanolic extract, 1 ml of 10% AlCl<sub>3</sub> and 1 ml of sodium acetate (1 M) were added and incubated at room temperature for 45 min in a dark chamber. The absorbances were taken at 415 nm. The TFC was calculated from the standard calibration curve graph which was obtained by using quercetin as a standard. The final result was expressed in mg quercetin equivalent (QE)/g of dried extract. The assays were carried out in triplicates and only the mean values are reported.

#### DPPH radical scavenging activity

A DPPH radical scavenging activity of the extracts of *V. simonsii* leaf and fruit was determined following the method described by Clarke et al. [14] with minor modifications. 1 ml of methanolic extract was mixed with 3 ml of DPPH reagent (0.2 mM) and incubated for 30 min at 37 °C in a dark chamber. A control was prepared by mixing 1 ml methanol (95%) and 3 ml DPPH reagent. The absorbances were read at 517 nm. Ascorbic acid was used as the standard antioxidant agent to compare the DPPH radical scavenging activity of the sample. The percentage of radical scavenging activity was calculated using the formula given in Eq. (1).

$$\%RSA = \frac{Ac - As}{Ac} \times 100 \quad (1)$$

where, %RSA = Radical scavenging activity percentage, Ac = Absorbance of control, As = Absorbance of sample.

IC<sub>50</sub> of the sample and standard was calculated from the regression curve equation obtained by plotting %RSA against various extract concentrations.

### FRAP assay

The FRAP assay of the extracts was done following the methods described by Benzie and Strain [4]. To 0.1 ml of methanolic extract, 3 ml of FRAP reagent (mixture of 0.3 M sodium acetate, 10 mM of TPTZ solution and 20 mM of FeCl<sub>3</sub> at a ratio of 10:1:1) was added and incubated for 15 min at 37 °C. The absorbances were recorded at 593 nm. A standard calibration curve graph was obtained using ascorbic acid of various concentrations (0.2–1.0 mM) as standard. The FRAP value of the extracts was calculated using Eq. (2) and expressed in μM ascorbic acid equivalent (AAE)/g of dried extract.

$$\text{FRAP value } (\mu\text{MAAE/g}) = c \times V \times \frac{t}{m} \quad (2)$$

where, c = Ascorbic acid equivalent in μM/ml, V = sample volume, t = dilution factor, m = weight of dried extract in gram (g).

### Antimicrobial activity assay

Antimicrobial activity assay of the crude methanolic extracts was done through agar-well diffusion method [56]. The assay was carried out against gram-positive (*Staphylococcus aureus* MTCC 11949, *Bacillus cereus* MTCC 8361), gram-negative (*Escherichia coli* MTCC 593, *Salmonella enterica* MTCC 1166) bacterial strains and fungus (*Candida albicans* MTCC 13013). The samples were prepared in Dimethyl sulfoxide (DMSO) at a concentration of 100 mg/ml. A 24 h culture was diluted with normal saline till the concentration of 1 × 10<sup>8</sup> cells/ml. Mueller Hinton Agar (MHA, HiMedia) for bacteria and Mueller Hinton Agar supplemented with 2% glucose and 5 μg/ml Methylene blue for fungus were used as the culture media for the assay. 100 μl of the diluted culture was spread onto solidified agar, and wells (8 mm) were bored. 100 μl of extract, DMSO (as negative control) and a ciprofloxacin 5 μg/100 μl (bacteria) and fluconazole 10 μg/100 μl (fungus) [as positive control] were placed onto the wells. After 24 h incubation at 37 °C, the diameter (mm) of the zone of growth inhibition was measured.

### FTIR analysis

The IR spectra of leaf and fruit sample of *V. simonsii* were recorded on a PerkinElmer Spectrum 100 spectrometer at ambient temperature. A small quantity of powdered plant sample was mixed with potassium bromide (KBr) and pressed into pellets. The spectra were recorded in the mid infra-red region (4000–400 cm<sup>-1</sup>). The spectral data were interpreted with the help of standard IR spectrum chart described by Pavia et al. [48].

### Gas chromatography-mass spectroscopy (GC–MS) analysis

A GC–MS analysis of the *V. simonsii* extracts (MEVL, MEVF) was carried out in a Thermo-Fischer Scientific model GC with a split/split less injection port and a split ratio of 1/100, coupled with an ISQ7000 mass spectrometer system and TG-5MS fused silica capillary column (30 m × 0.25 mm i.d, 0.25 μm film thickness). The temperature program was isothermal for 3 min at 60 °C, then increased to 230 °C at a rate of 5 °C/min. The injector temperature and transfer line temperature were set at 290 °C and 230 °C respectively. Ultrapure Helium was used as a carrier gas at a flow rate of 1 ml/min. The components were identified and confirmed by comparing the retention time (RT) index and mass spectrum with the authentic references provided in the NIST library. The peak area percentages of the spectrum were calculated automatically by using Chromeleon™ Software provided along with the instrument setup.

## Results

### Qualitative phytochemical screening

The qualitative phytochemical screening of the extracts revealed the presence of alkaloids, phenols, flavonoids, glycoside, tannin, steroids, terpenoids and saponins. The results for qualitative phytochemical screening of *V. simonsii* extracts are furnished in Table 1.

### Carbohydrate and protein content

The carbohydrate and protein content of the extracts were estimated by Anthrone's and Lowry's methods respectively. A carbohydrate content of 312.6 ± 0.74 mg/g (31.2%) was obtained in the fruit and 232.9 ± 0.64 mg/g (23.2%) in the leaf sample. Similarly, fruit and leaf samples showed 65.9 ± 1.79 mg/g and 34.6 ± 0.77 mg/g of protein content respectively. The measured carbohydrate and protein content of the *V. simonsii* extracts is furnished in Table 2.

**Table 1** Results of the qualitative phytochemical screening of *V. simonsii* extract

Tests	Leaf extract	Fruit extract
Alkaloid	+	+
Antraquinone	–	–
Glycoside	+	+
Flavonoid	+	+
Phenolic	+	+
Steroids	+	+
Saponins	+	+
Tannins	+	+
Terpenoids	+	+

(+) indicates presence and (-) indicates absence

**Table 2** Carbohydrate and Protein content of *V. simonsii*

Samples	Total carbohydrate (mg/g)	Total Protein (mg/g)
Leaf	232.9±0.64	34.6±0.77
Fruit	312.6±0.74	65.9±1.79

Values are present as mean ± SD

### Total phenols and flavonoid content

Phenols and flavonoids have a strong correlation with the antioxidant activities [9, 70]. The TPC and TFC of the leaf and fruit extracts of *V. simonsii* were determined by Folin-Ciocalteu and Aluminum Chloride methods respectively. The total phenol and flavonoid content of the extracts were calculated using the standard calibration curve graph (Fig. 2 and Fig. 3). The fruit extract displayed 250.20 ± 8.12 mgGAE/g of phenolic contents and 40.65 ± 1.31 mgQE/g of flavonoid contents. Whereas, leaf extract showed 127.03 ± 1.62 mgGAE/g and 45.83 ± 3.93 mgQE/g of phenolic and flavonoid content (Table 3).

### DPPH radical scavenging assay

The DPPH radical is a stable free radical. This is because of an odd electron delocalizing across the molecule which consequently inhibits dimer formation. The DPPH radical scavenging assay uses these free radicals to measure the ability of antioxidants to neutralize those free radicals. The reduction of the free radicals to a non-radical

state is indicated by the colour change from dark purple to yellow [68]. The reducing capacities of the extracts increase accordingly with the increase in concentration. IC<sub>50</sub> (half maximal inhibitory concentration) of free radical scavenging activity was calculated using various concentrations of the extracts. Fruit extract (MEVF) showed an IC<sub>50</sub> value of 131.35 ± 1.71 µg/ml and 872.71 ± 2.86 µg/ml was observed in leaf extract (MEVL) (Table 3). Further, the DPPH free radical scavenging activities of fruit and leaf extracts and standard ascorbic acid at various concentrations are displayed in Fig. 4.

### FRAP assay

The ferric reducing antioxidant power (FRAP) is based on the reduction of ferric-tripyridyl triazine (Fe<sup>3+</sup>-TPTZ) complex to ferrous-tripyridyl triazine (Fe<sup>2+</sup>-TPTZ) by antioxidants at low pH (3.6) [4]. The fruit extract showed highest ferric reducing ability with a FRAP value of 94.31 ± 0.67 µMAAE/g, whereas 32.57 ± 0.85 µMAAE/g of FRAP value was observed in the leaf extract (Table 3).

### Antimicrobial assay

The antimicrobial activities of the *V. simonsii* extracts were performed by agar-well diffusion method. The tested extracts showed varied inhibitory actions against tested bacteria and fungus. The results of the antimicrobial activity assay of the extracts are furnished in Table 4 and Fig. 5. Leaf extract (100 mg/ml) showed highest

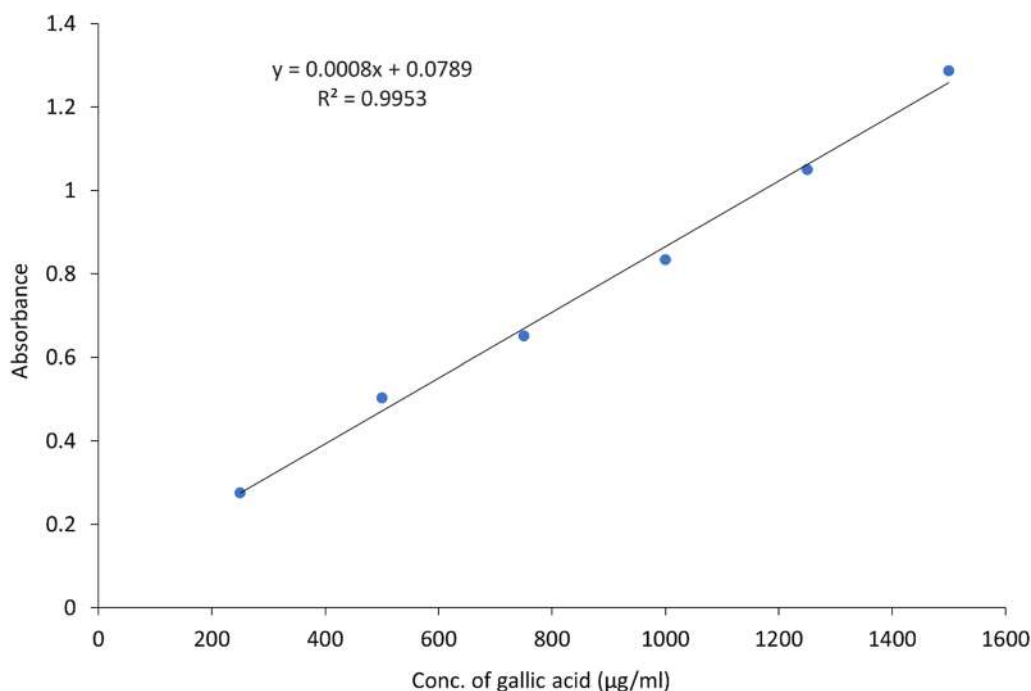


**Fig. 2** Calibration curve graph of gallic acid for TPC

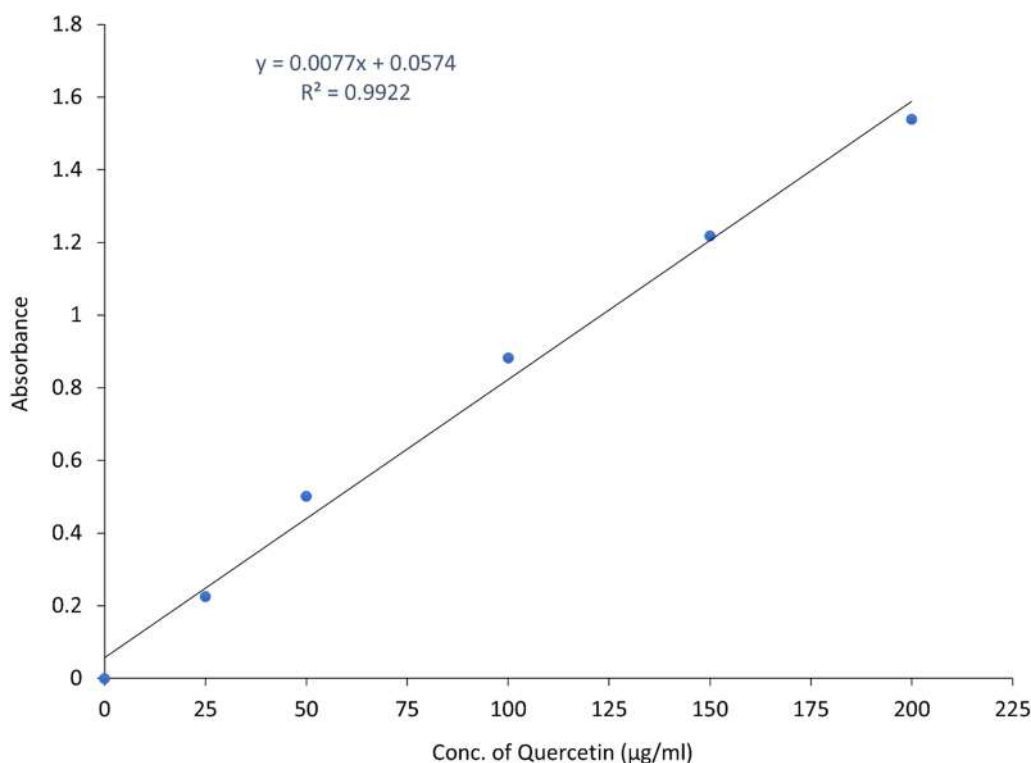


**Fig. 3** Calibration curve graph of quercetin for TFC

**Table 3** Phenolic, flavonoid, DPPH and FRAP values of *V. simonsii* extracts

Samples	Phenolic (mgGAE/g)	Flavonoid (mgQE/g)	DPPH IC <sub>50</sub> value (µg/ml)	FRAP value (µMAAE/g)
Leaf (MEVL)	127.03 ± 1.62	45.83 ± 3.93	872.71 ± 2.86	32.57 ± 0.85
Fruit (MEVF)	250.20 ± 8.12	40.65 ± 1.31	131.35 ± 1.71	94.31 ± 0.67

Values are present as mean ± SD

inhibition zone against *S. aureus* (17 mm) and lower zone against *B. cereus* (15 mm). Similarly, fruit extract (100 mg/ml) showed inhibition zone against *S. aureus* (13 mm) and *B. cereus* (15 mm). However, no inhibition zone was observed against gram-negative bacteria (*E. coli* and *S. enterica*) and fungus (*C. albicans*).

#### FTIR analysis

FTIR was done to identify the functional groups in the chemical constituents of the plant extracts. FTIR spectrum and spectral values of the extracts of *V. simonsii* is furnished in Fig. 6 and Table 5. Twelve (12) significant bands were detected in the range of 4000–400 cm<sup>-1</sup>. The peaks were observed at 3426 cm<sup>-1</sup>, 2927 cm<sup>-1</sup>, 1649 cm<sup>-1</sup>, 1387 cm<sup>-1</sup>, 1251 cm<sup>-1</sup> and 1066 cm<sup>-1</sup>. A broad absorbance at 3500–3400 cm<sup>-1</sup> denotes stretching vibration of OH in H bonded alcohol. Additionally, stretching vibration was observed at 1085–1050 cm<sup>-1</sup>,

thereby confirming the presence of phenolic compounds [45]. A C-H stretching vibration at 3000–2840 cm<sup>-1</sup> implies the presence of lipid. Absorption at 1649 cm<sup>-1</sup> can be referred to C=O vibration of carboxylic acid [20]. A stretching vibration of C-N was observed at 1321 cm<sup>-1</sup> which corresponds to amines. The stretching vibration of C-O at 1251 cm<sup>-1</sup> and 1148 cm<sup>-1</sup> implies the presence of ether. From Fig. 6, it can be seen that leaf (MEVL) and fruit (MEVF) extracts displayed peaks at the same band, however their absorption intensity was different.

#### GC-MS analysis

The GC-MS analysis of the methanolic leaf (MEVL) and fruit (MEVF) extracts of *V. simonsii* reveals the presence of a total of 21 and 13 bioactive compounds respectively. The chromatograms are displayed in Figs. 7 and 8, whereas the phytochemicals of MEVL and MEVF with their retention time (RT) and concentration (Peak area



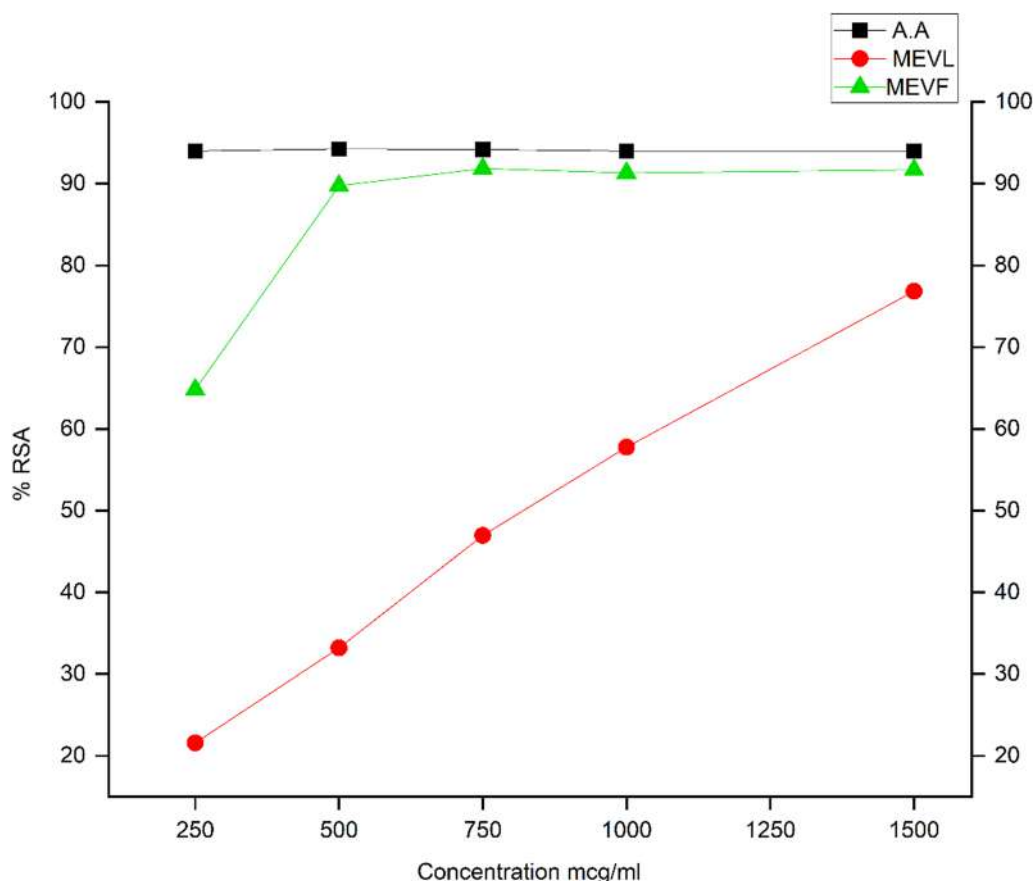


Fig. 4 DPPH assay of MEVL and MEVF. 'AA' denotes ascorbic acid

Table 4 The antimicrobial activity of *V. simonsii* extracts against gram-positive, gram-negative bacteria and fungus

Test sample	Concentration of extracts	Diameter of zone of inhibition (mm)				
		<i>E. coli</i>	<i>S. aureus</i>	<i>B. cereus</i>	<i>S. enterica</i>	<i>C. albicans</i>
MEVL (leaf)	100 mg/ml	ND	17.80±0.80	15.78±2.62	ND	ND
MEVF (Fruit)	100 mg/ml	ND	13.12±2.52	14.84±1.83	ND	ND
Positive control (Ciproflaxacin/ Fluconazole)	-	40.57±2.32	27.79±0.75	30.08±1.36	35.49±1.85	30.38±1.60
Negative control (DMSO)	-	NA	NA	NA	NA	NA

Values are present as mean ± SD, ND = Not Detected, NA = No Activity

%) are presented in Tables 6 and 7 respectively. Compounds obtained in MEVL are: 1,2,3,4-Cyclohexanetetrol (16.86%), α-Amyrin (15.95%), β-Amyrin (4.41%), β-Sitosterol (5.70%), Neophytadiene (4.96%), Lup-20(29)-en-3-ol, acetate, (3β)- (9.22%), Ergosta-5,22-dien-3-ol, acetate, (3β,22E)-, Benzoic acid, 4-ethoxy-, ethyl ester, Tridecanoic acid, 12-methyl-, methyl ester, cis-Z-a-Bisabolene epoxide, 1-Heptatriacotanol (2.07%), α-Tocopheryl acetate (1.48%). Similarly, compounds obtained in MEVF are: Glycerin (37.38%), Lupeol; Lup-20(29)-en-3-ol,

acetate, (3β)- (35.12%), Propanoic acid, 2-methyl-, 2-ethylhexyl ester (8.20%), Lupeol (2.84%), -, Benzoic acid, 4-ethoxy-, ethyl ester (3.90%), Benzene acetaldehyde, α,2,5-trimethyl, Eicosane, 2-methyl-, Pentadecanoic acid, 14-methyl-, methyl ester.

### Discussion

Bioprospecting of medicinal plants strictly demands pharmacognostic investigation of crude plant materials. Such investigations include screening of phytochemicals

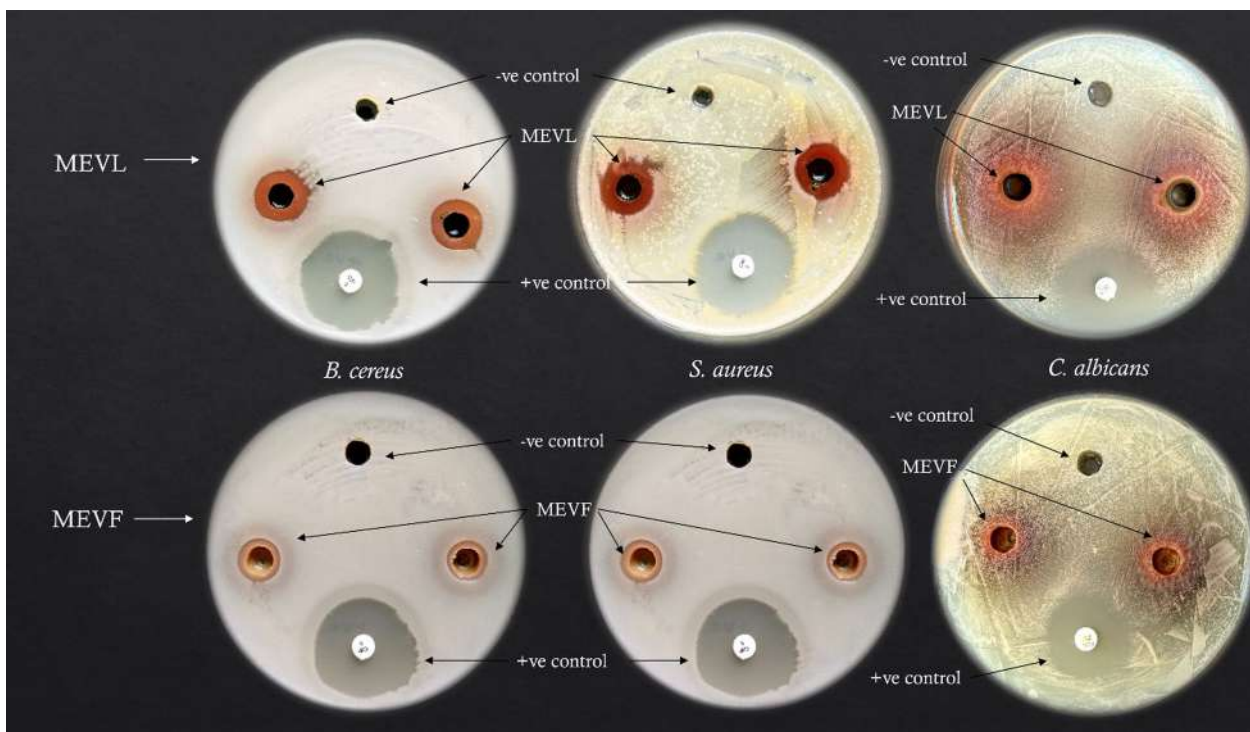


**Fig. 5** Antimicrobial activities of *V. simonsii* extracts

and biological activities [6]. The present study investigates the phytochemicals, antioxidant and antimicrobial activities of *V. simonsii* to validate its pharmaceutical potential. The presence or absence of phytochemicals play a crucial role in the biological activities of specific plant species [69]. In the present study, qualitative phytochemical screening revealed the presence of major phytochemicals such as alkaloid, phenols, flavonoid, steroids, etc. (Table 1). The result was concordant with the findings of the previous studies carried out on related species such as *V. opulus* [33], *V. coriaceum* [73], *V. foetens* [7] and *V. grandiflorum* [71]. However, anthraquinones, which were found in the aqueous and methanolic fraction of the aerial parts of *V. foetens* [7] and roots of *V. grandiflorum* [71], were absent in the species under investigation. This might be due to the fact that phytochemical distribution is diverse among the different parts of the same plant [53]. On the contrary, cardiac glycoside, which was reported absent in previously studied *Viburnum* species (*V. opulus* and *V. coriaceum*), was present in *V. simonsii*. Nevertheless, it is confirmed by previous studies that phenols, flavonoids, alkaloids, tannins and saponins are chiefly responsible for antioxidant and antimicrobial activities [3, 65].

It is worth mentioning that the majority of the therapeutically valued plants are employed in the development of nutraceutical products. Therefore, investigation of

the nutritional profile of plants including carbohydrate, protein, fats and minerals are indispensable. As these nutritional compounds execute an essential role in making healthy organ systems in human beings [52]. Also, they are crucial elements in the selection of plant species for nutraceutical significance [45]. In comparison to the other related species such as *Viburnum mullaha* [40], the carbohydrate content of the species under study was found higher. However, it was found lower in comparison to wild vegetables such as *Dryopteris filixmas*, *Corchorus capsularis*, *Ipomoea aquatica* etc. [60] and wild edible plants such as *Gnetum gnemon*, *Prenanthes hookeri*, *Smilax perfoliata*, *Blumea lanceolaria* etc., consumed by the local tribes of Meghalaya [61]. The protein content of the studied species was in close proximity to a previous report on *V. opulus* [50] and *V. mullaha* [40]. Furthermore, Vishwakarma and Karma [74], reported protein content of edible herbs in the range of 3.1–13.6% and regarded them as a good protein source. Therefore, owing to the considerable content of carbohydrates and proteins, plant materials of *V. simonsii*, (both fruit and leaf) can be utilized in dietary supplement products.

Qualitative phytochemical analysis of an extract is not sufficient enough to validate its pharmaceutical potential. The quantitative investigations of some of the important compounds such as phenols, flavonoids, alkaloids, terpenoids also account most in this regard. Besides, a strong

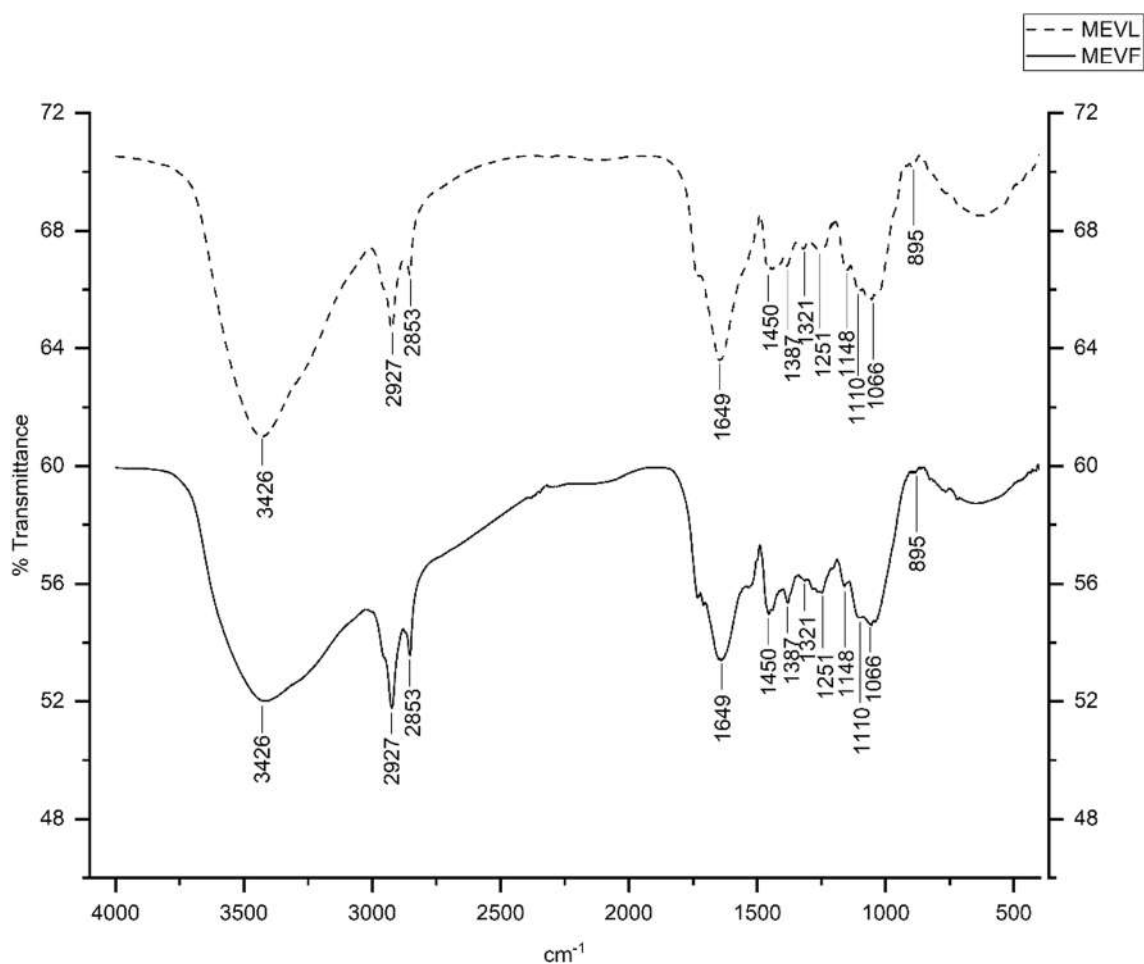


**Fig. 6** FTIR spectrum of MEVL and MEVF

correlation also exists between the quantity of phenolic compounds and antioxidant activities [9, 70]. Flavonoids, the most diverse and widely distributed phenol

**Table 5** FTIR spectral values and their corresponding functional groups in *V. simonsii*

	Absorption (cm <sup>-1</sup> )	Appearance	Group	Compound class
1	3500-3400	Stretching	O-H	Alcohol
2	3000-2840	Stretching	C-H	Alkane
3	3000-2840	Stretching	C-H	Alkane
4	1650-1600	Stretching	C=O	Carboxylic acid
5	1450-1375	Bending	C-H	Alkane
6	1450-1375	Bending	C-H	Alkane
7	1390-1310	Stretching	C-N	Amine
8	1275-1200	Stretching	C-O	Alkyl aryl ether
9	1150-1085	Stretching	C-O	Aliphatic ether
10	1124-1087	Stretching	C-O	Secondary alcohol
11	1085-1050	Stretching	C-O	Primary alcohol
12	895-885	Bending	C=O	Alkene

of natural products, possess free radical scavenging and antimicrobial activities [15]. Similarly, it is crucial to analyse the free radical scavenging potential of the extracts along with phenolic content assay to substantiate antioxidant property. Since free radicals are of different chemical entities, different tests are required to prove the free radical scavenging capability through various mechanism [29]. In this regard, DPPH and FRAP assay methods are often employed. In terms of phenolic content, the values for *V. simonsii* fruit extract (250.20 mg/g) were higher than the fruit extract of *V. opulus* (131.99 mg/g) [59], *V. mullaha* (12.57 mg/g) [66] and *V. coriaceum* (29.75 mg/g) [73]. In contrast, the flavonoid content of *V. simonsii* fruit extract (40.65 mg/g) was higher than the fruit of *V. mullaha* (35.03 mg/g) [66]. Further, Česonienė et al. [12] and Polka et al. [50] demonstrated that *V. opulus* fruit has significant antioxidant activity with 10.07–37.3 mg/g of phenolic content and FRAP value of 0.19 μM/g. Undeniably, *V. opulus* was the most studied among the *Viburnum* species so far [66]. Besides, Levent et al. [35] also

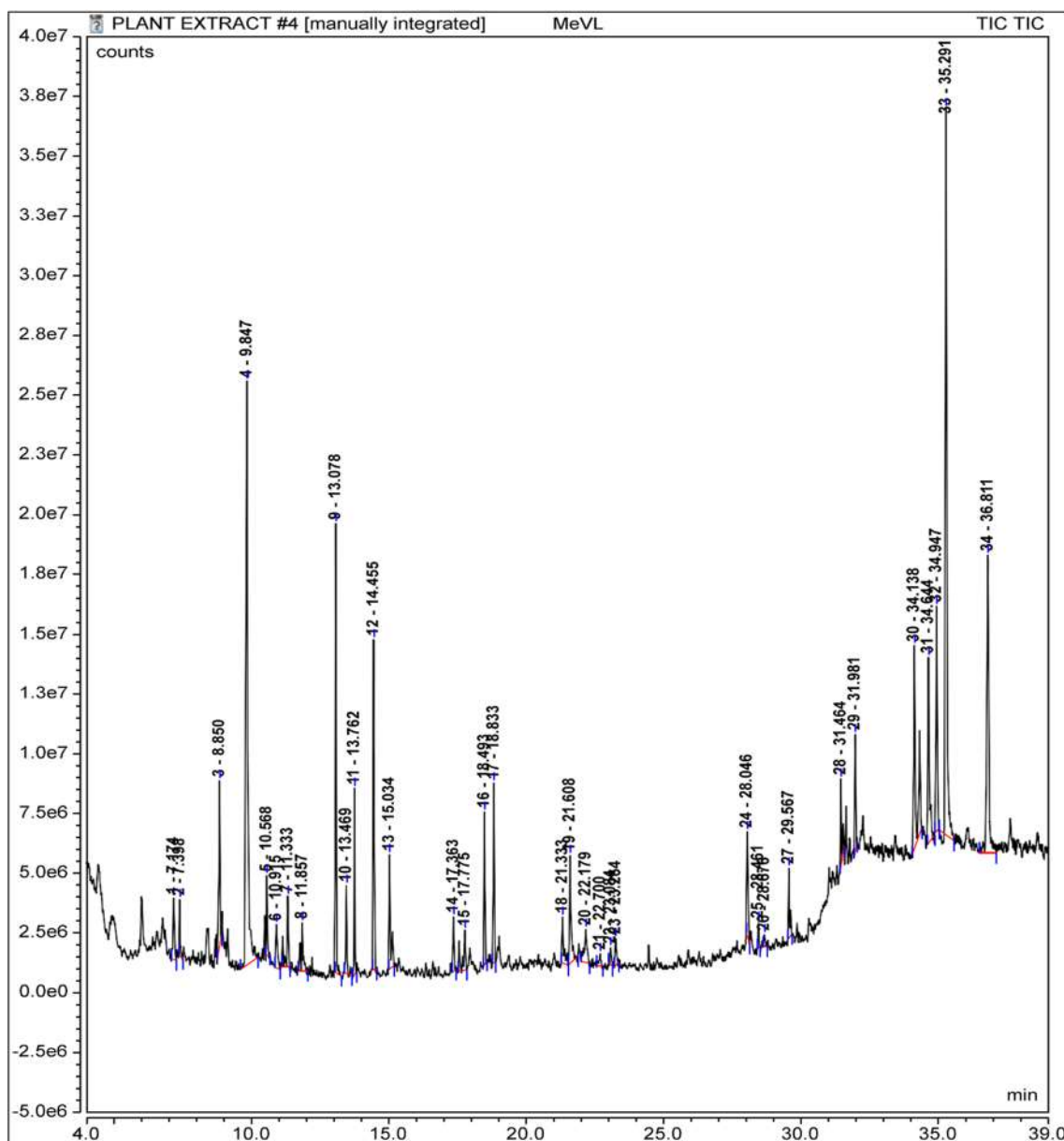


**Fig. 7** GC-MS chromatogram of MEVL

demonstrated the strong DPPH inhibition potency ( $IC_{50}$  85  $\mu\text{g}/\text{ml}$ ) of *V. lantana*. Vijaytha et al. [73] have also demonstrated a weak antioxidant activity of *V. coriaceum* ( $IC_{50}$  1500  $\mu\text{g}/\text{ml}$ ). However, considering the standard antioxidant property, the antioxidant values of the *V. simonsii* fruit extracts (MEVL) represent moderately strong free radical scavenging activity (Table 3). Because,  $IC_{50}$  values in the range of 10–100  $\mu\text{g}/\text{ml}$  represent very strong antioxidant properties, whereas  $>100$  represent moderate strong and  $>500$  represents weak properties [49].

In wake of recent advancements in modern medicine, there has been a rapid upsurge in multiple antibiotic resistant bacteria. Especially, gram-negative pathogenic bacteria are known to be resistant to many antibiotics [54]. Therefore, to combat antibiotic resistance of the pathogenic bacteria, alternative strategies are much essential. Further, it has been verified that medicinal plants exhibit good antimicrobial activity [55]. The antimicrobial activities of any plant extracts were found to have correlation with the presences of some phyto-compounds such as alkaloid, tannins, steroids, phenols,

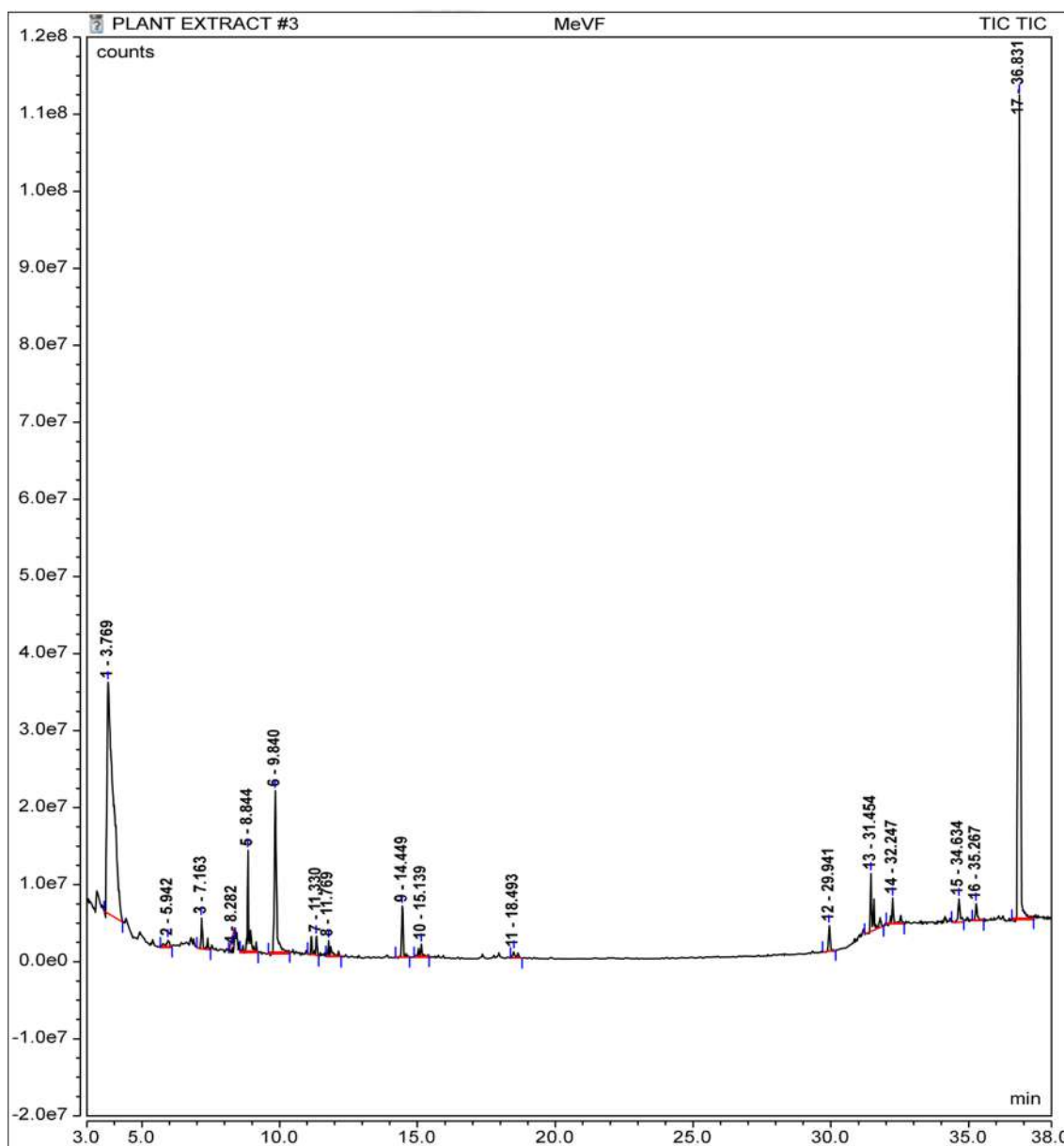


**Fig. 8** GC-MS chromatogram of MEVF

etc., [30]. Different mechanisms by which phytochemicals inhibit microbial growths were mentioned earlier [2]. For instance, destruction of cell membrane, inhibition of cell-wall and protein biosynthesis, DNA replication and repairing. Plants rich in polyphenolic compounds exhibited antibacterial activities against a broad spectrum of bacteria [8, 67]. These polyphenolic compounds were found to inhibit bacterial growth by restricting the activities of virulence factor, biofilm formation and cell-wall formation, and by reducing pH values [30]. The present findings showed that fruit and leaf extract

showed inhibitory action against gram-positive bacteria only (Table 4 and Fig. 5). These findings were in agreement with the findings reported by Wintola et al. [76], in which anti-dysenteric plant extracts showed 12–15 mm inhibitory zone against the same bacteria that were used in the present study. Additionally, Sagdic et al. [59] demonstrated that methanolic extracts of *V. opulus* showed 19–22 mm zone of inhibition against *B. cereus* and *S. aureus*. Roy et al. [57] reported that methanolic fractions of *V. foetidum* showed 18–20 mm inhibitory zone against the *B. cereus* and *S. aureus* bacteria. No activity against

**Table 6** GC MS spectral analysis of methanolic leaf extract of *Viburnum simonsii* (MEVL)

Sl. No	RT (min)	Name of the Compounds	Peak Area %
1	7.174	8-Methyl-3-oxo-2-oxabicyclo (4.4.0) deca-4,9-diene-6,8-carbolactone	1.32
2	7.398	t-Butyl-(2-[3-(2,2-dimethyl-6-methylene-cyclohexyl)-propyl]-[1, 3] dithian-2-yl)-dimethyl-silane	0.87
3	8.850	Benzoic acid, 4-ethoxy-, ethyl ester	2.51
4	9.847	1,2,3,4-Cyclohexanetetrol	16.86
5	10.568	Cyclohexanol, 3-ethenyl-3-methyl-2-(1-methylethenyl)-6-(1-methylethyl)-, [1R-(1a,2a,3β,6a)]-	0.94
6	11.333	Tridecanoic acid, 12-methyl-, methyl ester	1.59
7	13.078	Neophytadiene	4.96
8	13.762	3,7,11,15-Tetramethyl-2-hexadecen-1-ol	2.23
9	14.455	Hexadecanoic acid, methyl ester	4.04
10	15.034	n-Hexadecanoic acid	2.22
11	17.363	11-Octadecenoic acid, methyl ester	0.92
12	18.493	1-Heptatriacotanol	2.07
13	18.833	Doconexent	2.41
14	21.608	cis-Z-a-Bisabolene epoxide	2.50
15	28.046	Ergosta-5,22-dien-3-ol, acetate, (3β,22E)-	1.70
16	31.464	W-18	1.45
17	31.981	a-Tocopheryl acetate	1.48
18	34.138	β-Sitosterol	5.70
19	34.644	β-Amyrin	4.41
20	35.291	a-Amyrin	15.95
21	36.811	Lup-20(29)-en-3-ol, acetate, (3β)-	9.22

**Table 7** GC MS spectral analysis of methanolic fruit extract of *Viburnum simonsii* (MEVF)

Sl. No	R. T (min)	Name of the Compounds	Peak Area %
1	3.769	Glycerin	37.38
2	7.163	Benzeneacetaldehyde, a,2,5-trimethyl-	1.33
3	8.282	3-Pyridinecarboxylic acid, 1,6-dihydro-4-hydroxy-2-methyl-6-oxo-, ethyl ester	1.13
4	8.844	Benzoic acid, 4-ethoxy-, ethyl ester	3.90
5	9.840	Propanoic acid, 2-methyl-, 2-ethylhexyl ester	8.20
6	11.330	Cyclopentanetridecanoic acid, methyl ester	1.00
7	11.769	Eicosane, 2-methyl-	1.27
8	14.449	Pentadecanoic acid, 14-methyl-, methyl ester	1.49
9	15.139	Decane, 2,3,5,8-tetramethyl-	0.91
10	29.941	Lupeol, trifluoroacetate	0.76
11	31.454	Lupeol	2.84
12	32.247	Hexasiloxane, 1,1,3,3,5,5,7,7,9,9,11,11-dodecamethyl-	1.37
13	36.831	Lup-20(29)-en-3-ol, acetate, (3β)-	35.12

gram-negative bacteria and fungus might be due to the reason that some phytochemicals are target specific or might be due to the fact that gram-negative bacteria show highest resistance to broad spectrum of antibiotics [54]. For instance, coumarin (polyphenolic compound) shows activity against gram-positive and no activity against gram-negative bacteria [17]. In addition, Iqbal et al. [25], recently isolated three alkaloid compounds

(Viburnoate A, B, C) from *V. grandiflorum* and demonstrated that these alkaloid compounds showed maximum inhibition against gram-positive bacteria than gram-negative bacteria.

Many scientific investigations concerning antimicrobial and antioxidant activities of other *Viburnum* species [25, 50, 57, 73] have been undertaken previously. However, there is lack of scientific documentation on the efficacy

of currently studied species, especially on the aspects of antimicrobial and antioxidant activities. Therefore, the findings pertaining to free radical scavenging and antimicrobial potential of the *V. simonsii* extracts in the present study necessitates the need for identifying active antioxidant as well as antimicrobial components present in the extracts and speculating their subsequent commercial application.

FTIR was done in order to determine the functional groups present in the crude extract. The FTIR spectra implies the presence of alcohols (primary and secondary), ethers, amines, carboxylic acids and hydrocarbons (alkane, alkene and alkyne). In the FTIR spectra the fruit extract showed more absorption intensity than leaf extracts, which may be attributed to the presences of phytochemicals in larger quantity than the leaf extracts. The phytoconstituents of the *V. simonsii* extracts were identified by GC–MS analysis. The analysis revealed the presence of 21 compounds in fruit extract and 13 compounds in leaf extract. 1,2,3,4-Cyclohexanetetrol are polyols having highest peak area percentage (16.86%) in MEVL which act as glucosidase inhibitor [47]. Lup-20(29)-en-3-ol, acetate, (3 $\beta$ )- found in both MEVL (9.22%) and MEVF (35.12%) have anticancer, anti-inflammatory, antituberculosis, antimalarial, antimicrobial, antinociceptive and antioxidant activities [38, 51].  $\beta$ -Sitosterol (5.70%), have antitumor activities against breast, lung, prostate and colon cancer [31].  $\alpha$ ,  $\beta$ -Amyrins (15.95%, 4.41%) were reported to have antinociceptive, anti-inflammatory, antioxidant, anti-diabetic and anticancer, antihyperglycemic, gastroprotective and anticonvulsant properties [19, 46]. Neophytadiene (4.96%) have anti-inflammatory, anti-microbial, antioxidant, antipyretic, good analgesic properties [5, 11]. Further, Benzoic acid, 4-ethoxy-, ethyl ester, which is found in both MEVL and MEVF has cardioprotective, antimicrobial, antioxidant and anti-inflammatory properties [37]. Pentadecanoic acid, 14-methyl-, methyl ester, Tridecanoic acid, 12-methyl-, methyl ester, Hexadecanoic acid, methyl ester, n-Hexadecanoic acid, 11-Octadecenoic acid, methyl ester and 1-Heptatriacotanol were reported to have antimicrobial, anti-inflammatory, hypocholesterolemic, cancer preventive, antioxidant, hepatoprotective, and antiarthritic properties [18, 21]. cis-Z-a-Bisabolene epoxide increase sex hormone activity and has antitumor property [18]. In one of the previous studies on the related species such as *Viburnum odoratissimum* var *odoratissimum* dehydrovibsanin G (diterpenoid), (+)-9'-O-seneciopyllaricresinol (lignan) were isolated and reported to possess anticancer activity against breast cancer cell lines (human A431, T47D) [36]. Recently, five new terpenoids (two vibsane-type diterpenoids, three iridoid allosides) were isolated from *Viburnum odoratissimum*

var *sessiliflorum*, these compounds showed efficient anti-inflammatory and anticancer activities against colon cancer [78].

However, it is worth mentioning herein that FTIR and GC–MS studies are not conclusive for phytochemical investigations. Since IR and GC–MS studies cannot elucidate the structure of the bioactive compounds, higher techniques such as NMR spectroscopy is required. NMR provides insight into the different structures and functionalities of the various components and, hence, assists the interpretation of the results of the other analytical methods [43]. The study also necessitates the need for NMR spectroscopy (a part of planned future research activity) which is highly sought after in drug development for both molecule identification and structural elucidation [16].

## Conclusion

The use of plant-based medicine as an alternative to allopathic medicine is now becoming an increasingly attractive option for the management of human diseases. The medicinal plants secrete a diverse array of high value bio-actives (polyphenols, flavonoids, alkaloids, glycosides, terpenoids etc.) and consequently possess significant bioactivity. Additionally, medicinal plants are believed to impart lesser side effects in comparison to conventional allopathic medicine. *V. simonsii* in the present study showed high phenolic content and appreciable antioxidant and antibacterial activities. Qualitative phytochemical screening revealed the presence of high value bioactives. FTIR study also confirms the presence of functional groups which are usually present in phytochemicals. Further, GC–MS analysis demonstrated the presence of compounds which have anticancer, anti-inflammatory, antidiabetic, antimalarial, antituberculosis, and anti-nociceptive properties. Since the plant parts are already in use by the indigenous populace of Meghalaya, there lies tremendous scope for new area of investigations. Therefore, the present study warrants greater research capacities with specific emphasis on pure compound isolation, bioactivities (*in-vitro*, *in vivo* investigation of anticancer, antiviral, anti-diabetic, anti-inflammatory activity etc.) and *in silico* drug designing studies in order to validate its pharmaceutical potential.

## Abbreviations

V. simonsii:	Viburnum simonsii
V. opulus	Viburnum opulus
MEVL	Methanolic extract of V. simonsii leaf
MEVF	Methanolic extract of V. simonsii fruit
FTIR	Fourier transform infrared
GC–MS	Gas chromatography mass spectrometry
TPC	Total phenolic content
TFC	Total flavonoid content
DPPH	2,2-Diphenyl-1-picrylhydrazyl

FRAP	Ferric reducing antioxidant power
GAE	Gallic acid equivalent
QE	Quercetin equivalent
RSA	Radical scavenging activity
AAE	Ascorbic acid equivalent
DMSO	Dimethyl sulfoxide
NMR	Nuclear magnetic resonance
MHA	Mueller Hinton agar

### Acknowledgements

The first author (SRS) acknowledges the Ministry of Tribal Affairs, Govt. of India, for providing financial assistance in the form of National fellowship for Higher Studies for ST Students (NFST).

### Plant authentication

The plant species was identified and authenticated by referring to the existing herbarium specimen (Reference accession no: 90420) available in Botanical Survey of India, Eastern Region, Shillong, India

### Author contributions

SRS: Formal analysis, investigation, methodology, writing original draft and editing. MMP: Visualization, conceptualization, formal analysis, investigation, methodology, writing-original draft, reviewing and editing. VC: Formal analysis, investigation, methodology, writing original draft. DKV: Formal analysis, investigation, methodology and writing original draft. PB: Formal analysis, investigation, methodology and writing original draft. SK: Formal analysis and writing original draft. PPP: Formal analysis and writing original draft.

### Funding

No external funding was received to conduct the study.

### Availability of data and materials

All data and materials are available upon request.

### Declarations

#### Ethics approval and consent to participate

Not applicable.

#### Consent for publication

Not applicable.

#### Competing interests

The authors declare no competing interests.

#### Author details

<sup>1</sup>Department of Forestry, School of Sciences, Nagaland University, Lumami, Nagaland 798627, India. <sup>2</sup>Department of Chemistry, Government Digvijay Autonomous Postgraduate College, Rajnandgaon, Chhattisgarh 491441, India. <sup>3</sup>Department of Energy Engineering, Assam Science and Technology University, Guwahati, Assam 781013, India. <sup>4</sup>Department of Applied Biology, University of Science and Technology Meghalaya, Ri-Bhoi, Meghalaya 793101, India. <sup>5</sup>Department of Zoology, School of Sciences, Nagaland University, Lumami, Nagaland 798627, India.

Received: 13 September 2023 Accepted: 2 December 2023

Published online: 11 December 2023

### References

- Acharya J, Mukherjee A (2014) An account of *Viburnum* L. in the Eastern Himalayan region. *Acta Bot Hung* 56(3–4):253–262. <https://doi.org/10.1556/abot.56.2014.3-4.1>
- Álvarez-Martínez FJ, Barrajón-Catalán E, Herranz-López M, Micol V (2021) Antibacterial plant compounds, extracts and essential oils: An updated review on their effects and putative mechanisms of action. *Phytomedicine* 90:153626. <https://doi.org/10.1016/j.phymed.2021.153626>
- Barbieri R, Coppo E, Marchese A, Daglia M, Sobarzo-Sánchez E, Nabavi SF, Nabavi SM (2017) Phytochemicals for human disease: An update on plant-derived compounds antibacterial activity. *Microbiol Res* 196:44–68. <https://doi.org/10.1016/j.micres.2016.12.003>
- Benzie IFF, Strain JJ (1996) The ferric reducing ability of plasma (FRAP) as a measure of “antioxidant power”: the FRAP assay. *Anal Biochem* 239:70–76
- Bhardwaj M, Sali VK, Mani S, Vasanthi HR (2020) Neophytadiene from *Turbinaria ornata* suppresses LPS-induced inflammatory response in RAW 264.7 macrophages and Sprague Dawley rats. *Inflammation* 43:937–950. <https://doi.org/10.1007/s10753-020-01179-z>
- Bhat SG (2021) Medicinal Plants and Its Pharmacological Values. In: El-Shemy HA (ed.) *Natural Medicinal Plants*. IntechOpen, London, UK, pp 217–229.
- Bibi Y, Nisa S, Waheed A, Zia M, Sarwar S, Ahmed S, Chaudhary MF (2010) Evaluation of *Viburnum foetens* for anticancer and antibacterial potential and phytochemical analysis. *Afr J Biotechnol* 9(34):5611–5615. <https://doi.org/10.5897/AJB09.1867>
- Bouarab CL, Degraeve P, Ferhout H, Bouajila J, Oulahl N (2019) Plant antimicrobial polyphenols as potential natural food preservatives. *J Sci Food Agric* 99(4):1457–1474. <https://doi.org/10.1002/jsfa.9357>
- Cai Y, Luo Q, Sun M, Corke H (2004) Antioxidant activity and phenolic compounds of 112 traditional Chinese medicinal plants associated with anticancer. *Life Sci* 74(17):2157–2184. <https://doi.org/10.1016/j.lfs.2003.09.047>
- Capar TD, Dedebas T, Yalcin H, Ekici L (2021) Extraction method affects seed oil yield, composition, and antioxidant properties of European cranberrybush (*Viburnum opulus*). *Ind Crops Prod* 168:113632. <https://doi.org/10.1016/j.indcrop.2021.113632>
- Carretero ME, López-Pérez JL, Abad MJ, Bermejo P, Tillet S, Israel A, Noguera-p B (2008) Preliminary study of the anti-inflammatory activity of hexane extract and fractions from *Bursera simaruba* (Linneo) Sarg (Burseraceae) leaves. *J Ethnopharmacol* 116(1):11–15. <https://doi.org/10.1016/j.jep.2007.10.034>
- Česonienė L, Daubaras R, Viškelis P, Šarkinas A (2012) Determination of the total phenolic and anthocyanin contents and antimicrobial activity of *Viburnum opulus* fruit juice. *Plant Foods Hum Nutr* 67:256–261. <https://doi.org/10.1007/s11130-012-0303-3>
- Chen J, Shao J, Zhao C, Shen J, Dong Z, Liu W et al (2018) Chemical constituents from *Viburnum fordiae* Hance and their anti-inflammatory and antioxidant activities. *Arch Pharm Res* 41:625–632. <https://doi.org/10.1007/s12272-018-1026-2>
- Clarke G, Ting KN, Wiart C, Fry J (2013) High correlation of 2, 2-diphenyl-1-picrylhydrazyl (DPPH) radical scavenging, ferric reducing activity potential and total phenolics content indicates redundancy in use of all three assays to screen for antioxidant activity of extracts of plants from the Malaysian rainforest. *Antioxidants* 2(1):1–10. <https://doi.org/10.3390/antiox2010001>
- Daneshzadeh MS, Abbaspour H, Amjad L, Nafchi AM (2020) An investigation on phytochemical, antioxidant and antibacterial properties of extract from *Eryngium billardieri* F. Delaroché *J Food Meas Charact* 14:708–715. <https://doi.org/10.1007/s11694-019-00317-y>
- Emwas AH, Szczepski K, Poulson BG, Chandra K et al (2020) NMR as a “gold standard” method in drug design and discovery. *Molecules* 25(20):4597. <https://doi.org/10.3390/molecules25204597>
- Enioutina EY, Teng L, Fateeva TV, Brown JC, Job KM, Bortnikova VV et al (2017) Phytotherapy as an alternative to conventional antimicrobials: combating microbial resistance. *Exp Rev Clin Pharmacol* 10(11):1203–1214. <https://doi.org/10.1080/17512433.2017.1371591>
- Ganesh M, Mohankumar M (2017) Extraction and identification of bioactive components in *Sida cordata* (Burm. f.) using gas chromatography–mass spectrometry. *J Food Sci Technol* 54:3082–3091. <https://doi.org/10.1007/s13197-017-2744-z>
- Ghosh G, Panda P, Rath M, Pal A, Sharma T, Das D (2015) GC-MS analysis of bioactive compounds in the methanol extract of *Clerodendrum viscosum* leaves. *Pharmacognosy Res* 7(1):110–113. <https://doi.org/10.4103/0974-8490.147223>
- Gogoi K, Phukan MM, Dutta N, Pradeep SS, Sedai P, Kumar Konwar B, Maji TK (2014) Valorization and miscellaneous prospects of waste *Musa balbisiana* Colla pseudostem. *J Waste Manag* 2014:412156. <https://doi.org/10.1155/2014/412156>



21. Gomathi D, Kalaiselvi M, Ravikumar G, Devaki K, Uma C (2015) GC-MS analysis of bioactive compounds from the whole plant ethanolic extract of *Evolvulus alsinoides* (L.) L. *J Food Sci Technol* 52:1212–1217. <https://doi.org/10.1007/s13197-013-1105-9>
22. Harborne JB (1973) Methods of plant analysis. Phytochemical methods: a guide to modern techniques of plant analysis, 1–32.
23. Haridasan K, Rao RR (1985–1987) Forest flora of Meghalaya. Vol 1, II. Bishen Singh Mahendra Pal Singh, Dehra Dun India.
24. Hooker JD (1875) The flora of british India (Vol. 1). L. Reeve, London.
25. Iqbal N, Yasmin I, Ullah H et al (2022) Isolation, characterization and antibacterial studies of three new chemical constituents isolated from *Viburnum grandiflorum*. *Pharm Chem J* 56(4):480–486. <https://doi.org/10.1007/s11094-022-02663-6>
26. Jahan I, Ahmet O (2020) Potentials of plant-based substance to inhabit and probable cure for the COVID-19. *Turk J Biol* 44:228–241. <https://doi.org/10.3906/biy-2005-114>
27. Kajszczak D, Zaklos-Szyda M, Podśędek A (2020) *Viburnum opulus* L.—A review of phytochemistry and biological effects. *Nutrients* 12(11):3398. <https://doi.org/10.3390/nu12113398>
28. Kanjilal UN, Kanjilal PC, Das A, De RN, Bor NL (1934–1940) Flora of Assam. Vols. 1–5. Government of Assam, Shillong.
29. Kasote DM, Katyare SS, Hegde MV, Bae H (2015) Significance of antioxidant potential of plants and its relevance to therapeutic applications. *Int J Biol Sci* 11(8):982–991
30. Khameneh B, Eskin NM, Iranshahy M, Fazly Bazzaz BS (2021) Phytochemicals: a promising weapon in the arsenal against antibiotic-resistant bacteria. *Antibiotics* 10(9):1044. <https://doi.org/10.3390/antibiotics10091044>
31. Khan Z, Nath N, Rauf A, Emran TB, Mitra S et al (2022) Multifunctional roles and pharmacological potential of  $\beta$ -sitosterol: Emerging evidence toward clinical applications. *Chem Biol Interact* 365:110117. <https://doi.org/10.1016/j.cbi.2022.110117>
32. Khomarlou N, Aberomand-Azar P, Lashgari AP, Tebyanian H, Hakakian A, Ranjbar R, Ayatollahi SA (2018) Essential oil composition and in vitro antibacterial activity of *Chenopodium album* subsp. *striatum*. *Acta Biol Hung* 69(2):144–155. <https://doi.org/10.1556/018.69.2018.2.4>
33. Kraujalytė V, Venskutonis PR, Pukalskas A, Česonienė L, Daubaras R (2013) Antioxidant properties and polyphenolic compositions of fruits from different European cranberrybush (*Viburnum opulus* L.) genotypes. *Food Chem* 141(4):3695–3702. <https://doi.org/10.1016/j.foodchem.2013.06.054>
34. Kubo M, Nakai M, Harada K, Fukuyama Y (2019) Structure of seven new vibane-type diterpenoids from *Viburnum awabuki*. *Tetrahedron* 75(16):2379–2384. <https://doi.org/10.1016/j.tet.2019.02.049>
35. Levent AM, Saltan ÇG, Sever YB, Çoban T (2008) Antioxidant properties of *Viburnum opulus* and *Viburnum lantana* growing in Turkey. *Int J Food Sci Nutr* 59(3):175–180. <https://doi.org/10.1080/09637480701381648>
36. Li FJ, Yu JH, Wang GC, Zhang H, Yue JM (2015) Diterpenes and lignans from *Viburnum odoratissimum* var *odoratissimum*. *J Asian Nat Prod Res* 17(5):475–481. <https://doi.org/10.1080/10286020.2015.1041934>
37. Lipińska MM, Haliński ŁP, Gołębiowski M, Kowalkowska AK (2023) Active compounds with medicinal potential found in maxillariinae Benth (Orchidaceae Juss.) representatives—a review. *Int J Mol Sci* 24(1):739. <https://doi.org/10.3390/ijms24010739>
38. Liu K, Zhang X, Xie L, Deng M, Chen H, Song J et al (2021) Lupeol and its derivatives as anticancer and anti-inflammatory agents: Molecular mechanisms and therapeutic efficacy. *Pharmacol Res* 164:105373. <https://doi.org/10.1016/j.phrs.2020.105373>
39. Lowry OH (1951) Protein measurement with the folin phenol reagent. *J Biol Chem* 193:265–275
40. Maikhuri RK, Dhyani D, Tyagi Y, Singh D, Negi VS, Rawat LS (2012) Determination of nutritional and energy value of *Viburnum mullaha* Buch-Ham. Ex D. Don (Indian cranberry). *Ecol Food Nutr* 51(3):218–226
41. Mir AH, Upadhaya K, Choudhury H (2014) Diversity of endemic and threatened ethnomedicinal plant species in Meghalaya, North-East India. *Int Res J Environ Sci* 3(12):64–78
42. Mir AH, Upadhaya K, Roy DK, Deori C, Singh B (2019) A comprehensive checklist of endemic flora of Meghalaya. *India J Threatened Taxa* 11(12):14527–14561. <https://doi.org/10.11609/jott.4605.11.12.14527-14561>
43. Negahdar L, Gonzalez-Quiroga A, Otyuskaya D, Toraman HE, Liu L et al (2016) Characterization and comparison of fast pyrolysis bio-oils from pinewood, rapeseed cake, and wheat straw using  $^{13}\text{C}$  NMR and comprehensive GCx GC. *ACS Sustain Chem Eng* 4(9):4974–4985. <https://doi.org/10.1021/acssuschemeng.6b01329>
44. Neupane P, Lamichhane J (2020) Estimation of total phenolic content, total flavonoid content and antioxidant capacities of five medicinal plants from Nepal. *Vegetos* 33:360–366. <https://doi.org/10.1007/s42535-020-00116-7>
45. Nisar T, Wang ZC, Yang X, Tian Y, Iqbal M, Guo Y (2018) Characterization of citrus pectin films integrated with clove bud essential oil: Physical, thermal, barrier, antioxidant and antibacterial properties. *Int J Biol Macromol* 106:670–680. <https://doi.org/10.1016/j.ijbiomac.2017.08.068>
46. Nogueira AO, Oliveira YIS, Adjafre BL, de Moraes MEA, Aragao GF (2019) Pharmacological effects of the isomeric mixture of alpha and beta amyryrin from *Protium heptaphyllum*: a literature review. *Fundam Clin Pharmacol* 33(1):4–12. <https://doi.org/10.1111/fcp.12402>
47. Ogawa S, Asada M, Ooki Y, Mori M, Korenaga T (2005) Design and synthesis of glycosidase inhibitor 5-amino-1, 2, 3, 4-cyclohexanetetrol derivatives from (–)-vibo-queritol. *Bioorg Med Chem* 13(13):4306–4314. <https://doi.org/10.1016/j.bmc.2005.04.003>
48. Pavia DL, Lampman GM, Kriz GS, Vyvyan JA (2014) Introduction to spectroscopy. Cengage learning, Stamford, USA.
49. Phongpaichit S, Nikom J, Rungjindamai N, Sakayaroj J, Hutadilok-Towatana N, Rukachaisirikul V, Kirtikara K (2007) Biological activities of extracts from endophytic fungi isolated from *Garcinia* plants. *FEMS Microbiol Immunol* 51(3):517–525. <https://doi.org/10.1111/j.1574-695X.2007.00331.x>
50. Polka D, Podśędek A, Koziolkiewicz M (2019) Comparison of chemical composition and antioxidant capacity of fruit, flower and bark of *Viburnum opulus*. *Plant Foods Hum Nutr* 74:436–442. <https://doi.org/10.1007/s11130-019-00759-1>
51. Prachayasittikul S, Saraban P, Cherdtrakulkiat R, Ruchirawat S, Prachayasittikul V (2010) New bioactive triterpenoids and antimalarial activity of *Diospyros rubra* Lec. *Excli J* 9:1–10
52. Rahmatollah R, Mahbobeh R (2010) Mineral contents of some plants used in Iran. *Pharmacognosy Res* 2(4):267–270. <https://doi.org/10.4103/0974-8490.69130>
53. Raya KB, Ahmad SH, Farhana SF, Mohammad M, Tajidin NE, Parvez A (2015) Changes in phytochemical contents in different parts of *Clinacanthus nutans* (Burm. f.) lindau due to storage duration. *Bragantia* 74:445–452. <https://doi.org/10.1590/1678-4499.0469>
54. Rhetso T, Shubharani R, Roopa MS, Sivaram V (2020) Chemical constituents, antioxidant, and antimicrobial activity of *Allium chinense* G. Don *Futur J Pharm Sci* 6(1):1–9. <https://doi.org/10.1186/s43094-020-00100-7>
55. Rios JL, Recio MC (2005) Medicinal plants and antimicrobial activity. *J Ethnopharmacol* 100(1–2):80–84. <https://doi.org/10.1016/j.jep.2005.04.025>
56. Rojas R, Bustamante B, Bauer J, Fernández I, Albán J, Lock O (2003) Antimicrobial activity of selected Peruvian medicinal plants. *J Ethnopharmacol* 88(2–3):199–204. [https://doi.org/10.1016/S0378-8741\(03\)00212-5](https://doi.org/10.1016/S0378-8741(03)00212-5)
57. Roy S, Khatun R, Rahman MAA (2017) In vitro antimicrobial and cytotoxic activities of various methanolic fractions of *Viburnum foetidum* L. (Adoxaceae). *J pharmacogn phytochem* 6(5):183–186
58. Royal Botanic Garden, Kew (2023) <https://powo.science.kew.org/taxon/urn:lsid:ipni.org:names:149931-1>, Accessed on 01 September, 2023.
59. Sagdic O, Aksoy A, Ozkan G (2006) Evaluation of the Antibacterial and Antioxidant Potentials of Cranberry (Gilaburu, *Viburnum Opulus* L.) Fruit Extract. *Acta Aliment* 35(4):487–492. <https://doi.org/10.1556/aalim.35.2006.4.12>
60. Satter MMA, Khan MMRL, Jabin SA, Abedin N, Islam MF, Shaha B (2016) Nutritional quality and safety aspects of wild vegetables consume in Bangladesh. *Asian Pac J Trop Biomed* 6(2):125–131. <https://doi.org/10.1016/j.apjtb.2015.11.004>
61. Seal T, Chaudhuri K (2016) Nutritional analysis of some selected wild edible plants consumed by the tribal people of Meghalaya state in India. *Int J Food Sci Nutr* 1(6):39–43
62. Shao J-H, Chen J, Xu X-Q, Zhao C-C, Dong Z-L, Liu W-Y, Shen J (2019) Chemical constituents and biological activities of *Viburnum macrocephalum* f. *keteleeri*. *Nat Prod Res* 33(11):1612–1616
63. Sharifi-Rad J, Quispe C, Vergara CV et al (2021) Genus *Viburnum*: Therapeutic potentialities and agro-food-pharma applications. *Oxid Med Cell Longev* 2021:3095514. <https://doi.org/10.1155/2021/3095514>

64. Shen X, Xing S, Zhang L et al (2018) Vibsanin A sensitizes human acute myeloid leukemia cells to tyrosine kinase inhibitor-induced myeloid differentiation via activation of PKC and upregulation of Lyn. *Biochem Biophys Res Commun* 502(1):110–115. <https://doi.org/10.1016/j.bbrc.2018.05.129>
65. Shukla A, Desai K, Modi N (2020) In vitro antioxidant and antimicrobial potential of *Sterculia urens* Roxb root extract and its bioactive phytoconstituents evaluation. *Futur J Pharm Sci* 6(1):1–11. <https://doi.org/10.1186/s43094-020-00063-9>
66. Singh H, Lily MK, Dangwal K (2017) *Viburnum mullaha* D. DON fruit (Indian cranberry): A potential source of polyphenol with rich antioxidant, anti-elastase, anti-collagenase, and anti-tyrosinase activities. *Int J Food Prop* 20(8):1729–1739. <https://doi.org/10.1080/10942912.2016.1217878>
67. Sun J, Liu JN, Fan B, Chen XN, Pang DR, Zheng J, Zhang Q, Zhao YF, Xiao W, Tu PF, Song YL, Li J (2019) Phenolic constituents, pharmacological activities, quality control, and metabolism of *Dracaena* species: a review. *J Ethnopharmacol* 244:112138. <https://doi.org/10.1016/j.jep.2019.112138>
68. Sundaram V SS, Chandrasekaran S NR, Pandian A (2021) *Strobilanthes heyneanus* root extract as a potential source for antioxidant and antimicrobial activity. *Futur J Pharm Sci* 7(91):1–12. <https://doi.org/10.1186/s43094-021-00242-2>
69. Sureshkumar J, Amalraj S, Murugan R, Tamilselvan A, Krupa J, Sriramavatharajan V et al (2021) Chemical profiling and antioxidant activity of *Equisetum ramosissimum* Desf. stem extract, a potential traditional medicinal plant for urinary tract infections. *Futur J Pharm Sci* 7:192. <https://doi.org/10.1186/s43094-021-00339-8>
70. Tsao R, Yang R, Xie S, Sockovie E, Khanizadeh S (2005) Which polyphenolic compounds contribute to the total antioxidant activities of apple? *J Agric Food Chem* 53(12):4989–4995. <https://doi.org/10.1021/jf048289h>
71. Uddin G, Alam M, Siddiqui BS, Rauf A (2013) Preliminary phytochemical profile and antibacterial evaluation of *Viburnum grandiflorum* Wall. *Glob J Pharm* 7(2):133–137. <https://doi.org/10.5829/idosi.gjp.2013.7.2.1106>
72. Upadhaya K (2015) Structure and floristic composition of subtropical broad-leaved humid forest of Cherapunjee in Meghalaya. *Northeast India J Biodivers Manage Forestry* 4:4
73. Vijaytha V, Anupama RV, Haridas M (2020) Phytochemical profiling, and anti-oxidant, anti-bacterial, and anti-inflammatory properties of *Viburnum coriaceum* Blume. *Futur J Pharm Sci* 6:1–13. <https://doi.org/10.1186/s43094-020-00098-y>
74. Vishwakarma KL, Dubey V (2011) Nutritional analysis of indigenous wild edible herbs used in eastern Chhattisgarh, India. *Emirates J Food and Agriculture* 23:554–560
75. Wang D, Yang Y, Shi X, Yang K, Yin K, Wang F et al (2020) *Viburnum foecoides* A-D, 1-O-isovalerylated iridoid 11-O-alloside derivatives from *Viburnum foetidum* var. *ceanothoides*. *Fitoterapia* 143:104601. <https://doi.org/10.1016/j.fitote.2020.104601>
76. Wintola OA, Afolayan AJ (2015) The antibacterial, phytochemicals and antioxidants evaluation of the root extracts of *Hydnora africana* Thunb. used as antidiarrheic in Eastern Cape Province. *South Africa BMC Complement Altern Med* 15:1–12. <https://doi.org/10.1186/s12906-015-0835-9>
77. Wu B, Wu S, Qu H, Cheng Y (2008) New antioxidant phenolic glucosides from *Viburnum dilatatum*. *Helv Chim Acta* 91(10):1863–1870. <https://doi.org/10.1002/hlca.200890199>
78. Yang LI, Yajiao JIAN, Fan XU, Yongxin LUO, Zhixuan LI, Yi OU et al (2023) Five new terpenoids from *Viburnum odoratissimum* var *sessiliflorum*. *Chin J Nat Med* 21(4):298–307. [https://doi.org/10.1016/S1875-5364\(23\)60438-8](https://doi.org/10.1016/S1875-5364(23)60438-8)
79. Yarazari SB, Jayaraj M (2022) GC–MS analysis of bioactive compounds of flower extracts of *calycopteris floribunda* lam.: a multi potent medicinal plant. *Appl Biochem Biotechnol* 194(11):5083–5099. <https://doi.org/10.1007/s12010-022-03993-7>
80. Yemm EW, Willis A (1954) The estimation of carbohydrates in plant extracts by anthrone. *Biochem J* 57:508–514. <https://doi.org/10.1042/bj0570508>
81. Zhang Y, Zhou WY, Song XY, Yao GD, Song SJ (2020) Neuroprotective terpenoids from the leaves of *Viburnum odoratissimum*. *Nat Prod Res* 34(10):1352–1359. <https://doi.org/10.1080/14786419.2018.1514400>
82. Zhao CC, Zhang XH, Chen J, Shao JH, Zhao ZY, Tang YY (2022) Lignans with  $\alpha$ -glucosidase, protein tyrosine phosphatase 1B, and aldose reductase inhibitory activities from the fruits of *Viburnum cylindricum*. *Ind Crops Prod* 178:11460
83. Zhu QF, Qi YY, Zhang ZJ, Fan M, Bi R, Su J, Wu XD, Shao LD, Zhao QS (2018) Vibsan-type Diterpenoids from *Viburnum odoratissimum* and their cytotoxic and hsp 90 inhibitory activities. *Chem Biodivers* 15(5):800049. <https://doi.org/10.1002/cbdv.201800049>

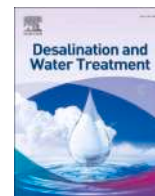
## Publisher's Note

Springer Nature remains neutral with regard to jurisdictional claims in published maps and institutional affiliations.

Submit your manuscript to a SpringerOpen® journal and benefit from:

- Convenient online submission
- Rigorous peer review
- Open access: articles freely available online
- High visibility within the field
- Retaining the copyright to your article

Submit your next manuscript at ► [springeropen.com](https://www.springeropen.com)



## Persistent pesticides: Accumulation, health risk assessment, management and remediation: An overview



Iqbal Ansari<sup>a</sup>, Maha M. El-Kady<sup>b</sup>, Alaa El Din Mahmoud<sup>c,d</sup>, Charu Arora<sup>e,\*</sup>, Aazad Verma<sup>e</sup>, Ravikumar Rajarathinam<sup>a</sup>, Priyanka Singh<sup>f</sup>, Dakeshwar Kumar Verma<sup>f</sup>, Jyoti Mittal<sup>g</sup>

<sup>a</sup> Department of Biotechnology, Vel Tech Rangarajan Dr. Sagunthala R&D Institute of Science and Technology, Avadi 600062, Chennai, India

<sup>b</sup> Department of Self-pollinated Vegetables Crops, Horticulture Research Institute (HRI), Agriculture Research Centre (ARC), Giza, Egypt

<sup>c</sup> Environmental Sciences Department, Faculty of Science, Alexandria University, Alexandria 21511, Egypt

<sup>d</sup> Green Technology Group, Faculty of Science, Alexandria University, Alexandria 21511, Egypt

<sup>e</sup> Department of Chemistry, Guru Ghasidas Vishwavidyalaya, Bilaspur 495009, Chhattisgarh, India

<sup>f</sup> Department of Chemistry, Govt. Digvijay Autonomous Postgraduate College, Rajnandgaon 491441, Chhattisgarh, India

<sup>g</sup> Department of Chemistry, Maulana Azad National Institute of Technology, India

### ARTICLE INFO

#### Keywords:

Persistent pesticides  
Organochlorine  
DDT  
Endosulfan  
Biomagnification  
Health risk assessment

### ABSTRACT

Pesticides are being employed for large-scale agricultural purposes, leading to global environmental issues. Organochlorine pesticides (dieldrin, DDT, and aldrin) are persistent due to their stable nature. Organochlorine pesticide (OCPs) residues present in various foodstuffs, blood serum, air, water, soil and sediments have generated a global surge due to their severe health as well as environmental ill effects. It pollutes air, soil, water resources and gets transferred into the tropic level through food chains and food webs. Studies reveal that insecticides (pesticides) may harm pulmonary, fertility, circulatory, neuronal, hormonal and endocrine functions leading to severe health ailments. In the present article, the fate of persistent pesticides in different ecosystems has been reviewed. Challenges and policies of pest management have been critically discussed.

### 1. Introduction

Organochlorine pesticides are also called persistent pesticides because they are quite steady and not likely to disintegrate or change in the environment for a longer duration. They also resist biological, physical, photochemical, or chemical breakdowns. Organo-chlorinated persistent pesticides belong to heterogeneous categories of organic substances and primarily consist of hydrogen, carbon and many atoms of chlorine per molecule. According to statistics made on various pesticides, 40% of all used pesticides belong to the class of organo-chlorines [1]. They have properties similar to other persistent organic pollutants (POPs), such as polychlorinated dibenzo-p-dioxins/furans (PCDDs/Fs) and polychlorinated biphenyls (PCBs). Once they are introduced into the environment, organo-chlorine pesticides have the capacity for long-term persistence. For example, Dichlorodiphenyltrichloroethane (DDT) was used widely in agriculture to control insects during the period 1940 s-1970 s. It was also used on a large scale to control malaria and typhus. But it may persist for 50 years. Therefore, it has been banned in most developed countries [2]. Although such

chemical properties made the insecticides very effective, they also made them hazardous to the environment as they were transported via different food chains and tropic levels to humans and animals. They are lipophilic therefore, they have a tendency to accumulate in the fatty tissues of humans and animals and break down in the body.

There are different ways of exposure to persistent pesticides, such as eating contaminated foods such as vegetables and leafy roots, fish, fatty meats and poultry products. Persistent pesticide exposure can happen in various ways, such as consuming imported food from countries that use these pesticides, inhalation of contaminated air or drinking water, absorption through the skin, and even through human breast milk for infants [3]. Exposure to large doses of organochlorine pesticides has severe effects on the nervous system. Organochlorine accumulation in the body by persistent exposure such as in people who work with or use organochlorine pesticides for a long time can cause liver damage. Moreover, some early studies made on organochlorine exposure, particularly DDT found a relationship between breast cancer and its levels in the body. According to a study conducted by [4], there may be a correlation between elevated levels of persistent organic pollutants

\* Corresponding author.

E-mail address: [charuarora77@gmail.com](mailto:charuarora77@gmail.com) (C. Arora).

found in human blood serum and the development of diabetes. The persistent pesticides' negative effects are also extended to the marine environment, including an increase in sponges and algae, a reduction in live coral cover, and seagrass bed damage.

## 2. Persistent organic pollutants (POPs) classification

Organochlorine pesticides are categorized into four broad groups:

Hexa-chloro-cyclo-hexane (HCH): It was first identified as a new insecticide in the mid-20th century. The compound was first available commercially as an insecticide in France, while, Michael Faraday was probably the first one to synthesize it in 1825 [5,6]. Also, it was found that the exceptional properties of HCH as insecticide are associated with one of the isomers only and it was called "Ganarnexane", which was isolated for the first time at the beginning of the 20th century by van der Linden (and it is called "lindane" in his honor). This new substance replaced derris quickly, which was used for controlling the flea beetle, further, it also demonstrated to be very efficient not only for controlling many horticultural and agricultural pests but also against locusts and manufacturing insects such as flies, bed bugs, crickets, cockroaches, etc. In addition, it was introduced in the 1950 s as a scabicide for human use for the first time [5]. Hexa-chloro-cyclo-hexane (HCH) is a cyclic saturated chlorinated compound that has eight isomers. Although, that toxic substance had been banned in the majority of countries, but still regularly detected in marine environments, the use and production of HCH have decreased over time. In 2006, the United States Environmental Protection Agency (EPA) banned the end substance uses of lindane. Lindane was also banned in Europe, Canada and Mexico.

Four isomers of HCH only had been considered commercially important ( $\beta$ ,  $\alpha$ ,  $\gamma$  and  $\delta$ ). The gamma-hexa-chloro-cyclo-hexane ( $\gamma$ -HCH) isomer was a pure form and used widely as a powerful pesticide. Thus, when hexachlorocyclohexane pesticide products contain more than 99%  $\gamma$ -HCH, then the substance is called lindane. From a technical degree  $\alpha$ -HCH,  $\beta$ -HCH and HCH are considered to be potentially carcinogenic for humans. There is some evidence that suggests that lindane ( $\gamma$ -HCH) may be carcinogenic. Hyperplastic nodules can develop as a result of prolonged exposure to alpha-HCH, as observed in the livers of mice and rats. Furthermore, it has been found to induce cancerous tumors in the liver of these animals. [7–14]. In 1953 Danopoulos et al. discovered the first evidence that  $\gamma$ -HCH could be toxic for humans. In their experiment, seventy-nine people exposed to a mixture of HCH isomers used in the house, including on bed covers, clothes and skin were specified with primary symptoms like vertigo, headaches, myalgia and lassitude followed by intestinal colic, diarrhea and stomatitis [5]. Central nervous system (CNS) symptoms were also observed, including mental confusion, blindness, dysarthria and convulsions. Furthermore, one patient died as a result of kidney and liver failure. Recently, there have been many studies focusing on HCH toxicity in humans, including evidence of their carcinogenicity [15]. In addition, in the north of India [16] Singh et al., (2013) studied exposure to  $\beta$ -HCH and they discovered that direct association may cause a risk of Alzheimer's disease in the population.

DDT and related compounds DDD and DDE: DDT was used extensively worldwide as an agricultural pesticide and for malaria and typhus vector control in the 20th century from the forties to the seventies. According to its intensive use, DDT has become omnipresent in the ecological system. Thus, throughout the ecological system, p, p'-DDT breaks down into p'-DDD (1,1-dichloro-2,2-bis(4-chlorophenyl) ethane) and p, p'-DDE (1,1-dichloro-2,2-bis(4-chlorophenyl) ethene). DDE is more persistent than its precursor, DDT. Additionally, DDT and its two degradation products, DDD and DDE, are known as persistent organic pollutants (POPs) that exhibit tissue-specific toxicity in the adrenal cortex, potentially leading to cell death. Due to  $\alpha$ , p'-DDD specific tissue toxicity, it has been used as a chemotherapy drug for adrenal cancer in humans. However, DDD strength and efficacy are low

and treatment with it is associated with hazardous side effects. Therefore, DDE has been suggested as another possible therapeutic tool [17]. DDT is extremely toxic to aquatic living organisms (some amphibian species and fishes). In another study on mice, DDT increased lung tumor incidence and both DDD and DDE are carcinogenic in mice [18]. DDE can cause mortality in young or developing birds of prey by inducing a reduction in the thickness of their eggshells [19].

Cyclodienes (heptachlor, aldrin etc.): Cyclodienes are toxic organochlorine insecticides that can cause neurological damage by disrupting the normal functioning of the GABAA receptor and  $\text{Ca}^{2+}$  -  $\text{Mg}^{2+}$  + ATPase in the nervous system [20]. Cyclodienes are polycyclic chlorinated hydrocarbon compounds and are used as insecticides. Cyclodienes also cause developmental as well as hepatotoxicity, furthermore can change the endocrine and immune systems. Most cyclodienes have been categorized as potential carcinogens for humans. Moreover, they are extremely toxic to marine lifeforms, birds, bees and earthworms. These substances pose a danger to human well-being and the natural world; consequently, these items have been entirely banned from production and usage in most advanced countries. The known cyclodienes are endrin, isodrin, dieldrin, aldrin, chlordane, toxaphene, endosulfan, telodrin (isopentane) and heptachlor. Between a period of time from the 1970 s to the 1990 s, the selling and use of all cyclodienes, except endosulfan, was banned from the European Union, the United States, and numerous countries worldwide. Endosulfan was allowed to be usable until 2016. The danger of human exposure still exists owing to their persistence in the environment.

Mirex and chlordecone: These are similar to highly chlorinated derivatives obtained from cyclopentadiene. Mirex and chlordecone merely differ in structure as the former has two bridgehead chlorine atoms while the latter has a carbonyl oxygen atom. Mirex was first launched commercially in 1959 in the USA for use in pesticide formulation and as a fire retardant for industrial purposes; later Mirex was eliminated from use in the United States and Europe in 1978. While chlordecone was first used to control banana root borer in the United States, it was utilized for controlling other pests worldwide. All goods with chlordecone content were canceled in the year 1978. Waste site residents were probably exposed to chlordecone or mirex through skin contact or eating plants cultivated in contaminated soils since these substances link with soil particles. Another way of exposure for people living near waste sites is ingestion or eating animals or fishes which bioconcentrated mirex and chlordecone. However, chlordecone or mirex intake from drinking water is improbable because of their limited solubility in water [20]. Also, chlordecone or mirex inhalation exposure after volatilization from contaminated sites is uncommon because these chemical compounds are nonvolatile. According to animal studies, exposure to mirex may result in grave health effects for the exposed populations. The major organs in experimental animals affected by mirex include liver, thyroid and kidney disturbances. Ocular injury includes cataract development in the eyes of young people if they get exposed to mirex immediately after birth, while in the thyroid, follicles breakdown or an increase in cystic follicles had been observed. Exposure to mirex in animals causes cardiovascular disturbances, cataracts and increased stillbirths. It is also a liver carcinogen in animals. While, chlordecone exposure in experimental animals affects the endocrine system, nervous system, kidneys, reproductive system and liver. Studies suggest that exposure to chlordecone in an occupational setting can impair nervous system functioning, cause liver damage, and potentially affect fertility. Symptoms like increase in cerebrospinal fluid pressure, blurring of vision and headache were observed in workers coming in contact with a high level of chlordecone during its manufacturing process. Furthermore, numerous workers had severe effects on the liver, for example, enhanced microsomal enzyme activity, hepatomegaly, fatty degeneration and mild inflammatory changes, and reproductive toxicity such as altered sperm motility and decreased sperm count [21,22].

### 3. Global actions made to control POPs

International Conventions dealing with POPs and Pesticides:

The United Nations Environment Programme (UNEP) widened its investigation and research area on POPs, in May 1995, with a premier focus on “Dirty Dozen”. It is a group of twelve extremely toxic and persistent compounds: chlordane, aldrin, dieldrin, DDT, heptachlor, endrin, mirex, hexachlorobenzene, polychlorinated dibenzo-p-dioxins, polychlorinated biphenyls, toxaphene and polychlorinated dibenzofurans. A lot of these pesticides are not used in agriculture, however, some of them are continuously used in some developing countries. Moreover, some additional compounds like certain brominated flame-retardants, carcinogenic polycyclic aromatic hydrocarbons (PAHs) and organometallics like tributyltin (TBT) have been included in the POP list. According to the UNEP global report, levels of numerous persistent pesticides especially chlordane, heptachlor and DDT, in the industrial country’s environment are decreasing in comparison with the levels in the 1980 s or 1990 s

Stockholm Convention on POPs, aimed to decrease these chemicals released a global Stockholm Convention by the UNEP (United Nations Environment Programme) in 2001 in Sweden. The main purpose of that convention was to create a pollutants list including these persistent pollutants through participating countries. The primary list included the first 12 pollutants. Nevertheless, this list had been increased over time to include other pollutants of concern. The convention became effective on May 17th, 2004. POPs namely aldrin, alpha hexachlorocyclohexane, beta hexachlorocyclohexane, chlordane, chlordecone, dieldrin, endrin, heptachlor, hexabromobiphenyl, hexabromodiphenyl ether and heptabromodiphenyl ether, hexachlorobenzene, lindane, mirex, pentachlorobenzene, polychlorinated biphenyls, tetrabromodiphenyl ether and pentabromodiphenyl ether, toxaphene or camphechlor were described in the Stockholm Convention’s Annexes. Some pesticides have been restricted for use such as DDT, and perfluorooctane sulphonic acid (PFOS). Some pesticides are formed unintentionally during the manufacturing of other chemicals and pesticides like dioxins, furan, hexachlorobenzene (hcb), polychlorinated biphenyls (PCBs) and pentachlorobenzene.

### 4. Human exposure and health hazards

Organochlorine pesticides (OCPs) are man-made chemicals that draw huge global issues because of their bioaccumulation and adverse effects along with their persistent and toxic nature [21,22]. Organochlorines are chemicals that can endure for long periods of time and accumulate in fatty tissues over time. [23–26]. OCPs are typically persistent, hydrophobic, degradation-resistant and are present everywhere [27,28]. Meanwhile, [27] has opined that the field half-life time of a few organochlorines like DDT, DDE and DDD is 15 years. However, the field half-life time for toxaphene and aldrin is 9 and 365 days, respectively. Furthermore, it has been found that only 0.1% of pesticides applied actually reach their intended target, with 99.9% instead being released into the environment via channels such as runoff, infiltration, and crop residue retention [28–30]. These chemicals can then travel a great distance throughout the biosphere [31]. After entering the biological system, these compounds get accumulated and biomagnified in the food chain owing to their lipophilic nature, thus resulting in a high degree of contamination observed at higher trophic levels [32]. Pesticide exposure results into several neurological ailments like coordination and memory loss decreased visual ability with motor signaling. Meanwhile, ingestion of OCPs leads to light, sound and touch hypersensitivity as well as dizziness, tremors, seizures, nausea, vomiting, confusion and nervousness [33]. The presence of endocrine disruptors shows adverse effects due to mimicking or provoking natural body hormones. Moreover, chronic exposure to pesticides has been associated with lasting health effects in people, including decreased cognitive function, developmental abnormalities, certain cancers, and

**Table 1**

Levels of chlorinated pesticides in both serum and adipose samples, reporting the results in parts per billion [41].

S. No	Compound	Serum	Adipose
1.	HCB	< 0.3	135
2.	Endrin	< 0.3	168
3.	Beta-BHC	< 0.3	1657
4.	Gamma-BHC	< 0.3	121
5.	Heptachlor	< 0.3	63
6.	Hep-epoxide	< 0.3	33
7.	Oxychlordane	0.4	72
8.	Trans-Nonachlor	0.3	123
9.	Dieldrin	< 0.3	36
10.	DDE	14.2	284
11.	DDT	< 0.3	222

damage to the endocrine system [34–36] even when low doses are involved.

In addition, Venkataraman et al. have noted that pesticides can have lethal effects on biological processes, especially the activity of cholinesterase [37]. They reported the inhibition of AChE activity owing to the relationship between RBC cholinesterase and methyl parathion. The presence of OCPs was reported in blood samples.  $\alpha$ -endosulfan and  $\beta$ -endosulfan were found in higher quantities, 1.565 mg/kg and 1.233 mg/kg, respectively. Bioconcentration and biomagnification of these chemicals and various health issues have been reported in Karachi city [38].

Residues of numerous chlorinated hydrocarbons - specifically DDT, DDE, DDD, aldrin, dieldrin, heptachlor, heptachlor epoxide, and PCBs - have been detected in the adipose tissue of individuals from general populations in Denmark and Greenland [39]. Similarly, the adipose samples obtained from women in several European countries illustrated the regular presence of DDE [40]. Another adipose study in Israel showed the presence OCPs in human bodies [41]. The presence of chlorinated pesticides in blood serum and adipose samples (ppb) has been illustrated in Table 1.

According to Table 1, there are disparities in the levels of chlorinated pesticides detected in serum versus adipose samples taken from a single person. While collecting adipose samples, it should be kept in mind that the sample must be taken from three different sites in order to ensure uniform toxin distribution. Laboratories specializing in the test of these compounds provide results in ng/ml of blood instead of toxin per gram of lipid along with a reference range of their specific laboratory averages which may not be the “normal ranges” preferred in the USA.

In this context, Bayoumi et al. [41] have studied the effect of endosulfan, aldrin and dieldrin on CHO-K1 cultures. Aldrin resulted in an increase in membrane leakage as well as peroxide production at very low concentrations. However, dieldrin and endosulfan resulted in an increase in membrane fragility at higher concentrations. Marcela et al. have also reported the detection of heptachlor, 4,4- DDE, aldrin, gamma-chlordane, dieldrin, chlordane,  $\alpha$ -endosulfan, endosulfan,  $\beta$ -endosulfan, oxychlordane, 4,4-DDT, and 2,4-DDT in serum samples obtained from 99 individuals by using chromatography. OCs have been found in human fluids like serum, urine and breast milk [42–45].

Endosulfan may amplify the abnormal sperm number in the epididymis along with necrosis of Leydig cells and seminiferous tubules [46–48]. It can also affect hormonal synthesis in male kids along with a delay in sexual maturity [49]. It may increase irregular spermatozoa and reduce sperm count as well as motility [50]. Dioxins are polychlorinated aromatic hydrocarbons that lead to developmental, reproductive as well as immunologic toxicities in addition to carcinogenicity. Oxidative stress in is produced in the epididymis and epididymal sperm due to reduction of antioxidant enzymes, reduction in fertility rate and delayed puberty has been noticed due to exposure to Tetrachlorodibenzo-p-dioxin (TCDD) [51].

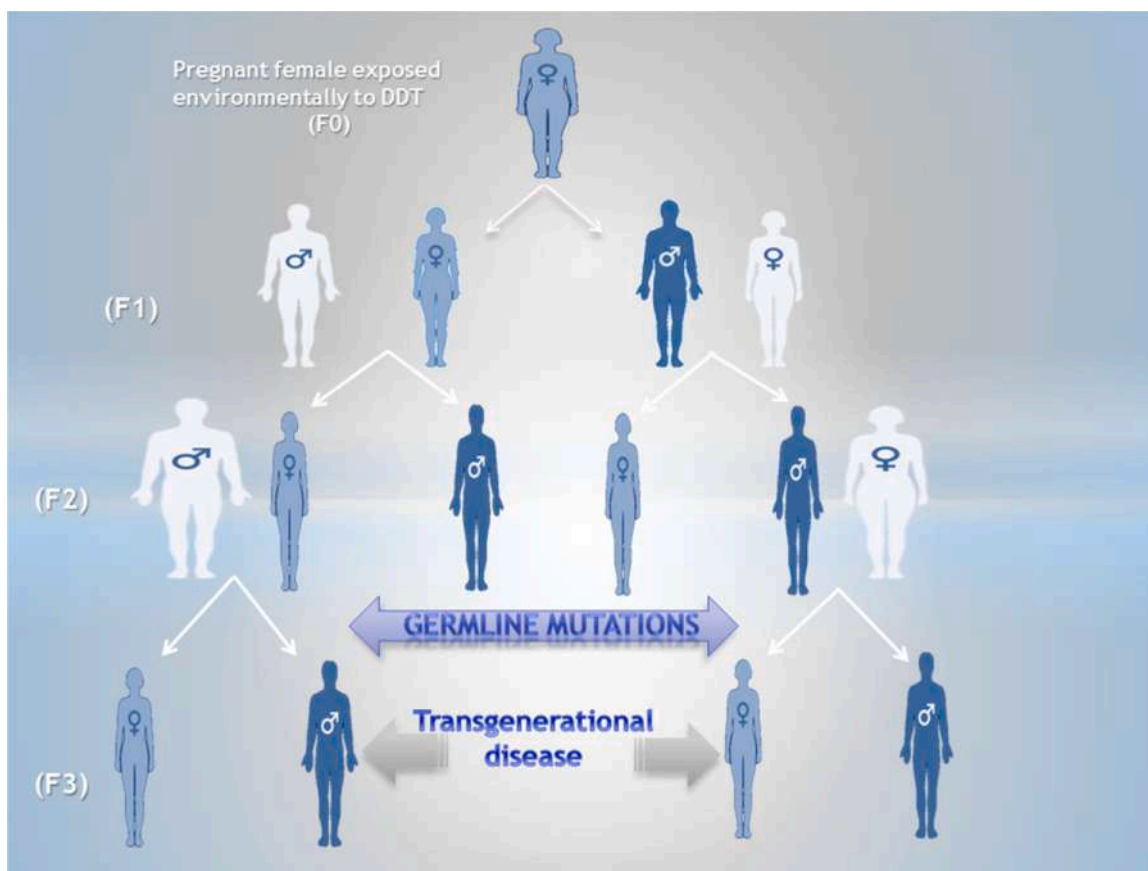


Fig. 1. Epigenetic transgenerational inheritance of disease induced by DDT (adapted and modified from [52]).

Kabasenche & Michael [52] have studied the impacts of DDT transgenerational effects in non-DDT exposed progeny and generations (Fig. 1). The use of DDT has been banned for the last thirty years; however, DDT has been utilized in Africa in recent years for malaria prevention.

DDT (dichlorodiphenyltrichloroethane) application has been prohibited in the United States and most of the developed countries. However, in some nations, it has been widely employed as an insecticide for killing malaria larvae. The Stockholm Convention of UNEP anticipated the removal of 12 chemical substances that induced DDT in 2001 [53]. The risk of human exposure increases by indoor spraying of DDT [54]. Some toxic effects in humans like neurological disease, reproductive disease [55] developmental abnormalities [56] and cancer [57] have been observed via direct DDT exposure. Skinner et al. have studied the epigenetic transgenerational actions of DDT which include obesity and diseases related to the kidney, testis and ovary [58].

#### 4.1. Fate in aquatic ecosystem

Organochlorine pesticides (OCPs) are pollutants present in aquatic environments worldwide [59]. Run-off discharge from agricultural fields and sewage systems are their major sources in the environment. OCPs are highly attracted to the fatty tissues present in humans, plants and animals leading to their considerable accumulation [60,61].

Olga et al. studied contamination of organic pollutants during 1997–1998 [62]. The presence of OCPs and PCBs has been detected by GC-MS. Their results showed that bioaccumulation of persistent OCPs was found in the trophic chain. Fig. 2 shows by the process of biomagnifications how DDT gets transferred from one trophic level to another in the aquatic food chain and gets accumulated in the tissues of organisms.

#### 4.2. Exposure in avian populations

An avian population plays a vital role in proper ecosystem functioning [75]. Organochlorines (OCs) could pollute virtually at the tissue level of almost all life forms [36]. Organochlorine pesticides (OCPs) are lipophilic and are thus get accumulated mainly in the fatty tissues of the body. Their metabolic rate is also slow, in birds, it has half-lives in the order of 1 year. *p, p* 0-DDE exposure reduces reproductive success rates in birds like *osprey Pandion haliaetus* and bald eagle *Haliaeetus leucocephalus* [76,77]. According to the findings of the US National Academy of Sciences, exposure to DDE, a DDT metabolite, in bald eagles has led to a decrease in their numbers in the US, as well as a decline in the strength of their eggshells [78]. Abnormal behaviors in some breeding gulls associated with organochlorine pollutants have been observed in Lake Ontario and southern California, [79,80]. This might be due to estrogenic effects caused by *o,p'*-DDT, mirex as well as some PCBs at environmental concentrations [81,82]. Several experimental approaches have successfully used blood sample investigations of avian species such as migrating raptors, nestling bald eagles, peregrine falcons, gyrfalcons nestlings and Egyptian vultures [83–86]. The presence of OCPs in some species of birds has been also reported in India in several studies [87,88]. Moreover, Venugopal et al. studied the presence of OCPs in the blood plasma of thirteen species of birds in the Ahmedabad city of India [89].

#### 4.3. Treatment process

##### 4.3.1. Bioremediation by microbes

The UNEP Stockholm Convention held in 2011 recognized endosulfan as a persistent organic pollutant. Hence, it was removed from the international market in the year 2012 [89]. At present, degradation of the endosulfan sulfate is the chief concern due to its toxic nature,

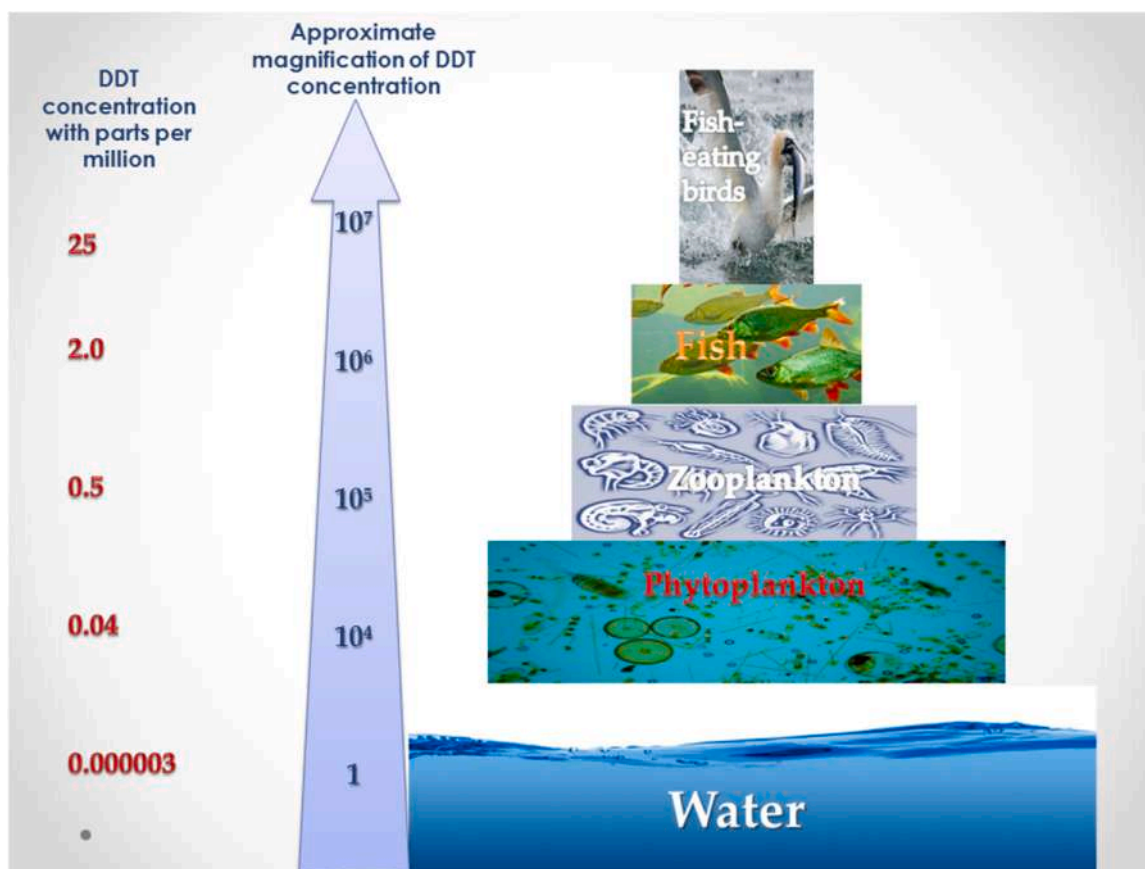


**Fig. 2.** Bioaccumulation of DDT concentrations (ppm) in the aquatic food chain. Contaminants accumulate at the highest level of the food chain, resulting in the topmost trophic level possessing the greatest concentration of harmful substances. Despite its adverse effects, endosulfan, a cyclodiene pesticide, is still prevalent across the globe [63,64]. Endosulfan remains present in water anywhere from a few days to a consecutive month, depending on its physicochemical nature [65]. Compared to other cyclodiene insecticides, endosulfan displays distinctive physical and chemical characteristics that influence its environmental and biological fate [66]. The substance is highly lethal to aquatic organism. In 1984, The United States Fish and Wildlife Service (USFW) categorized endosulfan as the most lethal. In some fish species, the  $LC_{50}$  value ranges between 0.011 to  $3.0 \mu\text{g l}^{-1}$  [67]. Endosulfan leads to gonadal toxicity in mammals, genotoxicity and neurotoxicity [68–70]. The tadpoles of the Australian frog *Limnodynastes peronii* exposed to sublethal concentrations of endosulfan led to a decrease in tadpole length as compared to control tadpoles. Endosulfan exposure also leads to declining growth and feeding behaviour of tadpoles along with decreased predator avoidance [71]. Endosulfan acts on the fish's central nervous system directly, which further leads to hyperactivity, convulsions, and mortality, in severe cases [72]. The toxicity of endosulfan was also studied in juvenile rainbow trout (*Oncorhynchus mykiss*) The Histological results reveal that endosulfan damaged the gills, lamella, epithelia, liver, kidney and spleen of fish [73,74].

higher persistence and bioaccumulation perspective [66]. In India, endosulfan which is a chlorinated pesticide is being broadly used for various agricultural protection activities in cotton, tea, sugarcane and vegetables [90]. Endosulfan and its derivatives naturally get degraded under alkaline conditions and UV light photooxidation in the environment [91]. The biological transformation process helps in the production of endosulfan sulfate, whereas, the diol is produced from endosulfan under alkaline conditions [92]. Microbes have gained popularity in the degradation of contaminants due to their cost-effective and efficient way. Naturally, the presence of these microorganisms reduces the toxicity of endosulfan by its degradation [93–97]. Previous investigations revealed the formation of several intermediates such as the sulfate, diol, ether, lactone, hydroxy ether and dialdehyde derivatives of endosulfan as a result of microbial degradation of endosulfan [91,92].

Endosulfan biodegradation occurs either by oxidation or hydrolysis. A toxic metabolite, endosulfan sulfate is obtained upon oxidation of endosulfan. However, hydrolysis yields lesser toxic metabolite, endosulfan diol [91,93,98,99]. Endosulfan diol can be broken down to endosulfan hydroxyl ether, endosulfan ether, endosulfan lactone and endosulfan dialdehyde which are less toxic. Hence degradation of endosulfan through hydrolysis is a much better detoxification pathway [100].

Several bacterial species like *Klebsiella oxytoca*, *Bacillus sp.* and *Pandoraea sp.* [91,101,102], have been accounted to degrade endosulfan in soils and solutions. Similarly, Gi-Seok et al., 2005 have reported that the bacterium KE-8 species are capable of biodegrading endosulfan and endosulfan sulfate. Further, the degradation constants for  $\alpha$ -endosulfan,  $\beta$ -endosulfan and endosulfan sulfate were found to be 0.3084, 0.2983 and  $0.2465 \text{ day}^{-1}$ , respectively in 4 days of the experiment [91]. The Bacterial strain of *Alcaligenes faecalis* JBW4 degraded  $\alpha$ - and  $\beta$ -endosulfan by 87.5% and 83.9%, respectively within 5 days. Their results suggested endosulfan degradation through a non-oxidative path [103].

Another microbial approach for the biodegradation of endosulfan, involved the application of *Aspergillus niger*, as a fungal soil isolate. The isolated culture of *Aspergillus niger* could tolerate  $400 \text{ mg/ml}^{-1}$  technical-grade endosulfan. After 12 days of incubation, endosulfan was entirely degraded. In addition, the complete mineralization of the substance is indicated by the emission of  $\text{CO}_2$  during its metabolism. The metabolization of endosulfan engenders various intermediates, including endosulfan diol, endosulfan sulfate, as well as an unknown metabolite, as confirmed by Thin Layer Chromatography (TLC) results [90]. Similarly, several fungi species such as *Aspergillus terreus*, *Aspergillus niger*, *Cladosporium oxysporum*, *Mucor thermohyalospora*, *Fusarium ventricosum*, *Scenedesmus sp.*, *Anabaena sp.*, *Chlorococcum sp.*, etc. have been assessed for their ability of degrading endosulfan [102,104–107].

Cyanobacteria are freely existing, photoautotrophic microbes that have the potential to degrade natural as well as synthetic chemicals, particularly pesticides [108–110]. Hence, cyanobacteria can be an effective means to transform and bioremediate highly persistent and toxic materials from the environment. For instance, some species of blue-green algae such as *Synechococcus elongates*, *Phormidium tenue* and *Nostoc linckia* have been effective in degrading monocrotophos and quinalphos present in soil [108]. Sung-Eun et al. have reported the biotransformation of endosulfan into endosulfan diol (endodiol) and small amounts of endosulfan lactone and endosulfan hydroxy ether by *Anabaena flos-aquae* and *Anabaena sp.* PCC 7120, blue-green algal species isolated from the soil environment [111]. During the study, two species of *Anabaena* treated with  $\alpha$ -endosulfan yielded small amounts of  $\beta$ -endosulfan after incubation for one day. This might be possible due to the action of the isomerase enzyme present in the *Anabaena* species.

#### 4.3.2. Challenges and policies of persistent pesticides management

Around the world, the agriculture sector requires the application of pesticides. Pests and diseases damaged 30% of crops worldwide [112,113]. Hence, pest management is mandatory in agriculture for food security [114]. The major issue of pesticide management is that most of them are imported illegally, locally synthesized and uncontrolled. Extensive pesticide usage for agricultural practices leads to the loss of biodiversity and increases [115] pest resistance. For instance, high concentrations of fungicides (i.e. chlorothalonil) were detected in Edward Island, Canada. They affected the potato yield and the increase in the concentration of carbofuran and methamidophos in the air caused serious issues for wildlife. In Nigeria, the farmers suffered from vomiting (58.0%), headache (83.3%), nausea (86.0%) because of the increase in the concentration of insecticides (23.5%), fungicides (28.2%) and herbicides (48.3%) [115]. When we have a look at the Group of Eastern Africa which includes Ethiopia, Kenya, Tanzania and Uganda. It is found that Ethiopia imported large quantities of pesticides in the following order: 72% insecticides, 25% herbicides, 2.6% fungicides and 1.3% rodenticides or disinfectants whereas Uganda imported 47% more pesticides in 2004 than in 1980 [116].

The challenge of persistent pesticides is their storage and disposal because they can accumulate and reach different components of the ecosystem [117]. There is always insufficient information on pesticide management when the farmers use it. Furthermore, the content and concentrations of these pesticides are not clear and accessible to the public [116]. It is logical that farmers should use pesticides following the guidelines on spraying time and pesticide concentration mentioned in the packages. However, most farmers cannot read the labels of the packages, so they do not follow the guidelines and follow their own experience. Machezano et al. carried out face-to-face interviews using a structured questionnaire among farmers in Botswana [118]. Their study indicated that the majority of small-scale farmers, 62.7%, were unaware of Integrated Pest Management strategies, while 93.1% had no prior exposure to such practices, along with 79.4% of respondents being unacquainted with biological control methods. The use of many chemical pesticides such as aldrin, hexachlorobenzene, DDT and toxaphene is prohibited owing to their toxic effects on humans as well as environment. They are known as persistent organic pollutants (POPs) and are regulated by the Stockholm Convention of the United Nations Environment Program [119]. Pesticide management requires comprehensive policies to reach suppliers, farmers and consumers. Europe is the leader in implementing pesticide policies such as the maximum residue limits for pesticides that can be detected in agricultural products and regulatory frameworks [120]. Fig. 3 illustrates a comprehensive approach to pesticide policies.

Assessment of pesticide contamination is required using integrative approaches. Further details can be found in the work of [119] as they highlighted several trials in in-situ techniques such as weight of evidence, effects-directed analysis and toxicity identification evaluation.

Thuy et al. recommend the interplay between legislation, control and education for management improvements [121]. There has been advancement in the detection and determination of pesticide residues through nanotechnology-based colorimetric methods. Such techniques are very promising and can be simple, cheap and allow faster sensing of analytes. The colorimetric technique depends on the color change of colloidal nanoparticles upon interaction with pesticides in a few minutes. Several nanoparticles can be considered [122,123]. For instance, the yellow color of silver nanoparticles (AgNPs) turns to brown-red and becomes agglomerated. Further details about nanosensors for pesticides can be found in the work of [124].

The data presented in the article has been summarized in Table 2.

#### 4.3.3. Integrated pesticide management (IPM)

The World Health Organization's database states that Highly Hazardous Pesticides (HHPs), as defined by the International Code of Conduct on Pesticide Management, pose significant acute or chronic hazards and are capable of causing severe, lasting harm to human health and the environment. The purpose of this international code of conduct is to promote the best practice of producing, transporting, storing and using pesticides [125]. It is documented that around 90% of the used pesticides are lost to affect the ecosystem and farmers due to regular agricultural pest management [126]. It is notable that Goal number 12 of the Sustainable Development: "Responsible Consumption and Production" has a target to achieve sustainable administration of chemicals and wastes all the way through their life cycles. The reduction process of pesticides involves three steps; i) identification (check WHO classification), ii) assessment (actual impacts, survey, exposure monitoring, and models of risk assessment), and iii) mitigation risks (prohibition, restrictions, limited use, application by licensed applicators).

The preventive pesticide measures are the use of protective equipment, crop rotation, integrated pest management and regulation policy in pesticide application [127]. However, the lack of awareness and stringent regulations of using persistent pesticides cause adverse impacts on terrestrial and aquatic ecosystems (pest/disease resistance and high rate of bioaccumulation) and those effects can reach the whole food chain [112]. Van den Berg et al., 2020 concluded that proper pesticide legislation was lacking in several countries, especially low-income countries. Therefore, the current trend of management is applying a controlled release system because it can diminish the adverse impacts of persistent pesticides through single dosages, eliminating multiple dosing, reducing leaching and interacting with the target pests effectively.

Herein, we focus on Integrated Pesticide Management (IPM). Earlier IPM focused only on ecological aspects of pest management [128]. Recently, IPM is an approach to fight against pests, pathogens and weeds using a sustainable strategy. It is the amalgamation of protective and curative actions to become less reliant on synthetic pesticides [129]. Its program also includes monitoring, forecasting, and decision tools to control the needed chemicals. The foundation of an IPM approach is the use of preventive crop measures, which depends on understanding environmental conditions, pests and the use of practical measures to manage pests [130]. The implementation of IPM is a vital step towards sustainable agriculture to assure profitability for the farmers, affordability to consumers and food security [127,128]. The IPM framework is applicable to various crops, different soil types, ecological conditions, pests, pathogens and agricultural practices, etc. This should be considered by all countries because the planting of Pesticide-Treated Seeds is an unsustainable practice that involves treating seeds with synthetic pesticides which needs re-evaluation from environmental, economic and social aspects [131]. In 1888, the introduction of the Vedalia ladybird beetle to manage the cottony-cushion scale in the USA was successful in getting rid of the pest in 2 years and in 1945–1946, the introduction of *Chrysolina hypericin* and *Chrysolina quadrigemina* reduced the invasive



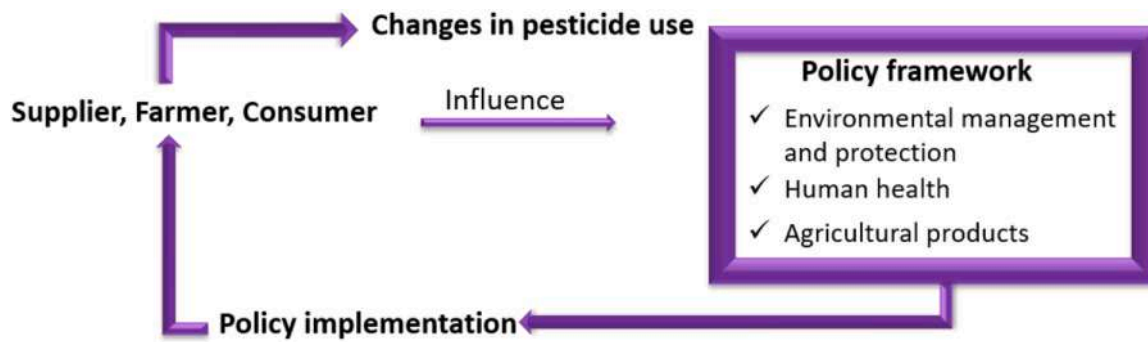


Fig. 3. A comprehensive approach to pesticide policies.

**Table 2**  
Recapitulative table summarizing the data presented in the article.

Pesticide	Adsorbent Type	References
Pentachlorophenol	Mesoporous silica material	[51,97]
DDT	Mesoporous silica material	[98–101]
DDE	Mesoporous silica material	[98,99]
DDD	Mesoporous silica material	[98,99]
Heptachlor	Mesoporous silica material	[98]
Endosulfan	Mesoporous silica material	[98]
Aldrin	Mesoporous silica material	[98]
Dieldrin	Mesoporous silica material	[98]
Methoxychlor	Mesoporous silica material	[98]
Diazinon	Mesoporous silica material	[102,103]
Fenitrothion	Mesoporous silica material	[103]
Acephate	Mesoporous silica material	[104]
Folimat	Zeolite	[104]
Phoxim	Mesoporous silica material	[104]
Chlorpyrifos	Zeolite	[104]
Dipterex	Mesoporous silica material	[104]
2,4-D	Zeolite	[52,105]
Carbendazim	Mesoporous silica material	[104]
Imidacloprid	Zeolite	[104]
Mesosulfuron-methyl	Mesoporous silica material	[107]
Glyphosate	Zeolite	[108]
Avermectin	Mesoporous silica material	[109]
Paraquat	Mesoporous silica material	[110–112]
DEET	Zeolite	[113]
Bentazone	Mesoporous silica material	[114–116]
$\alpha$ -endosulfan	Zeolite	[106,114,115,117]
Fipronil	Zeolite	[118]
Clopyralid	Zeolite	[119]
Imidacloprid	Zeolite	[120]
Metalaxyl-m	Zeolite	[120]
Isoproturon	Zeolite	[120]
Simazine	Zeolite	[120]
Atrazine	Zeolite	[123–125]
Linuron	Zeolite	[126–128]
Nicosulfuron	Zeolite	[127]
		[129–132]

population of *Hypericum perforatum* which is toxic to livestock [132]. Farmers applied molluscicide like metaldehyde to their lands in the autumn and winter season to keep crops from slug damage [133]. It is recommended that its maximum application is 210 g of metaldehyde/ha. Chowdhury et al. applied biopesticide in combination with chemical pesticides for combating pests in *Jatropha curcas* [134]. They

found that the combined pesticide application reduces the cost and use of excessive chemical pesticides which have a detrimental effect on the environment.

Singh et al. [112] highlighted and reviewed the classification of the controlled release system based on the materials used (polymeric, metallic, and clay). Anderson et al. summarized the major challenges and

possible solutions for the successful implementation of the IPM strategy [130]. They concluded that the strategy of IPM is to vary the approaches of pest management, and not rely on one single technique.

We can also think about the integration of nanotechnology in the advanced controlled release system to increase its efficiency. However, there are many factors to consider before real application such as social acceptance, economic aspects and ecological footprint.

## 5. Conclusion

There is an urgent need for innovative approaches that prioritize sustainability and environmental health in agriculture. These include embracing agricultural reforms and transitioning towards food production methods that prioritize sustainability in order to attain food independence. To achieve this, it is important to choose natural pesticides that can serve as a substitute for conventional chemical pesticides. Alternatively, adopting green chemistry-based practices in the agricultural sector can contribute significantly towards sustainable food production and environmental preservation.

## Declaration of Competing Interest

The authors declare that they have no known competing financial interests or personal relationships that could have appeared to influence the work reported in this paper.

## References

- [1] Gupta PK. Pesticide exposure—Indian scene. *Toxicology* 2004;198:83–90. <https://doi.org/10.1016/j.tox.2004.01.021>.
- [2] Aktar W, Sengupta D, Chowdhury A. Impact of pesticides use in agriculture: their benefits and hazards. *Interdiscip Toxicol* 2009;2:1–12. <https://doi.org/10.2478/v10102-009-0001-7>.
- [3] Perera FP, Rauh V, Whyatt RM, Tang D, Tsai WY, Bernert JT, Tu YH, Andrews H, Barr DB, Camann DE, Diaz D, Dietrich J, Reyes A, Kinney PL. A Summary of recent findings on birth outcomes and developmental effects of prenatal ETS, PAH, and pesticide exposures. *NeuroToxicology* 2005;26:573–87. <https://doi.org/10.1016/j.neuro.2004.07.007>.
- [4] Lee D-H, Lee I-K, Song K, Steffes M, Toscano W, Baker BA, Jacobs Jr DR. A strong dose-response relation between serum concentrations of persistent organic pollutants and diabetes: results from the National Health and Examination Survey 1999–2002. *Diabetes Care* 2006;29:1638–44.
- [5] Danopoulos E, Melissinos K, Katsas G. Serious poisoning by hexachlorocyclohexane. Clinical and laboratory observations on five cases. *Arch Indust Hyg Occup Med* 1953;8:582–7.
- [6] Szydio ZA. Michael Faraday the educator - an essay to commemorate the 150<sup>th</sup> anniversary of Faraday's Death. *Chem-Didact-Ecol-Metrol* 2017;22:43–57. <https://doi.org/10.1515/cdem-2017-0002>.
- [7] Hanada M, YUTANI C, MIYAJI T. Induction of hepatoma in mice by benzene hexachloride, GANN. *Jpn J Cancer Res* 1973;64:511–4.
- [8] Ito N, Nagasaki H, Arai M, Sugihara S, Makiura S. Histologic and ultrastructural studies on the hepatocarcinogenicity of benzene hexachloride in mice. *J Natl Cancer Inst* 1973;51:817–26.
- [9] Ito N, Nagasaki H, Arai M, Makiura S, Sugihara S, Hirao K. Histopathologic studies on liver tumorigenesis induced in mice by technical polychlorinated biphenyls and its promoting effect on liver tumors induced by benzene hexachloride. *J Natl Cancer Inst* 1973;51:1637–46.
- [10] Ito N, Nagasaki H, Sugihara S, Miyata Y, Arai M, Shirai T. Brief communication: development of hepatocellular carcinomas in rats treated with benzene hexachloride. *J Natl Cancer Inst* 1975;54:801–5.
- [11] Ito N, Hananouchi M, Sugihara S, Shirai T, Tsuda H, Fukushima S, Nagasaki H. Reversibility and irreversibility of liver tumors in mice induced by the  $\alpha$  isomer of 1, 2, 3, 4, 5, 6-hexachlorocyclohexane. *Cancer Res* 1976;36:2227–34.
- [12] NAGASAKI H, KawABATA H, MIYATA Y, INOUE K, HIRAO K, AOE H, ITO N. Effect of various factors on induction of liver tumors in animals by the  $\alpha$ -isomer of benzene hexachloride, GANN. *Jpn J Cancer Res* 1975;66:185–91.
- [13] Schulte-Hermann R, Parzefall W. Failure to discriminate initiation from promotion of liver tumors in a long-term study with the phenobarbital-type inducer  $\alpha$ -hexachlorocyclohexane and the role of sustained stimulation of hepatic growth and monooxygenases. *Cancer Res* 1981;41:4140–6.
- [14] Tryphonas L, Iverson F. Sequential histopathologic analysis of  $\alpha$ -hexachlorocyclohexane-induced hepatic megalocytosis and adenoma formation in the HPB mouse. *J Natl Cancer Inst* 1983;71:1307–18.
- [15] Bradley AE, Shoenfelt JL, Durda JL. Carcinogenicity and mode of action evaluation for alpha-hexachlorocyclohexane: Implications for human health risk assessment. *Regul Toxicol Pharmacol* 2016;76:152–73.
- [16] Singh N, Chhillar N, Banerjee B, Bala K, Basu M, Mustafa M. Organochlorine pesticide levels and risk of Alzheimer's disease in north Indian population. *Hum Exp Toxicol* 2013;32:24–30. <https://doi.org/10.1177/0960327112456315>.
- [17] Cantillana T. Toxicologically important DDT metabolites: Synthesis, enantioselective analysis and kinetics, PhD Thesis, Department of Environmental Chemistry, Stockholm University, 2009. <https://www.diva-portal.org/smash/record.jsf?pid=diva2:212562> (accessed November 30, 2023).
- [18] Falandysz J, Strandberg B. Persistent Organochlorine Compounds in Sludge and Sediments from the Gdańsk Region, Baltic Sea., *Polish Journal of Environmental Studies*. 13 (2004). <https://citeseerx.ist.psu.edu/document?repid=rep1&type=pdf&doi=02cb3ebf3cfd7f9988fcbcd8dd366ea983601b3> (accessed November 30, 2023).
- [19] Tan L, He M, Men B, Lin C. Distribution and sources of organochlorine pesticides in water and sediments from Daliao River estuary of Liaodong Bay, Bohai Sea (China). *Estuar, Coast Shelf Sci* 2009;84:119–27.
- [20] Kenaga EE. Correlation of bioconcentration factors of chemicals in aquatic and terrestrial organisms with their physical and chemical properties. *Environ Sci Technol* 1980;14:553–6. <https://doi.org/10.1021/es0165a001>.
- [21] Dan Y, Shi-Hua QI, ZHANG J-Q, Ling-Zhi TAN, ZHANG J-P, Zhang Y, Feng XU, Xin-Li X, Ying HU, Wei C. Residues of organochlorine pesticides (OCPs) in agricultural soils of Zhangzhou City, China. *Pedosphere* 2012;22:178–89.
- [22] Parween M, Ramanathan Al, Khillare PS, Raju NJ. Persistence, variance and toxic levels of organochlorine pesticides in fluvial sediments and the role of black carbon in their retention. *Environ Sci Pollut Res* 2014;21:6525–46. <https://doi.org/10.1007/s11356-014-2531-6>.
- [23] Waliszewski SM, Gomez-Arroyo S, Infanzon RM, Villalobos-Pietrini R, Maxwell Hart M. Comparison of organochlorine pesticide levels between abdominal and breast adipose tissue. *Bull Environ Contam Toxicol* 2003;71:156–62. <https://doi.org/10.1007/s00128-003-0143-9>.
- [24] Waliszewski SM, Hernández MVM, Infanzón RM, Trujillo P, Guzmán MIM. Niveles de plaguicidas organoclorados persistentes en mujeres con carcinoma mamario en Veracruz. *Rev Int De Contam Ambient* 2003;19:59–65.
- [25] Waliszewski \* SM, Gomez-Arroyo S, Infanzon RM, Carvajal O, Villalobos-Pietrini R, Trujillo P, Maxwell M. Persistent organochlorine pesticide levels in bovine fat from Mexico. *Food Addit Contam* 2004;21:774–80. <https://doi.org/10.1080/02652030410001712736>.
- [26] Ragab S, El Sikaily A, El Nemr A. Concentrations and sources of pesticides and PCBs in surficial sediments of the Red Sea coast, Egypt. *Egypt J Aquat Res* 2016;42:365–74.
- [27] Sparling DW. Organochlorine pesticides. *Ecotoxicol Essentials*, (2016).
- [28] Pimentel D. Amounts of pesticides reaching target pests: environmental impacts and ethics. *J Agric Environ Ethics* 1995;8:17–29. <https://doi.org/10.1007/BF02286399>.
- [29] Miller GT. *Sustaining the Earth 9*. Pacific Grove, California: Thompson Learning, Inc.; 2004. p. 211–6.
- [30] Zhang W, Jiang F, Ou J. Global pesticide consumption and pollution: with China as a focus. *Proc Int Acad Ecol Environ Sci* 2011;1:125.
- [31] El-Shahawi MS, Hamza A, Bashammakh AS, Al-Saggaf WT. An overview on the accumulation, distribution, transformations, toxicity and analytical methods for the monitoring of persistent organic pollutants. *Talanta* 2010;80:1587–97.
- [32] Poon BHT, Leung CKM, Wong CKC, Wong MH. Polychlorinated biphenyls and organochlorine pesticides in human adipose tissue and breast milk collected in Hong Kong. *Arch Environ Contam Toxicol* 2005;49:274–82.
- [33] I. Mahmood, S.R. Imadi, K. Shazadi, A. Gul, K.R. Hakeem, Effects of pesticides on environment, Plant, Soil and Microbes: Volume 1: Implications in Crop Science. (2016) 253–269.
- [34] Brouwer A, Longnecker MP, Birnbaum LS, Cogliano J, Kostyniak P, Moore J, Schantz S, Winneke G. Characterization of potential endocrine-related health effects at low-dose levels of exposure to PCBs. *Environ Health Perspect* 1999;107:639–49.
- [35] Crisp TM, Clegg ED, Cooper RL, Wood WP, Anderson DG, Baetcke KP, Hoffmann JL, Morrow MS, Rodier DJ, Schaeffer JE. Environmental endocrine disruption: an effects assessment and analysis. *Environ Health Perspect* 1998;106:11–56.
- [36] Hurley PM. Mode of carcinogenic action of pesticides inducing thyroid follicular cell tumors in rodents. *Environ Health Perspect* 1998;106:437–45. <https://doi.org/10.1289/ehp.98106437>.
- [37] Venkataraman BV, Naga Rani MA, Andrade C, Joseph T. Correlation of time course of blood cholinesterases activity and toxic manifestation of acute methylparathion in antidote treated rats. *Indian J Physiol Pharmacol* 1994;38. 214–214.
- [38] Khwaja S, Mushtaq R, Yousuf M, Attaullah M, Tabbassum F, Faiz R. Monitoring of biochemical effects of organochlorine pesticides on human health. *Health* 2013;2013 [https://www.scirp.org/html/21-8202207\\_35567.htm](https://www.scirp.org/html/21-8202207_35567.htm) (accessed December 2, 2023).
- [39] Jensen GE, Clausen J. Organochlorine compounds in adipose tissue of greenlanders and southern danes. *J Toxicol Environ Health* 1979;5:617–29. <https://doi.org/10.1080/15287397909529774>.
- [40] Sanz-gallardo MI, Guallar E, Van P, Veer T, Longnecker MP, Strain JJ, Martin BC, Kardinaal AFM, Fernández-Crehuet J, Thamm M, Kohlmeier L, Kok FJ, Martín-moreno JM. Determinants of p,p'-dichlorodiphenyldichloroethane (DDE) concentration in adipose tissue in women from five European cities. *Arch Environ Health* Int J 1999;54:277–83. <https://doi.org/10.1080/00039899909602486>.
- [41] Bayoumi AE, García-Fernández AJ, Ordóñez C, Pérez-Pertejo Y, Cubría JC, Reguera RM, Balana-Fouce R, Ordóñez D. Cyclo-diene organochlorine insecticide-induced alterations in the sulfur-redox cycle in CHO-K1 cells. *Comp Biochem Physiol Part C: Toxicol Pharmacol* 2001;130:315–23.
- [42] Varona ME, Díaz-Criollo SM, Lancheros-Bernal AR, Murcia-Orjuela AM, Henao-Londoño GL, Idrovo AJ. Organochlorine pesticide exposure among agricultural

- workers in Colombian regions with illegal crops: an exploration in a hidden and dangerous world. *Int J Environ Health Res* 2010;20:407–14. <https://doi.org/10.1080/09603123.2010.491855>.
- [43] Campoy C, Jimenez M, Olea-Serrano MF, Frias MM, Canabate F, Olea N, Bayés R, Molina-Font JA. Analysis of organochlorine pesticides in human milk: preliminary results. *Early Hum Dev* 2001;65:S183–90.
- [44] Burns JS, Williams PL, Sergeev O, Korrirk SA, Lee MM, Revich B, Altschul L, Del Prato JT, Humblet O, Patterson DG, Turner WE, Starovoytov M, Hauser R. Serum concentrations of organochlorine pesticides and growth among Russian boys. *Environ Health Perspect* 2012;120:303–8. <https://doi.org/10.1289/ehp.1103743>.
- [45] Ntow WJ, Tagoe LM, Drechsel P, Kelderman P, Gijzen HJ, Nyarko E. Accumulation of persistent organochlorine contaminants in milk and serum of farmers from Ghana. *Environ Res* 2008;106:17–26.
- [46] Faqi AS, Dalsenter PR, Ligensa A, Merker HJ, Chahoud I. Effect on male fertility and testis concentrations of low dose of 2, 3, 7, 8-tetrachlorodibenzo-p-dioxin (TCDD) in offspring of rats exposed during pregnancy and lactation. *Teratology* 1997;56:403.
- [47] Jaiswal A, Parihar VK, Kumar MS, Manjula SD, Krishnanand BR, Shanbhag R, Unnikrishnan MK. 5-Aminosalicylic acid reverses endosulfan-induced testicular toxicity in male rats. *Mutat Res/Genet Toxicol Environ Mutagen* 2005;585:50–9.
- [48] Saradha B, Vaithinathan S, Mathur PP. Lindane induces testicular apoptosis in adult Wistar rats through the involvement of Fas-FasL and mitochondrial-dependent pathways. *Toxicology* 2009;255:131–9.
- [49] Narayana K, Narayan P, D'Souza UJA. Letter To Editor-Is our drinking water a slow poison?, (2004). <https://tspace.library.utoronto.ca/bitstream/1807/7583/1/ms04087.pdf> (accessed December 2, 2023).
- [50] Rao M, Narayana K, Benjamin S, Baiyya KL. L-ascorbic acid ameliorates postnatal endosulfan induced testicular damage in rats. *Indian J Physiol Pharmacol* 2005;49:331.
- [51] Bell DR, Clode S, Fan MQ, Fernandes A, Foster PM, Jiang T, Loizou G, MacNicol A, Miller BG, Rose M. Toxicity of 2, 3, 7, 8-tetrachlorodibenzo-p-dioxin in the developing male Wistar (Han) rat. I: No decrease in epididymal sperm count after a single acute dose. *Toxicol Sci* 2007;99:214–23.
- [52] Kabasche WP, Skinner MK. DDT, epigenetic harm, and transgenerational environmental justice. *Environ Health* 2014;13:62. <https://doi.org/10.1186/1476-069X-13-62>.
- [53] Davies K. Strategies for eliminating and reducing persistent bioaccumulative toxic substances: common approaches, emerging trends, and level of success. *J Environ Health* 2006;69:9–16.
- [54] Aneck-Hahn NH, Schulerberg GW, Bornman MS, Farias P, De Jager C. Impaired semen quality associated with environmental DDT exposure in young men living in a malaria area in the Limpopo Province, South Africa. *J Androl* 2007;28:423–34. <https://doi.org/10.2164/jandrol.106.001701>.
- [55] Hauser R, Singh NP, Chen Z, Pothier L, Altschul L. Lack of an association between environmental exposure to polychlorinated biphenyls and p, p'-DDE and DNA damage in human sperm measured using the neutral comet assay. *Hum Reprod* 2003;18:2525–33.
- [56] Longnecker MP, Klebanoff MA, Zhou H, Brock JW. Association between maternal serum concentration of the DDT metabolite DDE and preterm and small-for-gestational-age babies at birth. *Lancet* 2001;358:110–4.
- [57] Jaga K, Brosius D. Pesticide exposure: human cancers on the horizon. *Rev Environ Health* 1999;14. <https://doi.org/10.1515/REVEH.1999.14.1.39>.
- [58] Skinner MK, Manikkam M, Tracey R, Guerrero-Bosagna C, Haque M, Nilsson EE. Ancestral dichlorodiphenyltrichloroethane (DDT) exposure promotes epigenetic transgenerational inheritance of obesity. *BMC Med* 2013;11:228. <https://doi.org/10.1186/1741-7015-11-228>.
- [59] Pandit GG, Rao AM, Jha SK, Krishnamoorthy TM, Kale SP, Raghu K, Murthy NBK. Monitoring of organochlorine pesticide residues in the Indian marine environment. *Chemosphere* 2001;44:301–5.
- [60] Bentzen TW, Follmann EH, Amstrup SC, York GS, Wooller MJ, Muir DCG, O'Hara TM. Dietary biomagnification of organochlorine contaminants in Alaskan polar bears. *Can J Zool* 2008;86:177–91. <https://doi.org/10.1139/Z07-124>.
- [61] Swackhamer DL, Hites RA. Occurrence and bioaccumulation of organochlorine compounds in fishes from Siskiwit Lake, Isle Royale, Lake Superior. *Environ Sci Technol* 1988;22:543–8. <https://doi.org/10.1021/es00170a010>.
- [62] Poliakova OV, Lebedev AT, Petrosyan VS, Hanninen O, Renzoni A, Sawa D, Walker C. Accumulation of persistent organic pollutants in the food chain of lake baikal. *Toxicol Environ Chem* 2000;75:235–43. <https://doi.org/10.1080/02772240009358907>.
- [63] Goebel H, Gorbach S, Knauf W, Rimpau RH, Huttenbach H. Properties, effects, residues, and analytics of the insecticide Endosulfan. *Properties, Effects, Residues, and Analytics of the Insecticide Endosulfan* New York, NY: Springer New York; 1982. p. 1–165. [https://doi.org/10.1007/978-1-4612-5712-7\\_1](https://doi.org/10.1007/978-1-4612-5712-7_1).
- [64] Shen L, Wania F, Lei YD, Teixeira C, Muir DCG, Bidleman TF. Atmospheric Distribution and Long-Range Transport Behavior of Organochlorine Pesticides in North America. *Environ Sci Technol* 2005;39:409–20. <https://doi.org/10.1021/es049489c>.
- [65] Naqvi SM, Vaishnavi C. Bioaccumulative potential and toxicity of endosulfan insecticide to non-target animals. *Comp Biochem Physiol Part C: Comp Pharmacol* 1993;105:347–61.
- [66] Sutherland TD, Weir KM, Lacey MJ, Horne I, Russell RJ, Oakeshott JG. Enrichment of a microbial culture capable of degrading endosulphate, the toxic metabolite of endosulfan. *J Appl Microbiol* 2002;92:541–8.
- [67] Verschueren K. Handbook of environmental data on organic chemicals, (1985). [https://journals.lww.com/soilsci/Citation/1985/04000/Handbook\\_of\\_Environmental\\_Data\\_on\\_Organic.14.aspx](https://journals.lww.com/soilsci/Citation/1985/04000/Handbook_of_Environmental_Data_on_Organic.14.aspx) (accessed December 2, 2023).
- [68] Singh SK, Pandey RS. Effect of sub-chronic endosulfan exposures on plasma gonadotrophins, testosterone, testicular testosterone and enzymes of androgen biosynthesis in rat. *Indian J Exp Biol* 1990;28:953–6.
- [69] Chaudhuri K, Selvaraj S, Pal AK. Studies on the genotoxicity of endosulfan in bacterial systems. *Mutat Res/Genet Toxicol Environ Mutagen* 1999;439:63–7.
- [70] Paul V, Balasubramanian E. Effects of single and repeated administration of endosulfan on behaviour and its interaction with centrally acting drugs in experimental animals: a mini review. *Environ Toxicol Pharmacol* 1997;3:151–7.
- [71] Broomhall SD. Egg temperature modifies predator avoidance and the effects of the insecticide endosulfan on tadpoles of an Australian frog. *J Appl Ecol* 2004;41:105–13. <https://doi.org/10.1111/j.1365-2664.2004.00883.x>.
- [72] Harri ML, van den Heuvel MR, Rouse J, Martin PA, Struger J, Bishop CA, Takacs P. Pesticides in Ontario, a critical assessment of potential toxicity of agricultural products to wildlife, with consideration for endocrine disruption, 2004. [https://islandscholar.ca/islandora/object/ir%3Aair-batch6-5317?solr\\_nav%5Bid%5D=8a461a6b5578cca6b00e&solr\\_nav%5Bpage%5D=3&solr\\_nav%5Boffset%5D=4](https://islandscholar.ca/islandora/object/ir%3Aair-batch6-5317?solr_nav%5Bid%5D=8a461a6b5578cca6b00e&solr_nav%5Bpage%5D=3&solr_nav%5Boffset%5D=4) (accessed December 2, 2023).
- [73] Capkin E, Altinok I, Karahan S. Water quality and fish size affect toxicity of endosulfan, an organochlorine pesticide, to rainbow trout. *Chemosphere* 2006;64:1793–800.
- [74] Beyger L, Orrego R, Guchardi J, Holdway D. The acute and chronic effects of endosulfan pulse-exposure on *Jordanella floridae* (Florida flagfish) over one complete life-cycle. *Ecotoxicol Environ Saf* 2012;76:71–8.
- [75] Şekercioğlu ÇH, Daily GC, Ehrlich PR. Ecosystem consequences of bird declines. *Proc Natl Acad Sci* 2004;101:18042–7.
- [76] Anderson DW. Eggshell changes in certain North American birds. *Proc XVth Int Orn Congr* 1972:514–40.
- [77] Wiemeyer SN, Bunck CM, Krynitsky AJ. Organochlorine pesticides, polychlorinated biphenyls, and mercury in osprey eggs—1970–79—and their relationships to shell thinning and productivity. *Arch Environ Contam Toxicol* 1988;17:767–87.
- [78] Liroff RA. Balancing risks of DDT and malaria in the global POPs treaty. *Pest Saf N* 2000;4.
- [79] Fox GA, Gilman AP, Peakall DB, Anderka FW. Behavioral abnormalities of nesting Lake Ontario herring gulls. *J Wildl Manag* 1978:477–83.
- [80] Hunt Jr GL, Hunt MW. Female-female pairing in western gulls (*Larus occidentalis*) in southern California. *Science* 1977;196:1466–7.
- [81] Fry DM, Toone CK. DDT-induced feminization of gull embryos. *Science* 1981;213:922–4. <https://doi.org/10.1126/science.7256288>.
- [82] Fry DM, Toone CK, Speich SM, Peard RJ. Sex ratio skew and breeding patterns of gulls: demographic and toxicological considerations. *Stud Avian Biol* 1987;10:26–43.
- [83] Elliott JE, Norstrom RJ. Chlorinated hydrocarbon contaminants and productivity of bald eagle populations on the Pacific coast of Canada. *Environ Toxicol Chem* 1998;17:1142–53. <https://doi.org/10.1002/etc.5620170622>.
- [84] Elliott JE, Shutt L. Monitoring organochlorines in blood of sharp-shinned hawks (*Accipiter striatus*) migrating through the great lakes. *Environ Toxicol Chem* 1993;12:241–50. <https://doi.org/10.1002/etc.5620120207>.
- [85] Dykstra CR, Meyer MW, Warnke DK, Karasov WH, Andersen DE, Bowerman IV WW, Giesy JP. Low reproductive rates of Lake Superior bald eagles: low food delivery rates or environmental contaminants? *J Gt Lakes Res* 1998;24:32–44.
- [86] Gómara B, Ramos L, Gangoso L, Donázar JA, González MJ. Levels of polychlorinated biphenyls and organochlorine pesticides in serum samples of Egyptian Vulture (*Neophron percnopterus*) from Spain. *Chemosphere* 2004;55:577–83.
- [87] Muralidharan S. Aldrin poisoning of Sarus cranes (*Grus antigone*) and a few granivorous birds in Keoladeo National Park, Bharatpur, India. *Ecotoxicology* 1993;2:196–202. <https://doi.org/10.1007/BF00116424>.
- [88] Muralidharan S, Dhananjayan V, Risebrough R, Prakash V, Jayakumar R, Bloom PH. Persistent organochlorine pesticide residues in tissues and eggs of white-backed vulture, *Gyps bengalensis* from different locations in India. *Bull Environ Contam Toxicol* 2008;81:561–5.
- [89] Chakrabarty S, Rajakumar A, Raghuvver K, Sridevi P, Mohanachary A, Prathibha Y, Bashyam L, Dutta-Gupta A, Senthilkumaran B. Endosulfan and flutamide, alone and in combination, target ovarian growth in juvenile catfish, *Clarias batrachus*. *Comp Biochem Physiol Part C: Toxicol Pharmacol* 2012;155:491–7.
- [90] Bhalerao TS, Puranik PR. Biodegradation of organochlorine pesticide, endosulfan, by a fungal soil isolate, *Aspergillus niger*. *Int Biodeterior Biodegrad* 2007;59:315–21.
- [91] Kwon G-S, Sohn H-Y, Shin K-S, Kim E, Seo B-I. Biodegradation of the organochlorine insecticide, endosulfan, and the toxic metabolite, endosulfan sulfate, by *Klebsiella oxytoca* KE-8. *Appl Microbiol Biotechnol* 2005;67:845–50.
- [92] Martens R. Degradation of [8,9-<sup>14</sup>C]endosulfan by soil microorganisms. *Appl Environ Microbiol* 1976;31:853–8. <https://doi.org/10.1128/aem.31.6.853-858.1976>.
- [93] Hussain S, Arshad M, Saleem M, Khalid A. Biodegradation of  $\alpha$ - and  $\beta$ -endosulfan by soil bacteria. *Biodegradation* 2007;18:731–40.
- [94] Goswami S, Singh DK. Biodegradation of  $\alpha$  and  $\beta$  endosulfan in broth medium and soil microcosm by bacterial strain *Bordetella* sp. B9. *Biodegradation* 2009;20:199–207.
- [95] Li W, Dai Y, Xue B, Li Y, Peng X, Zhang J, Yan Y. Biodegradation and detoxification of endosulfan in aqueous medium and soil by *Achromobacter xylosoxidans* strain CSS. *J Hazard Mater* 2009;167:209–16.
- [96] Elsaid OEG, Abdelbagi AO, Elsheikh EAE. Microbial degradation of endosulfan in carbon free media and selective media. *Res J Agric Biol Sci* 2010;6:257–62.
- [97] Kataoka R, Takagi K, Sakakibara F. A new endosulfan-degrading fungus, *Mortierella* species, isolated from a soil contaminated with organochlorine pesticides. *J Pestic Sci* 2010;35:326–32.

- [98] Horne I, Sutherland TD, Harcourt RL, Russell RJ, Oakeshott JG. Identification of an *opd* (Organophosphate Degradation) Gene in an *Agrobacterium* Isolate. *Appl Environ Microbiol* 2002;68:3371–6. <https://doi.org/10.1128/AEM.68.7.3371-3376.2002>.
- [99] Kwon G-S, Kim J-E, Kim T-K, Sohn H-Y, Koh S-C, Shin K-S, Kim D-G. *Klebsiella pneumoniae* KE-1 degrades endosulfan without formation of the toxic metabolite, endosulfan sulfate. *FEMS Microbiol Lett* 2002;215:255–9.
- [100] Shivaramaiah HM, Sanchez-Bayo F, Al-Rifai J, Kennedy IR. The Fate of Endosulfan in Water. *J Environ Sci Health, Part B* 2005;40:711–20. <https://doi.org/10.1080/03601230500189311>.
- [101] Awasthi N, Singh AK, Jain RK, Khangarot BS, Kumar A. Degradation and detoxification of endosulfan isomers by a defined co-culture of two *Bacillus* strains. *Appl Microbiol Biotechnol* 2003;62:279–83.
- [102] Siddique T, Okeke BC, Arshad M, Frankenberger WT. Biodegradation Kinetics of Endosulfan by *Fusarium ventricosum* and a *Pandoraea* Species. *J Agric Food Chem* 2003;51:8015–9. <https://doi.org/10.1021/jf030503z>.
- [103] Kong L, Zhu S, Zhu L, Xie H, Su K, Yan T, Wang J, Wang J, Wang F, Sun F. Biodegradation of organochlorine pesticide endosulfan by bacterial strain *Alcaligenes faecalis* JBW4. *J Environ Sci* 2013;25:2257–64.
- [104] Mukherjee I, Gopal M. Degradation of beta-endosulfan by *Aspergillus Niger*. *Toxicol Environ Chem* 1994;46:217–21. <https://doi.org/10.1080/02772249409358115>.
- [105] Mukherjee I, Mittal A. Bioremediation of endosulfan using *Aspergillus terreus* and *Cladosporium oxysporum*. *Bull Environ Contam Toxicol* 2005;75.
- [106] Shetty PK, Mitra J, Murthy NBK, Namitha KK, Savitha KN, Raghu K. Biodegradation of cyclodiene insecticide endosulfan by *Mucor thermohyalospora* MTCC 1384. *Curr Sci* 2000;1381–3.
- [107] Sethunathan N, Megharaj M, Chen ZL, Williams BD, Lewis G, Naidu R. Algal Degradation of a Known Endocrine Disrupting Insecticide,  $\alpha$ -Endosulfan, and Its Metabolite, Endosulfan Sulfate, in Liquid Medium and Soil. *J Agric Food Chem* 2004;52:3030–5. <https://doi.org/10.1021/jf035173x>.
- [108] Megharaj M, Venkateswarlu K, Rao AS. Metabolism of monocrotophos and quinalphos by algae isolated from soil. *Bull Environ Contam Toxicol* 1987;39:251–6.
- [109] Megharaj M, Madhavi DR, Sreenivasulu C, Umamaheswari A, Venkateswarlu K. Biodegradation of methyl parathion by soil isolates of microalgae and cyanobacteria. *Bull Environ Contam Toxicol* 1994;53:292–7.
- [110] Yan GA, Jiang JW, Wu G, Yan X. Disappearance of linear alkylbenzene sulfonate from different cultures with *Anabaena* sp. HB 1017. *Bull Environ Contam Toxicol* 1998;60:329–34.
- [111] Lee S-E, Kim J-S, Kennedy IR, Park J-W, Kwon G-S, Koh S-C, Kim J-E. Biotransformation of an Organochlorine Insecticide, Endosulfan, by *Anabaena* Species. *J Agric Food Chem* 2003;51:1336–40. <https://doi.org/10.1021/jf0257289>.
- [112] Singh R, Kumar N, Mehra R, Kumar H, Singh VP. Progress and challenges in the detection of residual pesticides using nanotechnology based colorimetric techniques. *Trends Environ Anal Chem* 2020;26:e00086.
- [113] Dotaniya ML, Meena VD, Saha JK, Dotaniya CK, Mahmoud AED, Meena BL, Meena MD, Sanwal RC, Meena RS, Dautaniya RK, Solanki P, Lata M, Rai PK. Reuse of poor-quality water for sustainable crop production in the changing scenario of climate. *Environ Dev Sustain* 2023;25:7345–76. <https://doi.org/10.1007/s10668-022-02365-9>.
- [114] Savary S, Willocquet L, Pethybridge SJ, Esker P, McRoberts N, Nelson A. The global burden of pathogens and pests on major food crops. *Nat Ecol Evol* 2019;3:430–9.
- [115] Oluwole O, Cheke RA. Health and environmental impacts of pesticide use practices: a case study of farmers in Ekiti State, Nigeria. *Int J Agric Sustain* 2009;7:153–63. <https://doi.org/10.3763/ijas.2009.0431>.
- [116] Loha KM, Lamoree M, Weiss JM, de Boer J. Import, disposal, and health impacts of pesticides in the East Africa Rift (EAR) zone: a review on management and policy analysis. *Crop Prot* 2018;112:322–31.
- [117] Chaukura N, Muzawazi ES, Katengeza G, Mahmoud AED. Remediation technologies for contaminated soil systems. *Emerging Contaminants in the Terrestrial-Aquatic-Atmosphere Continuum*. Elsevier; 2022. p. 353–65 <https://www.sciencedirect.com/science/article/pii/B9780323900515000195> (accessed December 3, 2023).
- [118] Machekano H, Mvumi BM, Nyamukondiwa C. *Plutella xylostella* (L.): pest status, control practices, perceptions and knowledge on existing and alternative management options in arid small-scale farming environments. *Int J Pest Manag* 2020;66:48–64. <https://doi.org/10.1080/09670874.2018.1552380>.
- [119] Cuevas N, Martins M, Costa PM. Risk assessment of pesticides in estuaries: a review addressing the persistence of an old problem in complex environments. *Ecotoxicology* 2018;27:1008–18.
- [120] Möhring N, Ingold K, Kudsk P, Martin-Laurent F, Niggli U, Siegrist M, Studer B, Walter A, Finger R. Pathways for advancing pesticide policies. *Nat Food* 2020;1:535–40.
- [121] Thuy PT, Van Geluwe S, Nguyen V-A, Van B. der Bruggen, Current pesticide practices and environmental issues in Vietnam: management challenges for sustainable use of pesticides for tropical crops in (South-East) Asia to avoid environmental pollution. *J Mater Cycles Waste Manag* 2012;14:379–87.
- [122] Mahmoud AED. Eco-friendly reduction of graphene oxide via agricultural by-products or aquatic macrophytes. *Mater Chem Phys* 2020;253:123336.
- [123] Khan AH, Tirth V, Fawzy M, Mahmoud AED, Khan NA, Ahmed S, Ali SS, Akram M, Hameed L, Islam S, Das G, Roy S, Dehghani MH. COVID-19 transmission, vulnerability, persistence and nanotherapy: a review. *Environ Chem Lett* 2021;19:2773–87. <https://doi.org/10.1007/s10311-021-01229-4>.
- [124] Mahmoud AED, Fawzy M. Nanosensors and Nanobiosensors for Monitoring the Environmental Pollutants. In: Makhlof ASH, Ali GAM, editors. *Waste Recycling Technologies for Nanomaterials Manufacturing* Cham: Springer International Publishing; 2021. p. 229–46. [https://doi.org/10.1007/978-3-030-68031-2\\_9](https://doi.org/10.1007/978-3-030-68031-2_9).
- [125] van den Berg H, Gu B, Grenier B, Kohlschmid E, Al-Eryani S, da Silva Bezerra HS, Nagpal BN, Chanda E, Gasimov E, Velayudhan R. Pesticide lifecycle management in agriculture and public health: Where are the gaps? *Sci Total Environ* 2020;742:140598.
- [126] Ghormade V, Deshpande MV, Paknikar KM. Perspectives for nano-biotechnology enabled protection and nutrition of plants. *Biotechnol Adv* 2011;29:792–803.
- [127] Sharma AK, Sharma D, Chopra AK. An overview of pesticides in the development of agriculture crops. *J Appl Nat Sci* 2020;12:101–9.
- [128] Dara SK. The new integrated pest management paradigm for the modern age. *J Integr Pest Manag* 2019;10:12.
- [129] Karlsson Green K, Stenberg JA, Lankinen Å. Making sense of integrated pest management (IPM) in the light of evolution. *Evolut Appl* 2020;13:1791–805. <https://doi.org/10.1111/eva.13067>.
- [130] Anderson JA, Ellsworth PC, Faria JC, Head GP, Owen MD, Pilcher CD, Shelton AM, Meissle M. Genetically engineered crops: importance of diversified integrated pest management for agricultural sustainability. *Front Bioeng Biotechnol* 2019;7:24.
- [131] Lamichhane JR. Parsimonious use of pesticide-treated seeds: an integrated pest management framework. *Trends Plant Sci* 2020;25:1070–3.
- [132] DeBach P, Rosen D. *Biological control by natural enemies*, CUP Archive, 1991. [https://books.google.com/books?hl=en&lr=&id=K6dOAAAIAAJ&oi=fnd&pg=PR9&dq=+DeBach+P,+Rosen+D.+\(1991\).+Biological+control+by+natural+enemies,+CUP+Archive.&ots=vMYEN5mG2O&sig=KxAxUnRrUIRPxZweMcdmreYlQU](https://books.google.com/books?hl=en&lr=&id=K6dOAAAIAAJ&oi=fnd&pg=PR9&dq=+DeBach+P,+Rosen+D.+(1991).+Biological+control+by+natural+enemies,+CUP+Archive.&ots=vMYEN5mG2O&sig=KxAxUnRrUIRPxZweMcdmreYlQU) (accessed December 3, 2023).
- [133] Castle GD, Mills GA, Gravell A, Jones L, Townsend I, Cameron DG, Fones GR. Review of the molluscicide metaldehyde in the environment. *Environ Sci: Water Res Technol* 2017;3:415–28.
- [134] Chowdhury J, Al Basir F, Takeuchi Y, Ghosh M, Roy PK. A mathematical model for pest management in *Jatropha curcas* with integrated pesticides-An optimal control approach. *Ecol Complex* 2019;37:24–31.



## Research Article

## Exploring ZnO nanoparticles: UV–visible analysis and different size estimation methods

Sanju Singh<sup>a</sup>, Jaya V. Gade<sup>b</sup>, Dakeshwar Kumar Verma<sup>c</sup>, Berdimurodov Elyor<sup>d,e,f</sup>, Bhawana Jain<sup>a,\*</sup><sup>a</sup> Department of Chemical Sciences, Siddhachalam Laboratory, Raipur, Chhattisgarh, 493221, India<sup>b</sup> Department of Analytical Chemistry, SNDT Women's University, Mumbai, 400049, Maharashtra, India<sup>c</sup> Department of Chemistry, Govt. Digvijay Autonomous Postgraduate College, Rajnandgaon, Chhattisgarh, 491441, India<sup>d</sup> Chemical & Materials Engineering, New Uzbekistan University, 54 Mustaqillik Ave., Tashkent, 100007, Uzbekistan<sup>e</sup> Medical School, Central Asian University, Tashkent, 111221, Uzbekistan<sup>f</sup> Faculty of Chemistry, National University of Uzbekistan, Tashkent, 100034, Uzbekistan

## ARTICLE INFO

## Keywords:

UV-Visible analysis

Zinc oxide nanoparticle size methods

ANOVA statistical study

Brus equation

Effective mass approximation

## ABSTRACT

The study investigates several theoretical and empirical methods for determining the size of zinc oxide nanoparticles (ZnO NPs) and studies their characteristics by using solely UV–visible spectroscopy. The investigation begins with the green synthesis of three samples of ZnO NPs using three different reducing agents *Aspergillus Niger* fungal biomass (AN), *Aloe barbadensis* Mille (ABM) and *Ocimum tenuiflorum* (OT) leaves, respectively with Zinc Sulphate as a precursor involving precipitation method. The study analyses the UV–visible data of each sample to obtain optical bandgap, Urbach energy, refractive index, optical conductivity. and apply several methods or Models such as Effective Mass Approximation (EMA) or Brus Equation (BE), Hyperbolic Band Model (HBM), Meulenkamp's Expression (ME), Tight Binding Model (TBM) and a simplified version of EMA (SEMA) to estimate the size of ZnO NPs. The effectiveness of size-determining models was assessed using two sets of one-way analysis of variance (ANOVA) for each ZnO sample and models Followed by Tukey post-hoc analysis to identify the exact sample that is different from other samples.

## 1. Introduction

ZnO is a semiconductor with a high melting point and thermal conductivity, large elastic constants, and a large band gap it also exhibits multifunctional properties, including antibacterial, anti-inflammatory and bio-imaging capabilities [1,2]. These properties of ZnO NPs depend on their physical characteristics such as the bandgap, which are influenced by their size due to the quantum confinement of charge carriers [3]. Therefore, having a reliable method for evaluating this dimension is crucial. Among the available techniques for size assessment, transmission electron microscopy (TEM) offers precise measurements of nanoscale structures' shape and size. Despite its accuracy, TEM is not the most suitable for swiftly measuring multiple sets of samples routinely. Therefore, it is necessary to apply alternative methods based on data derived from optical absorption measurements to estimate nanoparticle size.

UV–visible spectroscopy is a credible technique that plays a crucial

role in the study and primary characterization of synthesized nanoparticles [4]. It has been used extensively for 37 years due to its simplicity, variety, precision, speed, and cost-effectiveness, and has become a crucial analytical instrument in modern laboratories [5]. It provides extensive experimental data into the electronic structure of NPs and can be specifically significant to characterize and determine the size of all kinds of nanoparticles, including semiconductor nanoparticles like ZnO [6]. Other traditional methods like dynamic light scattering (DLS), scanning electron microscopy (SEM) and TEM have limitations like real-time monitoring, aggregation data, and sample prep challenges and can be problematic in complex matrices or reactive environments [7,8]. On the other hand, these instruments may not always be cost-effective or readily available [9] everywhere. Therefore, researchers face difficulties in accurately sizing the nanoparticles due to the limited availability of cost-effective techniques. To address these challenges UV–visible spectrometers can become an alternate option to obtain the accurate size of nanoparticles due to their low cost, easy accessibility and availability in

\* Corresponding author.

E-mail address: [bhawanajain123@gmail.com](mailto:bhawanajain123@gmail.com) (B. Jain).

almost all research laboratories [10].

Several theoretical studies have been attained to understand the fundamental dependency of size on the optical characteristics of NPs [11]. In 2012, Martinez E. et al. introduced a method for accurately determining the diameter of gold NPs using UV–vis spectra. However, their strategy applies only to gold and silver NPs [12]. In 2020, Rodríguez-Mas et al. compared four different methods to estimate the diameter of CdS nanoparticles from optical absorption measurements [13]. In 2020 (Upadhyay et al., 2020), reported the comparison of the synthesis of ZnO NP synthesized by leaves extract of *Ocimum Tenuiflorum* and by chemical route method using an organic capping agent (Upadhyay et al., 2020), but they use advanced techniques for characterization. Similarly, numerous kinds of literature are available that explore UV–visible characterization and their use in size determination with the help of different theoretical and practical models [14]. Despite this, there is hardly any literature available that compares the size obtained by using UV–visible data for different samples of ZnO NPs which are synthesized by using different green reducing agents.

In this context, we aim to explore the significance of UV–visible spectroscopy in the characterization and measurement of the size of different samples of ZnO NP that are specifically synthesized by the green synthesis approach, which is more economical and environment-friendly than the high-cost, laborious and toxic compounds involved chemical approaches [15,16]. We have compared various approaches, incorporating both theoretical and empirical methods, for determining the dimensions of ZnO nanoparticles by using UV–visible spectroscopy to overcome the challenges associated with traditionally used methods like DLS, TEM and SEM and offer a practical alternative for researchers seeking precise size estimation. The study focuses on ZnO nanocrystals synthesized through the precipitation method using three different reducing agents, optical absorption spectra were recorded, and the absorption edge was determined using the Tauc relation. Additionally, four established methods (Brus equation, Hyperbolic Band Model, Meulenkamp expression, Tight Binding Model, and simplified form of Effective mass approximation) were employed to estimate the size calculation. Subsequently, we have employed one-way ANOVA in all the methods to assess their effectiveness and identify the most reliable method for each ZnO sample.

## 2. Materials and method

### 2.1. Materials

Zinc sulphate heptahydrate ( $\text{ZnSO}_4 \cdot 7\text{H}_2\text{O}$ ) 99 % pure form and sodium hydroxide (NaOH), biomass of *Aspergillus Niger*, plant extract of *Aloe barbadensis miller* and *Ocimum tenuiflorum* and Potato Dextrose Agar (PDA) Media for growth of *Aspergillus Niger* were used in the experiments. All the chemicals used were of analytical reagent grade obtained from E. Merck Mumbai, India and PDA media was purchased from Hi-Media laboratories, Maharashtra, India. The deionized water was used to prepare all the solutions.

### 2.2. Procedure

#### 2.2.1. Preparation of fungal biomass

The fungus cells of *Aspergillus Niger* were cultivated in PDA media, at 32 °C for 72 h [17] to obtain a significant growth of mycelium. After a sufficient growth of fungal, the mycelium was detached from the media and dried under sunlight for 24 h (Fig. 1). Then fungus biomass is harvested from the culture and centrifuged to make a suspension with water (Mekky et al., 2021).

#### 2.2.2. Preparation of *Aloe barbadensis miller* leaf extract

Fresh *Aloe barbadensis miller* leaves were properly cleaned in distilled water to remove external impurities and soil. Then it was cut into medium-sized parts to facilitate the extraction process. 20 g of finely chopped skin of leaves were mixed with 100 ml of distilled water in a 250 ml glass conical flask to prepare the extract. The combined mixture was heated to 60 °C in a water bath for 10 min (Fig. 1). The aqueous solution's colour transitioned from watery to pale green. The extract was filtered through Whatman filter paper No. 1 and stored in a refrigerator for later use [18].

#### 2.2.3. Preparation of *Ocimum tenuiflorum* leaf extracts

Fresh leaves of *Ocimum tenuiflorum* were properly cleaned in distilled water and dried in sunlight for 5–6 days. The extract was made by combining 10 g of each dry leaf with 100 ml of distilled water in a

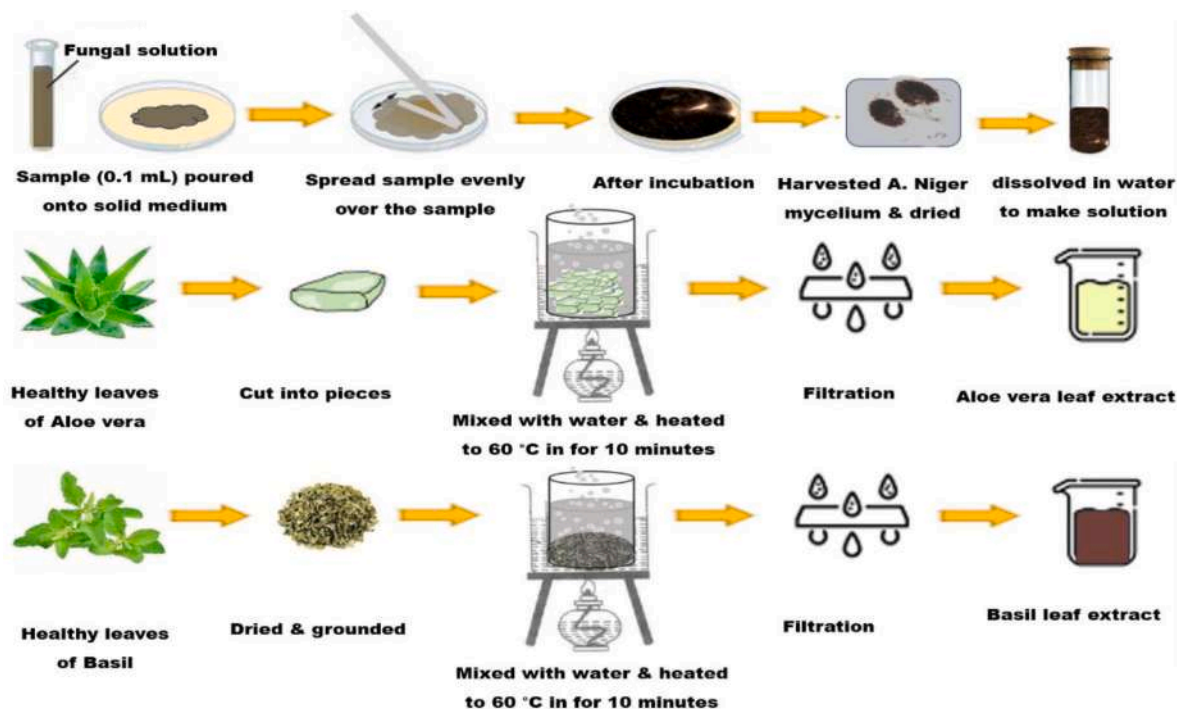


Fig. 1. Preparation of fungus biomass, *Aloe barbadensis miller* Leaf Extract and *Ocimum tenuiflorum* leaf extracts.

250 ml conical flask. The mixture was heated for 10 min to 90 °C in a water bath. The colour of the aqueous solution changed from watery to filtered to reddish brown (Fig. 1). The extract was centrifuged for 5 min at 5000 rpm, and filtered through Whatman filter paper No. 1. The prepared solution is stored in a refrigerator for further use [19,20].

### 2.3. Synthesis of ZnO nanoparticles

Fig. 2 represents the step-by-step process of synthesis of ZnO samples. To prepare three samples of ZnO NP's, ZnSO<sub>4</sub>·7H<sub>2</sub>O was dissolved in distilled water in three different beakers (labelled ZnO-AN, ZnO-ABM, ZnO-OT) to create 1 M solution of each sample. Zinc oxide nanoparticles were created using a previously published procedure with a few minor adjustments. In summary, 100 mL of extract (AN/ABM/OT) was mixed with 1 M of zinc sulphate heptahydrate (ZnSO<sub>4</sub>•7H<sub>2</sub>O) and allowed to sit at 70 °C for 2 h on a magnetic stirrer. After the reaction was finished, the mixture was centrifuged for 10 min at 10,000 rpm while being allowed to cool at 25 °C. The supernatant was discarded, and the remaining pellet was then placed separately within a hot air oven set at 70 °C for an overnight period to enable the evaporation of any remaining alcohol. This process gave the dry powder which was finally calcined in the air in a muffle furnace at 800 °C for 1 h [21,22].

### 2.4. Characterization of ZnO nanoparticles

To validate the formation of ZnO the synthesized nanoparticle samples were characterized by using a UV–visible spectrophotometer (Shimadzu UV–visible Spectrometer, Japan) at the wavelength range of 200–800 nm, and distilled water was used as the blank reference. The absorbance spectrum was analyzed to ascertain optical properties, and their band gap energy was determined using Tauc's equation [23]. Other key parameters were also calculated using the obtained value of the optical band gap and absorption peak.

### 2.5. Determination methods/models of size of zinc oxide NPS by UV–Visible spectroscopy data

The size of the nanoparticles has a significant impact on how the material's properties are altered. To investigate the properties of the materials, the size evolution of semiconducting nanoparticles becomes extremely important. It is suggested that the absorption onset from UV–vis absorption spectra can also be utilized to determine the average particle size of a Nano colloid [24]. After thoroughly reviewing the literature, this article obtained the following approaches to determine a relationship between the bandgap energy/absorption edge and nanoparticle size.

#### 2.5.1. Brus Equation (BE)/Effective Mass Approximation (EMA)

One of the first theoretical methods to calculate the size of nanoparticles using absorption spectra was proposed by L. E. Brus. He used an effective mass approximation for the kinetic energy and a higher frequency dielectric solution technique for the potential energy to solve the Schrödinger equation for the first excited state [25]. Brus investigated the relationship between the cluster's size and electronic structure and connected the effects of quantum confinement to the nanoparticle's radius [26]. Brush theoretically explained the quantum confinement effect as the variation in absorbance wavelength with particle size, considering the exciton being contained inside the physical dimensions of the nanocrystal core and proposed a theoretical model based on effective masses of electrons and holes in bulk. He proposed the following expression state (sometimes also referred to as Brus equation) to yield the energy of the lowest 1s-excited which can be used to obtain the radius of the nanoparticles:

$$E^* = E_g^{bulk} + \frac{\hbar^2 \pi^2}{2eR^2} \left( \frac{1}{m_e^* m_0} + \frac{1}{m_h^* m_0} \right) - \frac{1.8 e}{4\pi\epsilon\epsilon_0 R} - \frac{0.124e^3}{\hbar^2 (4\pi\epsilon\epsilon_0)^2} \left( \frac{1}{m_e^* m_0} + \frac{1}{m_h^* m_0} \right)^{-1} \quad (1)$$

Here  $E_g$  is the bulk semiconductor band gap, which is a size-induced shift in the energy of the lowest excited state (the traditional conduc-

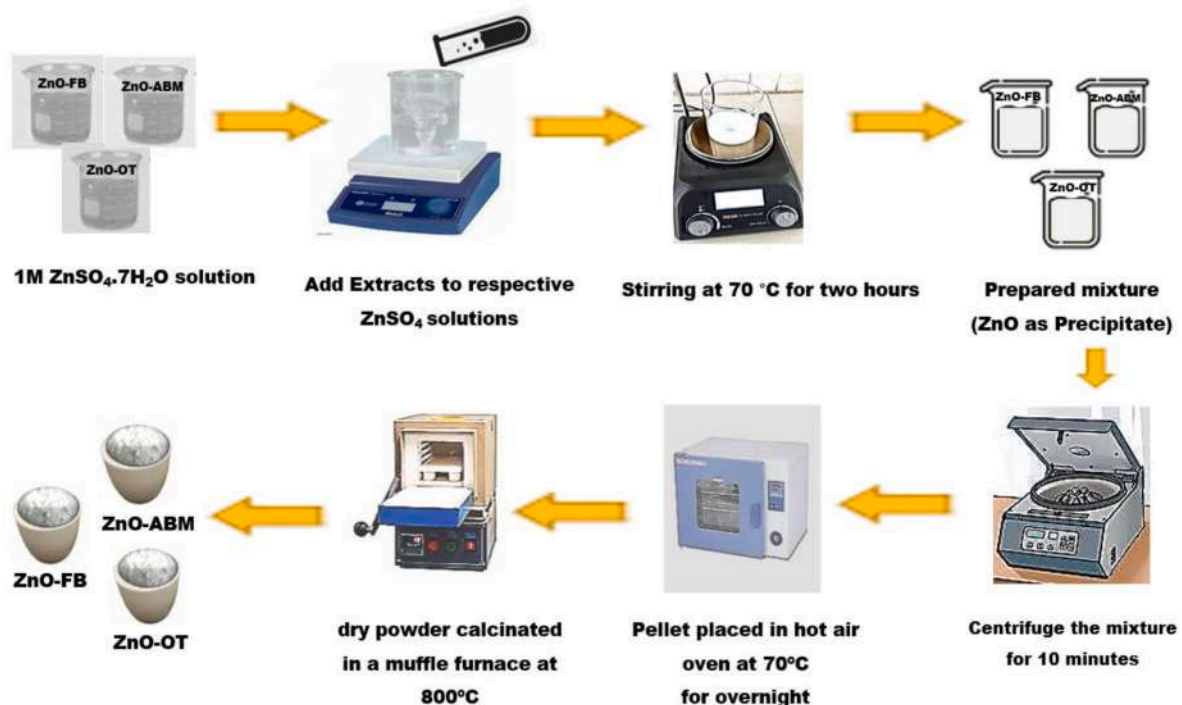


Fig. 2. Synthesis of different samples of ZnO NPs.

tion band),  $R$  is the particle radius,  $e$  is the electron charge,  $\epsilon_1$  is the dielectric constant of the material,  $\epsilon_0$  is the relative dielectric constant. In this equation  $\frac{1}{m_e^* m_0} + \frac{1}{m_h^* m_0}$  is the sands for the effective mass of the exciton which can be also replaced by  $m_1$ :

$$\Delta E = \frac{\hbar^2 \pi^2}{2m_1 R^2} - \frac{1.8e^2}{\epsilon_1 R} - \frac{0.248m_1 e^4}{2\epsilon_1^2 \hbar^2} \quad (2)$$

The first term in Equation (2) represents the particle-in-box localization energy, specifically the kinetic energy term and the second part of the equation accounts for the screened coulomb interaction energy ( $E_C$ ) between the electron and hole. The third term is polarization term represented by Rydberg energy ( $E_R$ ) which is a size-independent component related to the electron-hole correlation and denoting the loss of solvation energy [27,28]. This term is very small does not affect the equation and can be omitted [29]. This method has been proved to be reliable for sizes larger than 4 nm and the model essentially assumes that electrons and holes are contained within an infinite square well and links the characteristics of the absorbed light to the size of the nanoparticles [25,30]. The numerical values for Brus equation are given in equation (3) [31]:

$$E_g = 3.37 - \frac{1.35}{d} + \frac{8.47}{d^2} \quad (3)$$

### 2.5.2. Expression suggested by Meulenkamp (ME)

Another convenient and practical approach to calculating the particle size is described by Meulenkamp [32]. This method relates the bandgap energy calculated from the wavelength ( $\lambda$ ) at which the absorption is 50 % of that at the excitonic peak, with the cluster diameter. The expression for this method can be written as:

$$\frac{1240}{\lambda^{1/2}} = A + \frac{B}{D^2} - \frac{C}{D} \quad (4)$$

It involves equating diameter ( $D$ ) in Å, with the wavelength ( $\lambda$ ) which is half from the shoulder denoted as  $\lambda_{1/2}$  (nm). Where  $A$ ,  $B$  and  $C$  are constants whose values are  $A = 3.301$ ,  $B = 294.0$  and  $C = 1.09$  for ZnO nanoparticles. He used XRD data to estimate the particle size and connected that size to the wavelength at which the first absorption maximum occurred while moving from longer wavelengths. Another form of his equation  $n$  which is utilized to calculate the size of nanoparticles in nanometers is provided in equation (5) and has the same functional structure as Brus relation [33].

$$E_g = 3.301 + \frac{0.109}{d} + \frac{2.94}{d^2} \quad (5)$$

### 2.5.3. Hyperbolic Band Model (HBM)

The Hyperbolic band model (HBM) is another approach for connecting UV-VIS data (bandgap) and radius. According to Wang et al., small nanoparticles do not considerably benefit from the size-dependent Coulomb interaction of the Schrödinger equation for the excited crystallite state [13]. Therefore, they offer a straightforward effective approximation that accurately describes the band gap of nanoparticles without the need for large Coulomb corrections. This approximation is based on the assumptions that only two bands are significant for calculating the band gap, namely those that at the L point constitute the highest occupied valence band and the lowest unoccupied conduction band, and that the lowest excitation of the particle lattice involves a straightforward electron transfer from one constituting ion to another at a cost in energy equal to the bulk band gap  $E_g$  Ref. [34]. Thus, the HBM was developed which is given in equation (6):

$$R = \sqrt{\frac{2\pi^2 \hbar^2 E_g^{bulk}}{m^* (E_{g,nano}^2 - E_{g,bulk}^2)}} \quad (6)$$

The radius of NPs,  $m^*$  is an effective mass of the specimen,  $E_{g,bulk}$  is

the bandgap of a particle in bulk form,  $\hbar$  is Planck's constant and  $E_{g,nano}$  is the bandgap of a particle at the nanoscale. In this equation, the effective mass ( $m^*$ ) is determined by the mass of the electrons inside the semiconductor and the free mass ( $m_0$ ) outside the semiconductor. On the other hand, the value of  $E_{g,nano}$  can be calculated by the formula [35]:

$$E_g^{nano} = \frac{\hbar c}{\lambda_p} \quad (7)$$

Where  $C$  denotes the velocity of light ( $3 \times 10^8$  m/s),  $\hbar$  is the Planck constant ( $6.6 \times 10^{-34}$  Js) and  $\lambda_{peak}$  is the absorption peak obtained from UV-visible spectra (Fig. 1). In the BE investigation, we found that potential changes in  $m_e^*$  and  $m_h^*$  could affect the outcomes of calculating NP sizes. However, the HBM model simplifies the electron and hole effective masses into a single mass, using the following equation:

$$\frac{1}{m^*} = \frac{1}{m_e^*} + \frac{1}{m_h^*} \quad (8)$$

Where,  $m^*$  is the effective mass and  $m_e^*$  and  $m_h^*$  are the effective masses of electrons and holes, respectively. The dependence of  $m^*$  on  $m_e^*$  and  $m_h^*$  (Equation (8)) makes the study of both variables necessary. Then, for a proper application of theoretical models to determine the size of the nanoparticles, both the calculation of the absorption edge and an exact value of the effective mass became essential. It's noteworthy that when the energy levels are close to the bulk bandgap, the HBM tends to predict larger nanoparticle diameters compared to the BE. This outcome is because the BE lies on the principle of infinite square well-type of quantum confinement, which means the model assumes that nanoparticles behave as if their electrons and holes are confined within an infinite square well due to their small size [36].

### 2.5.4. Tight Binding Model (TBM)

The more common approach used by several researchers is the empirical expression of Viswanatha et al. [37], which is based on the cluster equation given in equation (9) and is referred to as R. Viswanatha 1 or Tight Binding Model (TBM) or TB strategy.

$$E_g = 3.35 + \frac{1.67}{d^{1.4}} \quad (9)$$

The method has several advantages over the other approaches mentioned above. This method significantly increases the result's accuracy as compared to EMA [38]. The best-fit expression of this method is given in equation (10) and is referred to as R. Viswanatha 2.

$$E_g = 3.35 + \frac{100}{18.1 d^2 + 14.4 d - 0.8} \quad (10)$$

$d$  is the mean diameter for the nanoparticle,  $E_g$  is the bandgap in the nanocrystal of diameter  $d$ . Viswanatha et al. demonstrated that the Brus model did not produce findings that were satisfactory for ZnO particles smaller than 5–6 nm and instead tended to overestimate the size. They tried a different theoretical approach and performed a real space calculation to provide the variation of the bandgap as a function of the nanocrystal size. They calculated the shift in the band gap with particle size using a tight binding model and related their results to experimental data where the particle size was assessed using XRD data and imitated Brus' functional dependence to adjust the exponents in equation (8) which provided the greatest fit but somewhere it is not satisfactory, especially for large nanocrystal sizes. To obtain a better description of the entire range of sizes, they provide another expression which is given in equation (9), in which the coefficients are determined from a least-squared-error procedure. They claim that the theoretically estimated bandgap shifts obtained from their model are in agreement with the entire range of sizes. Therefore, incorporating TBM for calculating the band gap shift with particle size provides a more accurate and reliable prediction of band gap variations compared to other empirical models as it offers a comprehensive description of the entire range of nanocrystal



sizes, addressing the limitations of other models that may not provide satisfactory results for very small or very large nanocrystals. By relating theoretical calculations to experimental data obtained from techniques like X-ray diffraction (XRD), it allows researchers to validate and refine their models, ensuring consistency between theoretical predictions and experimental observations. Overall, TBM contributes to a deeper understanding of nanocrystal behaviour by providing accurate and comprehensive insights into their optical and electronic properties as a function of size [39].

### 2.5.5. Simplified version of EMA/particle radius as a function of peak absorbance wavelength (SEMA)

Some researchers including Talam et al., Samuel et al., and Pesika et al. also utilized the more simplified equation (4) of Brus equation, which describes the particle size (radius) as a function of peak absorbance wavelength for monodispersed ZnO nanoparticles. The equation is derived from an effective mass model given in equation (1) with small mathematical simplification and is used to find the size of the particle from the absorbance spectra [23]. The following equation can denote the simplified equation:

$$r(\text{nm}) = \frac{-0.3049 + \sqrt{-26.23012 + \frac{10240.72}{\lambda_p(\text{nm})}}}{-6.3829 + \frac{2483.2}{\lambda_p(\text{nm})}} \quad (11)$$

Where  $r$  is the radius of NP and  $\lambda_p$  is the absorbance peak obtained through UV-visible data.

## 2.6. Statistical study

The calculated sizes were subjected to two sets of one-way ANOVA from Origin Pro 2023b to determine statistically significant differences among models between the sample of ZnO synthesized. Post-hoc tests (Tukey test) were employed for further pairwise comparisons of models.

## 3. Result and discussion

### 3.1. X-Ray Diffraction (XRD)

Fig. 3 displays the X-ray diffraction analysis of all samples of ZnO NPs. The XRD was conducted to characterize the crystalline structure and particle size of three samples of ZnO NPs synthesized via a green

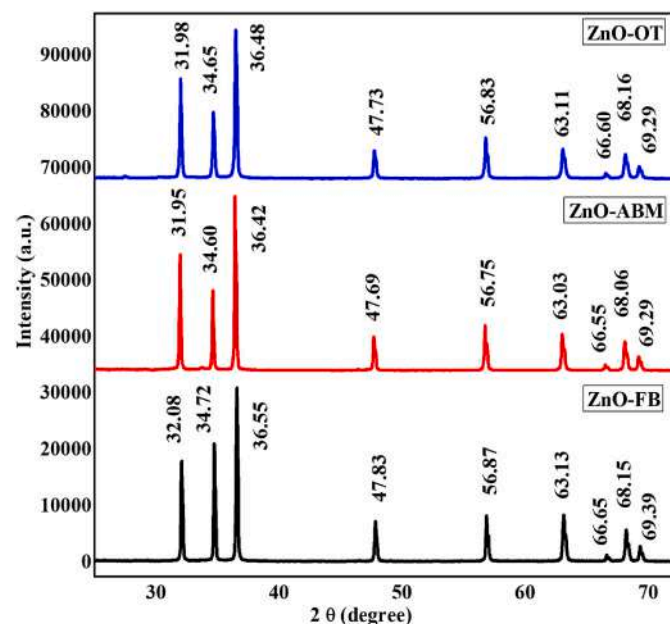


Fig. 3. X-ray diffraction analysis of all samples of ZnO NPs.

synthesis approach. From this XRD patterns analysis, we determined peak intensity, position and width, and full-width at half-maximum (FWHM) data as mentioned in Table 1. The XRD patterns of all three samples exhibited distinct peaks, which corresponds to various crystallographic planes (hkl values) of ZnO NPs samples (Table: 1) with lattice constants  $a = b = 0.324$  nm and  $c = 0.521$  nm (JPCDS card number: 36–1451) [24].

The observed peaks and plans were consistent with the hexagonal wurtzite crystal structure of ZnO, confirming the crystalline nature of our nanoparticles synthesized via the green approach further, it also confirms the synthesized nanopowders were free of impurities as it does not contain any characteristics XRD peaks other than ZnO peaks. Analysis of peak broadening using variations in the Full Width at Half Maximum (FWHM) among different samples synthesized using different bio-reducing agents and conditions reflect differences in crystallinity and structural defects. The synthesized ZnO nanoparticle diameter was calculated using Debye-Scherrer formula [40,41]:

$$D = K\lambda/\beta \cdot \cos\theta \quad (12)$$

where  $K = 0.89$  is Scherrer's constant,  $\lambda$  is the wavelength of X-rays,  $\theta$  is the Bragg diffraction angle, and  $\beta$  is the full width at half-maximum (FWHM) of the diffraction peak corresponding to the plane. The average particle sizes of the ZnO nanoparticles synthesized via the green approach were found to be in the range of 44.6 nm–51.7 nm. These sizes are consistent with the typical dimensions of ZnO nanoparticles synthesized using bio-reducing agents via the precipitation method and revealed variations in crystallite size and strain among the samples synthesized using different reducing agents. ZnO-OT exhibited a crystallite size of 45.0 nm, while ZnO-ABM and ZnO-FB showed sizes of 51.7 nm and 44.6 nm, respectively. The differences in crystallite size may be attributed to variations in the bio-reducing agents and their interactions with the precursor materials. Comparing the XRD patterns of the three samples synthesized using different bio-reducing agents, it was observed that the peak intensities and positions were similar, indicating similar crystallographic orientations and phase purity. However, slight variations in peak broadening were observed, suggesting differences in crystallinity and microstructural characteristics influenced by the choice of bio-reducing agent [42].

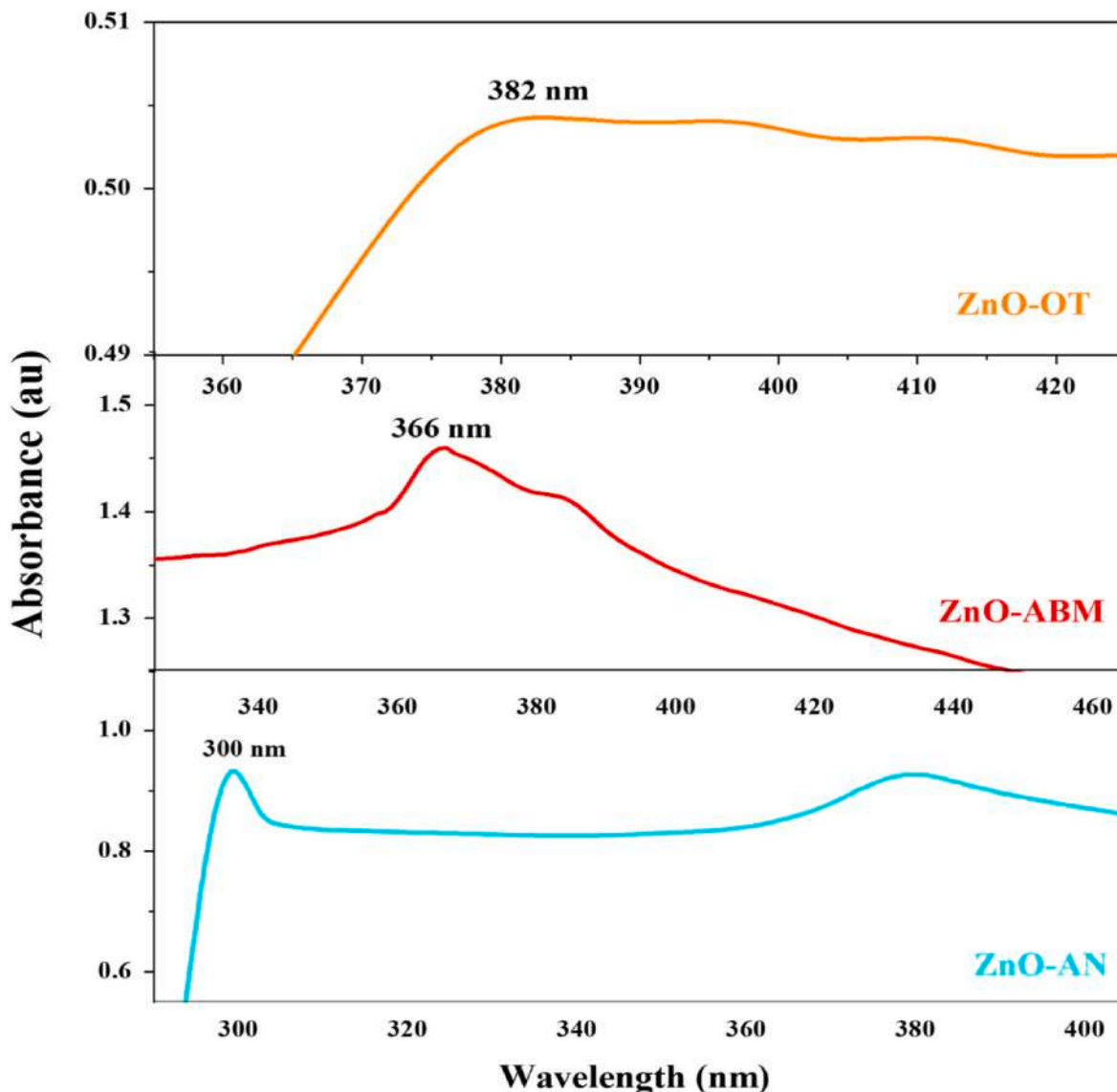
### 3.2. Absorption spectrum of ZnO nanoparticles

Fig. 4 shows the optical absorption spectrum of all the synthesized samples of ZnO NPs. Sample ZnO-AN exhibits a strong absorption band at about 380 nm [43] and an excitonic absorption peak at about 300 nm, on the other hand, samples ZnO-ABM and ZnO-OT show a single excitonic peak at around 366 nm and 382 nm, respectively. All the excitonic absorption peaks confirm the presence of ZnO NPs in the sample (Fig. 4). The significant acute absorption proves that the distribution of nanoparticles is monodispersed and the broad absorption band at 380 nm in sample FB that ranges towards longer wavelength might be owing to the movement of the electronic cloud on the overall skeleton of the ZnO NPs [44]. The absorption peaks for ZnO-AN and ZnO-ABM are noticeably blue-shifted compared to the bulk absorption edge, which generally appears at 380 nm at ambient temperature [45], it is due to the quantum size effect, which is thought to be responsible for this orderly shift of the absorption edge towards shorter wavelengths or higher energy as the nanoparticle size decreases and known as blue shift [46].

The absorption peak for ZnO-OT does not exhibit any blue shift as it remains in the position that is very close to bulk ZnO or comparatively red shifted towards a higher wavelength. This excitonic absorption peak at 300 nm, 366 nm and 382 nm indicates the energy level at which electronic transitions occur within ZnO nanoparticles. Specifically, this peak corresponds to the creation of excitons, which are bound pairs of electrons and holes generated when electrons are excited from the valence band to the conduction band. Another absorption band in ZnO-

**Table 1**  
XRD pattern analysis data.

ZnO-OT			ZnO-ABM			ZnO-ABM		
Bragg's angle (2θ)	all values	FWHM	Bragg's angle (2θ)	hkl values	FWHM	Bragg's angle (2θ)	hkl values	FWHM
31.98	100	0.2	31.95	100	0.2	32.08	100	0.2
34.65	0,0,2	0.2	34.60	0,0,2	0.2	34.72	0,0,2	0.2
36.48	101	0.2	36.42	101	0.2	36.55	101	0.2
47.73	102	0.3	47.69	102	0.2	47.83	102	0.3
56.83	110	0.3	56.75	110	0.3	56.87	110	0.3
63.11	103	0.3	63.03	103	0.4	63.13	103	0.3
66.60	200	0.3	66.55	200	0.2	66.65	200	0.3
68.19	112	0.4	68.06	112	0.4	68.15	112	0.2
69.29	201	0.4	69.29	201	0.4	69.39	201	0.3



**Fig. 4.** UV-visible absorption spectra of ZnO-AN, ZnO-ABM, ZnO-OT.

AN at around 380 nm represents a broader range of wavelengths where absorption occurs. It may be due to the transitions of electrons between energy states within the conduction and valence bands or may also involve other complex processes like defect-related absorption.

**3.3. Optical bandgap for ZnO nanoparticles**

The band gap energy of nanoparticles can be determined by either

Tauc plot method or by using the following equation [47]:

$$E_g = 1240 / \lambda \tag{13}$$

It relates the band gap energy ( $E_g$ ) to the wavelength ( $\lambda$ ) of the excitonic absorption peak. Where the band gap energy ( $E_g$ ) is taken in eV and the excitonic absorption peak ( $\lambda_{peak}$ ) is in nanometers (nm). The estimated band gap energies for ZnO nanoparticles based on this equation are approximately 4.13, 3.38 and 3.24 eV for Sample ZnO-AN, ZnO-

ABM and ZnO-OT respectively. The Tauc plot method was used to calculate band gap energy [48]. This technique establishes a correlation between the absorption coefficient ( $\alpha$ ) and the incident photon energy ( $h\nu$ ) in proximity to the absorption edge which is articulated through Equation (14) as follows:

$$(\alpha h\nu) = B (h\nu - E_g)^n \quad (14)$$

Within the equation  $\alpha$  signifies the absorption coefficient,  $h\nu$  represents the photon energy (directly associated with the wavelength),  $E_g$  stands for the bandgap energy,  $B$  is a constant factor, and  $n$  corresponds to the exponent value which characterizes the nature of the electronic transition between the valence band and conduction band, it may have values  $1/2$ ,  $2$ ,  $3/2$ , and  $3$  corresponding to the allowed direct, allowed indirect, forbidden direct, and forbidden indirect transitions, respectively.

A graph (Fig. 3) between  $(\alpha h\nu)^2$  and  $h\nu$  was plotted by following equation (14) For transition  $n = 1/2$ , in which the value of absorption coefficient ( $\alpha$ ) is obtained through absorbance (in Fig. 1) and the sample thickness ( $L$ ) using the relationship:

$$\log I/I_0 = \log e - \alpha L \sim \log I/I_0 = -\alpha L (\log e) \\ \sim \log I_0/I = \alpha L (0.4343) \sim A = \alpha L / 2.303 \quad (15)$$

Where,  $\log I_0/I = \text{Absorbance (A)}$ , in this way  $\alpha = 2.303 A/L$ . In our case, the Standard value of  $L$  is 1 cm. Therefore, the Overall absorption coefficient  $\alpha$  can be calculated by:

$$\alpha = 2.303 \times A \quad (16)$$

Fig. 5 displays the estimated band gap for ZnO nanoparticles from the Tauc plot of  $(\alpha h\nu)^2$  vs.  $h\nu$ . We have obtained the  $E_g$  by extrapolating the straight section to the energy axis at  $= 0$ . The synthesized samples of ZnO NPs have band gaps around 4.00, 3.53 and 3.43 eV for ZnO-AN, ZnO-ABM and ZnO-OT, respectively. These changes in the band gaps are attributed to variations in the structural parameters of all samples [49]. The value of  $n = 1/2$  is taken in the Tauc relation plot (Fig. 5), which indicates the direct allowed transitions in ZnO NPs of all samples [50]. It can be determined that the mode of transition in every sample of ZnO NPs is direct since the band gap energy is larger for the directly permitted transition when calculated using a taut plot for both values of  $n$ [51]. The value of band gap energies represents the semiconductor behaviour of ZnO NPs with a wide band gap, which requires

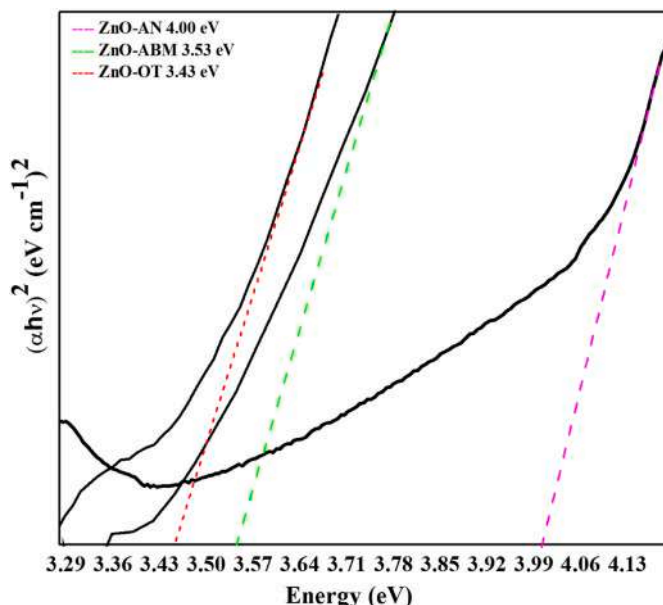


Fig. 5. Band gap of samples of ZnO-AN, ZnO-ABM, ZnO-OT Nanoparticle.

approximately between 3.43 and 4.00 eV of energy to promote an electron from the valence band to the conduction band.

Comparatively, to the bulk band gap of ZnO which has a direct band structure with a wide bandgap of 3.37eV, which leads to its transparent nature [52] this value is slightly higher, which may be caused by the strain during ZnO nanoparticle production, and it is a result of the quantum confinement effects. A wider band gap also indicates higher transparency and potential for UV absorption.

### 3.4. Urbach Energy

The Urbach energy is a parameter that provides insights into the broadening of the absorption edge in the optical spectrum of a semiconductor material like ZnO as well as used to quantify the degree of disorder or defects in the bandgap. The ZnO imperfections create Local electrical fields, which have an impact on band tailing or donor levels enlarging into impurity bands that combine with the conduction band to cause band tailing [50]. The Urbach law describes the exponential dependence of fundamental absorption edge into photon energy [53]. This exponential behaviour of absorbance coefficient arises from the electronic transition between localised states and their density falls off exponentially with photon energy. The width of the localised state is called Urbach energy and its relationship with the absorbance coefficient is described as follows:

$$\alpha = \alpha_0 e^{\frac{h\nu}{E_u}} \quad (17)$$

where  $\alpha$  is the absorbance coefficient,  $\alpha_0$  is a constant and  $E_u$  is the Urbach energy [54,55]. To determine Urbach Energy a graph between  $\ln(\alpha)$  and photon energy ( $h\nu$ ) has been plotted separately for all the samples, shown in Fig. 6. The value of  $E_u$  was estimated by taking the reciprocal of the slopes of the linear part in the lower photon energy area of the curve [56]. The value of Urbach energy was found to be 3.67 (0.00367 eV), 5.03 (0.005 eV), and 50.51 meV (0.05eV) for the sample ZnO-AN, ZnO-ABM, ZnO-OT, respectively, which suggests that there is some degree of disorder or defects present in the bandgap of synthesized nanoparticles. This could be attributed to factors such as surface defects, impurities, or structural imperfections in synthesized nanoparticles, which can impact the material's optical properties and may have implications for its applications in optoelectronics or other fields. Our interpretation predicted the Urbach energy of ZnO-AN and ABM was lower than that of the ZnO-OT nanoparticles. It is suggested the molecules with larger band gap energy have lower Urbach tail/energy or less localized states and more crystallinity order. As a result, in this instance, there might be greater ordering in the ZnO-AN because the Urbach energy in this sample is less than that of the ZnO-ABM and ZnO-OT (Table 2). The higher Urbach energy of NPs ZnO-OT and ZnO-ABM may be due to an increase in electron concentration, which raises the probability of electron-electron and electron-impurity scattering as well as band tailing in the forbidden gap. This increase in electron concentration can be due to the involvement of different reducing agents during the synthesis process.

The value for sample ZnO-OT is relatively much higher than the other two. It may imply that there may be structural irregularities, lattice imperfections, or defects present in your ZnO nanoparticles, contributing to a greater degree of disorder in the material [57] or the creation of additional interband between the valence and conduction bands. In certain research contexts, an extremely high Urbach energy may be of interest because it suggests a highly disordered or amorphous material, which could have unique optical or electronic properties [58].

### 3.5. Refractive index

The refractive index ( $n$ ) is a fundamental parameter of optical materials that plays a very significant role in the design of optical devices. Thus, controlling this parameter in nanoparticles makes them crucial for

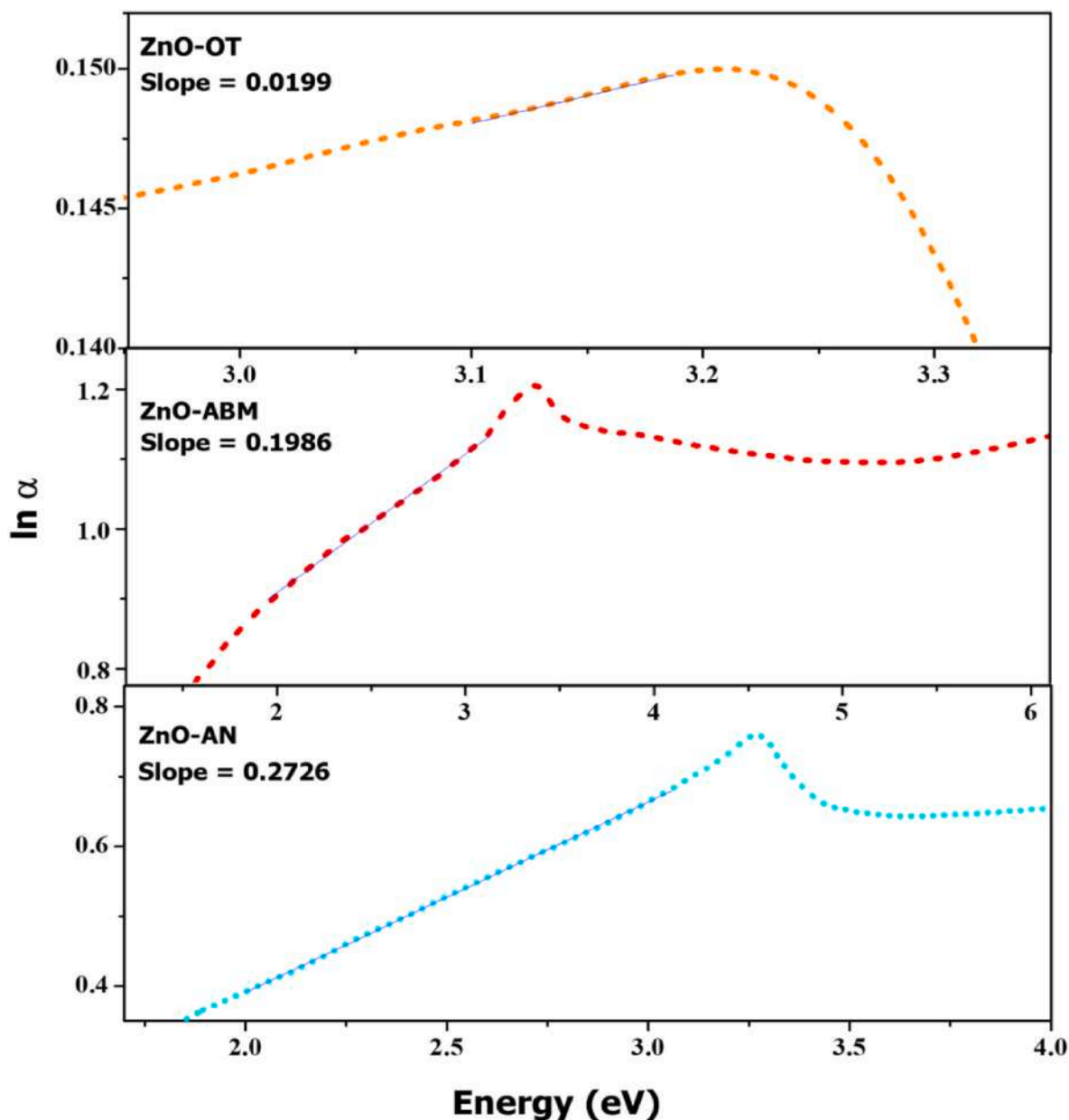


Fig. 6. Plot between  $\ln(\alpha)$  vs. Energy representing the slope to determine Urbach Energy.

**Table 2**

Obtained values of different parameters observed by UV-visible spectroscopy for ZnO-AN, ZnO-ABM, ZnO-OT.

Properties	Calculated Values		
	ZnO-AN	ZnO-ABM	ZnO-OT
Absorbance Peak (nm)	300	366	382
Band gap (eV)	4.00	3.43	3.53
Refractive Index	2.55	2.60	2.70
Optical Conductivity ( $10^9$ per second)	1.30	1.97	7.10
Urbach energy (meV)	3.67	5.03	50.51

a variety of industrial and medical applications [59]. According to the empirical relationships, the value of the refractive index ( $n$ ) was related to the band gap value with the help of the following equation:

$$n = \sqrt{\frac{12.417}{\sqrt{E_g - 0.365}}} \quad (18)$$

The linear relationship in empirical equation (18) was proposed by Reddy et al. [60] and used to calculate the values of refractive indexes here. The empirical formula provides the values 2.55, 2.6 and 2.7 for ZnO-AN, ZnO-ABM and ZnO-OT respectively, which are very close to each other. The values indicate the strong ability of the synthesized ZnO NP samples to refract light, making them suitable for optical applications. It also denotes the sample's high transparency in the visible and UV spectrum region, which enhances their potential towards optical devices like photodetectors and solar cells, and offers opportunities for optical enhancement and material characterization.

### 3.6. Optical conductivity

Optical conductivity is a material property that quantifies how a material conducts electric current in response to the absorption of photons in the optical range. It is a key parameter for understanding the optical and electrical behaviour of materials, particularly in the context of optoelectronic devices and optical coatings. Here we have calculated

the value of optical conductivity  $\sigma_{opt}$  of all the samples of ZnO nanoparticles using the formula [14]:

$$\sigma_{opt} = \frac{anc}{4\pi} \quad (16)$$

Where, absorption coefficient ( $\alpha$ ) and the refractive index ( $n$ ), the speed of light ( $c$ ) in space was involved in the calculation. The calculated values of the optical conductivity for the samples ZnO-AN were  $1.3 \times 10^9 \text{ s}^{-1}$ , for ZnO-ABM was  $1.97 \times 10^9 \text{ s}^{-1}$  and for the ZnO-OT was  $7.1 \times 10^{10} \text{ s}^{-1}$ , as can be seen in Table 2.

The magnitude of  $\sigma_{opt}$  is related to the material's ability to absorb and re-emit photons, which is important in various optoelectronic applications, including solar cells, photodetectors, and light-emitting devices. Higher values often indicate better optical response and may be desirable for certain optical device designs [61]. In our study, all the calculated optical conductivity values might be considered high and indicative of efficient optical response, which can be advantageous for optoelectronic applications. The sample ZnO-OT has the highest value among all three samples denoting the highest potential of electrons in particular NPs to absorb photons and become excited at a rate of  $7.1 \times 10^{10} \text{ s}^{-1}$  times per second when exposed to light within the considered energy range [59].

### 3.7. Determination of size of ZnO NPs

In this section, the size of a synthesized nanoparticle was calculated by using 5 different approaches with the data obtained from the optical spectra. The results obtained by the five models were compared to analyse their accuracy.

#### 3.7.1. Brush model

The first approach used to determine the size of the nanoparticles was the Effective mass approximation mentioned in section 2.5.1. The solved form of the Brus equation from Equation number (3) was used to calculate the size of all samples. Equation (1) was utilized to derive the numerical values in equation (3) in which the values of  $m_e^* = 0.19m_0$  and  $m_h^* = 0.80m_0$  were employed, which was also utilized by Brus et al. in their investigation [62]. Different values of the effective masses of the electrons and holes were utilized by different researchers. For illustration, Monticone et al. and Pesika et al. utilized the following parameters  $m_e = 0.26m_0$ ,  $m_h = 0.59m_0$  ( $m_0$  denoting the free electron mass), Dielectric constants of ZnO = 3.7 and surrounding liquid ( $\epsilon_0$ ) = 8.5 in their work to derive equation (2) [11,63]. While Praus et al. provided the values  $m_e^* = 0.18m_0$  and  $m_h^* = 0.80m_0$  and Dey et al. reported  $m_e^* = 0.42m_0$  and  $m_h^* = 0.61m_0$ . It is important to note that small changes in the effective mass values have the potential to have a big impact on the computed sizes of NPs, that is why we have used the same which was utilized by Brus et al. to prevent any calculation errors in the Brus equation.

The Brus equation predicts that materials that have smaller energy gaps, need to have larger crystal sizes before they can absorb light at the same energy level as the bulk material. On the other hand, materials with larger energy gaps can reach this point at intermediate crystal sizes, which are around 60 Å in diameter. This happens because a balance occurs between two factors, quantum effects that try to confine the electrons and electrostatic forces that try to spread them out. However, when the crystal size is even smaller, the simple equation predicts a significant increase in energy (a blue shift). To get accurate results in such cases, we can't rely on the basic equation alone. We need to use a more advanced analysis that considers how the charge is distributed on the surface of the crystal (L. E. [62]).

Our results also show that the relationship between bandgap energy and nanoparticle size aligns with the fundamental assumptions of the Brus equation and we observed that smaller bandgap energies correspond to larger nanoparticle sizes. ZnO-AN has the highest bandgap energy ( $E_g = 4.00 \text{ eV}$ ), and its estimated nanoparticle size is 2.56 nm

whereas, ZnO-ABM, with a bandgap energy of 3.43 eV, exhibits a larger nanoparticle size of 5.58 nm, on the other hand ZnO-OT, having a bandgap energy of 3.53 eV, falls in between, with an estimated nanoparticle size of 4.40 nm. Our results provide valuable insights into the relationship between bandgap energy and nanoparticle size, confirming the applicability of the Brus equation to our experimental conditions. However, major computational efforts and difficulties do not allow for the calculation of the properties of large-sized nanocrystals (Sapra & Sarma, 2004b) as well and the simplifications made in applying the Brus equation are some limitations while applying this equation.

#### 3.7.2. Empirical formula suggested by Meulenkamp (ME)

The next approach used to calculate the particle size of ZnO nanoparticles was proposed by Meulenkamp who introduced equation (5) mentioned in section 2.5.2 which correlates the particle sizes to  $\lambda_{1/2}$  [32]. Meulenkamp suggested using a band gap calculated from  $\lambda_{1/2}$  (nm), which is a wavelength at which absorption becomes half the absorption compared to the first absorption maximum when going from lower energy (half of that at the shoulder). But here we have used the same value of band gap that we have used for other methods because it was comparatively difficult to obtain an approximate value of  $\lambda_{1/2}$  in the case of Sample ZnO-OT, as the first absorption value of this sample is already at a higher wavelength than the other two. Because of this, we were getting a very high low value of  $E_g$  which may not provide a real number after solving the equation. Therefore, to make similarity in the calculation for all samples, we choose to take the band gap energy obtained from the Tauc plot method (Fig. 2) and obtained the particle diameter 1.96 nm for Zn-AN, 6.02 nm for ZnO-ABM and 4.3 nm for ZnO-OT, which are in the good agreement with the sizes obtained from Brus equation.

#### 3.7.3. Hyperbolic Band Model (HBM)

In the second approach, the particle size is determined by the relationship between the absorption band gap and radius using equation number (6) as mentioned in 2.5.3 known as the hyperbolic band model [64]. In this equation the value of effective mass ( $m^*$ ) =  $29.15 \times 10^{-31} \text{ kg}$  for ZnO,  $E_{g\text{bulk}} = 3.37 \text{ eV}$ , Planck's constant  $h = 6.626 \times 10^{-34} \text{ Js}$ , and  $E_{g\text{nano}} = 4 \text{ eV}$ , 3.43 eV and 3.53 eV derived from the absorption spectra (Fig. 2) were used to calculate the average particle size [65]. The average particle size obtained from this formula is 4.6, 9.5, and 15.7 nm for samples ZnO-AN, ABM, and OT, respectively. The obtained size suggests that these ZnO nanoparticles are in the nanoscale range and can have promising characteristics for various applications, especially in the field of nanotechnology and optoelectronics. However, the sizes calculated by this method are larger than the previous methods used, This may be due to irregularity in the shapes of the particles in the sample because to determine the particle's exact size using the hyperbolic band model the particle should have an accurate circular form [64].

#### 3.7.4. Tight Binding Model (TBM)

Another approach used to obtain the average particle diameter was a tight binding model (TBM) or the empirical expression suggested by Viswanatha et al. which is mentioned in section 2.5.4 in equation (10). In this case, the estimated particle sizes were 2.0, 4.5 and 7.2 nm for ZnO-AN, ZnO-ABM and ZnO-OT, respectively, which also correspond to the nanoscale regime. The values for  $E_g$  used here were the same as in the previous methods. The size obtained for ZnO-AN was in good agreement with the Brus equation but the size calculated for sample ZnO-OT was larger than Brus and Mulenkamp's methods. The disagreement can be due to the applicability of different methods of synthesis of the nanoparticle.

#### 3.7.5. Simplified version of EMA(SEMA)

Finally, the radius of all samples was calculated by a simple equation (11) mentioned in section 2.5.5 which utilized the inflexion point in the absorption vs. wavelength spectrum, where  $\lambda_p$  is the peak absorbance

wavelength in nm. The values  $m_e = 0.26 m_0$ ,  $m_h = 0.59 m_0$ ,  $m_0$  is the free electron mass,  $\hbar = 8.5$ , and  $E_{g,bulk} = 3.3$  eV was used in the derivation of the simplified equation [23]. The prepared ZnO nanoparticle samples exhibited the absorbance peak at about 300 nm (ZnO-AN), 366 nm (ZnO-ABM), 382 nm (ZnO-OT) which corresponds to the particle size of 2.7 nm, 5.1 nm and 7.7 nm respectively. The result is in good agreement with TBM but slightly varies with that of the Brush equation.

### 3.8. Comparative study

The size dependence of the optical characteristics of nanoparticles is one of its most striking features. A semiconductor nanoparticle's absorption edge shifts to shorter wavelengths as its size decreases, signalling an expanding band gap. As the size of the particles lowers, colours will shift if the semiconductor's band gap is within the energy range of visible light. It has been observed that there is good agreement between the sizes estimated from the above-mentioned methods, but we can also observe some discrepancies in some cases. It is because the accuracy of these formulas depends on various factors such as precursor and method used to synthesise NPs, material's composition, structure and specific conditions.

It is important to note that the formula mentioned is mostly empirical, and while it may provide a reasonable estimate of size for many materials, it may not capture all the range of ZnO NPs. Similarly, to obtain the exact size of the particle using the hyperbolic band model, the particle should be exactly circular [64]. A comparative chart of size for all nanoparticles can be seen in Table 3, in which we can see in the case of ZnO-AN, BE (equation (3)), ME (equation (5)) and SEMA (equation (11)) give similar values of particle diameter while for nanoparticle ZnO-ABM, only the diameter provided by Brus equation and Meulenkamp's Formula is in good agreement. On the other hand, in the case of nanoparticle ZnO-OT, only BE, ME and TBM provided the values close to each other. Size estimated from HBM, TBM and SEMA is mostly in less agreement with other methods. In contrast, the values provided by BE and ME are much closer than the others in most of the cases. In addition, all samples synthesized in similar conditions with a different reducing agent have no similar size of the nanoparticle, which indicates the interaction of the reducing agent with the property of the nanoparticle.

The comparative graph presented in Fig. 7 indicates that the size of the nanoparticles is inversely related to their bandgap as we move down to the energy of the bandgap. A decrease in the size of nanoparticles can be easily noted for all synthesized nanoparticles, that is the key assumption of most of the methods used in this study. Our results validate that all methods apply to our experimental settings and offer insightful information on the connection between bandgap energy and nanoparticle size. But occasionally, significant computational work and challenges make it laborious and time-consuming as well, and the precise bandgap value without any adjustments is required to obtain an accurate assessment of the size.

## 4. Statistical study (Analysis of variance)

One-way ANOVA was used in this study to statistically assess the applicability of all reducing agent for their synthesis and methods to calculate the size of nanoparticles. This study used two settings of one-way ANOVA (single factor) with a 95 % confidence interval ( $\alpha = 0.05$ ) to assess if the size of nanoparticles synthesized by three different reducing

**Table 3**

Size of ZnO nanoparticles obtained using UV-visible data by applying different approaches.

Samples	BE (nm)	SEMA (nm)	ME (nm)	TBM (nm)	HBM (nm)
ZnO-AN	2.7	2.7	2.1	2.0	4.6
ZnO-ABM	4.2	5.1	3.8	4.5	9.5
ZnO-OT	5.1	7.7	5.2	7.2	15.7

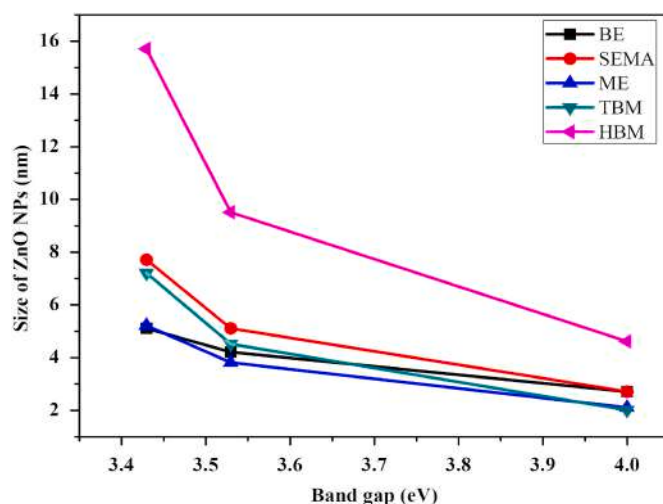


**Fig. 7.** Comparison between calculated Size value of all samples and their relation with Bandgap.

agents, calculated by 5 different Models differed significantly from one another or not.

In our first set of ANOVAs, we targeted the sample of ZnO NP synthesized by using 3 different reducing agents to identify the statistical difference in the size of nanoparticles with the choice of reducing agent. ZnO-AN, ZnO-ABM and ZnO-OT were the targeted variables and the hypotheses for the two-tailed test were as follows:

The Null Hypothesis (H0): There are no significant differences in the estimated sizes of ZnO nanoparticles synthesized by using different reducing agents.

The Proposed Hypothesis (H1): There are significant differences in the estimated sizes of ZnO nanoparticles synthesized by using different reducing agents.

In this case, the null hypothesis was rejected since the significance value ( $p = 0.041$ ) was less than the significance level of 95 %, which denotes that there was a statistically significant difference between the populations. The results of our analysis are summarized in Table 4. The ANOVA analysis provided a p-value of 0.041 which is smaller than the used significance level of 0.05, Which does not support the null hypothesis and signifies that there is statistically significant variation in the estimated sizes of ZnO nanoparticles synthesized by using different reducing agents.

To reveal the detailed analysis of all populations we performed post-hoc analysis after ANOVA. We have chosen Tukey Test as posthoc analysis to compare the data in pair and it may be inferred from the executed Tukey test (Table 5) that in pairwise comparisons, the differences between the sample ZnO-AN and ZnO-OT are statistically significant ( $p\text{-value } 0.03 < \alpha = 0.05$ ) at 0.05 level, where the significance values between sample FB (Mean =  $2.82 \pm 0.47$ , Standard Deviation = 1.05) and ZnO-OT (Mean =  $8.18 \pm 1.95$ , Standard Deviation = 4.36) are 1 (Table 4). However, the sample ZnO-AN and ZnO-ABM (Mean =  $5.42 \pm 1.04$ , Standard Deviation = 2.33) as well as ZnO-ABM and ZnO-OT have a significance value of 0, which indicates that the samples ZnO-

**Table 4**

One Way ANOVA on the source of ZnO.

Properties	Source of variation	Sum of squares	Degree of freedom	Mean Square	F Value	P Value > F
Source of ZnO NPs	Between groups	71.85	2	35.92	4.22	0.0441
	within groups	102.2	12	8.52	–	–
	Total	174.05	14	–	–	–

**Table 5**

Tukey posthoc analysis for pairwise comparison of sources of ZnO NP.

Sample	Mean	Standard deviation	Comparisons	Mean Difference	SEM	q Value	Prob (p-value)	Sig
ZnO-AN	2.82 ± 0.47	1.05	ABM - AN	2.60	1.85	1.99	0.37	0
ZnO-ABM	5.42 ± 1.04	2.33	OT - AN	5.36	1.85	4.11	0.03	1
Zno-OT	8.18 ± 1.95	4.36	OT - ABM	2.76	1.85	2.11	0.33	0

AN to ZnO-ABM ( $p$  value =  $0.37 > \alpha = 0.05$ ) and ZnO-OT to ZnO-ABM ( $p$  value =  $0.33 > \alpha = 0.05$ ) are not significantly different. Therefore, it may be possible that the reducing agent used to synthesise the ZnO nanoparticle can considerably affect the size of the nanoparticle.

In our second set of ANOVA Brus Equation (EMA), the Hyperbolic Band Model, Meulenkamp formula, Tight Binding Model and Simplified EMA were the targeted variables. The hypotheses for the test were as follows:

The Null Hypothesis ( $H_0$ ): There are no significant differences in the estimated sizes of ZnO nanoparticles among the different approaches/methods.

The Proposed Hypothesis ( $H_1$ ): There are significant differences in the estimated sizes of ZnO nanoparticles among the different approaches/methods.

In our case, the null hypothesis was not rejected since the significance value was not less than the significance level ( $\alpha = 0.05$ ), which denotes that there was not any statistically significant difference between the two populations. The results of the analysis are summarized in Table 6. The ANOVA analysis provided a p-value of 0.16323 which is higher than the used significance level of 0.05, Which supports our null hypothesis and signifies that there is no statistically significant variation in the estimated sizes of ZnO nanoparticles between the various models or approaches. This indicates that the final ZnO nanoparticle size may not be considerably affected by the estimation technique selection, according to the data and analysis.

## 5. Conclusion

This study successfully characterizes ZnO NPs using UV-visible spectroscopy and presents alternative formulas for size determination. Although the formulas utilized to calculate different parameters are mostly empirical and based on observed relationships rather than a theoretical model or fundamental physical laws. Therefore, the obtained results and characteristics of synthesized ZnO NP samples have some discrepancies and are influenced by factors such as particle size, shape, synthetic process, environmental conditions, and surface characteristics. From ANOVA analysis, we can conclude that there is no statistically significant variance in estimated sizes via the formulas employed, indicating that any of the formulas can be employed to calculate the size of NPs via low-cost, real-time, less laborious alternative methods using UV-visible data. Moreover, the accuracy of these formulas also depends on the material's composition, structure, and the specific conditions under which they are used. Additionally, the calculated optical bandgap of all samples indicates semiconductor behaviour, and XRD analysis revealed a crystalline structure and crystal size ranging from 44.6 nm to 51.7 nm for ZnO nanoparticles. The ZnO NP sample synthesized via biomass is the smallest, and the ZnO sample synthesized via OT is larger, despite all having a high value of Urbach energy suggesting the presence of defects, while very close values of refractive index and optical conductivity demonstrate their optical transparency and near suitability for optoelectronic applications.

## 6. Future scope

The findings of this investigation open doors for further research in different directions. Future studies can focus on comparing the results obtained through applied UV-visible-based methods with other more reliable techniques to understand the precision and error percentage in

**Table 6**

One Way ANOVA on methods of determination of Size of synthesized NPs.

Properties	Source of variation	Sum of squares	Degree of freedom	Mean Square	F Value	P Value > F
Models or Methods	Between groups	78.37	4	19.59	2.05	0.16
	Within groups	95.68	10	9.57	-	-
	Total	174.05	14	-	-	-

the value obtained through the present methods as well as refining the accuracy of size determination approaches to the nanoparticles synthesized using different model can also be promising for further investigation. Additionally, the impact of defects on ZnO NP properties and exploration towards novel applications of ZnO NPs in optoelectronic devices, photodetectors, solar cells, and light-emitting devices is also worthwhile. Moreover, investigations into optimizing ZnO NP synthesis methods and tailoring their properties for specific applications can be pursued for practical advancements in materials science and nanotechnology.

## CRedit authorship contribution statement

**Sanju Singh:** Writing – original draft, Methodology, Investigation, Funding acquisition, Formal analysis, Data curation, Conceptualization, Project administration, Resources, Software. **Jaya V. Gade:** Writing – review & editing. **Dakeshwar Kumar Verma:** Writing – review & editing. **Berdimurodov Elyor:** Writing – review & editing. **Bhawana Jain:** Validation, Supervision, Methodology, Writing – review & editing.

## Declaration of competing interest

The authors declare that they have no known competing financial interests or personal relationships that could have appeared to influence the work reported in this paper.

## Data availability

Data will be made available on request.

## Acknowledgement

The authors would like to thank Siddhachalam Laboratory, Raipur 492001, Chhattisgarh, India for providing all the required materials, support and constant encouragement of its members to conduct the research successfully.

## Appendix A. Supplementary data

Supplementary data to this article can be found online at <https://doi.org/10.1016/j.optmat.2024.115422>.

## References

- [1] G. Dutta, A. Sugumaran, Bioengineered zinc oxide nanoparticles: chemical, green, biological fabrication methods and its potential biomedical applications, J. Drug

- Deliv. Sci. Technol. 66 (2021) 102853, <https://doi.org/10.1016/j.jddst.2021.102853>.
- [2] M.M. Kadhim, S.A. Abdullaha, T.Z. Taban, T.S. Alomar, Na Ahmed Al-Masoud, S. K. Hachim, The effect of Stone-Wales defect on the sensitivity of a ZnO monolayer in detection of PH<sub>3</sub> and AsH<sub>3</sub> gases: a DFT study, *Appl. Phys. A* 129 (2) (2023) 159, <https://doi.org/10.1007/s00339-023-06405-7>.
- [3] S. Kumar, R. Seth, S. Panwar, K.K. Goyal, V. Kumar, R.K. Choubey, Morphological and optical studies of ZnO-silica nanocomposite thin films synthesized by time dependent CBD, *J. Electron. Mater.* 50 (6) (2021) 3462–3470, <https://doi.org/10.1007/s11664-021-08863-2>.
- [4] X.-F. Zhang, Z.-G. Liu, W. Shen, S. Gurunathan, Silver nanoparticles: synthesis, characterization, properties, applications, and Therapeutic approaches, *Int. J. Mol. Sci.* 17 (9) (2016) 1534, <https://doi.org/10.3390/ijms17091534>.
- [5] S. Mourdikoudis, R.M. Pallares, N.T.K. Thanh, Characterization techniques for nanoparticle comparison and complementarity upon studying nanoparticle properties, *Nanoscale* 10 (27) (2018) 12871–12934, <https://doi.org/10.1039/C8NR02278J>.
- [6] F. Al-dolaimy, M.H. Kzar, U.A.-R. Hussein, A.T. Kareem, T.L. Mizal, A.A. Omran, H. A. Nasser, A.H. Alawadi, F.A. Ali, A. Alsaalamy, A. Fawaz, Green synthesis and characterization of inorganic nanoparticles with focus on Au nanoparticles for investigation of E-coli detection and treatment, *J. Inorg. Organomet. Polym. Mater.* (2023), <https://doi.org/10.1007/s10904-023-02844-0>.
- [7] M. Anbuvarnan, M. Ramesh, G. Viruthagiri, N. Shanmugam, N. Kannadasan, Synthesis, characterization and photocatalytic activity of ZnO nanoparticles prepared by biological method, *Spectrochim. Acta Mol. Biomol. Spectrosc.* 143 (2015) 304–308, <https://doi.org/10.1016/j.saa.2015.01.124>.
- [8] S.S. Kumar, P. Venkateswarlu, V.R. Rao, G.N. Rao, Synthesis, characterization and optical properties of zinc oxide nanoparticles, *Int. Nano Lett.* 3 (1) (2013) 30, <https://doi.org/10.1186/2228-5326-3-30>.
- [9] I. Khan, K. Saeed, I. Khan, Nanoparticles: properties, applications and toxicities, *Arab. J. Chem.* 12 (7) (2019) 908–931, <https://doi.org/10.1016/j.arabj.2017.05.011>.
- [10] F. Rocha, A. Gomes, C. Lunardi, S. Kaliaguine, G. Patience, Experimental methods in chemical engineering: ultraviolet visible Spectroscopy|UV-vis, *Can. J. Chem. Eng.* 96 (2018), <https://doi.org/10.1002/cjce.23344>.
- [11] S. Monticone, R. Tufeu, A.V. Kanaev, Complex nature of the UV and visible fluorescence of colloidal ZnO nanoparticles, *J. Phys. Chem. B* 102 (16) (1998) 2854–2862, <https://doi.org/10.1021/jp973425p>.
- [12] E.J.C. Martinez, N. Chequer, J. Solis, T. Cordova, Alternative methodology for gold nanoparticles characterization diameter using PCA technique and UV-VIS spectrophotometry, *Nanosci. Nanotechnol.* 2 (2012), <https://doi.org/10.5923/j.nn.20120206.06>.
- [13] F. Rodríguez-Mas, J.C. Ferrer, J.L. Alonso, D. Valiente, S. Fernández de Ávila, A comparative study of theoretical methods to estimate semiconductor nanoparticles' size, *Crystals* 10 (3) (2020), <https://doi.org/10.3390/cryst10030226>. Article 3.
- [14] R. Das, S. Pandey, Comparison of optical properties of bulk and nano crystalline thin films of CdS using different precursors, *Int. J. Mater. Sci.* 1 (1) (2011) 35–40.
- [15] S. Faisal, H. Jan, S.A. Shah, S. Shah, A. Khan, M.T. Akbar, M. Rizwan, F. Jan, Wajidullah, N. Akhtar, A. Khattak, S. Syed, Green synthesis of zinc oxide (ZnO) nanoparticles using aqueous fruit extracts of myristica fragrans: their characterizations and biological and environmental applications, *ACS Omega* 6 (14) (2021) 9709–9722, <https://doi.org/10.1021/acsomega.1c00310>.
- [16] M. Liaqat, A. Basit, T. Iqbal, S. Afsheen, I. Maryam, A. Younas, R.R.M. Khan, N. Al-Zaqri, I. Warad, Investigate the effect of ZnO/Bi<sub>2</sub>O<sub>3</sub> nanocomposite: a synergistic versatile approach for biomedical and environmental applications, *Colloids Surf. A Physicochem. Eng. Asp.* 681 (2024) 132773, <https://doi.org/10.1016/j.colsurfa.2023.132773>.
- [17] Y. Rilda, R. Rinaldi, S. Syukri, A. Armaini, R. Refinel, A. Agustien, H. Pardi, Biosynthesis of zinc oxide (ZnO) using culture biomass of *Aspergillus Niger*: the influence of pH on textile morphology and antimicrobial activity, <https://doi.org/10.21203/rs.3.rs-793590/v1>, 2021.
- [18] K. Ali, S. Dwivedi, A. Azam, Q. Saqib, M.S. Al-Said, A.A. Alkhedairy, J. Musarrat, Aloe vera extract functionalized zinc oxide nanoparticles as nano antibiotics against multi-drug resistant clinical bacterial isolates, *J. Colloid Interface Sci.* 472 (2016) 145–156, <https://doi.org/10.1016/j.jcis.2016.03.021>.
- [19] R.M.I. Elsamra, M.S. Masoud, A.A. Zidan, G.M.E. Zokm, M.A. Okbah, Green synthesis of nanostructured zinc oxide by *Ocimum tenuiflorum* extract: characterization, adsorption modeling, cytotoxic screening, and metal ions adsorption applications, *Biomass Conversion and Biorefinery* (2023), <https://doi.org/10.1007/s13399-022-03709-1>.
- [20] S. Raut, D.P.V. Thorat, R. Thakre, Green synthesis of zinc oxide (ZnO) nanoparticles using *Ocimum tenuiflorum* leaves 4 (5) (2013).
- [21] S. Sabir, M. Arshad, S.K. Chaudhari, Zinc oxide nanoparticles for revolutionizing agriculture: synthesis and applications, *Sci. World J.* 2014 (2014) e925494, <https://doi.org/10.1155/2014/925494>.
- [22] O.M. Elshayb, K.Y. Farroh, H.E. Amin, A.M. Atta, Green synthesis of zinc oxide nanoparticles: fortification for rice grain yield and nutrients uptake enhancement, *Molecules* 26 (3) (2021) 584, <https://doi.org/10.3390/molecules26030584>.
- [23] S. Samuel, L. S. Bose, K. George, Optical Properties of ZnO Nanoparticles, 2009.
- [24] S. Talam, S.R. Karumuri, N. Gunnam, Synthesis, characterization, and spectroscopic properties of ZnO nanoparticles, *ISRN Nanotechnology* 2012 (2012) 1–6, <https://doi.org/10.5402/2012/372505>.
- [25] L.E. Brus, Electron-electron and electron-hole interactions in small semiconductor crystallites: the size dependence of the lowest excited electronic state, *J. Chem. Phys.* 80 (9) (1984) 4403–4409, <https://doi.org/10.1063/1.447218>.
- [26] N.V. Hullavarad, S.S. Hullavarad, P.C. Karulkar, Cadmium sulphide (CdS) nanotechnology: synthesis and applications, *J. Nanosci. Nanotechnol.* 8 (7) (2008) 3272–3299, <https://doi.org/10.1166/jnn.2008.145>.
- [27] G. Taka, T.D. Das, Synthesis of ZnO nanoparticles through a simple wet chemical precipitation method, *IOP Conf. Ser. Earth Environ. Sci.* 1042 (1) (2022) 012017, <https://doi.org/10.1088/1755-1315/1042/1/012017>.
- [28] S. Kumar, H.C. Jeon, T.W. Kang, R. Singh, J.K. Sharma, R.K. Choubey, Structural and optical properties of silica capped ZnS:Mn quantum dots, *J. Mater. Sci. Mater. Electron.* 26 (6) (2015) 3939–3946, <https://doi.org/10.1007/s10854-015-2928-0>.
- [29] C. Dushkin, K. Papazova, N. Dushkina, E. Adachi, Attenuated quantum confinement of the exciton in semiconductor nanoparticles, *Colloid Polym. Sci.* 284 (1) (2005) 80–85, <https://doi.org/10.1007/s00396-005-1327-0>.
- [30] L. Brus, Electronic wave functions in semiconductor clusters: experiment and theory, *J. Phys. Chem.* 90 (12) (1986) 2555–2560, <https://doi.org/10.1021/j100403a003>.
- [31] L. Spanhel, Colloidal ZnO nanostructures and functional coatings: a survey, *J. Sol. Gel Sci. Technol.* 39 (1) (2006) 7–24, <https://doi.org/10.1007/s10971-006-7302-5>.
- [32] E.A. Meulenkaamp, Size dependence of the dissolution of ZnO nanoparticles, *J. Phys. Chem. B* 102 (40) (1998) 7764–7769, <https://doi.org/10.1021/jp982305u>.
- [33] T.J. Jacobsson, Synthesis and characterisation of ZnO nanoparticles. An experimental investigation of some of their size dependent quantum effects. <https://urn.kb.se/resolve?urn=urn:nbn:se:uu:diva-121715>, 2010.
- [34] Y. Wang, A. Suna, W. Mahler, R. Kasowski, PbS in polymers. From molecules to bulk solids, *J. Chem. Phys.* 87 (12) (1987) 7315–7322, <https://doi.org/10.1063/1.453325>.
- [35] T. Kundu, N. Karak, P. Barik, S. Saha, Optical properties of ZnO nanoparticles prepared by the chemical method using poly (vinylalcohol) (PVA) as capping agent, *IJSCSE* 1 (2011) 19–24.
- [36] R. Koole, E. Groeneveld, D. Vanmaekelbergh, A. Meijerink, C. De Mello Donegá, Size effects on semiconductor nanoparticles, in: C. De Mello Donegá (Ed.), *Nanoparticles*, Springer Berlin Heidelberg, 2014, pp. 13–51, [https://doi.org/10.1007/978-3-662-44823-6\\_2](https://doi.org/10.1007/978-3-662-44823-6_2).
- [37] R. Viswanatha, S. Sapra, B. Satpati, P.V. Satyam, B.N. Dev, D.D. Sarma, Understanding the quantum size effects in ZnO nanocrystals, *J. Mater. Chem.* 14 (4) (2004) 661–668, <https://doi.org/10.1039/B310404D>.
- [38] S. Sapra, D.D. Sarma, Evolution of the electronic structure with size in II-VI semiconductor nanocrystals, *Phys. Rev. B* 69 (12) (2004) 125304, <https://doi.org/10.1103/PhysRevB.69.125304>.
- [39] A. Sharma, B.P. Singh, S. Dhar, A. Gondorf, M. Spasova, Effect of surface groups on the luminescence property of ZnO nanoparticles synthesized by sol-gel route, *Surf. Sci.* 606 (3–4) (2012) L13–L17, <https://doi.org/10.1016/j.susc.2011.09.006>.
- [40] P.P. Mahamuni, P.M. Patil, M.J. Dhanavade, M.V. Badiger, P.G. Shadija, A. C. Lokhande, R.A. Bohara, Synthesis and characterization of zinc oxide nanoparticles by using polyol chemistry for their antimicrobial and antibiofilm activity, *Biochemistry and Biophysics Reports* 17 (2019) 71–80, <https://doi.org/10.1016/j.bbrep.2018.11.007>.
- [41] S. Monga, N. Sharma, R.K. Choubey, Y.K. Mishra, R.S. Katiyar, A. Singh, Prospects of non-linear optical behaviour of PZT/ZnO heterostructures, *Ceram. Int.* 49 (8) (2023) 11737–11752, <https://doi.org/10.1016/j.ceramint.2022.11.297>.
- [42] H. Naseer, T. Iqbal, Green synthesis of silver-doped zinc oxide nanoparticles for investigation of their photocatalytic activity and shelf life applications, *Biomass Conversion and Biorefinery* (2023), <https://doi.org/10.1007/s13399-023-04380-w>.
- [43] Y.D. Jin, J.P. Yang, P. Heremans, M. Van der Auweraer, E. Rousseau, H.J. Geise, G. Borghs, Single-layer organic light-emitting diode with 2.0% external quantum efficiency prepared by spin-coating, *Chem. Phys. Lett.* 320 (2000) 387–392, [https://doi.org/10.1016/S0009-2614\(00\)00279-7](https://doi.org/10.1016/S0009-2614(00)00279-7).
- [44] W. Muhammad, N. Ullah, M. Haroon, B. Haider Abbasi, Optical, morphological and biological analysis of zinc oxide nanoparticles (ZnO NPs) using *Papaver somniferum* L, *RSC Adv.* 9 (51) (2019) 29541–29548, <https://doi.org/10.1039/C9RA04424H>.
- [45] V. Prasad, C. D'Souza, D. Yadav, A.J. Shaikh, N. Vigneshwaran, Spectroscopic characterization of zinc oxide nanorods synthesized by solid-state reaction, *Spectrochim. Acta Mol. Biomol. Spectrosc.* 65 (1) (2006) 173–178, <https://doi.org/10.1016/j.saa.2005.10.001>.
- [46] A. Younas, T. Iqbal, A. Almohammed, S. Afsheen, Experimental and theoretical comparative analysis of pure WO<sub>3</sub> and La doped WO<sub>3</sub> for degradation of MB, *Opt. Quant. Electron.* 55 (13) (2023) 1172, <https://doi.org/10.1007/s11082-023-05446-9>.
- [47] J. Liu, J. Cao, Z. Li, G. Ji, S. Deng, M. Zheng, Low-temperature solid-state synthesis and phase-controlling studies of CdS nanoparticles, *J. Mater. Sci.* 42 (2007) 1054–1059, <https://doi.org/10.1007/s10853-006-0964-0>.
- [48] P. Samanta, A. Saha, T. Kamilya, Chemical synthesis and optical properties of ZnO nanoparticles, *J. Nano- Electron. Phys.* 6 (2014).
- [49] S. Kumar, Kavita, H.S. Bhatti, K. Singh, S. Sharma, V. Kumar, R. K. Choubey, Effect of glutathione capping on the antibacterial activity of tin doped ZnO nanoparticles, *Phys. Scripta* 96 (12) (2021) 125807, <https://doi.org/10.1088/1402-4896/ac1eb3>.
- [50] V. Perumal, S. Kalyanaraman, B. Santoshkumar, Dr R. Thangavel, Estimation of electron-phonon coupling and Urbach energy in group-I elements doped ZnO nanoparticles and thin films by sol-gel method, *Mater. Res. Bull.* 77 (2016), <https://doi.org/10.1016/j.materresbull.2016.01.015>.



- [51] P. Bindu, S. Thomas, Optical properties of ZnO nanoparticles synthesised from a polysaccharide and ZnCl<sub>2</sub>, *Acta Phys. Pol., A* 131 (2017) 1474–1478, <https://doi.org/10.12693/APhysPolA.131.1474>.
- [52] L.K. Sharma, D. Mandal, R.K. Choubey, S. Mukherjee, On the correlation of the effect of defects on the microstructural, optical and magnetic properties of doped ZnO, *Phys. E Low-dimens. Syst. Nanostruct.* 144 (2022) 115370, <https://doi.org/10.1016/j.physe.2022.115370>.
- [53] P. Bindu, S. Thomas, Optical properties of ZnO nanoparticles synthesised from a polysaccharide and ZnCl<sub>2</sub>, *Acta Phys. Pol., A* 131 (6) (2017) 1474–1478, <https://doi.org/10.12693/APhysPolA.131.1474>.
- [54] F. Urbach, The long-wavelength edge of photographic sensitivity and of the electronic absorption of solids, *Phys. Rev.* 92 (5) (1953) 1324, <https://doi.org/10.1103/PhysRev.92.1324>, 1324.
- [55] L. Ding, M. Friedrich, M. Fronk, O. Gordan, D. Zahn, L. Chen, D. Zhang, C. Cobet, N. Esser, Correlation of band gap position with composition in high-k films, *J. Vac. Sci. Technol. B: Microelectronics and Nanometer Structures* 32 (2014), <https://doi.org/10.1116/1.4866399>, 03D115-03D115.
- [56] M. Caglar, S. Ilican, Y. Caglar, Influence of dopant concentration on the optical properties of ZnO: in films by sol-gel method, *Thin Solid Films* 517 (17) (2009) 5023–5028, <https://doi.org/10.1016/j.tsf.2009.03.037>.
- [57] W. Al-Taa'y, M. Abdul Nabi, R.M. Yusop, E. Yousif, B.M. Abdullah, J. Salimon, N. Salih, S.I. Zubairi, Effect of nano ZnO on the optical properties of poly(vinyl chloride) films, *International Journal of Polymer Science* 2014 (2014) e697809, <https://doi.org/10.1155/2014/697809>.
- [58] O.R. Vasile, I. Serdaru, E. Andronescu, R. Truşcă, V.A. Surdu, O. Oprea, A. Ilie, B.Ş. Vasile, Influence of the size and the morphology of ZnO nanoparticles on cell viability, *Compt. Rendus Chem.* 18 (12) (2015) 1335–1343, <https://doi.org/10.1016/j.crci.2015.08.005>.
- [59] G.M. Abdelghani, A.B. Ahmed, A.B. Al-Zubaidi, Synthesis, characterization, and the influence of energy of irradiation on optical properties of ZnO nanostructures, *Sci. Rep.* 12 (1) (2022), <https://doi.org/10.1038/s41598-022-24648-x>. Article 1.
- [60] R.R. Reddy, Y.N. Ahammed, A study on the Moss relation, *Infrared Phys. Technol.* 36 (5) (1995) 825.
- [61] O. Gh. Abdullah, S.B. Aziz, K.M. Omer, Y.M. Salih, Reducing the optical band gap of polyvinyl alcohol (PVA) based nanocomposite, *J. Mater. Sci. Mater. Electron.* 26 (7) (2015) 5303–5309, <https://doi.org/10.1007/s10854-015-3067-3>.
- [62] L.E. Brus, Electron–electron and electron-hole interactions in small semiconductor crystallites: the size dependence of the lowest excited electronic state, *J. Chem. Phys.* 80 (9) (1984) 4403–4409, <https://doi.org/10.1063/1.447218>.
- [63] N.S. Pesika, K.J. Stebe, P. Searson, Determination of the particle size distribution of quantum nanocrystals from absorbance spectra, *Adv. Mater.* 15 (2003) 1289–1291, <https://doi.org/10.1002/adma.200304904>.
- [64] M.K. Debanath, S. Karmakar, Study of blueshift of optical band gap in zinc oxide (ZnO) nanoparticles prepared by low-temperature wet chemical method, *Mater. Lett.* 111 (2013) 116–119.
- [65] S. Jankovic, D. Gajic, T. Okolić, D. Jelić, Preparation and Characterization of ZnO Nanoparticles by Solvent Free Method, *Contemporary Materials* 9 (2018), <https://doi.org/10.7251/COMEN1801048J>.

Cite this: *Sustainable Food Technol.*,  
2024, 2, 689

## Microbial bioconversion of food waste to bio-fertilizers†

Pramod Kumar Mahish,<sup>a</sup> Dakeshwar Kumar Verma,<sup>b</sup> Anjali Ghritlahare,<sup>c</sup>  
Charu Arora<sup>d</sup> and Paz Otero<sup>e</sup>

Food waste is a matter of concern in our society. A large amount of waste has been reported in municipalities (households, markets, food courts, and ceremonies), the agriculture sector, food-based industries and airports. Food wastage involves economic losses and entails the use of resources and has an environmental impact that could be avoided by educating society in environmental values and looking for new revalorization strategies. Food waste contains organic matter in a rich amount which depends on the type of waste such as oils, fruits, agro-industrial waste, bakery, dairy, meat etc. A number of strategies are applied for the management of food waste such as recycling, bioconversion, animal feed etc. Among them microbial bioconversion is now becoming popular. It employs a biochemical process in which organic waste is converted into manure that improves soil quality while taking part in the sustainable development of society and contributing to our environment. Some bacteria, fungi, and actinomycete fermentations have been described to perform this upcycling since they present many advantages such as ease, safety, cost-effectiveness, eco-friendliness, and a rapid process. A microbial bio-converted fertilizer also meets quality and safety which enhances the growth of crops. Therefore, the present work aims to present the sources and types of food waste, recent food waste scenarios around the world, the diversity of microbes that convert food waste to fertilizers, the mechanism of bioconversion, and the use of the converted fertilizer.

Received 8th March 2023  
Accepted 19th January 2024

DOI: 10.1039/d3fb00041a

rsc.li/susfoodtech

### Sustainability spotlight

Food waste is a matter of concern in our society. In this context, the use of microbial capacity to decompose organic matter is a very vibrant technique to valorize food waste. Several sources and types of food waste such as waste cooking oils, agro-industrial wastes such as vegetables, fruit, juice, wheat, rice, potato, sugarcane, bakery waste, dairy waste and different types of meat, fish and poultry wastes have been proven to be profitable sources for their use for bioconversion. And some bacteria, fungi, and actinomycete fermentations have been described to perform this upcycling since they present many advantages such as ease, safety, cost-effectiveness, eco-friendliness, and a rapid process. The present work aims to present the sources and types of food waste, recent food waste scenarios around the world, the diversity of microbes that convert food waste to fertilizers, the mechanism of bioconversion, and the use of the converted fertilizer.

## 1. Introduction

According to the Food and Agriculture Organization (FAO), the difference between food loss and food waste is that the former

refers to loss of food due to quantitative or qualitative reasons, whereas if the food is expired or soiled due to carelessness of the consumer, then it is defined as food waste.<sup>1</sup> In addition, the FAO points out that food waste is a waste of inputs, land, and labor (FAO 2011).<sup>2</sup> In parallel, the EPA explains that it is a little different than that in a residence or commercial establishment where uneaten food or food preparation residues have been known as food waste.<sup>3</sup> Therefore, food waste is foodstuff of all types excluded from the food supply chain fit for the consumption of humans. While 98% of the hunger population lives in developing countries among which 15% suffer from malnutrition<sup>4</sup> and nutritional deficiency and hunger challenges, that billions of people are suffering nowadays,<sup>5</sup> the situation in developed societies is entirely different. From one side, wealthier civilization with home delivery, better food chain systems, and supermarkets act as simple accessibility of food;

<sup>a</sup>Department of Biotechnology, Govt. Digvijay Autonomous Postgraduate College Rajnandgaon, Chhattisgarh, 491441, India

<sup>b</sup>Department of Chemistry, Govt. Digvijay Autonomous Postgraduate College Rajnandgaon, Chhattisgarh, 491441, India. E-mail: dakeshwarverma@gmail.com

<sup>c</sup>Subject Matter Specialist (Soil Science), KVK Rajnandgaon (Affiliated to Indira Gandhi Agriculture University), Raipur, Chhattisgarh, 491441, India

<sup>d</sup>Department of Chemistry, Guru Ghasidas (Central) University Bilaspur, Chhattisgarh, 495009, India

<sup>e</sup>Analytical & Food Chemistry Department, Faculty of Science, University of Vigo, E32004 Ourense, Spain. E-mail: paz.otero@uvigo.es

† Electronic supplementary information (ESI) available. See DOI: <https://doi.org/10.1039/d3fb00041a>



however, this modern food delivery scenario brings challenges in terms of urban food waste increase and thus, has an impact on the environment and sustainable development and food safety and security.<sup>6</sup> In addition, the anaerobic digestion of food waste makes a contribution to the greenhouse gases in the environment.<sup>7</sup> Leachate is another environmental challenge linked to food waste. Apart from environmental challenges, several other difficulties arise from food waste, which are listed in Fig. 1. In this context, food safety and security are a globally important challenge nowadays because they are sandwiched between the commodity demand increase from the increase in population and the shortage of agricultural land due to urbanization and industrialization.<sup>8</sup> Increasing consumption rates and shrinking crop areas are major concerns related to sustainable food demand.<sup>9</sup> Related to safety and security, wasting food is another burning issue, of which about one-third is produced for human feasting.<sup>2</sup> This is related to post-harvesting, pre-consumption, and post-consumption levels. An increase in greenhouse gases is directly proportional to food waste.<sup>10</sup> Food waste creates a burden on production and demand which reflects the use of crop fields, the use of irrigated water, manpower & inputs, and fertilizers.<sup>11</sup> The loss of biodiversity is also related to habitat destruction by agricultural areas.<sup>12</sup>

In industrialized countries, governments and authorities demand limitations on waste generation in the whole food supply chain, commencing with primary production, processing, and whole food distribution, in individual households, restaurants and food services. Households account for up to 45% food waste and its amount is increasing over time.<sup>13–16</sup> In a recent study of Russia, overproduction and consumer leftovers have been found to be the reasons for food waste and about 14 tons of food waste was averaged per restaurant per year.<sup>17</sup> The United States Department of Agriculture-The Economic Research Service (USDA-ERS) (USA), Waste &



**Dakeshwar Kumar Verma**

Department of Chemistry, Govt. Digvijay Autonomous Postgraduate College, Rajnandgaon, Chhattisgarh, India 491441 [dakeshwarverma@gmail.com](mailto:dakeshwarverma@gmail.com). Dr Dakeshwar Kumar Verma, holding a PhD, serves as an Assistant Professor of Chemistry at Govt. Digvijay Autonomous Postgraduate College in Rajnandgaon, Chhattisgarh, India, with the postal code 491441. Driven by a profound passion for scientific exploration, his research focuses primarily on the preparation and design of organic compounds for diverse applications. With an impressive track record, Dr Verma has authored over 100 research papers, review articles, and book chapters that have found their place in esteemed peer reviewed international journals, including those published by ACS, RSC, Wiley, Elsevier, Springer, and Taylor & Francis, among others. This extensive body of work showcases his dedication to contributing to the collective knowledge of the scientific community. Beyond his role as an author, Dr Verma is an active and valued participant in the peer-review process. He serves as a reviewer for high-impact journals such as the *Journal of Molecular Liquids* (Elsevier), *Materials Chemistry and Physics* (Elsevier), and *Scientific Reports* (Nature), underscoring his commitment to maintaining the rigor and quality of scientific research. As a testament to his academic influence, Dr Verma has taken on editorial responsibilities (editor and author) for published as well as upcoming books slated to be published by renowned publishers such as ACS, RSC, Wiley, Taylor & Francis, Elsevier, Springer and De Gruyter. This role highlights his dedication to shaping and disseminating knowledge in various scientific domains. With a cumulative citation count of over 1800, an h-index of 24, and an i-10 index of 34, Dr Verma's impact is evident through the recognition and relevance of his work in the scientific community. Furthermore, his commitment to fostering the growth of future scholars is evident in his supervision of two full-time PhD research scholars. Dr Verma's dedication to research excellence has been acknowledged through prestigious awards such as the Council of Scientific and Industrial Research Junior Research Fellowship award in 2013. During his PhD journey in 2013, he also availed of the MHRD National Fellowship, further solidifying his commitment to academic growth and advancement. In essence, Dr Dakeshwar Kumar Verma's biography exemplifies his unwavering dedication to advancing the realm of chemistry through prolific research contributions, editorial engagements, and mentorship of emerging scholars. His multifaceted role as a researcher, reviewer, editor, and mentor underscores his substantial impact on the academic landscape. Google Scholar link: <https://scholar.google.com/citations?user=J663VtkAAA&hl=en>, SCOPUS link: <https://www.scopus.com/authid/detail.uri?authorId=56835167300>, WOS/PUBLONS ID: <https://publons.com/researcher/4446851/dr-dakeshwar-kumar-verma>.



**Pramod Kumar Mahish**

Pramod Kumar Mahish is presently serving as Assistant Professor of Biotechnology at Govt. Digvijay Autonomous Postgraduate College, Rajnandgaon (Chhattisgarh), India, with the postal code 491441. He had 10 years of teaching and 13 years of research experience. Dr Mahish had published 21 research papers, 10 books and 21 book chapters (including Wiley, Springer, De-Gruyter, Elsevier and IGI). He had completed 3

research projects and is presently guiding 2 PhD scholars. He has received a UGC National Fellowship (New Delhi) for doing his PhD. He is also a fellow member of the World Researchers Association. Dr Mahish is engaged in the editing of 2 books on the American Chemical Society and Tylor and Francis platforms.



Resources Action Programme (WRAP) (UK), FAO (UN) and UNEP (UN) are some national agencies and organizations of government that are actively engaged in the prevention of food waste and FUSION and REFRESH programs have been funded by the European Commission for sustainable utilization of food resources.<sup>18</sup> The quantification of food waste in each sector and food chain process plays an important role in the global management of food waste. Bakery products such as bread, fruits and vegetables, and meat have been recorded as a major proportion of urban food waste.<sup>19</sup> Apart from these, cereals, root crops, oilseeds, dairy, and fish waste form 20–50% of the waste

worldwide.<sup>2</sup>

Food waste could be mainly measured by direct and indirect methods. Direct methods are based on measuring, counting and waste composition analysis, *i.e.*, based on the primary data of infield observation. For example, weighing is one of the traditional direct methods by which food waste can be weighed in hospitals, households, schools, restaurants, *etc.*<sup>20</sup> In the household collection of garbage, waste is collected from homes and food waste is separated from others to measure the actual quantity.<sup>21</sup> When physical access to food waste is not possible, then the application of indirect methods with the use of coefficients and mass balance is employed. Indirect methods use statistical tools, modern computational software, and modeling based on mathematical formulae to estimate the quantity of food waste, so that data from indirect measurement are derived from the primary record of the direct method. In the EU, the most recommended method for all processes in the agri-food supply chains is the direct measurement and analysis of the waste composition.<sup>22</sup>

### 1.1 Methodology

The most popular bibliographic databases have been used to search for literature in the study *viz.* Scopus, Web of Science and Google Scholar. The key words used are – “Food waste”; “Food loss”; “Biofertilizer from food”; “Bioconversion of food waste”; “Valorization of food waste” and so on. The literature obtained from the database has been filtered. Books and review and research articles have been selected and other literature has been eliminated. Literature published in English has been selected and literature in other languages has been excluded. Valorization of food waste other than microbial methods was also excluded. Literature studies were also selected according to the publication period. The selected literature studies have been read and analyzed to satisfy the objective of the study.



**Anjali Ghritlahare**

*Anjali Ghritlahare is presently working as Subject Matter Specialist of Soil Science at Krishi Vigyan Kendra (Agriculture Science Centre) in Rajnandgaon affiliated with Indira Gandhi Agriculture University, Raipur (Chhattisgarh), India. She has obtained her Bachelors (Agriculture) from the BTC College of Agriculture & Research Station, Sarkanda, Bilaspur, India and Masters (Soil Science) from Junagarh*

*Agriculture University, Gujrat, India. She has been engaged in the research, extension, field trials and training of farmers since 2012. She was awarded a gold medal as a merit student in her MS program. Her former institute was awarded the Best National Institute Award in 2017.*



**Charu Arora**

*Dr Charu Arora, working as Professor of Chemistry at Guru Ghasidas University (a central university), Bilaspur, C. G., India, has 21 years of teaching and research experience. Her areas of interest and research are Environmental Chemistry, Kinetics and Natural Product Chemistry. She has completed her PhD and postgraduation in Chemistry at GK University, Haridwar and the Indian Institute of Technology, Roorkee in*

*2003 and 1995 respectively. She received the SARC Gold Medal Award 2011 conferred by the Scientific and Applied Research Centre, CCS University, Meerut for her outstanding contribution in the field of Chemistry Research. She has published more than 60 research papers, one book and 17 book chapters with reputed publishers *viz.* Elsevier, Bentham Science, Wiley, Academic Excellence, Springer *etc.* Dr Arora is an editor, co-editor and author of several books on the Wiley science, Elsevier and De-Gruyter platforms.*



**Paz Otero**

*Dr Paz Otero received her bachelor's degree in Food Science from the University of Santiago de Compostela (USC), Spain, in 2006. She obtained a PhD from the Pharmacology Department of the Veterinary Faculty at the same university. Dr Otero has held postdoctoral research positions at the Limerick Institute of Technology, Ireland (2014–2017), and the Institute of Food Science Research, Autonomous University of Madrid (2017–*

*2018). She has published extensively in the fields of food chemistry, toxicology, analytical chemistry, and nutrition with more than fifty-three research articles, seventy contributions to international congresses, and ten book chapters to her credit. Dr Otero also serves as an invited reviewer for several research journals and a guest editor for special issues.*



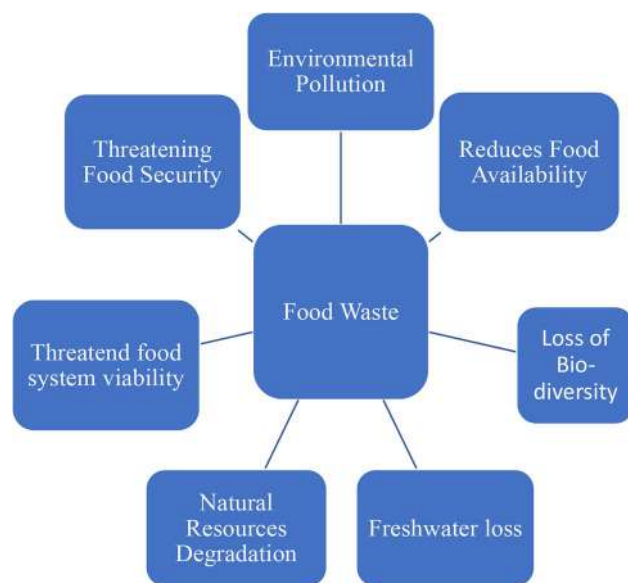


Fig. 1 Effect of food waste on the environment and sustainable development.

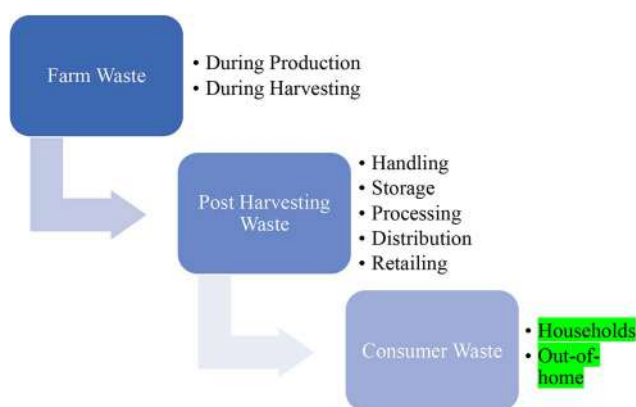


Fig. 2 Loss of food waste in the various steps of food production and transport to the consumer.

## 2. Sources and management of food waste

Households and surroundings that are directly or indirectly related to individuals are the major sources of food waste after production and processing.<sup>23</sup> Our neighbors, friends, educational institutes, markets, and working places such as physical settings influence the wastage of food.<sup>24</sup> In a household, dependence on each other, togetherness, and structure of the family affect the use or misuse of food.<sup>25,26</sup> Fig. 2 indicates a step-by-step loss of food from land to the consumer and Fig. 3 is related to the reasons for food losses in the different steps. The quantification of overall waste in the food chain is a little challenging because it depends on harvested items, situation, process utilized *etc.* A study in the US suggests about 20% food waste at the production stage, 20% in processing and

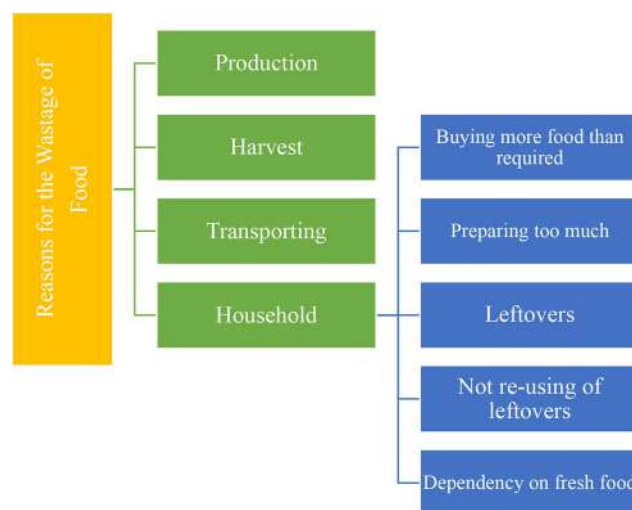


Fig. 3 Reasons for the wastage of food from production to use in households.

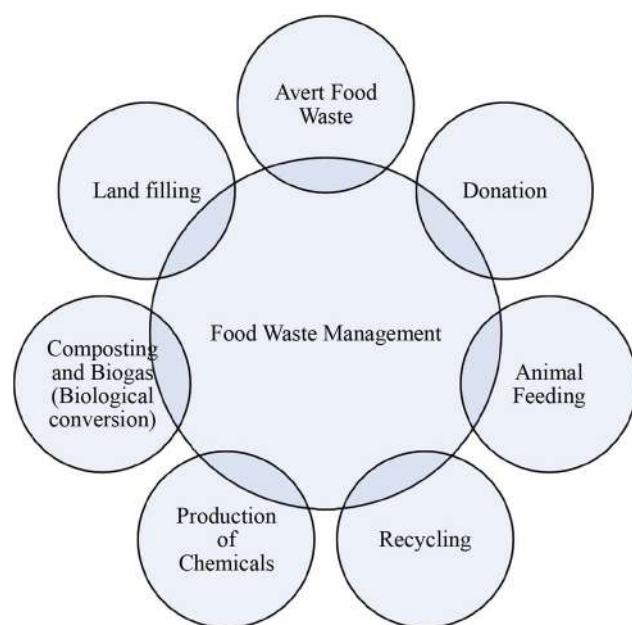
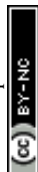


Fig. 4 Main management strategies for food waste.

distribution and the rest (60%) in the consumption stage.<sup>27</sup> Food losses are also observed to be much higher in low-income countries due to infrastructure, deprived technology, a lack of awareness about environmental parameters and market coordination.<sup>28</sup> About 26% of food waste is recorded at the production stage in South Africa and nearly half (13%) is observed in Canada in the overall food chain. These data may vary according to foods such as cereals, fruits and vegetables and meats. Post-harvest food waste also depends on the food type. Cereal waste was observed to be maximum at post-harvest and storage steps; fruit and vegetables at the production step; meat, fish, milk and eggs at the retailing step due to a lack of coolant facility. Household or consumer waste is more in high



income countries. About 40–50% household food waste has been recorded in the European Union and Canada.<sup>29</sup>

There are several possibilities for managing food waste.<sup>43</sup> Averting food waste, landfills, donations, animal feeding, recycling, production of chemicals, composting and biogas are among the most applied waste management methods on large and moderate scales (Fig. 4). All of them show advantages and disadvantages (Table 1). For example, in a fast urban lifestyle averting food waste is not possible except for some exceptions. Landfilling is a simple disposal practice; however, it presents some environmental concerns since in the long term, this method can produce contamination and pollution of the surrounding environment with a negative impact on air and groundwater.<sup>30</sup> In addition, it contributes to leachate

production, unpleasant smell around the site and sources of pathogenic microorganisms. Animal feeding is a common method found in countries with a high demand for animal food such as South Korea and the United States since it does not lead to negative environmental impacts.<sup>44</sup> Nevertheless, this is not a profitable method for low livestock production countries. Moreover, it has to follow strict guidelines as in the case of low salt content or caffeine free products, as they can cause harmful effects on animals.<sup>34</sup> Donation is another waste management practice currently successfully implemented in the UAE in which supermarkets, hotels and restaurants donate excess food to families in need. However, the collected food for donation represents a very small amount of the total waste. Other management methods, such as recycling food waste, seem very

**Table 1** Advantages and disadvantages of some possible management methods for food waste

S. no.	Method of management	Advantages	Disadvantages	References
1	Landfill	Easy method; no tools/equipment required; no need for scientific knowledge	Contamination and pollution; negative impact on groundwater; emission of greenhouse gases; unpleasant odor; leachate formation; growth of mosquitoes and other insects	6 and 30
2	Donation	Fulfills the needs of underprivileged communities	Improper disposal of food by the receiver	31
3	Animal feed	No environmental impact; more nutrients for animals	Risk of contamination for animals	32
4	Pyrolysis	No emission of harmful gases; conversion to biofuels and biochar	Needs equipment setup with high energy requirements	33
5	Incineration	No need for land; minimum requirement of human resources; generation of energy from waste	Release of toxic gas and ash; need for setup	34 and 35
6	Gasification	Less environmental concern; production of future fuels	High temperature and high energy requirement; release of hydrocarbons and ash	36
7	Transesterification	Minimizes soil and water pollution by oils; production of biodiesel from waste oil	Complex methodology; requirement of high energy; release of water	37 and 38
8	Composting	Bioconversion to green manure; no environmental concern; bioremediation of harmful chemicals	Very slow process; need for setup with skilled knowledge; generates unpleasant smell	39
9	Anaerobic digestion	Bioconversion of food waste to green manure and biogas; no environmental concern	Need for a digester; low capacity; needs scientific knowledge to maintain pH and temperature	40
10	Anaerobic fermentation	Bioconversion of food waste to alcohols and acids; production of future fuels and green manure; less emission of CO <sub>2</sub> and greenhouse gases; high efficiency	Need for a fermenter or reactor; costly method; need for scientific knowledge; difficulty in product recovery	41
11	Hydrogen production	Bioconversion of food waste to green energy; use of byproducts as manure	Need for production setup with skilled manpower; low capacity	42





Fig. 5 Scheme of organic fertilizer and biogas energy production from household food waste [Copyright 2022 @ BioEnergy Consult from Zafar S.<sup>46</sup> source: <https://www.bioenergyconsult.com/renewable-energy-food-residuals/>].

poor because of their rapid degradation. On the other hand, chemical conversion methods are relatively new and only implemented recently at a moderate scale; therefore they still need intensive implementation and development. Finally, composting is a suitable method for the management of food waste that involves the conversion of organic matter to ammonia-nitrogen, carbon dioxide or humic substances under an aerobic atmosphere.<sup>45</sup> The collection of food waste in wheeled bins followed by the separation of waste on the basis of texture (dryness or wetness), source (organic or synthetic), nature (metallic or nonmetallic) and approach (recyclable or non-recyclable) is increasing in developed countries. Fig. 5 shows the organic fertilizer and biogas energy production process from household food waste. In this sense, household food waste can be recycled into biogas energy and organic fertilizers. However, the fertilizer can be used to improve crop growth, which could be beneficial for society and biogas generation could not fulfill the high demand of society.

### 3. Organic composition and valorization of some food waste

In general, food waste has a good nutritional value because it is rich in high quality organic nutrients since it was intended for human consumption (see the figure in the ESI†). Produce from farms, restaurants, and manufacturing facilities, such as fruits, vegetables, meats, and cereals, make up the majority of food waste that affects every aspect of daily life. Plant-based food losses from the farming land to the customer are over 40% and cumulative. This contains vegetables which are not gathered due to inappropriate maturity, do not satisfy strict excellence stipulations by the superstores, and are disallowed harvests or parts or fiber/pomace after extracting juice by processing industries.<sup>47</sup> However, food waste typically has high moisture content in the range of 50–85%, which reduces shelf-life and makes food waste collection and use for animal feeding difficult

because of the possible spoilage.<sup>32</sup> Therefore, a good option is its use for bioconversion. The nutritional composition of some food waste is presented in Fig. 6.

#### 3.1 Waste cooking oils

Cooking oil waste is rich mainly in saturated fatty acids such as palmitic acid, monounsaturated fatty acids such as oleic acid

Waste Cooking oils	• Saturated and polyunsaturated fatty acids
Fruit and Juices Waste	• Polysaccharides, proteins, fibers, pectin
Wheat and Rice	• Cellulose, hemicellulose, lignin, pectin
Potato and sugarcane	• Fructose, sucrose and glucose, cellulose, lignin, and fiber
Bakery waste	• Starch, sucrose, fructose, lipids, phosphorus
Dairy waste	• Lactose, fatty acids, whey protein and casein
Meat, fish, and Poultry waste	• Amino acid and Fatty acids
Vegetable waste	• Protein, lignin, cellulose, hemicellulose, pectin

Fig. 6 Organic matter of some common food waste for possible valorisation to biofertilizers.



and polyunsaturated fatty acids such as linolenic and linoleic acids.<sup>48,49</sup> Due to this composition, cooking oils have been biologically converted into fuel, acids, metabolites, enzymes, polymers, *etc.*, using microorganisms. Biodiesel is one of the important products obtained from waste cooking oils.<sup>48,50</sup> Waste cooking oils have been observed as the source of lactic acid and citric acids bio-converted by *Rhizopus* microspores and *Lichtheimia corymbifera*.<sup>51,52</sup> Metabolites such as polyhydroxyalkanoates and carotenoids were produced from the waste of cooking oil by *Paracoccus* sp. strain LL1.<sup>53</sup> Bioplastics are another important product produced from *Escherichia coli* in the presence of waste cooking oils as substrates.<sup>54</sup> *Lichtheimia corymbifera* is also used for the production of single-cell oils and lipase from waste cooking oils.<sup>52</sup>

### 3.2 Fruit and juice waste

Fruit waste has been reported worldwide because of its high content of protein, fiber, and carbohydrates which could be recovered and re-used. Waste oranges contain D-limonene, a type of monoterpene.<sup>55</sup> Cellulose, hemicellulose, pectin, lignin, and sugar have been reported from pineapple waste.<sup>56</sup> Similarly, banana peel is rich in various organic materials such as polysaccharides, proteins, fibers, and pectin.<sup>57</sup> Fiber, proteins, and lipids are the major components of waste pomegranates and tangerines.<sup>58,59</sup> The bioconversion of waste fruit and juices is a virtuous idea because many fruits contain only 30–50 percent edible parts while the other part is related to the peel that generally wastes after fruit consumption. Tangerine biomass has 40–50% peel, pomegranates 50%, and bananas have 30–40% peel.<sup>60</sup> Therefore, half of the fruit contains waste having organic materials which possibly valorizes useful products. Methane as a source of fuel has been obtained from the bioconversion of passion fruit peel, cashew bagasse, and D-limonene of orange peel by the presence of microbes in anaerobic digestion.<sup>55,61</sup> Biologically derived adsorbents have been obtained from pomegranate peel, orange juice, and tangerines.<sup>60,62</sup> Biosorbents produced from the pomegranate peel and orange juice were able to remove phenol from the wastewater. Orange peel has been biologically converted to bioelectricity by *Pseudomonas*<sup>63</sup> while bio-pigments are produced by *Monascus purpureus* ATCC 16365 and *Penicillium purpurogenum* CBS 113139.<sup>64</sup> Orange peel waste is also used to produce biofertilizers.<sup>65</sup> Pineapple waste has been utilized for the production of ethanol, phenolic anti-oxidants, citric acid, lactic acid, biogas, and fiber, those are achieved by *Saccharomyces cerevisiae* and *Zymomonas mobilis* (ethanol), *Rhizopus oligosporus* (phenol), *Aspergillus niger* (citric acid) and *Lactobacillus lactis* (lactic acid).<sup>56</sup> Biochar and environmentally friendly substances have been produced from the banana peel.<sup>66</sup> Banana peel is also used for the synthesis of single cell proteins biologically converted by *Rhodotorula glutinis* NRRL Y-1091 and *Ganoderma wiiroense*.<sup>67</sup> Biofertilizers and biogas have been produced from peels of fruits such as pomegranates, sweet lime, bananas, and tangerines.<sup>60,65</sup>

### 3.3 Agro-industrial waste – wheat and rice

Agro-industrial waste is a rich source of cellulose, chitin, hyaluronic acid, inulin, and pectin, *i.e.*, organic nutrients which are

important substrates for biochemical conversion.<sup>68</sup> For example, paddy straw and wheat straw particularly contain cellulose, hemicellulose, and lignin.<sup>69</sup> In this sense, agro-industrial waste has been converted to cellulase, xylanase, and other industrially important enzymes with the aid of microorganisms such as *Aspergillus flavus* under solid-state fermentation.<sup>70,71</sup> Economically significant acids such as acetic acid have been produced from agro waste by fermentative bacteria *Bacillus* sp. PM06 and butyric acid is obtained from *Clostridium tyrobutyricum*.<sup>72,73</sup> Similarly, vanillic acid is synthesized from corn bran biologically converted by *Pseudomonas putida* KT2440.<sup>74</sup> Future fuel bioethanol is synthesized from agro waste by *Bacillus* sp. PM06, *Saccharomyces cerevisiae* MTCC 4780 and mushrooms.<sup>72,75,76</sup> Other future energies such as biohydrogen, bioelectricity, and biobutanol were also produced from agro-industrial waste.<sup>76</sup>

### 3.4 Agro-industrial waste – potato and sugarcane

Potatoes are composed of carbohydrates, especially starch. Potatoes contain three main types of sugars: fructose, sucrose and glucose and other compounds such as cellulose, hemicellulose, lignin, and fiber.<sup>77</sup> In the study, ash, proteins, lipids, total sugar, fiber, starch, and phosphorus were recovered from potato processing waste.<sup>78</sup> Bioethanol is obtained from the waste of sugarcane biochemically converted by *Saccharomyces cerevisiae*.<sup>79</sup> Sugarcane bagasse is used for the production of biohydrogen by the thermophilic Clostridiales consortium.<sup>42</sup> In this study, hydrogen production (1.71 mL H<sub>2</sub> per mL culture) and yield (586.19 mL H<sub>2</sub> per g carbohydrate) produced by Clostridiales were augmented by 113.75% and 32.48% equated with that of fermentation from solely pretreated sugarcane bagasse.

Mannooligosaccharides are obtained from potato peel and sugarcane bagasse by *Penicillium oxalicum* KUB-SN2-1.<sup>80</sup> *Monascus rubber* has been used for the production of natural pigments from sugarcane.<sup>81</sup> Lactic acid has been obtained from the nutrients available in the waste of potatoes from the conversion of *Lactobacillus pentosus*.<sup>82</sup> Sugarcane molasses is used for the production of polyhydroxybutyrate, a bioplastic produced by the action of *Bacillus cereus* 2156.<sup>83</sup> Another biodegradable composite has been obtained from the waste of potato and sugarcane bagasse.<sup>84</sup> *Cellulomonas* sp., *Klebsiella* sp., *Proteus* sp., *Enterobacter* sp., and *Salmonella* sp. have been used to obtain organic compost. This compost was found to be rich with carbon content (26.75%) and C:N ratio (12.44%). In parallel, it increased the nitrogen (2.34%), phosphorus (1.15%), and potassium (1.37%) content along with the population of microorganisms *i.e.*, bacteria, fungi, and actinomycetes.<sup>85</sup>

### 3.5 Bakery waste

Bakery waste contains high protein materials, although this waste is also rich in starch, sucrose, fructose, lipids, phosphorus, *etc.*<sup>86</sup> Due to the availability of such nutrients, bakery waste has been used as a media nutrient for the growth of bakery yeast.<sup>87</sup> Succinic acid is one of the important products synthesized from bakery waste biologically converted from





*Actinobacillus succinogenes*.<sup>86,88</sup> *Thermomyces* sp. and *Monascus purpureus* have been studied to produce some important enzymes such as glucoamylase<sup>89,90</sup> and protease<sup>89</sup> from bakery waste. Future fuels bioethanol and biohydrogen have also been produced from bakery waste by the action of *Saccharomyces cerevisiae*<sup>91</sup> and *Rhodo pseudomonas palustris* 42OL.<sup>92</sup> Bakery waste is utilized for the production of bio-pigments by *Monascus purpureus*<sup>89</sup> and lactate by *Lactobacillus amylovorus* DSM 20532.<sup>92</sup> Environmentally friendly bioplastic (PBH) has also been obtained from the waste of bakeries.<sup>88</sup>

### 3.6 Dairy waste

Dairy waste is mainly composed of lactose and fatty acids. The other components are whey protein and casein.<sup>93,94</sup> Dairy waste is converted to bioethanol by *Lactococcus lactis*.<sup>95</sup> Lactose bioconversion has also been used for the production of bioethanol by microbes.<sup>96</sup> Another future fuel biodiesel is produced from dairy wastewater by *Chlamydomonas polyphyrenoideum*.<sup>97</sup> By the action of microbes, bioplastics and biosurfactants have also been produced from the waste of dairy.<sup>98</sup> Single-cell proteins are another valuable product obtained by microbial action from dairy waste<sup>96</sup> and panner whey.<sup>99</sup> *Kluyveromyces marxianus* was used for the production of single-cell proteins from paneer whey. Kasmi<sup>96</sup> also used lactose bioconversion for the production of lactic acid, citric acid, and biopolymers from dairy waste. Green manure has been obtained from the conversion of *Hermetia illucens* from dairy waste.<sup>100</sup> Similarly, a liquid biofertilizer was obtained from dairy waste by the action of some geosphere microbes.<sup>101</sup>

### 3.7 Meat, fish, and poultry waste

Animal meat and its waste contain a high volume of fatty acids and amino acids. Fatty acids – palmitic acid, eicosapentaenoic acid (EPA), and docosahexaenoic acid (DHA) have been recorded in some fish such as pink perch (*Nemipterus japonicus*), Indian mackerel (*Rastrelliger kanagurta*) and Indian oil sardine (*Sardinella longiceps*).<sup>102</sup> *Lactobacillus plantarum* has been used for fish waste fermentation and the product was utilized as broiler chicken feed.<sup>103</sup> Similarly, microbial bioconversion has been utilized to produce biodiesel/biogas, dietetic products (chitosan), natural pigments, and cosmetics (collagen) from the waste of fish.<sup>104</sup> Bioactive peptides have been obtained from the waste of meat and have relevant physiological effects such as antihypertensive, antioxidant, antidiabetic, and antimicrobial.<sup>105</sup> Waste bone meal and meat were utilized as absorbents for the removal of lead from the aqueous solution.<sup>106</sup> Protein hydrolysates, enzymes, and polyunsaturated fatty acids have been recovered from chicken waste.<sup>107</sup> High protein feed and gelatin are utilized in the food industry and cosmetics have been obtained from the waste of meat.<sup>108</sup> Biofuel has also been produced from the same waste. Biofertilizers are also obtained from the conversion of waste from meat and poultry<sup>108,109</sup> *Aspergillus niger* was utilized for the conversion of poultry waste to biofertilizers. Similarly, *Bacillus megaterium* has been used for the production of liquid phosphate fertilizers from the waste of animal bones.<sup>110</sup>

### 3.8 Vegetable waste

Proteins, dry matter, organic matter, lignin, cellulose, hemicellulose, pectin, and digestible nutrients have been obtained from waste fruit and vegetables.<sup>111,112</sup> Lignin (19%), hemicellulose (14%), cellulose (50%), and pectin have been specially obtained from tomato waste.<sup>113</sup> Vegetable waste has been biologically converted to so many types of valuable products with the aid of microbial conversion. Lactic acid was obtained from the waste of vegetables by the conversion of lactic acid bacteria and *Penicillium* sp. The same waste is used to get protein extracts by *Bacillus subtilis*, *Rhizopus oligosporus*, and *Fusarium flocciferum*. *Aspergillus*, *Yarrowia*, and *Trichoderma* species have been used to obtain carbohydrates and glycosidases from the above waste.<sup>114</sup> Leafy vegetable waste contains pigments of photosynthetic importance. Pigments such as anthocyanins, betalains, carotenoids, and chlorophylls have been obtained by Usmani *et al.*<sup>98</sup> and have been used in the food, pharma, and cosmetic industries. Several bioactive compounds such as antioxidants, oils, fiber, fatty acids, isoprenoids, lipids, proteins, saponins, and phytoestrogens have been isolated from vegetable waste by Jiménez-Moreno *et al.*<sup>115</sup> Nano-emulsions of some bioactive compounds such as carotenoids and polyphenols have also been made from vegetable waste by Saini *et al.*<sup>116</sup> Bayram *et al.*<sup>117</sup> synthesized food packing materials such as biopolymers and bio-composites, edible films, and coatings from the waste of vegetables. Valuable products such as fermented beverages, single-cell proteins, single-cell oils, bio-colors, flavors, fragrances, polysaccharides, biopesticides, and plant growth regulators have been obtained from the waste of vegetables through the conversion of microbes.<sup>118</sup> Sources of energy such as bioethanol, biogas, methane, and biohydrogen have been produced from the waste of vegetables by microbial action.<sup>113,118,119</sup> Vegetable waste has been biologically converted into biofertilizers by *Trichoderma reesei*.<sup>119</sup> A similar conversion was also noted by Fritsch *et al.*<sup>113</sup> from the waste of tomatoes.

## 4. Mechanism of bioconversion of food waste by microbes

A number of microbial groups have demonstrated their ability to convert food waste to valuable products. These microbial groups mainly belong to bacteria, actinomycetes, yeast and molds. The microbes belong to various functional groups such as aerobic nitrogen fixers, ammonifiers, denitrifiers, and nitrifiers capable of converting nutrients from food waste to fertilizers and biogas.<sup>120</sup> To achieve this bioconversion microorganisms produce a number of enzymes *viz.* amylase, cellulase, xylanase and pectinase.<sup>121</sup>

The methods and mechanisms applied to the valorization of food waste into useful products play a very important role because the product quality is dependent on the process used. Food waste can be converted to produce different organic fertilisers and soil amendments by a wide range of biological, physical and chemical methods following different procedures such as composting, anaerobic digestion, dehydration, biochar production, and chemical hydrolysis. Among these, anaerobic



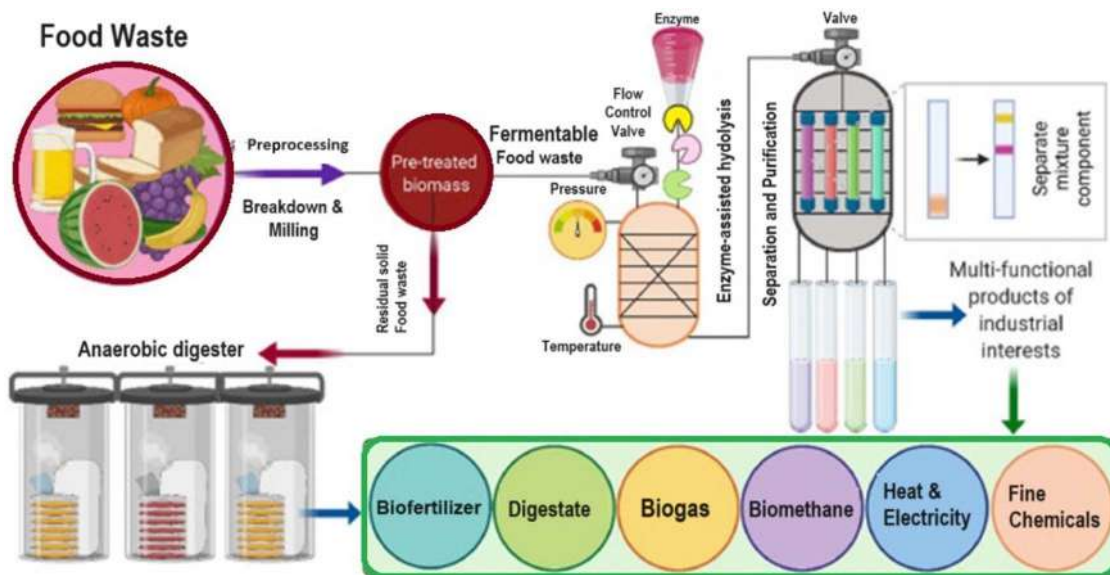


Fig. 7 Microbial bioconversion methods of food waste resulting in various valuable products including biofertilizers. This conversion is achieved by methods such as anaerobic digestion, composting, fermentation by microbes of microbial enzymes, etc. [Copyright © 2022 Elsevier from Sufficiency *et al.*<sup>133</sup>].

fermentation and composting are the main large-scale conversion methods currently used.<sup>122</sup> In addition, Fig. 7 represents some methods of microbial bioconversion of food waste to various products including biofertilizers. The incubation period, temperature, and moisture content parameters play a crucial role in the bioconversion of waste. However, emerging conversion methods for food waste such as biochar production, dehydration, and chemical hydrolysis have shown promising properties, which also makes them useful approaches for food waste bioconversion.<sup>123</sup> Sometimes both physical and biological approaches were used for the valorization of food waste. For example, Mahmood *et al.*<sup>124</sup> first utilized a household garbage dryer & processor for the valorization of vegetable and fruit peels and leftover food to dry the biomass, and then, favourable moisture waste was treated with *Aspergillus niger* UY2015\_11.

The bibliography shows a wide range of food waste bioconversion processes by anaerobic fermentation using different sources and types of microorganisms. For instance, an anaerobic digestion method was applied by Dahunsi *et al.*<sup>125</sup> for the bioconversion of *Carica papaya* (pawpaw) fruit peels into green fertilizers using bovine rumen as a source of microbes. For this, preliminary peel was converted to a slurry which was then treated with the rumen in a reactor to carry out the fermentation under anaerobic conditions for 28–34 days. Li *et al.*<sup>126</sup> utilized *Pseudomonas aeruginosa* for the digestion of kitchen waste to obtain biofertilizers. However, in this study, the authors used a glass flask to produce anaerobic conditions at the laboratory experimental scale. Fermentation strategies play an important role in direct production or enhancement of production of biomolecules. Various fermentation methods have been applied to produce astaxanthin from food waste by *Phaffia rhodozyma*.<sup>127,128</sup>

In another study, a 40-L-biogas reactor was utilized for biogas production from the digestion of boiled rice, boiled cassava products, bread, boiled yam, and boiled maize by using different genera of bacteria such as *Escherichia*, *Citrobacter*, *Bacillus*, *Pseudomonas*, *Proteus*, *Klebsiella*, *Clostridium*, *Bacteroides*, *Enterobacter*, *Staphylococcus*, *Salmonella*, *Streptococcus*, *Aspergillus*, *Mucor*, *Rhizopus* and *Penicillium*.<sup>129</sup> The biogas reactor design contained various manometers for temperature and pH control and a plastic tube for the collection of gas produced during digestion. Wang *et al.*<sup>130</sup> used a mixture of bread, cabbage, pork, and rice with sawdust for the composting and production of manure for seed germination. The mixture was placed in a 20-L reactor with a controlled temperature and moisture. After day 35 of incubation nutritional profiling and seed germination of compost have been carried out.

The composting method was also applied by Tsai *et al.*<sup>132</sup> in which a mechanical composter has been used to valorise food waste collected from restaurants. Initially, the food waste was chopped and mixed with sawdust to maintain moisture for favourable fermentation inside the composter. Strains of *Streptomyces thermonitrificans* NTU-88, isolate CH18, *Brevibacillus borstelensis* SH168 and *Bacillus stearothermophilus* ATCC 10149 were utilized for composting over 28 days. A typical composter was used by Sangamithirai *et al.*<sup>133</sup> for the bioconversion of vegetable and fruit waste. Mesophilic bacteria were responsible for the composting over 3 months with mixing at regular intervals. Composting of huge volumes of food waste was performed by Lin *et al.*<sup>134</sup> Sawdust and mature compost were mixed with about 800 kg of pre-sheared food waste and allowed for composting in a large reactor. Moisture content and temperature were maintained to allow for fermentation.



Stabnikova *et al.*<sup>135</sup> obtained organic fertilizers from the waste of some food materials. The mechanism was adopted as an aerobic bioconversion of food waste by the bacterial strain *Bacillus thermoamylovorans* SW25. It took 10 days to convert food waste into organic fertilizers in a pilot scale reactor. Jiang *et al.*<sup>136</sup> performed thermophilic anaerobic digestion reactions over 230 days with the aid of *Methano sarcina* and *Methano thermobacter* to digest food waste. Coffee pulp and husk were valorized by the method of composting by Dadi *et al.*<sup>137</sup> A mixture of coffee waste, cow dung, and rock phosphate was treated with *Bacillus megaterium* in a cement cistern. The compost was turned into a consistent interlude for up to 120 days. The final products were dried in shade and fortified with some minerals before application.

## 5. Advanced bioprocessing methods used for the conversion of food waste to fertilizers

The bioconversion of solid waste rich in organic matter is usually performed by conventional biowaste valorisation technologies such as anaerobic digestion or composting which have been widely adopted for food waste management. Some systematic techniques are presented in Fig. 8 describing the valorisation of food waste by microbes to meet the end product as a biofertilizer.

However, they can sometimes be limited due to their high operation costs, low recovery efficiency and system instability.<sup>138</sup> Advanced tools and techniques have emerged in the last few

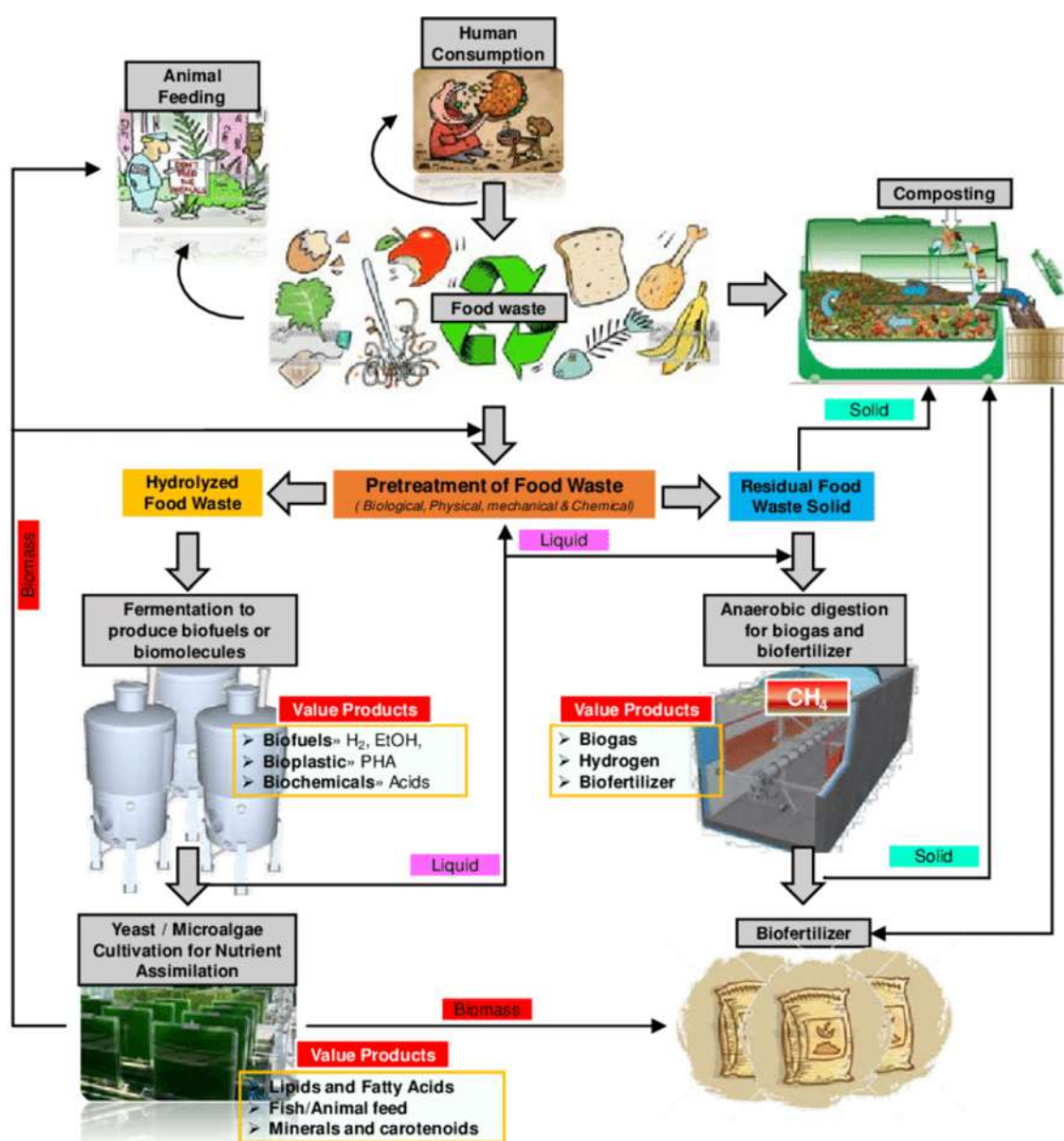
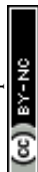


Fig. 8 Techniques and methods employed for the production of biofertilizers from food waste. The steps also generate many other valuable products [Copyright 2023; Karthikeyan *et al.*<sup>141</sup>].



years to cover new uses and needs as they are easy, accurate, and cost-effective methods. Food waste was composted by Lin<sup>134</sup> using a pilot-scale active aeration reactor. This is a negative-pressure fermentation technology which is a good system for maintaining proper moisture, promoting the growth of prolific active thermophilic microorganisms and reducing  $\text{NH}_3$  formation during the composting process while reducing the composting time. Evans *et al.*<sup>139</sup> proposed a large bioreactor plant for the bioconversion of food waste, able to convert 30 000 tonnes of food waste per year resulting in more than 13 000 tonnes of biofertilizer as well as a huge volume of electricity and natural gas. An advanced pilot-scale reactor for the bioconversion of food waste to fertilizers was used by Stabnikova *et al.*<sup>135</sup> The reactor was designed with an inlet and outlet of air, an agitator, a motor, a control panel, a cooling tower, and other necessary devices for an anaerobic reaction. *Bacillus thermoamylovorans* SW25 has been used for the valorization of food waste into fertilizers.

Chung *et al.*<sup>138</sup> utilized microbial electrochemical technology for the biological conversion of food waste to compost and biogas. This technology has been highly promising for efficiently harvesting high value-added products from food waste. Microbial electrochemical technology is used to convert the chemical energy from organic substrates to electrical energy by using special types of biocatalysts, electrodes and bacteria resulting in the production of compost and energy gas. This technology has various advantages over conventional composting methods such as low operation cost, high recovery efficiency, system stability, and high process kinetics.

Microbial fuel cells are another advanced method utilized nowadays for the production of energy from waste and recovery of resources also gives rise to solid matter readily converted to fertilizers. This method was utilized by Xin *et al.*<sup>140</sup> for the anaerobic digestion of food waste for energy production followed by solid matter for fertilizers. Fungal cells were used to prepare microbial fuel cells. The microbial fuel cell allows ultra-fast hydrolysis of waste and is therefore ideal for the production of fertilizers.<sup>112</sup>

## 6. Bio-fertilizers produced from food waste by microbes

Biofertilizers produced from food waste need to meet some requirements to increase soil fertility and crop production such as being rich in organic sources and macro- and microelements and having an appropriate C:N ratio, among others. In this sense, biofertilizers have been identified as an alternative to chemical fertilizers for the improvement of crop production in sustainable farming<sup>142,143</sup> Some quality parameters of biofertilizers produced from food waste by microorganisms and listed in Fig. 9 are a balanced C:N ratio, low coliform bacteria, an increase of microbiota, organic matter and essential micro- and macroelements, a decrease of lignin cellulose and better phosphate solubilisation. Some studies confirming these properties are shown below.

Tsai *et al.*<sup>132</sup> collected food waste from restaurants on the university campus to produce an organic fertilizer. The

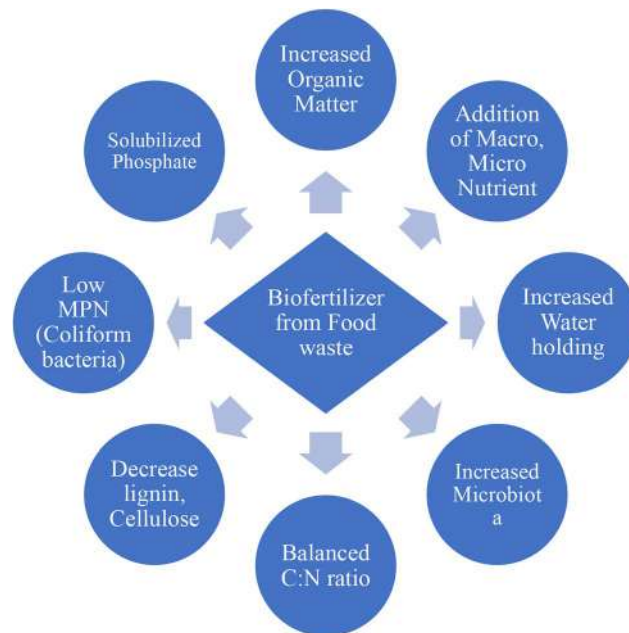


Fig. 9 Quality properties of a biofertilizer produced from food waste by microorganisms.

experiment was performed in bioreactor A, in which thermophilic lipolytic microbes were inoculated with food waste and bioreactor B was taken as a control without microbes. The fertilizer made from microbes has been proven to be a quality fertilizer by an increase in total nitrogen from 2.01% to 2.10%, ash increased from 24.94% to 29.21%, crude fat decreased from 4.88% to 1.34% and the C/N ratio decreased from 18.02 to 17.65. To produce this fertilizer *Streptomyces therrmonitrificans* NTU-88, isolate CH18, *Brevibacillus borstelensis* SH168, and *Bacillus stearothermophilus* ATCC 10149 were used. Sangamithirai *et al.*<sup>133</sup> produced a biofertilizer from the combination of fruit and vegetable waste that has advantages such as high water holding capacity that is useful for tolerance to droughts. The quality is field tested with the germination of cucumber seeds. A significant increase in the germination index was observed and shoot and root length increased compared to the control. Mesophilic bacteria were used to produce biofertilizers from the waste. Food waste was used to obtain compost through thermophilic bacteria.<sup>134</sup> The resulting compost was advanced when pH drop from 5.2 to 4.3 on the first day, followed by a gradual pH gain to 7.4 on the 60th day. After 60 days, the C/N ratio dropped from 32 to below 20. The final compost contains 1.6% nitrogen, 0.6% phosphate, and 1.4% potassium with total coliforms below 3 MPN/100 mL. Lower coliform is a sign of the absence of various pathogenic organisms and hence the compost is suitable for field applications.

*Aspergillus niger* UY2015\_11 was used for the production of green fertilizers from the waste of vegetable and fruit peels and leftover food that comes from diverse meat and vegetable menus by Mahmood *et al.*<sup>124</sup> During the bioconversion of waste, phosphate has been solubilized by the fungus through the production of citric acid. The solubilization of phosphate is easily available for the utilization of plants during the growth



stage. Similarly, iron- and calcium-based inorganic phosphates were also recorded for solubilization by the fungus. Zhu *et al.*<sup>144</sup> used a combination of seaweed, plant ash, animal proteins, and edible mushroom residues for the bioconversion of these waste to biofertilizers with the aid of *Bacillus criculans*, *Bacillus sphaericus*, *Bacillus firmus*, *Bacillus schlegelii*, *Bacillus stearothermophilus*, *Bacillus subtilis*, *Candida tropicalis*, and *Lactobacillus delbrueckii*. The application of the fertilizer to the field has increased organic matter by 1.31 and 1.55-fold compared with soil without fertilization as well as increased the quality of humus and aggregation of large particles.

The fruit peel waste of *Carica papaya* (pawpaw) was used for the production of organic fertilizers by Dahunsi *et al.*<sup>125</sup> This valorization was achieved by the anaerobic digestion of waste in the presence of microbes. The obtained fertilizer was found to

be advantageous over the chemical fertilizer with an increase of nitrogen, phosphorus, and potassium by 28, 40, and 22% respectively. However, improvements in many other macro- and microelements were also recorded. *Trichoderma reesei* was used for the anaerobic digestion followed by aerobic digestion of fruit and vegetable waste for biofertilizers and biogas production by Chakravarty *et al.*<sup>119</sup> The obtained biofertilizer achieved a C : N ratio of 10–11 and a decrease in lignin by 64% in the case of food waste and 70% in the case of vegetable waste. Dadi *et al.*<sup>137</sup> used coffee pulp waste for the production of an organic fertilizer. The C : N ratio of compost materials has decreased with the advancement of the period of decomposition from 17.6 to 7.25. Greater reduction in lignin content (37.54% to 28.46%), cellulose content (25.95 to 16.75%), and total phenol content (76.75 mg/100 g to 38.8 mg/100 g) with an increase in humic

**Table 2** Promotion of growth in plants by application of bio-fertilizers obtained from food waste

S. no.	Food waste	Valorisation method	Crop to which fertilizers were applied	Outcome of the application of bio-fertilizers	Reference
1	<i>Carica papaya</i> (pawpaw) fruit peels	Anaerobic digestion	Maize	Better performance in terms of number of leaves, leaf area, plant height, stem girth, total shoot and root biomass, and length of the root as compared to chemical fertilizers	125
2	Rice bran, rapeseed mill cake and fish processing waste	Use of lactic acid bacteria, yeast and phototrophic bacteria	Tomato ( <i>L. esculentum</i> L. cv. Momotaro T 96)	More active young leaves and developed more young fruit as compared to chemical fertilizers. Fruit yield is higher in the later growth stage and vitamin C is higher in the fruit as compared to chemical fertilizers	145
3	Vegetable and fruit peels and leftover food	Use of <i>Aspergillus niger</i> UY2015_11	Lettuce and <i>Brassica rapa</i>	Similar growth was recorded from the green fertilizer obtained from fruit and vegetable waste as compared to chemical and rapeseed oil cake organic fertilizers. Therefore, no significant difference was observed	124
4	Kitchen waste oil	Use of <i>Pseudomonas aeruginosa</i> PA-3	Cabbage	Plant height reached 7.83 cm in 12 days, while that of the control group was 5.17 cm. Leaf area on the 12th day and 15th day was 1.08 cm <sup>2</sup> and 1.35 cm <sup>2</sup> , respectively while in the control it was recorded to be 0.56 cm <sup>2</sup> and 0.71 cm <sup>2</sup> . Similarly the stem diameter of cabbage plants was also increased with the addition of a fertilizer obtained from kitchen waste oil as compared to the control	126
5	Vegetable and fruit waste	Use of mesophilic bacteria	Cucumber	A significant increase in cucumber shoots and root length. A germination index of more than 80% was obtained showing phytotoxic-free and mature compost	133
6	Food waste	Use of <i>Streptomyces thermonitrificans</i> NTU-88, <i>Brevibacillus borstelensis</i> SH168 and <i>Bacillus stearothermophilus</i> ATCC 10149	Alfalfa	The germination rate of alfalfa seed increased from 10.50 (day 7) to 97.50% (day 28)	132
7	Food waste	<i>Bacillus thermoamylovorans</i> SW25	<i>Ipomoea aquatica</i> (kang kong plant)	The addition of organic fertilizers to the subsoil increased the yield and growth of the plant by 1.5 to 2 times	135



substances (40.65%) was recorded during the composting period.

Biofertilizers and their nutritional composition help promote the growth of crops and play a crucial role because a food waste fertilizer serves as a source of nutrients.<sup>122</sup> Therefore, it is necessary to understand the promotion of plant growth by biofertilizers obtained from the valorisation of food waste (Table 2).

## 7. Safety concerns of biofertilizers obtained from the valorisation of food waste

Increasing the biological origin fertilizer technology has brought forward the safety of plants from the co-existence of pathogenic microbes' growth during production steps. Exceptionally, *Salmonella*, *Klebsiella* and total coliforms have been obtained from the fertilizer produced from food waste.<sup>129</sup> However, this kind of fertilizer may be used for the crop field once the pathogen has been treated. But pathogen-free fertilizers do not require such chemical treatment to kill the pathogen. The biofertilizer obtained from the valorization of household waste, slaughter residues, and some organic food waste does not support the growth of some pathogens such as *S. enterica* and *L. monocytogenes* even after supplementation with rich substrates in the waste sources containing carbon sources and other trace elements.<sup>146</sup> Therefore, this provides a promising alternate biofertilizer with crop safety.

A pilot-scale active aeration reactor was studied for composting food in which a biological filter bed was used to remove  $\text{NH}_3$  from the emission by Lin.<sup>134</sup> Using this composting system less than 1 ppm  $\text{NH}_3$  was recorded which is below the detectable limit and prevents its emission into the ambient atmosphere. This fermentation reaction system is also advantageous to promote the growth of active thermophilic microorganisms. The acidification and the growth of thermophilic microbes disinfect the compost to eliminate pathogenic microorganisms. With decreasing pH and increasing temperature during the initial stage of the composting process, the number of total coliforms decreases. On the first day, the compost pH was about 4.3, the temperature was 65 °C, and total coliforms dropped to 240 MPN/100 mL. After the process enters the thermophilic fermentation period (higher than 65 °C in this case) on the 14th day, the total coliforms decrease to below 3 MPN/100 mL which is the LDL (lowest detection limit) for MPN.

The biofertilizer obtained from vegetable and food waste was found to have good hygienic quality, since, pathogenic bacteria such as *Escherichia coli* and *Salmonella dysenteriae* were not detected in the mature compost.<sup>133</sup> During the experimental stage low  $\text{CO}_2$  emission was also recorded in environmentally friendly production of compost from food waste. Food waste (including vegetable and fruit peels and leftover food which comes from diverse meat and vegetable menus) collected from the university restaurant was used to produce a green fertilizer using *Aspergillus niger* UY2015\_11. Results showed that one strain of *Aspergillus niger* UY2015\_11 significantly inhibited the

growth of *Fusarium*. Mahmood *et al.*<sup>124</sup> worked with 112 strains, of which 16 inhibited the growth of *Fusarium* spp.

## 8. Economic aspects of bioconversion of food waste

Food waste management with traditional ways such as landfilling could not be economically sustainable because an expenditure is needed to collect, transport and landfill waste, while microbial bioconversion gives rise to products such as fertilizers, bioelectricity, and biofuels which can have value. In an estimate by Yong *et al.*<sup>147</sup> biofertilizers and biogas produced from waste provide a sustainable economy as well as protection of the environment in Malaysia. Revenue from the sale of biofertilizers and biogas electricity to the grid is estimated to be much higher and profitable. The initial expenditure to make a setup for production of fertilizers from waste was recovered from the year 4 and the business estimate was profitable from the same year. A similar observation is noted in the study by Ma *et al.*<sup>148</sup> The estimated co-location of food waste and municipal waste water treatment gives rise to a profitable corporation. The energy expenditure for waste water treatment in a year (16.86 billion kW h) and recoverable electric energy from food waste (26.44 billion kW h) provides about 9.58 billion kW h of surplus electric energy in China for year 2012. Therefore, bioconversion of food waste to fertilizers and their co-products definitely contributes to a green environment as well as a sustainable economy.

## 9. Conclusion and future prospects

Increasing global population, demographic shifting, urbanization, economic growth, and evolution of life standards are some very important reasons for the generation of enormous amounts of food waste. It is necessary to minimize food loss to increase food safety; however, this is multifaceted as losses are found in the crop production and stock cycling process. Food waste from household ingestion contributes mainly to food loss as demonstrated in various studies. Urban waste is among the top priorities and an important challenge for authorities. Various alternate management systems such as landfilling, burning, and dumping are traditional and non-environmentally friendly methods that contribute to the toxic emissions in the atmosphere. Therefore, the use of microbial capacity to decompose organic matter is a very vibrant technique to valorize food waste. Several sources and types of food waste such as waste cooking oils, agro-industrial wastes such as vegetables, fruit, juice, wheat, rice, potato, sugarcane, bakery waste, dairy waste and different types of meat, fish and poultry wastes have been proven to be profitable sources for their use for bioconversion. Nowadays composting, anaerobic and aerobic digestion, and fermentation are the most likely utilized methods for bioconversion of food waste to biofertilizers, organic compost, biochar, and biogas.

However, scientific communities are now utilizing genetically engineered microbes for the valorization of urban waste as



a valuable product. These engineering approaches include gene deletion, overexpression, modification in a targeted manner, or addition of metabolic routes.<sup>149</sup> Similar approaches are now utilized to valorize organic waste as a valuable product. Liu *et al.*<sup>150</sup> recently expressed an *A. niger* pectinase in *Pichia pastoris* to enable oligogalacturonide (OG) production directly from ground mandarin and orange peel waste. Recombinant yeast *Yarrowia lipolytica* was used to produce long chain fatty acid from waste.<sup>151</sup> Grohmann *et al.*<sup>152</sup> used a recombinant strain of *Escherichia coli* KO11 for the fermentation of sugar present in orange peel. The most recent genetically engineered strains of microorganisms have been utilized for better composting and digestion capacity for the valorization of food waste.<sup>153</sup>

## Author contributions

Pramod Kumar Mahish: preparation of TOC, literature review, manuscript writing, drawing of figures. Dakeshwar Kumar Verma: initial editing, plagiarism check, supervision. Anjali Ghritlahare: manuscript writing, drawing of figures, reference arrangement, copyright. Charu Arora: conceptualization, final editing. Paz Otero: final modification, supervision.

## Conflicts of interest

The authors declare no conflict of interest.

## References

- Food and Agriculture Organization, Mitigation of Food Wastage: Societal Costs and Benefits, 2014, <https://www.fao.org/documents/card/en?details=a530f2ad-499c-400f-b9c0-6c8988f2ee9d/>.
- Food and Agriculture Organization, Global Food Losses and Food Waste: Extent, Causes and Prevention, 2011, <https://www.fao.org/3/mb060e/mb060e00.htm>.
- United States Environmental Protection Agency, Terms of Environment: Glossary, Abbreviations and Acronyms, 2008, <http://www.epa.gov/OCEPAterms/fterms.html>.
- World Food Programme, The Year in Review, 2012, <https://www.wfp.org/publications/year-review-2012-0>.
- Food and Agriculture Organization, Food Wastage Footprint: Impacts on Natural Resources, 2018, <https://www.fao.org/documents/card/en?details=000d4a32-7304-5785-a2f1->.
- M. Melikoglu, C. C. Lin and C. Webb, Analysing global food waste problem: Pinpointing the facts and estimating the energy content, *Cent. Eur. J. Eng.*, 2013, 3(2), 157–164, DOI: [10.2478/s13531-012-0058-5](https://doi.org/10.2478/s13531-012-0058-5).
- J. O'Connor, B. S. Mickan, J. Rinklebe, H. Song, K. H. Siddique, H. Wang, M. B. Kirkham and N. S. Bolan, Environmental implications, potential value, and future of food-waste anaerobic digestate management: A review, *J. Environ. Manage.*, 2022, 318, 115519, DOI: [10.1016/j.jenvman.2022.115519](https://doi.org/10.1016/j.jenvman.2022.115519).
- P. Alexander, C. Brown, A. Arneeth, J. Finnigan, D. Moran and M. D. Rounsevell, Losses, inefficiencies and waste in

- the global food system, *Agric. Syst.*, 2017, 53, 190–200, DOI: [10.1016/j.agry.2017.01.014](https://doi.org/10.1016/j.agry.2017.01.014).
- D. Tilman and M. Clark, Global diets link environmental sustainability and human health, *Nature*, 2014, 515, 518–522, DOI: [10.1038/nature13959](https://doi.org/10.1038/nature13959).
  - S. D. Porter, D. S. Reay, P. Higgins and E. Bomberg, A half-century of production-phase greenhouse gas emissions from food loss & waste in the global food supply chain, *Sci. Total Environ.*, 2016, 571, 721–729, DOI: [10.1016/j.scitotenv.2016.07.041](https://doi.org/10.1016/j.scitotenv.2016.07.041).
  - C. Chen, A. Chaudhary and A. Mathys, Nutritional and environmental losses embedded in global food waste, *Resour., Conserv. Recycl.*, 2020, 160, 104912, DOI: [10.1016/j.resconrec.2020.104912](https://doi.org/10.1016/j.resconrec.2020.104912).
  - A. Chaudhary and T. M. Brooks, National consumption and global trade impacts on biodiversity, *World Dev.*, 2019, 121, 178–187, DOI: [10.1016/j.worlddev.2017.10.012](https://doi.org/10.1016/j.worlddev.2017.10.012).
  - C. Beretta, F. Stoessel, U. Baier and S. Hellweg, Quantifying food losses and the potential for reduction in Switzerland, *Waste Manage.*, 2013, 33(3), 764–773, DOI: [10.1016/j.wasman.2012.11.007](https://doi.org/10.1016/j.wasman.2012.11.007).
  - M. Gjerris and S. Gaiani, Household food waste in Nordic countries: Estimations and ethical implications, *Nord. J. Appl. Ethics*, 2013, 14, 6–23, DOI: [10.5324/eip.v7i1.1786](https://doi.org/10.5324/eip.v7i1.1786).
  - Waste & Resources Action Programme, Household Food and Drink Waste: A Product Focus, 2016, <https://wrap.org.uk/resources/report/household-food-drink-waste-product-focus>.
  - FUSIONS, Food Waste Data Set for EU-28, 2015, <https://www.wur.nl/en/Publication-details.htm?publicationId=publication-way-353033373834>.
  - V. Filimonau and V. A. Ermolaev, A sleeping giant? Food waste in the foodservice sector of Russia, *J. Cleaner Prod.*, 2021, 297, 126705, DOI: [10.1016/j.jclepro.2021.126705](https://doi.org/10.1016/j.jclepro.2021.126705).
  - L. Xue and G. Liu, Introduction to global food losses and food waste, in *Saving Food*, Academic Press, 2019, pp. 1–31, DOI: [10.1016/B978-0-12-815357-4.00001-8](https://doi.org/10.1016/B978-0-12-815357-4.00001-8).
  - S. Kirkpatrick and V. Tarasuk, The relationship between low income and household food expenditure patterns in Canada, *Public Health Nutr.*, 2003, 6, 589–597, DOI: [10.1079/PHN2003517](https://doi.org/10.1079/PHN2003517).
  - C. Dias-Ferreira, T. Santos and V. Oliveira, Hospital food waste and environmental and economic indicators—A Portuguese case study, *Waste Manage.*, 2015, 46, 146–154, DOI: [10.1016/j.wasman.2015.09.025](https://doi.org/10.1016/j.wasman.2015.09.025).
  - B. E. Gutiérrez-Barba and A. Ortega-Rubio, Household food-waste production and a proposal for its minimization in Mexico, *Life Sci. J.*, 2013, 10(3), 1772–1783, DOI: [10.7537/marslsj100313.266](https://doi.org/10.7537/marslsj100313.266).
  - S. Łaba, M. Niedek, K. Szczepański, R. Łaba and A. Kamińska-Dwórznička, Regulation of the food waste measuring in the EU in the light of the need of counteracting the food wastage, *Environ. Nat. Resour.*, 2019, 4(82), 1–6, DOI: [10.2478/oszn-2019-0015](https://doi.org/10.2478/oszn-2019-0015).
  - M. Boulet, A. C. Hoek and R. Raven, Towards a multi-level framework of household food waste and consumer

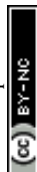


- behavior: Untangling spaghetti soup, *Appetite*, 2021, **156**, 104856, DOI: [10.1016/j.appet.2020.104856](https://doi.org/10.1016/j.appet.2020.104856).
- 24 M. Story, K. M. Kaphingst, R. Robinson-O'Brien and K. Glanz, Creating healthy food and eating environments: policy and environmental approaches, *Annu. Rev. Public Health*, 2008, **29**(1), 253–272, DOI: [10.1146/annurev.publhealth.29.020907.090926](https://doi.org/10.1146/annurev.publhealth.29.020907.090926).
- 25 A. Scott, C. Oates and W. Young, Conceptual framework of the adoption and practice of environmental actions in households, *Sustain*, 2015, **7**(5), 5793–5818, DOI: [10.3390/su7055793](https://doi.org/10.3390/su7055793).
- 26 D. R. Forsyth, *Group Dynamics*, Wadsworth, 2012.
- 27 M. Griffin, J. Sobal and T. A. Lyson, An analysis of a community food waste stream, *Agric. Human Values*, 2009, **26**, 67–81, DOI: [10.1007/s10460-008-9178-1](https://doi.org/10.1007/s10460-008-9178-1).
- 28 L. Manzocco, M. Alongi, S. Sillani and M. C. Nicoli, Technological and consumer strategies to tackle food wasting, *Food Eng. Rev.*, 2016, **8**, 457–467, DOI: [10.1007/s12393-016-9149-z](https://doi.org/10.1007/s12393-016-9149-z).
- 29 L. Xue, G. Liu, J. Parfitt, X. Liu, E. Van Herpen, Å. Stenmarck, C. O'Connor, K. Östergren and S. Cheng, Missing food, missing data? A critical review of global food losses and food waste data, *Environ. Sci. Technol.*, 2017, **51**(12), 6618–6633, DOI: [10.1021/acs.est.7b00401](https://doi.org/10.1021/acs.est.7b00401).
- 30 T. N. B. Dung, B. Sen, C. C. Chen, G. Kumar and C. Y. Lin, Food waste to bioenergy via anaerobic processes, *Energy Procedia*, 2014, **61**, 307–312, DOI: [10.1016/j.egypro.2014.11.1113](https://doi.org/10.1016/j.egypro.2014.11.1113).
- 31 J. A. Aitken, B. Alaybek, R. Hartman, G. Mika, E. M. Broad Leib, R. Plekenpol, K. Branting, D. Rao, L. Leets and A. Sprenger, Initial assessment of the efficacy of food recovery policies in US States for increasing food donations and reducing waste, *Waste Manage.*, 2024, **176**, 149–158, DOI: [10.1016/j.wasman.2023.12.051](https://doi.org/10.1016/j.wasman.2023.12.051).
- 32 A. Georganas, E. Giamouri, A. C. Pappas, G. Papadomichelakis, F. Galliou, T. Manios, E. Tsiplakou, K. Fegeros and G. Zervas, Bioactive Compounds in Food Waste: A Review on the Transformation of Food Waste to Animal Feed, *Foods*, 2020, **9**, 291, DOI: [10.3390/foods9030291](https://doi.org/10.3390/foods9030291).
- 33 S. Elkhalfifa, T. Al-Ansari, H. R. Mackey and G. McKay, Food waste to biochars through pyrolysis: A review, *Resour., Conserv. Recycl.*, 2019, **144**, 310–320, DOI: [10.1016/j.resconrec.2019.01.024](https://doi.org/10.1016/j.resconrec.2019.01.024).
- 34 F. H. Pour and Y. T. Makkawi, A review of post-consumption food waste management and its potentials for biofuel production, *Energy Rep.*, 2021, **7**, 7759–7784, DOI: [10.1016/j.egypr.2021.10.119](https://doi.org/10.1016/j.egypr.2021.10.119).
- 35 H. A. Rahman, Incinerator in Malaysia: really needs?, *Int. J. Chem. Environ. Biol. Sci.*, 2013, **1**, 678–681.
- 36 R. Muangrat, A review: utilization of food wastes for hydrogen production under hydrothermal gasification, *Environ. Technol. Rev.*, 2013, **2**(1), 85–100, DOI: [10.1080/21622515.2013.840682](https://doi.org/10.1080/21622515.2013.840682).
- 37 B. Kayode and A. Hart, An overview of transesterification methods for producing biodiesel from waste vegetable oils, *Biofuels*, 2019, **10**(3), 419–437, DOI: [10.1080/17597269.2017.1306683](https://doi.org/10.1080/17597269.2017.1306683).
- 38 F. Moazeni, Y. C. Chen and G. Zhang, Enzymatic transesterification for biodiesel production from used cooking oil, a review, *J. Cleaner Prod.*, 2019, **216**, 117–128, DOI: [10.1016/j.jclepro.2019.01.181](https://doi.org/10.1016/j.jclepro.2019.01.181).
- 39 S. Fan, A. Li, A. ter Heijne, C. J. Buisman and W. S. Chen, Heat potential, generation, recovery and utilization from composting: A review, *Resour., Conserv. Recycl.*, 2021, **175**, 105850, DOI: [10.1016/j.resconrec.2021.105850](https://doi.org/10.1016/j.resconrec.2021.105850).
- 40 C. Jin, S. Sun, D. Yang, W. Sheng, Y. Ma, W. He and G. Li, Anaerobic digestion: An alternative resource treatment option for food waste in China, *Sci. Total Environ.*, 2021, **779**, 146397, DOI: [10.1016/j.scitotenv.2021.146397](https://doi.org/10.1016/j.scitotenv.2021.146397).
- 41 M. Y. Areeshi, Recent advances on organic biofertilizer production from anaerobic fermentation of food waste: Overview, *Int. J. Food Microbiol.*, 2022, **374**, 109719, DOI: [10.1016/j.ijfoodmicro.2022.109719](https://doi.org/10.1016/j.ijfoodmicro.2022.109719).
- 42 S. J. Chen, X. Chen, B. B. Hu, M. Y. Wei and M. J. Zhu, Efficient hydrogen production from sugarcane bagasse and food waste by thermophilic clostridiales consortium and Fe–Mn impregnated biochars, *Renewable Energy*, 2023, **211**, 166–178, DOI: [10.1016/j.renene.2023.04.114](https://doi.org/10.1016/j.renene.2023.04.114).
- 43 X. Xiong, I. K. M. Yu, D. C. W. Tsang, N. S. Bolan, Y. Sik Ok, A. D. Igalavithana, M. B. Kirkham, K.-H. Kim and K. Vikrant, Value-added chemicals from food supply chain wastes: State-of-the-art review and future prospects, *Chem. Eng. J.*, 2019, **375**, 121983, DOI: [10.1016/j.cej.2019.121983](https://doi.org/10.1016/j.cej.2019.121983).
- 44 N. B. D. Thi, G. Kumar and C.-Y. Lin, An overview of food waste management in developing countries: Current status and future perspective, *J. Environ. Manage.*, 2015, **157**, 220–229, DOI: [10.1016/j.jenvman.2015.04.022](https://doi.org/10.1016/j.jenvman.2015.04.022).
- 45 K. M. Kibler, D. Reinhart, C. Hawkins, A. M. Motlagh and J. Wright, Food waste and the food-energy-water nexus: A review of food waste management alternatives, *Waste Manage.*, 2018, **74**, 52–62, DOI: [10.1016/j.wasman.2018.01.014](https://doi.org/10.1016/j.wasman.2018.01.014).
- 46 S. Zafar, Food Waste to Energy Plant | BioEnergy Consult, <https://www.bioenergyconsult.com/tag/food-waste-to-energy-plant/>, (accessed September 3, 2023).
- 47 T. A. A. Nasrin and M. A. Matin, Valorization of Vegetable Wastes, in *Food Processing By-Products and Their Utilization*, John Wiley & Sons, Ltd, Chichester, UK, 2017, pp. 53–88, DOI: [10.1002/9781118432921.ch4](https://doi.org/10.1002/9781118432921.ch4).
- 48 M. Sharma, Z. Usmani, V. K. Gupta and R. Bhat, Valorization of fruits and vegetable wastes and by-products to produce natural pigments, *Crit. Rev. Biotechnol.*, 2021, **41**, 535–563, DOI: [10.1080/07388551.2021.1873240](https://doi.org/10.1080/07388551.2021.1873240).
- 49 A. Mannu, G. Vlahopoulou, P. Urgeghe, M. Ferro, A. Del Caro, A. Taras, S. Garroni, J. P. Rourke, R. Cabizza and G. L. Petretto, Variation of the chemical composition of waste cooking oils upon bentonite filtration, *Resources*, 2019, **8**, 108, DOI: [10.3390/resources8020108](https://doi.org/10.3390/resources8020108).
- 50 Sahar, S. Sadaf, J. Iqbal, I. Ullah, H. N. Bhatti, S. Nouren, Habib-ur-Rehman, J. Nisar and M. Iqbal, Biodiesel





- production from waste cooking oil: an efficient technique to convert waste into biodiesel, *Sustain. Cities Soc.*, 2018, **41**, 220–226, DOI: [10.1016/j.scs.2018.05.037](https://doi.org/10.1016/j.scs.2018.05.037).
- 51 T. Yuwa-amornpitak and K. Chookietwatana, Bioconversion of waste cooking oil glycerol from cabbage extract to lactic acid by *Rhizopus microspores*, *Braz. J. Microbiol.*, 2018, **49**, 178–184, DOI: [10.1016/j.bjm.2018.06.007](https://doi.org/10.1016/j.bjm.2018.06.007).
- 52 A. H. Hashem, A. M. Khattab and M. Abdelraof, A facile one-pot bioconversion of frying oil waste to single cell oils and related products using fungi *via* response surface methodology, *Biomass Convers. Biorefin.*, 2022, **13**, 16711–16721, DOI: [10.1007/s13399-021-02165-7](https://doi.org/10.1007/s13399-021-02165-7).
- 53 P. Kumar and B. S. Kim, *Paracoccus* sp. strain LL1 as a single cell factory for the conversion of waste cooking oil to polyhydroxyalkanoates and carotenoids, *Appl. Food Biotechnol.*, 2019, **6**(1), 53–60, DOI: [10.22037/afb.v6i1.21628](https://doi.org/10.22037/afb.v6i1.21628).
- 54 Y. Li, Z. Cheng, C. Zhao, C. Gao, W. Song, L. Liu and X. Chen, Reprogramming *Escherichia coli* metabolism for bioplastics synthesis from waste cooking oil, *ACS Synth. Biol.*, 2021, **10**, 1966–1979, DOI: [10.1021/acssynbio.1c00155](https://doi.org/10.1021/acssynbio.1c00155).
- 55 M. A. Martín, J. A. Siles, A. F. Chica and A. Martín, Biomethanization of orange peel waste, *Bioresour. Technol.*, 2010, **101**, 8993–8999, DOI: [10.1016/j.biortech.2010.06.133](https://doi.org/10.1016/j.biortech.2010.06.133).
- 56 A. Upadhyay, J. P. Lama and S. Tawata, Utilization of pineapple waste: a review, *J. Food Sci. Technol.*, 2013, **6**, 10–18, DOI: [10.3126/jfstn.v6i0.8255](https://doi.org/10.3126/jfstn.v6i0.8255).
- 57 J. K. Bediako, A. K. Sarkar, S. Lin, Y. Zhao, M.-H. Song, J.-W. Choi, C.-W. Cho and Y.-S. Yun, Characterization of the residual biochemical components of sequentially extracted banana peel biomasses and their environmental remediation applications, *Waste Manage.*, 2019, **89**, 141–153, DOI: [10.1016/j.wasman.2019.04.009](https://doi.org/10.1016/j.wasman.2019.04.009).
- 58 M. Xu, G. Tian, C. Zhao, A. Ahmad, H. Zhang, J. Bi, H. Xiao and J. Zheng, Infrared drying as a quick preparation method for dried tangerine peel, *Int. J. Anal. Chem.*, 2017, **1**–11, DOI: [10.1155/2017/6254793](https://doi.org/10.1155/2017/6254793).
- 59 P. Kandylis and E. Kokkinomagoulos, Food applications and potential health benefits of pomegranate and its derivatives, *Foods*, 2020, **9**, 122, DOI: [10.3390/foods9020122](https://doi.org/10.3390/foods9020122).
- 60 A. El Barnossi, F. Moussaid and A. Iraqi Housseini, Tangerine, banana and pomegranate peels valorisation for sustainable environment: A review, *Biotechnol. Rep.*, 2021, **29**, e00574, DOI: [10.1016/j.btre.2020.e00574](https://doi.org/10.1016/j.btre.2020.e00574).
- 61 L. A. d. Santos, R. B. Valença, L. C. S. d. Silva, S. H. d. B. Holanda, A. F. V. d. Silva, J. F. T. Jucá and A. F. M. S. Santos, Methane generation potential through anaerobic digestion of fruit waste, *J. Cleaner Prod.*, 2020, **256**, 120389, DOI: [10.1016/j.jclepro.2020.120389](https://doi.org/10.1016/j.jclepro.2020.120389).
- 62 M. Ververi and A. M. Goula, Pomegranate peel and orange juice by-product as new biosorbents of phenolic compounds from olive mill wastewaters, *Chem. Eng. Process.*, 2019, **138**, 86–96, DOI: [10.1016/j.ccep.2019.03.010](https://doi.org/10.1016/j.ccep.2019.03.010).
- 63 W. Miran, M. Nawaz, J. Jang and D. S. Lee, Conversion of orange peel waste biomass to bioelectricity using a mediator-less microbial fuel cell, *Sci. Total Environ.*, 2016, **547**, 197–205, DOI: [10.1016/j.scitotenv.2016.01.004](https://doi.org/10.1016/j.scitotenv.2016.01.004).
- 64 A. Kantifedaki, V. Kachrimanidou, A. Mallouchos, S. Papanikolaou and A. A. Koutinas, Orange processing waste valorisation for the production of bio-based pigments using the fungal strains *Monascus purpureus* and *Penicillium purpurogenum*, *J. Cleaner Prod.*, 2018, **185**, 882–890, DOI: [10.1016/j.jclepro.2018.03.032](https://doi.org/10.1016/j.jclepro.2018.03.032).
- 65 M. Nossier, Impact of organic fertilizers derived from banana and orange peels on tomato plant quality, *Arab Univ. J. Agric. Sci.*, 2021, **29**(1), 459–469, DOI: [10.21608/ajs.2021.46495.1278](https://doi.org/10.21608/ajs.2021.46495.1278).
- 66 T. A. Sial, M. N. Khan, Z. Lan, F. Kumbhar, Z. Ying, J. Zhang, D. Sun and X. Li, Contrasting effects of banana peels waste and its biochar on greenhouse gas emissions and soil biochemical properties, *Process Saf. Environ. Prot.*, 2019, **122**, 366–377, DOI: [10.1016/j.psep.2018.10.030](https://doi.org/10.1016/j.psep.2018.10.030).
- 67 S. Chaturvedi, A. Kumari, A. Bhattacharya, A. Sharma, L. Nain and S. K. Khare, Banana peel waste management for single-cell oil production, *Energy, Ecol. Environ.*, 2018, **3**, 296–303, DOI: [10.1007/s40974-018-0101-3](https://doi.org/10.1007/s40974-018-0101-3).
- 68 M. A. d. Souza, I. T. Vilas-Boas, J. M. Leite-da-Silva, P. d. N. Abrahão, B. E. Teixeira-Costa and V. F. Veiga-Junior, Polysaccharides in Agro-Industrial Biomass Residues, *Polysaccharides*, 2022, **3**, 95–120, DOI: [10.3390/polysaccharides3010005](https://doi.org/10.3390/polysaccharides3010005).
- 69 C. M. Hussain and R. K. Kadeppagari, *Biotechnology for Zero Waste: Emerging Waste Management Techniques*, Wiley & Sons, Limited, John, 2021.
- 70 R. Ravindran, S. Hassan, G. Williams and A. Jaiswal, A review on bioconversion of agro-industrial wastes to industrially important enzymes, *Bioengineering*, 2018, **5**(4), 93, DOI: [10.3390/bioengineering5040093](https://doi.org/10.3390/bioengineering5040093).
- 71 A. Singh, S. Bajar, A. Devi and N. R. Bishnoi, Adding value to agro-industrial waste for cellulase and xylanase production *via* solid-state bioconversion, *Biomass Convers. Biorefin.*, 2021, **1**–10, DOI: [10.1007/s13399-021-01503-3](https://doi.org/10.1007/s13399-021-01503-3).
- 72 R. Rajesh and S. N. Gummadi, Production of multienzymes, bioethanol, and acetic acid by novel *Bacillus* sp. PM06 from various lignocellulosic biomass, *Biomass Convers. Biorefin.*, 2022, DOI: [10.1007/s13399-022-02418-z](https://doi.org/10.1007/s13399-022-02418-z).
- 73 T. Akhtar, A. S. Hashmi, M. Tayyab, A. A. Anjum, S. Saeed and S. Ali, Bioconversion of agricultural waste to butyric acid through solid state fermentation by *Clostridium tyrobutyricum*, *Waste Biomass Valorization*, 2018, **11**, 2067–2073, DOI: [10.1007/s12649-018-0475-7](https://doi.org/10.1007/s12649-018-0475-7).
- 74 P. Upadhyay, N. K. Singh, R. Tupe, A. Odenath and A. Lali, Biotransformation of corn bran derived ferulic acid to vanillic acid using engineered *Pseudomonas putida* KT2440, *Prep. Biochem. Biotechnol.*, 2019, **50**, 341–348, DOI: [10.1080/10826068.2019.1697935](https://doi.org/10.1080/10826068.2019.1697935).
- 75 T. Agrawal, S. K. Jadhav and A. Quraishi, Bioethanol production from an agro-waste, deoiled rice bran by *Saccharomyces cerevisiae* MTCC 4780 *via* optimization of fermentation parameters, *EnvironmentAsia*, 2019, **12**, 20–24, DOI: [10.14456/ea.2019.3](https://doi.org/10.14456/ea.2019.3).



- 76 A. Kosre, D. Koreti, P. K. Mahish and N. K. Chandrawanshi, Current perspective of sustainable utilization of agro waste and biotransformation of energy in mushroom, in *Energy: Crises, Challenges and Solutions*, John Wiley & Sons, Inc., Hoboken, New Jersey, 2021, p. 352.
- 77 N. V. Hoang, A. Furtado, L. Donnan, E. C. Keeffe, F. C. Botha and R. J. Henry, High-throughput profiling of the fiber and sugar composition of sugarcane biomass, *BioEnergy Res.*, 2016, **10**, 400–416, DOI: [10.1007/s12155-016-9801-8](https://doi.org/10.1007/s12155-016-9801-8).
- 78 M. Leonel, E. L. do Carmo, A. M. Fernandes, R. P. Soratto, J. A. M. Eburneo, É. L. Garcia and T. P. R. dos Santos, Chemical composition of potato tubers: the effect of cultivars and growth conditions, *J. Food Sci. Technol.*, 2017, **54**, 2372–2378, DOI: [10.1007/s13197-017-2677-6](https://doi.org/10.1007/s13197-017-2677-6).
- 79 K. C. Khaire, V. S. Moholkar and A. Goyal, Bioconversion of sugarcane tops to bioethanol and other value-added products: an overview, *Mater. Sci. Energy Technol.*, 2021, **4**, 54–68, DOI: [10.1016/j.mset.2020.12.004](https://doi.org/10.1016/j.mset.2020.12.004).
- 80 S. Chantorn, C. Piyapittayanun and P. Dangpram, Bioconversion of agricultural wastes to mannooligosaccharides and their prebiotic potential, *Chiang Mai J. Sci.*, 2018, **45**(1), 60–67, <http://epg.science.cmu.ac.th/ejournal/>.
- 81 R. Terán Hilaes, R. A. de Souza, P. F. Marcelino, S. S. da Silva, G. Dragone, S. I. Mussatto and J. C. Santos, Sugarcane bagasse hydrolysate as a potential feedstock for red pigment production by *Monascus ruber*, *Food Chem.*, 2018, **245**, 786–791, DOI: [10.1016/j.foodchem.2017.11.111](https://doi.org/10.1016/j.foodchem.2017.11.111).
- 82 J. de Oliveira, L. Porto de Souza Vandenberghe, P. Zwierchczewski de Oliveira, A. Fátima Murawski de Mello, C. Rodrigues, P. Singh Nigam, V. Faraco and C. R. Soccol, Bioconversion of potato-processing wastes into an industrially-important chemical lactic acid, *Bioresour. Technol. Rep.*, 2021, **15**, 100698, DOI: [10.1016/j.biteb.2021.100698](https://doi.org/10.1016/j.biteb.2021.100698).
- 83 S. S. Suryawanshi, S. S. Sarje, P. C. Loni, S. bhujbal and P. P. Kamble, Bioconversion of sugarcane molasses into bioplastic (polyhydroxybutyrate) using *Bacillus cereus* 2156 under statistically optimized culture conditions, *Anal. Chem. Lett.*, 2020, **10**, 80–92, DOI: [10.1080/22297928.2020.1746197](https://doi.org/10.1080/22297928.2020.1746197).
- 84 R. Jumaidin, S. N. Mohd Zainel, N. W. Adam, M. S. F. Hussin, A. F. Ab Ghani, M. Mohammad Taha, M. R. Mansor, M. Y. Yaakob, M. N. Ahmad, N. A. Maidin, M. K. Wahid, N. A. Mohamad Yatim, M. H. Ab Rahman and M. H. Osman, Thermal Degradation and Mechanical Characteristics of Sugarcane Bagasse Reinforced Biodegradable Potato Starch Composites, *J. Adv. Res. Fluid Mech. Therm. Sci.*, 2020, **78**, 157–166, DOI: [10.37934/arfmts.78.1.157166](https://doi.org/10.37934/arfmts.78.1.157166).
- 85 T. C. Sarker, M. A. Mannan, P. C. Mondol, A. H. Kabir, S. M. Parvez and M. F. Alam, Physico-chemical profile and microbial diversity during bioconversion of sugarcane press mud using bacterial suspension, *Not. Sci. Biol.*, 2013, **5**, 346–353, DOI: [10.15835/nsb539080](https://doi.org/10.15835/nsb539080).
- 86 A. Y.-z. Zhang, Z. Sun, C. C. J. Leung, W. Han, K. Y. Lau, M. Li and C. S. K. Lin, Valorisation of bakery waste for succinic acid production, *Green Chem.*, 2013, **15**, 690, DOI: [10.1039/c2gc36518a](https://doi.org/10.1039/c2gc36518a).
- 87 O. Benabda, M. Kasmi, F. Kachouri and M. Hamdi, Valorization of the powdered bread waste hydrolysate as growth medium for baker yeast, *Food Bioprod. Process.*, 2018, **109**, 1–8, DOI: [10.1016/j.fbp.2018.02.007](https://doi.org/10.1016/j.fbp.2018.02.007).
- 88 R. A. D. Arancon, C. S. K. Lin, K. M. Chan, T. H. Kwan and R. Luque, Advances on waste valorization: new horizons for a more sustainable society, *Energy Sci. Eng.*, 2013, **1**, 53–71, DOI: [10.1002/ese3.9](https://doi.org/10.1002/ese3.9).
- 89 M. A. Haque, V. Kachrimanidou, A. Koutinas and C. S. K. Lin, Valorization of bakery waste for biocolorant and enzyme production by *Monascus purpureus*, *J. Biotechnol.*, 2016, **231**, 55–64, DOI: [10.1016/j.jbiotec.2016.05.003](https://doi.org/10.1016/j.jbiotec.2016.05.003).
- 90 A. Cerda, M. El-Bakry, T. Gea and A. Sánchez, Long term enhanced solid-state fermentation: inoculation strategies for amylase production from soy and bread wastes by *Thermomyces* sp. in a sequential batch operation, *J. Environ. Chem. Eng.*, 2016, **4**, 2394–2401, DOI: [10.1016/j.jece.2016.04.022](https://doi.org/10.1016/j.jece.2016.04.022).
- 91 F. Ebrahimi, M. Khanahmadi, S. Roodpeyma and M. Taherzadeh, Ethanol production from bread residues, *Biomass Bioenergy*, 2008, **32**, 333–337, DOI: [10.1016/j.biombioe.2007.10.007](https://doi.org/10.1016/j.biombioe.2007.10.007).
- 92 A. Adessi, M. Venturi, F. Candelieri, V. Galli, L. Granchi and R. De Philippis, Bread wastes to energy: sequential lactic and photo-fermentation for hydrogen production, *Int. J. Hydrogen Energy*, 2018, **43**, 9569–9576, DOI: [10.1016/j.ijhydene.2018.04.053](https://doi.org/10.1016/j.ijhydene.2018.04.053).
- 93 M. Romero-Huelva, E. Ramos-Morales and E. Molina-Alcaide, Nutrient utilization, ruminal fermentation, microbial abundances, and milk yield and composition in dairy goats fed diets including tomato and cucumber waste fruits, *J. Dairy Sci.*, 2012, **95**, 6015–6026, DOI: [10.3168/jds.2012-5573](https://doi.org/10.3168/jds.2012-5573).
- 94 S. Roufou, S. Griffin, L. Katsini, M. Polańska, J. F. M. Van Impe and V. P. Valdramidis, The (potential) impact of seasonality and climate change on the physicochemical and microbial properties of dairy waste and its management, *Trends Food Sci. Technol.*, 2021, **116**, 1–10, DOI: [10.1016/j.tifs.2021.07.008](https://doi.org/10.1016/j.tifs.2021.07.008).
- 95 J. Liu, S. H. Dantoft, A. Würtz, P. R. Jensen and C. Solem, A novel cell factory for efficient production of ethanol from dairy waste, *Biotechnol. Biofuels*, 2016, **9**(1), 1–11, DOI: [10.1186/s13068-016-0448-7](https://doi.org/10.1186/s13068-016-0448-7).
- 96 M. Kasmi, Biological processes as promoting way for both treatment and valorization of dairy industry effluents, *Waste Biomass Valorization*, 2016, **9**, 195–209, DOI: [10.1007/s12649-016-9795-7](https://doi.org/10.1007/s12649-016-9795-7).
- 97 R. Kothari, R. Prasad, V. Kumar and D. P. Singh, Production of biodiesel from microalgae *Chlamydomonas polypyrenoidum* grown on dairy industry wastewater, *Bioresour. Technol.*, 2013, **144**, 499–503, DOI: [10.1016/j.biortech.2013.06.116](https://doi.org/10.1016/j.biortech.2013.06.116).
- 98 Z. Usmani, M. Sharma, J. Gaffey, M. Sharma, R. J. Dewhurst, B. Moreau, J. Newbold, W. Clark, V. K. Thakur and



- V. K. Gupta, Valorization of dairy waste and by-products through microbial bioprocesses, *Bioresour. Technol.*, 2022, **346**, 126444, DOI: [10.1016/j.biortech.2021.126444](https://doi.org/10.1016/j.biortech.2021.126444).
- 99 M. Babu, S. P. Raj, C. B. Nirmala, M. Deccaraman and E. Sagadevan, Production of Single Cell Protein using *Kluyveromyces marxianus* isolated from paneer whey, *Int. J. Biomed. Adv. Res.*, 2014, **5**(05), 255–257.
- 100 K. u. Rehman, R. Ur Rehman, A. A. Somroo, M. Cai, L. Zheng, X. Xiao, A. Ur Rehman, A. Rehman, J. K. Tomberlin, Z. Yu and J. Zhang, Enhanced bioconversion of dairy and chicken manure by the interaction of exogenous bacteria and black soldier fly larvae, *J. Environ. Manage.*, 2019, **237**, 75–83, DOI: [10.1016/j.jenvman.2019.02.048](https://doi.org/10.1016/j.jenvman.2019.02.048).
- 101 M. Gogoi, S. Banerjee, S. Pati and S. Ray Chaudhuri, Microbial Bioconversion of Dairy Wastewater in Packed Bed Biofilm Reactor into Liquid Biofertilizer, *Geomicrobiol. J.*, 2022, **39**(3–5), 249–258, DOI: [10.1080/01490451.2021.1980921](https://doi.org/10.1080/01490451.2021.1980921).
- 102 A. K. Rai, H. C. Swapna, N. Bhaskar and V. Baskaran, Potential of seafood industry by products as sources of recoverable lipids: Fatty acid composition of meat and nonmeat component of selected Indian marine fishes, *J. Food Biochem.*, 2011, **36**, 441–448, DOI: [10.1111/j.1745-4514.2011.00549.x](https://doi.org/10.1111/j.1745-4514.2011.00549.x).
- 103 A. Shabani, F. Boldaji, B. Dastar, T. Ghoorchi and S. Zerehdaran, Preparation of fish waste silage and its effect on the growth performance and meat quality of broiler chickens, *J. Sci. Food Agric.*, 2018, **98**, 4097–4103, DOI: [10.1002/jsfa.8926](https://doi.org/10.1002/jsfa.8926).
- 104 K. Jayathilakan, K. Sultana, K. Radhakrishna and A. S. Bawa, Utilization of by products and waste materials from meat, poultry and fish processing industries: a review, *J. Food Sci. Technol.*, 2011, **49**, 278–293, DOI: [10.1007/s13197-011-0290-7](https://doi.org/10.1007/s13197-011-0290-7).
- 105 F. Toldrá, L. Mora and M. Reig, New insights into meat by-product utilization, *Meat Sci.*, 2016, **120**, 54–59, DOI: [10.1016/j.meatsci.2016.04.021](https://doi.org/10.1016/j.meatsci.2016.04.021).
- 106 D. Vamvuka, S. Dermitzakis, D. Pentari and S. Sfakiotakis, Valorization of meat and bone meal through pyrolysis for soil amendment or lead adsorption from wastewaters, *Food Bioprod. Process.*, 2018, **109**, 148–157, DOI: [10.1016/j.fbp.2018.04.002](https://doi.org/10.1016/j.fbp.2018.04.002).
- 107 A. Lasekan, F. Abu Bakar and D. Hashim, Potential of chicken by-products as sources of useful biological resources, *Waste Manage.*, 2013, **33**(3), 552–565, DOI: [10.1016/j.wasman.2012.08.001](https://doi.org/10.1016/j.wasman.2012.08.001).
- 108 U. u. Rahman, A. Sahar and M. A. Khan, Recovery and utilization of effluents from meat processing industries, *Food Res. Int.*, 2014, **65**, 322–328, DOI: [10.1016/j.foodres.2014.09.026](https://doi.org/10.1016/j.foodres.2014.09.026).
- 109 F. Z. Ozi, N. Boutaleb, M. Hadidi, B. Bahlaouan, M. Bennani, A. Silkina and S. El Antri, Production of bio-fertilizer by biotransformation of poultry waste enriched with molasses and algae, *Environ. Qual. Manag.*, 2022, **32**(3), 123–134, DOI: [10.1002/tqem.21868](https://doi.org/10.1002/tqem.21868).
- 110 A. Saeid, M. Labuda, K. Chojnacka and H. Górecki, Valorization of bones to liquid phosphorus fertilizer by microbial solubilization, *Waste Biomass Valorization*, 2013, **5**, 265–272, DOI: [10.1007/s12649-013-9238-7](https://doi.org/10.1007/s12649-013-9238-7).
- 111 J. S. Lamba, M. Wadhwa and M. P. S. Bakshi, Methane Production Potential of Fruit and Vegetable Wastes in Vitro, *Anim. Nutr. Feed Technol.*, 2016, **16**, 363–372, DOI: [10.5958/0974-181x.2016.00032.9](https://doi.org/10.5958/0974-181x.2016.00032.9).
- 112 N. G. Das, K. S. Huque, S. M. Amanullah, S. Dharmapuri and H. P. S. Makkar, Study of chemical composition and nutritional values of vegetable wastes in Bangladesh, *Vet. Anim. Sci.*, 2018, **5**, 31–37, DOI: [10.1016/j.vas.2018.02.003](https://doi.org/10.1016/j.vas.2018.02.003).
- 113 C. Fritsch, A. Staebler, A. Happel, M. Cubero Márquez, I. Aguiló-Aguayo, M. Abadias, M. Gallur, I. Cigognini, A. Montanari, M. López, F. Suárez-Estrella, N. Brunton, E. Luengo, L. Sisti, M. Ferri and G. Belotti, Processing, valorization and application of bio-waste derived compounds from potato, tomato, olive and cereals: A review, *Sustainability*, 2017, **9**, 1492, DOI: [10.3390/su9081492](https://doi.org/10.3390/su9081492).
- 114 C. Sabater, L. Ruiz, S. Delgado, P. Ruas-Madiedo and A. Margolles, Valorization of vegetable food waste and by-products through fermentation processes, *Front. Microbiol.*, 2020, **11**, 581997, DOI: [10.3389/fmicb.2020.581997](https://doi.org/10.3389/fmicb.2020.581997).
- 115 N. Jiménez-Moreno, I. Esparza, F. Bimbela, L. M. Gandía and C. Ancín-Azpilicueta, Valorization of selected fruit and vegetable wastes as bioactive compounds: Opportunities and challenges, *Crit. Rev. Environ. Sci. Technol.*, 2019, **50**, 2061–2108, DOI: [10.1080/10643389.2019.1694819](https://doi.org/10.1080/10643389.2019.1694819).
- 116 A. Saini, P. S. Panesar and M. B. Bera, Valorization of fruits and vegetables waste through green extraction of bioactive compounds and their nanoemulsions-based delivery system, *Bioresour. Bioprocess.*, 2019, **6**, 26, DOI: [10.1186/s40643-019-0261-9](https://doi.org/10.1186/s40643-019-0261-9).
- 117 B. Bayram, G. Ozkan, T. Kostka, E. Capanoglu and T. Esatbeyoglu, Valorization and application of fruit and vegetable wastes and by-products for food packaging materials, *Molecules*, 2021, **26**(13), 4031, DOI: [10.3390/molecules26134031](https://doi.org/10.3390/molecules26134031).
- 118 S. K. Panda, R. C. Ray, S. S. Mishra and E. Kayitesi, Microbial processing of fruit and vegetable wastes into potential biocommodities: a review, *Crit. Rev. Biotechnol.*, 2017, **38**, 1–16, DOI: [10.1080/07388551.2017.1311295](https://doi.org/10.1080/07388551.2017.1311295).
- 119 I. Chakravarty and S. A. Mandavgane, Valorization of fruit and vegetable waste for biofertilizer and biogas, *J. Food Process Eng.*, 2020, **44**(2), e13512, DOI: [10.1111/jfpe.13512](https://doi.org/10.1111/jfpe.13512).
- 120 A. El Barnossi, F. Moussaid and A. Iraqi Housseini, Quantitative Research of Systematic and Functional Microbial Groups Associated with Decaying Solid Green Household Waste in Water and Soil, *Pol. J. Environ. Stud.*, 2020, **29**, 2631–2639, DOI: [10.15244/pjoes/112365](https://doi.org/10.15244/pjoes/112365).
- 121 S. Dantroliya, C. Joshi, A. Mohapatra, D. Shah, P. Bhargava, S. Bhanushali, R. Pandit, C. Joshi and M. Joshi, Creating wealth from waste: An approach for converting organic waste in to value-added products using microbial



- consortia, *Environ. Technol. Innovation*, 2022, 25, 102092, DOI: [10.1016/j.eti.2021.102092](https://doi.org/10.1016/j.eti.2021.102092).
- 122 J. O'Connor, S. A. Hoang, L. Bradney, S. Dutta, X. Xiong, D. C. W. Tsang, K. Ramadass, A. Vinu, M. B. Kirkham and N. S. Bolan, A review on the valorisation of food waste as a nutrient source and soil amendment, *Environ. Pollut.*, 2021, 272, 115985, DOI: [10.1016/j.envpol.2020.115985](https://doi.org/10.1016/j.envpol.2020.115985).
- 123 J. O'Connor, S. A. Hoang, L. Bradney, J. Rinklebe, M. B. Kirkham and N. S. Bolan, Value of dehydrated food waste fertiliser products in increasing soil health and crop productivity, *Environ. Res.*, 2022, 204, 111927, DOI: [10.1016/j.envres.2021.111927](https://doi.org/10.1016/j.envres.2021.111927).
- 124 A. Mahmood, R. Iguchi and R. Kataoka, Multifunctional food waste fertilizer having the capability of *Fusarium*-growth inhibition and phosphate solubility: A new horizon of food waste recycle using microorganisms, *Waste Manage.*, 2019, 94, 77–84, DOI: [10.1016/j.wasman.2019.05.046](https://doi.org/10.1016/j.wasman.2019.05.046).
- 125 S. O. Dahunsi, S. Oranusi, V. E. Efeovbokhan, A. T. Adesulu-Dahunsi and J. O. Ogunwole, Crop performance and soil fertility improvement using organic fertilizer produced from valorization of *Carica papaya* fruit peel, *Sci. Rep.*, 2021, 11, 4696, DOI: [10.1038/s41598-021-84206-9](https://doi.org/10.1038/s41598-021-84206-9).
- 126 Y. Li, T. Cui, Y. Wang and X. Ge, Isolation and characterization of a novel bacterium *Pseudomonas aeruginosa* for biofertilizer production from kitchen waste oil, *RSC Adv.*, 2018, 8(73), 41966–41975, DOI: [10.1039/c8ra09779h](https://doi.org/10.1039/c8ra09779h).
- 127 J.-X. Lai, X. Chen, J. Bu, B.-B. Hu and M.-J. Zhu, Direct production of astaxanthin from food waste by *Phaffia rhodozyma*, *Process Biochem.*, 2022, 113, 224–233, DOI: [10.1016/j.procbio.2022.01.003](https://doi.org/10.1016/j.procbio.2022.01.003).
- 128 J. Lai, W. Liu, J. Bu, X. Chen, B. Hu and M. Zhu, Enhancement of astaxanthin production from food waste by *Phaffia rhodozyma* screened by flow cytometry and feed application potential, *Biotechnol. Appl. Biochem.*, 2023, 70, 1817–1829, DOI: [10.1002/bab.2484](https://doi.org/10.1002/bab.2484).
- 129 H. I. Owamah, S. O. Dahunsi, U. S. Oranusi and M. I. Alfa, Fertilizer and sanitary quality of digestate biofertilizer from the co-digestion of food waste and human excreta, *Waste Manage.*, 2014, 34, 747–752, DOI: [10.1016/j.wasman.2014.01.017](https://doi.org/10.1016/j.wasman.2014.01.017).
- 130 X. Wang, A. Selvam and J. W. C. Wong, Influence of lime on struvite formation and nitrogen conservation during food waste composting, *Bioresour. Technol.*, 2016, 217, 227–232, DOI: [10.1016/j.biortech.2016.02.117](https://doi.org/10.1016/j.biortech.2016.02.117).
- 131 E. Sufficiency, S. A. Qamar, L. F. R. Ferreira, M. Franco, H. M. N. Iqbal and M. Bilal, Emerging biotechnological strategies for food waste management: A green leap towards achieving high-value products and environmental abatement, *Energy Nexus*, 2022, 6, 100077, DOI: [10.1016/j.nexus.2022.100077](https://doi.org/10.1016/j.nexus.2022.100077).
- 132 S.-H. Tsai, C.-P. Liu and S.-S. Yang, Microbial conversion of food wastes for biofertilizer production with thermophilic lipolytic microbes, *Renewable Energy*, 2007, 32, 904–915, DOI: [10.1016/j.renene.2006.04.019](https://doi.org/10.1016/j.renene.2006.04.019).
- 133 K. M. Sangamithirai, J. Jayapriya, J. Hema and R. Manoj, Evaluation of in-vessel co-composting of yard waste and development of kinetic models for co-composting, *Int. J. Recycl. Org. Waste Agric.*, 2015, 4, 157–165, DOI: [10.1007/s40093-015-0095-1](https://doi.org/10.1007/s40093-015-0095-1).
- 134 C. Lin, A negative-pressure aeration system for composting food wastes, *Bioresour. Technol.*, 2008, 99(16), 7651–7656, DOI: [10.1016/j.biortech.2008.01.078](https://doi.org/10.1016/j.biortech.2008.01.078).
- 135 O. Stabnikova, H.-B. Ding, J.-H. Tay and J.-Y. Wang, Biotechnology for aerobic conversion of food waste into organic fertilizer, *Waste Manage. Res.*, 2005, 23(1), 39–47, DOI: [10.1177/0734242x05049768](https://doi.org/10.1177/0734242x05049768).
- 136 M. Jiang, W. Qiao, Y. Wang, T. Zou, M. Lin and R. Dong, Balancing acidogenesis and methanogenesis metabolism in thermophilic anaerobic digestion of food waste under a high loading rate, *Sci. Total Environ.*, 2022, 824, 153867, DOI: [10.1016/j.scitotenv.2022.153867](https://doi.org/10.1016/j.scitotenv.2022.153867).
- 137 D. Dadi, G. Daba, A. Beyene, P. Luis and B. Van der Bruggen, Composting and co-composting of coffee husk and pulp with source-separated municipal solid waste: a breakthrough in valorization of coffee waste, *Int. J. Recycl. Org. Waste Agric.*, 2019, 8, 263–277, DOI: [10.1007/s40093-019-0256-8](https://doi.org/10.1007/s40093-019-0256-8).
- 138 T. Hyun Chung and B. Ranjan Dhar, A multi-perspective review on microbial electrochemical technologies for food waste valorization, *Bioresour. Technol.*, 2021, 125950, DOI: [10.1016/j.biortech.2021.125950](https://doi.org/10.1016/j.biortech.2021.125950).
- 139 T. D. Evans, M. Boor and D. MacBrayne, Presented in Part at the 12th CIWEM European Biosolids & Biowastes Conference, West Yorkshire, 2007.
- 140 X. Xin, Y. Ma and Y. Liu, Electric energy production from food waste: Microbial fuel cells versus anaerobic digestion, *Bioresour. Technol.*, 2018, 255, 281–287, DOI: [10.1016/j.biortech.2018.01.099](https://doi.org/10.1016/j.biortech.2018.01.099).
- 141 O. P. Karthikeyan, S. Mehariya and J. W. Wong, Presented in Part at the 4th International Conference on Energy and Environment Research (ICEER), Porto, Portugal, 2017.
- 142 C. Du, J. J. Abdullah, D. Greetham, D. Fu, M. Yu, L. Ren, S. Li and D. Lu, Valorization of food waste into bio-fertilizer and its field application, *J. Cleaner Prod.*, 2018, 187, 273–284, DOI: [10.1016/j.jclepro.2018.03.211](https://doi.org/10.1016/j.jclepro.2018.03.211).
- 143 O. Oyetunji, N. Bolan and G. Hancock, comprehensive review on enhancing nutrient use efficiency and productivity of broadacre (arable) crops with the combined utilization of compost and fertilizers, *J. Environ. Manage.*, 2022, 317, 115395, DOI: [10.1016/j.jenvman.2022.115395](https://doi.org/10.1016/j.jenvman.2022.115395).
- 144 L. Zhu, X. Jia, M. Li, Y. Wang, J. Zhang, J. Hou and X. Wang, Associative effectiveness of bio-organic fertilizer and soil conditioners derived from the fermentation of food waste applied to greenhouse saline soil in Shan Dong Province, China, *Appl. Soil Ecol.*, 2021, 167, 104006, DOI: [10.1016/j.apsoil.2021.104006](https://doi.org/10.1016/j.apsoil.2021.104006).
- 145 H.-L. Xu, R. Wang and M. A. U. Mridha, Effects of organic fertilizers and a microbial inoculant on leaf photosynthesis and fruit yield and quality of tomato



- plants, *J. Crop Prod.*, 2001, 3(1), 173–182, DOI: [10.1300/j144v03n01\\_15](https://doi.org/10.1300/j144v03n01_15).
- 146 J. Södergren, C. U. Larsson, L. Wadsö, K.-J. Bergstrand, H. Asp, M. Hultberg and J. Schelin, Food waste to new food: Risk assessment and microbial community analysis of anaerobic digestate as a nutrient source in hydroponic production of vegetables, *J. Cleaner Prod.*, 2022, 333, 130239, DOI: [10.1016/j.jclepro.2021.130239](https://doi.org/10.1016/j.jclepro.2021.130239).
- 147 Z. J. Yong, M. J. K. Bashir and M. S. Hassan, Biogas and biofertilizer production from organic fraction municipal solid waste for sustainable circular economy and environmental protection in Malaysia, *Sci. Total Environ.*, 2021, 776, 145961, DOI: [10.1016/j.scitotenv.2021.145961](https://doi.org/10.1016/j.scitotenv.2021.145961).
- 148 Y. Ma and Y. Liu, Turning food waste to energy and resources towards a great environmental and economic sustainability: An innovative integrated biological approach, *Biotechnol. Adv.*, 2019, 37, 107414, DOI: [10.1016/j.biotechadv.2019.06.013](https://doi.org/10.1016/j.biotechadv.2019.06.013).
- 149 S. Cheon, H. M. Kim, M. Gustavsson and S. Y. Lee, Recent trends in metabolic engineering of microorganisms for the production of advanced biofuels, *Curr. Opin. Chem. Biol.*, 2016, 35, 10–21, DOI: [10.1016/j.cbpa.2016.08.003](https://doi.org/10.1016/j.cbpa.2016.08.003).
- 150 M.-Q. Liu, X.-J. Dai, L.-F. Bai and X. Xu, Cloning, expression of *Aspergillus niger* JL-15 endo-polygalacturonase A gene in *Pichia pastoris* and oligo-galacturonates production, *Protein Expression Purif.*, 2014, 94, 53–59, DOI: [10.1016/j.pep.2013.10.025](https://doi.org/10.1016/j.pep.2013.10.025).
- 151 P. Gajdoš, J. Hambalko, O. Slaný and M. Čertík, Conversion of waste materials into very long chain fatty acids by the recombinant yeast *Yarrowia lipolytica*, *FEMS Microbiol. Lett.*, 2020, 367(6), fnaa042, DOI: [10.1093/femsle/fnaa042](https://doi.org/10.1093/femsle/fnaa042).
- 152 K. Grohmann, R. G. Cameron and B. S. Buslig, *Fermentation of Orange Peel Hydrolysates by Ethanologenic Escherichia coli*, Humana Press, Totowa, NJ, 1996.
- 153 I. Ben Tahar and P. Fickers, Metabolic engineering of microorganisms for urban waste valorization, *Case Stud. Chem. Environ. Eng.*, 2021, 4, 100148, DOI: [10.1016/j.cscee.2021.100148](https://doi.org/10.1016/j.cscee.2021.100148).





# Synergistic mixture of the *Dactyloctenium aegyptium* extract and KI as an environment friendly and highly efficient corrosion inhibitor for steel in 0.5 M HCl

Raghvi<sup>a</sup>, Akhil Saxena<sup>a,\*</sup>, Jasdeep Kaur<sup>a,\*\*</sup>, Elyor Berdimurodov<sup>b,c,d</sup>, Dakeshwar Kumar Verma<sup>e</sup>

<sup>a</sup> Department of Chemistry, Chandigarh University, Gharuan, Mohali, Punjab, India

<sup>b</sup> Chemical & Materials Engineering, New Uzbekistan University, 54 Mustaqillik Ave., Tashkent, 100007, Uzbekistan

<sup>c</sup> University of Tashkent for Applied Sciences, Str. Gavhar 1, Tashkent, 100149, Uzbekistan

<sup>d</sup> Department of Physical Chemistry, National University of Uzbekistan, Tashkent, 100034, Uzbekistan

<sup>e</sup> Department of Chemistry, Govt. Digvijay Autonomous Postgraduate College, Rajnandgaon, Chhattisgarh, 491441, India

## ARTICLE INFO

### Keywords:

*Dactyloctenium aegyptium* extract (DAE)

Weed management

Eco-inhibition

Electrochemical investigations

SEM

Computational studies

## ABSTRACT

To prevent steel from corroding in HCl solution, a cost-effective inhibitor of *Dactyloctenium aegyptium* and KI is presented. UV-Vis, infrared spectroscopy, and scanning electron microscopy analysis are used to undertake a comprehensive experimental evaluation of the inhibitors and their interactions with the steel. The optimum concentration of the *Dactyloctenium aegyptium* extract (DAE) with the maximum corrosion protection efficacy is found via electrochemical measurements. The bioactive constituents of the DAE such as Tricin, Vanillic acid, *p*-hydroxybenzaldehyde, and *p*-hydroxybenzoic acid conferred a maximum inhibition efficiency of 95.7 % at 800 ppm. The inhibitory activity of its ethanolic extract increased with increasing concentration. Further various adsorption isotherm models including Langmuir, Temkin and Freundlich were used to understand the adsorption of the DAE on the metal surface. The DFT based investigations show that the active constituents of the DAE are highly polarized, soluble in aqueous solution and adsorb on the steel surface efficiently.

## 1. Introduction

Steel, a predominantly iron and carbon alloy, can be commonly found in things as small as a needle to as enormous as construction marvels. Renowned for its remarkable strength, toughness, and resistance to a range of climatic conditions, steel is one of the most significant materials in contemporary civilization because of the versatility and functionality it provides which are further enhanced through the addition of other alloying elements. According to the World Steel Association report on 'World Steel in 2023', India marks its place in the top 64 % of countries to produce 97 % of the world's crude steel. It stands 2nd in crude steel production and use of finished steel goods succeeding China, whereas it's placed 7th as a global steel exporter. Industrial market plays a crucial role in backing-up a nation's economy and steel in turn is pivotal in backing-up the industries. From construction bars, steel plates, pipelines, boilers and machinery parts small to big, almost all is

constituted of steel in one way or the other. In industries highly concentrated acids are used to clean the steel surfaces but it causes acidic corrosion.

The indispensability of steel, however, makes it an easy prey for corrosion. Prolonged exposure to environmental and chemical agents deteriorates its structural integrity as well as operations through corrosion. Though being an important part of industrial equipment, machinery and pipelines, steel commonly suffers acidic corrosion caused by 'steel pickling', a common process practiced for degreasing, descaling, and cleaning the pipes and parts by the use of concentrated acids such as hydrochloric acid and sulphuric acid known as pickling agents. The persistent use of such aggressive acids causes gradual electrochemical surface reactions or in other words, 'eats up' the steel surface, thereby changing its composition and ultimately causing massive loss on the whole [1].

Many corrosion inhibition techniques have been developed over the

\* Corresponding author.

\*\* Corresponding author.

E-mail addresses: [akhil.uis@cumail.in](mailto:akhil.uis@cumail.in) (A. Saxena), [jasdeep.e9012@cumail.in](mailto:jasdeep.e9012@cumail.in) (J. Kaur).

<https://doi.org/10.1016/j.jics.2024.101317>

Received 23 May 2024; Received in revised form 20 July 2024; Accepted 18 August 2024

Available online 20 August 2024

0019-4522/© 2024 Indian Chemical Society. Published by Elsevier B.V. All rights are reserved, including those for text and data mining, AI training, and similar technologies.

**Table 1**  
Brief of some latest plants studied for their anticorrosive properties on steel in acidic media.

S. No.	Plant	Metal	Corrosive Medium	Efficiency	Plant extract concentration	Methods	Reference No.
1.	<i>Datura stramonium</i>	Mild Steel	1 M HCl	94.2 %	0.2 g/L	Weight loss, PDP, EIS, UV-Vis., SEM/EDX	[6]
2.	<i>Syzygium aromaticum</i>	Mild Steel	0.5 M HCl	94 %	4 g/L	PDP, EIS, Computational studies	[7]
3.	<i>Salvia rosmarinus</i>	Mild Steel	1 M HCl	87 %	800 ppm	Weight loss, PDP, EIS, FT-IR, UV-Vis., FE-SEM, AFM	[8]
4.	<i>Spinacia oleracea</i>	Carbon Steel	1 M HCl	93 %	500 ppm	Weight loss, PDP, EIS, AAS	[9]
5.	<i>Ammi visnaga</i> L.	Carbon Steel	1 M HCl	84 %	700 ppm	Weight loss, PDP, EIS, SEM, Computational studies	[10]
6.	<i>Hedera helix</i>	XC18 Steel	1 M HCl	92.67 %	1000 ppm	Weight loss, PDP, EIS, SEM, Computational studies	[11]
7.	<i>Urtica dioica</i> L.	×38 Mild Steel	0.5 M H <sub>2</sub> SO <sub>4</sub>	90 %	4 g/L	Weight loss, PDP, EIS, SEM, Computational studies	[12]
8.	<i>Pelargonium graveolens</i>	Mild Steel	0.5 M H <sub>2</sub> SO <sub>4</sub>	92.6 %	200 ppm	PDP, EIS, SEM/EDX	[13]
9.	<i>Mimosa pudica</i>	Stainless Steel	0.5 M H <sub>2</sub> SO <sub>4</sub>	92 %	500 ppm	Weight loss, PDP, EIS, AFM, Computational studies	[14]
10.	<i>Petroselinum crispum</i>	Carbon Steel	1 M H <sub>2</sub> SO <sub>4</sub>	90.2 %	300 ppm	Weight loss, PDP, EIS, FT-IR, XPS	[15]
11.	<i>Terminalia bellerica</i>	Steel	1 M H <sub>2</sub> SO <sub>4</sub>	91.79 %	4000 ppm	Weight loss, PDP, EIS, SEM, Computational studies	[16]
12.	<i>Eupatorium adenophora spreng/KI</i>	Cold Rolled Steel	0.5 M H <sub>2</sub> SO <sub>4</sub>	93.3 %	–	Gravimetric, PDP, EIS, SEM, AFM	[17]

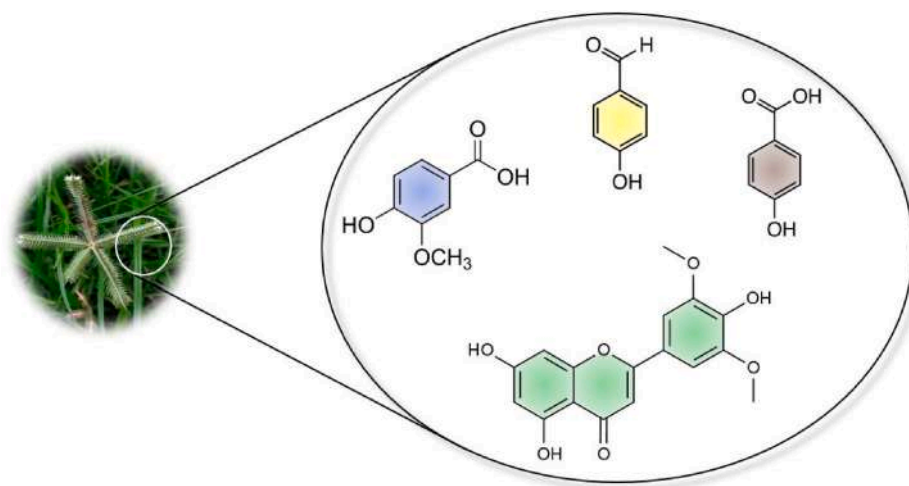


**Fig. 1.** Active phytochemical constituents present in *Dactyloctenium aegyptium*.

years to tackle this problem such as the use of paints, galvanization and corrosion inhibitors. All of these practices work by the development of a coating on the surfaces of metals, thus isolating it from the direct attack of corrosive agents. Eliminating cracks, proper drainage, and ventilation have also been a few examples of good design practices to help stop moisture buildup and reduce corrosion rate.

Rest being traditional practices, there has been a surge in the development and use of corrosion inhibitors over the past few years. Corrosion inhibitors are broadly divided into synthetic and natural, based on the source of derivation. As their names say, synthetic inhibitors are lab-developed chemical substances. Compounds of zinc, phosphates, surfactants, and paints fall under this type. Natural corrosion inhibitors on the other hand originate from natural sources such as plant extracts, oils, and minerals [2–5].

The potential of natural corrosion inhibitors has been in extensive exploration over the past 15–20 years owing to their profitability in biodegradability and abundance coming from renewable sources. Not only do they align with the green initiatives by being environmentally benign, but natural corrosion inhibitors are also net cost-effective and provide additional synergic benefits such as antimicrobial and anti-fungal properties over synthetic corrosion inhibitors. The rationale behind the use of natural corrosion inhibitors is the presence of bioactive compounds such as alkaloids, flavonoids, terpenoids, etc. known as

Phytochemicals, which are rich in heteroatoms. These heteroatoms aid in the adsorption of the inhibitor onto the metal surface through lone pair donation to the metal's empty orbitals. Corrosion inhibition efficacy of a few lately reported plants has been compiled in Table 1 [6–17].

*Dactyloctenium aegyptium*, commonly known as Durban crowfoot or Egyptian crowfoot grass, grows in loamy and damp soil conditions and is native to Africa and Asia. Often used as fodder for ruminants, it's classified as a Category 2 invasive weed by the 'Florida Exotic Pest Plant Council' (FLECCP). It is easily available in abundance along the roadside, in fields, and in gardens. The literature survey renders the presence of many notable phytochemicals in its extract. But out of these, *p*-hydroxybenzaldehyde, *p*-hydroxybenzoic acid, Tricin, and Vanillic acid play a major role owing to the availability of rich heteroatoms, functional groups and  $\pi$ -ring systems [18] (Fig. 1). *Dactyloctenium aegyptium* has already been studied for its pharmacological, biofuel, antioxidant, antibacterial, and anti-fertility properties [19–22], however, there has been no investigation on its anticorrosive behaviour yet.

Applying natural corrosion inhibitors in the acidic environment has been a good tactic to reduce the corrosion rate of metals. However, at times the plant extract solely is not capable of exhibiting a reduced corrosion rate of metals due to certain factors. Certain studies have addressed this problem by presenting the enhanced corrosion inhibition effectiveness of the plant extracts when combined with small amounts of

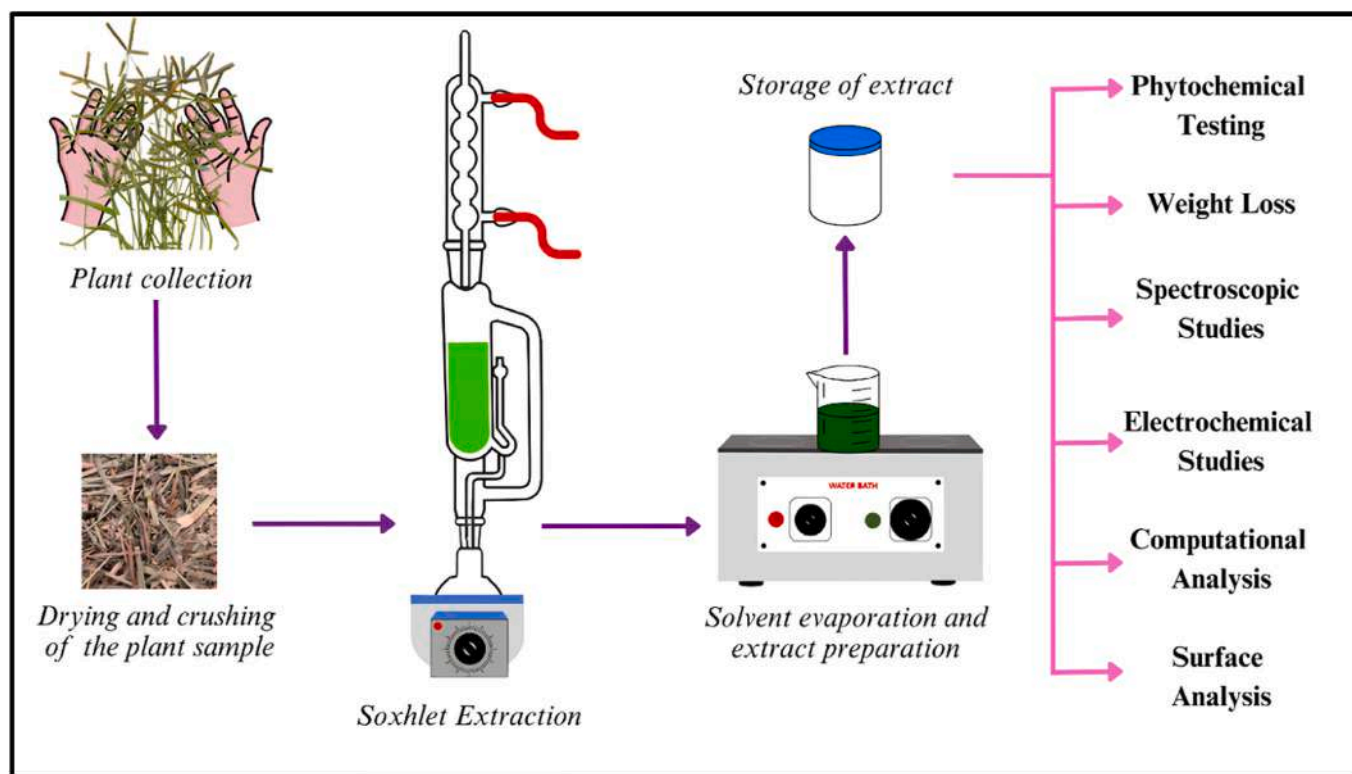


Fig. 2. A schematic diagram of preparation of the *Dactyloctenium aegyptium* extract and methodology.

inorganic salts containing  $I^-$ ,  $Cl^-$  and  $Br^-$  [23–27]. Therefore, the present study aims to explore the anticorrosive effectiveness of *Dactyloctenium aegyptium*, a commonly found grass weed and also to check its efficacy in the presence of KI under the acidic conditions of 0.5 M HCl on steel.

## 2. Experimental

### 2.1. Preparation of corrosive medium

The corrosive medium was prepared using the laboratory-available hydrochloric acid by Chemigens Research & Fine Chemicals, diluting it to 0.5 M in distilled water by applying the basic molarity equation  $M_1V_1 = M_2V_2$ . 100 mL of this 0.5 M aggressive solution of HCl was used for the forthcoming studies.

### 2.2. Preparation of steel specimens

Steel sheet was purchased from Metal & Hardware Store in Industrial Area, Chandigarh. The sheet was cut into 1 cm × 1 cm square pieces and made smooth using high grades of emery paper. These were later washed thoroughly with distilled water and dried well in the folds of filter paper before use. The composition of the steel was acquired from the Central Institute of Hand Tools Jalandhar. The steel used in this work contains 99.2 % Fe, 0.120 % Si, 0.105 % C, 0.378 % Mn and 0.079 % S.

### 2.3. Preparation of extract

*Dactyloctenium aegyptium* was collected with roots, thoroughly cleaned under tap water and air dried in the shade. Once completely dry, it was ground into semi-coarse powder and put on Soxhlet for 5 Hrs using 200 mL of 95 % (v/v) ethanol as the solvent. The extract was then filtered and kept on the water bath until a solid concentrate was obtained. The concentrate was stored in an air-tight bottle for further studies. A schematic diagram of the preparation of DAE extract is shown

Table 2

Qualitative phytochemical testing.

Phytochemical	Test Performed	Expected Positive Result
Alkaloids	Wagner's test: the extract was subjected to Wagner's reagent (1:5 mixture of aqueous iodine and potassium iodide)	Reddish-brown precipitates
Flavonoids	Few drops of dil. NaOH was added to the extract	Appearance of yellow color
Saponins	5 mL water and 5 mL of the extract filtrate was mixed vigorously	Steady foam formation
Coumarin	A few drops of alcoholic NaOH were added to 2 mL of the extract	Appearance of yellow color
Sugars	Fehling solutions A & B were taken in a 1:1 ratio and boiled for 1 min. They were added to 1 mL of extract and heated for 5–10 min on the water bath	Appearance of yellowish or brick-red precipitates
Tannins	Two drops of 5 % $FeCl_3$ were added to the extract	Greenish precipitates
Terpenoids	Salkowski test: 2 mL chloroform was mixed with 2 mL of extract. To this 3 mL conc. $H_2SO_4$ was added slowly	Reddish-brown color at the interface

in Fig. 2.

### 2.4. Phytochemical testing

The filtrate of ethanolic extract was subjected to the following tests given in Table 2 to check for the presence of constituent phytochemicals [28].

### 2.5. Weight loss measurements

In each 250 mL beaker, different concentrations of the *Dactyloctenium aegyptium* extract (DAE) were prepared up to 100 mL by diluting with the corrosive medium. Initial weights of clean steel pieces were



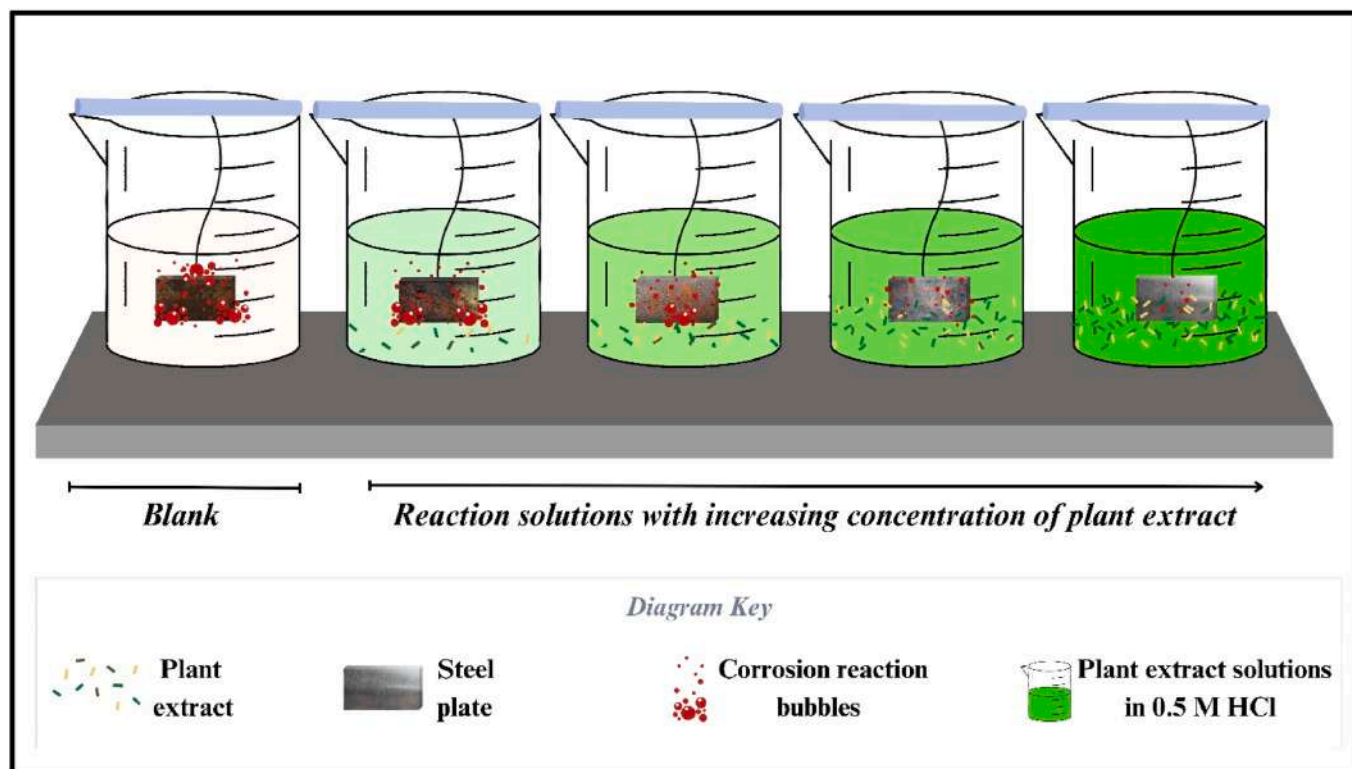


Fig. 3. A schematic diagram of the weight loss measurements at room temperature.

taken. They were tied with a thread and each was suspended in a different plant extract solution with the help of capillaries. One steel piece was suspended in only 0.5 M HCl which served as a blank solution (Fig. 3). After keeping for 24 h at room temperature, the pieces were taken out and air dried completely followed by noting their final weights. Weight loss was repeated with similar concentrations of the plant extract but 0.1 g KI was added to each this time. Triplicate tests were performed for each concentration. The corrosion inhibition efficiency ( $\eta$ ) and surface coverage ( $\theta$ ) were calculated with equations (1) and (2), respectively [29].

$$\eta \% = \frac{W_0 - W_e}{W_0} \times 100 \quad (1)$$

$$\theta = \frac{W_0 - W_e}{W_0} \quad (2)$$

where,  $W_0$ : difference in weight of steel plate dipped in blank solution (g).

$W_e$ : difference in weight of steel plate dipped in plant extract solution (g).

## 2.6. Adsorption isotherm

### 2.6.1. Langmuir adsorption isotherm

For a better understanding of the inhibitor's adsorption process onto the steel surface, a theoretical approach of using the adsorption isotherm was adopted. Generally used Langmuir Adsorption Isotherm comprises plotting a graph between  $C$  v/s  $C/\theta$  using the results of weight loss to obtain a best-fit line having  $R^2 \approx 1$ . Extent of adsorption is determined from  $K_{ads}$  as calculated from the inhibitors optimal concentration and the slope of the graph. Having high values of  $K_{ads}$  and slope  $\approx 1$  are ideally desired, implying strong adsorption of the inhibitor onto the metal surface [30–32].

Langmuir Adsorption Isotherm can be written as mentioned in equation (3)-

$$\frac{C}{\theta} = \frac{1}{K_{ads}} + C \quad (3)$$

where  $C$  refers to the optimal concentration of DAE used,  $\theta$  is the surface coverage and  $K_{ads}$  is the adsorption equilibrium constant.

### 2.6.2. Freundlich Isotherm

The Freundlich isotherm model describes a multiple-layer adsorption process on a heterogeneous adsorbent substrate, dismissing the lateral interactions. Theoretically, binding sites that are more energetically favorable are initially occupied, and binding strength declines as coverage increases, along with irregular enthalpy distribution. The non-linear and linear form of Freundlich isotherm is expressed by equations (4) and (5), respectively. A graph between  $\log \theta$  and  $\log C$  is plotted to best fit, wherein the value of slope represents  $n$  and intercept gives the  $K_{ads}$  values.

$$\theta = K_{ads} C^n \quad (4)$$

$$\log \theta = \log K_{ads} + n \log C \quad (5)$$

### 2.6.3. Temkin Isotherm

According to this isotherm, a multiple-layer adsorbent-adsorbate interactions ( $\alpha$ ) diminish the heat of adsorption of all molecules in the layer linearly rather than logarithmically as surface coverage increases. Adsorption involves a consistent distribution of binding energies, up to an optimal binding energy. The non-linear and linear form of Temkin isotherm is expressed by (vi) and (vii), respectively. Graphical representation of Temkin isotherm involves a best fit plot of  $\theta$  versus  $\log C$ .

$$e^{-2a\theta} = K_{ads} C \quad (6)$$

$$\theta = \frac{-2.303 \log K_{ads}}{2\alpha} + \frac{-2.303 \log C}{2\alpha} \quad (7)$$

where,  $C$  refers to the optimal concentration of DAE used,  $\theta$  is the surface

coverage and  $K_{ads}$  is the adsorption equilibrium constant. Graphs are plotted to best fit for each of these isotherms using the weight loss data and regression coefficient ( $R^2$ ) obtained. Having a higher  $R^2$  value usually  $\approx 1$  is desired to confirm the prevalence of either of the isotherm [33,34].

## 2.7. Potentiodynamic polarization estimation

Using a three-electrode setup of PGSTAT-204 Metrohm Autolab electrochemical workstation, polarization measurements were performed at 298 K using 100 mL of corrosive medium. The working electrode was prepared by covering the steel rod in Araldite resin in such a way that only 1 cm<sup>2</sup> region was left exposed for the reaction. Once dry, the periphery of the resin along with the exposed steel surface was polished smooth with high grades of emery paper. As a counter electrode, a platinum electrode was employed and as a reference electrode, a saturated calomel electrode was used. The working electrode was initially left undisturbed in the corrosive liquid for around 60 min to settle the OCP. Polarization graphs were produced between potentials of  $-0.1$  V and  $+0.1$  V in a current range of 100 nA to 1 mA at a scan rate of 0.001 V/s. Triplicate experiments were performed for all electrochemical measurements [30]. Tafel extrapolation gave the corrosion inhibition efficiency using the given formula-

$$\eta \% = \frac{I_{0corr} - I_{icorr}}{I_{0corr}} \times 100 \quad (8)$$

where  $I_{0corr}$  and  $I_{icorr}$  are corrosion densities in the absence and presence of plant extract, respectively.

## 2.8. EIS: electrochemical impedance spectroscopy

An identical electrochemical cell and workstation used for polarization estimations were utilized to perform electrochemical impedance spectroscopy in the frequency range of  $1 \times 10^5$  Hz–0.1 Hz with 10 frequencies per decade. The OCP amplitude was 0.01 V. Working electrode was left in the corrosive media for around 60 min. The Nyquist and Bode charts were used to get impedance information [35]. The effectiveness of inhibition was estimated using formula 9-

$$\eta \% = \frac{R_{ct} - R_{ct}^0}{R_{ct}} \times 100 \quad (9)$$

where  $R_{ct}$  and  $R_{ct}^0$  stand for charge transfer resistances with and without the inhibitor, respectively.

## 2.9. UV-visible spectroscopy

The similar plant extract concentrations used in weight loss measurements were subjected to UV-visible spectroscopic inspection using a Shimadzu UV-1900 spectrophotometer. Initially, the spectral analyses was done for plant extract solutions without dipping the steel piece and later taken for the same plant extract solutions after being dipped with the steel pieces for 24 h. It was crucial in inferring the adsorption mechanism of the inhibitor on the steel surface [31].

## 2.10. Surface morphological analyses

Surface morphological studies have been quite a valuable technique in visualizing and comprehending the impact of coatings and inhibitors on varied materials of profound interest and applicability. Using JEOL JSM-IT500A, the current study examined the surface morphology of steel under four conditions i.e. clean non-corroded steel piece, maximum corroded steel piece in 0.5 M HCl and inhibited steel piece by 800 ppm of DAE solution without and with KI. SEM images were collected for all four and contrasted to apprehend the inhibitor protection and adsorption onto the metal surface [32,36].

**Table 3**

Results of Phytochemical tests of the *Dactyloctenium aegyptium* extract.

PHYTOCHEMICAL	TEST PERFORMED	RESULT
• Alkaloids	Wagner's test	++
• Flavonoids	Dil. NaOH test	++
• Saponins	Foam test	++
• Coumarin	Alcoholic NaOH test	--
• Sugars	Fehling's test	++
• Tannins	Ferric Chloride test	++
• Terpenoids	Salkowski test	++

**Table 4**

Corrosion inhibition efficiency and surface coverage of *Dactyloctenium aegyptium* extract without and with KI in 0.5 M HCl.

(a) <i>Dactyloctenium aegyptium</i> extract without KI				
Concentration (ppm)	Weight Loss ( $\Delta W$ ) (g)	Inhibition Efficiency ( $\eta$ ) (%)	Surface Coverage ( $\theta$ )	Standard Deviation ( $\sigma$ )
0	0.201 $\pm$ 0.002	–	–	–
200	0.103 $\pm$ 0.003	48.7	0.487	0.880
400	0.096 $\pm$ 0.001	52.2	0.522	0.498
600	0.072 $\pm$ 0.004	64.1	0.641	0.531
800	0.060 $\pm$ 0.001	70.1	0.701	0.725
(b) <i>Dactyloctenium aegyptium</i> extract with 0.1 g KI				
Concentration (ppm)	Weight Loss ( $\Delta W$ ) (g)	Inhibition Efficiency ( $\eta$ ) (%)	Surface Coverage ( $\theta$ )	Standard Deviation ( $\sigma$ )
0	0.316 $\pm$ 0.010	–	–	–
200	0.097 $\pm$ 0.001	69.3	0.693	0.612
400	0.038 $\pm$ 0.001	87.9	0.879	1.189
600	0.024 $\pm$ 0.003	92.4	0.924	0.410
800	0.014 $\pm$ 0.002	95.5	0.955	0.294

## 2.11. DFT-based theoretical investigations

The DFT calculations are extensively used to understand the relationship between corrosion inhibition and molecular structures at the atomic level. This approach is particularly valuable because experimental investigations at the atomic scale often do not provide sufficient depth for comprehending corrosion inhibition [37–40]. Various sub-methods of DFT were applied to establish the theoretical foundation of corrosion inhibition for selected organic compounds [41]. For this study, the GAMESS-US software [42,43] with the 6-21G basis sets [44], along with density functional theory (DFT) and B3LYP (three-parameter Lee–Yang–Parr correlation function by Becke) [45,46] methods, were utilized to investigate Pistiphlorogluciny, Pistaciaphenyl ethers, and Naringenin as corrosion inhibitors. Visualization and analysis were performed using wxMacMolPlt [47] and Avogadro [48,49].

## 3. Results & discussion

### 3.1. Inferring the phytochemicals

On subjecting the ethanolic filtrate of DAE to the standard qualitative phytochemical testing, it was found that except coumarin, all other tested phytochemicals were present as reported in Table 3. The richness of such varied classes of phytochemicals in the taken plant extract

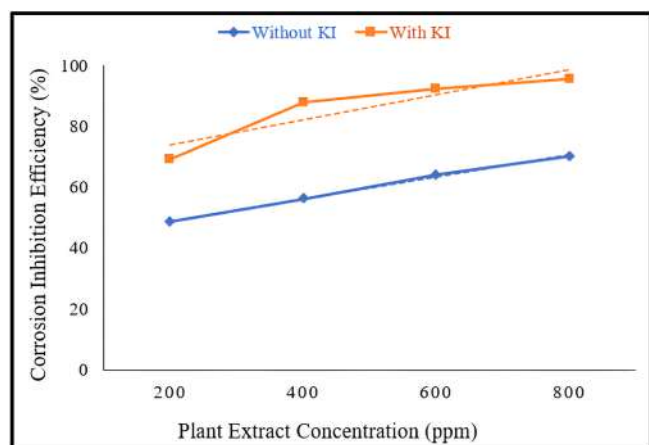


Fig. 4. Corrosion inhibition efficiency of the DAE extract in 0.5 M HCl without and with KI.

implied that the inhibitor shows a high chance of strong adsorption onto the metal surface due to the numerous available heteroatoms comprised by its diverse bioactive constituents [50].

### 3.2. Weight loss measurements

Weight loss studies were carried out at room temperature using 200 ppm, 400 ppm, 600 ppm, and 800 ppm of the DAE with and without the

addition of KI. Its maximum solubility was 800 ppm in the corrosive solution. As inferred from Table 4, the corrosion inhibition efficiency increased with increasing concentration of the plant extract either with its sole use or when combined with KI. This implied the greater extent of adsorption by the donation of electron lone pairs of the heteroatoms present in the inhibitor into the empty d-orbitals of the metal surface as more and more phytochemicals are available with the extract's increasing concentration. However, the corrosion inhibition efficiency of the inhibitor combined with KI is more than the extract solely over all the concentrations. This reason for some synergism between the extract and KI resulting in enhanced and stronger adsorptive inhibition of the steel against the corrosive acidic medium. Surface coverage has also been reported which aligns with the trend of inhibition efficiency i.e. more and more surface of the steel piece is being protected by the plant extract with increasing concentrations of the active constituents, that of extract with KI yet being greater than the extract alone. Fig. 4 provides a graphical comprehension of the corrosion inhibition efficiency of the plant extract with and without KI.

### 3.3. Adsorption isotherm study

Following the adsorption isotherms as discussed in section 2.6., Fig. 5(a), (b) and (c) illustrates the plot of Langmuir, Freundlich and Temkin adsorption isotherms respectively without and with the addition of KI. A higher regression coefficient ( $R^2$ ) value can be seen in Fig. 5 (a) hence a clear indicative of its overall prevalence in the present study. The values of  $R^2$ , slope, and  $K_{ads}$  as calculated for the plant extract in the absence and presence of KI using the Langmuir adsorption isotherm are

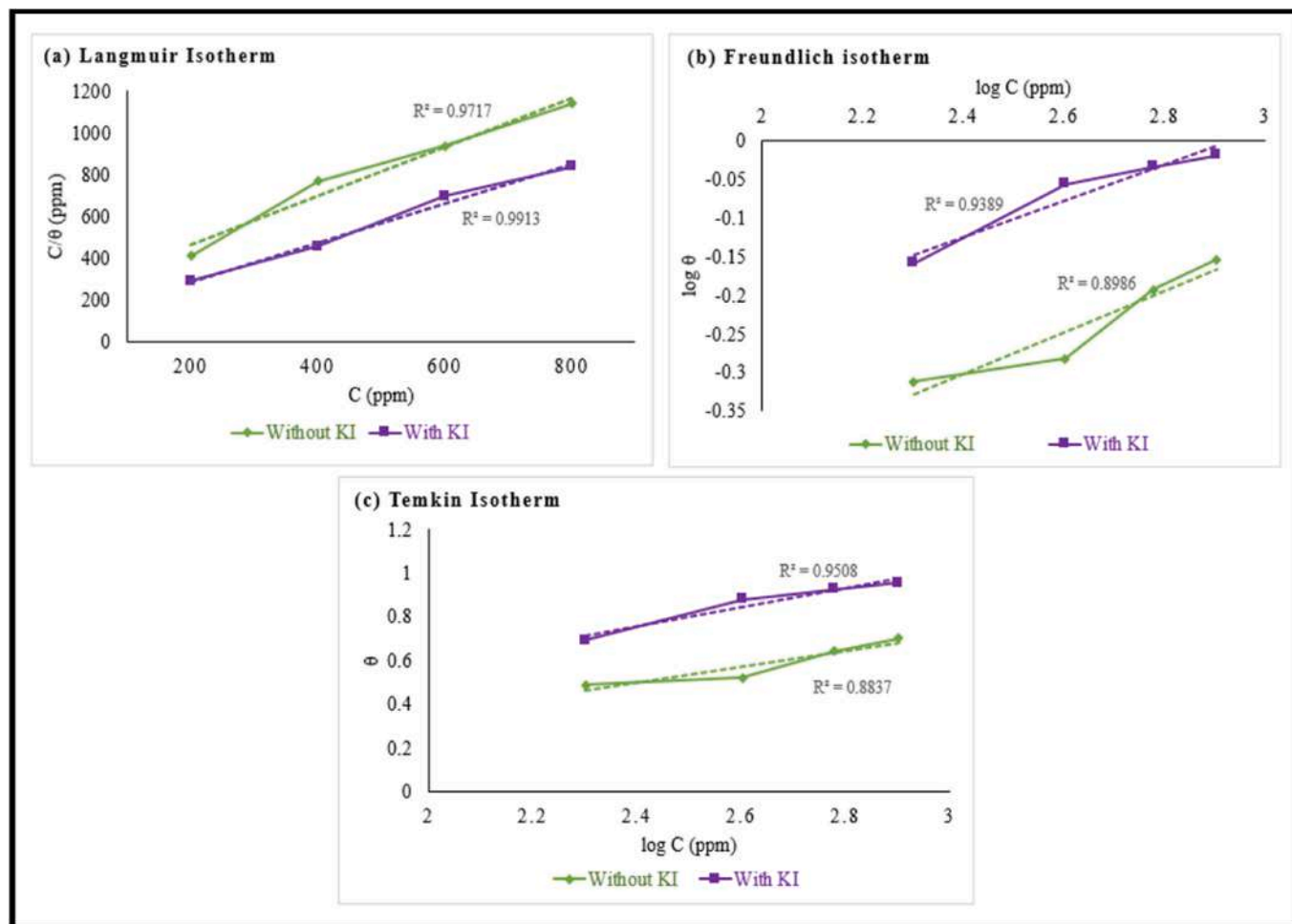
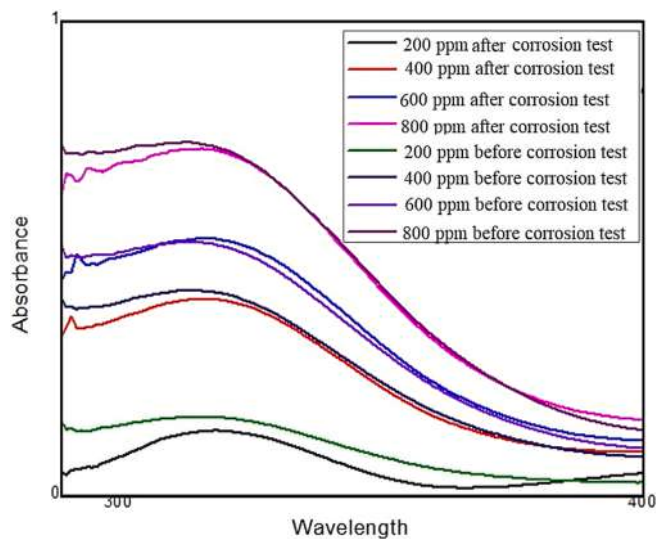


Fig. 5. Plot of Langmuir Adsorption Isotherm (a), Freundlich Isotherm (b) and Temkin Isotherm (c) for *Dactyloctenium aegyptium* extract.

**Table 5**

Values of  $R^2$ , equilibrium adsorption constant and slope for *Dactyloctenium aegyptium* extract as obtained from Langmuir Adsorption Isotherm.

<i>Dactyloctenium aegyptium</i> extract	$K_{ads}$ (ppm <sup>-1</sup> )	Slope	$R^2$
In absence of KI	$0.293 \times 10^{-2}$	1.18071	0.9717
In presence of KI	$2.652 \times 10^{-2}$	0.94328	0.9913

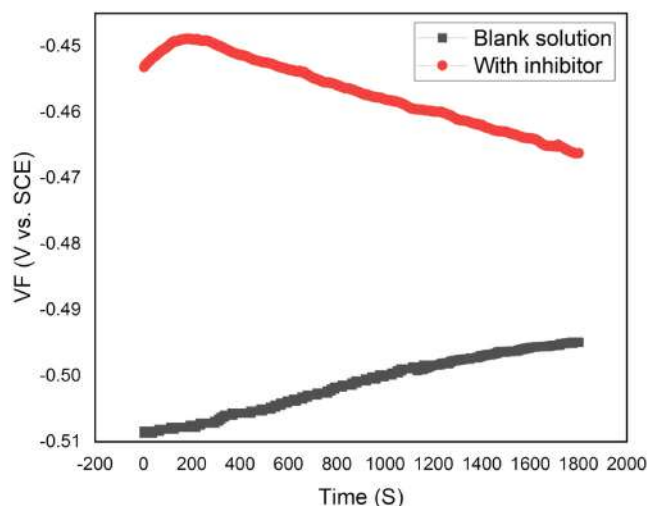


**Fig. 6.** Comparative UV-Vis. Spectrum for the adsorption of active constituents in varied concentrations of *Dactyloctenium aegyptium* extract onto the steel piece before and after immersion.

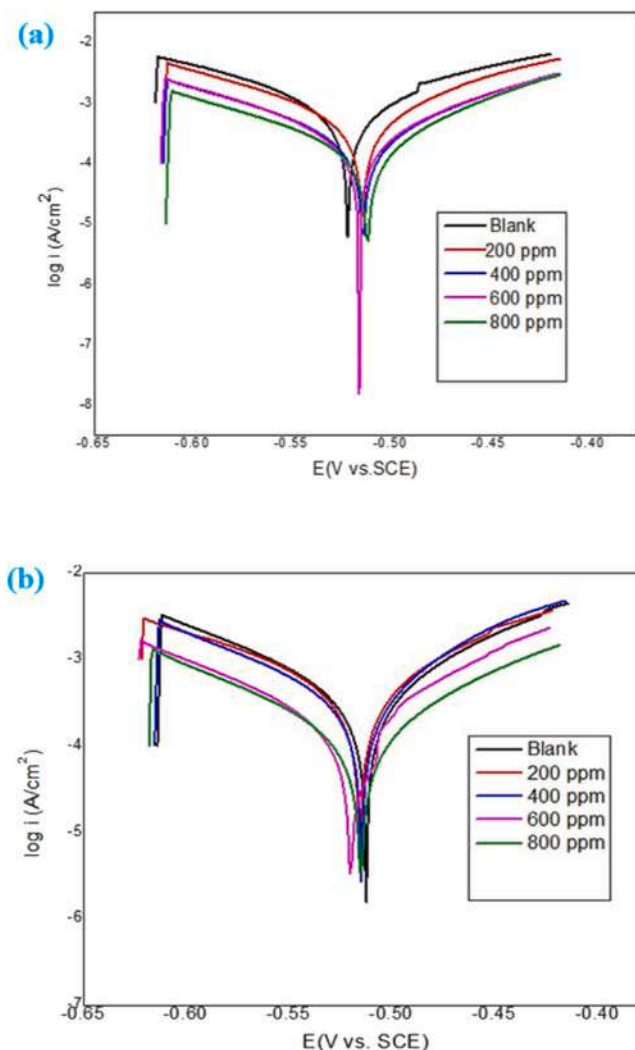
reported in Table 5. It can be seen that the value of  $K_{ads}$  is higher for extract combined with KI as compared to the extract solely, signifying the greater extent of adsorption and corrosion inhibition in the former than the latter. The slope too, in both cases, is  $\approx 1$  which means both cases of plant extract show desirable inhibition. Though lower than the Langmuir isotherm, the regression coefficient for DAE + KI system in the Freundlich isotherm is likewise near to unity. This observation suggested the likelihood of some extent of monolayer adsorption due to enhanced physisorption between the iodide and the phytochemicals present in the plant extract. Similar specific observations are made for the DAE/KI system in Temkin isotherm implying uniform surface coverage by the plant extract on the steel's surface [51]. These parameters indicate that the inhibitor is exhibiting strong and effective adsorption onto the steel surface.

### 3.4. UV-visible spectroscopy

This spectral study is intended to check whether the plant extract is getting adsorbed onto the steel or not hence, the UV-visible spectra of the DAE solution at varied concentrations in the presence of KI have been shown in Fig. 6 under the conditions of before and after 24 h dipping of the steel piece in the solution. A clear comparison can be made of the spectra wherein the absorbance is seen to be decreasing after the immersion of the steel piece in all concentrations which can be attributed to the reduction of the active constituents in the solution due to their adsorption onto the steel piece on dipping. Whereas the plant extract solution initially has all the active constituents intact, thus contributing to higher absorbance. This indicates that *Dactyloctenium aegyptium* is working as a promising inhibitor by showing strong adsorption onto the steel surface.



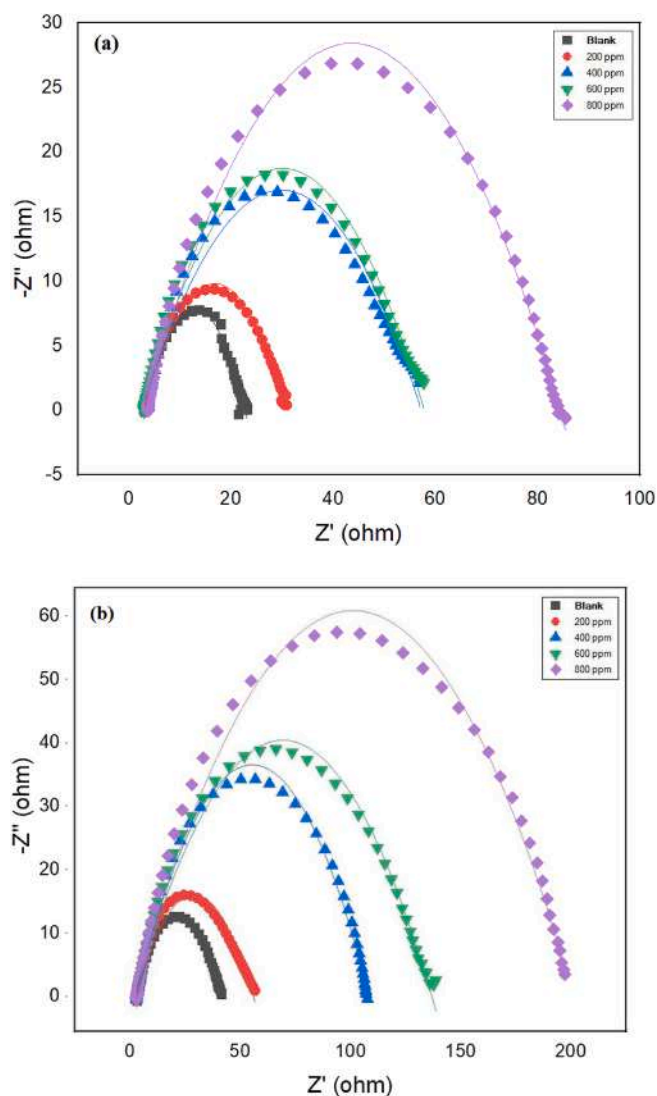
**Fig. 7.** OCP vs. Time plot for steel in 0.5 M HCl in the absence and presence of optimum concentration (800 ppm) of inhibitor.



**Fig. 8.** Tafel polarization curves in 0.5 M HCl for varied concentrations of *Dactyloctenium aegyptium* extract (a) in absence of KI and (b) in presence of 0.1 g KI.

**Table 6**Polarization parameters for steel with varied concentrations of *Dactyloctenium aegyptium* extract without and with addition of KI in 0.5 M HCl.

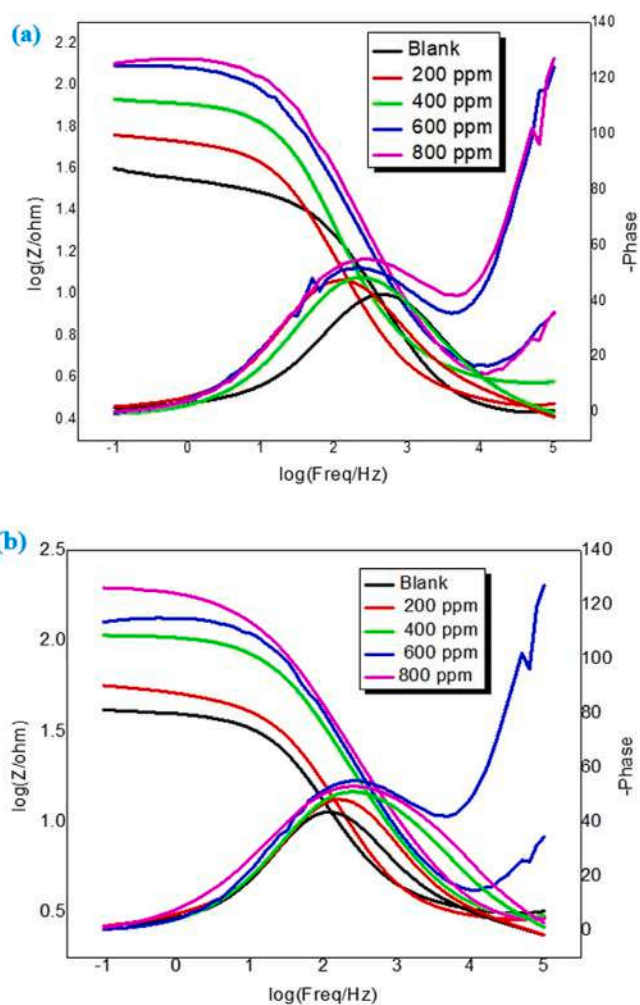
(a) Plant extract in absence of KI						
Extract concentration (ppm)	$E_{\text{corr}}$ (V versus SCE)	$\beta_a$ (V/dec)	$\beta_c$ (V/dec)	$I_{\text{corr}}$ ( $\text{A cm}^{-2}$ )	Corrosion rate (mm/y)	Inhibition Efficiency ( $\eta$ %)
0	$-0.521 \pm 0.020$	0.0950	0.0792	$6.4 \times 10^{-4} \pm 0.0001$	7.521	–
200	$-0.511 \pm 0.004$	0.0937	0.0895	$3.2 \times 10^{-4} \pm 0.0010$	3.784	50.0
400	$-0.513 \pm 0.010$	0.0826	0.0866	$2.1 \times 10^{-4} \pm 0.0002$	2.499	67.1
600	$-0.515 \pm 0.001$	0.0680	0.0750	$1.7 \times 10^{-4} \pm 0.0003$	1.989	73.4
800	$-0.531 \pm 0.002$	0.0900	0.0810	$1.5 \times 10^{-4} \pm 0.0001$	0.762	76.5
(b) Plant extract in presence of 0.1 g KI						
Extract concentration (ppm)	$E_{\text{corr}}$ (V versus SCE)	$\beta_a$ (V/dec)	$\beta_c$ (V/dec)	$I_{\text{corr}}$ ( $\text{A cm}^{-2}$ )	Corrosion rate (mm/y)	Inhibition Efficiency ( $\eta$ %)
0	$-0.512 \pm 0.003$	0.0740	0.0790	$2.6 \times 10^{-4} \pm 0.0001$	3.124	–
200	$-0.514 \pm 0.002$	0.0630	0.0880	$2.4 \times 10^{-5} \pm 0.00002$	2.904	90.7
400	$-0.513 \pm 0.004$	0.0490	0.0629	$1.6 \times 10^{-5} \pm 0.00003$	1.930	93.8
600	$-0.519 \pm 0.001$	0.0790	0.0950	$1.4 \times 10^{-5} \pm 0.00001$	1.800	94.6
800	$-0.530 \pm 0.001$	0.0870	0.0830	$1.1 \times 10^{-5} \pm 0.00002$	0.668	95.7

**Fig. 9.** Nyquist plot for steel in 0.5 M HCl and various concentrations of DAE without the addition of KI (a) and with the addition of 0.1 g KI (b).

### 3.5. Electrochemical measurements

#### 3.5.1. OCP measurement

The working electrode was dipped in the corrosive solution without

**Fig. 10.** Bode diagrams for steel in 0.5 M HCl with various concentrations of DAE without KI (a) and with 0.1 g KI (b).

and with optimum concentration of the inhibitor and left the arrangement undisturbed for 30 min to reach a stable open circuit potential as shown in Fig. 7. From Fig. 7 it is clear that the OCP is well settled and the further electrochemical measurements can be performed.

#### 3.5.2. Potentiodynamic polarization estimations

Fig. 8(a) and (b) depict the cathodic and anodic polarization studies of steel pieces in the corrosive solution with varying extract

**Table 7**

EIS parameters for steel in 0.5 M HCl with various concentrations of DAE in absence and presence of KI.

(a) Plant extract in absence of KI					
Extract concentration (ppm)	$R_s$ ( $\Omega$ )	$R_{ct}$ ( $\Omega$ )	CPE ( $\mu\text{Fcm}^{-2}$ )	n	Inhibition efficiency (%)
0	3.30 $\pm 0.04$	20.67 $\pm 0.03$	$0.595 \times 10^{-4}$ $\pm 0.0002$	0.87	–
200	1.09 $\pm 0.01$	35.50 $\pm 0.03$	$0.594 \times 10^{-5}$ $\pm 0.00002$	0.83	41.7
400	3.80 $\pm 0.02$	48.44 $\pm 0.02$	$0.624 \times 10^{-5}$ $\pm 0.00001$	0.80	57.3
600	3.33 $\pm 0.02$	50.91 $\pm 0.01$	$0.656 \times 10^{-5}$ $\pm 0.00003$	0.80	59.4
800	3.65 $\pm 0.01$	70.41 $\pm 0.02$	$0.670 \times 10^{-5}$ $\pm 0.00001$	0.80	70.6
(b) Plant extract in presence of 0.1 g KI					
Extract concentration (ppm)	$R_s$ ( $\Omega$ )	$R_{ct}$ ( $\Omega$ )	CPE ( $\mu\text{Fcm}^{-2}$ )	n	Inhibition efficiency (%)
0	3.42 $\pm 0.01$	23.94 $\pm 0.02$	$0.629 \times 10^{-4}$ $\pm 0.0001$	0.80	–
200	3.18 $\pm 0.02$	56.20 $\pm 0.04$	$0.644 \times 10^{-5}$ $\pm 0.00001$	0.80	57.4
400	3.64 $\pm 0.03$	99.63 $\pm 0.03$	$0.559 \times 10^{-5}$ $\pm 0.00002$	0.80	75.9
600	3.05 $\pm 0.03$	120.89 $\pm 0.01$	$0.600 \times 10^{-5}$ $\pm 0.00002$	0.81	80.2
800	1.38 $\pm 0.02$	268.00 $\pm 0.01$	$0.569 \times 10^{-5}$ $\pm 0.00001$	0.79	91.1

concentrations without and with 0.1 g KI, respectively. Table 6 includes the corresponding corrosion data, Tafel slopes ( $\beta_a$  &  $\beta_c$ ) and inhibition efficiency. PDP research is used to compute the corrosion current density ( $I_{\text{corr}}$ ) and corrosion potential ( $E_{\text{corr}}$ ) by extrapolating the linear sections of cathodic and anodic curves. Tafel curves show that the cathodic and anodic sections of current density decrease in the presence of DAE. The findings of the PDP study revealed the confirmation of the hydrogen evolution.

The Tafel curves for steel with different concentrations of the DAE, reveal that the inhibitor influences cathode  $\text{H}_2$  gas evolution and interferes with the iron dissolving process of the steel piece, indicating suppression of both cathodic and anodic corrosion processes by DAE in 0.5 M HCl. As a consequence addition of more plant extract should aid in preventing steel corrosion, suggesting that the more the plant extract, the lesser the corrosion process.

Table 6 also shows that increasing the concentration of DAE lowers corrosion current density in either of the cases. The corrosion current density obtained for 800 ppm of DAE without KI was  $1.5 \times 10^{-4} \text{ A/cm}^2$  with an inhibition efficiency of 76.5 %, whereas with the addition of 0.1 g KI, the combined synergism further lowered the corrosion current density to  $1.1 \times 10^{-5} \text{ A/cm}^2$  and elevated the inhibition efficiency to 95.7 %. A drop in corrosion rate for both systems was also seen in Table 6. Thus, it is clear that in the presence of 0.1 g KI along with DAE, the inhibition efficiency increases when compared to DAE without the addition of KI. It is because of the formation of an iodide bridge between the metal surface and the extract when KI is used.

### 3.5.3. Electrochemical impedance spectroscopy

Electrochemical impedance spectroscopy is a non-destructive method to test the corrosion resistance of materials on metal surfaces. Fig. 9(a) and (b) illustrate the Nyquist diagrams while Fig. 10(a) and (b) show the Bode diagrams for the DAE without and with KI, respectively at room temperature. Table 7 depicts the corresponding EIS findings. The resistance and capacitance were measured by fitting the spectra to an electrochemical equivalent circuit ( $R_s + R_{ct}$ ) using Nova software, as shown in the inset of Fig. 11, where  $R_s$  is the solution resistance between the reference and working electrodes,  $R_{ct}$  is the charge transfer resistance between the interface between the working electrode and the electrolyte, and CPE is the constant phase element arising from the double-layer capacitance of non-ideal rough metal surfaces.

Fig. 9 illustrates how the introduction of the inhibitor significantly decreased steel dissolving, as seen by the widening of the capacitive loops in both systems when the extract was present compared to when it wasn't. The working electrode's (steel) roughness and corrosion-induced inhomogeneity are the reasons for the semicircles' divergence.

The EIS curves exhibit identical behavior, as demonstrated by their similar semicircular plot. The only difference between the curves is their area, which was determined to represent the change in charge-transfer resistance from a higher to a lower frequency. In the corrosive medium, the steel specimens were effectively shielded from corrosion.

EIS data indicates that when the *Dactyloctenium aegyptium* extract concentrations and  $R_{ct}$  values increase, CPE values decrease. This suggests that slower rates of metal dissolution were caused by extract molecules adsorbing on the steel surface and displacing water molecules at the metal-to-water contact.

On comparing the Nyquist plots for DAE without and with 0.1 g KI, it is observed that the diameter of semicircles increases for each concentration of DAE/KI system than DAE alone, this increase being more than 2x times at 800 ppm when KI is present than its absence. It evidently indicates that the charge transfer value ( $R_{ct}$ ) for the DAE/KI system is higher than that of DAE alone thus, showing greater inhibition efficiency. This implies enhanced adsorption of the DAE in the presence of KI.

The Bode angle graphs show that the curves widen and shift to the

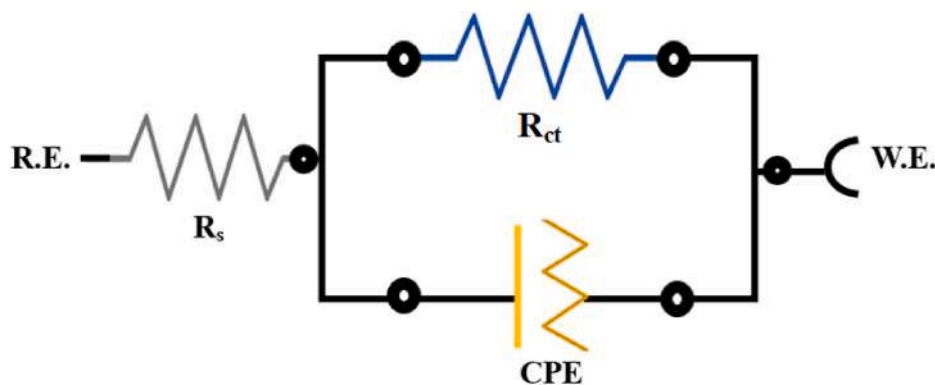


Fig. 11. Equivalent circuit of constant phase element (CPE).

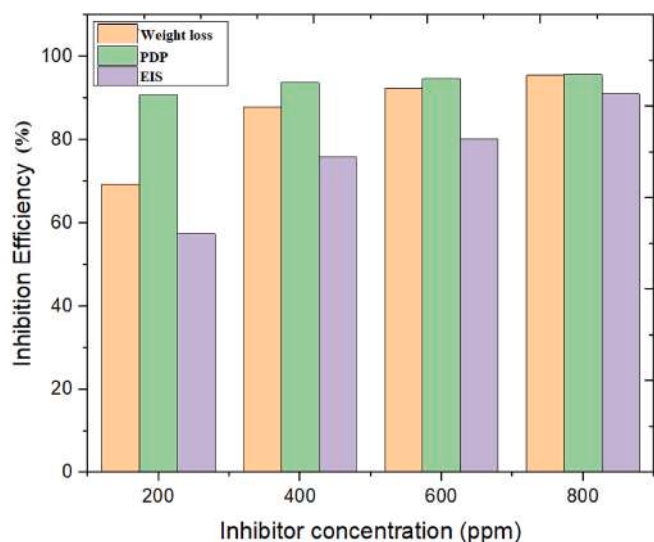


Fig. 12. Comparison of the Inhibition efficiency of the DAE extract obtained from weight loss method, PDP and EIS analysis.

left, or to lower frequencies, when a protective layer forms on the steel surface right after the inhibitor is infused. The findings in Table 7 further reveal that raising the inhibitor's quantity raises both the  $R_{ct}$  and inhibition efficiency values, suggesting that the DAE is effectively adsorbable onto the steel surface, with 800 ppm representing the greatest efficiency. Non-ideal capacitors caused by electrode flaws and/or surface reactions are reflected by the slightly flattened semi-circles. "n," where  $0 < n < 1$  (a pure capacitor with  $n = 1$ ), indicates variations in capacitor behavior. As shown in Table 7,  $n$  was found to be 0.80 concordantly in this inquiry.

The inhibition efficiency obtained from the PDP study and EIS study are in good agreement. A comparative graphical representation of the inhibition efficiency obtained from various methods is shown in Fig. 12.

### 3.6. Surface morphological analyses

SEM analyses of the steel piece have been done under four conditions as depicted in Fig. 13. The Surface of the plain non-corroded steel piece is shown in Fig. 13 (a), whereas the highly corroded steel piece when kept in the blank solution of 0.5 M HCl has been shown in Fig. 13 (b). The steel when dipped in blank solution can be seen to be adversely affected by the corrosive medium having a highly rough coral-like surface when compared to the steel surface unexposed to the corrosive

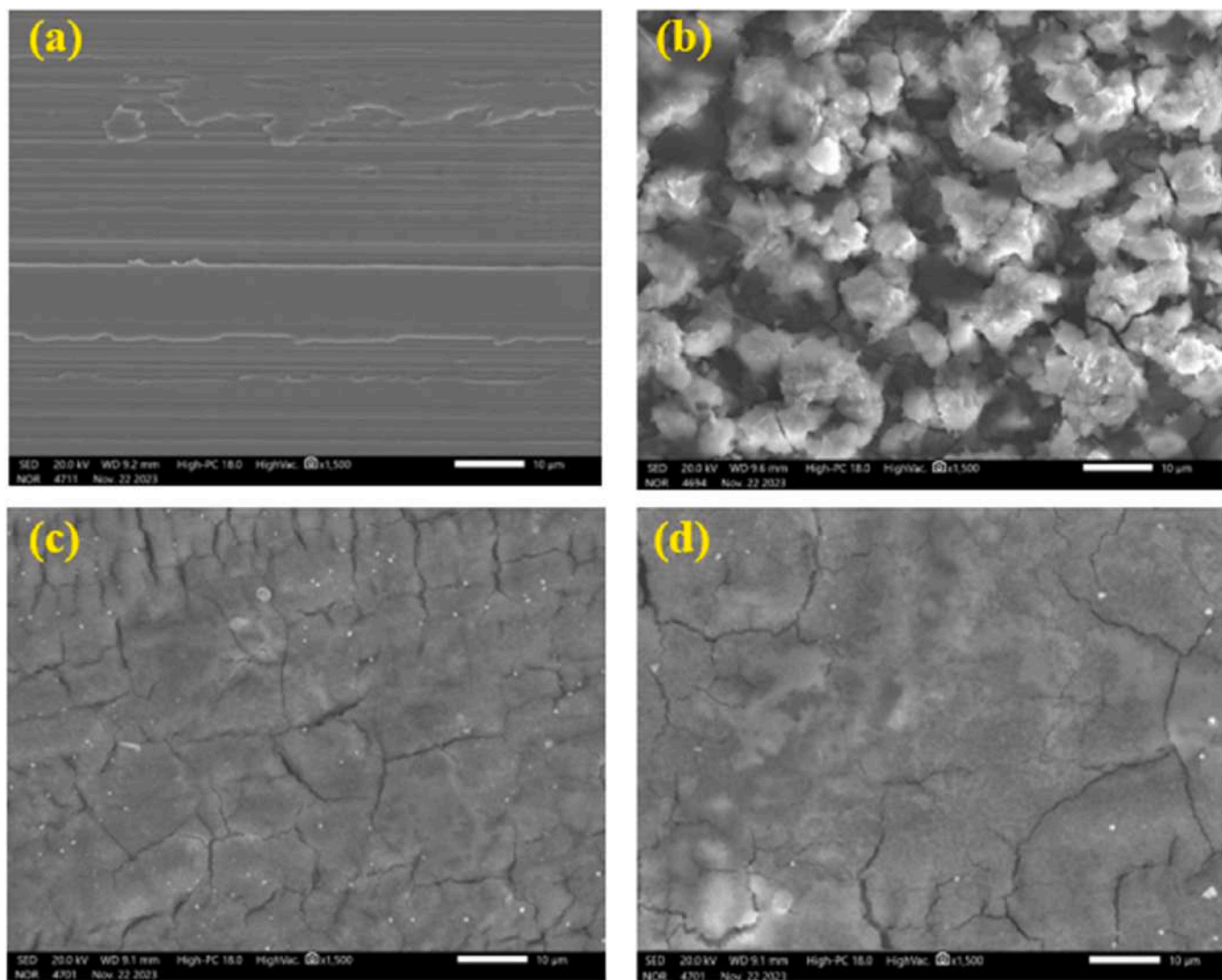


Fig. 13. SEM imaging of plain steel coupon (a), later being dipped in 0.5 M HCl (b), 800 ppm of *Dactyloctenium aegyptium* extract solution without KI (c) and 800 ppm of *Dactyloctenium aegyptium* extract with 0.1 g KI solution (d).

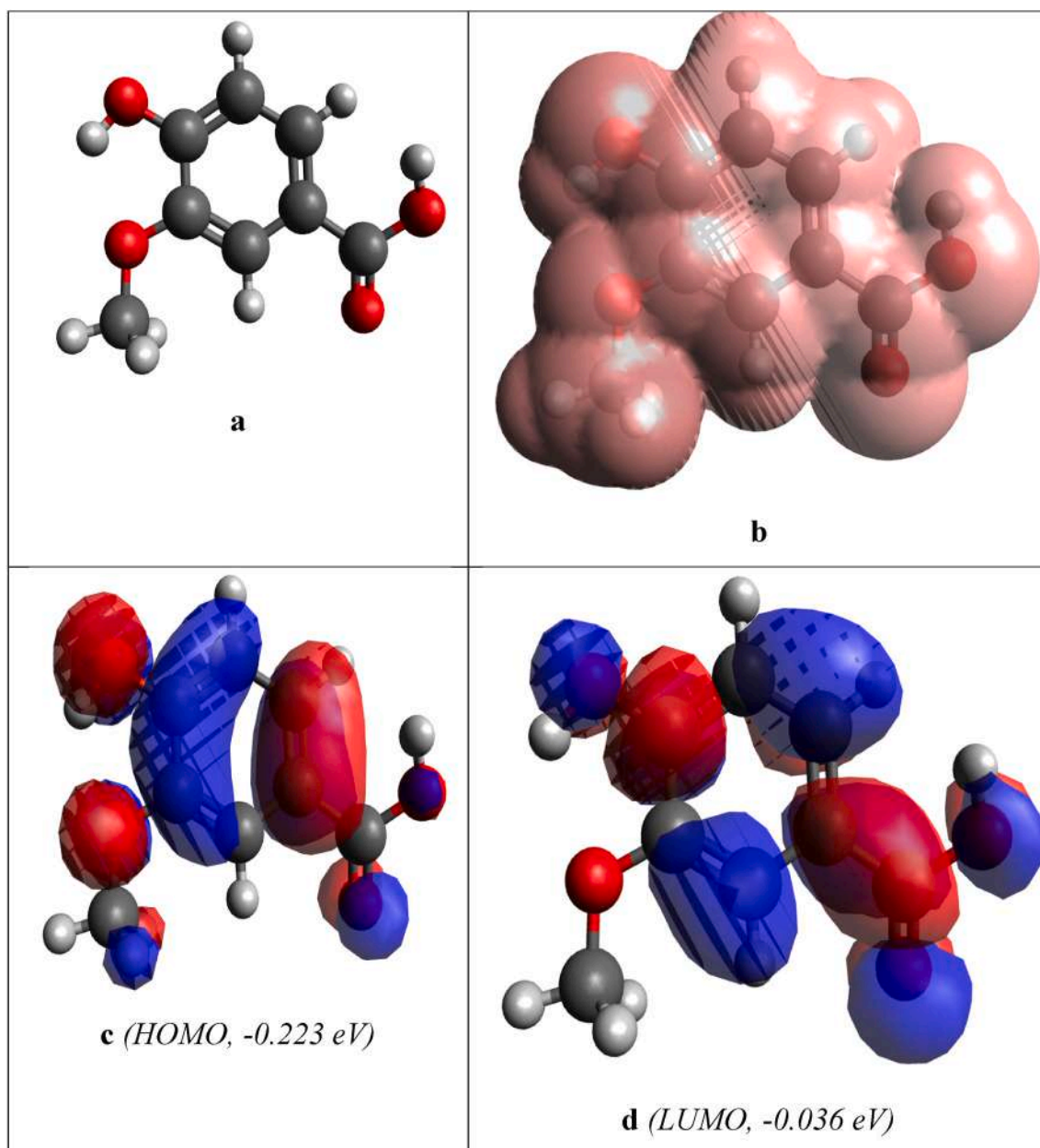


Fig. 14. (a) Optimised structure, (b) MEP, (c) HOMO and (d) LUMO of 4-hydroxy-3-methoxybenzoic acid corrosion inhibitor.

environment in Fig. 13 (a). On the other hand, Fig. 13(c) and (d) show the steel surface when exposed to the corrosive solution containing 800 ppm of DAE in the absence and presence of KI, respectively, which exhibit a significant decrease in surface roughness albeit rather shows smoothness slightly similar to non-corroded steel piece when compared to Fig. 13 (b). However, an improved surface morphology can be seen for steel inhibited by DAE/KI than DAE alone. Successful adsorption of the DAE onto the steel surface can thus be inferred as resulting in the formation of a protective layer and reducing the corrosion by the acidic medium.

### 3.7. DFT-based theoretical investigations

#### 3.7.1. Optimization investigations

The corrosion inhibition performances of 4-hydroxy-3-methoxybenzoic acid, 4-hydroxybenzoic acid, 4-hydroxybenzaldehyde, and 5,7-dihydroxy-2-(4-hydroxy-3,5-dimethoxyphenyl)-4H-chromen-4-one were evaluated through DFT-based optimization analyses. The

optimised structures revealed that these compounds are highly polarized, enhancing their solubility in aqueous solutions and their adsorption performance on metal surfaces. Key findings from the optimization investigations include the high polarization index of these compounds, with 5,7-dihydroxy-2-(4-hydroxy-3,5-dimethoxyphenyl)-4H-chromen-4-one demonstrating the highest polarization, facilitated by delocalized  $\pi$ -electrons and functional groups contributing to their polar nature (Figs. 14–17).

#### 3.7.2. Charge distribution investigations

Charge distribution analysis indicates that the values in charge of atoms in the studied inhibitors change slowly, influenced by stereochemical, chemical, physical, or planar nature of functional groups, heteroatoms, and  $\pi$ -systems. The oxygen atoms in the hydroxyl groups of these compounds are more negatively charged, making them effective adsorption centers on metal surfaces. For instance, all four compounds—4-hydroxy-3-methoxybenzoic acid, 4-hydroxybenzoic acid, 4-hydroxybenzaldehyde, and 5,7-dihydroxy-2-(4-hydroxy-3,5-



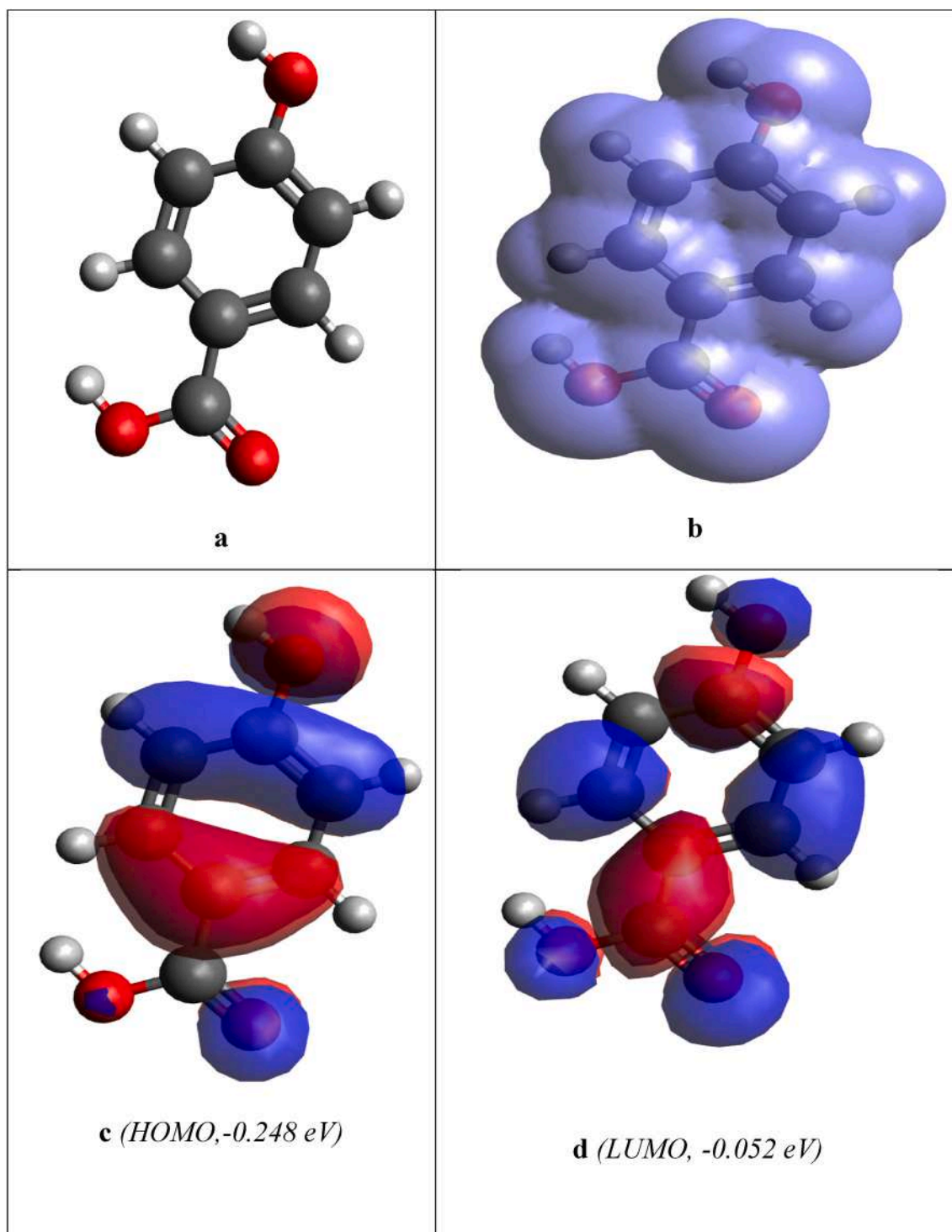


Fig. 15. (a) Optimised structure, (b) MEP, (c) HOMO and (d) LUMO of 4-hydroxybenzoic acid corrosion inhibitor.

dimethoxyphenyl)-4H-chromen-4-one—show negative charges predominantly located on oxygen atoms, which enhances their adsorption properties [52–54].

### 3.7.3. Molecular electrostatic potential (MEP) investigations

Molecular electrostatic potential (MEP) analysis identifies electrophilic (red areas) and nucleophilic (blue areas) regions in the molecular structures of the corrosion inhibitors. These maps highlight favorable nucleophilic regions that contribute to the adsorption performance of the inhibitors, with aromatic rings and functional groups serving as

centers of MEP regions. Each of the compounds—4-hydroxy-3-methoxybenzoic acid, 4-hydroxybenzoic acid, 4-hydroxybenzaldehyde, and 5,7-dihydroxy-2-(4-hydroxy-3,5-dimethoxyphenyl)-4H-chromen-4-one—exhibits multiple nucleophilic regions, enhancing their inhibition performance due to effective adsorption on metal surfaces. These investigations provide a detailed understanding of the molecular characteristics and adsorption mechanisms of the studied corrosion inhibitors, supporting their effectiveness in preventing corrosion (Figs. 14–17).

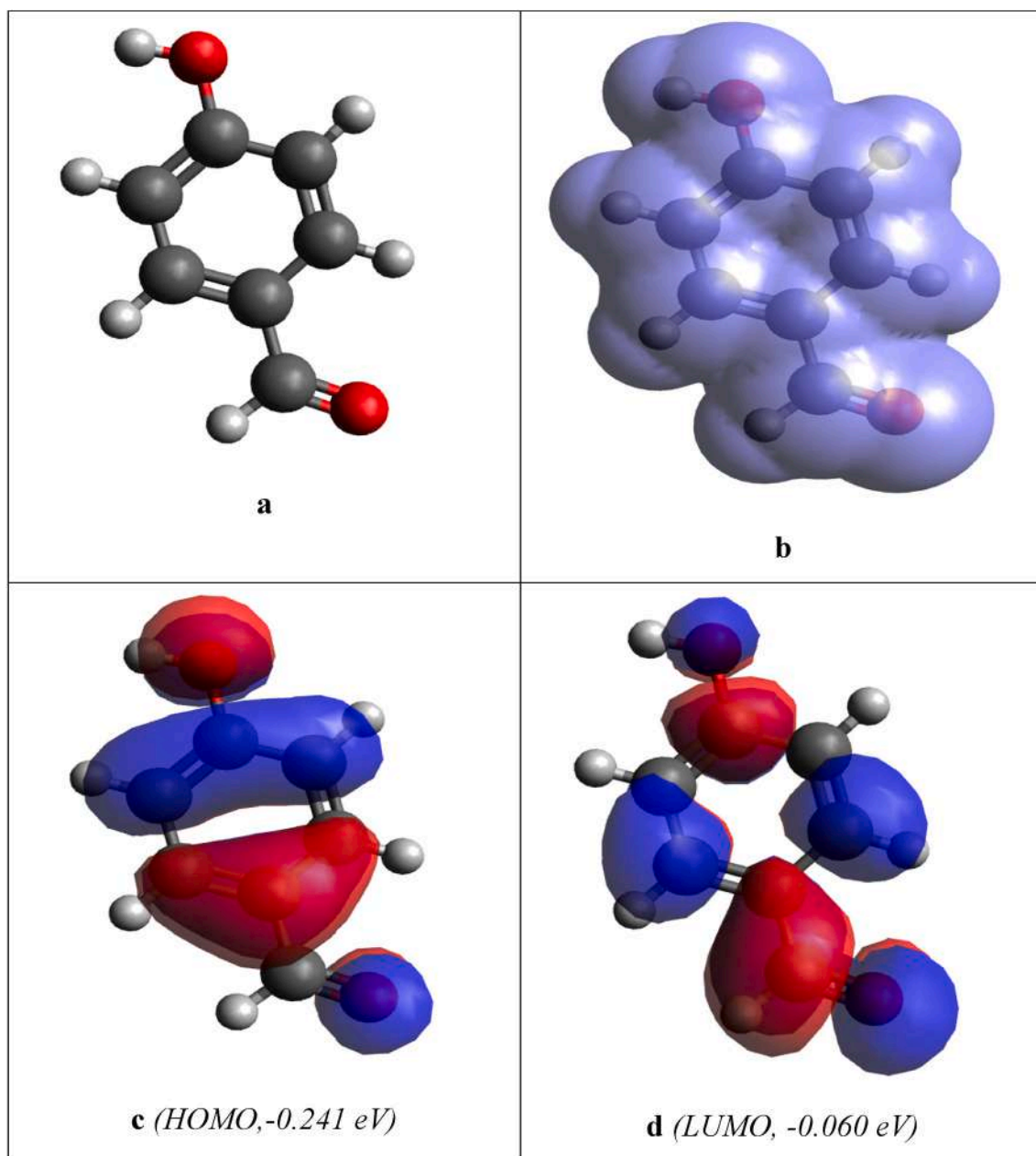


Fig. 16. (a) Optimised structure, (b) MEP, (c) HOMO and (d) LUMO of 4-hydroxybenzaldehyde corrosion inhibitor.

### 3.7.4. Frontier molecular orbital (FMO) investigations

The FMO analysis was performed to estimate the electron distribution in the Highest Occupied Molecular Orbital (HOMO) and Lowest Unoccupied Molecular Orbital (LUMO) regions of the studied compounds. The results show that the HOMO regions are mainly localized around specific carbon atoms and double bonds in each molecule [55–57]. This indicates that the molecules are negatively charged in these regions, which are crucial for their interaction with metal surfaces. For instance, the energy of HOMO orbitals for the selected compounds follows the order: 4-hydroxybenzaldehyde > 4-hydroxybenzoic acid > 4-hydroxy-3-methoxybenzoic acid > 5,7-dihydroxy-2-(4-hydroxy-3,5-dimethoxyphenyl)-4H-chromen-4-one, suggesting that 4-hydroxybenzaldehyde is the most efficient corrosion inhibitor among them (Figs. 14–17). The LUMO regions, on the other hand, indicate the antibonding orbitals that are suitable for electron acceptance, promoting chemical bonding formation between the metal surface and the corrosion inhibitor [58–67].

### 3.7.5. Molecular reactivity investigations

The molecular reactive parameters of organic compounds were estimated using the energy difference ( $\Delta E_{Inh}^{DFT}$ ) between the HOMO ( $E_{HOMO(Inh)}^{DFT}$ ) and LUMO ( $E_{LUMO(Inh)}^{DFT}$ ) according to Equations (10)–(19) and the calculated parameters are reported in Table 8.

$$\Delta E_{Inh}^{DFT} = E_{LUMO(Inh)}^{DFT} - E_{HOMO(Inh)}^{DFT} \quad (10)$$

$$I_{Inh}^{DFT} = -E_{HOMO(Inh)}^{DFT} \quad (11)$$

$$A_{Inh}^{DFT} = -E_{LUMO(Inh)}^{DFT} \quad (12)$$

$$\eta_{Inh}^{DFT} = \frac{1}{2} (I_{Inh}^{DFT} - A_{Inh}^{DFT}) \quad (13)$$

$$\epsilon_{Inh}^{DFT} = \frac{1}{\omega_{Inh}^{DFT}} \quad (14)$$

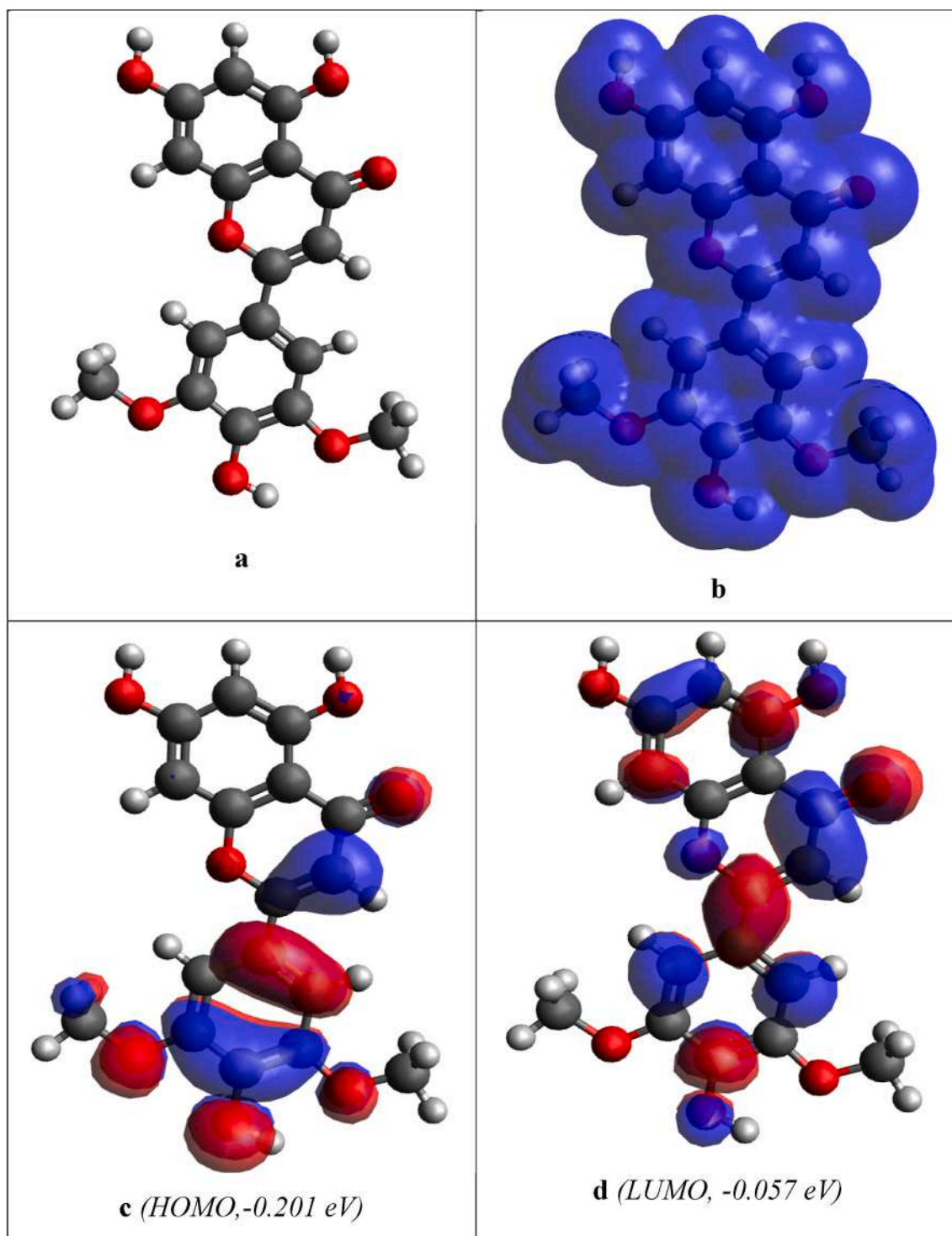


Fig. 17. (a) Optimised structure, (b) MEP, (c) HOMO and (d) LUMO of 5,7-dihydroxy-2-(4-hydroxy-3,5-dimethoxyphenyl)-4H-chromen-4-one corrosion inhibitor.

$$-\mu_{Inh}^{DFT} = \chi_{Inh}^{DFT} = \frac{1}{2} (I_{Inh}^{DFT} + A_{Inh}^{DFT}) \quad (15)$$

$$\omega_{Inh}^{DFT} = \frac{(\chi_{Inh}^{DFT})^2}{2\eta_{Inh}^{DFT}} \quad (16)$$

$$\sigma_{Inh}^{DFT} = \frac{1}{\eta} \quad (17)$$

$$\Delta N_{Inh}^{DFT} = \frac{(\chi_{Fe} - \chi_{Inh}^{DFT})}{2(\eta_{Fe} + \eta_{Inh}^{DFT})} \quad (18)$$

$$\psi_{Inh}^{DFT} = \frac{(\chi_{Fe} - \chi_{Inh}^{DFT})}{4(\eta_{Fe} + \eta_{Inh}^{DFT})} \quad (19)$$

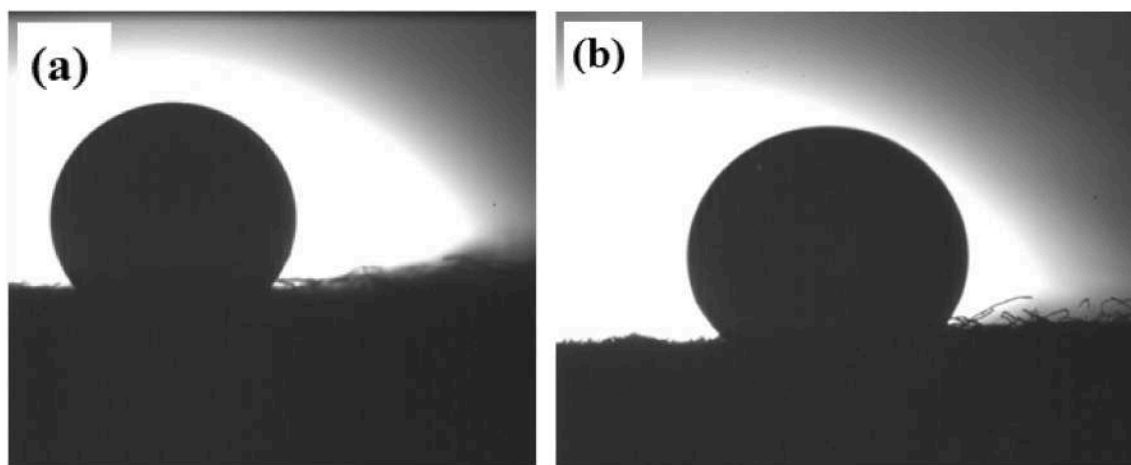
where  $\eta_{Fe}$  is 0 eV mol<sup>-1</sup> and  $\chi_{Fe}$  is 7 eV mol<sup>-1</sup>.

The theoretical parameters for the corrosion inhibitors, analyzed using DFT, B3LYP, and 6-31G basis sets, reveal significant insights into

**Table 8**

Theoretical parameters for corrosion inhibitors (DFT, B3LYP and 6-31G basis sets).

Parameters, eV	4-hydroxy-3-methoxybenzoic	4-hydroxybenzoic acid	4-hydroxybenzaldehyde	5,7-dihydroxy-2-(4-hydroxy-3,5-dimethoxyphenyl)-4H-chromen-4-one
$E_{HOMO}^{DFT}(inh)$	-0.223	-0.248	-0.241	-0.201
$E_{LUMO}^{DFT}(inh)$	-0.036	-0.052	-0.060	-0.057
$\Delta E_{inh}^{DFT}$	0.187	0.196	0.181	0.144
$\sigma_{inh}^{DFT}$	5.349	5.102	5.525	6.944
$\omega_{inh}^{DFT}$	0.234	0.257	0.224	0.124
$\eta_{inh}^{DFT}$	0.0935	0.098	0.0905	0.072
$\chi_{inh}^{DFT}$	0.1295	0.150	0.1505	0.129
$I_{inh}^{DFT}$	0.223	0.248	0.241	0.201
$A_{inh}^{DFT}$	0.036	0.052	0.060	0.057
$\mu_{inh}^{DFT}$	-0.1295	-0.150	-0.1505	-0.129
$\epsilon_{inh}^{DFT}$	4.273	3.889	4.464	8.065
$\Delta N_{inh}^{DFT}$	0.0425	0.033	0.0315	0.048
$\psi_{inh}^{DFT}$	0.085	0.066	0.063	0.096

**Fig. 18.** Contact angle analysis of the steel in the absence (a) and presence of the DAE extract (b).

their effectiveness. The HOMO and LUMO energies indicate that 5,7-dihydroxy-2-(4-hydroxy-3,5-dimethoxyphenyl)-4H-chromen-4-one has the highest energy gap, suggesting high reactivity. The energy gap ( $\Delta E_{inh}^{DFT}$ ) decreases from 4-hydroxy-3-methoxybenzoic acid (0.187 eV) to 5,7-dihydroxy-2-(4-hydroxy-3,5-dimethoxyphenyl)-4H-chromen-4-one (0.144 eV), indicating the latter's higher reactivity. Chemical softness ( $\sigma_{inh}^{DFT}$ ) increases from 4-hydroxybenzaldehyde (5.525 eV) to 5,7-dihydroxy-2-(4-hydroxy-3,5-dimethoxyphenyl)-4H-chromen-4-one (6.944 eV), highlighting its softness and reactivity. The electrophilicity index ( $\omega_{inh}^{DFT}$ ) is highest for 4-hydroxybenzoic acid (0.257 eV) and lowest for 5,7-dihydroxy-2-(4-hydroxy-3,5-dimethoxyphenyl)-4H-chromen-4-one (0.124 eV), indicating the latter's greater electron donation tendency. Chemical hardness ( $\eta_{inh}^{DFT}$ ) is lowest for 5,7-dihydroxy-2-(4-hydroxy-3,5-dimethoxyphenyl)-4H-chromen-4-one (0.072 eV), signifying its high reactivity. Electronegativity ( $\chi_{inh}^{DFT}$ ), ionization potential ( $I_{inh}^{DFT}$ ), and electron affinity ( $A_{inh}^{DFT}$ ) show minor variations among the inhibitors, with 4-hydroxybenzoic acid exhibiting the highest values. Chemical potential ( $\mu_{inh}^{DFT}$ ) values are similar across the inhibitors, while electrophilicity ( $\epsilon_{inh}^{DFT}$ ) is notably higher for 5,7-dihydroxy-2-(4-hydroxy-3,5-dimethoxyphenyl)-4H-chromen-4-one, suggesting a strong electron-donating ability. The fraction of electron transfer ( $\Delta N_{inh}^{DFT}$ ) is highest for this compound (0.048), indicating the most significant electron transfer to the metal surface, and its electrophilicity ( $\psi_{inh}^{DFT}$ ) is also highest (0.096), further supporting its strong electron-donating capability. Overall, these parameters suggest that 5,7-dihydroxy-2-(4-hydroxy-3,5-dimethoxyphenyl)-4H-chromen-4-one is the most reactive and effective corrosion inhibitor among the studied compounds,

followed by 4-hydroxybenzaldehyde, 4-hydroxybenzoic acid, and 4-hydroxy-3-methoxybenzoic acid.

### 3.8. Contact angle analysis

Contact angle analysis of the steel in the absence and presence of the optimum concentration (800 ppm) of the DAE extract provides additional details about the hydrophilic or hydrophobic nature of the layer formed on the steel surface (Fig. 18). The contact angle of the steel in the absence of the DAE extract is 82.44° while when the DAE extract is coated on the steel surface, then the contact angle becomes 90.42°. This increase in the contact angle of the steel surface in the presence of the DAE extract indicates the hydrophobic layer formation on the steel surface which protects the steel specimen from the corrosive attack [68].

### 3.9. Proposed mechanism of corrosion inhibition

It was observed during the weight loss studies performed with the blank solution of 0.5 M HCl that the more rapid the reaction occurs, the more are hydrogen bubbles seen indicating strong corrosion. However, on the gradual increase of the DAE concentration from 200 ppm to 800 ppm, the production of hydrogen bubbles decreased or occurred at a very slow rate, thereby slowing down the corrosion of the immersed steel pieces. This is because the electron lone pairs on the various active constituents of DAE donate into the metal's empty orbitals, forming a dative bond and getting adsorbed onto the surface. Moreover, the  $\pi$ -electron ring system of the phytochemicals also exhibits retrodonation type bonding with the metal. As a consequence, the DAE layers onto the

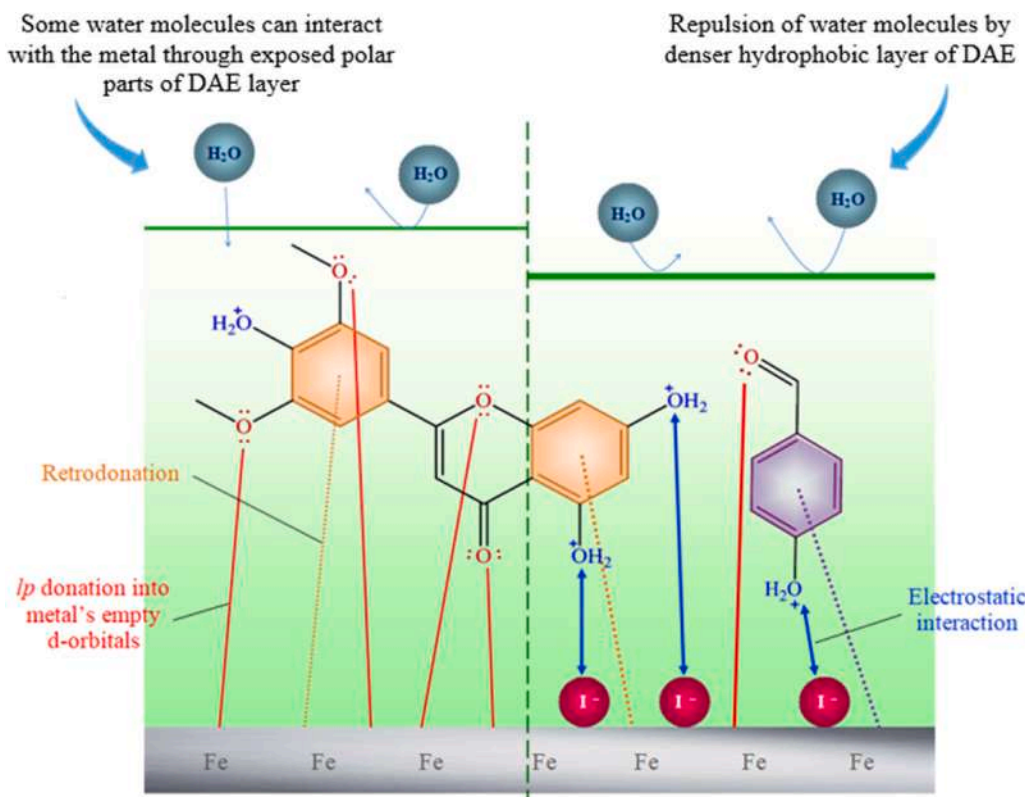


Fig. 19. Proposed corrosion inhibition mechanism of *Dactyloctenium aegyptium* extract on steel in absence and presence of KI.

metal surface shielding it from corrosion causing attack by water molecules in the solution and other groups.

But DAE in synergism with KI was able to show higher corrosion inhibitions compared with solely DAE which can be understood from the increased interaction and adherence between the DAE and steel surface through iodide acting as a bridge that was initially not present. Iodide furnished by KI first adheres to the steel surface through van der Waals interaction and later bonds with the protonated parts of DAE by electrostatic interaction. Hence, any polar charged part initially present in the sole DAE later remained unavailable for even a slight interaction with corrosive groups. This in turn forms a stronger hydrophobic barrier by the plant extract and shows enhanced protection of steel against corrosion. A schematic diagram of the proposed mechanism of the corrosion inhibition of the DAE extract is shown in Fig. 19.

#### 4. Conclusion

Preliminary screening of *Dactyloctenium aegyptium* as a corrosion mitigator for steel in 0.5 M HCl gave favorable results being rich in various phytochemicals such as alkaloids, flavonoids, sugars, etc. Except coumarin. DAE also exhibited satisfactory inhibition efficiency in weight loss measurements. Further, electrochemical measurements were also found to be in unison with the aforementioned observations pointing to enhanced corrosion inhibition with increasing concentrations of plant extract. The maximum inhibition efficiency of DAE was found to be 76.5 % at a concentration as low as 800 ppm which increased to 95.7 % in the presence of KI. This can be attributed to the adsorption of the phytochemicals onto the steel surface through their heteroatoms forming a protective layer against rapid corrosion, which is supported by Langmuir adsorption isotherm, UV-Vis. and SEM analyses. In this study, no toxic chemical was used for the preparation of the plant extract. Further the methods used for determining the anti-corrosive properties of the *Dactyloctenium aegyptium* extract are non-destructive so the studied inhibitor can be understood as an efficient eco-friendly green corrosion

inhibitor for steel. Optimised geometries and smaller  $\Delta E$  between the phytochemicals drawn from computational studies suggest them to be stable and have enduring inhibitory effects. Although *Dactyloctenium aegyptium* stands as a conclusive weed for corrosion inhibition of steel, the *Dactyloctenium aegyptium*/KI system however, is found to be more effectual owing to the increased interactions due to the introduction of iodide, resulting in stronger and denser protective extract layer onto the steel surface.

#### CRediT authorship contribution statement

**Akhil Saxena:** Validation, Supervision, Conceptualization. **Jasdeep Kaur:** Validation, Supervision, Conceptualization. **Elyor Berdimurodov:** Software. **Dakeshwar Kumar Verma:** Software, Writing – original draft.

#### Declaration of competing interest

The authors declare that they have no known competing financial interests or personal relationships that could have appeared to influence the work reported in this paper.

#### Acknowledgement

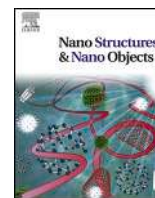
We (the authors of this manuscript) express our heartfelt thankfulness to Dr. Amanpreet Singh, Assistant Professor, Department of Chemistry, Chandigarh University Mohali, India for helping us in the contact angle measurements.

#### References

- [1] A. Saxena, D. Prasad, R. Haldhar, G. Singh, A. Kumar, Use of *Sida cordifolia* extract as green corrosion inhibitor for mild steel in 0.5 M  $H_2SO_4$ , *J. Environ. Chem. Eng.* 6 (2018) 694.

- [2] A. Amiery, W. Isahak, W. Azzawi, Corrosion inhibitors: natural and synthetic organic inhibitors, *Lubricants* 11 (2023) 174.
- [3] H. Yang, Role of organic and eco-friendly inhibitors on the corrosion mitigation of steel in acidic environments—a state-of-art review, *Molecules* 26 (2021) 3473.
- [4] H. Wei, B. Heidarshenas, L. Zhou, G. Hussain, Q. Li, K. Ostrikov, Green inhibitors for steel corrosion in acidic environment: state of art, *Materials Today Sustainability* 10 (2020) 100044.
- [5] J. Kaur, A. Saxena, Heterocyclic as corrosion inhibitors for petrochemical industries, *Handbook of Heterocyclic Corrosion Inhibitors 1* (2023) 271.
- [6] K. Hjouji, E. Chihbi, I. Atemni, M. Ouakki, T. Ainane, M. Taleb, Z. Rais, *Datura stramonium* plant seed extracts as a new green corrosion inhibitor for mild steel in 1 M HCl solution: experimental and surface characterization studies, *Sustainable chemistry and pharmacy* 34 (2023) 101170.
- [7] A. Acidi, A. Sedik, A. Rizi, R. Bouasla, K. Rachedi, M. Berredjem, et al., Examination of the main chemical components of essential oil of *syzygium aromaticum* as a corrosion inhibitor on the mild steel in 0.5 M HCl medium, *J. Mol. Liq.* 391 (2023) 123423.
- [8] A. Dehghani, B. Ramezanzadeh, Rosemary extract inhibitive behavior against mild steel corrosion in tempered 1 M HCl media, *Ind. Crop. Prod.* 193 (2023) 116183.
- [9] R. Hameed, M. Aleid, D. Mohammad, M. Badr, B. Huwaimel, M. Suliman, et al., *Spinacia oleracea* extract as green corrosion inhibitor for carbon steel in hydrochloric acid solution, *Int. J. Electrochem. Sci.* 17 (2022) 221017.
- [10] A. Zaher, R. Aslam, H. Lee, K. Azzeddine, B. Moncef, A. Alrashdi, et al., A combined computational & electrochemical exploration of the ammi visnaga L. Extract as a green corrosion inhibitor for carbon steel in HCl solution, *Arab. J. Chem.* 15 (2022) 103573.
- [11] H. Ahchouch, A. Noor, A. Hadfi, A. Driouiche, L. Bammou, M. Belkhaouda, et al., From nature to protection: unleashing the protective potential of heder helix leaves against corrosion in harsh acidic environments using experimental and theoretical insights, *Arab. J. Chem.* 17 (2024) 105593.
- [12] R. Maizia, A. Zaabar, A. Djermoune, D. Amoura, S. Martemianov, A. Thomas, et al., Experimental assessment and molecular-level exploration of the mechanism of action of nettle (*urtica dioica* L.) plant extract as an eco-friendly corrosion inhibitor for X38 mild steel in sulfuric acidic medium, *Arab. J. Chem.* 16 (2023) 104988.
- [13] O. Boussalem, Y. Bouazzaoui, A. Habsaoui, A. Amri, D. Mhanni, N. Dkhireche, et al., The study of the methanolic extract of *Pelargonium graveolens* as a green corrosion inhibitor of mild steel in H<sub>2</sub>SO<sub>4</sub> 0.5 M, *Chemical data collections* 48 (2023) 101084.
- [14] D. Prasad, R. Maithani, B. Ibrahim, *Mimosa pudica* extract corrosion inhibitive nature for stainless steel in 0.5 mol L<sup>-1</sup> sulfuric acid media, *J. Mol. Liq.* 389 (2023) 122940.
- [15] H. Elabbasy, M. Elmagar, A. Fouda, Surface interaction and corrosion inhibition of carbon steel in sulfuric acid using *petroselinum crispum* extract, *J. Indian Chem. Soc.* 100 (2023) 100988.
- [16] A. Abuelela, J. Kaur, A. Saxena, M. Bedair, D. Verma, E. Berdimurodov, Electrochemical and DFT studies of *Terminalia bellerica* fruit extract as an eco-friendly inhibitor for the corrosion of steel, *Sci. Rep.* 13 (2023) 19367.
- [17] H. Wang, S. Deng, J. Xu, D. Xu, D. Shao, G. Du, et al., Synergistic mixture of eupatorium adenophora spreng stems extract/KI as an efficient inhibitor for the corrosion of steel in H<sub>2</sub>SO<sub>4</sub>, *J. Ind. Eng. Chem.* 130 (2023) 218.
- [18] A. Kayed, M. Elghaly, A. Hela, New epoxy megastigmane glucoside from *Dactyloctenium aegyptium* L.P.beauv wild (crowfoot grass), *Journal of Scientific and Innovative Research* 4 (2015) 237.
- [19] K. Janbaz, F. Saqib, Pharmacological evaluation of *Dactyloctenium aegyptium*: an indigenous plant used to manage gastrointestinal ailments, *Bangladesh J. Pharmacol.* 10 (2015) 295.
- [20] H. Alhumade, O. Alayed, M. Iqbal, A. Shahid, T. Iqbal, M. Ahmad, et al., Exploration of the bioenergy potential of *Dactyloctenium aegyptium* through pyrolysis, kinetics, and thermodynamic parameters to produce clean fuels and biochemical, *Fuel* 341 (2023) 127663.
- [21] A. Ti, I. Ej, A. Adebayo, Evaluation of antioxidant and antimicrobial properties of silver nanoparticles biosynthesized using weed (*Dactyloctenium aegyptium*) extracts for sustainable environment, agriculture and ethno medicine, *Mater. Today: Proc.* (2023).
- [22] B. Naik, N. Dangi, H. Sapkota, N. Wagle, S. Nagarjuna, R. Sankaranand, Phytochemical screening and evaluation of anti-fertility activity of *Dactyloctenium aegyptium* in male albino rats, *Asian Pacific Journal of Reproduction* 5 (2016) 51.
- [23] J. Jacob, A. Raj, Synergistic effect of salts on the corrosion inhibitive action of plant extract: a review, *J. Adhes. Sci. Technol.* 35 (2020) 133.
- [24] S. Umoren, M. Solomon, Effect of halide ions on the corrosion inhibition efficiency of different organic species – a review, *J. Ind. Eng. Chem.* 21 (2015) 8.
- [25] S. Sanad, A. Ismail, N. Mahmoud, Inhibition effect of potassium iodide on corrosion of stainless steel in hydrochloric acid solution, *J. Mater. Sci.* 27 (1992) 5706.
- [26] A. Yaro, A. Khadom, S. Lahmod, Kinetics of the corrosion inhibition reaction of steel alloys in acidic media by potassium iodide, *React. Kinet. Mech. Catal.* 109 (2013) 417.
- [27] S. Aziz, A. Azaly, Synergistic effect of potassium iodide with some heterocyclic compounds on the corrosion inhibition of 304 stainless steel in hydrochloric acid solution, *Journal of bio- and tribo-corrosion* 3 (2017) 49.
- [28] J. Shaikh, M. Patil, Qualitative tests for preliminary phytochemical screening: an overview, *Int. J. Chem. Stud.* 8 (2020) 603.
- [29] A. Saxena, J. Kumar, Phytochemical screening, metal-binding studies and applications of floral extract of *Sonchus oleraceus* as a corrosion inhibitor, *Journal of Bio-and Tribo-Corrosion* 6 (2020) 55.
- [30] J. Kaur, A. Saxena, P. Reddy, D. Sathiaraj, M. Agrawal, K. Saxena, *Lepidium didymium* plant extract as eco-friendly corrosion inhibitor for steel in acidic medium, *Indian J. Eng. Mater. Sci.* 30 (2023) 256.
- [31] A. Sowmyashree, A. Somya, S. Rao, C. Kumar, A. Romaizan, M. Hussain, et al., Potential sustainable electrochemical corrosion inhibition study of citrus limetta on mild steel surface in aggressive acidic media, *J. Mater. Res. Technol.* 24 (2023) 984.
- [32] D. Prasad, R. Singh, S. Kaya, B. Ibrahim, Natural corrosion inhibitor of renewable eco-waste for SS-410 in sulfuric acid medium: adsorption, electrochemical, and computational studies, *J. Mol. Liq.* 351 (2022) 118671.
- [33] V. Shikuku, C. Kowenje, F. Kengara, Errors in parameters estimation using linearized adsorption isotherms: sulfadimethoxine adsorption onto kaolinite clay, *Chemical science international journal* 23 (2018) 1.
- [34] O. Ogunleye, A. Arinkoola, O. Eletta, O. Agbade, Y. Osho, A. Morakinyo, et al., Green corrosion inhibition and adsorption characteristics of *Luffa cylindrica* leaf extract on mild steel in hydrochloric acid environment, *Heliyon* 6 (2020) 03205.
- [35] R. Hsissou, M. Azogagh, F. Benhiba, S. Echihi, M. Galai, A. Shaim, M. Rafik, Insight of development of two cured epoxy polymer composite coatings as highly protective efficiency for carbon steel in sodium chloride solution: DFT, RDF, FVV and MD approaches, *J. Mol. Liq.* 360 (2022) 119406.
- [36] Y. Dewangan, D. Verma, E. Berdimurodov, R. Haldhar, O. Dagdag, M. Tripathi, V. Mishra, P. Kumar, N-hydroxypyrazine-2-carboxamide as a new and green corrosion inhibitor for mild steel in acidic medium: experimental, surface morphological and theoretical approach, *J. Adhes. Sci. Technol.* (2022) 1–21.
- [37] E. Berdimurodov, A. Kholikov, K. Akbarov, L. Guo, S. Kaya, D. Verma, M. Rbaa, O. Dagdag, Novel glycoluril pharmaceutically active compound as a green corrosion inhibitor for the oil and gas industry, *J. Electroanal. Chem.* 907 (2022).
- [38] O. Dagdag, R. Haldhar, S. Kim, L. Guo, M. Gouri, E. Berdimurodov, O. Hamed, S. Jodeh, E. Akpan, E. Ebenso, Recent progress in epoxy resins as corrosion inhibitors: design and performance, *J. Adhes. Sci. Technol.* (2022) 1–22.
- [39] E. Berdimurodov, A. Kholikov, K. Akbarov, L. Guo, S. Kaya, K. Katin, D. Verma, M. Rbaa, O. Dagdag, R. Haldhar, Novel gossypol–indole modification as a green corrosion inhibitor for low-carbon steel in aggressive alkaline–saline solution, *Colloids and Surfaces A Physicochemical and Engineering Aspect* 637 (2022) 128207.
- [40] C. Akalezi, A. Maduabuchi, C. Enenebeaku, E. Oguzie, Experimental and DFT evaluation of adsorption and inhibitive properties of *Moringa oleifera* extract on mild steel corrosion in acidic media, *Arab. J. Chem.* 13 (2020) 9270.
- [41] G. Barca, C. Bertoni, L. Carrington, D. Datta, N. Silva, J. Deustua, D. Fedorov, J. Gour, A. Gunina, E. Guidez, Recent developments in the general atomic and molecular electronic structure system, *J. Chem. Phys.* 152 (2020) 154102.
- [42] M. Schmidt, K. Baldrige, J. Boatz, S. Elbert, M. Gordon, J. Jensen, S. Koseki, N. Matsunaga, K. Nguyen, S. Su, General atomic and molecular electronic structure system, *J. Comput. Chem.* 14 (1993) 1347.
- [43] R. Krishnan, J. Binkley, R. Seeger, J. Pople, Self-consistent molecular orbital methods. XX. A basis set for correlated wave functions, *J. Chem. Phys.* 72 (1980) 650.
- [44] A. Becke, Density-functional thermochemistry. III. The role of exact exchange, *J. Chem. Phys.* 98 (1993) 5648.
- [45] C. Lee, W. Yang, R. Parr, Development of the Colle-Salvetti correlation-energy formula into a functional of the electron density, *Phys. Rev. B* 37 (1988) 785.
- [46] B. Bode, M. Gordon, *MacMolPlt*: a graphical user interface for GAMESS, *J. Mol. Graph. Model.* 16 (1998) 133.
- [47] M. Hanwell, D. Curtis, D. Lonie, T. Vandermeersch, E. Zurek, G. Hutchison, Avogadro: an advanced semantic chemical editor, visualization, and analysis platform, *J. Cheminf.* 4 (2012) 1–17.
- [48] D. Bajaj, P. Khurpade, An eco-friendly *mangifera indica* leaves extract corrosion inhibitor for stainless steel in acidic medium, *Nat. Environ. Pollut. Technol.* 23 (2024) 139.
- [49] S. Adejo, M. Ekwenchi, F. Momoh, E. Odiniya, Adsorption characterization of ethanol extract of leaves of *Portulaca oleracea* as green corrosion inhibitor for corrosion of mild steel in sulphuric acid medium, *International Journal of Modern Chemistry* 1 (2012) 125.
- [50] A. Fouda, K. Shalabi, M. Shaaban, Synergistic effect of potassium iodide on corrosion inhibition of carbon steel by *Achillea santolina* extract in hydrochloric acid solution, *Journal of Bio-and Tribo-Corrosion* 5 (2019) 71.
- [51] E. Berdimurodov, A. Kholikov, K. Akbarov, L. Guo, Experimental and theoretical assessment of new and eco-friendly thioglycoluril derivative as an effective corrosion inhibitor of St2 steel in the aggressive hydrochloric acid with sulfate ions, *J. Mol. Liq.* 335 (2021) 116168.
- [52] A. Shahmoradi, M. Ranjbarhane, A. Javidparvar, L. Guo, E. Berdimurodov, B. Ramezanzadeh, Theoretical and surface/electrochemical investigations of walnut fruit green husk extract as effective inhibitor for mild-steel corrosion in 1 M HCl electrolyte, *J. Mol. Liq.* 338 (2021) 116550.
- [53] R. Haldhar, S. Kim, E. Berdimurodov, D. Verma, C. Hussain, Corrosion inhibitors: industrial applications and commercialization, in: *Sustain. Corros. Inhib. II Synth. Des. Pract. Appl.* American Chemical Society, 2021, p. 10.
- [54] E. Berdimurodov, L. Guo, A. Kholikov, K. Akbarov, M. Zhu, MOFs-based corrosion inhibitors, *Supramol. Chem. Corros* (2021) 287.
- [55] A. Radwan, C. Mannah, M. Sliem, N. Qahtani, P. Okonkwo, E. Berdimurodov, A. Mohamed, A. Abdullah, Electrospun highly corrosion-resistant polystyrene–nickel oxide superhydrophobic nanocomposite coating, *J. Appl. Electrochem.* 51 (2021) 1605.
- [56] E. Berdimurodov, A. Kholikov, K. Akbarov, L. Guo, S. Kaya, K. Katin, D. Verma, M. Rbaa, O. Dagdag, R. Haldhar, Novel bromide–cucurbit[7]uril supramolecular

- ionic liquid as a green corrosion inhibitor for the oil and gas industry, *J. Electroanal. Chem.* 901 (2021) 115794.
- [57] A. Magri, R. Hsissou, A. Hmada, A. Berisha, N. Dkhireche, S. Vaudrueil, Development of new polymer composites formulated by glass as a potential protective coating for 3D printed H13 steel in acidic medium: DFT, MC and MD computational, *J. Mol. Liq.* 387 (2023) 122690.
- [58] R. Hsissou, R. Lachhab, A. Magri, S. Echihi, H. Vanaei, M. Galai, M. Touhami, M. Rafik, Synthesis characterization and highly protective efficiency of tetraglycidyl ether pentan epoxy prepolymer as a potential corrosion inhibitor for mild steel in 1 M HCl medium, *Polymers* 14 (2022) 3100.
- [59] A. Molhi, R. Hsissou, M. Damej, A. Berisha, M. Bamaarouf, M. Seydou, M. Benmessaoud, S. Hajjaji, Performance of two epoxy compounds against corrosion of C38 steel in 1 M HCl: electrochemical, thermodynamic and theoretical assessment, *Int. J. Corros. Scale Inhib.* 10 (2021) 812.
- [60] R. Hsissou, B. Benzidia, N. Hajjaji, A. Elharfi, Elaboration and electrochemical studies of the coating behavior of a new pentafunctional epoxy polymer: pentaglycidyl ether pentabisphenol A phosphorus on E24 carbon Steel in 3.5% NaCl, *J. Chem. Technol. Metall* 53 (2018) 898.
- [61] R. Hsissou, B. Benzidia, N. Hajjaji, A. Elharfi, Elaboration and electrochemical studies of the coating behavior of a new nanofunctional epoxy polymer on E24 steel in 3.5% NaCl, *Port. Electrochim. Acta* 36 (2018) 259.
- [62] R. Hsissou, B. Benzidia, N. Hajjaji, A. Elharfi, Elaboration, electrochemical investigation and morphological study of the coating behavior of a new polymeric polyepoxide architecture: cross linked and hybrid decaglycidyl of phosphorus pentamethylene dianiline on E24 carbon steel in 3.5% NaCl, *Electrochem. Acta* 37 (2019) 179.
- [63] R. Hsissou, H. Benassaoui, F. Benhiba, N. Hajjaji, A. Elharfi, Application of a new tri-functional epoxy prepolymer, triglycidyl ethylene ether of bisphenol a, in the coating of e24 steel in 3.5 % NaCl, *Journal of chemical technology and metallurgy* 52 (2017) 431.
- [64] I. Lebkiri, B. Abbou, R. Hsissou, Z. Safi, M. Sadiku, A. Berisha, A. Lebkiri, Investigation of the anionic polyacrylamide as a potential adsorbent of crystal violet dye from aqueous solution: equilibrium, kinetic, thermodynamic, DFT, MC and MD approaches, *J. Mol. Liq.* 372 (2023) 121220.
- [65] L. Kadiri, A. Ouass, R. Hsissou, Z. Safi, N. Wazzan, Y. Essaadaoui, A. Lebkiri, Adsorption properties of coriander seeds: spectroscopic kinetic thermodynamic and computational approaches, *J. Mol. Liq.* 343 (2021) 116971.
- [66] A. Amri, L. Kadiri, R. Hsissou, A. Lebkiri, Z. Wardighi, A. Lebkiri, Investigation of Typha Latifolia (TL) as potential biosorbent for removal of the methyl orange anionic dye in the aqueous solution. Kinetic and DFT approaches, *J. Mol. Struct.* 1272 (2023) 134098.
- [67] J. Bensalah, A. Idrissi, M. Faydy, G. Doumane, A. Staoui, R. Hsissou, Z. Abdelkader, Investigation of the cationic resin as a potential adsorbent to remove MR and CV dyes: kinetic, equilibrium isotherms studies and DFT calculations, *J. Mol. Struct.* 1278 (2023) 134849.
- [68] R. Hsissou, M. Azogagh, F. Benhiba, S. Echihi, M. Galai, A. Shaim, M. Rafik, Insight of development of two cured epoxy polymer composite coatings as highly protective efficiency for carbon steel in sodium chloride solution: DFT, RDF, FFV and MD approaches, *J. Mol. Liq.* 360 (2022) 119406.



## Graphene based nanocomposites enhanced Fenton process for azo dye degradation

Bhawana Jain<sup>a</sup>, Walid Daoudi<sup>b,\*</sup>, Ajaya K. Singh<sup>h,\*</sup>, Garima Pravin Pandey<sup>c</sup>, Surendra Prasad<sup>d,\*</sup>, Dakeshwar Kumar Verma<sup>e</sup>, Elyor Berdimurodov<sup>f,g</sup>

<sup>a</sup> Department of Chemical Sciences, Siddhachalam Laboratory, Raipur, Chhattisgarh, 493221, India

<sup>b</sup> Laboratory of Molecular Chemistry, Materials and Environment (LCM2E), Departement of chemistry, Multidisciplinary Faculty of Nador, University Mohamed I, Nador 60700, Morocco

<sup>c</sup> Department of Chemistry, Rani Durgavati University, Jabalpur, Madhya Pradesh 482001, India

<sup>d</sup> Discipline of Biological and Chemical Sciences, School of Agriculture, Geography, Environment, Ocean and Natural Science (SAGEONS), The University of South Pacific, Suva, Fiji

<sup>e</sup> Department of Chemistry, Govt. Digvijay P.G. Autonomous College, Rajnandgaon 491441, India

<sup>f</sup> Chemical & Materials Engineering, New Uzbekistan University, 54 Mustaqillik Ave, Tashkent 100007, Uzbekistan

<sup>g</sup> Medical School, Central Asian University, Tashkent 111221, Uzbekistan

<sup>h</sup> Department of Chemistry, Govt. V. Y. T. PG. Autonomous, College, Durg, Chhattisgarh, 491001, India

### ARTICLE INFO

#### Keywords:

GO-CeO<sub>2</sub> nanocomposites  
Methyl violet  
Methyl violet degradation  
Azo dye degradation  
Heterogeneous Fenton's process

### ABSTRACT

The design and fabrication of smart and low-cost nanocomposites (NCs) is still an area of challenge in wastewater treatment. In this context, firstly individual graphene oxide (GO) and cerium oxide (CeO<sub>2</sub>) nanoparticles (NPs) were synthesized by precipitation method. This was followed by synthesis of GO-CeO<sub>2</sub>-NCs by mixing GO and CeO<sub>2</sub>-NPs in natural surfactant which was characterized by UV-visible absorption spectroscopy. The morphology of the synthesized GO-CeO<sub>2</sub>-NCs was established by scanning electron microscopy (SEM) studies while high resolution transmission electron microscopy (HRTEM) analysis revealed shape and particle size of the synthesized NCs. Fourier transform infrared spectroscopy (FTIR) was used to confirm the presence of different functional groups in the synthesized GO-CeO<sub>2</sub>-NCs and thermal stability was determined by thermal gravimetric analysis (TGA). The synthesized GO-CeO<sub>2</sub>-NCs was used as catalyst in heterogeneous Fenton process for the degradation of methyl violet (MV) dye. The effects of various experimental parameters, i.e., pH, H<sub>2</sub>O<sub>2</sub>, GO-CeO<sub>2</sub> NCs for MV degradation were investigated to have optimum condition. The optimum conditions for effective degradation with 98 % was achieved just within 100 minutes, at pH=8, [H<sub>2</sub>O<sub>2</sub>] 80×10<sup>-4</sup> M, and [GO-CeO<sub>2</sub>] 18 mg/L for 3×10<sup>-3</sup> M degradation. The experimental observations have led up to propose a most plausible mechanism for GO-CeO<sub>2</sub>-NCs enhanced Fenton's degradation of MV. GO-CeO<sub>2</sub> nanocomposites with H<sub>2</sub>O<sub>2</sub> shows amazing removal capacities in the elimination of MV. In summary, synthesized GO-CeO<sub>2</sub> nanocomposites demonstrate remarkable efficiency in present work, and offering a promising solution for the effective degradation of methyl violet dye in wastewater treatment.

### 1. Introduction

With the rapid growth of industries, especially textile industries, the tremendous use of dyes has become a serious issue for the environment [1]. In this regard, extensive efforts have been dedicated to explore highly efficient material as heterogeneous catalyst for wastewater treatment via Fenton process [2,3]. Therefore, new type of precursors and rationally designed hetero-structured materials has been strongly

desired to achieve outstanding results in dye degradation. Among all nanomaterial, graphene based nanocomposites (NCs) synthesis has inflame worldwide researchers due to their excellent properties of high electrical, optical, thermal conductivity and large active surface area [4–7]. The graphene plays vital role because of sp<sup>2</sup>-hybridized monolayer of carbon with honeycomb array, which provide great space to make NCs with other metal oxide [8–10]. Additionally, graphene oxide (GO) incorporates non-oxidized benzene rings along with six-membered

\* Corresponding authors.

E-mail addresses: [walid.daoudi@ump.ac.ma](mailto:walid.daoudi@ump.ac.ma) (W. Daoudi), [ajayaksingh\\_au@yahoo.co.in](mailto:ajayaksingh_au@yahoo.co.in) (A.K. Singh), [prasad\\_su@usp.ac.fj](mailto:prasad_su@usp.ac.fj) (S. Prasad).

<https://doi.org/10.1016/j.nanoso.2024.101329>

Received 9 March 2024; Received in revised form 31 July 2024; Accepted 4 September 2024

Available online 16 September 2024

2352-507X/© 2024 Elsevier B.V. All rights are reserved, including those for text and data mining, AI training, and similar technologies.



aliphatic rings and produces exfoliated GO through chemical oxidation by attaching many more oxygen containing functional groups in the adjacent layers of graphite. This makes GO highly soluble in water as well as its aromatic region is conjugated easily with aromatic molecules through  $\pi$ - $\pi$  interaction. This distinctive nature of GO instigated the establishing of various metal oxide nanoparticles (NPs) on its surface. Owing to these attractive properties of GO, the imprinting of functional nanomaterials on this highly conductive GO nanosheets (NSs) is an effective tool to design a promising NCs. Graphene sheets can easily accommodate with metal oxide with uniform dispersion on it [11–13]. CeO<sub>2</sub> is an important high refractive index rare earth oxide which has high oxygen storage capacity and other extensive properties such as sensor, insulator, catalyst [14–16]. Because of tremendous physical and chemical properties of CeO<sub>2</sub>, it has fascinated much attention in recent years [17–19]. Hence, in the current study, CeO<sub>2</sub> has successfully been decorated on GO-NPs which show a synergistic effect for the development of material with remarkable properties. Whereas, the combination of GO-CeO<sub>2</sub> makes it magical NCs for several applications [14,20–24], this has motivated us to use it as heterogeneous catalyst.

Fenton process involves in situ generation of powerful radicals such as •OH under mild acidic conditions through electron transfer process from metal ion to H<sub>2</sub>O<sub>2</sub> [25]. For the first time, Fenton process used FeSO<sub>4</sub> and H<sub>2</sub>O<sub>2</sub> to produce radical but it had some disadvantages, i.e., sludge creation and pH maintenances [26]. To overcome this problem, FeSO<sub>4</sub> has now been substituted by various NPs-NCs as heterogeneous catalyst, which can easily be separated and recycled [27]. The NPs-NCs act as efficient heterogeneous catalyst because of their very small size and large surface area for reaction. Furthermore, Fenton process constitutes promising, effective and environment friendly process to remove pollutants from wastewater [28–32]. Thus, there is an urgent need of a best combination of H<sub>2</sub>O<sub>2</sub> and heterogeneous catalyst to remove dye containing wastewater. The textile industries play a vital role in the economic growth of any nation along with generation of employment. However, it also generates a large amount of textile wastes and wastewater that are damaging to the environment. Therefore, attention has been paid by researchers and industries on the reduction as well as purification of textile wastewater through environmentally friendly techniques [33,34]. The most difficult constituents in textile wastewater are dyes which have complex chemical structures. Dyes in textiles or any wastewater reduces the quality of the water and its dependent habitats and environment. Dyes also jeopardize to human and environment as even at very low concentration they have carcinogenic effects [35–37]. Treatment of textile effluent i.e., wastewater containing dye is quite complicated and efforts have been directed to develop effective treatment technologies for wastewater containing dyes [38,39]. However, there has not been very satisfactory method for remediating broad diversity of textile wastewater. The classical techniques like coagulation/flocculation, membrane separation (ultrafiltration, reverse osmosis) or removal by activated carbon adsorption just incorporate phase transfer of dyes [40–42]. The biological treatment of textile wastewater has also not been a complete solution to problem as many dyes are biologically resistant [43,44]. Methyl violet (MV), a model pollutant, also called as MV 10B (C<sub>25</sub>H<sub>30</sub>N<sub>3</sub>Cl) has frequently been used in textile and paper dyeing by several industries. However, it acts as a mutagen and mitotic poison and its presence in wastewater causes harmful impact on the environment. Generally, methods such as chemical bleaching, biodegradation and photo catalytic degradation have been used for the removal of crystal violet or MV dye from wastewater [45–47]. However, it has been reported that Fenton process gave better results for the degradation of MV dye [48–54], as compare to other process [55–57]. We have been working on treatment and removal of organic pollutants and dyes involving homogeneous and heterogeneous Fenton and Fenton like processes [25,29,32]. Thus, in continuation of our work, we have applied GO-CeO<sub>2</sub>-NCs as potential candidate for the treatment of MV dye containing wastewater. Therefore, the present paper reports a successful synthesis of GO-CeO<sub>2</sub>-NCs and its

characterization followed by its use as heterogeneous catalyst for MV degradation and study on recycle stability of GO-CeO<sub>2</sub>-NCs.

## 2. Experimental

### 2.1. Materials & method

All the reagents used were of analytical reagent (AR) grade. Graphite powder was purchased from Global Nanotech, Nagpur, India and used as a precursor for the synthesis of GO, H<sub>2</sub>O<sub>2</sub>, potassium nitrate (KNO<sub>3</sub>), potassium permanganate (KMnO<sub>4</sub>), and hydrochloric acid (HCl) and NH<sub>4</sub>OH were acquired from Merck, Mumbai, India. Cerium sulphate (Ce (SO<sub>4</sub>)<sub>2</sub>) was obtained from S. D. Fine chemicals, Mumbai, India while MV prevailed from Sigma Aldrich, Bengaluru, India. Sodium hydroxide (NaOH) and sulfuric acid (H<sub>2</sub>SO<sub>4</sub>), obtained from Merck, Mumbai, India, were used to maintain the pH. Triple distilled water (TDW) was used for all the reactions. First of all, GO was prepared by modified Hummers method [58]. In brief, 23 mL of H<sub>2</sub>SO<sub>4</sub> was taken in an Erlenmeyer flask and placed in an ice bath. This was followed by gradual addition 1 g of graphite powder and 0.5 g of KNO<sub>3</sub> with continuous stirring. Then slowly 3 g KMnO<sub>4</sub> was added and kept in water bath to attain temperature up to 35 °C and magnetic stirred for 2 h to get thick brown paste. Subsequently, 23 mL TDW was slowly added to the reaction mixture and the suspension was maintained at 98 °C for 30 min. The reaction mixture then diluted with TDW to 140 mL. To reduce residual KMnO<sub>4</sub> and MnO<sub>2</sub>, the solution was treated with H<sub>2</sub>O<sub>2</sub> (30 %). The resulting deep brown slurry was dialyzed in dialysis membrane against TDW for 7 days. Then further exfoliation was done through ultra-sonication for 1 h. Non-exfoliated GO layers were removed by centrifugation. The GO powders were obtained after drying the sample in a vacuum oven for 24 h at 60 °C. Cerium oxide (CeO<sub>2</sub>) was prepared by simple chemical precipitation method, using cerium sulphate as precursor [59]. In a typical experiment, 0.1 M aqueous solution of Ce(SO<sub>4</sub>)<sub>2</sub> was mixed with 25 % ammonia (NH<sub>4</sub>OH) solution (10 mL) and 0.1 M of cetyltrimethylammonium bromide (CTAB). The solution was then keeping the solution for continuous stirring for 2 h. The resultant yellow colored precipitate [Ce(OH)<sub>4</sub>] was washed with water/ethyl alcohol and calcined at 600 °C for 2 hrs to obtain CeO<sub>2</sub>. For the preparation of GO-CeO<sub>2</sub> NCs, 30 mL of 10 M NaOH solution and 10 mL reetha (natural surfactant) solution were mixed in a 500 mL beaker and keep in Orbital shaking incubator for 1 h. This was followed by addition of 1 mg GO to the above mixture and again shaken for 1 h. Then, 1 mg of CeO<sub>2</sub> was added and shaken for next 1 h. The reaction mixture was placed in sonicator for 6 h and filtered through Whatman filter paper 40 and left for 24 h for cooling. The sample was then autoclaved and washed with HNO<sub>3</sub> acid and subsequently with TDW times to remove impurities, if any. The washed graphene CeO<sub>2</sub> based NCs sample was placed in an oven to dry at 80 °C for 12 h. Thus, prepared GO-CeO<sub>2</sub>-NCs were subjected to characterization for further use.

### 2.2. Characterization studies

To validate the formation of GO-CeO<sub>2</sub> NCs the synthesized nanoparticle samples were characterized by using a UV–visible spectrophotometer (Shimadzu UV–visible Spectrometer, Japan) at the wavelength range of 200–800 nm, and DMSO was used as the blank reference. The synthesis of GO-CeO<sub>2</sub>-NCs absorbs in the wavelength range ~250–370 nm.

X-ray diffraction (XRD) study was carried out on Bruker D-8 advance X-ray diffractometer using CuK $\alpha$  X-ray radiation with  $\lambda = 0.154$  nm operated at 40 kV and 40 mA in the  $2\theta$  range of 10–80° to determine crystallinity and crystal size of the synthesized GO-CeO<sub>2</sub>-NCs. JEOL-JSM 6390 was used for scanning electron microscopy (SEM) analysis to find the surface morphology of the synthesized GO-CeO<sub>2</sub>-NCs for getting particle size of NCs. High resolution transmission electron microscopy (HRTEM) analysis was carried out on a Zeiss EM 912  $\Omega$  instrument at an

acceleration voltage of 120 kV. To find out physical and chemical changes in GO-CeO<sub>2</sub>-NCs during high temperature, TGA determination were carried out by using Perkin Elmer, Diamond instrument with a heating rate of 20 °C /min. FTIR spectrum of NCs was taken using FTIR 8400S, Shimadzu (Japan).

### 2.3. Kinetic study

The kinetic study of the degradation of MV by heterogeneous Fenton oxidation process was investigated by UV-visible spectroscopy at the maximum absorbance wavelength ( $\lambda_{\max}$ ) of MV at 580 nm. The concentration of the dye in the reaction mixture at different reaction times was determined by measuring the absorbance at  $\lambda_{\max}$  = 580 nm. The pH of the reaction mixture was adjusted at 8 using dilute NaOH. The oxidation of MV ( $3 \times 10^{-3}$  M) was achieved by addition of H<sub>2</sub>O<sub>2</sub> ( $80 \times 10^{-4}$  M) and GO-CeO<sub>2</sub>-NCs (18 mg/L) at 25 °C and stirred at a magnetic stirrer. The reaction was initiated by adding H<sub>2</sub>O<sub>2</sub> to the reaction bottle containing MV, GO-CeO<sub>2</sub>-NCs and sodium hydroxide. After every 10 min of the reaction, 4.5 mL of reaction mixture was taken out and was then analyzed in the spectral range from 200 to 800 nm periodically. Each experiment was replicated three times. The degradation percentage (%) of the dye was calculated using the following Eq. (1), where C is the initial concentration of the dye and C<sub>0</sub> is the concentration after degradation at given time t. The removal (R, %) was calculated from Eq. (2) and adsorption capacity (q<sub>e</sub>, mg L<sup>-1</sup>) from Eq. (3), as follows:

$$\text{Dye Degradation}(\%) = \left( \frac{C - C_0}{C} \right) \quad (1)$$

$$q_e = \left( \frac{C_0 - C_e}{m} \right) \times V \quad (2)$$

$$q_t = \left( \frac{C_0 - C_t}{m} \right) \times V \quad (3)$$

Where R, q<sub>e</sub> and q<sub>t</sub> (kinetic adsorption capacity of MV dye) were calculated by Eqs. (1)–(3), respectively, where C<sub>0</sub> and C<sub>e</sub> are the initial

and equilibrium concentrations of MV (mg/ L), respectively, C<sub>t</sub> is the concentration of MV at a given time t, m is the adsorbent mass (g) and V is the dye solution volume (mL). Furthermore, the kinetics of MV dye removal was examined using pseudo-first order and pseudo-second order kinetics.

## 3. Results and discussion

### 3.1. Characterization of GO-CeO<sub>2</sub>-NCs

The pure graphene absorption spectrum has an UV- absorption peak without hump between ~250–370 nm. The UV-visible spectrum of synthesized GO-CeO<sub>2</sub>-m-NCs, showed a peak without hump between ~258–330 nm (Figure SI.1). Which confirmed that the absorption edge was red shifted compared to graphene [60]. The optical band gap is an important parameter for NCs to know their photocapacity, photo-electrode or photodegradation application for dye degradation. A large amount of research has been devoted to modifying the band gap to modifying its optical absorption properties. These can be tuned by different synthesis methods, dopant, temperature etc [61–63].

Thus, optical band gap energy (E<sub>g</sub>) of the synthesized GO-CeO<sub>2</sub>-NCs was calculated using Tauc plot between the  $(\alpha h\nu)^2$  on the ordinate against  $h\nu$  (Figure SI.2) [64], where  $\alpha$  is the linear absorption coefficient of the material. The band gap was determined by extrapolating the linear portion of the Tauc plot as 2.1 eV (Figure SI.2).

To find the crystalline phase purity and structural information of the synthesized GO-CeO<sub>2</sub>-NCs the X-ray diffraction (XRD) was carried out. The XRD patterns of GO-NPs, CeO<sub>2</sub>-NPs and GO-CeO<sub>2</sub>-NCs have been depicted in Fig. 1, CeO<sub>2</sub> shows cubic fluorite structure with XRD peaks at 28.54°, 47.48° and 56.33° 2 $\theta$ , which were assigned to (111), (400) (311) reflection, respectively while GO shows a peak at 12.28° 2 $\theta$  which resemble to (001) reflection [65,66]. The XRD peaks of GO-CeO<sub>2</sub>-NCs clearly show that the diffraction peaks resembled exactly to those seen in GO with (001) reflection and in CeO<sub>2</sub> with (111) reflection. The most intense peak in the XRD pattern of GO-CeO<sub>2</sub> was found at 2 $\theta$ =10.69° while less intense broad peak obtained at 2 $\theta$ =28.08° and these two peaks were very much present in GO and CeO<sub>2</sub>, respectively. In case of

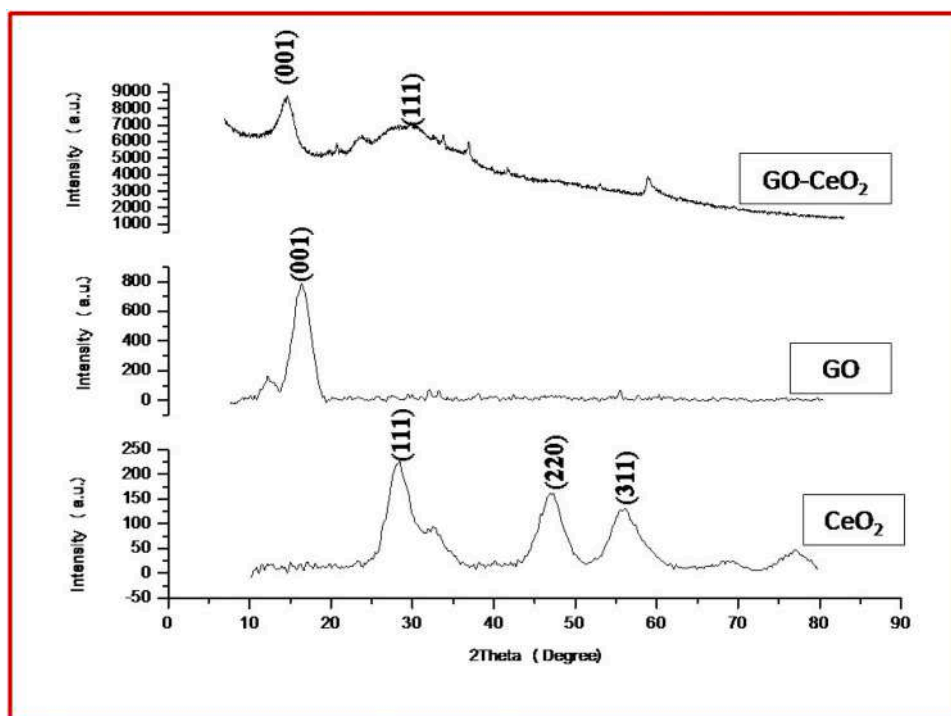


Fig. 1. XRD pattern of the synthesized GO, CeO<sub>2</sub> NPs and GO-CeO<sub>2</sub> NCs.

GO-CeO<sub>2</sub>-NCs a sharp and intense peak was not observed. This must be due to the formation of [CeOH(CO<sub>3</sub>)] on the surface of the particle during composite preparation. The Debye Sherrer equation was used to calculate average crystalline size of the particle [67], Bragg's equation helped to find the d-spacing [68], and the average micro-strain was calculated by Stokes-Wilson equation [69], where size and strain correlated broadening show a dependency on  $\theta$ . Value of interlayer spacing is affected by strain present in the crystallite, i.e., compressive stress reduced the interlayer spacing and increased tensile strength. The Williamson-Smallman's method [70], was to calculate dislocation density as a measure of irregularity inside the crystal which can affects the properties of the crystals. Larger the dislocation density higher the hardness of the crystal and lower the crystal size. Table 1 shows all the microstructural properties calculated, i.e., particle size, d-spacing, micro strain and dislocation density of GO-NPs, CeO<sub>2</sub>-NPs, GO-CeO<sub>2</sub>-NCs.

The scanning electron microscopic (SEM) image shown in Fig. 2 revealed morphology of GO-CeO<sub>2</sub>-NCs. It clearly shows GO-CeO<sub>2</sub>-NCs rough surface area with crumpled and wrinkled GO sheets (Fig. 2). It is clear from SEM image of GO-CeO<sub>2</sub> that CeO<sub>2</sub>-NPs anchored on exfoliated GO-NPs.

The energy dispersive X-ray (EDX) spectrum of the synthesized GO-CeO<sub>2</sub>-NCs is shown in Figure SI.3 which displays its elemental composition. The EDX spectrum confirmed the presence of carbon (C), cerium (Ce) and oxygen (O) in the synthesized GO-CeO<sub>2</sub>-NCs. Inset Table in Figure SI.3 contains atomic % of C, Ce and O which are quite comparable to the value reported in literature [66].

In order to get morphology and particle size of the synthesized GO-CeO<sub>2</sub>-NCs, high resolution transmission electron microscopy (HRTEM) analysis was carried out. HRTEM images of GO-CeO<sub>2</sub> are shown in Fig. 3 where exfoliated GO sheet is clearly visible. Fig. 3 A&B show that GO-CeO<sub>2</sub>-NCs is transparent with some clear visible wrinkles of GO while only small amount of CeO<sub>2</sub>-NPs are visible in Fig. 3 C&D. The shape of the synthesized GO-CeO<sub>2</sub>-NCs is confirmed to be hexagonal (Fig. 3C). Fig. 4 shows the selected area electron diffraction (SAED) pattern of the synthesized GO-CeO<sub>2</sub>-NCs. The SAED pattern contains a series of bright rings which show that the synthesized GO-CeO<sub>2</sub>-NCs is polycrystalline with clear boundaries.

In GO-CeO<sub>2</sub>-NCs, cerium should attach to carbon structure through carboxyl group. The FT-IR spectrum of the synthesized GO-CeO<sub>2</sub>-NCs is shown in Figure SI.4 which shows a strong band at 3417.11 cm<sup>-1</sup> that appeared due to symmetric and asymmetric stretching of water molecule, which came from improper handling KBr pallet. Methylene group showed less intense band in the range of 2851.76–2926.32 cm<sup>-1</sup> while the band appeared at 1728.96 cm<sup>-1</sup> is due to presence of carboxyl group. The band at 479.20 cm<sup>-1</sup> confirmed the presence of CeO<sub>2</sub> in NCs and due to stretching vibration mode of Ce-O<sub>2</sub>. The weak shoulder bands at 1728.96 cm<sup>-1</sup> and 1383.03 cm<sup>-1</sup> have been attributed to carboxyl group. The band at 1246.35 cm<sup>-1</sup> was obtained because of interaction between CeO<sub>2</sub> and atmospheric CO<sub>2</sub> while C=C vibration showed an intense band at 1627.51 cm<sup>-1</sup> [20].

Figure SI.5 shows the thermogravimetric analysis (TGA) curve of the synthesized GO-CeO<sub>2</sub>NCs. The TGA curve clearly shows a narrow decomposition process with sharp weight loss at 198°C and little mass loss at 550°C which have been attributed to GO decomposition and

**Table 1**

Microstructural properties of the GO NPs and CeO<sub>2</sub> NPs and GO-CeO<sub>2</sub> NCs obtained from XRD data.

Microstructural properties	GO NPs	CeO <sub>2</sub> NPs	GO-CeO <sub>2</sub> NCs
Crystal size, D (nm)	2.97 ±0.82	2.4±1.21	1.25±1.68
Interlayer spacing, d (nm)	0.72 ±0.02	0.31 ±0.05	0.41–0.84 ±0.03
Micro strain, $\epsilon \times 10^{-3}$	0.01096	0.069000	0.3821
Dislocation density, $\delta \times 10^{-14}$ (lines/m <sup>2</sup> )	11.33	17.36	80.00

burning of carboxyl and epoxy groups.

### 3.2. Heterogeneous fenton degradation of MV

The degradation of MV by heterogeneous Fenton process in aqueous solution at pH=8 was carried out in a conical flask on magnetic stirrer taking MV, GO-CeO<sub>2</sub> NCs and H<sub>2</sub>O<sub>2</sub> in sequence at room temperature. Reaction mixture was finally taken in 1 cm quartz cuvette to study MV degradation in UV-visible photometer where spectrum was recorded in the range of 310–910 nm. Figure SI.6 shows UV-visible absorption spectrum of MV containing reaction mixture which shows the maximum absorption at 580 nm. Various parameters that affect the degradation process investigated were: concentrations of MV, H<sub>2</sub>O<sub>2</sub>, and GO-CeO<sub>2</sub>, and pH of the medium.

To understand the effect of synthesized GO-CeO<sub>2</sub>-NCs on the degradation of the dye MV, the studies were carried out separately first with H<sub>2</sub>O<sub>2</sub> and then in the presence of GO-CeO<sub>2</sub> NCs. This was followed by degradation involving Fenton reaction, i.e., in the presence of H<sub>2</sub>O<sub>2</sub> and GO-CeO<sub>2</sub>-NCs together. It was observed that the dye MV was sluggishly degraded by H<sub>2</sub>O<sub>2</sub> while little fast in the presence of GO-CeO<sub>2</sub> and quite effectively degraded by Fenton process in which H<sub>2</sub>O<sub>2</sub> and GO-CeO<sub>2</sub> were used together. The results of the degradation of the dye MV are shown in Figure SI.7 where remaining concentration of MV (C/C<sub>0</sub>) is plotted against time.

The optimization of pH for the degradation of the dye MV is the most important parameter for study during Fenton process [28,59]. To determine optimal pH for the best degradation efficiency, a series of experiments at different pH 2, 4, 6, 8, 10, and 12 were carried out and the results obtained were plotted in terms of degradation (C/C<sub>0</sub>) against pH as shown in Figure SI.8. Thus, it was concluded that after pH 8–12, the maximum degradation occurs. At pH 8 optimum degradation obtained was 97 % at room temperature. As it is well known that before discharging any treated water into the environment, it is essential to maintain its pH, so pH 8 was taken as optimum which is close to neutral pH. Thus, for further study, the pH of the reaction mixture in Fenton process was maintained at 8.

The oxidation (degradation) of MV by oxidant hydroxyl radical (•OH) which comes from hydrogen peroxide (H<sub>2</sub>O<sub>2</sub>) via its action as catalyst. The degradation of MV was studied at different concentration of H<sub>2</sub>O<sub>2</sub> from 20 to 160 × 10<sup>-3</sup> M up to 100 minutes. As the concentration of H<sub>2</sub>O<sub>2</sub> increased, the degradation (%) of the dye MV was also increased. The results obtained are shown in Figure SI.9, which clearly shows that the maximum degradation was obtained with [H<sub>2</sub>O<sub>2</sub>] = 80 × 10<sup>-3</sup> M in 100 minutes.

In the Fenton process the catalyst GO-CeO<sub>2</sub> plays a significant role in the generation of •OH radical because in the absence of the catalyst GO-CeO<sub>2</sub>, H<sub>2</sub>O<sub>2</sub> acts as a weak oxidant and cannot generate sufficient amount of •OH to degrade MV. Thus, to find out the effect of the catalyst (GO-CeO<sub>2</sub>) and to optimize its concentration, MV degradation study was carried out at different concentration of the catalyst (6–30 mg/L), taking initial concentration of MV as 3 × 10<sup>-3</sup> M. The result of the degradation of MV at different concentration of GO-CeO<sub>2</sub> catalyst are shown in Figure SI.10, which concluded that 18 mg/L of the catalyst was the optimum amount for the degradation of MV. At amount less than 18 mg/L of GO-CeO<sub>2</sub>, the degradation of MV was damn slow while at higher than 18 mg/L it showed almost similar degradation (Figure SI.10). Thus, 18 mg/L of the catalyst GO-CeO<sub>2</sub> was taken as optimum in Fenton degradation of MV. The (•OH) hydroxyl radical generation from H<sub>2</sub>O<sub>2</sub> is responsible for the dye MV degradation which is activated only by the addition of GO-CeO<sub>2</sub> catalyst. However, excess active sites in catalyst slow down the degradation process, because of the fact that high concentration of GO-CeO<sub>2</sub> acts as •OH radical scavenger.

### 3.3. Evidence for •OH radical generation in Fenton process

As a confirmation of the hydroxyl (•OH) generation and its use in

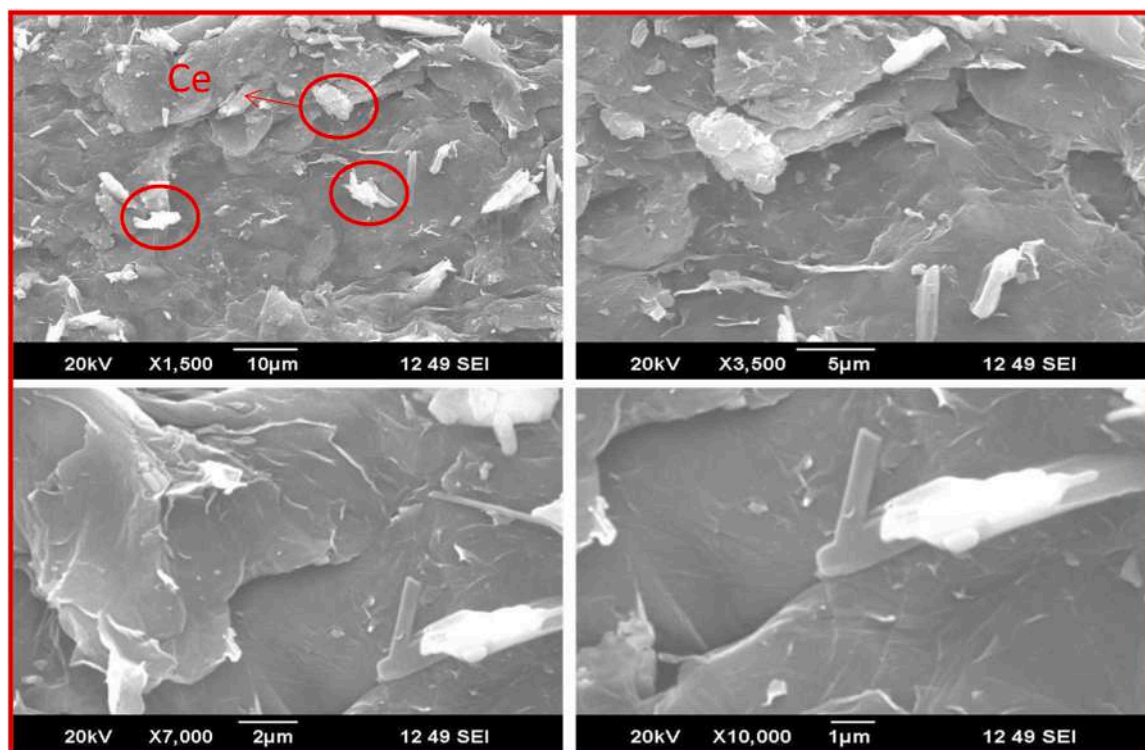


Fig. 2. SEM images of the synthesized GO-CeO<sub>2</sub> NCs where cerium oxide (CeO<sub>2</sub>) nanoparticles (indicated by circle) spread on graphene (GO) sheets.

Fenton process was it's investigated by radical trapping experiments. When a well-known •OH scavenger, t-butyl alcohol (TBA), was added to the reaction mixture the MV degradation was dropped to 32 % compare to blank experiment 98 % (Figure SI.11). The MV degradation was also studied with another •OH scavenger, benzoquinone (BQ), which caused only 19 % MV degradation (Figure SI.11). These studies confirmed the generation of •OH radicals which plays important role in the dye MV degradation.

### 3.4. Kinetics model

The effect of contact time on MV removal by GO-CeO<sub>2</sub> NCs and H<sub>2</sub>O<sub>2</sub> was presented in Fig. 5 A,B. A good removal was found as the adsorption started and time approached 50 min. The MV adsorption kinetics was explained by predictive theoretical pseudo first order and pseudo second order models [71]. Adsorption kinetics was used to test the linearity between time and adsorption capacity. The usual models include the pseudo-first-order kinetic Eq. (4) and the pseudo-second-order kinetic Eq. (5) [72]. Pseudo first order kinetic model has the following equation:

$$\log(q_e - q_t) = \log(q_e) - \frac{K_1}{2.303} \times t \quad (4)$$

Where  $q_e$  (mg/g) and  $q_t$  (mg/g) are the adsorption capacities at equilibrium and at a given time  $t$  and  $k_1$  ( $\text{min}^{-1}$ ) is the rate constant, determined from the slope. Fig. 5 A shows  $\log(q_e - q_t)$  versus  $t$  plot. The pseudo second order kinetic model has this equation:

$$\frac{1}{q_e - q_t} = \frac{1}{q_e} + K_2 \times t \quad (5)$$

Where  $q_e$  and  $q_t$  are the same as above, and  $k_2$  ( $\text{g/mg min}^{-1}$ ) is the rate constant. The values of  $q_e$  and  $k_2$  are calculated from the intercept and slope of the plot of  $t/q_t$  versus  $t$  shown in Fig. 5 B. The pseudo second order kinetic model shows an excellent correlation coefficient (above 0.99) at room temperature. This showed that chemisorptions were the rate controlling step of MV adsorption onto GO-CeO<sub>2</sub> NCs.

The high correlation coefficient obtained for pseudo second order kinetics indicated that the model nicely represented the experimental data.

### 3.5. Reusability of catalysts

Two crucial catalyst criteria are sustainability and reusability. Recycling tests were carried out for the removal of MV in order to investigate the stability and durability of the as-prepared GO-CeO<sub>2</sub> NCs. Following each cycle, the catalyst was separated by centrifugation, and the separated particles were subsequently cleaned with ethanol and heated to 100 degrees to eliminate any remaining moisture and contaminants. Finally, the catalyst's catalytic activity was terminated by reusing it. In three cycles, over 20.4 % of the catalyst was lost (Figure SI.12). After three successive cycles, Figure SI.12 demonstrates that very little degrading efficiency is lost. As a result, during the degrading process, GO-CeO<sub>2</sub> NCs might be regarded as reusable and stable nanocomposites.

### 3.6. Mechanism

Based on the optimization of the degradation process and other experimental observations it was concluded that •OH radical generated through heterogeneous Fenton process attacks on benzene ring of MV molecules and break it into small molecules in several steps. The Fenton process for the degradation of MV is shown in scheme 1 in Eqs. (2) to (4). Initially generated •OH radicals degrade MV into Michler's ketone which finally decomposed into very small molecules shown in Eqs. (3) and (4) (Fig. 5) [66].

## 4. Conclusions

GO-CeO<sub>2</sub>-NCs was fruitfully synthesized where percentage of GO in NCs was much higher than CeO<sub>2</sub>-NPs. The synthesis of GO-CeO<sub>2</sub>-NCs was used as heterogeneous catalyst in Fenton process for the degradation of MV at pH=8. The present experimental results concluded that

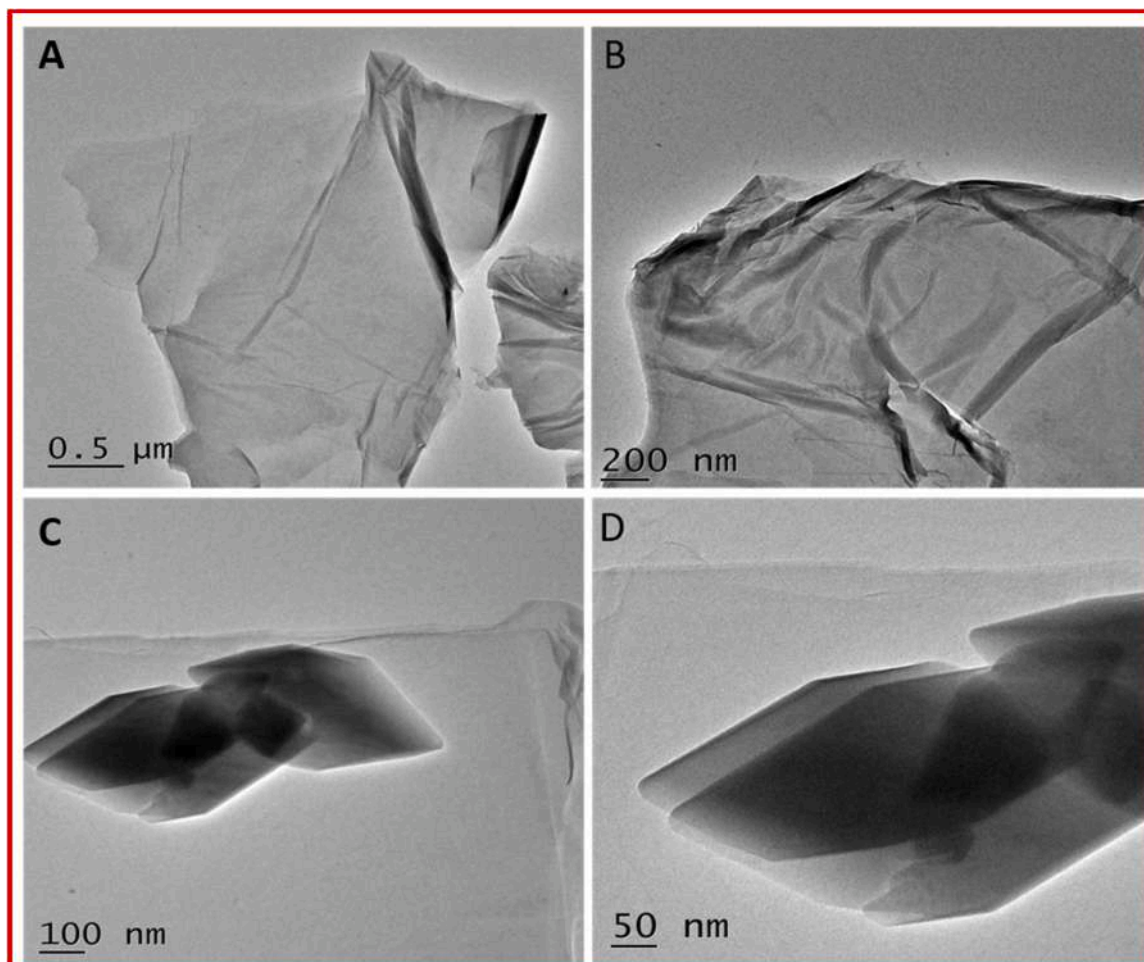


Fig. 3. HRTEM images of the synthesized of GO-CeO<sub>2</sub>-NCs with different magnifications.

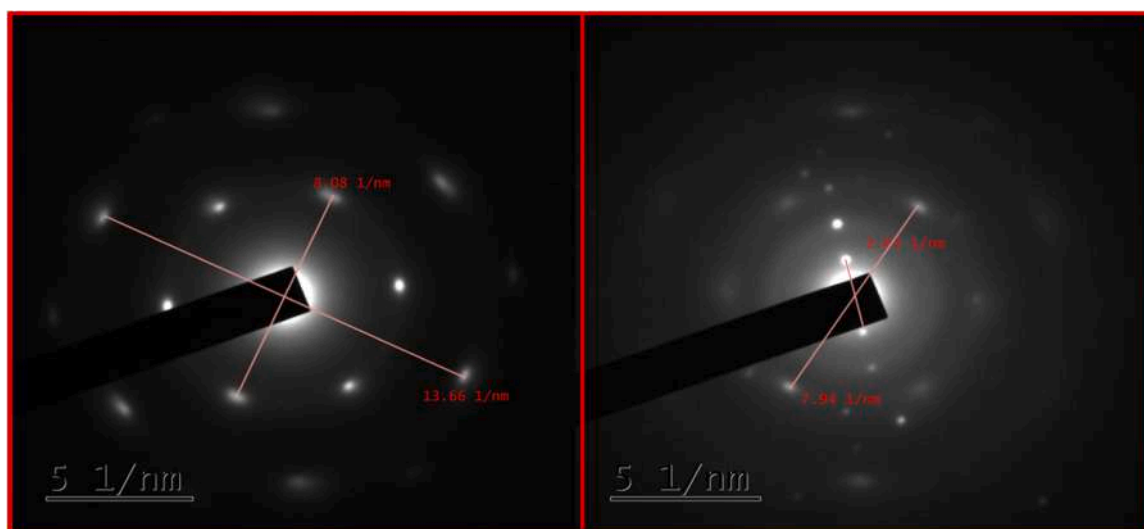


Fig. 4. Selected area electron diffraction (SAED) pattern of the synthesized GO-CeO<sub>2</sub>-NCs.

effective degradation of the dye MV by heterogeneous Fenton process is quite fast. It requires small amount of H<sub>2</sub>O<sub>2</sub> and GO-CeO<sub>2</sub>-NCs and the degradation process takes place at room temperature. The present report opens new way to treat wastewater containing MV as a low cost technique and with ease of implementation. This study clearly explains that

interaction of rare earth metal, cerium, with non-metal graphene has potential scope for water treatment involving Fenton's process.

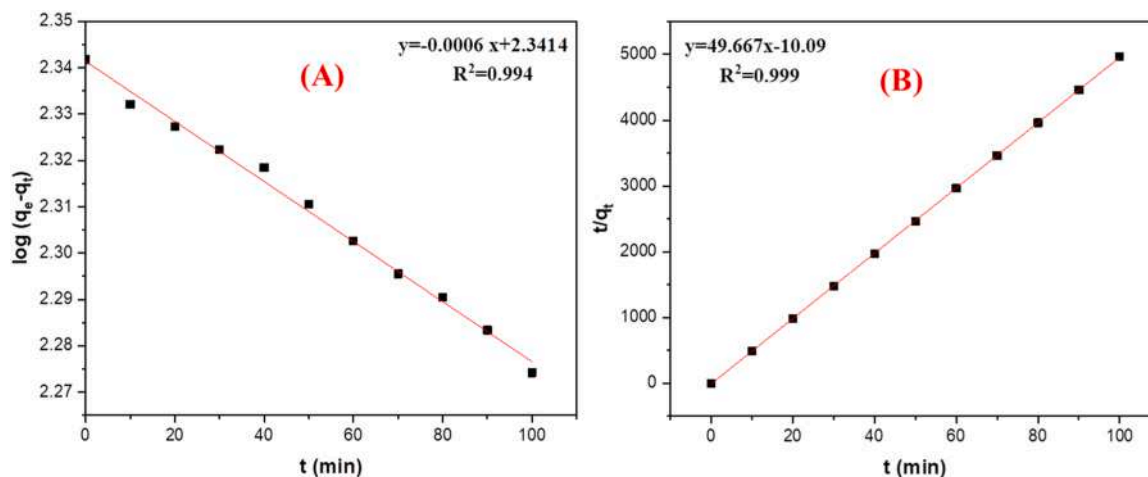


Fig. 5. (A) MV degradation via heterogeneous Fenton process using GO-CeO<sub>2</sub> NCs fitted with the pseudo-first-order model and (B) with the pseudo-second-order model.

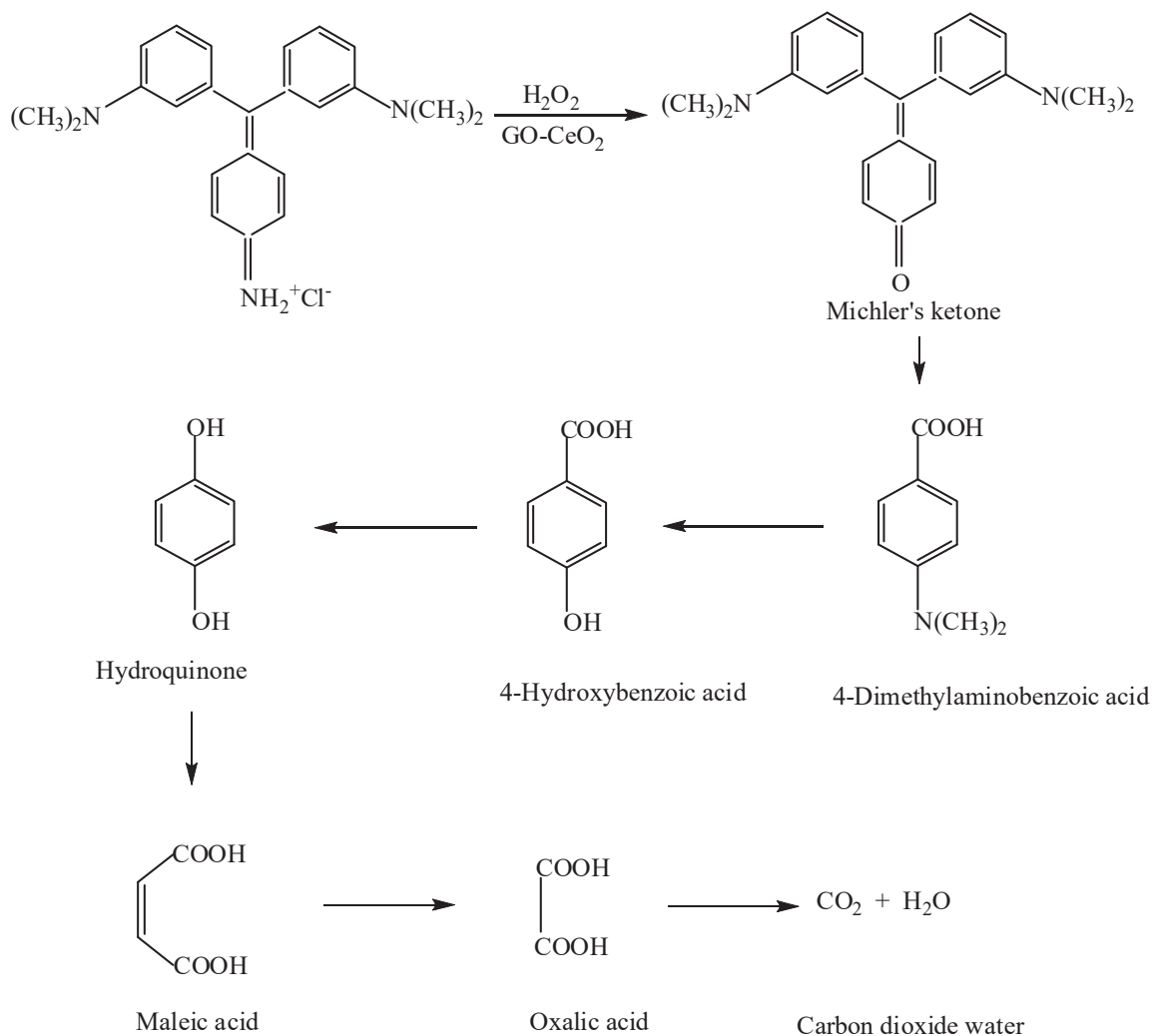


Fig. 6. Schematic pathway for the dye MV degradation by heterogeneous Fenton process.

#### CRediT authorship contribution statement

**Surendra Prasad:** Resources, Methodology, Investigation, Formal analysis, Data curation. **Dakeshwar Kumar Verma:** Writing – review &

editing, Supervision, Methodology, Investigation, Formal analysis. **Ajaya K. Singh:** Writing – original draft, Software, Formal analysis. **Garima Pravin Pandey:** Methodology, Formal analysis, Data curation, Conceptualization. **Walid Daoudi:** Writing – review & editing,

Visualization, Validation, Formal analysis. **Bhawana Jain:** Writing – original draft, Visualization, Software, Funding acquisition, Formal analysis. **Elyor Berdimurodov:** Writing – review & editing, Validation, Supervision.

### Declaration of Competing Interest

The authors declare that they have no known competing financial interests or personal relationships that could have appeared to influence the work reported in this paper.

### Data Availability

No data was used for the research described in the article.

### Acknowledgement

This work was financially supported by The University Grants Commission through Woman Post Doctoral Fellowship award (F.15-1/2013-14/PDFWM-2013-14-GE-CHH-18784(SA-II)). Authors are thankful to Government V. Y. T. PG. Autonomous College, Durg, for providing basic instrumental facilities. Authors also thank SAIF Cochin for characterization analysis of nanocomposites.

### Appendix A. Supporting information

Supplementary data associated with this article can be found in the online version at [doi:10.1016/j.nanoso.2024.101329](https://doi.org/10.1016/j.nanoso.2024.101329).

### References

- [1] E. Kianfar, V. Cao, Polymeric membranes on base of PolyMethyl methacrylate for air separation: a review, *J. Mater. Res. Technol.* 10 (2021) 1437–1461, <https://doi.org/10.1016/j.jmrt.2020.12.061>.
- [2] N. Thomas, D.D. Dionysiou, S.C. Pillai, Heterogeneous Fenton catalysts: a review of recent advances, *J. Hazard. Mater.* 404 (2021) 124082.
- [3] A. Rodríguez, G. Ovejero, J.L. Sotelo, M. Mestanza, J. García, Heterogeneous Fenton Catalyst Supports Screening for Mono Azo Dye Degradation in Contaminated Wastewaters, *Ind. Eng. Chem. Res.* 49 (2010) 498–505, <https://doi.org/10.1021/ie901212m>.
- [4] P.M. Ashraf, S.N. Thomas, L. Edwin, Development of graphene–nanometre-sized cerium oxide-incorporated aluminium and its electrochemical evaluation, *Appl. Nanosci.* 6 (2016) 149–158, <https://doi.org/10.1007/s13204-015-0438-2>.
- [5] A. Kausar, I. Ahmad, M.H. Eisa, M. Maaza, Graphene nanocomposites in space sector—fundamentals and advancements, *C* 9 (2023) 29, <https://doi.org/10.3390/c9010029>.
- [6] G. Bertoni, L. Calmels, A. Altibelli, V. Serin, First-principles calculation of the electronic structure and EELS spectra at the graphene/Ni(111) interface, *Phys. Rev. B* 71 (2005) 075402, <https://doi.org/10.1103/PhysRevB.71.075402>.
- [7] R. Bhargava, S. Khan, Enhanced optical properties of Cu<sub>2</sub>O anchored on reduced graphene oxide (rGO) sheets, *J. Phys.: Condens. Matter* 30 (2018) 335703, <https://doi.org/10.1088/1361-648X/aad2b2>.
- [8] K.S. Novoselov, A.K. Geim, S.V. Morozov, D. Jiang, Y. Zhang, S.V. Dubonos, I. V. Grigorieva, A.A. Firsov, Electric field effect in atomically thin carbon films, *Science* 306 (2004) 666–669, <https://doi.org/10.1126/science.1102896>.
- [9] O. Akhavan, Photocatalytic reduction of graphene oxides hybridized by ZnO nanoparticles in ethanol, *Carbon* 49 (2011) 11–18, <https://doi.org/10.1016/j.carbon.2010.08.030>.
- [10] C.N.R. Rao, A.K. Sood, K.S. Subrahmanyam, A. Govindaraj, Graphene: the new two-dimensional nanomaterial, *Angew. Chem. Int. Ed.* 48 (2009) 7752–7777, <https://doi.org/10.1002/anie.200901678>.
- [11] J. Du, X. Lai, N. Yang, J. Zhai, D. Kisailus, F. Su, D. Wang, L. Jiang, Hierarchically ordered macro–mesoporous TiO<sub>2</sub>–graphene composite films: improved mass transfer, reduced charge recombination, and their enhanced photocatalytic activities, *ACS Nano* 5 (2011) 590–596, <https://doi.org/10.1021/nn102767d>.
- [12] Y. Liang, Y. Li, H. Wang, J. Zhou, J. Wang, T. Regier, H. Dai, Co<sub>3</sub>O<sub>4</sub> nanocrystals on graphene as a synergistic catalyst for oxygen reduction reaction, *Nat. Mater.* 10 (2011) 780–786, <https://doi.org/10.1038/nmat3087>.
- [13] M.U. Rahman, U.Y. Qazi, T. Hussain, N. Nadeem, M. Zahid, H.N. Bhatti, I. Shahid, Solar driven photocatalytic degradation potential of novel graphitic carbon nitride based nano zero-valent iron doped bismuth ferrite ternary composite, *Opt. Mater.* 120 (2021) 111408, <https://doi.org/10.1016/j.optmat.2021.111408>.
- [14] L. Jiang, M. Yao, B. Liu, Q. Li, R. Liu, H. Lv, S. Lu, C. Gong, B. Zou, T. Cui, B. Liu, G. Hu, T. Wågberg, Controlled synthesis of CeO<sub>2</sub>/graphene nanocomposites with highly enhanced optical and catalytic properties, *J. Phys. Chem. C* 116 (2012) 11741–11745, <https://doi.org/10.1021/jp3015113>.
- [15] R. Si, Y.-W. Zhang, L.-P. You, C.-H. Yan, Rare-earth oxide nanopolyhedra, nanoplates, and nanodisks, *Angew. Chem. Int. Ed. Engl.* 44 (2005) 3256–3260, <https://doi.org/10.1002/anie.200462573>.
- [16] S. Yu, Q. Liu, W. Yang, K. Han, Z. Wang, H. Zhu, Graphene–CeO<sub>2</sub> hybrid support for Pt nanoparticles as potential electrocatalyst for direct methanol fuel cells, *Electrochim. Acta* 94 (2013) 245–251, <https://doi.org/10.1016/j.electacta.2013.01.149>.
- [17] C. Xu, X. Qu, Cerium oxide nanoparticle: a remarkably versatile rare earth nanomaterial for biological applications, e90–e90, *NPG Asia Mater.* 6 (2014), <https://doi.org/10.1038/am.2013.88>.
- [18] D. Parimi, V. Sundararajan, O. Sadak, S. Gunasekaran, S.S. Mohideen, A. Sundaramurthy, Synthesis of positively and negatively charged CeO<sub>2</sub> nanoparticles: investigation of the role of surface charge on growth and development of drosophila melanogaster, *ACS Omega* 4 (2019) 104–113, <https://doi.org/10.1021/acsomega.8b02747>.
- [19] J.C. McGinnis Swanand Patil, Sudipta Seal, F. James, Rare Earth Nanoparticles Prevent Retinal Degeneration Induced by Intracellular Peroxides, in: *Nano-Enabled Medical Applications*, Jenny Stanford Publishing, 2020.
- [20] M.F.P. da Silva, H.C. de, J.F. da Costa, E.R. Triboni, M.J. Politi, P.C. Isolani, Synthesis and characterization of CeO<sub>2</sub>–graphene composite, *J. Therm. Anal. Calorim.* 107 (2011) 257–263, <https://doi.org/10.1007/s10973-011-1924-8>.
- [21] Y. Wang, C.X. Guo, J. Liu, T. Chen, H. Yang, C.M. Li, CeO<sub>2</sub> nanoparticles/graphene nanocomposite-based high performance supercapacitor, *Dalton Trans.* 40 (2011) 6388–6391, <https://doi.org/10.1039/C1DT10397K>.
- [22] G. Wang, J. Bai, Y. Wang, Z. Ren, J. Bai, Preparation and electrochemical performance of a cerium oxide–graphene nanocomposite as the anode material of a lithium ion battery, *Scr. Mater.* 65 (2011) 339–342, <https://doi.org/10.1016/j.scriptamat.2011.05.001>.
- [23] M. Lei, Z.B. Wang, J.S. Li, H.L. Tang, W.J. Liu, Y.G. Wang, CeO<sub>2</sub> nanocubes-graphene oxide as durable and highly active catalyst support for proton exchange membrane fuel cell, *Sci. Rep.* 4 (2014) 7415, <https://doi.org/10.1038/srep07415>.
- [24] S. Fatima, M. Iqbal, H.N. Bhatti, M. Iqbal, N. Alwadai, M. Al Huwayz, A. Nazir, Synthesis of oval-shaped Bi<sub>2</sub>Al<sub>4</sub>O<sub>9</sub> nanoparticles and their applications for the degradation of acid green 25 and as fuel additives, *ACS Omega* 8 (2023) 30868–30878, <https://doi.org/10.1021/acsomega.3c01245>.
- [25] B. Jain, A.K. Singh, H. Kim, E. Lichtfouse, V.K. Sharma, Treatment of organic pollutants by homogeneous and heterogeneous Fenton reaction processes, *Environ. Chem. Lett.* 16 (2018) 947–967, <https://doi.org/10.1007/s10311-018-0738-3>.
- [26] B. Jain, A.K. Singh, V.K. Sharma, Degradation of naphthylazo anionic dye by Fenton and Fenton-like processes: a comparative study with Fast sulphon black-F, *Desalin. Water Treat.* 62 (2017) 252–256.
- [27] B. Jain, A.K. Singh, A. Hashmi, Md.A.B.H. Susan, J.-P. Lellouche, Surfactant-assisted cerium oxide and its catalytic activity towards Fenton process for non-degradable dye, *Adv. Compos. Hybrid. Mater.* 3 (2020) 430–441, <https://doi.org/10.1007/s42114-020-00159-z>.
- [28] Treatment of pharmaceutical wastewater by heterogeneous Fenton process: an innovative approach - ProQuest, (n.d.). <https://www.proquest.com/openview/7e647e0a973da92a3e874058f53d2232/1?pq-origsite=gscholar&cbl=4402877> (Accessed January 29, 2024).
- [29] B. Jain, A. Hashmi, S. Sanwaria, A.K. Singh, Md.A.B.H. Susan, A. Singh, Zinc oxide nanoparticle incorporated on graphene oxide: an efficient and stable photocatalyst for water treatment through the Fenton process, *Adv. Compos. Hybrid. Mater.* 3 (2020) 231–242, <https://doi.org/10.1007/s42114-020-00153-5>.
- [30] M. Hartmann, S. Kullmann, H. Keller, Wastewater treatment with heterogeneous Fenton-type catalysts based on porous materials, *J. Mater. Chem.* 20 (2010) 9002–9017, <https://doi.org/10.1039/C0JM00577K>.
- [31] P. Zhong, Q. Yu, J. Zhao, S. Xu, X. Qiu, J. Chen, Degradation of bisphenol A by Fe-Al layered double hydroxides: A new synergy of homo- and heterogeneous Fenton systems, *J. Colloid Interface Sci.* 552 (2019) 122–133, <https://doi.org/10.1016/j.jcis.2019.05.040>.
- [32] B. Jain, A. Hashmi, S. Sanwaria, A.K. Singh, Md.A.B.H. Susan, S.A.C. Carabineiro, Catalytic Properties of Graphene Oxide Synthesized by a “Green” Process for Efficient Abatement of Auramine-O Cationic Dye, *Anal. Chem. Lett.* 10 (2020) 21–32, <https://doi.org/10.1080/22297928.2020.1747536>.
- [33] S. Yadav, A. Asthana, R. Chakraborty, B. Jain, A.K. Singh, S.A.C. Carabineiro, M.A. B.H. Susan, Cationic Dye Removal Using Novel Magnetic/Activated Charcoal/β-Cyclodextrin/Alginate Polymer Nanocomposite, *Nanomaterials* 10 (2020) 170, <https://doi.org/10.3390/nano10010170>.
- [34] A.K. Singh, S. Bano, B. Jain, Mechanistic investigation of osmium(VIII)catalyzed oxidation of brilliant green dye by chloramine-T in alkaline medium: a spectrophotometric kinetic study, *SN Appl. Sci.* 2 (2020) 245, <https://doi.org/10.1007/s42452-020-2030-y>.
- [35] B. Lellis, C.Z. Fávoro-Polonio, J.A. Pamphile, J.C. Polonio, Effects of textile dyes on health and the environment and bioremediation potential of living organisms, *Biotechnol. Res. Innov.* 3 (2019) 275–290, <https://doi.org/10.1016/j.biori.2019.09.001>.
- [36] S. Kobylewski, M.F. Jacobson, Toxicology of food dyes, *Int. J. Occup. Environ. Health* 18 (2012) 220–246, <https://doi.org/10.1179/1077352512Z.00000000034>.
- [37] J. Manzoor, M. Sharma, Impact of Textile Dyes on Human Health and Environment, in: *Impact of Textile Dyes on Public Health and the Environment*, IGI Global, 2020, pp. 162–169, <https://doi.org/10.4018/978-1-7998-0311-9.ch008>.
- [38] L. Zhou, C. Gao, W. Xu, Magnetic Dendritic Materials for Highly Efficient Adsorption of Dyes and Drugs, *ACS Appl. Mater. Interfaces* 2 (2010) 1483–1491, <https://doi.org/10.1021/am100114f>.
- [39] H.S. RAI, M.S. BHATTACHARYYA, J. SINGH, T.K. BANSAL, P. VATS, U. C. BANERJEE, Removal of Dyes from the Effluent of Textile and Dyestuff

- Manufacturing Industry: A Review of Emerging Techniques With Reference to Biological Treatment, *Crit. Rev. Environ. Sci. Technol.* 35 (2005) 219–238, <https://doi.org/10.1080/10643380590917932>.
- [40] K. Tanaka, K. Padermpole, T. Hisanaga, Photocatalytic degradation of commercial azo dyes, *Water Res.* 34 (2000) 327–333, [https://doi.org/10.1016/S0043-1354\(99\)00093-7](https://doi.org/10.1016/S0043-1354(99)00093-7).
- [41] A. Ahmad, S. Hamidah Mohd-Setapar, C. Sing Chuong, A. Khatoun, W.A. Wani, R. Kumar, M. Rafatullah, Recent advances in new generation dye removal technologies: novel search for approaches to reprocess wastewater, *RSC Adv.* 5 (2015) 30801–30818, <https://doi.org/10.1039/C4RA16959J>.
- [42] T.M. Pizzolatto, E. Carissimi, E.L. Machado, I.A.H. Schneider, Colour removal with NaClO of dye wastewater from an agate-processing plant in Rio Grande do Sul, Brazil, *Int. J. Miner. Process.* 65 (2002) 203–211, [https://doi.org/10.1016/S0301-7516\(01\)00082-5](https://doi.org/10.1016/S0301-7516(01)00082-5).
- [43] N.Y. Donkadokula, A.K. Kola, I. Naz, D. Saroj, A review on advanced physico-chemical and biological textile dye wastewater treatment techniques, *Rev. Environ. Sci. Biotechnol.* 19 (2020) 543–560, <https://doi.org/10.1007/s11157-020-09543-z>.
- [44] D. Bhatia, N.R. Sharma, J. Singh, R.S. Kanwar, Biological methods for textile dye removal from wastewater: A review, *Crit. Rev. Environ. Sci. Technol.* 47 (2017) 1836–1876, <https://doi.org/10.1080/10643389.2017.1393263>.
- [45] C. Yatome, S. Yamada, T. Ogawa, M. Matsui, Degradation of Crystal violet by *Nocardia corallina*, *Appl. Microbiol. Biotechnol.* 38 (1993) 565–569, <https://doi.org/10.1007/BF00242956>.
- [46] C. Sahoo, A.K. Gupta, A. Pal, Photocatalytic degradation of Crystal Violet (C.I. Basic Violet 3) on silver ion doped TiO<sub>2</sub>, *Dyes Pigments* 66 (2005) 189–196, <https://doi.org/10.1016/j.dyepig.2004.09.003>.
- [47] X. Ou, C. Wang, F. Zhang, H. Sun, Wuyunna, Degradation of methyl violet by Fenton's reagent: kinetic modeling and effects of parameters, *Desalin. Water Treat.* 51 (2013) 2536–2542, <https://doi.org/10.1080/19443994.2012.749000>.
- [48] F. Rehman, M. Sayed, J.A. Khan, L.A. Shah, N.S. Shah, H.M. Khan, R. Khattak, Degradation of Crystal Violet Dye by Fenton and Photo-Fenton Oxidation Processes, *Z. für Phys. Chem.* 232 (2018) 1771–1786, <https://doi.org/10.1515/zpch-2017-1099>.
- [49] C. Bouasla, M.E.-H. Samar, F. Ismail, Degradation of methyl violet 6B dye by the Fenton process, *Desalination* 254 (2010) 35–41, <https://doi.org/10.1016/j.desal.2009.12.017>.
- [50] S. Hashemian, M. Tabatabaee, M. Gafari, Fenton Oxidation of Methyl Violet in Aqueous Solution, *J. Chem.* 2013 (2012) e509097, <https://doi.org/10.1155/2013/509097>.
- [51] H.-J. Fan, S.-T. Huang, W.-H. Chung, J.-L. Jan, W.-Y. Lin, C.-C. Chen, Degradation pathways of crystal violet by Fenton and Fenton-like systems: Condition optimization and intermediate separation and identification, *J. Hazard. Mater.* 171 (2009) 1032–1044, <https://doi.org/10.1016/j.jhazmat.2009.06.117>.
- [52] B.A. Ünnü, G. Gündüz, M. Dikkancı, Heterogeneous Fenton-like oxidation of crystal violet using an iron loaded ZSM-5 zeolite, *Desalin. Water Treat.* 57 (2016) 11835–11849, <https://doi.org/10.1080/19443994.2015.1044915>.
- [53] H. Zhang, H. Gao, C. Cai, C. Zhang, L. Chen, Decolorization of Crystal Violet by ultrasound/heterogeneous Fenton process, *Water Sci. Technol.* 68 (2013) 2515–2520, <https://doi.org/10.2166/wst.2013.539>.
- [54] M.R.R. Kooh, M.K. Dahi, L.B.L. Lim, Removal of the methyl violet 2B dye from aqueous solution using sustainable adsorbent *Artocarpus odoratissimus* stem axis, *Appl. Water Sci.* 7 (2017) 3573–3581, <https://doi.org/10.1007/s13201-016-0496-y>.
- [55] K. Mohanty, J.T. Naidu, B.C. Meikap, M.N. Biswas, Removal of Crystal Violet from Wastewater by Activated Carbons Prepared from Rice Husk, *Ind. Eng. Chem. Res.* 45 (2006) 5165–5171, <https://doi.org/10.1021/ie060257r>.
- [56] M.R. Kulkarni, T. Revanth, A. Acharya, P. Bhat, Removal of Crystal Violet dye from aqueous solution using water hyacinth: Equilibrium, kinetics and thermodynamics study, *Resour. -Effic. Technol.* 3 (2017) 71–77, <https://doi.org/10.1016/j.reffit.2017.01.009>.
- [57] O. B. Akpor, J. E. Deborah, O. M. Oluba, Comparative Decolouration of Crystal Violet Dye using Chicken Feather Fibre, *Chemical Oxidation and Bacterial Cells, J. Environ. Sci. Technol.* 11 (2018) 246–253.
- [58] M. Sohail, M. Saleem, S. Ullah, N. Saeed, A. Afridi, M. Khan, M. Arif, Modified and improved Hummer's synthesis of graphene oxide for capacitors applications, *Mod. Electron. Mater.* 3 (2017) 110–116, <https://doi.org/10.1016/j.moem.2017.07.002>.
- [59] H. Li, G. Wang, F. Zhang, Y. Cai, Y. Wang, I. Djerdj, Surfactant-assisted synthesis of CeO<sub>2</sub> nanoparticles and their application in wastewater treatment, *RSC Adv.* 2 (2012) 12413–12423, <https://doi.org/10.1039/C2RA21590J>.
- [60] M.E. Khan, M.M. Khan, M.H. Cho, CdS-graphene Nanocomposite for Efficient Visible-light-driven Photocatalytic and Photoelectrochemical Applications, *J. Colloid Interface Sci.* 482 (2016) 221–232, <https://doi.org/10.1016/j.jcis.2016.07.070>.
- [61] A.K. Singh, P.K. Vishwakarma, S.K. Pandey, R. Pratap, R. Giri, A. Srivastava, A comparative study of band gap engineered in-situ and ex-situ MWCNTs/TiO<sub>2</sub> heterostructures for their enhanced photocatalytic activity under visible light, *Inorg. Chem. Commun.* 150 (2023) 110540, <https://doi.org/10.1016/j.inoche.2023.110540>.
- [62] D. Sharma, B.R. Mehta, Nanostructured TiO<sub>2</sub> thin films sensitized by CeO<sub>2</sub> as an inexpensive photoanode for enhanced photoactivity of water oxidation, *J. Alloy. Compd.* 749 (2018) 329–335, <https://doi.org/10.1016/j.jallcom.2018.03.228>.
- [63] D. Sharma, V.R. Satsangi, R. Shrivastav, U.V. Waghmare, S. Dass, Understanding the photoelectrochemical properties of nanostructured CeO<sub>2</sub>/Cu<sub>2</sub>O heterojunction photoanode for efficient photoelectrochemical water splitting, *Int. J. Hydrog. Energy* 41 (2016) 18339–18350, <https://doi.org/10.1016/j.ijhydene.2016.08.079>.
- [64] J. Tauc, Optical properties and electronic structure of amorphous Ge and Si, *Mater. Res. Bull.* 3 (1968) 37–46, [https://doi.org/10.1016/0025-5408\(68\)90023-8](https://doi.org/10.1016/0025-5408(68)90023-8).
- [65] M.J. McAllister, J.-L. Li, D.H. Adamson, H.C. Schniepp, A.A. Abdala, J. Liu, M. Herrera-Alonso, D.L. Milius, R. Car, R.K. Prud'homme, I.A. Aksay, Single Sheet Functionalized Graphene by Oxidation and Thermal Expansion of Graphite, *Chem. Mater.* 19 (2007) 4396–4404, <https://doi.org/10.1021/cm0630800>.
- [66] A.S. Dezfali, M.R. Ganjali, H.R. Naderi, P. Norouzi, A high performance supercapacitor based on a ceria/graphene nanocomposite synthesized by a facile sonochemical method, *RSC Adv.* 5 (2015) 46050–46058, <https://doi.org/10.1039/C5RA02957K>.
- [67] A. Hashmi, A.K. Singh, B. Jain, A. Singh, Muffle atmosphere promoted fabrication of graphene oxide nanoparticle by agricultural waste, Fuller., Nanotub. Carbon Nanostruct. 28 (2020) 627–636, <https://doi.org/10.1080/1536383X.2020.1728744>.
- [68] A. Hashmi, A.K. Singh, B. Jain, S.A.C. Carabineiro, Chloramine-T/N-Bromosuccinimide/FeCl<sub>3</sub>/KIO<sub>3</sub> Decorated Graphene Oxide Nanosheets and Their Antibacterial Activity, *Nanomaterials* 10 (2020) 105, <https://doi.org/10.3390/nano10010105>.
- [69] A.R. Stokes, A.J.C. Wilson, The diffraction of X rays by distorted crystal aggregates - I, *Proc. Phys. Soc.* 56 (1944) 174, <https://doi.org/10.1088/0959-5309/56/3/303>.
- [70] G.K. Williamson, W.H. Hall, X-ray line broadening from filed aluminium and wolfram, *Acta Metall.* 1 (1953) 22–31, [https://doi.org/10.1016/0001-6160\(53\)90006-6](https://doi.org/10.1016/0001-6160(53)90006-6).
- [71] A.E. Nemr, Potential of pomegranate husk carbon for Cr(VI) removal from wastewater: kinetic and isotherm studies, *J. Hazard Mater.* 161 (2009) 132–141, <https://doi.org/10.1016/j.jhazmat.2008.03.093>.
- [72] S. Gupta, B.V. Babu, Removal of toxic metal Cr(VI) from aqueous solutions using sawdust as adsorbent: Equilibrium, kinetics and regeneration studies, *Chem. Eng. J.* 150 (2009) 352–365, <https://doi.org/10.1016/j.cej.2009.01.013>.





## Synthesis and characterization of halloysite-cerium nanocomposite for removal of manganese

Purnima Mishra<sup>a,b</sup>, Lakhvinder Kaur<sup>c</sup>, Rajmani Patel<sup>a</sup>, Raghvendra Kumar Mishra<sup>d</sup>,  
Dakeshwar Kumar Verma<sup>b,\*</sup>, Walid Daoudi<sup>e,\*</sup>

<sup>a</sup> Hemchand Yadav University, Durg, Chhattisgarh 491001, India

<sup>b</sup> Department of Chemistry, Govt. Digvijay Autonomous Postgraduate College, Rajnandgaon, Chhattisgarh 491441, India

<sup>c</sup> Department of Nutrition and Dietetics, Manav Rachna International Institute of Research and Studies, Sector-43, Aravalli Hills, Delhi-Surajkund Road, Faridabad, Haryana 121004, India

<sup>d</sup> School of Aerospace, Transport and Manufacturing, Cranfield University, MK430AL, United Kingdom

<sup>e</sup> Laboratory of Molecular Chemistry, Materials and Environment (LCM2E), Department of Chemistry, Multidisciplinary Faculty of Nador, University Mohamed I, Nador 60700, Morocco

### ARTICLE INFO

#### Keywords:

Halloysite  
Adsorption  
Composite  
Pollution  
Manganese

### ABSTRACT

This study explores the use of a Halloysite composite to efficiently remove manganese from water through adsorption. We optimized experimental parameters, such as dosage (3 g/L), contact time, pH levels (ranging from 2 to 12), and initial Mn concentration (20 ppm), first in distilled water and then in polluted water. The main objective is to create an environmentally friendly material for practical manganese removal, especially important for at-risk populations like young individuals exposed to manganese. Using an oxidation-reduction approach, we synthesized a Halloysite-mediated nanocomposite for manganese removal through adsorption. The composite's crystallinity increased from 70.88 % to 77.4 % after manganese adsorption, indicating successful adsorption. At a transition temperature of 303 K, the composite showed an impressive 93 % manganese removal efficiency. We conducted comprehensive analyses using Scanning Electron Microscope (SEM), Energy Dispersive X-ray Spectroscopy (EDS), Transmission Electron Microscope (TEM), Fourier Transform Infrared Spectroscopy (FT-IR), X-ray diffraction (XRD), and UV-visible spectrophotometry to compare the composite's performance before and after adsorption. These results provide valuable insights into the structural changes and performance characteristics of the synthesized composite in manganese removal. Optimized experimental parameters and methodology lay the groundwork for further exploration of eco-friendly materials for water decontamination.

### 1. Introduction

Water, a fundamental necessity for living organisms, faces severe pollution due to the direct or indirect dumping of pollutants into the environment without adequate treatment. Widespread pollution is causing harmful impacts on ecosystems, becoming a critical environmental issue [1,2]. The swift advancement of technology is contributing to a rise in pollution. Nitrogen and nitrates come from different sources, such as agricultural runoff, industrial discharges, and urban drainage. These substances pose significant threats to the quality of water [3,4]. The surge in industries worldwide further exacerbates environmental degradation by compromising both air and water quality [5–7]. Manganese pollution in water poses a significant challenge, stemming from

natural deposits, industrial discharges, and agricultural practices. Elevated levels of manganese in water sources are contributed by mining operations, industrial discharges, and the use of manganese-containing fertilizers in agriculture [8,9]. Persistent contact with increased levels of manganese in drinking water carries health hazards, particularly for infants and young children. This exposure may lead to neurodevelopmental issues and symptoms akin to those found in Parkinson's disease in adults [10].

To address manganese pollution, effective water treatment procedures are essential. Several techniques, such as oxidation and filtration, ion exchange, biological treatment, and reverse osmosis, are used to eliminate manganese from water [10]. Despite being the fifth most common metal on Earth, excessive amounts of manganese can be

\* Corresponding authors.

E-mail addresses: [dakeshwarverma@gmail.com](mailto:dakeshwarverma@gmail.com) (D.K. Verma), [walid.daoudi@ump.ac.ma](mailto:walid.daoudi@ump.ac.ma) (W. Daoudi).

<https://doi.org/10.1016/j.jece.2024.114611>

Received 17 March 2024; Received in revised form 17 October 2024; Accepted 28 October 2024

Available online 29 October 2024

2213-3437/© 2024 Elsevier Ltd. All rights reserved, including those for text and data mining, AI training, and similar technologies.

neurotoxic. This leads to early toxic symptoms known as Locura Man-ganica [11,12]. The impact of manganese on water quality includes undesirable taste, metallic flavor, and discoloration of clothing and utensils [13,14]. Researchers have explored different methods to separate pollutants from water, including coagulation and precipitation, electrodialysis, membrane separation, photocatalysis and chemical catalysis, bioremediation, adsorption, disinfection, and mixed processes. These methods have been tested for their efficacy in removing various pollutants, including microbial contaminants [15]. Traditional techniques for demagnetization rely on transforming soluble  $Mn^{2+}$  into removable, insoluble precipitates. Theoretically, mechanical aeration of water can facilitate the oxidation of  $Mn^{2+}$  by atmospheric oxygen. However, this process is pH-dependent and requires accelerated alkali-zation [16].  $Mn^{2+}$  oxidation can be accomplished even at near-neutral pH by employing oxidizing agents such as potassium permanganate or ozone, but these methods are expensive. Additionally, they can oxidize other substances found in water, increasing the need for oxidants [17].

The sand filter getting clogged and producing large amounts of sludge are two drawbacks of this technology. For the reasons mentioned above, it would be advantageous to create a different manganese removal technique that is less dependent on pH levels, more affordable, and technically simpler [18]. Cation exchange and adsorption are two other techniques for removing  $Mn^{2+}$ . Several materials, including activated carbon [19], oxidized multi-walled carbon nanotubes [20], bio-matrix made from various plant wastes [21], zeolites [22], and modified multivalent metal ions [23], have been used for this purpose. These adsorbents remove  $Mn^{2+}$  from aqueous solutions with considerable efficiency, but the cost of these methods is largely due to the high dosages required. Adsorbents made from waste materials can reduce expenses. However, using them to treat drinking water can be problematic, especially if the adsorbent contains unwanted components that may leach into the treated water [24]. Halloysite-based adsorbents possess unique characteristics such as high cation-exchange capacity, vast surface area, and a high density of functional hydroxyl groups on the adsorbent surface [25]. These adsorbents have been studied for the removal of dyes [26], methylene blue [27], tetracycline [28], heavy metal ions [29], iodide [30], uranium [31], and iron [32]. The application of halloysite-based adsorbents for the highly effective removal of metals or radionuclides has received special attention [33]. However, as far as we know, there hasn't been any research done on the effectiveness and practicality of halloysite-based adsorbents for  $Mn^{2+}$  removal during drinking water treatment. The study explores the application of ecologically acceptable halloysite nanotubes and derivatives as adsorbents for pollutant removal. The study highlights the significance of addressing water pollution, particularly manganese contamination. It emphasizes the use of innovative materials, such as halloysite-based composites, for this purpose. The research contributes to improving our understanding of effective water treatment methods. Additionally, it brings attention to the potential of halloysite in various environmental applications.

## 2. Experimental methods

### 2.1. Materials

Materials from Sigma Aldrich—halloysite, sodium hydroxide, hexamethylene tetramine, and ceric ammonium nitrate—were used. Materials were chosen based on properties. Halloysite's tubular structure enhances adsorption, and Halloysite provides nanoscale channels for pollutant removal. Sodium hydroxide adjusts pH for optimal performance. Hexamethylene tetramine stabilizes material integrity. Ceric ammonium nitrate contributes to oxidation, and aids in oxidation reactions.

### 2.2. Synthesis of halloysite–cerium composite

To synthesize the halloysite-Ce composite, sodium hydroxide solutions were prepared at concentrations of 0.001 N, 0.01 N, 0.1 N, 0.5 N, and 1 N using double-distilled water. Halloysite solutions were then created by adding the appropriate amount of halloysite to 2 % weight/volume solutions of sodium hydroxide with continuous stirring. The resulting mixtures were heated to 90°C and sonicated to generate halloysite suspensions, left undisturbed overnight. The next day, a centrifugation process at 7000 rpm for 20 minutes separated the product from the supernatant. Multiple washes with deionized water followed, continuing until a neutral pH was reached. The Halloysite extract, produced with different sodium hydroxide concentrations, was then dispersed in 500 ml of distilled water under ultrasonication for 40 minutes. Subsequently, ceric ammonium nitrate was added, and stirring continued for half an hour. Hexamine was then introduced to each beaker while stirring for two hours. The resulting residual powdered solid was filtered, washed numerous times with water, freeze-dried overnight, and identified as HallCe 0.001, HallCe 0.01, HallCe 0.1, HallCe 0.5, and HallCe 1. Fig. 1 outlines the synthesis steps of the halloysite-Ce composite.

### 2.3. Adsorption experiment

To create the manganese stock solution, a 1000 ppm concentration certified reference material (CRM) was diluted with double-distilled water. The CRM, known for its accuracy and traceability, ensured experiment reliability. Optimal conditions were determined through systematic experiments. This work has been carried out triplicate manner to justify the work. Varying one condition at a time while keeping others constant. Adsorption isotherm experiments covered manganese concentrations from 1 to 20 mg/L. In the pH effect test, the manganese solution's pH was adjusted from 2.0 to 12.0 using 0.1 mol/L NaOH and HCl solutions. Kinetics tests at a pH of 7.0 involved recording Mn content at various stages.

The adsorbent's regeneration capacity was tested three times with a 1 mol/L NaOH desorption solution. For optimizing the composite's efficiency in manganese removal, different weight ratios were explored. This aimed to create a stable and effective Halloysite-Ce composite. In practical testing, 50 ml manganese solutions with varying concentrations were taken in wide-mouth conical flasks at room temperature. Different quantities of the prepared composite material were added, and the solutions were stirred well with a magnetic stirrer for approximately 5 minutes. Analyses were conducted triplicate at different time intervals to determine the optimal adsorption period. Buffer solutions were added to assess the pH effect. Manganese concentration was determined using a UV-Visible Spectrophotometer (Merk-Pharo 300) calibrated with a concentration curve.

### 2.4. Analysis of coexisting ions

The concentrations of  $Mn^{2+}$  and coexisting cations ( $Ca^{2+}$ , and  $Mg^{2+}$ ) were measured both before and after adsorption using inductively coupled plasma optical emission spectrometry (ICP OES, Optima 2000 DV, Perkin-Elmer, USA). To determine the concentrations of coexisting anions ( $Cl^-$ ,  $SO_4^{2-}$ ), two different methods were employed. Chloride ( $Cl^-$ ) concentration was measured using the argentometric Mohr method according to IS 3025 part 32, with potassium chromate as an indicator and a standard silver nitrate solution of 0.0141 Normal. Sulfate ( $SO_4^{2-}$ ) concentration was measured gravimetrically using barium chloride, following IS 3025 Part 24. Each sample measurement was performed in triplicate to ensure an error margin of no more than 3 %. Additionally, due to concerns about potential titanium toxicity, the residual concentration of titanium in the solution was also measured post-adsorption using ICP OES. Parameters for comparing adsorption were established by following equation [34].

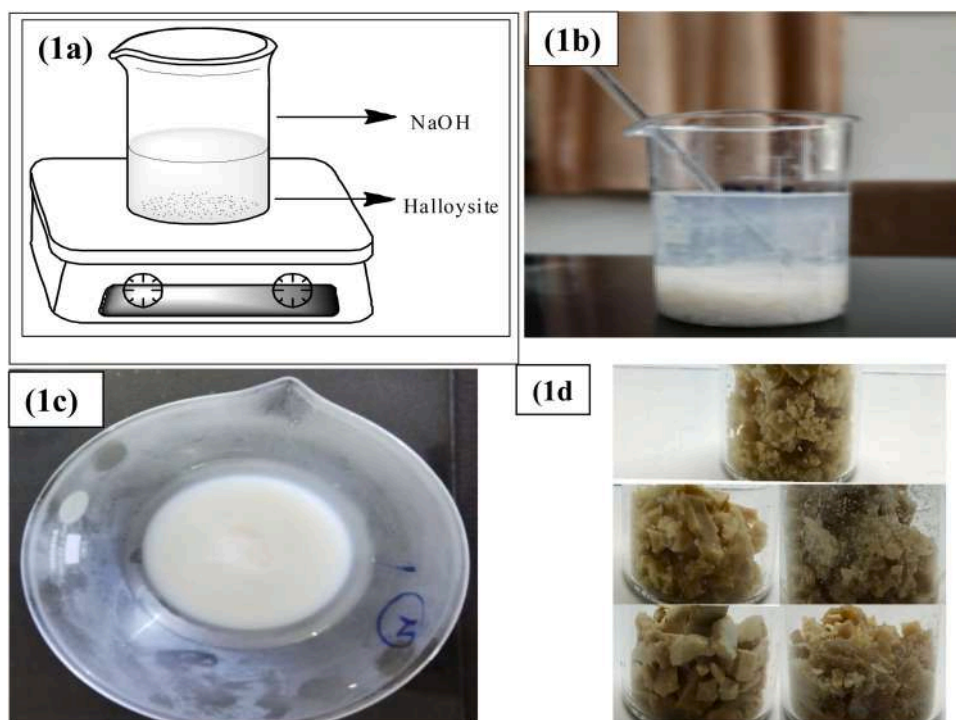


Fig. 1. (1a) Initial Mixing and Stirring of Halloysite in NaOH, (1b) Formation of Cloudy Sol and Heating, (1c) Freeze-Drying, (1d) Synthesised composites.

$$\text{Adsorption Capacity : } q_e = \frac{(C_0 - C)}{W} \times V \quad (1)$$

$$\text{Removal Efficiency : } EI(\%) = \frac{(C_0 - C)}{C_0} \times 100 \quad (2)$$

Where  $C_0$  and  $C$  are initial and final adsorption concentration in mg/L respectively and  $W$  is the mass of nano composite material in gm,  $V$  is the volume of the test sample taken in L,  $q_e$  is amount of adsorbate in mg/g (Mn) adsorbed at equilibrium. Higher the adsorption capacity better is the adsorbent.

Eq. 3 was employed to calculate crystallinity percentages [35]. In this process, the area of crystalline peaks was compared to the total area of all peaks. This comparison took into account both crystalline and amorphous components in X-ray diffraction (XRD) analysis [36].

$$\text{Crystallinity} = \frac{\text{Area of crystalline peak}}{\text{Area of all peaks(Crystalline + Amorphous)}} \times 100 \quad (3)$$

The Eq. (4) represents the adsorption capacity at equilibrium and is defined as:

$$q_e = \frac{(C_i - C_e)}{W} \times V \quad (4)$$

Where  $q_e$  is adsorption capacity at equilibrium,  $C_i$  is initial concentration of Manganese (before adsorption),  $C_e$  is equilibrium concentration of Manganese (after adsorption),  $W$  is adsorbent weight in grams and  $V$  is working volume in Liter.

Using the linear form of the Langmuir isotherm equation, this is given as Eq. (5):

$$\frac{1}{q_e} = \left[ \left( \frac{1}{k_L \times q_{\max}} \right) \times \frac{1}{q_e} \right] + \frac{1}{q_{\max}} \quad (5)$$

Non-linear form of the Langmuir isotherm equation is given as Eq. (6):

$$q_e = \frac{q_{\max} \times k_L \times C_e}{(1 + k_L \times C_e)} \quad (6)$$

Where  $k_L$  is (in L/mg) Langmuir constant related to the affinity of the binding sites [37].  $q_{\max}$  (mg/g) is the maximum adsorption capacity and  $R_L$  is separation Factor.

$$R_L = \frac{1}{1 + (C_i \times k_L)} \quad (7)$$

Table SI.3 presents the experimental data for the Langmuir isotherm. This table likely includes the essential parameters and values obtained during the experimental analysis using the Langmuir model. The Langmuir isotherm is widely used to describe the relationship between adsorbate and adsorbent in adsorption processes.

## 2.5. Characterization methods

Physical properties of the synthesized composite materials underwent characterization through Fourier Transform Infrared (FT-IR), X-ray Diffraction (XRD), Scanning Electron Microscopy with Energy Dispersive X-ray Spectroscopy (SEM-EDS), and High-Resolution Transmission Electron Microscopy (HRTEM) [38]. FT-IR spectra were acquired with a BRUKER FT-IR spectrophotometer (Model ALPHA II, Germany) in ATR mode at room temperature, utilizing KBr pellets [39]. This qualitative technique identified functional groups on the adsorbent surface, revealing hydroxyl (-OH) groups between 3600 and 3200  $\text{cm}^{-1}$  and stretching vibrations of Si-O and Al-O bonds in the halloysite structure between 1200 and 1000  $\text{cm}^{-1}$  [40–42]. XRD, a method for examining crystal structure, utilized a Bruker D8 Advance diffractometer with Ni-filtered Cu K-Alpha radiation. The XRD patterns provided details about the crystal lattice arrangement and identified crystalline phases present in halloysite [43]. HRTEM, operating at 200 kV, offered atomic-level structural information. Images were captured using a Jeol/JEM 2100 electron microscope, achieving a lattice resolution of 0.14 nm [44]. Scanning Electron Microscopy (SEM) was utilized to examine and analyze the surface characteristics, texture, and

topography of the composite material. SEM produced high-resolution images that revealed surface features such as roughness, porosity, and particle arrangement. This technique was applied to monitor changes in the surface morphology of the composite and evaluate the uniformity of surface grafting. Upon comparing the grafted surface to the un-grafted matrix, SEM analysis showed a more relaxed structure and a noticeable increase in surface roughness. The reaction between the composite

and manganese was determined using UV-visible spectrophotometry (Merck Pharo 300). Standard methods (IS 3025 and APHA 24th edition) were applied, utilizing the APHA 3500-Mn-B method at 525 nm wavelength with Certified Reference Material (CRM) approved by NIST [45]. The calibration graph ensured spectrophotometer accuracy. UV-visible spectroscopy assessed changes in pollutant concentration before and after adsorption by the Nano composite materials [46].

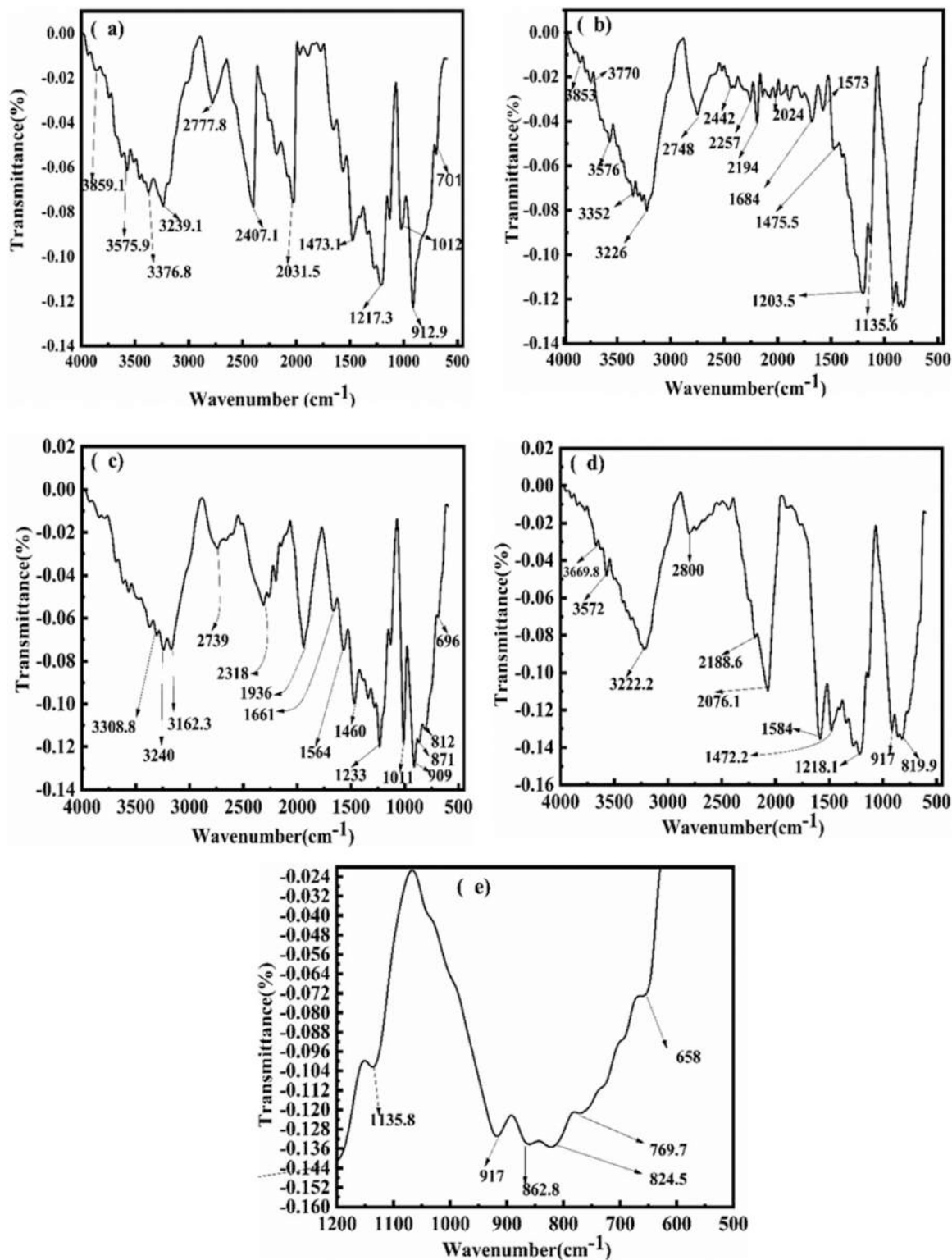


Fig. 2. FT-IR spectra of (a) halloysite (b) halloysite before cerium loading (c) Hallo-Ce composite (d) after adsorption of manganese solution of 10 ppm, (e) enlarged part of graph 2d.

Assessing manganese levels in water samples was vital, considering the possibility of soluble manganese undergoing oxidation and precipitation, especially on container walls. For precise analysis, it was essential to promptly measure the levels of manganese immediately after collecting the samples. This involved employing suitable analytical methods, such as a spectrophotometer or atomic absorption spectroscopy. In cases where delayed analysis was inevitable, a proactive strategy included acidifying the sample at the collection time. For rapid and accurate analysis, the water sample was quickly analyzed using a spectrophotometer or atomic absorption spectroscopy. However, in cases where delayed analysis was necessary and a determination of total manganese content was still desired, acidification of the sample at the time of collection was recommended. The presence of silver nitrate facilitated per-sulfate oxidation of soluble manganous compounds, producing permanganate. The resulting color, if too high per-sulfate and no organic materials were present, persisted for at least 24 hours. Boiling with  $\text{HNO}_3$  was employed to eliminate high concentrations of  $\text{Cl}^-$ , while  $\text{HgSO}_4$  in a special reagent addressed any residual  $\text{Cl}^-$  interference. The final colorimetric stage accounted for colored solutions resulting from additional inorganic ions. It was noted that samples exposed to air might yield unsatisfactory results due to manganese precipitation. To address this, 1 drop of 30 % hydrogen peroxide ( $\text{H}_2\text{O}_2$ ) was added to the sample after mixing a special reagent to re-dissolve precipitated manganese. Prior to the analysis, the spectrophotometer was calibrated with distilled water as a blank reagent. A calibration curve, using manganese solutions of varying concentrations, was plotted, and the concentration of manganese was determined before and after the addition of the prepared composite using ultraviolet spectroscopy (Figure SI.1). Different amounts of the composite were added to manganese-containing solutions of varying concentrations, and the study was conducted at 525 nanometers, considering the time course of the composite's effect [3].

### 3. Results and discussion

#### 3.1. Fourier transform infrared spectroscopy FT-IR

FT-IR analysis was employed to scrutinize the spectra of a halloysite-cerium composite before and after manganese adsorption. This examination disclosed the production and stabilization of nanoparticles. In past studies, it was noted that NaOH interacts efficiently with tetrahedral silicate. This interaction leads to the formation of silanol groups, identified as Si-OH. Extended exposure to a concentrated NaOH solution exceeding 1 mol/L has the potential to dissolve the external surface of HNTs. The peaks identified at 3690 and 3622  $\text{cm}^{-1}$  corresponded to the stretching vibration of hydroxyl groups bonded to aluminum (Al-OH). Additionally, the peak at 690  $\text{cm}^{-1}$  was attributed to the stretching vibration of Si-O bonds [40,47]. Our study revealed notable alterations, including peaks at 3337  $\text{cm}^{-1}$  to 3321  $\text{cm}^{-1}$  and 1636  $\text{cm}^{-1}$ . These peaks were associated with the stretching and bending vibrations of the -OH group of water molecules, respectively [24]. For pure halloysite, the strong absorption peaks (Fig. 2a) were seen at 3575.9  $\text{cm}^{-1}$ , 3376.8  $\text{cm}^{-1}$ , 3222.2  $\text{cm}^{-1}$ , 2777.8  $\text{cm}^{-1}$ , 2407  $\text{cm}^{-1}$ , 2031.5  $\text{cm}^{-1}$ , 2800  $\text{cm}^{-1}$ , 1473  $\text{cm}^{-1}$ , 1217.3  $\text{cm}^{-1}$ , and 912.9  $\text{cm}^{-1}$ . FTIR spectrum at 3700–3600  $\text{cm}^{-1}$  is associated with the hydroxyl groups (OH), Bands at 1630–1650  $\text{cm}^{-1}$  corresponding to the bending vibrations of water molecules (H-O-H), broad bands at 1000–1100  $\text{cm}^{-1}$  indicative of Si-O stretching in the tetrahedral layer, 900–950  $\text{cm}^{-1}$  [48]. Bands are due to the bending vibrations of Al-OH groups and Si-O-Al linkages. When halloysite treated with NaOH, band (Fig. 2b) at 1630–1650  $\text{cm}^{-1}$  altered due to the interaction with NaOH. Bands at 900–950  $\text{cm}^{-1}$  significantly altered, due to the dihydroxylation and breakdown of the alumina layers in the halloysite [49]. On loading Cerium strong peaks (Fig. 2c) appeared at 1936  $\text{cm}^{-1}$ , 1460  $\text{cm}^{-1}$ , 1233  $\text{cm}^{-1}$ , 1011  $\text{cm}^{-1}$  and at 909  $\text{cm}^{-1}$  and some new weak peaks are appeared at 871  $\text{cm}^{-1}$ , 812  $\text{cm}^{-1}$  and at 696  $\text{cm}^{-1}$ . After adsorption of 10 ppm Manganese

solution (Figs. 2d and 2e) the absorption bands at 1472  $\text{cm}^{-1}$ , 1281  $\text{cm}^{-1}$ , and 917  $\text{cm}^{-1}$  are related to Mn atoms through O-H bending vibrations. The absorption band at 2076  $\text{cm}^{-1}$ , on the other hand, results from radically differing levels of hydrogen bonding in the material.

#### 3.2. X-ray diffraction (XRD)

The investigation aimed to explore subtle structural changes in Halloysite on treatment with NaOH, before and after Cerium loading, as well as the changes in composite before and after manganese adsorption. Advanced techniques, including X-ray Diffraction (XRD), were employed for this purpose. The main goal was to understand the interactions at the nanoscale and detect crystallographic changes within the composite material. Through XRD examination, the crystal structure of the composite was unveiled. In Fig. 3a and Fig. 3b, a direct comparison was presented between XRD peaks and reference patterns of Halloysite both before and after sodium hydroxide treatment. This comparison revealed noticeable changes in both the positions and intensities of the peaks, indicating distinct alterations in the material's characteristics. These comparisons provided insights into the developing crystalline phases within the Halloysite. The XRD peaks of halloysite (Fig. 3a) showed d-values of 7.44, 4.46, and 3.35 Å, corresponding to the (001), (110), and (111) reflections, respectively. The d001-value of 7.74 Å<sup>0</sup> confirms the presence of Halloysite-7 Å. The Halloysite reflections remain evident in the XRD patterns even after treatment with NaOH (Fig. 3b), indicating that the crystalline structure of halloysite is preserved. However, the intensity of the (001) reflections decrease after the reaction with NaOH, suggesting that NaOH etching induces disorder along the c-axis. The XRD pattern of halloysite after treatment with sodium hydroxide and subsequent loading with cerium oxide (Fig. 3c) shows a strong peak at d spacing 4.37 Å<sup>0</sup> (2 theta - 18.2°), replacing the original peak of 7 Å. This shift might be due to the significant structural change of combined effects of NaOH treatment and cerium oxide loading, resulting in a more compact or differently organized layer structure in the halloysite.

When halloysite is treated with sodium hydroxide and put into manganese water without loading cerium, its XRD pattern is shown in Fig. 3d. XRD of studied materials observed three main peaks at 2 theta -11.7°, 20.1° and 24.9° exhibits d-values of 7.13, 4.45, and 3.37 Å<sup>0</sup>, which correspond to the (002), (110), and (111) reflections, no new peak was found in its XRD pattern. The XRD pattern of halloysite loaded with cerium oxide, without prior treatment with NaOH, Fig. 3f shows the characteristic peaks of both halloysite and cerium oxide, with halloysite's interlayer spacing largely unchanged.

An essential aspect of the study was evaluating crystallinity, as shown in Fig. 3c. The percentages were obtained through a thorough analysis of XRD data, which considered peak heights, FWHM values, d-spacing values, and Miller indices. This highlighted structural changes due to manganese adsorption. They clearly showed how the composite responded to external stimuli. The halloysite-mediated composite had a crystallinity of 70.88 %. After manganese adsorption, the crystallinity increased to 77.4 %, signifying the adsorption of manganese. The XRD data revealed various characteristics for each peak, including 2θ values, peak heights, FWHM values, d-spacing values, relative intensities, and Miller indices (h k l). After manganese adsorption (Fig. 3e), the strongest peak (100 % relative intensity) appeared at 2θ -20.5°, with a d-value of 4.37 and Miller indices of (110). Other strong peaks were identified at 2θ - 31.4°, 44.9° and 2θ - 48.7°, corresponding to the (02-2), (31-1) and (310) planes, respectively. This result thoroughly explores the structural dynamics of the Halloysite-Ce Composite during manganese adsorption. The combination of XRD analysis, crystallinity assessment provides our comprehension of nanoscale interactions and crystallographic details in the composite. Table SI.1 and Table SI.2 provides a complete perspective about d-spacing, Miller indices, and the structural changes caused by manganese adsorption.

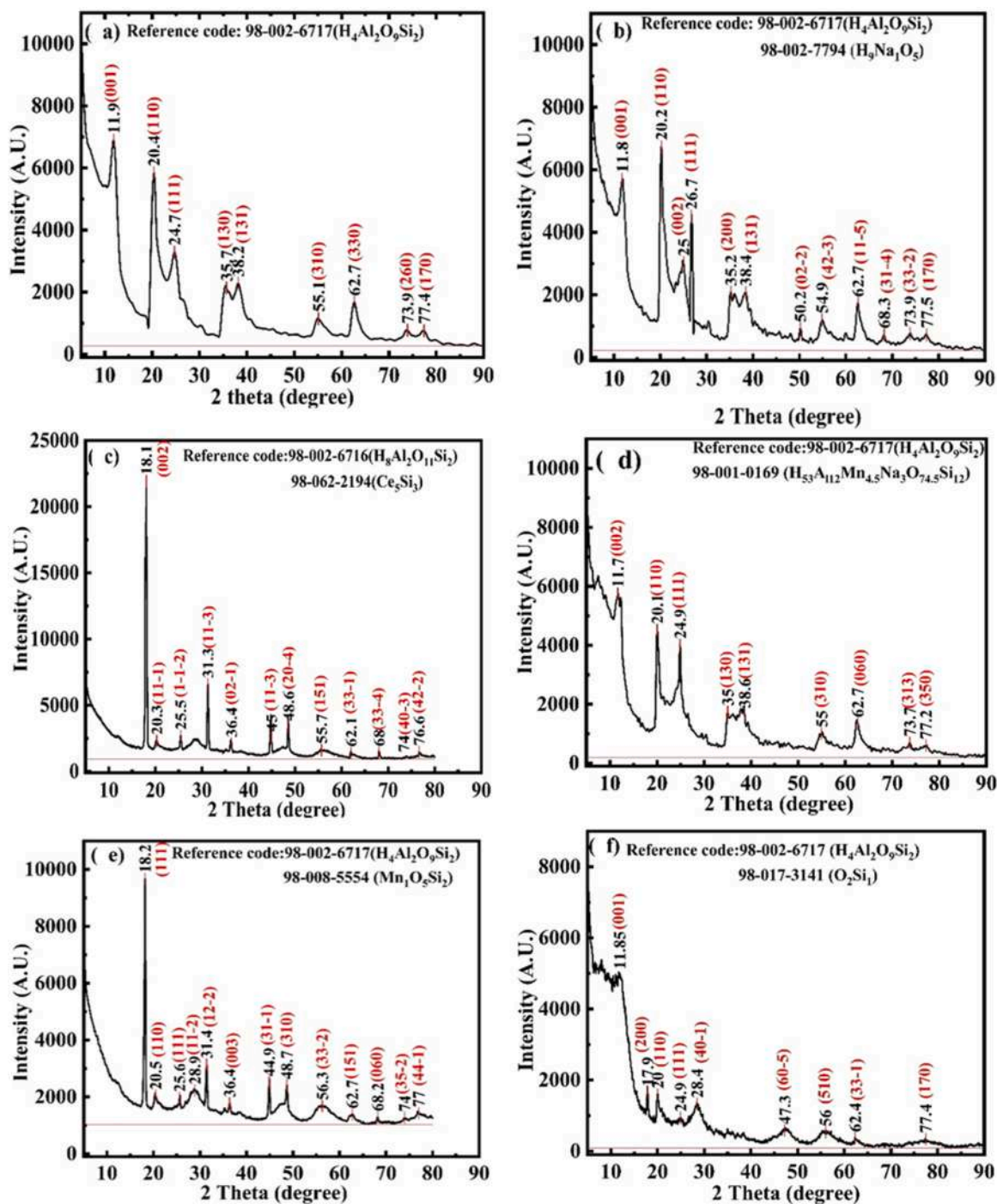
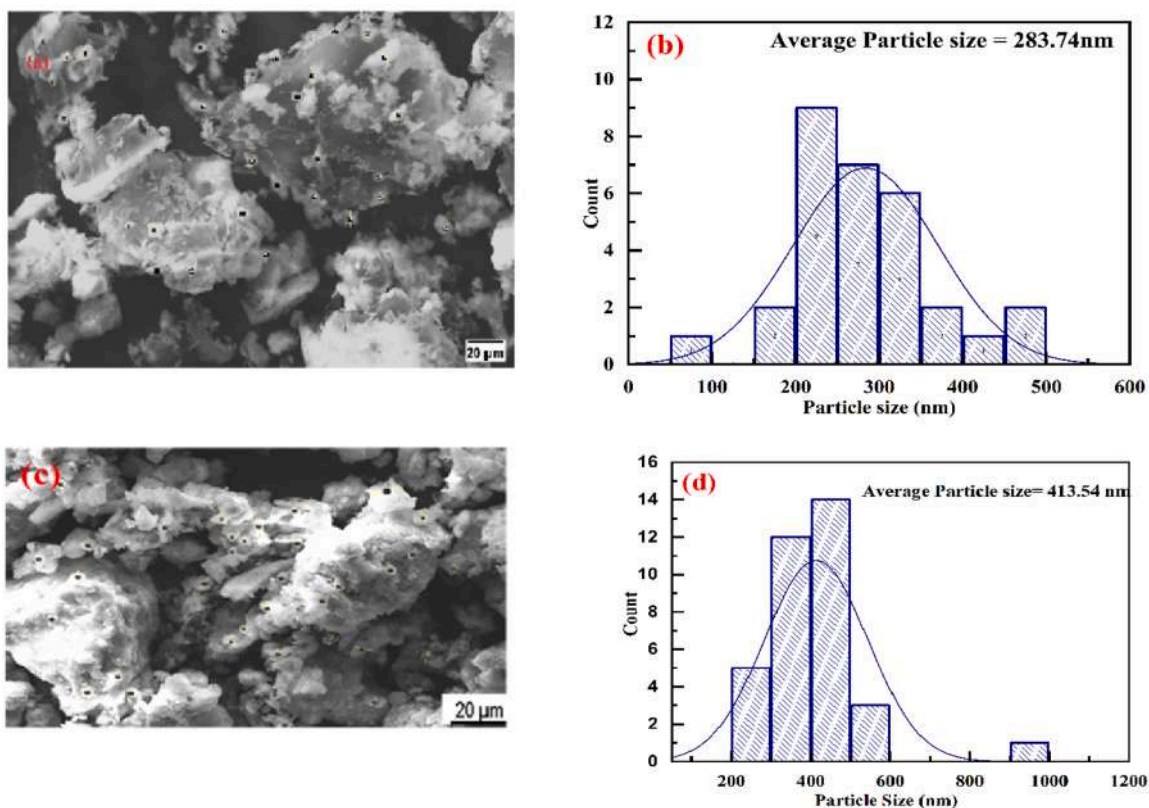


Fig. 3. Peaks with reference pattern peak position and miller indices (a) Halloysite (b) Halloysite treated with NaOH (c) cerium loaded on halloysite with NaOH treatment (d) without cerium loaded halloysite with Mn (e) manganese on the cerium loaded composite.

### 3.3. Scanning electron microscopy (SEM)

SEM images in Fig. 4a and Fig. 4b displayed the composite of halloysite and cerium, indicating an average particle size of 283.74 nm. These images clearly depicted particles covering the clay's surface, enabling the detection of applied cerium oxide. Subsequently, Fig. 4c and Fig. 4d displayed SEM images of the composite after application work, revealing an average particle size of 413.54 nm. Following the application of manganese, an additional adsorption process occurred, resulting in an increased average particle size from 283.74 nm to 413.54 nm. The data suggest that applying cerium oxide and subsequent

manganese adsorption lead to the formation of layers on the halloysite surface. These layers comprise cerium oxide and manganese compounds, contributing to an increased average particle size. The combination of cerium oxide and manganese particles induces particle aggregation on the halloysite surface, further increasing particle size. This phenomenon involves the production of coatings or adsorbed layers on the halloysite particles, contributing to an overall increase in particle size. The introduction of different materials induces structural changes in the halloysite composite, resulting in an observable increase in particle size. This study offers valuable insights into the surface characteristics and structural modifications of the composite material, as



**Fig. 4.** (a) SEM image of halloysite -cerium composite at 20 μm, (b) Graph of particle size obtained by SEM image of halloysite -cerium composite, (c) SEM image of halloysite -cerium composite at 20 μm with average particle size after adsorption of manganese on halloysite -cerium composite, (d) Graph of particle size obtained by SEM image after adsorption of manganese on halloysite -cerium composite.

revealed through SEM analysis. The SEM images in Fig. 4, coupled with the particle size data, help to understand the dynamic interactions and morphological changes resulting from applying cerium oxide and subsequent manganese adsorption.

In this study, Energy-Dispersive X-ray Spectroscopy (EDS) analysis was employed to verify the formation of the Halloysite-Cerium composite and the subsequent adsorption of Manganese (Table 1 and Fig. 5). The EDS measurements focused on specific points, and the resulting peaks are illustrated in Fig. 5a and b. Spectrum 5a displayed atomic percentages for N, Al, O, Si, and Ce in the composite material as 5.05, 69.5, 10.92, 11.34, and 3.19, respectively. Following Manganese adsorption, Spectrum 5b revealed values of 6.02, 68.35, 10.99, 11.27, 3.26, and 0.11 at% for N, Al, O, Si, Ce, and Mn, confirming the successful adsorption of Manganese onto the composite. The EDS analysis provides essential elemental composition data, contributing to our understanding of compositional changes in the Halloysite-Cerium composite during the adsorption process. When integrated with the earlier SEM and XRD analyses, this information contributes to a thorough exploration of the structural dynamics and morphological alterations induced by the application of cerium oxide and the subsequent adsorption of manganese on the halloysite surface.

**Table 1**

EDS Weight ratio of electro-spun of halloysite-Ce composite before and after adsorption of manganese.

Spectrum	Components											
	N		O		Al		Si		Ce		Mn	
	Weight %	Atomic %	Weight %	Atomic %	Weight %	Atomic %	Weight %	Atomic %	Weight %	Atomic %	Weight %	Atomic %
<b>Spectrum 5a</b>	3.15	5.05	49.57	69.5	13.13	10.92	14.2	11.34	19.95	3.19	Nil	Nil
<b>Spectrum 5b</b>	3.74	6.02	48.53	68.35	13.16	10.99	14.05	11.27	20.25	3.26	0.27	0.11

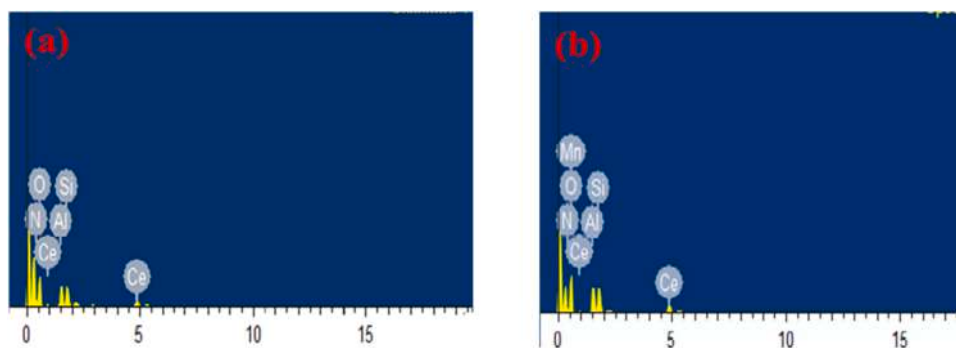


Fig. 5. (a) EDS spectrum of halloysite-Ce composite material, (b) EDS spectrum of halloysite-Ce composite material after adsorption of manganese.

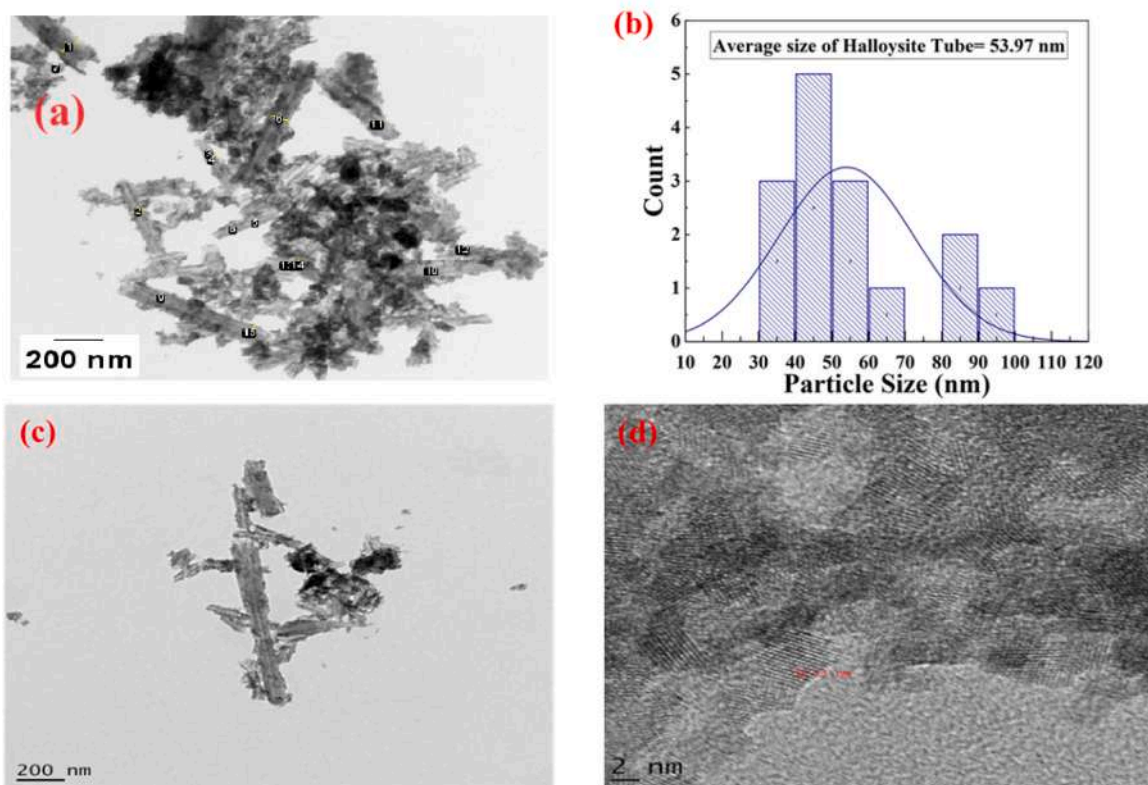


Fig. 6. (a) TEM image of Halloysite-Ce composite, (b) Graph showing average Particle Size (c) TEM image of Halloysite-Ce composite after adsorption of Manganese (d) TEM image obtained with high resolution showing interplanar distance.

### 3.5. Adsorption isotherm

In our investigation, adsorption isotherms played a crucial role in determining the equilibrium adsorption activity. These isotherms, including the Langmuir, Freundlich, and Temkin models, elucidate the relationship between the adsorbate amount on the surface and its concentration in the bulk phase at equilibrium. Through rigorous experimentation and analysis using Freundlich, Langmuir, and Temkin isotherms, we identified the Langmuir model as the most fitting, supported by the highest  $R^2$  value. This finding indicates that the Langmuir isotherm aptly describes the adsorption behaviour observed in our study. The Langmuir isotherm is particularly relevant when adsorption reaches a point where time no longer significantly influences the process. This isotherm assumes adsorption occurs on a surface with a finite number of identical, independent adsorption sites. Once these sites are occupied, further adsorption becomes negligible, indicating that the process has reached its maximum and attained equilibrium. This insight

into the adsorption behaviour enhances our understanding of the dynamics governing the interaction between the adsorbate and the adsorbent surface. The experimental data points aligned with the Langmuir model, providing a visual representation of the agreement between the model and observed adsorption behavior. This agreement is further substantiated by the calculated  $R^2$  value, emphasizing the suitability of the Langmuir isotherm for our specific study. The comprehensive analysis of adsorption isotherms contributes to the robustness of our findings and supports the validity of the Langmuir model in describing the equilibrium adsorption process in our experimental setup.

The fitting graphs of the three models and the results are listed in Table SI.4. This indicates that equilibrium adsorption data is better fitted by Langmuir linear model, suggesting that the adsorption of Manganese by Halloysite-Ce composite is the single-layer adsorption of uniform medium surface.



### 3.6. Thermodynamic parameter

The  $\Delta G^0$  value is a key indicator of thermodynamic feasibility in the adsorption process, with a negative value signifying spontaneity [50]. Our findings show that  $\Delta G^0$  remains negative only up to 303 K, indicating the energetic favorability of metal ion adsorption on the nano-composite material within this temperature range. With increasing temperature,  $\Delta G^0$  becomes positive, signaling a shift towards non-spontaneity at higher temperatures [51]. Determining  $\Delta H^0$  unveils the thermodynamic nature of adsorption, distinguishing between exothermic (negative  $\Delta H^0$ ) and endothermic (positive  $\Delta H^0$ ) reactions [52]. Our study unveiled a negative  $\Delta H^0$ , signaling an exothermic process where heat is released during adsorption. Higher temperatures are less favorable for this exothermic reaction. The entropy change ( $\Delta S^0$ ) in the adsorption process indicates the degree of disorder. A negative  $\Delta S^0$  suggests increased order as adsorption progresses, with system components organized more structurally [53]. This study found a negative  $\Delta S^0$ , indicating a trend toward increased orderliness during adsorption. This insight enhances our understanding of the thermodynamic behavior in metal ion adsorption on nano-composite materials (Table 2).

### 3.7. Kinetics of adsorption process

The rate of adsorption is affected by the concentration of adsorbate in the bulk phase, temperature, adsorbent surface area, and the nature of the adsorbent-adsorbate. To optimize Manganese adsorption on the halloysite-Ce composite material, various kinetic models were examined, including pseudo-first order, and pseudo-second order. On applying pseudo first order kinetics, the linear form of pseudo first order is expressed by Eq. (8) [54]:

$$\ln(q_e - q_t) = \ln q_e - k_1 t \quad (8)$$

To find value of  $k_1$  and  $q_e$  a graph plotted in between  $\ln(q_e - q_t)$  and  $t$  (time). Shown in Fig. 7 that  $R^2$  is the correlation coefficient, from the result it is clear that value of  $R^2$  is 0.48855 (not closer to 1) and Value of  $q_e$  (calculated) and  $q_e$  (experimental) are not closed to each other, so it is not suitable for our experiment [55]. Comparison of kinetic model is given in Tables SL.5, SL.6 and SL.7.

The correlation coefficient for the pseudo-second order kinetic model was 0.999, indicating that the data matched more pseudo-second order kinetics. Meanwhile, the  $q_e$  experimental and  $q_e$  calculated values indicated a significant difference for pseudo first order, indicating that it was a poor fit for Mn adsorption on the surface of nanocomposite material. For pseudo second-order kinetics, the  $q_e$  experimental values was very close to the  $q_e$  calculated values [56]. These results reveal that Mn adsorption using a Halloysite-Ce composite pseudo-second order. The rate-controlling phase in the pseudo-second order kinetic model is chemical sorption, which involves valence forces via electron sharing or exchange between sorbent and sorbate.  $0.02799 \text{ g mg}^{-1} \text{ min}^{-1}$  was found as the pseudo second-order rate constant [57].

### 3.8. Effect of various parameters

Manganese is found in water in three main oxidation states: Mn(II), Mn(III), and Mn(IV), with Mn(II) and Mn(IV) being the most readily found [58]. pH, redox potential, and the existence of complexing agents

**Table 2**  
Thermodynamic parameter for manganese adsorption on halloysite composite.

Temp. (K)	$K_L$	$\Delta G^0$ (KJ mol <sup>-1</sup> )	$\Delta H^0$ (KJ mol <sup>-1</sup> )	$\Delta S^0$ (J K <sup>-1</sup> )	$R^2$
298	4.476671	-3.714	-128.38	-416.22	0.9728
303	3.66347	-3.27			
308	0.96875	0.0813			
328	0.04893	8.228			

are some of the variables that affect the distribution of these manganese species. Mn(II) is more soluble and the chemical precipitation mechanisms are simpler, manganese removal under acidic conditions is frequently more effective [59]. The production of insoluble Mn(III) and Mn(IV) compounds at neutral to alkaline pH levels can make removal more difficult because these forms may need more strong oxidants and extensive treatment plans. So acidic environments are preferable for manganese removal over neutral and alkaline ones. Fig. 8 visually illustrates it. This study examines how pH levels and the dosage of adsorbent influence the efficiency of manganese removal from aqueous solutions. It specifically investigates the effects of varying the weight of the adsorbent on the removal process. In this study, we systematically investigated the impact of various parameters on manganese removal, conducting experiments at temperatures up to 303 K and a rotation speed of 200 rpm [60]. The removal efficiency showed a significant increase with pH, peaking at pH=3. However, a subsequent pH increase led to a decline in both adsorption capacity and the percentage of manganese removal. This can be attributed to reduced adsorption-free energy at low pH and increased negative charge on the adsorbent surface beyond pH=6, causing repulsion of adsorbent and adsorbate. Concerning adsorbent dosage, an initial rise in removal efficiency was observed with higher dosages due to increased availability of exchangeable sites. At 3 g/L adsorbent dosage, maximum removal efficiency reached 93 %. However, further increases in dosage led to a reduction in active sites due to manganese ion aggregation, resulting in decreased removal percentage [61]. To explore the influence of adsorbent weight on manganese removal, we selected an experimental condition of pH 3.0. Manganese removal increased with rising adsorbent dosage, peaking at 94 % efficiency at 3 g/L. However, removal efficiency declined beyond this concentration, indicating saturation. The heightened removal efficiency at increased dosages is attributed to a corresponding rise in available active sites for adsorption [62]. Conversely, at larger dosages, particle aggregation occurred, leading to a decrease in the percentage of manganese removal.

### 3.9. Regeneration experiment

Fig. 9 shows the removal effectiveness of manganese using Hallo-Ce composite following four cycles of adsorption and desorption. Regeneration refers to restoring an adsorbent material's capacity after saturation. As adsorption progresses, the material becomes saturated with the adsorbate, leading to a gradual decline in its ability to absorb more of the target substance until reaching maximum capacity. To maintain effectiveness, regeneration becomes necessary. An efficient adsorption material should not only demonstrate high adsorption efficiency but also show good reuse performance and recyclability [63]. In investigating the Hall-Ce composite's regeneration, a 1 mol/L NaOH desorption solution was used. After the initial regeneration, the composite retained 90 % of its saturated adsorption capacity. Following three additional cycles, the Manganese adsorption capacity slightly decreased but remained at 98 % of the initial value. These findings underscore the composite's ability to easily recover its active adsorption sites, ensuring effective reuse. This exploration emphasizes the significance of regeneration in preserving the efficacy of adsorbent materials. The Hall-Ce composite's consistent retention of a substantial portion of its adsorption capacity after multiple regeneration cycles highlights its potential for sustainable and effective use.

### 3.10. Effect of co-existing ions of removal of manganese

The presence of anions did not significantly affect the  $\text{Mn}^{2+}$  removal efficiency. In contrast, the coexisting cations were found to reduce the  $\text{Mn}^{2+}$  removal efficiency. The decrease in adsorbed  $\text{Mn}^{2+}$  was most notable with divalent cations, while the presence of monovalent cations caused only a slight reduction. For instance, without any additional ions, the  $\text{Mn}^{2+}$  removal efficiency was 99 % at an initial concentration of

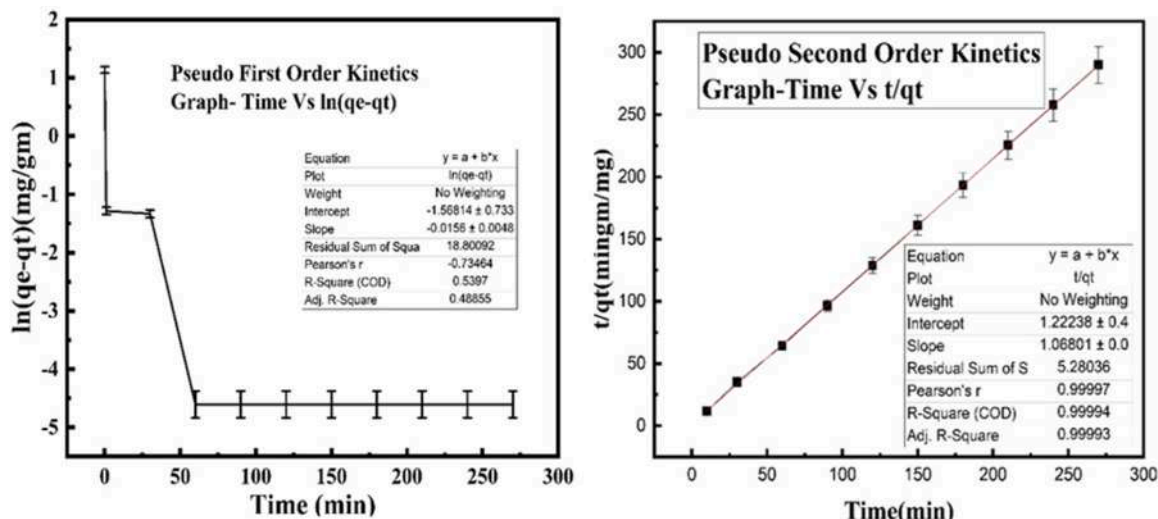


Fig. 7. Pseudo first order kinetics, and Pseudo second order kinetics.

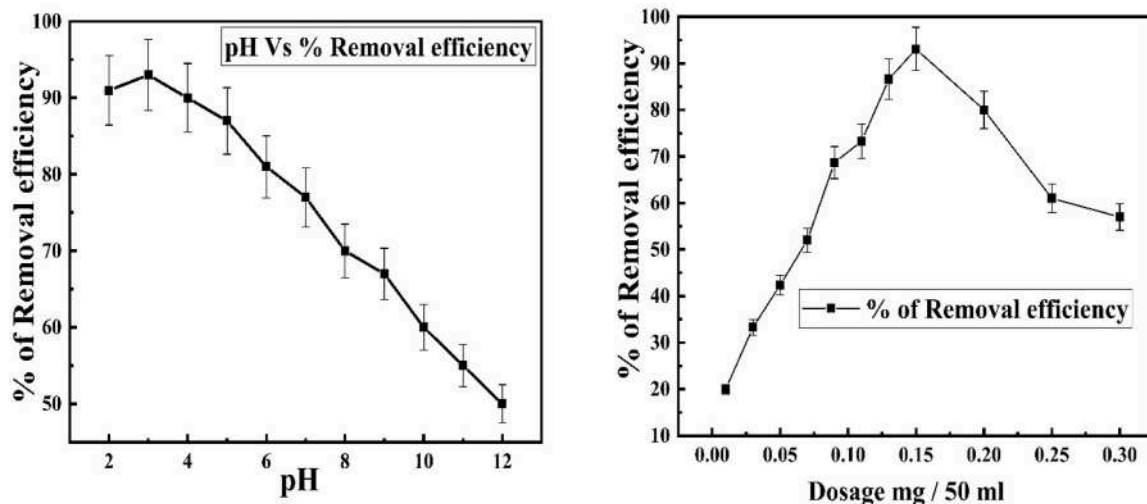


Fig. 8. (a) Effect of pH on Mn removal, and(b) Effect of adsorbent dosage on Mn removal.

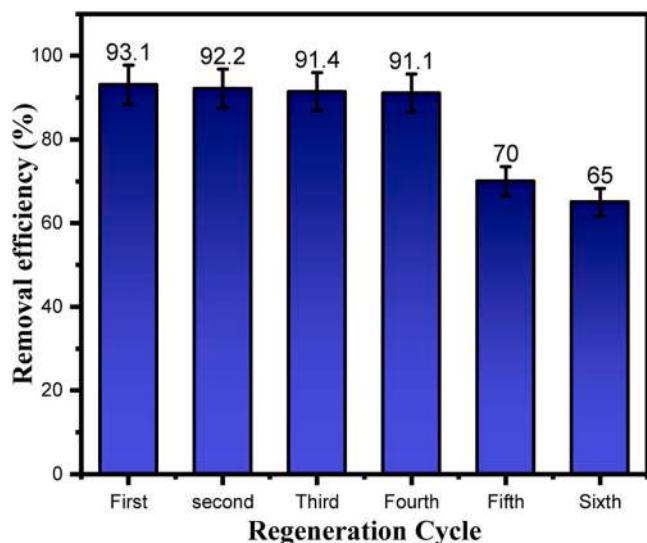


Fig. 9. The findings of Mn adsorption across six regeneration cycles.

0.5 mg L<sup>-1</sup>. When Na<sup>+</sup> or K<sup>+</sup> ions were present, the efficiency slightly decreased to 96 %. However, the addition of Ca<sup>2+</sup> and Mg<sup>2+</sup> ions caused the Mn<sup>2+</sup> removal efficiency to drop to 40 % and 74 %, respectively. The inhibitory effect of coexisting cations on Mn<sup>2+</sup> removal followed the order: Ca<sup>2+</sup> > Mg<sup>2+</sup> > K<sup>+</sup> > Na<sup>+</sup>.

### 3.11. Comparison of adsorption properties

This study's adsorbent Exhibits optimal adsorption efficiency of 93.1 % in the pH range of 3–4, making it suitable for acidic conditions. from Table 3 Halloysite /poly (amidoamine) is suitable for removal for Cr (VI) and Adsorbent Polyvinyl alcohol- chitosen, which also operates optimally within the same pH range but with slightly lower efficiency (84.6 %).Our composite material achieves a high removal efficiency of 93.1 %, indicating it can effectively remove a significant portion of the target contaminant from the solution and has an adsorption capacity of 3.0 mg/g, which indicates the amount of contaminant that can be adsorbed per gram of the adsorbent. the high removal efficiency suggests that our adsorbent is highly effective even at lower capacities, possibly due to its high selectivity and fast adsorption kinetics.

**Table 3**  
List of reported maximum adsorption capacities of adsorbents for pollutants.

Sr No	Material used	Material removed	pH	Adsorption capacity/Percentage removal	Interfering ions	Reusability	Ref.
1	Hallo nanotubes -Fe <sub>3</sub> O <sub>4</sub>	Cd (II)		11.4 mg/g	No	Three	[64]
2	Halloysite-chitosan	Tetracycline	3.3–7.7	88.28 %	...	-	[65]
3	Polyphosphazene-coated halloysite	Uranium (VI)		98.78 %	-	-	[16]
4	Halloysite/Ag <sub>2</sub> O	Iodide	5–9	39.99 mg/gm	Cl <sup>-</sup> , Br <sup>-</sup> , or SO <sub>4</sub> <sup>2-</sup>	-	[66]
5	Silanized halloysite	Fe(II), Fe(III)	3–7	96 %, 91 %	-	Five	[67]
6	Halloysite/Cerium catalytic material	cyclohexane carboxylic acid	4–7	99.5 %	...	-	[68]
7	Halloysite	Brilliant Green and Acid Red	6, and 2	12.5 mg g <sup>-1</sup> , and 13.9 mg g <sup>-1</sup>	KNO <sub>3</sub>	Four	[30]
8	Activated carbon	Mn (II)	4.5	20 mg/L (96.92 %)	No	-	[31]
13	M.stenopetala tree (bark and seed)	Mn (II)	1–7.5	79.53 % -bark 88.93 % - seeds	-	-	[69]
14	Halloysite-Ce composite	Mn (II)	3	93.1 % 3.10 mg/gm		Four	<b>This study</b>

### 3.12. Adsorption mechanism

Figure SI.3 illustrates the effectiveness of cerium-loaded halloysite in removing manganese. The halloysite without cerium loading shows a noticeable color appearance of manganese, indicating that it is not effective in removing manganese. However, after loading with cerium, no color appeared, signifying that the cerium-loaded halloysite composite material successfully removed the manganese. This visual evidence and analysis in the UV Spectrophotometer support the conclusion that cerium enhances the halloysite's ability to remove manganese from the solution. The Halo-Ce Composite was synthesized by treatment of halloysite with NaOH after that reacted with cerium oxide. NaOH can deprotonate the hydroxyl groups of the halloysite. This increases the negative charge density on the halloysite surface, enhancing its ability to adsorb positively charged ions and also introduce additional hydroxyl group. The cerium oxide component, in the form of CeO<sub>2</sub>, imparts catalytic and redox properties that are beneficial for the removal of metal ions. The initial step in the removal mechanism involves the exchange of manganese ions (Mn<sup>2+</sup>) in the solution with ions (such as H<sup>+</sup> or Na<sup>+</sup>) present on the surface of the Halo-Ce Composite. The negatively charged sites on the halloysite nanotubes and the cerium oxide bind positively charged manganese ions where manganese ions are directly bonded to the oxygen atoms of the cerium oxide (Ce–O–Mn).

## 4. Conclusion

In conclusion, this study successfully explored the effectiveness of a Halloysite composite for removing manganese from water through adsorption. The optimization of experimental parameters, including a dosage of 3 g/L, varied pH levels (ranging from 2 to 12), contact time, and an initial Mn concentration of 20 ppm, produced promising outcomes in both distilled and polluted water. The composite exhibited a significant increase in crystallinity from 70.88 % to 77.4 % after manganese adsorption, indicating successful adsorption. At a transition temperature of 303 K, the composite demonstrated an impressive 93 % manganese removal efficiency, establishing its effectiveness under specific conditions. The critical role of pH in manganese removal was highlighted, with optimal efficiency observed around pH 3.0. Beyond this threshold, the negative charge on the adsorbent surface triggered repulsive effects, resulting in a reduction in removal efficiency. Additionally, increasing the adsorbent dosage positively influenced manganese removal, indicating an enhanced availability of active adsorption sites. These insights have practical implications for refining manganese removal procedures using the composite material in environmental and water treatment applications.

### Ethics approval

This is not applicable.

### Consent to participate

Not applicable.

### Consent for publication

Not applicable.

### Funding

Not applicable

### CRediT authorship contribution statement

**Purnima Mishra:** Writing – original draft, Validation, Methodology, Investigation, Formal analysis. **Lakhvinder Kaur:** Methodology, Formal analysis. **Rajmani Patel:** Validation, Methodology, Investigation, Data curation, Conceptualization. **Raghvendra Kumar Mishra:** Software, Resources, Methodology, Investigation. **Dakeshwar Kumar Verma:** Visualization, Supervision, Methodology, Investigation, Data curation. **Walid Daoudi:** Writing – review & editing, Validation, Software, Formal analysis.

### Declaration of Competing Interest

The authors declare that they have no known competing financial interests or personal relationships that could have appeared to influence the work reported in this paper.

### Acknowledgements

Authors grateful to Principal, Govt. Digvijay College Ranjnandgaon for providing basic and lab facilities, also thankful to HOD and all the members of the Department of Chemistry for their valuable suggestions and support. Dr A.K. Singh, Associate Professor, Govt. VYT College, Durg for his encouragement and support. The authors would also like to thank Govt. VYT College, Durg for FTIR analysis and NIT Raipur for SEM/EDS and XRD analysis, Sophisticated Test and Instrumentation Centre Cochin University of Science & Technology Campus, Kochi, Kerala for TEM analysis.

### Appendix A. Supporting information

Supplementary data associated with this article can be found in the online version at [doi:10.1016/j.jece.2024.114611](https://doi.org/10.1016/j.jece.2024.114611).

### Data availability

No data was used for the research described in the article.

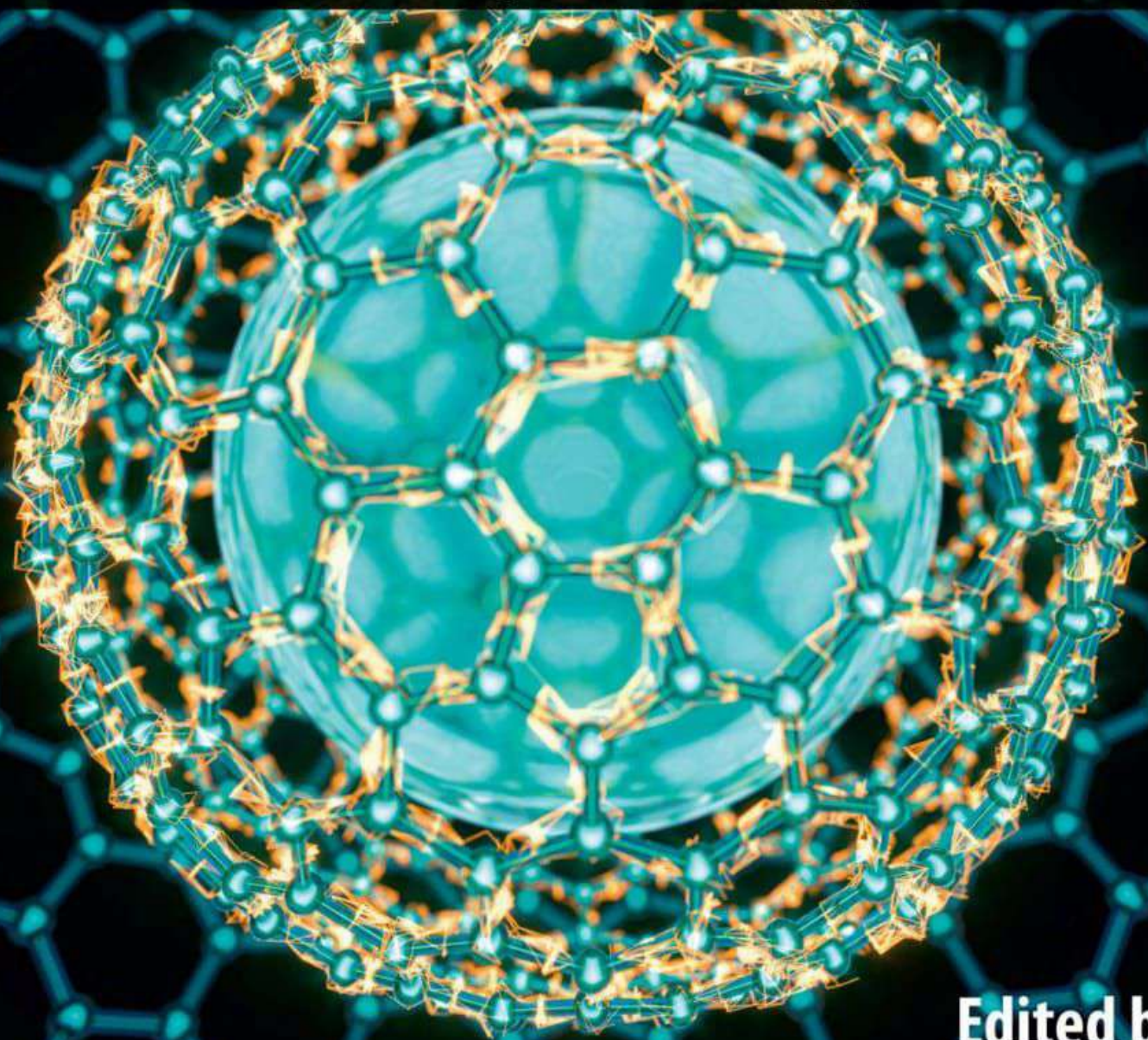
## References

- [1] F.O. Ajibade, B. Adedun, K.H. Lasisi, et al., Chapter 25 - Environmental pollution and their socioeconomic impacts, in: A. Kumar, V.K. Singh, P. Singh, V.K. Mishra (Eds.), *Microbe Mediated Remediation of Environmental Contaminants*, Woodhead Publishing, 2021, pp. 321–354.
- [2] R.L. Singh, P.K. Singh, Global environmental problems, in: R.L. Singh (Ed.), *Principles and Applications of Environmental Biotechnology for a Sustainable Future*, Springer, Singapore, 2017, pp. 13–41.
- [3] I. Skenderovic, B. Kalac, S. Becirovic, Environmental pollution and waste management, *Balk. J. Health Sci.* 3 (2015) 2–10.
- [4] A.K. Roy Choudhury, Environmental impacts of the textile industry and its assessment through life cycle assessment, in: S.S. Muthu (Ed.), *Roadmap to Sustainable Textiles and Clothing: Environmental and Social Aspects of Textiles and Clothing Supply Chain*, Springer, Singapore, 2014, pp. 1–39.
- [5] G.R. Bhagure, S.R. Mirgane, Heavy metal concentrations in groundwaters and soils of Thane Region of Maharashtra, India, *Environ. Monit. Assess.* 173 (2011) 643–652, <https://doi.org/10.1007/s10661-010-1412-9>.
- [6] M. Jayakumar, U. Surendran, P. Raja, et al., A review of heavy metals accumulation pathways, sources and management in soils, *Arab J. Geosci.* 14 (2021) 2156, <https://doi.org/10.1007/s12517-021-08543-9>.
- [7] N. Verma, M. Rachamalla, P.S. Kumar, K. Dua, Chapter 6 - Assessment and impact of metal toxicity on wildlife and human health, in: S.K. Shukla, S. Kumar, S. Madhav, P.K. Mishra (Eds.), *Metals in Water*, Elsevier, 2023, pp. 93–110.
- [8] Md.A. Rahman, Md.A. Hashem, Md.S. Rana, Md.R. Islam, Manganese in potable water of nine districts, Bangladesh: human health risk, *Environ. Sci. Pollut. Res.* 28 (2021) 45663–45675, <https://doi.org/10.1007/s11356-021-14016-z>.
- [9] Organization WH, *Manganese in Drinking Water: Background Document for Development of WHO Guidelines for Drinking-water Quality*. World Health Organization, 2021.
- [10] M.J. Leonhard, E.T. Chang, A.E. Loccisano, M.R. Garry, A systematic literature review of epidemiologic studies of developmental manganese exposure and neurodevelopmental outcomes, *Toxicology* 420 (2019) 46–65.
- [11] G. Björklund, M.S. Chartrand, J. Aaseth, Manganese exposure and neurotoxic effects in children, *Environ. Res.* 155 (2017) 380–384, <https://doi.org/10.1016/j.envres.2017.03.003>.
- [12] J.A. Bauer, B. Claus Henn, C. Austin, et al., Manganese in teeth and neurobehavior: sex-specific windows of susceptibility, *Environ. Int.* 108 (2017) 299–308, <https://doi.org/10.1016/j.envint.2017.08.013>.
- [13] P. Sarin, V.L. Snoeyink, J. Bebee, et al., Iron release from corroded iron pipes in drinking water distribution systems: effect of dissolved oxygen, *Water Res.* 38 (2004) 1259–1269, <https://doi.org/10.1016/j.watres.2003.11.022>.
- [14] H.A. Aziz, P.G. Smith, Removal of manganese from water using crushed dolomite filtration technique, *Water Res.* 30 (1996) 489–492, [https://doi.org/10.1016/0043-1354\(95\)00178-6](https://doi.org/10.1016/0043-1354(95)00178-6).
- [15] S. Sharma, A. Bhattacharya, Drinking water contamination and treatment techniques, *Appl. Water Sci.* 7 (2017) 1043–1067, <https://doi.org/10.1007/s13201-016-0455-7>.
- [16] K. Fialova, M. Motlochova, L. Cermakova, et al., Removal of manganese by adsorption onto newly synthesized TiO<sub>2</sub>-based adsorbent during drinking water treatment, *Environ. Technol.* 44 (2023) 1322–1333, <https://doi.org/10.1080/09593330.2021.2000042>.
- [17] S. Saito, Y. Matsui, Y. Yamamoto, et al., Oxidative removal of soluble divalent manganese ion by chlorine in the presence of superfine powdered activated carbon, *Water Res.* 187 (2020) 116412, <https://doi.org/10.1016/j.watres.2020.116412>.
- [18] S. Kurtz, F. Bilek, J. Schlenstedt, H.-J. Kochan, Treating mine water contaminated with iron, manganese and high solid carbon loads under tropical conditions, in: *Proceedings of the Securing the Future and Eighth ICARD (2009)*.
- [19] M. Niksirat, R. Sadeghi, J. Esmaili, Removal of Mn from aqueous solutions, by activated carbon obtained from tire residuals, *SN Appl. Sci.* 1 (2019) 782, <https://doi.org/10.1007/s42452-019-0797-5>.
- [20] T.C. Egbosiuwa, A.S. Abdulkareem, A.S. Kovo, et al., Enhanced adsorption of As(V) and Mn(VII) from industrial wastewater using multi-walled carbon nanotubes and carboxylated multi-walled carbon nanotubes, *Chemosphere* 254 (2020) 126780, <https://doi.org/10.1016/j.chemosphere.2020.126780>.
- [21] Q. Wang, M. Xiao, K. Fang, et al., Enhancing manganese removal through pre-deposition of powdered activated carbon-manganese oxide (PAC-MnOx) film on gravity-driven ceramic membrane: the impact of biofilm integrity and fluid dynamics, *Sep. Purif. Technol.* 342 (2024) 127051, <https://doi.org/10.1016/j.seppur.2024.127051>.
- [22] X. Hu, L. Zhang, Y. An, et al., Simultaneous removal of manganese and ammonium nitrogen from mine water using sodium hexametaphosphate modified natural zeolite loaded by 3D MnOx, *J. Environ. Chem. Eng.* 12 (2024) 112509, <https://doi.org/10.1016/j.jece.2024.112509>.
- [23] M.H. Kanani-Jazi, S. Akbari, M. Haghghat Kish, Efficient removal of Cr (VI) from aqueous solution by halloysite/poly(amidoamine) dendritic nano-hybrid materials: kinetic, isotherm and thermodynamic studies, *Adv. Powder Technol.* 31 (2020) 4018–4030, <https://doi.org/10.1016/j.apt.2020.08.004>.
- [24] P. Yu, Y. Song, X. Jin, et al., Study on the efficiency of manganese oxide-bearing manganese sand for removing Mn<sup>2+</sup> from aqueous solution, *Microporous Mesoporous Mater.* 364 (2024) 112859, <https://doi.org/10.1016/j.micromeso.2023.112859>.
- [25] S.B.A. Boraei, F. Eshghabadi, R. Hosseinpour, et al., Halloysite nanotubes in biomedical applications: recent approaches and future trends, *Appl. Clay Sci.* 253 (2024) 107346, <https://doi.org/10.1016/j.clay.2024.107346>.
- [26] N.Q. Nguyen, Y. Jeong, L. Abelmann, et al., Enhanced magnetic halloysite nanotubes for dye removal at different pH conditions, *Colloids Surf. A: Physicochem. Eng. Asp.* 680 (2024) 132631, <https://doi.org/10.1016/j.colsurfa.2023.132631>.
- [27] S. Zhang, X. Fan, J. Xue, A novel magnetic manganese oxide halloysite composite by one-pot synthesis for the removal of methylene blue from aqueous solution, *J. Alloy. Compd.* 930 (2023) 167050, <https://doi.org/10.1016/j.jallcom.2022.167050>.
- [28] S. Erdem, M. Öztekin, Y. Sağ Açikel, Investigation of tetracycline removal from aqueous solutions using halloysite/chitosan nanocomposites and halloysite nanotubes/alginate hydrogel beads, *Environ. Nanotechnol., Monit. Manag.* 16 (2021) 100576, <https://doi.org/10.1016/j.enmm.2021.100576>.
- [29] W. Niu, X. Qiu, P. Wu, et al., Unrolling the tubes of halloysite to form dickite and its application in heavy metal ions removal, *Appl. Clay Sci.* 231 (2023) 106748, <https://doi.org/10.1016/j.clay.2022.106748>.
- [30] W. Yu, Q. Wan, D. Tan, et al., Removal of iodide from water using halloysite/Ag<sub>2</sub>O composites as efficient adsorbent, *Appl. Clay Sci.* 213 (2021) 106241, <https://doi.org/10.1016/j.clay.2021.106241>.
- [31] H. Yang, L. Zhao, R. Ju, et al., Construction of polyphosphazene-coated halloysite nanotube composite with in-situ released PO<sub>4</sub><sup>3-</sup> for efficient and rapid removal of uranium from wastewater, *Sep. Purif. Technol.* 314 (2023) 123668, <https://doi.org/10.1016/j.seppur.2023.123668>.
- [32] G. Pandey, M. Tharmavaram, G. Phadke, et al., Silanized halloysite nanotubes as 'nano-platform' for the complexation and removal of Fe (II) and Fe (III) ions from aqueous environment, *Sep. Purif. Technol.* 293 (2022) 121141, <https://doi.org/10.1016/j.seppur.2022.121141>.
- [33] G. Lazzara, G. Cavallaro, A. Panchal, et al., An assembly of organic-inorganic composites using halloysite clay nanotubes, *Curr. Opin. Colloid Interface Sci.* 35 (2018) 42–50, <https://doi.org/10.1016/j.cocis.2018.01.002>.
- [34] A. Mohamed, R.R. Atta, A.A. Kotp, et al., Green synthesis and characterization of iron oxide nanoparticles for the removal of heavy metals (Cd<sup>2+</sup> and Ni<sup>2+</sup>) from aqueous solutions with Antimicrobial Investigation, *Sci. Rep.* 13 (2023) 7227, <https://doi.org/10.1038/s41598-023-31704-7>.
- [35] S. Ruan, C.A. Schuh, Electrodeposited Al-Mn alloys with microcrystalline, nanocrystalline, amorphous and nano-quasicrystalline structures, *Acta Mater.* 57 (2009) 3810–3822, <https://doi.org/10.1016/j.actamat.2009.04.030>.
- [36] D.G. Chukhchin, A.V. Malkov, I.V. Tyshkunova, et al., Diffractometric method for determining the degree of crystallinity of materials, *Crystallogr. Rep.* 61 (2016) 371–375, <https://doi.org/10.1134/S1063774516030081>.
- [37] N. Kumari, C. Mohan, Basics of clay minerals and their characteristic properties, *Clay Clay Min.* 24 (2021) 1–29.
- [38] M.S. Geetha, H. Nagabhushana, H.N. Shivananjaiah, Green mediated synthesis and characterization of ZnO nanoparticles using Euphorbia Jatropha latex as reducing agent, *J. Sci. Adv. Mater. Devices* 1 (2016) 301–310.
- [39] P. Wang, Y. Tang, Y. Liu, et al., Halloysite nanotube@carbon with rich carboxyl groups as a multifunctional adsorbent for the efficient removal of cationic Pb(II), anionic Cr(VI) and methylene blue (MB), *Environ. Sci. Nano* 5 (2018) 2257–2268, <https://doi.org/10.1039/C8EN00561C>.
- [40] G. Zeng, Y. He, Y. Zhan, et al., Novel polyvinylidene fluoride nanofiltration membrane blended with functionalized halloysite nanotubes for dye and heavy metal ions removal, *J. Hazard. Mater.* 317 (2016) 60–72, <https://doi.org/10.1016/j.jhazmat.2016.05.049>.
- [41] S. Zeng, C. Reyes, J. Liu, et al., Facile hydroxylation of halloysite nanotubes for epoxy nanocomposite applications, *Polymer* 55 (2014) 6519–6528, <https://doi.org/10.1016/j.polymer.2014.10.044>.
- [42] B. Zsírka, E. Horváth, P. Szabó, et al., Thin-walled nanoscrolls by multi-step intercalation from tubular halloysite-10Å and its rearrangement upon peroxide treatment, *Appl. Surf. Sci.* 399 (2017) 245–254, <https://doi.org/10.1016/j.apsusc.2016.12.053>.
- [43] M.N. Prabhakar, G.M. Raghavendra, B.V.D. Vijaykumar, et al., Synthesis of a novel compound based on chitosan and ammonium polyphosphate for flame retardancy applications, *Cellulose* 26 (2019) 8801–8812, <https://doi.org/10.1007/s10570-019-02671-y>.
- [44] Zheng K., Gao Y., Bai X., et al (2018) In situ TEM: theory and applications. In: Wang R, Wang C, Zhang H, et al (eds) *Progress in Nanoscale Characterization and Manipulation*. Springer, Singapore, 381–477.
- [45] Island P.E., Scotia N., Territories N. (2016) *Manganese in Drinking Water*. Federal-Provincial-Territorial Committee on Drinking Water (Ed.) Government of Canada.
- [46] A.M. El-Khawaga, H. Tantawy, M.A. Elsayed, A.I.A. Abd El-Mageed, Synthesis and applicability of reduced graphene oxide/porphyrin nanocomposite as photocatalyst for waste water treatment and medical applications, *Sci. Rep.* 12 (2022) 17075, <https://doi.org/10.1038/s41598-022-21360-8>.
- [47] X. Song, L. Zhou, Y. Zhang, et al., A novel cactus-like Fe<sub>3</sub>O<sub>4</sub>/Halloysite nanocomposite for arsenite and arsenate removal from water, *J. Clean. Prod.* 224 (2019) 573–582, <https://doi.org/10.1016/j.jclepro.2019.03.230>.
- [48] S. Vahur, L. Kiudorv, P. Somelar, et al., Quantitative mineralogical analysis of clay-containing materials using ATR-FT-IR spectroscopy with PLS method, *Anal. Bioanal. Chem.* 413 (2021) 6535–6550, <https://doi.org/10.1007/s00216-021-03617-9>.
- [49] M.F. Mubarak, A.H. Ragab, R. Hosny, et al., Enhanced performance of chitosan via a novel quaternary magnetic nanocomposite chitosan/grafted halloysitenanotubes@Zn<sub>7</sub>Fe<sub>3</sub>O<sub>4</sub> for uptake of Cr (III), Fe (III), and Mn (II) from wastewater, *Polymers* 13 (2021) 2714, <https://doi.org/10.3390/polym13162714>.
- [50] H.I. Adekola, F.A. Adekola, M.N. Abdulraheem, Kinetic and thermodynamic studies on adsorption of sulphate from aqueous solution by magnetite, activated

- carbon and magnetite-activated carbon composites, *Niger. J. Chem. Res.* 22 (2017) 39–69.
- [51] M.S. Silva, L.S. Silva, F.J.L. Ferreira, et al., Study of interactions between organic contaminants and a new phosphated biopolymer derived from cellulose, *Int. J. Biol. Macromol.* 146 (2020) 668–677, <https://doi.org/10.1016/j.ijbiomac.2019.12.121>.
- [52] X. Zhang, X. Han, Y. Liu, et al., Remediation of water tainted with noxious aspirin and fluoride ion using UiO-66-NH<sub>2</sub> loaded peanut shell, *Environ. Sci. Pollut. Res.* 30 (2023) 93877–93891, <https://doi.org/10.1007/s11356-023-28906-x>.
- [53] F. Al-Badaii, R. Hassan, N. Jalil, A. Halim, Adsorptive removal of boron from aqueous solutions using peels of jering seeds (*Archidendron pauciflorum*): isotherm, kinetic and thermodynamic studies, *Desalin. Water Treat.* 312 (2023) 139–157.
- [54] N. Sazali, Z. Harun, N. Sazali, A review on batch and column adsorption of various adsorbent towards the removal of heavy metal, *J. Adv. Res. Fluid Mech. Therm. Sci.* 67 (2020) 66–88.
- [55] S.M. Al-Mahmoud, Kinetic, isothermal and thermodynamic investigations for the use of pumpkin seed husks as low-cost biosorbent of solochrome cyanine R from aqueous solutions, *Egypt. J. Chem.* (2020), <https://doi.org/10.21608/ejchem.2020.24327.2445>.
- [56] Y.M. Vargas-Rodríguez, A. Obaya, J.E. García-Petronilo, et al., Adsorption studies of aqueous solutions of methyl green for halloysite nanotubes: kinetics, isotherms, and thermodynamic parameters, *Am. J. Nanomater.* 9 (2021) 1–11.
- [57] S.S. Kolluru, S. Agarwal, S. Sireesha, et al., Heavy metal removal from wastewater using nanomaterials-process and engineering aspects, *Process Saf. Environ. Prot.* 150 (2021) 323–355, <https://doi.org/10.1016/j.psep.2021.04.025>.
- [58] X. Wang, Q. Wang, P. Yang, et al., Oxidation of Mn(III) species by Pb(IV) oxide as a surrogate oxidant in aquatic systems, *Environ. Sci. Technol.* 54 (2020) 14124–14133, <https://doi.org/10.1021/acs.est.0c05459>.
- [59] Y. Li, H. Huang, Z. Xu, et al., Mechanism study on manganese(II) removal from acid mine wastewater using red mud and its application to a lab-scale column, *J. Clean. Prod.* 253 (2020) 119955, <https://doi.org/10.1016/j.jclepro.2020.119955>.
- [60] Chiew C.S.C. (2016) Halloysite/alginate nanocomposite beads for Pb<sup>2+</sup> removal from aqueous solution. PhD Thesis, Monash University.
- [61] N.N. Rudi, M.S. Muhamad, L.T. Chuan, et al., Evolution of adsorption process for manganese removal in water via agricultural waste adsorbents, *Heliyon* 6 (2020), <https://doi.org/10.1016/j.heliyon.2020.e05049>.
- [62] P. Muhizi, The efficiency of clay-based adsorbent in fluoride removal from groundwater: adsorption process, *J. Min. Environ.* 14 (2023) 839–851, <https://doi.org/10.22044/jme.2023.12933.2348>.
- [63] M. Arshadi, Manganese chloride nanoparticles: a practical adsorbent for the sequestration of Hg(II) ions from aqueous solution, *Chem. Eng. J.* 259 (2015) 170–182, <https://doi.org/10.1016/j.cej.2014.07.111>.
- [64] M. Amjadi, A. Samadi, J.L. Manzoori, A composite prepared from halloysite nanotubes and magnetite (Fe<sub>3</sub>O<sub>4</sub>) as a new magnetic sorbent for the preconcentration of cadmium(II) prior to its determination by flame atomic absorption spectrometry, *Microchim. Acta* 182 (2015) 1627–1633, <https://doi.org/10.1007/s00604-015-1491-y>.
- [65] N. Esfandiari, B. Nasernejad, T. Ebadi, Removal of Mn(II) from groundwater by sugarcane bagasse and activated carbon (a comparative study): application of response surface methodology (RSM), *J. Ind. Eng. Chem.* 20 (2014) 3726–3736, <https://doi.org/10.1016/j.jiec.2013.12.072>.
- [66] I. Kara, D. Tunc, F. Sayin, S.T. Akar, Study on the performance of metakaolin based geopolymer for Mn(II) and Co(II) removal, *Appl. Clay Sci.* 161 (2018) 184–193, <https://doi.org/10.1016/j.clay.2018.04.027>.
- [67] H.A. Ibrahim, W.I. El-DougDoug, H.H. Hefni, et al., Removal of Ni (II), Mn (II) and Zn (II) from crude yellow cake aqueous solution by cross-linked chitosan and polyvinyl alcohol, *Egypt. J. Pet.* 30 (2021) 61–69.
- [68] A.Z. Melaku, Removal of manganese from wastewater using *Moringa stenopetala* plant parts as an adsorbent material, *Heliyon* 9 (2023), <https://doi.org/10.1016/j.heliyon.2023.e22517>.
- [69] M.A. Abdel-Fadeel, N.S. Aljohani, S.R. Al-Mhyawi, et al., A simple method for removal of toxic dyes such as Brilliant Green and Acid Red from the aquatic environment using Halloysite nanoclay, *J. Saudi Chem. Soc.* 26 (2022) 101475.

# HANDBOOK OF BIOMOLECULES

Fundamentals, Properties, and Applications



Edited by  
**Chandrabhan Verma**  
**Dakeshwar Kumar Verma**

EMERGING MATERIALS AND TECHNOLOGIES

# Biosorbents

Diversity, Bioprocessing,  
and Applications

Edited by

**PRAMOD KUMAR MAHISH,  
DAKESHWAR KUMAR VERMA,  
and SHAILESH KUMAR JADHAV**



**CRC Press**  
Taylor & Francis Group

# Metal Organic Frameworks

Fundamentals to Advanced

Edited by  
Bhawana Jain  
Dakeshwar Kumar Verma  
Ajaya Kumar Singh  
Jai Singh





WILEY-VCH

Edited by Dakeshwar Kumar Verma and  
Jeenat Aslam

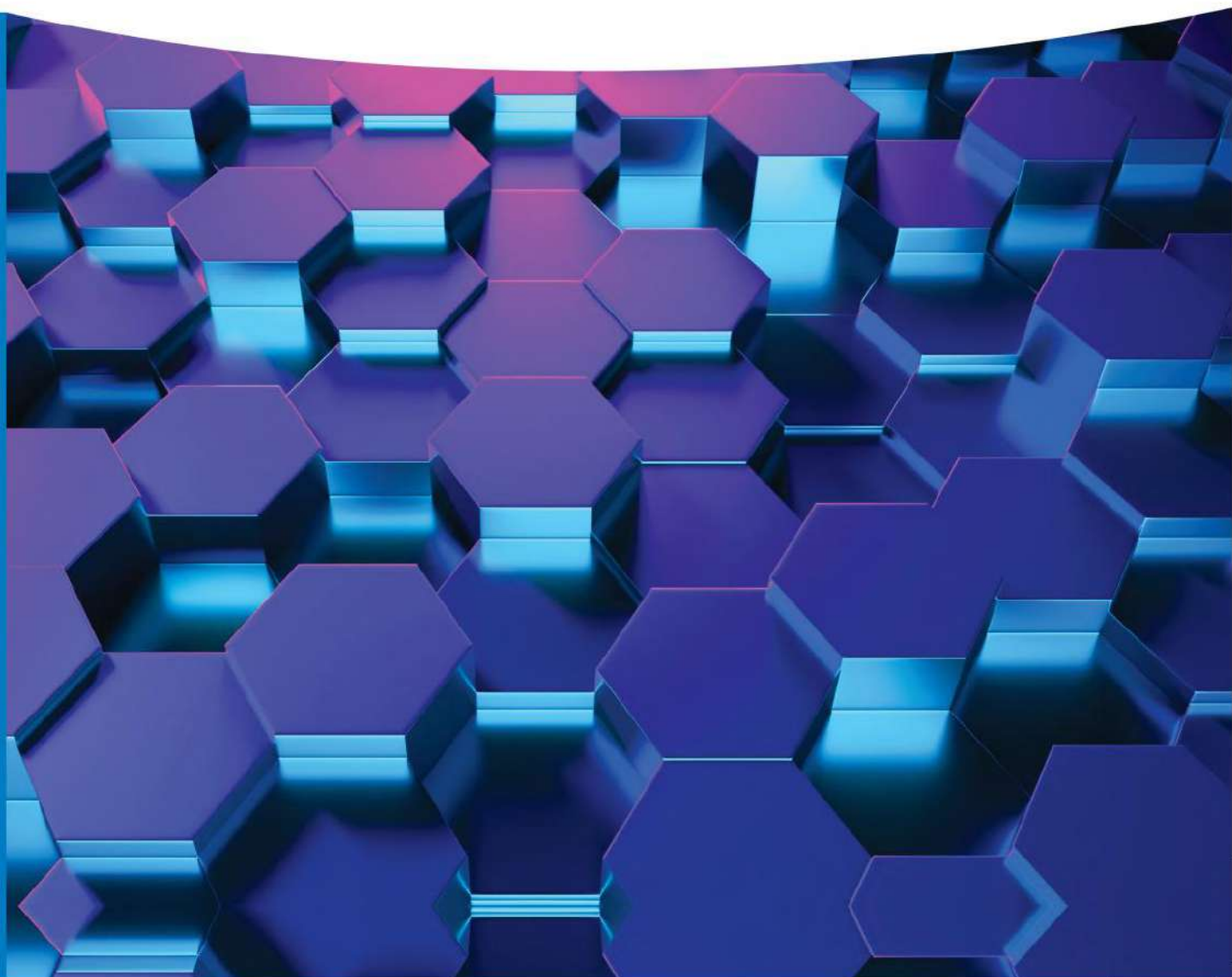
# Organometallic Compounds

Synthesis, Reactions, and Applications

Verma, Dakeshwar Kumar  
Aslam, Jeenat (Eds.)

Organometallic Compounds

WILEY-VCH





DE GRUYTER

# CARBON ALLOTROPES

NANOSTRUCTURED ANTI-CORROSIVE MATERIALS

*Edited by Jeenat Aslam, Chandrabhan Verma,  
Dakeshwar Kumar Verma, Ruby Aslam*

DE  
G

# **HANDBOOK OF** **ORGANIC NAME** **REACTIONS**

**REAGENTS, MECHANISM AND APPLICATIONS**



**Dakeshwar Kumar Verma**  
**Yeestdev Dewangan**  
**Chandrabhan Verma**

WILEY-VCH

Edited by Dakeshwar Kumar Verma,  
Chandrabhan Verma, and Paz Otero Fuertes

# Green Chemical Synthesis with Microwaves and Ultrasound

Verma, Chandrabhan Verma, Otero Fuertes (Eds.)

Green Chemical Synthesis with

WILEY-VCH



# ESSENTIAL OILS

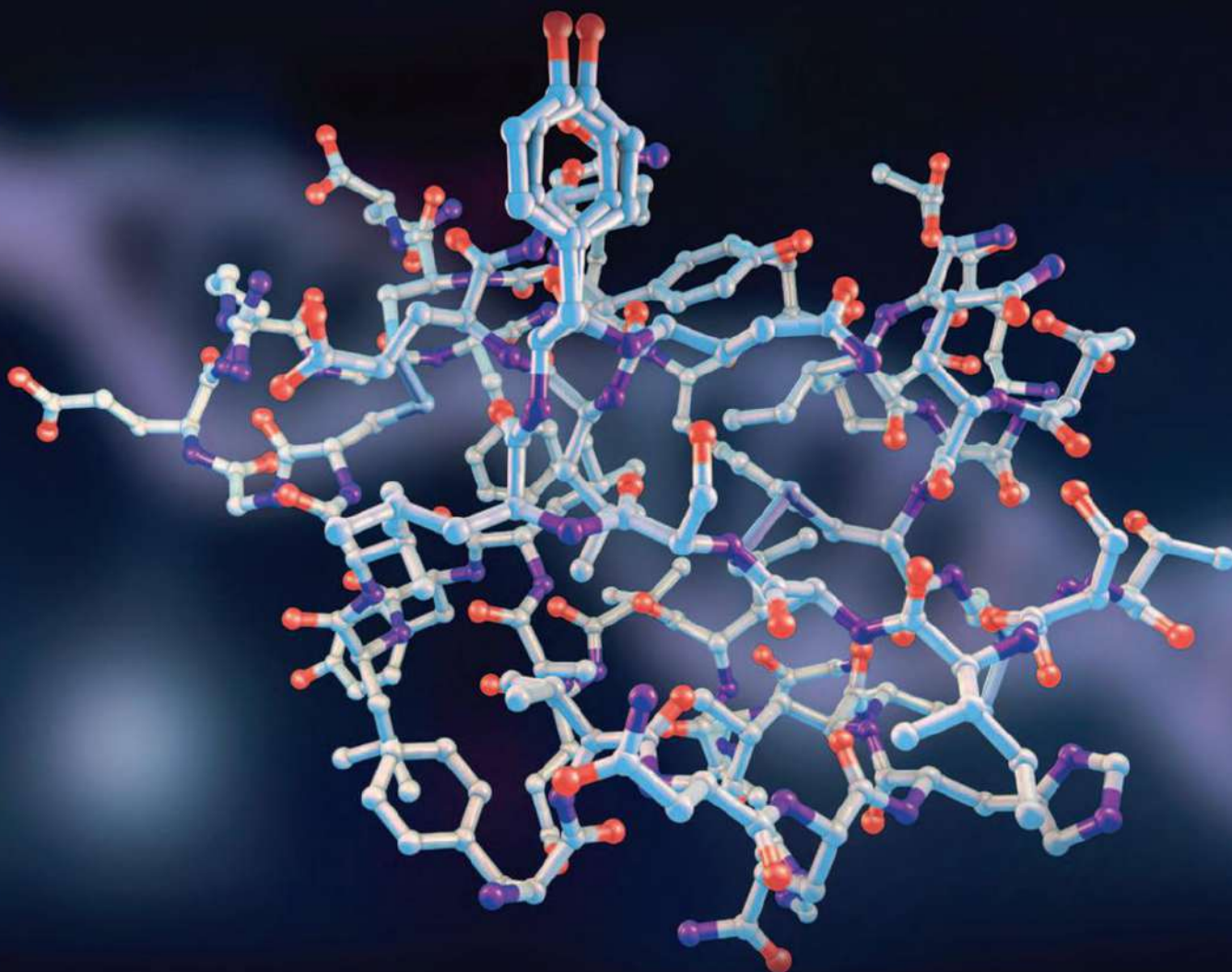
SOURCES, PRODUCTION AND APPLICATIONS

*Edited by Rajendra C. Padalia,  
Dakeshwar K. Verma, Charu Arora  
and Pramod K. Mahish*



# COMPUTATIONAL MODELING AND SIMULATIONS FOR DESIGNING OF CORROSION INHIBITORS

Fundamentals and Realistic Applications



Edited by

Dakeshwar Kumar Verma

Chandrabhan Verma

Jeenat Aslam





# MARINE MOLECULES FROM ALGAE AND CYANOBACTERIA

Extraction, Purification, Toxicology and Applications

Edited by

Paz Otero Fuertes · Dakeshwar Kumar Verma



DE GRUYTER

STEM

# PHYTOCHEMICALS IN MEDICINAL PLANTS

BIODIVERSITY, BIOACTIVITY AND DRUG DISCOVERY

*Edited by Charu Arora, Dakeshwar K. Verma,  
Jeenat Aslam, Pramod K. Mahish*



DE  
G



ACS SYMPOSIUM SERIES

# HEAVY METALS IN THE ENVIRONMENT

MANAGEMENT STRATEGIES FOR GLOBAL POLLUTION



**D. K. VERMA, C. VERMA  
& P. K. MAHISH**



ACS Publications



DE GRUYTER

STEM

# CARBON DOTS IN BIOLOGY

SYNTHESIS, PROPERTIES, BIOLOGICAL  
AND PHARMACEUTICAL APPLICATIONS

*Edited by Berdimurodov Elyor Tukhliyivich  
and Dakeshwar Kumar Verma*

DE  
GRUYTER



# **BARRIERS TO ENGLISH COMMUNICATION** (ITS CONCEPTS AND PROBLEMS)

**Patron**

**Dr. K L Tandekar**

**Edited by**

**Dr. Anita Shankar  
Dr. Neelu Shrivastava**

**Co-Editors**

**Dr. Anita Shaha  
Ms. Manjari Singh**

# Content

1.	E-Learning, Mobile-Learning: Merits and Demerits, Dr. Anita Shankar	09
2.	Barriers to English Communication in Professional Colleges, Dr. Neelu Shrivastava	16
3.	Barrier to Effective Communication in English, Ms. Manjari Singh	29
4.	Teaching English to Rural Students, Dr. Anita Saha	36
5.	Fusion of English Language in Hindi Cinema, Dr. Aradhana Goswami	44
6.	Importance of Language Lab in ELT, Dr. Shiela Vijay, Dr. Neeta Sharma	54
7.	The Impact of Mother Tongue on Learning English Language, Dr. Harpreet Kaur Garcha	61
8.	Role of Forums in Promoting English Language Learning, Dhanesh Ram Sinha	67
9.	Impact of Social Networks on English Language, Teaching and Learning, Dr. Sunayana Mishra	76
10.	Literature as a Catalyst for Language Teaching, Dr. Merily Roy	84
11.	Importance of English Language in Career Enhancement, Dr Reshma Lakesh, Rimsha Lakesh	89

**BARRIERS TO ENGLISH COMMUNICATION  
(ITS CONCEPTS AND PROBLEMS)**

ISBN- 978-81-972535-3-9



*Published by*  
**Sarvpriya Prakashan**  
1569, First Floor Church Road,  
Kashmiri Gate, Delhi-110006  
e-mail : sarvapriyapublishing@gmail.com  
e-mail : Mob.: 9425358748

Cover Design : Kanhaiya Sahu  
First Edition : 2024  
Price: Rs. 250  
Copy Right : Author



*Published by*  
**Sarvpriya Prakashan**  
1569, First Floor Church Road,  
Kashmiri Gate, Delhi-110006  
  
*Raipur Office*  
Changora Bhatta, Road  
Behind Emerald Hotel, P.S. City -492013  
Mob.: 9425358748 e-mail : sarvapriyapublishing@gmail.com  
First Edition : 2024  
Price: Rs.100.00

कार्यालय मुख्य निर्वाचन पदाधिकारी  
छत्तीसगढ़

इन्द्रावती खण्ड, पुराना मंत्रालय परिसर, रायपुर फोन न. 0771-2236685

E mail-ceoraipur.cg@gov.in

फा क्र.01/स्वीप/इंडलाईन सर्वे/2024/636।

रायपुर दिनांक 18 JUL 2024

// वित्तीय स्वीकृति आदेश //

भारत निर्वाचन आयोग नई दिल्ली के निर्देशानुसार लोकसभा आम निर्वाचन-2024 के दृष्टिगत मतदाताओं के मतदान के प्रति उनके रुझान रुचि, ज्ञान एवं विश्वास KAP (Knowledge, Attitude and Practices) का आंकलन करने हेतु छत्तीसगढ़ राज्य के सभी 05 संभाग के समस्त 33 जिलों के सभी 90 विधानसभा क्षेत्रों के संभागवार Endline Survey Report (2024) कार्य कराये जाने हेतु छत्तीसगढ़ राज्य के निम्नानुसार शासकीय उच्च शैक्षणिक संस्थानों को उनके नाम के समक्ष कॉलम में अंकित राशि की स्वीकृति प्रदान की जाती है-

स.क्र	संस्थान-	संभाग	राशि रु
01	कुलसचिव, पंडित रविशंकर शुक्ल विश्वविद्यालय रायपुर (छ०ग०)	रायपुर,	6,80,000
02	प्राचार्य, राजीव गांधी शासकीय स्नातकोत्तर महाविद्यालय अंबिकापुर सरगुजा (छ०ग०)	सरगुजा	6,16,000
03	प्राचार्य, शासकीय बिलासा कन्या स्नातकोत्तर महाविद्यालय बिलासपुर (छ०ग०)	बिलासपुर	8,16,000
04	प्राचार्य, शासकीय भानुप्रताप देव स्नातकोत्तर महाविद्यालय कांकेर (छ०ग०)	बस्तर	5,88,000
05	प्राचार्य, शासकीय दिग्विजय स्नातकोत्तर महाविद्यालय राजनांदगांव (छ०ग)	दुर्ग,	6,80,000
योग-			33,80,000

(तींति स लाख अस्सी हजार रूपये) मात्र

अतः उपरोक्तानुसार शासकीय उच्च शैक्षणिक संस्थानों को आबंटित किये जाने वाले कुल राशि रु 33,80,000/- (तींति स लाख अस्सी हजार रूपये) मात्र अग्रिम आहरण किये जाने की स्वीकृति प्रदान की जाती है।

उपरोक्तानुसार देयक के भुगतान पर होने वाला व्यय राशि रु 33,80,000/- (तींति स लाख अस्सी हजार रूपये) मात्र FY 2024-25 हेतु राज्य शासन से प्राप्त आबंटन मांग संख्या 29-2015-निर्वाचन, (3307)-103-मतदाता सूचियों की तैयारी एवं मुद्रण #09-विज्ञापन एवं प्रचार-प्रसार मद से विकलनीय होगा।

(मुनिप. द्वारा अनुमोदित)

उप संचालक (वित्त)  
कार्यालय मुख्य निर्वाचन पदाधिकारी  
छत्तीसगढ़, रायपुर

योजना भवन, नार्थ ब्लॉक, सेक्टर-19 नवा रायपुर अटल नगर, छत्तीसगढ़  
टेलीफैक्स : 0771-2511223 ईमेल: ms.cgspc@gov.in

// स्वीकृति आदेश //

नवा रायपुर अटल नगर, दिनांक 02/05/2023

क्रमांक 1134 /F2(SS)-04/रायोआ/2023 : छत्तीसगढ़ शासन, वित्त निर्देश 30/2016 द्वारा प्रत्यायोजित अधिकारों का उपयोग करते हुए एतद् द्वारा Dr.Mahesh Shrivastava, Asst. Prof. Govt. Digvijay P.G. College Rajnandgaon को उनके द्वारा प्रस्तुत अध्ययन प्रस्ताव "A Critical analysis of Government Programmes for the upliftment of Baiga Tribe in Chhattisgarh" हेतु राशि रु.4.50 लाख (चार लाख पचास हजार रुपये मात्र) को तीन किश्तों में प्रदाय की स्वीकृति प्रदान की जाती है।

2/ उक्त स्वीकृति उच्चस्तरीय "अनुमोदन समिति" की बैठक दिनांक 14/03/2023 में प्रदत्त अनुमोदन के आधार पर जारी की जा रही है।

3/ निम्नानुसार मदवार राशि रु.4.50 लाख प्रदाय की स्वीकृति प्रदाय की जाती है -

(अ) अनावर्ती व्यय- रु.0.50 लाख

(ब) आवर्ती व्यय- रु.4.00 लाख

**A. Non-Recurring (Equipment if required) Maximum Rs 1.00 lakhs (Rupees One Lakh Only)**

SN	Name of Equipment/ Facilities to procure	Specification of equipment	No. of Units	Estimated cost (Rs.) as on date
1.	Camera/Handy cam	Photographs & Videography	1	40,000
2	Books/Journals	Research work	-	10,000
<b>Total :</b>				<b>50,000</b>

**B. Recurring**

SN	Item	Budget/ Justification	No. of Units	Total
<b>Honorarium to Manpower</b>				
1.	Honorarium to Human Resources			
	(a) Research Assistant	@Rs.16000 PM X5	01	80,000
	(b) Field Investigator	@Rs.15000 PM X5	02	1,50,000
	(c) Part time Typist	@Rs.8000 PM X5	01	40,000
2.	Contingencies			10,000
3.	Travel and Field work			1,20,000
<b>Total :</b>				<b>4,00,000</b>
<b>Grand Total :</b>				<b>4,50,000</b>

(रूपये चार लाख, पचास हजार मात्र)

उपरोक्तानुसार योजना के नियम, शर्त के आधार पर उक्त कार्य हेतु प्रथम किश्त के रूप में स्वीकृत राशि का 40 प्रतिशत यथा रु.1.80 लाख प्रदाय की स्वीकृति प्रदान की जाती है। उक्त कार्य हेतु 04 माह की अवधि निर्धारित की गई है। संपूर्ण अध्ययन कार्य इस अवधि में पूर्ण किया जाना आवश्यक होगा। उक्त अवधि के अंत में प्रथम किश्त जारी दिनांक रो की जावेगी।

उपरोक्तानुसार व्यय मांग संख्या-31 योजना, अर्थिक एवं सांख्यिकी विभाग से संबंधित व्यय, क्रमांक 7639-राज्य योजना का सुदृढीकरण मूल्यांकन एवं अनुसंधान के अंतर्गत #10 व्यवसायिक हेतु अदायगियां, उपशीर्ष 003- परामर्श सेवाएं मद से विकल्पनीय होगी।

राज्य योजना आयोग द्वारा योजना अंतर्गत पत्र क्रमांक 1611 दिनांक 17/08/2022 द्वारा जारी केंद्र प्रासंगिक एवं विकासोन्मुखी विषयों पर अध्ययन प्रस्ताव प्राप्त करने हेतु दिशा-निर्देश तथा MoU निहित समस्त नियम एवं शर्तों का पूर्ण रूप से पालन करना अनिवार्य होगा।





# पर्यटन उद्योग

विकास, चुनौतियाँ एवं संभावनाएँ



प्रधान संपादक  
डॉ. के.एल. टाण्डेकर

पुस्तक लेखक : डॉ. राजेश कुमार

ISBN-978-93-93901-24-2

लेखक

डॉ. राजेश कुमार

1269, First Floor Church Road,  
Kashmiri Gate, Delhi-110006  
मि. 9425328748

आवृत्ति : प्रथम संस्करण

2024

मूल्य : ₹ 320.00

लेखक का पता : दिल्ली

Published by

Sarvriya Prakashan

1269, First Floor Church Road,

Kashmiri Gate, Delhi-110006

Rajpur Office

Changora Bhatia, Road

Behind Imperial Hotel, P.S. City-492013

Mob.: 9425328748 e-mail: sarvriyaprakashan@gmail.com

First Edition : 2024

Price : ₹ 320.00

पर्यटन उद्योग : विकास, चुनौतियाँ  
एवं संभावनाएँ  
Challenges, Development And Possibility In  
Tourism Industry

●  
प्रधान सम्पादक  
डॉ. के. एल. टाण्डेकर  
प्राचार्य

●  
सम्पादक  
डॉ. डी. पी. कुर्रे  
विभागाध्यक्ष, अर्थशास्त्र  
डॉ. एस. के. उके  
विभागाध्यक्ष, वाणिज्य

●  
सह.-सम्पादक  
डॉ. एच. सी. जैन  
डॉ. महेश श्रीवास्तव  
डॉ. रागिनी पराते  
शासकीय दिग्विजय स्वशासी स्नातकोत्तर महाविद्यालय,  
राजनांदगांव (छ.ग.)




सर्वप्रिय प्रकाशन

दिल्ली-रायपुर

# दलित सशक्तिकरण के सामाजिक-आर्थिक आयाम

डॉ. डी.पी. कुर्रे

प्राध्यापक, अर्थशास्त्र  
शासकीय दिग्विजय स्वशासी स्नातकोत्तर  
महाविद्यालय  
राजनांदगांव, (छ.ग.)

सम्यक्  प्रकाशन

पर्यटन उद्योग : विकास, चुनौतियाँ एवं संभावनाएँ

ISBN- 978-93-93901-54-5

●  
प्रकाशक

**सर्वप्रिय प्रकाशन**

1569, प्रथम मंजिल, चर्च रोड,  
कश्मीरी गेट, दिल्ली-110006  
मो. 94253-58748

आवरण सज्जा : कन्हैया

प्रथम संस्करण : 2024

मूल्य : 350.00 रुपये

**कॉपीराइट** : लेखकाधीन

●  
*Published by*

**Sarvpriya Prakashan**

1569, First Floor Church Road,  
Kashmiri Gate, Delhi-110006

*Raipur Office*

Changora Bhatha, Road

Behind Imrald Hotel , P.S. City -492013

Mob.: 9425358748 e-mail : sarvapriyaprakashan@gmail.com

First Edition : 2024

Price : Rs.350.00

# छत्तीसगढ के आर्थिक विकास में पर्यटन उद्योग का योगदान

डॉ. डी. पी. कुरे


प्राध्यापक, अर्थशास्त्र

शासकीय दिग्विजय स्वशासी स्नातकोत्तर महाविद्यालय,  
राजनांदगांव (छ.ग.)

डॉ. विनोद कुमार जोशी

प्राध्यापक, अर्थशास्त्र

डॉ. राधाबाई शासकीय नवीन कन्या स्नातकोत्तर  
महाविद्यालय, रायपुर (छ.ग.)

सम्यक्  प्रकाशन

प्रथम संस्करण : 2024 (बुद्धाब्द 2568)

प्रकाशक : सम्यक प्रकाशन

32/3, पश्चिमपुरी, नई दिल्ली-110063

Web : [www.samyakprakashan.in](http://www.samyakprakashan.in)

© सर्वाधिकार लेखकाधीन

**ISBN: 978-81-19945-78-8**

मूल्य : 450 रुपये

रचना : दलित सशक्तिकरण के सामाजिक-आर्थिक आयाम

रचनाकार : डॉ. डी.पी. कुर्रे

आवरण : शांत कला निकेतन

शब्दांकन : संदीप आर्ट एण्ड ग्राफिक्स

मुद्रक : बालाजी ऑफसेट प्रिंटर्स, नई दिल्ली

दलित  
कित  
तो  
प्रथम  
अनुभ  
आधि  
के स  
जा  
भारत  
बेहत  
उत्थ  
लक्ष्य  
आजि  
पर  
निच  
थें।  
साम  
योज  
भी  
कोरि  
की  
हैं।  
देश

पर्यटन उद्योग : विकास, चुनौतियाँ एवं संभावनाएँ

ISBN- 978-93-93901-54-5

●  
प्रकाशक

**सर्वप्रिय प्रकाशन**

1569, प्रथम मंजिल, चर्च रोड,  
कश्मीरी गेट, दिल्ली-110006  
मो. 94253-58748

आवरण सज्जा : कन्हैया

प्रथम संस्करण : 2024

मूल्य : 350.00 रुपये

**कॉपीराइट** : लेखकाधीन

●  
*Published by*

**Sarvpriya Prakashan**

1569, First Floor Church Road,  
Kashmiri Gate, Delhi-110006

*Raipur Office*

Changora Bhatha, Road

Behind Imrald Hotel , P.S. City -492013

Mob.: 9425358748 e-mail : sarvapriyaprakashan@gmail.com

First Edition : 2024

Price : Rs.350.00



87

13. छत्तीसगढ़ का प्रमुख दार्शनिक, ऐतिहासिक,  
धार्मिक पर्यटन स्थल डोंगरगढ़  
– डॉ. के. एल. टाण्डेकर 164  
– श्रीमती अंकिता शर्मा

96

14. पर्यटन एवं रोजगार के अवसर  
– डॉ. निधि मोनिका शर्मा 173  
– कु. प्रीति जंघेल

111

15. शैक्षणिक पर्यटन में पर्यावरण की भूमिका  
– डॉ. अमित कुमार 182

118

16. पर्यटन उद्योग : विकास चुनौतियाँ एवं संभावनाएँ  
– डॉ. समित ल. माहोरे 191  
– डॉ. गुलाबचंद चिखलौंडे

17. विश्व पर्यटन उद्योग में भारत की भागीदारी का अध्ययन  
– संजय कुमार देवांगन 211  
– एच .सी. जैन

132

18. खैरागढ़, छुईखदान, गण्डई जिला क्षेत्र में पर्यटन विकास  
की संभावनाएँ – सुश्री निरुपा साहू 223  
– विजय कुमार

140

19. आर्थिक विकास में पर्यटन उद्योग की भूमिका  
– नीलू गुप्ता 230  
– डॉ. डी. पी. कुर्रे

154

20. पर्यटन उद्योग में रोजगार के अवसर एवं सरकारी योजनाएँ  
– ऋषि सिंह भाटिया 240  
– डॉ. एच. एस. भाटिया
21. ग्रामीण पर्यटन के विकास में आधारभूत ढांचे की भूमिका  
– डॉ. के. एल. टाण्डेकर 248  
– डॉ. युगेश्वरी साहू

पर्यटन उद्योग : विकास, चुनौतियाँ एवं संभावनाएँ // 5

- 87
13. छत्तीसगढ़ का प्रमुख दार्शनिक, ऐतिहासिक,  
धार्मिक पर्यटन स्थल डोंगरगढ़  
– डॉ. के. एल. टाण्डेकर 164  
– श्रीमती अंकिता शर्मा
- 96
14. पर्यटन एवं रोजगार के अवसर  
– डॉ. निधि मोनिका शर्मा 173  
– कु. प्रीति जंघेल
- 111
15. शैक्षणिक पर्यटन में पर्यावरण की भूमिका  
– डॉ. अमित कुमार 182
- 118
16. पर्यटन उद्योग : विकास चुनौतियाँ एवं संभावनाएँ  
– डॉ. समित ल. माहोरे 191  
– डॉ. गुलाबचंद चिखलोंडे
- 132
17. विश्व पर्यटन उद्योग में भारत की भागीदारी का अध्ययन  
– संजय कुमार देवांगन 211  
– एच .सी. जैन
- 140
18. खैरागढ़, छुईखदान, गण्डई जिला क्षेत्र में पर्यटन विकास  
की संभावनाएँ – सुश्री निरुपा साहू 223  
– विजय कुमार
- 154
19. आर्थिक विकास में पर्यटन उद्योग की भूमिका  
– नीलू गुप्ता 230  
– डॉ. डी. पी. कुर्रे
- 4
20. पर्यटन उद्योग में रोजगार के अवसर एवं सरकारी योजनाएँ  
– ऋषि सिंह भाटिया 240  
– डॉ. एच. एस. भाटिया
21. ग्रामीण पर्यटन के विकास में आधारभूत ढांचे की भूमिका  
– डॉ. के. एल. टाण्डेकर 248  
– डॉ. युगेश्वरी साहू

पर्यटन उद्योग : विकास, चुनौतियाँ एवं संभावनाएँ // 5



# पर्यटन उद्योग

विकास, चुनौतियाँ एवं संभावनाएँ



प्रधान संपादक  
डॉ. के.एल. टाण्डेकर

UGC Approved Journal No. 49321

Impact Factor : 6.125

ISSN : 0976-6650

# Shodh Drishti

An International Peer Reviewed Refereed Research Journal

---

Vol. 14, No. 9.1

Year - 14

September, 2023

---

PEER REVIEWED JOURNAL

*Editor in Chief*

**Prof. Abhijeet Singh**

*Editor*

**Dr. K.V. Ramana Murthy**

Principal

Vijayanagar College of Commerce

Hyderabad

**Dr. Anil Kumar**

Assistant Professor, Department of History

Rajdhani College, University of Delhi

*Published by*

**SRIJAN SAMITI PUBLICATION**

**VARANASI**

E-mail : shodhdristivns@gmail.com, Website : shodhdrishti.com, Mob. 9415388337

## *Contents*

↵	Right to Privacy in India; Gradual Development through Judicial Decisions <b>Dr. Shyam Ji Nigam &amp; Dr. Suhel Azim Qureshi</b>	1-6
↵	Development with Disparity in India: Socio-Legal Perspectives <b>Dr. Dhiraj Kumar Mishra</b>	7-12
↵	Role and Impact of Indian Cinema on Education System and Society <b>Dr. Aradhana Goswami</b>	13-17
↵	Locating Masculinity within Korean Television and Indian Television <b>Sushmita Pandey</b>	18-24
↵	Isolation and Characterization of Cadmium-Resistant Fungi from Riverain Soils of Agra <b>Dr. Krati Trivedi</b>	25-26
↵	Marital Rape Law in India : Need to Change the Narrative <b>Mahesh Kumar Pandey</b>	27-32

**MONOTONE GENERALIZED  $(\alpha, \beta)$ -NONEXPANSIVE MAPPINGS IN  
ORDERED HYPERBOLIC METRIC SPACES**

SAMIR DASHPUTRE AND KAVITA SAKURE

ABSTRACT. In this paper, we discuss SPK iterative algorithm for approximating fixed point of monotone generalized  $(\alpha, \beta)$ -nonexpansive mapping in the setting of partially ordered hyperbolic spaces. Indeed, we present some convergence results for SPK iterative algorithm for monotone generalized  $(\alpha, \beta)$ -nonexpansive mapping. Moreover, we provide an application of our results to nonlinear integral equations.

REFERENCES

- [1] B. Abdullatif, B. Dehaish and M.A. Khamsi: *Browder and Göhde fixed point theorem for monotone nonexpansive mappings*, Fixed Point Theory Appl., **2016**(2016), No. 1, 1-9.
- [2] R.P. Agarwal, D. O'Regan and D.R. Sahu: *Iterative construction of fixed points of nearly asymptotically nonexpansive mappings*, J. Nonlinear Convex Anal., **8**(2007), No. 1, 61-79.
- [3] F. Akutsah and O.K. Narain: *On generalized  $(\alpha, \beta)$ -nonexpansive mappings in Banach spaces with applications*, Nonlinear Funct. Anal. Appl., **26**(2021), No. 4, 663-684.
- [4] K. Aoyama and F. Kohsaka: *Fixed point theorem for a nonexpansive mappings in Banach spaces*, Nonlinear Anal., **2011**(2011), No. 13, 4387-4391.
- [5] B.A. Bin Dehaish and M.A. Khamsi: *Browder and Göhde fixed point theorem for monotone nonexpansive mappings*, Fixed Point Theory Appl., **2016**(2016), No. 1, 1-9.
- [6] H. Busemann: *Spaces with non-positive curvature*, Acta Math., **80**(1948), 259-310.
- [7] F.E. Browder: *Nonexpansive nonlinear operators in a Banach space*, Proc. Natl. Acad. Sci. USA, **54**(1965), No. 4, 1041-1044.
- [8] K. Goebel and W.A. Kirk: *Iteration processes for nonexpansive mappings*, Contemp. Math., **21**(1983), 115-123.
- [9] D. Göhde: *Zum Prinzip der kontraktiven Abbildung*, Math. Nachr., **30**(1965), 251-258.
- [10] M. Gromov, M. Katz, P. Pansu and S. Semmes: *Metric Structures for Riemannian and non-Riemannian Spaces*, Birkhäuser Boston, 1999.
- [11] M. Imdad and S. Dashputre: *Fixed point approximation of picard normal s-iteration process for generalized nonexpansive mappings in hyperbolic spaces*, Math. Sci., **10**(2016), No. 3, 131-138.
- [12] S. Ishikawa: *Fixed points by a new iteration method*, Proc. Amer. Math. Soc., **44**(1974), No. 1, 147-150.
- [13] A.R. Khan, H. Fukhar-ud-din and M. Khan: *An implicit algorithm for two finite families of nonexpansive maps in hyperbolic spaces*, Fixed Point Theory Appl., **54**(2012), No. 12, 1-12.
- [14] W.A. Kirk: *A fixed point theorem for mappings which do not increase distances*, Amer. Math. Monthly, **72**(1965), No. 9, 1004-1006.
- [15] W.A. Kirk and B. Panyanak: *A concept of convergence in geodesic spaces*, Nonlinear Anal., **68**(2008), 3689-3969.
- [16] Jong Kyu Kim, Samir Dashputre, Padmavati . Sudha and Kavita Sakure: *Generalized  $\alpha$ -nonexpansive mappings in hyperbolic spaces*, Nonlinear Funct. Anal. Appl., **27**(2022), No. 3, 449-469.

---

Received: December 25, 2023. Revised: March 29, 2024.

2020 Mathematics Subject Classification: 47H10, 54H25.

Key words and phrases: Partial ordered hyperbolic spaces, monotone nonexpansive mappings, SPK iterative algorithm,  $\Delta$ -convergence.

- [17] U. Kohlenbach: *Some logical metatheorems with applications in functional analysis*, Trans. Amer. Math. Soc., **357**(2005), No. 1, 89-128.
- [18] L. Leuştean: *A quadratic rate of asymptotic regularity for CAT(0) spaces*, J. Math. Anal. Appl., **325**(2007), No. 1, 386-399.
- [19] L. Leuştean: *Nonexpansive iterations in uniformly convex  $W$ -hyperbolic spaces*, in *Nonlinear analysis and optimization I. Nonlinear analysis*, Contemp. Math., **513**(2010), pp. 193-209.
- [20] T.C. Lim: *On the center of convex set*, Proc. Amer. Math. Soc., **81**(1981), No. 2, 345-346.
- [21] W.R. Mann: *Mean value methods in iteration*, Proc. Amer. Math. Soc., **4**(1953), 506-610.
- [22] M.A. Noor: *New approximation schemes for general variational inequalities*, J. Math. Anal. Appl., **251**(2000), No. 1, 217-229.
- [23] R. Pandey, R. Pant, V. Rakočević and R. Shukla: *Approximating fixed points of a general class of nonexpansive mappings in Banach spaces with applications*, Results Math., **74**(2019), Art. No. 7.
- [24] S. Reich and I. Shafrir: *Nonexpansive iterations in hyperbolic spaces*, Nonlinear Anal., **15**(1990), No. 6, 537-558.
- [25] H.F. Senter and W.G. Dotson: *Approximating fixed points of nonexpansive mappings*, Proc. Amer. Math. Soc., **44**(1974), 375-380.
- [26] T. Suzuki: *Fixed point theorems and convergence theorems for some generalized nonexpansive mappings*, J. Math. Anal. Appl., **340**(2008), No. 2, 1088-1095. 2008.
- [27] W. Takahashi: *A convexity in metric space and nonexpansive mappings, I*, Kodai Math. Sem. Rep., **22**(1970), No. 2, 142-149.

*Department of Mathematics*  
*Govt. College*  
*Arjunda, Balod, Chhattisgarh, India*  
*E-mail address: samir231973@gmail.com*

*Department of Mathematics*  
*Govt. Digvijay Auto. P.G. College*  
*Rajnandgaon, Chhattisgarh, India*  
*E-mail address: kavitaage@gmail.com*



# कार्यालय-प्राचार्य, शासकीय दिग्विजय स्वशासी स्नातकोत्तर महाविद्यालय, राजनांदगांव (छ.ग.)

Web site- [www.gdcr.ac.in](http://www.gdcr.ac.in)

Email: [principal@digvijaycollege.com](mailto:principal@digvijaycollege.com)

☎ : 07744-225036

## अग्रणी दिग्विजय : NEP 2020

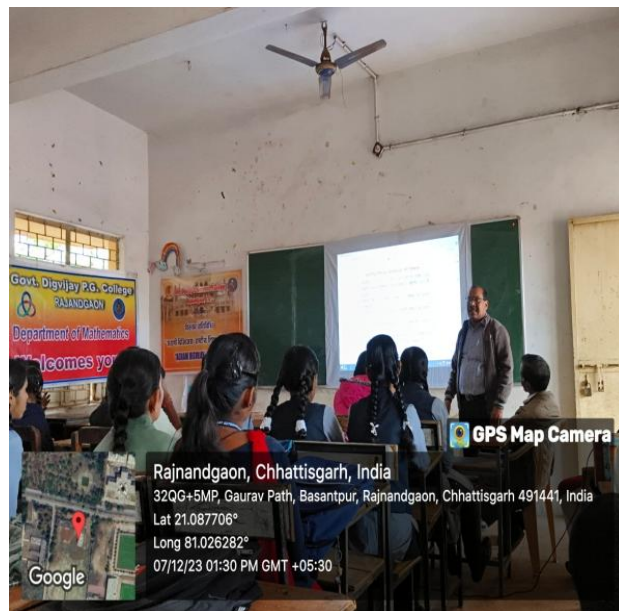
### गणित विभाग द्वारा गुजराती विद्यालय, राजनांदगाँव में NEP की जानकारी दी गयी

शासकीय दिग्विजय महाविद्यालय के गणित विभाग द्वारा दिनांक 07.12.2023 को प्राचार्य डॉ के एल टांडेकर के मार्गदर्शन एवं विभागाध्यक्ष डॉ शबनम खान एवं सहायक प्राध्यापक डॉ. के. के. देवांगन के नेतृत्व में गुजराती राष्ट्रीय उच्चतर माध्यमिक विद्यालय, राजनांदगाँव में कक्षा 10 वीं, 11 वीं एवं कक्षा 12 वीं के विद्यार्थियों को राष्ट्रीय शिक्षा नीति 2020 की PPT के माध्यम से विस्तृत जानकारी प्रदान की। विभागाध्यक्ष डॉ शबनम खान ने NEP 2020 के बारे में बताया कि राष्ट्रीय शिक्षा नीति के अंतर्गत सभी प्रकार की शिक्षा हर विद्यार्थी को दी जा रही है। गुजराती राष्ट्रीय उच्चतर माध्यमिक विद्यालय, राजनांदगाँव के प्राचार्य श्री डी. आर. नावेलकर ने बताया कि शासकीय दिग्विजय महाविद्यालय, राजनांदगाँव जिले का सबसे पुराना महाविद्यालय है तथा वह स्वयं इस महाविद्यालय के विद्यार्थी रहे हैं। बहुआयामी प्रतिभा वाले विद्यार्थी इस महाविद्यालय से उत्तीर्ण हुए हैं, चाहे कला के क्षेत्र में, चाहे खेल के क्षेत्र में, चाहे पढाई के क्षेत्र में, चाहे सांस्कृतिक गतिविधि में, राष्ट्रीय स्तर पर नाम रोशन किया है।





NEP 2020 के बारे में डॉ. के. के. देवांगन के विस्तार से PPT के माध्यम से बताया कि कालेज में सेमेस्टर के पढ़ाई निरंतर है, क्रेडिट पॉइंट सिस्टम से ग्रेड दिया जाता है और NEP 2020 के फायदे बताये | इस कार्यक्रम के अंतर्गत विद्यार्थियों को राष्ट्रीय शिक्षा नीति का मूल आधार, प्रारूप, उद्देश्य, आयु निर्धारण, भारत की उच्च शिक्षा की प्रमुख समस्याएं एवं उनके दूर करने के प्रयास, कौशल आधारित शिक्षा, कुअशल शिक्षा की विशेषताएं, DSC, AECC, GE कोर्स और Value Added Course, महाविद्यालय की दृष्टि से राष्ट्रीय शिक्षा नीति 2020 के नवीन प्रावधान एवं पद्धति इत्यादि की जानकारी प्रदान की। साथ ही विद्यार्थियों को करियर मार्गदर्शन भी प्रदान किया गया।



गणित विभाग ने अतिथि व्याख्याता श्री रवि सोनकर, स्नातकोत्तर गणित के 20 विद्यार्थियों ने भी इस कार्यक्रम में सहभागिता प्रदान की। उन्होंने विद्यार्थियों का गणित से भय दूर करने हेतु विभिन्न तरीको से गणित को पढाया।



GPS Map Camera

Rajnandgaon, Chhattisgarh, India  
 32QG+5MP, Gaurav Path, Basantpur, Rajnandgaon, Chhattisgarh 491441,  
 India  
 Lat 21.087711°  
 Long 81.026298°  
 07/12/23 02:12 PM GMT +05:30

Google

GPS Map Camera

Rajnandgaon, Chhattisgarh, India  
 32QG+66G, Gaurav Path, Basantpur, Rajnandgaon, Chhattisgarh 491441,  
 India  
 Lat 21.087815°  
 Long 81.026099°  
 07/12/23 02:14 PM GMT +05:30

GPS Map Camera

Rajnandgaon, Chhattisgarh, India  
 32QG+5MP, Gaurav Path, Basantpur, Rajnandgaon, Chhattisgarh 491441,  
 India  
 Lat 21.087645°  
 Long 81.026353°  
 07/12/23 02:16 PM GMT +05:30

Google

इस कार्यक्रम के अन्त में विद्यालय के विद्यार्थियों से फीडबैक प्रपत्र भरवाया गया। इस कार्यक्रम में बड़ी संख्या में विद्यालय के 10 वीं, 11 वी एवं 12 वीं के विद्यार्थी सम्मिलित हुए।



# गणित विभाग द्वारा गुजराती विद्यालय में एनईपी की दी जानकारी

गणित विभाग द्वारा गुजराती विद्यालय में एनईपी की दी जानकारी

राजनांदगांव (दावा)। शासकीय दिग्विजय महाविद्यालय के गणित विभाग द्वारा प्राचार्य डॉ.के.एल. टांडेकर के मार्गदर्शन एवं विभागाध्यक्ष डॉ. शबनम खान एवं सहायक प्राध्यापक डॉ. के. के. देवांगन के नेतृत्व में गुजराती राष्ट्रीय उच्चतर माध्यमिक विद्यालय, राजनांदगांव में कक्षा 10 वीं, 11 वीं एवं कक्षा 12 वीं के विद्यार्थियों को राष्ट्रीय शिक्षा नीति 2020 की NEP के माध्यम से विस्तृत जानकारी प्रदान की। विभागाध्यक्ष डॉ. शबनम खान ने NEP-2020 के बारे में बताया कि राष्ट्रीय शिक्षा नीति के अंतर्गत सभी प्रकार की शिक्षा हर विद्यार्थी को दी जा रही है।

गुजराती राष्ट्रीय उच्चतर माध्यमिक विद्यालय के प्राचार्य डी.आर. नावेलकर ने बताया कि शासकीय दिग्विजय



महाविद्यालय, राजनांदगांव जिले का सबसे पुराना महाविद्यालय है तथा वह स्वयं इस महाविद्यालय के विद्यार्थी रहे है। बहुआयामी प्रतिभा वाले विद्यार्थी इस महाविद्यालय से उत्तीर्ण हुए है, चाहे कला के क्षेत्र में, चाहे खेल के क्षेत्र में, चाहे पढ़ाई के क्षेत्र में, चाहे सांस्कृतिक गतिविधि में, राष्ट्रीय स्तर पर नाम रोशन किया है। NEP 2020 के बारे में डॉ. के. के. देवांगन के विस्तार से पीपीटी के माध्यम से बताया कि कॉलेज में सेमेस्टर के पढ़ाई निरंतर है, क्रेडिट पॉइंट सिस्टम से ग्रेड दिया जाता



है और NEP 2020 के फायदे बताये। इस कार्यक्रम के अंतर्गत विद्यार्थियों को राष्ट्रीय शिक्षा नीति का मूल आधार, प्रारूप, उद्देश्य, आयु निर्धारण, भारत की उच्च शिक्षा की प्रमुख समस्याएं एवं उनके दूर करने के प्रयास, कौशल आधारित शिक्षा, कुशल शिक्षा की विशेषताएं, DSC, AECC, GE कोर्स। Value Added Course महाविद्यालय की दृष्टि से राष्ट्रीय शिक्षा नीति 2020 के नवीन प्रावधान एवं पद्धति इत्यादि की जानकारी प्रदान की। साथ ही विद्यार्थियों को करियर मार्गदर्शन

भी प्रदान किया गया। गणित विभाग ने अतिथि व्याख्याता रवि सोनकर, स्नातकोत्तर गणित के 20 विद्यार्थियों ने भी इस कार्यक्रम में सहभागिता प्रदान की।

उन्होंने विद्यार्थियों का गणित से भय दूर करने हेतु विभिन्न तरीकों से गणित को पढ़ाया। इस कार्यक्रम के अन्त में विद्यालय के विद्यार्थियों से फीडबैक प्रपत्र भरवाया गया। इस कार्यक्रम में बड़ी संख्या में विद्यालय के 10वीं, 11वीं एवं 12वीं के विद्यार्थी सम्मिलित हुए।

के ए बा वि पर इस् क प्र प्रा पर अ स श्री दे के प्रा प्रि शा स् शा स् उ सां सा कुं



MONOTONE GENERALIZED  $(\alpha, \beta)$ -NONEXPANSIVE MAPPINGS IN  
ORDERED HYPERBOLIC METRIC SPACES

SAMIR DASHPUTRE AND KAVITA SAKURE

ABSTRACT. In this paper, we discuss SPK iterative algorithm for approximating fixed point of monotone generalized  $(\alpha, \beta)$ -nonexpansive mapping in the setting of partially ordered hyperbolic spaces. Indeed, we present some convergence results for SPK iterative algorithm for monotone generalized  $(\alpha, \beta)$ -nonexpansive mapping. Moreover, we provide an application of our results to nonlinear integral equations.

REFERENCES

- [1] B. Abdullatif, B. Dehaish and M.A. Khamsi: *Browder and Göhde fixed point theorem for monotone nonexpansive mappings*, Fixed Point Theory Appl., **2016**(2016), No. 1, 1-9.
- [2] R.P. Agarwal, D. O'Regan and D.R. Sahu: *Iterative construction of fixed points of nearly asymptotically nonexpansive mappings*, J. Nonlinear Convex Anal., **8**(2007), No. 1, 61-79.
- [3] F. Akutsah and O.K. Narain: *On generalized  $(\alpha, \beta)$ -nonexpansive mappings in Banach spaces with applications*, Nonlinear Funct. Anal. Appl., **26**(2021), No. 4, 663-684.
- [4] K. Aoyama and F. Kohsaka: *Fixed point theorem for a nonexpansive mappings in Banach spaces*, Nonlinear Anal., **2011**(2011), No. 13, 4387-4391.
- [5] B.A. Bin Dehaish and M.A. Khamsi: *Browder and Göhde fixed point theorem for monotone nonexpansive mappings*, Fixed Point Theory Appl., **2016**(2016), No. 1, 1-9.
- [6] H. Busemann: *Spaces with non-positive curvature*, Acta Math., **80**(1948), 259-310.
- [7] F.E. Browder: *Nonexpansive nonlinear operators in a Banach space*, Proc. Natl. Acad. Sci. USA, **54**(1965), No. 4, 1041-1044.
- [8] K. Goebel and W.A. Kirk: *Iteration processes for nonexpansive mappings*, Contemp. Math., **21**(1983), 115-123.
- [9] D. Göhde: *Zum Prinzip der kontraktiven Abbildung*, Math. Nachr., **30**(1965), 251-258.
- [10] M. Gromov, M. Katz, P. Pansu and S. Semmes: *Metric Structures for Riemannian and non-Riemannian Spaces*, Birkhäuser Boston, 1999.
- [11] M. Imdad and S. Dashputre: *Fixed point approximation of picard normal s-iteration process for generalized nonexpansive mappings in hyperbolic spaces*, Math. Sci., **10**(2016), No. 3, 131-138.
- [12] S. Ishikawa: *Fixed points by a new iteration method*, Proc. Amer. Math. Soc., **44**(1974), No. 1, 147-150.
- [13] A.R. Khan, H. Fukhar-ud-din and M. Khan: *An implicit algorithm for two finite families of nonexpansive maps in hyperbolic spaces*, Fixed Point Theory Appl., **54**(2012), No. 12, 1-12.
- [14] W.A. Kirk: *A fixed point theorem for mappings which do not increase distances*, Amer. Math. Monthly, **72**(1965), No. 9, 1004-1006.
- [15] W.A. Kirk and B. Panyanak: *A concept of convergence in geodesic spaces*, Nonlinear Anal., **68**(2008), 3689-3969.
- [16] Jong Kyu Kim, Samir Dashputre, Padmavati . Sudha and Kavita Sakure: *Generalized  $\alpha$ -nonexpansive mappings in hyperbolic spaces*, Nonlinear Funct. Anal. Appl., **27**(2022), No. 3, 449-469.

---

Received: December 25, 2023. Revised: March 29, 2024.

2020 Mathematics Subject Classification: 47H10, 54H25.

Key words and phrases: Partial ordered hyperbolic spaces, monotone nonexpansive mappings, SPK iterative algorithm,  $\Delta$ -convergence.

- [17] U. Kohlenbach: *Some logical metatheorems with applications in functional analysis*, Trans. Amer. Math. Soc., **357**(2005), No. 1, 89-128.
- [18] L. Leuştean: *A quadratic rate of asymptotic regularity for CAT(0) spaces*, J. Math. Anal. Appl., **325**(2007), No. 1, 386-399.
- [19] L. Leuştean: *Nonexpansive iterations in uniformly convex  $W$ -hyperbolic spaces*, in *Nonlinear analysis and optimization I. Nonlinear analysis*, Contemp. Math., **513**(2010), pp. 193-209.
- [20] T.C. Lim: *On the center of convex set*, Proc. Amer. Math. Soc., **81**(1981), No. 2, 345-346.
- [21] W.R. Mann: *Mean value methods in iteration*, Proc. Amer. Math. Soc., **4**(1953), 506-610.
- [22] M.A. Noor: *New approximation schemes for general variational inequalities*, J. Math. Anal. Appl., **251**(2000), No. 1, 217-229.
- [23] R. Pandey, R. Pant, V. Rakočević and R. Shukla: *Approximating fixed points of a general class of nonexpansive mappings in Banach spaces with applications*, Results Math., **74**(2019), Art. No. 7.
- [24] S. Reich and I. Shafrir: *Nonexpansive iterations in hyperbolic spaces*, Nonlinear Anal., **15**(1990), No. 6, 537-558.
- [25] H.F. Senter and W.G. Dotson: *Approximating fixed points of nonexpansive mappings*, Proc. Amer. Math. Soc., **44**(1974), 375-380.
- [26] T. Suzuki: *Fixed point theorems and convergence theorems for some generalized nonexpansive mappings*, J. Math. Anal. Appl., **340**(2008), No. 2, 1088-1095. 2008.
- [27] W. Takahashi: *A convexity in metric space and nonexpansive mappings, I*, Kodai Math. Sem. Rep., **22**(1970), No. 2, 142-149.

*Department of Mathematics*  
*Govt. College*  
*Arjunda, Balod, Chhattisgarh, India*  
*E-mail address: samir231973@gmail.com*

*Department of Mathematics*  
*Govt. Digvijay Auto. P.G. College*  
*Rajnandgaon, Chhattisgarh, India*  
*E-mail address: kavitaage@gmail.com*

# Convergence results for Picard Normal S-iterative algorithm with applications

Samir Dashputre, Padmavati and Kavita Sakure

**Keywords.** Nonlinear functional integral equations, Condition (E), nonexpansive mapping, strong convergence, weak convergence.

**AMS classification.** 47H10, 54H25.

**Abstract.** In this article, we enquire for some weak and strong convergence results for a class of mappings satisfying Condition (E) via Picard Normal S-iterative algorithm (PNSA) in the setting of uniformly convex Banach space (UCBS). Eventually, we furnish an example to substantiate our attained findings and numerically compare PNSA with that of some other well-known iterative algorithms. Additionally, we discuss the existence of the solution of a nonlinear functional integral equation as an application of our result.

## 1 Introduction

Throughout this article,  $\mathbb{N}$  stands for a set of natural numbers. Assume that  $S$  is self-map defined on nonempty subset  $U$  of Banach space  $(Y, \|\cdot\|)$  and that  $F(S)$  stands for the set of all fixed points of  $S$ . The mapping  $S$  is called nonexpansive, if

$$\|Su_1 - Su_2\| \leq \|u_1 - u_2\|, \quad \text{for all } u_1, u_2 \in U.$$

The self-map  $S$  on  $U$  is quasi-nonexpansive, if  $F(S) \neq \emptyset$  and

$$\|Su_1 - u^*\| \leq \|u_1 - u^*\|, \quad \text{for all } u_1 \in U, u^* \in F(S).$$

The theory for the existence of fixed points of nonexpansive mappings, at the outset, discussed by Browder [2], Göhde [6] and Kirk [9], independently. After many researchers have obtained numerous generalizations from their results.

Suzuki [22], in 2008, introduced Suzuki's generalized nonexpansive mapping which is a generalization of nonexpansive mappings.

**Definition 1.1.** The mapping  $S : U \rightarrow U$  is known as Suzuki's generalized nonexpansive mapping (SGNM), if

$$\frac{1}{2}\|u_1 - Su_2\| \leq \|u_1 - u_2\| \Rightarrow \|Su_1 - Su_2\| \leq \|u_1 - u_2\|, \quad \text{for all } u_1, u_2 \in U.$$

García-Falset *et al.* [3], in 2011, extended the class of SGNM and came up with an exciting collection of satisfying Condition  $(E_\mu)$  which contains the class of SGNM.

**Definition 1.2.** A self mapping  $S$  defined on nonempty subset  $U$  of Banach space of  $Y$  is called to satisfy condition  $(E_\mu)$  on  $U$ , if there is  $\mu \geq 1$  such that

$$\|u_1 - Su_2\| \leq \mu\|u_1 - Su_2\| + \|u_1 - u_2\|, \quad \text{for all } u_1, u_2 \in U.$$

If for some  $\mu \geq 1$ ,  $S$  satisfies the Condition  $(E_\mu)$  on  $U$ . Then  $S : U \rightarrow U$  is called to satisfy Condition (E) on  $U$ .

In the literature, there are some iterative processes that are used for elucidating fixed points for nonexpansive mappings, SGNM, and mapping satisfying condition  $(E_\mu)$ ,  $\mu \geq 1$  [15] and generalized nonexpansive mappings via Mann [11], Ishikawa [7], Noor [13], Garodia [4, 5], generalized F-iterative [16] iteration processes. Some authors implemented previously defined iterative algorithms in different spaces successfully (see [25, 26]) and some of the applications of iterative algorithms are found in [10, 18, 20, 23, 24, 27].

Agarwal *et al.* [1] introduced S-iteration algorithm as follows:

$$\begin{cases} t_1 \in U \\ t_{m+1} = (1 - \alpha_m)St_m + \alpha_m Su_m \\ u_m = (1 - \beta_m)t_m + \beta_m St_m, \quad \forall m \in \mathbb{N}, \end{cases} \quad (1.1)$$

where  $\{\alpha_m\}$  and  $\{\beta_m\}$  are sequences in  $(0, 1)$ .

Sahu [17] introduced normal S-iteration algorithm (NSA, in brief) as follows:

$$\begin{cases} t_1 \in U \\ t_{m+1} = Su_m \\ u_m = (1 - \alpha_m)t_m + \alpha_m St_m, \quad \forall m \in \mathbb{N}, \end{cases} \quad (1.2)$$

where  $\{\alpha_m\}$  is sequence in  $(0, 1)$ .

In 2014, Kadioglu and Yildirim [8] introduced the Picard normal S-iterative algorithm (PNSA, in brief) as follows:

$$\begin{cases} t_1 \in U \\ t_{m+1} = Su_m \\ u_m = (1 - \alpha_m)v_m + \alpha_m Sv_m \\ v_m = (1 - \beta_m)t_m + \beta_m St_m, \quad \forall m \in \mathbb{N}, \end{cases} \quad (1.3)$$

where  $\{\alpha_m\}$  and  $\{\beta_m\}$  are real sequences in  $(0, 1)$ .

This research article is structured into seven sections. In Section 2, we collect some basic definitions and results which are playing key roles in this manuscript. In Section 3, we establish the strong and weak convergence results utilizing PNSA (1.3) for a mapping satisfying Condition (E) in UCBS and an example designed for such mapping is presented in Section 4. The comparison of the convergence behaviour of PNSA (1.3) with some known aforementioned iterative algorithms is presented in Section 5 and we establish existence results for solutions of the nonlinear functional integral equation as an application of our result in Section 6. The Section 7 summarizes this paper in a form of a conclusion.

## 2 Preliminaries

In this section, we give some essential definitions and results which help us to establish our main results. Assume that  $U$  is a nonempty, closed and convex subset of Banach space  $Y$ . For bounded sequence  $\{t_m\}$  in  $Y$ , denote

- $r(t, \{t_m\}) = \limsup_{m \rightarrow \infty} \|t - t_m\|$ ;
- asymptotic radius of  $\{t_m\}$  with respect to  $U$  by  $r(U, \{t_m\}) = \inf\{r(t, \{t_m\}) : t \in U\}$ ;
- asymptotic center of  $\{t_m\}$  with respect to  $U$  by  $A(U, \{t_m\}) = \{t \in U : r(t, \{t_m\}) = r(U, \{t_m\})\}$ .

**Definition 2.1.** [21] Assume that  $S$  is self-mapping defined on nonempty subset  $U$  of Banach space  $Y$ . A sequence  $\{t_m\}$  in  $D$  is said to be approximate fixed point sequence (A.F.P.S.), if  $\lim_{m \rightarrow \infty} \|St_m - t_m\| = 0$ .

**Proposition 2.2.** [3] Assume that  $S$  is a function satisfying the Condition (E) defined on nonempty subset  $U$  of Banach space  $Y$  and  $F(S) \neq \emptyset$ , then  $S$  is quasi-nonexpansive.

**Theorem 2.3.** [3] Assume that  $S$  is a function satisfying the Condition (E) defined on compact subset  $U$  of Banach space  $Y$ , then  $U$  admits A.F.P.S. if and only if  $S$  has fixed point in  $U$ .

Opial [14] gave the condition termed as Opial's condition which is useful in the investigation of demiclosedness principle of nonlinear mappings.



**Definition 2.4.** A Banach space  $Y$  is said to satisfy the Opial's condition, if for any sequence  $\{t_m\}$  with  $t_m \rightarrow t^*$  in  $Y$  such that

$$\liminf_{m \rightarrow \infty} \|t_m - t^*\| < \liminf_{m \rightarrow \infty} \|t_m - u\|$$

for all  $u \in Y$  with  $t^* \neq u$ .

**Example 2.5.** The space  $\ell^p$  ( $1 < p < \infty$ ) and Hilbert space satisfy the Opial's condition, but  $\mathcal{L}^p[0, 2\pi]$ , ( $1 < p \neq 2$ ) does not satisfy the Opial's condition.

**Lemma 2.6.** [19, Theorem 2.3.13] Suppose that  $Y$  is a UCBS and  $\{a_m\}$  is sequence in  $[\theta, 1 - \theta]$  for  $\theta \in (0, 1)$ . The sequences  $\{t_m\}$  and  $\{u_m\}$  in  $Y$  are such that  $\limsup_{m \rightarrow \infty} \|t_m - t^*\| \leq l$ ,  $\limsup_{m \rightarrow \infty} \|u_m - t^*\| \leq l$ , and  $\limsup_{m \rightarrow \infty} \|a_m(t_m - t^*) + (1 - a_m)(u_m - t^*)\| = l$  for some  $l \geq 0$  and  $t^* \in Y$ . Then  $\lim_{m \rightarrow \infty} \|t_m - u_m\| = 0$ .

### 3 Main Results

In the following section, we present strong and weak convergence results for a sequence  $\{t_m\}$  generated by PNSA (1.3).

**Theorem 3.1.** Suppose that  $S$  is mapping satisfying Condition (E) defined on convex and closed subset  $U$  of uniformly convex Banach space  $Y$ . Assume that  $\{t_m\}$  is a sequence generated by PNSA (1.3) and  $u^* \in F(S)$ . Then  $\lim_{m \rightarrow \infty} \|t_m - u^*\|$  exists.

*Proof.* Assume that  $m \in \mathbb{N}$ , Using Proposition 2.2 and (1.3),

$$\begin{aligned} \|v_m - u^*\| &\leq (1 - \beta_m)\|t_m - u^*\| + \beta_m\|St_m - u^*\| \\ &\leq (1 - \beta_m)\|t_m - u^*\| + \beta_m\|t_m - u^*\| \\ &\leq \|t_m - u^*\|. \end{aligned} \tag{3.1}$$

Using Proposition 2.2, (1.3) and (3.1),

$$\begin{aligned} \|u_m - u^*\| &\leq (1 - \alpha_m)\|v_m - u^*\| + \alpha_m\|Sv_m - u^*\| \\ &\leq (1 - \alpha_m)\|v_m - u^*\| + \alpha_m\|v_m - u^*\| \\ &\leq \|v_m - u^*\| \\ &\leq \|t_m - u^*\|. \end{aligned} \tag{3.2}$$

Using Proposition 2.2, (1.3), (3.1) and (3.2),

$$\begin{aligned} \|t_{m+1} - u^*\| &= \|Su_m - u^*\| \\ &\leq \|u_m - u^*\| \\ &\leq \|v_m - u^*\| \\ &\leq \|t_m - u^*\|. \end{aligned} \tag{3.3}$$

Now, from (3.1), (3.2) and (3.3), we get

$$\max \{ \|t_{m+1} - u^*\|, \|u_m - u^*\|, \|v_m - u^*\| \} \leq \|t_m - u^*\|.$$

The inequality (3.3) shows that  $\{\|t_m - u^*\|\}$  is non-increasing monotonic sequence and hence  $\{\|t_m - u^*\|\}$  is bounded sequence and therefore  $\lim_{m \rightarrow \infty} \|t_m - u^*\|$  exists.  $\square$

**Theorem 3.2.** Suppose that  $S$  is mapping satisfying Condition (E) defined on convex and closed subset  $U$  of uniformly convex Banach space  $Y$ . Assume that  $\{t_m\}$  is a sequence generated by PNSA (1.3) with  $t_1 \in U$ . Then  $\{t_m\}$  is bounded and  $\lim_{m \rightarrow \infty} \|St_m - t_m\| = 0$  if and only if  $F(S)$  is nonempty.

*Proof.* Suppose that  $\{t_m\}$  is bounded and  $\lim_{m \rightarrow \infty} \|St_m - t_m\| = 0$ . We claim that  $F(S) \neq \emptyset$ . Assume that  $u^* \in A(U, \{t_m\})$ . Then

$$r(Su^*, \{t_m\}) = \limsup_{m \rightarrow \infty} \|t_m - Su^*\|.$$

Now, since  $S : U \rightarrow U$  satisfies the Condition (E), therefore

$$\begin{aligned} r(Su^*, \{t_m\}) &= \limsup_{m \rightarrow \infty} \|t_m - Su^*\| \\ &\leq \mu \limsup_{m \rightarrow \infty} \|St_m - t_m\| + \limsup_{m \rightarrow \infty} \|t_m - u^*\| \\ &= r(u^*, \{t_m\}). \end{aligned} \quad (3.4)$$

Since asymptotic center of the sequence  $\{t_m\}$  is unique, therefore, by (3.4),

$$Su^* = u^*,$$

which shows that  $u^* \in F(S)$  and hence  $F(S) \neq \emptyset$ .

For converse part, assume that  $F(S) \neq \emptyset$  and we will prove that  $\{t_m\}$  is bounded and  $\lim_{m \rightarrow \infty} \|St_m - t_m\| = 0$ . Assume that  $u^* \in F(S)$  because  $F(S) \neq \emptyset$ . Then by Theorem 3.1,  $\lim_{m \rightarrow \infty} \|t_m - u^*\|$  exists. Assume that

$$\lim_{m \rightarrow \infty} \|t_m - u^*\| = l. \quad (3.5)$$

From Proposition 2.2 and (3.3),

$$\limsup_{m \rightarrow \infty} \|St_m - u^*\| \leq l. \quad (3.6)$$

From (3.1) and (3.3),

$$\limsup_{m \rightarrow \infty} \|v_m - u^*\| \leq \lim_{m \rightarrow \infty} \|t_m - u^*\| = l. \quad (3.7)$$

From Proposition 2.2 and (3.7),

$$\limsup_{m \rightarrow \infty} \|Sv_m - u^*\| \leq l. \quad (3.8)$$

From (3.2) and (3.3),

$$\limsup_{m \rightarrow \infty} \|u_m - u^*\| \leq \lim_{m \rightarrow \infty} \|t_m - u^*\| = l. \quad (3.9)$$

From Proposition 2.2 and (3.9),

$$\limsup_{m \rightarrow \infty} \|Su_m - u^*\| \leq l. \quad (3.10)$$

Now, from (1.3) and (3.9),

$$\begin{aligned} \limsup_{m \rightarrow \infty} \|(1 - \alpha_m)(v_m - u^*) + \alpha_m(Sv_m - u^*)\| &= \limsup_{m \rightarrow \infty} \|(1 - \alpha_m)v_m + \alpha_m Sv_m - u^*\| \\ &\leq \limsup_{m \rightarrow \infty} \|u_m - u^*\| \\ &\leq l. \end{aligned} \quad (3.11)$$

From (1.3) and (3.3),

$$\begin{aligned} \liminf_{m \rightarrow \infty} \|t_{m+1} - u^*\| &= \liminf_{m \rightarrow \infty} \|Su_m - u^*\| \\ &\leq \liminf_{m \rightarrow \infty} \|u_m - u^*\| \\ &= \liminf_{m \rightarrow \infty} \|(1 - \alpha_m)v_m + \alpha_n Sv_m - u^*\| \\ &= \liminf_{m \rightarrow \infty} \|(1 - \alpha_m)(v_m - u^*) + \alpha_m(Sv_m - u^*)\|, \end{aligned}$$

and hence

$$l \leq \liminf_{m \rightarrow \infty} \|(1 - \alpha_m)(v_m - u^*) + \alpha_m(Sv_m - u^*)\|. \tag{3.12}$$

From (3.11) and (3.12),

$$\lim_{m \rightarrow \infty} \|(1 - \alpha_m)(v_m - u^*) + \alpha_m(Sv_m - u^*)\| = l. \tag{3.13}$$

Now, (3.7), (3.8), (3.13) and Lemma 2.6 provides

$$\lim_{m \rightarrow \infty} \|Sv_m - v_m\| = 0.$$

Now, from (1.3) and (3.3),

$$\begin{aligned} \limsup_{m \rightarrow \infty} \|(1 - \beta_m)(t_m - u^*) + \beta_m(St_m - u^*)\| &= \limsup_{m \rightarrow \infty} \|(1 - \beta_m)t_m + \beta_t St_m - u^*\| \\ &\leq \limsup_{m \rightarrow \infty} \|t_m - u^*\| \\ &\leq l. \end{aligned} \tag{3.14}$$

From (1.3) and (3.3),

$$\begin{aligned} \liminf_{m \rightarrow \infty} \|t_{m+1} - u^*\| &= \liminf_{m \rightarrow \infty} \|Su_m - u^*\| \\ &\leq \liminf_{m \rightarrow \infty} \|u_m - u^*\| \\ &\leq \liminf_{m \rightarrow \infty} \|v_m - u^*\| \\ &= \liminf_{m \rightarrow \infty} \|(1 - \beta_m)t_m + \beta_m St_m - u^*\| \\ &= \liminf_{m \rightarrow \infty} \|(1 - \beta_m)(t_m - u^*) + \beta_m(St_m - u^*)\|, \end{aligned}$$

and hence,

$$l \leq \liminf_{m \rightarrow \infty} \|(1 - \beta_m)(t_m - u^*) + \beta_m(St_m - u^*)\|. \tag{3.15}$$

From (3.14) and (3.15),

$$\lim_{m \rightarrow \infty} \|(1 - \beta_m)(t_m - u^*) + \beta_m(St_m - u^*)\| = l. \tag{3.16}$$

Now, from (3.3), (3.6), (3.16) and Lemma 2.6, we have  $\lim_{m \rightarrow \infty} \|St_m - t_m\| = 0$ . □

The following Theorem presents the weak convergence result for a sequence  $\{t_m\}$  generated by PNSA (1.3) using Opial’s property.

**Theorem 3.3.** *Suppose that  $S$  is mapping satisfying Condition (E) defined on convex and closed subset  $U$  of uniformly convex Banach space  $Y$ . Assume that  $\{t_m\}$  is a sequence generated by PNSA (1.3). Suppose that  $F(S) \neq \emptyset$  and  $Y$  satisfies Opial’s property. Then sequence  $\{t_m\}$  generated by (1.3) weakly converges to element of  $F(S)$ .*

*Proof.* We have  $\lim_{m \rightarrow \infty} \|St_m - t_m\| = 0$  and sequence  $\{t_m\}$  generated by PNSA (1.3) is bounded, due to Theorem 3.1, therefore  $Y$  is reflexive and it implies that there is subsequence  $\{t_{m_k}\}$  of  $\{t_m\}$  such that  $\{t_{m_k}\}$  weakly converges to some  $u^* \in U$ . Now, due to Opial’s property, the sequence  $\{t_m\}$  weakly converges to  $u^* \in U$ . □

The following Theorem presents the strong convergence result for sequence  $\{t_m\}$  generated by PNSA (1.3) using Opial’s property.

**Theorem 3.4.** *Suppose that  $S$  is mapping satisfying Condition (E) defined on convex and closed subset  $U$  of uniformly convex Banach space  $Y$ . Assume that  $t_1 \in U$ . Also assume that  $F(S) \neq \emptyset$  and closed. Then the sequence  $\{t_m\}$  generated by PNSA (1.3) strongly converges to element of  $F(S)$ , if  $\liminf_{m \rightarrow \infty} d(t_m, F(S)) = 0$ , where  $d(u^*, F(S))$  represents the distance of  $u^*$  from the set  $F(S)$ .*

*Proof.* Assume that  $\liminf_{m \rightarrow \infty} d(t_m, F(S)) = 0$ . Then there is a subsequence  $\{u_m\}$  of  $\{t_m\}$  such that

$$\liminf_{m \rightarrow \infty} d(u_m, F(S)) = 0.$$

Assume that  $\{u_{m_k}\}$  is subsequence of  $\{u_m\}$  such that  $\|u_{m_k} - v_k\| \leq \frac{1}{2^k} \forall k \geq 1$ , where  $\{v_k\}$  is sequence of fixed points of mapping  $S$ . Now, by Theorem 3.1,

$$\|u_{m_{k+1}} - v_k\| \leq \|u_{m_k} - v_k\| \leq \frac{1}{2^k}.$$

Now from (3), we set

$$\|v_{k+1} - v_k\| \leq \|v_{k+1} - u_{m_{k+1}}\| + \|u_{m_{k+1}} - v_k\| \leq \frac{1}{2^{k+1}} + \frac{1}{2^k} < \frac{1}{2^{k-1}}$$

which ensure that  $\{v_k\}$  is Cauchy sequence in  $F(S)$ . Now, since  $F(S)$  is closed and  $\{v_k\}$  converges to some fixed point of mapping  $S$ , say  $v \in F(S)$ . Therefore,

$$\|u_{m_k} - v\| \leq \|u_{m_k} - v_k\| + \|v_k - v\|,$$

as  $m \rightarrow \infty$ ,  $\{u_{m_k}\}$  strongly converges to  $v \in F(S)$  and from Theorem 3.1,  $\lim_{m \rightarrow \infty} \|t_m - v\|$  exists and consequently  $\{u_m\}$  strongly converges to  $v \in F(S)$ .  $\square$

The following Theorem presents the strong convergence result for sequence  $\{t_m\}$  generated by PNSA (1.3) using Condition (I).

**Theorem 3.5.** *Suppose that  $S$  is mapping satisfying Condition (E) and Condition (I) defined on convex and closed subset  $U$  of uniformly convex Banach space  $Y$ . Assume that  $t_1 \in U$ . Assume that  $t_1 \in U$ . Also, assume that  $F(S) \neq \emptyset$  and closed. Then the sequence  $\{t_m\}$  generated by PNSA (1.3) strongly converges to element of  $F(S)$ .*

*Proof.* Since  $S$  satisfies the Condition (I), therefore

$$\|t_m - St_m\| \geq g(d(t_m, F(S))). \quad (3.17)$$

Due to Theorem 3.1, we have

$$\liminf_{m \rightarrow \infty} \|St_m - t_m\| = 0. \quad (3.18)$$

From (3.17) and (3.18),

$$\liminf_{m \rightarrow \infty} g(d(t_m, F(S))) = 0.$$

By the property of function  $g : [0, \infty] \rightarrow [0, \infty]$ ,

$$\liminf_{m \rightarrow \infty} d(t_m, F(S)) = 0.$$

Now, due to Theorem 3.4, the sequence  $\{t_m\}$  strongly converges to fixed point of mapping  $S$ .  $\square$

## 4 Numerical Example

**Example 4.1.** Assume that  $U = [-1, 2] \subseteq \mathbb{R}$  with usual norm. The mapping  $S : U \rightarrow U$  is given by

$$Su = \begin{cases} -\frac{u}{7}, & \text{if } u \in [-1, 0) \\ -u, & \text{if } u \in [0, 1] \setminus \{\frac{1}{7}\} \\ 0, & \text{if } u = \frac{1}{7}. \end{cases}$$

If  $u_1 = \frac{1}{7}$  and  $u_2 = 1$ , then

$\frac{1}{2}\|u_1 - Su_1\| = \frac{1}{14}$  and  $\|u_1 - u_2\| = \frac{6}{7}$ , therefore

$$\frac{1}{2}\|u_1 - Su_1\| < \|u_1 - u_2\|.$$

Here  $\|Su_1 - Su_2\| = 1$ , therefore

$$\|Su_1 - Su_2\| > \|u_1 - u_2\|,$$

which shows that  $S$  is not SGNM. We will prove that  $S$  is a function satisfying Condition (E). For this, we can consider the following cases:

**Case I :** If  $u_1, u_2 \in [-1, 0)$ ,

$$\begin{aligned} \|u_1 - Su_2\| &\leq \|u_1 - Su_1\| + \|Su_1 - Su_2\| \\ &= \|u_1 - Su_1\| + \frac{1}{7}\|u_1 - u_2\| \\ &\leq \|u_1 - Su_1\| + \|u_1 - u_2\|. \end{aligned}$$

**Case II :** If  $u_1, u_2 \in [0, 1] \setminus \{\frac{1}{7}\}$ ,

$$\begin{aligned} \|u_1 - Su_2\| &\leq \|u_1 - Su_1\| + \|Su_1 - Su_2\| \\ &= \|u_1 - Su_1\| + \|u_1 - u_2\|. \end{aligned}$$

**Case III :** If  $u_1 \in [-1, 0)$  and  $u_2 = \frac{1}{7}$ ,

$$\begin{aligned} \|u_1 - Su_2\| &= \|u_1\| \leq \frac{8}{7}\|u_2\| + \|u_2 - \frac{1}{7}\| \\ &= \|u_1 - Su_1\| + \|u_1 - u_2\|. \end{aligned}$$

**Case IV :** If  $u_1 \in [-1, 0)$  and  $u_2 \in [0, 1] \setminus \{\frac{1}{7}\}$ ,

$$\begin{aligned} \|u_1 - Su_2\| &= \|u_1 + u_2\| \leq \|u_1\| + \|u_2\| \\ &\leq \frac{8}{7}\|u_1\| + \|u_1 - u_2\| \\ &= \|u_1 - Su_1\| + \|u_1 - u_2\|. \end{aligned}$$

**Case V :** If  $u_1 \in [0, 1] \setminus \{\frac{1}{7}\}$  and  $u_2 = \frac{1}{7}$ ,

$$\begin{aligned} \|u_1 - Su_2\| &= \|u_1\| \leq 2\|u_1\| + \|u_1 - \frac{1}{7}\| \\ &= \|u_1 - Su_1\| + \|u_1 - u_2\|. \end{aligned}$$

Therefore the mapping  $S$  satisfies condition (E) and its fixed point is 0.

## 5 Numerical Results

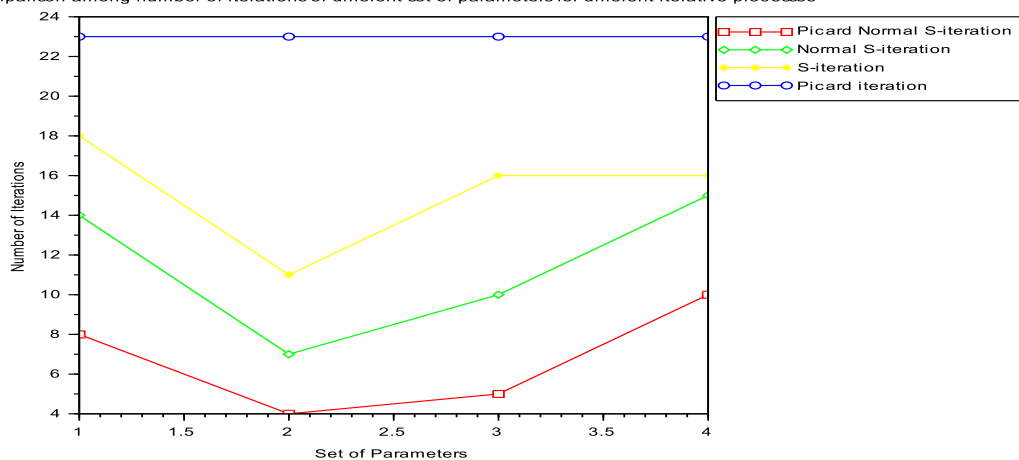
In this section, a comparison of the convergence behaviour of PNSA (1.3) with NSA (1.2), S-iterative algorithm (1.1) and Picard iterative algorithm for a mapping satisfying Condition (E) defined in Example 4.1 is presented. We select the different set of parameters of  $\alpha_m, \beta_m, \gamma_m$  and stopping criteria  $\|t_m - u^*\| \leq 10^{-11}$ . The influence of initial values of PNSA (1.3), NSA (1.2), S-iterative algorithm (1.1) and Picard iterative algorithm is examined in Table 1 using  $\alpha_m = \frac{2m}{3m+21}, \beta_m = \frac{3m}{4m+51}$ .

**Observations:** Here one can note that it is exhibited in Table 1, Table 2 and Figure 1, PNSA (1.3) is faster than NSA (1.2), S-iterative algorithm (1.1) and Picard iterative algorithm for a different set of parameters and initial values for a mapping satisfying Condition (E) defined in Example 4.1.

**Table 1.** Comparison of number of iterations of PNSA (1.3) with other iterative algorithms for Example 4.1

Initial Value	PNSA	NSA	S-iteration	Picard
-1	11	13	19	23
-0.8	11	13	19	23
-0.6	11	13	18	22
-0.4	11	13	18	22
-0.2	10	12	18	22
0.2	11	13	19	23
0.4	11	13	19	23
0.6	11	13	19	23
0.8	11	13	19	24
1	11	13	19	24

Comparison among number of iterations of different set of parameters for different iterative processes

**Figure 1.** Comparison among number of iterations of PNSA (1.3) for initial value 0.4 for Example 4.1

**Table 2.** Comparison of number of iterations of PNSA (1.3) with other iterative algorithms for different parameters for Example 4.1

Iteration	Initial Values									
	-1	-0.8	-0.6	-0.4	-0.2	0.2	0.4	0.6	0.8	1
For $\alpha_m = \frac{m^2}{2m^2+71}, \beta_m = \frac{m^3}{3m^3+11}$										
PNSA	8	8	8	8	8	8	8	8	8	8
NSA	14	14	14	14	13	14	14	14	14	14
S-iteration	18	18	18	17	17	17	18	18	19	19
Picard	23	23	22	22	22	23	23	23	24	24
For $\alpha_m = \frac{1}{(3m+7)^{\frac{1}{8}}}, \beta_m = \frac{1}{(7m+2)^{\frac{1}{9}}}$										
PNSA	4	4	4	4	4	4	4	5	5	5
NSA	7	7	7	7	7	7	7	7	8	8
S-iteration	10	10	9	9	9	10	11	11	11	11
Picard	23	23	22	22	22	23	23	23	24	24
For $\alpha_m = \frac{4m}{7m+11}, \beta_m = \frac{m}{3m+55}$										
PNSA	5	5	5	5	5	5	5	6	6	6
NSA	10	10	9	9	9	10	10	10	10	10
S-iteration	16	16	16	15	15	15	16	16	17	17
Picard	23	23	22	22	22	23	23	23	24	24
For $\alpha_m = \frac{3m}{6m-1}, \beta_m = \frac{1}{(2m+7)^{\frac{2}{13}}}$										
PNSA	10	10	10	10	10	10	10	11	11	11
NSA	16	16	16	15	15	15	15	15	16	16
S-iteration	17	17	17	17	16	16	16	16	16	16
Picard	23	23	22	22	22	23	23	23	24	24

## 6 Application

In the following section, we discuss the application to substantiate one of our obtained results. Consider  $C[0, 1]$  as space of continuous functions defined on  $\mathcal{E} = [0, 1] \subset \mathbb{R}_+$  and nonlinear functional integral equation (FIE, in brief)

$$\varphi(u) = f(u) + \lambda_1 \int_0^u \kappa(u, s)g(s, \varphi(s))ds + \lambda_2 \int_0^1 \bar{\kappa}(u, s)\bar{g}(s, \varphi(s))ds \quad (6.1)$$

for all  $u, s \in \mathcal{E}$ ,  $\lambda_1, \lambda_2$  are positive constants and  $f : \mathcal{E} \rightarrow \mathbb{R}_+$ ,  $g, \bar{g} : \mathcal{E} \times \mathbb{R} \rightarrow \mathbb{R}_+$ ,  $\kappa, \bar{\kappa} : \mathcal{E} \times \mathcal{E} \rightarrow \mathbb{R}_+$ . We have the following conditions.

(**K<sub>1</sub>**) The function  $f : \mathcal{E} \rightarrow J$  is continuous.

(**K<sub>2</sub>**) The functions  $\kappa, \bar{\kappa} : \mathcal{E} \times J \rightarrow \mathbb{R}_+$  are continuous such that for all  $u, s \in \mathcal{E}$

$$\int_0^u \kappa(u, s)ds \leq K_1 \quad \text{and} \quad \int_0^1 \bar{\kappa}(u, s)ds \leq K_2.$$

(**K<sub>3</sub>**) The functions  $g, \bar{g} : \mathcal{E} \times \mathbb{R} \rightarrow \mathbb{R}$  are continuous and there are two constants  $L_1, L_2$  such that for all  $u \in \mathcal{E}; \varphi_1, \varphi_2 \in C$ ,

$$\begin{aligned} |g(u, \varphi_1) - g(u, \varphi_2)| &\leq L_1|\varphi_1(u) - \varphi_2(u)| \\ |\bar{g}(u, \varphi_1) - \bar{g}(u, \varphi_2)| &\leq L_2|\varphi_1(u) - \varphi_2(u)| \end{aligned}$$

(**K<sub>4</sub>**)  $\lambda_1 L_1 K_1 + \lambda_2 L_2 K_2 = 1$ .

The following result represents the existence of the solution of FIE (6.1).

**Theorem 6.1.** Assume that  $U$  is compact subset of  $Y = C[0, 1]$ , where supremum norm is defined by  $\|\varphi_1 - \varphi_2\| = \sup_{u \in \mathcal{E}} |\varphi_1(u) - \varphi_2(u)|$  and assumptions from (**K<sub>1</sub>**) to (**K<sub>4</sub>**) are true. The mapping  $S : U \rightarrow U$  is defined by

$$S\varphi(u) = f(u) + \lambda_1 \int_0^u \kappa(u, s)g(s, \varphi(s))ds + \lambda_2 \int_0^1 \bar{\kappa}(u, s)\bar{g}(s, \varphi(s))ds.$$

Then  $S$  admits A.F.P.S. if and only if nonlinear FIE (6.1) has solution in  $Y$ .

*Proof.* Assume that  $\varphi_1, \varphi_2 \in U$ . Then

$$\begin{aligned} |\varphi_1(u) - S\varphi_2(u)| &= \left| \varphi_1(u) - \left( f(u) + \lambda_1 \int_0^u \kappa(u, s)g(s, \varphi_1(s))ds + \lambda_2 \int_0^1 \bar{\kappa}(u, s)\bar{g}(s, \varphi_1(s))ds \right) \right. \\ &\quad \left. + \left( f(u) + \lambda_1 \int_0^u \kappa(u, s)g(s, \varphi_1(s))ds + \lambda_2 \int_0^1 \bar{\kappa}(u, s)\bar{g}(s, \varphi_1(s))ds \right) \right. \\ &\quad \left. - f(u) - \lambda_1 \int_0^t \kappa(u, s)g(s, \varphi_2(s))ds + \lambda_2 \int_0^1 \bar{\kappa}(u, s)\bar{g}(s, \varphi_2(s))ds \right| \\ &\leq |\varphi_1(u) - S\varphi_1(u)| + \lambda_1 \int_0^u \kappa(u, s)|g(s, \varphi_1(s)) - g(s, \varphi_2(s))|ds \\ &\quad + \lambda_2 \int_0^1 \bar{\kappa}(u, s)|\bar{g}(s, \varphi_1(s)) - \bar{g}(s, \varphi_2(s))|ds \\ &\leq |\varphi_1(u) - S\varphi_1(u)| + \lambda_1 \int_0^u \kappa(u, s)L_1|\varphi_1(s) - \varphi_2(s)|ds \\ &\quad + \lambda_2 \int_0^1 \bar{\kappa}(u, s)L_2|\varphi_1(s) - \varphi_2(s)|ds. \end{aligned}$$

On taking supremum of both the sides, we get

$$\begin{aligned} \|\varphi_1 - S\varphi_2\| &\leq \|\varphi_1 - S\varphi_1\| + (\lambda_1 K_1 L_1 + \lambda_2 K_2 L_2)\|\varphi_1 - \varphi_2\| \\ &= \|\varphi_1 - S\varphi_1\| + \|\varphi_1 - \varphi_2\|. \end{aligned}$$



This shows that the  $S$  is mapping satisfying the Condition (E) on  $U$  with  $\mu = 1$ . By Theorem 2.3, nonlinear FIE (6.1) has solution in  $U$ .  $\square$

**Corollary 6.2.** Assume that  $U$  is compact subset of  $Y = C[0, 1]$ , where supremum norm is defined by  $\|\varphi_1 - \varphi_2\| = \sup_{u \in \mathcal{E}} |\varphi_1(u) - \varphi_2(u)|$  and assumptions from  $(\mathbf{K}_1)$  to  $(\mathbf{K}_4)$  are true. The mapping  $S : U \rightarrow U$  is defined by

$$S\varphi(u) = f(u) + \lambda_1 \int_0^u \kappa(u, s)g(s, \varphi(s))ds.$$

Then the nonlinear FIE

$$\varphi(u) = f(u) + \lambda_1 \int_0^u \kappa(u, s)g(s, \phi(s))ds$$

has solution in  $Y$  if and only if  $S$  admits A.F.P.S.

*Proof.* On setting  $\bar{\kappa}(t, s) \equiv 0$ , we get the desired result.  $\square$

The following Corollary is the result of Pandey *et al.* [15, Theorem 6.1]

**Corollary 6.3.** Assume that  $U$  is compact subset of  $Y = C[0, 1]$ , where supremum norm is defined by  $\|\varphi_1 - \varphi_2\| = \sup_{u \in \mathcal{E}} |\varphi_1(u) - \varphi_2(u)|$  and assumptions from  $(\mathbf{K}_1)$  to  $(\mathbf{K}_4)$  are true. The mapping  $S : U \rightarrow U$  is defined by

$$S\varphi(u) = f(u) + \lambda_2 \int_0^1 \bar{\kappa}(u, s)\bar{g}(s, \varphi(s))ds.$$

Then the nonlinear FIE

$$\varphi(u) = f(u) + \lambda_2 \int_0^1 \bar{\kappa}(u, s)\bar{g}(s, \varphi(s))ds$$

has solution in  $Y$  if and only if  $S$  admits A.F.P.S.

*Proof.* On setting  $\kappa(t, s) \equiv 0$ , we get the desired result.  $\square$

**Example 6.4.** Let us consider the following nonlinear FIE : For  $u, s \in [0, 1]$ ,

$$\phi(u) = (u^2 + 4) + \frac{3}{20} \int_0^u [(u^3 + 1)(2s + 4)] \frac{|\varphi(s)|}{3} ds + \frac{5}{12} \int_0^1 [u^2(2s + 5)] \frac{|\varphi(s)|}{5} ds. \tag{6.2}$$

If we take

$$\begin{aligned} \lambda_1 &= \frac{3}{20}, \quad \lambda_2 = \frac{5}{12}, \quad f(u) = u^2 + 4; \\ \kappa(u, s) &= (u^3 + 1)(2s + 4), \quad \bar{\kappa}(u, s) = u^2(2s + 5); \\ g(s, \varphi(s)) &= \frac{|\varphi(s)|}{3} \quad \bar{g}(s, \varphi(s)) = \frac{|\varphi(s)|}{5}. \end{aligned}$$

Then nonlinear FIE (6.2) will be in form of (6.1).

It is clear that function  $f(u) = u^2 + 4, \forall u \in [0, 1]$  is continuous.

For each  $u, s \in [0, 1]$ ,

$$\int_0^1 \kappa(u, s) = \int_0^1 (u^3 + 1)(2s + 4)ds \leq 10;$$

$$\int_0^1 \bar{\kappa}(u, s) = \int_0^u u^2(2s + 5)ds \leq 6.$$

For  $\varphi_1, \varphi_2 \in U; s \in [0, 1]$ ,

$$\begin{aligned} |g(s, \varphi_1(s)) - g(s, \varphi_2(s))| &= \left| \frac{|\varphi_1(s)|}{3} - \frac{|\varphi_2(s)|}{3} \right| \\ &= \frac{1}{3} \left| |\varphi_1(s)| - |\varphi_2(s)| \right| \\ &\leq \frac{1}{3} \left| \varphi_1(s) - \varphi_2(s) \right| \end{aligned}$$

$$\begin{aligned} |\bar{g}(s, \varphi_1(s)) - \bar{g}(s, \varphi_2(s))| &= \left| \frac{|\varphi_1(s)|}{5} - \frac{|\varphi_2(s)|}{5} \right| \\ &= \frac{1}{5} \left| |\varphi_1(s)| - |\varphi_2(s)| \right| \\ &\leq \frac{1}{5} \left| \varphi_1(s) - \varphi_2(s) \right| \end{aligned}$$

Since all assumptions of Theorem 6.1 are satisfied with  $K_1 = 10, K_2 = 6$  and  $\lambda_1 K_1 L_1 + \lambda_2 K_2 L_2 = 1$ . Therefore nonlinear FIE (6.2) has a solution.

## 7 Conclusion

It concludes that we have established convergence theorems for mapping satisfying Condition (E) via PNSA (1.3) in UCBS. Further, a comparison of the rate of convergence of PNSA (1.3) for such mappings is done and it is observed that PNSA (1.3) is faster, numerically, than well-known iteration processes such as Picard iterative algorithm, NSA (1.2) and S-iterative algorithm (1.1). As existence results for nonlinear FIE discussed in Pandey *et al.* [15], so one can note that our obtained result improves those of due to Pandey *et al.* [15].

## Acknowledgement

The authors are grateful to the referees for their valuable comments and suggestions which improve the paper.

## References

- [1] R.P. Agarwal, D. O'Regan and D.R. Sahu, Iterative construction of fixed points of nearly asymptotically nonexpansive mappings, *J. Nonlinear Convex Anal.* **8** (1), 61–79 (2007).
- [2] F.E. Browder, Nonexpansive nonlinear operators in a Banach space, *Proc. Natl. Acad. Sci. U.S.A.* **54** (4), 1041–1044.
- [3] J. García-Falset, E. Llorens-Fuster and T. Suzuki, Fixed point theory for a class of generalized nonexpansive mappings, *J. Math. Anal. Appl.* **375** (1), 185–195 (2011).
- [4] C. Garodia and I. Uddin, A new iterative method for solving split feasibility problem, *Journal of Applied Analysis and Computation* **10**(3), 986–1004 (2020).
- [5] C. Garodia, I. Uddin and S.H. Khan, *Approximating common fixed points by a new faster iteration process*, *Filomat* **34** (6), 2047–2060 (2020).
- [6] D. Göhde, Zum Prinzip der kontraktiven Abbildung, *Math. Nachr.* **30**, 251–258 (1965).
- [7] S. Ishikawa, Fixed points by a new iteration method, *Proc. Am. Math. Soc.* **44** (1), 147–150 (1974).
- [8] N. Kadioglu and I. Yildirim, Approximating fixed points of nonexpansive mappings by faster iteration process, *J. Adv. Math. Stud.* **8** (2), 257–264 (2015).
- [9] W.A. Kirk, A fixed point theorem for mappings which do not increase distances, *Amer. Math. Monthly* **72** (9) (1965), 1004–1006.
- [10] S.Khatoun, I. Uddin and D. Baleanu, Approximation of fixed point and its application to fractional differential equation, *J. Appl. Math. Comput.* **66**, 507–525 (2021).
- [11] W.R. Mann, Mean value methods in iteration, *Proc. Am. Math. Soc.* **4** (1953), 506–610.

- [12] K. Nakajo and W. Takahashi, Strong convergence theorems for nonexpansive mappings and nonexpansive semigroups, *J. Math. Anal. Appl.* **279** (2) (2003), 372–379.
- [13] M.A. Noor, New approximation schemes for general variational inequalities, *J. Math. Anal. Appl.* **251** (1), 217–229 (2000).
- [14] Z. Opial, Weak convergence of the sequence of successive approximations for nonexpansive mappings, *Bull. Amer. Math. Soc.* **73** (4), 591–597 (1967).
- [15] R. Pandey, R. Pant, V. Rakoevi, R. Shukla, Approximating fixed points of a general class of nonexpansive mappings in Banach spaces with applications, *Results Math.* **2019** 74:7 (2019).
- [16] S. Rezapour, M. Iqbal, A. Batool, S. Etemad and T. Botmart, A new modified iterative scheme for finding common fixed points in Banach spaces: application in variational inequality problems, *AIMS Mathematics*, **8**(3), 5980-5997 (2023).
- [17] D.R. Sahu, Application of the s-iteration process to constrained minimization problems and feasibility problems, *Fixed Point Theory* **12**, 187–204 (2011).
- [18] D.R. Sahu, Applications of accelerated computational methods for quasi-nonexpansive operators to optimization problems, *Soft Comput* **24**, 17887–17911 (2020).
- [19] D.R. Sahu, D. O'Regan and R.P. Agarwal, Fixed Point Theory for Lipschitzian-type Mappings with Applications, *Springer New York*, (2009).
- [20] D.R. Sahu, A. Pitea and M. Verma, A new iteration technique for nonlinear operators as concerns convex programming and feasibility problems, *Numer. Algor.* **83**, 421–449 (2020).
- [21] H.F. Senter and W.G. Dotson, Approximating fixed points of nonexpansive mappings, *Proc. Am. Math. Soc.* **44**, 375–380 (1974).
- [22] H.F. Senter and W.G. Dotson, Approximating fixed points of nonexpansive mappings, *Proc. Am. Math. Soc.* **44**, 375–380 (1974).
- [23] I. Uddin, C. Garodia and T. Abdeljawad, Convergence analysis of a novel iteration process with application to a fractional differential equation, *Adv. Cont. Discr. Mod.* **2022**, 16 (2022).
- [24] I. Uddin, C. Garodia and J.J. Nieto, Mann iteration for monotone nonexpansive mappings in ordered CAT(0) space with an application to integral equations, *J. Inequal. Appl.* **2018**, 339 (2018).
- [25] I. Uddin and M. Imdad, On certain convergence of S-Iteration scheme in CAT(0) spaces, *Kuwait J. Sci.* **42** (2), 93-106 (2015).
- [26] I. Uddin and M. Imdad, Convergence of SP-iteration for generalized nonexpansive mapping in Hadamard spaces, *Haceteppe Journal of Mathematics and Statistics* **47** (6) (2018), 1595–1604.
- [27] H.K. Xu and D.R. Sahu, Parallel normal S-iteration methods with applications to optimization problems, *Numerical Functional Analysis and Optimization*, **42** (16), 1925-1953 (2021).
- [28] Y. Yao, Y.J. Cho, Y.C. Liou, Algorithms of common solutions of variational inclusions, mixed equilibrium problems and fixed point problems, *Eur. J. Oper. Res.* **212** (2), 242–250 (2011).

### Author information

Samir Dashputre, Department of Mathematics, Govt. College, Arjunda, Balod, Chhattisgarh, India.  
E-mail: samir231973@gmail.com

Padmavati, Department of Mathematics, Govt. V.Y.T. Autonomous P.G. College, Durg, Chhattisgarh, India.  
E-mail: padmavati.sudha62@gmail.com

Kavita Sakure, Department of Mathematics, Govt. Digvijay Auto. P.G. College, Rajnandgaon, Chhattisgarh, India.  
E-mail: kavitaage@gmail.com

# Reliability Modeling and Analysis of an Industrial System with one Main Unit with Two Subunit

Hemant Kumar Saw<sup>1</sup>, Iti Sao<sup>2</sup>, Prachi Singh<sup>3</sup>

<sup>1</sup>Government. Digvijay P.G. Autonomous College Rajnandgaon, Chhattisgarh, India

<sup>2,3</sup>Government V. Y.T. Autonomous. P.G. College, Durg Chhattisgarh, India

**Abstract:** *The paper deals with Reliability modelling and analysis of an industrial system with one main unit with two sub unit. The system consists of one main unit and two sub unit. System will be operable when main unit and at least one subunit is in operative mode. It is assumed that only one job is taken for processing at a time. There is a single server who visits the system immediately when preventive maintenance and repair required. The unit works as new after preventive maintenance and repair. The failures of the unit are distributed exponentially while the distribution of PM and repair time are taken is arbitrary. Semi-Markov and Markov regenerative point techniques are used to calculate various reliability parameters.*

**2020 Mathematics Subject Classification:** 90B25,60K10.

**Keywords:** Main time between failure (MTBF), Preventive maintenance (PM), Regenerative point technique ,semi-Markov process

## 1. Introduction

It is obvious that a system is composed of a number of components and to achieve high reliability of the system; we have to use high reliable components. In many cases when it is not possible to produce such type of components, we can increase the system reliability by incorporating the redundancies of the corresponding components. Reliability models for system have widely been analyzed by a number of authors under various assumption, including Saw and Manker [4] develop a stochastic reliability model of a one-unit main system with two associate units along with sub - unit. Gopalan [2] analyzed cost benefit analysis of one server two-unit cold standby system with repair and preventive maintenance, Nakagawa and Osaki [7] studies model which describes single unit system with scheduled maintenance and variation in demand. Pathak, and Mehata [8] developed the configuration modelling of wire rod system, Singh and Singh [6] analysis cost-benefit analysis of a single unit system with scheduled maintenance and variation in demand. Gupta 2007 [1] discussed benefit analysis of distillery plant system studies some reliability models in real data of failure and repair rates in such system. Saw, Pathak and Chaturvedi [5] analysis stochastic model for analysis real industrial system modal of a RO membrane used in water purification system. Bhatt, Chitkara and Bhardwaj [3] analysis two identical unit cold standby system with single repairman has been discussed. This modal present Reliability modelling and Analysis of an industrial system with one main unit with two sub unit. Also, the involvement of preventive maintenance in the modal increases the reliability of the functioning units.

## 2. Materials and Method

In this study, the stochastic reliability of the system is analyzed by using semi-Markov process and regenerative point techniques expression for various reliability measures like Mean time between failure. The steady state Availability, the Busy period of the server due to repair of a

failed unit at  $t = 0$ . Busy period of the server due to preventive maintenance at  $t = 0$ . Expected down time at  $t = 0$ . Expected number of visits by server at  $t = 0$ . Profit incurred to the system.

### System Description

The system consists of three units namely one main unit M and two associate unit U and R. Hear the associate unit U and R dependents upon the main unit M. The main unit is employed to rotate U and R. As soon as job arrives, all the units work with load. It is assumed that only one job is taken for processing at a time. There is a single repairman who repair the failed units on a priority basis. Using regenerative point technique, several system characteristics such as transition probabilities, mean sojourn times, availability and busy period of the repairman are evaluated. In the end, the expected profit is also calculated.

### Assumptions

- 1) The system consists of one main unit and two associate units.
- 2) The associate units U and R starts with the help of the main unit.
- 3) There is a single repairman who repairs the failed units on a priority basis.
- 4) After repair system work in good state.
- 5) The repair starts immediately upon failure of units.
- 6) After a random period of time, the whole system goes to preventive maintenance.

### Notations

$P_{ij}$  = Transition probabilities from  $S_i$  to  $S_j$

$\mu_i$  = Mean Sojourn time at time t

$x_1/x_2/x_3$  = Constant repair rate of Main unit M/Associate unit U/Associate unit R

$\alpha_1/\alpha_2/\alpha_3$  = Failure rate of Main unit M/Associate unit U/Associate unit R

Volume 12 Issue 12, December 2023

[www.ijsr.net](http://www.ijsr.net)

Licensed Under Creative Commons Attribution CC BY

$f_1/f_2/f_3$  = Probability density function of repair time of Main unit M/Associate unit U/Associate Unit R

$\overline{F}_1/\overline{F}_2/\overline{F}_3$  = Cumulative distribution function of repair time of Main unit M/Associate unit U/Associate unit R

$a(t)$  = Probability density function of preventive maintenance,

$b(t)$  = Probability density function of preventive maintenance completion time,

$\overline{G}(t)$  = Cumulative distribution functions of preventive maintenance,

$\overline{H}(t)$  = Cumulative distribution functions of preventive maintenance completion time,

$\$$  = Symbol for Laplace-Stieltjes transforms,

$\phi$  = Symbol for Laplace-convolution

$Q_{i,j}(t)$  = Cumulative distribution function of transition time from  $S_i$  to  $S_j$

$B_0(t)$  = Busy period of the server for repair due to failed unit at time  $t=0$

$B$  = Set of regenerative states

$\pi_i(t)$  = CDF of time to system failure when starting from state  $B_0 = S_i \in B$

$\mu_i(t)$  = Mean Sojourn time in the state  $B_0 = S_i \in B$ ,

$D_i(t)$  = Repairman is busy in the repair at time  $t$

$B_0 = S_i \in B$ ,

**Symbols**

$M_0/M_G/M_r$ - Main unit 'M' under operation/good and non-operative mode/repair mode,

$R_0/R_g/R_r$  — Associate unit 'R' under operation/good and non-operative mode/repair mode

$U_0/U_g/U_r$ -Associate unit 'U' under operation/good and non-operative mode/repair mode,

P.M. — System under preventive maintenance

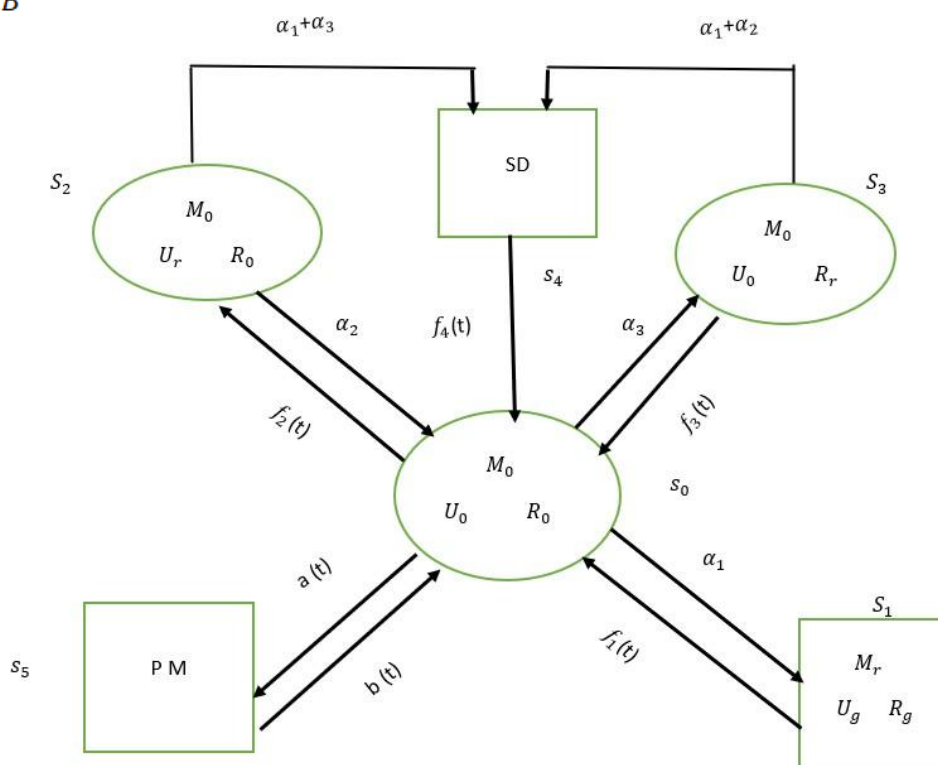
**Up States**

$S_0 = (M_0, U_0, R_0), S_2 = (M_0, U_r, R_0), S_3 = (M_0, U_0, R_r)$

**Down States**

$S_1 = (M_r, U_g, R_g), S_4 = (S. D.), S_5 = (P. M.)$

State transition diagram



**Mathematical Analysis of the System**

**Transition Probabilities and Mean Sojourn Times**

Simple probabilistic considerations yield the following non-zero transition probabilities:

$$Q_{01}(t) = \int_0^t \alpha_1 e^{-(\alpha_1 + \alpha_2 + \alpha_3)t} \overline{G}(t) dt$$

$$Q_{02}(t) = \int_0^t \alpha_2 e^{-(\alpha_1 + \alpha_2 + \alpha_3)t} \overline{G}(t) dt$$

$$Q_{03}(t) = \int_0^t \alpha_3 e^{-(\alpha_1+\alpha_2+\alpha_3)t} \bar{G}(t) dt$$

$$Q_{24}(t) = \int_0^t (\alpha_1 + \alpha_3) e^{-(\alpha_1+\alpha_3)t} \bar{F}_2(t) dt$$

$$Q_{05}(t) = \int_0^t a(t) e^{-(\alpha_1+\alpha_2+\alpha_3)t} dt$$

$$Q_{34}(t) = \int_0^t (\alpha_1 + \alpha_2) e^{-(\alpha_1+\alpha_2)t} \bar{F}_3(t) dt$$

$$Q_{10}(t) = \int_0^t f_1(t) dt$$

$$Q_{50}(t) = \int_0^t b(t) dt$$

$$Q_{20}(t) = \int_0^t f_2(t) e^{-(\alpha_1+\alpha_3)t} dt$$

$$Q_{40}(t) = \int_0^t f_4(t) dt$$

$$Q_{30}(t) = \int_0^t f_3(t) e^{-(\alpha_1+\alpha_2)t} dt$$

The nonzero element  $P_{ij}$  can be obtained as

$$P_{ij} = \lim_{Pt \rightarrow \infty} C_{ij}(t)$$

$$P_{01}(t) = \int_0^\infty \alpha_1 e^{-(\alpha_1+\alpha_2+\alpha_3)t} \bar{G}(t) dt = \frac{\alpha_1 [1 - f^*(\alpha)]}{\alpha}$$

$$P_{02}(t) = \int_0^\infty \alpha_2 e^{-(\alpha_1+\alpha_2+\alpha_3)t} \bar{G}(t) dt = \frac{\alpha_2 [1 - f^*(\alpha)]}{\alpha}$$

$$P_{03}(t) = \int_0^\infty \alpha_3 e^{-(\alpha_1+\alpha_2+\alpha_3)t} \bar{G}(t) dt = \frac{\alpha_3 [1 - f^*(\alpha)]}{\alpha}$$

$$P_{05}(t) = \int_0^\infty a(t) e^{-(\alpha_1+\alpha_2+\alpha_3)t} dt = f^*(\alpha)$$

$$P_{20}(t) = \int_0^\infty e^{-(\alpha_1+\alpha_3)t} f_2(t) dt = f_2^*(\alpha_1 + \alpha_3)$$

$$P_{30}(t) = \int_0^\infty e^{-(\alpha_1+\alpha_2)t} f_3(t) dt = f_3^*(\alpha_1 + \alpha_2)$$

$$P_{24}(t) = \int_0^\infty (\alpha_1 + \alpha_3) e^{-(\alpha_1+\alpha_3)t} \bar{F}_2(t) dt = 1 - f_2^*(\alpha_1 + \alpha_3)$$

$$P_{34}(t) = \int_0^\infty (\alpha_1 + \alpha_2) e^{-(\alpha_1+\alpha_2)t} \bar{F}_3(t) dt = 1 - f_3^*(\alpha_1 + \alpha_2)$$

$$P_{10}(t) = \int_0^\infty f_1(t) dt = 1$$

$$P_{50}(t) = \int_0^\infty b(t) dt = 1$$

It can be easily verified that;

$$P_{01} + P_{02} + P_{03} + P_{05} = 1$$

$$P_{20} + P_{24} = 1, P_{30} + P_{34} = 1$$

defined as the time of stay in that state before transition to any other state.

$$\mu_0 = \frac{[1 - f^*(\alpha)]}{\alpha}$$

$$\mu_1 = \int_0^\infty \bar{F}_1(t) dt$$

$$\mu_2 = \frac{[1 - f_2^*(\alpha_1 + \alpha_3)]}{\alpha_1 + \alpha_3}$$

The main sojourn times ( $\mu_i$ ) in the generative state  $i$  is

$$\mu_3 = \frac{[1 - f_3^*(\alpha_1 + \alpha_2)]}{\alpha_1 + \alpha_2}$$

$$\mu_4 = \int_0^\infty \bar{F}_4(t) dt$$

$$\mu_5 = \int_0^\infty \bar{H}(t) dt$$

Laplace Stieltjes transform of  $C_{ij}(t)$  we get.

$$\bar{Q}_{ij}(s) = \int_0^\infty e^{-st} C_{ij}(t) dt = L[C_{ij}(t)] = q_{ij}^*(s)$$

$$\bar{Q}_{01}(s) = \int_0^\infty \alpha_1 e^{-(s+\alpha)t} \bar{G}(t) dt = \frac{\alpha_1 [1 - g^*(s + \alpha)]}{s + \alpha}$$

$$\bar{Q}_{26}(s) = \int_0^\infty (\alpha_1 + \alpha_3) e^{-(s+\alpha_1+\alpha_3)t} \bar{F}_2(t) dt = \frac{\alpha_1 + \alpha_3 [1 - f_2^*(s + \alpha_1 + \alpha_3)]}{s + \alpha_1 + \alpha_3}$$

$$\bar{Q}_{30}(s) = \int_0^\infty e^{-(s+\alpha_1+\alpha_2)t} f_3(t) dt = f_3^*(s + \alpha_1 + \alpha_2)$$

$$\bar{Q}_{36}(s) = \int_0^\infty (\alpha_1 + \alpha_2) e^{-(s+\alpha_1+\alpha_2)t} \bar{F}_3(t) dt = \frac{\alpha_1 + \alpha_2 [1 - f_3^*(s + \alpha_1 + \alpha_2)]}{s + \alpha_1 + \alpha_2}$$

$$\bar{Q}_{50}(s) = \int_0^\infty e^{-st} b(t) dt = b^*(s)$$

$$\bar{Q}_{40}(s) = \int_0^\infty e^{-st} f_6(t) dt = f_6^*(s)$$

We define  $m_{ij}$  as follows:

$$m_{ij} = - \left[ \frac{d\bar{Q}_{ij}(s)}{ds} \right]_{s=0} = -Q'_{ij}(0)$$

It can be easily verified

$$m_{01} + m_{02} + m_{03} + m_{05} = \mu_0$$

$$m_{20} + m_{24} = \mu_2$$

$$m_{30} + m_{34} = \mu_3$$

Where  $\alpha_1 + \alpha_2 + \alpha_3 = \alpha$  Main Time Between Failure

$\pi_i(t)$  is defined as the CDF of first passage time from

$i^{th}$  state to a failed state.

$$A_0(t) = M_0(t) + q_{01}(t)\phi A_1(t) + q_{02}(t)\phi A_2(t) + q_{03}(t)\phi A_3(t) + q_{05}(t)\phi A_5(t)$$

$$A_1(t) = q_{10}(t)\phi A_0(t)$$

$$A_2(t) = M_2(t) + q_{20}(t)\phi A_0(t) + q_{24}(t)\phi A_4(t)$$

$$\bar{Q}_{02}(s) = \int_0^\infty \alpha_2 e^{-(s+\alpha)t} \bar{G}(t) dt = \frac{\alpha_2 [1 - g^*(s + \alpha)]}{s + \alpha}$$

$$\bar{Q}_{03}(s) = \int_0^\infty \alpha_3 e^{-(s+\alpha)t} \bar{G}(t) dt = \frac{\alpha_3 [1 - g^*(s + \alpha)]}{s + \alpha}$$

$$\bar{Q}_{05}(s) = \int_0^\infty e^{-(s+\alpha)t} a(t) dt = g^*(s + \alpha)$$

$$\bar{Q}_{10}(s) = \int_0^\infty e^{-st} f_1(t) dt = f_1^*(s)$$

$$\bar{Q}_{20}(s) = \int_0^\infty e^{-(s+\alpha_1+\alpha_3)t} f_2(t) dt = f_2^*(s + \alpha_1 + \alpha_3)$$

$$\pi_0(t) = Q_{01}(t) + Q_{02}\pi_2(t) + Q_{03}(t)\pi_3(t) + Q_{05}(t)$$

$$\pi_2(t) = Q_{20}\pi_0(t) + Q_{26}(t)$$

$$\pi_3(t) = Q_{30}\pi_0(t) + Q_{36}(t)$$

Taking Laplace- Stieltjes Transforms (L.S.T.) on both side and solving we get, The MTBF when the system starts from

the state  $S_0$  is given by.

$$E(T) = - \left[ \frac{d\bar{\pi}_0(s)}{ds} \right]_{s=0} = \frac{D(0) - N(0)}{D(0)}$$

$$= \frac{\mu_2 P_{02} + \mu_3 P_{03} - \mu_0}{1 - P_{02} P_{20} - P_{03} P_{30}}$$

#### Availability Analysis

Using probabilistic argument, we have the following recursive relations

$$A_3(t) = M_3(t) + q_{30}(t)\phi A_0(t) + q_{34}(t)\phi A_4(t)$$

$$A_4(t) = q_{40}(t)\phi A_0(t)$$

$$A_5(t) = q_{50}(t)\phi A_0(t)$$

Where

$$M_0(t) = e^{-(\alpha_1+\alpha_2+\alpha_3)t}\overline{G}(t)$$

$$M_2(t) = e^{-(\alpha_1+\alpha_3)t}\overline{F}_2(t)$$

$$M_3(t) = e^{-(\alpha_1+\alpha_2)t}\overline{F}_3(t)$$

Taking Laplace-Stieltjes Transforms (L.S.T.) of above equation and solving the steady -state availability is given by.

$$A_0^* = \lim_{s \rightarrow 0} sA_0^*(s) = \frac{N_1(0)}{D(0)}$$

Where

$$N_1(0) = \mu_2 P_{02} + \mu_3 P_{03} - \mu_0$$

$$D(0) = 1 - P_{02}P_{20} - P_{03}P_{30}$$

### Busy Period Analysis

Using probabilistic argument, we have the following recursive relation for

$$B_0(t) = q_{01}(t)\phi B_1(t) + q_{02}(t)\phi B_2(t) + q_{03}(t)\phi B_3(t) + q_{05}(t)\phi B_5(t)$$

$$B_1(t) = W_1(t) + q_{10}(t)\phi B_0(t)$$

$$B_2(t) = W_2(t) + q_{20}(t)\phi B_0(t) + q_{24}(t)\phi B_4(t)$$

$$B_3(t) = B_3(t) + q_{30}(t)\phi B_0(t) + q_{34}(t)\phi B_4(t)$$

$$B_4(t) = q_{40}(t)\phi B_0(t)$$

$$B_5(t) = q_{50}(t)\phi B_0(t)$$

Where

$$W_1(t) = \overline{F}_1(t), W_2(t) = \overline{F}_2(t), W_3(t) = \overline{F}_3(t),$$

Taking Laplace transform of above equation and solving for

$$B_0(s)$$

$$B_0(s) = \frac{N_2(s)}{D_2(s)}$$

Where

$$N_2(s) = \mu_2 P_{02} + \mu_3 P_{03} - \mu_0$$

$$D_2(s) = 1 - P_{02}P_{20} - P_{03}P_{30}$$

### Profit Analysis

$G(t)$  = Expected total revenue earned by the system in  $(0, t]$

- Expected repair cost of the failed units
- Expected repair cost of the repairman in preventive maintenance
- Expected repair cost of the Repairman in shut down

$$G(t) = C_0 A_0 - C_1 B_0 - C_2 B'_0 - C_3 B''_0$$

Where

$C_0$  be the per unit time revenue by the system

$C_1, C_2$  and  $C_3$  be the per unit time for which the system is under simple repair, preventive maintenance and shut down repair, respectively.

### References

- [1] Gupta R. and Kumar, K. *cost benefit analysis of distillery plant system*, Int J. Agricult. stat. Science. Vol. **3(2)**, pp 541-554. 2007(2007).
- [2] M.N. Gopalan and H.E. Nagarwala, *cost benefit analysis of one-server two unit cold standby system with repair and P.M.*, microelectron. Reliab Vol. **25(2)**(1985), pp267-26, 1985.
- [3] Bhatti, Jasdev, Ashok Chitkara, and nitin Bhardwaj. *Profit analysis of two unit cold standby system with two types of failure under inspection policy and discrete distribution*. "International journal of science and engineering research 2.2(2011); **1-7**.
- [4] Sao Hemant, and H.L. Manker. *Reliability Modeling of a System with One Main Unit and two associate Units along with sub-unit*, Communications in Mathematics and Applications **13.1**(2022)
- [5] Saw, H.K., Pathak, and Chaturvedi, R. *Stochastic Modelling and Reliability Analysis of a RO Membrane System Used in Water Purification System with Patience -time for repair*.
- [6] S.K. Singh and S.P. Singh, *The configuration modelling and analysis of wire rod mill system*, Aligarh Journal of Statistics **22** (2000), 43 – 62.
- [7] T. Nakagawa and S. Osaki, *Stochastic behavior of a two-unit priority stand by redundant system with repair*, Microelectronic and Reliability **14(3)** (1975), 309 – 313, DOI: 10.1016/0026-(75)90708-8.
- [8] V.K. Pathak, K. Mehata, S. Sahu and A. Namdeo, *Comparative study of reliability parameter of a system under different types of distribution functions*, African Journal of Mathematics and Computer Science Research **7(4)** (2014), 47 – 54, DOI: 10.5897/AJMCSR2014.0539



[Home](#) [Drug Delivery and Translational Research](#) [Article](#)

# Investigation of human hair keratin-based nanofibrous scaffold for skin tissue engineering application

Original Article Published: 17 August 2023

Volume 14, pages 236–246, (2024) [Cite this article](#)

## Drug Delivery and Translational Research

[Aims and scope](#)[Submit manuscript](#)

[Keshaw R. Aadil](#) , [Akash Nathani](#), [Archana Rajendran](#), [Chandra S. Sharma](#) , [Nibedita Lenka](#)  & [Pratima Gupta](#) 

 632 Accesses  2 Citations  5 Altmetric [Explore all metrics](#) →

## Abstract

Keratin-based nanofibers were fabricated using the electrospinning technique, and their potential as scaffolds for tissue engineering was investigated. Keratin, extracted from the human hair, was blended with poly(vinyl alcohol) (PVA) in an aqueous medium.

Morphological characterizations of the fabricated PVA-keratin nanofiber (PK-NF) random and aligned scaffolds performed using a scanning electron microscope (SEM) revealed the



# Introduction to Microbiology

**Dr. Shama A. Baig**  
**Dr. Sanju Sinha**



# Introduction to Microbiology



**First Volume**

**Editors**

Dr. Shama. A. Baig  
Dr. Sanju Sinha



# Contents

1	History and Development of Microbiology ..... <i>Dr. Kiran Jain and Samiksha Jain</i>	1-19
2	Classification System ..... <i>Dr. Anita Mahiswar and Dr. Shama A. Baig</i>	20-29
3	Virology ..... <i>Dr. Arpita Mukherjee</i>	30-50
4	Bacteriology ..... <i>Dr. Seema Sahu</i>	51-77
5	Archaeobacteria (Archaea) ..... <i>Miss. Samiksha Mishra</i>	78-90
6	Mycology ..... <i>Dr. Reena Kulshrestha</i>	91-105
7	Phycology ..... <i>Dr. Sweta Gaikwad</i>	106-126
8	Protozoology ..... <i>Dr. Sanju Sinha and Dr. Alka Mishra</i>	127-162
9	Microscopy ..... <i>Amit Kumar Sahu</i>	163-173
10	Sterilization and Staining Techniques in Microbiology ..... <i>Dr. Sanju Sinha</i>	174-189
11	Isolation and Staining Techniques ..... <i>Ms. Yogita Lokhande</i>	190-200

# Chapter 1

## History and Development of Microbiology



*Dr. Kiran Jain & Samiksha Jain*

- 
1. **Fundamentals of Microbiology**
  2. **History**
  3. **Development of Microbiology**
  4. **Golden Era of Microbiology, Fields of Microbiology**
  5. **Major groups, Role of Microbes in Daily Life**
  6. **Pioneers of Microbiology Antony von Leeuwenhoek**
  7. **Louis Pasteur, Robert Koch**
  8. **Joseph Lister, Alexander Fleming**
  9. **Martinus W. Beijerinck**
  10. **Sergei N. Winogradsky**
  11. **Selman A. Waksman**
  12. **Paul Ehrlich**
  13. **Elie Metchnikoff**
  14. **Edward Jenner**

**Hans Christian Gram.**

### **Introduction**

Microbiology is formed by "Mikros" + Bios+ Logos Mikros meaning Small, Bios- life and Logos. Science.

Microbiology is the study of living organisms that are not visible through naked eyes and can be studied under microscope. Microorganisms are unicellular to multicellular, ubiquitous in distribution and an important role in Ecosystem. Micro organisms include bacteria, fungi, algae, protozoan, & viruses (at the borderline of living & non-living). It includes the study of their forms, distribution, structure, reproduction, physiology, metabolism, and classification. Relationship of microorganisms with microbes as well as with other living organisms, plants, animals and human beings are also studied.

# Chapter 2

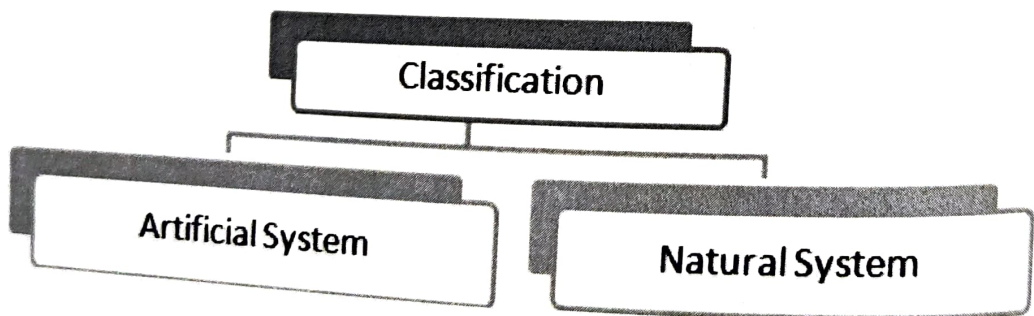
## Classification System



*Dr. Anita Mahiswar and Dr. Shama A. Baig*

1. Principles of Classification
2. Binomial Nomenclature
3. Haeckel's three Kingdom
4. Whittaker's five Kingdom
5. Carl Woese's 3 domain system
6. Concept of Prokaryotic and Eukaryotic Microorganisms.

Classification is the process of arranging organisms, both living and extinct, into groups based on similar characteristics. The major purpose of classification is identification of species and to show the degree of relatedness amongst. It plays an important role to provide idea about ancestry and lineage of an organism. The science of naming and classifying organisms is called taxonomy. The term is derived from the Greek taxis ("arrangement") and nomos ("law").



**Principles of Classification:** Characterization, classification and identification are major objectives in all branches of the biological sciences. In order to identify and classify microorganisms, we must first learn their characteristics. The major characteristics of microorganisms fall into the following categories:-

- **Morphological characteristics:** Cell shape, size, structure, cell arrangement, occurrence of special structure and developmental forms, staining reactions and motility and flagellar arrangement.

## ABOUT AUTHORS



**Dr. Shama Afroze Baig** is Assistant Professor and Head of Department (Microbiology) at Swami Shri Swaroopanand Saraswati Mahavidyalaya HUDCO Bhilai and she has also been Head of Microbiology Dept. in Govt Digvijay Autonomous P.G. College, Rajnandgon, CG and Assistant professor in Govt VYTPG Autonomus College, Durg , C.G. She was also a JRF, SRF and RA in Pandit Ravishankar Shukla University, Raipur, M.P. She has been graduated (BSc) and pursued her MSc. And Ph.D Courses from Pt. Ravi Shankar Shukla University , Raipur Chhattisgarh .She has completed PG Diploma in Yoga and M.A. Philosophy from Hemchand Yadav University, Durg, C.G. She has been honoured with 12th M.P Young Scientist Award 1997, Award of Excellence (IUFRO Symposi um) 2011, and Best Designer Award (Navbharat) 2007 and qualified GATE (JRF). She has a lifetime membership in many Professional Bodies ( MBSI, MPCG Darshan Parishad, Advances in Life Sciences, Trends in Bio Sciences, Society for Science and Environment , ICPEP, Indian Journal of Ecology and Indian Botanical Society ). She has a membership in around 20 Committees. She has attended 45 above Conferences and 33 Webinars at National and International levels and presented paper in it. She has published 22 research papers and 3 patents (2 National, 1 German).



**Dr. Sanju Sinha**, Assistant Professor, Govt. V.Y.T. PG Autonomous College, Durg, Chhattisgarh, 490 001. She passed her M.Sc. from Govt. V.Y.T. PG Autonomous College, Durg. She obtained her M.Phil. (with gold Medal) and Ph.D. degree from Pt Ravishankar Shukla University, Raipur. She has more than 25 years of research experience with work on Environmental Biology, Pollution Biology, Biodiversity with extensive works on protozoa of Chhattisgarh. She has more than 10 research papers in National and International Journals. To her credit she has published 6 books. She had served as Senior Scientific Officer in Chhattisgarh Council of Science and Technology for more then 9 Years. Presently she is working as an Assistant Professor of Zoology in Govt. V.Y.T. PG Autonomous College, Durg and is guiding 5 students for Ph.D.

This book is published in online version with e ISBN: 978-93-5747-507-5



Selfpage Developers Pvt Ltd

ISBN: 978-93-5747-933-2



9 789357 479332

MRP Rs. 499/-